Volume 22, No. 1

January–February, 1960

COLLOID JOURNAL

(KOLLOIDNYI ZHURNAL)

A publication of the Academy of Sciences of the USSR

IN ENGLISH TRANSLATION

Year and issue of first translation:
Vol. 14 No. 1 Jan.-Feb. 1952

545-157
8

Annual subscription *$80.00*
Single issue *20.00*

Copyright 1960
CONSULTANTS BUREAU ENTERPRISES, INC.
227 West 17th Street, New York, N. Y.

Editorial Board
(KOLLOIDNYI ZHURNAL)

P. N. Antipov-Karataev, B. V. Deriagin, B. A. Dogadkin
(Acting Editor), A. V. Dumanskii, V. A. Kargin,
S. M. Lipatov, P. A. Rebinder, I. P. Serdobolskii
(Secretary), M. P. Volarovich

A complete copy of any paper in this issue may be purchased from the publisher for $7.50

Note: The sale of photostatic copies of any portion of this copyright translation is expressly prohibited by the copyright owners.

Printed in the United States of America

VOLATILIZATION OF INGREDIENTS FROM POLYMERS

L. G. Angert, A. I. Zenchenko, and A. S. Kuz'minskii

Scientific Research Institute of the Rubber Industry, Moscow
(Translated from: Kolloidnyi Zhurnal Vol. 22, 22, No. 1, pp. 2-8, January-February, 1960)
(Original article submitted December 7 1958)

Some of the ingredients present in polymers may evaporate (or volatilize) under vacuum or by the action of heat. Volatilization of ingredients occurs during treatment of polymers at high temperatures, during curing of rubber goods in pans, during accelerated thermal aging of polymeric materials in thermostats, and from certain articles in use. The loss of ingredients increases with the free volume in which the polymer is present. Softeners, plasticizers, antioxidants, and free sulfur readily volatilize from various rubbers.

Volatilization of the most important ingredients present in polymeric materials has an adverse effect on their main physicochemical and mechanical properties, and their performance deteriorates accordingly. Moreover, volatilization of ingredients is accompanied by their migration from one polymer material into another when different materials are aged together in thermostats, and this leads to erroneous estimates of their heat stability [1].

Much information on the subject of migration has been published by ISO [2]. Until recently volatilization of various additives from polymers has not been studied widely enough from the scientific aspect. The only process to be studied in any detail was volatilization of plasticizers from plastics under atmospheric pressure and under vacuum [3].

The present investigation was undertaken in order to establish the empirical relationships which characterize the behavior of ingredients in raw and cured rubbers under various conditions, and for a theoretical examination of the problem.

In these investigations the volatilization of antioxidant from a rubber plate heated in a stream of gas was studied. The antioxidant was phenyl-β-naphthylamine.

The investigation procedure was as follows: Sodium butadiene rubber (SKB without antioxidant) was mixed in a micro roll mill with phenyl-β-naphthylamine; plates of the required thickness were molded from the resultant mix at 70°. The antioxidant was volatilized from rubber plates of standard surface area (150 × 10 mm) in glass tubes 18 mm in diameter; the rubber specimens were placed on glass supports. The tube was placed in a horizontal tubular surface heated by silicone fluid circulated from a Wobser thermostat (Fig. 1). A current of nitrogen passing through the tube removed the antioxidant vapor from the heated part of the tube into an attached trap immersed in freezing mixture. The antioxidant condensed in the trap and was estimated quantitatively by a colorimetric method. Volatilization was studied at temperatures above 100°.

Volatilization of the ingredient may depend both on the characteristics of the test specimen (plate thickness, initial concentration of ingredient in the specimen, etc.) and on the experimental conditions (temperature, velocity of the nitrogen stream, etc.).

Accordingly, the investigation consisted of determinations of the process kinetics in relation to the above-named factors.

Figure 2 represents the kinetics of volatilization of phenyl-β-naphthylamine (Neozone D, initial concentration 2%) from a plate of SKB 1.35 mm thick in a current of nitrogen flowing at 140 ml/minute at various temperatures. The curves are satisfactorily represented by the expression:

$$\frac{c}{c_0} = 1 - e^{-Kt}, \tag{1}$$

where c is the amount of ingredient lost at time t, as percent by weight of rubber; c_0 is the initial content of ingredient in the rubber, in % by weight; K is a constant.

Differentiation of Eq. (1) with respect to t gives an expression for the rate of volatilization:

$$v = \frac{dc}{dt} = K(c_0 - c) = Kc_1, \tag{2}$$

where c_1 is the amount of ingredient present in the rubber at time t, as percent by weight of rubber.

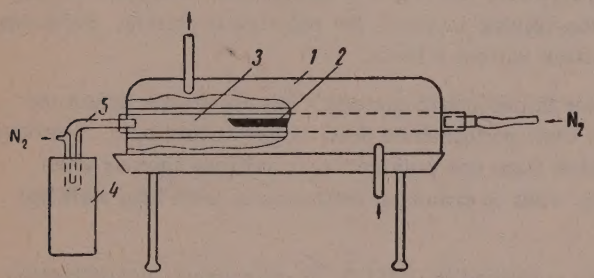


Fig. 1. Apparatus for studying the kinetics of ingredient volatilization from raw and cured rubbers in a current of gas: 1) Horizontal tubular furnace; 2) plate of raw or cured rubber; 3) glass tube, d = 18 mm; 4) Dewar flask; 5) detachable trap.

This expression corresponds to the equation for a reaction of the first order, and accordingly the constant K is the volatilization rate constant. The values of K for different temperatures were calculated by rectification of the corresponding kinetic curves in $\ln(1 - c/c_0) - t$ coordinates and calculation of the slopes of the straight lines so obtained. The effect of temperature on the volatilization rate constant is represented in Fig. 3. The activation energy of the process was found to be 14 kcal/mole.

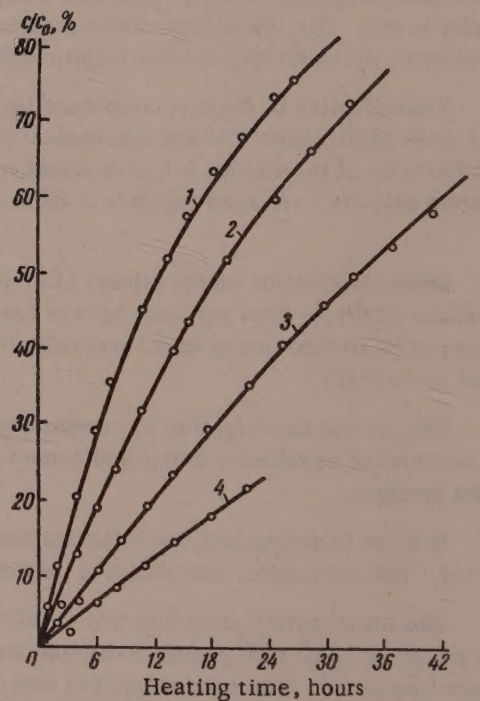


Fig. 2. Kinetics of volatilization of phenyl-β-naphthylamine from SKB at various temperatures: 1) 150°; 2) 140°; 3) 130°; 4) 120°.

The relationship between the volatilization rate and plate thickness was studied for specimens of R from 0.45 to 2.65 mm. The results show (Fig. 3, Curve 1) that the volatilization rate drops sharply with increasing plate thickness. The constant K is inversely proportional to the plate thickness (Fig. 4, Curve 2).

For studies of the influence of the initial antioxidant concentration on its rate of volatilization from rubber, plates in which the antioxidant concentration was varied from 0.3 to 1.5% were used. The relationship between the volatilization rate constant and the initial concentration of the ingredient in this concentration range is linear (Fig. 5) and is represented by the equation

$$K = K'(1 + ac_0), \tag{3}$$

where a is a constant calculated from the experimental data (the equation is valid at c > 0).

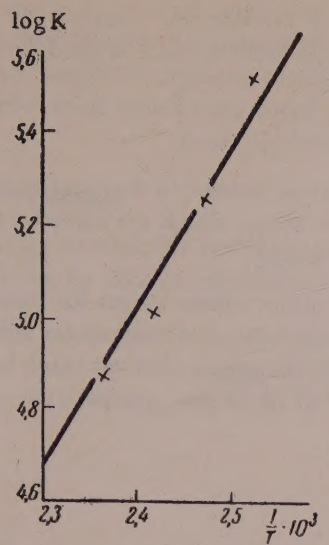


Fig. 3. Effect of temperature on the rate constant K of volatilization of phenyl-β-naphthylamine from SKB.

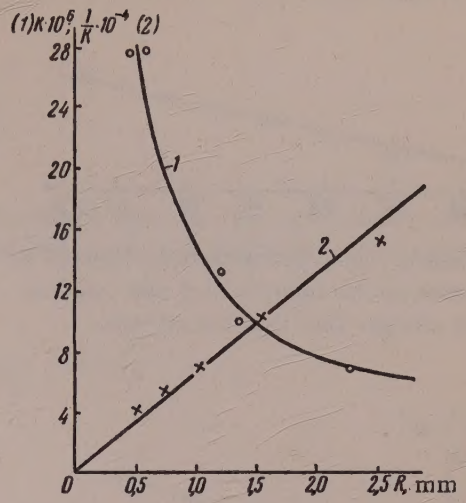


Fig. 4. Effect of plate thickness on the rate constant of volatilization of phenyl-β-naphthylamine at 140° and nitrogen velocity 140 ml/min.

Polymers and rubber products in use are often surrounded by moving air. We therefore studied volatilization of phenyl-β-naphthylamine from rubber in a current of nitrogen the flow rate of which was varied from 15 to 1000 ml/minute. The results are plotted in Fig. 6. It is clear from Fig. 6 (Curve 1) that the rate of volatilization increases with the flow rate of the nitrogen stream (W). Curve 1 is rectified in W/K − W coordinates (Curve 2), and the relationship between K and the gas flow rate can be represented by the following function:

$$K = K'' \left(\frac{W}{b+W}\right), \tag{4}$$

where b is a constant determined experimentally.

On the basis of these experimental results, we can write the following expression for the volatilization rate constant:

$$K = K_0 e^{-E/RT} \left(\frac{W}{b+W}\right)(1+ac_0)\cdot\frac{1}{R}, \tag{5}$$

where E is the activation energy of the volatilization process in kcal/mole; K is a constant which depends on the nature of the polymer and ingredient.

Equations (1) and (5) can be used for finding the amounts of ingredients volatilized from different polymers under various conditions. The values of K_0 and E for a given system are found experimentally.

It is likely that these relationships are of the same character in volatilization of other ingredients.

As already noted, the question of volatilization of ingredients from cured rubbers, which differ from polymers by the presence of a spatial network, is of great practical interest. It was accordingly necessary to study how the volatilization process changes in the transition from raw rubber to vulcanizates with different densities of the spatial network.

The vulcanizates were prepared by irradiation of rubber plates 1 mm thick in TRTs-ZA x-ray tubes for radiochemical investigations, developed by the Institute of Physical Chemistry of the Academy of Sciences, USSR,

under nominal tube conditions of 80 kv and 200 ma. The density of the vulcanization network was characterized by the equilibrium modulus (E_∞), the value of which varied from 13 to 38 kg/cm^2.

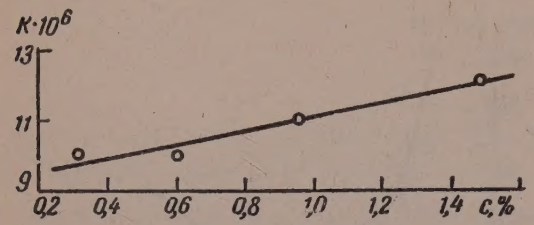


Fig. 5. Effect of initial concentration of phenyl-β-naphthylamine on the volatilization rate constant at 140° and nitrogen flow rate 140 ml/min.

Figure 7 shows that the volatilization rate of phenyl-β-naphthylamine falls sharply with increasing density of the spatial network. It follows that ingredients must volatilize much more slowly from cured rubbers than from uncured polymers.

It was also of interest to find how volatilization is influenced by fillers, which are essential ingredients of most rubber stocks.

Figure 8 shows kinetic curves for volatilization of phenyl-β-naphthylamine from rubber without filler and from rubber containing channel black and chalk in the proportions of 60 weight parts per 100 weight parts of rubber.

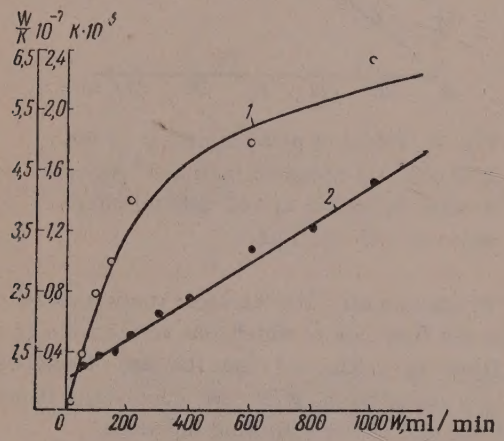


Fig. 6. Effect of nitrogen flow rate at 140° on the rate constant of volatilization of phenyl-β-naphthylamine.

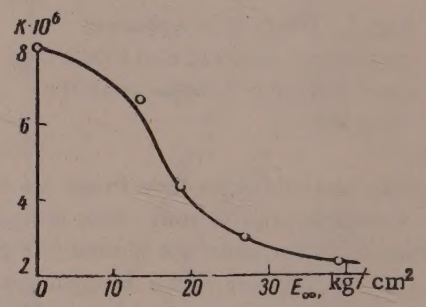


Fig. 7. Variations of the volatilization rate constant with the equilibrium modulus of the vulcanizate at 130° and nitrogen flow rate 160 ml/min.

The results show that both fillers reduce the volatilization rate of phenyl-β-naphthylamine appreciably, and channel black has a greater decreasing effect than chalk.

The effect of the nature of the polymer on volatilization kinetics was then studied. The experiments showed that the volatilization rate of phenyl-β-naphthylamine decreases in the following series of polymers: polyethylene > fluoroprene rubber > SKB > SKS-30 > SKN-26 > Nairit (Fig. 9).

This series coincides almost completely with the series of polymers in order of solubility and heat of solution of phenyl-β-naphthylamine in them [4, 5]. Accordingly, the differences in the rates of volatilization of the antioxidant from different polymers may be attributed to mutual influence of the solute and polymer molecules, leading to different values of the vapor pressure of phenyl-β-naphthylamine over the polymers. Variations of vapor pressure influence the volatilization rate.

In the light of the modern theory of evaporation of liquids [6] and of the mechanism of diffusion of substances of low molecular weight in polymers [4, 7] it may be postulated that in general the volatilization of ingredients from polymers proceeds in two stages: 1) Diffusion of the substance through the plate of polymer, and 2) removal of molecules of the substance from the plate surface.

The first stage of volatilization conforms to Fick's law

$$\frac{\partial c(x, t)}{dt} = D \frac{\partial^2 c(x, t)}{\partial x^2}, \qquad (6)$$

where $\frac{\partial^2 c}{\partial x^2}$ is the derivative of the concentration gradient; D is the coefficient of diffusion.

In the second stage the rate of removal of the substance from the surface must be proportional to the surface concentration of the substance (c_s), or

$$\frac{dQ}{dt} = mc_s, \tag{7}$$

where m is a constant.

By analogy of diffusion and heat conduction, the volatilization process may be represented by the following equation, derived by suitable transformation of the equation for heat conduction under analogous conditions [8]:

$$\frac{c_1(x, t)}{c_0} = \sum_{n=1}^{\infty} \frac{2 \sin \mu_n}{\mu_n + \sin \mu_n \cdot \cos \mu_n} \cdot \cos \mu_n \frac{x}{R} \cdot e^{-\frac{\mu_n^2 Dt}{R^2}}, \tag{8}$$

where $\mu_n = HR \cot \mu_n$, and $H = m/D$; c_1 is the concentration (wt. %) of the substance in the plate at a distance x from the covered surface at time t; c_0 is the initial concentration of the substance (wt. %); R is the thickness of the plate (cm); D is the coefficient of diffusion (cm^2/sec). In Eq. (8), when x is equal to the plate thickness (R), c_1 is equal to c_s.

Substituting the expression for c_s into Eq. (8) and transforming, we have the following expression for the volatilization kinetics

$$\frac{dQ}{dt} = mc_0 \sum_{n=1}^{\infty} \frac{\sin 2\mu_n}{\mu_n + \frac{\sin 2\mu_n}{2}} \cdot e^{-\mu_n^2 \frac{Dt}{R^2}}. \tag{9}$$

At the same time, it may be assumed that the amount of substance volatilized (per unit surface) is proportional to its total content in the plate, i.e.,

$$dQ = Rdc. \tag{10}$$

Substituting this expression into Eq. (9), we have the following expression for the volatilization rate:

$$\frac{d(c/c_0)}{dt} = \frac{m}{R} \times \sum_{n=1}^{\infty} \frac{\sin 2\mu_n}{\mu_n + \frac{\sin 2\mu_n}{2}} \cdot e^{-\mu_n^2 \frac{Dt}{R^2}} \tag{11}$$

It has been shown that in the case of heat transfer the mechanism of the process is determined by the value of HR. Thus, when HR < 0.1 the rate is limited by the rate of heat loss to the surroundings, which in the case of volatilization corresponds to the rate of removal of the substance from the plate surface. When 100 > HR > 0.1, the volatilization rate is determined both by the rate of heat loss to the surroundings and by the rate of diffusion through the plate.

By substitution of our experimental data into Eq. (11) the value of HR can be determined. It was found that in volatilization of phenyl-β-naphthylamine from rubber at temperatures above 100° HR < 0.1. Hence, it may be concluded that the kinetics of the process is determined by the rate of removal of the ingredient from the plate surface. Diffusion of the substance in the polymer is not a determining factor under these conditions.

At such low values of HR $\sin \mu_n$ can be replaced by μ_n, and μ_n^2 by HR. Moreover, in this case the first term in the sum of Eq. (11) is sufficient.

With these simplifications we have the following expression for the volatilization rate:

$$\frac{d(c/c_0)}{dt} = \frac{m}{R} e^{-\frac{m}{R}t}. \quad (2)$$

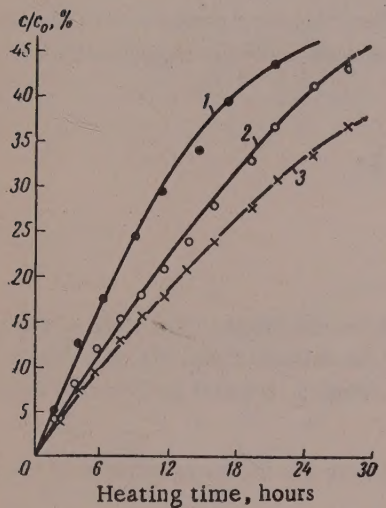


Fig. 8. Kinetics of volatilization of phenyl-β-naphthylamine from SKB at 150° and nitrogen flow rate 160 ml/min: 1)Rubber without filler; 2) rubber with 60 wt. parts of chalk; 3) rubber with 60 wt. parts of channel black.

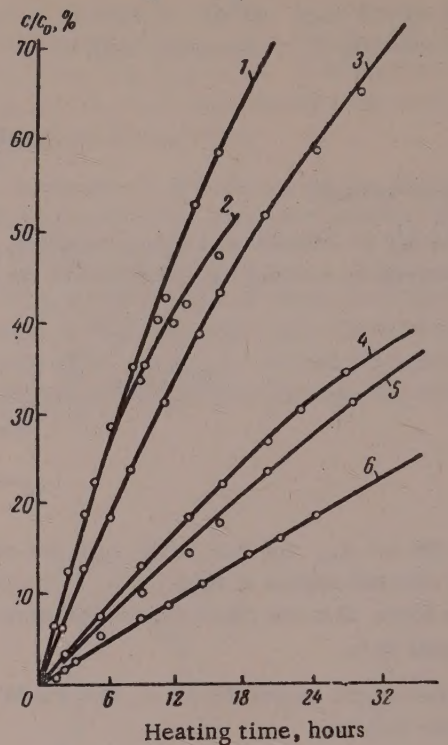


Fig. 9. Kinetics of volatilization of phenyl-β-naphthylamine from different polymers at 140° and nitrogen flow rate 140 ml/min: 1) Polyethylene; 2) SKF-32; 3) SKB; 4) SKS-30; 5) SKN-26; 6) Nairit.

In the integral form, Eq. (12) becomes:

$$\frac{c}{c_0} = 1 - e^{-\frac{m}{R}t}. \quad (13)$$

It is easy to see that this equation is analogous to the empirical function given above, which represents the kinetic curves for volatilization of ingredients [Eq. (1)]. This agreement confirms the validity of the foregoing concepts of the mechanism of volatilization.

SUMMARY

1. The rate of volatilization of phenyl-β-naphthylamine from a rubber plate depends on the flow rate of gas over the plate, the plate thickness, and the initial concentration of the ingredient. The activation energy of the volatilization process is 14.0 kcal/mole.

2. The rate of volatilization of phenyl-β-naphthylamine diminishes in the following polymer series: polyethylene > fluoroprene rubber > SKB > SKS-30 > SKN-26 > Nairit.

3. The volatilization rate drops sharply with increase of the density of the vulcanization network, and decreases in presence of fillers.

4. The mechanism postulated for volatilization of ingredients from polymers is confirmed by theoretical calculations.

LITERATURE CITED

[1] A. E. Yuve and R. Shearer, India Rubber World 128, 5, 623 (1953); R. N. Thomson and N. S. Grace, India Rubber World 128, 216 (1953); W. J. Schonlau, India Rubber J. 127, 7, 4 (1954).

[2] M. B. Fackler and G. S. Rugg, International Organization for Standardization, ISO/TK, Documents No. 107, 98, 102.

[3] K. Zöhrer and A. Merz, Kunststoffe 45, 1 (1955); H. M. Quackenbos, Ind. Eng. Chem. 46, 6, 1935 (1954); R. F. Boyer, J. Appl. Phys. 20, 540 (1949); R. E. Morris and A. E. Barrett, Rubber Age 75, 76 (1954); K. Thinius, J. prakt. Chem. 3, 50 (1956).

[4] A. S. Kuz'minskii, S. A. Reitlinger, and E. V. Shemastina, in the book: Aging and Fatigue of Raw and Cured Rubbers and Increase of Their Endurance [In Russian] (1955), p. 130.

[5] S. A. Reitlinger and A. S. Kuz'minskii, Zhur. Priklad. Khim. 27, 2, 214 (1954).*

[6] S. I. Sklyarenko and M. K. Baranaev, Zhur. Fiz. Khim. 8, 1, 51 (1936); S. I. Sklyarenko and M. K. Baranaev, Zhur. Fiz. Khim. 7, 549 (1936); M. K. Baranaev, Zhur. Fiz. Khim. 13, 1635 (1939).

[7] R. Barrer, Diffusion In and Through Solids [Russian Translation] (IL, Moscow, 1948); A. S. Kuz'minskii, S. A. Reitlinger, and E. V. Shemastina, Kolloid Zhur. 18, 707 (1956);* A. R. Kemp, F. S. Malm, G. G. Winspear, and B. Stiratelli, Ind. Eng. Chem. 32, 1075 (1940).

[8] A. V. Lykov, Heat Conduction in Nonsteady Processes [In Russian] (Gosenergoizdat, 1948), p. 42.

* Original Russian pagination. See C. B. Translation.

A STUDY OF THE ADSORPTION PROPERTIES OF HYDROLYTIC LIGNIN

V. I. Vanina, A. M. Gutman, A. P. Zakoschikov,

S. A. Zakoshchikov, and V. M. Rotleider

Higher School of Industrial Cooperation, Cherkizovo, Moscow Province
(Translated from: Kolloidnyi Zhurnal Vol. 22, No. 1, pp. 9-15 January-February, 1960)
(Original article submitted October 29, 1958)

In hydrolysis of wood and various agricultural plant wastes, enormous amounts (hundreds of thousands of tons per year) of hydrolytic lignin are obtained as a by-product, in the proportion of 30-35% on the weight of processed material; no rational use for this product in the national economy has yet been found in practice.

Suggested uses of hydrolytic lignin are numerous. The simplest way of utilizing hydrolytic lignin is to burn it [1]. Many suggestions refer to the pyrolysis of lignin [2]. There is a definite value in methods for the use of hydrolytic lignin, together with sulfite liquor concentrates, for acceleration of clinker grinding in the cement industry and as plastifiers for the cement so obtained. Introduction of 0.3-0.5% of lignin on the weight of clinker raises mill output by up to 15% [3]. Lignin treated with 20-25% caustic soda at 180-200° for 4-6 hours becomes soluble in alkalies; in this form it mixes readily with latexes of synthetic rubbers (such as SKS-3) and can be used for rubber reinforcement [4].

If hydrolytic lignin is treated with 61% nitric acid (sp. gr. 1.38) up to 35% by weight of oxalic acid is obtained.

There are many patents on the use of hydrolytic lignin as filler in molding powders, in particular for replacing the costly and scarce wood flour. Lignin for this purpose must be neutral; it is therefore washed, or dried at high temperatures (150-170°) [5]. There have also been many proposals for the use of hydrolytic lignin in plastics production [6]. Preparation of phenol – lignin resins was studied by Ushakov and Matveev [7]; they gave them the name of FL resins; the hardening agent for such resins is hexamethylenetetramine. Lignin obtained in hydrolysis of wood by concentrated hydrochloric acid can be extensively used for production of bakelite powder [1], with up to 30% saving of phenol.

Special interest attaches to searches for methods of using lignin without additional complex treatments. Since lignin and cellulose are the main components of wood and are most intimately bound together, there should be much in common between the properties of cellulose and lignin (at least in the native form), and this should suggest a number of new ways of using lignin. Unfortunately, the physicochemical properties and in particular the adsorption properties of hydrolytic lignins have been studied very little.

The present investigation is of a preliminary character and is not claimed to clarify the question exhaustively.

The material taken for the investigation was technical hydrolytic lignin, which was not purified, and no attempt was made to isolate from it any more homogeneous fraction closer in composition to native lignin. Hydrolytic lignin is a complex mixture of native lignin modified under harsh hydrolysis conditions, huminlike products formed by decomposition of sugars by the action of dilute mineral acid (0.5-1.0% H_2SO_4) at 175-190°, residual unhydrolyzed polysaccharides, and various acid-insoluble components of the raw material (fats, waxes, resins, phlobaphenes, some ash components, etc.).

Wood lignin is a substance of aliphatic – aromatic character; its basis is the 4-hydroxy-3-methoxyphenylpropane group condensation of which gives rise to the molecule of native lignin [8].

The question of the functional groups in lignin has not been finally settled. Whereas the presence of methoxyl, phenolic, and hydroxyl groups in the lignin molecules is undoubted, the opinions of different workers vary with regard to the presence of acetyl, formyl, and carbonyl groups and of double bonds. A very important hypothesis is the highly probable presence of keto- enol groups in lignin, which have been studied in particular detail by Nikitin [9].

The functional groups of hydrolytic lignin may differ significantly in composition from the functional groups of native lignin or of lignin preparations isolated by other methods. The nature of the functional groups in polymeric lignin determines its surface properties. Our task was to investigate these properties in relation to various substances and to determine how substances absorbed on the surface of lignin modify the properties of that surface, in particular with regard to adsorption of other substances.

Our experiments were performed with hydrolytic lignin obtained from the Leningrad Hydrolysis Works. The lignin had the following composition:

Moisture	8.3%
Ash	1.24%
Undissolved sugars (calculated as glucose)	3.8%
Hydrolyzable carbohydrates	11.01%
OCH_3-groups	8.58%
"Lignin" content (by Kõnig's method)	84.47%

If lignin is previously demineralized by dilute sulfuric, hydrochloric, or phosphoric acid solution, washed, and dried, it does not adsorb acids from dilute solutions. The adsorptive capacity of lignin for bases is not less than that of cellulose, and for caustic alkalies, it is greater. Lignin is a very active sorbent for moisture and adsorbs more from air than does cellulose under the same conditions.

Lignin has the advantage over cellulose in that it is dyed very well not only by direct (substantive) dyes, but also by basic dyes. Quite unexpected was the fact that it could be also dyed by acid dyes, but these dyeings are much less fast to water than those produced by basic or substantive dyes.

Basic dyes are adsorbed well by hydrolytic lignin even in the cold. The adsorption of a basic dye (Malachite Green) by lignin was determined with the aid of the FÉK-M photoelectric colorimeter, which was first used for determination of a calibration curve (Table 1).

TABLE 1

Adsorption of Malachite Green by Hydrolytic Lignin from the Leningrad Works. Liquor Ratio (Weight of Solution to Weight of Lignin) = 50

Temperature (°)	Adsorption time, min	Concentration of Malachite Green, %		Temperature (°)	Adsorption time, min	Concentration of Malachite Green, %	
		in solution	adsorbed, on weight of lignin			in solution	adsorbed, on weight of lignin
20	30	0,0045	0,175	100	30	0,10	3,75
20	30	0,0079	0,180	100	30	0,20	6,75
20	30	0,0118	0,430				
20	30	0,0180	0,60	20	60	0,20	4,75

Table 1 shows that the amount of dye adsorbed increases with increasing dye concentration in the bath; much more dye is adsorbed at the boil than in the cold. Prolonged washing of the dyed lignin in water showed that the dye does not pass from the lignin into water. If up to 1% of dye is applied to lignin the color produced

is a mixture of the color of the dye and of the yellow-brown color of the lignin itself, but in presence of only 1.5-2% of dye the lignin background becomes imperceptible and purer colors are obtained. Other basic dyes behave similarly to Malachite Green. When lignin is dyed by Methylene Blue a grass-green color is obtained, of a different shade than that given by Malachite Green.

Lignin dyed by basic dyes can be additionally colored by dyes of other classes, such as acid, which are then firmly bound on the lignin, forming stable lakes with the basic dyes. Similar additional coloring can be effected by many substantive dyes; this is an example of the influence of an adsorbed substance on the properties of the adsorbent surface.

Direct (substantive) dyes, like basic dyes, give good and fast dyeings on hydrolytic lignin (Table 2).

TABLE 2

Adsorption of Direct Scarlet by Lignin from Solutions of Different Concentrations at 18°, Dyeing Time 30 Minutes (Liquor Ratio = 50)

Concentration of Direct Scarlet solution, %	0.032	0.125	1.160
Dye adsorbed, % on weight of lignin	1.035	1.080	2.085

It follows from Table 2 that the amounts of direct dye taken up are considerably less than those found previously for basic dyes, and therefore dye absorption must be intensified by addition of electrolytes at the end of dyeing and by regulation of temperature, the solution not being allowed to boil. To mask the color of the lignin itself, it is necessary, as before, to have 1.5-2.0% of dye on the weight of lignin.

Acid dyes are taken up by lignin, but the dyeings are not fast to water. For fast dyeings the lignin was previously mordanted by a basic aluminum salt which was fixed by silicate treatment.

Vat dyes. Insoluble vat dyes color lignin well by adsorption of the soluble leuco compounds from alkaline maths followed by oxidation of the leuco compounds by air or by treatment with oxidizing agents. There were no difficulties in oxidizing dyes which were indigo derivatives, and anthraquinone dyes (Vat Red KKh, Vat Golden Yellow ZhKh, Vat Brilliant Violet K, Vat Brilliant Greeen ZK, etc.), but oxidation of leuco indigo is extremely difficult and normal blue dyeings could not be obtained even if acidified dichromate solutions were used for oxidation. The dye vats are prepared and applied in the usual way. Leuco compounds are best oxidized by dilute acidified dichromate solutions, as the powdered mass of dyed lignin containing large amounts of water is oxidized very slowly in air.

Sulfur dyes, applied to lignin by the usual method from baths containing sodium sulfide are taken up well by lignin, but the dyeings are dirty and very dark, unlike the dyes used, and are of no practical interest.

Dyeing of lignin by oxidation of aniline (Aniline Black). Lignin takes up aniline well from solutions of aniline hydrochloride, and also the free base. Aniline Black is easily formed on lignin by the usual univalent method for production of this pigment, and is very fast on the lignin. If smaller amounts of aniline are taken for the dyeing, the colors produced are a fine shade of brown rather than black. This is a very interesting fact, as the formation of substances with a brown color when aniline is oxidized on vegetable fibers is unknown. The black and brown pigments formed by oxidation of aniline on lignin are very fast to light and are undoubtedly of practical interest.

Insoluble azoic pigments are formed on lignin by coupling, on the fiber, of the so-called Azotols (naphthols and other compounds capable of coupling with diazo compounds to form insoluble colored pigments) with diazotized aromatic amines (Azoamines). Our experiments showed that hydrolytic lignin, being a substance of aromatic character, can couple with diazo compounds with formation of colors different from that of lignin itself, and of no practical value.

Lignin takes up Azotols well and therefore normal insoluble azoic colors such as are commonly used in the textile and paint industries can be obtained on it.

Table 3 contains results of experiments on adsorption of caustic soda from aqueous solutions by samples of lignin previously dyed by Aniline Black, Cold Bordeaux, and Methylene Blue. The adsorption of Aniline Black was 10% of the lignin weight, and of Cold Bordeaux and Methylene Blue, approximately 2.0%.

TABLE 3

Effect of Dyeing of Hydrolytic Lignin on Adsorption of Caustic Soda at 18° During 1 Hour (Liquor Ratio = 50)

Dye applied to lignin	Amount of caustic soda adsorbed from solution containing NaOH (% on weight of lignin)			
	0.124	0.208	0.512	1.004
Lignin not dyed	2.25	3.18	5.71	6.17
Aniline Black	2.80	3.94	7.12	9.25
Methylene Blue	2.32	3.45	6.49	8.75
Cold Bordeaux	1.70	1.33	3.17	–

It follows from Table 3 that lignin takes up considerable amounts of alkali. These values are much higher than the literature values for cellulose. Lignin takes up other bases equally well; these include aniline, naphthylamines, and others used in the form of their salts.

Dyes applied to lignin surface sharply change the properties of that surface. Thus, the adsorption of caustic soda by lignin is increased by Aniline Black and Methylene Blue, whereas the insoluble azoic dye formed from β-naphthol and α-naphthylamine (Cold Bordeaux) lowers it sharply.

Table 4 contains data on sorption of moisture by lignin from air at different relative humidities.

TABLE 4

Effect of Dyeing of Hydrolytic Lignin on Adsorption of Water Vapor (at 18°)

Dye on lignin	Amount of water adsorbed, % on weight of lignin, on exposure over saturated salt solutions		
	$Ca(NO_3)_2$, humidity 55%	NH_4NO_3 humidity 65%	Na_2CO_3, humidity 92%
Lignin not dyed	5.60	7.20	15.10
Aniline Black	5.57	6.85	11.19
Methylene Blue	6.36	7.22	12.50
Cold Bordeaux	12.77	18.30	33.42

Lignin samples were kept at 18° for over a month in desiccators over saturated salt solutions.

Table 4 shows that aniline takes up no less water than does cellulose under the same conditions. Aniline Black makes the lignin surface hydrophobic, decreasing the amount of water adsorbed. At lower relative humidities of the air Methylene Blue somewhat increases the amount of water adsorbed by lignin, but on increase of the relative humidity of the air to 92% the amount of adsorbed water decreases. Variations in the influence of the dyeing at different relative humidities of the air are probably associated with changes in the mechanism of moisture sorption (with prevailing capillary condensation in sorption of more than 8-10% water). The azoic dye Cold Bordeaux makes the lignin surface very strongly hydrophilic, the amount of water taken up in its presence being roughly double that for undyed lignin.

Table 5 contains results of experiments with films from polyvinyl chloride resin (PVCR) to which lignin had been added. The films were made from a mixture of 60 wt. parts of plasticizer and 20 wt. parts of lignin per 100 wt. parts of PVCR.

Five specimens of such films were prepared (the control film specimen did not contain lignin). The other specimens contained either undyed lignin or lignin dyed with Methylene Blue, Direct Light Fast Diazo Bordeaux, Sulfur Green, and Aniline Black (the first three in the proportion of approximately 2%, and Aniline Black in the proportion of 10% on the weight of lignin). The mixes were allowed to swell in a thermostat at 70° for 3-4 hours with periodic stirring, and then masticated in a roll mill for 10-15 minutes at 90-100°. The masses were formed into films in a hot press at 140-150° under 150 atmos pressure and cooled to 40° under pressure (Table 5).

TABLE 5

Physical and Mechanical Properties of Polyvinyl Chloride Films Filled with Hydrolytic Lignin (20 wt. parts), Undyed and Dyed by Various Dyes

Dye applied to lignin	Film thickness, mm	Tensile strength, kg/cm²	Elongation at break, %	Residual elongation, %	Specific gravity
Without lignin	1,28	102,8	280,0	49,3	1,19
Undyed	1,49	76,0	166,7	18,7	1,18
Methylene Blue	1,40	109,8	171,7	22,0	1,21
Direct Diazo Boredeaux	1,02	102,0	209,0	34,7	1,20
Sulfur Green	0,96	106,6	263,3	44,7	1,21
Aniline Black	1,28	91,3	116,7	8,7	1,19

Table 5 shows that addition of 20% of undyed lignin to a PVC film has an adverse effect on its mechanical properties. Unsatisfactory results are also obtained with lignin dyed by Aniline Black. The strength of films containing lignin dyed by a basic dye (Methylene Blue), a direct dye, or a sulfur dye is not less than that of the control specimen; the elongation at break and residual elongation are somewhat lower.

Insoluble azoic dyes do not interact with polyvinyl chloride resin. Polyvinyl chloride film containing lignin dyed by an azoic dye (from β-naphthol and p-nitroaniline) has a metallic color resembling that of copper under reflected light.

The results of experiments on PVC films with additions of different amounts of lignin dyed by a direct dye — Light Fast Diazo Bordeaux — are given in Table 6.

TABLE 6

Film Formulations

Film components	Contents, parts by weight							
	control	film specimen No.						
		6	7	8	9	10	11	12
Polyvinyl chloride resin	100	100	100	100	100	100	100	100
Dibutyl phthalate	60	60	60	60	60	60	60	—
Undyed lignin	—	20	—	—	—	—	—	—
Lignin dyed by Light Fast Diazo Bordeaux	—	—	10	20	30	40	50	75

Test data on the films artificially aged by the accelerated method (exposure in a thermostat at 70° for 72 hours) are presented in Table 7.

The data in Table 7 confirm the results of the previous experiments, according to which dyed lignin may be introduced into PVC films in amounts of up to 30% without adverse effect on the mechanical properties of the films. This is a result of practical significance which is being utilized in experimental work on the production of linoleum.

TABLE 7

Physical and Mechanical Properties of PVC Films Containing Different Amounts of Dyed Lignin

Film No. (Table 6)	Film thickness, mm	Tensile strength, kg/cm²	Relative elongation, %	Residual elongation, %	Specific gravity	Volatile content, %
			Before aging			
Control	0,58	127,6	266,6	36,3	1,2	—
6	0,62	120,7	192,2	24,6	1,2	—
7	0,70	125,8	262,7	36,7	1,2	—
8	0,69	125,8	221,3	34,6	1,24	—
9	0,60	128,8	195	28,6	1,23	—
10	0,56	107,8	142	19,0	1,23	—
11	0,59	111,0	113,6	13,3	1,22	—
12	0,59	103	89,5	11,3	1,22	—
			After aging			
Control	0,53	120,9	197,5	18,7	1,21	2,78
6	0,62	115,5	190,3	23,6	1,22	2,68
7	0,76	118,2	197,0	28	1,23	2,36
8	0,53	119,7	185	25,6	1,24	4,53
9	0,60	124,1	159,2	19,7	1,24	3,29
10	0,57	114	105,0	13,0	1,23	4,38
11	0,61	115,5	78,3	7,3	1,24	5,46
12	0,59	118,9	26,6	3,7	1,23	6,64

SUMMARY

1. Hydrolytic lignin has much in common with cellulose in its adsorption properties. Lignin can be used as a substrate for insoluble dyes such as Aniline Black and various insoluble azoic dyes obtained from diazotized amines and various atomatic compounds which couple with diazo compounds.

2. Dyes applied to lignin surface alter its adsorption properties, including the adsorptive capacity for alkali and water.

3. Dyed lignin can be used as a filler for polyvinyl chloride products (films, linoleum).

LITERATURE CITED

[1] S. I. Sukhanovskii and M. I. Chudakov, Utilization of Hydrolytic Lignin [In Russian] (Central Bureau of Technical Information, Moscow, 1958).

[2] N. P. Mel'nikov, S. I. Sukhanovskii, and N. V. Chalov, Tr. Lesotekhn. Akad. im. S. M. Kirova 75 (1956); G. G. Plachenov, S. I. Sukhanovskii, M. I. Chudakov, and E. I. Akhmina, Proc. Conference on Wood Pyrolysis [In Russian] (Acad. Sci. Latvian SSR, 1957); V. G. Panasyuk and N. S. Maksimenko, Gidrolizn. i Lesokhim. Prom. SSSR 1 (16-17) (1958).

[3] S. I. Sukhanovskii and N. V. Mukhin, Gidrolizn, Prom. SSSR 2 (1951).

[4] S. I. Sukhanovskii, M. I. Chudakov, and A. Z. Yakovenko, Gidrolizn. i Lesokhim. Prom. SSSR 3 (1956).

[5] B. D. Bogomolov, Gidrolizn. Prom. SSSR 4 (1951).

[6] I. P. Losev and V. S. Kalininskii, Lesokhim. Prom. 4 (1939); J. Scheiber, Chemistry and Technology of Artificial Resins [Russian translation] (Goskhimizdat, 1949), p. 545.

[7] S. N. Ushakov and I. I. Matveev, Girdolizn. Prom. SSSR 4 (1948).

[8] N. N. Shorygina and T. Ya. Kefeli, Zhur. Obshchei Khim. 17, 2058 (1947); 18, 528 (1948).

[9] N. I. Nikitin, Chemistry of Wood [In Russian] (1951); V. N. Nikitin, Chemistry of Wood and Cellulose [In Russian] (State Wood and Paper Press, 1951); V. N. Nikitin, Tr. Leningrad Lesotekhn. Akad. 75 (1956).

INVESTIGATION OF THE DIELECTRIC AND RHEOLOGICAL PROPERTIES OF PLASTIC DISPERSE SYSTEMS

Yu. F. Deinega, A. V. Dumanskii, G. V. Vinogradov, and V. P. Pavlov

Institute of General and Inorganic Chemistry, Academy of Sciences, Ukrainian SSR, Kiev

(Translated from: Kolloïdnyi Zhurnal Vol. 22, No. 1, pp. 16-22, January-February, 1960)
(Original article submitted June 15, 1959)

Combined polarization-optical and rheological studies of plastic disperse systems, exemplified by lubricant greases (soap pseudogels) provided new information on the nature of these systems and on deformation processes taking place in them [1]. A feature of special interest was the formation of a frozen flow structure when the lubricant flow was rapidly arrested [1]. However, optical methods are not applicable to concentrated systems of low transparency which are widely used in practice. Accordingly, combined investigations of the electrical and rheological properties of plastic disperse systems may be of importance.

The dielectric and rheological determinations were conducted in the apparatus [2] shown in Fig. 1. The body 1, with an accurate cylindrical channel in its lower portion, contains the internal cylinder, a rotor 3, mounted on two precision bearings 3. The working surfaces of the body and rotor are smooth and strictly concentric. The radial gap between these surfaces can be varied between 0.25 and 1.00 mm by means of a range of rotors with working parts between 6.25 and 5.50 mm in radius. The height of the working gap between body and rotor was 50 mm. The nut 4, intended for variation of the clearance and regulation of the bearings, prevents axial displacement of the rotor; its shaft 5 is rigidly coupled to reducing gear and a DVS-U1 synchronous electric motor. The rotor was rotated at speeds of 0.192; 0.96; 4.8; 24; 120; 600 rpm. The torque set up in the concentric gap by the deforming material is balanced by twisting of the torsion wire 6 through a definite angle. This angle was measured by rotation of a graduated disk fixed to the drum 7. The torque was transmitted to the dynamometer through a flexible metallic wire 8. Shearing stresses (τ) between 0.25 and 430 kg/cm^2 could be measured by means of a range of torsion wires.

The material under test was introduced into the working gap of the apparatus by means of a device screwed into the lower end of the body 1. When the cap 9 is screwed down the sample is fed by means of the piston 10 into the gap between the body and the rotor. The upper end of the piston has a cup 11. Filling of the apparatus is indicated by appearance of the sample in the control windows closed by the screws 12.

An alternating electrical potential was applied to the rotor by means of a sliding contact on its shaft, and to the body through a metal wire connecting it to the dynamometer. The body and rotor of the instrument thus acted as the plates of a capacitor. The rotor was insulated from the body of the instrument by means of the plastic collar 13 and washer 14. The capacity (dielectric constant ϵ) and tangent of the loss angle ($\tan \delta$) were measured in the range of 0.4 to 10 kilocycles/second by the substitution method with the MLE-1 sonic bridge.

Typical plastic disperse systems were used for studying the dielectric and rheological properties. The following plastic greases were investigated: konstalin, solidol, and grease 201, made by thickening of mineral oils by Na soaps of castor-oil acids, hydrated Ca soaps of cottonseed-oil acids, and technical lithium stearate, respectively.

The reproducibility of the yield value (τ_y) determinations and of stresses corresponding to steady flow corresponds to maximum deviations of about ± 3% from the mean values. Variations of ϵ in deformation of plastic greases were determined to an accuracy of 0.3%. The error in determinations of tan δ varied between ± 0.0006 and ± 0.003 in accordance with the nature of the sample.

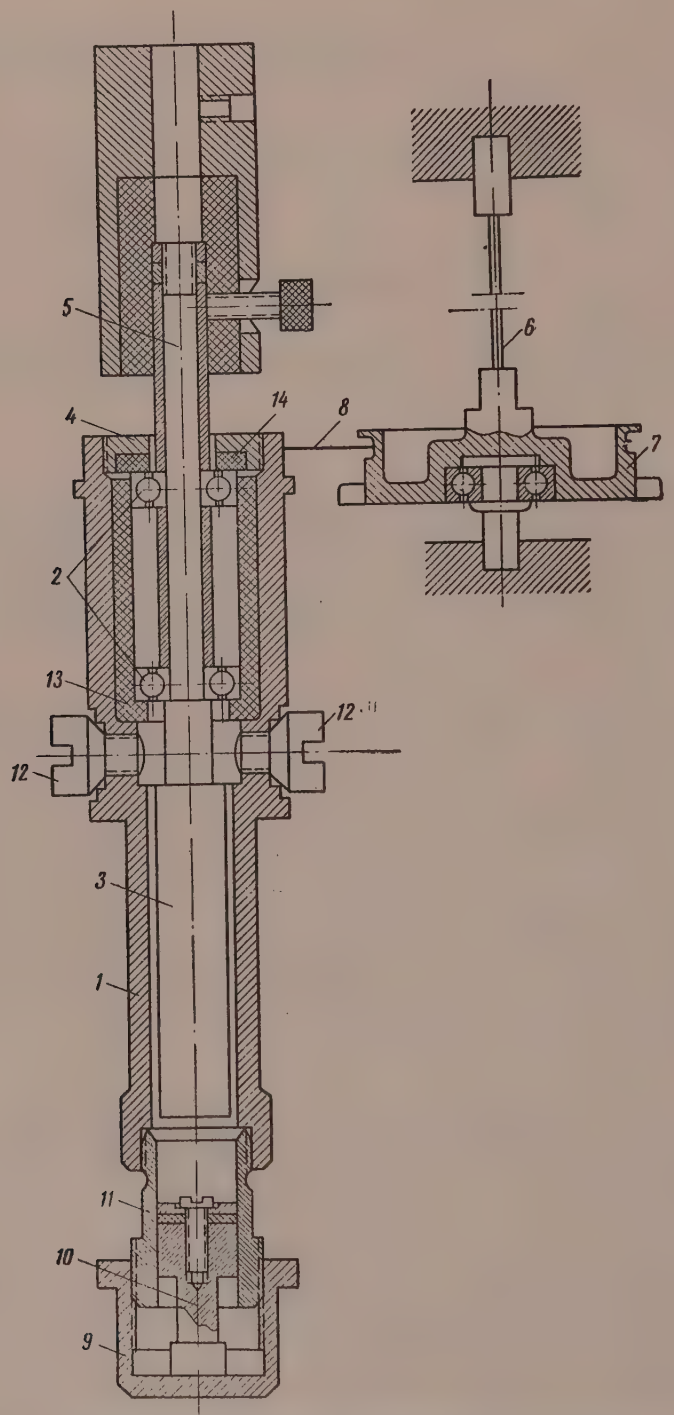


Fig. 1. Apparatus for simultaneous investigation of electrical and rheological properties of plastic disperse systems.

Studies of the structure of lubricant greases by means of the electron microscope [3] showed that the particles of disperse phase in them are ribbon-shaped or acicular soap crystallites. When the grease flows, the optically anisotropic particles of the disperse phase undergo orientation, which results in flow birefringence [1]. It has been demonstrated [4] that the dielectric properties of greases change in flow in accordance with these structural characteristics. However, in that investigation, which is apparently the only one hitherto concerned with dielectric properties of greases in flow, the formation of a frozen flow structure when the flow was suddenly stopped was not observed. However, such an effect is to be expected by analogy with the results obtained in studies of optical polarization of greases. This effect may be very important for investigation of numerous details of the correlation of rheological and dielectric properties of plastic disperse systems.

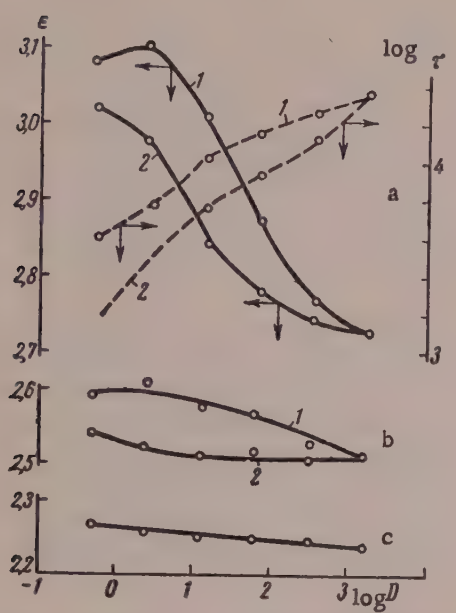


Fig. 2. Flow curves and variations of the dielectric constant of greases with the velocity gradient.

The results of a study of variations of ϵ with the velocity gradient (D, sec^{-1}) for konstalin (a), solidol (b), and grease 201 (c) at 20° and 0.4 kc/sec are plotted in Fig. 2. In the case of konstalin the dash lines represent $D(\tau)$ flow curves, with τ expressed in dynes/cm^2. All the points used for plotting of the curves correspond to steady flow conditions. Curves marked 1 represent transitions from lower to higher values of D, and curves marked 2 correspond to decreasing D.

Figure 2 shows that konstalin undergoes the greatest changes of ϵ with D. This effect diminishes with increasing frequency in the range of 0.4 to 10 kc/sec.

The decrease of ϵ and increase of birefringence with increase of D are due to orientation of the anisotropic particles in the flow direction. It is difficult to account for differences in the sensitivity of ϵ for the systems studied to the rate of shear merely on the basis of differences in the optical anisotropy and the shape and dimensions of the particles of the disperse phase. It is likely that the tendency of greases to surface polarization plays an important role in the dielectric sensitivity to deformation.

In the case of konstalin, when D is decreased from high values, hysteresis loops appear on the $\epsilon(D)$ and $\tau(D)$ curves (Fig. 2); these indicate changes undergone by the systems at high values of D. The main cause of the changes in the rheological properties of greases under the influence of high D is irreversible breakdown of the particles of the disperse phase — homogenization of the systems. As the result of intensive homogenization of greases (D of the order of 10^4 sec^{-1}) consecutive increase and decrease of D within the range of its average values corresponds to a single $D(\tau)$ curve;

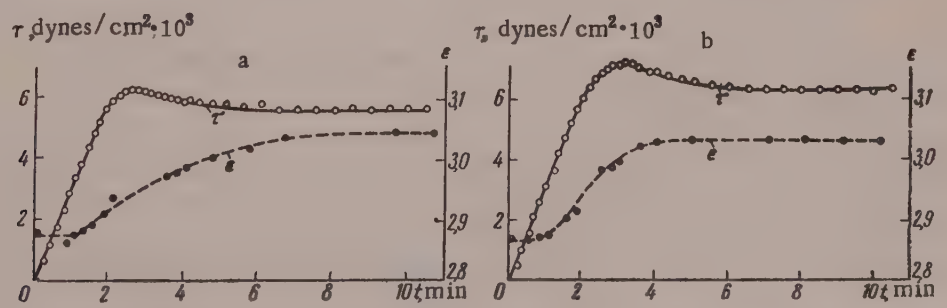


Fig. 3. Variations of shear stress and dielectric constant with time at constant rate of load in konstalin with a frozen anisotropic structure.

i.e., under these conditions hysteresis effects are eliminated. Homogenization lowers the viscous resistance of greases; its influence on the dielectric properties of greases had not been studied, although such investigations are of great interest as they would establish the relationship between the dielectric properties and structure of plastic disperse systems.

It was found in studies of the dielectric properties of greases that rapid arrest of flow results in the value of ϵ becoming fixed at the level observed in flow under the deformation conditions immediately preceding the arrest. This means that plastic disperse systems of the grease type can show electrical effects of frozen flow similar to those found previously in optical polarization studies [1]. Thus, both dielectric and optical polarization studies confirm that the flow structure of greases can be "frozen" when the flow is suddenly arrested. Frozen flow structures can be retained for long periods without change.

The possibility of using different methods (rheological, dielectric, and optical) for observation of anisotropy in plastic disperse systems facilitates studies of structure formation and breakdown. In this connection great interest attaches to simultaneous studies of rheological behavior and dielectric properties of greases in deformation of a frozen orientated structure corresponding to high shear rates. Such experiments were performed with konstalin. It should be noted that the π-effect is observed in the case of konstalin [5]. Frozen orientated flow structures were obtained by two methods. In the first method the body of the instrument, disconnected from the dynamometer, was turned by hand through about 180° and then stopped almost instantly. Rapid turning of the body draws the grease layers distant from the rotor into the flow, which is equivalent to homogenization of the grease. As a result, the influence of the π-effect is reduced somewhat and the yield value measured in an instrument with smooth working surfaces is increased. Instantaneous arrest of grease flow gives a frozen orientated structure.

In the second method of producing a frozen orientated structure in greases the rotor, rotating at a definite speed, was quickly stopped. This method was used for obtaining frozen structures corresponding to various, including high, values of D.

Let us consider an investigation, by the electrical method, of transition through the yield value for konstalin. The first method was used to produce a frozen anisotropic structure in konstalin. The rotor of the instrument was then rotated at 0.96 rpm in the direction in which the structure of the system had been orientated. The modulus of the dynamometer used for these experiments was 30 $g \cdot cm \cdot radian^{-1}$. The results are plotted in Fig. 3. Here the continuous lines represent plots of τ against $\underline{t}$, and dash lines correspond to the function $\epsilon(t)$, where $\underline{t}$ is the time. Figure 3, a shows that slow rotation of the rotor produces flow in the previously orientated grease. Thermal motion results in disorientation of the disperse-phase particles, which occurs before the yield value [maximum on the $\tau(t)$ curve] is passed, and which corresponds to a decrease of the shearing modulus described earlier [6].

In the other similar experiment the body of the instrument was initially rotated rapidly in direction opposite to that of the subsequent slow rotation of the rotor (Fig. 3, b). The higher value of τ_{max} is due to reorientation of the structural elements in the system [6]. If the particles of the disperse phase undergo reorientation a longer time is required to reach equilibrium values of ϵ. This can be seen from a comparison of the $\epsilon(t)$ curves in Fig. 3, a and 3, b.

The reason why the yield value is sharply manifested in presence of intensive relaxation processes, detected by determinations of ϵ, is due to the fact that transition of the yield value is caused by movement of large particles of the disperse phase [6] on which the influence of thermal motion is weak.

After the yield value has been passed and the structural framework has broken down, equilibrium orientation is attained during slow flow; this had not been reached in the experiments represented by Fig. 3. Therefore, the right-hand branches of the $\tau(t)$ curves lie at somewhat different levels.

Determinations of ϵ in deformation of the frozen orientated structure corresponding to high values of D showed that the states of konstalin at low values of D were not equivalent; whereas in one case this state was reached by a gradual decrease of D, in others it was attained by increase of D from the frozen structure of rapid flow. The results of these experiments are plotted in Fig. 4. (Here the abscissa axis is shown with a gap so that it could show the log D scale and the value $D = 0$ corresponding to static determinations of ϵ for the grease).

A system with a high degree of particle orientation in flow was obtained by deformation at high values of D (point A in Fig. 4). Gradual decrease of D gave the curve ABC. When D is decreased new equilibrium states are reached with less perfect orientation of the particles of the disperse phase. When the flow was rapidly arrested the freezing of flow was represented electrically by a value of ϵ close to 2.8 (point E). Deformation of this system with subsequent increase of D gave the Curve EDBA.

Properties of systems with frozen structure of rapid flow are characterized by nonequivalence of states C and D.

Figure 5 gives the results obtained in determinations of tan δ for konstalin (a), solidol (b), and 201 grease (c) at various values of D. The values of tan δ rose with increase of D owing to increased conductivity in flow, probably as the result of impacts between the particles [4]. The influence of D on tan δ is greatest for solidol. Hysteresis effects are also the most pronounced in this case. Therefore, in the graph for solidol (Fig. 5, b) variations of tan δ with increasing (Curve 1) and decreasing D are shown. Rapid arrest of flow results in instantaneous decrease of tan δ for konstalin and grease 201. In the case of solidol tan δ continues to decrease for several hours.

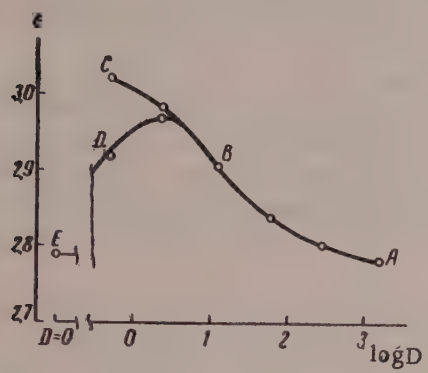


Fig. 4. Variations of the dielectric constant of konstalin with the velocity gradient under different deformation conditions.

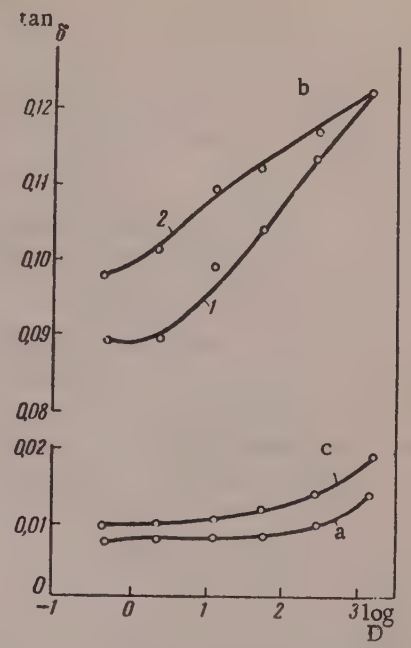


Fig. 5. Effect of velocity gradient on the tangent of the dielectric loss angle of greases.

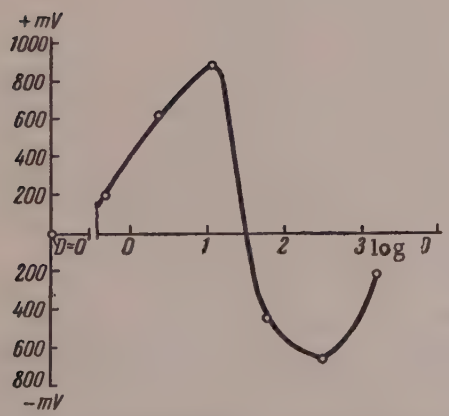


Fig. 6. Electrification of grease during deformation at different rates.

The fact that the frozen flow structure, evaluated electrically from the values of ε, remains constant in time while tan δ decreases more or less rapidly when the flow is arrested confirms the view [6] that the specific properties of plastic disperse systems such as greases are determined by the presence, on the one hand, of large particles of the disperse phase, which are only slightly influenced by thermal motion, and on the other, of small particles which are under the influence of thermal motion. The particles which are affected relatively little by thermal motion cause the greases to have a low tendency to stress relaxation and determine the rigidity of the structural framework and anisotropy of the frozen flow structure. The very small particles, involved in thermal motion, influence elastic after-effects, the tendency of stress relaxation at high stresses, thixotropic restoration and gradual decrease of tan δ after arrest of the flow, and disorientation of the particles of the disperse phase in anisotropic structures before the yield value has been passed.

It was observed that deformation of the greases was accompanied by a strong electrification effect, the existence of which was first noted in studies of the efflux of greases from capillaries [7]. Typical results obtained in experiments with konstalin are plotted in Fig. 6. Here, the potentials recorded at the instrument rotor are shown on the ordinate axis. The abscissa axis is of the type shown in Fig. 4.

SUMMARY

1. Typical plastic disperse systems — konstalin, solidol, and grease 201 — differed in the sensitivity of their dielectric properties to deformation at velocity gradients from 0.5 to $1.5 \cdot 10^3$ sec^{-1} in the frequency range between 0.4 and 10 kc/second. The dielectric constant (ϵ) of konstalin and solidol decreases with increase of the velocity gradient (D), owing to flow orientation of the soap particles. The tangent of the loss angle (tan δ) of greases may increase with increasing velocity gradient. With consecutive increase and decrease of the velocity gradient the values of dielectric constant, tangent of the loss angle, and shear stress showed hysteresis effects.

2. Rapid arrest of flow of konstalin and solidol results in formation of anisotropic structures, with frozen flow demonstrated electrically, analogously to frozen flow demonstrated optically. The dielectric constant of a frozen anisotropic structure is stable in time. The dielectric losses decrease at various rates with time.

3. By determinations of the dielectric constant during deformation of anisotropic frozen structures, it is possible to investigate disorientation and reorientation of particles of the disperse phase in the transition from elastic deformations through the yield value to steady flow. Disorientation of soap crystallites begins under the influence of thermal motion in the course of plastic flow before the yield value is passed, and terminates when a state of viscous flow is reached. Reorientation of the particles of the disperse phase raises the yield value of konstalin and changes the form of the plot of the dielectric constant against the shearing stress.

4. Deformation of greases may be accompanied by electrification, which depends on the rate of deformation.

5. The peculiar combination of rheological, optical, and dielectric properties discussed in this paper is the consequence of the presence of both large and small particles of disperse phase in plastic disperse systems of the grease type.

LITERATURE CITED

[1] G. V. Vinogradov, Proc. Third All-Union Conference on Colloid Chemistry [In Russian] (Kiev, Acad. Sci. Ukrainian SSR, 1952), p. 249.

[2] V. P. Pavlov, Summary of Work on Chemistry and Technology of Petroleum and Gas in 1956 [In Russian] (Institute of Petroleum, Acad. Sci. USSR, Moscow, 1957), p. 69.

[3] G. V. Vinogradov, Zhur. Priklad. Khim. 28, 52 (1955)*; V. V. Sinitsyn et al., Khimiya i Tekhnologiya Topliv i Masel 11, 51 (1958).

[4] A. Bondi and C. Penther, J. Phys. Chem. 57, 72 (1953).

[5] G. V. Vinogradov and V. V. Sinitsyn, Doklady Akad. Nauk SSSR 86, 573 (1952).

[6] G. V. Vinogradov and V. P. Pavlov, Izvest. Akad. Nauk SSSR, Otdel Tekhn. Nauk, Mekhanika i Mashinostroenie 2, 134 (1959); Kolloid Zhur. 20, 248 (1958).*

[7] V. V. Sinitsyn, "Viscous properties and wall slippage of plastic greases," [In Russian] Candidate's Dissertation (Institute of Petroleum, Acad. Sci. USSR, Moscow, 1954).

* See C. B. translation.

EXPERIMENTAL INVESTIGATIONS OF LAMINAR SYSTEMS

25. ELECTRON-MICROSCOPIC INVESTIGATION OF THE STRUCTURE AND FORMATION MECHANISM OF ULTRATHIN FILMS OF COPPER HYDROXIDE FORMING ON A SOLID SURFACE

E. M. Kazakov, G. A. Kitaev, and S. G. Mokrushin

The S. M. Kirov Ural Polytechnic Institute, Sverdlovsk
(Translated from: Kolloidnyi Zhurnal Vol. 22, No. 1, pp. 23-24, January-February, 1960)
(Original article submitted July 14, 1958)

In studies of the formation of hydroxide films with a colloidal structure on the surfaces of aqueous solutions of complex ammine salts of copper and nickel [1-3], it was observed that similar films are formed on the vessel walls under the layers of solution. Such films exhibit interference colors, are transparent to transmitted light, and have considerable mechanical strength. The present communication is concerned with a discussion of the results of an electron-microscopic study of the structure and formation mechanism of ultrathin films from colloidally-adsorbed copper hydroxide at the liquid —solid interphase.

The cupric hydroxide sols were prepared in Petri dishes from 0.025 M solutions of cupric sulfate tetrammine containing a certain amount of excess ammonia. When the latter is removed the cupric ammine complex is decomposed, and this leads to hydrolysis of cupric ions and formation of the colloidally-dispersed hydroxide. The sol particles constitute the material from which films are formed both on solution surfaces [4] and on glass.

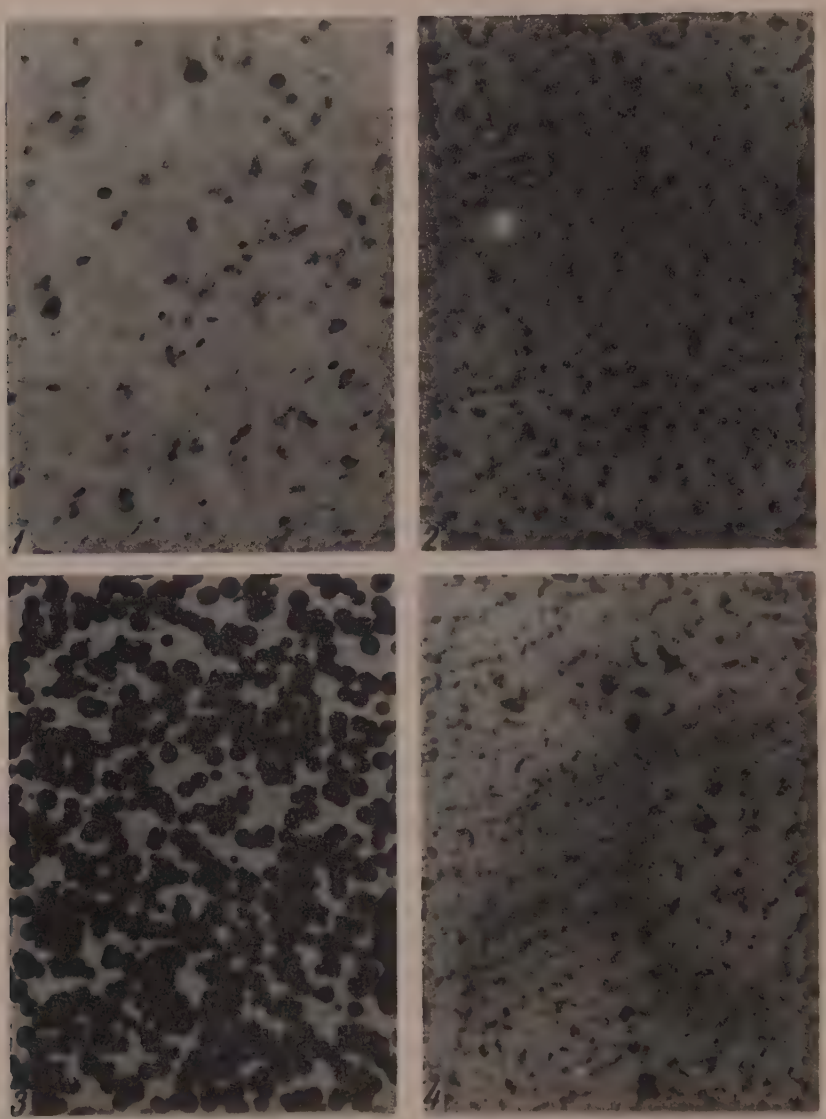
In view of the techniques of specimen preparation in electron microscopy we prepared the hydroxide films on collodion supports. The supports were fixed in metal loops and lowered to the bottom of a dish containing the solution prepared for film formation. Readiness of the solution was indicated by the formation of extremely thin film on its surface. After various time intervals the specimens were withdrawn, washed repeatedly, dried, and then examined in the EM-3 electron microscope at a direct optical magnification of 6,500.

Electron-microscopic examination of hydroxide films formed on solid surfaces in times varying from 15 minutes to 3 hours showed that at the initial stage film formation occurs by adsorption of primary amorphous very small colloidal particles on the solid surface (Photo 1). As the result of subsequent surface coagulation, the particles grow and form colloidal aggregates of regular spherical form (Photo 2, 3). Evidence of surface coagulation is provided by the fact that the colloidal particles adsorbed on the collodion support in the course of 15 minutes from a solution which had been aged for three hours are considerably smaller (Photo 4) than the particles which form the film after a three-hour exposure (Photo 3). The larger particles present in the solution are not adsorbed on the support surface.

It follows from these observations that the film is formed by adsorption, on a solid surface, of colloidal particles of a definite high degree of dispersion, and this is followed by surface coagulation.

Denser and thicker films could not be examined in the electron microscope, as the collodion supports burned away. However, the observations indicate that these films, like those formed on solution surfaces [2, 3] have a porous structure and are polymicellar. Electron-diffraction patterns confirmed that the hydroxide particles forming the films are amorphous.

It should also be noted that the process under consideration is analogous to formation of metallic semi-transparent film layers on solid surfaces by cathodic sputtering or thermal sublimation under vacuum. Workers who studied these effects [4] support colloidochemical concepts.



Electron micrographs of ultrathin $Cu(OH)_2$ films (× 13,000) formed during: 1) 15 minutes; 2, 3) 1.5 and 3 hours; 4) 15 minutes from a solution aged for three hours.

Our results are consistent with the views of Kargin and his associates [5] on the mechanism of formation of colloidal particles in solutions, according to which the first stage in the formation of a new colloidal phase consists of the formation of relatively large amorphous rounded grains.

SUMMARY

1. Electron micrographs of ultrathin $Cu(OH)_2$ films made by precipitation from colloidal solutions showed that such films are formed by adsorption of very small colloidal particles on solid surfaces, followed by surface coagulation.

2. The amorphous nature of the copper hydroxide particles forming the films was confirmed by means of electron diffraction studies.

LITERATURE CITED

[1] S. G. Mokrushin and P. S. Konyaev, Zhur. Fiz. Khim. 6, 95 (1935); S. G. Mokrushin, Zhur. Fiz. Khim. 5, 1082 (1934); Kolloid Zhur. 10, 305 (1948); S. G. Mokrushin and G. A. Kitaev, Kolloid Zhur. 19, 93 (1957).*

[2] S. G. Mokrushin, G. A. Kitaev, and O. K. Shabalina, Doklady Akad. Nauk SSSR 94, 1109 (1954).

[3] N. V. Demenev, N. N. Buinov, and M. I. Milyutina, Kolloid. Zhur. 12, 252 (1950); S. G. Mokrushin, Yu. D. Tkachev, and O. K. Shabalina, Kolloid. Zhur. 19, 597 (1957).*

[4] G. V. Rozenberg, Uspekhi Fiz. Nauk 58, 478 (1956); F. Joliot-Curie, Selected Works (Acad. Sci. USSR Press, Moscow, 1957) [Russian translation].

[5] Z. Ya. Berestneva and V. A. Kargin, Uspekhi Khimii 24, 249 (1955); Kolloid. Zhur. 17, 196 (1955);* Z. Ya. Berestneva, G. A. Karetskaya, and V. A. Kargin, Kolloid. Zhur. 12, 338 (1950); 13, 323 (1951).

* See C. B. translation.

HEAT AND ENTROPY OF ADSORPTION OF BENZENE AND n-HEXANE VAPORS ON MAGNESIUM HYDROXIDE

A. V. Kiselev and D. P. Poshkus

Chemical Faculty of the M. V. Lononosov University, Moscow, Adsorption Laboratory

Institute of Physical Chemistry of the Academy of Sciences, USSR, Laboratory of Sorption Processes

(Translated from: Kolloidnyi Zhurnal Vol. 22, No. 1, pp. 25-30, January-February, 1960)
(Original article submitted September 23, 1958)

In the preceding investigations of this series [1, 2] we determined the adsorption isotherms for benzene and hexane vapors on magnesium hydroxide surfaces dehydrated to different extents. It was shown that in the region of relative vapor pressures corresponding to predominant filling of a monolayer on magnesium oxide the adsorption of hexane is greater than that of benzene, whereas on magnesium hydroxide with a weakly dehydrated surface the adsorption of hexane is less than the adsorption of benzene. In the present investigation, we determined the heats and entropies of adsorption of these vapors on magnesium hydroxide with a weakly dehydrated surface.

Method of investigation. The adsorbent used was a sample of $Mg(OH)_2$ - 3 magnesium hydroxide evacuated at 20°; as is indicated by earlier work [1], the surface of this material is weakly dehydrated. The preparation and structural characteristics of this sample were described earlier [2].

The differential heat of adsorption Q_a was found from the isotherms of adsorption on this sample of magnesium hydroxide, determined at two temperatures T_1 and T_2 (10 and 30°), from the formula

$$Q_a = \frac{RT_1T_2}{T_2 - T_1}\left[\ln\left(\frac{p}{p_s}\right)_{T_2} - \ln\left(\frac{p}{p_s}\right)_{T_1}\right]_a + L,$$

where L is the heat of condensation of the adsorbate, and p/p_s is the relative vapor pressure. The method used for determination of the adsorption isotherms and the degree of accuracy were the same as in the preceding investigation [3]. The accuracy of determination of the heat of adsorption ΔQ_a was estimated for each individual case by means of the theory of errors.

The differential entropy of transition of a mole of adsorbate from the free liquid into the adsorption layer, ΔS_a, was calculated from the formula

$$\Delta S_a = -\frac{RT\left(\ln\frac{p}{p_s}\right)_{a,T} + (Q_a - L)}{T},$$

for T = 293.2° (20° C); the value of $RT \ln \frac{p}{p_s}$, the differential work of adsorption at that temperature, was found from the isotherms given previously [2]. The accuracy of determination of the differential entropy of adsorption $\Delta(\Delta S_a)$ was estimated by means of the expression $\Delta(\Delta S_a) = \Delta Q_a/T$.

Figure 1 shows isotherms for adsorption of benzene and hexane vapors on $Mg(OH)_2$-3 sample at 10 and 30°.

Plots of the differential heats of adsorption Q_a of benzene and hexane vapors against the absolute adsorption α, calculated from the adsorption isotherms at two temperatures, for $Mg(OH)_2$-3 sample are presented in Fig. 2. The vertical continuous lines indicate the accuracy of determination of the heats of adsorption at the given degrees of adsorption. In the region of intermediate surface coverage the accuracy of determination of the heats of adsorption is about ± 0.1, ± 0.2 kcal/mole. The horizontal dash lines indicate the heats of condensation of benzene and hexane vapors, and the corresponding vertical dash lines show the capacities α_m of benzene and hexane monolayers.*

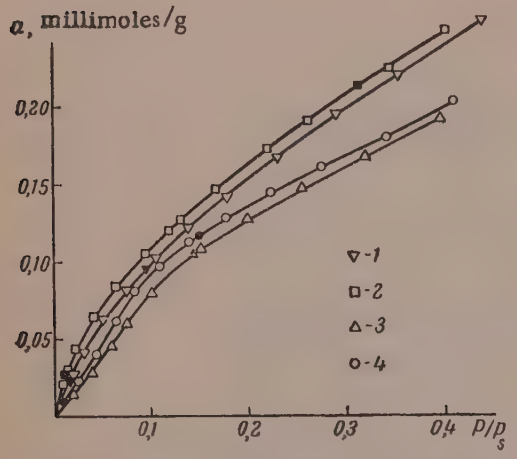


Fig. 1. Isotherms for adsorption of benzene vapor at 30° (1) and 10° (2) and hexane vapor at 30° (3) and 10° (4) on $Mg(OH)_2$-3 sample.

The differential heat of adsorption of benzene (Fig. 2, a) decreases continuously with increasing surface coverage. The heat of adsorption of hexane (Fig. 2, b) falls sharply during filling of the first 25% of the surface; in the region of intermediate coverage it increases somewhat and passes through a maximum; when the monomolecular layer becomes filled and predominant adsorption in the second layer begins the value gradually decreases and approaches the heat of condensation of the gases.

Calculated values of the differential entropy of adsorption of benzene and hexane vapors at 20° on $Mg(OH)_2$-3 are plotted against the absolute adsorption α in Fig. 3. The vertical continuous lines indicate the accuracy of determination of the entropy of adsorption. Dash lines indicate values of α. In the region of intermediate filling of the monolayer, the accuracy of determination of the entropy of adsorption is approximately ± 0.5 cal/degree · mole.

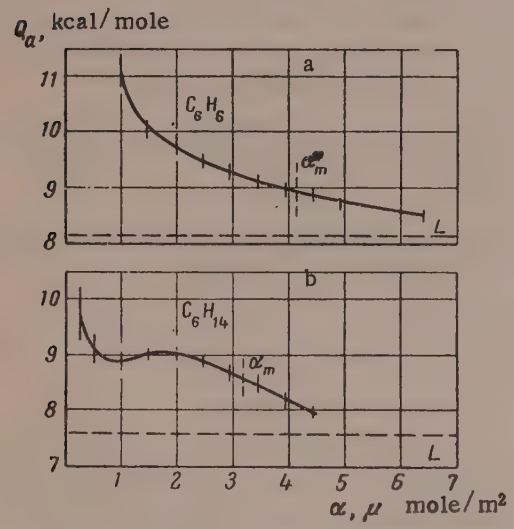


Fig. 2. Variations of the differential heats of adsorption of benzene (a) and n-hexane (b) vapors on $Mg(OH)_2$-3 with the absolute adsorption.

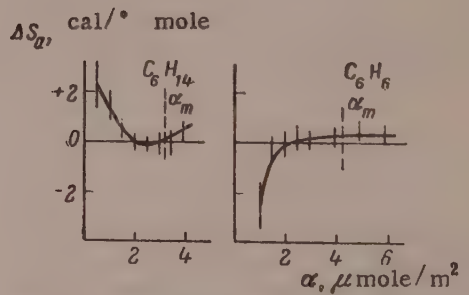


Fig. 3. Variation of the differential entropy of adsorption of n-hexane and benzene vapors on $Mg(OH)_2$-3 with the absolute adsorption.

* The monolayer capacities α_m per unit adsorbent surface for benzene and n-hexane vapors were determined by division of the specific capacities of the monolayers α_m, found from linear plots of the corresponding adsorption isotherms in BET coordinates (see [2]), by the specific surfaces of the sample, found from adsorption of nitrogen vapor as determined by the BET method; the area occupied by a nitrogen molecule in a compact monolayer was taken as $\omega_m = 16.2$ A.

The differential entropy of transition of a mole of hexane from the free liquid to the surface of $Mg(OH)_2$-3 magnesium hydroxide (Fig. 3), is initially positive and falls sharply with increasing degree of coverage; when the monolayer is complete it passes through a minimum, when its value is close to zero. In the region of transition to adsorption in the second layer, the value of entropy for hexane increases. The entropy of adsorption of benzene is initially negative and rises sharply with increase of surface coverage θ to 0.5 (Fig. 3), while in the remaining region of monolayer filling and in transition to adsorption in the second layer it is almost constant and close to zero.

Heat of adsorption and nature of the adsorption of benzene and hexane vapors on magnesium hydroxide. In the general case, the heat of adsorption is the sum of the energy of interaction of the adsorbed molecules with the adsorbent and the energy of interaction between the adsorbed molecules. In the case of adsorption of nonpolar molecules on a polar adsorbent, in addition to dispersional interaction between the adsorbed molecules there is also interaction between dipoles induced in the adsorbed molecules by the electric field over the adsorbent. It follows that the monotonic decrease of the heat of adsorption of benzene on $Mg(OH)_2$-3 (Fig. 2, a) with increasing surface coverage may be due not only to energetic heterogeneity of the surface of this adsorbent with respect to benzene molecules, but also to increased repulsion between induced dipoles in the benzene molecules with increasing filling of the monolayer.*

The weak maximum on the plot of the differential heat of adsorption of hexane vapor against the adsorption (Fig. 2, b) in the region of moderate filling of the monolayer is probably the result of masking of the influence of surface heterogeneity and repulsion between induced dipoles in the hexane molecules by the influence of strong dispersional attraction between these molecules [5]. No such maximum is found in the plot of the differential heat of adsorption of benzene on magnesium hydroxide against the adsorption during filling of the monolayer (Fig. 2, a), probably because benzene molecules are more sensitive than hexane molecules to heterogeneity of the magnesium hydroxide surface and because the attraction in the adsorption layer is weaker between benzene molecules than between hexane molecules [4, 5].

For quantitative comparisons of the heats of adsorption of different adsorbates on different adsorbents, it is convenient to use heats of adsorption for degree of surface coverage $\theta = 0.5$, as in this region of monolayer filling the influence of surface heterogeneity on the heat of adsorption is already small, whereas horizontal interaction between the adsorbed molecules is still weak [5]. The differential heats of adsorption at $\theta = 0.5$ are known as the standard values [5] and are denoted by Q_a^0.

The standard differential heats of adsorption Q_a^0 of benzene and hexane vapors on $Mg(OH)_2$-3 magnesium hydroxide, magnesium oxide, hydrated and dehydrated silica gels, and graphitized carbon black are compared in the table.

Standard Heats of Adsorption Q_a^0 of Benzene and Hexane on Different Adsorbents, in kcal/mole

Adsorbent	Adsorbate		$Q^0_{a\,C_6H_6} - Q^0_{a\,C_6H_{14}}$
	C_6H_6	C_6H_{14}	
$Mg(OH)_2$-3	9,6	9,0	+0,6
Silica gel containing 12.8 μmoles of OH per m^2 surface area	10,4 [6]	8,8 [7]	+1,6
The same, 1 μmole OH per m^2 surface area	8,5 [8]	8,6 [8]	−0,1
	9,2 [9]	9,4 [9]	−0,2
Graphitized carbon black	10,0 [4]	12,1 [5]	−2,1

* Interaction between the constant multipoles of benzene molecules is probably small, as the differential heat of adsorption of benzene vapor on a nonpolar adsorbent (graphitized carbon black [4]) does not diminish with increase of surface coverage to $\theta \approx 1$.

It is seen in the table that the standard heat of adsorption of benzene on polar adsorbents with strongly hydrated surfaces (magnesium hydroxide and hydrated silica gel) is considerably greater than that of hexane; on polar adsorbents which have few or no hydroxyl groups in the surface (dehydrated silica gel and MgO) the standard heats of adsorption of benzene and hexane are approximately equal. The heat of adsorption of benzene vapor on a nonpolar adsorbent (graphitized carbon black) is approximately 2 kcal/mole less than the heat of adsorption of hexane vapor. Since benzene and hexane are adsorbed only by the action of dispersional forces on graphite [9], the heats of adsorption of benzene and hexane molecules should remain in approximately the same ratio for adsorption on other adsorbents if only dispersional interaction took place between these molecules and the adsorbent and if we disregard any possible slight variations of the equilibrium distances of benzene and hexane molecules from the surface in adsorption on different adsorbents, which may lead to some alteration in the ratio of the dispersional interactions of these molecules with the adsorbent. However, the standard heat of adsorption of benzene on hydrated silica gel is greater than that of hexane by approximately 1.6 kcal/mole. This anomalous behavior of benzene, and of aromatic and unsaturated hydrocarbons, in general, in adsorption on hydrate silica gel surfaces is caused by additional interaction, further to the dispersional type, leading to formation of the so-called π-complexes [8, 10, 11]. Approximate calculations [12] show that increase of the heat of adsorption of benzene on hydrate silica gel surface may be attributed mainly to Coulomb forces between the benzene molecules and the electrostatic field created by the hydroxyl groups of the silica gel.

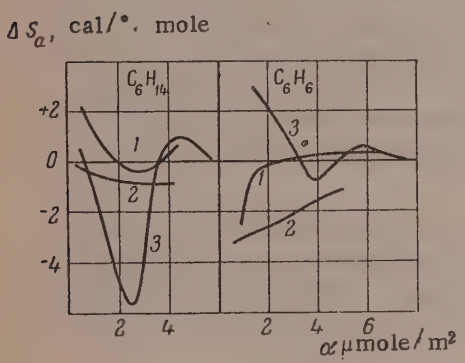


Fig. 4. Comparison of curves for the differential entropies of adsorption of n-hexane and benzene vapors on $Mg(OH)_2$-3 (1), hydrated silica gel (2), and graphitized carbon black (3).

Evidently, electrostatic interaction of the electric field above the magnesium hydroxide lattice (its principal plane is the basal plane, the surface layer of which consists of hydroxyl ions) with a benzene molecule is considerably greater than electrostatic interaction with a hexane molecule, so that the total heat of adsorption of benzene on magnesium hydroxide, as on hydrated silica gel, is greater than the heat of adsorption of hexane.

Retention of the electrostatic field, even though modified or weakened, on dehydration of silica gel surface probably accounts for the fact that the ratio of the heats of adsorption of benzene and hexane vapors on incompletely dehydrated silica gel is still somewhat greater than the ratio for graphitized black.

The similarity of the heats of adsorption of benzene and hexane on magnesium oxide (see table), which does not contain any hydroxyl groups, indicates that the increase of the ratio of the heats of adsorption of benzene and hexane in adsorption on polar adsorbents, relative to that found in adsorption on graphite, is due to electrostatic causes.

Benzene and hexane molecules lie flat on the adsorbent surface [1, 2, 4, 5]. The mean polarization of the benzene molecule ($10.3 \cdot 10^{-24}$ cm^3) and the polarization in a direction perpendicular to the plane of the benzene ring ($6.35 \cdot 10^{-24}$ cm^3) are less than the mean polarization of the hexane molecule $\alpha = 11.8 \cdot 10^{-24}$ cm^3 [13], and it follows that inductive interaction of the adsorbed molecules with the electric field cannot be responsible for increase of the heat of adsorption of benzene in comparison with hexane. This increase is probably caused by the greater Coulomb interaction of the benzene molecule than the hexane molecule with the electric field above the adsorbent, because of the peculiarities of the electrical structure of the benzene molecule: a higher concentration of negative charges, mainly π-electrons, at the periphery of the molecule on either side of the plane of the benzene ring, as the result of which the benzene molecule acts as a spatial quadrupole with a large moment.

Differential entropy of adsorption. In Fig. 4 are presented the curves for differential entropies of adsorption of benzene and hexane on magnesium hydroxide, silica gel with a hydrated surface [6], and graphitized carbon black [4, 5]. It follows from Fig. 4 that the curves for the differential entropy of adsorption of both hexane and benzene molecules on magnesium hydroxide are more similar to the corresponding curves for hydrated silica gel than those for graphitized carbon black. It follows that the state of these molecules in the adsorption layer on magnesium hydroxide is more similar to the state of these molecules on silica gel than on graphitized carbon black, and the entropy (and therefore the mobility) of both the hexane and the benzene molecules is greater in the first layer on magnesium hydroxide surface than on silica gel surface.

At the standard degree of surface coverage $\theta = 0.5$ for $Mg(OH)_2$-3 sample the differential entropy of adsorption of benzene is $\Delta S_a^0 \approx 0$ cal/degree·mole, and that of hexane is $\Delta S_a^0 \approx +0.5$ cal/degree·mole, whereas on silica gel the respective values are -2.6 and -0.6 cal/degree·mole, and on graphitized carbon black they are $+1.9$ and -2.9 cal/degree·mole.

SUMMARY

1. Curves for the differential heats and entropies of adsorption of benzene and hexane vapors were calculated from the adsorption isotherms determined at two different temperatures on magnesium hydroxide with a weakly hydrated surface.

2. The standard heat of adsorption of benzene vapor is greater than that of n-hexane vapor on magnesium hydroxide with a weakly hydrated surface.

3. Comparison of the standard heats of adsorption on different adsorbents shows that the heat of adsorption of benzene vapor on polar adsorbents is greater than or close to the heat of adsorption of hexane, whereas on a nonpolar adsorbent the heat of adsorption of benzene is considerably less than that of n-hexane. The higher value of the ratio of the heats of adsorption of benzene and n-hexane vapors on polar than on nonpolar adsorbents is mainly due to stronger Coulomb interaction of the benzene molecules with the electric field above the polar adsorbent surface.

LITERATURE CITED

[1] A. V. Kiselev and D. P. Poshkus, Kolloid. Zhur. 21, 590 (1959).*

[2] A. V. Kiselev and D. P. Poshkus, Kolloid. Zhur. 21, 653 (1959).*

[3] A. V. Kiselev, I. E. Neimark, D. P. Poshkus, and M. A. Piontkovskii, Izvest. Akad. Nauk SSSR, Otdel. Khim. Nauk 2, 232 (1959).*

[4] N. N. Avgul', G. I. Berezin, A. V. Kiselev, and I. A. Lygina, Izvest. Akad. Nauk SSSR, Otdel. Khim. Nauk 1304 (1956).*

[5] N. N. Avgul', G. I. Berezin, A. V. Kiselev, and I. A. Lygina, Zhur. Fiz. Khim. 30, 2106 (1956).

[6] A. A. Isirikyan and A. V. Kiselev, Zhur. Fiz. Khim. 32, 679 (1958).

[7] A. A. Isirikyan and A. V. Kiselev, Zhur. Fiz. Khim. 31, 2127 (1957).

[8] A. V. Kiselev, in the book: The Structure and Properties of Porous Materials (London, 1958), p. 195.

[9] N. N. Avgul', A. A. Isirikyan, A. V. Kiselev, I. A. Lygina, and D. P. Poshkus, Izvest. Akad. Nauk SSSR, Otdel. Khim. Nauk 1314 (1957).*

[10] A. A. Isirikyan and A. V. Kiselev, Doklady Akad. Nauk SSSR 115, 343 (1957).*

[11] L. D. Belyakova and A. V. Kiselev, Doklady Akad. Nauk SSSR 119, 298 (1958).*

[12] A. V. Kiselev and D. P. Poshkus, Doklady Akad. Nauk SSSR 120, 834 (1958).*

[13] Landolt-Börnstein, Tabellen, 6 Auflage, No. 3, p. 511.

* See C. B. translation.

STRENGTHENING OF STRUCTURAL BONDS IN CLAY SOILS AS THE RESULT OF ELECTROCHEMICAL STABILIZATION

G. N. Zhinkin

Leningrad Institute of Railroad Transport Engineers
(Translated from: Kolloidnyi Zhurnal Vol. 22, No. 1, pp. 31-36, January-February, 1960)
(Original article submitted September 17, 1958)

Electrochemical stabilization of soils is one of the important problems of colloid chemistry, as in the course of this process crystallization bonds are formed between particles in clay systems and crystallization structures are produced.

The first investigations in this field [1-4] showed that under the influence of direct electric current clay soils are dried and acquire increased strength and resistance to water. Between 1948 and 1953 the present author, on the advice of Professor A. V. Liverovskii, used this method for reinforcement of weak soils in railroad beds over five railroad regions under various geological, climatic, and hydrological conditions [2].

These and subsequent investigations demonstrated the effectiveness of electrochemical soil stabilization and gave some indications of ways of applying the method in practice. However, further progress was hindered by lack of data on irreversibility of the stabilization, i.e., on the permanence of the stabilized soil properties.

To establish whether the stabilization is irreversible we carried out periodic observations of the state of the above-named regions of railroad beds, accompanied by sampling of the soil for laboratory investigations. Comparison of the properties of unstabilized soils with those of stabilized soils several years after electrochemical treatment gave an indication of changes taking place in the stabilized soils and yielded some data on strengthening of their structural bonds.

Coagulation, crystallization, and structurization processes in clay soils are considerably more complicated than are such processes in ordinary suspensions and colloidal solutions. The diverse mineral composition and dispersity of the solid phase in soils, the composition of their exchange cations and of the ions of the soil water, genetic characteristics, and certain other factors complicate the general picture of structure formation.

It is known that a direct electric current influences primarily the most finely-dispersed (colloidal) part of soil [3]. Our investigations [4] confirm this and make it possible to deduce the nature of the bonds which arise between the colloidal particles in soil after electrochemical stabilization, with due regard to results of granulometric analysis.

To account for the nature of the structural changes taking place in stabilized soil we make use of the experimental studies and theoretical concepts of Rebinder and his school [5] in the field of structure formation in disperse systems. It has been shown that cohesion in a clay soil is caused by molecular forces, and depends on the number of particles and the area of contact between them. Moreover, cohesion depends on the thickness of the residual films of water at the points of contact between the particles; the thinner these films and the more numerous the particles (and therefore the contacts between them), i.e., the greater the density of the coagulation structure of the soil, the stronger is the soil.

When a direct current is passed through a soil, the soil becomes dried as the result of electroosmosis, with some compaction of the soil, decrease in the thickness of the water layers, and increase of the cohesion forces (structural strength). In addition to strengthening of molecular bonds, crystallization bonds arise between the particles as the result of formation and growth of coalescing crystallization centers of new solid phases.

At the start of electrochemical stabilization there is an intensive growth of molecular bonding, which at that stage represents the main force causing cohesion (strength) of the soil. These bonds are known to be reversible and are weakened on moistening. Subsequently, stronger and more stable bonds arise between the particles and the strength as a whole becomes of a coagulational-crystallizational character. Crystallization bonds begin to play the main role in soil stabilization, and determine the strength and its permanence in time. Increased cohesion between the soil particles results from an increase in the number of crystallization bonds, intensification of such bonding, and increase of the concretion contact area.

The ferric, aluminum, and calcium hydroxides formed in the course of electrochemical stabilization cement the soil particles together in such a way that any subsequent wetting or changes of electrokinetic conditions cannot break down the structural bonds which have been formed. The soil strength increases not only during the electrochemical stabilization, but also after the end of the process [6]; this is confirmed by the data presented below.

It was shown by laboratory experiments [7] that the dispersity of soils decreases after electrochemical stabilization. This process is most pronounced in the anode zone, and particles between 0.01 and 0.005 mm in size undergo the greatest aggregation.

To determine changes in the composition of a soil subjected to electrochemical stabilization in an earth work we compared its granulometric composition before and after stabilization. The table contains results obtained in a study of soil samples taken from the anode zone; the changes of composition in the cathode and intermediate zones are similar but less pronounced. The table shows that stabilization is immediately followed by a decrease in the content of particles < 0.01 mm in size and an increase in the content of particles > 0.01 mm.

Coarsening of the particle-size composition of the soil was accompanied by increase of its specific cohesion. Thus, the cohesion of a soil sample taken in the Leningrad region was 0.04 kg/cm^2 before and 0.19 kg/cm^2 after stabilization. Similar increases of cohesion were found in soils from the Arkhagel'sk (from 0.10 to 0.37 kg/cm^2) and Khar'kov (from 0.04 to 0.30 kg/cm^2) regions.

This increase of specific cohesion indicates that the soil is reinforced as the result of electrochemical stabilization; this is fully consistent with coarsening of its particle-size composition. Evidently, both effects, caused by the action of the direct current and electrolyte,* lead to considerable structural changes.

Particle-Size Composition of Soils Before and After Stabilization

Location of stabilized region	Type of sample	Weight % of fractions of particle diameter, mm							
		2,0—1,0	1,0—0,5	0,50—0,25	0,25—0,10	0,10—0,05	0,05—0,01	0,01—0,002	<0,002
Leningrad region	Before stabil.	1	1	1	4	6	29	40	18
	After stabil.	—	1	2	4	8	73	7	5
Arkhagel'sk region	Before stabil.	—	—	1	1	10	41	34	13
	After stabil.	—	—	—	2	14	45	29	10
Khar'kov region	Before stabil.	—	1	1	5	6	25	32	30
	After stabil.	—	—	1	3	8	32	29	27

The principal factors influencing structure formation are electroosmosis, electrolysis, and secondary chemical processes at the particle surfaces. Electrolysis leads to intensive saturation of the soil by cations of the chemical additive introduced through the anode and to accelerated increase of the concentration of the electrolytes in the dispersion medium, and thus creates suitable conditions for soil aggregation.

Electroosmosis favors saturation of the soil with the chemical additive and leads to dehydration of the soil. This creates favorable conditions for formation and growth of new crystalline substances and concretions of them,

* A 4% calcium chloride solution was introduced into the soil at the same time as the direct current was passed.

increase of molecular forces, and reinforcement of structure. The chemical processes on the particle surfaces, accelerated and directed by electrolysis and electroosmosis, lead to formation of a new crystallization structure.

It is known that highly disperse coagulation structures are thixotropic and can be broken down mechanically under certain conditions. It is therefore theoretically possible that the improvement in soil properties attained as the result of electrochemical stabilization may be lost with time. To determine whether the reinforcement and the structural changes are irreversible, we carried out observations on changes in the properties of soils in earth works for 2-5 years after stabilization.

Investigation of sample pieces taken several years after the stabilization showed that structural changes in stabilized soils continue in the same direction after stabilization; thus, their particle-size composition becomes coarser and the specific cohesion increases with time.

For example, the content of fractions smaller than 0.002 mm in soil from the Leningrad region was 5% immediately after stabilization (November, 1948), while six months later (May, 1949) it had fallen to 4%; in 1952 it remained at the same level (4%), and by 1953 it fell to 2%.

Samples from the Arkhagel'sk region showed similar changes in composition. In this case, the content of particles smaller than 0.002 mm fell to 10% after stabilization; a year later (1952), it fell further to 7%, and remained at approximately the same level in 1953. This was accompanied by an increase in the content of particles 0.05-0.01 mm in size: in 1951, immediately after stabilization, these particles comprised 45% of the soil, in 1952 the content reached 58%, but in 1953 it remained approximately the same (55%).

Similar effects were observed in soil samples from the Khar'kov region. Here the content of particles smaller than 0.002 mm fell to 27% after stabilization, six months later it was 14%, and subsequently remained at that level. The content of particles 0.10-0.05 mm in size showed a corresponding increase.

It follows from the above data that aggregation of soil particles even increases in time rather than being lost. This indicates that structural changes continue in soil after the end of the stabilization treatment.

The specific cohesion changes with time fully in accordance with changes in the particle-size composition. For example, in the case of the samples from the Leningrad region the soil strength increased after completion of the treatment in 1948 from 0.19 to 0.32 kg/cm^2 by 1953; thus, the strength was nearly doubled in five years.

The strength of soil taken from the Arkhagel'sk region increased from 0.37 to 0.77 kg/cm^2, i.e., it was doubled, during 1.5 years of observations.

In the soil from the Khar'kov region the cohesion of the soil was also almost doubled after stabilization during the observation period.

The above results show that structural reinforcement in a soil does not cease after treatment by a direct electric current is stopped; the reinforcement processes induced by the passage of the direct current, having received a suitable initial impetus, may develop in soil without any external influences.

It is known [8] that soils previously treated with salts may undergo peptization with breakdown of the original structure by the natural action of soil and surface waters. This did not occur under the influence of natural leaching of the stabilized soil by surface waters under our conditions.

Bezruk [9], in a study of the effects of alternate freezing and thawing of soil, found that the dispersity of soil increases as a result. It was therefore natural to expect a similar result under our conditions. However, as the above data showed, no peptization due to natural freezing and thawing of a soil stabilized by the electrochemical process could be eventually detected. It follows that this reinforcement of the soil structure prevails over the natural action referred to above, and this proves that the action of electrochemical soil stabilization is irreversible.

The initial thixotropic coagulational structure of a moist clay soil has low strength; the contacts of the soil particles are plastified by thin interlayers of solution, and therefore such soils have plasticoviscous properties. If a direct current is passed through the soil, especially if chemical additives are simultaneously introduced into the soil, the thixotropic coagulational structure becomes more compact in individual regions and is considerably reinforced. This effect is also favored to a great extent by electroosmotic dehydration of the soil. Decrease of the thickness of the solvation layers and increased concentration of ions in the diffuse layer, especially at the

points of contact between the solid particles or in regions where their relative positions are the most favorable, leads to formation of crystallization centers followed by concretion of the crystals.

The nature and constitution of the crystallization bonds formed in soils during electrochemical stabilization are being investigated by Korzhuev and Titkov [10] in relation to reinforcement of borehole walls.

It is important to note that electrochemical stabilization does not produce any appreciable decrease in the volume of the soil. Compaction of the particles is hindered by their anisodiametric shape at high dispersions. At the same time this particle shape has a favorable influence in formation of a spatial coagulation-crystallization structure within the stabilized soil.

The soil dehydration effected by electrochemical stabilization may be eventually lost under natural conditions. The sole factor which determines the permanency of the soil strength is the new crystallization structure, which causes irreversible transformation of the soil.

Reinforcement of the soil structure proceeds somewhat more slowly after the current has been passed than during the actual process of electrochemical stabilization. This is probably due to further conversion of coagulation into crystallization bonds, with simultaneous reinforcement of the crystallization bonds. Apparently, no new coagulation bonds are formed during this period, and reinforcement of the soil and coarsening of its particle-size composition take place owing to gradual conversion of the coagulation-crystallization structure into one of the crystallization-coagulation type, i.e., a structure in which crystallization bonds predominate. The formation of a crystallization structure in this case is induced by the action of weak molecular forces at the points of direct concretion of the crystals. These forces are apparently the same as those which form the crystal lattice [11].

As has already been stated, cohesion between the soil particles was doubled in the course of time after the end of the stabilization treatment, while in comparison with untreated soil the strength of stabilized soil increased approximately 8-fold (to the same extent for all three sampling regions). The increase of strength and coarsening of the particle-size composition of soils in time confirm the foregoing views on the changes in their structure.

The decrease in soil density observed after stabilization provides some indirect evidence of formation of new crystals. For example, the density of soil (determined in kerosene) from the Arkhagel'sk region fell from 2.73 to 2.68 g/cm^3 after stabilization; the density of soil from the Khar'kov region fell from 2.69 to 2.64 g/cm^3. Other samples showed average density decreases of 0.02-0.04 g/cm^3.

The decrease of soil density after stabilization, characteristic for all samples, probably occurs as the result of formation of individual crystals of groups of crystals in the soil, with density less than that of the soil particles themselves.

Our investigations were performed on soils in their natural formations,* which created special difficulties in clarification of the processes taking place in electrochemical soil stabilization and in interpretation of the individual effects. The next stage in our investigation is elucidation of the topochemical nature of the crystalline bridges of the new solid phase formed, and study of possible control of the stabilization process and of the strength of the treated soil by additional chemical influences (in relation to the composition of the injected solutions, nature of the electrolytes, etc.).

SUMMARY

1. The most significant characteristics of electrochemical stabilization are changes in the particle-size composition and specific cohesion of soils.

2. The action of direct electric current and calcium chloride solution on a clay soil changes its structure from the thixotropic coagulational to the coagulation-crystallization type. As a result, the strength of the soil is increased 3 to 4-fold.

3. When the stabilization treatment is ended the strength of the coagulation-crystallization soil structure continues to increase; this results in a further, approximately twofold increase of soil strength. On the whole, the strength of a soil is increased 7 to 8-fold after electrochemical stabilization.

* The experimental soils belong to the hydromica group with respect to the predominant mineral composition.

4. The strength increase of the soil which follows after electrochemical stabilization indicates that the stabilization is irreversible; this is important in practical applications of the process.

LITERATURE CITED

[1] B. A. Rzhanitsyn, Proceedings of Conference on Stabilization of Soils and Rocks [In Russian] (Izd. AN SSSR, 1941), p. 55; A. A. Dragi, Zheleznodorozhnyi Transport 5-6, 75 (1946); L. Casagrande, Bautechnik 1, 14 (1937); M. Lacroix, Ann. pouts et chaussees 5, 99 (1948).

[2] G. N. Zhinkin, Coll. Trans. Leningrad Inst. Railroad Transport Engineers [In Russian] (Transport and Railroad Press, 1952), 144, 64; (1956), 150, 72.

[3] K. K. Gedroits, Selected Works [In Russian] (Agricultural Press, 1955), 1, 122.

[4] G. N. Zhinkin, Doklady Akad. Nauk SSSR 71, 917 (1950).

[5] P. A. Rebinder, Proc. Conference on Engineering and Geological Properties of Rocks [In Russian] (Izd. AN SSSR, 1956), 1, 31; Vestnik AN SSSR 10, 32 (1957).

[6] G. N. Zhinkin, Coll. Trans. Leningrad Inst. Railroad Transport Engineers [In Russian] (Transport and Railroad Press, 1959), 157, 164.

[7] B. F. Rel'tov and L. V. Novikov, Izv. N.-I. In-ta Gidrotekhn. 31, 177 (1946); B. V. Tolstopyatov, Pochvovedenie 8, 67 (1940).

[8] L. N. Lomize, Proc. Conference on Soil Mechanics and Foundations [In Russian] (Gosenergoizdat, 1956), p. 172.

[9] V. M. Bezruk, Theoretical Principles of Soil Reinforcement by Cements [In Russian] (Automobile Transport Press, 1956), p. 139.

[10] A. S. Korzhuev and N. I. Titkov, Summaries of Papers at the 4th All-Union Conference on Colloid Chemistry [In Russian] (Izd. AN SSSR, 1958), p. 214.

[11] N. V. Mikhailov and P. A. Rebinder, Kolloid. Zhur. 17, 107 (1955).*

* See C. B. translation.

EMULSION POLYMERIZATION OF STYRENE IN PRESENCE OF EMULSIFIERS OF DIFFERENT MOLECULAR WEIGHTS

N. Ya. Ivanova and A. I. Yurzhenko

Ivan Franko University, L'vov
(Translated from: Kolloidnyi Zhurnal Vol. 22, No. 1, pp. 37-41, January-February, 1960)
(Original article submitted December 13, 1958)

In studies of emulsion polymerization many workers have shown that the surface-active emulsifier introduced into a polymerization system is not only an unreactive stabilizer for the emulsion of monomer and of the latex formed, but also acts as a factor which determines to a considerable extent the topochemistry of the polymerization process. It has been shown that the emulsifier acts as a kinetic factor with a significant influence on the rate of the polymerization process as a whole, and therefore on its constituent reactions [1, 2]. Studies of the relationship between particular properties of emulsifiers and the kinetics of emulsion polymerization are of both theoretical and practical interest.

The present investigation was concerned with the influence of the molecular weight of the emulsifier on the polymerization rate and on the molecular weights of the polymers formed.

Methods and materials. Emulsion polymerization of styrene was effected in dilatometers [3] in a water thermostat at 60°. A magnetic stirrer was used for agitation. Purified nitrogen was passed through the solutions of the components of the reaction mixture in order to remove free oxygen. The aqueous phase was deaerated before the dilatometer was placed in the thermostat. In all the experiments the ratio of monomer to water phases was 1 : 9. To keep the pH of the system constant, 0.1 g-equiv of Na_2CO_3 per liter was introduced into the aqueous phase in all cases.

The emulsifiers used were sodium salts of fatty-acid fractions of various molecular weights, containing from 7 to 21 carbon atoms and over, and sodium caprylate, prepared as described earlier [4].

The results of a study of the colloidochemical properties of the emulsifiers used, which have a definite influence on emulsion polymerization, are presented in a separate communication in this journal.

The polymerization catalyst was isopropylbenzene hydroperoxide (IHP) containing 78% active oxygen. The IHP concentration in all experiments was 0.01 M calculated for the hydrocarbon phase.

The rate of polymerization (v_p) in moles/liter·hour was calculated from the equation:

$$v_p = \left[\frac{\Delta S/\Delta\tau}{100}\mu \cdot \frac{1000\, d\mu}{M_0}\right] : \gamma,$$

where μ is the relative volume of the hydrocarbon phase; γ is the relative volume of the aqueous phase; $d\mu$ is the density of the monomer at the polymerization temperature; M_0 is the molecular weight of styrene; S is the extent of polymerization (percentage of monomer polymerized); τ is the time in hours; $\Delta S/\Delta\tau$ was determined from the tangent of the slope of the kinetic curve for each emulsifier in the homologous series.

The polymers obtained as the result of polymerization were purified in a Soxhlet apparatus and then reprecipitated by alcohol from benzene solution. The molecular weights of the polystyrenes were estimated from the intrinsic viscosities.

Figure 1 shows plots of the extent of polymerization against time for an emulsifier of average molecular weight 296.8, with various amounts of the emulsifier in the system. It is seen in Fig. 1 that the extent of polymerization increases regularly with the concentration of the emulsifier. Similar curves were obtained for other members of the series; these curves were used for calculating the polymerization rate for the linear region of the $S = f(\tau)$ curve.

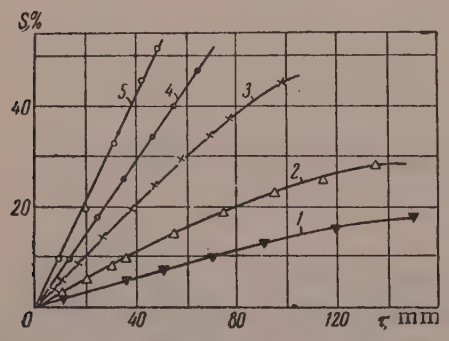


Fig. 1. Variation of the extent of polymerization with time with different contents of emulsifier (M = 296.8) in the polymerization system: 1) 0.001 mole/liter; 2) 0.005 mole/liter; 3) 0.01 mole/liter; 4) 0.025 mole/liter; 5) 0.05 mole/liter.

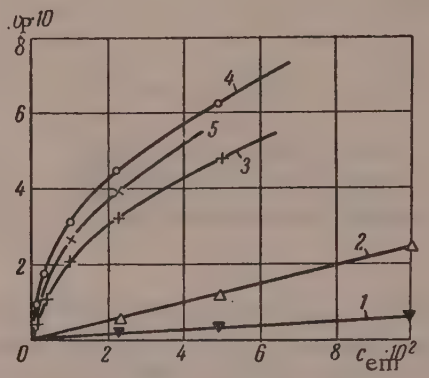


Fig. 2. Variation of the polymerization rate of styrene with the concentrations of emulsifiers of different molecular weights: 1) 166.2; 2) 176.6; 3) 240.6; 4) 296.8; 5) 336.0.

Data on polymerization rates in presence of emulsifiers of the homologous series are plotted in Fig. 2. As expected, the polymerization rate increases with emulsifier concentration for each member of the series; this is in agreement with literature data on other materials [1, 5].

The observed sharp increase of the polymerization rate in the region of low emulsifier concentrations, found from the lowest member of the series to the emulsifier of average molecular weight 296.8, must be attributed to transition of the soaps from the nonmicellar to the micellar state; this is confirmed by experimental data on the critical concentration of micelle formation (CCM). The course of polymerization of styrene is the same in presence of small amounts of sodium caprylate as in its absence; this indicates that when salts of low molecular weight are used at low concentrations, the solutions are virtually free from micelles and the polymerization proceeds at the greatest rate within the monomer droplets. The variation of the polymerization rate v_p with the molecular weight M_{em} of the emulsifier, shown in Fig. 3, indicates that the molecular weight of the emulsifier is an important kinetic factor in emulsion polymerization of unsaturated hydrocarbons. It may be seen on the left of the graph along the abscissa axis that the $v_p = f(M_{em})$ curve marks off a range of salts of low molecular weight in the series, which have weak colloidal properties and are incapable of associating in micelles. Because of this, these salts do not induce emulsion polymerization at an appreciable rate.

These are followed by emulsifiers in presence of which the polymerization rate increases almost linearly with their molecular weight. In this region of the homologous series the polymerization rate increases almost linearly with increase of the molecular weight of the emulsifier (the emulsifier concentration is 0.025 mole/liter in each case).

It is reasonable to attribute this increase of polymerization rate to lengthening of the hydrocarbon chain in the soap molecule which leads, as experiments show, to increased size of the emulsifier micelles and to greater solubilizing action. The conditions for growth of monomer-polymer particles are more favorable in larger emulsifier micelles.

Optimum polymerization (the highest polymerization rate at a given molar concentration of the emulsifier) occurs in presence of the emulsifier with average molecular weight 296.8 (with 17-19 carbon atoms in the molecule).

The results show that there is a limit to the increase in the rate of emulsion polymerization with increasing length of the hydrocarbon radical in the soap. The regular increase of the rate with the molecular weight of the emulsifier breaks down when fatty-acid salts of the C_{21} fraction and higher (molecular weight 336.0) are used as the emulsifier. In this case, the polymerization rate falls with increasing molecular weight of the emulsifier; this appears to be due to changes in the size and shape of emulsifier micelles. The formation of large asymmetric micellar aggregates hinders access of the monomer into the emulsifier micelles and thereby has an adverse effect on the polymerization rate.

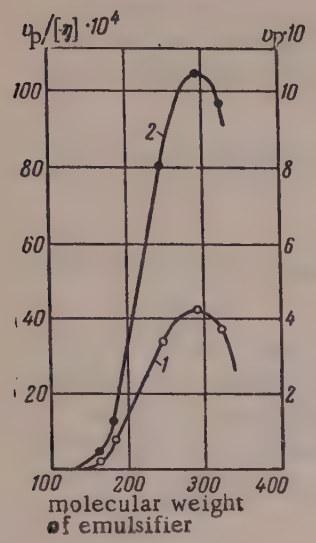


Fig. 3. Polymerization rate (1) and initiation rate (2) of styrene in presence of emulsifiers of different molecular weights.

In addition to determinations of the rate, we determined the molecular weights of the polymers formed under the conditions described. The results are presented in the table, which shows that the intrinsic viscosity of the polymer solutions increases for each individual soap with increase of emulsifier concentration. This increase of intrinsic viscosity and hence of the molecular weight with increasing emulsifier content of the system is explicable from the topochemical aspect, as the number of places where growth of active polymer chains is possible increases with the soap content of the reaction mixture.

It follows that increase of the polymerization rate in this case is effected by extension of the zone of the polymerization reaction at a given catalyst content, and this diminishes the probability of chain termination.

With regard to the influence of the molecular weight of the emulsifier on the molecular weight of the polymer, in this case, as in the case of the polymerization rate, increase of the length of the hydrocarbon chain in the soap leads to an increase of the molecular weight of the polymer. Increase of the molecular weight of the polymer when the first members of the homologous series are used as emulsifiers is consistent with our hypothesis concerning the topochemistry of the process and is associated with conversion of these fatty-acid salts into the micellar state. This conversion results in transfer of the polymerization process from the monomer droplets into the emulsifier micelles, which leads to a sharp change in the conditions for chain termination (the probability is reduced), so that the molecular weights of the forming polymers rise sharply.

Effect of Emulsifier Concentration on the Intrinsic Viscosity and Molecular Weight of Polymers

Average molecular weight of emulsifier	Emulsifier concentration, moles/liter	Intrinsic viscosity $[\eta]$	Average molecular weight of emulsifier	Emulsifier concentration, moles/liter	Intrinsic viscosity $[\eta]$
166,2	0,025	22,0	240,6	0,010	38,0
	0,050	28,0		0,025	42,0
	0,100	34,0		0,05	45,0
176,5	0,001	27,0	296,8	0,001	29,6
	0,010	30,0		0,010	35,0
	0,025	32,0		0,025	40,0
	0,050	39,0		0,050	43,0
	0,100	42,0	336,0	0,001	30,0
				0,010	34,0
				0,025	39,0

Increase of the molecular weight of the polymers with increase of the molecular weight of the emulsifier in the range of 166.2-296.8 is undoubtedly due to increased solubilization of the monomer, i.e., extension of

the zone of emulsion polymerization at a constant content of catalyst in the system. This, like increase of emulsifier concentration, should cause the molecular weight of the polymers to increase.

Thus, the remarkable specific action of a surface-active emulsifier as a kinetic factor in emulsion polymerization is manifested in the fact that the increase of the polymerization rate caused by increases in the concentration and molecular weight of the emulsifier is accompanied by a simultaneous increase in the molecular weight of the polymer. Exactly the opposite is found for such kinetic factors in polymerization as catalyst concentration and temperature (increase of polymerization rate is accompanied by a decrease in the molecular weight of the polymer formed).

From the rates of polymerization and the molecular weights of the polymers, it is possible to deduce the nature of the variations of the rate of initiation in the polymerization system with the molecular weight of the emulsifier (Fig. 3).

It is clear from Fig. 3 that the rate of initiation in polymerization systems stabilized by these emulsifiers varies symbatically with the polymerization rate.

We may conclude from these results that in selection of a surface-active emulsifier for synthesis of high polymers by polymerization of monomers, it is necessary to aim at certain definite micellar size in the aqueous phase of the original monomer emulsion. The optimum dispersity of an emulsifier corresponds to a definite value of its molecular weight. Clearly, this optimum may differ for different types of emulsifiers. The experiments show that for sodium salts of saturated aliphatic acids this optimum lies in the $C_{17}-C_{19}$ range.

SUMMARY

1. The rate of polymerization of styrene in emulsion in presence of Na salts of saturated fatty-acids of different molecular weight (from 166.2 to 336.0) increases linearly with increase of the molecular weight of the emulsifier from 166.2 to 296.8. On further increase of the molecular weight of the emulsifier, beyond the maximum, the polymerization process slows down. Fatty-acid salts with molecular weights below 166.2 do not induce any appreciable polymerization in emulsion.

These observations are correlated with changes in the size and structure of the emulsifier micelles, which are the main sites of emulsion polymerization.

2. The molecular weight of the polymers formed increases with the molecular weight of the emulsifier. This indicates that increase in the size of the emulsifier micelles (up to a certain limit) favors polymer chain growth.

3. In every instance, the molecular weight of the polymer formed (like the polymerization rate) increases with increasing concentration of the emulsifier; this must be attributed to extension of the zone of the polymerization reaction when fresh portions of emulsifier are added at a constant catalyst content.

It is our pleasant duty to thank F. V. Nevolin for supplying the fatty-acid fractions.

LITERATURE CITED

[1] N. S. Tsvetkov and A. I. Yurzhenko, Kolloid. Zhur. 15, 308 (1953).*

[2] N. A. Fermor and A. B. Peizner, Kolloid. Zhur. 15, 292 (1953).*

* See C. B. translation.

[3] N. P. Apukhtina and A. M. Lyagalova, Kolloid. Zhur. 17, 337 (1955);* C. W. Carr, J. M. Kolthoff, E. J. Meechan, and D. E. Williams, J. Polymer Sci. 5, 191 (1950); A. I. Yurzhenko and V. A. Puchin, Zavodskaya Lab. 21, 206 (1955).

[4] W. Harkins, J. Am. Chem. Soc. 51, 1675 (1929).

[5] A. P. Sheinker and S. S. Medvedev, Zhur. Fiz. Khim. 29, 250 (1955).

* See C. B. translation.

INFLUENCE OF FILLERS ON THE PROPERTIES OF POLYDIMETHYLSILOXANE

A. S. Novikov and F. S. Tolstukhina

Institute of the Rubber Industry, Moscow
(Translated from: Kolloidnyi Zhurnal Vol. 22, No. 1, pp. 42-48, January-February, 1960)
(Original article submitted December 23, 1958)

In the course of milling of rubber stocks, stable rubber-filler chemical bonds may be formed as the result of interaction between polymer radicals formed by mechanical degradation and the reactive regions of the surfaces of the filler particles [1]. Such bonds may be retained and additional ones may be formed during vulcanization. Naturally, the existence of such bonds in raw mixes and vulcanizates must influence their mechanical properties.

It is known that rubbers based on polysiloxane (SKT) have unsatisfactory mechanical properties because of their chemical structure. One way of improving them is by addition of fillers which react chemically with the rubber into SKT stocks. The influence of fillers on the properties of vulcanizates based on polydimethylsiloxane has been studied [2, 3], but the mechanism of their action is obscure.

In the present investigation an attempt was made to determine whether polymer– filler chemical bonds are formed in silicone rubber, to estimate the amounts of bonds formed in unvulcanized mixes and vulcanizates with different fillers, and to determine the influence of the degree of cross linking on mechanical properties. Silica fillers (Aerosil, Ultrasil, Microsil, and silica gel powder) and titanium dioxide were used. The weak intermolecular forces characteristic of polydimethylsiloxane make it a suitable material for such investigations, as it is possible to detect even very small effects produced by the fillers on its mechanical properties.

Effect of Fillers on the Structure and Mechanical Properties of Raw Mixes. Determination of Bound Rubber and Calculation of the Number of Effective Chains in the Gel Network

The swelling method which has been developed for vulcanizates [4, 5] was used for determination of the number of bonds constituting the spatial network structure in the raw rubber mix. The solvent used was methyl ethyl ketone, the Huggins constant μ for which is 0.498 [6]. Mixtures of polymer containing 5 parts of filler by volume were made under constant conditions in roll mills and stored for equal times.

Mix samples weighing about 1 g were placed on weighed wire gauze into weighing bottles, covered with 60 ml of methyl ethyl ketone, and left for 10 days at room temperature. The gel remaining on the gauze was then weighed in the closed bottle. The volume of solvent adsorbed was found by dividing the difference in weight between the swollen sample and the dry extracted sample by the density of the solvent.

The content of silicone rubber in the dry extracted gel, which had to be known for calculation of the volume fraction of the rubber in the swollen state, was determined by means of ultimate analysis. The content of effective network chains ν per unit volume was calculated from the equation [1, 2]

$$\nu = -\frac{1}{V_s}\,\frac{\ln(1-V_r)+V_r+\mu V_r^2}{V_r^{1/3}},$$

where V_r is the volume fraction of the polymer in the swollen sample; V_s is the molar volume of the solvent; μ is the Huggins constant.

TABLE 1

Effect of Silica Fillers on Formation of a Spatial Network in Raw Mixes Based on Polydimethylsiloxane

Filler in mix	Content of silicone rubber in dry extracted gel		Maximum swelling, Q_m	Vol. fraction of rubber in swollen sample, V_r	Mol. wt. M_c of chain segment between branch points $\times 10^{-3}$	Content of effective network chains per unit volume, mole/cm^3
	from results of ultimate analysis, %	Volume, cm^3				
Aerosil	80.0	0.426	6.36	0.135	53.6	$1.79 \cdot 10^{-5}$
Ultrasil	61.8	0.245	10.73	0.085	207.8	$4.61 \cdot 10^{-6}$
Powdered silica gel	44.3	0.087	23.38	0.041	988.2	$9.70 \cdot 10^{-7}$
Microsil	Gel not formed			Mixture completely soluble		

The results of analysis for polymer content in the dry extracted gel and calculation of the chain content in the gel network (Table 1) show that the fillers studied differ in their activity in network formation according to the size and structure of their particles. The greatest amount of bound rubber was found in the mix with Aerosil; the mix with Microsil is completely soluble in methyl ethyl ketone.

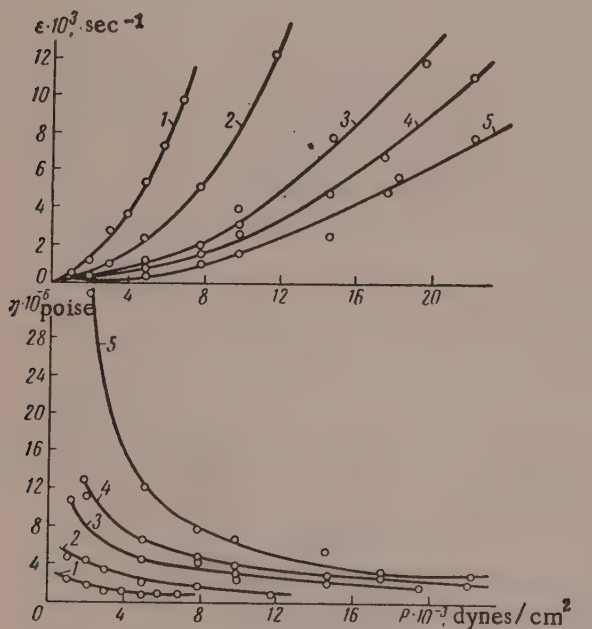


Fig. 1. Rheological curves: 1) Polydimethylsiloxane; 2) mixture with titanium dioxide; 3) mixture with powdered silica gel; 4) mixture with Microsil; 5) mixture with Ultrasil.

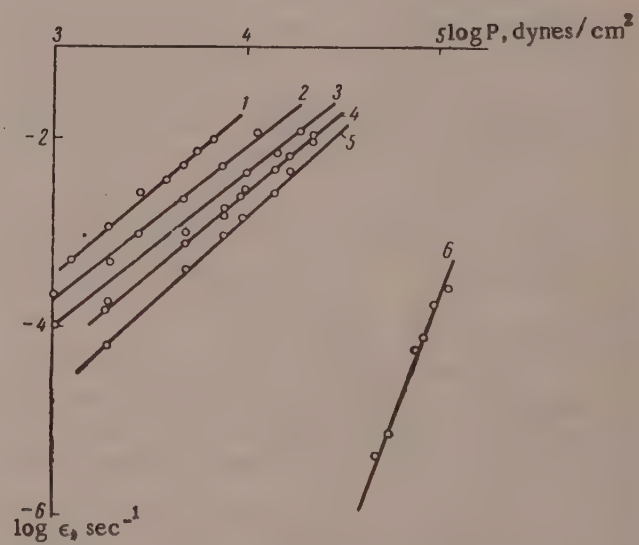


Fig. 2. Variation of the logarithm of the velocity gradient ϵ with the logarithm of the stress P: 1) Polydimethylsiloxane; 2) mixture with titanium dioxide; 3) mixture with powdered silica gel; 4) mixture with Microsil; 5) mixture with Ultrasil; 6) mixture with Aerosil.

The density of the spatial network of the gel in the mixture of SKT with Aerosil ($\nu = 1.79 \cdot 10^{-5}$ mole/cm^3) is approximately four times that in the mixture of SKT with Ultrasil ($\nu = 4.61 \cdot 10^{-6}$ mole/cm^3),

and twenty times the density of the gel network in the mixture of SKT with powdered silica gel (ν = $= 9.7 \cdot 10^{-7}$ mole/cm^2).

The mechanical properties of these mixtures were characterized by their shearing deformation at constant stress, as is widely done in studies of disperse systems [7-9].

The viscosity and elastic deformation were determined in steady flow at 82° under different applied stresses. The elastic deformation was found from the restoration of the sample dimensions after removal of the load. Figure 1 shows rheological curves for SKT polymer and filled mixtures. It is clear from Fig. 1 that flow is retarded in presence of fillers. The less active the filler, the closer does its curve lie to the curve for the pure polymer. The greatest decrease of the flow rate is found in the mixture with Aerosil, the flow curve for which does not fit into the scale used and which is plotted in logarithmic coordinates in Fig. 2. This retardation of flow is probably due both to formation of bonds of the van der Waals type and to formation of stable rubber-filler bonds which are not broken down either by the solvent or under the influence of small stresses and at 82°.

In the stress range used the flow curves can be quantitatively represented by the Ostwald and de Waele exponential equation $\epsilon = \varphi \tau^n$ (here ϵ is the velocity gradient, cm^{-1}); τ is the shearing stress in dynes/cm^2; φ and n are constants (Fig. 2).

The value of the constant n indicates the degree of deviation from Newtonian flow. (For Newtonian liquids $n = 1$). It follows from Fig. 2 (Table 2) that the more active the filler the higher the value of n, and the more does the flow curve for the mixture deviate from the Newtonian straight line. Mixtures with Aerosil are the most anomalous.

TABLE 2

Mechanical Properties of Unvulcanized Mixes with Silica Fillers

Mixes with	log φ	n	$E_2 \cdot 10^{-3}$, dynes/cm^2	Mixes with	log φ	n	$E_2 \cdot 10^{-3}$, dynes/cm^2
Polydimethylsiloxane	—8,27	1,64	3,50	Microsil	— 9,61	1,76	14,8
Titanium dioxide	—8,77	1,66	—	Ultrasil	—10,80	2,00	22,41
Powdered silica gel	—9,06	1,66	16,44	Aerosil	—21,78	4,40	75,10

In Fig. 3 the elastic deformation developing under steady flow conditions is plotted against the shearing stress. The slope E_2 of the approximately linear relationships can serve as a quantitative measure of the bonds formed in the polymer-filler system.

These values (Table 2) change almost 20-fold from $3.5 \cdot 10^3$ dynes/cm^2 for the unfilled polymer, where bonds are formed by mechanical tangling of the molecular chains, to $75 \cdot 10^3$ dynes/cm^2 for the mix with Aerosil.

Influence of Fillers on Structure and Properties of Vulcanizates

The influence of fillers on the amount of bonds formed by them in vulcanizates was evaluated from the quasiequilibrium modulus and swelling. The mixtures for vulcanization were prepared as previously, except that benzoyl peroxide was added in the proportion of 2 parts to 100 parts of polymer by weight. The samples were vulcanized for 10 minutes at 120°, and then heated in a thermostat for 6 hours at 200°.

The samples were swollen in methyl ethyl ketone at room temperature. The swollen samples, at intervals of 2 days up to 8 days, were dried between sheets of filter paper and weighed on a torsion balance at 10-second intervals up to 70 seconds. The weight of each swollen sample was found by extrapolation of the linear plots of sample weight against time to zero time. In calculations of the volume fraction of the swollen polymer a correction was applied for the filler content and possible extraction of polymer from the vulcanizate was taken into consideration. For this the volume of the dry extracted sample was found by weighing in anhydrous ethyl alcohol. The volume of the filler, calculated from the formulation and the initial sample weight, was subtracted from this volume.

The calculated values of the contents of effective network chains per unit volume (ν) are given in Table 3, which also indicates the influence of an increase of filler content on the amount of cross links in the vulcanizate.

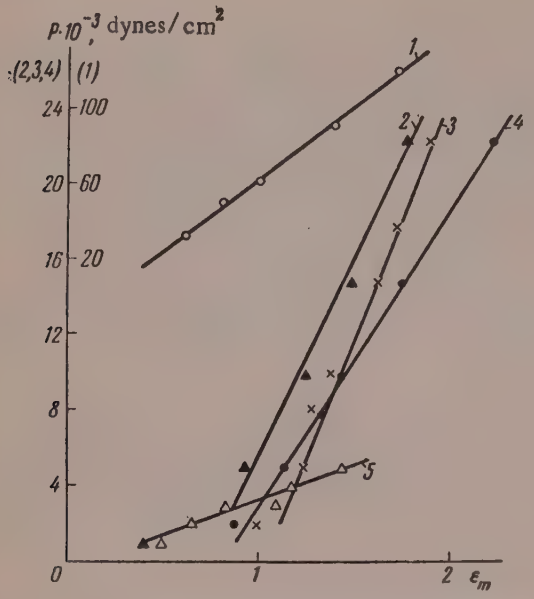


Fig. 3. Variations of the elastic deformation ϵ_m with the shearing stress P for SKT mixtures: 1) With Aerosil; 2) with powdered silica gel; 3) with Ultrasil; 4) with Microsil; 5) polydimethylsiloxane.

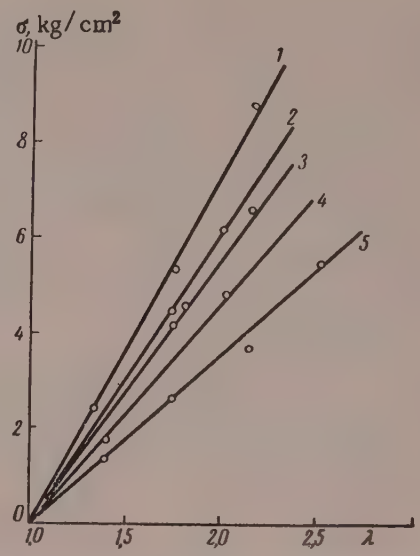


Fig. 4. Variations of the quasiequilibrium stress with relative elongation of vulcanizates containing: 1) Aerosil; 2) Ultrasil; 3) powdered silica gel; 4) without filler; 5) Microsil.

The quasiequilibrium stresses at fixed deformation were determined by means of a dynamometer of the Polanyi type at 80°.

TABLE 3

Effect of Filler Content on the Amount of Bonds in Vulcanizates

Filler in vulcanizate	Amount of filler, volumes per 100 wt. parts of polymer	Q_m	V_r	$\nu \cdot 10^4$, mole/cc	Filler in vulcanizate	Amount of filler, volumes per 100 wt. parts of polymer	Q_m	V_r	$\nu \cdot 10^4$, mole/cc
Aerosil	5	1,242	0,446	6,57	Powdered silica gel	5	1,450	0,408	4,92
	10	1,032	0,491	9,00		10	1,422	0,413	5,18
	20	0,888	0,529	11,72		15	1,242	0,446	6,56
Ultrasil	5	1,329	0,429	5,98		20	1,184	0,458	7,19
	10	1,135	0,468	7,84					
	15	1,027	0,493	9,31	Titanium dioxide	5	1,505	0,399	4,55
	20	0,977	0,506	9,98		10	1,353	0,425	5,62
						20	1,316	0,432	6,50
					Without filler	0	2,282	0,304	1,99

The data found for the swelling and the quasiequilibrium modulus show that in the presence of filler additional bonds appear in the vulcanizates, as the elasticity modulus and the content of effective chains in unit network volume are higher for vulcanizates with Aerosil, Ultrasil, and powdered silica gel than for the unfilled vulcanizate. Silica fillers are involved in formation of stable chemical bonds and differ in their activity in forming the spatial network. The greatest amount of stable bonds is formed in the vulcanizate with Aerosil, and the amount is less with Ultrasil and powdered silica gel. The quasiequilibrium modulus indicates that the vulcanizate with Microsil has a less dense network (Fig. 4) than the vulcanizate without filler, while according to swelling data, it is above the unfilled vulcanizate. This discrepancy is possibly caused by the low thermal stability of the polymer– Microsil bonds, which break down under applied stress. Under stresses of the order of 10^6 dynes/cm^2 at 80° the molecular chains probably slip off the filler particles; evidence of this is also provided by the higher rate of stress relaxation at constant deformation for vulcanizates with Microsil in comparison with the other fillers studied (Fig. 5). For the same relative elongation $\lambda = 1.75$ at 80° the rate of stress relaxation in vulcanizates with Microsil is double that in vulcanizates with powdered silica gel, and 7.4 times that in vulcanizates with Aerosil (Table 4).

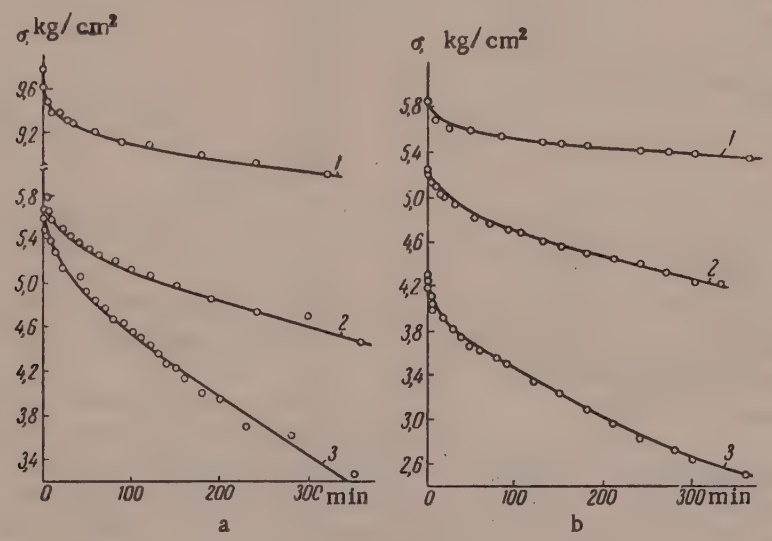


Fig. 5. Stress relaxation in vulcanizates: a) $\lambda = 1.75$ and 80°; b) $\lambda = 2.15$ and 80°. Fillers: 1) Aerosil; 2) powdered silica gel; 3) Microsil.

TABLE 4

Effect of Fillers on the Rate of Stress Relaxation*

Filler in vulcanizate	$\frac{\sigma_{in} - \sigma_{300}}{\sigma_{in}}$	
	λ=1,75	λ=2,15
Aerosil	0,051	0,098
Powdered silica gel	0,19	0,15
Microsil	0,38	0,40

* The rate of stress relaxation was determined in terms of the ratio of the change of stress during an arbitrary time interval of 5 hours to the initial stress $\left(\frac{\sigma_{in} - \sigma_{300}}{\sigma_{in}}\right)$.

Figure 6 represents the influence of filler content on the amount of bonds in vulcanizates containing from 5 to 20 volumes of filler per 100 weight parts of polymer. It is seen that the relationship is linear. At all the filler contents not only is the relative position of the fillers with regard to their ability to form stable bonds retained, but the content of effective network chains increases with the amount of filler in the studied range of 5 to 20 volumes. The rate of this increase, represented by the slope of the approximately straight lines, also varies with the activity of the filler, decreasing in the sequence: Aerosil, Ultrasil, powdered silica gel, titanium dioxide. It follows that with the less active fillers increase of filler content has less influence on the vulcanizate structure.

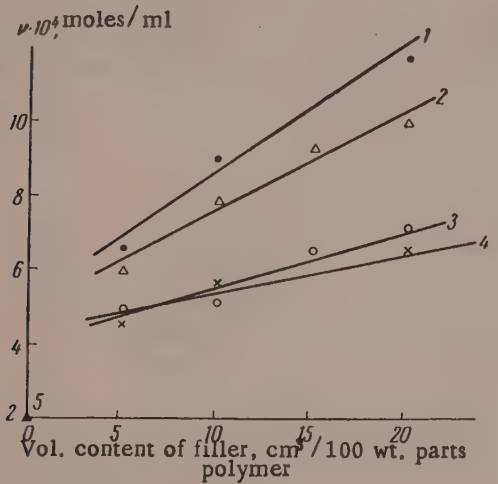


Fig. 6. Effect of filler content on the chain content ν in vulcanizates: 1) With Aerosil; 2) with Ultrasil; 3) with powdered silica gel; 4) with titanium dioxide.

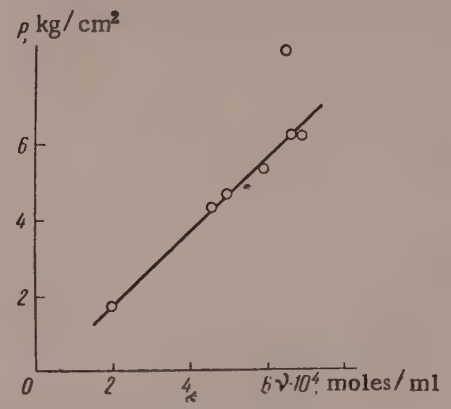


Fig. 7. Effect of the amount of cross links ν on the tensile strength P.

The influence of structure on the physical and mechanical properties of vulcanizates containing 5 parts of filler by volume is shown in Fig. 7. It is seen that the tensile strength is extremely sensitive to changes of ν. A comparison of the values found for ν for the mix gel, unfilled vulcanizate, and vulcanizate with filler shows that polymer – filler cross links are formed not only during mastication of the mixes in roll mills as the result of interaction between free radicals and the surface of the filler particles, but also during vulcanization as the result of interaction of free radicals, formed in the vulcanization process, with the filler particles.

SUMMARY

1. When SKT silicone rubber is masticated with silica fillers, stable polymer-filler chemical bonds are formed. The activity of the investigated silica filler diminishes in the following sequence: Aerosil, Ultrasil, powdered silica gel, Microsil.

2. The rubber-filler chemical bonds formed during mastication are not only retained during vulcanization, but are formed additionally during the process.

3. The rheological curves for filled mixtures deviate from the straight lines characteristic of Newtonian liquids; the deviation increases with increasing rubber-filler bonding.

4. The amount of rubber-filler chemical bonds formed increases linearly with the volume fraction of filler in the rubber.

5. The mechanical strength of vulcanizates increases in proportion to the ability of fillers to form stable bonds.

LITERATURE CITED

[1] W. F. Watson, Third Rubber Tech. Conference (London, 1954).

[2] E. J. Warrick and P. C. Lauterbur, Ind. Eng. Chem. 47, 486 (1955).

[3] E. J. Warrick, Rubber World 5, 193 (1955).

[4] P. J. Flory and J. Rehner, J. Chem. Phys. 11, 521 (1943).

[5] P. J. Flory, J. Chem. Phys. 18, 108 (1950).

[6] D. W. Scott, J. Am. Chem. Soc. 68, 1877 (1946).

[7] P. A. Rebinder, in the book: New Methods for Physicochemical Investigation of Surface Effects [In Russian] (Proc. Inst. Phys. Chem., Izd. AN SSSR, 1950).

[8] L. V. Chumakova and P. A. Rebinder, Doklady Akad. Nauk SSSR 81, 239 (1951).

[9] L. V. Chumakova and P. A. Rebinder, Kolloid Zhur. 18, 540 (1956).*

* See C. B. translation.

STRUCTURAL AND MECHANICAL PROPERTIES OF SOLUTIONS, GELS, AND COAGULATES (COACERVATES) OF GELATIN

V. A. Pchelin and N. Ya. Solomchenko

M. V. Lomonosov University, Moscow, Chemical Faculty,

Department of Colloid Chemistry
(Translated from: Kolloidnyi Zhurnal Vol. 22, No. 1, pp. 63-68, January-February, 1960)
(Original article submitted July 15, 1958)

Studies of structural and mechanical properties are important means for elucidation of the internal structure of disperse systems and changes in this structure under the influence of external factors [1, 2].

Applied to polymer solutions, and in particular to polyelectrolytes [2], this method provides conclusive solutions to a number of problems relating to their molecular structure and the mechanism of a number of processes leading to changes in it. This is shown by the results of numerous studies of the structural and mechanical properties of polymers, including gelatin [3, 4]. In these studies gelatin was used both in solution and in the form of gels and air-dry films.

It is also known that the action of a number of substances in gelatin solutions leads to formation of a new phase in the form of drops consisting mainly of the same aqueous gelatin solution but at a higher concentration, and containing various amounts of the third component which induced the process.

This formation of a new phase is also observed in solutions of other polymers, and is known in the literature as the coacervation effect [5].

It is still uncertain whether gelatin retains its molecular structure after conversion into the new phase, and, if not, what changes take place in it.

In the present investigation an attempt was made to solve this problem by studies of the structural and mechanical properties of gelatin converted into the new phase state by the action of sodium sulfate and resorcinol (these are typical substances causing coacervation, and at the same time they differ sharply in their chemical nature).

Methods and apparatus. The methods described previously [6] were used to convert gelatin into the new phase state. It should merely be noted that after addition of sodium sulfate or resorcinol to the gelatin solution gelatin first separates out in the form of microscopic droplets (an emulsion of gelatin in water is formed). If Na_2SO_4 has been added, when such emulsions are kept at 50° the droplets coalesce and after 24 hours the system separates out completely into two layers. The bottom layer then contains almost all the gelatin taken originally. It was found that when droplets coalesce out of 10% gelatin solution, the concentration in the new phase is 31.35%. If resorcinol is added, the droplets do not coalesce and the coacervate is a stable emulsion.

The gelatin separated out in the form of the new phase (coacervate) was used in our further investigations. Parallel experiments were performed with ordinary gelatin.*

* Photographic gelatin, previously brought into the isoelectric state and demineralized by the Loeb method [7], was used in the work.

The independent variables in our experiments were the shearing stress and temperature. The temperature range was so chosen that the system would be obtained both in the liquid and in the gel state. The viscosity of solutions and the structural and mechanical properties of gelatin gels and coacervates were studied accordingly.

All the determinations were performed with an elastoviscosimeter of the rotational type, which differed from instruments described previously in a number of features* (Fig. 1).

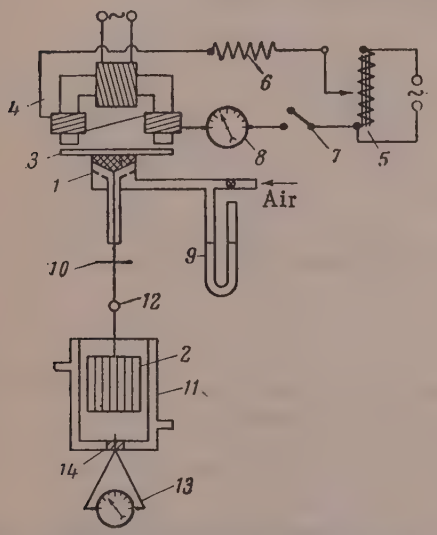


Fig. 1. Line diagram of elastoviscosimeter (explanation in text).

The essential part of the instrument is the air bearing 1, which ensures virtually total absence of friction in rotation of the internal cylinder 2, and provides for centering of the moving system. The load on the moving system is applied at a distance by means of an alternating-current electromagnetic motor. The motor consists of a light aluminum disk 3 and an electromagnet 4. The electromagnet consists of a core and three coils; the middle (large) coil is used for permanent magnetization, while the two outer ones are for transmission of torque to the aluminum disk 3. These coils are designed to carry current up to 10 amp, and are included in a circuit consisting of an autotransformer 5 (LATR-1), a loading resistance 6, a switch 7, and an ammeter 8. The sensitivity of the latter is chosen in accordance with the viscosity (elasticity) of the system under investigation. Alteration of the current strength in the circuit changes the torque transmitted to the disk 3, caused by Foucault currents set up in it. There is a strictly linear relationship between the current strength and the magnitude of the torque. The transformer 5 is used for smooth or stepwise loading, while the switch 7 can be used for applying or removing the load instantaneously. The manometer 9 is used to measure the pressure in the air bearing. A part of the air from the bearing passes downward through a tube along a rigid axis onto a light aluminum disk 10 which shields the surface of the system under investigation.** The outer stationary cylinder 11 is surrounded by a water jacket connected to an ultrathermostat, and is fitted with a thermocouple 14 and millivoltmeter 13 for temperature measurement.

For expression of the torque in absolute units (dynes · cm) the apparatus was calibrated against liquids of known viscosity (sucrose solutions); a current of 1 amp corresponded to a torque of 352 dynes · cm acting on the cylinder 2. The viscosities of liquid systems were measured by determination of the rate of rotation of the disk 3 under different loads. The structural and mechanical properties of gel systems were studied with the aid of kinetic curves representing the development and decrease of deformation at constant shearing stress and with instantaneous loading and unloading of the system. These curves were recorded automatically on photographic paper; for this the instrument was provided with a special attachment (not shown in Fig. 1) consisting of a drum rotated at various fixed speeds by means of an electric motor. The photographic paper was attached to the drum, and a light spot was reflected onto it through a slit from a light source by means of the mirror 12 (Fig. 1).

It was observed in unpublished experiments by one of us jointly with N. V. Grigor'eva, and in a published research [4], that the elasticity modulus of gelatin gel increases (the aging effect) over a considerable period, and does not reach a constant value even after 50 days. Because of this, and also in view of the fact that only relative values were required, we reduced the duration of the experiments to a minimum and established standard times for performance of the individual operations. Shortening of the duration of the experiments is also desirable from other points of view. For example, addition of various antiseptics to the system becomes unnecessary, there

* The elastoviscosimeter used in the investigation was designed by one of us jointly with S. P. Alekhin. A detailed account of the design will be given in a special communication.

** In addition, evaporation in all the experiments was prevented by application of a thin layer of pure liquid petrolatum.

is no risk of error owing to thermolysis of gelatin in experiments at higher temperatures and to solubilization of the nonpolar solvent used to protect the system from evaporation, etc.

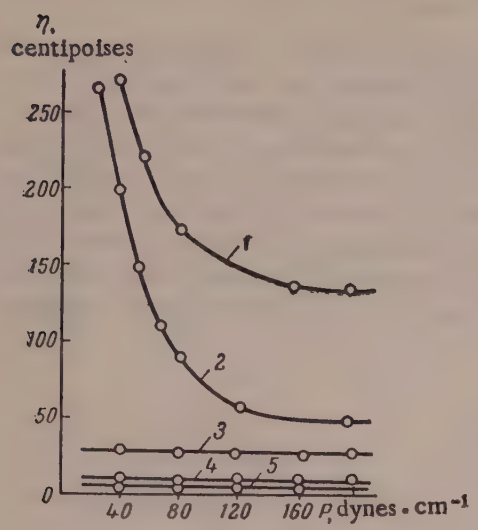


Fig. 2. Variations of the viscosity of 31.35% gelatin solution with the shearing stress: 1) 30°; 2) 31°; 3) 32°; 4) 40°; 5) 50°.

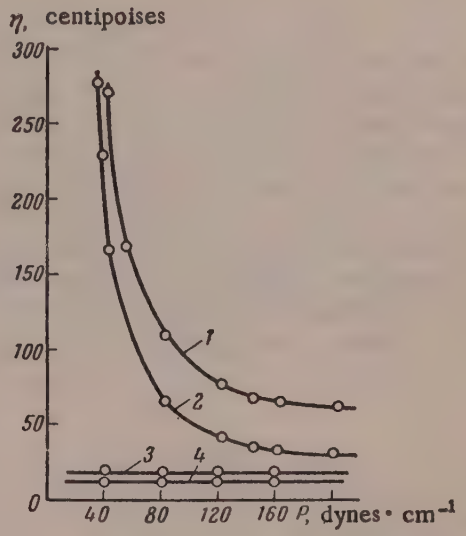


Fig. 3. Variations of the viscosity of gelatin + Na_2SO_4 coacervate with the shearing stress: 1) 36°; 2) 37°; 3) 40°; 4) 50°.

Viscosity variations of gelatin solutions and coacervates with the shearing stress at various temperatures are plotted in Figs. 2, 3, and 4. The viscosity falls with rise of temperature in all three systems, but they differ significantly in all other respects. Thus, gelatin solution (Fig. 2) and the coacervate produced by the action of Na_2SO_4 (Fig. 3) have a well-defined structure which disappears over a narrow temperature range. This takes place in the 31-32° range for 31.35% gelatin solution, and in the 37-40° range for the coacervate. The behavior of the gelatin + resorcinol coacervate (emulsion) (Fig. 4) is sharply different. In the 31-50° range this system behaves like a Newtonian liquid, and the viscosity-temperature relationship is linear, in contrast to the first two cases (see Fig. 5).

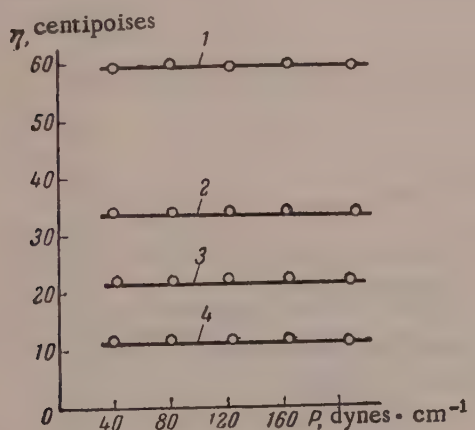


Fig. 4. Variations of the viscosity of gelatin + resorcinol coacervate with the shearing stress: 1) 31°; 2) 36°; 3) 40°; 4) 50°.

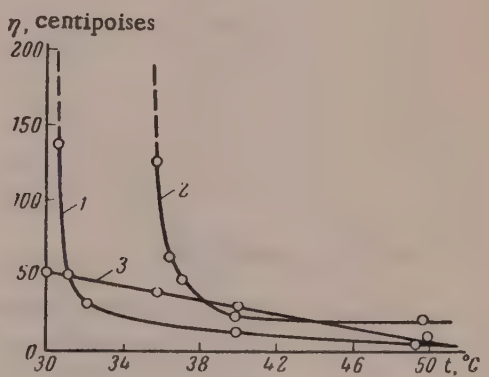


Fig. 5. Effect of temperature on the viscosity of: 1) 31.35% gelatin solution; 2) gelatin + + Na_2SO_4 coacervate; 3) gelatin + resorcinol coacervate.

The considerable general decrease in the viscosity of this system is also noteworthy.

For studies of the kinetics of growth and decrease of deformation at constant shearing stress in relation to the temperature the materials used were 10 and 31.35% gelatin gels and gelatin + Na_2SO_4 coacervates. The gelatin + resorcinol coacervate cannot be investigated by this method because of its fluidity.

The loads used in these experiments were considerably less than in the viscosity experiments, to ensure the greatest preservation of the structure and to allow fuller observations of changes in the relationship between elasticity and fluidity. The results of the determinations, plotted in Figs. 6, 7, and 8, show that the structural and mechanical properties of the systems change sharply over a narrow temperature range. This is shown by the fact that the flow rate increases sharply with rise of temperature, indicating breakdown of contact between the molecular chains of gelatin and relative displacement of these chains. At the same time all three systems retain elastic properties, which can be easily measured, even at the highest temperatures (50°). The magnitude of the nominal-instantaneous deformation at constant P increases with rise of temperature. Evidently, the breakdown of contacts and relative displacement of the macromolecules is accompanied by further chain straightening and orientation in direction of the acting shearing stress.

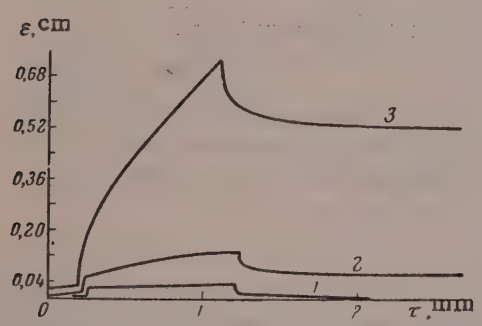


Fig. 6. Kinetics of development and decrease of deformation of 10% gelatin solution at P = = 12.5 dynes · cm^{-1}: 1) 24°; 2) 25°; 3) 26°.

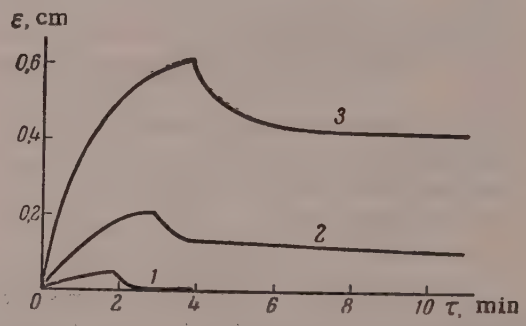


Fig. 7. Kinetics of development and decrease of deformation of 31.35% gelatin solution at P = 15.6 dynes · cm^{-1}; 1) 30°; 2) 31°; 3) 32°.

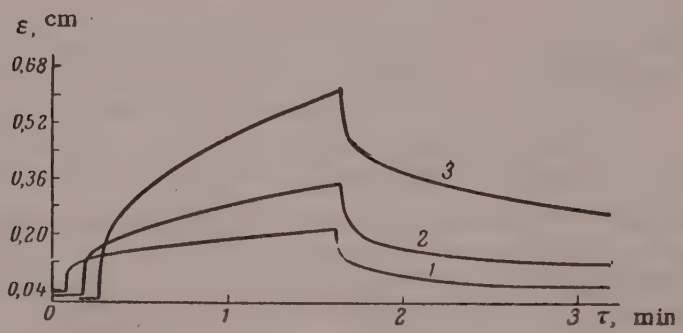


Fig. 8. Kinetics of development and decrease of deformation of gelatin + Na_2SO_4 coacervate at P = 22.0 dynes · cm^{-1}: 1) 36.5°; 2) 37°; 3) 37.5°.

The form of these curves indicates that there are no qualitative peculiarities about the development and decrease of deformation in the three systems. The sole difference is the temperature range in which flow begins. For clarity, the effects of temperature are plotted in Fig. 9, which shows that the temperature at which flow begins rises with increase of gelatin concentration. The behavior of the coacervate is like that of gelatin taken

at an even higher concentration. Since in reality the concentration of the coacervate is equal to that of the gelatin (31.35%), the observed effect may be attributed to increase of the number of contact in the gel network owing to partial dehydration of the gelatin by sodium sulfate.

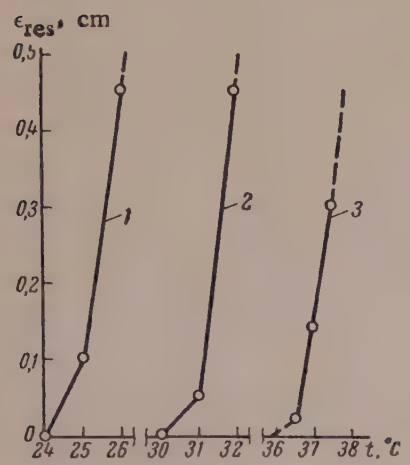


Fig. 9. Effect of temperature on residual deformation: 1) 10% gelatin solution; 2) 31.35% gelatin solution; 3) gelatin + Na_2SO_4 coacervate.

It has already been pointed out that the structural and mechanical properties of the other coacervate studied, gelatin + resorcinol, are highly specific. Absence of structure formation in this system and its stability indicate that in the interaction of gelatin with resorcinol a peculiar mechanism is involved in the formation of the new phase.

Formation of the new phase in this concentrated two-component system is probably caused by changes in the configuration of the gelatin macromolecules owing to formation of bridges consisting of resorcinol molecules linked by hydrogen bonds to the functional groups of the protein chains.

Since resorcinol is a weak dibasic acid, formation of bridges of the salt type may also be postulated.

The macromolecules in concentrated gelatin solutions are greatly intertangled and have all possible configurations, and therefore it may be assumed that bridge formation may be both intra- and intermolecular. This reinforcement of the structure prevents coalescence of the coacervate droplets.

SUMMARY

1. An elastoviscosimeter of a new type was used for studying the viscosity and deformation characteristics of gelatin converted into a new phase state (coacervate) by the action of sodium sulfate and resorcinol.

2. The gelatin coacervate made by the action of sodium sulfate qualitatively retains the structural and mechanical properties of gelatin but has higher elasticity and a higher melting point.

3. The gelatin coacervate made by the action of resorcinol behaves like a Newtonian liquid of a considerably lower viscosity than the original gelatin solution. It is suggested that resorcinol changes the configuration of the gelatin macromolecules by formation of hydrogen and salt-type bonds between the gelatin molecules and resorcinol.

The authors are deeply grateful to Academician P. A. Rebinder for valuable advice.

LITERATURE CITED

[1] P. A. Rebinder, Vestnik Akad. Nauk SSSR 10, 32 (1957).

[2] P. A. Rebinder and L. V. Ivanova-Chumakova, Advances in Polymer Chemistry and Technology [In Russian] (Goskhimizdat, Moscow, 1957), p. 146.

[3] P. I. Zubov, Z. N. Zhurkina, and V. A. Kargin, Kolloid. Zhur. 9, 109, 367 (1947); 16, 109 (1954);* Doklady Akad. Nauk SSSR 67, 659 (1949).

[4] L. V. Ivanova-Chumakova, P. A Rebinder, and G. I. Krus, Kolloid. Zhur. 18, 682 (1956).*

* See C. B. translation.

[5] T. N. Evreinova, Uspekhi Sovrem. Biol. 37, 177 (1954).

[6] W. J. Holleman, H. G. Bungenberg de Jong, and R. S. Tjaden Modderman, Kolloid-Beihefte 39, 334 (1934).

[7] J. Loeb, Proteins and the Theory of Colloidal Behavior [Russian translation] (State Light Industry Press, 1933), p. 52.

RADIOACTIVE TRACER STUDIES OF THE GELATION OF RUBBER LATEXES

D. M. Sandomirskii and M. K. Vdovchenkova

Scientific Research Institute for Rubber and Latex Products, Moscow

(Translated from: Kolloidnyi Zhurnal Vol. 22, No. 1, pp. 69-73, January-February, 1960)

(Original article submitted May 20, 1958)

Gelation of latex is one of the important methods used for manufacture of rubber products directly from latex [1]. This term is used in latex technology only in cases when conversion of the latex to a gel takes place under the influence of destabilizing ions which form slowly in the latex mixture itself. One method of bringing this about is by introduction of zinc oxide and ammonium salts into the latex. The formation of zinc ammine cations in this process, and their interaction with the globules, have been studied in a number of investigations [2, 3], but as yet they cannot be regarded as fully understood.

Our previous investigations [4, 5] showed that radioactive isotopes can be used with success for studying latex coagulation and ionic deposition. The present investigation was concerned with the use of $Zn^{65}O$ for coagulation of Nairit L-3 and L-4 polychloroprene latexes, SKS-50 butadiene-styrene latex, and polychloroprene latex stabilized by sodium paraffinate and sodium tridecylate labeled with C^{14} in the carboxyl group (VKh-2 latex).

The aqueous $Zn^{65}O$ paste was prepared as follows. Metallic zinc, to serve as carrier, was mixed with Zn^{65}, and the mixture was dissolved in HCl (1 :1) to give $ZnCl_2$. After removal of iron (by precipitation with $CaCO_3$) ammonia was added to precipitate $Zn(OH)_2$, which was calcined to give ZnO.

The radioactive zinc oxide was mixed thoroughly with inactive zinc oxide. The zinc oxide paste was prepared by the usual method in an aqueous solution of NF dispersing agent. In experiments with VKh-2 latex a paste of inactive zinc oxide was used. Different amounts of paste were introduced into latex mixtures consisting of 10 ml latex, 1 ml of 10% ammonia solution, and 1 ml of 5% ammonium chloride solution.

To determine whether gelation of the latex is accompanied by chemical binding of zinc, and whether all the zinc introduced into the latex is so bound, the gels formed with $Zn^{65}O$ paste were washed with ammoniacal ammonium nitrate solution and the radioactivity of the latter was determined. Two hours of washing was sufficient to remove uncombined zinc from the gel. The washed and dried gel was burned in a muffle furnace, and the activity of the ash was determined by the usual method. It was found that during gelation a part of the zinc is bound firmly in the gel and is not extracted when the latter is washed with ammonium nitrate solution. The amount of bound zinc depends on the type of latex. Latex L-4 binds 0.94 meq of zinc per g of latex, L-3 binds 0.69, SKS-50 binds 0.52, and VKh-2 binds 0.61 meq.

Extraction of VKh-2 latex gels with ethyl alcohol, which dissolves sodium tridecylate, showed that much more of the protective substance is bound with the electrolyte in gelation than in coagulation [4] or ionic deposition (see below). In the case of 38% latex 84% of the tridecylic acid is bound, and if the latex is diluted to 30%, 94-100% of the tridecylic acid is bound.

These experiments therefore show that formation of insoluble products from the zinc ammine ions with the protective substances plays the principal role in latex gelation.

It was of interest to determine how far the amount of bound zinc can serve to characterize a particular latex, as in coagulation or ionic deposition [4, 5].

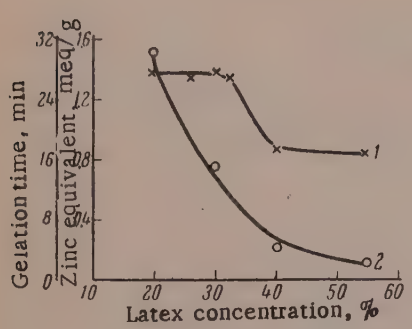


Fig. 1. Variations of the amount of bound zinc and gelation time with the concentration of L-4 latex: 1) Bound zinc; 2) gelation time.

It is known from everyday technological experience that the gelation rate of latex increases very rapidly with the amount of zinc oxide added. It was therefore also of interest to elucidate the relationship between the gelation rate and the amount of bound zinc. For this purpose the influence of zinc oxide concentration in the latex mixture and of the concentration of the latex itself on the amount of bound zinc was studied. The results (see Table 1 and Fig. 1) show that the amount of zinc bound in gelation, calculated per g of rubber, is independent of the amount of zinc oxide added. The latter has a significant influence on the gelation rate, but irrespective of the time required for gelation the amount of bound zinc depends only on the composition of the particular latex, i.e., on its content of substances which form insoluble compounds with the zinc ammine ions.

It is thus possible to speak of the zinc equivalent of a given latex, analogous to the calcium equivalent in ionic deposition [5]. However, the relationship between the cation equivalent and the latex concentration is not the same in gelation as in ionic deposition [5].

TABLE 1

Variations of the Amount of Bound Zinc and the Gelation Rate with the Zinc Oxide Content of L-4 Latex

ZnO concentration, % on the rubber	Amount of bound zinc, meq/g	Gelation time, min
13	1.48	Instantaneous
6.5	1.50	4
6.5*	1.52	20
3.75	1.52	~200

* The amount of ammonium salt was decreased in this experiment.

The existence of two regions for the diluted latex is clearly seen in Fig. 1. In each of these regions the amount of bound zinc is almost independent of the latex concentration, but dilution of the original latex in the 40-32% concentration range results in a sharp increase of the zinc equivalent. This effect may be explained as follows. With uniform distribution of the zinc oxide paste throughout the volume of the latex mixture desorption of the protective substance from the globule surfaces, which occurs on dilution of the latex, cannot influence the amount of electrolyte bound. However, dilution of the latex has a significant effect on the structure of the forming gel. In the original latex a dense and strong gel is rapidly formed, while in the dilute latex a very loose gel is formed slowly. In this case, the zinc ammine ions have time to react with almost all the protective substance in the latex. In dense gels, formed during rapid gelation from undiluted latex, the zinc ammine ions do not have time to react with all the protective substances, so that the amount of bound zinc is less. Experiments with VKh-2 latex also show that the amount of protective substance combining with the gelating ions increases with dilution of the latex.

However, it must be pointed out that the absolute amounts of bound protective substance found for latex made with tridecylic acid cannot be referred directly to latexes made with other emulsifiers. These values can be used only for comparing the effects taking place in different methods of electrolyte action on latex, such as coagulation [4], ionic deposition [5], and gelation.

SURFACE-CHEMICAL EFFECTS AND STRUCTURE FORMATION IN ASKANGEL SUSPENSIONS*

S. N. Papuashvili and M. E. Shishniashvili

Institute of Chemistry, Academy of Science, Georgian SSR,

Laboratory of Colloid Chemistry, Tbilisi
(Translated from: Kolloidnyi Zhurnal Vol. 22, No. 1, pp. 49-56, January-February, 1960)
(Original article submitted July 4, 1958)

The mechanism of electrolyte action on thixotropic structure formation in colloidal disperse systems of natural aluminosilicates (clays, soils, etc.) has not been studied adequately as yet.

Dumanskii and his associates [1] showed that formation of colloidal systems with thixotropic properties depends mainly on the degree of lyophily of the disperse phase. According to Rebinder and his school [2], thixotropic structure formation in aqueous suspensions of clays containing asymmetric particles is favored by the highly hydrophilic character of the greater part of the particle surfaces. In the formation of a thixotropic coagulation structure cohesion between the particles is effected most easily by impacts at the corners or edges, which are the least hydrophilic regions.

Most workers [3-7] have considered hydrophily, stability, and the nature of structure formation in clay suspensions in relation to the cation-exchange processes which take place on the particle surfaces under the influence of electrolytes. However, the tendency to correlate the mechanism of thixotropic structure formation in clay suspensions with simple cation-exchange processes often fails to yield satisfactory results. For example, the amount of water held by clay in presence of electrolytes is not directly related to the hydration capacity of the cations but depends more on the strength of the bonds between the ions and the clay particles and on the nature of the anions [8]. According to Uskov [9] changes in the structural and mechanical properties of clay suspensions depend not on cation-exchange processes but on the excess amount of added electrolyte. In Mattson's view [10], the dispersity, hydrophily, plasticity, and other properties of aluminosilicate colloids are primarily correlated with the chemical nature of the particle surface, which alters when the particles interact with electrolytes.

Our investigations [11] have shown that when electrolytes interact with clays and other aluminosilicates the simple cation-exchange effects are accompanied by more complex surface-chemical processes in which the anions of the added electrolytes play a significant role. The compounds formed on the surface, including readily soluble (mobile) compounds of aluminum and silicon, very often determine the nature of structure formation, while the role of cation-exchange processes is merely secondary.

The purpose of the present investigation was to study the mechanism of action of various electrolytes on thixotropic structure formation in suspensions of askangel from the Tsikhis-ubani deposits in the Georgian SSR. The structural and mechanical properties of these suspensions were studied in relation to the adsorptional, electrokinetic, and other surface-chemical changes taking place in the interaction of askangel with various electrolytes.

* Presented at the Fourth All-Union Conference on Colloid Chemistry in Tbilisi, 1958.

Changes in the structural and mechanical properties of suspensions of askangel which had been electrodialyzed or treated with alkali greatly depend on variations in the nature and content of readily soluble compounds of aluminum and silicon. Curve 1, Fig. 1 shows that the amount of mobile aluminum (basic and trivalent aluminum ions) formed on the particle surfaces during electrodialysis increases sharply with decrease of the suspension pH. The structural viscosity and dynamic shearing stress of the electrodialyzed suspension, determined by the capillary method, diminish with fall of pH while water loss rises sharply. After prolonged interaction with increasing amounts of NaOH the amounts of mobile aluminum and silicon compounds in the askangel suspension increase considerably. For example, as the pH rises from 8.85 to 10.9 the Na_2SiO_3 content of a 4.5% suspension increases from 50.4 to 693 mg of SiO_2 per 100 g of clay. The difference between the amounts of aluminum dissolved out after treatment of the suspension with hydrochloric acid (decrease of pH from 10.9 to 3 and from 8.85 to 3) is 915 mg Al_2O_3 per 100 g of clay. The mobile aluminum is probably present on the particles of the treated suspension in the form of aluminates and compounds of the "permutite" type.

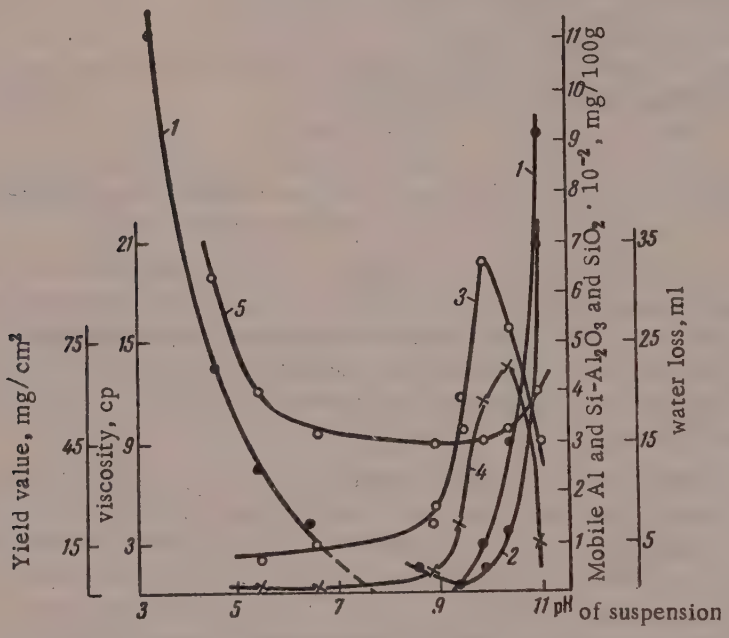


Fig. 1. Effect of the pH of the medium on the properties of 4.5% suspensions of electrodialyzed and alkali-treated askangel: 1) Mobile Al; 2) mobile Si; 3) viscosity; 4) yield value; 5) water loss.

The content of dissolved silicates in the alkali-treated suspension increases severalfold on rise of temperature from 25 to 130°. The abrupt change in the structural and mechanical properties of the suspension with change of pH coincides with the start of abundant formation of mobile aluminum and silicon (Fig. 1).

It is interesting to note that the different effects of electrolytes (NaCl, NaOH, and NaF) on the structural and mechanical properties of electrodialyzed askangel suspensions [11, 12] are easily explained in the light of our work [13] which showed that electrodialyzed askangel is Al-askangel and not H askangel. The reason is that the surface-chemical processes between the exchange aluminum and the anions of the added electrolytes proceed differently. In presence of NaCl cation exchange results mainly in displacement of aluminum ions into solution, whereas in presence of NaOH and NaF the compounds $Al(OH)_3$ and $NaAlF_6$, respectively, are formed on the particle surfaces.

The effects of different electrolytes [Na_2SiO_3, $(NaPO_3)_6$, $Na_4P_2O_7$, NaOH, $NaAlO_2$, Na_2CO_3, etc.] on the structural and mechanical properties of suspensions of fine askangel fractions were studied individually. In this series of experiments, the kinetics of thixotropic reinforcement and deformation of the suspension was studied

by means of the Veiler-Rebinder apparatus [14]. The $\epsilon = f(t)$ deformation curves were used to find the elasticity moduli for nominal instantaneous deformation (E_1) and creep (E_2), the yield value (P_k), and plastic viscosity η [15]. As already stated, for elucidation of the mechanism of action of the above-named electrolytes on structure formation a study was also carried out of anion adsorption from solutions of certain electrolytes, changes of electrokinetic potential, and contents of soluble silicic acid. The experimental results showed that thixotropic structure formation in suspensions treated with increasing amounts of Na_2SiO_3, $Na_4P_2O_7$, and $(NaPO_3)_6$ is approximately the same in character in all cases. With a low content of sodium silicate in the suspension the rate of thixotropic strengthening of its structure falls sharply (Fig. 2). The other structural parameters: $(P_m)_{max}$, D_1, E_2, P_k, η also decrease (see table and Figs. 2 and 3). Further increase of Na_2SiO_3 concentration results in a sharp rise of yield value and other characteristics of structural reinforcement. The coefficient of thixotropy

$$\left(K_T = \frac{P_{max} - P_{min}}{P_{min}}\right).$$

also increases sharply.

Influence of Na_2SiO_3 on the Properties of Highly Disperse Askangel Suspensions. Suspension Volume 200 ml After Treatment, Concentration 6 g of Clay per 100 ml

Expt. No.	Amount of Na_2SiO_3, mole · 10^4	pH of suspension	Amount of adsorbed SiO_3^{2-}, g-equiv · 10^4	P_k, dynes/cm²	$E_1 \times 10^{-3}$, dynes/cm²	$E_2 \cdot 10^{-3}$, dynes/cm²	$\eta \times 10^{-4}$ poises
1	0,0	8,40	—	80	12,6	68,9	1,47
2	2,40	8,64	3,6	70	10,12	41,4	1,12
3	4,79	8,98	7,9	—	—	—	—
4	9,59	9,31	15,1	50	4,66	31,75	1,08
5	19,17	9,92	25,5	45	5,23	29,4	0,37
6	38,33	10,22	38,9	60	8,09	43,6	0,98
7	76,67	11,0	81,2	—	—	—	—

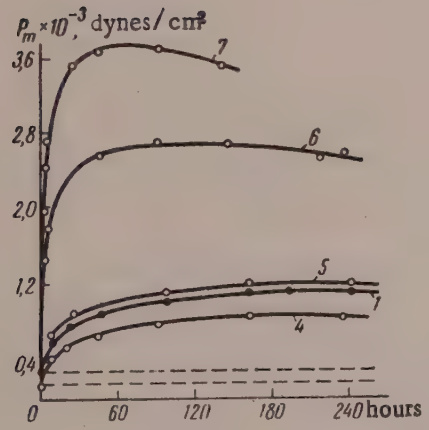


Fig. 2. Kinetics of thixotropic reinforcement of 6% askangel suspensions treated with increasing amounts of Na_2SiO_3. The curve numbers correspond to experiment numbers in the table.

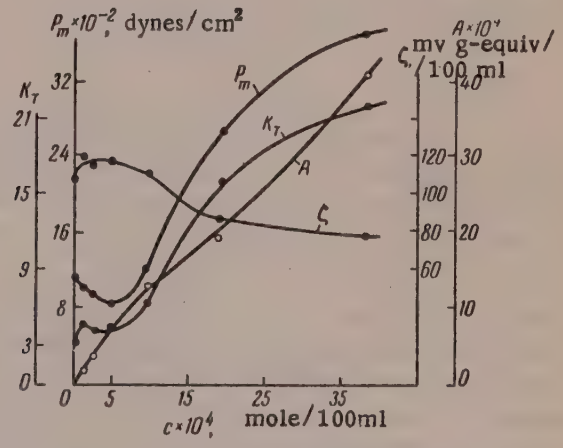


Fig. 3. Influence of sodium silicate on the properties of 6% askangel suspension: P_m) Maximum yield stress; K_T) coefficient of thixotropy; A) adsorption of SiO_3^{2-}; ζ) electrokinetic potential.

It should be noted that in presence of large amounts of Na_2SiO_3 the strength of the thixotropic coagulation structure gradually falls after each consecutive breakdown and gradual buildup, as the result of developing aggregative coagulation (Fig. 2, Curves 6 and 7). A similar effect was observed by Serb-Serbina and Rebinder [2] in treatment of electrodialyzed gilyabi clay by fairly large amounts of NaOH. However, they sought the cause of this effect in gradual replacement of hydrogen ions by sodium ions.

In our view, this kind of variation of the structural and mechanical properties of askangel suspensions treated with Na_2SiO_3, $(NaPO_3)_6$ and $Na_4P_2O_7$ is caused mainly by anion adsorption and other physicochemical changes on the particle surfaces. For example, adsorption of SiO_3 ions greatly increases with increase of Na_2SiO_3 concentration (see table and Fig. 3). If the suspension contains relatively small amounts of Na_2SiO_3, the SiO_3 anions, adsorbed on the hydrophobic regions of the particle surfaces, lower the probability of particle cohesion or weaken the existing bonds between the structural elements. This process is probably also favored by the high values of the electrokinetic potential, which remains virtually constant in this range of electrolyte concentrations (Fig. 3). On further increase of the Na_2SiO_3 concentration intensive adsorption of SiO_3 ions may result in the formation of shells of semicolloidal silicic acid (of a polymeric character) around the particles. In addition, the zeta-potential decreases appreciably owing to the presence of excess electrolyte. Both these factors favor the formation of a strong thixotropic structure, the strength of which gradually decreases with time as the result of developing aggregative coagulation of the particles.

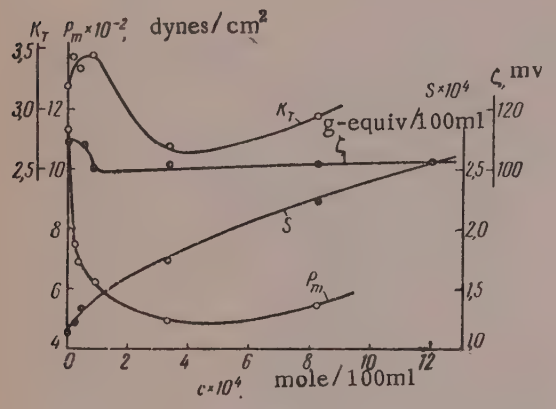


Fig. 4. Influence of $(NaPO_3)_6$ on properties of askangel suspensions: P_m) Maximum yield stress; K_T) coefficient of thixotropy; S) content of SiO_3^{2-} in filtrates; ζ) electrokinetic potential.

As the concentration of these sodium polyphosphates increases in solution, there is an increase in the amount of silicic acid going into solution as the result of chemisorptive interaction of multivalent phosphate ions with the clay particle surfaces (Fig. 4). The possible formation of chemical surface compounds of the aluminophosphate type is not excluded. According to our results [16] and other data, adsorption of phosphate ions on native and synthetic aluminosilicates occurs even in an alkaline medium, and eventually passes into chemisorption.

Figure 4 shows that in the range of sodium hexametaphosphate concentrations studied the zeta-potential of the suspension remains almost unchanged. For such cases, the predominant influence of anions of the added electrolytes on thixotropic structure formation was also demonstrated by studies of the influence of NaOH and $(NaPO_3)_6$ on the kinetics of thixotropic strengthening of suspensions of highly disperse Na-askangel (Fig. 5).

The strong coagulation structure formed by the action of NaOH on a structureless Na-askangel suspension, disappears again almost entirely on addition of small amounts of sodium hexametaphosphate. It is evident that in this case there can be no cation-exchange processes, and the change in the structure formation is caused in this instance only by interaction of the electrolyte cations with the particle surfaces.

The results of another series of experiments (Figs. 6 and 7) showed that the influence of various truly-soluble aluminum compounds (sodium aluminate, and the new basic salt aluminum oxychloride, prepared in our laboratory) on thixotropic structure formation and other properties of suspensions is approximately the same in each case, but differs strongly from the influence of Na_2SiO_3, $(NaPO_3)_6$ and $Na_4P_2O_7$. The explanation is that when sodium aluminate or aluminum oxychloride is added to the suspension the particle surfaces become enriched with aluminum compounds as the result of intensive adsorption of these electrolytes, which form sparingly-soluble compounds of various compositions and properties with the readily-soluble silicic acid in the askangel suspension. Therefore the SiO_3^{2-} content of filtrates diminishes with increasing concentration even of a strongly alkaline electrolyte — sodium aluminate. The influence of sodium aluminate on the zeta-potential also differs from the influence of sodium silicate or polyphosphates. The zeta-potential decreases mainly in the range of low concentrations of sodium aluminate.

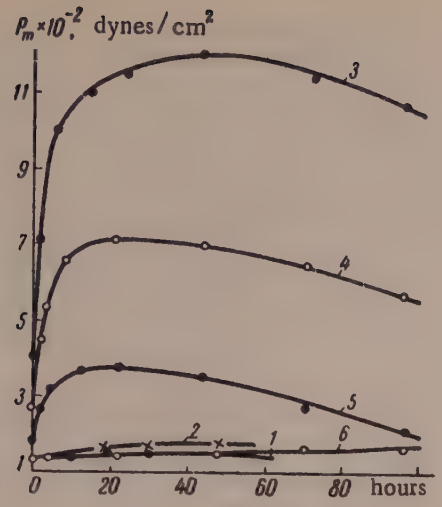


Fig. 5. Effect of additions of NaOH and $(NaPO_3)_6$ on thixotropic strengthening of a 4.32% Na-askangel suspension: 1) Without addition; 2) 0.036% NaOH; 3) 0.36% NaOH; 4) 0.36% NaOH and 0.036% $(NaPO_3)_6$; 5) 0.36% NaOH and 0.18% $(NaPO_3)_6$; 6) 0.18% $(NaPO_3)_6$.

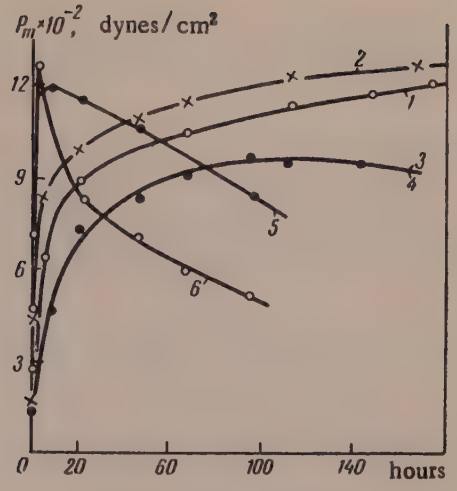


Fig. 6. Kinetics of thixotropic strengthening of 6% askangel suspensions with addition of various amounts of $NaAlO_2$ solution (moles × × 10^{-4}/ 200 ml suspension): 1) 0; 2) 1.39; 3) 3.48; 4) 6.95; 5) 13.9; 6) 23.66.

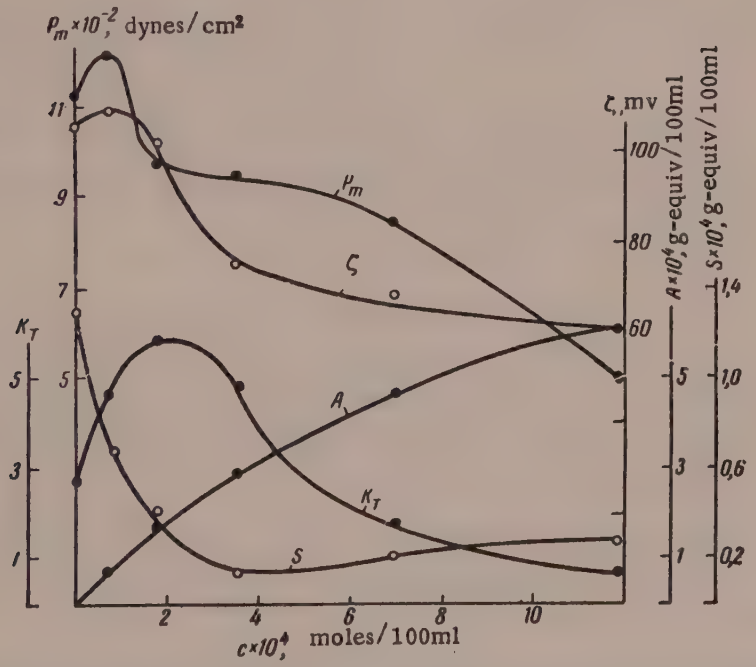


Fig. 7. Influence of sodium aluminate on the properties of 6% askangel suspension: P_m) After 100 hours of strengthening; K_T) coefficient of thixotropy; ζ) electrokinetic potential; S) contents of SiO_3^{2-} in filtrates; A) adsorption of aluminate.

It was also found that in presence of relatively small amounts of sodium silicate or polyphosphates, the water loss of the suspension decreases, whereas in presence of aluminate or oxychloride it increases.

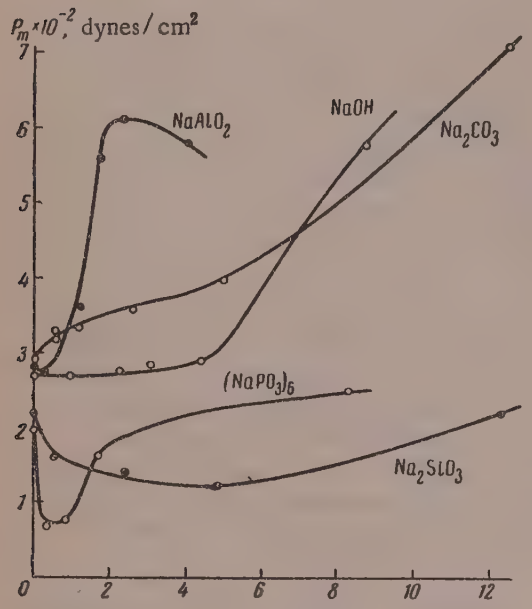


Fig. 8. Strength of structure after 100 hours of strengthening of 7.5% highly disperse askangel suspension as a function of the added electrolyte concentrations.

Thus, enrichment of the surface of the askangel particles with different aluminum compounds and loss of readily-soluble compounds of silicon and anions of the potential-determining layer leads to a sharp decrease in the hydrophilic regions and an increase of nonthixotropic bonds between the particles in the coagulation structure or to actual aggregative coagulation of the suspension in presence even of small amounts of these electrolytes.

It must also be pointed out that if sodium aluminate and silicate (in various proportions) are added simultaneously to the suspension, the thixotropic structure formation of the suspension passes through a maximum. At a definite quantitative ratio of these electrolytes, the structure formed has the highest strength and thixotropy. This is probably because aluminosilicate compounds of the "permutite" type are formed on the particle surfaces as the result of chemical interaction between sodium aluminate and silicate. The character of structure formation in the suspension greatly depends on variations of the $Al_2O_3 : SiO_2$ molar ratio in these compounds.

Other alkaline electrolytes — sodium carbonate and hydroxide — differ considerably from the above-named sodium electrolytes in their influence on thixotropic strengthening. In particular, this is illustrated by the fact that in Fig. 8, the curve for variations of the yield value of 7.5% askangel suspension treated with NaOH occupies an intermediate position between the curves for suspensions to which $NaAlO_2$ and Na_2SiO_3, respectively, had been added. This may be because when NaOH interacts with the clay mobile compounds of silicon and aluminum in the form of the corresponding silicates and aluminates are simultaneously formed on the particle surfaces.

SUMMARY

1. Variations of the structural, mechanical and physicochemical properties of electrodialyzed askangel suspensions greatly depend on the amounts of mobile (exchange) aluminum and on the nature of the surface-chemical processes taking place between the aluminum and the added electrolyte anions. Different electrolytes (Na_2SiO_3, $Na_4P_2O_7$, $(NaPO_3)_6$, $NaAlO_2$, NaOH, Na_2CO_3, etc.) differ in their influence of thixotropic structure formation.

2. When askangel suspensions interact with Na_2SiO_3, $(NaPO_3)_6$ and $Na_4P_2O_7$ fully reversible thixotropic structures are formed owing to intensive adsorption of multivalent anions, increase in the amount of readily-soluble silicon compounds on the particle surfaces, and high values of the zeta-potential.

3. Electrolytes which enrich the surface of the clay particles by aluminum compounds, cause loss of soluble silicon compounds from it, or decrease the amount of anions in the potential-determining layer, favor increase of nonthixotropic bonding between the particles in the spatial structure. NaOH and Na_2CO_3 occupy an intermediate position between these two types of differently-acting electrolytes.

LITERATURE CITED

[1] A. V. Dumanskii, Kolloid Zhur. 12, 319 (1950); A. V. Dumanskii and P. A. Demchenko, Doklady Akad. Nauk SSSR 78, 277 (1951); A. V. Dumanskii, P. A. Demchenko, and L. G. Demchenko, Kolloid. Zhur. 14, 164 (1952).*

[2] P. A. Rebinder, Proceedings of Conference on Viscosity of Liquids and Colloidal Solutions [In Russian] (Izd. AN SSSR, Moscow-Leningrad, 1941), 1, 361; N. N. Serb-Serbina and P. A. Rebinder, Kolloid. Zhur. 9, 381 (1947); P. A. Rebinder, Proceedings of Third All-Union Conference on Colloid Chemistry [In Russian] (Izd. AN SSSR, 1957), p. 7; L. A. Abduragimova, P. A. Rebinder, and N. N. Serb-Serbina, Kolloid. Zhur. 17, 184 (1955).*

[3] N. N. Serb-Serbina, Proceedings of Conference on Viscosity of Liquids and Colloidal Solutions [In Russian] (Izd. AN SSSR, Moscow-Leningrad, 1941), 1, 381; N. N. Serb-Serbina and S. A. Nikitina, Kolloid. Zhur. 8, 63 (1946).

[4] V. S. Baranov and Z. B. Buks, Chemical Treatment of Clay Suspensions in Oil-Well Drilling [In Russian] (State Fuel Tech. Press, 1945).

[5] L. V. Lyutin, Stabilization of Mineral Suspensions [In Russian] (Moscow-Leningrad, 1947).

[6] H. Broun and J. Richter, Kolloid. Zhur. 113, 20 (1946).

[7] S. Filatov, Bentonite Clays of Georgia [In Russian] (Acad. Sci. Georgian SSR Press, 1953), p. 27.

[8] G. V. Kukolev and Ya. M. Syrkin, Kolloid. Zhur. 17, 90 (1955).*

[9] I. A. Uskov, Kolloid. Zhur. 19, 511 (1957).*

[10] S. Mattson, Soil Colloids [In Russian] (State Agricultural Press, 1938).

[11] S. N. Papuashvili, M. E. Shishniashvili, and L. D. Agladze, Trudy In-ta Khimii Akad. Nauk Gruz. SSR 13, 3 (1957); 14, 73 (1958).

[12] E. I. Kobakhidze, M. E. Shishniashvili, and N. N. Serb-Serbina, Kolloid. Zhur. 19, 299 (1957).*

[13] S. N. Papuashvili, M. E. Shishniashvili, and L. D. Agladze, Trudy In-ta Khimii Akad. Nauk Gruz. SSR 12, 23 (1956).

[14] S. Ya. Veiler and P. A. Rebinder, Doklady Akad. Nauk SSSR 49, 354 (1945).

[15] E. E. Segalova and P. A. Rebinder, Doklady Akad. Nauk SSSR 71, 85 (1950); E. E. Segalova, P. A. Rebinder, and L. S. Sentyuryukhina, Kolloid. Zhur. 13, 461 (1951).

[16] M. E. Shishniashvili and S. N. Papuashvili, Trudy In-ta Khimii Akad. Nauk Gruz. SSR 9, 1 (1948); M. E. Shishniashvili and L. L. Batsanadze, Kolloid. Zhur. 8, 269 (1946).

[17] M. E. Shishniashvili, V. A. Kargin, and A. L. Batsanadze, Zhur. Fiz. Khim. 21, 391 (1947); Trudy In-ta Khimii Akad. Nauk Gruz. SSR 7, 33 (1946).

ADHESION OF HIGH POLYMERS

4. INFLUENCE OF MECHANICAL FACTORS ON ADHESION OF HIGH POLYMERS

A. P. Pisarenko, A. I. Shapovalova, and S. S. Voyutskii

All-Union Scientific Research Institute of Artificial Leather (VNIIK), Moscow
(Translated from: Kolloidnyi Zhurnal Vol. 22, No. 1, pp. 57-62, January-February, 1960)
(Original article submitted September 22, 1958)

Effects which form the basis of specific adhesion were considered in our preceding publications [1-3]. The present communication is concerned with the influence of mechanical factors on adhesive strength.

It is known that bonding merely by specific adhesion is rarely found in practice; it is more often accompanied by mechanical adhesion, or wedging of the adhesive in the pores and cracks of the substrate surface.

The available information [4] does not embrace the whole range of effects in mechanical adhesion and does not provide answers to questions which arise in practice. Therefore, studies of the influence of mechanical factors are of great practical importance as well as of theoretical interest.

The following adhesives were used in the present investigation: natural rubber; SKN-40 butadiene-acrylonitrile copolymer containing 37.7% acrylonitrile; SKS-50 butadiene- styrene copolymer containing 50% styrene; and polyisobutylene of 200 grade. In some experiments SKN-26 and SKN-18 butadiene – acrylonitrile copolymers and polyisobutylenes of different molecular weights were also used as adhesives.

This group of adhesives was chosen because their specific adhesion to the substrate was low, so that the joint was broken down at the adhesive – substrate boundary in the tests. This made it possible to observe variations of bonding strength with increasing damage of the substrate surface. The adhesives were applied to the substrate in solution form in solvents generally used for preparation of rubber adhesives (ligroine, benzene, dichloroethane).

The substrate used in the earlier experiments was a cellulose-fiber model – cellophane with different degrees of surface damage. The cellophane, washed free of glycerol and dried in the stretched state [2], was subjected to mechanical treatment by emery paper. The surface damage was estimated in terms of light transmission through the specimen and of the optical density of the treated cellophane, determined by means of the FM universal photometer. The light transmission τ naturally decreased with increasing surface damage, while the optical density D increased correspondingly.

Table 1 contains data on the degree of mechanical damage of the cellophane surfaces used in the experiments.

In further experiments, the substrates were different fabrics made from cellulose fibers. Since the chemical nature of cellophane and the fibers is the same, the influence of specific adhesion could be eliminated in experiments concerned with studies of mechanical adhesion.

The preparation and separation of the joints were carried out under strictly standard conditions by a procedure developed previously [2].

Table 2 contains data on the resistance to separation of the above-named polymers from cellophane with different degrees of surface damage.

TABLE 1

Effects of Mechanical Treatment of Specimen Surface on Light Transmission and Optical Density of Cellophane

Type of cellophane	Code mark for degree of surface damage	Light transmission τ, %	Optical density D
Original	—	82	0,085
Washed	—	84	0,075
The same, treated	1/1	57	0,25
The same	3/3	25	0,60
	5/5	20,5	0,69

It follows from Table 2 that high-strength elastic adhesives which have low specific adhesion are attached much more firmly to a surface of the same nature if its surface is mechanically damaged. The resistance to separation increases continuously with increasing degree of surface damage.

With the greatest degree of surface damage the resistance to separation is increased more than sevenfold in the case of natural rubber, threefold in the case of SKN-40 copolymer, elevenfold in the case of SKS-50 copolymer, and almost threefold in the case of polyisobutylene.

Since there is little reason to believe that joints of the "rivet" type can be formed in experiments with cellophane in which the surface has been damaged by treatment with emery paper, the increased resistance to separation must be attributed mainly to increase of the contact area between the adhesive and substrate. It is also possible that increased resistance to separation is also due to increasing specific adhesion because of removal of the surface cellophane layer, which probably has higher density and thereby hinders diffusion of the molecules of adhesive into the substrate.

TABLE 2

Effect of Mechanical Treatment of Cellophane on Adhesion of Various Elastomers

Code mark for degree of surface damage	Resistance to separation*, g/cm			Code mark for degree of surface damage	Resistance to separation*, g/cm		
	least	greatest	average		least	greatest	average
Adhesive — natural rubber				Adhesive — SKS-50			
Not damaged	13	25	18	Not damaged	2,5	22	14
1/1	48	101	69	1/1	78,0	125	103
3/3	80	106	90	3/3	135,0	155	145
5/5	115	137	129	5/5	148,0	173	160
Adhesive — SKN-40				Adhesive — polyisobutylene grade 200			
Not damaged	80	124	103	Not damaged	60	71	68
1/1	158	219	189	1/1	88	107	100
3/3	263	283	270	3/3	98	135	125
5/5	295	325	308	5/5	137	148	142

* Separation of the adhesive type.

In bonding of fabrics with a more extensively developed surface, the relief of which favors formation of "rivet" joints, bond strength increases still further. This is seen in Table 3 which contains the results of tests on joints in which a cotton fabric (percale) was used as the substrate.

The data in Table 3 indicate that in this case the bond strength is tens or even hundreds of times as great as the specific adhesion. For example, comparison of the data in Tables 2 and 3 shows that the strength of bonding by natural rubber is increased 20-fold, by SKS-50 copolymer more than 150-fold, by SKN-40 copolymer nearly 27-fold, and by polyisobutylene 23-fold. It is important to note that, as far as could be judged from the appearance of the separated joints, the separation was of the mixed or adhesive character.

If, in addition to "rivet" joints, bonding is also effected by projecting hairs from the fabric penetrating into the adhesive layer, the bond strength is increased still further. This is clear from Table 3, which contains data on the strength of bonding of staple fabric, the surface of which has numerous hairs.

TABLE 3

Resistance to Separation of Specimens of: I) Pairs of Percale Strips; II) Pairs of Viscose Staple Strips; Bonded by Different Elastomers

Substrate	Type of separation	Resistance to separation, g/cm		
		greatest	least	average
Smooth cellophane	Adhesive	60	71	68
Cellophane after mechanical treatment, 5/5	Cellophane after mechanical treatment, 5/5	137	148	142
Cotton fabric AST-100	Mixed	1089	1133	1112
Percale cotton fabric	Adhesive	1472	1613	1572
Viscose staple fabric		1950	2.)	2078

Comparison of data on the strength of bonding of percale and staple fabric by polyisobutylene (Table 3) shows that the bond strength is increased by almost 25% as the result of embedment of hairs in the adhesive layer. Certain conclusions concerning the influence of the nature of the adhesive on the bonding of fabrics may also be drawn from the data in Table 3. It was shown in one of our investigations [3] that specific adhesion to cellophane is greatest for SKN-18 polymer and least for SKN-40 polymer. It follows from Table 3 that if the adhesive is wedged in the fabric pores and hairs are embedded in the adhesive layer the strength of bonding by butadiene – acrylonitrile copolymers changes in the reverse sequence. The strength of bonding of two fabric strips by means of SKN-40 copolymer is over 40 times as great as the specific adhesion determined in the experiment with untreated cellophane, since in separation of the joint the fabric breaks when the load reaches 4 kg/cm. If the fabric strips are bonded by means of SKN-18 copolymer the bonding strength remains at the level of the specific adhesion. This reversal of the sequence should, of course, be attributed to the fact that in presence of mechanical adhesion the bond strength is determined by the cohesive strength of the adhesive, which is considerably greater for SKN-40 polymer than for SKN-18.

The strength of bonding of fabrics also depends to a considerable extent on the nature of the fibers, the spinning process used, and type of weave. This is clearly illustrated by the data in Table 4, indicating the strength of bonding of different types of cellulose-fiber fabrics by polyisobutylene 200. For comparison, Table 4 also includes data on the resistance to separation of joints made from untreated and mechanically-treated cellophane with polyisobutylene 200.

Table 4 shows that bond strength increases continuously with increasing development of the surface relief of the substrate. This is clear from the results for cellophane and especially for fabrics. As we pass from a fabric with a less-developed surface and relatively coarser relief (AST-100) to a finer and denser fabric (percale) the bond strength increases from 1112 to 1572 g/cm, and in the case of viscose staple fabric it reaches 2078 g/cm, which is more than 30 times the specific adhesion to cellophane.

It is evident from the above data that polyisobutylene is bonded firmly to fabric made from viscose fibers, the surface of which is in general quite smooth. This bonding is effected both by penetration of the adhesive into the spaces between the threads and fibers of the fabric, and by embedment of individual hairs into the adhesive layer. In other words, to effect separation force is needed not only to overcome intermolecular forces

between the adhesive and substrate and to break down "rivet" joints, but also to pull out the fibrils from the adhesive layer or to break them. The appearance of the separated joints indicates that the separation is of the adhesive type, suggesting that the joints are broken at the fiber – adhesive contact boundary.

TABLE 4

Effects of the Character of Cellophane Surface and Fabric Type on the Strength of Bonding by Polyisobutylene 200

Substrate	Type of separation	Resistance to separation, g/cm		
		greatest	least	average
Smooth cellophane	Adhesive	60	71	68
Cellophane after mechanical treatment, 5/5	The same	137	148	142
Cotton fabric AST-100	»	1089	1133	1112
Percale cotton fabric	Mixed	1472	1613	1572
Viscose staple fabric	Adhesive	1950	2230	2078

In conclusion, we consider the influence of the molecular weight of the adhesive on the resistance of fabric joints to separation. Table 5 contains data on the strength of bonding of percale strips by means of polyisobutylenes of different molecular weights.

Table 5 shows that the bond strength decreases with decreasing molecular weight and falling mechanical strength of polyisobutylene, while the type of separation, as was to be expected, changes from adhesive or mixed to cohesive.

TABLE 5

Effect of Molecular Weight of Polyisobutylene on the Strength of Bonding of Percale Cotton Fabric

Molecular weight of adhesive	Type of separation	Resistance to separation, g/cm		
		least	greatest	average
200 000 (polyisobutylene 200)	Mixed	1472	1613	1572
150 000	Mixed – adhesive	1385	1584	1513
118 000	The same	1306	1446	1378
50 000	Mixed	1185	1398	1304
20 000	Cohesive	259	363	335
7 000	The same	0	0	0

Our experiments revealed the interesting fact that in the case of polyisobutylene of molecular weight 200,000 the type of separation of the joint and resistance to separation are the same both in absence and in presence of mechanical adhesion. The explanation is, of course, that in both cases, the destruction of the joint is of the cohesive type because of the low mechanical characteristics of the adhesive used.

SUMMARY

1. The effects of mechanical adhesion on the strength of bonding by different elastomers were investigated and it was shown that the strength of bonding of polymers of low specific adhesion is tens or hundreds of times as great if the degree of mechanical damage of the surface is increased, the porosity becomes greater, or projecting fibrils are present on the fabric surface.

2. In presence of mechanical adhesion the bond strength is generally determined by the cohesive strength of the adhesive. The influence of cohesive strength is especially pronounced when surface irregularities of the substrate (such as fabric hairs) are firmly embedded in the adhesive layer.

3. It was found in the earlier investigations that the variation of the specific adhesion of polyisobutylene with its molecular weight is represented by a curve with a maximum at molecular weight 20,000. In the present investigation, it was shown that in presence of mechanical adhesion the bonding strength is greatest for polyisobutylene with molecular weight 200,000 and least for polyisobutylene with molecular weight 20,000.

LITERATURE CITED

[1] S. S. Voyutskii, A. I. Shapovalova, and A. P. Pisarenko, Doklady Akad. Nauk SSSR 105, 1000 (1955).

[2] A. I. Shapovalova, S. S. Voyutskii, and A. P. Pisarenko, Kolloid. Zhur. 18, 485 (1956).*

[3] S. S. Voyutskii, A. I. Shapovalova, and A. P. Pisarenko, Kolloid. Zhur. 19, 274 (1957).*

[4] N. A. de Bruyne and R. Houwink (Editors), Adhesion [Russian translation] (IL, 1954).

* See C. B. Translation.

STRUCTURAL AND MECHANICAL PROPERTIES OF SOLUTIONS, GELS, AND COAGULATES (COACERVATES) OF GELATIN

V. A. Pchelin and N. Ya. Solomchenko

M. V. Lomonosov University, Moscow, Chemical Faculty,

Department of Colloid Chemistry
(Translated from: Kolloidnyi Zhurnal Vol. 22, No. 1, pp. 63-68, January-February, 1960)
(Original article submitted July 15, 1958)

Studies of structural and mechanical properties are important means for elucidation of the internal structure of disperse systems and changes in this structure under the influence of external factors [1, 2].

Applied to polymer solutions, and in particular to polyelectrolytes [2], this method provides conclusive solutions to a number of problems relating to their molecular structure and the mechanism of a number of processes leading to changes in it. This is shown by the results of numerous studies of the structural and mechanical properties of polymers, including gelatin [3, 4]. In these studies gelatin was used both in solution and in the form of gels and air-dry films.

It is also known that the action of a number of substances in gelatin solutions leads to formation of a new phase in the form of drops consisting mainly of the same aqueous gelatin solution but at a higher concentration, and containing various amounts of the third component which induced the process.

This formation of a new phase is also observed in solutions of other polymers, and is known in the literature as the coacervation effect [5].

It is still uncertain whether gelatin retains its molecular structure after conversion into the new phase, and, if not, what changes take place in it.

In the present investigation an attempt was made to solve this problem by studies of the structural and mechanical properties of gelatin converted into the new phase state by the action of sodium sulfate and resorcinol (these are typical substances causing coacervation, and at the same time they differ sharply in their chemical nature).

Methods and apparatus. The methods described previously [6] were used to convert gelatin into the new phase state. It should merely be noted that after addition of sodium sulfate or resorcinol to the gelatin solution gelatin first separates out in the form of microscopic droplets (an emulsion of gelatin in water is formed). If Na_2SO_4 has been added, when such emulsions are kept at 50° the droplets coalesce and after 24 hours the system separates out completely into two layers. The bottom layer then contains almost all the gelatin taken originally. It was found that when droplets coalesce out of 10% gelatin solution, the concentration in the new phase is 31.35%. If resorcinol is added, the droplets do not coalesce and the coacervate is a stable emulsion.

The gelatin separated out in the form of the new phase (coacervate) was used in our further investigations. Parallel experiments were performed with ordinary gelatin.*

* Photographic gelatin, previously brought into the isoelectric state and demineralized by the Loeb method [7], was used in the work.

The independent variables in our experiments were the shearing stress and temperature. The temperature range was so chosen that the system would be obtained both in the liquid and in the gel state. The viscosity of solutions and the structural and mechanical properties of gelatin gels and coacervates were studied accordingly.

All the determinations were performed with an elastoviscosimeter of the rotational type, which differed from instruments described previously in a number of features* (Fig. 1).

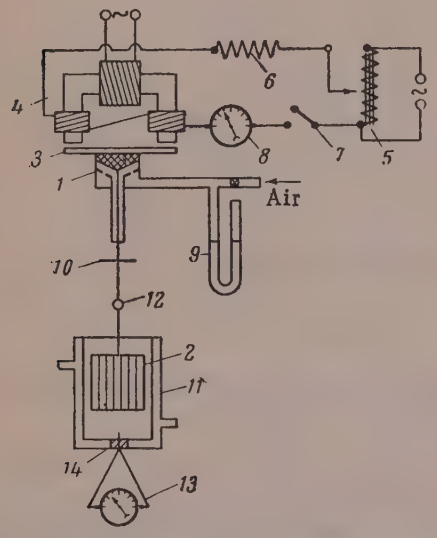


Fig. 1. Line diagram of elastoviscosimeter (explanation in text).

The essential part of the instrument is the air bearing 1, which ensures virtually total absence of friction in rotation of the internal cylinder 2, and provides for centering of the moving system. The load on the moving system is applied at a distance by means of an alternating-current electromagnetic motor. The motor consists of a light aluminum disk 3 and an electromagnet 4. The electromagnet consists of a core and three coils; the middle (large) coil is used for permanent magnetization, while the two outer ones are for transmission of torque to the aluminum disk 3. These coils are designed to carry current up to 10 amp, and are included in a circuit consisting of an autotransformer 5 (LATR-1), a loading resistance 6, a switch 7, and an ammeter 8. The sensitivity of the latter is chosen in accordance with the viscosity (elasticity) of the system under investigation. Alteration of the current strength in the circuit changes the torque transmitted to the disk 3, caused by Foucault currents set up in it. There is a strictly linear relationship between the current strength and the magnitude of the torque. The transformer 5 is used for smooth or stepwise loading, while the switch 7 can be used for applying or removing the load instantaneously. The manometer 9 is used to measure the pressure in the air bearing. A part of the air from the bearing passes downward through a tube along a rigid axis onto a light aluminum disk 10 which shields the surface of the system under investigation.** The outer stationary cylinder 11 is surrounded by a water jacket connected to an ultrathermostat, and is fitted with a thermocouple 14 and millivoltmeter 13 for temperature measurement.

For expression of the torque in absolute units (dynes · cm) the apparatus was calibrated against liquids of known viscosity (sucrose solutions); a current of 1 amp corresponded to a torque of 352 dynes · cm acting on the cylinder 2. The viscosities of liquid systems were measured by determination of the rate of rotation of the disk 3 under different loads. The structural and mechanical properties of gel systems were studied with the aid of kinetic curves representing the development and decrease of deformation at constant shearing stress and with instantaneous loading and unloading of the system. These curves were recorded automatically on photographic paper; for this the instrument was provided with a special attachment (not shown in Fig. 1) consisting of a drum rotated at various fixed speeds by means of an electric motor. The photographic paper was attached to the drum, and a light spot was reflected onto it through a slit from a light source by means of the mirror 12 (Fig. 1).

It was observed in unpublished experiments by one of us jointly with N. V. Grigor'eva, and in a published research [4], that the elasticity modulus of gelatin gel increases (the aging effect) over a considerable period, and does not reach a constant value even after 50 days. Because of this, and also in view of the fact that only relative values were required, we reduced the duration of the experiments to a minimum and established standard times for performance of the individual operations. Shortening of the duration of the experiments is also desirable from other points of view. For example, addition of various antiseptics to the system becomes unnecessary, there

* The elastoviscosimeter used in the investigation was designed by one of us jointly with S. P. Alekhin. A detailed account of the design will be given in a special communication.

** In addition, evaporation in all the experiments was prevented by application of a thin layer of pure liquid petrolatum.

is no risk of error owing to thermolysis of gelatin in experiments at higher temperatures and to solubilization of the nonpolar solvent used to protect the system from evaporation, etc.

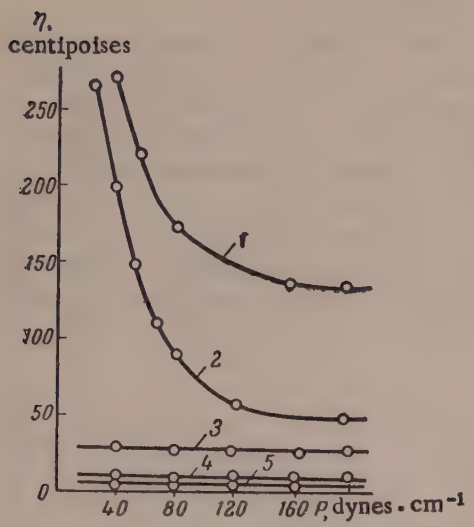


Fig. 2. Variations of the viscosity of 31.35% gelatin solution with the shearing stress: 1) 30°; 2) 31°; 3) 32°; 4) 40°; 5) 50°.

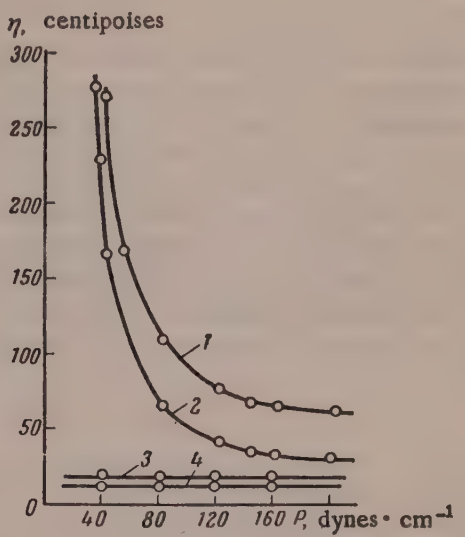


Fig. 3. Variations of the viscosity of gelatin + Na_2SO_4 coacervate with the shearing stress: 1) 36°; 2) 37°; 3) 40°; 4) 50°.

Viscosity variations of gelatin solutions and coacervates with the shearing stress at various temperatures are plotted in Figs. 2, 3, and 4. The viscosity falls with rise of temperature in all three systems, but they differ significantly in all other respects. Thus, gelatin solution (Fig. 2) and the coacervate produced by the action of Na_2SO_4 (Fig. 3) have a well-defined structure which disappears over a narrow temperature range. This takes place in the 31-32° range for 31.35% gelatin solution, and in the 37-40° range for the coacervate. The behavior of the gelatin + resorcinol coacervate (emulsion) (Fig. 4) is sharply different. In the 31-50° range this system behaves like a Newtonian liquid, and the viscosity-temperature relationship is linear, in contrast to the first two cases (see Fig. 5).

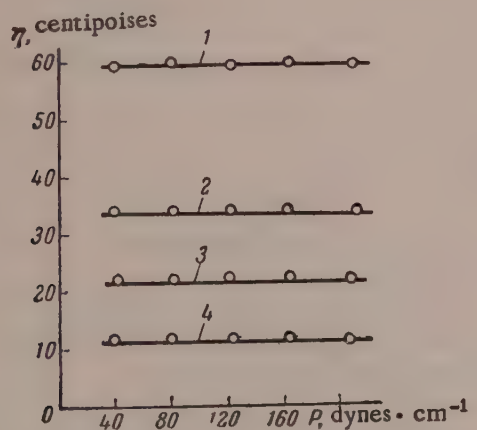


Fig. 4. Variations of the viscosity of gelatin + resorcinol coacervate with the shearing stress: 1) 31°; 2) 36°; 3) 40°; 4) 50°.

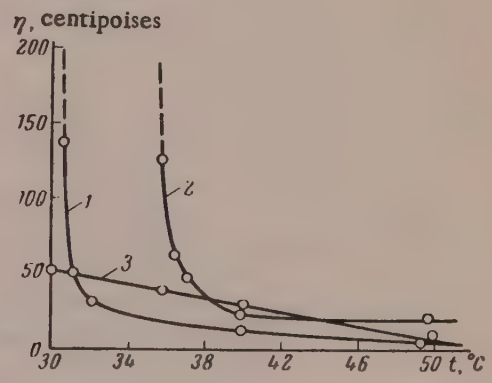


Fig. 5. Effect of temperature on the viscosity of: 1) 31.35% gelatin solution; 2) gelatin + + Na_2SO_4 coacervate; 3) gelatin + resorcinol coacervate.

The considerable general decrease in the viscosity of this system is also noteworthy.

For studies of the kinetics of growth and decrease of deformation at constant shearing stress in relation to the temperature the materials used were 10 and 31.35% gelatin gels and gelatin + Na_2SO_4 coacervates. The gelatin + resorcinol coacervate cannot be investigated by this method because of its fluidity.

The loads used in these experiments were considerably less than in the viscosity experiments, to ensure the greatest preservation of the structure and to allow fuller observations of changes in the relationship between elasticity and fluidity. The results of the determinations, plotted in Figs. 6, 7, and 8, show that the structural and mechanical properties of the systems change sharply over a narrow temperature range. This is shown by the fact that the flow rate increases sharply with rise of temperature, indicating breakdown of contact between the molecular chains of gelatin and relative displacement of these chains. At the same time all three systems retain elastic properties, which can be easily measured, even at the highest temperatures (50°). The magnitude of the nominal-instantaneous deformation at constant P increases with rise of temperature. Evidently, the breakdown of contacts and relative displacement of the macromolecules is accompanied by further chain straightening and orientation in direction of the acting shearing stress.

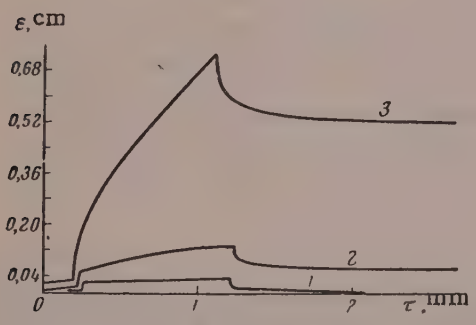


Fig. 6. Kinetics of development and decrease of deformation of 10% gelatin solution at P = = 12.5 dynes · cm^{-1}: 1) 24°; 2) 25°; 3) 26°.

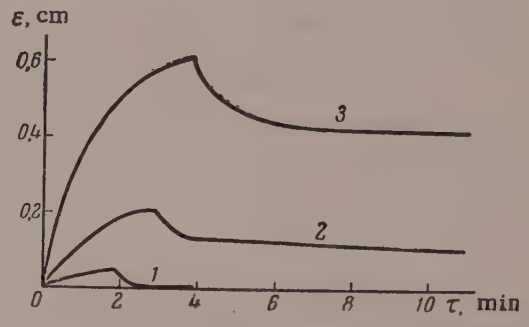


Fig. 7. Kinetics of development and decrease of deformation of 31.35% gelatin solution at P = 15.6 dynes · cm^{-1}; 1) 30°; 2) 31°; 3) 32°.

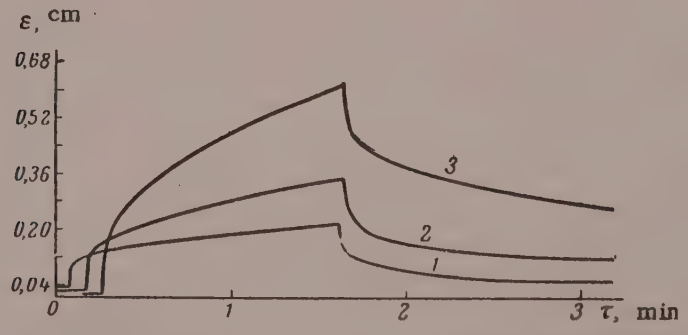


Fig. 8. Kinetics of development and decrease of deformation of gelatin + Na_2SO_4 coacervate at P = 22.0 dynes · cm^{-1}; 1) 36.5°; 2) 37°; 3) 37.5°.

The form of these curves indicates that there are no qualitative peculiarities about the development and decrease of deformation in the three systems. The sole difference is the temperature range in which flow begins. For clarity, the effects of temperature are plotted in Fig. 9, which shows that the temperature at which flow begins rises with increase of gelatin concentration. The behavior of the coacervate is like that of gelatin taken

at an even higher concentration. Since in reality the concentration of the coacervate is equal to that of the gelatin (31.35%), the observed effect may be attributed to increase of the number of contact in the gel network owing to partial dehydration of the gelatin by sodium sulfate.

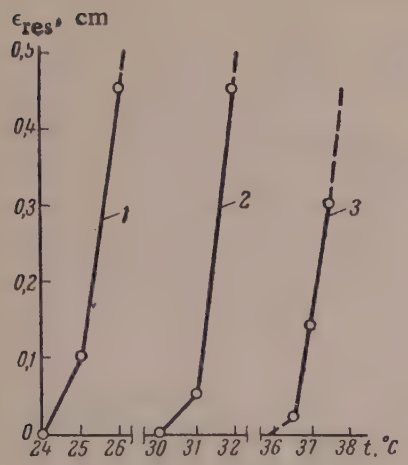


Fig. 9. Effect of temperature on residual deformation: 1) 10% gelatin solution; 2) 31.35% gelatin solution; 3) gelatin + Na_2SO_4 coacervate.

It has already been pointed out that the structural and mechanical properties of the other coacervate studied, gelatin + resorcinol, are highly specific. Absence of structure formation in this system and its stability indicate that in the interaction of gelatin with resorcinol a peculiar mechanism is involved in the formation of the new phase.

Formation of the new phase in this concentrated two-component system is probably caused by changes in the configuration of the gelatin macromolecules owing to formation of bridges consisting of resorcinol molecules linked by hydrogen bonds to the functional groups of the protein chains.

Since resorcinol is a weak dibasic acid, formation of bridges of the salt type may also be postulated.

The macromolecules in concentrated gelatin solutions are greatly intertangled and have all possible configurations, and therefore it may be assumed that bridge formation may be both intra- and intermolecular. This reinforcement of the structure prevents coalescence of the coacervate droplets.

SUMMARY

1. An elastoviscosimeter of a new type was used for studying the viscosity and deformation characteristics of gelatin converted into a new phase state (coacervate) by the action of sodium sulfate and resorcinol.

2. The gelatin coacervate made by the action of sodium sulfate qualitatively retains the structural and mechanical properties of gelatin but has higher elasticity and a higher melting point.

3. The gelatin coacervate made by the action of resorcinol behaves like a Newtonian liquid of a considerably lower viscosity than the original gelatin solution. It is suggested that resorcinol changes the configuration of the gelatin macromolecules by formation of hydrogen and salt-type bonds between the gelatin molecules and resorcinol.

The authors are deeply grateful to Academician P. A. Rebinder for valuable advice.

LITERATURE CITED

[1] P. A. Rebinder, Vestnik Akad. Nauk SSSR 10, 32 (1957).

[2] P. A. Rebinder and L. V. Ivanova-Chumakova, Advances in Polymer Chemistry and Technology [In Russian] (Goskhimizdat, Moscow, 1957), p. 146.

[3] P. I. Zubov, Z. N. Zhurkina, and V. A. Kargin, Kolloid. Zhur. 9, 109, 367 (1947); 16, 109 (1954); Doklady Akad. Nauk SSSR 67, 659 (1949).

[4] L. V. Ivanova-Chumakova, P. A Rebinder, and G. I. Krus, Kolloid. Zhur. 18, 682 (1956).*

* See C. B. translation.

[5] T. N. Evreinova, Uspekhi Sovrem. Biol. 37, 177 (1954).

[6] W. J. Holleman, H. G. Bungenberg de Jong, and R. S. Tjaden Modderman, Kolloid-Beihefte 39, 334 (1934).

[7] J. Loeb, Proteins and the Theory of Colloidal Behavior [Russian translation] (State Light Industry Press, 1933), p. 52.

RADIOACTIVE TRACER STUDIES OF THE GELATION OF RUBBER LATEXES

D. M. Sandomirskii and M. K. Vdovchenkova

Scientific Research Institute for Rubber and Latex Products, Moscow

(Translated from: Kolloidnyi Zhurnal Vol. 22, No. 1, pp. 69-73, January-February, 1960)

(Original article submitted May 20, 1958)

Gelation of latex is one of the important methods used for manufacture of rubber products directly from latex [1]. This term is used in latex technology only in cases when conversion of the latex to a gel takes place under the influence of destabilizing ions which form slowly in the latex mixture itself. One method of bringing this about is by introduction of zinc oxide and ammonium salts into the latex. The formation of zinc ammine cations in this process, and their interaction with the globules, have been studied in a number of investigations [2, 3], but as yet they cannot be regarded as fully understood.

Our previous investigations [4, 5] showed that radioactive isotopes can be used with success for studying latex coagulation and ionic deposition. The present investigation was concerned with the use of $Zn^{65}O$ for coagulation of Nairit L-3 and L-4 polychloroprene latexes, SKS-50 butadiene-styrene latex, and polychloroprene latex stabilized by sodium paraffinate and sodium tridecylate labeled with C^{14} in the carboxyl group (VKh-2 latex).

The aqueous $Zn^{65}O$ paste was prepared as follows. Metallic zinc, to serve as carrier, was mixed with Zn^{65}, and the mixture was dissolved in HCl (1 :1) to give $ZnCl_2$. After removal of iron (by precipitation with $CaCO_3$) ammonia was added to precipitate $Zn(OH)_2$, which was calcined to give ZnO.

The radioactive zinc oxide was mixed thoroughly with inactive zinc oxide. The zinc oxide paste was prepared by the usual method in an aqueous solution of NF dispersing agent. In experiments with VKh-2 latex a paste of inactive zinc oxide was used. Different amounts of paste were introduced into latex mixtures consisting of 10 ml latex, 1 ml of 10% ammonia solution, and 1 ml of 5% ammonium chloride solution.

To determine whether gelation of the latex is accompanied by chemical binding of zinc, and whether all the zinc introduced into the latex is so bound, the gels formed with $Zn^{65}O$ paste were washed with ammoniacal ammonium nitrate solution and the radioactivity of the latter was determined. Two hours of washing was sufficient to remove uncombined zinc from the gel. The washed and dried gel was burned in a muffle furnace, and the activity of the ash was determined by the usual method. It was found that during gelation a part of the zinc is bound firmly in the gel and is not extracted when the latter is washed with ammonium nitrate solution. The amount of bound zinc depends on the type of latex. Latex L-4 binds 0.94 meq of zinc per g of latex, L-3 binds 0.69, SKS-50 binds 0.52, and VKh-2 binds 0.61 meq.

Extraction of VKh-2 latex gels with ethyl alcohol, which dissolves sodium tridecylate, showed that much more of the protective substance is bound with the electrolyte in gelation than in coagulation [4] or ionic deposition (see below). In the case of 38% latex 84% of the tridecylic acid is bound, and if the latex is diluted to 30%, 94-100% of the tridecylic acid is bound.

These experiments therefore show that formation of insoluble products from the zinc ammine ions with the protective substances plays the principal role in latex gelation.

It was of interest to determine how far the amount of bound zinc can serve to characterize a particular latex, as in coagulation or ionic deposition [4, 5].

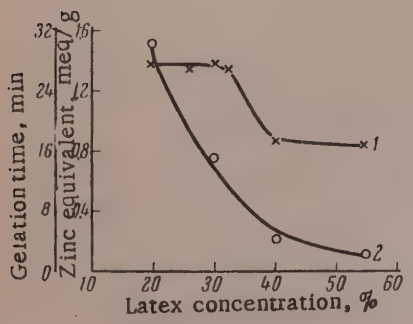


Fig. 1. Variations of the amount of bound zinc and gelation time with the concentration of L-4 latex: 1) Bound zinc; 2) gelation time.

It is known from everyday technological experience that the gelation rate of latex increases very rapidly with the amount of zinc oxide added. It was therefore also of interest to elucidate the relationship between the gelation rate and the amount of bound zinc. For this purpose the influence of zinc oxide concentration in the latex mixture and of the concentration of the latex itself on the amount of bound zinc was studied. The results (see Table 1 and Fig. 1) show that the amount of zinc bound in gelation, calculated per g of rubber, is independent of the amount of zinc oxide added. The latter has a significant influence on the gelation rate, but irrespective of the time required for gelation the amount of bound zinc depends only on the composition of the particular latex, i.e., on its content of substances which form insoluble compounds with the zinc ammine ions.

It is thus possible to speak of the zinc equivalent of a given latex, analogous to the calcium equivalent in ionic deposition [5]. However, the relationship between the cation equivalent and the latex concentration is not the same in gelation as in ionic deposition [5].

TABLE 1

Variations of the Amount of Bound Zinc and the Gelation Rate with the Zinc Oxide Content of L-4 Latex

ZnO concentration, % on the rubber	Amount of bound zinc, meq/g	Gelation time, min
13	1.48	Instantaneous
6.5	1.50	4
6.5*	1.52	20
3.75	1.52	~200

* The amount of ammonium salt was decreased in this experiment.

The existence of two regions for the diluted latex is clearly seen in Fig. 1. In each of these regions the amount of bound zinc is almost independent of the latex concentration, but dilution of the original latex in the 40-32% concentration range results in a sharp increase of the zinc equivalent. This effect may be explained as follows. With uniform distribution of the zinc oxide paste throughout the volume of the latex mixture desorption of the protective substance from the globule surfaces, which occurs on dilution of the latex, cannot influence the amount of electrolyte bound. However, dilution of the latex has a significant effect on the structure of the forming gel. In the original latex a dense and strong gel is rapidly formed, while in the dilute latex a very loose gel is formed slowly. In this case, the zinc ammine ions have time to react with almost all the protective substance in the latex. In dense gels, formed during rapid gelation from undiluted latex, the zinc ammine ions do not have time to react with all the protective substances, so that the amount of bound zinc is less. Experiments with VKh-2 latex also show that the amount of protective substance combining with the gelating ions increases with dilution of the latex.

However, it must be pointed out that the absolute amounts of bound protective substance found for latex made with tridecylic acid cannot be referred directly to latexes made with other emulsifiers. These values can be used only for comparing the effects taking place in different methods of electrolyte action on latex, such as coagulation [4], ionic deposition [5], and gelation.

It was desired to determine how the zinc equivalent depends on previous treatment of the latex, and in particular on aging and dialysis. These experiments were performed with L-4 latex.

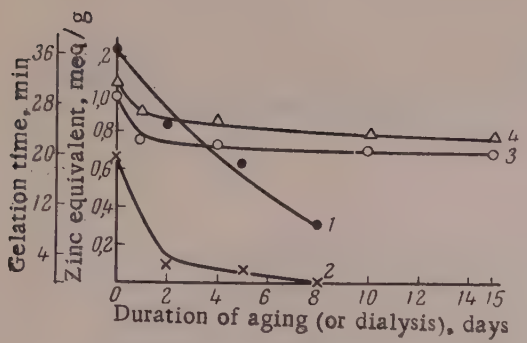


Fig. 2. Variations of the zinc equivalent and gelation time during artificial aging (at 70°) and dialysis of L-4 latex: 1) Zinc equivalent during aging; 2) gelation time during aging; 3) gelation time during dialysis; 4) zinc equivalent during dialysis.

Figure 2 shows that dialysis and aging of the latex (especially the latter) lead to appreciable decrease of the zinc equivalent and accelerated gelation. Similar effects were observed by us for the calcium equivalent in ionic deposition [5]. The hypothesis was put forward that decrease of latex stability during aging leads to particle aggregation and therefore to a decrease of the specific surface of the disperse phase. Some of the protective substance is then trapped within the aggregates and does not interact with the electrolyte.

To test this hypothesis, electron micrographs were taken of the polychloroprene latex before and after aging, and also after dialysis.*

The photographs in Fig. 3 show clearly that globule aggregation does occur during aging of the latex.

As was to be expected, removal of a part of the protective substance during dialysis of the latex reduces the zinc equivalent and increases the gelation rate, although not as much as aging does. Electron micrographs show that some aggregation takes place in this case also, although the globule retain their individuality to a greater extent.

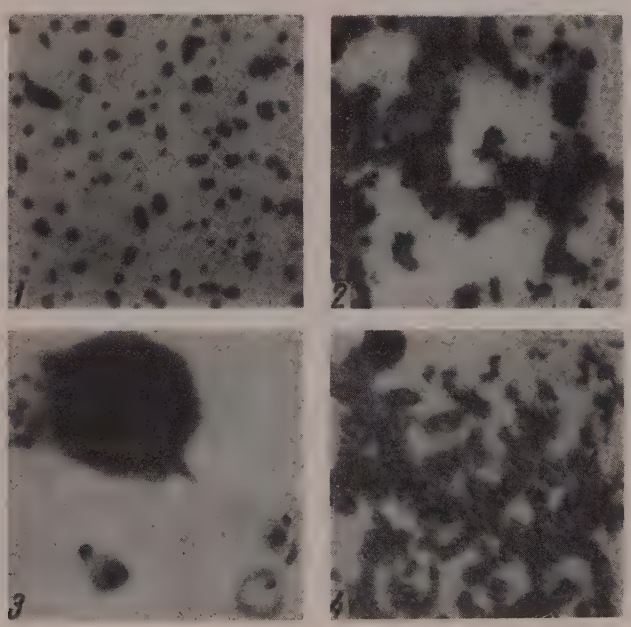


Fig. 3. Aggregation of globules in polychloroprene latex during artificial aging and dialysis (× 7500): 1) Original latex; 2) after aging for 5 days at 50°; 3) same, at 70°; 4) after dialysis for 15 days.

* We are deeply grateful to B. V. Shtarkh for taking the micrographs.

Just as decrease of the calcium equivalent accelerates ionic deposition [5], decrease of the zinc equivalent accelerates gelation.

It follows that in gelation, as in ionic deposition and in coagulation of latex by calcium chloride solutions, the protective substances react with the cations to form insoluble compounds. A coagulum or gel with a concentration and structure which depend on the conditions is formed.

It was of interest to compare the amounts of electrolyte bound in different instances. The relevant data are presented in Table 2. The amounts of protective substance bound (in experiments with VKh-2 latex) are also shown.

TABLE 2

Amounts of Bound Electrolyte and Protective Substances in Different Methods for Production of the Coagulum or Gel

Latex	Coagulation		Ionic deposition		Gelation
	calcium number	zinc number	calcium equivalent	zinc equivalent	zinc equivalent
	Amount of bound electrolyte, meq/g				
L-4	0.063	0.11	0.40	0.50	1.07
	Amount of bound tridecylic acid, %				
VKh-2	26		38		84-95

In order to compare different cations, the amounts of zinc bound by 1 g of rubber in coagulation of latex by means of $Zn^{65}Cl_2$ (the zinc number) and in ionic deposition with $Zn^{65}Cl_2$ solution as the fixing agent were determined.

More zinc than calcium salt is needed for coagulation or ionic deposition. This is probably because zinc chloride can form autocomplexes of zinc zincate ions in solution [6]. This effect also probably accounts for the slower ionic deposition if zinc is used as the fixing agent [7].

The amount of cations bound is greatest in gelation, followed by ionic deposition, and binding is least in coagulation. This is consistent with the fact that in gelation by means of zinc oxide nearly all (or most) of the protective substance present in the latex is bound, while in ionic deposition from the same latex by means of calcium chloride only approximately 38% is bound, and in coagulation, approximately 26% [4].

A possible cause of this is the difference between the rates of interaction of the protective substance and the electrolyte in these cases. In gelation by means of zinc oxide, the process is fairly slow and results in formation of a relatively loose structure through which the destabilizing ions can diffuse further and can combine with any unchanged protective substance. In coagulation, a relatively large amount of electrolyte (considerably in excess of the threshold value) is added to the latex at once, when a fairly dense coagulum is formed rapidly and prevents further diffusion of the electrolyte. Ionic deposition apparently represents an intermediate case. The gel formed is less dense than the coagulum but its concentration is lower than that of the gel formed in gelation of latex by means of zinc oxide [8, 9]. The rate of gel formation is also higher in ionic deposition than in gelation.

SUMMARY

1. It is shown that when gelation of rubber latexes is effected by means of zinc oxide the protective substances of the latex react with zinc ammine ions to form zinc salts insoluble in water.

2. The number of milliequivalents of zinc bound by 1 g of rubber (the zinc equivalent) depends on the type of latex, is independent of the amount of gelating agent added, and decreases on artificial aging and dialysis of the latex.

3. The zinc equivalent increases with dilution of the latex owing to formation of less dense gels during gelation.

4. Most of the protective substance becomes bound during gelation of the latex.

5. Aging of latex results in aggregation of the globules.

6. The amount of insoluble compounds formed by reaction of the protective substance in the latex with the electrolyte in coagulation, ionic deposition, and coagulation of latex decreases with increasing rate of destabilization of the latex and with increasing density of the coagulum or gel formed.

LITERATURE CITED

[1] R. Noble, Latex in Industry (New York, 1953).

[2] S. S. Voyutskii, R. M. Panich, and K. A. Kal'yanova, Kolloid. Zhur. 12, 50 (1950); 13, 89 (1951).

[3] M. Van den Tempel, Trans. Inst. Rubber Ind. 31, 33 (1955).

[4] D. M. Sandomirskii and M. K. Vdovchenkova, Kolloid. Zhur. 20, 80 (1958).*

[5] D. M. Sandomirskii and M. K. Vdovchenkova, Kolloid. Zhur. 20, 214 (1958).*

[6] B. V. Nekrasov, Course of General Chemistry [In Russian] (Moscow, 1953), p. 662.

[7] N. Martinon, Rev. Gen. du Caoutchouc 28, 43 (1951).

[8] D. M. Sandomirskii, in the book: Production and Uses of Synthetic Latexes [In Russian] (Moscow-Leningrad, 1953), p. 32.

[9] D. M. Sandomirskii and V. V. Chernaya, Trudy In-ta Rezinov. Prom-sti 1, 22 (1954).

* See C. B. translation.

STRUCTURE FORMATION DURING HYDRATION HARDENING OF CALCIUM OXIDES OF DIFFERENT DEGREES OF DISPERSION

E. E. Segalova, S. I. Kontorovich, and P. A. Rebinder

Institute of Physical Chemistry, Academy of Sciences, USSR,

Division of Disperse Systems

Moscow University, Department of Colloid Chemistry

(Translated from: Kolloidnyi Zhurnal Vol. 22, No. 1, pp. 74-80, January-February, 1960)

(Original article submitted August 22, 1959)

Although quicklime, recommended as a hydration mortar by Smirnov and Osin [1], has been used for more than 25 years, the mechanism of pure hydration hardening of calcium oxide is still very little understood.

It was shown in studies of the hydration of calcium oxide in dilute suspensions [2] that it has metastable solubility which ensures high degrees of supersaturation with respect to the newly-formed stable $Ca(OH)_2$. The hydration of CaO, like that of other hydration mortars and cements, consists of dissolution of the original calcium oxide and crystallization of the hydrated form, $Ca(OH)_2$, from the resultant supersaturated solution.

Studies of the hydration hardening of pure calcium oxide present considerable difficulties owing to the high heat of reaction. In studies of the hardening of lime-sand mortars hydration hardening is accompanied by formation of calcium hydrosilicate [3], which complicates studies of the hydration behavior of calcium oxide.

In the present investigation structure formation was studied with suspensions which contained large amounts of an inert filler in addition to calcium oxide, so that the water-lime ratio (W/S) could be increased (and the process of structure formation thereby retarded) without segregation taking place in the system, and the evolution of heat was reduced.

The inert filler was pure calcium carbonate; its nominal specific surface, determined by means of the Tovarov apparatus, was 0.2 m^2/g. This filler does not cause hardening in mixtures with calcium hydroxide in absence of CO_2 and is virtually without effect on the solubilities of CaO and $Ca(OH)_2$ because its own solubility is low.

The mechanical properties of the concentrated suspensions were investigated by measurements of the plastic strength by means of the cone plastometer [4]. The specimens were kept in a desiccator over saturated $Ca(OH)_2$ solution and were not protected from the action of atmospheric carbon dioxide, as it was found in special experiments that atmospheric CO_2 has hardly any effect for several hours on the hardening structure if the plastometer cone is immersed to a depth of not less than 3-5 mm for the measurements.

The rate of hydration of calcium oxide was determined in a calorimeter with an automatically-regulated adiabatic jacket [5], whereby the hydration of calcium oxide could be observed for several hours.

Figure 1 shows characteristic kinetic curves for crystallization structure formation in suspensions containing 25% CaO and 75% $CaCO_3$, and curves for the rate of hydration (found from the amount of heat evolved) of CaO in these suspensions, determined in parallel experiments.

A sharp increase of plastic strength due to crystallization of most of the $Ca(OH)_2$ is followed by a strength decrease, clearly seen at all the investigated water-solid (W/S) ratios. At W/S = 0.4 (Fig. 1, a) the strength increases instead of decreasing; the increase stops at the instant of complete hydration.

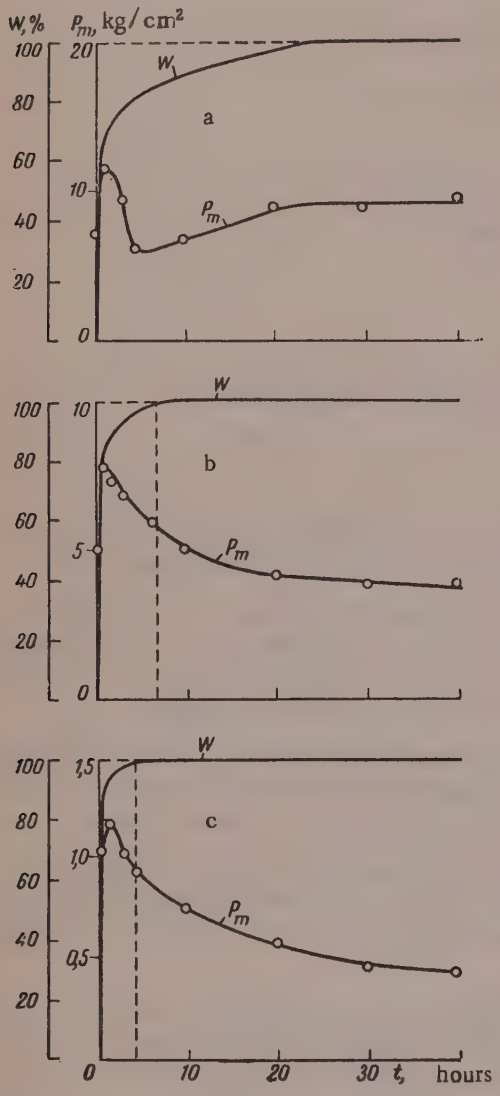


Fig. 1. Course of crystallization structure formation (P_m) and hydration (W) (from heat evolution) in CaO suspensions with S = = 3.0 m^2/g at different W/S ratios: Composition of suspension 25% CaO + 75% $CaCO_3$; a) W/S = 0.4; b) W/S = 0.5; c) W/S = 0.6.

The strength decrease observed during storage of the samples under moist conditions, occurring after the end of hydration, may be attributed (as was shown earlier [6]) to dissolution of crystallization contacts which are not in thermodynamic equilibrium. The rate of this decrease increases with increasing porosity of the sample, i.e., with increasing volume of the solution in which recrystallization processes can take place. At low W/S ratios recrystallization is very slow and the strength decrease due to dissolution of crystallization contacts is difficult to detect even if the solubility of the substance constituting the crystallization structure is fairly high. These relationships are fully confirmed in studies of the kinetics of structure formation in CaO suspensions. It follows from Fig. 1 and from the table which is based on the same data that as W/S increases the strength decrease after the end of hydration becomes more rapid. At W/S = 0.4, although there is some tendency to a fall in strength after the end of hydration, the strength values determined 12 hours after preparation of the suspension did not differ to any practical extent from the values corresponding to the instant at which hydration was completed.

In addition to this strength decrease, it follows from Fig. 1 that CaO suspensions undergo a decrease of strength before the end of hydration, i.e., during formation of the hardening structure while the newly-formed substances are crystallizing out. The rate of this strength decrease is greater at lower W/S ratios (see table); it is caused by partial breakdown of the crystallization structure at its weakest regions under the influence of stresses arising during the growth of crystals firmly bonded by concretion contacts [7].

The growth of crystals constituting the hardening structure on the one hand strengthens this structure, and on the other it gives rise to internal tensile stresses which cause partial breakdown of the structure and lower its strength. The dual nature of this process results in an inflection on the strength-increase curve (Fig. 1, a), because after partial breakdown of the structure and the associated dissipation of stresses, the predominant part is played by strengthening of the structure caused by increase in the size of its constituent crystals.

A study of the relationship between the final strength of the structure and the degree of dispersion of the original cementing material, performed with suspensions of the α and β forms of calcium sulfate hemihydrate [6] and tricalcium aluminate [8], showed that there is a certain optimum degree of dispersion at which a crystallization structure of maximum strength is formed. Since ordinary CaO is usually very finely-dispersed and therefore has an enormous total rate of solution [2], it could be assumed that the strength of the crystallization structure of $Ca(OH)_2$ would increase with decreasing dispersity of the original CaO.

For preparation of calcium oxide of different degrees of dispersion a CaO sample (calcium oxide, "pure" grade) of nominal specific surface 3 m^2/g was calcined* for 3 hours in a Kryptol furnace at 1800° and then ground in a vibratory mill to nominal specific surfaces of 0.14 and 0.51 m^2/g.

Effect of W/S Ratio on the Strength of the Hardening Structure

W/S	Plastic strength P_m, kg/cm²			Strength decrease, %	
	maximum, $(P_m)_{max}$	at instant of complete hydration, $(P_m)_{max}$	4 hours after end of hydration, $(P_m)_{max}$	$\frac{(P_m)_{max} - (P_m)_H}{(P_m)_{max}}$	$\frac{(P_m)_H - (P_m)_4}{(P_m)_H}$
0,40	12,0	9,0	9	25	0
0,50	7,5	6,0	3,8	20	37
0,60	1,2	1,05	0,45	12,5	57,1

It is known that at high temperatures calcium oxide undergoes recrystallization leading to a sharp increase in the size of the original crystals [9], and unaccompanied by changes in the crystal lattice [10]. It follows from Fig. 2, a that the rate of hydration slows down rapidly with decrease of the dispersity (S) of calcium oxide; this is probably due not only to a decrease of the total rate of solution because of the decreased total surface area of CaO, but also to increased retardation by the protective coatings formed by the newly-formed substances on the surface of the original calcium oxide particles.

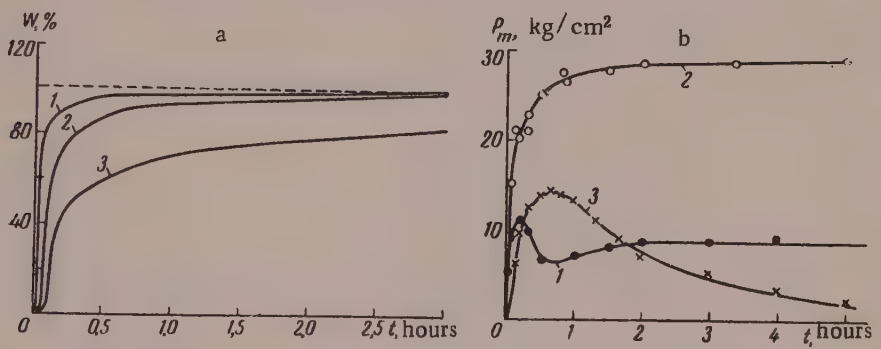


Fig. 2. Course of hydration (a) and crystallization structure formation (b) in CaO suspensions of different degrees of dispersion (S): Composition of suspension 25% CaO + 75% $CaCO_3$; W/S = 0.40; 1) S = 3.0 m^2/g; 2) S = 0.51 m^2/g; 3) S = = 0.14 m^2/g.

The strength of the crystallization structure first rises sharply with decreasing dispersity of the original CaO (Curve 2, Fig. 2, b) and then falls; structure formation in these suspensions has the following characteristics. At the initial dispersity of the CaO (S = 0.51 m^2/g) hardening is accompanied by noticeable expansion of the suspension but, as is clear from Fig. 2, b, the strength does not fall.

At S = 0.14 m^2/g the strength reaches its maximum value very rapidly, long before the end of hydration, and then begins to fall continuously; this fall is associated with considerable expansion of the suspension, which eventually disintegrates with complete loss of strength.

* The sintering of calcium oxide was carried out by us in the Refractories Institute (Khar'kov). We thank Professor A. S. Berezhnoi and Professor G. V. Kukolev for their help.

This spontaneous breakdown of the structure in the course of its development is caused by internal stresses which result in expansion of the structure and its ultimate total breakdown. The magnitude of these stresses greatly increases with decreasing dispersity of the original CaO, since the total rate of dissolution of CaO falls in the process, and therefore high supersaturations in the liquid phase are maintained for a relatively shorter time, so that the conditions are less favorable for formation of new crystallization centers and more favorable for growth of crystals which are already present. The appearance of stresses and expansion of the structure, as has already been pointed out, are due not to formation of new crystallization centers which might be located in the pores of the hardening structure, but to directed growth of crystals already linked by stable concretion contacts.

If the initial dispersity is high, most of the CaO is hydrated at high supersaturations, which leads to the formation of a crystallization structure framework consisting of very small hydroxide crystals. The relatively small amount of substance which remains for further growth of this framework, i.e., for growth of its constituent crystals, should not give rise to large stresses, because the surface on which crystallization takes place is very large. Therefore, it may be assumed that the low strength found when the dispersity of the original material is high is due to excessive comminution of the crystals which compose the crystalline hardening structure and not to the appearance of high internal stresses. Conversely, the low strength found when the original material is coarsely dispersed is due to the appearance of considerable internal stresses which accompany the hardening process and which cause partial or even complete breakdown of the structure.

These hypotheses are confirmed by the results obtained in investigations of the dependence of the strength of the hardening structure on the CaO and $Ca(OH)_2$ contents of the mixture and on the water-solid ratio, carried out at the two extreme degrees of dispersion of calcium oxide, 3.00 and 0.14 m^2/g.

Figure 3 represents variations of the specific strength, or the strength per gram of the cementing material, with the total CaO content of a mixture containing filler ($CaCO_3$). All the suspensions were prepared at the same W/S ratio, 0.4.

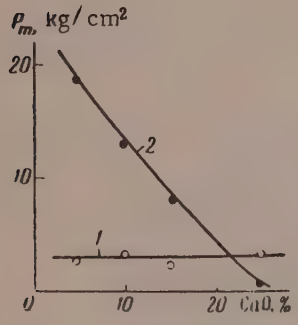


Fig. 3. Variations of the specific strength of the crystallization structure with the CaO content (%) of the suspension, at W/S = = 0.40: dispersity of the original CaO: 1) S = 3.0 m^2/g; 2) S = 0.14 m^2/g.

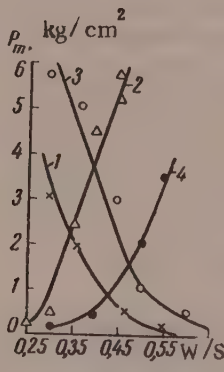


Fig. 4. Variations of the strength of the crystallization structure (at the end of hydration) with the W/S ratio of suspensions containing CaO of different degrees of dispersion (S): Compositions of suspensions 1 and 2) 10% CaO + 90% $CaCO_3$; 3 and 4) 20% CaO + + 80% $CaCO_3$; 1) S = 3.00 m^2/g; 2) S = 0.14 m^2/g; 3) S = 3.0 m^2/g; 4) S = 0.14 m^2/g.

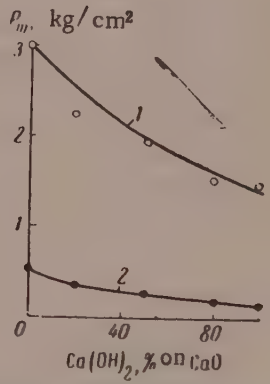


Fig. 5. Effect of additions of hydrated calcium oxide on the strength of the structure formed in CaO suspensions, S = 3.0 m^2/g: composition of suspension: 10% CaO + 90% [$CaCO_3$ + + $Ca(OH)_2$]; 1) W/S = = 0.30; 2) W/S = 0.45.

Figure 3 shows that when the dispersity of CaO is high the specific strength is virtually independent of the lime content; in other words, the final strength of the structure at the given W/S ratio is directly proportional to the content of cementing material in the sample. If the material is coarsely dispersed (Curve 2, Fig. 3) the specific strength at the same W/S ratio falls sharply with increasing CaO content in the system, as this is accompanied by increases in the internal stresses leading to breakdown of the structure.

Figure 4 represents variations of the strength of the hardening structure with W/S ratio for mixtures containing 10 and 20% CaO. In the case of the original CaO ($S^* = 3.00$ m^2/g) the strength falls sharply with increase of W/S ratio, whereas in the case of the coarse CaO ($S^* = 0.14$ m^2/g), on the contrary, the strength increases with increasing W/S ratio. This increase cannot be attributed to better placement characteristics of the mixture, as the pastes were adequately mobile in working (during sample preparation) at all the investigated W/S ratios. The internal stresses diminish sharply with increase of W/S ratio, and in this instance the resultant strength increase prevails considerably over the fall of strength due to increased porosity of the structure.

As was shown earlier [6], repeated agitation of suspensions of binding materials during structure formation or increase of the first mixing time of the suspension result in partial breakdown of the structure formed and a decrease of its final strength. A similar effect is produced by addition of hydrated lime to the suspension; this sharply accelerates hydration and structure formation and lowers the strength of the structure.

It was found that these relationships, like the usual dependence of strength on the amount of cementing material or the water-solid ratio, are valid only if the final strength of the hardening structure is not influenced decisively by the internal stresses which arise during its development. For example, in the case of highly disperse CaO, increase of the stirring time in the initial mixing leads to a very sharp decrease in the strength of the resultant structure; additions of $Ca(OH)_2$ have a similar effect (Fig. 5).

The behavior of suspensions of coarse CaO is different. Figure 6 represents the course of structure formation in a suspension of coarse calcium oxide which was stirred 30 and 60 minutes after preparation, when the strength of the original suspension had already reached its maximum value. It follows from Fig. 6 that in this instance repeated stirring results in a considerable increase of the strength of the resultant structure, as this mechanical action eliminates the stresses which cause total breakdown of the structure in the original suspension.

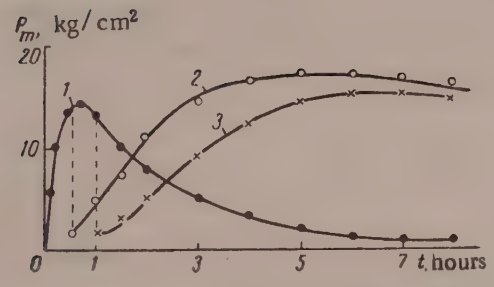


Fig. 6. Effect of the time of repeated stirring of the structure on the course of hardening in CaO suspensions, $S = 0.14$ m^2/g; composition of suspension: 25% CaO + 75% $CaCO_3$; W/S = 0.40; stirring times: 1) 1 minute; 2) 30 minutes; 3) 60 minutes.

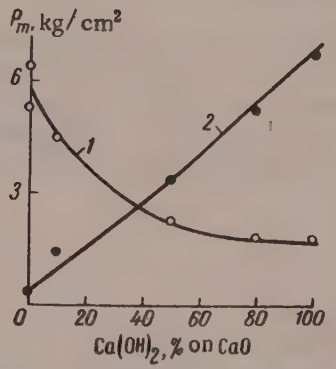


Fig. 7. Effect of additions of calcium hydroxide on the strength of the structure formed in CaO suspensions; $S = 0.14$ m^2/g; composition of suspension 10% CaO + 90% [$CaCO_3$ + $Ca(OH)_2$]. 1) W/S = 0.45; 2) W/S = 0.30.

The strength is also increased if fairly large amounts of hydrated lime are introduced into the suspension because in that case, as in mechanical stirring, there is a reduction in the number of crystallization contacts which bind together the crystals of the newly-formed substances, and this reduces the tensile stresses which arise during development of the hardening structure. It must be noted that a strength increase on addition of $Ca(OH)_2$

to the suspension is observed only at low W/S ratios, at which the internal stresses are particularly prominent, whereas at high W/S ratios, when the stresses are much lower, additions of the hydroxide to the same suspension lower the strength of the resultant structure (Fig. 7).

All these experiments show that at a given W/S ratio the internal tensile stresses are considerably more prominent if the original material is coarsely dispersed. It must be emphasized, however, that stresses occur in any process of crystallization structure formation, and they may have a decisive influence on the strength of the resultant hardening structure even if the dispersity of the original material is high. This occurs if structure formation proceeds under unfavorable conditions which favor the appearance of internal stresses; for example, at very high contents of the cementing material in the mixture or at very low W/S ratios. This is precisely what happens in slaking of quicklime, when the internal stresses completely break down the weak crystallization framework formed during the first instants of interaction of the calcium oxide with water. For a hardening structure of the maximum strength with minimum expenditure of lime (i.e., for the maximum "specific strength") it is necessary to have a certain optimum degree of fineness at which, on the one hand, the crystals of the newly-formed substances are not excessively fine, and on the other, there are no considerable internal stresses which could result in large decreases of the strength of the structure in the course of its development. The experiments described above show that the optimum fineness of the material in question should depend on the amount of it in the mixture, the water-solid ratio, and the experimental temperature, which influences both the dissolution rate of the original material and its solubility, i.e., the degree of supersaturation in the liquid phase of the suspension.

SUMMARY

1. Development of the hardening structure in calcium oxide suspensions is accompanied by appearance of internal stresses which reduce the strength of the forming structure even before hydration is complete. The strength decrease caused by the internal stresses is greater at lower water-solid ratios and at higher contents of lime in the suspension (i.e., at lower contents of filler).

If the samples are stored under moist conditions after the end of hydration, the strength decreases owing to dissolution of crystallization contacts which are not in thermodynamic equilibrium. The intensity of this process increases with increase of the water-solid ratio.

2. A hardening structure with the maximum strength is formed only at a certain optimum degree of dispersion of the original lime. The decrease of strength found when lime of a higher degree of dispersion than this is used is due to excessive comminution of the crystals composing the hardening structure, while the strength decrease at degrees of dispersion below the optimum value is the result of high internal stresses which lead to considerable or even total breakdown of the structure.

LITERATURE CITED

[1] I. V. Smirnov, Quicklime [In Russian] (Profizdat, Moscow, 1950); B. V. Osin, Quicklime as a New Cement Material [In Russian] (Industrial Construction Press, Moscow, 1954).

[2] E. E. Segalova, S. N. Kontorovich, and P. A. Rebinder, Doklady Akad. Nauk SSSR 123, 3, 509 (1958).*

[3] V. F. Abrosenkova, G. I. Logginov, and P. A. Rebinder, Doklady Akad. Nauk SSSR 115, 3, 509 (1957).*

[4] P. A. Rebinder and N. A. Semenenko, Doklady Akad. Nauk SSSR 64, 835 (1949).

[5] O. I. Luk'yanova, E. E. Segalova, and P. A. Rebinder, Kolloid. Zhur. 19, 460 (1957);* V. F. Kiselev, Proc. Conference on Cement Chemistry [In Russian] (Industrial Construction Press, 1956), p. 243.

* See C. B. translation.

[6] E. E. Segalova and V. N. Izmailova, Kolloid. Zhur. 20, 601 (1958).*

[7] E. E. Segalova, S. I. Kontorovich, and P. A. Rebinder, Doklady Akad. Nauk SSSR (1959) (in press).*

[8] E. S. Solov'eva, Dissertation [In Russian] (Moscow, 1958).

[9] J. Wuhrer, Zement-Kalk-Gips 6, 354 (1953); V. J. Asbe, Rock. Proc. 57, 2 (1954); H. R. Stalley, and S. H. Greenfeld, Industr. and Engng. Chem. 41, 520 (1949).

[10] N. P. Tabunshchikov, Trudy Vsesoyuz. In-ta Sodovoi Prom. 6 (1952); Kei-iti Aliyama, Chem. Abs. 2670 (1940).

* See C. B. translation.

EFFECTS OF DEFORMATION AND DISPERSION OF COLLOIDAL SYSTEMS IN THE VICINITY OF ELECTRIFIED SURFACES*

M. F. Serebrenaya and N. A. Krotova

Institute of Physical Chemistry, Academy of Sciences, USSR, Moscow

(Translated from: Kolloidnyi Zhurnal Vol. 22, No. 1, pp. 82-89, January-February, 1960)

(Original article submitted November 24, 1958)

Our preliminary communication is concerned with a range of phenomena which have been studied very little and which relate to the behavior of certain oleophilic colloidal systems near the surfaces of dielectrics electrified by friction. Investigation of such effects is very important not only scientifically but also from the practical aspect, as they may form the basis of certain new technological processes in which an electrostatic field causes deformation or dispersion of the elements in a colloidal system.

Spraying in an electrical field with the aid of high-tension sources is now used as a method for application of varnish and paint coatings [1]. The process is generally accompanied by formation of a highly disperse aerosol (mist), a sprayed colloidal system in which the disperse phase consists of pigment particles. This effect is highly undesirable, as it leads to losses of paint. Mists are often formed from charged paint particles when paint passes between rapidly-rotating rollers [2]. Spraying by the action of an electric field and formation of electric charge on particles formed by mechanical dispersion are allied processes which are opposite in character. In the former case, the action of an electric field causes mechanical dispersion, whereas in the second charged particles are formed as the result of mechanical dispersion.

The purpose of the present work was to study processes of the first type in relation to printing inks and certain model colloidal systems. Studies of processes taking place in such complex systems as printing inks cannot give conclusive results.

However, there are publications [3] concerned with spraying of pure solvents under the influence of high voltages. It was found that solvents with large dipole moments are sprayed more easily, whereas nonpolar solvents are dispersed with great difficulty. These experiments [3] were conducted with the aid of laboratory apparatus for paint spraying in an electrostatic field, designed on the same principle as industrial equipment.

Vannegut and Neubauer [4] designed an apparatus for spraying of liquids of low conductivity (such as distilled water, alcohol, or lubricating oils). If a potential of the order of 5-10 kv is applied to a liquid slowly dripping out of a fine capillary which is positively charged, a monodisperse aerosol can be obtained. Spraying can be effected either by direct or by alternating current. In the former case, highly charged droplets are formed at a rate of about 100 per second; they are approximately 10^{-2} cm in diameter and bear charges of the same sign. In the second case, the aerosol formed is electrically neutral as a whole, but it can be separated into two fractions with opposite charges. The authors [4] present high-speed photographs of the spraying process and attribute the observed effects to mutual repulsion of like charges on the surface of the charged drops emerging from the capillary. The repulsion forces act in the opposite direction to the forces of surface tension. If the total charge is high enough the repulsion forces overcome surface tension and the drop begins to disintegrate.

* Presented at the Fourth All-Union Conference on Colloid Chemistry, Tbilisi, 1958.

The spraying effect can also be achieved without the use of high-voltage sources; this was demonstrated in our experiments which are described in this paper. The experiments were performed as follows.



Fig. 1. Drop of liquid petrolatum near an electrified surface; the tip of the needle carrying the drop is in contact with the surface (a), and at a distance from the surface (b); the effect does not occur.

A stationary drop hanging from the point of a needle or the tip of a capillary was placed near the polished surface of an ebonite block, charged by friction against a chamois roller rotated by an electric motor at 1500 rpm. The treatment time was 10 minutes. The potential of the surface was of the order of 100-200 v (measured by means of an electrostatic voltmeter). It was found experimentally that the surface potential remains unchanged with increase of the treatment time under these conditions. The sign of the charge, determined by means of an electronic electroscope, was negative.

If an electrified surface is brought toward a drop of liquid petrolatum on the point of a needle, the drop remains stationary even if the projecting point of the needle touches the ebonite surface (Fig. 1). However, if the electrified surface is brought toward a drop of 5% suspension of carbon black in liquid petrolatum, the drop becomes deformed and begins to slide off the needle point (Fig. 2, a); under certain conditions it becomes dispersed (Fig. 2, b). The drop may be caused to pulsate if the ebonite surface is periodically moved toward and away from it. As the dispersion medium remains inert near the electrified surface, it may be regarded as a dielectric medium in which particles of a conducting disperse phase move under the influence of the field; these particles may draw the medium along with them in their motion.

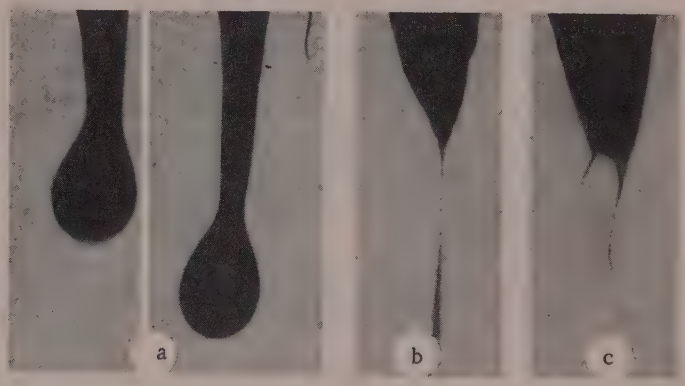


Fig. 2. Drop of carbon black suspension in liquid petrolatum; flow of drop from the tip on approach to an electrified surface (a); spraying of drop from the tip (b); rotation of the centers of spraying of the drop (c).

High-speed motion photography was used for investigating the observed processes of drop deformation and spraying. The SKS high-speed camera (with a magnifying sighting device for focusing directly onto the film) was used. The filming rate was varied between 800 and 1500 frames per second. The time was recorded with the aid of a periodically-flashing neon lamp (with a half period of +0.01 second when supplied with mains alternating current).

Shadow photography was used, with the light source placed behind the objective; in another method the object was illuminated by a powerful source. The former method was more convenient for studying drop deformation and spraying processes. The process of spray printing in an electric field, studied by us for the first time, was investigated by the second method. Heat filters ($CuSO_4$ solution) were used to prevent heating of the specimens by the light sources. The linear dimensions of the images on the frames were measured by means of

the MIR-1 comparator. The number of particles sprayed in unit time was determined by projection of the frames onto a screen by a narrow-film projector. In certain cases, the linear dimensions were also measured on a screen or by means of a frame analyzer.

Suspensions of carbon black in liquid petrolatum were used in the investigation. Spheron black with a specific surface of 120 m^2/g and thermal black with a specific surface of 45 m^2/g were used. The suspensions were prepared in two stages: First weighed quantities of the black were ground in a mortar with small amounts of liquid petrolatum and a few drops of oleic acid as stabilizer, and the rest of the petrolatum was then added. Suspensions of other substances were investigated in addition to carbon black.

Under these experimental conditions, drop deformation and spraying is observed clearly only with a conducting disperse phase in a nonconducting dispersion medium. If the disperse phase has the properties of a dielectric the effect is either absent or is very weak. Suspensions of semiconductors in general behave similarly to suspensions of conductors.

In addition to the systems described above, printing inks were also tested; primarily black newspaper ink in which the pigment is carbon black, and also a number of colored inks containing both mineral and organic pigments. Undiluted industrial inks did not exhibit the effect, probably because of their high viscosity. The effect was observed very distinctly when the inks were diluted with machine oil in 1:5 ratio. After being aged for a year the inks became quite inactive and did not exhibit any deformation effects in an electric field (under the experimental conditions used). The loss of the properties initially observed in the ink might have been attributed to formation of a three-dimensional structure (the so-called "resinification" of the ink), breakdown of which would require additional force. This process should evidently be accompanied by changes in the structural and mechanical properties of the ink. However, determinations in the Veiler-Rebinder apparatus showed that the inks after aging did not have structural viscosity.* It is possible that more delicate methods might reveal structural and mechanical differences between an inactive aged ink and a fresh ink.

Application of the methods of high-speed motion photography to studies of the behavior of a certain small volume of a colloidal system in an electric field made it possible to establish different types of processes taking place and to perform certain quantitative determinations.

Two principal processes may be observed in suspensions of carbon black.

1. Detachment of large drops, assuming a spherical shape in flight, drop diameter 3-6 mm.

2. Detachment of small droplets in rapid succession (at an average rate of 100 droplets per second). The droplet size varies between 0.1 mm and 10^{-3} mm. Very often, it is possible to observe formation of small droplets (spraying) which begins immediately after the fall of a large drop. The two processes may alternate. Addition of a stabilizer (oleic acid) to the carbon-black suspension has little influence on its behavior in an electric field; however, it is evident that in a stabilized suspension which does not separate out the carbon particles move only under the influence of the field, whereas in an unstabilized suspension sedimentation also occurs.

The experiments showed that the finer suspension of Spheron black tends to give predominant spraying in an electric field, whereas a suspension of the coarser thermal black forms large drops. Suspensions of Spheron black sometimes exhibit an interesting type of spraying — the centers of spraying migrate over the drop surface and appear to rotate; this is seen especially clearly when a film is examined (Fig. 2, c). This effect is in all probability due to local heterogeneity of the electric field.

Printing inks are systems with elasticoplastic properties and considerably higher viscosity than the model suspensions of carbon black studied. The same processes of drop detachment and spraying may be observed in printing inks as in suspensions of carbon black, but the detaching drops and droplets become elongated in flight. This is because during the short time of flight (of the order of 10^{-2} - 10^{-3} second) the drop of ink which is deformed during detachment cannot attain an equilibrium spherical shape, as the time of stress relaxation in the drop is considerably more than the duration of its flight.

* The determinations were performed by N. N. Serb-Serbina.

The effects associated with the elasticoplastic properties of the system include the observed pronounced deformation of a hanging drop with the formation of an elongated element which gradually extends toward the electrified surface and eventually touches it. In Fig. 3, the deformation L of such an element is plotted against the distance h from the electrified surface. Evidently, here the deformation is a function of the force of electrostatic attraction. The formation and deformation of such elements is seen especially clearly when the mass of the drop is fairly large and the drop is attached to a flat base. This effect may form the basis of a method of electrostatic printing with transfer of the ink from the form to the paper.

As the electrified surface approaches printing ink contained in a capillary, the ink meniscus begins to pulsate. The pulsation has a period of the order of 10^{-2} second and amplitude A from 0.01 to 0.12 mm (Fig. 4). These effects may be attributed to periodic charging and discharging of the surface [5].

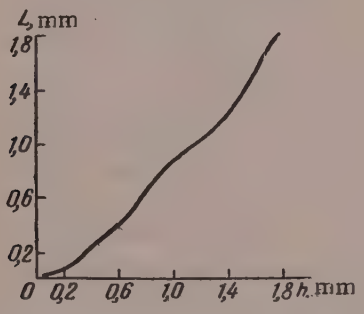


Fig. 3. Deformation of an element of printing ink as a function of the distance from an electrified surface.

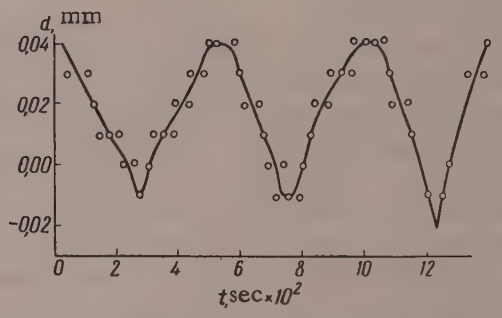


Fig. 4. Pulsation of ink meniscus near an electrified surface; d) changes of the meniscus level, mm.

If a drop of ink is placed on paper placed on an electrified surface, the drop assumes a branched or spiral shape, evidently conforming to the distribution of the lines of force of the field, which is in general homogeneous but which reveals local concentrations of lines of force (Fig. 5).

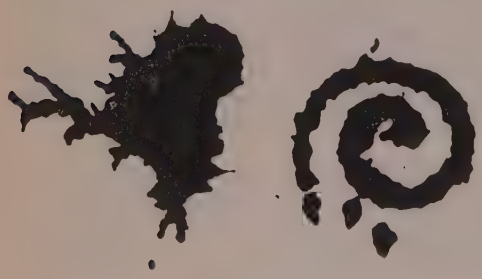


Fig. 5. Drops of printing ink placed on an electrified surface.

In interpretation of these effects observed in carbon-black suspensions and printing inks it must be remembered that both volume and surface processes may take place under the experimental conditions. The volume processes comprise deformation and detachment of a certain element of the colloidal system under the influence of electrical forces. The surface processes consist of formation, at the surface of this element, of minute droplets in the region of maximum concentration of the lines of force of the field. The resultant mist sometimes consists of such fine particles that the spraying cannot be detected by our methods of high-speed photography with enlargement during the filming or on a screen. However, the fine mist is revealed on paper, placed on the electrified ebonite surface, as a very fine spray in the form of a corona. Under slight, often undetected, changes in the experimental conditions a drop which is initially deformed begins to disintegrate. Alternation of the deformation and spraying processes may be explained as follows. In model colloidal systems (suspensions of carbon black) the pure solvent (liquid petrolatum) does not undergo any appreciable changes in the electric field. If it contains a conducting disperse phase (particles of carbon black), this phase becomes charged by induction, with a charge of opposite sign, near the electrified ebonite surface and is attracted by the latter. This causes deformation and displacement of the drop as a whole. As a result, the first drop is usually detached. In the following detaching drops the disperse phase is already displaced to a considerable extent and is concentrated at the surface directed toward the ebonite, and concentration of similarly-charged particles causes their mutual repulsion.

As a result (as in the experiments of Vannegut and Neubauer) very minute droplets rapidly leaving the needle point are formed. It follows that the surface charge must reach a critical value for spraying to begin. Printing inks also undergo spraying in the field of an electrified surface and, as in the case of the model colloidal systems studied, detachment of large drops alternates with spraying.

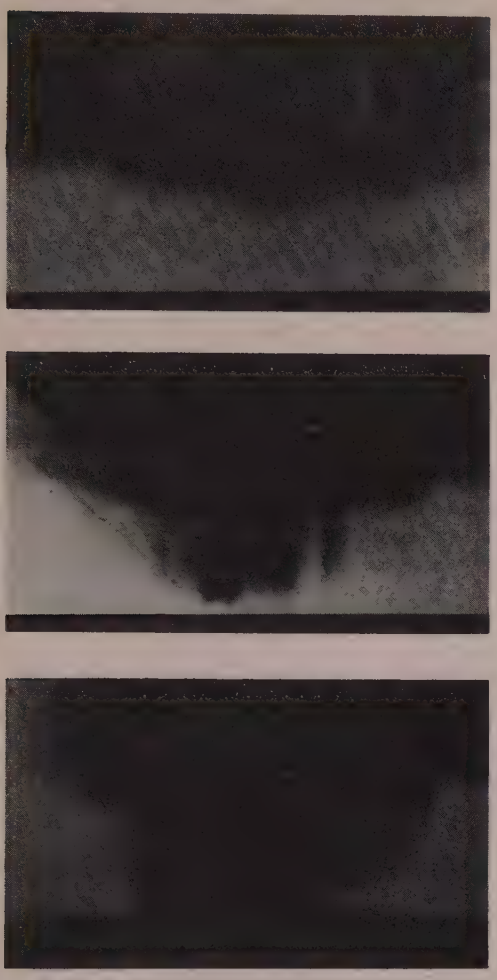


Fig. 6. Transfer of ink from type face to paper; high-speed frames; end view.

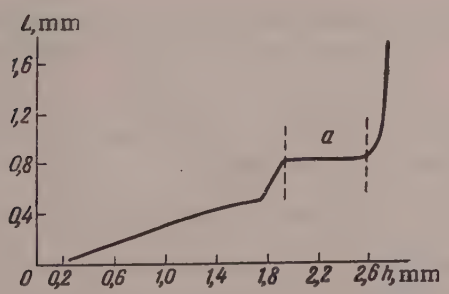


Fig. 7. Variation of the deformation L of an ink element with the distance h from the electrified surface; a) is the spraying region.

This behavior of printing ink near an electrified surface is of interest with regard to practical applications. Deformation and transfer of elements of the ink from the support to an electrified surface can be used for printing in an electrostatic field without use of pressure. The formation of minute droplets which fall on a moving electrified field in the form of a fine fog can be used as the basis for a new technological process of spray printing in an electrostatic field. If the surface is stationary, this method can be used for producing a very fine surface spray.

Printing is usually effected by pressure of inked type face on paper. The ink adheres to the paper, while its inner layers are broken. Thus, both the adhesive and the cohesive properties of the ink play a predominant part in the printing process. Close contact between the ink particles and the paper, which is effected by pressure, is required for adhesive bonding between them.

The principle of contactless printing is that the particles are charged by induction near an electrified paper surface and are attracted to it, forming a stable adhesive bond.

The transfer of printing ink from type was also studied by high-speed photography. The type (letter H) coated with newspaper black ink was fixed in a clamp and an electrified ebonite surface with a strip of printing paper fixed on top was brought up to it from below. At a definite distance, it could be seen that the ink was drawn out from the projecting regions of the type and transferred to the paper surface. The transfer of the principal and subsidiary lines in the type was not simultaneous because of the difficulties in ensuring that the planes of the paper and the printing type were parallel (Fig. 6). This main process is accompanied by partial spraying of the ink, as shown by examination of the photographic frames (Fig. 7). The prints obtained by this method are of the appearance shown in Fig. 8.

Trials of this method for printing were carried out with the aid of a simple laboratory unit in which charging was effected by friction of a rapidly-rotating ebonite ring against a chamois pad. A strip of paper is wound from one roller onto another and slides slowly over the ring. The printing type consists of squares of different areas. The type is fixed on a metal ring of the same diameter as the ebonite ring. When contact is established as the result of transfer of ink to the paper across the narrow gap between the type and the paper, the metal roller begins to move in a direction opposite to that of

the paper, but at the same speed, leaving an imprint. This unit represents the first attempt in this direction, and gives very imperfect although quite conclusive results. It is important to note that transfer of the ink and production of an imprint occurs without the use of high-tension sources.*

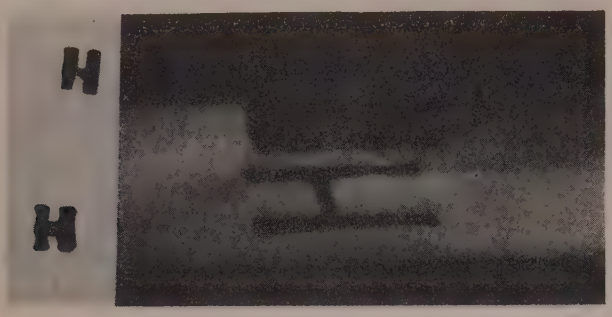


Fig. 8. Imprint of the letter H formed in an electric field.

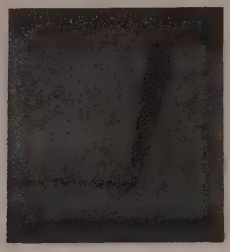


Fig. 9. Transfer of ink onto a moving paper strip.

When an electrified surface with an attached paper strip moves relative to a spraying drop of printing ink, a very fine dotted line remains on the paper, with regular alternation of large and small drops (Fig. 9). If the surface is in translational and vibratory motion, it is possible to obtain a sinusoidal curve or to record any displacements on a plane. This principle may be applied to the operation of a recording device which operates without contact between the paper and the stylus; this is evidently a considerable advantage, as friction between paper and stylus is eliminated.

The recording is effected by means of simple equipment consisting of an ebonite ring driven by a motor; a paper band slides slowly over this ring and is wound onto a takeup roller. The band is electrified by friction against the rapidly-rotating ebonite roller so that its inner surface is negatively charged. The ink is contained in a curved capillary fixed on a support so that its tip is close to the inner surface of the paper band; the ink is transferred onto the band in the form of a dotted line a few microns thick.

SUMMARY

1. Deformation of small volumes of carbon-black suspensions in liquid petrolatum and of printing inks in the uniform field of an electrified surface is attributed to migration of charged particles of the disperse phase, carrying the dispersion medium with them, toward the surface.

2. In absence of a disperse phase the solvent (under the experimental conditions used) does not react to the approach of a charged surface.

3. When sufficient charged particles have accumulated at the drop surface the drop disintegrates as the result of repulsion of like charges and decrease of surface tension. Deformation and disintegration (spraying) occur alternately.

4. High-speed photography was used to measure the deformation as a function of the distance from the charged surface, the dimensions and shape of the sprayed particles, and the rate of spraying.

5. The observed effects may be applied in contactless printing and electrostatic spray printing.

We thank Corresponding Member of the Academy of Sciences, USSR, B. V. Deryagin for valuable advice, and N. E. Golynskaya and B. A. Fadeev for assistance in the experimental work.

* Experiments were recently carried out on transfer of printing ink from a printing surface with application of potentials from 1.5 to 2.5 kv at a distance of several millimeters between the printing surface and the paper.

LITERATURE CITED

[1] M. N. Livshits, Electrical Methods of Painting, Enameling, and Glazing [In Russian] (Industrial Construction Press, 1956); R. Tilney, Metal Finishing J. 2, 274 (1956); Kipling, J. Oil and Color Chem. Assoc. 39, 641 (1956); S. Panzer, Ind. Lack Betrieb 2, 3137 (1957).

[2] B. A. Berezin, Printing Papers and Their Applications [In Russian] (1949); B. A. Berezin and A. A. Zagorinskaya, Printing Materials [In Russian] (Art Press, Moscow, 1955).

[3] Q. Osami, J. Electrochem. Soc. Japan 22, 1, 20 (1954); 24, 5, 229 (1956).

[4] Tanks, Phys. Rev. 48, 562 (1935); B. Vannegut and R. Neubauer, J. Coll. Sci. 7, 616 (1952).

[5] N. A. Kantsov, Corona Discharge and Its Use in Electrical Filters [In Russian] (State Tech. Press, 1947).

EXPERIMENTAL INVESTIGATIONS OF THE SCATTERING OF LIGHT BY A COAGULATING AEROSOL

O. M. Todes, V. F. Fedortsev, and A. A. Chekunov

Leningrad

(Translated from: Kolloidnyi Zhurnal Vol. 22, No. 1, pp. 90-96, January-February, 1960)

(Original article submitted September 17, 1958)

In an earlier paper [1], we derived a simple interpolation relationship for the effective cross section of light scattering $F\,(cm^2)$ by aerosol particles, in the form

$$F = \frac{B\omega^2}{1 + \frac{B}{A}\omega^{4/3}}, \tag{1}$$

where the numerical coefficient $A = \sqrt[3]{\frac{9\pi}{2}} = 2{,}42$; $\omega = \frac{4}{3}\pi r^3$ (cm^3) is the volume of a particle; B is a coefficient which depends on the wavelength λ of the scattered light (cm) and the refractive index $\underline{m}$ of the particle material in accordance with the equation

$$B = \frac{24\pi^3}{\lambda^4}\left(\frac{m^2 - 1}{m^2 + 1}\right)^2. \tag{2}$$

In the limiting cases of small and large particles, Eq. (1) passes into the equations for Rayleigh [2] and geometrical [3] scattering respectively, while in the intermediate range of particle sizes, of the same order as the wavelength ($\omega \approx \lambda^3$), the theoretical diffraction peaks are smoothed out. This smoothing corresponds to real conditions, since in practice it is necessary to use light which is not strictly monochromatic and polydisperse aerosols.

The linear coefficient of light scattering $K\,(cm^{-1})$ for a polydisperse aerosol medium of particle concentration $N\,(cm^{-3})$ and weight concentration $M\,(g \cdot cm^{-3})$, with average particle volume ω and particle density $\delta\,(g \cdot cm^{-3})$ may be calculated from the equation

$$K = FN = F\frac{M}{\delta \cdot \omega}. \tag{3}$$

Equations (1) and (3) give the final interpolation equation for the so-called hiding power $(K/M,\ cm^2/g)$ of an aerosol as a function of the average particle volume ω:

$$\frac{K}{M} = \frac{B}{\delta}\frac{\omega}{1 + \frac{B}{A}\omega^{4/3}}. \tag{4}$$

In a real polydisperse aerosol medium the average particle size is changing continuously. It has been shown [4] that the particle concentration of an aerosol contained in a constant volume varies, owing to coagulation, with the time t (seconds) according to the asymptotic law:

$$\frac{1}{N} = \frac{8{,}8\,kT}{3\eta}\,t, \tag{5}$$

where η is the viscosity of air, k is the Boltzmann constant, and T is the absolute temperature.

The expression $\frac{8.8\ kT}{3\eta}$, the coagulation constant for a polydisperse aerosol, is 10% greater than the constant calculated by Smoluchowski [5] for a monodisperse aerosol. Accordingly, the average particle volume at time t is given by the expression:

$$\omega = \frac{M}{\delta N} = \frac{8{,}8\ kT}{3\eta}\,\frac{M}{\delta}\,t. \tag{6}$$

In an aerosol cloud spreading in the atmosphere, the particle concentration alters owing to simultaneous processes of coagulation and growth of the cloud volume. For a cloud formed from a linear source, this alteration is represented by the equation [6]:

$$\frac{1}{n} = \frac{1}{NV} = \frac{1}{n_i}\left(1 + \frac{K_C N_0 x_0}{u}\ln\frac{x + x_0}{x_0}\right), \tag{7}$$

where n is the number of particles in volume V; n_i is the number of particles in the initial volume of the cloud which has spread to a distance x_0 from the source; N_0 is the initial particle concentration of aerosol in the cloud; x is the distance traversed by the cloud during its time of existence t (seconds) under the influence of wind of velocity u (cm/second); K_C is the coagulation constant.

Accordingly, the average particle volume ω in the cloud at a distance $x = ut$ from the source is

$$\omega = \omega_i\left(1 + \frac{K_C N_0 x_0}{u}\ln\frac{x + x_0}{x_0}\right), \tag{8}$$

where ω_i is the initial particle volume.

By substituting the values found for ω into Eq. (4), we can find the hiding power of an aerosol medium at a given instant t.

For an aerosol medium coagulating in a constant volume (V = const), after introduction of the scale

$$\omega_0 = \left(\frac{A}{B}\right)^{3/4} = \frac{\lambda^3}{4\pi^2\sqrt[4]{12}}\left(\frac{m^2+2}{m^2-1}\right)^{3/2} \tag{9}$$

and the dimensionless variables

$$\theta = \frac{\sqrt[4]{12}}{6\pi}\cdot\frac{K\delta\lambda}{M}\left(\frac{m^2+2}{m^2-1}\right)^{1/2} = \frac{K\delta\lambda}{10{,}1\,M}\left(\frac{m^2+2}{m^2-1}\right)^{1/2} \tag{10}$$

and

$$\tau = \frac{\omega}{\omega_0} = \frac{8{,}8}{3}\,4\pi^2\sqrt[4]{12}\,\frac{M}{\delta}\,\frac{kT}{\eta\lambda^3}\left(\frac{m^2-1}{m^2+2}\right)^{3/2}t = 215\,\frac{M}{\delta}\,\frac{kT}{\eta\lambda^3}\left(\frac{m^2-1}{m^2+2}\right)^{3/2}t, \tag{11}$$

all the constant factors in Eq. (4) cancel out and it assumes the simple form:

$$\theta = \frac{\tau}{1 + \tau^{4/3}}, \tag{12}$$

without the numerical constants incorporated in the scales of the dimensionless variables.

For an aerosol medium spreading in the atmosphere ($V \neq$ const) the value of θ in Eqs. (4), (8), and (10), is given by an expression similar to (12) but with the value

$$\tau = \tau' = \left(\frac{B}{A}\right)^{3/4} \omega_1 \left(1 + \frac{K_c N_0 x_0}{u} \ln \frac{x + x_0}{x_0}\right). \tag{13}$$

The relationship (12) is plotted in Fig. 1. The curve has a maximum for $\theta = \frac{3^{3/4}}{4} = 0.57$ at $\tau = 3^{3/4} = 2.28$. By returning to dimensional coordinates, we can find the maximum hiding power of the aerosol

$$\left(\frac{K}{M}\right)_{\max} = \frac{5{,}76}{\delta\lambda} \sqrt{\frac{m^2 - 1}{m^2 + 2}}. \tag{14}$$

In coagulation at constant volume the time required to reach this maximum is

$$t_{\max} = 0{,}0106 \frac{\delta}{M} \frac{\eta\lambda^3}{kT} \left(\frac{m^2 + 2}{m^2 - 1}\right)^{3/2}. \tag{15}$$

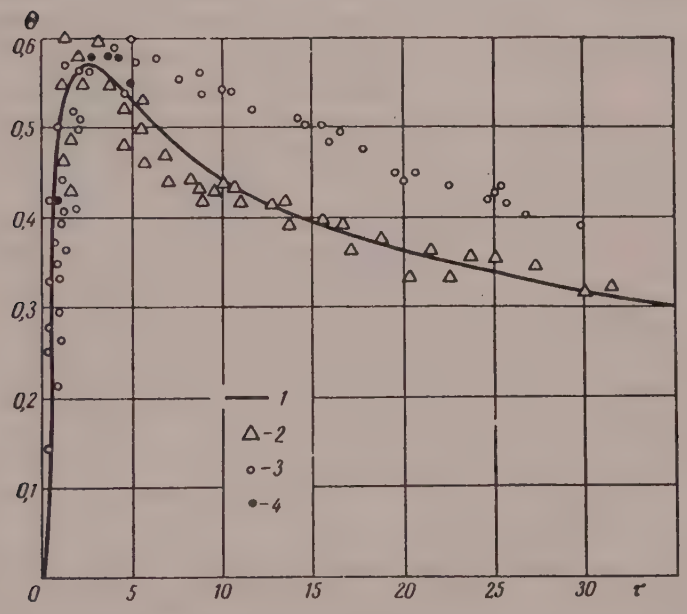


Fig. 1. Theoretical relationship between θ and τ, and experimental data: 1) Theoretical relationship; 2) sulfuric acid mist; 3) phosphoric acid mist; 4) oil mist.

Equation (12) was derived previously [1] by a more complicated method, from the complete particle-size distribution curves of the coagulating aerosol. Unfortunately, some errors crept into the numerical coefficients of the variables θ and τ.

It follows from Eqs. (14) and (15) that increase of the weight concentration M of the aerosol does not alter the maximum hiding power, but results in a proportional decrease in the time required to reach $(K/M)_{max}$ owing to a corresponding acceleration of coagulation. Increase of the refractive index m increases the maximum hiding power in proportion to $\sqrt{\frac{m^2-1}{m^2+2}}$, and reduces the particle volume ω_0 at which this maximum is reached by a factor of $\sqrt{\left(\frac{m^2-1}{m^2+2}\right)^3}$

Accordingly, the time required to reach ω_0 and $(K/M)_{max}$ is also reduced by a factor of $\sqrt{\left(\frac{m^2-1}{m^2+2}\right)^3}$ Finally, with increase of the wavelength λ of the scattered light $(K/M)_{max}$ decreases in proportion to λ, while ω_0 and t_{max} increase in proportion to λ^3.

In coagulation and scattering of an aerosol in the atmosphere the type of variation of θ with the distance depends significantly on the values $Q = \omega_1 (B/A)^{3/4}$ and $\rho = \frac{K_c \cdot N_0}{u/x_0}$.

The function $\theta = f\left(\frac{x+x_0}{x_0}\right)$ for $Q = 1$ and $\rho = 0.5$, 1.0, and 2.0, is plotted in Fig. 2.

Figure 2 shows that under these conditions the hiding power of aerosol particles in a cloud spreading in the atmosphere changes little. This is due to the influence of scattering of the cloud on particle growth as the result of coagulation. With increase of ρ, which represents the ratio of the coagulation rate to the scattering rate, the time required to reach maximum values of K/M becomes less, and reduction of the hiding power during subsequent motion of the aerosol particles becomes more pronounced.

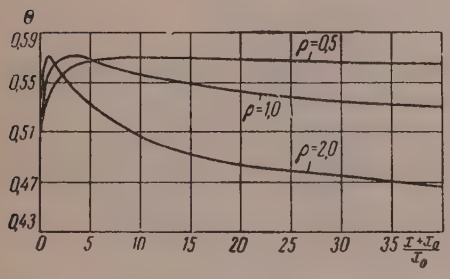


Fig. 2. Variation of the optical properties of aerosol particles in a cloud scattering in the atmosphere.

To verify these qualitative conclusions and the quantitative results given by our theory special experiments were carried out in order to determine the scattering of light by various aerosols coagulating at constant volume, at different weight concentrations, and at values of λ in the visible and infrared regions of the spectrum. The latter condition was due to the desire to obtain experimental data not only for the descending ($\tau > 2.28$) but also for the ascending ($\tau < 2.28$) branch of the curve in Fig. 1. The experiments were conducted in a specially-equipped chamber with aerosols of sulfuric and phosphoric acids, and with fumes of heavy oil (mazut).

Mazut fumes were made by evaporation of mazut (average boiling point 360°) with subsequent condensation of the vapor on admission of the heated stream into the cloud chamber. Sulfuric acid aerosols were made by evaporation of definite weights of liquid sulfur trioxide on a heated metal surface. Phosphoric acid aerosols were made by combustion of weighed amounts of phosphorus directly in the chamber. Large evaporation and combustion surfaces were used in order to ensure that the substance was converted into aerosol form in a relatively short time, not greater than 15-20 seconds. Special propeller stirrers were used to distribute the aerosols throughout the chamber space as uniformly as possible.

The duration of each experiment was considerable, up to 60-80 minutes, because it was required to observe variations of the aerosol hiding power with time. In such long time intervals, the weight concentration of an aerosol diminishes appreciably owing to sedimentation and deposition of the larger particles on the chamber walls. In the case of mazut fumes, because of the heterogeneous composition, the more volatile fractions gradually evaporated.

In the case of the strongly hygroscopic aerosols of sulfuric and phosphoric acids further growth of the particles was possible owing to the moisture present in the chamber.

Because of all these factors and the duration of the experiments, the condition M = constant on which the derivation of the theoretical Eq. (12) was based was not fully satisfied. Accordingly, samples of the aerosols were

taken at intervals of 5-10 minutes on filters, and the concentrations M_t at those instants were determined and correlated with the corresponding extinction coefficients K_t, determined simultaneously.

The apparatus for determination of the radiant energy intensity I was placed at a definite distance l from a source emitting a parallel light beam. K was calculated from the equation:

$$K = \frac{2.3}{l} \log \frac{I_0}{I}, \tag{16}$$

where I_0 is the instrument reading in absence of the aerosol.

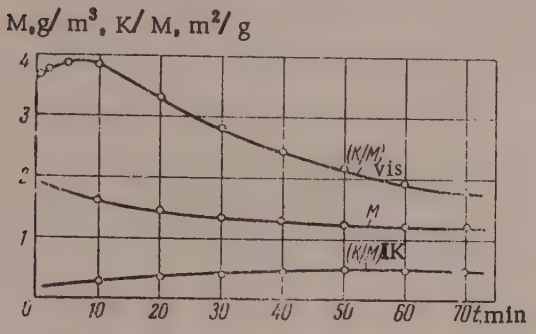


Fig. 3. Variations of M and K/M in a phosphoric acid mist.

The intensity of visible light was determined by a selenium photoelectric cell with a correcting filter which reduced the spectral characteristics of the cell to the sensitivity of the human eye. In accordance with this the wavelength in the determinations in the visible region of the spectrum was taken to be $\lambda = 0.55\ \mu$.

The source of infrared radiation was a heated Silit resistor, and the receiver was a thermopile. An interference light filter was used to isolate the spectral region between 3 and 4 μ, with a sharp transmission maximum at the calculated wavelength $\lambda = 3.4\ \mu$.

The results of one of the experiments with phosphoric acid mist are plotted in Fig. 3.

In analysis of the experimental data the density (δ) of mazut was assumed to be 0.95 g/cm³, and the refractive index was found to be 1.5. The sulfuric acid mist at 40-45% moisture content and 16-18° was calculated to have the equilibrium composition 60-65% H_2SO_4; the density was taken to be $\delta = 1.5$ g/cm³, and the refractive index m = 1.39. For the phosphoric acid aerosols under the experimental conditions $\delta = 1.42$ g/cm³, m = 1.35.

Value of the Coefficients α and β on the Visible of the Spectrum for Analysis of Aerosols

Aerosol	α $\frac{g}{m^2}$	β $\frac{m^3}{g \cdot min}$
Mazut fumes	0.097	2.9
Sulfuric acid mist	0.168	1.33
Phosphoric acid mist	0.166	1.21

If Eqs. (10) and (11) are written in the form

$$0 = \alpha \frac{K}{M} \text{ and } \tau = \beta Mt$$

the values given in the table are found for the coefficients α and β after substitution of the corresponding values of δ and m, in the visible region of the spectrum.

To calculate the coefficients α and β for the infrared region, it is necessary to know the refractive index at $\lambda = 3.4\ \mu$. Owing to lack of such data, we had to modify somewhat the analysis of the experimental data by introduction of a new variable:

$$z = 0\tau^{1/3} = \frac{\delta}{10,1} \sqrt[3]{215 \frac{kT}{\delta\eta}} \cdot \frac{K}{M} (Mt)^{1/3}, \tag{17}$$

which does not include the refractive index. It follows from Eqs. (12) and (17) that

$$z = \frac{\tau^{4/3}}{1+\tau^{4/3}} \quad \text{or} \quad \tau = \left(\frac{z}{1-z}\right)^{3/4} \tag{18}$$

In other words, the value of $\left(\frac{z}{1-z}\right)^{3/4}$ calculated from the experimental data by Eqs. (17) and (18) is directly proportional to the product Mt, while the ratio

$$\frac{\left(\frac{z}{1-z}\right)^{3/4}}{Mt} = \frac{215\,kT}{\delta\eta\lambda^3}\left(\frac{m^2-1}{m^2+2}\right)^{3/} \tag{19}$$

remains constant. According to the results of some experiments with phosphoric acid mist, this ratio for the middle region of the curve varied between 0.020 and 0.012, and had the average value of 0.016 $m^3 \cdot g \cdot$ minute. The refractive index calculated from Eq. (19) for phosphoric acid in the infrared region of the spectrum was m = = 1.9. By taking this value, we find for θ and τ in the infrared region:

$$\theta = 0{,}7\,\frac{g}{m^2} \cdot \frac{K}{M} \text{ and } \tau = 0{,}016\,\frac{m^3}{g \cdot \text{min}} \cdot Mt. \tag{20}$$

In our experiments the initial weight concentrations M of the aerosols were varied between 3.1 and 0.08 g/m^3. The weight concentration fell by 30-40% in 80 minutes.

The results of a series of experiments, recalculated in accordance with Eqs. (10) and (11), are presented in Fig. 1. In the calculations the experimental values of the extinction coefficients of the radiant energy in the visible region of the spectrum were diminished by 10% to allow for light absorption by aerosol particles of mazut and phosphoric acid, and by 30% in the case of sulfuric acid [7]. Figure 1 shows that the experimental variations of the hiding power with time are close to the theoretical. The results of other experiments give a similar fit with the theoretical curve.

Since λ^3 in the infrared region is 236 times the corresponding value for the visible region, it follows from Eq. (10) that the time scale is very much extended. Accordingly, the experimental data lie on the left-hand portion of the theoretical curve, before the maximum.

The experimental values of θ for phosphoric acid mist in the visible region lie somewhat above the theoretical curve, probably because the published values for light absorption by particles [7] are somewhat low, and the τ scale is somewhat too high.

In view of the fact that in our experiments the weight concentration M gradually decreased and variations of the particle composition and refractive index m during the experiments were difficult to estimate, the agreement of the experimental data for different aerosols with the theoretical expression (12) must be regarded as satisfactory for a very wide range of the determining parameters (the initial weight concentration varied from 3.1 to 0.08 g/m^3, and the wavelength from 0.55 to 3.4 μ).

Equation (12) can therefore be recommended for approximate calculation of changes in the hiding power of a coagulating polydisperse aerosol with time, over a wide range of wavelengths of the scattered light and of weight concentrations of the aerosol.

SUMMARY

1. It is shown theoretically that increase in the size of aerosol particles due to coagulation changes the degree of light extinction. This change is represented by Eq. (12). For coagulation at constant volume the dimensionless time parameter is determined from Eq. (11), and for coagulation in a cloud which is being dispersed in the atmosphere, from Eq. (13).

When a cloud is scattered in the atmosphere, coagulation at some distance from the source leads to only slight changes in the size of the aerosol particles. Accordingly, the changes of their optical properties are also slight.

2. The theoretical Eq. (12) was confirmed experimentally by experiments with aerosols of sulfuric and phosphoric acids and with mazut fumes, over wide ranges in the initial weight concentrations of the aerosols and wavelengths of the scattered light.

LITERATURE CITED

[1] O. M. Todes and A. A. Chekunov, Kolloid. Zhur. 19, 633 (1957).*

[2] Lord Rayleigh, Phil. Mag. 5, 47, 375 (1899).

[3] K. S. Shifrin, Light Scattering in a Turbid Medium [In Russian] (State Tech. Theoret. Press, 1951).

[4] O. M. Todes, in the book: Problems of Kinetics and Catalysts [In Russian] (1949), 7, 157.

[5] M. Smoluchowski, Z. Phys. Chem. 92, 129 (1917).

[6] O. M. Todes and A. A. Chekunov, Kolloid. Zhur. 19, 4, 490 (1957).*

[7] Yu. M. Veitser and G. P. Luchinskii, Masking Smokes [In Russian] (Goskhimizdat, 1947).

* See C. B. translation.

STATES OF AGGREGATION OF COMPOUNDS OF HIGH MOLECULAR WEIGHT

6. TENSILE CHARACTERISTICS OF AN ANISOTROPIC POLYCAPROLACTAM FILM

R. I. Fel'dman and S. I. Sokolov

Moscow Institute of Chemical Machinery Construction

N. K. Krupskaya Moscow Region Pedagogic Institute

(Translated from: Kolloidnyi Zhurnal Vol. 22, No. 1, pp. 97-100, January-February, 1960)

(Original article submitted May 20, 1958) May 15, 1958)

In our earlier considerations [1] of two extreme types of macromolecular packing in polymers present in the condensed states it was noted that in many cases a folded type of packing is possible, such that regions (segments) of a single macromolecule are packed parallel to each other as the result of rotation through 180° at definite points. The depth of the folds or the length of the segments in parallel orientation may vary. If the folds are sufficiently deep, the diffraction pattern found by x-ray or electron-diffraction methods becomes indistinguishable from the corresponding pattern for parallel orientation of the macromolecules without folds. We proposed the terms flexural and rectile, respectively for packings with and without folds.

In our view, the presence of folds should be revealed primarily by high values for the elongation of some polymeric materials when they are stretched under conditions favorable for unfolding without rupture of the chains themselves. This applies, for example, to the "cold drawing" effect observed predominantly in crystallizing polymers such as polyamide films and threads, polyethylene, etc. In some instances, such effects are also observed in amorphous polymers, especially those which have a tendency to form relatively ordered regions in the mass of amorphous substance.

It was assumed that, if a polymer has no particular predominant orientation of the folds, unfolding during stretching should begin at the folds which are orientated at right angles to the direction of the force. Separation of pairs of segments with consecutive breakdown of intermolecular bonds should be easier than displacement along a chain with simultaneous breakdown of all the forces of interaction with neighboring chains. If the tensile force acts at an angle φ to the direction of the folds, the detaching component f_{det} must be equal to the total force f_0 multiplied by sin φ, i.e.,

$$f_{det} = f_0 \sin \varphi.$$

When the angle φ is 30°, the detaching component is one-half the total force. It may be assumed that at temperatures which are not too close to the temperature of total softening (melting, in the case of crystalline polymers) cold drawing should involve to a greater extent those folds which lie at relatively large angles, close to 90°, to the stretching direction. Some of the folds remain folded; their number increases with decrease of the angle φ. It was therefore of interest to study the extension of films in a variety of directions after the films had been subjected to cold drawing in one direction. The results may, first, give further confirmation of the hypothesis concerning folded packing of polymer chains and, second, provide a basis for important practical conclusions concerning the mechanical properties characteristic of orientated anisotropic polymers.

The tests were performed on polycaprolactam specimens cut from an anisotropic film in different directions at 15° intervals. The polycaprolactam film was made by the works process, by melt extrusion through a slit onto a water-cooled drum with subsequent approximately 300% stretching in one direction on a stretching machine. The molecular weight of the polyamide was approximately 14,000. The specimens had working length 25 mm, width 5 mm, and thickness 0.06 mm.

The load-elongation curves were plotted up to the breaking point, with the aid of a dynamometer of the Polanyi type. The extension rate was 2 mm/min at $t = 20 \pm 0.5°$.

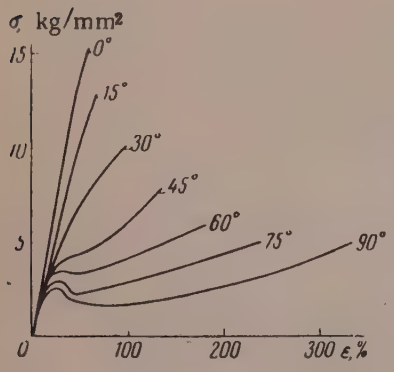


Fig. 1. Tensile curves for polycaprolactam specimens cut from an anisotropic films at various angles to the direction of orientation.

The relative elongation (ϵ) was expressed as a percentage of the initial specimen length (l), and the stress (σ, kg/mm^2) was calculated for the initial cross section. The form of the load-elongation curves gradually changes with the angle between the direction of orientation and the direction of the tensile strength, between 0 and 90°. For illustration, Fig. 1 shows load-elongation curves for specimens cut at angles of 0, 15, 45, 60, 75, and 90° to the direction of orientation formed in the course of manufacture; this corresponds to the angles between the direction of orientation and the direction of the tensile force in dynamometer tests. Twelve or more specimens were tested for each direction. Analysis of the average tensile characteristics shows that the relative elongation at break (ϵ_b) increases, and the breaking strength (σ_b) decreases with increase of the angle between the direction of initial orientation and the direction of the tensile force; this is illustrated by the relationships plotted in Fig. 2. Evaluation of the experimental data showed that in the first approximation the relative elongation at break ϵ_x for specimens cut at an angle x between the direction of orientation and the direction of the tensile force can be expressed as

$$\varepsilon_x = A(1 - \cos x) + B = A[1 - \sin(90° - x)] + B. \quad (1)$$

The constants in Eq. (1) are: $A = \epsilon_{90} - \epsilon_0$ and $B = \epsilon_0$. Substitution of the values of A and B into Eq. (1) gives

$$\varepsilon_x = \varepsilon_0 + (\varepsilon_{90} - \varepsilon_0)[1 - \sin(90° - x)]. \quad (2)$$

The following expression may be used for the tensile stress σ_x:

$$\sigma_x = C(1 - \sin x) + D. \quad (3)$$

The constants in Eq. (3) are: $C = \sigma_0 - \sigma_{90}$ and $D = \sigma_{90}$, and consequently

$$\sigma_x = \sigma_0 - (\sigma_0 - \sigma_{90}) \sin x. \quad (4)$$

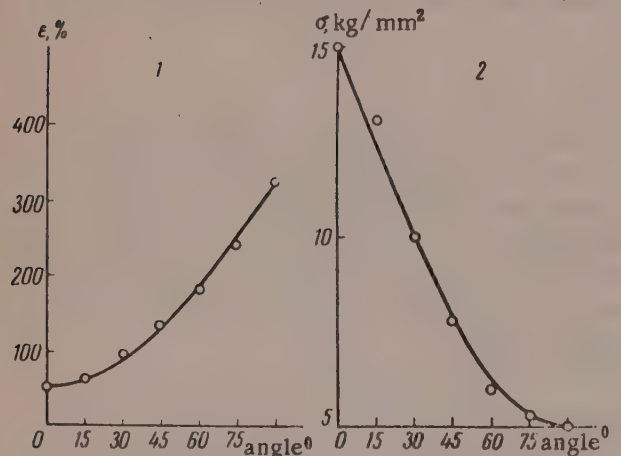


Fig. 2. Variations of the tensile characteristics of anisotropic polycaprolactam film with the angle between the direction of orientation and the direction of the tensile stress: 1) Relative elongation at break; 2) tensile strength.

Figure 2 shows the results in the form of curves calculated from the proposed Eqs. (2) and (4). The agreement between the calculated values of the relative elongation at break and the tensile strength, and the corresponding experimental values (indicated in Fig. 2 by circles), may be regarded as quite satisfactory. Equations (2) and (4) are suitable for calculating the tensile characteristics of articles cut from anisotropic polycaprolactam films when stresses at various angles to the orientation direction arise in them when in use.

Our results may be interpreted as follows in the light of our hypothesis of unfolding of flexural formations during stretching [1]. During the initial stretching of the film (during manufacture) the flexural aggregates were unfolded to an increasing extent with increase of the angle φ.

The rest of the aggregates accordingly remained folded. During subsequent extension at different angles to the orientation direction (x) the remaining aggregates are unfolded. This unfolding gives rise to the additional deformations ($\epsilon_x - \epsilon_0$), reaching the maximum value of ($\epsilon_{90} - \epsilon_0$) when the angle x is 90°. It should be noted that the initial extension of the film was approximately 300%, whereas the additional elongation (at break) in the same direction ($x = 0°$) was approximately 50%. Thus, the total elongation in this direction, approximately 350%, is approximately equal to the elongation in the direction at right angles to it ($x = 90°$) as found in our experiments. If the average breaking stress for the same specimens, calculated for the initial cross section and equal to 15 and 5 kg/mm^2, respectively, is calculated for the true cross section at break by multiplication by $(1 + \alpha)$, where the relative elongation at break is $\alpha = \Delta l/l$, the strength difference between the specimens disappears, and the following condition is satisfied:

$$\sigma_0(1 + \alpha_0) = \sigma_{90}(1 + \alpha_{90}). \quad (5)$$

SUMMARY

1. The elongation at break (ϵ) and breaking strength (σ) of specimens of anisotropic polycaprolactam film cut at different angles to the orientation direction were determined.

2. Expressions were derived for the relative elongation at break (ϵ_x) and tensile strength (σ_x) as functions of the angle between the directions of orientation and the tensile stress (x):

$$\varepsilon_x = \varepsilon_0 + (\varepsilon_{90} - \varepsilon_0)[1 - \sin(90° - x)] \text{ and}$$
$$\sigma_x = \sigma_0 - (\sigma_0 - \sigma_{90})\sin x,$$

where ϵ_0, σ_0, ϵ_{90}, and σ_{90} are the relative elongations at break (%) and tensile strengths (kg/mm^2) when the angle x is 0 and 90°, respectively.

3. Differences between the values of the tensile strength in different directions can be attributed entirely to changes in the cross-sectional area of the specimens as the result of elongation.

Accordingly, the tensile characteristics conform to the expression:

$$\sigma_0(1 + \alpha_0) = \sigma_{90}(1 + \alpha_{90}),$$

where $\alpha = \Delta l/l$ is the relative elongation at break.

4. These results are interpreted in the light of the hypothesis of flexural packing of crystalline polymer chains and of opening of the folds during stretching.

The authors thank N. I. Fel'dman for his interest in the work and for discussion of the results.

LITERATURE CITED

[1] S. I. Sokolov and R. I. Fel'dman, Kolloid. Zhur. 21, 5, 630 (1959).*

* See C. B. translation.

EFFECT OF TEMPERATURE ON CERTAIN STRUCTURAL AND MECHANICAL CHARACTERISTICS OF CLAY PASTES*

V. B. Chernogorenko

Scientific Research Institute of Building Materials and Products, Kiev
(Translated from: Kolloidnyi Zhurnal Vol. 22, No. 1, 101-104, January-February, 1960)
(Original article submitted May 26, 1958)

For determination of the optimum heating temperature in molding of clay pastes from six Ukrainian clays the efflux curves of the pastes and the strengths of the structure formed were studied at temperatures between 20 and 80°

Efflux of the pastes was studied in an apparatus of the Hoeppler type by means of a capillary viscosimeter with an attachment 22 mm long and 10.8 mm in internal diameter. The capillary was grooved to eliminate the wall slippage effect.

The experimental curves for the efflux pressure against the paste flow rate at various temperatures were used for calculating the nominal dynamic yield value (P_{K_2}), the Bingham viscosity (η^*_m), and the Volarovich plasticity ($\varphi = P_{K_2} \mid \eta^*_m$) [1].

The strength of the structure formed — the limiting shear stress P_m — was determined by the Rebinder method [2] by means of the cone plastometer. Since clay pastes are strongly thixotropic, all the determinations were performed with the same time of structure formation, 30 minutes. The values of P_m were found from the initial portions of the curves, where the strength of the structure increases linearly with time.

For pastes of Krasnogvardeiskoe and Chasov Yar clay (Fig. 1, a; 2, b) P_m increases and P_{K_2} decreases with rise of temperature. For pastes of Glukhov kaolin (Fig. 3, a) P_{K_2} increases up to 40° and then decreases, with a simultaneous fall in the value of P_m. For pastes of Gorbsk bentonite (Fig. 3, b) P_{K_2} is independent of temperature. Similar effects were observed by Malyshev and Tsarevich [3] in studies of dilute suspensions of a number of bentonite clays. At the same time, the structural strength P_m of pastes from Gorbsk bentonite increases with rise of temperature. The values of P_{K_2} and P_m for pastes of Belaya Tserkov' losses increase with temperature. For pastes of spondylic clay P_m increases with temperature (Fig. 2, a); P_{K_2} first decreases up to 50°, and then increases.

Agranat and Volarovich [4] put forward the view, confirmed in a number of instances, that the nominal dynamic yield value P_{K_2} (the limiting shear stress, in their terminology) can be determined by means of the Rebinder cone plastometer. It follows from the results given that the values of P_m and P_{K_2} coincide only for some pastes at a definite temperature. This is the case for pastes of Krasnogvardeiskoe and spondylic clays at 20° and for pastes of Glukhov kaolin at 40°. In all other cases, these values do not coincide and vary differently with the temperature. This shows that the limiting shear stress P_m determined in the cone plastometer is independent of the other value — the nominal dynamic yield value P_{K_2} — and characterizes the strength of the structure. The mutual independence of these structural and mechanical characteristics was demonstrated experimentally by Kobakhidze and Shishniashvili [5], who showed that $P_m > P_{K_2}$ for suspensions of bentonite clays.

* Paper at the Fourth All-Union Conference on Colloid Chemistry, Tbilisi, May, 1958.

This inequality is also confirmed by our results. The relationship $P_{K_2} > P_m$ was found only for pastes of Belaya Tserkov' losses.

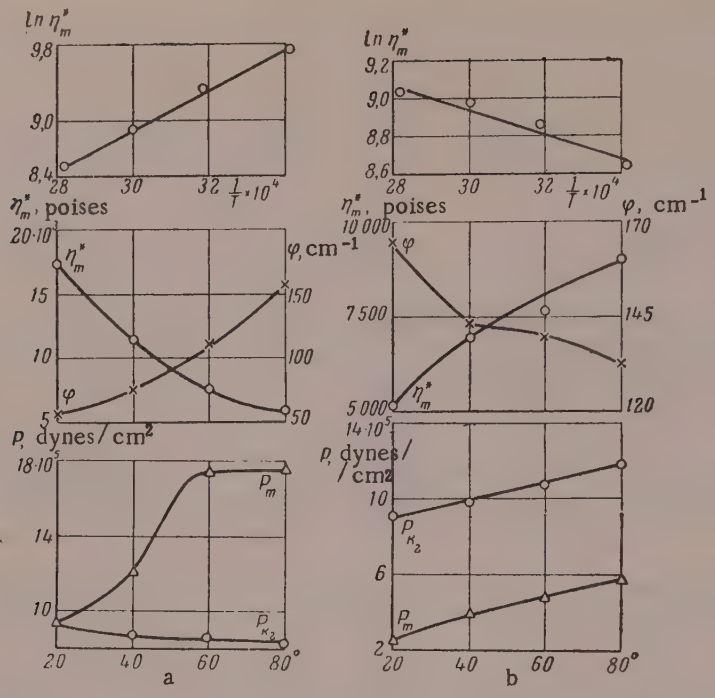


Fig. 1. Effects of heating temperature on the structural and mechanical characteristics of pastes of Krasnogvardeiskoe clay, W = 26.0% (a), and Belaya Tserkov' loess, W = 23.4% (b); time of structure formation 30 minutes.

At constant moisture content the Bingham viscosity of pastes of Krasnogvardeiskoe clay (Fig. 1, a) and Gorbsk bentonite (Fig. 3, b) falls steadily with increase of temperature. For pastes of Glukhov kaolin (Fig. 3, a) the Bingham viscosity (accuracy ± 10%) remains constant. In the case of Belaya Tserkov' loess (Fig. 1, b) the viscosity increases with temperature. The viscosity curve for pastes of spondylic clay (Fig. 2, a) has a distinct minimum at 50°, while for pastes of Chasov Yar clay (Fig. 2, b) this minimum is at 60°.

In view of the fact that steady viscosity values, corresponding to ultimate structural breakdown of the pastes, could not be reached even at high efflux pressures, we studied the effects of temperature on the plastic viscosity corresponding to a considerable degree of structural breakdown. We plotted $\eta^*_m = Ae^{\frac{B}{T}}$ curves, as usual in $\ln \eta^*_m$ $\frac{1}{T}$ coordinates (Figs. 1-3). In the case of spondylic and Chasov Yar clays, this relationship is represented by pairs of straight lines (Fig. 2, a and 2, b).

It is known that colloidal systems consisting of fine particles associated in aggregates are sensitive to temperature [6]. The degree of coagulation structure formation depends, in addition to other factors, on the number of particles per unit volume [7] and on the temperature of structure formation, as was shown by Serb-Serbina and Polonskii [8] for dilute suspensions of some bentonite clays.

Peptization and dispersion effects in pastes increase with rise of temperature, i.e., with increasing Brownian motion. The clay aggregates disintegrate into their constituent particles and the viscosity falls. Owing to the increased number of particles per unit volume of paste, the number of effective collisions between the clay particles increases. This intensifies coagulation structure formation, with an increase of the structural strength determined in the cone plastometer. It is only for pastes of Glukhov kaolin, containing particles of weakly-hydrophilic kaolinite, that the thermal dispersion effect is small and the viscosity remains virtually constant

(Fig. 3, a). The strength of the structure composed of kaolinite particles diminishes with rise of temperature. It may be assumed that in pastes of spondylic clay (Fig. 2, a), disaggregation of the clay particles takes place up to 50°. The Bingham viscosity of the paste decreases with decreasing size of the structural elements. Above that temperature, dispersion and peptization processes are suppressed by processes of coagulation structure formation. During efflux of the pastes, the minimum plastic viscosity increases owing to increasing size of the structural

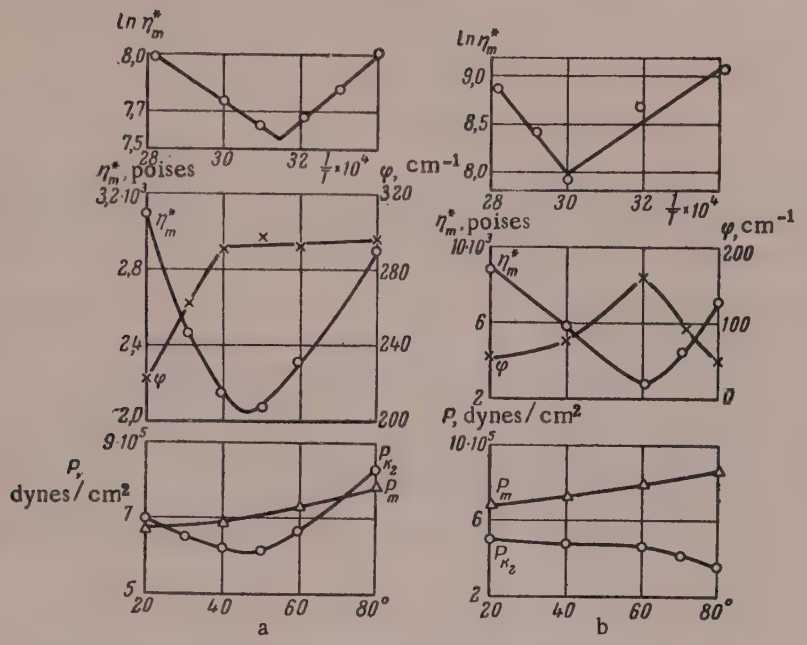


Fig. 2. Effects of heating temperature on the structural and mechanical characteristics of pastes of spondylic clay, W = = 32.8% (a), and Chasov Yar clay, W = 37.9% (b); time of structure formation 30 minutes.

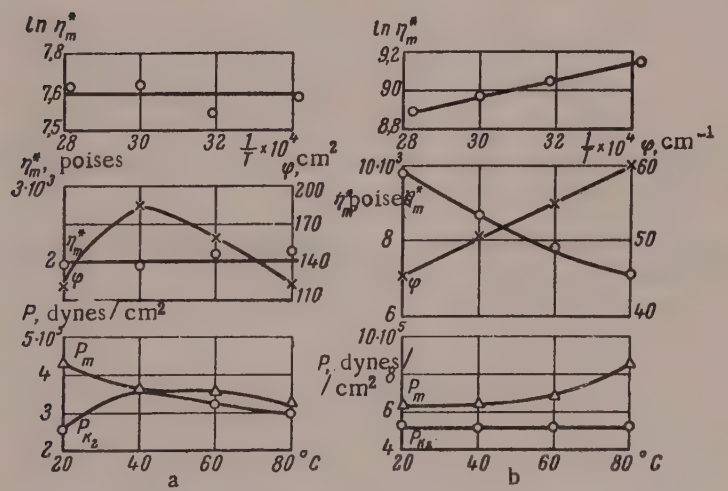


Fig. 3. Effects of heating temperature on the structural and mechanical characteristics of pastes of Glukhov kaolin, W = = 42.8% (a), and Gorbsk bentonite, W = 49.0% (b); time of structure formation 30 minutes.

elements. The same effect occurs with Chasov Yar clay (Fig. 2, b). As already noted, Belaya Tserkov' loess occupies a special position with regard to the effect of temperature on its structural and mechanical properties. The Bingham viscosity of loess pastes increases with rise of temperature. This shows that coagulation structure formation leads to growth of the structural elements (particle aggregation) which begins at room temperature.

The curves for variations of Volarovich plasticity (φ) in Figs. 1-3 characterize the molding properties of heated ceramic pastes and indicate the optimum heating temperatures. Only in the case of pastes of Belaya Tserkov' loess heating is not recommended, as it lowers the plasticity. This is fully consistent with the behavior of these pastes in production.

SUMMARY

1. The nominal dynamic yield value, Bingham viscosity, Volarovich plasticity and structural strength as indicated by the limiting shear stress have been determined between 20 and 80° for pastes of the normal molding moisture content made from six different Ukrainian clays.

2. The nominal dynamic yield value P_{K_2} and the limiting shear stress P_m are mutually-independent structural and mechanical characteristics. The value of P_m may be greater than, equal to, or less than P_{K_2}, in accordance with the nature of the clay and the temperature. Generally $P_m > P_{K_2}$.

3. The effect of temperature on Bingham viscosity is associated with the nature of the clay. The logarithm of the Bingham viscosity is a linear function of the reciprocal temperature. For pastes of Chasov Yar and spondylic clays, this relationship is represented by pairs of straight lines.

It is my pleasant duty to thank Academician P. A. Rebinder for valuable comments on this paper.

LITERATURE CITED

[1] M. P. Volarovich, Trudy In-ta Prikladnoi Mineralogii B66 (1934); M. P. Volarovich and D. M. Tolstoi, Zhur. Fiz. Khim. 4, 815 (1933).

[2] P. A. Rebinder and N. A. Semenenko, Doklady Akad. Nauk SSSR 64, 835 (1949).

[3] A. I. Malyshev and K. A. Tsarevich, Neftyanoe Khozyaistvo 1, 34 (1934).

[4] N. N. Agranat and M. P. Volarovich, 19, 3 (1957).

[5] E. I. Kobakhidze and M. E. Shishniashvili, Kolloid. Zhur. 19, 59 (1957).*

[6] A. I. Rabinerson, Problems of Colloid Chemistry [In Russian] (United State Technical Press, Leningrad, 1937).

[7] N. N. Serb-Serbina, Conference on Viscosity of Liquids and Colloidal Solutions [In Russian] (Izd. AN SSSR, Moscow-Leningrad, 1941), 1, 381.

[8] N. N. Serb-Serbina and T. M. Polonskii, Doklady Akad. Nauk SSSR 96, 104 (1954); T. M. Polonskii, Vestnik Akad. Nauk Beloruss. SSR, ser. tekhn. 2, 147 (1956).

* See C. B. translation.

INFLUENCE OF DRYING OIL ON STABILIZATION OF CARBON-BLACK SUSPENSIONS

B. N. Shakhkel'dyan

Moscow Polygraphic Institute

(Translated from: Kolloidnyi Zhurnal Vol. 22, No. 1, pp. 106-110, January-February, 1960)

(Original article submitted December 23, 1958)

It is known that black printing inks are suspensions of carbon black in mineral oils with additions of various resinous and polymeric substances. The viscosity characteristics and therefore the printing behavior of such suspensions depends on the stabilizing power of the additives. It has been shown [1] that additions of small amounts of drying oil to nonpolar petrolatum stabilize suspensions of gas channel black previously extracted in boiling benzene. The stabilization is manifested in a decrease of the relative viscosity of the suspension. The effect has a certain limit. Addition of more than 30% of drying oil to the dispersion medium has no further influence on the minimum constant relative viscosity of the structure broken down to the limit at high velocities.

To elucidate the influence of surface-active substances present in the carbon black on the viscosity characteristics of printing inks, suspensions of unextracted technical carbon black were studied. It was found that unextracted carbon black in pure petrolatum forms suspensions which thicken less than those with extracted black at high deformation rates (Fig. 1). Addition of a certain amount of drying oil to the petrolatum has almost no effect on thickening of suspensions of unextracted black, whereas in the case of extracted black the relative viscosity is lowered.

It seems that surface-active substances formed by oxidation during manufacture of the black favor formation of a stabilizing layer from the petrolatum hydrocarbons on the surface of the particles of unpurified black. As increasing amounts of drying oil are introduced into the dispersion medium, the petrolatum hydrocarbons in the solvation layer are gradually replaced by components of the drying oil. The stabilizing effect remains unchanged, as is shown by the fact that Curves 1-4 in Fig. 1 coincide.

The rebuilding of the solvation layer is apparently completed when the content of drying oil in the dispersion medium has reached 20%, as above this concentration the relative viscosity falls, indicating a qualitative change in the nature of adsorption. The relative viscosity of the suspension continues to fall with increase of drying-oil content to 80%, after which the concentration of drying oil ceases to influence the relative viscosity.

A similar limit to adsorption was reached in suspensions of extracted carbon black when the concentration of drying oil was 30%. It follows that surface-active substances favor more complete adsorption of the drying-oil components. As is clear from Fig. 2, the higher adsorption activity results in a greater stabilizing effect in suspensions of unextracted carbon black.

An interesting fact is that despite the differences at the initial and final values of the $(\eta/\eta_0)_{min} = f(c_{do})$ curves for suspensions of extracted and unextracted black, these curves coincide for suspensions containing 30% drying oil, which is the concentration corresponding to maximum adsorption on the surface of extracted carbon black. This may indicate that the stabilizing effect is directly related to the amount of substances adsorbed. The differences in relative viscosity are attributable, at low concentrations of drying oil, to adsorption of hydrocarbons from the mineral oil on the surface of unextracted carbon black, and at high concentrations to increased adsorption of the drying-oil components.

The constant thickening of suspensions of extracted carbon black at low drying-oil concentrations [start of the $(\eta/\eta_0)_{min} = f(c_{do})$ curve] is due to insufficient adsorption and not to stabilization by hydrocarbons of the mineral oil. In contrast to suspensions of unextracted black, in this case, constant thickening is found over a narrow range of drying-oil concentrations.

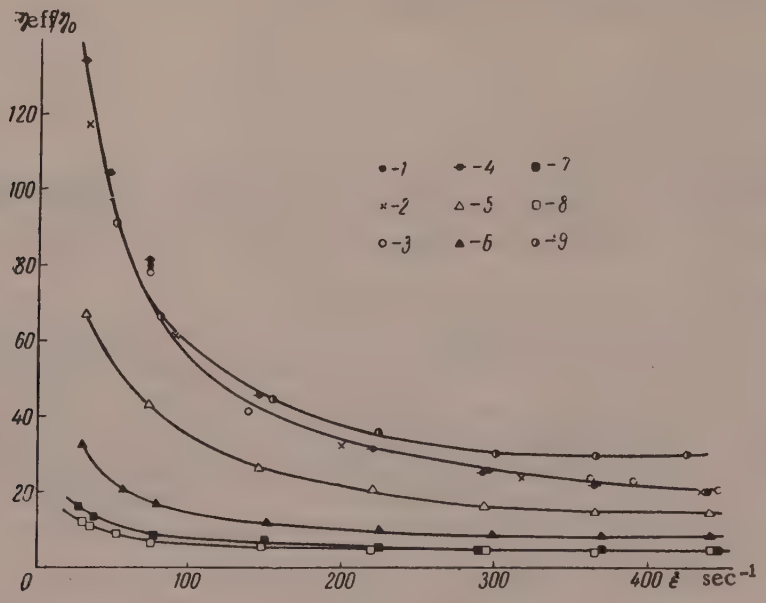


Fig. 1. Effects of deformation rate and composition of the dispersion medium on the relative viscosity of suspensions of unextracted (1-8) and extracted (9) carbon black. Dispersion medium: 1, 9) Petrolatum; 2) same, with 5% drying oil; 3) same, with 10% drying oil; 4) same, with 20% drying oil; 5) same, with 30% drying oil; 6) same, with 50% drying oil; 7) same, with 80% drying oil; 8) drying oil.

The surface of the unextracted carbon black particles apparently varies in its adsorptive power. At low concentrations of drying oil adsorption occurs at the more active regions of the carbon-black surface. These regions are capable of adsorbing nonpolar hydrocarbons from the mineral oil when polar components of the drying oil are absent or present in insufficient quantity. Complete saturation of these regions is reached when the content of drying oil in the petrolatum reaches about 20% (with 11.9% of carbon black by volume in the suspension). Other, less active regions of the carbon-black surface adsorb only the polar components of the drying oil, and only after the more active regions have become saturated. Removal of the surface-active substances by extraction in hot benzene lowers the adsorption activity and, in particular, prevents adsorption of nonpolar hydrocarbons from the mineral oil.

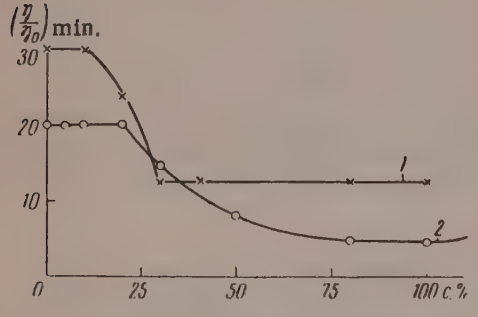


Fig. 2. Effect of the content of drying oil (c) in the dispersion medium on the relative viscosity of suspensions after ultimate breakdown of the structure: 1) Extracted carbon black; 2) unextracted carbon black.

The surface heterogeneity of unextracted carbon black results in differences in the character of stabilization of the suspension when adsorption takes place at regions differing in activity. At high deformation rates unextracted carbon black produces less thickening effect than extracted black on the petrolatum, but the relative viscosities of suspensions of both

types of black converge with decrease of the deformation rate. It follows that the solvation which occurs as the result of adsorption on the more active regions of the particles cannot prevent particle aggregation at low deformation rates, whereas at drying-oil concentrations above that required for saturation of the active regions the relative viscosity decreases over the entire range of deformation rates.

The explanation of the fact that the minimum relative viscosity of the suspensions is independent of the composition of the dispersion medium at limiting adsorption of the surface-active components of drying oil (Curves 7 and 8 in Fig. 1, and 4-7 in Fig. 2 [1]) is that in such systems the degree of aggregation and the shape and size of the structural elements are similar at high rates of deformation. However, the same systems exhibit significant differences in the region of anomalous viscosity: As the deformation rate decreases, the increase of relative viscosity becomes more rapid with decrease of the amount of drying oil in the dispersion medium.*

These differences are probably caused by flow disorientation of the particles, which occurs and intensifies with decrease of the deformation rate. Such disorientation has been reported by Voet [2] who, in a study of the relationship between the dielectric constant of carbon-black suspensions and the deformation rate attributed the existence of minima on the $E = f(\epsilon)$ curves to coiling of the linear aggregates in suspensions stabilized by surface-active substances on decrease of the rate of deformation.

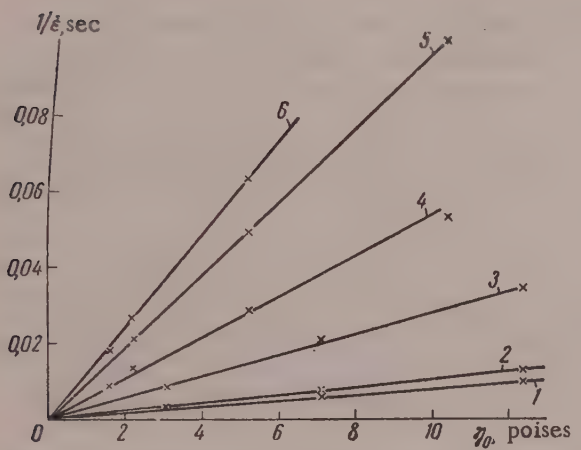


Fig. 3. Relationship between the deformation rate and the viscosity of the medium (η_0) for carbon-black suspensions of the same relative viscosity. Relative viscosities: 1) 6.5; 2) 7; 3) 12.5; 4) 22 [1]; 5) 27 [1]; 6) 30 [1].

If it is postulated that in systems with limiting adsorption, with the same ultimate relative viscosity, the kinetic particles have the same structure, it follows that equal increases of relative viscosity with decrease of the deformation rate should occur at equal degrees of disorientation. Since decrease of the deformation rate should favor disorientation, while increase of the viscosity of the medium should hinder it, there should be an inverse relationship between the viscosity medium and the velocity gradient at which different suspensions with limiting stabilization exhibit equal thickening in the region of anomalous viscosity.

To verify this hypothesis, the experimental data plotted in Fig. 1 and earlier results [1] were used to determine the deformation rates corresponding to equal given relative viscosities for different systems at the limiting degree of stabilization. Figure 3 shows that the viscosity of the medium is proportional to the reciprocal of the deformation rate at which suspensions with different amounts of drying oil in the dispersion medium have the same relative viscosity. This confirms the hypothesis of an orientational mechanism of anomalous viscosity at the limiting degree of adsorption.

If the differences in the relative viscosities of suspensions at the limiting degree of stabilization are caused by disorientation, which is retarded in more viscous media, then the static characteristics of structure formation, independent of the deformation rate, should be the same for all systems stabilized to the limit. The yield value of the maximum thixotropic structure can be used as such a characteristic. Accordingly, the yield values were determined by means of the Veiler-Rebinder apparatus [3], and thixotropic increase of structural strength in the suspensions was investigated. The yield value was determined from the minimum extension of the spring which causes irreversible displacement of the plate detectable through the telescope at 10-fold magnification. All the

* Figure 1 shows $\eta/\eta_0 = f(\epsilon)$ curves determined with a decrease of the rotation rate of the viscosimeter cylinder after the minimum constant viscosity of the structure after ultimate breakdown had been reached.

investigated suspensions were first thoroughly stirred, and the apparatus was filled under constant conditions. The first determination of the yield value was carried out as soon after the stirring as the preparation of the apparatus allowed (in practice, within 3 minutes after the end of the stirring).

Thixotropic Strengthening of Carbon-Black Suspensions

Suspension No.	Content of drying oil in dispersion medium, %	Yield value, g/cm² at different intervals after stirring					
		2 min	10 min	60 min	2 days	10 days	30 days
1	0	6,7	6,9	Slippage			
2	5	6,7	6,7	7,15	Slippage		
3	10	6,1	7,0	11,3	13,6	Slippage	
4	20	5,2	6,95	10,6	11,6	Slippage	
5	30	1,31	1,7	2,23	—	5,6	6,6
6	50	0,7	1,32	1,9	3,54	5,03	5,2
7	80	0,62	1,15	1,61	3,42	4,56	4,6
8	100	0,25	0,78	1,15	2,77	4,50	4,6

The results of these determinations, presented in the table, show that the yield values of the suspensions decrease regularly with increase of drying-oil content. Suspensions Nos. 1-4, containing up to 20% drying oil in the dispersion medium, have almost the same yield values in the freshly-stirred state. This is consistent with the identity of the $\eta/\eta_0 = f(\epsilon)$ curves and is accounted for by the hypothesis presented above concerning adsorption of mineral oil components on the more active regions of the unextracted carbon-black surface. Nevertheless, the thixotropic structures built up progressively in these systems differ both in strength and in nature. The lower the content of drying oil, the greater the strength of the thixotropic structure and the more prominent is the wall slippage, which is not eliminated completely even if riffled plates are used.

For systems with higher contents of drying oil (suspensions No. 7 and No. 8; see table), with equal relative viscosities at high deformation rates, the yield values differ at first after the stirring, but they converge during thixotropic strengthening and become equal at the maximum buildup; this confirms the hypothesis that these suspensions are similar in structure. The differences between the yield values of these systems in the freshly-stirred state are probably due to a lower rate of thixotropic structure formation in the more viscous suspension No. 8.

SUMMARY

1. The surface-active substances contained in gas channel black favor stabilization of suspensions in petrolatum and increase the degree of stabilization in presence of drying oil.

2. The surface of the carbon-black particles varies in its adsorptive power. Regions of higher activity are capable of adsorbing the nonpolar components of petrolatum.

3. The anomalous viscosity of suspensions at the maximum degree of stabilization, observed on decrease of the deformation rate after the structure has been broken down, is attributable to disorientation of the particles, which is greater at lower viscosities of the medium.

LITERATURE CITED

[1] B. N. Shakhkel'dyan, Kolloid. Zhur. 20, 498 (1958).*

[2] A. Voet, Am. Ink Maker 35, 4, 34 (1957).

[3] S. Ya. Veiler and P. A. Rebinder, Doklady Akad. Nauk SSSR 49, 354 (1945); B. N. Shakhkel'dyan, Nauchn. Trudy Mosk. Poligr. In-ta 4, 137 (1957).

* See C. B. translation.

THERMODYNAMICS OF THIN LIQUID LAYERS

L. M. Shcherbakov

Tula Mechanical Institute

(Translated from: Kolloidnyi Zhurnal Vol. 22, No. 1, pp. 111-116, January-February, 1960)

(Original article submitted October 25, 1958)

It has been shown by the work of B. V. Deryagin's school [1] that thin liquid layers (less than 1 micron thick) have a number of anomalous properties. For quantitative investigation of these anomalies Deryagin introduced a new thermodynamic characteristic for such layers, the "disjoining pressure," and developed methods for experimental determination of this quantity.

In the phenomenological approach, the disjoining pressure of thin layers can be regarded as an example of the so-called capillary effects of the second kind [2]. This eliminates the gap between ordinary capillary effects and anomalies of thin liquid layers, so that they can all be considered within the framework of a single thermodynamic theory.*

Thermodynamic analysis of equilibrium conditions in heterogeneous systems shows that growth of the interfacial area has a dual effect on equilibrium in a system. In addition to its direct influence which can be estimated by means of the well-known Laplace and Kelvin equations,** there is an indirect effect. The latter is due to changes in the surface tension itself as the interfacial area increases. Accordingly, we can distinguish two classes of capillary phenomena [2]:

1) The usual capillary phenomena, or capillary effects of the first kind, due to the direct influence of increasing liquid surface.

2) Capillary effects of the second kind, due to changes of surface tension with variations of the geometrical parameters of the surface (drop radius, thickness of the layer) which determine the dimensions of the liquid phase.

Evidently effects of the second kind play a particularly important role in highly disperse systems, in which the interfacial tension differs appreciably from values given in standard tables.

Effects of the second kind can be studied in the pure form in systems which have been described as having a constant interfacial area [2]. Consider a very thin (h of the order of 10^{-5} to 10^{-7} cm) layer of pure liquid (indicated ') contained in a cylinder at constant temperature, in equilibrium with its own vapor (indicated "). For such a system the usual capillary effects may be disregarded, as the area of the liquid – vapor interface remains unchanged whatever changes may occur in the volume of the layer.*** The only factor which can influence equilibrium of the system under these conditions is variation of the excess surface energy of the layer with changes in its thickness. The free energy of the system in question is given by the expression:

$$F = F' + F'' + 2\sigma S,$$

* This was first done in 1940 by Deryagin [1].

** For example, see [3].

*** Variations of the area of the regions of the surface where the liquid is in contact with the cylinder walls may be disregarded.

where S is the area of the base of the layer, and σ is the specific excess free surface energy of the layer, regarded as a function of the thickness $\underline{h}$ and temperature T.

The equilibrium conditions of the system are determined from the principle of minimum free energy. The system must also be under conditions of constant temperature and mechanical isolation:

$$\left.\begin{aligned} T' = T_s = T'' = \text{const}, \\ V' + V'' = \text{const}, \\ m' + m'' = \text{const} \\ S = \text{const}. \end{aligned}\right\}$$

Variation of F with the additional conditions taken into account gives the general equilibrium conditions for the system:

$$\mu'(P', T) = \mu''(P'', T);\ P' - P'' = 2\left(\frac{\partial\sigma}{\partial h}\right)_{T,S}, \tag{1}$$

where $\mu^{(i)}$ is the chemical potential of the i-th phase.

If we remove the restriction of constant S, i.e., if we take ordinary capillary effects into consideration also, we similarly find the equilibrium conditions for a layer with variable surface area:

$$\mu'(P', T) = \mu''(P'', T);\ P' - P'' = 2\frac{\sigma}{h} + 2\left(\frac{\partial\sigma}{\partial h}\right)_{T,S}. \tag{2}$$

Here the first term in the right-hand side of the second equation represents the capillary effect of the first kind.

Differentiating these conditions with respect to $\underline{h}$*, and taking into account the fact that $(\partial\mu/\partial P) = v$, the molar volume of the phase in question, we have:

$$\frac{\partial P'}{\partial h} = \frac{v''}{v'' - v'}\frac{\partial}{\partial h}\left(2\frac{\sigma}{h} + 2\frac{\partial\sigma}{\partial h}\right) \cong \frac{\partial}{\partial h}\left(2\frac{\sigma}{h} + 2\frac{\partial\sigma}{\partial h}\right).$$

Integration between the limits $h = \infty$ and $h = h$, gives the pressure in the layer:

$$P' = P_0 + 2\frac{\sigma}{h} + 2\frac{\partial\sigma}{\partial h}.$$

For systems of constant surface area this equation becomes:

$$P' = P_0 + 2\frac{\partial\sigma}{\partial h}. \tag{4}$$

This equation determines the "disjoining pressure" of the layer, which is [4] $p(h) = P_0 - P'$.**

---

* The relationship between $\mu^{(i)}$ and $\underline{h}$ is defined through the intermediate variable $P^{(i)}$.

** For a layer of pure liquid in contact with its own vapor $p(h) < 0$; therefore, strictly speaking, it is a "joining" rather than "disjoining" pressure; see [5].

For calculations, the concrete relationship between σ and h must be known. It was shown by Deryagin and Abrikosova [6] that for very thin layers it may be assumed that $p(h) = 2\frac{\partial\sigma}{\partial h} \sim \frac{1}{h^3}$. Hence, we have for the specific excess free surface energy of the layer:

$$\sigma = \sigma_\infty (1 - k/h^2).$$

Here σ_∞ is the value of σ corresponding to $h = \infty$, which is none other than the usual tabulated value for the surface tension of the liquid. To determine k we use the physically obvious condition: $\sigma \to 0$ at $h \to \delta$ (here δ is the thickness of the intermediate surface layer separating the liquid and gas phases), and hence we have $k = \delta^2$.* Therefore, we have the following first approximation for the relationship between the specific excess free surface energy of the layer and its thickness:

$$\sigma = \sigma_\infty (1 - \delta^2/h^2). \tag{5}$$

We now consider the influence of the thickness of the layer on the pressure of its saturated vapor. Differentiation of the layer equilibrium conditions (2) with respect to h, and reasoning similar to that used in the derivation of Eq. (3), gives the following expression for the change of saturated vapor pressure:

$$\frac{\partial P''}{\partial h} = \frac{v'}{v'' - v'} \frac{\partial}{\partial h}\left(2\frac{\sigma}{h} + 2\frac{\partial\sigma}{\partial h}\right) \approx \frac{v'}{v''} \frac{\partial}{\partial h}\left(2\frac{\sigma}{h} + 2\frac{\partial\sigma}{\partial h}\right).$$

If the vapor is assumed to be an ideal gas, we have $v'' = RT/P''$. Integrating, on this assumption, the last equation in the limits between $h = \infty$ and $h = h$, we have for the saturated vapor pressure of a thin layer:

$$P'' = P_0 \exp\left[\frac{v'}{RT}\left(2\frac{\sigma}{h} + 2\frac{\partial\sigma}{\partial h}\right)\right]. \tag{6}$$

For a layer of constant surface area this expression becomes**

$$P'' = P_0 \exp\left[\frac{v'}{RT}\left(2\frac{\partial\sigma}{\partial h}\right)\right]. \tag{7}$$

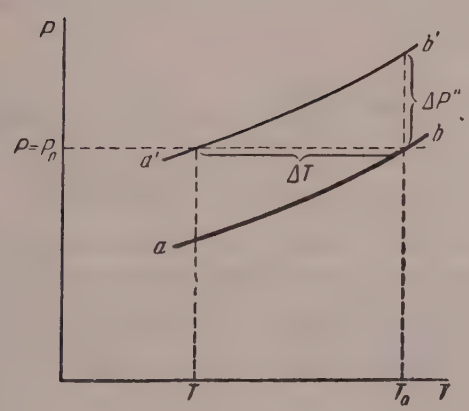


Fig. 1

In passing to analysis of the influence of decreasing layer thickness on the temperature of phase transition, we consider the equilibrium diagram (Fig. 1). The transition temperature may be defined as the temperature at which the two phases at a given pressure (or pressures) coexist in equilibrium. In the present instance, this is the equilibrium temperature of the liquid at which its saturated vapor pressure reaches the given value. It follows from Fig. 1 that with decrease of the layer thickness the evaporation curve ab on the equilibrium diagram is displaced by

$$\Delta P'' = P'' - P_0 = P_0\left[\exp\left(\frac{v'\varphi}{RT}\right) - 1\right]$$

(for brevity, φ is used to represent the expression $2\frac{\sigma}{h} + 2\frac{\partial\sigma}{\partial h}$)

* According to the Gibbs theory of surface phases (see, for example, [7]) $\delta \approx -(\partial\sigma/\partial P)_T$ while the last coefficient can be estimated (at least in order of magnitude) from such data as the experimental relationship between σ and P [8].

** The resultant equation is analogous to the equation derived by B. V. Deryagin [1] in his theory of capillary condensation.

and takes up the position a'b'. Therefore, the given saturated vapor pressure is now reached at T and not at T_0.

For the lowering of the transition temperature, we have from the diagram:

$$\Delta T = -(T_0 - T) = -\frac{\Delta P''}{dP''/dT} \approx -\frac{P_0 \frac{v'\varphi}{RT}}{dP''/dT}, \tag{8}$$

where dP^*/dT is the slope of the evaporation curve a*b*. Over a short length the curves a*b* and ab may be regarded as parallel. Therefore the slope factor dP^*/dT may be replaced by the slope factor dP_0/dT for the original curve ab. The latter is determined by the usual Clausius-Clapeyron equation (for a considerable mass of liquid)

$$\frac{1}{P_0}\frac{dP_0}{dT} = \frac{\lambda_0}{RT_0}$$

(λ_0 is the molar heat of evaporation at temperature T_0). Substituting the value of the slope factor into Eq. (8), we find the lowering of the transition temperature for a thin layer

$$\frac{\Delta T}{T_0} = -\frac{v'}{\lambda_0}\left(2\frac{\sigma}{h} + 2\frac{\partial\sigma}{\partial h}\right). \tag{9}$$

For a layer with constant interfacial area the first term in this equation, corresponding to the capillary effect of the first kind, is omitted.

We now consider transition from one equilibrium state, defined by the values of T and $\underline{h}$ to another infinitely close equilibrium state: $T + dT$; $h + dh$. From the conditions (2), we have for this transition:

$$d\mu' = d\mu''; \; dP' - dP'' = d\left(2\frac{\sigma}{h} + 2\frac{\partial\sigma}{\partial h}\right). \tag{10}$$

Since for the change of chemical potential, we have $d\mu = vdP + \eta dT$ ($\underline{v}$ and η are the molar volume and entropy of the phase under consideration), we can write the first of the above equations in the form

$$v^* dP' + \eta' dT = v'' dP'' + \eta'' dT.$$

Further, since $\eta^* - \eta' = \lambda/T$ (λ is the molar heat of evaporation of the layer), we have from (10) the system of equations:*

$$v'' dP'' - v' dP' = \frac{\lambda}{T} dT; \; dP' - dP'' = d\left(2\frac{\sigma}{h} + 2\frac{\partial\sigma}{\partial h}\right) \tag{11}$$

which represents an extension of the Clausius-Clapeyron equation to systems with extensive interfacial areas.

To find the relationship between the heat of evaporation and the layer thickness it is convenient to use the enthalpy: $H = U + PV$. If the system contains a surface phase, it is necessary to consider the surface enthalpy H_s, defined by the expression [10]: $H_s = \epsilon S - \sigma$,** where ϵ is the specific total excess surface energy of the layer. The relationship between the latter and the layer thickness may be represented in the first approximation by an equation analogous to Eq. (5)

$$\varepsilon = \varepsilon_\infty (1 - \delta^2/h^2) \tag{12}$$

* See also [9].

** In contrast to a volume phase, for which the work of expansion is taken as positive, for a surface phase the work of surface contraction is taken as positive.

[here ϵ_∞ is the tabular value of the specific total free surface energy of the liquid; δ is a parameter of approximately the same value as in Eq. (5)].

Consider a quantity of vapor (saturated with respect to the layer) so large that evaporation of the liquid layer in it has no appreciable effect on its pressure. The enthalpy change in evaporation of the layer is:

$$\Delta H = H'' - (H' + H_s).$$

Differentiation of this expression with respect to the evaporated mass (in moles) gives the following expression for the molar heat of evaporation of the layer:

$$\lambda = H''_{\text{mol}} - H'_{\text{mol}} - \frac{\partial H_s}{\partial m}. \tag{13}$$

By definition,

$$H'_{\text{mol}} = u'_{\text{mol}} + P'v'; \quad H''_{\text{mol}} = u''_{\text{mol}} + P''v''.$$

But for the liquid phase $v' \approx v'_0$, and the value of P' is determined by Eq. (3); for the gas phase, assumed to be approximately an ideal gas, we have $P''v'' = P_0 v''_0$, and hence

$$H'_{\text{mol}} = u'_{\text{mol}} + \left(P_0 + 2\frac{\sigma}{h} + 2\frac{\partial\sigma}{\partial h}\right)v' \cong (u'_{\text{mol}} + P_0 v'_0) +$$

$$+ v'_0\left(2\frac{\sigma}{h} + 2\frac{\partial\sigma}{\partial h}\right) = H'_{\text{mol},0} + v'_0\left(2\frac{\sigma}{h} + 2\frac{\partial\sigma}{\partial h}\right);$$

$$H''_{\text{mol}} = u''_{\text{mol}} + P''v'' = u''_{\text{mol}} + P_0 v''_0 = H''_{\text{mol},0}.$$

Further, we have:

$$\frac{\partial H_s}{\partial m} = \frac{1}{S}v'\frac{\partial H_s}{\partial h} = v'\left[\left(2\frac{\epsilon}{h} + 2\frac{\partial\epsilon}{\partial h}\right) - \left(2\frac{\sigma}{h} + 2\frac{\partial\sigma}{\partial h}\right)\right] \cong$$

$$\cong v'_0\left[\left(2\frac{\epsilon}{h} + 2\frac{\partial\epsilon}{\partial h}\right) - \left(2\frac{\sigma}{h} + 2\frac{\partial\sigma}{\partial h}\right)\right]$$

(v'_0 is the molar volume of the layer). Substitution of H'_{mol}, H''_{mol} and $\frac{\partial H_s}{\partial m}$ into Eq. (13) gives for the molar heat of evaporation of the thin layer:

$$\lambda = \lambda_0 - v'_0\left(2\frac{\epsilon}{h} + 2\frac{\partial\epsilon}{\partial h}\right), \tag{14}$$

Therefore, the heat of evaporation is less for a thin layer than for a considerable mass of liquid.

Assuming that the relationship between ϵ and $\underline{h}$ is represented by Eq. (12), and the relationship between σ and $\underline{h}$ by Eq. (5), we have from Eqs. (9) and (14)

$$\frac{\Delta\lambda}{\lambda_0} = \frac{\Delta T}{T_0}\cdot\frac{\epsilon_\infty}{\sigma_\infty},$$

i.e., the relative lowering of the heat of evaporation caused by decrease of layer thickness is somewhat greater than the corresponding lowering of the transition temperature.

SUMMARY

1. In consideration of equilibria in thin liquid layers, it is necessary to take into account effects of the second kind ("disjoining pressure" of the layers) in addition to the usual capillary effects. The effects of the second kind can be correlated with the relationship between the thickness of the layer and its excess surface energy.

2. It has been shown by the methods of thermodynamics that the phase-transition temperature is lower for a liquid in a thin layer than for a considerable mass of liquid. The lowering of the transition temperature is

$$\frac{\Delta T}{T_0} = -\frac{v'}{\lambda_0}\left(2\frac{\sigma}{h} + 2\frac{\partial\sigma}{\partial h}\right),$$

where h is the thickness of the layer.

3. The heat of phase transition also decreases with decreasing layer thickness. The relative decrease of the heat of phase transition is somewhat greater than the relative lowering of the transition temperature.

In conclusion, the author offers his deep gratitude to Corresponding Member of the Academy of Sciences, USSR, B. V. Deryagin, for discussion and valuable advice.

LITERATURE CITED

[1] B. Deryagin and E. Pbukhov, Kolloid. Zhur. 1, 385 (1935); B. V. Deryagin and M. M. Kusakov, Izvest. Akad. Nauk SSSR, Ser. Khim. 5, 1119 (1937); B. V. Deryagin, M. M. Kusakov and L. S. Lebedeva, Doklady Akad. Nauk SSSR 23, 670 (1939); B. Deryagin, Zhur. Fiz. Khim. 14, 137 (1940).

[2] L. M. Shcherbakov, Dissertation [In Russian] (Institute of Physical Chemistry, Acad. Sci. USSR, Moscow, 1950); Trudy Tul'skogo Mekhanicheskogo In-ta 7, 117 (1958); 8, 173 (1958).

[3] L. M. Shcherbakov, Uch. Zap. Kishinevskogo Un-ta 1, 23 (1949); Kolloid. Zhur. 20, 502 (1958).*

[4] B. V. Deryagin, Kolloid. Zhur. 17, 207 (1955).*

[5] B. V. Deryagin and A. S. Titievskaya, Doklady Akad. Nauk SSSR 89, 1041 (1953).

[6] B. V. Deryagin and I. I. Abrikosova, Zhur. Eksperim. i Teoret. Fiz. 21, 425 (1951); Doklady Akad. Nauk SSSR 108, 214 (1956);* Zhur. Fiz. Khim. 32, 442 (1958).

[7] V. K. Semenchenko, Surface Effects in Metals and Alloys [In Russian] (Tech. Theoret. Lit. Press, 1957), p. 24.

[8] L. M. Shcherbakov, Kolloid. Zhur. 14, 379 (1952);* L. M. Shcherbakov and A. S. Bolotin, Uch. Zap. Kishinevskogo Un-ta 11, 153 (1954).*

[9] L. M. Shcherbakov, Uch. Zap. Kishinevskogo Un-ta 5, 117 (1952).

[10] Guggenheim, Modern Thermodynamics [Russian translation] (Moscow-Leningrad, 1941), p. 149.

* See C. B. translation.

EFFECT OF THE ANGLE OF SCATTERING ON THE SECOND VIRIAL COEFFICIENT OF POLYMER SOLUTIONS, DETERMINED BY THE LIGHT-SCATTERING METHOD

V. E. Éskin

Institute of High Polymers, Academy of Sciences, USSR, Leningrad
(Translated from: Kolloidnyi Zhurnal Vol. 22, No. 1, pp. 117-119, January-February, 1960)

(Original article submitted July 18, 1958)

The original theory in which the influence of intermolecular forces on the angular distribution of light scattering in polymer solutions was taken into account [1] yielded a relationship between the scattering angle θ and the coefficient B of the term including the square of the concentration c in the series

$$\frac{Hc}{I_0^u} = \frac{1}{MP(\theta)} + Ac + Bc^2 + \ldots, \qquad (1)$$

where H is an optical constant of the solution; I_θ^u is the excess intensity (after subtraction of scattering in the solvent) of light scattering by the solution at an angle θ to the primary light beam; M is the molecular weight of the dissolved polymer; $P(\theta)$ is the Debye function allowing for intramolecular interference; and A and B are coefficients in the series.

The coefficient A was found to be independent of the scattering angle. In later and more detailed theories [2, 3] it was shown that the coefficient A of the first power of the concentration in the Series (1) also depends on the scattering angle. According to these theories, there should be an apparent decrease of the second virial coefficient with increase of the scattering angle in good solvents. This is confirmed experimentally in a number of instances. We observed such variations of the second virial coefficient for the system methyl methacrylate-chloroform.

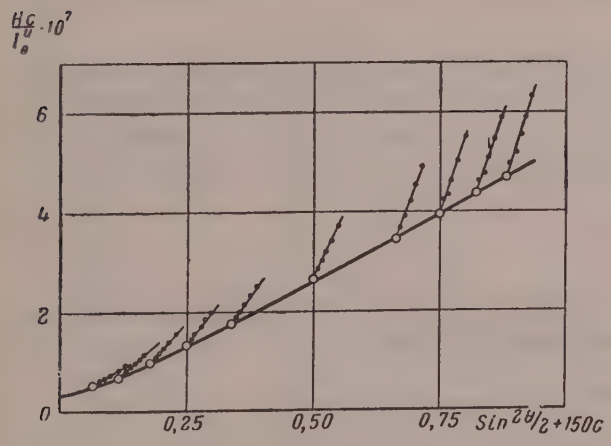


Fig. 1. Angular distribution of light scattering by solutions of poly-p-tert-butylphenyl methacrylate in acetone ($M \approx 25 \cdot 10^6$).

However, in some system the opposite effect is observed — an increase of the second virial coefficient with increase of the scattering angle θ.

Figure 1 shows results obtained in determinations of the angular distribution of light scattering by solutions of polymeric p-tert-butylphenyl methacrylate ($M \approx 25 \cdot 10^6$) in acetone. Solutions at five concentrations, from 0.036 to 0.006 g/100 ml, were investigated. Figure 1 clearly shows a more than fivefold increase of A_2 (slope of the straight lines for constant θ) as the angle θ changes from 30 to 140°.

Figure 2 represents analogous results obtained for light scattering by solutions of poly-β-vinylnaphthalene ($M = 3.5 \cdot 10^6$) for five concentrations

from 0.088 to 0.012 g/100 ml in benzene. In this case, A_2 increases rather less than threefold over the same range of scattering angles.

The angular distribution of light scattering by the solutions was determined by means of a photoelectric nephelometer [4]. The excess scattering by the solutions was 8 to 36 times the scattering by the pure solvent in the former case, and 3 to 17 times in the latter. Before the determinations dust was removed from the solutions by centrifugation for 40 minutes in a gravitational field of 15,000 g.

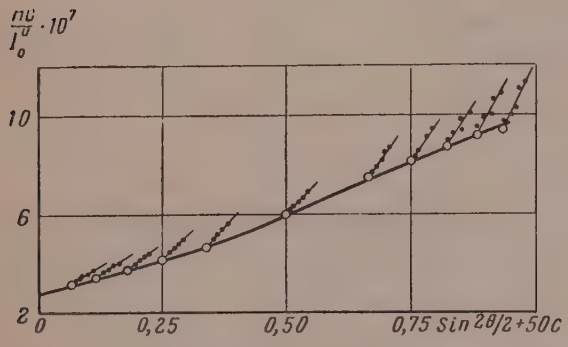


Fig. 2. Angular distribution of light scattering by solutions of poly-β-vinylnaphthalene in benzene ($M = 3.5 \cdot 10^6$).

It must be pointed out that the observed increase of the second virial coefficient with the scattering angle could not have been caused by inadequate purification of the solutions. In presence of dust, the measured asymmetry of light scattering increases on dilution; in this instance the reverse was the case.

It follows that investigation of light scattering by some polymer-solvent systems shows that the existing theories of the relationship between the virial coefficients in Series (1) and the scattering angle are inadequate.

We consider that the observed facts may be qualitatively explained by the following considerations. It is known that the factors which cause an increase in the size of the molecular coils simultaneously distort the scattering indicatrix, decreasing it at large scattering angles. This applies both to volume effects in good solvents [5, 6] and to chain rigidity [7]. Intermolecular forces (repulsion) should weaken effects of this kind. However, on dilution intermolecular collisions ("contacts") become less frequent, and deformation of the indicatrix should be more prominent with decrease of concentration. It is easy to see that this gradual decrease of the indicatrix with decreasing concentration should be manifested experimentally as an increase of the slope of the lines for constant θ with increase of θ.

It is of interest in this connection to correlate our values for the dimensions of the polymer coils with the volumes of solution per macromolecule. The coil dimensions were determined from the initial slopes of the curves [8] in Figs. 1 and 2, and were found to be $(\overline{h^2})^{1/2} \approx 4000$ A in the first case and $(\overline{h^2})^{1/2} = 1700$ A in the second [here $(\overline{h^2})^{1/2}$ is the root mean square distance between the ends of the macromolecular coil]. Taking $0.36\ (\overline{h^2})^{3/2}$ as the "volume" of the coil [9], we find $0.23 \cdot 10^{-13}$ and $1.8 \cdot 10^{-15}$ cm^3, respectively, for this quantity.

Simple calculations show that the volume of solution per molecule at the initial concentration of the light-scattering determinations is $1.2 \cdot 10^{-13}$ and $4.6 \cdot 10^{-15}$ cm^3, respectively. Thus, in both cases the initial concentrations approximately corresponded to "critical" concentrations of molecular "contact" in solution. It is obvious that 6 to 7 fold dilution of the solutions reduced considerably the influence of intermolecular contacts.

SUMMARY

1. It is shown that the second virial coefficient increases with the angle of scattering for solutions of poly-p-tert-butylphenyl methacrylate and poly-β-vinylnaphthalene in benzene.

2. A qualitative explanation of this effect is put forward.

LITERATURE CITED

[1] B. H. Zimm. J. Chem. Phys. 16, 1093 (1948).

[2] A. C. Albrecht, J. Chem. Phys. 27, 1014 (1957).

[3] P. T. Flory and A. M. Bueche, J. Polymer Sci. 27, 219 (1958).

[4] V. E. Eskin, Zhur. Tekhn. Fiz. 28, 7 (1958).

[5] O. B. Ptitsyn, Zhur. Fiz. Khim. 31, 1091 (1957).

[6] H. Benoit, Compt. rend. 245, 2244 (1957).

[7] A. Peterlin, Macromol. Chem. 9, 224 (1953).

[8] B. H. Zimm. J. Chem. Phys. 16, 1099 (1948).

[9] W. Kuhn, Kolloid. Zhur. 76, 258 (1936).

INFLUENCE OF SALTS OF FATTY ACIDS ON POLYMERIZATION OF STYRENE IN EMULSION

A. I. Yurzhenko and S. S. Ivanchov

Ivan Franko University, L'vov, Department of Physical and Colloid Chemistry

(Translated from: Kolloidnyi Zhurnal Vol. 22, No. 1, pp. 120-127, January-February, 1960)

(Original article submitted July 5, 1958)

In emulsion polymerization of unsaturated compounds the aqueous phase of the reaction system often contains electrolytes; they may be introduced into the system as polymerization catalysts (such as $K_2S_2O_8$), as inevitable impurities in the emulsifiers, as pH regulators, or as components of initiating redox systems in low-temperature polymerization.

Added electrolytes may have a strong influence on the colloidochemical properties of an emulsifier. Thus, in their presence the critical concentration of micelle formation falls sharply [1] and the micellar weight of emulsifiers increases [2]. The solubilizing power of emulsifiers is changed sharply on addition of electrolytes; the nature of the electrolyte is significant in this respect [3]. Electrolytes may also influence the course of decomposition of the polymerization catalyst [4].

If it is taken into account that emulsion polymerization of monomers which are insoluble or sparingly soluble in water takes place mainly in the emulsifier micelles, it is clear that the state of these micelles (their size and shape) must be a factor in the process kinetics. The state of the emulsifier micelles also determines the dispersity of the resultant latexes and to some extent the physical and mechanical properties of the polymers formed.

Thus, electrolytes introduced into a polymerization system, having a significant influence on the colloidal state of the emulsifier, may alter the polymerization kinetics and the properties of the resultant polymers.

The effects of inorganic salts (mainly sulfates and chlorides of alkali metals) on emulsion polymerization have been repeatedly studied by a number of workers [3, 5-7].

In the present investigation, it was decided to extend the range of these salts by studying the effects of sodium salts of fatty acids, from sodium formate to sodium palmitate, on the kinetics of emulsion polymerization. With this range of salts, it is possible to study the influence of the hydrocarbon radicals in their anions on emulsion polymerization, and to estimate the significance of their increasing surface activity; this is of practical importance. The technical emulsifiers of the fatty-acid salt type used in production of synthetic rubber are often mixtures of salts of different acids, both higher and lower. The role of the latter, and the need to remove them, is still obscure.

The published literature contains no data on the influence of salts of the lower fatty acids on emulsion polymerization.

Starting materials and methods. The monomer used was styrene. Before use, it was freed from inhibitors by treatment with 20% alkali solution followed by threefold vacuum distillation. The emulsifier was Nekal (sodium dibutylnaphthalenesulfonate), which is often used in the production of polymers by the emulsion process. Electrolyte impurities were removed from Nekal by twofold reprecipitation from absolute alcohol. Potassium presulfate was used as the polymerization catalyst.

The sodium acetate and sodium palmitate were chemically pure. Sodium formate was prepared by neutralization of formic acid by caustic soda and the resultant salt was purified by threefold recrystallization from water. The sodium salts of propionic, butyric, caproic, and caprylic acids, the C_7-C_9 fractions, and lauric acid were prepared by neutralization of the corresponding acids with sodium ethylate by the Harkins method [8]. In accordance with this method, sodium was dissolved in absolute alcohol and the resultant solution was titrated with the acid. The mixture was heated on a water bath for two hours, after which the alcohol was distilled off and the salt was dried and washed with ether in a Soxhlet apparatus.

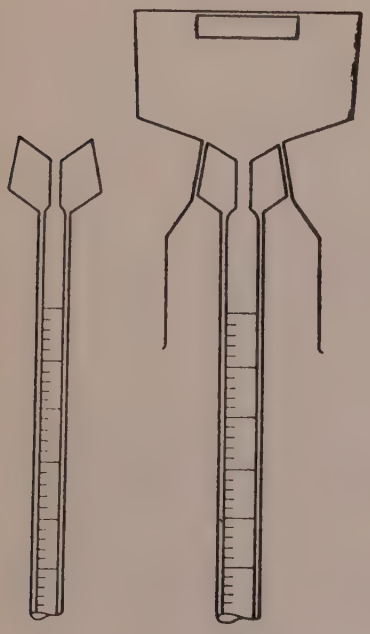


Fig. 1. Dilatometer with gas outlet for determination of the rate of emulsion polymerization.

Polymerization was effected in a dilatometer with a magnetic stirrer, shown in Fig. 1. In distinction from the dilatometer described by Puchin and Yurzhenko [9], the capillary of this dilatometer had a free outlet for the gases which could be formed in small amounts by decomposition of the catalyst ($K_2S_2O_8$) during the polymerization. If these gases are not removed from the dilatometer as soon as they are formed, a distorted picture of the process kinetics is obtained. The dilatometer capillary was filled with styrene. The polymerization was carried out at 50 ± 0.1°. The ratio of the nonaqueous to aqueous phase was 1 :9. The catalyst was used at 0.4% (0.0298 N) concentration, which corresponds to the maximum catalytic activity of persulfate [10]. The nickel concentration was 1% (0.029 N). The concentration of the added salts was varied, and did not exceed 0.3 mole/liter.

The latexes were coagulated by 30% sulfuric acid solution; the polymers were washed with water and then with alcohol in a Soxhlet apparatus.

The molecular weights of the polymers were determined from the intrinsic viscosities of their solutions in benzene at 25 ± 0.1°.

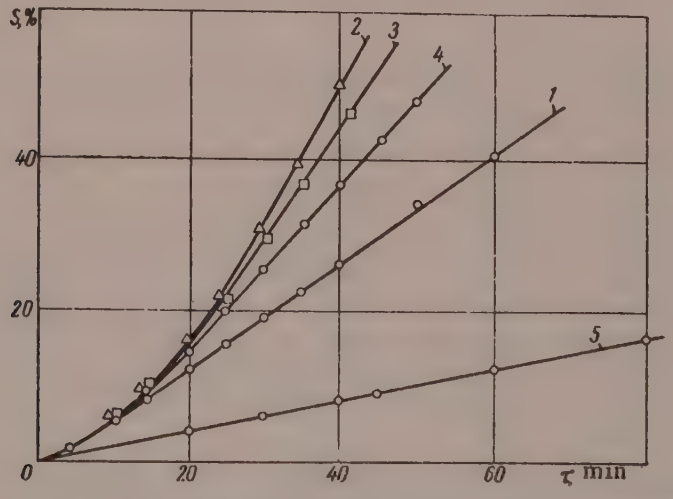


Fig. 2. Yield of polystyrene as a function of time in presence of various amounts of sodium butyrate: 1) No addition; 2) 0.0078 N; 3) 0.025 N; 4) 0.09 N; 5) 0.237 N.

In Fig. 2 the extent of polymerization S (the percentage of monomer polymerized) of styrene is plotted against time τ with different amounts of sodium butyrate in the system. It is clear from Fig. 2 that even small amounts of sodium butyrate increase the yield of polystyrene. At low concentrations of sodium butyrate the

acceleration of polymerization is proportional to the butyrate concentration in the polymerization system. The maximum yield of polymer per unit time is obtained when the sodium butyrate concentration is approximately 0.02 N (calculated for the aqueous phase). On further increase of the amount of butyrate in the polymerization system, the polymerization rate falls with the concentration of sodium butyrate.

The results are qualitatively similar with additions of sodium acetate, propionate, and formate to the polymerization system. In the case of sodium caprylate and higher members of the series, the polymer yield increases continuously with the concentration of the added salt; this is shown in Fig. 3 for sodium laurate.

The graphical relationship between the extent of polymerization S and time τ in the linear region was used to calculate the polymerization rates of styrene in presence of different additions of salts of the fatty-acid series from the equation

$$v = \frac{\Delta S/\Delta\tau}{100} \cdot \frac{\mu}{\gamma} \cdot \frac{1000\, d_M}{M_0},$$

where v is the polymerization rate, μ and γ, respectively, are the relative fractions of monomer and aqueous phase in the polymerization system, and d_M and M_0 are the density and the molecular weight of the monomer.

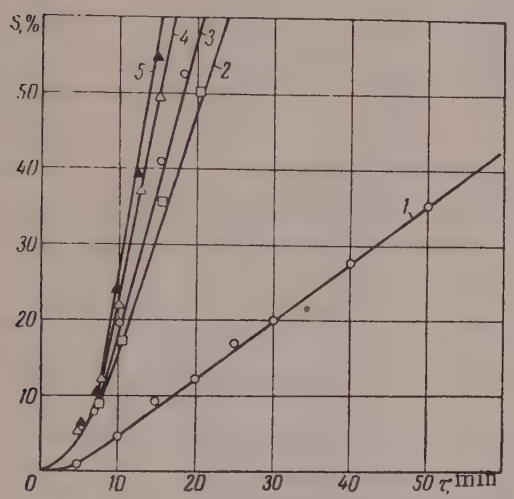


Fig. 3. Yield of polystyrene as a function of time in presence of various concentrations of sodium laurate in the polymerization system (concentration calculated for the aqueous phase): 1) No addition; 2) 0.0098 N; 3) 0.026 N; 4) 0.047 N; 5) 0.088 N.

The results obtained for all the investigated electrolytes are presented in Fig. 4, which shows that, on introduction of the first portions of the salts into the polymerization system up to 0.02 N concentration, the polymerization rate increases in every instance. This increase in the rate of the process depends on the length of the chain in the salt anion — the longer the hydrocarbon radical in the anion, the more pronounced the increase.

On addition of the investigated salts to the polymerization system at concentrations > 0.02 N the polymerization rate alters in different ways with different salts in the series. With additions of salts of the lower fatty acids up to sodium caprate inclusively, the polymerization rate is at a maximum at about 0.02 N concentration. On further additions of these salts to the polymerization system the rate of the process falls. Additions of sodium caprylate at concentrations > 0.02 N have almost no effect on the polymerization rate over the entire concentration range investigated. Salts of acids above caprylic increase the polymerization rate with increase of their concentration; this effect is more pronounced with increase of the length of the hydrocarbon radical in the electrolyte anion.

It follows that in their influence on the polymerization rate the sodium salts of this series of organic acids can be conveniently divided into two groups: the first group of salts of the lower fatty acids (from sodium formate to sodium caproate) which suppress polymerization (at concentrations above 0.02 N), and the second group of salts of fatty acids above caprylic, which continuously accelerate the process with increasing contents in the polymerization system. The action of the salts within each group varied regularly with increase of the hydrocarbon chain in the anion. An exception to this is sodium formate, which has a more pronounced accelerating effect on polymerization than sodium acetate and butyrate, which have longer hydrocarbon chains. With additions of sodium formate the maximum polymerization rate is shifted in the direction of higher concentrations.

The effects of these salts on the molecular weights of the polymers formed are represented in Fig. 5. Addition of salts of this series to the polymerization system produces sharp changes in the intrinsic viscosity $[\eta]$ of solutions of the resultant polymers. The variations of $[\eta]$ of the polymer solutions with the concentrations of the added salts differ in accordance with the length of the hydrocarbon radical in the anion. The intrinsic

viscosity rises sharply on addition of salts of the lower fatty acids – sodium acetate, propionate, butyrate, or caproate – in amounts up to 0.04 N to the polymerization system. Further additions of the same salts up to approximately 0.09-0.12 N result in a decrease of $[\eta]$. In the range from sodium acetate to sodium caproate, there is no difference in the effects of the salts on the intrinsic viscosity; the curves for $[\eta]$ against the salt concentrations coincide. With sodium formate $[\eta]$ for the polymers is considerably lower than with other salts of the same series.

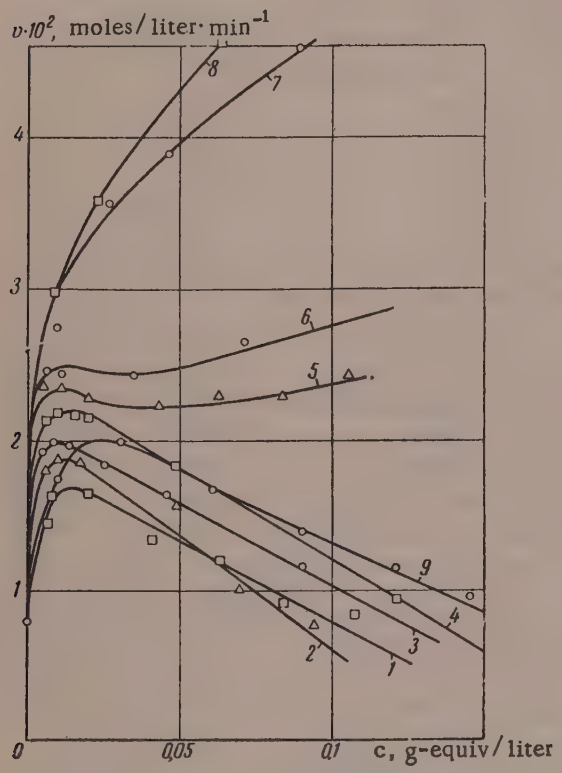


Fig. 4. Variations of polymerization rate with concentration of added sodium salts of fatty acids: 1) Sodium acetate; 2) propionate; 3) butyrate; 4) caproate; 5) caprylate; 6) sodium salts of C_7-C_9 acid fraction; 7) laurate; 8) palmitate; 9) formate.

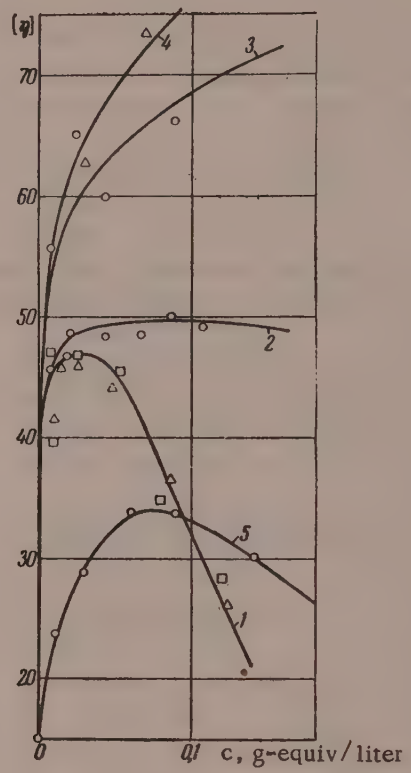


Fig. 5. Variations of the intrinsic viscosity of polymers with the concentration of added salts of fatty acids in the aqueous phase: 1) Sodium acetate to caproate; 2) caprylate; 3) laurate; 4) palmitate; 5) formate.

On addition of sodium caprylate to the polymerization system the intrinsic viscosity increases (on introduction of the first portions), and then remains almost constant over the entire concentration range studied. Addition of salts of acids above caprylic result in a continuous increase of the intrinsic viscosity; this effect is more pronounced with increase in the length of the hydrocarbon radical in the anion.

It is interesting to note that polymers obtained in presence of these salts always have considerably higher $[\eta]$ than polymers formed in polymerization without added salts.

It is easy to see that the relationships between the polymerization rates and intrinsic viscosities of the polymers and the concentrations and nature of the added salts are analogous. At low concentrations, the salts increase simultaneously the polymerization rate and the molecular weights of the polymers formed (since the intrinsic viscosity is proportional to the molecular weight) in all cases. At higher concentrations, the decrease of polymerization rate is accompanied by decreases in the molecular weights of the polymers, although the molecular weight maxima are found at higher salt concentrations than the maxima on the polymerization-rate curves.

The behavior of sodium formate shows some peculiarities; its accelerating effect on polymerization is more pronounced than in the case of sodium acetate, propionate, or butyrate, but $[\eta]$ of the polymers formed is considerably lower than it is in the case of the other salts. The maximum polymerization rate and intrinsic viscosity are found at higher concentrations in the case of sodium formate.

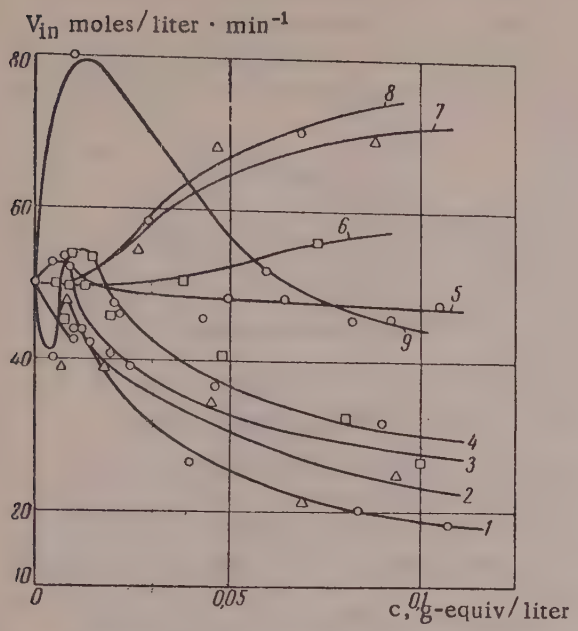


Fig. 6. Effects of concentrations of added salts on the rate of initiation of the polymerization reaction: 1) Sodium acetate; 2) propionate; 3) butyrate; 4) caproate; 5) caprylate; 6) C_7-C_9 fraction; 7) laurate; 8) palmitate; 9) formate.

Data on the polymerization rates and variations of $[\eta]$ for the polymers were used for calculating the relative rates of initiation of polymerization in presence of added salts. With small amounts of added salts of this type (up to 0.01 N) the initiation rates exhibit small maxima. Further, with the lower salts there is a decrease in the initiation rate, which is more pronounced for shorter radicals in the salt anions, while with the higher salts, on the contrary, the initiation rate increases and this effect is intensified with increase in the length of the anion radical. In the case of sodium caprylate, which occupies an intermediate position, the initiation rate remains virtually constant at all concentrations. Here again sodium formate exhibits some peculiarities. With addition of sodium formate, the initiation rate first rises very sharply, passes through a maximum at 0.01 N concentration, and then falls.

The data on polymerization and initiation rates and on the intrinsic viscosities of the resultant polymers can be used to divide these fatty acid salts into two groups in accordance with their influence on the polymerization process: 1) Salts which suppress the polymerization rate at concentrations above 0.02 N, and 2) salts which raise the polymerization rate continuously. Furthermore, the members of the first group (fatty acid salts from sodium formate to sodium caproate) give maxima in the polymerization rates and the molecular weights of the polymers formed and cause a decrease in the initiation rate with increasing concentration in the polymerization system. The second group of salts (salts of acids above caprylic) increase the polymerization and initiation rates and the molecular weights of the polymers when added to the polymerization system. Sodium caprylate occupies an intermediate position.

It follows from Fig. 6 that the salts can also be divided into two groups in accordance with their influence on the rate of initiation of the polymerization reaction: salts (up to sodium caprylate) which suppress the initiation reaction, and salts (above sodium caprylate) which accelerate it. The salts of the first group give rise to small maxima of the initiation rates only in the region of very low concentrations. Sodium formate differs in its action from the other salts in giving rise to a sharp maximum of the initiation rate.

We consider that to account for these results the following effects caused by additions of these salts must be taken into consideration:

1. Changes in the pH of the aqueous phase of the emulsion caused by hydrolysis of the added salts. It was found (with the aid of a glass electrode) that the pH of the aqueous phase varies between 6.8 and 9.5. It was shown earlier [10, 4] that polymerization of styrene in presence of $K_2S_2O_8$ is more rapid when the medium is alkaline. The sharp increase of polymerization rate in presence of small amounts of these salts is caused by this hydrolysis effect. In analogous experiments conducted in presence of Na_2CO_3 (0.1 N), hydrolysis of which resulted in a pH value of 9.5 in the aqueous phase, there was no abrupt increase of polymerization rate on addition of small amounts of the fatty-acid salts (Figs. 7 and 8).

2. These salts may have different salting-out effects on the emulsifier, with corresponding decreases in the critical concentration of micelle formation (CCM).

3. As a result of the surface activity which increases in this salt series from the lower to the higher members, there are increasing stabilization and solubilization effects. At a certain length of the hydrocarbon radical in the salt these effects may predominate over the salting-out action.

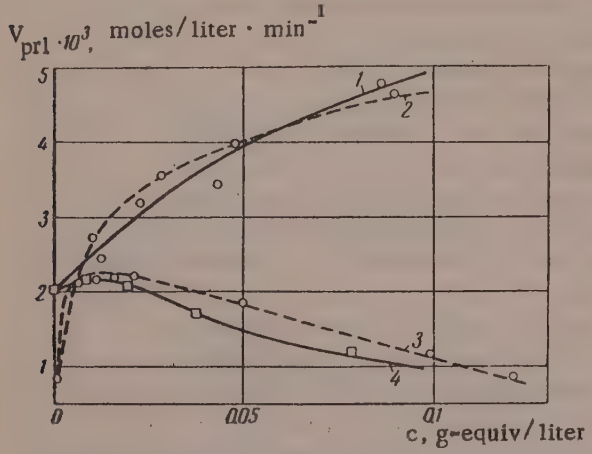


Fig. 7. Variations of the rate of emulsion polymerization with the concentrations of sodium laurate (1, 2) and butyrate (3, 4) in the aqueous phase in soda-buffered (1 and 4) and unbuffered systems (2, 3); Na_2CO_3 concentration 0.015 N.

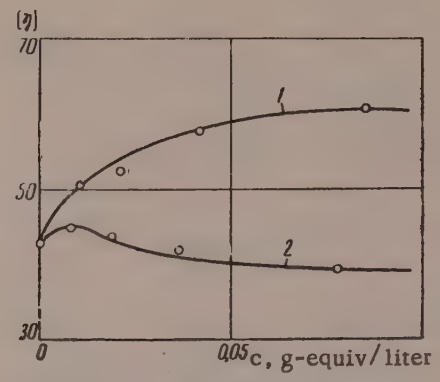


Fig. 8. Variations of the intrinsic viscosity of polymers with concentration of sodium laurate (1) and butyrate (2) in the aqueous phase buffered with Na_2CO_3.

This accounts for the subdivision of the salt series into two groups: 1) The lower members, where the salting-out effect predominates, so that they suppress (at concentrations above 0.22 N) the polymerization process in general and the initiation reaction in particular; 2) salts above caprylate, which continuously accelerate the polymerization process and the initiation reaction.

Increasing additions of salts above caprylate result in a continuous extension of the polymerization zone in the aqueous phase at a given catalyst content, and this is accompanied by an effect specific for emulsion polymerization: increase of the process rate with a simultaneous increase in the molecular weight of the polymer formed.

Conversely, additions of salts below caprylate and the resultant salting out of the emulsifier narrows the zone of the polymerization reaction in the aqueous phase of the monomer emulsion at constant catalyst content, and this produces the reverse effect – decrease of polymerization rate with a simultaneous decrease in the molecular weight of the polymer formed.

The results of investigations of such colloidal properties of emulsifiers as the CCM, turbidity, and tendency to solubilization in presence of the investigated salts are consistent with the foregoing considerations and form the subject of our next communication. On addition to the polymerization system, these salts may have a further effect – change of the decomposition rate of the catalyst.

Our investigation of the kinetics of $K_2S_2O_8$ decomposition in presence of these salts [11] showed that decomposition of the catalyst varies analogously to the polymerization rate. Additions of sodium formate sharply accelerate decomposition of the catalyst, and this accounts for its effect on the polymerization process. This specific behavior of sodium formate can naturally be attributed to the presence of an aldehyde group, which has the properties of an activator in the polymerization system.

SUMMARY

1. Salts of fatty acids can be divided into two groups according to their influence on emulsion polymerization of styrene (this influence varies regularly with increasing length of the hydrocarbon radical): Group I, salts of acids above caprylic, which continuously increase the rate of the process when introduced into the reaction mixture; group 2, salts of acids below caprylic, which suppress polymerization.

2. These salts have an analogous influence on the rate of initiation of the polymerization reaction and on the molecular weights of the resultant polymers: Salts of group 1 increase the initiation rate and the molecular weight, whereas salts of group 2 decrease them after a certain initial increase.

3. These facts are correlated with changes produced by the added salts in the zone of the polymerization reaction in the aqueous phase of the emulsion: an extension in presence of salts of group 1, and a contraction in presence of salts of group 2. This interpretation is consistent with data on changes in the colloidal state of the emulsifier and the dispersity of the synthetic latexes formed in presence of these salts.

LITERATURE CITED

[1] E. D. Goddar, O. Harva, and T. G. Jones, Trans. Faraday Soc. 49, 8 (1953).

[2] A. I. Yurzhenko and R. V. Kucher, Kolloid. Zhur. 13, 226 (1951); 14, 219 (1952).*

[3] N. P. Apukhtina and A. M. Lyagalova, Kolloid. Zhur. 17, 416 (1955);* 18, 3 (1956).*

[4] A. I. Yurzhenko, O. P. Brazhnikova, and N. I. Likholet, Ukrain. Khim. Zhur. 21, 586 (1956).

[5] C. E. Fryling and W. M. John, Industr. and Engng. Chem. 42, 2164 (1950).

[6] W. M. John, C. A. Uraneck, and C. F. Fryling, J. Polymer Sci. 7, 159 (1951).

[7] N. S. Tsvetkov and A. I. Yurzhenko, Kolloid. Zhur. 18, 362 (1956).*

[8] W. Harkins, J. Amer. Chem. Soc. 51, 1675 (1929).

[9] V. A. Puchin and T. I. Yurzhenko, Zavodskaya Lab. 21, 205 (1955).

[10] A. I. Yurzhenko and N. S. Tsvetkov, Kolloid. Zhur. 15, 136 (1953).*

[11] S. S. Ivanchov and A. I. Yutzhenko, Izv. VUZ, Khimiya i Khimicheskaya Tekhnologiya 4, 13 (1958).

* See C. B. translation.

LETTER TO THE EDITOR

THEORY OF DRIFT OF AN AEROSOL PARTICLE IN A STANDING ACOUSTIC WAVE

S. S. Dukhin

Institute of General and Inorganic Chemistry, Academy of Sciences,

Ukrainian SSR, Kiev

(Translated from: Kolloidnyi Zhurnal Vol. 22, No. 1, pp. 128-130, January-February, 1960)

(Original article submitted October 15, 1959)

In a standing acoustic wave suspended particles tend to concentrate either at the antinodes or at the nodes. The periodicity in the distribution of dispersed particles is usually attributed to the so-called "sound pressure" under the influence of which the particles drift toward the nearest antinode or, in other cases, toward a node. King's formula [1] for the sound pressure on a small sphere in a standing acoustic wave is widely used in this connection:

$$F_s = \frac{5}{2} km' (v - u)^2 f \sin 2kx, \tag{1}$$

where $k = \frac{2\pi}{\lambda}$; λ is the wavelength; m' is the mass of the medium displaced by the particle; v and u are the velocity amplitudes of the particle and medium; f is a factor which depends on the density ratio (of the order of unity) of the particle and medium. In derivation of this formula King disregarded the viscosity of the medium, so that Eq. (1) cannot be used in the present instance, where we are concerned with minute particles, the vibrational motion of which relative to the medium is characterized by a Reynolds number less than unity.

In such cases, the action of the acoustic wave on the particle is effected mainly by means of viscosity forces, and to study particle drift it is sufficient to consider the equation for the vibratory motion of a particle [2] in the second approximation, which is equivalent to taking into account anharmonicity of the vibrations:

$$\left(m + \frac{m'}{2}\right) \dot{v} + 6\pi\eta r \left(v + \frac{r}{\sqrt{\pi\nu}} \int_{-\infty}^{t} \frac{v(\tau)\, d\tau}{\sqrt{t - \tau}}\right) =$$

$$= \frac{3}{2} m\dot{u} + 6\pi\eta r \left(u + \frac{r}{\sqrt{\pi\nu}} \int_{-\infty}^{t} \frac{\dot{u}(\tau)\, d\tau}{\sqrt{t - \tau}}\right), \tag{2}$$

where m is the mass of the particle, η and ν are the viscosity and the kinematic viscosity of the medium; r is the particle radius; t is the time; $v = \dot{x}$ is the velocity of the particle; $u = A \sin kx \cdot \sin \omega t$ is the velocity distribution in the standing wave. It may be noted that Eq. (2) represents motion in a rapidly-oscillating field [3], so that Kapitsa's method [4] may be used. Since the vibration amplitude A is much smaller than the wavelength, x in the right-hand side of Eq. (2) may be assumed constant in the course of one period, $x = x_0$. Solution of Eq. (2) with this approximation represents harmonic vibration of the particle about the point $x = x_0$

$$x - x_0 = A' \sin kx_0 \cos(\omega t + \psi), \tag{3}$$

where

$$A' = A\left[\frac{\left(1+3\beta+\frac{9}{2}\beta^2+\frac{9}{2}\beta^3+\frac{9}{4}\beta^4\right)}{\frac{4}{9}\left(\frac{m}{m'}+\frac{1}{2}\right)^2+2\beta\left(\frac{m}{m'}+\frac{1}{2}\right)+\frac{9}{2}\beta^2+\frac{9}{2}\beta^3+\frac{9}{4}\beta^4}\right]^{1/2},$$

$$\tan\psi = \frac{(1+\beta)\beta(1-m/m')}{\left[\frac{m}{m'}\left(\frac{2}{3}+\beta\right)+\frac{1}{3}+2\beta+\frac{9}{2}\beta^2+\frac{9}{2}\beta^3+\frac{9}{4}\beta^4\right]}, \quad \beta = \frac{1}{r}\sqrt{\frac{2\nu}{\omega}}.$$

The right-hand side of Eq. (2) may be regarded as a quasiperiodic force with a slowly-changing amplitude, under the influence of which the particle oscillates and simultaneously undergoes a mean displacement in each period. Since we are concerned only with these displacements, consecutive summation of which represents the particle drift, we find the mean value of Eq. (2) for the period, first resolving sin kx into a series relative to the point $x = x_0$: $\sin kx = \sin kx_0 + k\cos kx_0 \cdot (x - x_0)$, where Eq. (3) should be used for substitution of $x - x_0$. The equation so derived gives the trajectory of the particle, averaged over the period $x_0(t)$

$$\left(m+\frac{m'}{2}\right)\ddot{x}_0 + 6\pi\eta r\left(\dot{x}_0 + \frac{r}{\sqrt{\pi\nu}}\int_{-\infty}^{t}\frac{\ddot{x}_0(\tau)\,d\tau}{\sqrt{t-\tau}}\right) = F(x_0), \tag{4}$$

where

$$F(x_0) = \frac{k}{4}A'A\omega^2 m\left[\sin\psi\cdot\frac{9}{4}(\beta^2+\beta) - \cos\psi\left(\frac{3}{2}+\frac{9}{4}\beta\right)\right]\sin 2kx_0. \tag{5}$$

In the case under consideration, when the Reynolds number is less than unity, it can be shown that the first and third terms in Eq. (4) are small in comparison with the second, and hence

$$6\pi\eta r\dot{x}_0 = F(x_0). \tag{4'}$$

The right-hand side of Eq. (4), which has the meaning of the average force over the period, is greater by several orders of magnitude than the sound pressure calculated from Eq. (1) when $m/m' \sim 10^3$ and at not very high frequencies ($\beta^2 \gtrsim m/m'$), which corresponds to almost complete entrainment of the particles by vibrations of the medium. This result is, in our opinion, very significant, because it indicates that more effective collection of minute particles in the nodal planes is possible than was hitherto believed. In particular, Eq. (4') gives a value of the order of 1 second for the collection time ($\lambda = 3$ cm, $r = 1\ \mu$, acoustic energy density $\Omega = 100$ ergs/cm^3), whereas Eq. (1) gives $\theta \sim 10^3$ seconds.

The acoustic beam should be in a vertical orientation to prevent sedimentation of the particles under gravity. Then the equilibrium distribution of the particles near a nodal plane, reached after time of the order of θ, is determined by the condition of compensation of the particle weight by the force $F(x_0)$.

$$mg = F(x_0). \tag{6}$$

It follows, for example, that at $\lambda = 3$ cm and $\Omega = 100$ ergs/cm^3 particles of radius $r < 1$ are continued over a range $\Delta x \sim 3\cdot 10^{-2}$ cm near the node.

Estimates of the root mean square displacement by thermal motion, carried out by means of the Einstein equation, show that, at least if the particle size is greater than 0.1 μ, thermal motion cannot prevent predominant concentration of the particles near the nodes.

LITERATURE CITED

[1] L. King, Proc. Roy. Soc. 147A, 212 (1934).

[2] N. A. Fuks, Mechanics of Aerosols [In Russian] (Izd. AN SSSR, Moscow, 1955), p. 20.

[3] L. D. Landau and E. M. Lifshits, Mechanics [In Russian] (Phys.-Math. State Press, Moscow, 1958).

[4] P. L. Kapitsa, Zhur. Tekh. Fiz. 21, 5 (1951).

BOOK REVIEWS

Bibliographic Survey of Colloid Chemistry in the USSR, No. 3 [In Russian] (Academy of Sciences, Ukranian SSR Press, Kiev, 1958)

A. V. Dumanskii and Z. M. Vashchenko

(Translated from: Kolloidnyi Zhurnal Vol. 22, No. 1, pp. 131, January-February, 1960)

This book is the third issue of the well-known work by A. V. Dumanskii with his pupils and associates.

The literature cited in this issue comprises 20,000 titles published in the Soviet scientific literature during the period 1942-1952, and is almost exhaustive. As in the previous issues, the literature references are preceded by brief surveys of the publications which appeared during the relevant time intervals. There are three such surveys: for 1942-1945, for 1946-1949, and for 1950-1952. These surveys make the literature lists easier to use by giving a general outline of the work and the main research trends during these intervals.

The book is provided with good alphabetical subject and author indexes.

This book, like the previous two issues, is a valuable aid for every worker engaged in teaching or research. It is especially important for research workers concerned with the history of Soviet chemistry, and in particular of colloid chemistry.

A. V. Dumanskii's book is an important and essential stage in the production of a history of Soviet colloid chemistry. It makes the work of the research scientist and teacher very much easier in searches and selection of necessary literature on colloid chemistry.

It is noted in the preface to the third issue that it contains a list of titles published before the start of "Referativnyi Zhurnal Khimiya," which can completely replace books of the type under review provided that all Soviet publications on general and applied colloid chemistry are exhaustively abstracted. The printing of the third issue (3000 copies) is small in relation to the demand. The first issue was published in 1000 copies, and the second in 3000. Publication of all three issues of the Bibliographical Survey in a single volume would be most desirable. Moreover, the Academy of Sciences, Ukrainian SSR Press should ensure better distribution of this book outside Kiev.

Certain faults, consisting of inaccuracies and misprints, should be corrected when the Bibliographical Survey of Colloid Chemistry in the USSR is republished.

The large and important work by A. V. Dumanskii, the value of which cannot be overestimated, must be welcomed.

V. I. Nazarov

Solutions of High Polymers [In Russian] (Goskhimizdat, Leningrad, 1958) (Ordered Edition), 128 pages.

S. S. Voyutskii

This book forms part of a general course of colloid chemistry given by the author in the Institute of Fine Chemical Technology. The first four chapters constitute an introduction necessary for the subsequent presentation.

Chapter 5 — Nature of polymer solutions — is a critical and interesting account of the micellar and molecular theories of polymer solutions; the molecular nature of these solutions is demonstrated very clearly. The applicability of the phase rule to polymer solutions is demonstrated and illustrated, and association phenomena in such solutions are discussed. A very important section, both practically and theoretically, is concerned with swelling and dissolution of polymers. Thermodynamic aspects of the problem are presented in a framework necessary for further understanding of the material.

In Chapter 6 — Swelling and dissolution of polymers — the characteristics of swelling and dissolution are described as fully as is required in a textbook. It is shown that swelling may be regarded as the first stage of dissolution; the first and second stages of swelling are admirably discussed; the question of the so-called limited swelling is considered in adequate detail, which is lacking in the existing textbooks (which are, it is true, very much out of date). The empirical formulas proposed by J. R. Katz for calculations of contraction and heat of swelling are given. The very important fact is mentioned that swelling may be significantly influenced by the shape of the specimen, as erroneous conclusions may very often be reached if this is disregarded. The data on integral and differential heats of swelling are important.

In Chapter 7 — Some properties of polymer solutions — it is shown in a discussion of the applicability of Raoult's law to polymer solutions that deviations from this law in real solutions may be attributed not only to energy interaction between the two components but also to the manner in which the molecules of solute and solvent are arranged relatively to each other. However, in considering the applicability of Raoult's law for determination of molecular weights of dissolved polymers, the author uses the concept of a "segment," which has not yet been firmly adopted in science; it is hardly advisable to use it in a textbook.

The author shows that in the light of modern data, it may be assumed that the phenomena of swelling and osmosis do not differ from each other in principle. However, it should be taken into account that there is a significant difference between the osmotic pressure of a gel in equilibrium with an external liquid and the osmotic pressure of a polymer solution separated from an external liquid by a semipermeable membrane. The author points out that in application of diffusion phenomena in polymer solutions to determination of molecular weights it is necessary to take into account the shape of the macromolecules, concentration, and other factors influencing the accuracy of the results.

In a discussion of the optical properties of high polymers, it is pointed out that the molecular weight of a solute may be determined by the light-scattering method. The section on viscosity of polymer solutions is presented in adequate detail.

The chapter is concluded by a discussion of the aggregative stability of polymer solutions, and the distinction between the mechanisms of coagulation of colloidal solutions and salting out of polymer solutions is pointed out; the coacervation effect is discussed and explained in the light of modern theories.

In an examination of the so-called aging of polymer solutions the author demonstrates its difference from aging of colloidal solutions and considers that polymer solutions do not undergo an aging process as such. However, we are of the opinion that aging processes should be interpreted more widely.

Chapter 8 — Concentrated solutions of high polymers — contains a discussion of systems which are of great interest, for example, to teaching institutions in the food industry. The effect and mechanism of plasticization are very interesting, as is the question of mutual solutions of high polymers.

Chapter 9 — Solutions of polymeric electrolytes — is too brief in view of the importance of these substances in the most diverse branches of chemistry. Chapter 9 should be expanded in the light of the interests of teaching establishments in the food, textile and other industries.

Chapter 10 — Gelation and syneresis — is, regrettably, also very brief, despite its great interest, and should likewise be expanded.

The whole book is presented in a clear style and is at a high scientific and theoretical level. The field of polymer solutions is so important theoretically and practically that every new work on the subject is most desirable.

It must be noted that the author of this book is not a mere compiler, but presents his views firmly without ignoring other viewpoints and statements. Because of this, the book is to some extent in the nature of a monograph.

There is no doubt that the uses of this book will extend beyond the institute for which it was written. It is only to be hoped that the author will expand the range of his work by introducing some sections of an applied nature, and thus produce a monograph on the subject.

In view of the great importance of polymers in the course of fulfillment of the decisions of the XXI st Congress of the CPSU concerning the extensive growth of the chemical industry, S. S. Voyutskii's book will prove most valuable.

V. I. Nazarov

The Structure and Properties of Porous Materials, edited by D. H. Everett and F. S. Stone (Butterworths, London, 1958)

(Translated from: Kolloidnyi Zhurnal Vol. 22, No. 1, pp. 131-132, January-February, 1960)

This book contains the papers (and the subsequent discussions) presented at the International Symposium on the Structure and Properties of Porous Materials, organized by the Colston Research Society in Bristol in March, 1958.

The paper by Rideal, which was of a general introductory character, was followed by a survey paper by Barrer (London), entitled "Aspects of sorption in porous crystals." The main difference between porous crystals and ordinary porous sorbents (charcoals, silica gels, porous glasses, etc.) lies in the regular and repeating pore shape, determined by their crystal-chemical structure; the pores are very small, down to 10 A or somewhat greater, so that the crystals act as molecular sieves. The shapes and sizes of pores found in crystals of various origins, distribution of sorbed molecules in these pores, and the influence of the chemical nature of cations on their sorption and molecular-sieve properties are discussed in the paper. The question of the mobility of molecules in the very limited space available in the pores of porous crystals was raised in the discussion.

The paper by Wynne-Jones (Newcastle on Tyne, England): "Surface characteristics of carbons," contained data on the surface area, structure, and chemical composition of fine-pored carbons. It was suggested that the structure of such carbons consists of more or less randomly arranged carbon crystallites at the edges of which carbon atoms are linked to hydrogen, oxygen, sulfur, and nitrogen. The acidic properties of carbon surfaces were studied, and experiments on electrochemical oxidation were carried out. Doubts were expressed in the discussion concerning the reliability of determining the surface area of such fine-pored sorbents as these carbons by the classical adsorption methods. The possible sintering mechanism of carbons during thermal treatment was also discussed.

In his communication "Energetics of sorption" Kington (London) analyzed theoretically the causes of surface heterogeneity of ionic porous crystals of the chabazite type; determinations of the heats of adsorption of various gases on them led to the conclusion that for such adsorbents the role of electrostatic energy is greater than that of dispersional energy in giving rise to heterogeneity, and that the quadrupole moments of the adsorbed molecules are of great significance. In the discussion Barrer made the interesting suggestion that the expected severalfold increase of the heat of adsorption of a molecule within the cavity of a porous crystal as compared with adsorption on a face is considerably less in practice owing to the fact that the number of atoms per unit volume of such an adsorbent is several times less than in a continuous solid.

The next two papers were concerned with adsorption methods for studying the structure of porous bodies. Until very recently, the great majority of investigations in this field have been based on the concept of cylindrical capillaries, although sorbents differing greatly in nature, known to differ very much in pore shape, were investigated. At best, it was merely noted that the pore-size distribution so determined is conventional in character. However, there is an increasing need for more precise concepts of true pore shape and for methods which give out conventional but real pore-size distributions in real adsorbents. Both these papers fill this gap to some extent. In the first of these, entitled "Shapes of capillaries," de Boer (Holland) gave a classification of the known types of hysteresis in sorption isotherms. He distinguished five types of hysteresis loops. Fifteen models of different pore shapes were considered and it was shown how capillary condensation in each or in combinations of them leads to different types of loop. The results were illustrated by experimental data and excellent electron micrographs, and the prevalence of different types of sorption hysteresis was indicated. Important views were put forward on the width of the hysteresis loop and its relation to the adsorbent structure. In the discussion attention was drawn to possible reversible capillary condensation around the contact points between particles in corpuscular structures. Experimental evidence was adduced in favor of using the desorption branch of the isotherm for calculation of pore-size distribution.

In the second of these papers: "Some problems in the investigation of porosity of adsorption methods," Everett (Bristol) noted the importance of studying the volume-surface ratio of pores. This ratio differs for different pore models, and yet it is not a definite characteristic of a given model, and other independent methods such as electron microscopy, x-ray techniques, etc., are needed for determinations of pore type or the shape of the particles in the adsorbent skeleton. Everett made the very interesting suggestion that the behavior of individual elements of certain structures in the course of desorption is not completely independent; the form of the desorption branch of the isotherm depends on the way in which the elements are grouped in the structure. For such structures the usual method for finding the pore-size distribution from the desorption branch does not give correct results. Possibly the significance of this suggestion is not very wide because in many structures each pore communicates with its neighbors through several (4-6 or even 8) "windows," and the probability that any structural element is surrounded by necessarily smaller neighbors is apparently not high, although it should be taken into account.

In the following two papers, the flow of gases through porous bodies was considered. In the paper by Dacey and Fendley (Canada) entitled "Flow of low-boiling gases through Saran charcoal" an account was given of a study of the flow of hydrogen, argon, neon, and methane through fine-pored charcoal at low adsorptions; it was found that it conforms to the mechanism of Knudsen and surface diffusion. The activation energy of surface diffusion proved to be somewhat less than the heat of adsorption for these gases. Wiggs (London), in his paper, "Relation between gas permeability and pore structure of solids," considered the motion of gases through porous solids by mechanisms of viscous molecular and mixed flow. It follows from the data presented in the paper that permeability due to molecular flow varies in proportion to the pore size, and that due to viscous flow, in proportion to the square of the pore size. Examples were given of the influence of porosity on gas permeability and on penetration of mercury through several typical porous structures. The general conclusion was drawn that there is no unique correlation between permeability and pore-size distribution, but semiempirical formulas can nevertheless be derived for certain materials.

Whereas the physical properties of homogeneous solid particles, determined by the specific properties of their constituent material, have been extensively studied, the statistics of heterogeneous assemblies of such particles and the influence of statistical factors on the properties of solid bodies have been considered very little in the past. This gap is partially filled by the paper by Flood (Canada): "Statistical descriptions, correlation factors, and physical properties of granular and porous solids." The paper contains a simplified statistical description of heterogeneous assemblies, with examples of the influence of certain statistical factors on the

general physical properties of the systems, such as Poiseuille flow, adsorptive expansion of porous materials, and others.

The paper by A. Kiselev (Moscow): "Structure of certain corpuscular adsorbents and its influence on their adsorption properties" contained the results of studies of geometrical and chemical modification of silica gels, carbon blacks, and magnesium hydroxide and oxide. The influence of geometrical modification was studied by calculations of equilibria for adsorbent models composed of spherical particles packed in different ways, and by experimental determinations of adsorption isotherms for unpressed and pressed samples of silica gel and carbon black in conjunction with investigations by electron microscopy. The influence of chemical modification of the surface was illustrated by the relationship between adsorption of a wide range of substances and the degree of surface hydration in silica gel and nonporous silicas. Kiselev's equations for isotherms of adsorption of vapors on homogeneous surfaces, with interaction of the adsorbed molecules taken into account, were also considered. The subsequent discussion dealt extensively with all aspects of geometrical and chemical methods of adsorbent modification.

The paper by Foster and Thorp (London): "Preparation and adsorptive properties of silica gels" dealt with studies of the influence of solution pH in gel formation on the properties of the resultant silica gel. It was shown in experiments on adsorption of water and ethanol that the pore size increases with rise of pH. The influence of acid extraction of ferric oxide on the structure of mixed silica-ferric oxide gel was also studied.

Schofield (Oxford), in his paper entitled, "Influence of surface charges on the properties of porous materials," discussed the results of a study of the ion-exchange properties of soils, with estimations of the surface charges and potentials of soil particles.

The paper by Mougey, Francois-Rossetti, and Imelik (Paris): "Influence of adsorption of cations on the texture and structure of silica gels" was concerned with the influence of the nature and concentration of cations adsorbed from solutions, and of the temperature and pressure in the subsequent heat treatment, on the texture of silica gels which was studied by adsorption of nitrogen vapor. They established the very interesting fact that the texture of silica gels containing ferric ions is stable but in presence of calcium, sodium, and potassium ions, it is variable.

In the communication by Kavtaradze (Moscow): "Structure of porous metal films and its influence on chemisorption properties" it was shown that changes in the structure of films of nickel and other metals as the result of consecutive condensation of their vapors or as the result of recrystallization do not have a significant influence on chemisorption properties per unit surface area.

The next two papers were concerned with the structure of porous materials. The pores in paper are spaces between fibers, mainly cellulose, orientated in the sheet plane. Studies of the shape, size, and configuration of these fibers are important for understanding of the mechanical, optical, filtration, and other properties of paper. The paper by Rance (Beaconsfield, England): "Porous structure of paper" contained a review of methods used for studying the structure of paper. Determination of the volume and surface area of pores in paper by the mercury-penetration method and by penetration of gases displacing an inert liquid was considered in detail. The subsequent discussion also dealt with filtration through paper and its application to structure determinations. The next paper, by King (Leeds, England): "Interaction of swelling agents with wool and nylon," was in the nature of a review of different theories of sorption of swelling agents by polymers (such as nylon), forms of bonding between the active groups in polymers and these agents, the partially crystalline nature of polymers, and changes in their permeability as the result of swelling. These questions were discussed in the light of experimental data on sorption of various solvents by polymers and dissolution of the latter, and on x-ray analysis and infrared spectroscopy.

Honeyborne and Harris (Garston, England) showed in their paper entitled, "Structure of porous building stone and its relation to weathering behavior" that studies of the structure of building stone may give useful information on its resistance to weathering, frost, and other atmospheric conditions. Convenient practical methods for structure determination were described and discussed, and compared with the methods generally used in the building industry.

The last paper, by Preston (Leeds): "Ascent of sap and movement of soluble carbohydrates in stems of higher plants" contained a discussion of possible mechanisms of upward movement of sap and descent of carbohydrate solutions. The author's views on the mechanism of the two movements were substantiated by the results of experiments with growing trees and electron micrographs of microtome sections.

The above brief review of the papers presented at the symposium shows that the structure and properties of a very wide range of natural and synthetic porous materials were considered and discussed. The participants discussed the investigation methods and the various theories which account for the observed facts.

The symposium proceedings are very valuable for those concerned with studies, production, and applications of various porous materials; i.e., for a wide circle of scientists and engineers.

A. P. Karnaukhov

SIGNIFICANCE OF ABBREVIATIONS MOST FREQUENTLY ENCOUNTERED IN SOVIET PERIODICALS

FIAN	Phys. Inst. Acad. Sci. USSR.
GDI	Water Power Inst.
GITI	State Sci.-Tech. Press
GITTL	State Tech. and Theor. Lit. Press
GONTI	State United Sci.-Tech. Press
Gosenergoizdat	State Power Press
Goskhimizdat	State Chem. Press
GOST	All-Union State Standard
GTTI	State Tech. and Theor. Lit. Press
IL	Foreign Lit. Press
ISN (Izd. Sov. Nauk)	Soviet Science Press
Izd. AN SSSR	Acad. Sci. USSR Press
Izd. MGU	Moscow State Univ. Press
LEIIZhT	Leningrad Power Inst. of Railroad Engineering
LET	Leningrad Elec. Engr. School
LETI	Leningrad Electrotechnical Inst.
LETIIZhT	Leningrad Electrical Engineering Research Inst. of Railroad Engr.
Mashgiz	State Sci.-Tech. Press for Machine Construction Lit.
MEP	Ministry of Electrical Industry
MES	Ministry of Electrical Power Plants
MESEP	Ministry of Electrical Power Plants and the Electrical Industry
MGU	Moscow State Univ.
MKhTI	Moscow Inst. Chem. Tech.
MOPI	Moscow Regional Pedagogical Inst.
MSP	Ministry of Industrial Construction
NII ZVUKSZAPIOI	Scientific Research Inst. of Sound Recording
NIKFI	Sci. Inst. of Modern Motion Picture Photography
ONTI	United Sci.-Tech. Press
OTI	Division of Technical Information
OTN	Div. Tech. Sci.
Stroiizdat	Construction Press
TOE	Association of Power Engineers
TsKTI	Central Research Inst. for Boilers and Turbines
TsNIEL	Central Scientific Research Elec. Engr. Lab.
TsNIEL-MES	Central Scientific Research Elec. Engr. Lab.—Ministry of Electric Power Plants
TsVTI	Central Office of Economic Information
UF	Ural Branch
VIESKh	All-Union Inst. of Rural Elec. Power Stations
VNIIM	All-Union Scientific Research Inst. of Meteorology
VNIIZhDT	All-Union Scientific Research Inst. of Railroad Engineering
VTI	All-Union Thermotech. Inst.
VZEI	All-Union Power Correspondence Inst.

Note: Abbreviations not on this list and not explained in the translation have been transliterated, no further information about their significance being available to us. — Publisher.

EXPERIMENTAL STUDY OF THE RHEOLOGICAL PROPERTIES OF HIGHLY DISPERSE MINERAL SUSPENSIONS

U. Ts. Andres

Institute of Combustible Minerals, Academy of Sciences, USSR, Moscow

Translated from: Kolloidnyi Zhurnal Vol. 22, No. 2, pp. 137-142, March-April, 1960

Original article submitted January 3, 1959

The extensive utilization of fine mineral suspensions as separation media for beneficiation of useful minerals makes it necessary to study the effects of concentration (c) and dispersity of the solid phase on the rheological properties of separation media. The literature contains much data on dilute suspensions of spherical particles, conforming to the Einstein equation or to its modified form for concentrated suspensions (Vand's equation). Much less work has been done on highly disperse suspensions, between the particles of which structural forces arise, and as the result of which the suspensions have yield values in addition to purely hydrodynamic interaction.

Dispersity Data on the Powders Used for Preparation of the Suspensions Studied

Barite, $\rho = 4.5$ g/cm^3		Ferrosilicon, $\rho = 5.1$ g/cm^3		Magnetite, $\rho = 5.2$ g/cm^3	
d, μ	S*, cm^2/g	d, μ	S, cm^2/g	d, μ	S, cm^2/g
3.26	4085	4.97	2340	1.510	7620
2.19	6050	4.0	3520	0.995	11600
1.88	7050	2.91	3980	0.867	13300
1.25	10650	1.35	8400	0.657	17600
		0.77	14800		
		0.35	32400		

* The specific surface (S), found by direct experiment, is connected with the particle diameter (d) by the simple relationship $S = \frac{60{,}000}{d\rho}$.

In view of the fact that in industrial media the finest fractions of a suspension play the most important role in flocculation of the solid-phase particles, the greatest interest attaches to studies of the rheological parameters of highly disperse suspensions.

The materials used as the disperse phases of the suspensions were barite, ferrosilicon, and magnetite, which are the commonest types of weighting agents for mineral suspensions used in beneficiation technology. Finely ground disperse phases of different degrees of dispersity (see table) were made by wet vibratory grinding with different residence times in the mill.

The rheological characteristics (dynamic yield value τ_d, static yield value τ_s, and plastic viscosity η*) were determined in a plastoviscosimeter of the Couette type with fluted coaxial cylinders. The cylinder height

was 60 mm; the gap width was 1 mm. Volarovich and Tolstoi [1] were the first to show that the mechanical properties of highly disperse mineral suspensions can be studied in apparatus of this type.

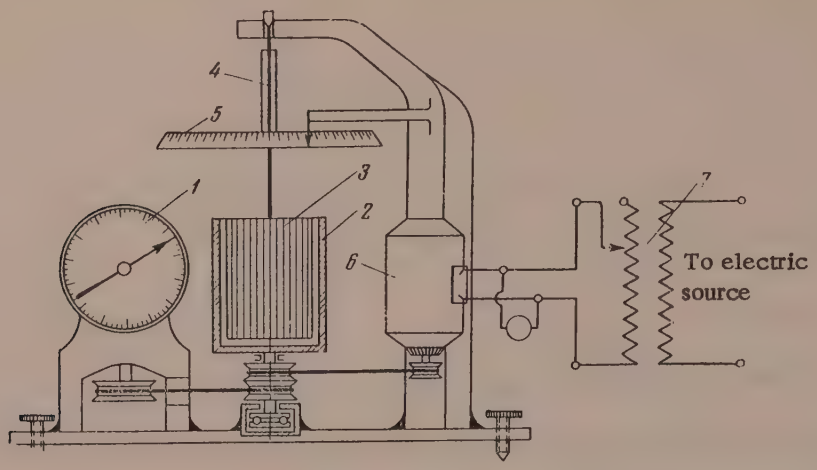


Fig. 1. Diagram of plastoviscosimeter for determination of τ_d and η': 1) Tachometer; 2) outer rotating cylinder; 3) suspended cylinder; 4) torsion wire; 5) graduated dial; 6) motor; 7) autotransformer.

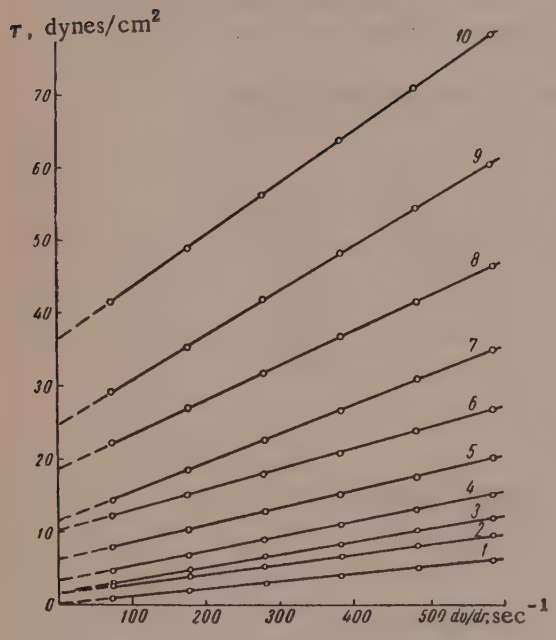


Fig. 2. The $\tau = f(dv/dr)$ relationship for aqueous barite suspensions; $d = 3.26\ \mu$, volume concentrations of barite: 1) Without barite; 2) 0.057; 3) 0.086; 4) 0.142; 5) 0.143; 6) 0.174; 7) 0.200; 8) 0.228; 9) 0.257; 10) 0.286.

Figure 1 is a line diagram of the apparatus, with the rotation speed of the outer cylinder variable by means of a rheostat. This apparatus was used for determinations of τ_d and η'. A similar apparatus with a slowly rotating outer cylinder (rotation speed of 0.2 rpm) was used for determinations of τ_s. Two wires, with constants of 0.374 and 1.186 dyne/cm^2 · degree, were used in the plastoviscosimeters, in accordance with the structural strength of the suspension. The determinations were performed after the system had been allowed to rest in the annular gap for 1 minute. For each system six points were determined for plotting of the flow curve. The velocity gradient was varied in the range of 50 to 600 sec^{-1}, and the data were determined over a period of 30-40 seconds from higher to lower rates of rotation. Each determination was performed 3 times. The reproducibility was generally good. The deviation from mean values did not exceed 2.5%, the average deviation being 0.8%. The strengths of the coagulation structures under static conditions (τ_s) were also determined after the suspensions had been at rest for 1 minute. The deviation of τ_s from the average value for three determinations did not exceed 3.2%; the mean value was 1.4%.

In analysis of the influence of sedimentation on the accuracy of the determinations of the shearing strength of the structures, it must be noted that the concentration gradient of the solid phase up the cylinder [which had the average value of 8% during the experiment for the concentration range of 0 to 0.15 (by volume), and 2.4% for the concentration range of 0.15 to 0.30] had no appreciable influence on the values found for any of the suspensions. The data indicate (see Figs. 3 and 4) that in the concentration range from 0 to 0.15 the function $\tau_d = f(c)$ is linear and τ_d is proportional to the average concentration of the solid phase in

the suspension volume. In the concentration range between 0.15 and 0.30 the $\tau_d = f(c)$ relationship deviates slightly from linearity owing to slight sedimentation at high suspension concentrations. All the determinations were carried out at 18 ± 0.5°.

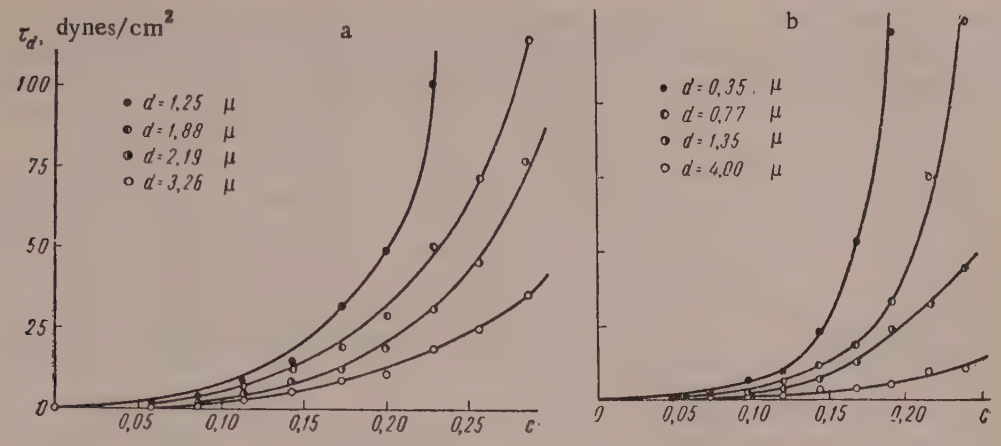


Fig. 3. The $\tau_d = f(c)$ relationship for suspensions of barite (a) and ferrosilicon (b).

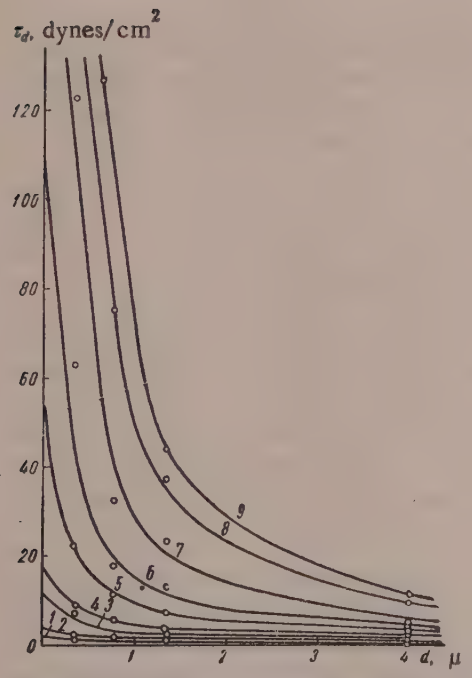


Fig. 4. The $\tau_d = f(d)$ relationship for aqueous ferrosilicon suspensions with ferrosilicon concentrations: 1) 0.048; 2) 0.718; 3) 0.097; 4) 0.119; 5) 0.143; 6) 0.167; 7) 0.192; 8) 0.216; 9) 0.240.

Four barite fractions and four ferrosilicon fractions were used for determinations of τ_d at different concentrations of the solid phase. Each fraction was used for preparation of 8-10 suspensions of different concentrations, with densities of: 1; 1.2; 1.3; 1.4; 1.5; 1.6; 1.7; 1.8; 1.9; 2.0 g/cm^3. The relationship between the concentration (c), density of the weighting agent (ρ), and density of the suspension (ρ_s) was found from the equation $c = \frac{(\rho_s - 1)}{(\rho - 1)}$.

In the studied range of velocity gradients, all the suspensions behave as Shvedov-Bingham viscoplastic bodies. The suspension viscosities were calculated from the equation $\eta' = \frac{(\tau - \tau_d)}{(dv/dr)}$.

Figure 2 shows the results obtained in determinations of $\tau = f(dv/dr)$ at various volume concentrations and dispersities for aqueous barite suspensions. In Fig. 3 the $\tau_d = f(c)$ relationships for barite and ferrosilicon suspensions are given. It follows from Fig. 3 that a certain critical concentration divides each $\tau_d = f(c)$ curve for ferrosilicon suspensions (Fig. 3, b) into two regions. On the average, the critical point corresponds to $c \approx 0.15$. In barite suspensions, the structural strength of the systems increases monotonically (Fig. 3, a).

Figure 4 shows variations of the shear strength of the structure with the dispersity for ferrosilicon suspensions. It follows from Fig. 4 that the $\tau_d = f(d)$ relationship becomes sharply pronounced at a certain concentration and near a certain dispersity. Thus, these limits are at $c > 0.114$ and $d < 3.5$ μ for barite suspensions, and at $c > 0.967$ and $d < 4.5$ μ for ferrosilicon suspensions. The differences between the numerical values of the critical points indicate that in addition to the concentration and dispersity of the solid phase in the suspension there is a further factor which is associated with the physicochemical properties of the substance and which influences the formation of orientation structures and therefore the dynamic yield value.

It should be noted that one of the principal distinctions between the apparent viscosity of a non-Newtonian liquid such as a fine mineral suspension and the true viscosity of a Newtonian liquid is that η', like τ_d, depends on the dispersity of the solid phase.

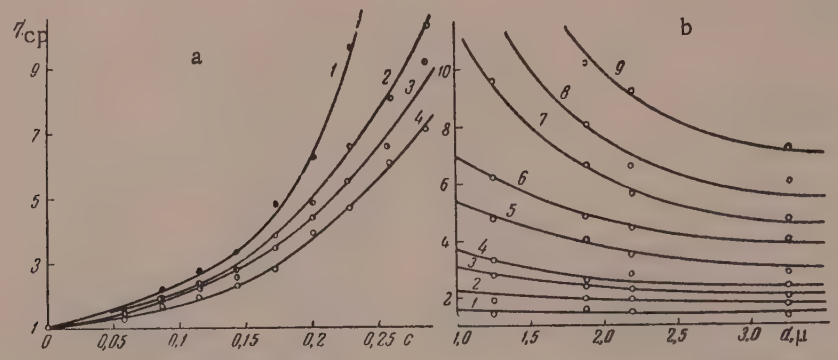


Fig. 5. Variations of η' with c for barite suspensions at different dispersities (a), and with d at different concentrations (b): a) Dispersity d, μ: 1) 1.25; 2) 1.88; 3) 2.19; 4) 3.26; b) Relative concentration: 1) 0.048; 2) 0.072; 3) 0.097; 4) 0.12; 5) 0.143; 6) 0.167; 7) 0.192; 8) 0.216; 9) 0.240.

Figure 5 represents variations of plastic viscosity with the concentration (a) and dispersity (b) of the solid phase in barite suspensions (the corresponding graphs for ferrosilicon suspensions are similar). These graphs are analogous in character to the graphs for yield value. The values of η' begin to be influenced by the dispersity of the solid phase at $c > 0.143$ and $d < 3.2\ \mu$ in barite suspensions and $c > 0.143$ and $d < 4.4\ \mu$ in ferrosilicon suspensions.

Figure 6 represents the $\eta'(\tau_d)$ relationship for barite suspensions (the corresponding graph for ferrosilicon suspensions is similar). It is clear from Fig. 6 that the function $\eta'(\tau_d)$ is close to a straight line

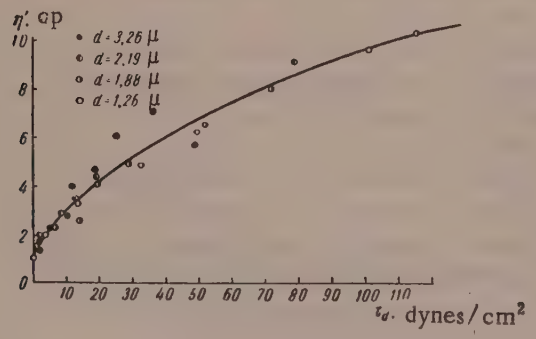


Fig. 6. Variations of η' with τ_d for barite suspensions.

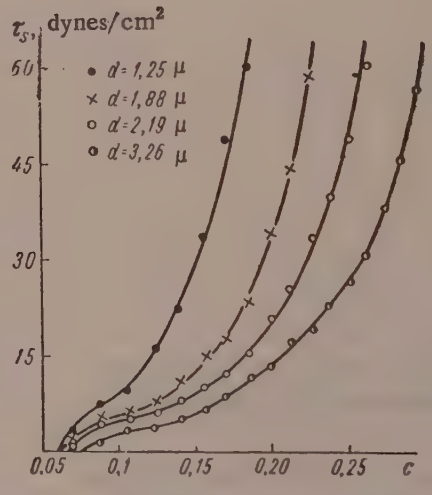


Fig. 7. Variations of τ_s with c for barite suspensions.

which does not pass through the coordinate origin. Figure 6 leads to the conclusion that a correlation exists be between τ_d and η', so that analysis of the data permits expression of one of these quantities in terms of the other, and this would significantly simplify the general expression for the relationship.

For static investigations of the shear strength of the structure arising as the result of growth of coagulation structures during a resting period of 1 minute, magnetite suspensions were studied in addition to barite and ferrosilicon. The relationship between the static yield value τ_s and c for barite, ferrosilicon, and magnetite

suspensions respectively is more complex than the relationship between the dynamic value τ_d and $\underline{c}$ (Fig. 7). The values of $\frac{d\tau_s}{dc}$ for the three cases are all different at similar concentrations and dispersities.

Figure 8 represents $\tau_s(d)$ relationships for ferrosilicon (a) and magnetite (b) suspensions. The influence of dispersity on formation of coagulation structures differs considerably for different suspensions. For example, in barite suspensions this influence becomes pronounced at $d > 3.0\ \mu$, in ferrosilicon suspensions at $d > 5.0\ \mu$, and in magnetite suspensions at $d > 1.6\ \mu$.

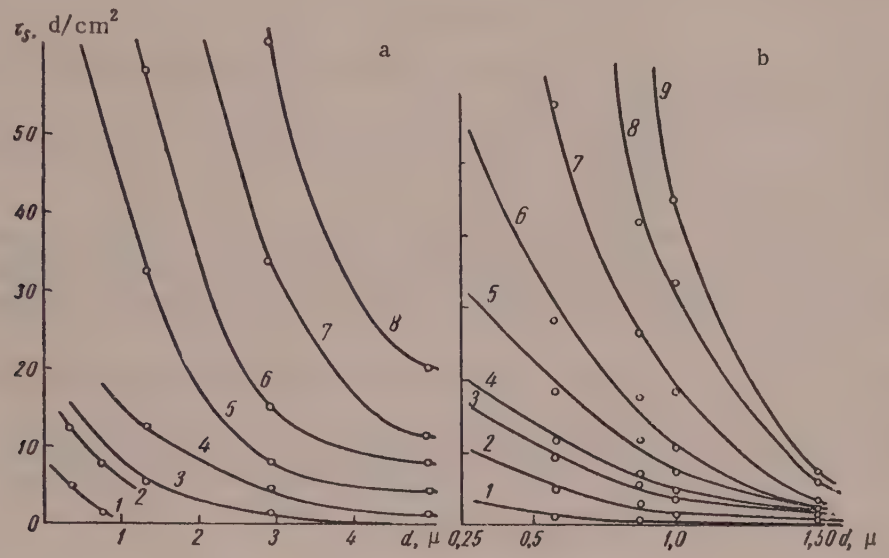


Fig. 8. Variations of τ_s with d at different concentrations: a) Ferrosilicon suspensions: 1) 0.14; 2) 0.164; 3) 0.225; 4) 0.262; 5) 0.288; 6) 0.314; 7) 0.341; 8) 0.367; b) Magnetite suspensions: 1) 0.071; 2) 0.088; 3) 0.104; 4) 0.121; 5) 0.137; 6) 0.154; 7) 0.170; 8) 0.187; 9) 0.203.

There have been several recent studies of the rheological properties of mineral suspensions used in technological beneficiation of useful minerals. Some authors disregard anomalous viscosity and consider such media as Newtonian liquids. As a result, they determine average effective viscosity parameters which depend on the instrument used and which do not represent the invariant characteristics of the medium. This applies to the work of Scala [2], who determined the viscosity of concentrated ferrosilicon suspensions at $\underline{c}$ up to 0.43 in a capillary viscosimeter, but did not take the yield value into consideration.

Volarovich and Tolstoi [1] used a coaxial-cylinder viscosimeter to demonstrate that the Shvedov-Bingham equation is applicable to the flow of a kaolinite suspension. In the present investigation this conclusion was confirmed for the systems studied in this instance. A similar conclusion was reached by Govier, Snook, and Lilge [3] who studied the mechanical properties of galenite, magnetite, and ferrosilicon suspensions in relation to the concentration of the solid phase by means of a Fann coaxial-cylinder viscosimeter (the velocity gradient was varied between 10 and 1000 sec^{-1}), and by Van der Welt and Fourie [4], who studied magnetite and shale suspensions in a modernized Stormer viscosimeter.

Numerous investigations have been concerned with the appearance of the properties of a non-Newtonian liquid in a suspension with increasing concentration of the solid phase. For example, Bingham recorded that in aqueous suspensions of diatomite clays τ_d appears at concentrations above $c = 0.129$. Oden found that the corresponding value of $\underline{c}$ for sulfur suspensions in water is 0.250, and Scott-Blair and Hauser found that in aqueous suspensions of bentonite clays τ_s appears in the concentration range between 0.02 and 0.001.

Our investigations show that in highly disperse suspensions τ_d appears at low concentrations, without any abrupt strengthening of the structure. Nevertheless, coagulation structures arise and τ_s appears after a certain concentration "threshold" has been passed. In our experiments, this threshold at various dispersities corresponds

to concentrations between 0.05 and 0.07 for barite suspensions, between 0.12 and 0.24 for ferrosilicon suspensions, and between 0.07 and 0.08 for magnetite suspensions.

Of the three types of suspensions studied, ferrosilicon suspensions have the highest fluidity and lowest structural strength under given conditions. As already noted, this fact may be attributed to differences in the physicochemical properties of the minerals studied, and is probably associated with the heat of wetting of the solid phase by the liquid.

SUMMARY

1. Highly disperse aqueous suspensions of barite and ferrosilicon are viscoplastic bodies, the flow of which conforms to the Bingham-Shvedov equation.

2. The dispersity of the solid phase, as well as its concentration, plays an important part in determining the rheological properties of these disperse systems.

3. In contrast to the dynamic yield value (τ_d), which begins to increase with increasing concentration of the solid phase virtually from zero in highly disperse suspensions, the static yield value (τ_s) appears abruptly after a concentration threshold, different for different substances, has been passed. The relationship between τ_s and concentration is more complex than the $\tau_d - c$ relationship.

4. Of the three types of suspensions studied, ferrosilicon suspensions had the highest fluidity at given values of c and d.

I am deeply grateful to Professor M. P. Volarovich for valuable advice in the course of this investigation.

LITERATURE CITED

[1] M. P. Volarovich and D. M. Tolstoi, Zhur. Fiz. Khim. 4, 815 (1933).

[2] K. Scala, Rudy 6, 1 (1958).

[3] M. Govier, L. Snook, and N. Lilge, Canad. Mining and Metallurg. Bull. 50, 541 (1957).

[4] P. S. Van der Welt and A. Fourie, J. S. Afric. Inst. of Mining and Metallurg. 57, 42 (1957).

INVESTIGATION OF THE MECHANISM OF FORMATION OF FILMS FROM VULCANIZED LATEX

2. FORMATION OF FILMS FROM SKS-30 ShKhP BUTADIENE-STYRENE LATEX

S. S. Voyutskii, D. M. Sandomirskii, N. M. Fodiman, R. M. Panich, and Z. M. Ustinova

The M. V. Lomonosov Institute of Fine Chemical Technology, Moscow Elastomer Laboratory

Translated from: Kolloidnyi Zhurnal Vol. 22, No. 2, pp. 143-147, March-April, 1960

Original article submitted January 27, 1959

It was shown in the preceding communication [1] that the strength of films formed from unvulcanized and vulcanized natural latexes is determined mainly by van der Waals forces. Latex films vulcanized in the dry state contain a more or less continuous network of rubber molecules linked by chemical bonds. It was suggested that, regardless of the vulcanization method used, rupture of films made from natural latex occurs generally in the rubber material of the globules and not at the strong interglobular interlayers at the protein-rubber boundary.

The present investigation is concerned with elucidation of the mechanism of film formation from vulcanized synthetic latex. In view of the nature of the protective substances generally used in emulsion polymerization (different from the native protein in natural latex), the lower degree of covering of the globules, and the different properties of the disperse phase, it is to be expected that in this case the mechanism of film formation would be different from the mechanism of film formation from natural latex.

The material used for the investigation was SKS-30 ShKhP butadiene-styrene latex containing 35.5% of the dry substance. Ammonium salts of paraffinic acids were used for stabilization during production of the latex. The influence of such factors as swelling of the films in water and petrolatum, test temperature on the tensile strength, and the behavior of films during mechanical treatment (milling) were studied. The experimental procedure is described in the previous investigation [1].

The vulcanized latex was prepared as follows: a latex mixture consisting of 100 weight parts of rubber (in latex form), 2 weight parts of sulfur,* 2 weight parts of zinc oxide, and 1 weight part of sodium diethyldithiocarbamate was heated up to 70° over a period of 45 minutes in a thermostat, and then vulcanized for 30 minutes at that temperature. An electron micrograph of a sample of the resultant latex showed that most of the globules become aggregated during vulcanization.

The following were investigated:

1) unvulcanized films made by drying of the original latex at room temperature;

* Sulfur and zinc oxide were introduced into the latex in the form of a 50% paste in Leikanol; the accelerator was dissolved directly in the latex.

2) films made by drying of vulcanized latex at room temperature;

3) films made by drying of a latex mixture of the composition given above at room temperature, and then vulcanized in a thermostat for 1 hour at 125°.

The results of experiments on swelling of the films in water vapor are given in the table.

Effect of Swelling in Water Vapor on the Properties of Films from SKS-30 ShKhP Butadiene-Styrene Latex

Film	Swelling, % of initial weight	Water-soluble substances lost in swelling, %	Tensile strength kg/cm²		Change of tensile strength after swelling, %
			before swelling	after swelling	
Not containing casein					
From unvulcanized latex	4,64	1,20	1,6	2,9	+81
From vulcanized latex	4,77	1,75	15,3	12,8	—17,6
Vulcanized in the dry state	3,95	1,16	14,0	13,8	—1,5
Containing casein					
From vulcanized latex	5,09	1,55	14,0	8,9	—36
Vulcanized in the dry state	5,20	1,80	16,7	14,2	—15,4

The data in the table show that, in contrast to films from natural latex [1], films from unvulcanized synthetic latex become stronger after swelling in water vapor, while the tensile strength of films from vulcanized latex decreases much less as the result of swelling. Swelling in water vapor has almost no effect on the strength of films vulcanized in the dry state. It should also be noted that the vulcanization conditions — either in latex form or in dry films — have virtually no effect on the tensile strength.

Figures 1 and 2 represent the effects of swelling in petrolatum and of the test temperature on the tensile strength of the films. The characteristic feature in both cases is that, in contrast to films from natural latex, films from vulcanized latex and films vulcanized in the dry state show approximately equal strength decreases.

It was shown previously [1] that behavior of films during mechanical treatment (milling) may give valuable information on the nature of the bonds between their structural elements. When films made from synthetic unvulcanized latex are treated in a microroll mill, a smooth continuous sheet is formed. Films made from vulcanized latex are somewhat less good, and give a less even sheet with occasional breaks. Films vulcanized in the dry state yield very uneven sheets. In the case of natural latex there are no differences in the behavior of vultex (vulcanized latex) and nonvulcanized latex films — both give good sheets, whereas films vulcanized in the dry state crumble during milling.

Films from synthetic and natural latex differ appreciably in a number of respects. Vulcanization results in a very large relative increase of strength in the case of SKS-30 ShKhP latex (9 to 10-fold), and a much smaller increase in the case of natural latex (3.5 to 4-fold). The vulcanization conditions (in latex form or in the dry state) influence the film strength in the case of natural latex but have almost no effect in the case of synthetic latex. Swelling in water vapor has little effect on the strength of films from synthetic latex, but has a very strong lowering effect on the tensile strength of films from vulcanized natural latex. The behavior of films from synthetic latex in swelling in petrolatum and on increase of temperature is almost independent of the vulcanization conditions, whereas these conditions influence the corresponding behavior of films from natural latex.

In mechanical treatment the differences between films from vulcanized and unvulcanized synthetic latex are very pronounced, whereas such differences are virtually nonexistent in the case of natural latex.

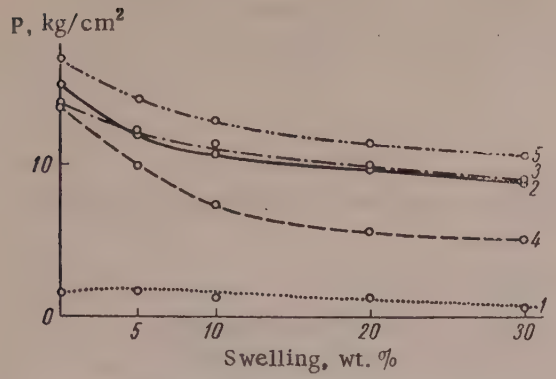


Fig. 1. Effect of swelling in petrolatum on the tensile strength of films from SKS-30 ShKhP butadiene-styrene latex: 1) Unvulcanized; 2) vulcanized; 3) vulcanized in the dry state; 4) vulcanized with 1.5% casein; 5) vulcanized in the dry state with 1.5% casein.

With regard to the problems with which we are concerned here (with the differences in the nature of the polymers disregarded), the main distinction between films from natural latex and films from SKS-30 ShKhP latex is that the protective layers in the latter consist of molecules of fatty-acid soaps and do not cover the whole globule surfaces. The rubber globules in natural latex are to a great extent covered by a protein coating (the soaps present in it do not play such an important part at the usual pH values). As the globules come closer together during drying of the latex, the protein coatings form an almost continuous network, the presence of which confers high strength to the unvulcanized rubber film [1, 2]. In production of vultex the protein coating evidently does not undergo any significant changes. In vulcanization in the dry state, rupture of the coating during film formation is easier at the higher temperatures; this increases the number of rubber – rubber contacts and the role of chemical bonding becomes more significant [1]. This accounts for the significant differences between vultex films and films vulcanized in the dry state. In the former, interglobular bonds due to van der Waals forces predominate; the latter contain continuous molecular networks characteristic of ordinary vulcanizates. Therefore, all factors which cause weakening of the protein layer (swelling in water) and of the intermolecular forces (increase of the distance between the globules during swelling in petrolatum; increase of temperature) result in a greater lowering of film strength in the case of vultex.

When a film is formed from SKS-30 ShKhP latex, the protective substance present in the latter cannot form a continuous network, and the film contains numerous rubber – rubber contacts. Naturally, this facilitates formation of a more or less continuous molecular network, i.e., of interglobular chemical bonds, during vulcanization in latex form as well as in the dry film. This is also favored by the formation of globule aggregates, which we observed in the latter instance. Thus, in the case of synthetic latex the qualitative differences between the structure of a film from vulcanized latex and that of a film vulcanized in the dry state are less prominent. Accordingly, they are almost equal in strength and are similarly influenced by swelling in water vapor, petrolatum, and increase of the test temperature.

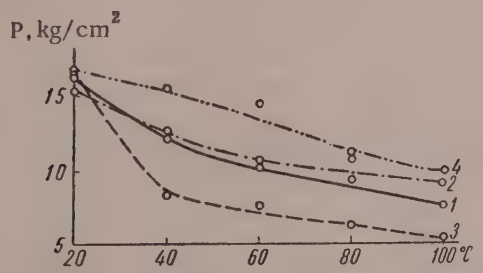


Fig. 2. Influence of test temperature on the tensile strength of films from SKS-30 ShKhP butadiene-styrene latex: 1) vulcanized; 2) vulcanized in the dry state; 3) vulcanized latex with 1.5% casein; 4) vulcanized in the dry state with 1.5% casein.

To confirm the foregoing views concerning the role of the protein coating on the globules, we studied the properties of films from SKS-30 ShKhP latex to which 1.5% of casein (calculated on the solids content) had been added in the form of 10% ammoniacal solution. This mixture was either vulcanized in latex form and then converted into films, or first made into films and then vulcanized in that form in the dry state.

The table shows that addition of casein has little influence on the tensile strength, but the influence of swelling in water vapor is greater than in films without casein.

Addition of casein results in a greater fall of strength in films from vulcanized latex when swollen in petrolatum (Fig. 1, Curve 4), and has little effect on the behavior of films vulcanized in the dry state (Curve 5). The same applies to the effect of increased test temperature (Curves 3 and 4). This factor has a greater influence on films from vulcanized latex in presence of casein.

Sheet formation from films during milling was improved considerably by addition of casein to the vultex. Casein-containing film vulcanized in the dry state became powdered during milling.

Thus, films made from SKS-30 ShKhP latex to which casein had been added approximated in some of their properties to films from natural latex. Strengthening of the protective coating increased the role of van der Waals forces.

SUMMARY

1. The effects of swelling in water vapor and in petrolatum, and of the test temperature, on the strength of rubber films made from SKS-30 ShKhP latex were studied.

2. The behavior of the films in mechanical treatment (milling) was investigated.

3. The strength of films from unvulcanized SKS-30 ShKhP synthetic latex is determined mainly by van der Waals forces, whereas the strength of films from vulcanized latex and films vulcanized in the dry state is determined by the presence of a continuous molecular network characteristic of vulcanizates.

4. Introduction of casein into the synthetic latex brings a number of properties of the films made from it closer to the properties of films from natural latex.

LITERATURE CITED

[1] S. S. Voyutskii, D. M. Sandomirskii, N. M. Fodiman, and R. M. Panich, Kolloid. Zhur. 21, 552 (1959).*

[2] D. M. Sandomirskii and I. K. Gagina, Kolloid. Zhur. 15, 448 (1953).*

* Original Russian pagination. See C. B. translation.

EFFECT OF DIFFUSION ON THE STREAMING POTENTIAL

B. V. Deryagin

Institute of Physical Chemistry, Academy of Sciences, USSR

Laboratory of Surface Phenomena, Moscow

Translated from: Kolloidnyi Zhurnal Vol. 22, No. 2, pp. 148-153, March-April, 1960

Original article submitted December 2, 1958

The accepted theory of streaming potentials is based on the assumption that in the steady state the convective surface electric current must be balanced by an opposing conduction current caused by the potential difference which arises between the two sides of the membrane.

This assumption ignores the fact that the electric charges are transported by two different carriers, anions and cations, and therefore two independent conditions must be considered: compensation of the convective surface flow of cations by an equal and opposite flow of cations across each section of the capillary (or system of capillaries) under the influence not only of the electrical but also of the chemical potential difference, i.e., under the influence of the cation concentration gradients, and an analogous condition for the anions.

An analogous idea formed the basis of a theory of the motion potential (Dorn effect) for bubbles [1], drops [2], and solid particles [3], which led to a formula containing, in contrast to Smoluchovski's equation [4], the ratio of the cationic and anionic mobilities. In the present paper we consider, on the same basis, the role of diffusion in the streaming potential — an effect identical in its mechanism to the Dorn effect. It will be shown that under certain conditions there should be sharp deviations from the classical theory, which give additional information on the structure of the double layer.

Consider an electrolyte solution in steady streamline flow, for simplicity, through a cylindrical capillary of circular section with radius a (up to the slippage plane at the capillary walls) and length L, under the influence of a pressure difference Δp. Let the solution contain cations of unit charge z^+, concentration c^+ moles/cm^3, and diffusion coefficient D^+. The corresponding values for the anions are denoted by z^-, c^-, and D^-; the solution viscosity is denoted by η.

Equating the difference of the pressure forces which tends to move the liquid through the capillary to the friction against the capillary walls, we have:

$$2\pi a L \eta \left(\frac{du}{dr}\right)_{r=a} = \pi a^2 \frac{dp}{dy} L, \tag{1}$$

where r is the distance from the capillary axis; y is the coordinate taken along the capillary axis toward the liquid stream.

Assume, for simplicity, that the thickness d of the double layer is small in comparison to a. In that case the total surface convective flows of cations and anions are, evidently, respectively equal:

$$2\pi a\left(\frac{du}{dr}\right)_{r=a}\int_0^\infty [c^+(h)-c^+(\infty)]\,hdh,$$

$$2\pi a\left(\frac{du}{dr}\right)_{r=a}\int_0^\infty [c^-(h)-c^-(\infty)]\,hdh, \qquad (2)$$

where h is the distance from the slippage plane; $c^\pm(h)$ and $c^\pm(\infty)$ are the concentrations of the ions at a distance h from the slippage plane and in the adjacent portions of the liquid volume. Subsequently, as in the previous paper [2], the argument ∞ is omitted from $c(\infty)$, but the concentration is regarded as possibly dependent on y, the distance from the capillary exit (Fig. 1).

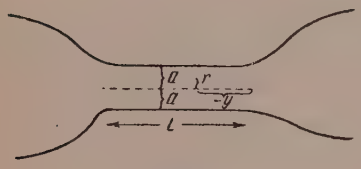


Fig. 1

In the steady state, the surface flows of ions in each section of the capillary must be balanced by opposing flows of three kinds.

1. Flows of electrical migration under the influence of the arising streaming potential and its electric field.

2. Diffusion flows under the influence of the concentration gradients of the corresponding ions.

3. Excess convection flows which depend on the excess concentration of ions in a given section of the capillary over the initial concentration of c_0 which persists at points in the volumes on each side of the porous membrane at distances from its surface which are large enough for disappearance of changes in the concentrations of the ions which arise at entry into the mouth of the capillary and at the exit from the latter (since some of the lines of flow of the liquid leave the main volume and enter the zone of the double layer, where the ion concentrations differ from the values in the main volume).

For the conditions of compensation of the surface flows (2) with Eq. (1) taken into account, we have

$$\frac{1}{\eta}\frac{dp}{dy}c^+\xi^+ = -\frac{FE}{RT}D^+z^+c^+ + D^+\frac{dc^+}{dy} - \bar{u}(c^+ - c_0^+),$$

$$\frac{1}{\eta}\frac{dp}{dy}c^-\xi^- = +\frac{FE}{RT}D^-z^-c^- + D^-\frac{dc^-}{dy} - \bar{u}(c^- - c_0^-), \qquad (3)$$

where E is the field intensity; F is the Faraday number; R is the gas constant; T is the absolute temperature

$$\xi^\pm = \frac{1}{c^\pm}\int_0^\infty [c^\pm(h)-c^\pm(\infty)]\,hdh;$$

and $\bar{u}$ is the average value for the capillary section of the linear velocity of the liquid flow. As a first approximation, we now assume that the liquid volume (beyond the limits of the double layer) is electrically neutral:

$$z^+c^+ = z^-c^-, \qquad (4)$$

and hence

$$c^\pm = z^\mp c, \qquad (5)$$

where c may be termed the molar concentration of the electrolyte (moles/cm^3).

The validity of conditions (4) and (5) as a basis for calculations of the first approximation and the magnitude of the error introduced may be estimated a posteriori. The parameters $\xi^\pm$ are connected with the Guggenheim moment of the double layer (ξ) and the zeta-potential (ζ) by the expression:

$$Fcz^+z^-(\xi^+ - \xi^-) = \xi = \frac{\varepsilon\zeta}{4\pi}. \tag{6}$$

Introducing the symbols ζ^+ and ζ^-:

$$\overline{\frac{\varepsilon\zeta^+}{4\pi}} = Fcz^+z^-\xi^+, \tag{7}$$

$$\overline{\frac{\varepsilon\zeta^-}{4\pi}} = -Fcz^+z^-\xi^-. \tag{8}$$

we can represent ζ in the form of a sum of two positive terms, cationic and anionic:

$$\zeta = \zeta^+ + \zeta^-, \tag{9}$$

each of which depends only on the distribution of the corresponding ion in the double layer. It may be noted that in contrast to $\zeta^\pm$ one of the coefficients $\xi^+\xi^-$ is always negative.

Using Eq. (5) we can represent Eq. (3) in the form:

$$\left.\begin{aligned}\frac{1}{\eta}\frac{dp}{dy}\xi^+ &= -\frac{FE}{RT}D^+z^+ + D^+\frac{1}{c}\frac{dc}{dy} - \overline{u}\frac{(c-c_0)}{c},\\ \frac{1}{\eta}\frac{dp}{dy}\xi^- &= +\frac{FE}{RT}D^-z^- + D^-\frac{1}{c}\frac{dc}{dy} - \overline{u}\frac{(c-c_0)}{c}.\end{aligned}\right\} \tag{10}$$

We now estimate the order of magnitude of Pe, the ratio of the last terms in the right-hand sides of Eq. (10), representing the role of convective diffusion to the penultimate terms representing ordinary diffusion; we have, assuming that

$$\frac{dc}{dy} \approx \frac{c-c_0}{L}, \qquad D_{\text{eff}} = \frac{D^+D^-(z^+ + z^-)}{z^+D^+ + z^-D^-},$$

$$\text{Pe} = \frac{\overline{u}L}{D_{\text{eff}}}, \tag{11}$$

where Pe is the dimensionless Peclet number, which determines the relative role of convective transfer in the diffusion process. If

$$\text{Pe} \gg 1\ldots, \tag{12}$$

then, for most of the capillary length the terms for ordinary diffusion in Eqs. (10) may be disregarded in comparison with the last terms of the right-hand sides. Then subtraction of the two equations term by term gives

$$\Delta V = -LE = \frac{1}{\eta}\frac{\Delta p}{\varkappa}Fcz^+z^-(\xi^+ - \xi^-) = \frac{\Delta p}{\eta\varkappa}\frac{\varepsilon\zeta}{4\pi}, \tag{13}$$

where

$$\varkappa = \frac{F^2}{RT}(z^+D^+ + z^-D^-)z^+z^-c, \tag{14}$$

here ΔV is the potential difference; Δp is the pressure difference between the two sides of the capillary; κ is the conductivity of the solution; i.e., we have the usual expression for the streaming potential.

We now consider the opposite case, when

$$\mathrm{Pe} \ll 1 \tag{15}$$

when the convection terms in the right-hand sides of Eqs. (10) may be neglected. Multiplying each term in Eqs. (10) by D^- and D^+, respectively, we have

$$\Delta V = -LE = \frac{1}{\eta}\frac{\Delta p}{\varkappa} Fcz^+z^- \frac{(D^-\xi^+ - D^+\xi^-)}{D_{\mathrm{eff}}} = \frac{\varepsilon}{4\pi\eta\varkappa}\Delta p \frac{(D^-\zeta^+ + D^+\zeta^-)}{D_{\mathrm{eff}}}, \tag{16}$$

which contains the effective coefficient of diffusion of the electrolyte:

$$D_{\mathrm{eff}} = \frac{D^+D^-(z^+ + z^-)}{z^+D^+ + z^-D^-}. \tag{17}$$

It is seen that at low velocities of flow through the capillary, the coefficient of proportionality between ΔV and dp changes, and is now determined not by $\zeta = \zeta^+ + \zeta^-$, but by some other combination of the cationic and anionic components of the ζ-potential with coefficients which depend on the ratio of the ionic mobilities D^+/D^-.

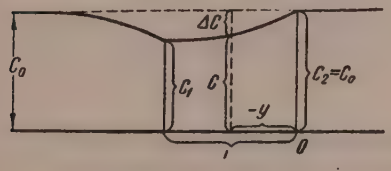


Fig. 2

It follows that by observing the streaming potential ΔV under two different sets of conditions, one satisfying Condition (12) and the other Condition (15), we can obtain two equations, from which ζ^+ and ζ^- or ξ^+ and ξ^- can be found separately. Thereby finding $\zeta = \zeta^+ + \zeta^-$, we can verify the Gouy-Chapman theory of the double layer whereby if ζ is known $\xi^\pm$ or $\zeta^\pm$ can be found.

It is easily seen that the change of the expression for E at low values of the Peclet number in comparison with high follows from the fact that in the former case the classic expression for the streaming potential contains an additional term which represents the diffusion potential due to the concentration difference between the ends of the capillary. Because of this, for actual determination of ΔV in accordance with Eq. (16) the electrodes must be situated in immediate proximity to the capillary ends; for example, in the case of a porous membrane they must be on the surface of the latter.

Another condition is conformity to the expression (15), from which it follows in conjunction with Eq. (11) and the Poiseuille equation that:

$$\frac{a^2\Delta p}{8\eta D_{\mathrm{eff}}} \ll 1. \tag{18}$$

Further, with Eq. (16) taken into account, condition (18) is transformed into

$$\Delta V \ll \frac{\varepsilon}{4\pi}\frac{1}{a^2}\frac{(D^-\zeta^+ + D^+\zeta^-)}{\varkappa} \tag{19}$$

or, disregarding the distinction between D^+ and D^- and taking into account Eq. (14) and the expression for the thickness of the double layer, we have

$$\frac{\Delta V}{\zeta} \ll \left(\frac{d}{a}\right)^2. \tag{20}$$

Since we assumed, to simplify the calculation, that $\underline{d}$ is much less than $\underline{a}$, taking as the permissible limit $a = 3d$, we finally have in this case the following condition for observability of the effect:

$$\Delta V \ll \frac{1}{9}\zeta. \tag{21}$$

We now consider the general case. Eliminating E from Eqs. (10), we have the following equation for determining the concentration distribution along the capillary:

$$\frac{d\Delta c}{dy} - \frac{\bar{u}\Delta c}{D_{\text{eff}}} = \frac{c}{\eta}\frac{dp}{dy}\frac{(D^-z^-\xi^+ + D^+z^+\xi^-)}{D^+D^-(z^+ + z^-)}, \tag{22}$$

where $\Delta c = c_0 - c$. We solve Eq. (22), assuming that relative changes of $\underline{c}$, and therefore of the whole right-hand side, are not large. For definite determination of Δc we require one boundary condition, to find which it is necessary to consider the concentration fields to the left and right of the capillary (Fig. 2). For simplicity, we assume that outside the capillary (or capillaries, in the case of a porous membrane) the liquid stream retains its unidimensional character in expanding. In that case, the concentration distribution should satisfy the equation

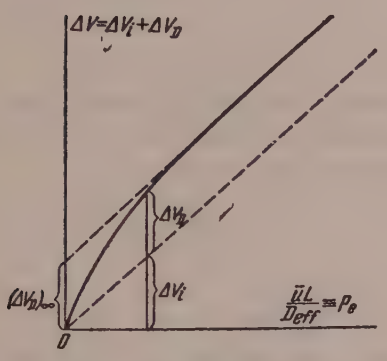


Fig. 3

$$\frac{d\Delta c}{dy} - \frac{\bar{u}\Delta c}{D_{\text{eff}}} = 0. \tag{22'}$$

For the zone before entry of the flow (on the left) into the capillary the solution of this equation is

$$\Delta c = Ce^{-\frac{\bar{u}y}{D_{\text{eff}}}} = (c_1 - c_0)e^{-\frac{\bar{u}(y-L)}{D_{\text{eff}}}},$$

where c_1 is the electrolyte concentration at the capillary end. For the zone beyond the capillary exit (on the right) the solution of Eq. (22') is

$$\Delta = (c_2 - c_0)e^{-\frac{\bar{u}y}{D_{\text{eff}}}},$$

where c_2 is the concentration at the capillary outlet. Since on the right the distances from the capillary exit (y) are negative, the following condition is necessary to avoid unlimited increase of concentration:

$$c_2 = c_0.$$

With the boundary condition taken into account, the integral of Eq. (22) becomes

$$\frac{\Delta c}{c_0} = \frac{c - c_0}{c_0} \approx \frac{1}{\eta\bar{u}}\frac{dp}{dy}\frac{(D^-z^-\xi^+ + D^+z^+\xi^-)}{(D^-z^- + D^+z^+)}\left[e^{-\frac{\bar{u}y}{D_{\text{eff}}}} - 1\right]. \tag{23}$$

Putting y = L, we have:

$$\frac{c_1 - c_2}{c_0} \equiv \frac{c_1 - c_0}{c_0} \approx \frac{1}{\eta\bar{u}}\frac{dp}{dy}\frac{(D^-z^-\xi^+ + D^+z^+\xi^-)}{(D^-z^- + D^+z^+)}\left[e^{-\frac{uL}{D_{\text{eff}}}} - 1\right]. \tag{24}$$

The streaming potential is found by addition of its ohmic component ΔV_i, which coincides with the "classic" value [Eq. (13)] to the concentration component, which is

$$\Delta V_D = -\frac{RT(D^+ - D^-)}{F(z^+D^+ + z^-D^-)}\frac{(c_1 - c_2)}{c_0} =$$

$$= \frac{\Delta p}{\eta}\frac{RT}{F}\frac{(D^+ - D^-)(D^-z^-\xi^+ + D^+z^+\xi^-)}{D^+D^-(z^+ + z^-)(D^+z^+ + D^-z^-)}\left[\frac{e^{-\frac{\bar{u}L}{D_{\text{eff}}}} - 1}{\bar{u}L/D_{\text{eff}}}\right]. \tag{25}$$

When $Pe = \frac{\bar{u}L}{D_{eff}} \ll 1$, summation of Eqs. (25) and (13) gives (16), which we derived independently. When $\frac{\bar{u}L}{D_{eff}} \to \infty$ we have at the limit

$$\Delta V = \Delta V_i + \Delta V_D = + \frac{\Delta p}{\eta \varkappa} Fcz^+z^- (\xi^+ - \xi^-) - \frac{8RT}{a^2F} \frac{(D^+ - D^-)(D^-z^-\xi^+ + D^+z^+\xi^-)}{(D^+z^+ + D^-z^-)^2} =$$

$$= \frac{Fcz^+z^-}{\varkappa} \left[\frac{\Delta p}{\eta} (\xi^+ - \xi^-) - \frac{8}{a^2} (D^+ - D^-) \frac{(D^-z^-\xi^+ + D^+z^+\xi^-)}{(D^+z^+ + D^-z^-)} \right]. \quad (26)$$

The limiting value (ΔV_D) at $Pe \to \infty$ may be in the range of 10-50 mv.

The relationship between $\Delta V = \Delta V_i + \Delta V_D$ and the Peclet number, shown schematically in Fig. 3, follows from Eqs. (13) and (25). It must be stressed once again that for verification of the theoretical Eq. (26) the electrodes must be in close contact with the surfaces of the porous membrane (or capillary ends), especially at the side where the stream enters the pores, and the liquid must not be agitated.

SUMMARY

1. In further development of the diffusion theory of the Dorn effect (potential due to motion of solid particles), the theory of the streaming potential in a cylindrical capillary has been examined. It is shown that the classical equation for the streaming potential is in reality valid not for limitingly low flow velocities but for velocities at which convective transport of ions along the capillary considerably exceeds diffusional transport, i.e., when the Peclet number, which in this case is the product of the average linear flow velocity and the capillary length divided by the diffusion coefficient of the ions, is much greater than unity.

2. At low Peclet numbers the equation for the streaming potential differs from the classical equation in that, instead of the zeta-potential, it contains a certain linear combination of the cationic and anionic components of the latter, with coefficients which depend on the mobilities of the cations and the anions. The two equations coincide only when these mobilities are equal.

3. To detect experimentally the deviations from the classical equation for the streaming potential the electrodes must be placed very close to the ends of the capillary (or capillaries in the case of a porous membrane). Such experiments should be of interest for verification of the double-layer theory and for obtaining more information on the structure of the double layer.

LITERATURE CITED

[1] S. S. Dukhin and B. V. Deryagin, Kolloid. Zhur. 20, 705 (1958).*

[2] S. S. Dukhin and B. V. Deryagin, Doklady Akad. Nauk SSSR 121, 503 (1958); Kolloid. Zhur. 21, 37 (1959).*

[3] B. V. Deryagin and S. S. Dukhin, Doklady Akad. Nauk SSSR 129, 1328 (1959).*

[4] M. Smoluchovski, Bull. de l'Acad. des Sciences de Cracove, Classe d., Sciences Mathem. et Natur. (1903), p. 182.

* Original Russian pagination. See C. B. translation.

BINDING OF WATER BY FINELY DIVIDED SEDIMENTS

3. INFLUENCE OF ADSORBENT STRUCTURE, DEGREE OF HYDRATION, AND CHARGES ON THE CATIONS ACCOMPANYING THE INDICATOR ION

O. I. Dmitrenko and G. A. Pavlova

Institute of Oceanology, Academy of Sciences, USSR, Moscow

Translated from: Kolloidnyi Zhurnal Vol. 22, No. 2, pp. 154-158, March-April, 1960

Original article submitted January 17, 1959

In the series of our investigations [1], molecular sorption of electrolytes by highly disperse sediments was estimated by its final result, i.e., disappearance of equivalent amounts of cations and anions from the equilibrium solutions.

This effect is associated with formation of undissociated molecules in aqueous solutions; it conforms to the law of mass action and is ultimately determined by the solubility of the adsorbed electrolytes, solvation of dissociated and undissociated components of the solution, electrostatic interaction between the ions, and conditions of distribution of water and electrolyte molecules between the solid and liquid phases of the system.

It may be concluded that molecular sorption of electrolytes from aqueous solutions depends on a number of conditions, of which two are the most important: interaction of the adsorbate with the solvent medium and influence of the structure of the adsorbent lattice.

The experiments carried out in the present investigation had the following aims: 1) to study the influence of the degree of hydration and charges of various cations accompanying the indicator anion on the sorption of water dipoles, and 2) to study the influence of adsorbent structure on the latter effect.

Determination of sorption of the solvent (water) by natural materials. Control experiments were performed by the method described earlier [2, 3] in order to obtain an idea of the influence of adsorbent composition on sorption of water.

Figure 1 represents binding of water by pure aleuritic sand from $MgCl_2$ solutions.

Negative values were obtained for the amounts of bound water corresponding to the different points on this curve over a wide range of equilibrium concentrations of the $MgCl_2$ solution (from 0.25 to 2 N). It seems likely that in this experiment there was positive binding of the electrolyte; with increasing concentration of the equilibrium solutions the amounts of molecularly bound magnesium chloride increase, being equal in magnitude but opposite in sign to the amounts of bound water. An explanation of this effect is provided by the postulate that the total number of electrolyte and water molecules adsorbed by colloidally disperse sediments is constant, and that they are interchangeable [2]. It is also seen that the maximum amounts of water negatively bound by aleuritic sand are not large; this is due to the nature of the adsorbent itself.

Determinations of the amount of water bound by Saratov chernozem from $CaCl_2$ solutions (Fig. 1) showed that this adsorbent is of great interest because of the very pronounced nonequivalence of its adsorption sites.

It was shown earlier that in adsorption of water from solutions of uni-univalent eluting electrolytes in experiments with kaolin, the amounts of water adsorbed are directly proportional to the concentration and solubility of the eluting electrolytes, while in experiments with montmorillonite they are inversely proportional ([3], Figs. 1 and 2). The curves obtained in experiments with kaolin were similar in shape to the curves found by Freundlich. The curves obtained in experiments with montmorillonite were their mirror images in direction. If these adsorbents are mixed, it is probable that water molecules are first bound by components similar to kaolin, and second by components similar to montmorillonite, because in the latter case binding of water within the adsorbent volume is predominant. Evidently reactions within the adsorbent volume may be of a retarded character.

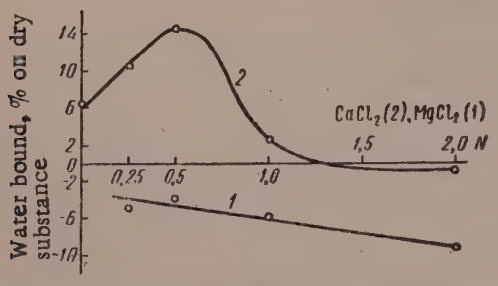


Fig. 1. Effect of adsorbent structure on the amount of bound water: 1) Binding of water by aleuritic sand; 2) binding of water by Saratov chernozem.

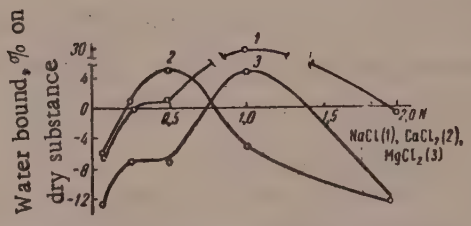


Fig. 2. Variations of the amounts of water bound by a mixed adsorbent with the charge of the ions accompanying the indicator ion: clay mud (sample 2); from solutions of: 1) NaCl; 2) $CaCl_2$; 3) $MgCl_2$.

Superposition of these two processes influences the shape of the resultant "additive" curves for binding of water by mixed adsorbents. When, at the maximum, binding of water by kaolin-like components of the mixture ends, a noticeable break appears on the curve. This is followed by binding of water by the mixture components resembling montmorillonite (volume binding); at this stage the water-binding curves asymptotically approach the abscissa axis. A similar process occurs in binding of water by Saratov chernozem (Fig. 1).

In subsequent experiments the adsorption properties of highly disperse marine sediments were studied. Some properties of these sediments are given in Table 1.

TABLE 1

Mechanical Composition and Moisture Contents of Two Samples of Clay Mud Taken from the Bottom of the Bering Sea

Samples	Moisture content, %	Sampling depth, m	Fractional composition, % fractions, mm			
			>0,25 and 0,25—0,1	0,1—0,05	0,05—0,01	<0,01
I	60,0	1580	0,8	16,8	48,5	33,9
II	57,0	2770	2,1	13,0	27,3	57,6

In Fig. 2, as previously, the abscissa axis gives the concentrations of equilibrium solutions of the electrolytes NaCl, $CaCl_2$, and $MgCl_2$ in terms of normality, while the ordinates give the amounts of water bound by the clay mud, given as percentages on the dry substance. Curves with maxima were obtained in all three experiments; this is characteristic of mixed adsorbents and indicates that here again the binding of water is additive in character. The amounts of bound water depend on the composition of the leaching electrolyte. The greatest amounts of bound water were found in experiments with sodium chloride; the maximum is at about 30% of bound water (Curve 1).

In the experiments with calcium and magnesium chlorides (Curves 2 and 3), a general decrease of the amount of bound water can be seen; the maxima are close to a value corresponding to 5% of bound water calculated on the dry substance of the adsorbents in each experiment. This leads to the conclusion that increase in the charge of the ions accompanying the indicator ion has an appreciable lowering effect on the amount of water bound by a particular mixed adsorbent.

Figure 3 shows curves for binding of water by clay mud (sample 1); the nature of these curves suggests that here we have not a mixture of adsorbents but a single adsorbent with an individual type of sorption similar to beidellite or montmorillonite. This result is of interest because it leads to the conclusion that in adsorption of water by individual adsorbents from solutions of bi-univalent electrolytes there is a direct relationship between solubility and sorption of water molecules. This result was found earlier in experiments with monomineral clays [3].

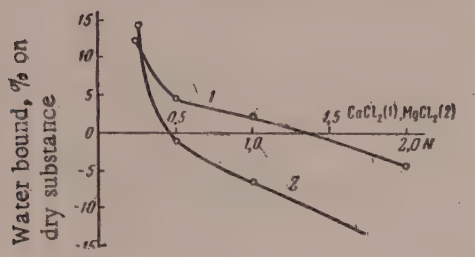


Fig. 3. Solubilities of the leaching electrolytes in relation to adsorption of water in experiments with an individual adsorbent: clay mud (sample 1); solutions of 1) $CaCl_2$; 2) $MgCl_2$.

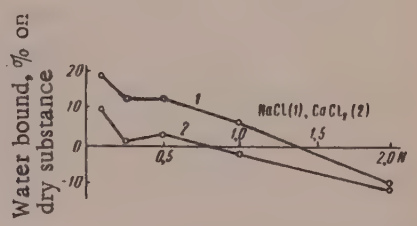


Fig. 4. Effects of adsorbent structure and composition of the leaching electrolyte on adsorption of water: clay mud (sample 3); solutions of: 1) NaCl; 2) $CaCl_2$.

It follows from Fig. 4 that Curve 1, found for leaching of a clay marine sediment (sample 3) with NaCl solution, lies above the curve for leaching of this sediment with $CaCl_2$ solution. It was found that in the former case, the amount of water bound was about 20-15%, and in the latter about 10-5%, calculated on the dry substance. The data in Fig. 4 indicate that the observed binding of water is characteristic of an adsorbent with a volume type of binding. Clay mud (sample 3) is not a mixed adsorbent, as the shape of the curves in Fig. 4 indicates.

Variations of the molecular sorption of salts with their solubility in different intermicellar liquids and with the sign and magnitude of the charge of marine sediments. Yarusov [4] found that in adsorption of certain salts by chernozem of the Sumy experimental station from various water-alcohol mixtures the adsorbability of the salts was in inverse ratio to their solubility.

Yarusov found appreciable values for adsorption of chloride by adsorbents carrying a negative charge. We showed in a series of experiments that typical gray and brown marine sediments are negatively charged. This made selection of the adsorbent arbitrary.

Gray marine mud was used in our experiments on molecular sorption from aqueous alcohol solutions. The sediment was first saturated for a long time with calcium from 0.5 N $Ca(NO_3)_2$ solution. Up to about five liters of this solution was used per 100 g sample. At the end of the saturation the wash liquors were tested for SO_4^{2-}, and the concentrations of the original and equilibrium $Ca(NO_3)_2$ solutions were compared. The sediment saturated with calcium was washed with water to remove excess saturating reagent, and then washed for a long time with a 1:1 mixture of 96% ethyl alcohol and water. The prepared samples were dried at 30°, ground in an agate mortar, passed through a screen of 0.025 mm mesh, and kept in stoppered bottles. To 5 g samples of the air-dry sediment, weighed on an analytical balance, there were added 50 ml lots of aqueous alcoholic solutions made up from 100 ml of 0.5, 1.0, or 2.0 N $CaCl_2$ solution and 300 ml of methyl, ethyl, or propyl alcohol. In each case 400 ml of aqueous alcohol solution was prepared.

In the adsorption experiments, the suspensions prepared as described above were shaken mechanically for 1 hour. The equilibrium solutions were then filtered off and their chloride contents determined by titration by the Mohr method. Control experiments were performed under the identical conditions.

The adsorption was determined from the difference between the chloride contents (meq) found in the original and equilibrium solutions in aqueous methyl, ethyl, or propyl alcohol. It follows from the results (Table 2) that adsorption of chloride from $CaCl_2$ solutions was negative in aqueous methyl alcohol, and positive in the ethyl and propyl alcohol mixtures. This is because of the very appreciably lower solubility of $CaCl_2$ in the latter two solvents. It is clear from Table 2 that the adsorption of ionic molecules of an electrolyte by finely divided adsorbents can be estimated analytically, so that it can be settled conclusively whether marine sediments of different types are similarly charged in all cases.

TABLE 2

Molecular Sorption of $CaCl_2$ from Aqueous Alcohol Solutions by Highly Disperse Gray Mud from the Bering Sea, Depth 85 m
(G. A. Pavlova's Experiments)

Concentration of aqueous alcohol solutions, N/4	Cl^- content in 5.005 ml of solution, meq		Molecular adsorption of $CaCl_2$, meq.	
	original	equilibrium	in experiment	calculated for 100 g of adsorbent in 1 liter
		Methyl alcohol		
0,5	0,6340	0,6357	—0,0017	—6,8
1,0	0,2695	1,2724	—0,0029	—11,6
2,0	2,5315	2,5428	—0,0113	—45,2
		Ethyl alcohol		
0,5	0,6295	0,6204	0,0091	36,4
1,0	1,2525	1,2328	0,0197	78,8
2,0	2,4680	2,4356	0,0324	129,3
		Propyl alcohol		
0,5	0,6185	0,6151	0,0034	13,4
1,0	1,2410	1,2238	0,0172	68,6
2,0	2,4630	1,5662	0,8967	3583 *

* The results obtained in the experiments with $CaCl_2$ solution in aqueous propyl alcohol were close to a state of saturation (phase separation).

It follows from Yarusov's experiments [4] and our work that adsorption of molecules (ionic associated groups) of electrolyte and water is independent of the sign of the adsorbent charge, but is determined to a greater extent by the dispersity of the adsorbent and the solubility of the adsorbed compounds in the intermicellar solution.

SUMMARY

1. Sorption of electrolytes (in molecular form or as ionic aggregates) from aqueous solutions depends on a number of conditions, the most important of which are interaction of adsorbate molecules with the solvent medium and the influence of adsorbent structure.

2. Binding of water by mixed adsorbents may be regarded as an additive process.

3. Sorption of water molecules by mixed and individual adsorbents decreases appreciably with increasing hydration and charge of the cations accompanying a particular indicator anion.

4. Molecular adsorption or adsorption of ionic aggregates is independent of the sign of the adsorbent charge, which only determines the orientation of the adsorbed components in the equilibrium solutions; the magnitude of adsorption is determined to a greater extent by the dispersity of the adsorbent and is in inverse ratio to the solubility of the adsorbed compounds in the intermicellar liquid.

LITERATURE CITED

[1] V. A. Kargin, P. S. Vasil'ev, and O. I. Dmitrenko, Zhur. Fiz. Khim. 13, 1837 (1939); 14, 1628 (1940); O. I. Dmitrenko, Khimizatsiya Sots. Zemledeliya 5 (1940); Collected Papers on Physical Chemistry [In Russian] (Izd. AN SSSR, Moscow-Leningrad, 1947) p. 376; O. I. Dmitrenko, V. A. Kargin, and A. A. Ryabinina, Kolloid. Zhur. 13, 3 (1951); O. I. Dmitrenko and A. A. Ryabinina, Kolloid. Zhur. 20, 163 (1958).*

[2] O. I. Dmitrenko, Kolloid. Zhur. 20, 163 (1958).*

[3] O. I. Dmitrenko and G. A. Pavlova, Kolloid. Zhur. 21, 419 (1959).*

[4] S. S. Yarusov, Khimizatsiya Sots. Zemledeliya 6 (1940).

* Original Russian pagination. See C. B. translation.

PRECIPITATION OF A UNIPOLARLY CHARGED AEROSOL IN AN ENCLOSED SPACE

V. F. Dunskii and A. V. Kitaev

Moscow

Translated from: Kolloidnyi Zhurnal Vol. 22, No. 2, pp. 159-167, March-April, 1960

Original article submitted January 27, 1959

When rooms are filled with aerosols for disinfection and disinfestation, the aerosol particles are deposited mainly on the floor, and formation of the required deposits on the ceiling and walls is possible only with excessive expenditure of the chemical agent. For uniform treatment of all the surfaces of a room it has been proposed [1, 2] to make use of the effect of electrostatic scattering, which occurs if the aerosol is unipolarly charged.

The precipitation of a unipolarly charged monodisperse aerosol in an enclosed space is considered in this paper, and the results of experiments and calculations are compared.

Precipitation of a monodisperse unipolarly charged aerosol in an enclosed space is first considered for the usual conditions in which convective motion of air inside the space is fairly intensive. The following simplifying assumptions are made for an approximate solution of this problem:

1. Because of the intensive motion of the air the numerical particle concentrations are equal at all points within the space.

2. Particle precipitation under the action of gravitational and electrostatic forces only is considered; precipitation caused by diffusion, inertia forces, thermophoresis, etc., is disregarded.

3. The aerosol particles are spherical; their charge and size do not change throughout the treatment cycle.

4. The mirror-image electrostatic forces acting on the particles in the wall layer are disregarded.

5. The particles move in conformity to the Stokes law.

With these assumptions, the velocity of a particle near the inner surface of the space is equal to the geometric sum of the falling velocity under gravity

$$\overline{W}_g = \frac{2g\gamma_l r^2}{9\eta} \qquad (1, a)$$

and the velocity under the influence of the electric field

$$\overline{W}_e = \overline{E}\, q/6\pi\eta_l r, \qquad (1, b)$$

where g is the acceleration due to gravity; γ_l is the density of the liquid; r is the particle radius; η is the dynamic viscosity of air; $\overline{E}$ is the field intensity; q is the particle charge.

If the space contains a distributed aerosol source of total capacity N (i.e., if N particles per second are introduced into the space), the number of particles deposited in time dt on the inner surface of the space is equal to the change in the number of particles suspended within the space,

$$ndt\int_{S_1}(\overline{W}_g+\overline{W}_e)d\overline{S}=\left(N-V\frac{dn}{dt}\right)dt$$

or

$$\frac{dn}{dt}=\frac{N}{V}-\frac{nW_eS_1}{V}-\frac{n}{V}\int_{S_1}\overline{W}_gd\overline{S}, \tag{2}$$

where n is the numerical concentration of the aerosol particles; t is the time; S is the area of the inner surface of the space; V is the volume of the space; W_e is the normal linear velocity of electrostatic precipitation of particles of radius r and charge q (the mean value for the whole surface).

Precipitation occurs only where the normal component of the vector $W_g + W_e$ is directed toward the surface S, i.e., in general, only on a part of the surface such that $S_1 < S$.

It may be assumed that when $W_e > W_g$ precipitation occurs over the entire enclosed surface S. Here $\int_S \overline{W}_g \cdot dS = 0$, since W_g is a constant vector, and Eq. (2) may be written:

$$\frac{dn}{dt}=\frac{N}{V}-\frac{nW_eS}{V}. \tag{3}$$

It is known [2] that in absence of an aerosol source (N = 0) the decrease of the numerical concentration of the aerosol particles owing to electrostatic scattering is

$$\frac{dn}{dt_{(N=0)}}=-\frac{2n^2q^2}{3\gamma_l r}. \tag{4}$$

Consequently,

$$W_e=\frac{2Vnq^2}{3S\gamma_l r}. \tag{5}$$

Substituting this value of W_e into Eq. (3), we have the equation for precipitation when $W_e > W_g$,

$$\frac{dn}{dt}=\frac{N}{V}-\frac{2n^2q^2}{3\gamma_l r}, \tag{6}$$

which differs from Eq. (4) for electrostatic scattering only by the presence of the aerosol source. It follows that at $W_e > W_g$ the total number of particles deposited on the inner surface of the space is determined by electrostatic scattering only, while gravity influences only the distribution of the precipitated particles over the surface S.

In the steady state (dn/dt = 0)

$$n_c=\sqrt{\frac{3\gamma N}{2q^2V}} \tag{7}$$

and the relative linear velocity of electrostatic precipitation is

$$(W_e/W_g)_c=\frac{q}{q\gamma_l S}\sqrt{\frac{27\eta NV}{2r^5}}. \tag{8}$$

It is interesting to note that at $W_e > W_g$ the mean intensity E of the electric field near the surface S is independent of the particle charge q:

$$E = \frac{6\pi\eta r W_e}{q} = \pi\sqrt{\frac{24VN\tau_1 r}{S^2}}.$$

At $W_e < W_g$ the precipitation Eq. (2)

$$dn/dt = \frac{N}{V} - \frac{nW_eS_1}{V} - \frac{n}{V}\int_{S_1}\overline{W}_g \cdot dS$$

is easily solved for a room of the usual shape (parallelepiped) where the particles are deposited only on the floor and walls and not on the ceiling. For example, for a cubical space of edge l the precipitation equation becomes:

$$\frac{dn}{dt} = \frac{N}{l^3} - \frac{5n^2q^2}{9\eta r} - \frac{2g\gamma_l\, nr^2}{9\eta l}. \qquad (9)$$

Unequal treatment of the room owing to the influence of gravity is represented, in the steady state, by the expressions

$$\varepsilon_1 = Q_{cg}/Q_{fr} = \left(\frac{W_e - W_g}{W_e + W_g}\right)_c \text{ and } \varepsilon_2 = Q_w/Q_{fr} = \left(\frac{W_e}{W_e + W_g}\right)_c,$$

where Q_{cg}, Q_{fr}, and Q_w are the amounts of liquid deposited per unit area of ceiling, floor, and walls, respectively.

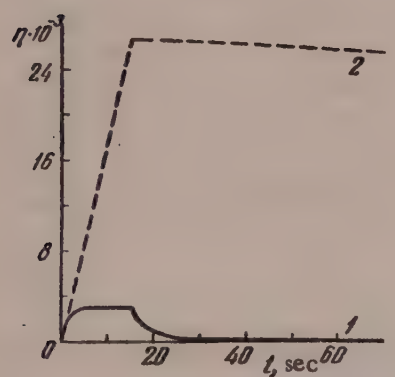


Fig. 1. Variations with time of the numerical particle concentration of a monodisperse aerosol in a cubical chamber. 1) With electrification of the aerosol; 2) without electrification.

However, when equipment of a high rate of output is used for disinfestation or disinfection, the space usually becomes quickly filled with the necessary amount of aerosol, when the aerosol supply is discontinued and the particles are precipitated relatively slowly. Therefore, the process takes place under nonequilibrium conditions: When the space is being filled with aerosol, the numerical particle concentration n increases together with the velocity of electrostatic precipitation W_e up to a maximum value which more or less approximates to an equilibrium value. The aerosol supply is then discontinued and precipitation continues at N = 0; the particle concentration falls, and the velocity W_e falls to a certain value W_{ek}, which corresponds to the residual concentration n_k.

The whole treatment cycle is represented by Eq. (2) under the following conditions:

$$0 \leqslant t \leqslant t_1, \quad 0 \leqslant n \leqslant n_1, \quad 0 \leqslant W_e \leqslant W_g;$$
$$t_1 \leqslant t \leqslant t_2, \quad n_1 \leqslant n \leqslant n_2, \quad W_g \leqslant W_e \leqslant W_2;$$
$$N = 0, \ t_2 \leqslant t \leqslant t_3, \quad n_2 \geqslant n \geqslant n_3, \quad W_2 \geqslant W_e \geqslant W_g.$$
$$N = 0, \ t_3 \leqslant t \leqslant T, \quad n_3 \geqslant n \geqslant n_k, \quad W_g \geqslant W_e \geqslant W_{e_k}.$$

For rooms of the usual shape (parallelepipeds) Eq. (2) is easily solved under these conditions.

As an example, we give the solution for a cubical space of edge l under the following conditions:

$$\gamma_l = 0{,}9\ \text{g/cm}^3, \ r = 2\cdot10^{-4}\ \text{cm}; \ \eta = 1{,}88\cdot10^{-4}\ \text{g/cm}\cdot\text{sec}$$
$$l = 105\ \text{cm}; \ N = 2{,}06\cdot10^9\ \text{sec}^{-1}; \ q = 3{,}27\cdot10^{-6}\ \text{CGSE}.$$

The space was filled with the aerosol during 15 seconds; the precipitation time at N = 0 was 30 minutes.

Here, in accordance with Eqs. (7) and (8), $n_c = 3080\ cm^{-3}$ and $(W_e/W_g)_c = 244$.

Variations of the numerical particle concentration $\underline{n}$ with time are shown in Fig. 1. In a different scale, the same graph represents variations of mean values of E and W_e with time. It follows from Curve 1 in Fig. 1 that when the aerosol is charged, the numerical particle concentration rapidly approaches the equilibrium concentration n_c and then remains almost constant until the supply of aerosol is discontinued, when it falls rapidly; after only one minute there is almost no aerosol in the space.

In treatment with an uncharged aerosol (Fig. 1, Curve 2) the numerical concentration rises almost linearly during the whole time of aerosol supply and reaches a value many times as large as that obtained with the charged aerosol, but still some tens of times less than the equilibrium value of n_c for an uncharged aerosol. After the supply is discontinued, $\underline{n}$ diminishes very slowly, and after 30 minutes about one-half of the total number of particles still remains in the suspended state.

Precipitation of a polydisperse aerosol. Generally polydisperse rather than monodisperse aerosols are used for fumigation of buildings. If an aerosol with a particle-size distribution represented by the function F(r) is introduced into the space, then Eq. (2) becomes:

$$\frac{\partial [nf(r, t)\, dr]}{\partial t} = \frac{NF(r)\, dr}{V} - \frac{nf(r, t)\, dr W_e S}{V} - \frac{nf(r, t)\, dr}{V} \int_S \overline{W}_g d\overline{S}, \tag{10}$$

where $f(r, t)$ is the size-distribution function for particles suspended in air within the space. In general $f(r, t)$ differs from F(r), just as the total numerical particle concentration $\underline{n}$ differs from the increase N/V in the number of particles per unit volume of the space.

For any fraction of a polydisperse aerosol Eq. (5) becomes

$$W_e = \frac{2V\rho q}{3S\tau_i r}, \tag{11}$$

where $\rho = \int_0^\infty qnf(r, t)\, dr$ is the volume-charge density of the aerosol.

When $W_e < W_g$, with Eq. (11) taken into account, the precipitation Eq. (10) becomes:

$$\frac{\partial [nf(r, t)\, dr]}{\partial t} = \frac{NF(r)\, dr}{V} - \frac{2\rho q nf(r, t)\, dr}{3\tau_i r}. \tag{12}$$

When $W_e < W_g$, for rooms of the usual shape (parallelepipeds), Eq. (10) can be simplified and reduced to a form analogous to (9).

In the steady state $\left(\frac{\partial [nf(r, t)\, dr]}{\partial t} = 0\right)$ Eq. (12) is easily solved

$$\frac{NrF(r)\, dr}{V} - \frac{2\rho_c q nf(r, t)\, dr}{3\eta} = 0,$$

$$\frac{N}{V}\int_0^\infty rF(r)\, dr - \frac{2\rho_c}{3\eta}\int_0^\infty qnf(r, t)\, dr = 0,$$

$$\frac{N}{V}\int_0^\infty rF(r)\, dr - \frac{2}{3\eta}\rho_c^2 = 0,$$

$$\rho_c = \sqrt{\frac{3\eta N}{2V}\int_0^\infty rF(r)\, dr} \tag{13}$$

and, with Eq. (11) taken into account,

$$\left(\frac{W_e}{W_g}\right)_c = \frac{3q}{g\gamma_l Sr^3}\sqrt{\frac{3\eta VN}{2}\int_0^\infty rF(r)dr} = \frac{3q}{g\gamma_l Sr^3}\sqrt{\frac{3\eta VNR}{2}}, \qquad (14)$$

where R is the average particle radius in accordance with the equation

$$R = \int_0^\infty rF(r)\,dr.$$

As an example, we assume the same conditions as in the example for a monodisperse aerosol. Further, we assume that the charge on a particle is proportional to its radius, $q = ar$, such that $a = 0.0196$ CGSE/cm and $R = 1.25 \cdot 10^{-4}$ cm.

Calculations give the values summarized in Table 1.

TABLE 1

Effects of Particle Radius on the Relative Linear Velocity of Electrostatic Precipitation and Precipitation Irregularity Factor in Treatment of a Space with a Polydisperse Aerosol

r, cm · 10^4	0.5	1,2	2	3,2	6	10	14	18	24	32
$(W_e/W_g)_c$	3580	621	224	87,5	24,8	8,95	4,57	2,76	1,55	0,875
Q_{cg}/Q_{fr}	~1	0,996	0,99	0,977	0,923	0,800	0,640	0,468	0,216	0

In the experiments, unipolar charging of the aerosols was effected by charging of a liquid film sprayed in an electric field. A sprayer designed by A. V. Kitaev (Fig. 2) was used. Air which ejected the liquid through the annular orifice of the nozzle 2 was forced under pressure through the annular gap between an insulated insert 1 and the nozzle 2. A negative potential (approximately 1000 v) was applied to the insert 1 while the nozzle 2 was grounded. The liquid flowing through the annular orifice of the nozzle was broken up by the air stream in the electric field between the insert and the nozzle 2. The particle surfaces facing the insert became positively charged by induction, while the negative charge leaked to ground through the unsprayed part of the liquid and the nozzle 2. Dispersion of the liquid gave a positively charged aerosol.

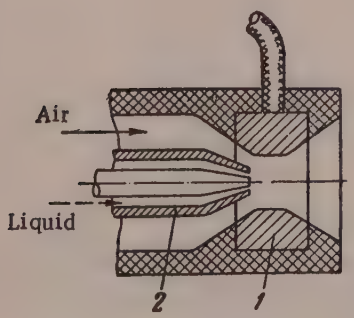


Fig. 2. Diagram of sprayer.

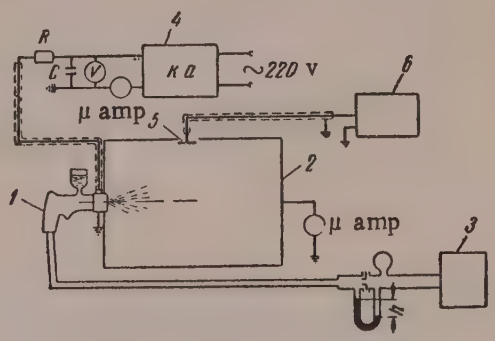


Fig. 3. Circuit of experimental unit.

Figure 3 is the circuit diagram of the experimental unit; the sprayer 1 was installed in the center of one of the walls of an insulated metal chamber 2, 1.2 m^3 in volume so that the aerosol stream was directed at the center of the opposite wall. Compressed air for dispersion of the liquid entered the sprayer from the compressor 3. The air rate was 10 m^3/hour, the air pressure was 3.5 atmospheres, and the liquid rate was 0.2 g/second. The source of constant potential was the kenotron unit 4; its potential, after half-wave rectification, was smoothed by means

of a 0.5 μF capacitor and, to ensure electrical safety of the sprayer, was fed through a resistor (0.75 megohm) to the insert. The convective current (charge introduced into the chamber with the droplets during 1 second of sprayer operation) was measured by grounding of the insulated chamber 2 through a microammeter. The convective current in the experiments was 2 microamperes. The field intensity in the chamber was measured at the center of the ceiling, where the transducer 5 was installed. The signals from the transducer were measured by means of the electron oscillograph 6.

The liquid used was spindle oil containing 8% of an aqueous alcoholic solution of potash soap. The latter was added to increase the conductivity of the liquid.

The amounts of liquid precipitated were determined by means of colorimetric analysis. Cells were attached by metal joints to the floor, ceiling, and walls of the chamber. After completion of the aerosol treatment the cells were taken out of the chamber. 0.1% of a fat-soluble dye was first dissolved in the liquid for the colorimetric determinations.

The particle-size composition of the precipitated droplets was determined microscopically. Microscope slides coated with a thin silicone layer [3] were placed at the center of the floor, ceiling, and each wall of the chamber. After the end of the treatment the slides were taken out and examined under a microscope with a graticule eyepiece at magnifications of × 120 and × 600. The precipitated drops were counted, the area examined was measured, and the droplets were grouped by size. About 50 drops of each size were taken; the slide area examined was gradually increased to approximately 1 cm^2.

The experiments were conducted as follows. The aerosol was fed into the chamber for 15 seconds (in experiments with glass slides) or 3 minutes (in experiments with colorimetric cells). The aerosol was allowed to settle for 30 minutes, air was blown through the chamber by means of a fan, and the slides or cells were taken out for analysis. It was confirmed by special tests that the effects of evaporation on droplet size may be disregarded.

The results obtained in determinations of the distribution of precipitated aerosols in the chamber experiments and in additional experiments carried out in a room 68 m^3 in volume are presented in Table 2.

TABLE 2

Distribution (in %) of Precipitated Aerosol (Colorimetric Determinations)

Conditions of aerosol preparation	Ceiling	Walls	Floor
Chamber 1.2 m^3 in volume			
Charged	4,06 – 4,07	34,4—53,6	44,4 – 61,5
Not charged	0,005 – 0,03	8,5—12	88,0—91,5
Room 68 m^3 in volume			
Charged	8,9	30,9	60,2
Not charged	0,003	8,4	91,6

The results demonstrate clearly that charging makes the treatment more uniform: about one-half of the liquid is deposited on the walls and ceiling, whereas without charging only 8.4-12% is deposited on the walls and ceiling. The effect was most pronounced in the case of the ceiling.

Comparison of the amounts of liquid used and the amounts of deposited liquid found showed that in these experiments most of the liquid was precipitated in the chamber; therefore the results of microscopic analysis of the precipitated droplets may be used for approximate estimation of the size range of the droplets in the aerosol stream formed by the sprayer. The distribution curves so determined (Fig. 4) show that under otherwise equal conditions, charging greatly increases the dispersity of the aerosol formed. This is probably due to decrease of the surface tension of the liquid as the result of charging, and also to a reduction of the rate of coagulation during spraying [4] as the result of electrostatic mutual repulsion of the charged droplets.

The results of microscopic analysis can be used for estimating the influence of charging on the irregularity of precipitation of droplets of different sizes. In Fig. 5, these results are presented in the form of plots of $\epsilon_1 = Q_{cg}/Q_{fr}$ and $\epsilon_2 = Q_w/Q_{fr}$ against the droplet radius.

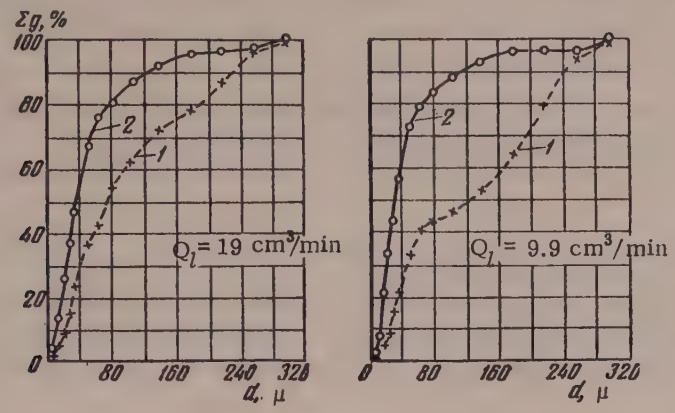


Fig. 4. Integral droplet-size distribution curves: Σg is the amount of liquid (%) contained in droplets of diameters between 0 and d (μ): 1) Not charged; 2) charged.

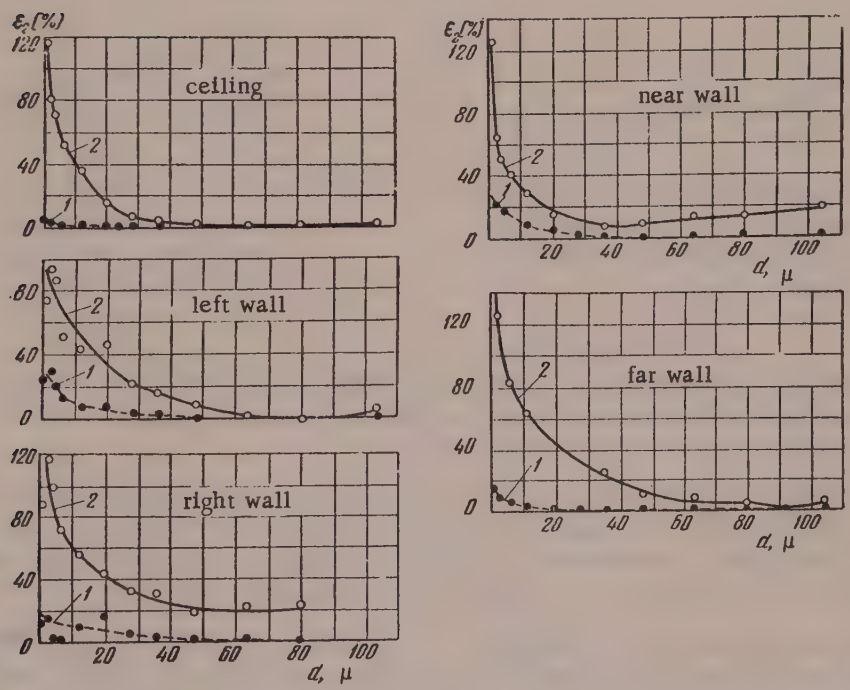


Fig. 5. Irregularity of precipitation of droplets of different sizes in the chamber: 1) Not charged; 2) charged.

In uncharged aerosols droplets of all sizes, down to the smallest ($r = 0.5\ \mu$), were deposited mainly on the floor; i.e., they were mainly under the influence of gravitational forces. In charged aerosols, the small droplets ($r < 2\mu$) were deposited approximately equally over all the chamber surfaces, i.e., the precipitation was effected mainly by the action of electrical forces. The role of gravitational forces increased with increasing r, and the larger droplets ($r > 50\ \mu$) were deposited mainly on the floor.

The average density of surface charge on the droplets can be found by division of the convective current by the surface area of the droplets in the aerosol; it is found to be 6.5 CGSE, whereas the surface charge density of the unsprayed liquid film in the sprayer is $\sigma = E/4\pi \approx 9$ CGSE. Here the field intensity (E) at the liquid surface was approximately estimated as the ratio of the applied potential (1000 v) to the width of the air gap between the liquid and the insert (0.3 mm). The fact that the values are of the same order of magnitude confirms that charging of the aerosol in this aprayer is inductive in character.

The experimental results can be used for approximate estimation of charge distribution by droplet size. If it is assumed that the charge distribution conforms to the exponential law

$$q = ar^m, \tag{15}$$

then the experimental results at once indicate the upper limit of the exponent m. As already stated, it follows from Fig. 5 that when r is small the numbers of droplets deposited on the floor and ceiling are approximately equal, but deposition on the floor begins to predominate as r increases. This means that as r increases, the gravitational forces, which are proportional to r^3, increase more rapidly than the electrostatic forces, and therefore $m < 3$.

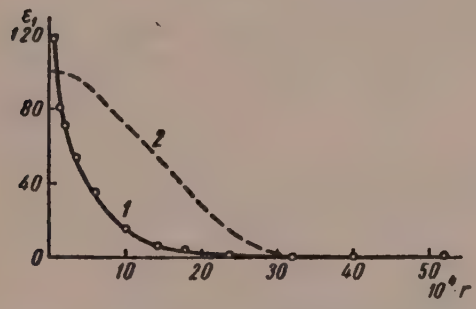


Fig. 6. Degree of irregularity (ϵ) of precipitation of droplets of different diameters (r) in the chamber: 1) Experimental data; 2) results calculated for m = 1.

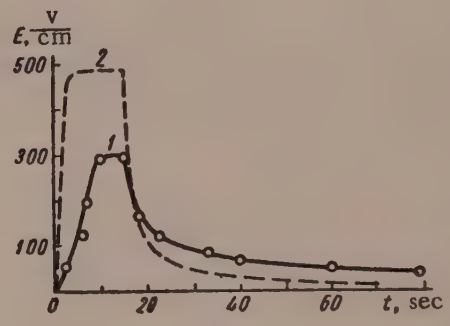


Fig. 7. Variations with time of the intensity E of a field created by a polydisperse aerosol in the chamber: 1) Experimental data; 2) results calculated for m = 1.

For comparison of the experimental results with the theory, Eqs. (10) and (12) were solved numerically with the aid of Eq. (15) in which m = 1 (the other values were assumed to be the same as in the experiments and in the example relating to the polydisperse aerosol).

Figure 6 shows the curve calculated for m = 1 compared with the experimental values of the degree of irregularity $\epsilon_1 = Q_{cg}/Q_{fr}$. Figure 7 represents changes in the average field intensity E calculated for m = 1 (Curve 2) and determined in the center of the ceiling (Curve 1). The experimental data are in satisfactory agreement with the calculated results. This confirms the assumptions made.

A distribution conforming to the condition $q \sim r$ may be the consequence of predominant formation of the smallest droplets from the part of the liquid which faces the air stream and the electric field, i.e., which carries most of the charge. It is possible that predominant transfer of charge to the projecting portions of the disintegrating liquid, from which the smaller droplets are probably formed, may also have an effect here. The highly charged fine droplets which are formed, first lower the intensity E at the surface of the rest of the disintegrating liquid in consequence of the shielding effect.

SUMMARY

1. An approximate theory is put forward for the precipitation of unipolarly charged monodisperse and polydisperse aerosols in an enclosed space.

2. A method has been developed and used for studying the precipitation of a unipolarly charged aerosol in a chamber 1.2 m^3 in capacity. The aerosol particles were charged in an electric field.

3. The experimental data are in approximate agreement with calculated results if it is assumed that the charge distribution over the droplets is proportional to the droplet radius. The possible causes of this type of charge distribution in the charging method used are discussed.

LITERATURE CITED

[1] A. G. Amelin et al., (Editors), Aerosols in Agriculture [In Russian] (Agricultural Press, Moscow, 1956) p. 77.

[2] N. A. Fuks, Mechanics of Aerosols [In Russian] (Izd. AN SSSR, Moscow, 1955).

[3] Z. M. Yuzhnyi, Kolloid. Zhur. 20, 507 (1958).*

[4] V. F. Dunskii, Zhur. Tekh. Fiz. 26, 1262 (1956).

* Original Russian pagination. See C. B. translation.

FLOW OF RUBBERLIKE POLYMERS AND THEIR MIXTURES WITH CARBON BLACK

N. V. Zakharenko, F. S. Tolstukhina, and G. M. Bartenev

Scientific Research Institute of the Rubber Industry, Moscow

Translated from: Kolloidnyi Zhurnal Vol. 22, No. 2, pp. 168-175, March-April, 1960

Original article submitted March 12, 1959

The mechanism of irreversible flow of polymers consists of displacement of small portions (segments) of their chains. This is confirmed by the low value of the activation energy of flow, comparable to that of viscous flow of compounds of low molecular weight, and by the fact that the activation energy is independent of the chain length [1].

It is also known that high polymers, and especially rubbers and their mixtures with carbon black, are systems with anomalous viscosity. This anomaly consists of a much more rapid increase of the flow rate with stress than is indicated by Newton's law of viscous flow.

Anomalous viscosity may be attributed to several causes: thixotropic structure of the material (characterized by reversible breakdown and restoration of bonds between the particles), changes in the shape of the chain molecules under stress (which may lead to transition from an isotropic to an anisotropic or oriented structure), and breakdown of the polymer chain molecules leading to a decrease of molecular weight [2].

The complex nature of polymer flow presents difficulties in the development of a theory of the process. This accounts for the lack of a satisfactory physical theory of polymer flow.

The present investigation consisted of a study of the flow of polymers and mixtures in a condensed phase in relation to the temperature and stress, in order to elucidate the laws governing the process. The materials used for the investigation were P-20 and P-118 polyisobutylene and its mixtures with rubber black, sodium butadiene rubber (SKB) and its mixtures with an active (lamp black) and an inactive (chalk) filler, and industrial rubber stocks used for production of rubber articles for technical purposes and of rubber footwear.

The flow of polymers and mixtures was studied by the method widely used for disperse systems, which is based on measurements of simple shear deformations at constant stress at low velocity gradients [3, 4].

Tolstoi's plastoelastometer [3] was used for determinations of effective viscosity. In this instrument (Fig. 1) the sample 1 is subjected to shear in a thin layer between two plane-parallel plates 2 and 3. The lower plate is stationary while the upper one is moved under the action of a load 4 over a pulley 5 which rests on needle bearings. The displacement of a micrometer scale 6, rigidly linked to the moving plate, is measured by means of a cathetometer to the nearest 0.0005 cm. The instrument is contained in a heat-insulated chamber in which the temperature is maintained constant to within $\pm 0.05^{\circ}$ by means of an ultrathermostat. The plates are grooved at right angles to the direction of displacement in order to improve cohesion and to prevent slippage.

A typical shear-deformation-time curve for polyisobutylene of P-118 grade (118 represents the molecular weight in thousands) is shown in Fig. 2. The nonlinear portion of the curve passes into a straight line; this indicates that a constant deformation rate becomes established. This linear portion of the curve represents the

increase of irreversible deformation; its slope can be used for finding the deformation rate and then the effective viscosity from the equation:

$$\sigma = \frac{\eta}{h} \cdot \frac{dx}{dt} \qquad (1)$$

where σ is the stress (dynes/cm^2); η is the effective viscosity (poises); x is the displacement (cm); t is the time (seconds); and h is the thickness of the layer of material (cm).

In order to refine the technique, the effects of layer thickness, groove depth, and plate size on the viscosity were investigated. The experiments were performed with different grades of polyisobutylene.

The thickness of the polyisobutylene layer was varied from 0.4 to 9 cm. It was found that the displacement velocity is proportional to the thickness, while the

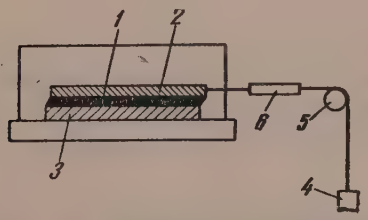


Fig. 1. Principle of the plasto elastometer.

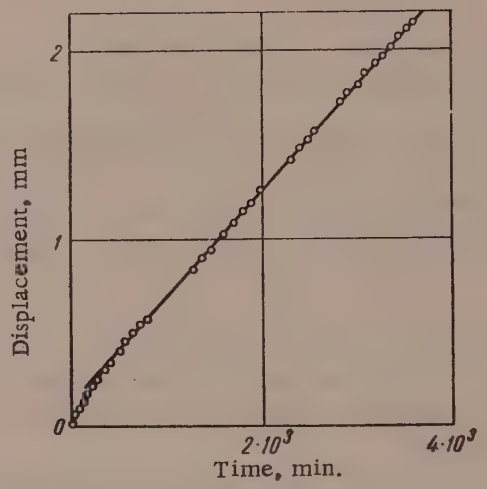


Fig. 2. Development of shear deformation in P-118 polyisobutylene; $\sigma = 3.9 \cdot 10^4$ dynes/cm^2; $t = 82°$.

viscosity is independent of the thickness up to about 3 mm. On further increase of layer thickness, the stressed state was no longer one of simple shear, and erroneous results were obtained. Specimens 1 mm thick were used in the subsequent experiments.

TABLE 1

Effect of Groove Depth on the Results of Viscosity Determinations with P-118 Polyisobutylene at 82°

Shear stress, $\times 10^{-4}$ dynes/cm^2	5.0	5.0	6.3	6.3
Groove depth, mm	0.1	0.3	0.1	0.3
Viscosity, $\times 10^{-9}$ poise	1.21	1.20	1.11	1.11

TABLE 2

Effect of Plate Size on Viscosity (Stress $19.6 \cdot 10^4$ dynes/cm^2)

Material	Temp. °C	Plate size, mm	Viscosity, poises
P-85 polyisobutylene	44	25 × 40	$8.5 \cdot 10^8$
		15 × 30	$8.7 \cdot 10^8$
Mixture based on SKB	57	25 × 40	$3.6 \cdot 10^7$
		15 × 30	$3.3 \cdot 10^7$

The experiments showed (Table 1) that the viscosity is also independent of the groove depth.

It follows that with grooves 0.1 and 0.3 mm deep, slippage of the polymer relative to the plate is excluded to an equal degree, and the material contained in the grooves does not undergo any significant deformation, so that the work expended in deformation of the material in the grooves may be disregarded. In the subsequent experiments, plates with grooves 0.1 mm deep were used.

Data on the effect of plate size on viscosity of P-85 polyisobutylene and a rubber mix containing SKB rubber are presented in Table 2. These results also show that the viscosity is almost independent of plate size.

The advantage of the method of shear in a plane-parallel layer is that the material is in a state of virtually homogeneous stress. Because of this, the velocity gradient and shear stress remain constant over a considerable section of the flow curve. However, a serious fault of the method is that at considerable relative displacements of the plate surfaces (at large deformations) the stress ceases to be constant.

Since there have not been any previous special investigations covering a wide range of stresses, it has not been determined whether there is a region of Newtonian flow in the case of polymers. It is known that such a region, characterized by constant viscosity independent of the stress, exists for disperse systems and structurized liquids at low stresses [5].

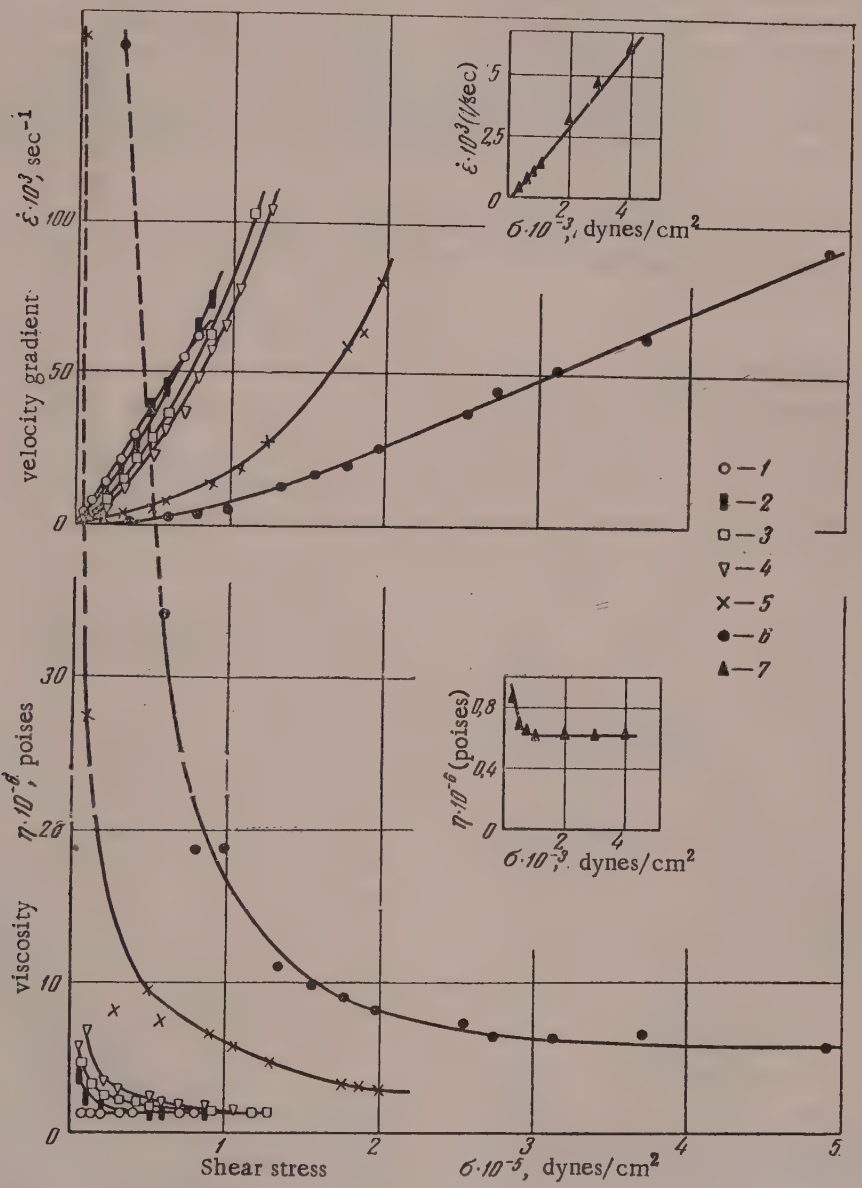


Fig. 3. Rheological curves for P-20 polyisobutylene with lamp black, t = 32°. 1) Without carbon black; 2) 20; 3) 25; 4) 30; 5) 65; 6) 80; 7) 3 weight parts of carbon black.

A region of Newtonian flow is found for P-20 polyisobutylene of low molecular weight (Fig. 3, Curve 1) in a 20-fold change of stress from $0.39\cdot10^4$ to $7.84\cdot10^4$ dynes/cm^2. It is seen that the velocity gradient is directly proportional to the stress and that the viscosity is independent of the stress. However, entirely different results

are obtained in studies of mixtures of polyisobutylene with lamp black (from 3 to 80 parts by weight per 100 parts by weight of polymer). No region of Newtonian flow was found for such mixtures (Fig. 3, Curves 2-6). In the region of small stresses, the viscosity changes very sharply. It is clear from Curve 7, Fig. 3, that even a small amount of carbon black (3 parts by weight) results in a deviation from Newtonian flow.

The greater viscosity of systems with carbon black (in the investigated range of stresses and carbon contents) in comparison with the pure polymer is attributable to formation of two types of bonds: unstable bonds of the van der Waals type which break down under the influence of small stresses, so that the viscosity decreases in the initial region of the flow curve, and more stable bonds which are formed, according to the modern view, by interaction of the free radicals formed during mechanical milling with the surfaces of the filler particles. As in the case of loaded mixtures, the region of Newtonian flow is smaller for pure polyisobutylene of high molecular weight. These facts can be explained if it is taken into account that in more complex systems than polyisobutylene of low molecular weight, there is a range of intermolecular bonds differing in stability and in the time of thixotropic recovery. As the stress and flow rate increase, some of the bonds with a greater restoration time fail to be restored after breakdown. This results in a decrease of the effective viscosity (despite an increase in the high-elasticity component of the deformation).

The deviation from Newtonian flow increases with filler content, as is seen from a comparison of the experimental data with the Ostwald-de Waele power equation

$$\dot{\varepsilon} = \frac{1}{\eta'} \sigma^n, \qquad (2)$$

where n represents deviation from Newtonian flow ($n \geq 1$); σ is the shear stress; η' is a constant for the material, which coincides with the viscosity η when $n = 1$.

It follows from Eq. (2) that $n = 1$ for materials which conform to Newton's law, but in all other cases n differs from 1, and increases with increasing deviation from Newton's law.

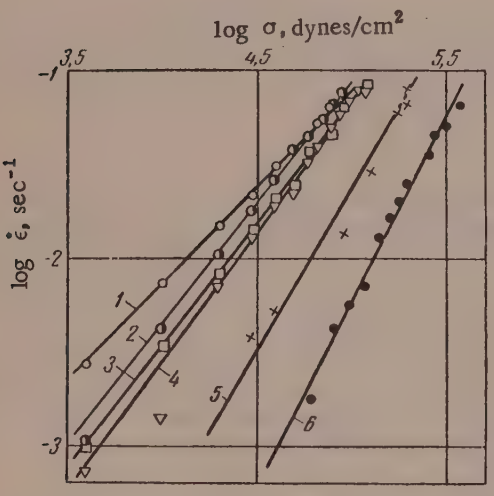


Fig. 4. The log $\dot{\varepsilon}$ (log σ) relationship for P-20 polyisobutylene with lamp black, $t = 32°$: 1) Without carbon black; 2) 20; 3) 25; 4) 30; 5) 65; 6) 80 weight parts of carbon black.

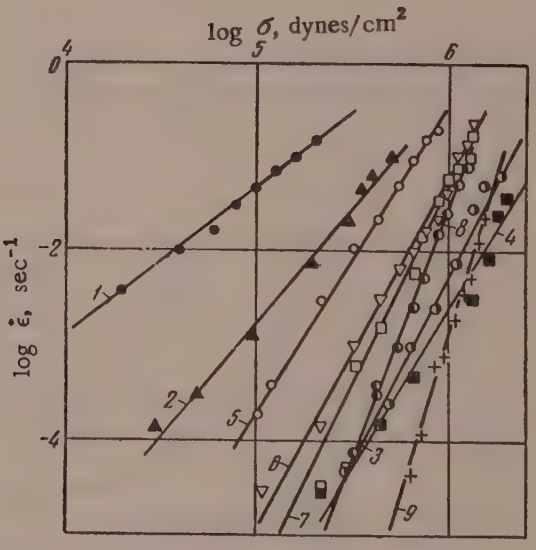


Fig. 5. The log $\dot{\varepsilon}$ (log σ) relationship for technical rubber stocks, $t = 82°$: 1, 2, 3, 4) Stocks for technical rubber products; 5, 6, 7, 8, 9) stocks for rubber footwear.

Data for P-20 polyisobutylene and its mixtures with carbon black are plotted in logarithmic coordinates in Fig. 4. The linear plots indicate that the flow of such mixtures is in practice represented by the Ostwald–de Waele equation. The slopes of the lines were used to calculate the deviations from Newtonian flow. It is

found that n is directly proportional to the filler content. The results may be represented by the formula $n = 1 + 0.012c$, where c is the filler content (weight parts per 100 weight parts of polymer).

Rheological curves similar to those given above for polyisobutylene mixtures (Fig. 3) were obtained by the same method at 82° for mixtures containing SKB and for technical rubber stocks.

Figure 5 shows that the flow of these materials, like the flow of polyisobutylene, conforms to the Ostwald–de Waele equation. The deviations n from Newtonian flow, calculated from these data, are given in Table 3, which shows that rubber stocks do not conform to Newton's law. For SKB-55 stocks, the deviation from Newtonian flow increases with the content of active filler. The value of n for stocks with inactive filler is the same as for stocks without filler. Technical rubber stocks differ in their deviation from Newtonian flow; n varies from 1.58 to 6.90.

Variations of viscosity of P-20 polyisobutylene and its mixtures with different amounts of carbon black with temperature are plotted in Fig. 6. The linear plots indicate that in the range between 20 and 80° the viscosity-temperature relationship approximately conforms to the exponential equation

$$\eta = Ae^{E/kT}, \tag{3}$$

where A is a constant; E is a quantity with the dimensions of activation energy.

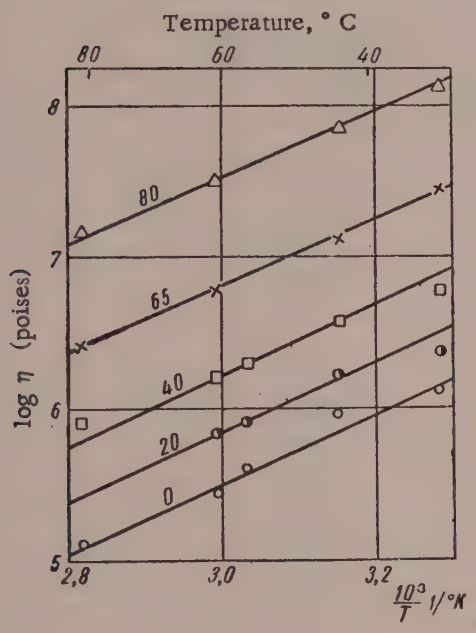


Fig. 6. The $\log \eta - \frac{1}{T}$ relationship for P-20 polyisobutylene and its mixtures with carbon black at $\sigma = 0.01$ kg/cm²; the numbers of the plots indicate the contents of lamp black in weight parts per 100 weight parts of polymer.

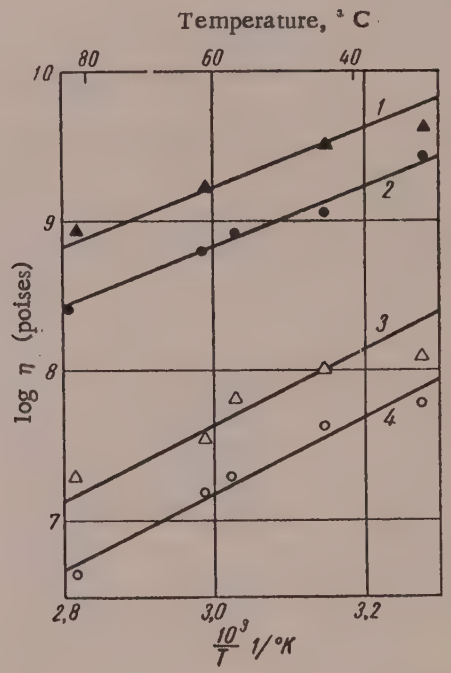


Fig. 7. The $\log \eta - \frac{1}{T}$ relationship at different shear stresses for P-85 polyisobutylene (1, 2) and stocks based on SKB-35 (3, 4); shear stress: 1) $0.98 \cdot 10^4$; 2) $29.4 \cdot 10^4$; 3) $19.6 \cdot 10^4$; 4) $39.2 \cdot 10^4$ dynes/cm².

The fact that the lines for the original polymer and of the mixtures all have the same slope indicates that the temperature coefficient of viscosity does not depend on the filler content, and therefore flow must occur by a diffusion mechanism of displacement of the rubber segments irrespectively of the presence of rubber-carbon bonds. The activation energy E in this case is 9.8 kcal/mole.

Straight lines were also obtained for rubber stocks in the same coordinate system; therefore these systems also conform to the exponential equation. The activation energies at a stress of $3.92 \cdot 10^5$ dynes/cm^2 were calculated:

Stocks based on	Activation energy
SKB-35	11.3 kcal/mole
Natural rubber	12 "
SKB-60	9.4 "
SKN-26	14.3 "
SKS-30 with reclaim	11.2 "
SKN-26 with reclaim	9.6 "
SKS-30	12.8 "

Figure 7 shows that the activation energy of viscous flow is almost unchanged with changes of shear stress. With changes of shear stress from $0.98 \cdot 10^4$ to $2.94 \cdot 10^5$ dynes/cm^2 for unfilled polyisobutylene, and from $1.96 \cdot 10^5$ to $3.92 \cdot 10^5$ dynes/cm^2 for a technical rubber stock based on SKB-35, the slope of the lines remains constant. It follows that the stress does not influence the activation energy (this requires more extensive verification) and only affects the preexponential term in Eq. (3). This indicates that both in complex systems and in pure polyisobutylene, the size of the elementary flow unit is not changed under the influence of stress.

TABLE 3

Deviations from Newtonian Flow (Values of n) for Rubber Stocks

Stocks	Based on SKB-55 rubber	n
Model	SKB-55	2.12
	SKB-55 + 20 chalk	2.12
	SKB-55 + 50 chalk	2.12
	SKB-55 + 20 black	2.10
	SKB-55 + 50 black	2.40
	SKB-55 + 80 black	2.65
For technical rubber products based on	NR	1.58
	SKB-35	2.44
	SKS-30	4.06
For rubber footwear, based on	SKN-26	3.46
	SKB-60	3.32
	SKS-30 + reclaim	3.78
	SKS-30 + reclaim	4.30
	NR + reclaim	5.50
	SKS-30	6.90

The values of the activation energy and the Eyring equation $H_{ev}/E = 4$ (where H_{ev} is the heat of evaporation of a segment) were used to determine the dimensions of the flow segment; it corresponds to 7 isobutylene units for P-20 and P-85 polyisobutylene, and to 7-11 rubber monomer units for technical rubber stocks.

Comparison of the curves in Figs. 6 and 7 shows that the activation energy of viscous flow is independent of the molecular weight of polyisobutylene; it follows from these curves that the activation energy for P-20 and P-85 polyisobutylene is 9.8 and 9.4 kcal/mole, respectively.

SUMMARY

1. The existence of Newtonian flow has been established for P-20 polyisobutylene in the region of small stresses, 10^3-10^4 dynes/cm^2. There is no region of Newtonian flow for systems containing carbon black in this stress range.

2. The rheological curves for complex rubber-carbon black systems conform to the Ostwald-de Waele empirical equation

$$\dot{\varepsilon} = \frac{1}{\eta'} \sigma^n.$$

in the stress range studied.

3. The index of deviation from Newtonian flow (n) increases with the content of active filler. The value of n is unchanged in presence of an inactive filler, and it remains the same as for the pure rubber.

4. The viscosity-temperature relationship for pure polyisobutylene, its mixtures with carbon black, and stocks based on various rubbers is represented by the exponential expression $\eta = Ae^{E/kT}$. The activation energies of viscous flow for these systems have been determined.

5. The temperature coefficient of viscosity and the activation energy are independent of the nature and amount of filler.

LITERATURE CITED

[1] P. J. Flory, J. Am. Chem. Soc. 62, 5, 1057 (1940); T. Y. Fox and P. J. Flory, J. Am. Chem. Soc. 70, 2384 (1948); A. Tobolsky, R. Powell, and H. Eyring, Chemistry of Large Molecules [Russian translation] (IL, Moscow, 1948).

[2] G. H. Piper and J. R. Scott, J. Rubber Res. 16, 135 (1947); 17, 151 (1948); W. Kauzman and H. Eyring, J. Am. Chem. Soc. 62, 3113 (1940).

[3] D. M. Tolstoi, Kolloid. Zhur. 10, 133 (1948).

[4] L. V. Chumakova and P. A. Rebinder, Doklady Akad. Nauk SSSR 81, 239 (1951).

[5] P. A. Rebinder, Vestnik Akad. Nauk SSSR 2 (1955); N. V. Mikhailov, Kolloid. Zhur. 17, 68 (1955); W. Philippoff, Wiskosität der Kolloide (Dresden-Leipzig, Steinkof, 1944); G. M. Bartenev, Zhur. Fiz. Khim. 29, 2007 (1955).

* Original Russian pagination. See C. B. translation

STRUCTURAL AND MECHANICAL PROPERTIES OF BITUMENS OXIDIZED BY DIFFERENT METHODS

A. I. Ivanov and N. V. Mikhailov

Scientific Research Institute for Building, Moscow

Translated from: Kolloidnyi Zhurnal Vol. 22, No. 2, pp. 176-185, March-April, 1960

Original article submitted May 26, 1959

In addition to the existing processes for bitumen production – exhaustive distillation of oil fractions from petroleum residues under vacuum (residual bitumens) and high-temperature air oxidation of petroleum asphalt in stills (oxidized bitumens)–a continuous emulsion oxidation process is now coming into use. In this last oxidation process the bitumens are in a high-temperature zone for a shorter time, with a considerable improvement of their rheological properties. Investigations by the Ufa Scientific Research Institute have demonstrated the advantages of this process and the improvements in the bitumen properties as indicated by the standard test data determined by immersion of a standard needle or by the ball and ring apparatus (B and R), the softening point, etc. These characteristics give an empirical idea of the structural and mechanical properties of bitumens and do not reflect the nature of the physical effects taking place in their structure during oxidation. We studied the structural and mechanical properties of bitumen oxidized by the emulsion process, with the aid of a continuous oxidation apparatus of the design described by Provinteev [1] which we modified by introduction of an additional cavitation unit (Fig. 1).

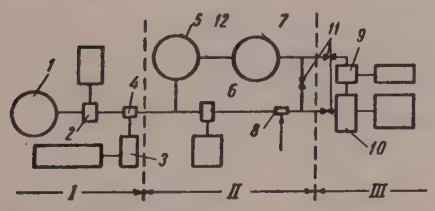


Fig. 1. Block diagram of the laboratory oxidation apparatus: I) Raw-material section; II) oxidation section; III) cavitation section.

The technological oxidation of asphalt in this apparatus is effected as follows: the asphalt is fed into the raw-material tank 1 where it is heated to 120-140° and dewatered; it is then fed by the gear pump 2 through the metering device 4 and mixer 8 into the coil of the oxidation reactor 7. The metering device 4 consists of a flanged stop valve with a regulator connected to an electric motor through the reducing gear 3. The valve is opened 15 times per minute and lets through definite amounts of asphalt. The angle through which the valve is turned is determined by a pointer, which is set separately for any given working conditions.

In passing through the mixer 8, the asphalt mixes with air fed from a compressor at 2-3 atmos pressure, and is oxidized in passing through the reactor coil. The bitumen mass then enters the expansion tank 5, where the light fractions are rapidly volatilized. The reactor and expansion tank are connected by a pipe $^1/_2$" in diameter.

The pipe is fitted with steam valves 11 which serve to direct the flow of the mass either through or away from the cavitation emulsifier and to regulate the feed rate. Asphalt can be oxidized by either a continuous or a batch process in this apparatus. In the former process, the bitumen flows continuously from the expansion tank. The oxidation time of the asphalt depends on the amount of air supplied and on the oxidation temperature. For further improvement of Provinteev's process it was decided to include a special emulsifier 10 with a pump 9 in the apparatus; this gave a cavitation effect and was therefore intended to increase the interfacial area considerably and thereby to accelerate the whole oxidation process. The cavitation emulsifier can operate at 1500 or 3000 rpm.

Petroleum asphalt from the Moscow refinery is used as the raw material for bitumen production. Bitumen samples from this refinery were taken in order to compare bitumens made by oxidation of the same raw material in a batch still and in the continuous unit by the emulsion process. Bitumen samples were taken during oxidation from the same still, 8 hours (bitumen III), 16 hours (bitumen IV), and 24 hours (bitumen V) after the start of oxidation. Asphalt was oxidized in the refinery in a 120 ton still at 255-270°, under 0.25 atmos air pressure in the still, and with an average air flow rate of 700 m^3/hour. Characteristics of the samples are given in Table 1.

TABLE 1

Physicochemical Properties of Asphalt and Bitumens, and Group Composition of Bitumens Oxidized in the Batch Still, Determined in Accordance with GOST Methods

Materials	Temperature, °C: softening B and R	Temperature, °C: flash point, Brenken	Penetration, 25°	Ductility, cm	Solubility in benzene, %	Water-soluble compounds, %	Group composition, %: oils	Group composition, %: tars	Group composition, %: asphaltenes
Asphalt	43	286	185	> 100	99,7	0,14	—	—	—
Bitumen III*	51	300	66	100	99,7	0,14	—	—	—
Bitumen IV	72	294	16	6	99,7	0,12	49,22	28,94	23,41
Bitumen V	93	282	6	2	99,6	0,12	47,36	23,01	30,94

* The group composition of bitumen III could not be determined, as the constituents are not coagulated by the method used.

The structural and mechanical properties of bitumen samples oxidized by the emulsion method were investigated with the aid of an electronic selsyn elastoviscosimeter [2] in conditions of pure homogeneous shear in a narrow gap between two coaxial cylinders at constant velocity gradient ($\dot{\epsilon}$ = const); development of the shear stress as a function of deformation was observed until an equilibrium value was reached. The absolute viscosity in poises was calculated for each velocity gradient from the results.

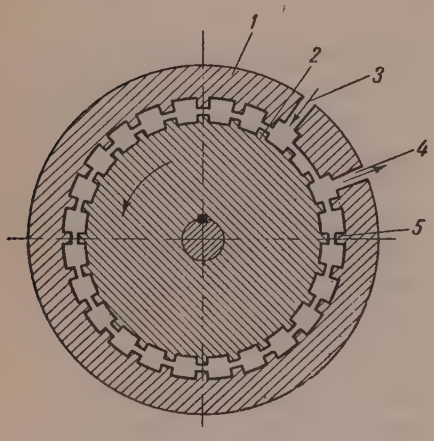


Fig. 2. Line diagram of cavitation emulsifier: 1) Stator; 2) rotor; 3) inlet; 4) outlet; 5) 0.5 mm gap between teeth.

The bitumen sample was dewatered, fed into the gap of the interchangeable coaxial cylinders, placed in a heat chamber at 180°, and then cooled down to the experimental temperature and held at that temperature for one hour. The torque at a given deformation rate was recorded oscillographically. The raw asphalt in the 40-70° temperature range, and bitumens in the 50-180° range, are quasiliquid (liquidlike) systems; therefore complete $\dot{\epsilon}$ (p) rheological curves could be obtained by investigations of equilibrium shear stress for given deformation rates.

The rheological curves for bitumens III are given in Fig. 3a, b, c, and d.

For comparison of the structural and mechanical properties of bitumens made from the same raw material by three different processes — in a batch still, in an emulsion apparatus, and in an emulsion-cavitation apparatus — their structural and mechanical characteristics were determined from the rheological curves in Fig. 3, the reference standard being the bitumen sample made in the still.

Petroleum asphalt and bitumens oxidized in the still. The following characteristics were determined for the petroleum asphalt and for bitumens oxidized in the still: highest ultimate viscosity of the practically undestroyed structure (η_0) and the minimum viscosity of the structure destroyed to the limit (η_m) (Table 2) as defined previously [3, 4].

Table 3 gives data on the relaxation time (τ_s), representing the hardness of the bitumen, average distances between the branch points of the structural network (δ), representing the strength of the structure, and values of the elasticity modulus (E) determined from the equations given earlier [5] at different temperatures

$$\tau_s = \frac{\eta_0 - \eta_m}{b}; \qquad \delta = \sqrt[3]{\frac{2kT}{b}}; \qquad E = \frac{\eta_0}{\eta_0 - \eta_m} \cdot P'_r,$$

where b, the critical stress coefficient (dynes · cm^2) is chosen separately for each temperature; k is the Boltzmann constant, equal to $1.38 \cdot 10^{-16}$ erg · degree; T is the absolute temperature; P'_r is the critical stress (dynes · cm^2) for the practically undestroyed structure, determined from the rheological curve for each given temperature.

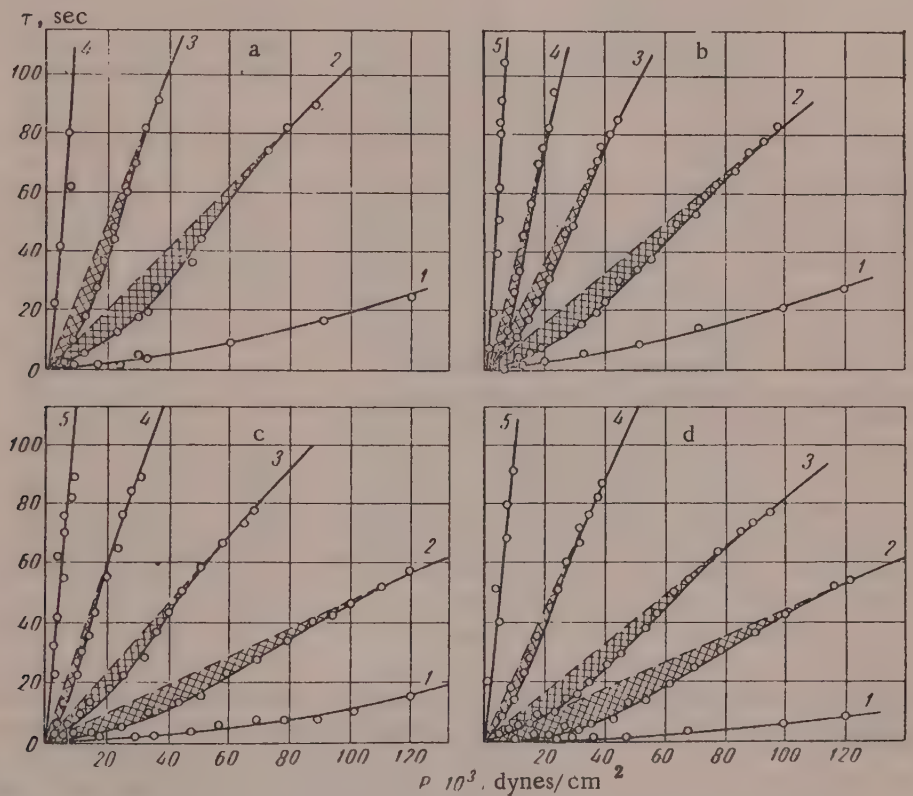


Fig. 3. Rheological $\dot{\varepsilon}(p)$ curves for asphalt and for bitumens III made by three different processes:
a) asphalt: 1) at 40°, $\eta_0 = 6.6 \cdot 10^3$; 2) at 50°, $\eta_0 = 2.5 \cdot 10^3$, $\eta_m = 0.96 \cdot 10^3$; 3) at 60°, $\eta_0 = 0.7 \cdot 10^3$, $\eta_m = 0.44 \cdot 10^3$; 4) at 70°, $\eta = 0.07 \cdot 10^3$
b) bitumen made in the still: 1) at 50°, $\eta_0 = 1.4 \cdot 10^4$; 2) at 60°, $\eta_0 = 4.5 \cdot 10^3$, $\eta_m = 1.22 \cdot 10^3$, $s = 560 \cdot 10^3$; 3) at 70°, $\eta_0 = 1.4 \cdot 10^3$, $\eta_m = 0.49 \cdot 10^3$, $s = 160 \cdot 10^3$; 4) at 80°, $\eta_0 = 0.5 \cdot 10^3$, $\eta_m = 0.19 \cdot 10^3$, $s = 56 \cdot 10^3$; 5) at 100°, $\eta = 0.062 \cdot 10^3$
c) bitumen made by the emulsion process: 1) at 50°, $\eta_0 = 1.8 \cdot 10^4$; 2) at 60°, $\eta_0 = 5.6 \cdot 10^3$, $\eta_m = 1.98 \cdot 10^3$, $s = 720 \cdot 10^3$; 3) at 70°, $\eta_0 = 2.0 \cdot 10^3$, $\eta_m = 0.85 \cdot 10^3$, $s = 242 \cdot 10^3$; 4) at 80°, $\eta_0 = 0.63 \cdot 10^3$, $\eta_m = 0.3 \cdot 10^3$, $s = 72 \cdot 10^3$; 5) at 100°, $\eta = 0.071 \cdot 10^3$
d) bitumen made by the emulsion-cavitation process: 1) at 50°, $\eta_0 = 2.1 \cdot 10^4$; 2) at 60°, $\eta_0 = 7.0 \cdot 10^3$, $\eta_m = 2.18 \cdot 10^3$, $s = 824 \cdot 10^3$; 3) at 70°, $\eta_0 = 2.8 \cdot 10^3$, $\eta_m = 1.2 \cdot 10^3$, $s = 398 \cdot 10^3$; 4) at 80°, $\eta_0 = 0.9 \cdot 10^3$, $\eta_m = 0.44 \cdot 10^3$, $s = 128 \cdot 10^3$; 5) at 100°, $\eta = 0.083 \cdot 10^3$.

TABLE 2

Limiting Values of Effective Viscosities η_0 and η_m, Velocity Gradients $\dot{\varepsilon}'_r$ and $\dot{\varepsilon}'_m$, and Shear Stresses P'_r and P'_m for Bitumens Oxidized in the Still at Various Temperatures

Materials	Temp. °C	η'_0, poises	$P'_m \cdot 10^3$, dynes · cm^{-2}	$\dot{\varepsilon}'_r$, sec^{-1}	η_m, poises	$P'_r \cdot 10^3$, dynes · cm^{-2}	$\dot{\varepsilon}'_m$, sec^{-1}
Asphalt	40	6600	20,0	3,0	—	—	—
	50	2500	2,5	1,0	960	70,0	73
	60	700	10,0	13,0	440	32,0	72
	70	71	70,0	80,0	71	70,0	80
Bitumen III	50	14000	14,0	1,0	—	—	—
	60	4500	2,0	0,45	1220	78,0	64
	70	1400	2,0	1,75	490	35,0	71
	80	500	1,0	2,0	190	15,0	76
	100	62	5,0	71,0	62	5,0	71
	120	17	1,7	98,0	17	1,7	98
	140	6	0,59	98,0	6	0,59	98
	160	2	0,19	98,0	2	0,19	98
	180	1	0,095	98,0	1	0,095	98
Bitumen IV	60	40000	80,0	2,0	—	—	—
	70	13700	27,4	2,0	—	—	—
	80	5000	15,0	3,0	—	—	—
	90	2200	22,0	10,0	1100	70,0	64
	100	800	10,0	13,0	390	33,0	82
	110	400	2,0	5,0	240	20,0	85
	120	77	5,0	70,0	77	5,0	70
	140	20	1,9	98,0	20	1,9	98
	160	3	0,295	98,0	3	0,295	98
	180	2,1	0,20	98,0	2,1	0,20	98
Bitumen V	80	18000	36,0	2,0	—	—	—
	100	6000	12,0	2,0	—	—	—
	110	2500	50,0	20,0	—	—	—
	120	1660	16,0	10,0	850	68,0	81
	130	710	10,0	15,0	310	26,0	86
	140	300	3,0	10,0	154	13,0	83
	150	62	6,0	80,0	62	5,0	80
	180	4,8	0,47	98,0	4,8	0,47	98

For determination of the degree of structure formation of bitumens made in the still, the rheological $\dot{\varepsilon}(p)$ curves and the equations derived earlier [5] were used to determine the total power H required to cause steady flow, and its components H_0 and ΔH. Table 4 contains quantitative values of H, H_0, and ΔH, the part of the power (%) expended in breaking down the structure in steady flow.

TABLE 3

Structural and Mechanical Characteristics δ, τ_s, and E for Bitumens Oxidized in the Still at Various Temperatures

Bitumens	Temp. °C	$\delta \cdot 10^6$, cm	τ_s, sec	$E \cdot 10^{-3}$, dynes × × cm^{-2}
Bitumen III	60	2,31	0,437	9,73
	70	3,24	0,325	3,28
	80	4,59	0,295	1,21
Bitumen IV	90	3,22	0,366	6,0
	100	4,29	0,351	2,3
	110	5,77	0,290	1,1
Bitumen V	120	3,56	0,337	4,50
	130	4,52	0,333	1,9
	140	6,23	0,319	0,9

In addition to the above characteristics, the distances δ between the branch points in the structural network (Table 3) and the percentage contents of asphaltenes from the group composition (Table 1) were used for determining the diameters (D) of the bitumen micelles in the branch points by means of the equations

$$V = \frac{4}{3}\pi R^3 \quad \text{and} \quad R = 0{,}6204 \cdot \sqrt[3]{V}$$

For bitumen IV, made in the still, D = 293 A at 100°, which is the temperature at which the group composition was determined. The bitumen micelles outside the branch points in the structural network are disregarded in this calculation.

Bitumens made in the emulsion and emulsion-cavitation apparatus. The same raw material was used for oxidation of asphalt by the emulsion process at 220–250° under 2.0-2.5 atmos pressure.

TABLE 4

Specific Power Required to Produce Steady Flow in Bitumens Made in the Still

Bitumen	Temp. °C	$\Delta H \cdot 10^{-3}$ erg × sec^{-1} × cm^{-3}	$H_0 \cdot 10^{-3}$ erg × sec^{-1} × cm^{-3}	$(H+\Delta H) \cdot 10^{-3}$ erg × sec^{-1} × cm^{-3}	$\frac{\Delta H}{H_0+\Delta H}$, %
Bitumen III	60	560	2600	3160	17,7
	70	160	1225	1385	11,5
	80	56	637	693	8,0
Bitumen IV	90	485	2275	2760	17,5
	100	250	1675	1925	12,5
	110	98	850	985	9,9
Bitumen V	120	540	2400	3140	18,4
	130	270	1570	1840	14,6
	140	105	713	818	12,8

In Fig. 4, log η_0 is plotted against the oxidation time (τ); it is seen that in the emulsion apparatus asphalt is oxidized 10 times as rapidly as in the still, while with the use of the cavitation emulsifier the oxidation rate is increased 40-fold with a considerable improvement in the quality of the bitumen. The accelerating effect of the cavitation emulsifier is due to the fact that the mass passed through the emulsifier is subjected to 37,000-75,000 vibrations per minute and the dispersion of air bubbles in the bitumen becomes greater, with a resultant increase of the interfacial area and therefore of the reaction surface.

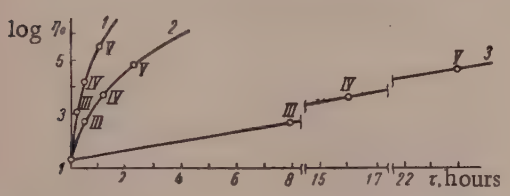


Fig. 4. Variations of log η_0 with oxidation time (τ) in production of bitumens III, bitumens IV, and bitumens V by different processes: 1) Emulsion-cavitation; 2) emulsion; 3) in batch still.

For investigation of the structural and mechanical properties of bitumens made in the emulsion and emulsion-cavitation apparatus, bitumen samples were taken with the same softening temperatures determined by the B and R method (51, 72, and 93°) as the bitumens made in the still. The same temperature conditions were used for the determinations in the electronic elastoviscosimeter as for the bitumens oxidized in the still. The results are presented in Tables 5 and 6.

It follows from the rheological curves (Fig. 3) and Tables 2 and 5 that all three bitumens made by the different processes differ from each other in their rheological properties. Bitumens made in the emulsion and emulsion-cavitation apparatus have higher strength characteristics. For example, at 60° the critical stress for the practically undestroyed structure (P'_T) is $2.0 \cdot 10^3$ dynes · cm^{-2} for bitumen III made in the still, $2.6 \cdot 10^3$ dynes · cm^{-2} for the same bitumen made in the emulsion apparatus, and $3.2 \cdot 10^3$ dynes · cm^{-2} in the emulsion-cavitation apparatus. For bitumen IV, the critical stress at 80° is $15.0 \cdot 10^3$ dynes · cm^{-2} for material made in the still, $21.0 \cdot 10^3$ dynes · cm^{-2} for material made in the emulsion apparatus, and $33 \cdot 10^3$ dynes · cm^{-2} for material made in the emulsion-cavitation apparatus. For bitumen V at 80°, $P'_T = 36 \cdot 10^3$ dynes · cm^{-2} if it is made in the still, $60 \cdot 10^3$ dynes · cm^{-2} in the emulsion apparatus, and $30 \cdot 10^3$ dynes · cm^{-2} in the emulsion-cavitation apparatus.

It follows from the data that the critical stress of the practically undestroyed structure is approximately 30% higher in the case of bitumen III made by the emulsion process, and approximately 60% higher in the case of the same bitumen made by the emulsion-cavitation process, than in the case of the same bitumen made in the still. For bitumen IV made by the emulsion process, P'_T is approximately 40% higher, and if made by the emulsion-cavitation process it is approximately 60% higher, than P'_T for bitumen made in the still. The value of P'_T for bitumen V made by the emulsion process is 67% higher, and for bitumen V made by the emulsion-cavitation process 130% higher, than the value of P'_T for the same bitumen made in the still.

TABLE 5

Limiting Values of Effective Viscosities η_0 and η_m, Velocity Gradients ϵ'_r and ϵ'_m, and Shear Stresses P'_r and P'_m for Bitumens Oxidized in the Emulsion and Emulsion-Cavitation Apparatus at Various Temperatures

Materials	Temp. °C	η_0, poises	$P'_r \cdot 10^3$, dynes × cm^{-2}	ϵ'_r, sec^{-1}	η_m, poises	$P'_m \cdot 10^3$ dynes × cm^{-2}	ϵ'_m, sec^{-1}
Asphalt	40	6600	20,0	3,0	—	—	—
	50	2500	2,5	1,0	960	70,0	73,0
	60	700	10,0	13,0	440	32,0	72
	70	71	70,0	80,9	71	70,0	80
Bitumen III from emulsion apparatus	50	18000	18,0	1,0	—	—	—
	60	5600	2,6	0,45	1980	105,0	53
	70	2000	3,5	1,75	850	51,0	60
	80	630	1,23	2,0	300	22,0	70
	100	72	6,0	80,0	72	6,0	80
	120	22	2,16	98,0	22	2,16	98
	140	7	0,685	98,0	7	0,685	98
	160	2,8	0,277	98,0	2,8	0,277	98
	180	1,4	0,135	98,0	1,4	0,135	98
Bitumen III from emulsion-cavitation apparatus	50	21000	21,0	1,0	—	—	—
	60	7000	3,2	0,45	2180	110,0	50
	70	2800	4,9	1,75	1200	75,0	62
	80	900	1,8	2,0	440	32,0	71
	100	83	7,0	80,0	83	7,0	80
	120	24	2,35	98,0	24	2,35	98
	140	8	0,76	98,0	8	0,76	98
	160	3	0,295	98,0	3	0,295	98
	180	1,6	0,160	98,0	1,6	0,160	98
Bitumen IV from emulsion apparatus	60	45000	90,0	2,0	—	—	—
	70	14000	28,0	2,0	—	—	—
	80	7000	21,0	8,0	—	—	—
	100	1200	15,6	13,0	610	5,0	82
	110	500	2,5	5,0	250	20,0	80
	120	120	10,0	83,0	120	10,0	83
	140	35	3,40	98,0	35	3,40	98
	160	3,5	0,34	98,0	3,5	0,34	98
	180	2,6	0,25	98,0	2,6	0,25	98
Bitumen IV from emulsion-cavitation apparatus	60	90000	180,0	2,0	—	—	—
	80	11000	33,0	8,0	—	—	—
	100	2400	31,0	13,0	1100	81,0	71,0
	120	600	2,4	4,0	300	25,0	80,0
	140	84	6,0	70,0	84	6,0	70,0
	160	4	0,38	98,0	4	0,38	98,0
	180	3	0,295	98,0	3	0,295	98,0
Bitumen V from emulsion apparatus	70	150000	75,0	0,5	—	—	—
	80	3000	60,0	2,0	—	—	—
	100	7000	14,0	2,0	—	—	—
	120	1900	19,0	10,0	970	78,0	80
	130	950	14,0	15,0	490	40,0	83
	140	410	4,9	10,0	200	15,0	77
	160	75	5,0	67,0	75	5,0	67
	180	6	0,58	98,0	6	0,58	98
Bitumen V from emulsion-cavitation apparatus	80	65000	130,0	2,0	—	—	—
	100	16000	32,0	2,0	—	—	—
	120	2500	25,0	10,0	1120	82,0	73
	140	500	5,0	10,0	250	20,0	80
	160	90	6,0	67,0	90	6,0	67
	180	8	0,79	98,0	8	0,79	98

The higher values of P'_r indicate a stronger structure in bitumens made by the emulsion and emulsion-cavitation processes. The values for the critical stress of the structure broken down to the limit (P'_m) also indicate that these bitumens have higher structural strength. For example, the value of P'_m at 80° for bitumen III is $15.0 \cdot 10^3$ dynes·cm^{-2} if it is made in the still, $22 \cdot 10^3$ dynes·cm^{-2} for the emulsion method, and $32.0 \cdot 10^3$ for the emulsion-cavitation method. The values for the critical stress of the structure broken down to the limit are considerably higher for bitumens IV and V.

Tables 3 and 6 also reveal differences in the rheological properties. The first relaxation time (τ_s) is greater for bitumens made by the emulsion and emulsion-cavitation processes; for example, for bitumen III $\tau_s = 0.325$ second if it is made in the still, 0.359 second if it is made by the emulsion process, and 0.390 second if it is made by the emulsion-cavitation process.

TABLE 6

Structural and Mechanical Characteristics δ, τ_s, and E and Group Composition of Bitumens Made in the Emulsion and Emulsion-Cavitation Apparatus

Bitumens	Temp. °C	$\sigma \cdot 10^6$, cm	τ_s, sec	$E \cdot 10^{-9}$ dynes × × cm^{-2}	Group composition, %		
					oils	tars	asphaltenes
Bitumen III from emulsion apparatus	60	2,26	0,452	14,94	—	—	—
	70	3,09	0,359	5,00	—	—	—
	80	4,45	0,300	1,75	—	—	—
Bitumen III from emulsion-cavitation apparatus	60	2,13	0,491	17,40	—	—	—
	70	2,85	0,390	6,39	—	—	—
	80	4,11	0,329	2,24	—	—	—
Bitumen IV from emulsion apparatus	100	4,00	0,368	3,2	50,20	26,81	23,55
	110	5,32	0,357	1,4			
Bitumen IV from emulsion-cavitation apparatus	100	3,36	0,481	5,9	55,54	23,44	21,11
	120	5,37	0,428	1,7			
Bitumen V from emulsion apparatus	120	3,42	0,344	5,5	49,70	23,05	27,68
	130	4,35	0,340	2,4			
	140	5,59	0,323	1,1			
Bitumen V from emulsion-cavitation apparatus	120	3,27	0,445	6,9	53,09	21,79	25,96
	140	5,45	0,357	1,5			

The data of Tables 3 and 6 show that δ is lower for bitumens made by the emulsion and emulsion-cavitation processes than those made in the still. For example, $\delta = 2.31 \cdot 10^6$ cm for bitumen made in the still, $2.26 \cdot 10^6$ cm for bitumen made by the emulsion process, and $2.13 \cdot 10^6$ cm for bitumen made by the emulsion-cavitation process; this indicates that they contain a stronger structural network, and this is confirmed by the smaller diameter of the bitumen micelles in the branch points of the structural network in such bitumens as compared with bitumens made in the still. For example, the diameters D of the bitumen micelles in the branch points of the structural network have the following values for bitumens IV at 100°:

Bitumen	D
Bitumen IV made in the still	293 A
Bitumen IV made by the emulsion process	282 A
Bitumen IV made by the emulsion-cavitation process	257 A

It follows from Tables 3 and 6 that bitumen III at 70° has elasticity modulus $E = 14.94 \cdot 10^{-3}$ dynes $\cdot$ cm^{-2} if made by the emulsion method, $17.4 \cdot 10^3$ dynes $\cdot$ cm^{-2} if made by the emulsion-cavitation method, and $9.73 \cdot 10^{-3}$ dynes $\cdot$ cm^{-2} if made in the still. Higher values of the elasticity modulus indicate a more elastic structure of the bitumens.

The data in Tables 4 and 7 indicate the degree of structurization in bitumens at different temperatures. For example, at 60° the degree of structurization of bitumen III made by the emulsion process is 156% greater, and of that made by the emulsion-cavitation process is 174% greater, than the structurization of bitumen made in the still; in the case of bitumens IV and V, the structurization is even greater. The degree of structurization of the system increases with the time during which the oxidized asphalt remains in the emulsion and especially in the emulsion-cavitation equipment.

For all bitumens III, total absence of structure is found at 100° (rheological curves in Fig. 3); for bitumens IV made in the still and by the emulsion process, at 120°, and made by the emulsion-cavitation process at 140°; for bitumens V made in the still, total absence of structure is observed at 150°, and for bitumens V made by the emulsion and emulsion-cavitation process, at 160°.

TABLE 7

Specific Power Required at Various Temperatures to Produce Steady Flow in Bitumens Made by the Emulsion and Emulsion-Cavitation Processes

Bitumen	Temp. °C	$\Delta H \cdot 10^{-3}$, erg × sec^{-1} × cm^{-3}	$H_0 \cdot 10^{-3}$, erg × sec^{-1} × cm^{-3}	$(H_0+\Delta H) \cdot 10^{-3}$, erg × sec^{-1} × cm^{-3}	$\frac{\Delta H}{H_0+\Delta H}$, %
Bitumen III from emulsion apparatus	60	720	2625	3345	21,5
	70	242	1560	1802	13,4
	80	72	770	842	8,5
Bitumen III from emulsion-cavitation apparatus	60	824	2725	3549	23,2
	70	398	2325	2723	14,6
	80	128	1237	1365	9,3
Bitumen IV from emulsion apparatus	100	398	2009	2407	16,5
	110	148	892	1040	14,2
Bitumen IV from emulsion-cavitation apparatus	100	617	2800	3417	18,0
	120	131	990	1121	11,6
Bitumen V from emulsion apparatus	120	650	2700	3350	19,3
	130	360	1935	2295	15,5
	140	126	785	802	13,9
Bitumen V from emulsion-cavitation apparatus	120	705	2800	3505	20,0
	140	135	800	935	14,4

The coefficients of thermal sensitivity determined from the equation $K = -\,d \log \eta_0/dT$ [6] over the 50-140° temperature range have the following values for bitumen III: made in the still, $K = 4.05 \cdot 10^{-2}$; made by the emulsion process, $3.5 \cdot 10^{-2}$; and made by the emulsion-cavitation process, $3.1 \cdot 10^{-2}$; these results show that bitumens oxidized by the emulsion and emulsion-cavitation processes have higher thermal stability.

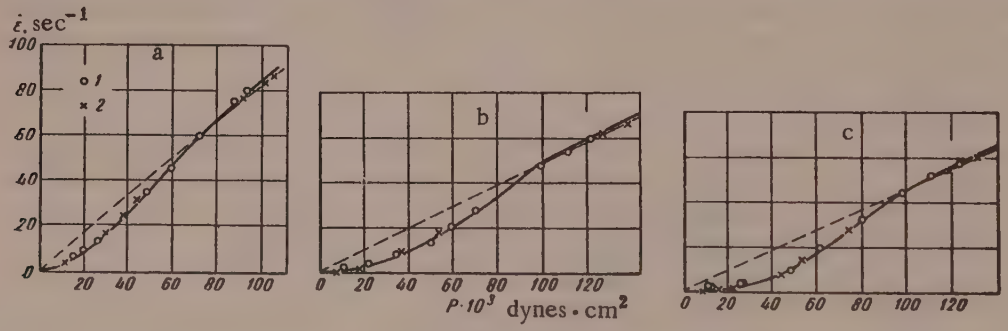


Fig. 5. Comparison of rheological $\dot{\varepsilon}(p)$ curves for 60° for bitumens III made in the still (a), by the emulsion process (b), and the emulsion-cavitation process (c): 1) Experimental curve; 2) theoretical curve.

Good agreement was obtained (Fig. 5, a, b, and c) between the experimental rheological curves and the theoretical values calculated from the equation [4]

$$\eta(P) = \eta_m + (\eta_0 - \eta_m)\frac{P/b}{sh\,P/b},$$

The slight discrepancies between the calculated and experimental curves are due to the use of an average value of the coefficient b in the equation.

SUMMARY

1. Bitumens made by the emulsion and emulsion-cavitation processes have higher structural strength as indicated by the values of P_r^* and P_m^*, higher viscosity as determined by the values of the practically undestroyed structure η_0 and the structure broken down to the limit η_m, and higher elasticity than bitumens made in the still.

2. Bitumens made by the emulsion and emulsion-cavitation processes are more highly structurized and their thermal stability is 15-20% higher.

3. The limiting maximum viscosity of the practically undestroyed structure η_0 at the operating temperature is a measure of the performance qualities of the bitumen, while η_m, the limiting minimum viscosity of the destroyed structure, represents the technological behavior (placement characteristics) of the bitumen. The viscosity of the destroyed structure at 180° shows differences of 2-3 poises between the different bitumens; therefore their performance characteristics differ little. However, their placement characteristics differ sharply.

4. By the continuous emulsion process for bitumen production asphalt can be oxidized 10 times as rapidly as in stills, while with the additional use of the cavitation effect as recommended by us the oxidation of asphalt is accelerated 40-fold and bitumens of better rheological properties are obtained.

LITERATURE CITED

[1] I. V. Provinteev, Stroitel'nye Materialy 11, 22 (1956).

[2] P. P. Budnikov, I. A. Semchenko, and N. V. Mikhailov, Stroitel'nye Materialy 9, 31 (1958).

[3] P. A. Rebinder, Trudy In-ta Fiz. Khimii AN SSSR 5 (1950).

[4] N. V. Mikhailov and P. A. Rebinder, Kolloid. Zhur. 17, 107 (1955).*

[5] N. V. Mikhailov and A. M. Likhtgeim, Kolloid. Zhur. 17, 364 (1955).*

[6] S. Ya. Shalyt and N. V. Mikhailov, Kolloid. Zhur. 18, 609 (1956).*

* Original Russian pagination. See C. B. translation.

TWO-DIMENSIONAL PROBLEM OF THE MOTION OF A VISCOPLASTIC DISPERSE SYSTEM BETWEEN TWO PLANES FORMING AN ACUTE ANGLE

A. Kh. Kim and M. P. Volarovich

The Kalinin Peat Institute

The Belorussian Polytechnic Institute

Translated from: Kolloidnyi Zhurnal Vol. 22, No. 2, pp. 186-194, March-April, 1960

Original article submitted December 14, 1958

Solutions of the problem of motion of a Shvedov-Bingham viscoplastic medium which have been published hitherto mainly refer to cases in which the differential equations are reduced to linear form and are easily integrated [1, 2]. Examples of these are problems of the motion of viscoplastic disperse systems in cylindrical pipes [3]. However, more complex problems, involving integration of nonlinear equations [4, 5] are important for practical purposes. Among these is the case considered in the present paper, concerned with the motion of a viscoplastic disperse system between two planes forming an angle 2α. Tyabin [6] attempted to solve this problem, but his extensive simplifications in the original equation led to results contrary to the boundary conditions of the problem.

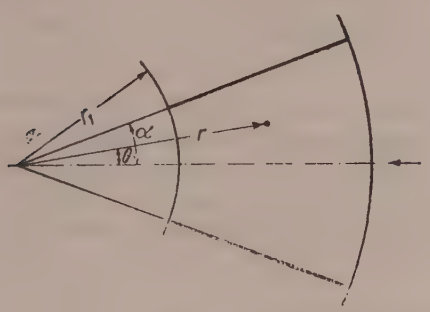


Fig. 1

Differential equations. Simultaneous solution of the equilibrium equation and the equation for the state of the viscoplastic medium gives a single equation in the polar coordinates r and θ [4, 7, 8]:

$$2\frac{\partial^2\lambda}{\partial r\partial\theta}+\frac{2}{r}\frac{d\lambda}{\partial\theta}+\frac{1}{r}\frac{\partial^2\tau}{\partial\theta^2}-r\frac{\partial^2\tau}{\partial r^2}-3\frac{\partial\tau}{\partial r}=$$

$$=\rho_0\left[\frac{\partial}{\partial\theta}\left(\frac{dv_r}{dt}\right)-\frac{\partial}{\partial r}\left(r\frac{dv_\theta}{dt}\right)\right], \qquad (1)$$

where

$$\lambda=2\frac{\partial v_r}{\partial r}\left(\frac{\tau_0}{h}+\eta\right); \qquad (2)$$

$$\tau=\left(\frac{1}{r}\frac{\partial v_r}{\partial\theta}+\frac{\partial v_\theta}{\partial r}-\frac{v_\theta}{r}\right)\left(\frac{\tau_0}{h}+\eta\right), \qquad (3)$$

where h is the intensity of the deformation rates; τ_0 is the yield value; ρ_0 is the density; η is the plastic viscosity. The velocity components v_r and v_θ must also satisfy the deformation continuity equation

$$\frac{\partial}{\partial r}(rv_r) + \frac{\partial v_\theta}{\partial \theta} = 0. \tag{4}$$

We introduce the flow function $\psi(r, \theta)$ satisfying the continuity condition. Expressing the velocity components through the flow function, we have

$$v_r = -\frac{1}{r}\frac{\partial \psi}{\partial \theta}, \quad v_\theta = \frac{\partial \psi}{\partial r}. \tag{5}$$

If we express λ and τ through the flow function and substitute the resultant expressions into Eq. (1), we obtain a nonlinear fourth-power equation in ψ. The boundary conditions for the function ψ are defined on the assumption that the system adheres to the solid walls, namely:

$$\left.\frac{\partial \psi}{\partial \theta}\right|_{\theta=\alpha} = 0, \quad \left.\frac{\partial \psi}{\partial r}\right|_{\theta=\alpha} = 0. \tag{6}$$

Moreover, the flow rate Q through all the radial sections of the diffuser must be constant,

$$\psi\Big|_{\theta=0} - \psi\Big|_{\theta=\alpha} = \pm\frac{Q}{2}, \tag{7}$$

where +Q is the flow rate for a diverging stream, and − Q is the flow rate for a converging stream.

Usually the problem of motion of a viscoplastic disperse system is solved on the basis of the fact that the system contains two regions: in one the particles undergo reversible elastic deformation, and in the other they are subjected to viscoplastic deformation [1]. At any point in the region of viscoplastic deformations, the maximum tangential stress is greater than the yield value τ_0. When the system moves in a cylinder, shearing takes place along planes parallel to the cylinder axis. When the external forces reach a certain value, the first shear layers originate at the solid walls and as the external load increases, the shear gradually extends toward the cylinder axis. Experiments on the transmission of x-rays through a number of disperse systems confirm the existence of a flow core in a system moving through a cylinder [9].

When a viscoplastic system moves through a conical diffuser, shear occurs in planes, the orientation of which relatively to the radius r differs at different points. The conclusions drawn below by consideration of the differential equations and experimental data [10] on flow of viscoplastic peat and lubricant greases in a cone, determined by the x-ray transmission method, show that a system moving in a cone cannot contain a flow core such as is usually observed in flow through a cylinder. In any event, this must be true if the cone angle is not too small and at low yield values τ_0.

Determination of the flow function. We write the flow function in the form

$$\psi = -\sum_1^\infty \frac{\omega_i}{r^{i-1}}. \tag{8}$$

where ω_i is a function of θ only. The velocity components then are

$$v_r = \sum_1^\infty \frac{\omega_i'}{r^i}, \quad v_\theta = \sum_1^\infty \frac{(i-1)\,\omega_i}{r^i}.$$

The flow function was expressed in this form in the solution of the problem of flow of a Newtonian viscous liquid in a circular cone [11].

In conformity to the boundary conditions (6), each function ω_i must satisfy the condition

$$\omega_i'\big|_{\theta=\alpha} = 0 \tag{9}$$

Moreover, for all the functions ω_i except ω_1 the following is true:

$$\omega_i\Big|_{\substack{\theta=\alpha\\ \theta=0}} = 0. \tag{10}$$

With regard to constancy of the flow rate Q, only the function ω_1 need satisfy this condition. The remaining functions ω_i, which are coefficients of l/r^{i-1} and satisfy the condition (10), have no influence on the flow-rate condition.

If $\underline{h}$, λ, and τ and their first and second derivatives are expressed in terms of the flow function and the expression obtained from Eq. (8) is substituted for ψ, we have the usual nonlinear equation in the following form:

$$\sum_{i\ldots\nu}\frac{(2\Phi_1+\Phi_2-\Phi_3)_{i\ldots z}\,(2\Phi_1+\Phi_2-\Phi_3)_{\delta\ldots\nu}}{r^{i+k+\ldots+\nu}} =$$

$$= \rho_0''^2\sum_{i\ldots d}\frac{I_{ik}I_{mn}S_{z\delta}S_{\mu\varepsilon}S_{\lambda\nu}S_{t\varphi}S_{\xi\varphi}S_{l\chi}S_{\rho\gamma}S_{\eta f}S_{qd}}{r^{i+k+\ldots+d+8}} -$$

$$- 2\eta'\rho_0'\sum_{i\ldots\rho}\frac{(2\theta_1+\theta_2-\theta_3)_{i\ldots z}\,I_{\delta\mu}S_{\varepsilon\lambda}S_{\nu t}S_{\varphi\xi}S_{\psi l}S_{\chi\rho}}{r^{i+k+\ldots+\rho+5}} +$$

$$+ \eta'^2\sum_{i\ldots\varphi}\frac{(2\theta_1+\theta_2-\theta_3)_{i\ldots z}\,(2\theta_1+\theta_2-\theta_3)_{\delta\ldots\nu}\,S_{t\varphi}}{r^{i+k+\ldots+\varphi+2}}, \tag{11}$$

где $\Phi_1 = m\left[\frac{3}{2}(n+z)-(i+k+m)+1\right]S_{nz}(S'_{ik}\omega'_m - 2S_{ik}\omega''_m)$,

$$\Phi_2 = \left(C''_iS_{km}+\frac{1}{2}C'_iS'_{km}-\frac{1}{2}C_iS''_{km}\right)S_{nz}-\frac{3}{2}S'_{nz}\left(C'_iS_{km}-\frac{1}{2}C_iS'_{km}\right),$$

$$\Phi_3 = \left[\frac{1}{2}(k+m)-i\right]\left[\frac{3}{2}(n+z)-(i+k+m)+2\right]C_iS_{km}S_{nz},$$

$$\theta_1 = 2m(i+k+m-n-z)\,\omega''_mS_{ik}S_{nz},$$

$$\theta_2 = C''_iS_{km}S_{nz},$$

$$\theta_3 = (i+1)(i+k+z-m-n-1)\,C_iS_{km}S_{nz},$$

$$I_{ik} = \omega'''_i\omega_k(k-1)-(k+1)\,\omega''_k\omega'_i+(i+k)(i-1)(k-i-1)\,\omega'_k\omega_i,$$

$$C_i = \omega''_i-(i^2-1)\,\omega_i,$$

$$S_{ik} = 4ik\omega'_i\omega'_k + C_iC_k,$$

$$\rho_0' = \frac{\rho_0}{\tau_0},\quad \eta' = \frac{\eta}{\tau_0}.$$

The indices i, k, m . . . , which assume the values 1, 2, 3, 4, . . . are in all cases in the following sequence:

$$i, k, m, n, z, \delta, \mu, \varepsilon, \lambda, \nu, t, \varphi, \xi, \psi, l, \chi, \rho, \gamma, \eta, f, q\ ,\ d.$$

Equating to zero the coefficients of l/r^u (u = 10, 11, 12 . . .), we obtain a system of equations from which the functions ω_1, ω_2, etc. are found.

We now consider the question of the flow core. Assume that a flow core exists (Fig. 2). Then it is more convenient to draw the radius vector $\underline{r}$ from the point Q_1 when the straight lines representing the boundary plane O_1A and the boundary of the flow core O_1B intersect.

From the condition of constant flow rate, we have

$$\int_0^{\alpha} v_r r\,d\theta = \text{const}. \tag{12}$$

This condition can be satisfied if the velocity v_r is written in the form

$$v_r = \frac{U(\theta)}{r} + \nu(r, \theta), \tag{13}$$

and

$$\int_0^{\alpha} \nu(r, \theta)\,d\theta = 0.$$

When $\theta = 0$, v_r is the velocity of the flow core and $\left.\frac{\partial v_r}{\partial r}\right|_{\theta=0} = 0$. Therefore, denoting the velocity of the flow core by D, we have

$$\frac{U(0)}{r} + \nu(r, 0) = D. \tag{14}$$

From the condition of adherence of the system to the solid wall, we have

$$\frac{U(\alpha)}{r} + \nu(r, \alpha) = 0. \tag{15}$$

It follows from Eqs. (14) and (15) that the function $\nu(r, \theta)$ must be of the form

$$\nu(r, \theta) = \varphi(\theta) - \frac{U(\theta)}{r}, \tag{16}$$

where

$$\varphi(0) = D, \quad \varphi(\alpha) = 0.$$

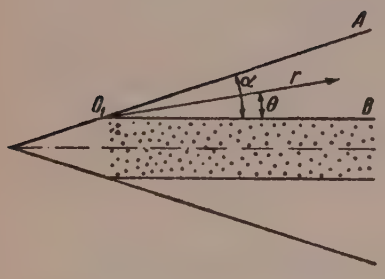


Fig. 2

The right-hand side of Eq. (16) may contain other terms, functions of r and θ, but they must all differ in form from $U(\theta)/r$. Hence, it follows that the conditions (12), (14), and (15) are incompatible. The conditions of adherence of the system to the solid wall and of constant flow rate represent the physical properties of a disperse system, and they must be accepted in the solution of the problem. Therefore, it follows that in this instance there cannot be a flow core.

We now find the basic function ω_1. The differential equation for this function is obtained by equating the coefficient of l/r^{10} to zero, namely:

$$[(4\omega_1'^2 + \omega_1''^2)[4\omega_1''(\omega_1'\omega_1''' - \omega_1''^2) + \omega_1''''[(4\omega_1'^2 + \omega_1''^2) - \omega_1''^2(4\omega_1'' + \omega_1'')] - \\ - 12\omega_1'\omega_1''(4\omega_1' + \omega_1''')(\omega_1'\omega_1''' - \omega_1''^2) = 0. \tag{17}$$

Put $\omega_1''/\omega_1' = p$, and then

$$\omega_1'''/\omega_1' = p' + p^2; \quad \omega_1''''/\omega_1' = p'' + 3pp' + p^3.$$

The differential Eq. (17) is rewritten in the form:

$$(4 + p^2)(4p'' + 16pp') - 12\,pp'(4 + p' + p^2) = 0.$$

If we put

$$4 + p' + p^2 = \Phi, \tag{18}$$

we have

$$(4 + p^2)\Phi' - 3pp'\Phi + 2pp'(4 + p^2) = 0 \quad \text{or}$$
$$(4 + p^2)\frac{d\Phi}{dp} - 3p\Phi + 2p(4 + p^2) = 0.$$

Integrating, we obtain

$$\Phi = C_1(4 + p^2)^{3/2} + 2(4 + p^2).$$

With the aid of Eq. (18) this last equation may be written:

$$\frac{dp}{d\theta} = C_1(4 + p^2)^{3/2} + 4 + p^2. \tag{19}$$

Integration gives the equation

$$\theta = f(p),$$

the right-hand side of which consists of different transcendental functions. This equation cannot be solved for p.

In view of the fact that the function ω_1 must be even, we resolve it into series in powers of $\theta (0 < \theta < 1)$

$$\omega_1 = \sum_{\nu=1} \frac{a_{(2\nu-1)}\theta^{2\nu-1}}{(2\nu - 1)!}.$$

Finding the coefficients of this series from Eq. (19), we have

$$\omega_1 = a_1\left[\theta + \frac{\gamma\theta^3}{6} + \frac{\gamma^2}{480}(8 + 3\gamma)\theta^5 - \frac{\gamma^3}{80640}(512 + 312\gamma + 9\gamma^2)\theta^7 + \ldots\right],$$

where $\gamma = a_3/a_1$.

If we confine ourselves to the first three terms of the resolution series, we have from (9)

$$\frac{32}{\alpha^4} + \frac{16}{\alpha^2}\gamma + \frac{8}{3}\gamma^2 + \gamma^3 = 0.$$

Put

$$p_1 = \frac{1}{3}\left(\frac{16}{\alpha^2} - \frac{64}{27}\right), \quad q_1 = \frac{16}{\alpha^4} - \frac{64}{9\alpha^2} + \frac{512}{729},$$

then

$$\gamma = -\frac{8}{9} + \sqrt[3]{-q_1 + \sqrt{q_1^3 + p_1^3}} + \sqrt[3]{-q_1 - \sqrt{q_1^2 + p_1^3}}.$$

Since $\alpha < 1$, $p_1 > 0$, it follows that γ must always be a real quantity less than zero. We determine α_1 from the condition (7):

$$a_1 = -\frac{Q}{2\alpha\left[1+\frac{\gamma\alpha^2}{6}+\frac{\gamma^2}{480}(8+3\gamma)\alpha^4\right]}$$

The differential equation for determination of ω_2 is found by equating the coefficient of l/r_{12} to zero:

$$U_i + 2U_k + 2U_n = 0,$$

where

$$U_i = \left(C_2''S_{11} + \frac{1}{2}C_2'S_{11}' - \frac{1}{2}C_2S_{11}''\right)S_{11} - \frac{3}{2}S_{11}\left(CS_{211}' - \frac{1}{2}C_2S_{11}'\right) + C_2S_{11}^2,$$

$$U_k = \left(C_i''S_{21} + \frac{1}{2}C_1'S_{21}' - \frac{1}{2}C_1S_{21}'\right)S_{11} - \frac{3}{2}S_{11}'\left(C_1'S_{21} - \frac{1}{2}C_1S_{21}'\right) - \frac{1}{2}C_1S_{21}S_{11},$$

$$U_n = 5S_{21}(S_{11}'\omega_1 - 2S_{11}\omega_1'') + \left(C_1''S_{11} + \frac{1}{2}C_1'S_{11}' - \frac{1}{2}C_1S_{11}''\right)S_{21} -$$
$$- \frac{3}{2}S_{21}'\left(C_1'S_{11} - \frac{1}{2}C_1S_{11}'\right).$$

In these expressions

$$C_2 = \omega_2'' - 3\omega_2;\ C_1 = \omega_1'';\ S_{11} = 4\omega_1'^2 + \omega_1''^2;$$
$$S_{21} + 8\omega_1'\omega_2' + (\omega_2'' - 3\omega_2)\,\omega_1''.$$

The initial values of the function are

$$\omega_2(0) = 0;\ \omega_2'(0) = b_1;\ \omega_2''(0) = (0);\ \omega_2'''(0) = b_3.$$

Finding the coefficients b_1 and b_3 from the boundary conditions

$$\omega_2(\alpha) = 0 \qquad \text{and} \qquad \omega_2'(\alpha) = 0,$$

we see that they are equal to zero. The other coefficients in the series of the function ω_2 are likewise zero.

We now determine the function ω_3. The differential equation is obtained by equating the coefficient of l/r^{14} to zero:

$$4\left[\left(C_1''S_{31} + \frac{1}{2}C_1'S_{31}' - \frac{1}{2}C_1S_{31}''\right)S_{11} - \frac{3}{2}S_{11}'\left(C_1''S_{31} - \frac{1}{2}C_1S_{31}'\right) -\right.$$
$$- S_{11}(S_{31}'\omega_1' - 2S_{31}\omega_1'') + 4S_{31}(S_{11}'\omega_1' - 2S_{11}\omega_1'') +$$
$$\left. + \left(C_1''S_{11} + \frac{1}{2}C_1'S_{11}' - \frac{1}{2}C_1S_{11}''\right)S_{31} - \frac{3}{2}S_{31}'\left(C_1'S_{11} - \frac{1}{2}C_1S_{11}'\right)\right] +$$
$$+ 2\left[\left(C_3''S_{11} + \frac{1}{2}C_3'S_{11}' - \frac{1}{2}C_3S_{11}''\right)S_{11} - 3S_{11}(S_{11}'\omega_3' - 2S_{11}\omega_3'') -\right.$$
$$\left. - \frac{3}{2}S_{11}'\left(C_3'S_{11} - \frac{1}{2}C_3S_{11}'\right)\right] - \eta'(4\omega_1'' + C_1'')\,S_{11}^{5/2} = 0,$$

where

$$C_3 = \omega_3'' - 8\omega_3;\ S_{31} = 12\omega_1'\omega_3' + (\omega_3'' - 8\omega_3)\,\omega_1''.$$

The initial values for the function ω_3 are the same as for the function ω_2, i.e.,

$$\omega_3(0) = 0,\ \omega_3'(0) = d_1,\ \omega_3''(0) = 0,\ \omega_3'''(0) = d_3.$$

Determining this function in the same way as the previous functions, we have

$$\omega_3 = \frac{\eta'\sigma_0\theta^5}{120} + d_1\left[\theta + \frac{\varphi\theta^3}{6} + (\sigma_2\varphi - \sigma_1)\frac{\theta^5}{120} + \ldots\right],$$

where

$$\varphi = \frac{d_3}{d_1};\quad \sigma_0 = a_1^2\left[4\gamma + \frac{\gamma 2}{4}(8 + 3\gamma)\right];$$
$$\sigma_1 = \frac{1}{4}\gamma(57\gamma + 18\gamma^2 + 48);\quad \sigma_2 = 3 + 13\gamma + \frac{9}{4}\gamma^2.$$

The constants d_1 and φ are found from the conditions $\omega_3(\alpha) = 0$ and $\omega_3^*(\alpha) = 0$, hence

$$\varphi = -12/\alpha^2 \qquad \text{and} \qquad d_1 = \frac{\eta'\sigma_0\alpha^4}{120 + 12\sigma_2\alpha^2 + \sigma_1\alpha^4}.$$

The function ω_1 is basic, and determines the flow rate. The remaining functions do not affect the flow rate and only correct the shape of the velocity profile. However, it has been found that the effect of these functions on the shape of the velocity profile is very slight. This is demonstrated by the following example. We find the functions ω_1 and ω_3 for the following data:

$$Q = 150\ \text{m}^2/\text{hr};\quad \alpha = 0{,}15;\quad \eta = 0{,}0002\ \text{kg}\cdot\text{sec}/\text{cm}^2;\quad \tau_0 = 0{,}1\ \text{kg}/\text{cm}^2.$$

Assume that the stream is convergent. Taking only the first three terms in the resolution of the function ω_1 into series, we find γ from the equation

$$1 + \frac{\gamma\alpha^2}{2} + \frac{\gamma^2}{96}(8 + 3\gamma)\alpha^4 = 0.$$

Putting $\alpha = 0.15$ into this equation we have $\gamma = -34.9$. If the first four terms are taken, we have the following equation for γ:

$$1 + \frac{\gamma\alpha^2}{2} + \frac{\gamma^2}{96}(8 + 3\gamma)\alpha^4 - \frac{\gamma^3}{11520}(512 + 312\gamma + 9\gamma^2)\alpha^6 = 0.$$

When $\alpha = 0.15$, this equation is satisfied by $\gamma = -34.85$. The difference between the values of γ in the two cases is less than 0.1%.

We now find the coefficient a_1

$$a_1 = -\frac{Q}{2\alpha\left[1 + \frac{\gamma\alpha^2}{6} + \frac{\gamma^2}{480}(8 + 3\gamma)\alpha^4 + \ldots\right]}.$$

Substitution of the numerical values gives

$$a_1 = -0{,}246\ \text{m}^2/\text{sec}.$$

The physical meaning of this result is that $\frac{a_1}{r}$ is the velocity at the diffuser axis, determined by the first (basic) function.

The general expression for the velocity determined by the first function is of the form

$$v_{r_1} = \frac{a_2}{r}\left[1 + \frac{\gamma\theta^2}{2} + \frac{\gamma^2}{96}(8 + 3\gamma)\theta^4 - \frac{\gamma^3}{11520}(512 + 312\gamma + 9\gamma^2)\theta^6 + \ldots\right].$$

We now find the parameters of the third correcting function

$$\sigma_0 = a_1^2\left[4\gamma + \frac{\gamma^2}{4}(8+3\gamma)\right] = -1780 \text{ m}^4/\text{sec};$$

$$\sigma_1 = \frac{1}{4}\gamma(57\gamma + 18\gamma^2 + 48) = -174000;$$

$$\sigma_2 = 3 + 13\gamma + \frac{9}{4}\gamma^2 = 2294; \quad \varphi = -12/a^3 = -533;$$

$$\eta' = \eta/\tau_0 = 0{,}002 \text{ sec};$$

$$d_1 = \frac{\tau_1'\sigma_0 a^4}{120 + 12\sigma_2 a^2 + \sigma_1 a^4} = -0{,}00000273 \text{ m}^4/\text{sec}.$$

Evidently $\frac{d_1}{r^3}$ is a correction for the radial velocity determined by the function ω_3. In this instance this correction for the velocity determined by the first function is $\frac{0.001}{r^2}\%$. It follows that it may be assumed with reasonable accuracy that the flow is radial.

Determination of pressure. In view of the small influence of the correcting functions on the velocity, we consider only the basic function ω_1 in determination of pressure.

The intensity h is

$$h = \frac{1}{r^2}\sqrt{4\omega_1'^2 + \omega_1''^2}.$$

We also find the functions λ and τ:

$$\lambda = -2\left(\frac{\tau_0\omega_1'}{\sqrt{4\omega_1'^2 + \omega_1''^2}} + \frac{\eta\omega_1'}{r^2}\right); \quad \tau = \frac{\tau_0\omega_1''}{\sqrt{4\omega_1'^2 + \omega_1''^2}} + \frac{\eta\omega_1''}{r^2}.$$

For determination of the pressure it is necessary to consider the equilibrium equations, which have the following form in projection on polar coordinate axes

$$-\frac{\partial p}{\partial r} + \frac{\partial\lambda}{\partial r} + \frac{1}{r}\frac{\partial\tau}{\partial\theta} + \frac{2\lambda}{r} = \rho_0\frac{dv_r}{dt}. \tag{20}$$

$$-\frac{\partial\rho}{r\partial\theta} - \frac{\partial\lambda}{rd\theta} + \frac{\partial\tau}{\partial r} + \frac{2\tau}{r} = \rho_0\frac{dv_\theta}{dt}. \tag{21}$$

Integration of Eq. (20) gives

$$p = \lambda + \int\frac{1}{r}\frac{\partial\tau}{\partial\theta}dr + 2\int\frac{\lambda}{r}dr - \rho_0\int\frac{dv_r}{dt}dr + U(\theta).$$

On completing the integration, we have

$$p = -\frac{2\tau_0\omega_1'}{\sqrt{4\omega_1'^2 + \omega_2''^2}} - \frac{\left(\tau_1\omega_1''' + \rho_0\omega_1'^2\right)}{2r^2} + \\ + \tau_0\left[\frac{\left(\omega_1''' - 4\omega_1'\right)}{\sqrt{4\omega_1'^2 + \omega_1''^2}} - \frac{\omega_1''^2\left(4\omega_1' + \omega_1'''\right)}{\left(4\omega_1'^2 + \omega_1''^2\right)^{\frac{3}{2}}}\right]\ln r + U(\theta). \tag{22}$$

This last equation is differentiated with respect to θ:

$$\frac{\partial p}{\partial \theta} = -2\tau_0 \frac{d}{d\theta}\left(\frac{\omega_1'}{\sqrt{4\omega_1'^2 + \omega_1''^2}}\right) + U'(\theta) + \Gamma(r, \theta). \tag{23}$$

Substituting the values of λ and τ into Eq. (21), we have

$$\frac{\partial p}{\partial \theta} = 2\tau_0 \frac{d}{d\theta}\left(\frac{\omega_1'}{\sqrt{4\omega_1'^2 + \omega_1''^2}}\right) + \frac{2\tau_0\omega_1''}{\sqrt{4\omega_1'^2 + \omega_1''^2}} + W(r, \theta). \tag{24}$$

Equating the right-hand sides of Eqs. (23) and (24), we have

$$U(\theta) = 4\tau_0 \frac{\omega_1'}{\sqrt{4\omega_1'^2 + \omega_1''^2}} + 2\tau_0 \int \frac{\omega_1'' d\theta}{\sqrt{4\omega_1'^2 + \omega_1''^2}} + D.$$

In general the functions $\Gamma(r, \theta)$ and $W(r, \theta)$ are not equal, as the solution is approximate. However, the difference between them is negligible for low absolute values of the correcting functions.

Substituting the value found for $U(\theta)$ into Eq. (22), we find the pressure difference between the diffuser exit and entry:

$$p_0 = \tau_0 \left[\frac{\omega_1''' - 4\omega_1'}{\sqrt{4\omega_1'^2 + \omega_1''^2}} - \frac{\omega_1''^2\left(4\omega_1' + \omega_1'''\right)}{\left(4\omega_1'^2 + \omega_1''^2\right)^{\frac{3}{2}}}\right] \ln\frac{r_2}{r_1} + \frac{\left(\eta\omega_1''' + \rho_0\omega_1'^2\right)}{2}\left(\frac{1}{r_1^2} - \frac{1}{r_2^2}\right),$$

where r_1 and r_2 are the radii of the outlet and inlet sections.

The average pressure at the diffuser entry is

$$p_{0av} = \frac{\tau_0}{\alpha} \ln\frac{r_2}{r_1} \int_0^{\alpha} \left[\frac{\omega_1''' - 4\omega_1'}{\sqrt{4\omega_1'^2 + \omega_1''^2}} - \frac{\omega_1''^2\left(4\omega_1' + \omega_1'''\right)}{\left(4\omega_1'^2 + \omega_1''^2\right)^{\frac{3}{2}}}\right] d\theta +$$

$$+ \frac{1}{2\alpha}\left(\frac{1}{r_1^2} - \frac{1}{r_2^2}\right) \int_0^{\alpha} \left(\eta\omega_1''' + \rho_0\omega_1'^2\right) d\theta. \tag{25}$$

It is important to note that the first term in the right-hand side of Eq. (25) is independent of the flow rate, while the second term becomes zero when $Q = 0$. It follows that the first term represents the initial pressure necessary to overcome the yield value. As in motion through a circular pipe, the $Q = f(p_{0av})$ curve does not pass through the coordinate origin.

SUMMARY

The Hencky-Ilyushin system of differential equations for viscoplastic flow, corresponding to a Shvedov-Bingham rheological body, has been considered in relation to the motion of a substance between two planes forming an acute angle. The problem was solved in r and θ polar coordinates. A differential equation in which the unknown functions were the velocity components v_r and v_θ was derived for the flow function $\psi(r, \theta)$. The boundary conditions for adherence of the medium to the solid walls were derived for the case when the shear extends throughout the medium and there is no solid flow core. With only the first two or three terms taken after resolution into series, an equation connecting the pressure and flow rate was derived.

LITERATURE CITED

[1] M. P. Volarovich, Kolloid. Zhur. 16, 3, 228 (1954).*

[2] M. Reiner, Ten Lectures on Theoretical Rheology [Russian translation] (State Tech. Press, 1947).

[3] M. P. Volarovich and A. M. Gutkin, Zhur. Tekh. Fiz. 8, 3, 321 (1946); A. Kh. Mirzadzhanade, Doklady Akad. Nauk SSSR 95, 5 (1954); Doklady Akad. Nauk Azer. SSR 13, 2, 139 (1957); N. V. Tyabin, Zhur. Tekh. Fiz. 25, 2, 339 (1955); A. Kh. Kim, Trudy Belorus. Politekhn. In-ta 56 (1958).

[4] A. M. Gutkin, Proc. 2nd All-Union Conference on Friction and Wear [In Russian] (Izd. AN SSSR, 1947), 1, 31.

[5] L. I. Kotova and B. V. Deryagin, Zhur. Tekh. Fiz. 27, 6, 1261 (1957); L. I. Kotova, Zhur. Tekh. Fiz. 27, 7, 1540 (1957).

[6] N. V. Tyabin, Doklady Akad. Nauk SSSR 84, 5, 943 (1952).

[7] M. P. Volarovich and A. M. Gutkin, Kolloid. Zhur. 15, 2, 155 (1953).*

[8] A. A. Ilyushin, Uchen. Zap. Mosk. Gos. Un-ta, Mekhanika 39 (1940).

[9] M. P. Volarovich, Kolloid. Zhur. 9, 5, 325 (1947).

[10] N. V. Lazovskaya, Kolloid. Zhur. 11, 2, 77 (1949).

[11] N. A. Slezkin, Matemat. Sbornik 42, 1, 43 (1935).

*Original Russian pagination. See C. B. translation.

INFLUENCE OF ADDED SURFACE-ACTIVE SUBSTANCES ON DEVELOPMENT OF A CRYSTALLIZATION HARDENING STRUCTURE IN CALCIUM OXIDES OF DIFFERENT DEGREES OF DISPERSION

S. I. Kontorovich, E. E. Segalova, and P. A. Rebinder

Department of Colloid Chemistry, Chemical Faculty, Moscow University

Division of Disperse Systems, Institute of Physical Chemistry,

Academy of Sciences USSR

Translated from: Kolloidnyi Zhurnal Vol. 22, No. 2, pp. 195-200, March-April, 1960

Original article submitted August 19, 1959

The use of added surface-active substances of the calcium lignosulfonate type (sulfite waste liquor, SSB) or glucose in the production of materials and components from quicklime [1] is based on their ability to retard hydration of calcium oxide, so that quicklime can be ground in the wet state for use as a cementing material, and placed and packed down without partial breakdown of the crystallization structure and decrease of ultimate strength.

It has been considered hitherto that the main cause of retarded hydration of cementing materials is formation of adsorption layers on the surface of the original substance, retarding the diffusion of water to the grain surface owing to the considerable resistance to diffusion in the intermediate layers [2]. However, our studies of the mechanism of the retarding action of SSB on the hydration of calcium oxide [3] showed that formation of adsorption layers on the surface of the original CaO is not the decisive and even not the only cause of the retarding effect of the additive.

Binding of the additive from the liquid medium of the suspension in the course of hydration of calcium oxide occurs mainly by adsorption of SSB on the nuclei of the newly formed compounds. Formation of an adsorption layer of the additive on the surfaces of the $Ca(OH)_2$ nuclei sharply suppresses their growth, and stabilizes their dimensions in the colloidal range. Formation of stabilized nuclei continues until almost all the additive has been adsorbed from the liquid medium of the suspension. It is only after this that nuclei capable of growth and concretion, i.e., formation of a crystallization structure, appear. However, even after all the additive has been adsorbed from the liquid medium of the suspension, hydration of the still unhydrated CaO proceeds at a rate considerably less than the normal, because by this time the suspension contains a large amount of colloidal $Ca(OH)_2$ particles stabilized by the additive; these, in accordance with Thomson's law, maintain a high degree of supersaturation with respect to $Ca(OH)_2$, so that the rate of CaO dissolution is reduced.

Figure 1 represents changes of temperature in mixing of mixtures containing 25% CaO ($S = 3.0\ m^2/g$) and 75% $CaCO_3$ (inert filler) with solutions containing SSB at different concentrations (0, 0.05, and 0.75 g per 100 ml of solution) and with colloidal solutions prepared as follows: 50 ml of 0.75% SSB solution was shaken for 10 minutes with 1.5 g CaO and the liquid phase of the resultant suspension was separated from the precipitate by two methods: by filtration through a filter with pores 2μ in diameter (solution A), or by decantation after the fairly large particles had settled (solution B). Solutions A and B had the same electrical conductivity $\kappa = 18 \cdot 10^{-3}$ $ohm^{-1} \cdot cm^{-1}$, corresponding to a solution supersaturated with respect to $Ca(OH)_2$ (for a saturated solution of $Ca(OH)_2$, $\kappa = 7.8 \cdot 10^{-3}$) but not saturated with respect to CaO (for a metastably saturated solution

of CaO $\kappa = 22 \cdot 10^{-3}$). The total SSB content, determined as described previously [3], of solutions A and B was 0.05 and 0.75 g per 100 ml of solution respectively.

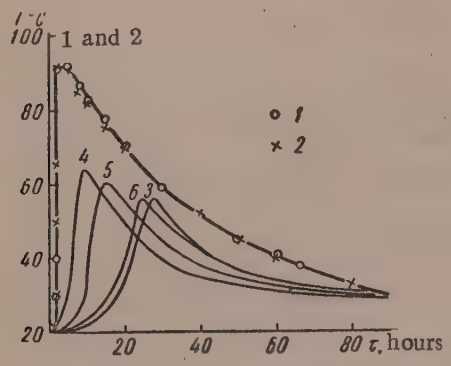


Fig. 1. Temperature changes in mixing of a mixture consisting of 25% CaO ($S = 3.0$ m^2/g) + 75% $CaCO_3$ with different solutions; W/S = 0.40: 1) Without SSB; 2) 0.05% SSB; 3) 0.75% SSB; 4) solution A; 5) same, after 24 hours; 6) solution B.

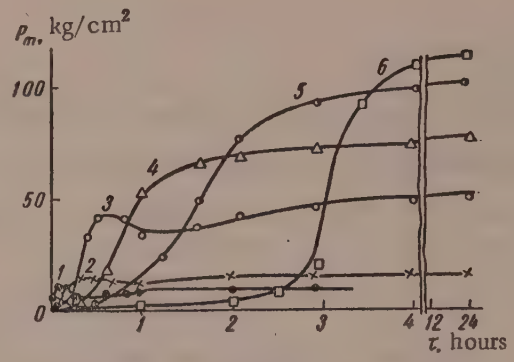


Fig. 2. Kinetics of crystallization structure formation in suspensions of calcium oxide ($S = 3.0$ m^2/g) in presence of added SSB: composition of suspension: 25% CaO + + 75% $CaCO_3$, W/S = 0.40; 1) Without SSB; 2) 0.14% SSB; 3) 0.4% SSB; 4) 0.72% SSB; 5) 1.44% SSB; 6) 7.2% SSB.

It follows from Fig. 1 (Curves 1 and 2) that addition of a solution containing 0.05 g SSB per 100 ml to the mixture does not have any appreciable retarding effect on hydration of CaO. However, if solution A of the same total SSB concentration, but with high supersaturation with respect to $Ca(OH)_2$ is used, the hydration rate is lower (Curve 4). Since the influence of added SSB can be disregarded in this case, the retardation of hydration can be attributed only to the influence of the high degree of supersaturation on the rate of dissolution of CaO.

When solution B, of the same electrical conductivity as solution A but with a considerably higher content of colloidal particles (the total content of $Ca(OH)_2$ determined by analysis in solution B is more than five times the $Ca(OH)_2$ content in solution A) is added to the mixture, the rate of hydration is reduced much more sharply than on addition of solution A, and reaches almost the same level as with the use of 0.75% SSB solution for the mixing (Curves 3, 6).

Thus, the higher the concentration of colloidal particles at a given initial degree of supersaturation, the longer the time during which a high degree of supersaturation is maintained, retarding the dissolution of calcium oxide and therefore the hydration process as a whole.

If solution B is kept for 24 hours, supersaturation in it decreases during that period as the result of recrystallization processes, and its conductivity becomes $14 \cdot 10^{-3}$, although the total contents of $Ca(OH)_2$ and SSB remain the same. The fact that hydration is retarded less effectively by a solution which has been aged in this manner (Curve 5) emphasizes the influence of the absolute degree of supersaturation on the rate of hydration of calcium oxide.

Therefore the main cause of the retarding action of SSB on hydration of CaO is decrease of the dissolution rate of calcium oxide under the influence of supersaturation maintained by colloidal $Ca(OH)_2$ particles, the growth of which is inhibited by the surface-active additive.

It was shown in earlier studies [4] of supersaturation kinetics in dilute suspensions of calcium oxide that the behavior of glucose is similar to that of SSB; it follows that retarded hydration in presence of added glucose is due to the same causes.

The present authors studied the effect of the dispersity of the original calcium oxide on the final strength of the crystallization structure; it was found that in the case of CaO [5], as for calcium sulfate hemihydrate [6] and tricalcium aluminate [7], a structure of maximum strength is formed only at a certain optimum degree of dispersion of the original cementing material.

The influence of dispersity on the strength of the structure formed is associated with variations of the over-all rate of dissolution of the cementing material. If the over-all rate of dissolution of calcium oxide is high (at high dispersity), most of the $Ca(OH)_2$ crystallizes out under conditions of high supersaturation corresponding to the metastable solubility of CaO. Under these conditions very small $Ca(OH)_2$ crystals are formed, and are bound together in a weak framework by means of crystallization contacts. The very fine crystals themselves are apparently the weak points in such a framework.

When the dispersity of the calcium oxide is low, and the rate of dissolution is therefore low also, the conditions are more favorable for formation of the crystallization structure framework, since because of the lower over-all rate of dissolution of CaO, formation of the crystals constituting the framework is accompanied by their growth. However, in this case too, much of the substance is used up in growth on the framework already formed, and this leads to formation of high tensile stresses which cause partial breakdown of the hardening structure.

It follows that only when calcium oxide of the optimum dispersity, and therefore with the optimum rate of dissolution, is hydrated is the ratio between the amounts of substance used to form the crystallization structure framework and to grow further crystals upon it, such that a structure of the maximum strength is formed.

It was of interest to study the effects of added SSB and glucose, which retard the dissolution of calcium oxide, on the conditions for formation of a crystallization hardening structure from CaO samples differing in specific surface and therefore in the over-all dissolution rate.

These investigations were carried out with concentrated suspensions containing 25% CaO and 75% $CaCO_3$; the latter was used as an inert filler so that the water-lime ratio could be increased without segregation of the suspension, and the heat evolution from the samples could thereby be reduced without artificial cooling. The kinetics of structure formation was characterized by variations of plastic strength measured by means of the cone plastometer [8].

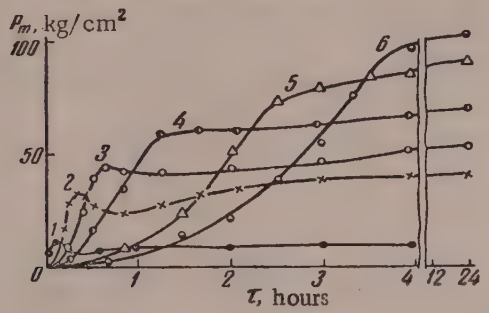


Fig. 3. Kinetics of crystallization structure formation in suspensions of calcium oxide (S = 3.0 m^2/g) in presence of glucose: composition of suspension: 25% CaO + + 75% $CaCO_3$; W/S = 0.40; 1) Without glucose; 2) 0.4%; 3) 0.8%; 4) 1.6%; 5) 4.0%; 6) 8% glucose solution.

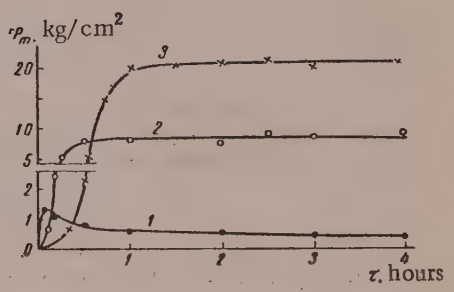


Fig. 4. Kinetics of crystallization structure formation in suspensions of calcium oxide (S = 3.0 m^2/g) in presence of glucose: composition of suspension: 25% CaO + 75% $CaCO_3$; W/S = 0.60; 1) Without glucose; 2) 0.4%; 3) 4.0% glucose solution.

For preparation of calcium oxides of different dispersities, CaO of "pure" grade (S = 3.0 m^2/g) was calcined in a Kryptol furnace at 1800° and then ground in a laboratory vibratory mill down to S = 0.14 and 0.51 m^2/g.

It is known [9] that such calcination causes recrystallization of calcium oxide, leading to a sharp increase in the size of the original crystals, and unaccompanied by changes in the crystal lattice [10].

Figures 2 and 3 represent the kinetics of structure formation in highly disperse calcium oxide (S = 3.0 m^2/g) in presence of various amounts of added SSB and glucose. It is clear from Figs. 2 and 3 that even small amounts of SSB and glucose greatly increase the strength of the structure. If the suspensions are mixed in solutions containing more than 2 g of additive per 100 ml, the strength of the structure continues to increase, but much less sharply. It follows that retardation of the dissolution of calcium oxide is favorable over the entire range of concentrations studied (from 0.14 to 8 g per 100 ml of solution).

It should be noted that the strength decrease due to partial breakdown of the structure by the action of tensile stresses diminishes with increase of the amount of additive. Moreover, even small amounts of added SSB and glucose prevent the strength decrease caused by dissolution of contacts which are not in thermodynamic equilibrium [6], which is most prominent at high water-solid (W/S) ratios.

Figure 4 represents the kinetics of structure formation in concentrated CaO suspensions at W/S = 0.6 in presence of various amounts of glucose. Whereas in absence of added glucose, the strength of the structure falls (by nearly 60% in 4 hours), there is no strength decrease at all in a structure containing small amounts of added glucose. The absence of a strength decrease in this case is explained by formation of numerous $Ca(OH)_2$ nuclei stabilized by the additive; these, because of their high dispersity, maintain supersaturations which prevent the dissolution of contacts not in thermodynamic equilibrium for a long time (for example, after 1.5 years the supersaturation in a dilute suspension of calcium oxide containing 0.4 g SSB per 100 ml of solution was 12%).

Figure 5 represents the kinetics of structure formation in concentrated suspensions of calcium oxide with specific surfaces of 0.51 and 0.14 m^2/g, in presence of different amounts of glucose. When glucose is added to a mixture containing CaO of S = 0.51 m^2/g, only small amounts of added glucose produce some increase in the strength of the structure. If solutions containing more than 0.4 g glucose per 100 ml are used for the mixing, there is a sharp decrease of strength, accompanied by a volume increase. The increase of strength on addition of small amounts of glucose to a suspension of CaO (S = 0.51 m^2/g) indicates that the rate of dissolution of this calcium oxide is somewhat higher than the optimum. Further retardation of dissolution, caused by additions of large amounts of glucose (1.6 g/100 ml), proves to be unfavorable. For the same reason introduction of additives which retard the dissolution rate into suspensions of coarse calcium oxide (S = 0.14 m^2/g), the dissolution rate of which is below the optimum, cannot increase the strength of the structure (Fig. 5, b). It should be noted that additions of SSB act similarly.

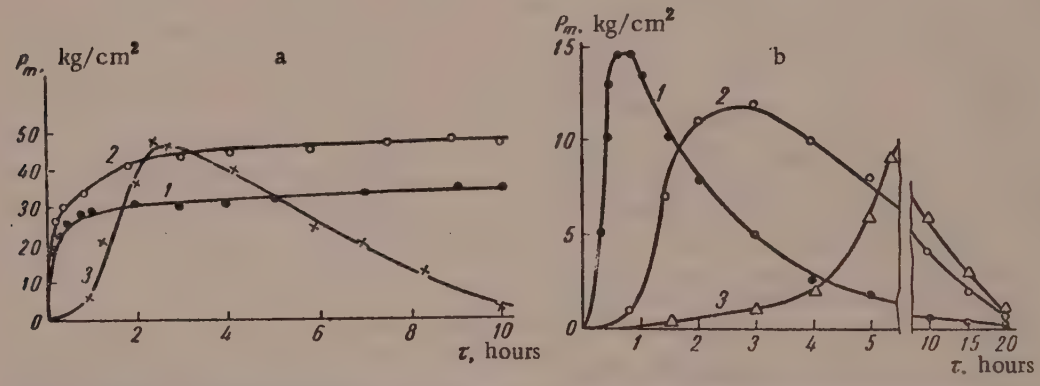


Fig. 5. Effects of added glucose on the kinetics of crystallization structure formation in suspensions of calcium oxide with S = 0.51 m^2/g (a) and S = 0.14 m^2/g (b): composition of suspensions: 25% CaO + 75% $CaCO_3$; W/S = 0.40; 1) Without glucose; 2) 0.4%; 3) 1.6% glucose solution.

It follows that SSB and glucose, introduced with the mixing water into calcium oxide suspensions, increase the strength of the hardening structure only if the rate of dissolution of calcium oxide is above the optimum.

SUMMARY

1. The main cause of the retarding effect of sulfite waste liquor (SSB) on hydration of CaO is decrease of the dissolution rate of calcium oxide under the influence of high supersaturation, maintained (in accordance with Thomson's law) by colloidal $Ca(OH)_2$ particles, the growth of which is inhibited by the surface-active additive.

2. When sulfite waste liquor (SSB) and glucose are added with the mixing water to calcium oxide suspensions they raise the strength of the hardening structure only if the dissolution rate of CaO is above the optimum. Thus,

additions of SSB or glucose in amounts from 0.14 to 8 g per 100 ml of solution to calcium oxide with S = 3.0 m^2/g produce a sharp increase in the final strength of the structure, and the decrease in the structural strength due to dissolution of contacts not in thermodynamic equilibrium is prevented.

Addition of SSB or glucose to calcium oxide which dissolves at a rate below the optimum (S = 0.14 and 0.51 m^2/g) leads to development of large internal tensile stresses which cause partial and in some cases complete breakdown of the crystallization hardening structure.

LITERATURE CITED

[1] G. I. Logginov, P. A. Rebinder, and V. P. Sukhova, Doklady Akad. Nauk SSSR 99, 4, 569 (1954).

[2] Yu. M. Butt and T. M. Berkovich, Cement Materials with Surface-Active Additives [In Russian] (Industrial Construction Press, Moscow, 1953); S. V. Shestoperov, T. Yu. Lyubimova, and F. M. Ivanov, Doklady Akad. Nauk SSSR 70, 6, 1045 (1956).

[3] S. I. Kontorovich, E. E. Segalova, and P. A. Rebinder, Doklady Akad. Nauk SSSR 129, 847 (1959).*

[4] E. E. Segalova, S. I. Kontorovich, and P. A. Rebinder, Doklady Akad. Nauk SSSR 123, 3, 509 (1958).*

[5] E. E. Segalova, S. I. Kontorovich, and P. A. Rebinder, Kolloid. Zhur. 22, 74 (1960).*

[6] E. E. Segalova and V. N. Izmailova, Kolloid. Zhur. 20, 5, 601 (1958).*

[7] E. S. Solov'eva, Dissertation [In Russian] (Moscow, 1959).

[8] P. A. Rebinder and N. A. Semenenko, Doklady Akad. Nauk SSSR 64, 835 (1949); E. E. Segalova, P. A. Rebinder, and O. I. Luk'yanova, Vestnik Mosk. Un-ta 17 (1954).

[9] J. Wuhrer, Zement-Kalk-Gips 6, 354, (1953); V. I. Asbe, Rock Prod. 57, 2 (1954); H. R. Stalley, and S. H. Greenfeld, Industr. and Engng. Chem. 41, 520 (1949).

[10] N. P. Tabunshchikov, Trudy Vses. In-ta Sodovoi Promyshlennosti 6 (1952); Kei Iche Akijame, cited in C. A. 2670[3] (1940).

* Original Russian pagination. See C. B. translation.

THE WEISSENBERG EFFECT

N. I. Malinin

Hydrodynamics Institute of the Siberian Division of the Academy of Sciences,

USSR, Novosibirsk

Translated from: Kolloidnyi Zhurnal Vol. 22, No. 2, pp. 201-210, March-April, 1960

Original article submitted November 25, 1958

Weissenberg [1, 2] and Garner and Nissan [3] discovered the phenomenon later named the Weissenberg effect. The nature of this effect is that in the flow of polymer solutions, normal stresses arise in perpendicular directions in addition to tangential stresses in the shear plane.

Figure 1, which is taken from Weissenberg's paper, illustrates the behavior of Newtonian liquids and Weissenberg liquids, which are polymer solutions, in a rotational apparatus. The rotor of the apparatus is the external cylinder; the stator may be of various designs or absent altogether. It follows from Fig. 1, a that in absence of a stator, the surface of a Newtonian or non-Newtonian liquid in a rotating cylinder assumes the form of a paraboloid of rotation in accordance with the laws of classical hydromechanics. The surface of a Newtonian liquid in presence of a stator tends to assume the same shape. The influence of the stator is generally slight. The situation with a Weissenberg liquid is quite different. Against the laws of classical hydromechanics, an anomalous liquid of this type rises up the walls of the internal cylinder overcoming gravitational and centrifugal forces (Fig. 1, b, c). If the internal cylinder contains a cavity, an anomalous liquid fills it partially or completely, dependent on the rotation rate. Figure 1, f represents a rotational apparatus with a stator in the form of a disk with piezometers. If the viscosimeter is filled with an anomalous liquid, the piezometers record higher pressures nearer the axis of rotation. If the disk stator can move in a vertical direction, then the anomalous liquid is capable of raising the disk together with a load placed on it to a certain height when the outer cylinder rotates.

The Weissenberg effect can be most conveniently studied experimentally with the aid of the Weissenberg-Roberts disk and cone rotational viscosimeter [4, 5], shown schematically in Fig. 2, a. This instrument contains a rotating cone, while the disk, made of transparent material, is stationary and has a number of orifices along its diameter; piezometers are inserted in the orifices. When the cone rotates, the liquid in the piezometers rises by virtue of the Weissenberg effect. The Weissenberg effect can be estimated quantitatively from the piezometer readings. When the angle between the disk and cone surfaces is small, the deformation field in the gap is almost homogeneous [6]. A rotational viscosimeter in which the liquid is contained between two disks is also very convenient for measurement of the Weissenberg effect. If the lower disk rotates, piezometers can be attached to the upper (stationary) disk for quantitative estimation of the pressure distribution due to the Weissenberg effect, as shown in Fig. 2, b.

Several experimental papers dealing with quantitative investigations of the Weissenberg effect have now been published. Roberts [6], Pollett [7], and Markovitz and Williamson [8] studied the Weissenberg effect by means of disk and cone viscosimeters, Padden and Dewitt [10] used a two-disk rotational instrument, and Ward and Lord [11] used a coaxial-cylinder rotational viscosimeter.

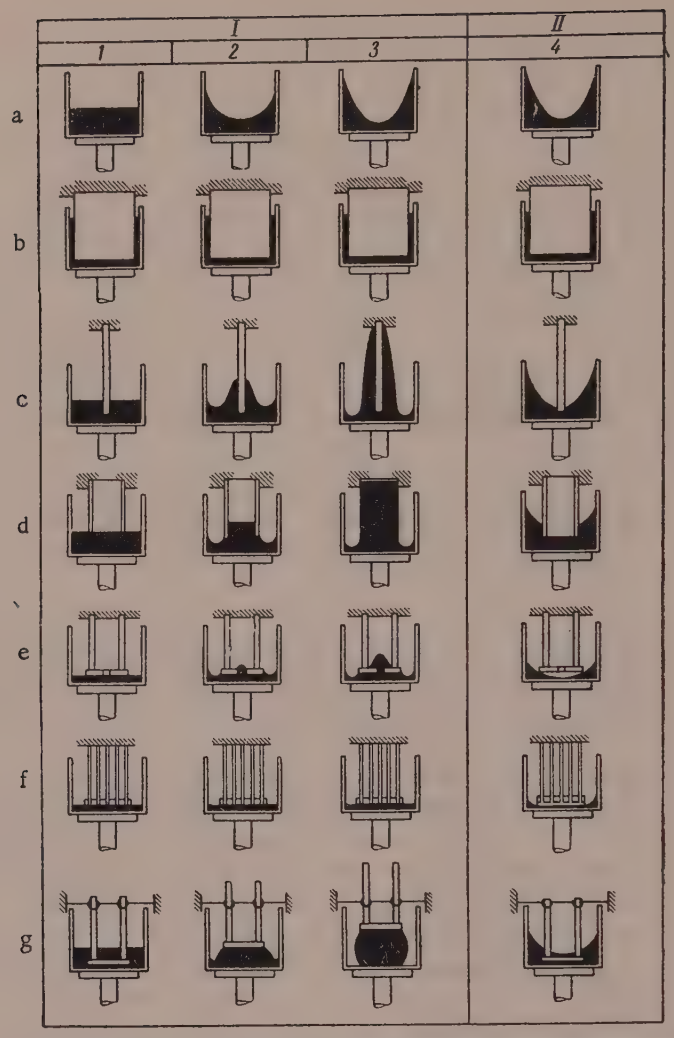


Fig. 1. Form of liquid surfaces in rotational instruments with different stator designs and rotation speeds: I) Weissenberg liquids with finite reversible deformation; II) Newtonian liquids with very small reversible deformation; shear rates: 1) Zero; 2) moderate; 3) high; 4) any; stator: a) Absent; b) cylinder; c) rod; d) open tube; e) tube with orifice, closed from below; f) disk with piezometers; g) disk.

Some workers have attempted to interpret the Weissenberg effect theoretically. Weissenberg [1] showed that liquids conforming to the equation

$$\frac{P_1 - P_2}{\lambda_1^2 - \lambda_2^2} = \frac{P_2 - P_3}{\lambda_2^2 - \lambda_3^2} = \frac{P_3 - P_1}{\lambda_3^2 - \lambda_1^2} = G, \qquad (1)$$

exhibit the effect named after him. Here P_i are the principal stresses, λ_i are the principal degrees of reversible* extension, and G is modulus of shear of the system. For pure shear Eq. (1) becomes:

* Here we are concerned not with thermodynamically reversible processes but reversible deformations which disappear instantaneously or in the course of time after removal of the load, as discussed by P. A. Rebinder [12].

$$\begin{vmatrix} P_1 - P_2 & \tau_{12} & 0 \\ \tau_{21} & 0 & 0 \\ 0 & 0 & 0 \end{vmatrix} = G \begin{vmatrix} \gamma_e^2 & \gamma_e & 0 \\ \gamma_e & 0 & 0 \\ 0 & 0 & 0 \end{vmatrix} \tag{2}$$

(γ_e represents the reversible components of shear, τ_{12} and τ_{21} are the corresponding components of the stress tensor). It follows from Eq. (2) that in pure shear normal stresses P_1 and P_2 should arise at the side faces of an element of the material subjected to shear.

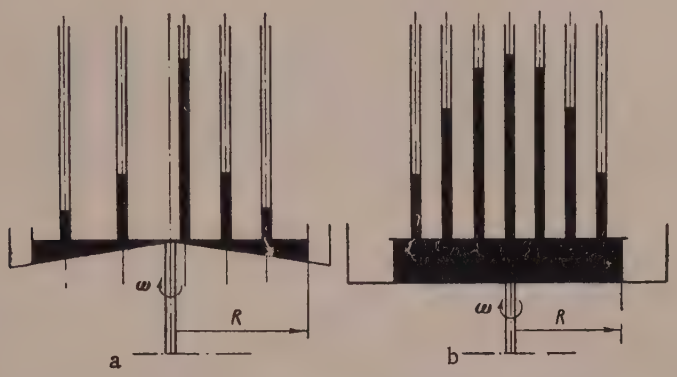


Fig. 2. Line diagrams of apparatus for quantitative measurement of the Weissenberg effect: a) Disk and cone rotational apparatus; b) two-disk rotational apparatus.

Equation (1) was also derived for rubberlike materials by Treloar, who based the derivation on the molecular network theory developed by Kuhn [13]. However, for space polymers the values of λ_i in Eq. (1) represent total degrees of extension, since in this instance we are concerned with almost completely reversible deformations of materials of the type of vulcanized rubbers.

To explain the Weissenberg effect, Reiner [14] advanced the hypothesis of the so-called cross viscosity η_c. Reiner writes the flow equation as follows:

$$P_{ij} = P\delta_{ij} + 2\eta\dot{\gamma}_{ij} + 4\eta_c \sum_{\alpha=1}^{\alpha=3} \dot{\gamma}_{i\alpha}\dot{\gamma}_{\alpha j}, \tag{3}$$

where P_{ij} is the stress tensor component, P is the average stress, δ_{ij} is Kronecker's delta, and $\dot{\gamma}_{ij}$, $\dot{\gamma}_{i\alpha}$, $\dot{\gamma}_{\alpha j}$ are the corresponding components of the deformation rate tensor. For pure shear in the 1-2 plane at velocity $\dot{\gamma}$, when $P_{33} = 0$, Eq. (3) is written in the form:

$$\begin{cases} P_{11} = P_{22} = \eta_c\dot{\gamma}^2 \\ \tau_{12} = \tau_{21} = \eta\dot{\gamma} \\ P = 2/3\,\eta_c\dot{\gamma}^2 \\ P_{33} = \tau_{23} = \tau_{31} = 0. \end{cases} \tag{4}$$

However, the attempts made by Roberts to confirm the existence of cross viscosity experimentally were unsuccessful [6].

Dewitt [15, 10] introduced special transverse terms, dependent on the circulation rate of the liquid, into the Maxwell equation in order to explain the Weissenberg effect.

Rivlin [16] developed a theory of a viscoelastic body which conforms to the following equation in flow:

$$P = \alpha_0 I + \alpha_1 A_1 + \alpha_2 A_2 + \alpha_3 A_1^2 + \alpha_4 A_2^2 + \alpha_5 (A_1 A_2 + A_2 A_1) + \\ + \alpha_6 (A_1^2 A_2 + A_2 A_1^2) + \alpha_7 (A_1 A_2^2 + A_2^2 A_1) + \alpha_8 (A_1^2 A_2^2 + A_2^2 A_1^2), \quad (5)$$

where **P** is the stress tensor $A_r = |A_{ij}^{(r)}|$ $(r = 1, 2)$ is a symmetrical tensor of rank two;

$$A_{ij}^{(1)} = \frac{\partial v_i}{\partial x_j} + \frac{\partial v_j}{\partial x_i},$$

$$A_{ij}^{(r+1)} = \frac{\partial A_{ij}^{(r)}}{\partial t} + v_e \frac{\partial A_{ij}^{(r)}}{\partial x_e} + A_{mj}^{(r)} \frac{\partial v_m}{\partial x_j} + A_{mj}^{(r)} \frac{\partial v_m}{\partial x_i},$$

I is a single tensor of rank two; v_i is the velocity of the body at the point under consideration in the direction of the x_i axis; α_0, α_1, etc. are the polynomials in the deformation velocity tensor invariants. The Weissenberg effect is a consequence of Eq. (5) since, according to the latter, each component of the stress tensor depends on any component of the deformation velocity tensor. However, it is still too early to speak of any practical applications of Eq. (5), as it is not clear how the functions $\alpha_0, \alpha_1, \ldots, \alpha_8$ can be determined experimentally.

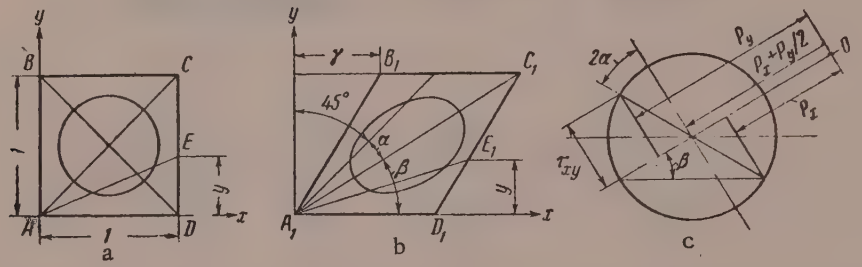


Fig. 3. Diagrams representing deformations and stresses in an elastic elementary body: a) An element of the body before shear; b) an element of the body after shear; c) Mohr's stress circle for the element.

It has been considered until now that only polymer solutions exhibit the Weissenberg effect. In this paper an attempt is made to prove theoretically the existence of the Weissenberg effect in all quasiliquid and quasisolid disperse systems having a certain elasticity of form.

Suppose that an elastic element ABCD before deformation has the shape of a cube with sides of unit length (Fig. 3, a). Consider a sphere within this element; this sphere is represented on the plane of the drawing by a circle. The diagonals AC and BD lie at angles of 45° to the cube faces. Let the element ABCD undergo a certain shear deformation γ (Fig. 3, b). It follows from Fig. 3, b that the diagonals AC and BD then deviate from their initial directions.

After deformation the principal elongation and therefore the principal normal stress P_1 are directed along the diagonal A_1C_1. This proposition is proved as follows.

We determine the relative elongation ϵ_y of the segment AE cutting the side CD at a certain distance from the base AD. Since we are dealing with a homogeneous deformation field, any straight line drawn in the body after deformation was straight before deformation. Therefore, simple geometrical considerations show that

$$\varepsilon_y = \frac{A_1 E_1}{AE} = \sqrt{\frac{(1 + \gamma y)^2 + \gamma^2}{1 + y^2}}.$$

To find how ϵ_y varies with height, we determine the derivative

$$\frac{d(\varepsilon_y)^2}{dy} = \frac{2[\gamma + \gamma y(\gamma - y)]}{(1 + y^2)^2}.$$

Since y can vary only between 0 and 1 and $\gamma > 0$, it follows that

$$\frac{d(\varepsilon_y)^2}{dy} > 0$$

and

$$\frac{d\varepsilon_y}{dy} > 0.$$

Therefore, the elongation increases with y. It follows that the principal elongation axis passing through the point A can cut the face C_1D_1 only at the point C_1. The point at which the principal elongation axis passing through the point A_1 cuts the face B_1C_1 can be investigated similarly. It is easy to show that if γ is not too large, the principal elongation axis can cut the face B_1C_1 only at the point C_1.

However, the diagonal A_1C_1 deviates from its initial direction by the angle α. It is easy to see that $\alpha = \arctan \frac{\gamma}{2}$. At low values of γ, $\alpha \approx \frac{\gamma}{2}$. The tangential stresses acting on the faces A_1D_1 and B_1C_1 can be found from the equation:

$$\tau_{xy} = \tau_{yx} = G\gamma. \tag{6}$$

Since the shear deformations $\gamma_{yz} = \gamma_{zx} = 0$ (by definition), the Mohr circle can be used for determination of the normal stresses P_x and P_y (Fig. 3, c).

From Fig. 3, c, we have:

$$P_y = \frac{P_x + P_y}{2} + \tau_{xy} \cdot 2\alpha = \frac{P_x + P_y}{2} + \tau_{xy}\gamma = \frac{P_x + P_y}{2} + G\gamma^2, \tag{7}$$

$$P_x = \frac{P_x + P_y}{2} - G\gamma^2. \tag{8}$$

Thus, it follows from Eqs. (7) and (8) that to bring about a finite shear deformation under the condition that the height of the specimen remains constant, a compressive stress must act in the direction of the y axis, and a tensile stress in the direction of the x axis. On the other hand, if these stresses are absent, extension should take place in the direction of the y axis, compression in the direction of the axis, with isotropic expansion. The first phenomenon was observed by Poynting and is known as the Poynting effect. The second was predicted by Kelvin, and is therefore known as the Kelvin effect [14].

It is quite obvious that Eqs. (7) and (8) are applicable to any elastic deformation whether it is accompanied by plastic deformations or not. However, if a body exhibits plastic in addition to elastic deformations, such as a Maxwell body, elastic deformations γ_e must be substituted into Eqs. (7) and (8) for calculation of the Weissenberg effect. For disperse systems and other complex bodies which exhibit elastic aftereffects [17-19] in addition to instantaneous elasticity and fluidity, the equilibrium modulus [18] G_p should be introduced instead of G into Eqs. (7) and (8).

In that case Eqs. (7) and (8) are written in the form:

$$P_y = \frac{P_x + P_y}{2} + G_p\gamma_e^2, \tag{9}$$

$$P_x = \frac{P_x + P_y}{2} - G_p\gamma_e^2. \tag{10}$$

For a Maxwell body $\tau_{xy} = \eta\dot{\gamma}_r$ (η is the viscosity and γ_r is the irreversible shear deformation), $\dot{\gamma}_e = \frac{\eta\dot{\gamma}_r}{G}$ and Eqs. (9) and (10) become:

$$P_y = \frac{P_x + P_y}{2} + \eta T \dot{\gamma}_r^2, \tag{11}$$

$$P_x = \frac{P_x + P_y}{2} - \eta T \dot{\gamma}_r^2, \tag{12}$$

where T is the relaxation time.

Equations (11) and (12) were derived by Weissenberg [5] in somewhat different mathematical form.

For a body represented by the Burgers model [18, 19] consisting of four elements

$$P_y = \frac{P_x + P_y}{2} + \eta^2 \left(\frac{1}{G_1} + \frac{1}{G_2}\right) \dot{\gamma}_r^2, \tag{13}$$

$$P_x = \frac{P_x + P_y}{2} - \eta^2 \left(\frac{1}{G_1} + \frac{1}{G_2}\right) \dot{\gamma}_r^2, \tag{14}$$

where G_1 and G_2 are the nominal instantaneous and elastic moduli, respectively, and η is the relaxation viscosity.

It follows from Eqs. (11) - (14) that the normal pressure generated by the Weissenberg effect is directly proportional to the square of the shear rate. Figure 4 shows the relationship between the pressure in the Weissenberg effect and the shear rate γ_r, determined by Markovitz and Williamson [8] for solutions of polyisobutylene in decalin. The data which are plotted in logarithmic coordinates in Fig. 4 were determined at different temperatures and concentrations, and are reduced to a single temperature and single concentration by means of the equations given by Padden and Dewitt. It follows from Fig. 4 that at lower shear rates the slope of the log P_b − log γ_r curves is approximately two, in agreement with Eqs. (11) - (14), but it diminishes with increasing rate of shear. This decrease is probably due to breakdown of structure in the systems, such as has been repeatedly observed in colloidal solutions of this type by Rebinder [18], Trapezenikov [20], Vinogradov and co-workers [21], and others, at high rates of shear.

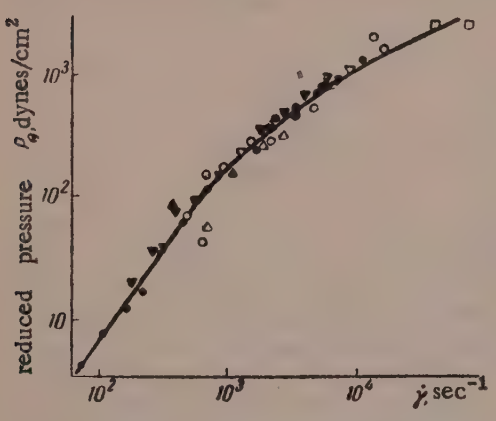


Fig. 4. Relation of normal pressure and shear rate for solutions of polyisobutylene in decalin, by the method of Morkovitz and Williamson [8].

It should be noted that the Weissenberg effect is very convenient for quantitative measurements of the influence of shear rate on the structural rheological characteristics of disperse systems. The pressure P_b which is due to the Weissenberg effect can be measured directly either with the aid of piezometers or from the magnitude of the force acting on the stator of the rotational instrument. From Eqs. (11) and (12), it follows that

$$P_b = \eta T \dot{\gamma}_r^2. \tag{15}$$

Since η can be found from measurements of the torque acting on the system and γ_r can be determined from the angular velocity of the rotor, Eq. (15) can be used for calculating the relaxation time T and the elasticity modulus G.

We now consider the behavior of a viscoelastic system subjected to shearing deformation in a disk and cone rotational viscosimeter of the type illustrated in Fig. 2, a, with small angles δ between the disk and cone surfaces. For this case, under steady conditions

$$\dot{\gamma}_r \approx \frac{\omega r}{r\delta} = \frac{\omega}{\delta}. \tag{16}$$

We use spherical coordinates r, φ, and θ. The tangential stresses are

$$\tau_{\varphi\theta} = \tau_{\theta\varphi} = \eta\dot{\gamma}_r = \eta\frac{\omega}{\delta}, \tag{17}$$

where $\tau_{r\varphi} = \tau_{\varphi r} = 0$, in consequence of the axial symmetry and $\tau_{r\theta} = \tau_{\theta r} = 0$ owing to absence of shear in these planes. Therefore, Eqs. (11) - (14) are applicable in the present instance, but the subscripts x and y are replaced by φ and θ, respectively.

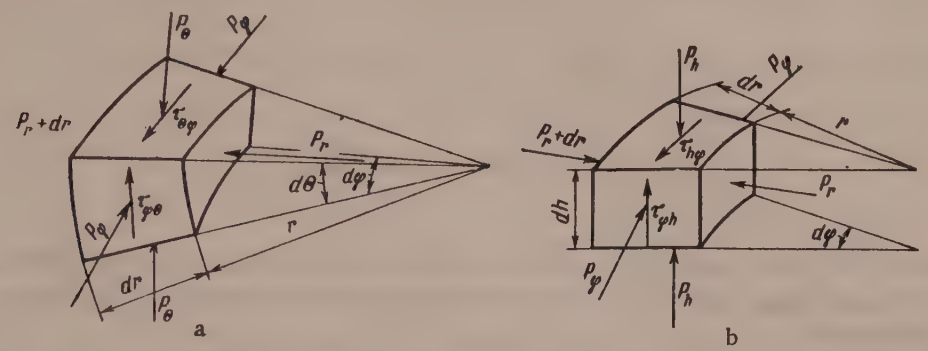


Fig. 5. Deformations and stresses in a viscoelastic elementary body: a) Element of a viscoelastic liquid in a disk and cone rotational apparatus; b) element of a viscoelastic liquid in a two-disk rotational apparatus.

Comparing the equilibrium equation for an element limited by the surfaces r = const, r + dr = const, φ = = const, $\varphi + d\varphi$ = const, θ = const, $\theta + d\theta$ = const (see Fig. 5, a) in calculation of the projections of the forces acting in different directions, we have

$$\frac{dP_r}{dr} + \frac{(2P_r - P_\varphi - P_\theta)}{r} = 0, \tag{18}$$

where P_r, P_φ and P_θ are the pressures in the directions of the r, φ, and θ axes. Owing to the spherical symmetry, the values of P_r, P_φ, and P_θ depend on r only. To solve Eq. (18) we use the results obtained by Roberts [6] and Pilpel [22], who showed experimentally that $P_r = P_\theta$. From Eqs. (11) and (12), we have

$$P_\theta - P_\varphi = 2\eta T\dot{\gamma}_r^2 = K,$$

where $K = 2\eta T\dot{\gamma}_r^2 = 2\eta T\frac{\omega^2}{\delta^2}$. For a medium which conforms to the Burgers model $K = 2\eta^2\left(\frac{1}{G_1} + \frac{1}{G_2}\right)\dot{\gamma}_r^2$.

Hence

$$dP_r + K\frac{dr}{r} = 0.$$

Integration of this equation gives

$$P_r = -K\ln r + C.$$

For determination of the integration constant C the condition is valid that the excess pressure on the free surface of the specimen, where r = R, is zero, and hence

$$P_r = P_\theta = K\ln\frac{R}{r} = 2\eta T\frac{\omega^2}{\delta^2}\ln\frac{R}{r};\ P_\varphi = K\left(\ln\frac{R}{r} - 1\right). \tag{19}$$

The diagonal components of the spherical tensor P (negative) are found from the equation:

$$P = \frac{P_r + P_\varphi + P_\theta}{3} = P_r - K/3.$$

The diagonal components of the stress deviator (which are also negative) are:

$$P_r = K/3; \quad P_\theta = K/3; \quad P_\varphi = -2K/3. \tag{20}$$

Equations (19) and (20) were derived in somewhat different form by Roberts [6] and verified experimentally by Roberts [6] and Markovitz [8, 9].

The total axial force Q acting on the disk and cone in presence of the Weissenberg effect is:

$$Q = K \int_0^R 2\pi r \ln \frac{R}{r} \cdot dr = \frac{\pi K R^2}{2}. \tag{21}$$

We consider by a similar method the behavior of a viscoelastic system in a layer between two rotating disks. The cylindrical coordinates r, h, and φ are used for solution of this problem. The shear rate γ_r can be found from the equation:

$$\dot{\gamma}_r = \frac{\omega}{H} r,$$

where H is the distance between the disks.

Consider an element of the body contained between the surfaces (r = const, r + dr = const, h = const, h + dh = const; φ = const, $\varphi + d\varphi$ = const) (see Fig. 5, b). The stresses are $\tau_{h\varphi} = \tau_{\varphi h} = \eta\dot{\gamma}_r = \dot{\eta}\frac{\omega}{H} r$, and $\tau_{r\varphi} = \tau_{\varphi r} = \tau_{hr} = \tau_{rh} = 0$, as before. From Eqs. (11) - (14) for a Maxwell body

$$P_h - P_\varphi = 2\eta T \dot{\gamma}_r^2 = 2\eta T \frac{\omega^2}{H^2} r^2 = K_1 r^2,$$

where $K_1 = 2\eta T \frac{\omega^2}{H^2}$. For a body conforming to the Burgers model $K_1 = 2\eta^2 \left(\frac{1}{G_1} + \frac{1}{G_2}\right) \frac{\omega^2}{H^2}$.

The equilibrium equation for the element in question is

$$\frac{dP_r}{dr} + \frac{P_r - P_\varphi}{r} = 0. \tag{22}$$

The motion of the layer adjacent to the rotating disk is very similar to the motion of the medium in a disk and cone viscosimeter at $\delta \to 0$. It is therefore to be expected that in a two-disk rotational apparatus $P_r = P_h$. Equation (22) then becomes:

$$\frac{dP_r}{dr} + K_1 r = 0; \quad P_r = -K_1 \frac{r^2}{2} + C.$$

The integration constant C is found from the condition at the specimen surface where $P_r = 0$. The system is retained in the gap between the disks, as in the disk and cone apparatus, by virtue of the Weissenberg effect (if, of course, the rotation speed of the rotor is high enough). Finally

$$P_r = P_h = \frac{K_1}{2}(R^2 - r^2), \tag{23}$$

$$P_\varphi = \frac{K_1}{2}(R^2 - 3r^2). \tag{24}$$

The diagonal components of the spherical stress tensor are:

$$P = \frac{P_r + P_h + P_\varphi}{3} = P_r - \frac{K_1 r^2}{3}. \tag{25}$$

The diagonal components of the stress deviator (negative) are:

$$P_r = P_h = \frac{K_1 r^2}{3}; \quad P_\varphi = -\frac{2}{3} K_1 r^2. \tag{26}$$

The axial pressure Q is found from the equation:

$$Q = \int_0^R 2\pi \frac{K_1}{2}(R^2 - r^2)\, r dr = \frac{\pi K_1 R^4}{4}. \tag{27}$$

Equations (23) - (27) may be used in calculations relating to circular pivots when it is necessary to determine the axial force transmitted to the lubricant; it is very desirable that they should be verified experimentally.

In conclusion, it should be noted that the Weissenberg effect should be of great importance in technology, especially in the case of bearings and pivots operating at high shaft speeds, because it eases lubrication of the frictional parts of the machinery. Unfortunately, apart from the investigations cited above, the effect has been studied very little.

SUMMARY

1. The Weissenberg effect should be found not only in solutions of high polymers, but in any disperse systems having some elasticity of form.

2. Equations have been derived for calculation of pressures which cause the Weissenberg effect, for the Maxwell and Burgers models which represent the behavior of viscoelastic bodies. In the case of a Maxwell body, these equations coincide with those derived in Weissenberg's theory.

3. The normal stresses arising in the Weissenberg effect between two disks one of which rotates and the other is stationary have been calculated for the case when the radial pressure equals the axial.

4. The axial forces in the Weissenberg effect have been calculated for relative rotation of two disks and a disk and a cone.

The author thanks Professor M. P. Volarovich for suggesting the problem and for his attention and interest.

LITERATURE CITED

[1] K. Weissenberg, Nature 159, 4035, 310 (1947).

[2] K. Weissenberg, Proc. of the 1st International Congress on Rheology (Scheveningen, 1948), pp. 1-29.

[3] F. H. Garner and A. H. Nissan, Nature 158, 4018, 634 (1946).

[4] S. M. Freeman and K. Weissenberg, Proc. of the 1st International Congress on Rheology (Scheveningen, 1948) pp. 11-12.

[5] A. Jobling and J. E. Roberts, in the book: Rheology, Theory and Applications 2 (New York, 1958), p. 503.

[6] J. E. Roberts, Proc. of the 2nd International Congress on Rheology (Oxford, 1954) p. 91.

[7] W. F. O. Pollett, Proc. of the 2nd International Congress on Rheology (Oxford, 1954) p. 85.

[8] H. Markovitz and R. B. Williamson, Trans. Soc. Rheology 1, 25 (1957).

[9] H. Markovitz, Trans. Soc. Rheology 1, 37 (1957).

[10] F. J. Padden and T. W. Dewitt, J. Appl. Phys. 25, 9, 1086 (1954).

[11] A. F. H. Ward and P. Lord, Proc. of the 2nd International Congress on Rheology (Oxford, 1954) p. 214.

[12] P. A. Rebinder, in the book: New Methods for Physicochemical Investigation of Surface Phenomena 1 [In Russian] (Inst. Phys. Chem. Acad. Sci. USSR, 1950) p. 5.

[13] L. Treloar, Physics of Rubber Elasticity [Russian translation] (IL, Moscow, 1953).

[14] T. M. Reiner, in the book: Rheology, Theory and Applications 1 (New York, 1956) p. 1.

[15] T. W. Dewitt, J. Appl. Phys. 26, 7, 889 (1955).

[16] R. S. Rivlin, J. Rational. Mech. and Analysis 5, 1, 179 (1956).

[17] M. P. Volarovich and R. A. Branopol'skaya, Investigation of the Physical and Mechanical Properties of Wheat Dough [In Russian] (Moscow-Leningrad, Food Industry Press, 1940).

[18] N. V. Mikhailov and P. A. Rebinder, Kolloid. Zhur. 17, 2, 107 (1955).*

[19] J. M. Burgers, First Report on Viscosity and Plasticity (Amsterdam, 1939).

[20] A. A. Trapeznikov and V. A. Fedotova, Proc. Third All-Union Conference on Colloid Chemistry [In Russian] (Izd. AN SSSR, 1956), p. 65.

[21] V. V. Sinitsyn, A. A. Konstantinov, and G. V. Vinogradov, Proc. Third All-Union Conference on Colloid Chemistry [In Russian] (Izd. AN SSSR, 1956) p. 113; V. P. Pavlov and G. V. Vinogradov, Doklady Akad. Nauk SSSR 122, 4, 464 (1958).*

[22] N. Pilpel, Trans. Faraday Soc. 50, 12, 1369 (1954).

* Original Russian pagination. See C. B. translation.

EFFECT OF THE DISPERSITY OF THE ORIGINAL PLASTER ON STRUCTURE FORMATION IN HARDENING OF CALCIUM SULFATE HEMIHYDRATE

Z. N. Markina, E. E. Segalova, and Ezhi Stoklosa

M. V. Lomonosov Moscow State University, Department of Colloid Chemistry

Translated from: Kolloidnyi Zhurnal Vol. 22, No. 2, pp. 211-216, March-April, 1960

Original article submitted September 8, 1959

The basic task in physicochemical investigations in the field of hardening of mineral cements is determination of the optimum conditions for formation of structures with the maximum strength.

In relation to this task, elucidation of the conditions of crystallization structure formation on the ultimate strength of the hardening structures is of determining significance. For example, determination of the influence of dispersity of cementing materials (including calcium sulfate hemihydrate) on structure formation during hydration hardening is of great practical value [1].

It is known [2] that increase of the dispersity of hemihydrate increases the strength of the structure of the dihydrate plaster formed. However, the problem of changes in the strength of the structure on further very great increase of dispersity has so far remained somewhat obscure. It was shown in [3] that there is a certain optimum of the hemihydrate dispersity beyond which the strength of the structure begins to decrease. In the case of β-gypsum this optimum approximately corresponds to a specific surface $S_1 \approx 12{,}000$ cm^2/g of the hemihydrate. As yet this fact is not generally accepted, let alone elucidated.

The present work was concerned with a more detailed study of this problem in relation to the α- and β-forms of calcium sulfate hemihydrate. First, for final confirmation of the existence of a dispersity optimum in relation to strength, we carried out numerous experiments on the kinetics of plastic-strength increase [4] in suspensions of hemihydrate of different degrees of dispersion. Nearly all the experiments were performed with a mixture consisting of 30% of calcium sulfate hemihydrate and 70% of washed and finely ground quartz sand. The apparent specific surface (S_1) of the hemihydrate used (ground either in jet or in vibratory mills) was determined by means of the Tovarov apparatus, and varied from 2000 to 17,000 cm^2/g.

It was found, in full agreement with earlier results [3] that structure formation is sharply accelerated with increased dispersity of the original hemihydrate (Figs. 1 and 2); the induction period is shortened and the maximum strength is reached much sooner because of an increase in the dissolution rate of the hemihydrate owing to increase of its surface area.

The fall of strength which replaces its rapid increase is attributable to dissolution, in moist storage conditions, of crystallization contacts of the structure which are not in thermodynamic equilibrium. The plot of the structural strength against the dispersity of the original hemihydrate passes through a maximum (Figs. 1, 2, and 3).

It is clear from Fig. 2 that in the case of the α-form of calcium sulfate hemihydrate, the strength decrease begins when the dispersity of the original hemihydrate is 9500 cm^2/g, but this decrease is small. In the case of the β-hemihydrate (Figs. 1 and 3), the strength maximum is found at $S_1 \approx 11{,}000$ cm^2/g.

The cause of the fall of structural strength with increase in the dispersity of the original plaster is undoubtedly associated with the influence of the dispersity of hemihydrate on the supersaturation kinetics in the liquid phase of the hardening suspension.

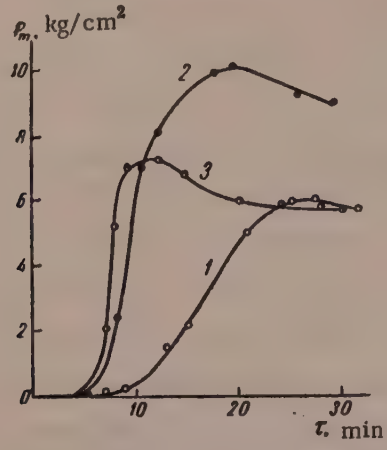


Fig. 1. Kinetics of structure formation in suspensions of calcium sulfate hemihydrate (β-form) of different degrees of dispersion. Composition of mixture: 30% of β-hemihydrate + 70% of ground quartz sand; W/S = 0.83. Apparent specific surface of the original hemihydrate: 1) 3400 cm^2/g; 2) 10,700 cm^2/g; 3) 16,500 cm^2/g.

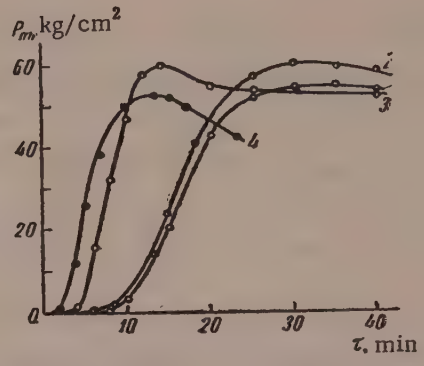


Fig. 2. Kinetics of structure formation in suspensions of calcium sulfate hemihydrate (α-form) of different degrees of dispersion. Composition of mixture: 30% of α-hemihydrate + 70% of ground quartz sand; W/S = 0.5. Apparent specific surface of the original hemihydrate: 1) 2940 cm^2/g; 2) 3400 cm^2/g; 3) 7700 cm^2/g; 4) 9500 cm^2/g.

As was shown earlier [3], development of a crystallization structure proceeds in two stages; the first stage is formation of a spatial framework of the crystallization structure, and the second is overgrowth of the resultant framework — increase in the size of its component crystals.

The existence of these two stages can be revealed by destruction of the partially hardened system after different time intervals. It is then found that rebuilding of the crystallization structure ceases considerably before the end of the hydration process [3]. This indicates that almost all the concretion contacts between the crystals are formed at the start of structure formation; subsequently the strength increase proceeds by overgrowth of the framework already formed. The ratio of the durations of the first and second stages of structure formation should alter with changes in the dispersity of the original material, as the over-all rate of dissolution of hemihydrate increases with increasing dispersity and high degrees of supersaturation are maintained relatively longer in the suspension; this should favor lengthening of the first stage of structure formation, at which crystallization contacts can arise.

In fact, determinations of supersaturation kinetics in dilute suspensions of calcium sulfate hemihydrate showed that the relative time during which high supersaturations are maintained in the suspension increases with increasing dispersity of the hemihydrate (Fig. 2). Supersaturation kinetics were studied by measurements of the electrical conductivity of the suspensions [3]. The ratio of the time during which the highest supersaturation is maintained in the liquid phase of the suspension to the total time of hydration is 0.47 for coarse and 0.56 for finely divided hemihydrate (Fig. 4).

In a concentrated hardening suspension of hemihydrate, the duration of the first stage of structure formation can be easily determined by repeated stirrings of the suspension at different intervals after the original mixing, and determination of the instant at which the suspension loses its power of repeated hardening. At this stage, despite the continuing hydration, formation of new crystallization contacts ceases in the suspension; this indicates the end of the first stage of structure formation.

Experiments on repeated destruction of the hardening suspension were conducted as follows. The suspension was put in several measurement vessels. A standard specimen hardened under the usual conditions, while the others were repeatedly stirred at a definite time after preparation to total breakdown of the crystallization structure which formed in them, and were then allowed to harden under the usual conditions (moist storage).

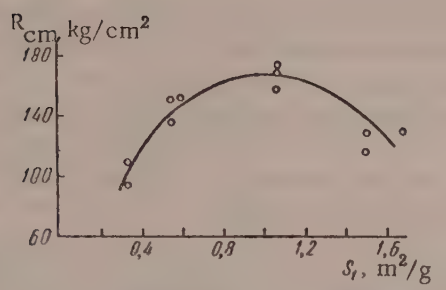


Fig. 3. Variations of the compressive strength of dry specimens of hardened plaster with the original specific surface (S_1) of the β-form of calcium sulfate hemihydrate, W/S = 0.7.

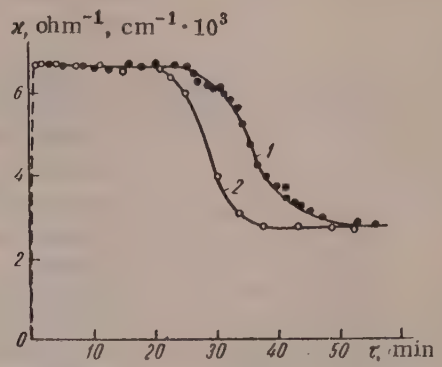


Fig. 4. Time variations of the conductivity (κ) of suspensions of the β-form of calcium sulfate hemihydrate at different degrees of dispersion; t = 20°. Specific surface of the original hemihydrate: 1) 3400 cm²/g; 2) 12,000 cm²/g.

The course of the plastic-strength increase was also investigated in the case of the repeatedly stirred suspensions. In Fig. 5, the ultimate strength of the structure (P_{max}) in these suspensions is plotted against the times at which they were repeatedly stirred, for hemihydrate of three different degrees of dispersion. The first point on the plot of P_{max} against time refers to the original suspension, stirred only once at the instant of preparation. The time corresponding to this point indicates the duration of stirring of the suspension during the mixing. These suspensions were stirred for a fairly long time when being prepared; this was necessary at the given W/S ratio to prevent segregation (W/S is the water-solid ratio).

It follows from Fig. 5 that the strength of the structure in a stirred suspension falls sharply with increase of the time of the repeated stirring, and complete loss of power of further structure formation occurs during a very short time interval.

Figure 1 shows that as the original dispersity of the hemihydrate increases, the maximum structural strength is attained after 26, 19, and 12 minutes, while from Fig. 5 it follows that the ability to form crystallization contacts is lost in the same suspensions after 11, 10, and 7 minutes. Hence, it follows that the relative duration of the first stage in the formation of a crystallization structure varies in the following manner as the dispersity of the original hemihydrate changes in the sequence of 3400, 10,700 and 16,500 cm²/g: 0.42, 0.52, and 0.58. This shows once again that the duration of the first stage of structure formation, when the formation of crystallization contacts is still possible, increases continuously with increasing dispersity of the original hemihydrate. However, strength determinations showed that great extension of the first stage of structure formation is unfavorable and leads to reduced strength of the plaster stone; this is especially pronounced in the case of the β-hemihydrate.

It was of interest to determine whether the strength decrease found at high degrees of dispersion of the original plaster is associated with the appearance of internal stresses in the specimen. The linear expansion of the structure, observed in the course of hardening, was measured for this purpose. The magnitude of the expansion is to some degree a measure of the stresses which arise in the system in the course of structure formation, because in general, growing crystals, in consequence of their directed growth, cause powerful stresses if their growth is hindered by mechanical obstacles [5]. The rigid crystallization framework, which is formed at the very beginning and prevents free distribution of the crystals, can itself be such an obstacle.

Linear expansion in the hardening of plaster was measured by means of the IZV-1 vertical optical gauge with 0.1 μ scale divisions. The design of this mass-produced instrument is described in [6]. The advantages of this instrument consist of the considerable accuracy of measurement, the possibility of measuring shrinkage as well as expansion, and the fact that, owing to preliminary balancing of the rod, the load on the plaster paste required to ensure constant contact between the rod and the specimen was only 0.09 g/cm^2. The readings were made by means of a microscope of × 60 magnification with a spiral micrometer eyepiece.

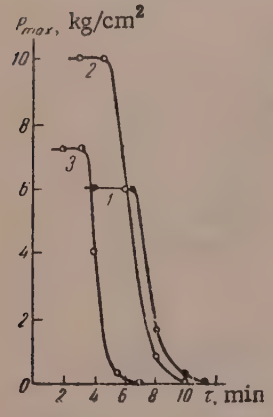


Fig. 5. Variations of the ultimate strength of the structure in suspensions of the β-form of calcium sulfate hemihydrate of different degrees of dispersion with the time of repeated stirring (τ). Composition of mixture: 30% of β-hemihydrate + + 70% of ground quartz sand; W/S = 0.83. Nominal specific surface of the hemihydrate: 1) 3400 cm^2/g; 2) 10,700 cm^2/g; 3) 16,500 cm^2/g.

The specimens under test were isolated from the atmosphere by means of a special plastic seal, so that during the hardening they were exposed only to the vapor of saturated calcium sulfate solution. The experimental procedure consisted of determination of the kinetics of linear expansion of plaster paste contained in a mold in the shape of a separable cylinder 100 mm long and 50 mm inside diameter. After the paste had been mixed and put into the cylinder, it was cut level with the edges of the mold and a waxed cover of light tin plate was placed on its exposed surface.

The start of elongation of the specimens coincides with the start of a rapid increase of the structural strength of the suspension. During the induction period, when there is as yet no continuous crystallization framework, there is even a decrease in the dimensions of the system owing to contraction. In order that the selection of the initial reading points should not be random, the minimum point corresponding to the end of contraction was taken as the initial length of the specimen. The relative linear expansion of the hemihydrate was expressed in percentages. The experimental results are presented in the table.

Analysis of the table shows that the fall of strength with increase in the dispersity of the original hemihydrate cannot be attributed to formation of large stresses in the hardening structure, as the expansion of hemihydrate diminishes with increase in its dispersity. This means that the linear expansion of hemihydrate is greater in cases in which the second stage of structure formation is longer. This is understandable, because at the first stage, when high supersaturations are still maintained in the suspension, new crystallization nuclei may arise in the pores of the hardening structure. At the second stage, new crystallization centers cannot be formed, and only growth of already-existing crystals takes place, and this produces tensile stresses, as the growing crystals are bound together into a rigid framework and are incapable of free displacement. This is also confirmed by the fact that at a given water-solids ratio (see table), expansion is greater in suspensions of the α- than of the β-form of calcium sulfate hemihydrate. The solubility of the α-form is lower than that of the β-form of calcium sulfate hemihydrate [7], and therefore in suspensions of the α-form, the conditions are more favorable for crystal growth and less favorable for formation of new crystallization centers than in suspensions of the β-form.

Relative Linear Expansion $\frac{\Delta L}{L_0}$ 100% of Hemihydrate Specimens Reached at the End of Hydration

Composition of Original Suspension: 30% Calcium Sulfate Hemihydrate + 70% Sand; W/S = 0.5

S_1, cm^2/g	α-$CaSO_4 \cdot 0{,}5H_2O$	β-$CaSO_4 \cdot 0{,}5H_2O$	S_1, cm^2/g	α-$CaSO_4 \cdot 0{,}5H_2O$	β-$CaSO_4 \cdot 0{,}5H_2O$
2940	0,40	—	9600	0,28	—
3400	0,38	0,25	10700	—	0,08
7700	0,31	—	16500	—	0,07

The strength decrease which accompanies a great decrease in the dispersity of the original hemihydrate is probably associated with excessive subdivision of the dihydrate crystals which constitute the hardening structure. This is favored by prolonged maintenance of high supersaturations in the suspension and by shortening of the second stage of structure formation, so that not enough material is left for overgrowth of the crystallites constituting the initial finely divided framework of the crystallization structure, so that its strength cannot increase substantially.

SUMMARY

1. The influence of dispersity of the α- and β-forms of calcium sulfate hemihydrate on crystallization structure formation during hydration. The apparent specific surface of the original hemihydrate was varied from 0.2 to 1.7 m^2/g.

2. There is an optimum dispersity of the hemihydrate which corresponds to the maximum strength of the forming crystallization structure.

3. The linear expansion of plaster stone during hardening was measured. The decrease in the strength of the hardening structure with increasing dispersity of the original plaster is not associated with internal stresses which develop in the course of hardening, but is apparently caused by excessive subdivision of the dihydrate crystals which constitute the hardening structure.

LITERATURE CITED

[1] Papers and Communications at the Conference on Modern Problems of Concrete Technology in the Production of Prefabricated Reinforced Concrete [In Russian] (Industrial Construction Press, Moscow, 1956).

[2] P. P. Budnikov, Gypsum, Its Investigation and Applications [In Russian] (Construction Press, 1943).

[3] V. N. Izmailova, E. E. Segalova, and P. A. Rebinder, Doklady Akad. Nauk SSSR 107, 3, 425 (1956);* E. E. Segalova, V. N. Izmailova, and P. A. Rebinder, Doklady Akad. Nauk SSSR 110, 5, 808 (1956); 114, 3, 594 (1957).*

[4] B. Ya. Yampol'skii and P. A. Rebinder, Kolloid. Zhur. 10, 6, 466 (1948).

[5] H. Buckley, Crystal Growth [Russian translation] (IL, Moscow, 1954).

[6] Yu. M. Butt, Practical Manual of Cement Technology [In Russian] (1953).

[7] K. Kelley, J. C. Southard, and C. T. Anderson, Thermodynamic Properties of Gypsum [Russian translation by S. S. Pechuro] (BT and Ministry of the Structural Materials Industry, 1949); T. I. Rozenberg and V. B. Ratinov, Collection: Trans. All-Union Scientific Research Institute of Reinforced Concrete [In Russian] (Industrial Construction Press, 1957) 1, 36.

* Original Russian pagination. See C. B. translation.

INVESTIGATION OF ADHESION EFFECTS IN BONDING OF RUBBER TO METAL BY "LEUKONAT" ADHESIVE

3. REACTION OF SODIUM BUTADIENE RUBBER WITH TRIPHENYLMETHANE TRIISOCYANATE

A. M. Medvedeva, B. V. Deryagin, and S. K. Zherebkov

Institute of Physical Chemistry, Academy of Sciences, USSR

Translated from: Kolloidnyi Zhurnal Vol. 22, No. 2, pp. 217-222, March-April, 1960

Original article submitted September 30, 1959

It was shown in earlier investigations [1, 2] that the strength of rubber-to-metal bonding by "Leukonat" adhesive (20% solution of triphenylmethane triisocyanate in dichloroethane) is determined by the ratio of the interaction intensities between the adhesive film and the contacting surfaces of the adhesive-rubber and the adhesive-metal interfaces. If these intensities are approximately equal, the bond strength is high, whereas if they differ sharply, the bond strength is low. Experiments showed that the interaction between the adhesive Leukonat film and the metal is influenced by the nature of the metal surface. The interaction between the adhesive film and rubber is influenced by the type of rubber in the vulcanizate, the nature of the filler, and the amount of filler used. One of the factors influencing the interaction between rubber and the adhesive film is variation of the thickness of the latter [2]. All these investigations show that it is possible to control the strength of rubber-metal bonding by Leukonat adhesive.

It was shown earlier that unfilled vulcanizates based on polar and nonpolar rubbers can be bonded to metal by means of Leukonat adhesive. The high bond strength at the polar rubber-adhesive film interface is due to the fact that oriented adsorption of polar groups takes place at this interface; the occurrence of a potential difference at the boundary between the two phases causes a redistribution of electrons between them which is equivalent to formation of an electric double layer with its layers in the two phases. The bond strength between the rubber and the adhesive film increases with increase in the content of polar groups in the rubber. It is evident that the role of oriented adsorption must be negligible in bonding between a nonpolar rubber and the adhesive film. The view was put forward that in this case adhesion at the rubber-adhesive film boundary is caused by forces of chemical interaction between the rubber and triphenylmethane triisocyanate.

To test this hypothesis, it was desired to study the interaction between rubber and isocyanate in solution and the vulcanizing effect of isocyanate on rubber. Since triphenylmethane triisocyanate is polyfunctional in character, it can interact simultaneously with several rubber molecules, and this should lead to the formation of a structural network similar to the network formed in vulcanization.

Interaction between rubber and isocyanate in solutions. Preliminary experiments showed that when triphenylmethane triisocyanate solution is added to rubber solutions, the viscosity of the rubber solutions increases considerably during storage and becomes structural in character. This is indicated by the fact that if the solution viscosity is determined by means of a Hoeppler viscosimeter, consecutive results differ from each other, and each successive result is always lower than the preceding one. Since structure formation in solution can be characterized by the increase of yield value with time, formation of spatial structures in the solutions was studied by means of the RV-7 viscosimeter [3, 4], which can be used for studying the properties of highly viscous liquids and concentrated disperse systems. With the aid of this instrument, it is possible to detect anomalous structural viscosity

in a system and at the same time to determine the yield value. The design of the instrument and the method of its use are described in detail in [4-6].

The experiments were performed with sodium butadiene rubber of RShch grade, without added phenyl-β-naphthylamine (Neozone D) antioxidant, so that any possible side reactions which might distort the course of the main process should be excluded. Solutions containing 1%, 2%, 3%, 4%, and 5% of sodium butadiene rubber in dichloroethane were prepared. After the rubber had completely dissolved, Leukonat adhesive was added to these solutions in the proportions of 1 weight part of isocyanate to 1 weight part of rubber. The resultant solutions were thoroughly stirred and their viscosities were immediately determined by means of a Hoeppler viscosimeter. Subsequently the rheological properties of the solutions were investigated at intervals during storage by means of the RV-7 viscosimeter.

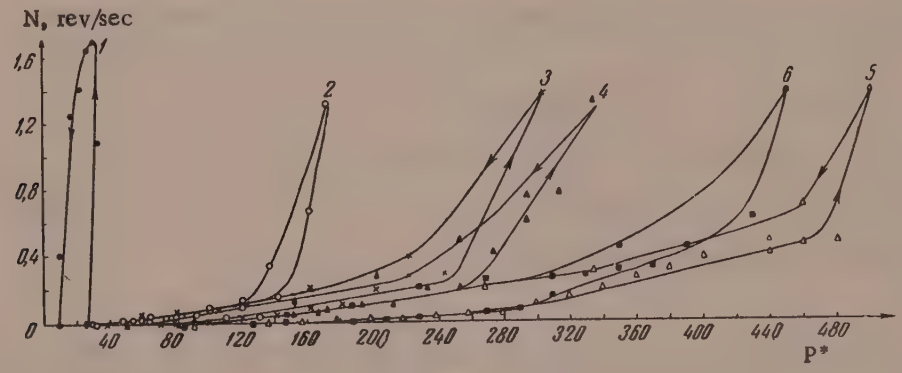


Fig. 1. Rheological curves characterizing the properties of 5% SKB solution containing isocyanate. Solutions kept for: 1) 20; 2) 30; 3) 40; 4) 50; 5) 60; 6) 70 days.

The loop-shaped curves in Fig. 1, for 50% SKB solutions with added isocyanate, represent variations of the rotation rate of the inner cylinder of the RV-7 viscosimeter with the applied rotating load. The lower branch of each curve represents a gradual increase and the upper a gradual decrease of the rotating load.

Figure 2 represents the influence of storage time on the viscosity of solutions of sodium butadiene rubber containing isocyanate. Variations of the yield values of the same solutions in course of storage are plotted in Fig. 3. It is clear from Figs. 2 and 3 that when isocyanate is added to 1% and 2% rubber solutions, their viscosity remains almost unchanged during storage. Addition of isocyanate to 3%, 4%, and 5% rubber solutions increases their viscosity by several tenth-powers, and they ultimately pass into gels. After the solutions had been stored for a certain time a structure appears in them, and the degree of its development, characterized by the yield value, is a function of the solution concentration and of the amount of isocyanate present.

It follows that the nature of the processes taking place in the rubber solutions is determined by their concentration and the isocyanate content.

The triphenylmethane triisocyanate introduced into the rubber solutions has three reactive groups in the molecule. In dilute solutions, where the distances between the rubber molecules are relatively large, structure formation either does not occur at all or proceeds at a very low rate. In concentrated solutions, the trifunctional isocyanate molecule can react simultaneously with several rubber molecules, which leads to the formation of a spatial network which is the cause of structural viscosity in these solutions. However, because of the reduced mobility of rubber molecules in concentrated solutions, and also because of the continuous viscosity increase, structure formation proceeds rather slowly.

The presence of hysteresis loops (Fig. 1) on the viscosity curves for such structurized solutions indicates that the structure is partially broken down during the testing of the solution. If the same solution is repeatedly tested, the structure is broken down to some extent, but a system with such a partially destroyed structure also has a yield value and its viscosity is considerably higher than that of the original solution (Fig. 5). If such a rubber solution with a partially destroyed structure was left to stand, the structure was not restored (Fig. 5, 4).

* Symbol indefinite in original-translator.

It is known [7] that structural networks formed by stable chemical bonds undergo virtually no relaxation at stresses below their yield value, while at stresses above this value they are irreversibly broken down. Thus, these experimental results confirm our hypothesis that chemical action takes place between the rubber and the isocyanate.

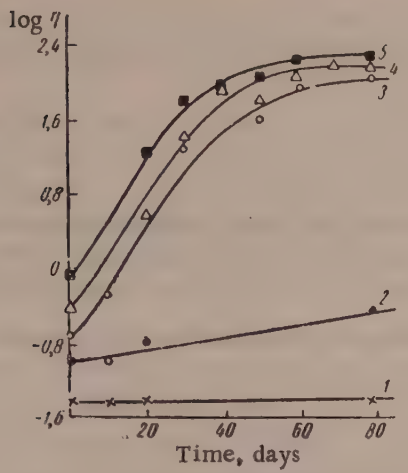


Fig. 2. Viscosity variations of 1%, 2%, 3%, 4%, and 5% rubber solutions containing isocyanates during storage: 1) 1%; 2) 2%; 3) 3%; 4) 4%; 5) 5% solution.

Vulcanizing action of isocyanate on rubber. Preliminary experiments showed that films made from SKB rubber with isocyanate and heated at 143° have limited swelling, which indicates that a spatial network is formed

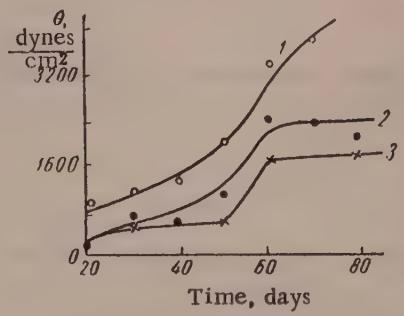


Fig. 3. Changes in the yield values of rubber solutions of different concentrations: 1) 5%; 2) 4%; 3) 3% solution.

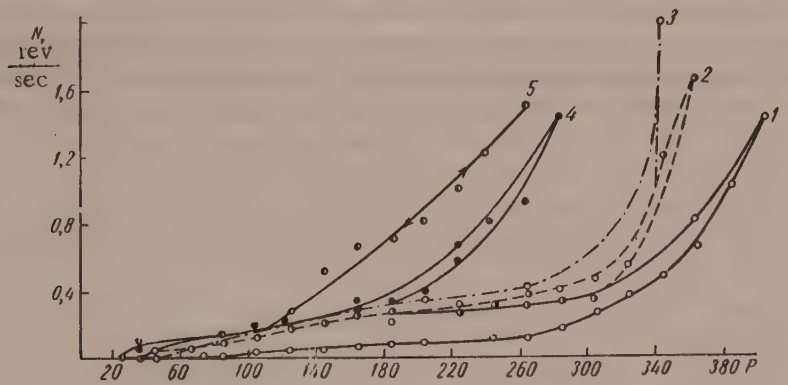


Fig. 4. Rheological curves representing changes in the properties of a 4% SKB solution during repeated testing in the RV-7 viscosimeter.

in them. However, this effect may be due to thermal vulcanization of films from sodium butadiene rubber [8] as well as to the action of isocyanate. It was necessary to determine the role of thermal vulcanization of the sodium butadiene rubber and of isocyanate as a vulcanization agent in this process. For this, a study was made of the behavior of three types of films, made from: rubber alone (T_1); from rubber with isocyanate (T_2); and from an ordinary unfilled mixture based on the same rubber (2.5 parts sulfur, 5 parts zinc oxide, 1.8 parts mercaptobenzothiazole, and 2.5 parts of stearic acid to 100 parts by weight of sodium butadiene rubber; T_3).

Films 0.2 mm thick were vulcanized in a press at 143° for 10, 30, and 50 minutes.

It is known [9, 10] that the maximum swelling of a vulcanizate depends on the number of cross links in the vulcanization structure. The density of the spatial network in a vulcanizate can be characterized in terms of the average molecular weight of the molecular segments contained between neighboring branch points in the spatial network. The density of the spatial network was determined by the swelling method [11].

The equilibrium swelling Q_e was determined from the formula [11]

$$Q_e = \frac{\rho_r}{\rho_s} \frac{P/P_0 - 1 + S}{F - S},$$

where P is the weight of the swollen specimen; P_0 is the weight of the original specimen; ρ_r and ρ_s are the densities of the rubber and the solvent; S is the content of soluble components; F is the rubber content of the original specimen.

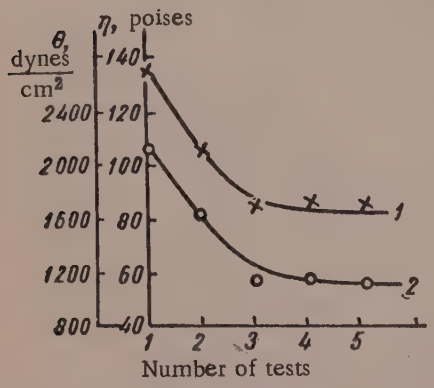


Fig. 5. Changes in the viscosity (1) and yield value (2) of 4% SKB solution containing isocyanate during repeated testing.

To determine S, the weight of each swollen specimen was found after it had been dried in a vacuum drying oven with complete removal of solvent. This weight usually differed from the initial weight of the specimen owing to dissolution of nonrubber admixtures from the vulcanizate and to removal of part of the polymer which did not form part of the regular network (Fig. 6).

If we know the equilibrium swelling (Q_e) and the parameter M, which is 0.410 for the system sodium butadiene rubber-benzene, we can use nomograms [11] for determining the density of the spatial network, characterized by the quantity M_c:

$$M_c = \rho_k V_S m_c$$

where ρ_r is density of the rubber; V_s is the molar volume of the solvent; m_c is found from a nomogram which represents the relationship of maximum swelling to the parameter M.

The test results, presented in Figs. 6 and 7, characterize maximum swelling and the density of the spatial network in vulcanizates of different compositions, based on sodium butadiene rubber. In the case of thermal vulcanizates T_1, the value of M_c is so large that it cannot be found by means of the nomogram. Films made from unfilled rubber, T_3, have the least values of equilibrium swelling and accordingly the lowest values of M_c. The weight of a swollen film remains almost unchanged after drying, which indicates the presence of a continuous vulcanization network.

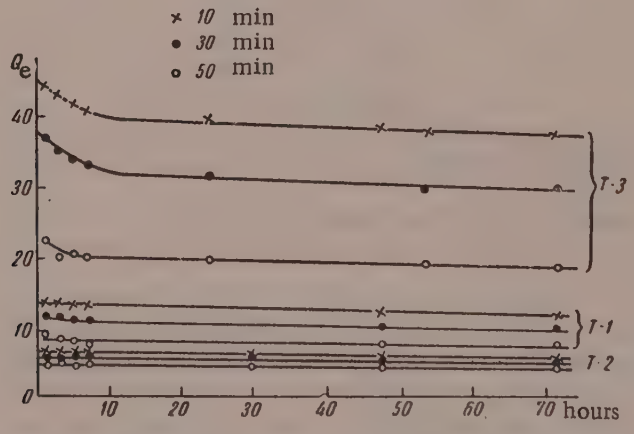


Fig. 6. Equilibrium swelling of vulcanizates of different compositions.

In accordance with existing views [9], films made from sodium butadiene rubber heated at 143° also have limited swelling, and the degree of maximum swelling decreases with increase of the heating time, but in this case, the equilibrium swelling alters in the range from 45 to 20, whereas in the case of a normal vulcanizate with sulfur it alters from 6.5 to 5. Moreover, swollen films made from SKB decrease considerably

in weight after drying, and therefore true equilibrium swelling cannot be attained. All these facts indicate that in this instance structure formation is insignificant. The T_2 film, containing isocyanate, is close in its properties to T_3 in its maximum swelling and the value of M_c; however, its maximum swelling is greater; it alters from 14 to 8. Moreover, the specimens partially dissolve during swelling. These facts show that in the case of T_2 rubber, structure formation is not so extensive as in a normal vulcanizate.

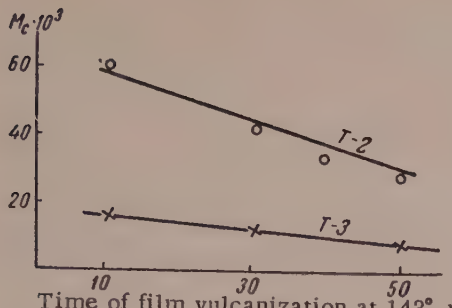


Fig. 7. Effect of vulcanization time on the value of M_c for T_2 and T_3 vulcanizates.

However, there is no doubt that structure formation does take place. Furthermore, structure formation is caused not by oxygen but by isocyanate, because in presence of isocyanate, the process is more intensive, whereas oxygen is present to the same extent in all cases.

These experiments show that chemical reaction takes place between rubber and isocyanate.

SUMMARY

1. Rubber in solution reacts with isocyanate solution; the course of the reaction differs in accordance with the contents of rubber and isocyanate in solution. The viscosity of 1-2% solutions of rubber to which isocyanate has been added during storage changes little. The viscosity of 3-5% rubber solutions increases by several orders of magnitude after addition of isocyanate. After some time, spatial structures appear in these solutions. Partial irreversible breakdown of the spatial structure takes place during repeated testing of such solutions.

2. Films of sodium butadiene rubber containing isocyanate and heated to 143° acquire the properties of vulcanizates, as is evident from their behavior in swelling.

3. These investigations confirm that chemical reactions take place between rubber and isocyanate even at ordinary temperatures. Therefore, it may be assumed that similar chemical action also takes place between rubber and isocyanate in the bonding of rubber to metal during vulcanization at 143-151°.

It is our pleasant duty to thank M. P. Volarovich for valuable advice in the course of this work.

LITERATURE CITED

[1] A. M. Medvedeva, B. V. Deryagin, and S. K. Zherebkov, Kolloid. Zhur. 19, 412 (1957).*

[2] B. V. Deryagin, S. K. Zherebkov, and A. M. Medvedeva, Kolloid. Zhur. 21, 558 (1959).*

[3] M. P. Volarovich, Zavodskaya Lab. 9, 831 (1945).

[4] M. P. Volarovich, Trudy In-ta Prikladnoi Mineralogii (1934).

[5] M. P. Volarovich and L. Ya. Ginzburg, Legkaya Promyshlennost 6, 22 (1952).

[6] M. P. Volarovich and L. Ya. Ginzburg, Kolloid. Zhur. 14, 20 (1952).*

[7] P. A. Rebinder and N. V. Mikhailov, Kolloid. Zhur. 17, 107 (1955).*

[8] B. A. Dogadkin and D. Pevzner, Collection: Investigations into the Physics and Chemistry of Rubber [In Russian] (State Chemistry Press, 1950) p. 17.

[9] B. A. Dogadkin et al., Collection: Vulcanization of Rubbers [In Russian] (State Chemistry Press, 1954) pp. 113, 173.

[10] P. Flory and J. Rehner, J. Chem. Phys. 11, 521 (1943).

[11] A. G. Shvarts, Kauchuk i Rezina 7, 31 (1957).

* Original Russian pagination. See C. B. translation.

PREPARATION AND SOME PROPERTIES OF LYOPHOBIC COLLOIDAL FORMS OF FIBER-FORMING POLYMERS

N. V. Mikhailov, V. I. Maiboroda, and S. S. Nikolaeva

Scientific Research Institute of Artificial Fibers, Mytishchi

Translated from: Kolloidnyi Zhurnal Vol. 22, No. 2, pp. 223-228, March-April, 1960

Original article submitted December 7, 1958

The use of various polymers in the form of aqueous dispersions has increased with the development of polymer chemistry. It is known that latexes of natural and synthetic rubbers and aqueous dispersions of vinyl polymers and cellulose derivatives are used in the production of insulating, anticorrosion, and decorative coatings [1]. Aqueous dispersions of polymers are also used on the large scale for production of films in various branches of technology. They are used especially extensively if the films must have strength, elasticity, resistance to repeated flexing, and stability in water. By the use of aqueous polymer dispersions, it is possible to avoid the use of inflammable, costly, and toxic solvents and the technological processes of film production can be simplified.

Despite the great practical significance of colloidal solutions of polymers, theoretical studies of their nature and properties are as yet at the initial stage, especially in the case of lyophobic colloids. Mention must be made of the work of Dogadkin, Voyutskii, Panich, Shtarkh, Sandomirskii, and others on the properties and conversion of latexes of synthetic and natural rubber [2]. Dogadkin [2] has developed and studied a process for production of aqueous dispersions of rubber by solvent substitution. Much interest attaches to the work of Glikman and Komarova [3] on the formation mechanism of lyophobic polymer sols and true solutions in organic solvents. However, this work was concerned with highly dilute systems and does not give the necessary information on the concentrated suspensions which are of practical importance.

Problems relating to the production of aqueous dispersions of fiber-forming polymers have hardly been studied at all. A knowledge of the nature of fiber-forming polymers may help in finding methods for producing concentrated suspensions and emulsions of relatively low viscosity.

At the present time, two principal methods are used for formation of fibers from synthetic polymers: from melts and from solutions. Conversion of highly viscous solutions and melts involves a number of difficulties associated with filtration and deaeration of the spinning solutions, toxicity of the solvents, and the need for evacuation and regeneration of the solvents.

Formation of fibers from aqueous colloidal polymer solutions may be a more effective method. The possibility of fiber production from suspensions is illustrated by methods for producing fibers from polytetrafluoroethylene [4] and latex [5].

There is particular interest in this method at the present time in relation to the discovery of new methods for synthesis of fiber-forming polymers in suspension form. In such cases, the use of high temperatures becomes unnecessary and it is possible to obtain polymers of high molecular weights, so that the physical and mechanical properties of the fibers can be improved considerably.

Colloidal solutions of fiber-forming polymers could probably be used as impregnating agents and coatings, and for production of films. Therefore, investigation of aqueous dispersions of fiber-forming polymers is of great theoretical and practical importance.

The purpose of the present work was to find methods for production of colloidal solutions of polycaprolactam and polyethylene terephthalate, and to study certain physicochemical properties of these solutions.

Methods for preparation of colloidal solutions of fiber-forming polymers. The condensation method, based on replacement of a solvent by a diluent, was used in the development of a method for preparing colloidal polycaprolactam solutions. The solvents used were formic acid (absolutely dry), sulfuric acid (38%), and glycerol. It was found that when 1% polycaprolactam solution in sulfuric acid was poured into a ten-fold volume of water in presence of Avirol or Leukanol, a stable sol is formed, containing 0.09-0.12% polycaprolactam. If a small amount of polycaprolactam solution in formic acid is added to a fivefold volume of water in presence of Avirol, a stable sol of somewhat higher concentration (0.5%) can be obtained. When a solution of polycaprolactam in glycerol is added to water in presence of the surface-active agent Karbozolin C, a 2% colloidal solution of polycaprolactam can be obtained.

Our technique for production of an aqueous suspension of polycaprolactam was as follows: 1-2 g of polycaprolactam was dissolved in 50 cc of glycerol, previously heated to 200°. The resultant solution was poured in a thin stream with vigorous stirring into an equal volume of 0.5% aqueous Karbozolin C solution, previously cooled to +5°. The colloidal solution must be constantly cooled during the preparation.

Colloidal solutions of polyethylene terephthalate were also prepared by a condensation method. Polyethylene terephthalate was dissolved in dimethylformamide at a bath temperature of 170-200°, as only one of the several samples of polyethylene terephthalate tested dissolved at 170°. To dissolve the other polymer samples, the bath temperature had to be at least 195°. When a solution of polyethylene terephthalate in dimethylformamide (polymer concentration not over 2%) is poured into water, a stable sol is formed without addition of stabilizers. With higher concentrations of polymer in the solution, it is necessary to add a stabilizer which favors the formation of a stable sol.

To prepare a 4.5% colloidal solution, 3.6 g of powdered polyethylene terephthalate resin was dissolved in 40 cc of dimethylformamide at a bath temperature of 170-200°. The resultant solution was not cooled, and was poured in a thin stream with vigorous stirring into an equal volume of a 2% solution of OS-20 agent at room temperature. After the solution of polyethylene terephthalate had been added, the stirring of the resultant colloidal solution was continued for some time.

These methods for preparation of colloidal polymer solutions are not intended to be used in production, but they can be used for scientific and certain practical purposes.

Investigation of certain physicochemical properties of lyophobic colloidal forms of fiber-forming polymers. To determine the effect of high temperatures during the dissolving on the molecular weight of the polymers, the specific viscosities of 0.5% solutions of polycaprolactam and polyethylene terephthalate in cresol were determined before and after they had been dissolved at high temperatures in the respective solvents (Table 1).

TABLE 1

Effect of Dissolution Temperature on the Viscosity of Solutions of Fiber-Forming Polymers

Polymer	Solvent	Dissolution temperature, °C	Specific viscosity	
			before dissolution	after dissolution
Polyethylene terephthalate sample 1	Dimethylformamide	180	0,245	0,260
Ditto, sample 2	Ditto	200	0,254	0,220
Ditto, sample 3	Ditto	200	0,241	0,210
Polycaprolactam	Glycerol	200	0,669	0,582

Table 1 shows that the molecular weights of the polymers present in the resultant colloidal suspensions are reasonably high.

The sign of the charge and the zeta-potential of the particles in the colloidal polymer solutions were determined by means of the Rabinovich and Fadiman apparatus [6]. The current strength during electrophoresis

did not exceed 10 ma. The voltage varied in accordance with the conductivity of the solution used. The auxiliary liquid was prepared from the same components as were used in the dispersion medium of the colloidal solution of the given polymer. The conductivities of the colloidal solution and of the corresponding auxiliary liquid were maintained equal; this was checked with the aid of a compensation bridge circuit for conductivity determination; the zeta-potential was calculated from the formula:

$$\zeta = \frac{K\Pi\eta u}{D}(300)^2,$$

where K is a numerical coefficient; η is the viscosity of the medium; $\underline{u}$ is the electrophoretic mobility; D is the dielectric constant.

The viscosity and dielectric constant of the dispersion medium were assumed to be equal to those of water. The surface tension of colloidal solutions was determined by Rebinder's method from the maximum bubble or drop pressure.

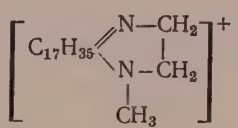
The relative viscosity of the colloidal solutions was determined in the ordinary Ostwald viscosimeter. The results are presented in Table 2.

TABLE 2

Physicochemical Properties of 1% Colloidal Solutions of Polycaprolactam and Polyethylene Terephthalate

Polymer	Sign of charge	ζ-potential, mv	Relative viscosity	Surface tension, dynes/cm	Conductivity, $ohm^{-1} \cdot cm^{-1}$
Polycaprolactam	+	33,3	1,24	34,7	$1,2 \cdot 10^{-5}$
Polyethylene terephthalate	—	10,8	1,03	7,02	$7,02 \cdot 10^{-6}$

The positive charge of the polycaprolactam suspension is evidently produced by adsorption, on the polymer particles, of the cation



of the cation-active agent Karbozolin C present during formation of the sol.

The negative sign of the charge on the polyethylene terephthalate particles may be attributed to the fact that when the polymer is dissolved at a high temperature, the end groups of the molecules are partially hydrolyzed to carboxyl. These groups confer a negative charge on the particles. The number of such groups in the molecule is small, as is indicated by the low values of the zeta-potential and the conductivity.

To confirm this hypothesis, we compared the conductivities ($ohm^{-1} \cdot cm^{-1}$) of the colloidal polymer solutions and of the corresponding dispersion media.

	Conductivity
Colloidal solution of polycaprolactam	$1.2 \cdot 10^{-5}$ $ohm^{-1} \cdot cm^{-1}$
Dispersion medium of the colloidal polycaprolactam solution	$1.19 \cdot 10^{-5}$ $ohm^{-1} \cdot cm^{-1}$
Colloidal solution of polyethylene terephthalate	$7.02 \cdot 10^{-6}$ $ohm^{-1} \cdot cm^{-1}$
Dispersion medium of colloidal polyethylene terephthalate solution	$3.2 \cdot 10^{-6}$ $ohm^{-1} \cdot cm^{-1}$

The fact that the conductivities of the colloidal polycaprolactam solution and of the dispersion medium are equal indicates that there is no appreciable dissociation of the polycaprolactam end groups themselves.

The conductivity of colloidal polyethylene terephthalate solution is almost double that of the corresponding dispersion medium, which indicates dissociation of the polar groups in the polyethylene terephthalate molecule.

A study was made of the influence of pH of colloidal polymer suspensions on their stability and on the zeta-potential of the particles. The Kolthoff and Vleeschhouwer citrate buffer with pH from 6.0 to 2.2 was used for the polyethylene terephthalate suspensions. Decrease of the suspension pH results in a gradual lowering of the zeta-potential and at pH 3.8 the isoelectric point is reached. Further decrease of pH leads to reversal of the charge on the particles.

It is interesting to note that polyethylene terephthalate sol prepared in presence of OS-20 stabilizer was not coagulated at the isoelectric point, whereas a sol of the same polymer prepared without stabilizer was coagulated at that point. This fact is in good agreement with Rebinder's views on the considerable role of the structuromechanical stabilization factor, determined in this instance by presence of the nonionic surface-active agent OS-20.

The pH of polycaprolactam suspensions was varied by means of Sorensen's borate buffer solutions with pH from 7.6 to 9.79, and citrate buffer solutions with pH from 6.0 to 2.2. Changes of suspension pH from 7.6 to 9.79 did not affect the particle stability or the magnitude of their charge, but at pH 6 the suspensions were instantly coagulated.

The particle size in the suspensions was determined visually by means of the Wikel-Zeiss microscope at 500 x magnification. The suspensions were examined both in ordinary and in polarized light. It was found that most of the particles were $< 1\ \mu$. The greater part of the particles in polyethylene terephthalate suspensions visible at 500 x magnification exhibit double refraction and have a regular leaflet shape. Polycaprolactam suspensions also contain birefringent particles, but they are much less numerous and are not so regular in shape [7]. Birefringence in sols may be due to two causes: it is caused either by orientation of asymmetric molecules, aggregates of which have amorphous structure, or by crystalline structure of the colloidal particles themselves.

To elucidate the structure of the colloidal polymer particles the suspensions were studied in the ÉM-3 electron microscope with a resolving power of 50 A.* For specimen preparation the suspension was diluted with redistilled water down to a concentration of about 0.001%, and a drop of the solution was placed on a collodion support and dried.

It was found that the particles in polycaprolactam and polyethylene terephthalate suspensions are of a regular globular shape. The size of these globules is 500-1000 A.

Electron-diffraction patterns of polyethylene terephthalate and polycaprolactam suspensions indicate that the polymers are of amorphous structure. The presence of several diffuse rings indicates a close-range arrangement of the polymer molecules.

The formation of aggregates of a chain or network structure may indicate changes in the colloidal systems with time. Berestneva, Koretskaya, and Kargin [8] attribute the presence of chain structures to the fact that regions of higher activity, at which cohesion occurs, are present on the surfaces of the spherical particles.

Further study of this question in relation to fiber-forming polymers is very important for finding methods of thread production.

SUMMARY

1. It is shown that 2% colloidal solutions of polycaprolactam and 4.5% colloidal solutions of polyethylene terephthalate can be prepared by the usual method of condensation precipitation from true solutions in glycerol and dimethylformamide.

* This part of the work was performed jointly with V. P. Kovaleva.

2. Colloidal polyethylene terephthalate sols are stable for several weeks. The charge is negative and the zeta-potential is 10.8 mv. The isoelectric state is reached at pH 3.8.

3. Colloidal polycaprolactam sols are stable for 5-6 days. The charge is positive, and the zeta-potential is 33.3 mv.

4. The particles in polycaprolactam and polyethylene terephthalate sols are amorphous in structure and have a regular globular shape.

LITERATURE CITED

[1] S. S. Voyutskii, Legkaya Promyshlennost' 2, 3, 4 (1946); H. A. Scholz, Ind. Eng. Chem. 45, 710 (1953); Ya. N. Kaplunov, P. I. Pavlovich, I. V. Plotnikov, V. M. Rogov, and A. M. Khomutov, Technology of Leather Substitutes [In Russian] (State Light Industry Press, Moscow, 1944), 2; T. P. Dagaev, Methods for Production of Reclaim Dispersions and Their Applications in Industry [In Russian] (All-Union Scientific Engineering and Technical Society of the Leather, Footwear and Fur Industries, 1946).

[2] B. A. Dogadkin, Zhur. Rezin. Prom. 5, 547 (1936); S. S. Voyutskii and B. V. Shtarkh, Kolloid. Zhur. 15, 77 (1952)*; D. Sandomirskii and K. Gagina, Kolloid. Zhur. 15, 448 (1953).*

[3] S. A. Glikman and L. V. Komarova, Kolloid. Zhur. 10, 189 (1948); S. A. Glikman, Papers at the Fourth Colloid Chemistry in Tbilisi [In Russian] (Acad. Sci. USSR Press, 1958); L. V. Komarova, Candidate's Dissertation [In Russian] (Saratov, 1946-1947).

[4] Plastics 22, 235, 113 (1957); A. J. Hall, Fibers 18, 239, 245 (1957).

[5] U. S. Patent 2,737,436, 6.03, Dow Chemical Co. (1956).

[6] A. I. Rabinovich and E. F. Fadiman, Zhur. Fiz. Khim. 8, 1 (1932).

[7] N. V. Mikhailov, V. I. Maiboroda, and S. S. Nikolaeva, Kolloid. Zhur. 21, 246 (1959).*

[8] Z. Ya. Berestneva, T. A. Koretskaya, and V. A. Kargin, Kolloid. Zhur. 12, 5 (1950).

* Original Russian pagination. See C. B. translation.

INFLUENCE OF VIBRATORY MILLING ON THE REINFORCING PROPERTIES OF CARBON BLACK

A. S. Fialkov, I. V. Temkin, and V. P. Toporova

Translated from: Kolloidnyi Zhurnal Vol. 22, No. 2, pp. 229-232, March-April, 1960

Original article submitted February 27, 1959

The use of carbon black as a filler considerably increases the moduli, tensile and tearing strength, and abrasion resistance of rubbers [1]. The reinforcing properties of carbon black depend on its specific surface and on the degree of development of the secondary structure, which is usually taken to mean the chains formed by the interconnected carbon particles.

The present authors have compared variations of the reinforcing properties of carbon blacks in relation to the degree of breakdown of the secondary structure. For this purpose, lamp and channel blacks were ground in a vibratory mill and then introduced into the rubber stocks.

It is known that a distinctive feature of vibratory mills is the high frequency of alternating action of the grinding bodies. This action weakens the structure and causes fatigue breakdown of the material at defect points [2].

The use of ultrasonic vibrations shortens grinding time by 10%. Accordingly, ultrasonic mills are used for production of finely divided materials.

Our samples of lamp and channel gas black were ground in an M-10 vibratory mill with a body 10 liters in volume, vibration amplitude 2.5 mm, and vibration frequency 25 cps under isothermal conditions. The grinding was conducted in cycles of 5, 10, 15, 20, 25, and 30 minutes. The temperature during grinding did not exceed 25-30°; the weight ratio of carbon black to grinding balls was constant in each case. The following values were determined for the ground specimens of carbon black: specific volume in the dry state and in "Galosha" gasoline, oil number, and the apparent specific surface by means of the FÉK-M photoelectric colorimeter.

The ground carbon black was introduced into the rubber stock which was formulated as follows:

Synthetic rubber SKB-50 av.	300 wt. parts
Rubberax grade A	9 "
Technical stearin	12 "
Captax	5.4 "
Zinc white, dry, M-1	15 "
Elemental gas sulfur, grade 1	4.5 "
Carbon black	180 "

The mixture was masticated in a laboratory 160 × 320 mm roll mill with a roll speed ratio of 24.6 : 31.2. The temperature of the rolls during the milling did not exceed 35-50°.

The components were mixed in the following sequence during the milling: 1 minute after the rubber, Rubberax was added; stearin was added at the 3rd minute after the start of milling; Captax at the 6th minute; and a mixture of carbon black with zinc white and sulfur at the 10th minute. After 22 minutes from the start of milling the mixture was run four times thin for 2 minutes, and then rolled for 2 minutes. The entire milling operation took 26 minutes.

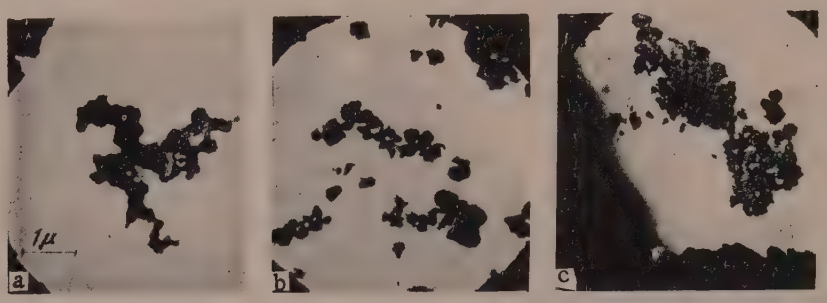


Fig. 1. Electron micrographs of lamp black: (a) Natural (b) ground in a vibratory mill for 2 hours; (c) ground for 16 hours; magnification 7000.

After the milled mixture had been left to rest at 15-30° for 2 hours, it was vulcanized in plate form at 143°; the cure time was 50 minutes.

After 2 hours of rest the vulcanized plates were tested in accordance with State All-Union Standards 269-53 and 270-53. The results are given in the table.

Variations of the Properties of Carbon Blacks and Rubber Mixtures with the Time of Grinding of the Carbon Black in a Vibratory Mill

Grinding time, min	Physical properties of carbon black			Physical properties of rubber mixtures			
	specific volume ml/g		oil number, ml/g	modulus at 300%, kg/cm²	tensile strength, kg/cm²	elongation, %	
	in dry state	in "Galosha" gasoline				relative	residual
			Lamp black				
0	8,0	24,0	1,10	57,0	80,0	510	24,0
5	3,0	11,0	0,58	37,0	76,0	650	35,0
10	3,0	9,0	0,58	36,0	71,0	620	28,0
15	3,0	6,0	0,50	29,0	78,0	652	31,0
20	2,0	5,0	0,50	31,0	82,0	636	26,0
25	2,0	4,0	0,48	33,0	87,0	622	25,0
30	1,0	4,0	0,48	32,0	80,0	602	22,0
			Gas channel black				
0	3,0	7,0	0,90	85,0	167,0	528	26,0
5	2,0	4,0	0,72	64,0	141,0	578	28,0
10	2,0	3,5	0,68	47,0	111,0	642	34,0
15	2,0	3,5	0,66	43,0	88,0	604	30,0
20	3,0	4,0	0,66	39,0	79,0	618	31,0

The table shows that after lamp and channel blacks are ground in the vibratory mill, their specific volumes in the dry state and in "Galosha" gasoline, and the oil number, decrease. These changes must be regarded as the result of intensive breakdown of the secondary structure; this is confirmed by the electron micrographs of ground and unground lamp black, given in Fig. 1.

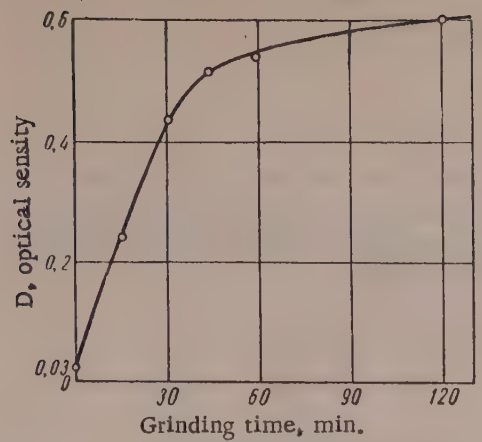


Fig. 2. Variation of the oxidation properties of lamp black with the time of grinding in a vibratory mill.

Breakdown of the secondary structure in carbon black is accompanied by liberation of a considerable number of active centers, which react with atmospheric oxygen. The carbon black becomes activated, as is shown by the data in Fig. 2 on changes in its properties. These properties were assessed in terms of the amount of I_2 liberated from KI solution, and were expressed as the optical density.

Introduction of ground carbon blacks into rubber stocks results in a decrease of modulus and increase of relative elongation (Fig. 3).

The decrease in tensile strength with ground channel black (see table) is particularly interesting. This sharp decrease in the tensile strength of rubber mixtures based on ground channel black is probably due to a greater breakdown of the secondary structure than in lamp black, and to more vigorous oxidation of the particles by atmospheric oxygen than is the case with lamp black.

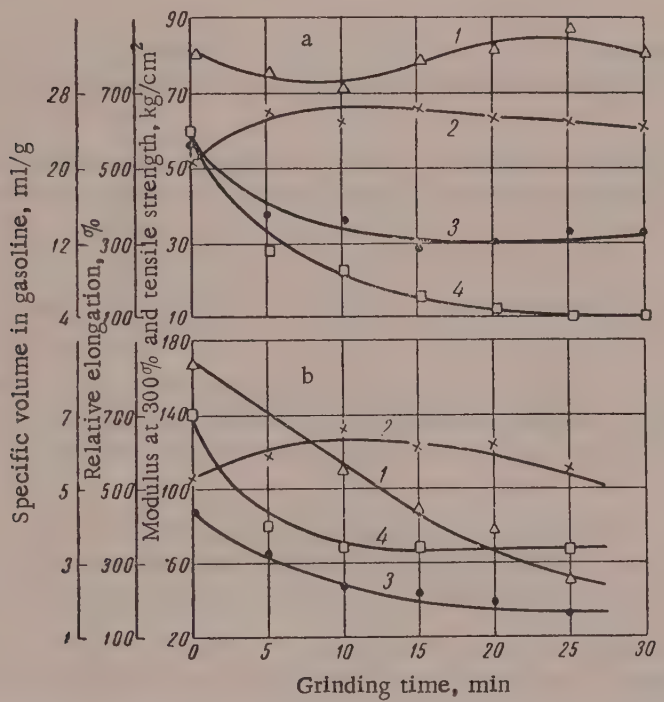


Fig. 3. Variations of the properties of lamp (a) and gas channel (b) blacks and of rubber mixtures containing them with the time of grinding in a vibratory mill: 1) Tensile strength; 2) relative elongation; 3) modulus at 300% elongation; 4) specific volume in "Galosha" gasoline.

X-ray structure analysis of lamp black ground in the vibratory mill for 16 hours did not reveal any changes in the crystallite structure of the carbon particles.

SUMMARY

1. Addition of carbon blacks ground in a vibratory mill to rubber mixtures lowers the modulus and increases the relative elongation of the mixtures.

2. Lamp and gas channel blacks ground in vibratory mills may be recommended for production of special types of rubber stocks, and as activators in granulation of ordinary carbon blacks.

LITERATURE CITED

[1] V. V. Kel'tsev and P. A. Tesner, Carbon Black, Its Properties, Production and Uses [In Russian] (State Fuel Technology Press, 1952); B. A. Dogadkin, K. A. Pechkovskaya, and A. A. Chernikina, Kolloid. Zhur. 8, 31 (1946); B. A. Dogadkin, K. A. Pechkovskaya, and M. Dashevskii, Kolloid. Zhur. 10, 357 (1948); Z. V. Chernykh and V. G. Epshtein, Kolloid. Zhur. 19, 644 (1957).*

[2] P. A. Rebinder, Kolloid. Zhur. 20, 527 (1958).*

[3] S. Kieskalt, Vereines. dtsch. Ingr. 91, 13, (1941).

* Original Russian pagination. See C. B. translation.

AN ELECTRON MICROSCOPE STUDY OF REINFORCED-RUBBER STRUCTURES

V. A. Shvetsov, A. P. Pisarenko, B. V. Shtarkh,

and A. S. Novikov

Scientific Research Institute of Film Materials and Artificial Leather

Scientific Research Institute of the Rubber Industry, Moscow

Translated from: Kolloidnyi Zhurnal Vol. 22, No. 2, pp. 233-236, March-April, 1960

Original article submitted February 7, 1959

The problem of rubber reinforcement by active fillers is one of great importance in the rubber industry; this explains why many investigators use the most recent research techniques for deeper studies into the structures formed by rubbers and active fillers.

Until recently, the structure and properties of natural and synthetic rubbers, rubber stocks, and vulcanizates were studied mainly by measurements of the elastic, plastic, and viscous properties of raw rubber stocks and mechanical properties of vulcanizates. Optical methods for visual study of disperse systems formed by rubbers and fillers have not been widely used because of the relatively low resolving power of optical microscopes.

In recent years disperse systems and polymer materials have been widely studied by means of electron microscopes, which have made the size range from 1000 to 20 A accessible to direct observation [1].

The results of electron microscope investigations are of much theoretical interest, and are of practical importance for studying certain materials and individual production processes. Special importance attaches to electron microscope studies of the degree of dispersion and configuration of the particles in powders used as fillers for rubber.

It is known that the low degree of dispersion of natural light-colored fillers (chalk, kaolin, diatomite, barytes, etc.), their tendency to aggregation and lumping, poor wettability by high polymers, and inability to form chain structures make them unsuitable for use as active fillers for rubbers.

Dogadkin and his co-workers [2] proved convincingly that the most important factor in the reinforcing action of carbon blacks is their ability to form chain and network structures in rubber mixtures.

The need to increase the activity of light-colored fillers prompted Soviet workers to carry out extensive investigations into the development of new methods for producing mineral active fillers capable of reinforcing synthetic rubbers to the same extent as carbon blacks.

It was shown [3] that it is possible to reinforce SKS-30 emulsion rubbers by light-colored fillers such as silicates of multivalent metals and colloidal silica, formed in the latex during formation of the rubber. Studies of the formation of filler particles and of their interaction with the rubber phase are of primary importance for an understanding of the mechanism of the reinforcing action of fillers.

Studies of the formation of colloidal silica outside the latex medium have been reported [4].

Aggregation and crystallization of colloidal silica lowers its value as an active filler for synthetic rubbers [5]. It was possible to show by means of electron microscope observations [5] that the action of added surface-active substances in formation of mineral fillers, in the light of the views of P. A. Rebinder and his school, is a

most important factor which determines such fundamental characteristics as high dispersity of the forming particles and the ability of these particles to yield chain and network structures.

Oriented adsorption of surface-active substances on the forming particles of silicate fillers renders them water-repellent and favors better dispersion in rubbers.

The important role of surface-active substances in the formation of silicate fillers and the valuable technological properties of butadiene-styrene rubbers prompted us to study the possibility of obtaining silicate and aluminate fillers in latexes of SKN-18 and SKN-26 nitrile rubbers, which are known to have high contents of surface-active substances. Silicate fillers were prepared from sodium silicate and calcium chloride, and aluminate fillers from sodium carbonate and aluminum sulfate.

The structurizing action of these fillers is so great that SKN-18 and SKN-26 rubbers did not dissolve in any of the usual solvents even at relatively low loadings. Solutions suitable for preparation of specimens for electron microscope observations could not be obtained by prolonged heating of finely divided samples of the rubbers in benzene, toluene, xylene, or chlorinated solvents. It was only when the rubber samples had been masticated for 10 minutes on cold rolls that it proved possible to obtain solutions of reinforced nitrile rubbers if they were heated in chlorobenzene on a water bath for 8 hours.

Solutions of the following rubber specimens were studied in the electron microscope:

Specimen 1: SKN-26, containing 24.2 wt. parts of silicate filler to 100 wt. parts of rubber.

Specimen 2: SKN-26, containing 52.8 wt. parts of silicate filler to 100 wt. parts of rubber.

Specimen 3: SKN-18, containing 32 wt. parts of aluminate filler to 100 wt. parts of rubber.

Specimen 4: This differed from Specimen 3 in that it had not been masticated before the dissolving. Although Specimen 4 only partially dissolved in chlorobenzene on heating, it was desired to determine whether the dissolved portion contained filler, and what its degree of dispersion was.

Specimen 5: SKN-26 containing 32 wt. parts of calcium silicate introduced during mastication.

The specimens for electron microscope investigation were made from 1% chlorobenzene solutions of the reinforced rubbers, and also from solutions diluted with chlorobenzene down to 0.1, 0.01, and 0.001% concentrations. The rubber solutions were perfectly clear in all cases. It must be noted that even in Specimen 2, which contained 52.8 wt. parts of silicate filler, the latter was bound so firmly with the rubber that not only were its chlorobenzene solutions clear and no filler separated out on standing, but even films of the raw rubber and vulcanizates were so transparent that print could be read through a millimeter thickness.

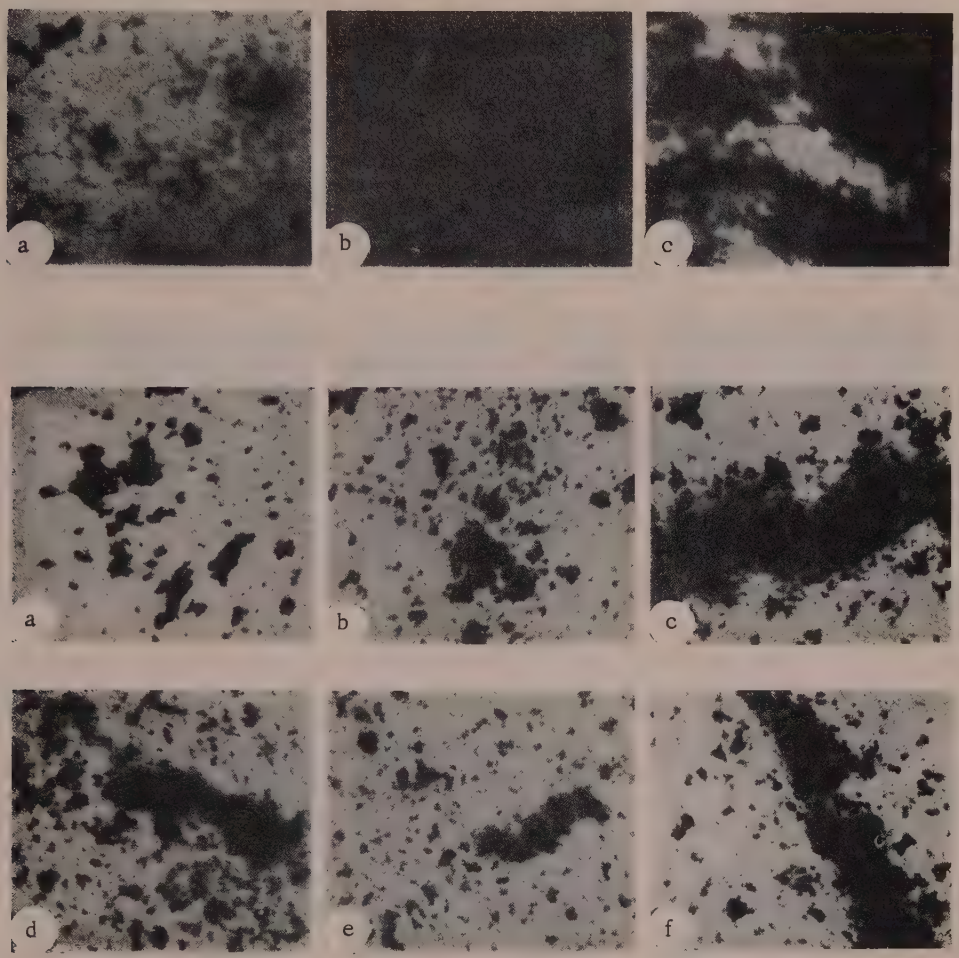
It is seen in the electron micrographs in Fig. 1, 1 and 1,2 that the elementary filler particles are similar in size, 50-100 mμ (7500 magnification). However, at a lower loading (Fig. 1, 1) the elementary filler particles have a lesser tendency to aggregation than at the higher degree of loading (Fig. 1, 2). Two characteristic facts may be deduced from the micrographs in Fig. 1, 2. The first is that with the higher filler content it has a more pronounced structurizing effect on the rubber, which is confirmed by the appearance of "threads" consisting of rubber gel fraction (Fig. 1, 2, c, d, f). It could be observed visually in the electron microscope that elementary filler particles are concentrated in these "threads." The sharp decrease in the diffusion solubility of rubber at higher loadings confirms the structurizing role of the filler.

A second characteristic feature of the solution of Specimen 2 (Fig. 1, 2) is the considerable number of rather dense and more or less large coagulated formations of elementary filler particles. It seems that when the filler concentration is increased, the conditions become more favorable for particle aggregation owing to interaction at the active centers on collision between particles formed in the latex.

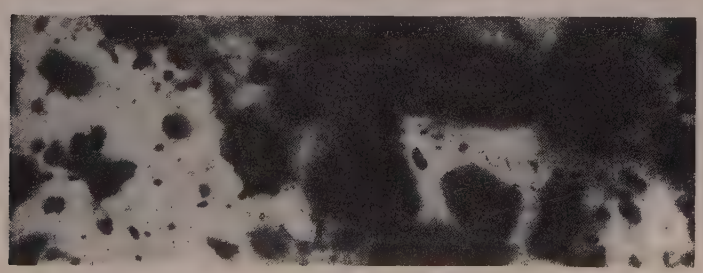
Figure 2, 1, shows electron micrographs of aluminate-containing nitrile rubber (Specimen 3) previously masticated and then dissolved in chlorobenzene, and Fig. 2, 2 corresponds to the same rubber (Specimen 4) which had not been masticated.

It is seen from Fig. 2, 1, that the elementary particles are much finer in the aluminate than in the silicate filler, and the particles lie at the limit of the resolving power of the ÉM-3 electron microscope used in our investigations (with 7500-fold electron microscopic magnification). Thus, it follows from Fig. 2, 1, e

and 2, 1, f that the size of the visible elementary particles is 30-50 mμ. In the specimen shown in Fig. 2, 2, f "clouds" can be seen; these probably consist of particle nuclei of the aluminate filler which had not yet reached the size at which they could be observed in the electron microscope.



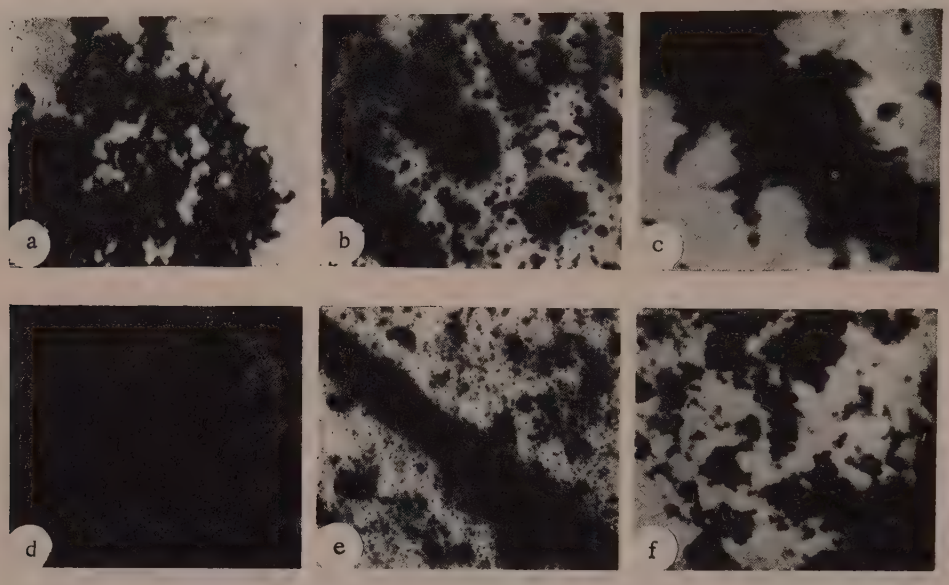
2



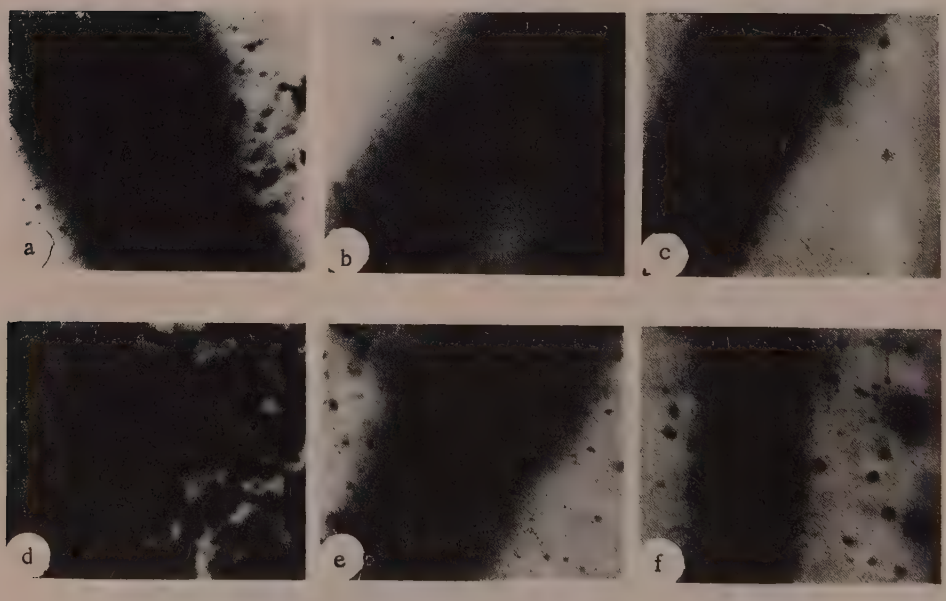
3

Fig. 1. Electron micrographs of SKN-26 rubber films with different contents of sodium silicate: 1) Specimen 1; 2) specimen 2; 3) specimen 5.

It must also be pointed out that aluminate filler has a pronounced structurizing effect on nitrile rubber. In Fig. 2, 1, c can be seen a characteristic "thread" of nitrile rubber gel fraction, with only part of the filler particles concentrated in this "thread." In Fig. 2, 1, e, it is seen that a considerable number of the filler particles has "gone into the thread" or become concentrated in the form of loose coagulated aggregates.



1



2

Fig. 2. Electron micrographs of SKN-18 rubber films containing 30 weight parts of aluminate filler, formed in the latex, per 100 weight parts of rubber: 1) Specimen 3; 2) specimen 4.

Figure 2, 1, a shows the typical loose coagulation structure generally characteristic of active gas blacks, which form coagulation structures in the form of thread, network, and chain formations.

Because of their high dispersity, low aggregation, and the ability to form loose coagulative network and chain structures, the activity of aluminate fillers should be high. This is fully confirmed by the data presented in the table.

Properties of SKN-26 Rubbers Containing Calcium Silicate and Aluminum Hydroxide Introduced at the Latex Stage and in Mastication

Filler, 60 wt. parts to 100 wt. parts rubber	Defoe hardness	Strength			Filler, 60 wt. parts to 100 wt. parts rubber	Defoe hardness	Strength		
		tensile, kg/cm²	tear, kg/cm	abrasion, cc/kw-hr			tensile kg/cm²	tear, kg/cm	abrasion, cc/kw-hr
Calcium silicate formed in the latex	5300	203	50	190	Aluminum hydroxide formed in the latex	5700	251	53	165
Ditto, introduced in mastication	3100	73	32	345	Ditto, introduced in mastication	4500	54	29	460

Figure 2, 2 shows electron micrographs of SKN-18 film (Specimen 4). A solution of this rubber which had been subjected to prolonged settling was taken for the electron microscope studies. It is seen in the micrographs in Fig. 2, 2 that the rubber still contains a considerable amount of filler particles, also concentrated in the "threads" of the rubber gel fraction (Fig. 2, 2, a, b, c, e, f).

It must be noted that despite the fact that the specimens were prepared from the upper, absolutely clear, portion of the solution, which should be expected to be the sol fraction, considerable more "threads" are observed in this instance, which confirms the strong structurizing effect of the aluminate filler.

For comparison, Fig. 1, 3 shows electron micrographs of SKN-26 solution containing calcium silicate introduced at the mastication stage. From a comparison of Fig. 1, 1 and 1, 3, it is seen that when the silicate filler is introduced at that stage its dispersion in the rubber is much worse, without formation of chain structures; this accounts for its considerably smaller reinforcing effect (see also table).

SUMMARY

1. Observations of solutions of reinforced rubbers in the electron microscope revealed the presence of rubber sol and gel fractions and secondary filler structures.

2. Most important factors in rubber reinforcement are high dispersity and low aggregation tendency of the fillers and the ability of aluminate and silicate fillers to form network and chain structures.

LITERATURE CITED

[1] A. L. Zaides and S. L. Pupko, Doklady Akad. Nauk SSSR 65, 2 (1959);* B. Dogadkin, K. Pechkovskaya, S. Pupko, and S. Simanovskaya, Tr. N.-i. in-ta Shinnoi Prom-sti (State Chemical Press, 1950); A. P. Pisarenko, A. B. Shekhter, and A. I. Echeistova, Doklady Akad. Nauk SSSR 76, 3 (1951); B. V. Shtarkh and A. P. Pisarenko, Legkaya Promyshlennost' 5 (1956).

[2] B. Dogadkin, K. Pechkovskaya, and V. Kuprianova, Tr. N.-i. in-ta Shinnoi Prom-sti (State Chemical Press, 1950).

[3] A. P. Pisarenko, A. P. Emel'yanova, and P. L. Zakharchenko, Kauchuk i Rezina 2 (1957); A. P. Pisarenko and A. P. Emel'yanova, Legkaya Prom-st' 2 (1957).

* See C. B. translation.

[4] Z. Ya. Berestneva, T. A. Koretskaya, and V. A. Kargin, Kolloid. Zhur. 11, 6, 369 (1949); 13, 5, 323 (1951).

[5] A. P. Pisarenko, B. V. Shtarkh, and A. P. Emel'yanova, Summaries of Papers at the Fourth All-Union Conference on Colloid Chemistry [In Russian] (Acad. Sci. USSR Press, Moscow, 1958).

INVESTIGATION OF CLAY MINERALS IN SOIL COLLOIDS

E. A. Yarilova and E. I. Parfenova

Soil Institute, Academy of Sciences, USSR, Moscow

Translated from: Kolloidnyi Zhurnal Vol. 22, No. 2, pp. 237-242, March-April, 1960

Original article submitted January 16, 1959

The first Soviet soil scientists to carry out detailed studies of soil-colloid minerals were N. I. Antipov-Karataev and his associates [1, 2]. Colloidal fractions of different soil types were studied by chemical and x-ray methods. With the exception of colloids from red soils, these fractions were characterized by fairly uniform $SiO_2:R_2O_3$ ratios which changed little within a given profile. X-ray investigations showed that clay minerals of the montmorillonite type* predominate in soils and their underlying accretions; large amounts of hydromicas are also characteristic. Minerals of the kaolinite group are rarely met, and occur mainly in red soils.

During the 20 years since the publication of those papers, investigation methods have been improved considerably, and new methods have been introduced which permit fuller and more accurate studies of the composition, structure, and properties of clay minerals in soils. However, the origin of soil clay minerals still remains obscure. The view most widely accepted is that clays are formed by breakdown and in situ metamorphosis of primary minerals (by dispersion and hydrolysis). Indeed, when soils are examined under the microscope, grains are always visible which are modified to some degree and which often represent pseudomorphoses of the clays from primary minerals. It has also been suggested that clay minerals are synthesized from the final amorphous decomposition products of primary minerals; in the opinion of Antipov-Karataev and Kader [4] this is the predominant process in the weathering crust and soils. A quite distinct position is held by Polynov [5], who considers that organisms play the main role in clay formation. On the one hand, they play an active part in conversion of primary minerals into argillaceous substances (as in pelitization of feldspars), and on the other, synthesis is effected from natural solutions which contain elements extracted from plants from the rocks and liberated during mineralization of the plant remains.

In our investigations, which were based on Polynov's views, we considered it necessary first to study thoroughly the composition and properties of the clay substance itself and to accumulate experimental data on various soils.

In micromorphological investigations of polished sections of soils with a pronounced illuvial process accumulations of a yellow, transparent, highly homogeneous colloidal argillaceous material are often observed in the micropores and cracks (Fig. 1); it stands out by its incrustation character, high birefringence and wave-like extinction due to the regular orientation of the clay particles in one direction. Earlier we studied clays of this type from illuvial levels of a number of soils [6] and put forward some suggestions concerning their possible synthetic origin. The present article contains the results of further studies of colloidal fractions from chestnut, chernozem, saline, and gray forest soils developed on loess and surface loams.

* Montmorillonite as an independent soil mineral is now being found only rarely [3].

For comparative studies of clay formation in different soils it is, of course, necessary to have material which is not contaminated by extraneous impurities. Since literature data indicate that fractions $> 0.2\ \mu$ still contain appreciable amounts of primary minerals, we isolated the $< 0.2\ \mu$ fractions and investigated them by chemical, x-ray, optical, and thermal methods.

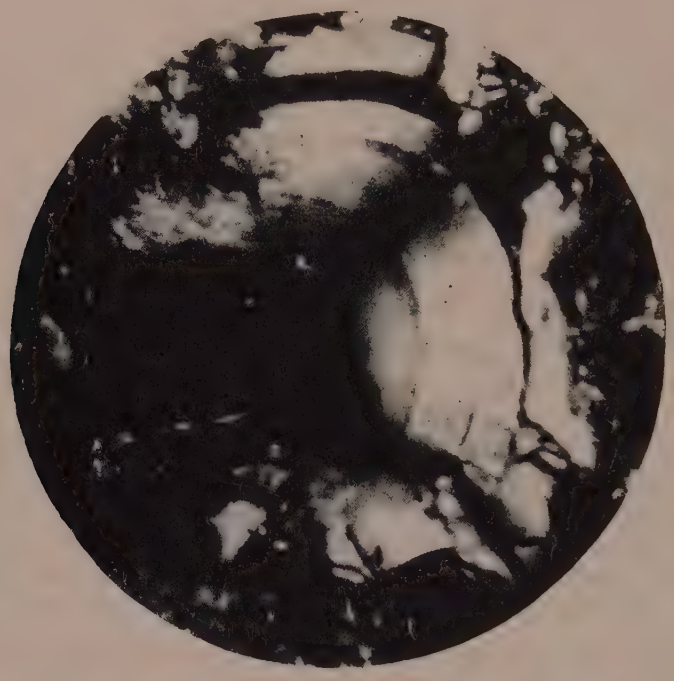


Fig. 1. Microphotograph of collomorphous clay mineral in a soil pore; magnification x 300, crossed nicols.

The x-ray patterns* of all the investigated samples are very similar; their common nature indicates a high degree of dispersion in the investigated minerals; there are few (12-13) lines and they are diffuse and weak. All the x-ray patterns have some degree of background indicating presence of amorphous substances. The first line in the x-ray pattern is very diffuse and broad, but relatively intense; its dimensions lie in the range 12.7 to 11.54 kX at the internal and 10.61 to 9.94 kX at the external diameter. The four other most intensive lines for different specimens have values in the following ranges: 4.56-4.64 kX, 3.38-3.36 kX, 2.60 kX, 1.51 kX. These values of d indicate that we are concerned here with three-layer clay minerals.

It is known that the 060 line, corresponding to the sixth order of the 0k0 reflections, can be used for determining the b constant of the unit cell and for finding whether a material belongs to the dioctahedral or the trioctahedral group of schistose minerals. In this instance, this line has the value 1.51 kX, which is characteristic of dioctahedral minerals [7]. The cell constant along the c axis, calculated from the 1.51 kX line, is 9.07 kX, while the value calculated from chemical structure formulas is 9.01-9.05 kX (Table 1). Thus, the different calculation methods gave very good agreement.

It might be supposed that the first line (band) in the x-ray pattern (12.7-9.9 kX) is due to a mixture of illite with weakly hydrated montmorillonite or to the presence of a mineral with random stratification of swollen and unswollen layers. Illite, a nonswelling mineral, has a constant interplanar spacing of 10 kX, whereas in montmorillonite it may vary with the degree of hydration from 10 kX in anhydrous montmorillonite to 21 kX in the case of montmorillonite completely saturated with water ($4H_2O$ molecules in the space between the sheets). To determine more precisely the nature of the material, oriented specimens treated with glycerol were

* The x-ray patterns were taken by N. A. Sharina.

prepared. However, their x-ray patterns proved to be identical with the powder patterns. This indicates the absence of montmorillonite as an impurity and supports the hypothesis of a probable presence of a small number of swelling layers.

TABLE 1

Structural Formulas of the Investigated Specimens

Section No.	Depth, cm	Octahedral layer				Tetrahedral layer			Total lattice charge	Sorbed cations %	K^{1+}	$(H_3O)^{1+}$	b, κX
		Al^{3+}	Fe^{3+}	Mg^{2+}	charge	Si^{4+}	Al^{3+}	charge					
64	0—10	1,19	0,60	0,21	0,21	3,26	0,74	0,74	0,95	0,31	0,33	0,31	9,05
	10—18	1,34	0,42	0,24	0,24	3,32	0,68	0,68	0,92	0,41	0,12	0,29	9,03
	25—35	1,22	0,58	0,20	0,20	3,31	0,69	0,69	0,89	0,32	0,28	0,29	9,04
	85—105	1,53	0,37	0,10	0,10	3,42	0,58	0,58	0,68	0,25	0,22	0,21	9,01
200	14—19	1,26	0,53	0,21	0,21	3,25	0,75	0,75	0,96	0,36	0,28	0,32	9,05
	30—40	1,30	0,52	0,18	0,18	3,33	0,67	0,67	0,85	0,42	0,09	0,34	9,04
	153—163	1,16	0,63	0,21	0,21	3,43	0,57	0,57	0,78	0,36	0,11	0,31	9,04
13	0—10	1,16	0,59	0,25	0,25	3,18	0,82	0,82	1,07	0,47	0,26	0,34	9,05
	10—20	0,81	0,55	0,64	0,64	3,12	0,88	0,88	1,52	1,03	0,31	0,18	9,09
	30—40	1,28	0,52	0,20	0,20	3,34	0,66	0,66	0,86	0,33	0,27	0,26	9,04
560	23—28	1,25	0,62	0,23	0,23	3,42	0,58	0,58	0,81	0,24	0,15	0,42	9,04
	80—85	1,03	0,74	0,23	0,23	3,39	0,61	0,61	0,84	0,36	0,19	0,29	9,05
	200—205	1,44	0,46	0,10	0,10	3,32	0,68	0,68	0,78	0,36	0,07	0,35	9,03

Thermal analysis of the soil colloids, carried out by E. A. Shurygina, indicates a close similarity between them. The thermograms have endothermic peaks at 95-125, 250-350, 500-550, 800-860° and an exothermic peak at 915-935°. According to these characteristics, the minerals are close to illite. The great depth of the first peak indicates the presence of a considerable amount of weakly bound water, while the peaks at 250-350° are due to the presence of certain amounts of sesquioxide minerals (Fig. 2).

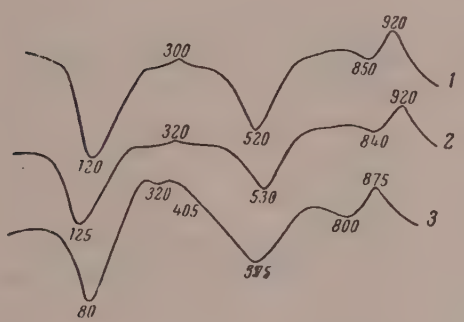


Fig. 2. Thermograms of colloidal soil fractions: 1) s. 560, 46-51 cm; 2) s. 560, 80-85 cm; 3) s. 13, 10-20 cm.

The results of total analyses (Table 2) were used to calculate the structural formulas of the clay minerals [8]. The calculation of the formulas must be based only on the amounts of elements present in the lattice. Since the colloids may contain admixtures of free oxides and hydroxides, these should be determined by appropriate extraction methods and the results excluded in calculation of the formulas. In the present instance, mobile SiO_2 comprised approximately 0.7% and Al_2O_3 approximately 1.3%, or 1.4 and 6.0% of the total contents respectively, while the free iron, determined by Deb's method [9] was from 1.2 to 2.7%, or 15-25% of the total.

On the basis of the results of x-ray and thermal analyses, we assumed a three-layer dioctahedral structure for the clay minerals in calculation of the formulas. This means that in one-half of the unit cell of the pyrophillite type $[Al_2Si_4O_{10}(OH)_2]$, the number of Al ions in the octahedral layer is two, and the number of Si^{4+} ions in the tetrahedral layer is four. In the clay mineral lattice, Al^{3+} of the octahedral layer can be replaced by other cations, either trivalent or bivalent (Fe^{3+}, Fe^{2+}, Mg^{2+}, etc.) while Si^{4+} of the tetrahedral layer can be replaced by Al^{3+}. Substitution of elements of higher valence by elements of lower valence leads to appearance of negative charges, balanced by the charges of adsorbed ions present in the interlayer space. In the light of these considerations, the calculation of formulas of the clay minerals is based on the general formula:

TABLE 2

Total Analyses of Soil Colloids in Percentages of Air-Dry Weights (Analyses Performed by É. F. Mochalova)

Soil and section No.	Depth, cm	Hygroscopic water, %	Calcination loss, %	Chemical composition, %										Molecular ratios	
				SiO_2	P_2O_5	Al_2O_3	Fe_2O_3 total	Fe_2O_3 free	CaO	MgO	MnO	K_2O	Na_2O	$\frac{SiO_2}{Al_2O_3}$	$\frac{SiO_2}{R_2O_3}$
64															
Chestnut, Altai region	0—10	5,98	17,57	39,04	—	19,71	9,60	2,05	2,08	2,47	0,23	3,12	0,19	3,42	2,51
	10—18	6,68	12,08	43,86	Tr.	22,75	7,28	1,61	1,64	4,51	Нет	1,18	0,02	3,28	2,72
	25—35	7,45	10,14	43,26	—	21,21	10,11	1,55	1,50	3,18	0,09	2,88	0,20	3,47	2,66
	85—105	8,20	9,18	46,11	—	24,21	6,78	Not deter.	0,04	2,78	0,09	2,38	0,23	3,24	2,74
200															
Chernozem, Altai region	14—19	6,65	15,68	40,04	—	21,05	8,65	»	1,86	3,15	0,09	2,68	0,20	3,23	2,56
	30—40	6,78	14,49	41,88	0,01	22,46	8,12	»	2,27	3,07	Сл.	0,88	0,03	3,17	2,58
	153—163	7,58	9,48	46,80	—	19,98	10,39	»	0,28	2,83	0,19	2,27	0,22	3,98	2,99
13															
Saline, Altai region	0—10	5,44	20,35	37,23	0,03	19,69	9,22	»	1,46	3,26	Нет	2,27	1,03	3,27	2,48
	10—20	5,55	12,82	37,61	0,02	17,33	8,81	»	7,02	5,34	0,19	2,96	2,38	3,69	2,78
	30—40	6,15	12,51	43,45	0,01	21,40	8,95	»	1,43	3,14	Сл.	2,74	0,22	3,82	2,70
560															
Gray forest, Tula province	23—28	5,68	13,04	42,63	0,02	20,80	11,31	2,68	2,27	2,46	0,14	1,60	0,12	3,48	2,58
	80—85	5,21	8,78	45,80	0,01	18,85	13,32	3,05	2,65	3,06	0,18	1,94	0,21	4,13	2,85
	200—205	6,41	10,42	45,05	0,01	24,44	8,32	2,33	1,46	3,06	Сл.	0,75	0,06	3,55	2,71

$$(Al_{a-x}Fe_bMg_c)\,[Al_xSi_{4-x}]\,O_{10}(OH)_2,$$

where $(Al_{a-x}Fe_bMg_c)$ represents ions of the octahedral layer, the sum of which should be 2; $[Al_xSi_{4-x}]$ represents ions of the tetrahedral layer, totalling 4; a, b, and c are the numbers of cations; $O_{10}(OH)_2$ is the anionic portion; x is the quantity of adsorbed cations. In addition to the adsorbed cations, the charges of the octahedral and tetrahedral layers can also be balanced by potassium and oxonium.

Our formulas for the clay minerals are not exact, because the amounts of adsorbed magnesium and bivalent iron, which influence the charge of the octahedral layer, are not accounted for separately; furthermore, the exact oxonium content is not known. Nevertheless, these formulas can be used for comparative characterization of the minerals.

The investigated soils are characterized (Table 1) by rather extensive replacement of silicon by aluminum in the tetrahedral layer of the clay mineral lattice ($^1/_5$ to $^1/_7$ of the total Si). We attempted to calculate the formulas of the clay minerals without free iron, but the results were not significantly different, and there was only a certain shift of the ratios between the elements within the layers.

If the formulas are compared with the formulas of montmorillonite and illite, the first thing to be noticed is the sharp distinction of our clay substance from montmorillonite. In the latter, replacement of silicon by aluminum in the tetrahedral layer is always slight, so that the lattice charge is mainly determined by the ions of the octahedral layer, whereas the reverse is the case in our formulas. Moreover, the total charge of the montmorillonite lattice is much lower. With regard to the composition of the octahedral layer, montmorillonite differs in generally having a somewhat higher aluminum content, a considerably higher magnesium content, and less iron. Potassium is hardly ever present in the interlayer cations of montmorillonite.

Our clay mineral formulas are closer to illite formulas, but here again there are noticeable differences. They primarily differ from illite by having a much lower potassium content and a higher iron content; this is highest in colloids from illuvial levels.

The investigated specimens are very similar to each other in their optical properties; their color is pale yellow or reddish yellow (in illuvial levels) and are transparent, but in upper levels they include finely dispersed humus. Pleochroism varies from greenish brown for Ng to straw-yellow for Np. There is no complete extinction, it is always wavelike. The refractive indices of all the samples are very similar, and vary in the following ranges: Ng' from 1.579 to 1.50; Np' from 1.555 to 1.545. Birefringence is high in all cases, and is within the range 0.017-0.024. Removal of free iron results in a considerable lowering of the refractive indices (Ng' 1.550; Np' 1.535).

The sorption capacity was determined for a number of samples. For most of them, the value varied between 55 and 65 meq per 100 g of colloids, which is intermediate between the capacities of montmorillonite and illite.

SUMMARY

1. The investigated soil colloids predominantly contain highly disperse dioctahedral (probably ditrioctahedral) clay minerals with a three-layer crystal lattice; they cannot be classified either as montmorillonite or as illite, and probably constitute a special group of clay minerals with mixed stratification, occurring in various soils.

2. They differ from montmorillonite by having a lower $SiO_2:Al_2O_3$ molecular ratio, the presence of appreciable amounts of potassium, in general a lower magnesium content, and a lower sorption capacity. The refractive indices differ sharply, and are considerably higher for our samples; neither their x-ray patterns nor their thermograms correspond to montmorillonite. The structural formulas also differ from the formulas of the latter.

3. There are similarities and differences between these colloids and illite. The molecular $SiO_2:Al_2O_3$ ratios are in most instances close to those of illite or slightly higher. The potassium content is about one-half that of illite, while the iron content is rather higher. The capacity is somewhat higher. The x-ray patterns differ in the first broad (from 10 to 12 kX) and diffuse line. The optical characteristics are similar. The thermograms

are also very similar. Their structural formulas are alike, except that the potassium content is lower and the oxonium content is therefore probably higher.

LITERATURE CITED

[1] I. N. Antipov-Karataev, B. K. Brunovskii, and A. A. Rode, Collection: The Soil Sorption Complex and Problems of Agriculture [In Russian] (The Lenin All-Union Academy of Agricultural Sciences, Moscow, 1937) p. 104.

[2] I. I. Antipov-Karataev, G. M. Ponomarev, and I. D. Sedletskii, Pochvovedenie 3-4, 54 (1942).

[3] N. I. Gorbunov, Pochvovedenie 2, 75 (1956).

[4] I. N. Antipov-Karataev and G. M. Kader, Tr. Pochvennogo in-ta Akad. Nauk SSSR 51, 98 (1956).

[5] B. B. Polynov, Selected Works [In Russian] (Acad. Sci. USSR Press, Moscow, 1956) pp. 395, 475.

[6] E. I. Parfenova and E. A. Yarilova, Pochvovedenie 4, 38 (1956); E. A. Yarilova and E. I. Parfenova, Pochvovedenie 9, 37 (1957); 2, 75 (1959).

[7] V. I. Mikheev, X-ray Key to Minerals [In Russian] (State Tech. Geological Press, Moscow, 1957).

[8] B. B. Zvyagin, Collection: Manual of Petrographic and Mineralogical Investigation of Clays [In Russian] (Proc. All-Union Geological Institute, State Tech. Geological Press, Moscow, 1957) p. 298.

[9] B. C. Deb, J. Soil. Sci. 1, 62, 212 (1950).

INFLUENCE OF THE SURFACE STATE OF GLASS ON THE PORE STRUCTURE OF FILMS PRODUCED BY ACID ETCHING ON UNSTABLE GLASSES

L. S. Yastrebova, A. K. Pogodaev, and D. P. Dobychin

S. I. Vavilov State Optical Institute, Leningrad

Translated from: Kolloidnyi Zhurnal Vol. 22, No. 2, pp. 243-246, March-April, 1960

Original article submitted December 26, 1958

It is known [1] that the surface of any silicate glass, with the exception of a freshly fractured surface, is always covered by a very fine film of hydrated silica; this is formed either by destruction of the glass by atmospheric moisture [2] or by the action of liquid water in the course of polishing of optical components. The thickness of this "natural" film (as it is often described) is, according to measurements with a polarization goniometer, some tens of angstroms [3]. Thicker films (about 1000-1400 A thick), formed by treatment of glasses in dilute acid solutions, are widely used for protection and clarification of optical components. The properties of these artificial films (which we shall for brevity term acid-etching films) depend to a considerable extent on their pore structure, which has been investigated [4] and systematically studied [5, 6] by the usual static technique of sorption measurement. Acid-etching films on powdered optical glasses were first used in such investigations. Subsequently, in view of the lack of direct data on the thickness of acid-etching films on powders, and also because films formed on the freshly-fractured glass surfaces are studied in experiments with powders, a technique was developed for investigating the pore structure of films formed directly on the polished surface of optical glass [7]. Control determinations by the two methods, performed on a porous glass specimen previously studied by means of the quartz spring balance, showed that the results (form of the isotherm, the predominant pore radius) given by all three methods are in agreement.

It is known that uniformity of the optical properties of etching films on unstable glasses depends considerably on the state of the glass surface before acid treatment. It was desired to find how differences in the surface state of powders and polished glass specimens affect the pore structure of acid-etching films formed on these surfaces. The experiments undertaken for this purpose were carried out with powders and polished specimens made from the same piece of TK-16 glass (pot-melted, of factory manufacture); this glass (heavy borosilicate crown containing considerable amounts of barium oxide) is among the optical glasses of the lowest chemical stability.

The 200-270 mesh powder fraction (average grain size 60 μ) was washed free of adhering fine particles by decantation with dry alcohol, and dried in a thermostat at 120°. To form the film, the powder was treated with 0.1 N aqueous acetic acid solution at 25° for 4 minutes.* At the end of that time the acid was quickly poured off and the powder was thoroughly washed first with distilled water and then with alcohol and dried for 2 hours at 120°; it was then used for the adsorption experiments. Freshly polished cubes were etched under the

* Calculations based on quantitative determination of barium dissolved out of the glass under these conditions showed that the thickness of the film formed should be about 1000 A.

same conditions for the time needed to form films of the required thickness. The film thickness was determined by investigation of the elliptical polarization of reflected light [1] and calculated by Obreimov's method [8].

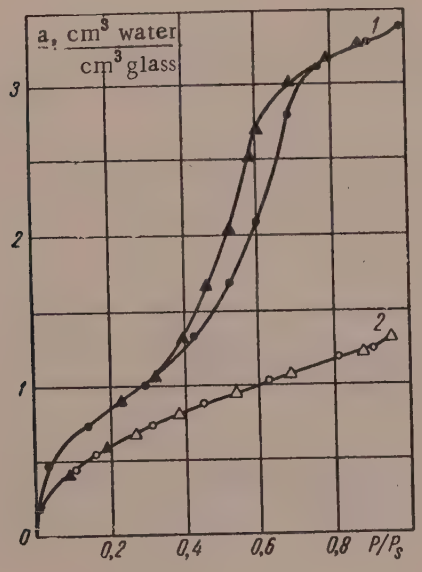


Fig. 1. Isotherms for adsorption of water on etching films formed on TK-16 glass powder: 1) Freshly prepared glass powder; 2) glass powder after 2.5 months of storage.

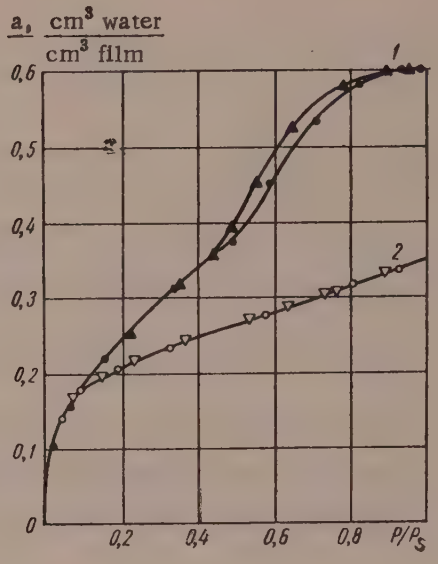


Fig. 2. Isotherms for adsorption of water on etching films formed on polished surfaces of TK-16 glass: 1) Glass surface treated with alkali solution after polishing; 2) freshly polished glass surface.

In the first experiments, freshly prepared powders and freshly polished specimens were subjected to acid etching. Isotherms for adsorption of water vapor on these films are given in Figs. 1 and 2. The adsorption isotherm for the film formed on the powder had a hysteresis loop (Fig. 1, Curve 1), whereas the isotherm for the film of a polished specimen (Fig. 2, Curve 2) did not have such a loop.

To elucidate the nature of this distinction, it was necessary to reduce the surfaces of the polished specimen and the powder to a similar state. This was achieved, on the one hand, by formation of a "natural" silica film on the TK-16 glass powder, which brought its surface state nearer to that of polished specimens. On the other hand, the film was removed from the surface of the polished specimens by means of alkali solution, which brought their surface state nearer to the surface of freshly powdered glass. Experiments were carried out with films made by acid etching of freshly polished specimens of TK-16 glass, treated with alkali solution (0.5 N NaOH at 20° for 10 minutes) to remove the surface silica film, and with etching films formed on powder from the same glass, stored after the powdering for 2.5 months with access of atmospheric air, the moisture of which corrodes the surface of the unstable glass and forms the above-mentioned silica film on its surface. The adsorption isotherms obtained in experiments with these films, given in Figs. 1 and 2, provide convincing evidence of the strong influence of the surface silica film on the structure of the forming acid-etching films. The presence of a "natural" silica film on the surface of TK-16 glass, both in powder form (Fig. 1, Curve 2), and on polished specimens (Fig. 2, Curve 2), leads to formation of an acid-etching film with such small pores that the isotherms for adsorption of water do not have hysteresis loops. Since the smallest pore radius in films on glass, recorded from the position of the hysteresis loop, is 8 A [9], it may be assumed that the pore radius of the investigated films is less than 8 A.

On the other hand, if there is no "natural" film on the glass surface, the films formed both on the powder (Fig. 1, Curve 1) and on polished specimens (Fig. 2, Curve 1), as the result of acid etching have considerably larger pores and yield water-adsorption isotherms with pronounced hysteresis loops. The pore radius is found to be similar in the two cases; 18-20 A for the powder and 21 A for the polished specimen. The thickness of the etching film formed on a freshly polished surface (i.e., in presence of the silica film) was 900 A, while on a surface "cleared" by alkali it was 1160 A.

Because of the absence of direct data on the thickness of films on powders, it is not possible to make a quantitative comparison between the isotherms for adsorption of water by films on powders and on polished specimens with similar initial surface states. Therefore the foregoing data are not evidence of quantitative agreement between the isotherms for adsorption on etching films on powders and on polished specimens, respectively, and therefore of exact similarity of their pore structures. The results refer to a similarity in the type and character of the isotherms, i.e., a qualitative likeness of the pore structures of etching films on powders to those on polished glass surfaces which both have (or do not have) "protective" silica films on their surfaces.

The results of these experiments can be regarded as proving the regulating influence of the primary ("natural") thin silica film on the pore structure of the thicker films formed on glass surfaces during acid etching.

SUMMARY

1. A study was made of the adsorption of water vapor on acid-etching films on polished specimens and powders of the unstable TK-16 glass, of the heavy crown type.

2. If a thin primary silica layer is present on the surface of the glass, acid etching leads to formation of microporous films with pores less than 8 A in radius.

3. In absence of a primary silica layer, acid etching of a glass surface leads to formation of films with pores about 20 A in radius and of a total volume which is nearly double that in films of about the same thickness, formed on specimens which had a primary silica film.

We thank K. S. Evstrop'ev for a number of valuable comments in the course of this work and in discussion of the results.

LITERATURE CITED

[1] I. V. Grebenshchikov, A. G. Vlasov, B. S. Neporent, and N. V. Suikovskaya, Clarification of Optical Glass [In Russian] (State Technical Press, 1946).

[2] I. V. Grebenshchikov and T. A. Favorskaya, Tr. Gosudarstvennogo Opticheskogo In-ta 7, 72 (1931).

[3] N. F. Timofeeva, Zhur. Éksper. Teoret. Fiz. 6, 71 (1936); Opt-Mekh. Prom. 9 (1937).

[4] S. P. Zhdanov, Collection: To the Memory of Academician I. V. Grebenshchikov, Tr. Gosudarstvennogo Opticheskogo In-ta 24, 145, 210 (1956).

[5] L. S. Yastrebova, Collection: to the Memory of Academician I. V. Grebenshchikov, Tr. Gosudarstvennogo Opticheskogo In-ta 24, 145, 172 (1956).

[6] L. S. Yastrebova and V. S. Molchanov, Zhur. Priklad. Khim. 31, 1628 (1958).*

[7] D. P. Dobychin and A. K. Pogodaev, Zhur. Fiz. Khim. 32, 2637 (1958).

[8] I. V. Obreimov, Zhur. Éksper. Teoret. Fiz. 14, 431 (1944).

[9] D. P. Dobychin, The Structure of Glass [In Russian] (1955), p. 318.

*Original Russian pagination. See C. B. translation.

LETTERS TO THE EDITOR

EFFECT OF THE THICKNESS OF THE SUPPORT ON THE FORCE OF DETACHMENT

V. A. Alekseeva, E. É. Karasik, and L. V. Korchagin

Artem Mining Institute, Dnepropetrovsk

Translated from: Kolloidnyi Zhurnal Vol. 22, No. 2, pp. 247-249, March-April, 1960

Original article submitted June 23, 1959

Freezing of coal, ores, and rocks to trolleys, railroad cars, dump cars, and truck bodies greatly complicates winter transport, as it involves additional labor for detaching the loads and increases standstill times.

We undertook an investigation in search of materials for lining the working surfaces of transport equipment in order to weaken the force of adhesion of frozen loads.

Samples of coal and rocks (0-1 mm grade, containing 25% moisture) were frozen at -9 or $-10°$ for 4 hours on the surfaces of various materials. The force required to detach the adhered materials was determined by means of the Michaelis lever instrument for extension and adhesion tests.

The adhesion area was 25 cm^2 in all the experiments; this was ensured by the use of a template. The thickness of the cake of wet raw material was 12 mm.

Average Force Required to Detach Frozen Coal from Various Materials*

Material	Thickness of material, mm	Detachment force, g/cm^2	Material	Thickness of material, mm	Detachment force, g/cm^2
Wood	2	250	Ebonite	2	30
	5	730		5	190
	14	>2000	Plexiglass	2	55
Iron	2	330		5	280
	5	800	Polyvinyl chloride	2	22
	10	>2000		5	130
Aluminum	2	130		10	420
	5	330	Polytetrafluoro-ethylene	2	15
				5	80
				10	300

* The experimental error did not exceed 8%.

Average values of the force required to detach frozen coal from various materials are given in the table.

The table shows that coal was frozen least firmly to polytetrafluoroethylene and polyvinyl chloride. It was also found that the bonding of coal by freezing increases with the thickness of the supporting material. This applies both to polished and to rough surfaces.

In studies of the freezing of various rocks to supports, the detachment forces were found to be approximately the same as in the case of coal.

When the initial thickness of the cake of coal or rock was increased from 12 to 24 and 36 mm the force of detachment remained almost without change.

It may be concluded from these results that in adhesion by freezing the decisive role is played by the material and thickness of the support, rather than by the material of the load.

The paradoxical relationship between the force of detachment and the support thickness can be explained on the assumption that in detachment from thin materials the latter are first subjected to bending deformation, so that the detachment proceeds nonuniformly over the contact area. Evidently, in such cases, a smaller force is needed for detachment than with thick supports, when the detachment occurs simultaneously over the whole contact area.

Similar results were obtained by Polyakov [1]. In bonding of a vinyl resin film to steel 2.28 mm thick, the force of adhesion was 25-30 kg/cm^2, whereas in bonding of vinyl resin to steel 4.3 mm thick, the force was 50-60 kg/cm^2.

To test the influence of water repellency of the surface on the freezing of coal and rocks to it, wetting of the different materials was investigated by measurements of the contact angle.

No correlation could be found between the force of attachment by freezing and the contact angle. This confirms the findings of Kobeko and Marei [2], according to whom water repellency of a surface is not a measure of the force of attachment by freezing of various substances to it.

The absence of any such correlation can be explained in terms of the electrical theory of adhesion advanced by Deryagin and Krotova [3].

Freezing of wet coal and rocks to various materials is caused by electrostatic attraction of the charges of the electric double layer formed at the ice-material interface. To separate the double layer, work must be done against the electrostatic forces. This work may be greater by several orders of magnitude than the work for separation of the surfaces at thermodynamic equilibrium, which is related to the contact angle by the Young-Dupré thermodynamic equation.

The Young-Dupré equation is inapplicable to nonequilibrium work or to the force of detachment. It is not surprising that the latter is not correlated with the contact angle.

In bonding of plastics 2-3 mm thick to iron the force required to detach frozen material increased 6-10-fold owing to the formation of a thickened metal-adhesive-plastic system and a decrease of the bending deformation.

When plastics were attached mechanically to iron (without adhesive) the force of detachment remained unchanged.

We thank Corresponding Member. Academy of Sciences, USSR B. V. Deryagin for reading the manuscript and for a number of valuable comments.

LITERATURE CITED

[1] K. A. Polyakov, Nonmetallic Chemically Resistant Materials [In Russian] (State Chemistry Press, 1952).

[2] P. P. Kobeko and F. I. Marei, Zhur. Tekh. Fiz. 12, 3, 277 (1946).

[3] B. V. Deryagin and N. A. Krotova, Doklady Akad. Nauk SSSR 61, 5, 849 (1948); Uspekhi Fiz. Nauk 38, 3, 387 (1948); Adhesion [In Russian] (Acad. Sci. USSR Press, Moscow, 1949); B. V. Deryagin, Vestnik Acad. Sci. USSR 7, 10 (1954).

MAXIMUM STRESS IN DEFORMATION AT A CONSTANT RATE

I. I. Gol'berg

Scientific Research Institute of Rubber and Latex Products, Moscow

Translated from: Kolloidnyi Zhurnal Vol. 22, No. 2, pp. 249-251, March-April, 1960

Original article submitted March 16, 1959

The causes of the occurrence of a stress maximum in deformation of a structurized liquid at a constant rate have been discussed by several scientists [1]. Two explanations of the effect have been offered: a stress maximum occurs either because a constant deformation rate is not attained instantaneously, or because of breakdown of the liquid structure during deformation. Explanation of this effect is important in relation to mechanical tests on a wide range of polymeric materials (such as rubbers, raw rubber stocks, etc.), and therefore a third explanation, which differs significantly from those mentioned, is offered below.

It has been shown [2] that simple Maxwellian liquids (the mechanical model of which consists of a spring and piston in series) cannot have a stress maximum at constant rate, which becomes established over a period of time, rising steadily from zero to the maximum value. This is also valid for more complex Maxwellian liquids. It follows that the first explanation is inapplicable to Maxwellian liquids.

However, a case is possible when a Maxwellian liquid (with the exception of a simple one) has a stress maximum in deformation at constant rate without breakdown of the structure. This can be shown most simply with a mechanical model. Let us consider a four-element model consisting of two Maxwell models joined in parallel (Fig. 1). Let τ_1 be the relaxation time in the first branch of the model, and τ_2 the relaxation time in the second branch, such that $\tau_1 > \tau_2$. A fairly rapid extension deformation is applied to the model and maintained until the stress in the second branch falls to a fairly small value (regarded as zero for practical purposes). Since $\tau_1 > \tau_2$, a certain stress still remains in the first branch. By repeating the stress and holding cycles we can accumulate a tensile stress, denoted by $2\sigma_0$, in the first branch. If the model is now released, the extended spring E_1 instantly contracts, causing compression of the spring E_2. Inertia forces are disregarded, and therefore contraction of spring E_1 ceases when spring E_2 has contracted down to stress σ_0. During this process, the pistons remain stationary because the deformation is instantaneous. The total stress on the model is zero,

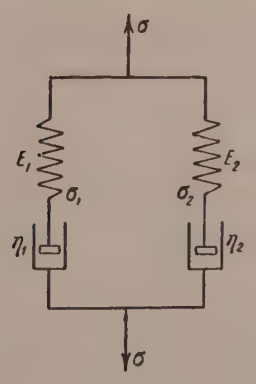


Fig. 1

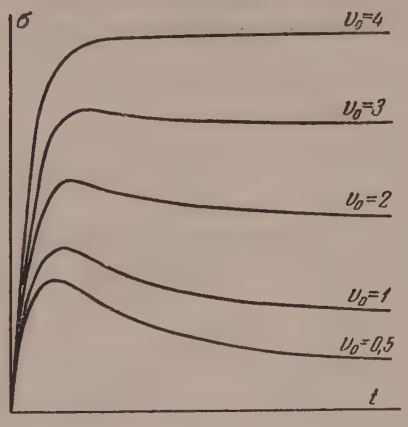


Fig. 2

but the model is "charged" with an internal stress σ_0.* This instant is taken as the zero time in subsequent deformation at constant rate.

A process similar to that described takes place, for instance, in mastication of raw rubber stocks. An internal stress may also arise when a narrow annular gap in a rotational viscosimeter is filled. It follows that an internal stress does not arise "ad hoc."

The equation for a four-element model is of the form

$$\frac{d^2\sigma}{dt^2}+\left(\frac{E_1}{\eta_1}+\frac{E_2}{\eta_2}\right)\frac{d\sigma}{dt}+\frac{E_1E_2}{\eta_1\eta_2}\sigma=(E_1+E_2)\frac{d^2\varepsilon}{dt^2}+E_1E_2\left(\frac{1}{\eta_1}+\frac{1}{\eta_2}\right)\frac{d\varepsilon}{dt}.$$

In deformation at constant rate $d\varepsilon/dt=v_0$, $d^2\varepsilon/dt^2=0$, and therefore

$$\frac{d^2\sigma}{dt^2}+\left(\frac{E_1}{\eta_1}+\frac{E_2}{\eta_2}\right)\frac{d\sigma}{dt}+\frac{E_1E_2}{\eta_1\eta_2}\sigma=E_1E_2\left(\frac{1}{\eta_1}+\frac{1}{\eta_2}\right)v_0. \tag{1}$$

The initial conditions are

$$\sigma=0,\ \sigma_1=-\sigma_2=\sigma_0,\ \text{at}\quad t=0, \tag{2}$$

where σ_1 is the stress in the first branch; σ_2 is the stress in the second branch. The solution of Eq. (1) for the initial conditions (2) is

$$\sigma=v_0\left[\eta_1(1-e^{-k_1t})+\eta_2(1-e^{-k_2t})\right]+\sigma_0(e^{-k_1t}-e^{-k_2t}), \tag{3}$$

here $k_1=\frac{1}{\tau_1}=\frac{E_1}{\eta_1}$, $k_2=\frac{1}{\tau_2}=\frac{E_2}{\eta_2}$

and, by the condition assumed earlier, $k_1 < k_2$.

When $v_0 = 0$, we derive from Eq. (3) an equation for the stress σ_0 in free "dissipation" of the initial stress

$$\sigma=\sigma_0(e^{-k_1t}-e^{-k_2t}). \tag{4}$$

The time to reach the maximum stress σ with free "dissipation" of the initial stress is

$$t^*=\frac{1}{k_2-k_1}\ln\frac{k_2}{k_1}. \tag{5}$$

In this case the time t^* is independent of σ_0, which is characteristic of linear systems. It follows from Eq. (4) that with short relaxation times (i.e., high values of k_1 and k_2) the initial stress σ_0 is rapidly "dissipated" and therefore cannot influence the total stress σ in subsequent deformation. The situation is different for substances with long relaxation times, such as bitumen or rubber stocks.

When $v_0 \neq 0$ the time required to reach the total stress maximum is given by the equation

$$t^*=\frac{1}{k_2-k_1}\ln\left(\frac{k_2}{k_1}\frac{\sigma_0+\eta_2v_0}{\sigma_0-\eta_1v_0}\right). \tag{6}$$

When the deformation rate reaches the value $v_0 = \sigma_0/\eta_1$, the time $t^* = \infty$, and therefore the stress σ must have a maximum at $v_0 < \sigma_0/\eta_1$ and does not have a maximum at $v_0 \geq \sigma_0/\eta_1$.

* The terms "extension" and "compression" commonly used in descriptions of the action of mechanical models have conventional significance. The stress and deformation considered here may be of any kind: extension, compression, or shear.

Curves calculated in accordance with Eq. (3) (Fig. 2) are in satisfactory qualitative agreement with the experimental curves given in [3]. The reservation must be made that the foregoing theory is applicable only within the validity limits of the superposition principle (linear theory).

To the best of the author's knowledge, the concept of a "charged" mechanical model is used here for the first time. It may possibly have applications in other cases.

LITERATURE CITED

[1] N. V. Mikhailov, Kolloid. Zhur. 17, 68 (1955)*; A. A. Trapeznikov, Kolloid. Zhur. 18, 496 (1956); G. V. Vinogradov and V. P. Pavlov, Kolloid. Zhur. 20, 248 (1958).

[2] I. I. Gol'berg, Present State of the Mathematical Theory of Mechanical Behavior of High Polymers [In Russian] (in the press).

[3] A. A. Trapeznikov and G. V. Assonova, Kolloid. Zhur. 20, 398 (1958).*

* Original Russian pagination. See C. B. translation.

PREPARATION AND ADSORPTION PROPERTIES OF A SYNTHETIC ZEOLITE

I. E. Neimark, M. A. Piontkovskaya, A. E. Lukash,
and R. S. Tyutyunnik

L. V. Pisarzhevskii Institute of Physical Chemistry, Academy of Sciences,
Ukr. SSR, Kiev

Translated from: Kolloidnyi Zhurnal Vol. 22, No. 2, pp. 251-252, March-April, 1960

Original article submitted November 17, 1959

Synthetic zeolites (molecular sieves) are crystalline aluminohydrosilicates of sodium, calcium, etc.; they have channels of strictly definite dimensions, which can be penetrated only by molecules of small size, and are impermeable to larger molecules. Because of their pronounced polarity, zeolites have especially high affinity for water, unsaturated hydrocarbons, carbon monoxide, etc. One of the most valuable properties of molecular sieves is their ability to adsorb large amounts of substances present in low concentrations and at high temperatures [1, 2]; they can also be used as highly effective drying agents and for extraction of ethylene, propylene, acetylene, and other hydrocarbons from petroleum gases and from waste gases in chemical plants.

Synthetic zeolites are not made in the USSR, and there has been no published work on their synthesis and properties.

We synthesized samples of crystalline sodium aluminosilicate by a nonhydrothermal method (in contrast to the methods described in the foreign patent literature), and studied their sorption isotherms for water vapor and carbon dioxide.

X-ray studies showed that our samples were identical in structure to the American zeolites 4A and 5A.

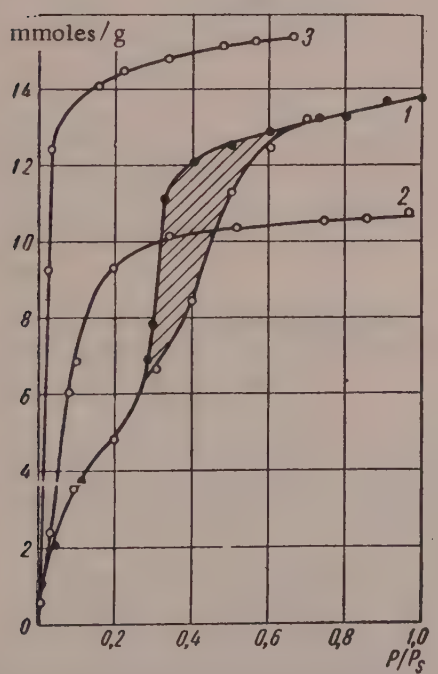


Fig. 1. Isotherms for sorption of water vapor by silica gel (1) American zeolite (2), and synthetic zeolite (3).

It is clear from Fig. 1 that the isotherm for sorption of water vapor by zeolites is almost rectangular; adsorption is practically complete at extremely low relative water-vapor pressures. The activity of zeolite with respect to water vapor at low values of p/p_s is 5 to 6 times the activity of silica gel. Because of this, substances can be dried to a higher degree than by means of existing adsorbents.

Figure 2 shows that the adsorption capacity of the zeolite samples for carbon dioxide is many times as high as that of silica gel, and somewhat higher than that of American zeolite 4A.

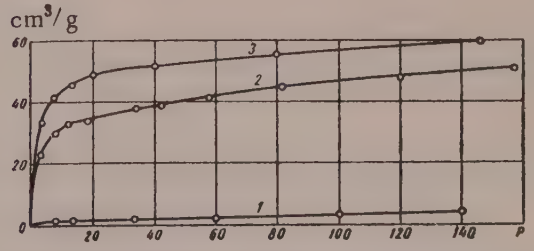


Fig. 2. Isotherms for sorption of carbon dioxide by silica gel (1), American zeolite (2), and synthetic zeolite (3).

Our synthetic sodium aluminosilicate samples can be used as starting materials in production of a range of artificial zeolites with different sorptional properties, which may be widely used in the chemical, petroleum, pharmaceutical, gas, and other industries.

LITERATURE CITED

[1] R. M. Barrer, Brenstoff-Chemie 35, 21/22 (1954).

[2] R. M. Barrer, Brit. Chem. Engng. May (1959).

STRUCTURE AND PROPERTIES OF VULCANIZATES FROM CARBOXYL-CONTAINING POLYMERS MADE BY THE SIMULTANEOUS ACTION OF METAL OXIDES AND IONIZING RADIATION

Z. N. Tarasova, B. A. Dogadkin, M. I. Arkhangel'skaya, and S. B. Petrova

Scientific Research Institute of the Tire Industry, Moscow

Translated from: Kolloidnyi Zhurnal Vol. 22, No. 2, pp. 253-255, March-April, 1960

Original article submitted November 9, 1959

Vulcanization of carboxyl-containing rubbers by means of metal oxides yields unfilled vulcanizates of high strength but low thermomechanical endurance, so that these vulcanizates begin to flow even at approximately 70°.

Studies of stress relaxation in butadiene-styrene copolymers containing from 1.25 to 10.9% methacrylic acid, vulcanized by means of calcium hydroxide, showed (see table) that the relaxation rate constant decreases with increase in the number of carboxyl groups in the chain, but remains 50-100 times the corresponding values for sulfur-vulcanized butadiene-styrene rubbers [1].

It is noteworthy that, in contrast to sulfur vulcanizates, the density of the vulcanization network in these vulcanizates of a carboxylated rubber remains almost unchanged during relaxation. In the case of butadiene polymer, the maximum swelling decreases owing to thermooxidative structure formation under relaxation conditions.

Salt-type bonds in vulcanized carboxylated rubbers are easily disrupted during swelling in organic solvents with added acetic acid [2], so that they dissolve completely under such conditions.

Investigation of changes in the osmotic and viscosimetric properties of solutions of raw mixes and vulcanizates before and after completion of the relaxation process, down to almost zero stress at 100°, showed that the molecular weight does not alter appreciably during relaxation. This observation, in conjunction with the above-mentioned fact that the cross-link content remains unchanged during relaxation, leads to the conclusion that the stress decrease during relaxation of vulcanized carboxylated rubbers containing cross links of the salt type is caused by breakdown of the latter and formation of equal amounts of new bonds as the result of exchange reactions.

Similar regrouping of bonds probably takes place in other thermomechanical processes under static and dynamic influences and during use of rubbers of this type, and is the cause of the good mechanical properties at relatively low temperatures.

The low thermomechanical stability of salt-type bonds necessitates additional introduction of stable bonds into the vulcanization network; this is usually achieved by combined vulcanization by means of metal oxides and tetramethylthiuram disulfide. However, this causes a considerable decrease in the strength characteristics (down to 100 kg/cm^2 in the case of unfilled vulcanizates).

Very interesting results were obtained by two-stage (stepwise) vulcanization by irradiation of preheated carboxylated rubbers (vulcanized by metal oxides) by means of a Co^{60} source at relatively low doses of 5 to 10 Mr. The resultant formation of a small number of $-C-C-$ cross links (approximately 1 per 1000 monomer units) gives vulcanizates of high thermomechanical endurance and strength. Whereas specimens vulcanized by metal oxides flow at 100° before irradiation, after irradiation with doses of 10 Mr the same specimens relax at a rate approximating to the relaxation rate of butadiene-styrene vulcanizates with sulfenamide accelerators,

Properties of Carboxylated Rubbers Vulcanized by Calcium Hydroxide (120 minutes at 150°)

Monomer type	Carboxyl group content, %	Tensile strength, kg/cm²	Modulus at 300%, kg/cm²	Relative elongation %	Relaxation rate constant at 100° and 40% $\epsilon \times 10^2$	Maximum swelling in toluene, % before relaxation	Maximum swelling in toluene, % after relaxation	Raw mixture $\eta_{sp/c}$ $c \to 0$	Raw mixture mol. wt.	Vulcanizate before relaxation $\eta_{sp/c}$ $c \to 0$	Vulcanizate before relaxation mol. wt.	Vulcanizate after relaxation $\eta_{sp/c}$ $c \to 0$	Vulcanizate after relaxation mol. wt.
Butadiene 70% and styrene 30%	0,65	160	31	920	Specimens flow	2260	2260	1,5	130 000	1,6	143 000	1,54	138 000
	0,65*	442	40,7	776,4	0,043	595	601	—	—	Insoluble			
	1,70	520	119	672	3,85	531	495	—	52 600	—	—	—	—
	3,00	339	183	565	1,20	424	429	0,82	—	1,09	80 600	1,04	75 300
	5,70	374	334	320	0,50	180	180	—	—	—	—	—	—
Butadiene	0,77	210,3	79,7	624	0,36	815	685	1,72	160 000	2,2	230 000	Insoluble	
	2,5	306	203	404	0,055	378	318	1,63	147 000	1,94	192 000	—	—

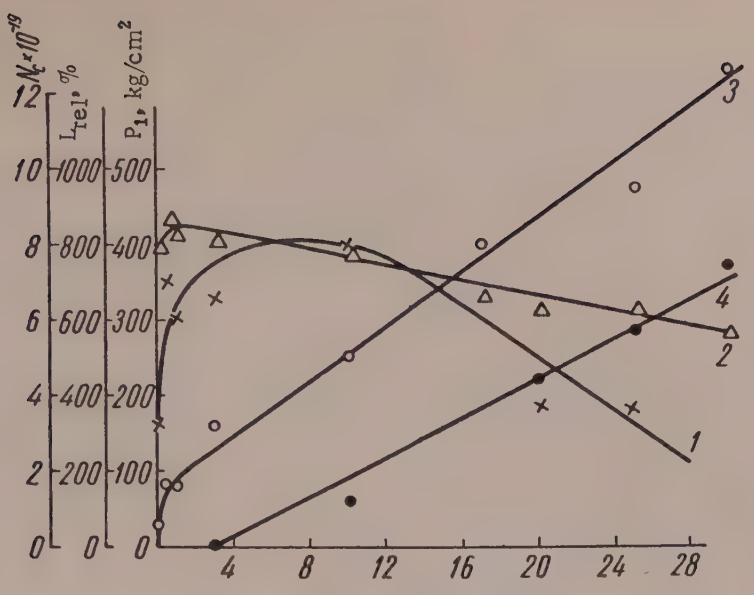
* After irradiation with Co^{60}, dose 10 Mr.

with a network density of $2 \cdot 10^{20}$ ml^{-1} (roughly one bond per 50 monomer units). The strength of such vulcanizates is over 400 kg/cm².

Comparison of data on the swelling of vulcanizates in pure solvent and in solvent with added acetic acid showed that when a carboxylated rubber previously heated with metal oxides is irradiated, the formation of stable bonds which are not broken down by acid is accompanied by formation of new bonds which break down during swelling in solvent containing acid. These bonds have a significant effect on the vulcanizate properties, and in particular on the strength (see figure). Vulcanizates formed by irradiation of carboxylated rubbers (without metal oxides) swell both in pure toluene and in toluene containing acetic acid to the same maximum value; this shows that when rubbers are irradiated without metal oxides, no bonds other than normal chemical ones are formed.

It follows that carboxylated rubber vulcanizates containing salt-type bonds and a thin network of stable $-C-C-$ bonds have high strength characteristics together with high thermomechanical endurance, which makes this type of rubber very promising for technical purposes. Rubbers of this type can be made not only by a two-stage vulcanization process by preliminary heating with metal oxides and other salt-forming compounds and subsequent treatment by ionizing radiation, but also by simultaneous application of these treatments.

Our observations concerning the influence of the structure of carboxylated rubber vulcanizates on their strength characteristics are general in character, and are of undoubted interest in relation to the formulation of the factors which determine the strength of cross-linked polymers [3]. The latter have high strength when, in addition to a relatively thin and uniform network of stable chemical bonds, they contain a network of less stable and easily regrouped bonds, redistribution of which favors dissipation of local excessive stresses which lead to formation and development of sites of polymer degradation.



Variations of the properties of SKS30-1 carboxylated rubber, vulcanized by means of calcium hydroxide, with the dose of irradiation by Co^{60}. The rubber contained 0.65% carboxyl groups: 1) Tensile strength (P_1); 2) relative elongation (L_{rel}); 3) total content of cross links (in ml); 4) content of cross links (in ml) not broken down by the action of acid.

LITERATURE CITED

[1] B. A. Dogadkin and Z. N. Tarasova, Kolloid. Zhur. 15, 347 (1953).*

[2] W. Cooper, J. Polymer Sci. 28, 195 (1958); I. Poddubnyi, E. Érenburg, and E. Starovoitova, Doklady Akad. Nauk SSSR 535 (1958).*

[3] B. A. Dogadkin, Z. N. Tarasova, M. Ya. Kaplunov, V. L. Karpov, and N. A. Klauzen, Kolloid. Zhur. 20, 260 (1958).*

* Original Russian pagination. See C. B. translation.

ADSORPTIONAL LOWERING OF THE STRENGTH OF QUARTZ AND RUBY IN SOLUTIONS OF NEUTRAL ELECTROLYTES

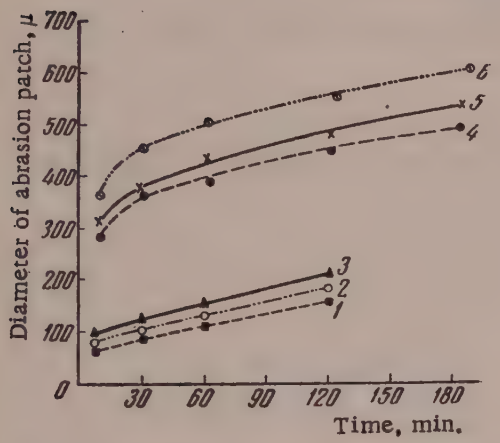
G. I. Fuks

Scientific Research Institute of the Horology Industry, Moscow

Translated from: Kolloidnyi Zhurnal Vol. 22, No. 2, pp. 256-258, March-April, 1960

Original article submitted August 10, 1959

Adsorption lowering of the strength of solids in surface-active media, discovered by Rebinder [1], has been studied in detail for metals [2] and for some nonmetallic materials (glass [3], graphite [4], and others [5]). Investigations carried out in our laboratory on microhardness (by means of the PMT-3 instrument [6]) and wear (by means of a modification of the four-ball tribometer [7]) of crystalline quartz and synthetic ruby (Al_2O_3 colored by 1.5% Cr_2O_3 and 0.004% TiO_2) showed that these minerals lose strength in water and in aqueous solutions of neutral electrolytes (see table and figure). Before the determinations, the surfaces of the mineral specimens were polished down to grade 13-14 surface finish and, for removal of surface-active substances, repeatedly washed by distilled solvents and rubbed over with activated carbon; in some control experiments the specimens were additionally heated under vacuum for 2 hours at 340-370°.



Wear of minerals by friction in water and electrolyte solutions. Minerals: 1, 2, and 3) ruby (contact pressure 375 kg/mm^2); 4, 5, and 6) quartz (contact pressure 95 kg/mm^2). Media: 1 and 4) H_2O; 2 and 5) 0.05 N KCl; 3) 0.05 N $K_4Fe(CN)_6$; 6) 0.05 N $Th(NO_3)_4$.

The effect (strength lowering) increases with increasing time of contact between the minerals and solvents, and the influence of solution concentration and nature of the ions can be established only after 30-45 minutes, but after 6-10 hours, the magnitude of the effect becomes stabilized. For example, the microhardness of one ruby specimen in 0.5 N KCl solution was 2050 kg/mm^2 after 10 minutes and 1640 kg/mm^2 after 18 hours of contact, while the diameter of the abrasion patch on quartz (abrasion time 5 minutes at a linear velocity of 0.54 cm/sec and total pressure 2.1 kg) was 210 μ after 30 minutes of preliminary exposure to 0.05 N KCl solution, and 229 μ after 60 minutes.

The magnitude of the effect increases with solution concentration and the charge of the ions, i.e., with increasing adsorption. An interesting fact is that the sign of the ionic charge does not appear to be of significance. The adsorption mechanism is also confirmed by reversibility of the process; after removal of the salt solutions, washing, and drying, the mineral specimens regain their original microhardness in air.

Microhardness (kg/mm^2) of Quartz and Ruby Specimens After Contact with Water and Aqueous Electrolyte Solutions for 1 Hour

Minerals	Air	Water	0,005*N* KCl	0,05*N* KCl	0,5*N* KCl	0,05*N* $CaCl_2$	0,05*N* K_2SO_4	0,05*N* $Th(NO_3)_4$	0,05*N* $K_4Fe(CN)_6$
Quartz	1170	1130	1010	980	930	910	910	900	900
Ruby	2270	2110	2090	2010	1960	1950	1940	1540	1660

The results of the experiments are of practical significance in relation to easier working of technical precision jewels. The observed changes in the hardness and wear resistance of inert and chemically homogeneous minerals illustrate the widespread occurrence of the adsorptional lowering of strength of solids and show that development of microcracks, which weaken brittle bodies, may be caused by adsorption of ions as well as by adsorption of surface-active substances [8].

LITERATURE CITED

[1] P. Rebinder, Z. Phys. 72, 191 (1931); P. A. Rebinder and N. A. Kalinovskaya, Zhur. Tekh. Fiz. 2, 726 (1932); P. A. Rebinder, Izvest. OMEN Akad. Nauk SSSR, ser. khim. 25, 639 (1936).

[2] V. I. Likhtman, P. A. Rebinder, and G. V. Karpenko, Influence of Surface-Active Media on Processes of Metal Deformation [In Russian] (Acad. Sci. USSR Press, 1954).

[3] M. S. Aslanova, Doklady Akad. Nauk SSSR 95, 1215 (1954); M. S. Aslanova and P. A. Rebinder, Doklady Akad. Nauk SSSR 96, 299 (1954).

[4] E. B. Matskevich and P. Yu. Butyagin, Kolloid. Zhur. 20, 665 (1958).*

[5] P. A. Rebinder, Physicochemical Mechanics [In Russian] ("Knowledge" Press, 1958).

[6] M. M. Khrushchev and E. S. Berkovich, The PMT-2 and PMT-3 Instruments for Microhardness Testing [In Russian] (Acad. Sci. USSR Press, 1950).

[7] G. I. Fuks, Zavodskaya Lab. 5, 594 (1956).

[8] G. V. Bartenev, I. V. Yudina, and P. A. Rebinder, Kolloid. Zhur. 20, 654 (1958);* E. D. Shchukin and P. A. Rebinder, Kolloid. Zhur. 20, 645 (1958).*

* Original Russian pagination. See C. B. translation.



NIKOLAI FEDOROVICH ERMOLENKO

(On his 60th Birthday and Completion of 36 Years of Scientific, Teaching, and Social Activity)

G. L. Starobinets and A. S. Barkan

Translated from: Kolloidnyi Zhurnal Vol. 22, No. 2, pp. 259-260, March-April, 1960

On January 29, 1960, the scientific community of Belorussia honored the eminent scientist, one of the pioneers of chemical science in the Belorussian SSR, Academician of the Academy of Sciences of the Belorussian SSR, Professor Nikolai Fedorovich Ermolenko.

He was born in a middle-class peasant family in the village of Klyukovka, Orshanka region, Vitebsk province. After successfully graduating at the 2nd Moscow University he worked from 1924 in the Department of General and Inorganic Chemistry of the University of Belorussia, and since 1930 to the present day, he has been head of this department. In 1932 Ermolenko organized the Colloid Laboratory of the Academy of Sciences, Belorussian SSR, of which he is still the head.

The range of his scientific interests is very wide and varied. In addition to researches in the fields of colloid chemistry, physical chemistry of high polymers, and adsorption from solutions, which are the main trends of his scientific research activity, he and his pupils have carried out serious investigations in general, inorganic, and applied chemistry, and also in the history of chemistry; the total comprises over 200 investigations.

Only the most important of his results can be mentioned here. In studies of thixotropy, Ermolenko discovered the effect of sedimentational thixotropy. As the result of studies of the swelling of high polymers in mixed media, Ermolenko and his associates demonstrated the dependence of swelling on the polarity of the medium, discovered the temperature hysteresis of swelling, carried out a very detailed investigation of the influence of added polar components on the occurrence of maxima and minima on swelling isotherms, and derived an original equation for the kinetics of swelling.

A series of investigations by Ermolenko and his co-workers is concerned with the mechanism of the action of inhibitors on oxidation of rubbers, effect of polymers on the solubility of metals and the oxidation of cellulose by halogens, and the influence of solvents on the solution state of cellulose derivatives; he also showed that the optical properties of colloidal systems change continuously in sol-gel and gel-sol transitions.

An extensive series of researches of Ermolenko and his co-workers is devoted to studies of adsorption from mixed media. In this work, the influence of polarity of the medium on the course of adsorption from solutions on carbon, mineral, and mixed adsorbents was established. At the same time the general relationship between solubility and adsorption of various substances was determined, and the influence of structure, nature, and position of substituents on adsorption of substances from homogeneous and mixed media was elucidated. In particular, it was shown that decreasing electronegativity of substituent groups in the molecules of aromatic acids favors increasing adsorption, and a relationship was established between the degree of adsorption, dipole moments of the substituent groups, and the dissociation constants of the acids.

In the course of these investigations, it was shown that suitable activation conditions can yield lignin and peat charcoals which are not inferior in activity to the best decolorizing wood charcoals.

During the Patriotic War Ermolenko (together with E. N. Novikova) carried out important work on adsorptive removal of sulfur compounds from petroleum. During the postwar years, a method for adsorptive purification of antibiotics and other medicinals was developed and introduced into practice.

He has given much effort and energy to providing a scientific and technological basis for the development of a number of branches of the chemical industry of the Belorussian SSR.

A talented teacher and eminent organizer of scientific research, Ermolenko has trained numerous chemists and has created a scientific school, members of which are successfully developing chemical science in the Academy of Sciences Belorussian SSR., the Belorussian University, and a number of other research institutions and teaching establishments of the Republic.

Nikolai Fedorovich Ermolenko, a leading scientist and communist, combines his extensive and diverse scientific and teaching activity with active participation in the life of the community. For many years he has led the work of the Minsk Division of the Mendeleev Society, and has been a permanent member of the Minsk Regional Soviet of Workers' Deputies during the last four congresses.

For his many years of fruitful scientific, teaching, and social activity N. F. Ermolenko has received the Order of Lenin, two Orders of the Red Banner of Labor, a medal "For Valiant Labor During the Great Patriotic War," and a Diploma of Honor of the Supreme Soviet of the Belorussian SSR; he has been given the honorary title of Distinguished Scientific Worker of the Belorussian SSR.

We wish him many years of health and fruitful work for the good of our Motherland.

SIGNIFICANCE OF ABBREVIATIONS MOST FREQUENTLY ENCOUNTERED IN SOVIET PERIODICALS

FIAN	Phys. Inst. Acad. Sci. USSR.
GDI	Water Power Inst.
GITI	State Sci.-Tech. Press
GITTL	State Tech. and Theor. Lit. Press
GONTI	State United Sci.-Tech. Press
Gosenergoizdat	State Power Press
Goskhimizdat	State Chem. Press
GOST	All-Union State Standard
GTTI	State Tech. and Theor. Lit. Press
IL	Foreign Lit. Press
ISN (Izd. Sov. Nauk)	Soviet Science Press
Izd. AN SSSR	Acad. Sci. USSR Press
Izd. MGU	Moscow State Univ. Press
LEIIZhT	Leningrad Power Inst. of Railroad Engineering
LET	Leningrad Elec. Engr. School
LETI	Leningrad Electrotechnical Inst.
LETIIZhT	Leningrad Electrical Engineering Research Inst. of Railroad Engr.
Mashgiz	State Sci.-Tech. Press for Machine Construction Lit.
MEP	Ministry of Electrical Industry
MES	Ministry of Electrical Power Plants
MESEP	Ministry of Electrical Power Plants and the Electrical Industry
MGU	Moscow State Univ.
MKhTI	Moscow Inst. Chem. Tech.
MOPI	Moscow Regional Pedagogical Inst.
MSP	Ministry of Industrial Construction
NII ZVUKSZAPIOI	Scientific Research Inst. of Sound Recording
NIKFI	Sci. Inst. of Modern Motion Picture Photography
ONTI	United Sci.-Tech. Press
OTI	Division of Technical Information
OTN	Div. Tech. Sci.
Stroiizdat	Construction Press
TOE	Association of Power Engineers
TsKTI	Central Research Inst. for Boilers and Turbines
TsNIEL	Central Scientific Research Elec. Engr. Lab.
TsNIEL-MES	Central Scientific Research Elec. Engr. Lab.—Ministry of Electric Power Plants
TsVTI	Central Office of Economic Information
UF	Ural Branch
VIESKh	All-Union Inst. of Rural Elec. Power Stations
VNIIM	All-Union Scientific Research Inst. of Meteorology
VNIIZhDT	All-Union Scientific Research Inst. of Railroad Engineering
VTI	All-Union Thermotech. Inst.
VZEI	All-Union Power Correspondence Inst.

Note: Abbreviations not on this list and not explained in the translation have been transliterated, no further information about their significance being available to us. — Publisher.

A. V. DUMANSKII

(On his 80th birthday)

Translated from Kolloidnyi Zhurnal Vol. 22, No. 3, pp. 265-271, May-June, 1960

Our scientific community honors the eightieth birthday and the completion of nearly sixty years of scientific activity of Active Member of the Academy of Sciences, Ukrainian SSR, and Corresponding Member, Acad. Sci. USSR, Anton Vladimirovich Dumanskii, who was born in Ivanovo-Voznesensk on June 22, 1880.

Dumanskii started to work on colloids while still a student at the Kiev Polytechnic Institute. His first paper, concerned with a study of the properties of colloidal silver, was published in Izvestia Kievskogo Polytekh. Inst. in 1903, and since that time he has worked continuously in the colloid field, being one of the founders of Russian colloid science. He was retained at the Kiev Polytechnic Institute, and there he founded the first colloid laboratory in Russia, and in 1913 he started to give the first systematic course on the subject.

From 1903 to 1907 he was concerned mainly with research on stability of colloidal silver and ferric hydroxide solutions, and carried out detailed studies of the conditions of their coagulation by the action of electrolytes and the chemistry of interaction between colloidal particles and simple electrolyte ions. Even at that time he was not satisfied with the primitive research methods then available to science, and he started extensive application of physicochemical methods, as he considered that the time had come to abandon the view that colloids were special, indefinite systems which cannot be studied by the methods of physical chemistry.

Dumanskii's foremost achievement was the first use of collodion films as semipermeable membranes; this made investigations of colloidal systems considerably simpler. From that time collodion membranes came into general use both in dialysis and ultrafiltration of sols, and in osmotic determinations on colloidal solutions. Having developed this technique, Dumanskii carried out the first studies of distribution of simple ions between a colloidal solution and an external liquid, separated by a seimpermeable membrane, and was the first to apply the precise conductivity method to studies of this distribution. In this work it was shown that the conductivity of a simple electrolyte increases if it causes coagulation of a colloid; conversely, if the amount of added electrolyte is obviously insufficient for coagulation, its conductivity in the external liquid decreases owing to adsorption of its ions by the colloidal particles. This adsorption effect was observed in urea solutions at concentrations insufficient for coagulation of the colloidal solution. Later this method was applied extensively by the Soviet scientist A. I. Rabinovich and the Viennese research worker Pauli.

During the same period an important advance in research on colloidal solutions was Dumanskii's application of centrifugal force for determination of colloidal particle size. In 1909 he published two papers: "Influence of centrifugal force on equilibrium in a chemical system," and "Influence of centrifugal force on certain solutions." In these studies a centrifuge operating at 4000 revolutions per minute was used, and an essentially new method for determination of colloidal particle size was proposed. This work was destined to play an exceptionally important role in our time. The Swedish scientist Svedberg, on the basis of Dumanskii's work, developed a method for determining molecular weights of polymers by means of the ultracentrifuge; this is now one of the most reliable research methods, which can with every justification be given the name of the Dumanskii–Svedberg method.



A. V. Dumanskii

All the above-mentioned researches were generalized in his dissertation "On colloidal solutions" (Voronezh, 1914). This was the first dissertation on colloids in Russia.

During the subsequent years Dumanskii, now a professor, organized a large scientific laboratory for colloid research in the Voronezh Agricultural Institute; this became the center of Russian colloid science. In this laboratory he carried out very important research on the viscosity of colloid solutions, and was the first to conclude that colloidal particles are coated with solvation layers. One year later these observations were confirmed by Hatschek, and ten years after by Kruyt. This started a new trend in studies of colloid solvation, which is being followed to this day. This concluded the first 15-year period of Dumanskii's work, during which he published 24 scientific papers.

The Great October Socialist Revolution found A. V. Dumanskii in full flower of his creative effort. Being a leading scientist linked with the people in all his activities, he sprang to the defense of the victories of the revolution from its earliest days and developed extensive scientific and organizational activity. It was during the Soviet period of his work that he proved to be a leading Soviet scientist, a first-rate organizer of Soviet science, and a sensitive and attentive teacher of Soviet youth. The Colloid Laboratory of the Voronezh Agricultural Institute, which expanded during the earliest years of Soviet power, attracted young people who wished to specialize in the colloid field from many towns of the Soviet Union. Young scientists from Moscow, Leningrad, Kiev, Khar'kov, Tashkent, Novocherkassk, Perm', and other towns could be found in this laboratory. They all received a most warm welcome and attentive treatment, and all left enriched by experience of research work in the colloid field. This yearning of young people for science, which gained an outlet even in the earliest years of Soviet power, grew continuously in later years and Dumanskii was soon surrounded by a large school of young scientists working both on fundamental theoretical problems and on tasks of importance to the national economy.

Among the theoretical studies of this period attention must be drawn to a large series of researches on the chemistry of colloidal particle formation. It was first shown that vanadium pentoxide sols, containing rod-like particles, have the remarkable property of passing on dilution from the colloidal state into true solutions containing complex ions, and then into ordinary true solutions. This work demonstrated that the chemical course of sol formation consists of formation of complex ions which gradually increase in complexity, and ultimately aggregate into colloidal particles. Thus, the formation of $(MoO_3)_n$ sol may be represented as $H_2MoO_4 \rightarrow H_2MoO_4(MoO_3)_3 \rightarrow$ $\rightarrow H_2MoO_4(MoO_3)_4 \rightarrow H_2MoO_4(MoO_3)_n$ (colloidal solution), from which it is evident that the stabilizer H_2MoO_4 is present on the surface of the newly formed colloidal particle. Dumanskii confirmed this mechanism of sol formation by studies of electronegative sols of heavy-metal hydroxides in alkaline media in presence of hydroxy acids, a method for preparation of which was worked out in his laboratory. It is important to note that it became necessary in the light of these results to revise the widely accepted theories of foreign scientists—Pauli, Fajans, and others—as they were oversimplified, while the Fajans theory was also in need of revision because it was based on the concept of a crystalline structure in the colloidal nucleus, whereas in reality at the initial instant of formation this nucleus is amorphous and only gradually becomes crystalline. Another of Dumanskii's investigations, concerned with the stability of colloidal solutions, should be mentioned in this connection. The stability of an arsenic trisulfide sol was measured continuously over a period of six years, and was found to remain absolutely constant; it was thus demonstrated that even hydrophobic colloids, if completely stabilized, can be classified as completely stable in the thermodynamic sense. This period of Dumanskii's work includes the publication of his monograph: Methods for Determination of Dispersities of Sols, Emulsions, and Suspensions (1928), which contained the theoretical principles of all modern methods of particle size determination.

It is characteristic of Dumanskii as a scientist that during his entire working life he did not confine himself to purely theoretical investigations, but always sought ways to apply his knowledge to the rapidly growing industry of Soviet Russia. Thus, when Lenin raised the question of electrification of the country, it became necessary to utilize various local forms of fuel. Peat was such a fuel in the case of Moscow and the Moscow region. Since at that time peat was obtained from its deposits by the action of streams of water, it was necessary to find a fairly rapid and efficient method for removing excess water from the peat slurry. Dumanskii undertook the work on this problem, and as the result of his investigations during 1921-1922 an effective method for dewatering of peat slurry was introduced by the State Institute for the Planning of Peat Industry Plants. The results of this research were reported in the paper entitled "Colloidal properties of peat" (1926). The so-called "Russian process" proved to be the best of the various methods of peat dewatering used in the world industry.

By 1932 the Colloid Laboratory of the Voronezh Agricultural Institute had expanded so much and had become so closely linked with industry that it could no longer cope with the demands of either the rapidly growing science or of the new industry. It therefore became necessary to expand considerably the work carried out under Dumanskii's guidance. By a decision of the Soviet government, the first institute of colloid chemistry in the world was established in Voronezh in 1932, under Dumanskii. The organization of this institute played a most important role in the development of colloid science in the USSR. The main tasks of the institute were: development of new methods for physicochemical analysis of colloidal systems, and study of the mechanism of binding of water by colloid particles. During this period the Institute of Colloid Chemistry made extensive use of N. S. Kurnakov's triangular diagram method. This method had a very favorable influence on the development of several branches of colloid chemistry; on the one hand, it provided a new approach to studies of such complex effects as coagulation, peptization, and fractionation, and on the other, it made it possible to detect and correct a number of inaccuracies in earlier work in which less accurate methods had been used. Dumanskii was awarded the Grand Mendeleev Prize in 1932 for his work in this field.

The extensive researches on binding of water by colloids not only yielded results of great theoretical importance, but also led to development of simple and convenient methods for determination of bound water, which were widely adopted in several branches of industry. Dumanskii's demonstration of the role played by bound water in technological processes of the food industry was an important achievement. His methods made it possible to investigate the sugar, fermentation starch and molasses, baking, and other industries and to eliminate incorrect procedures in them. Dumanskii also demonstrated the great importance of bound water in the resistance of plants to drought and frost.

The Colloid Institute, which grew out of the Colloid Laboratory of the Voronezh Agricultural Institute, very soon became the center of colloid science in the USSR and exerted a strong scientific and organizing influence on the development of this branch of science. Dumanskii also proved a first-rate scientific organizer in his convening of conferences on colloids. The first and very narrow conference was held in 1929; it was attended mainly by Dumanskii's co-workers and by Moscow scientists: S. A. Voznesenskii, B. A. Dogadkin, S. M. Lipatov, and P. A. Rebinder. At this conference Dumanskii was already able to report on the work of his laboratory, to draw attention to the rapid growth of colloid science in our country, and to propose the foundation not only of a special institute but also of a special journal, which would help to unite all Soviet scientists working in the colloid field. In 1934 the first All-Union conference on colloids was held at the Colloid Institute in Voronezh; this was attended by an enormous number of delegates and vividly demonstrated the unprecedented growth of this branch of science in the USSR. Before that conference many Soviet colloid scientists worked separately from each other, did not exchange their research results, and published their papers in various Soviet and foreign journals.

In view of this, Dumanskii undertook organization of Kolloidnyi Zhurnal. For a long time he, as chief editor, had to do all the main work on reading and editing of the papers. During the first years of the journal he believed that his main task as editor was to devote the maximum attention to young scientists in outlying districts, who were often without guidance and who lacked confidence in their first experiments. This attention played a considerable part in attracting young scientists to participation in development of the journal and of colloid science.

It has already been stated that Dumanskii devoted a great deal of attention in the Colloid Institute to studies of the mechanism of binding of various liquids by colloids. This was a new stage in his work, which up to then had been concerned with lyophobic colloids. This new direction was not accidental. By 1930 science and industry were confronted with new problems associated with development of new types of production: artificial fibers, plastics, synthetic rubber. With his characteristic breadth of approach Dumanskii attacked the problem of synthetic polymer formation and lyophilic properties. In 1932, at the request of Academician S. V. Lebedev, he found a catalyst for polymerization of butadiene. This work was associated with an attempt to elucidate the mechanism of the polymerization process.

Dumanskii showed that the modern theory of coagulation kinetics can be fully applied to studies of the polymerization process. However, the main direction in the work of Dumanskii and his school during this period was in the field of systematic studies of polymer lyophily. Having reviewed critically the state of the problem, Dumanskii showed in 1936 that a colloidal particle, or polymer macromolecule, is capable of binding a certain amount of liquid; the diffuse solvation layer can be broken down either by the action of heat or by introduction of extraneous soluble substances into the solution, and the higher their concentration the more pronounced their destructive effect

on the diffuse layers. Since the liquid attached to the particles is not a solvent for extraneous soluble substances (indicators) introduced into the same system, the amount of liquid bound by the colloid particles can be estimated from changes in the indicator concentration, while by variations of the indicator concentration it is possible to determine the thickness of the diffuse solvation layer (at low indicator contents) and the amount of firmly bound liquid (at high indicator concentrations).

The refractometric method developed by Dumanskii for determination of bound liquid is widely used as a rapid and accurate control method in various industrial processes. Dumanskii presented the results of his investigations in a monograph entitled Lyophily of Disperse Systems (1940), which contains a critical review of existing methods for determining the degree of solvation, a critical assessment of different theories of the effect, and a discussion of its industrial significance. This monograph retains its importance to the present day, being the only monography on the subject in the world's literature.

During the Great Patriotic War Dumanskii, as a true patriot, was engaged in defense problems; he organized production of fabrics proofed against mustard gas from local industry and production of activated charcoal, and developed a new method for decarbonizing internal combustion engines. At the end of the war he moved to Moscow, where he organized a colloid laboratory attached to the Ministry of the Food Industry, and a colloid committee of the All-Union Engineering and Technical Society of the Food Industry. At the same time he organized and led the colloid section of the D.I. Mendeleev All-Union Chemical Society. A conference on colloids in the food industry was held at Dumanskii's initiative in 1945, and its proceedings were published in the form of two volumes entitled Colloids in Processes of the Food Industry. Simultaneously with this he resumed editing of Kolloid. Zhurnal. In the same year he was elected an Active Member of the Academy of Sciences, Ukrainian SSR, and moved to Kiev. There he became head of the Institute of General and Inorganic Chemistry, and undertook the editorship of the Ukrainskii Khimicheskii Zhurnal. From this time he worked on a number of very important problems of polymer science with the aid of new physicochemical techniques. Among his researches of this period mention must first be made of a detailed study of the thermochemical aspects of solvation. On the assumption that water molecules are associated, he proposed the following thermochemical equation for hydration of starch and other polymers insoluble in water:

$$\Sigma Q = Q_1 + Q_2 + Q_{ads} + q_k$$

where ΣQ is the total quantity of heat, determined calorimetrically; Q_1 is the heat of dissociation of $(H_2O)_n$ into simple molecules; Q_{ads} is the heat of adsorption of simple water molecules by the polymer; Q_2 is the heat of association of the remaining simple water molecules, and q_k is the change of kinetic energy of simple water molecules in orientation on the polymer surface. Since association of water molecules and hydration are both effected by hydrogen bonding, it may be assumed that the number of hydrogen bonds is the same after hydration as before, and therefore $Q_1 + Q_2 + Q_{ads} = 0$ and $\Sigma Q = q_k$.

It follows that the heat of hydration is constant, equal to the change of kinetic energy of simple water molecules when they become attached to the polymer surface, for all insoluble polymers which are hydrated by means of hydrogen bonding. It was found experimentally that ΣQ is 1328 cal/mole of water, or 10^{-13} erg per molecule. These results are represented by the expression 5/2 RT = 1450 cal/mole. Since ΣQ is calculated per gram of solid polymer, the Dumanskii rule can be used to calculate the limiting amount of liquid bound by a polymer merely from the experimental value of ΣQ. Tests of Dumanskii's rule for certain polymers gave good agreement between calculated and experimental results.

Another group of Dumanskii's researches is concerned with the dielectric properties of polymers in solutions. This is an important problem which has been investigated very little as yet. This method was used for determination of the degree of hydration of polymers on the one hand, and for studies of polymer structure on the other. Dumanskii derived the following formula for calculating the degree of hydration:

$$n = \frac{(c_1 - c_2 p_f)\, d_w}{(p_w - p_f)\, G_k},$$

where n is the amount of water bound by one gram of polymer; p_w is the specific polarization of bound water; p_f is the specific polarization of free water; d_w is the density of free water; G_k is the weight of disperse phase per 100 g of solution. He showed that 1 g of protein binds 0.42 g of water, and the density of bound water is 1.7. He regards denaturation of proteins as an effect associated with a decrease of the amount of bound water (down to 0.26) and of its density.

It is assumed that in denaturation the density of the protein itself increases from 1.24 to 1.34. Determinations of dipole moments showed that the dipole moment decreases as the result of denaturation. These recent investigations mark a new trend in Dumanskii's work; there is no doubt that they will yield very important results in the future.

We cannot fail to mention Dumanskii's teaching work in various higher education establishments of the Soviet Union over a number of years. His extensive teaching experience is reflected in the books: Dispersity and the Colloidal State of Matter (1932), and Colloid Science (1935, 1937, 1948). These books summarize the work, both of Dumanskii himself and his school, and of other Soviet scientists, and young students are thus given a clear idea of the achievements of colloid sciences in the USSR.

Dumanskii is also an outstanding social and political worker. In 1919-1920 he took active part in the work of the Regional Council of National Economy in restoring the industry of the Voronezh province; in 1935 he was elected to the Voronezh City Soviet, in 1937, to the Voronezh Regional Executive Committee, and in 1939 he was elected as a deputy to the Voronezh Regional Workers' Soviet. For his scientific and organizing work during the Great Patriotic War the Supreme Soviet of the Kazakh SSR gave him in 1942 the honorary title of distinguished scientific worker. In November 1944 he was awarded the Order of Lenin, and in July 1945, the Order of the Red Banner of Labor. He has been a member of the Communist Party of the Soviet Union since April 1940.

It is impossible to give a full account of his varied activities in a short article. We merely aimed to show that in A. V. Dumanskii we have a leading Soviet scientist, an indefatigable organizer of Soviet science, and an excellent teacher of Soviet youth.

Dumanskii's scientific work has become an integral part of modern colloid science, and his activities provide an example of selfless service to our great country.

Editorial Board

INFLUENCE OF THE STRUCTURE AND LENGTH OF HYDROCARBON RADICALS IN DETERGENTS ON THEIR OLEOPHILIC PROPERTIES*

P. A. Demchenko and A. V. Dumanskii

Institute of General and Inorganic Chemistry, Academy of Sciences, UkrSSR, Kiev
Translated from Kolloidnyi Zhurnal, Vol. 22, No. 3, pp. 272-276
May-June, 1960
Original article submitted February 29, 1960

Studies of solubilizing power, critical concentration of micelle formation (CCM), and heats of wetting of various detergents are becoming increasingly important, scientifically and practically, for characterization of their lyophilic properties and elucidation of component binding in systems: surface-active agent (SA)–hydrocarbon–water and SA–hydrocarbon–polar substance–water [1-4]. No systematic investigations have as yet been carried out in this field; therefore, development of the theoretical principles underlying preparation of technically important systems of this type, with predetermined properties, has been retarded and their rational application in various branches of industry is delayed [4-8].

In this paper we present results obtained in studies of solubilization, heats of wetting, and critical concentrations of micelle formation of certain detergents. The materials used were prepared by neutralization of high-molecular organic acids by alkali, as described in earlier papers [1-3].

Solubilizing power and heats of wetting of certain detergents. The solubilizing power of detergent solutions was determined by the direct method [9] at 60°. The relative experimental error was ~3%. Earlier indirect methods for determining solubilization [8, 10] gave less concordant results. Experimental data on solubilization of heptane and toluene in 0.1 M aqueous solutions of saturated fatty-acid soaps and certain detergents containing hydrocarbon radicals differing in structure are given in the table and in Fig. 1 (Curve 1). It was found that in the cases of sodium palmitate, myristate, and laurate the solubilization of heptane decreases almost linearly with decrease in the length of the hydrocarbon radical from C_{18} to C_{12}. In solutions of soap homologs of lower molecular weight the decrease in solubilization of heptane is less rapid, as indicated by the lower portion of curve 1. Solutions of soap homologs containing less than seven carbon atoms in the radical do not form micellar solutions and therefore have no solubilizing action.

Similar results were obtained for solubilization of octane, synthine, and xylene in 0.1 M solutions of sodium soaps of synthetic fatty acids of different molecular weights [9] and chlorinated hydrocarbons in solutions of saturated fatty-acid soaps [14, 15]. The heats of wetting of individual soaps by certain hydrocarbons were determined earlier [3, 11], and it was shown that the heat of wetting is a measure of oleophilic properties.

The heats of wetting of saturated fatty-acid soaps, and of sodium oleate and ricinoleate were determined by the method described earlier [12, 13]; the results are given in Fig. 1 (Curve 2). The heats of wetting of sodium laurate, myristate, palmitate, and stearate by heptane were found to be 180, 230, 295, and 365 cal/mole, respectively.

Sodium ricinoleate, oleate, and stearate all have 18 carbon atoms in their hydrocarbon radicals, and similar molecular weights: 320, 304, and 306, respectively, but their heats of wetting and solubilizing powers of their solutions differ sharply. This is because of the presence of a double bond in the middle of the sodium oleate radical, and of a double bond and a hydroxy group in the sodium ricinoleate radical. The heats of wetting of sodium ricinoleate and oleate by heptane are 150 and 170 cal/mole, respectively. The solubilization of heptane in 0.1 M solutions of sodium ricinoleate, oleate, and stearate was 0.27, 0.45, and 0.81 mole per mole of soap, respectively.

*Paper presented at the Colloid Chemistry Section of the Eighth Mendeleev Congress (Moscow, March 23, 1959).

It is evident from the experimental data in this paper that the solubilizing powers and heats of wetting of soaps vary symbatically. Hence it is to be expected that the presence of oxygen in the hydrocarbon radical of a detergent should decrease its oleophilic character. This was confirmed by determination of the solubilizing power of the ether of potassium β-hydroxypropionate ($C_{10}H_{21}OCH_2CH_2COOK$); a 0.1 M aqueous solution of this substance solubilizes 0.88 mole of toluene per mole, whereas sodium stearate, which is of similar molecular weight but does not contain oxygen in the radical, solubilizes nearly 2.6 times as much toluene (see table).

Solubilization of toluene and heptane in 0.1 M aqueous solutions of sodium naphthenate, abietate, and dibutylnaphthalenesulfonate (Nekal) was studied. The experimental results are given in the table. The solubilizing power of aqueous detergent solutions diminishes with increasing cyclization of the hydrocarbon radicals.

Comparison of the experimental data shows that the solubilizing power of the investigated detergents depends on the length and structure of their hydrocarbon radicals. They form the following series in order of diminishing solubilization of hydrocarbons.

Sodium stearate > sodium naphthenate > sodium palmitate > sodium oleate > sodium myristate > sodium ricinate > sodium dibutylnaphthalenesulfonate > decyl etherof potassium β-hydroxypropionate> sodium laurate > sodium abietate.

The solubilization effect also depends on the structure of the solubilized hydrocarbon. The table shows that toluene and heptane, which have the same number of carbon atoms but differ in molecular structure, are not solubilized equally by solutions of various detergents.

Critical concentrations of micelle formation in solutions of detergent homologs. The critical concentration of micelle formation (CCM) is a reliable criterion for transition of a true solution of a surface-active agent (SA) into a colloidal two-phase state [4, 16-18]. The dependence of CCM on the molecular weights of individual detergents has been reported [4, 8, 16]. The influence of structure and size of hydrocarbon radicals and hydrophilic groups in surface-active agents on CCM has not been studied sufficiently. The critical concentration of micelle formation in solutions of napthenate soaps has not, apparently, been studied at all.

Several methods [8, 16], giving results in satisfactory agreement, have been recommended for investigations of CCM. In our investigations we used the relatively accurate volumetric method [19], which gives reproducible results (to ~ 2%), for determinations of CCM of detergents.

CCM determinations were carried out on homologs of sodium naphthenate soaps, alkyl benzenesulfonates, and sodium soaps of saturated fatty acids. The experimental results are plotted in Fig. 2. CCM rises steadily with decrease of molecular weight in the investigated series of soap homologs, especially when the molecules contain fewer than 12 carbon atoms. The positions of the CCM–molecular weight curves for the detergents in Fig. 2 show that the CCM of detergents is strongly influenced by the structure and length of the hydrocarbon radicals and their attached hydrophilic groups. For example, sodium palmitate, naphthenate, and alkyl benzenesulfonate, with similar molecular weights of 278, 270, and 279, have CCM of 0.9, 1.8, and 6.0 g/liter, respectively. It follows that cyclization of the radicals in detergents is accompanied by increase of CCM and decrease of solubilizing power. The investigated detergents form the following series in order of increasing CCM:

alkyl benzenesulfonates > alkyl sulfonates > sodium naphthenates > sodium soaps of saturated fatty acids.

Solutions of low-molecular detergent homologs: sodium enanthate $CH_3(CH_2)_5COONa$, heptyl sulfate $CH_2(CH_2)_5CH \cdot OSO_3Na$, butylbenzenesulfonate $CH_3(CH_2)_5CHC_6H_4SO_3Na$, and naphthenate, with molecular weights of 152, 218, 231, and 164, respectively, did not form micelles.

We term these molecular weights "critical," because only homologs of higher molecular weights form colloidal solutions with solubilizing power. The difference between the molecular weight M of a detergent forming micellar solutions and the critical molecular weight of the homolog M_{cr} may be termed the effective hydrocarbon radical. With increase of its length detergent molecules become capable of associating into micelles at lower concentrations, and of forming colloidal solutions with their specific properties. For the detergent homologs studied CCM was found to be inversely proportional to the third power of the effective hydrocarbon radical, and its value can be found from the formula $CCM = K/(M-M_{cr})^3$, g/liter, where K is a constant. The values of K for sodium soaps of saturated fatty acids, sodium salts of naphthenic acids, alkyl sulfates, and alkyl benzensulfonates are respectively: $1{,}8 \cdot 10^6$; $2 \cdot 10^6$; $5 \cdot 10^5$ and $7 \cdot 10^5$.

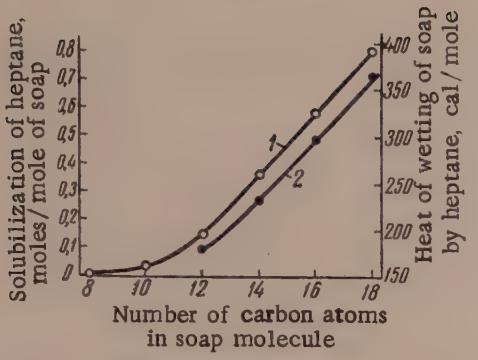


Fig. 1. Solubilization of heptane in 0.1 M solutions of sodium soaps of saturated fatty acids (1), and heats of wetting of the soaps by heptane (2)

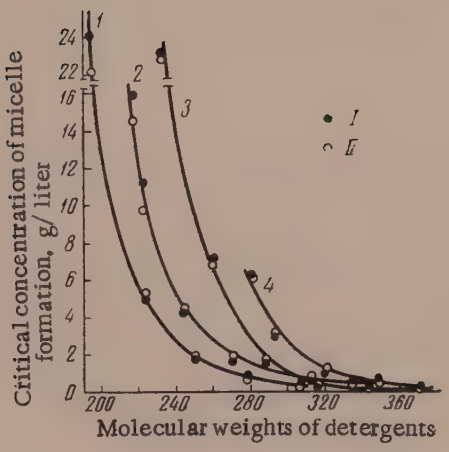


Fig. 2. Critical concentration of micelle formation as a function of molecular weight for sodium soaps of saturated fatty acids (1), sodium soaps of naphthenic acids (2), alkyl sulfonates (3), and alkyl benzenesulfonates (4). I) Experimental data; II) values calculated from the formula.

Influence of Radical Length and Structure in Detergents on Solubilization of Hydrocarbons by 0.1 M Solutions

Detergent	Molecular weight	No. of carbon atoms in molecule	Solubilization, moles/mole of soap	
			toluene	heptane
Sodium laurate	222	12	0,53	0,14
Sodium myristate	255	14	1,02	0,36
Sodium palmitate	278	16	1,68	0,55
Decyl ether of potassium β-hydroxypropionate	296	13	0,88	—
Sodium oleate	304	18	1,60	0,45
Sodium stearate	306	18	2,27	0,81
Sodium ricinoleate	320	18	—	0,27
Sodium abietate	324	20	0,41	0,11
Sodium naphthenate	326	—	1,85	0,57
Sodium dibutylnaphthalene--sulfonate (Nekal)	243	18	—	0,26

The values of CCM for the investigated detergent homologs, calculated from the formula, are in good agreement with the experimental data in Fig. 2. Typical detergents were found to have CCM of 0.3-7.0 g/liter. Detergents of high molecular weight, with CCM below 0.3 g/liter, have poor solubility and can be used only at high temperatures and in mixtures with homologs of lower molecular weight. Low-molecular detergent homologs with CCM over 7.0 g/liter have low detergent power and should be used as wetting and flotation reagents.

SUMMARY

1. The critical concentration of micelle formation, heat of wetting, and solubilizing power vary sharply with changes in the length and structure of hydrocarbon radicals in detergents.

2. The critical concentration of micelle formation and solubilizing power can be used as criteria for quantitative characterization of lyophilic and other important practical properties of detergents.

3. Homologs of alkyl benzenesulfonates, alkyl sulfates, sodium soaps of saturated fatty acids, and sodium naphthenates, which have detergent action, have critical concentrations of micelle formation in the range 0.3-7.0 g/liter and in 0.1 M solutions they solubilize more than 0.2-0.5 mole of hydrocarbon per mole of detergent.

Homologs of low molecular weight, with critical concentrations of micelle formation > 7 g/liter, have weak solubilizing detergent action.

4. A formula for calculating CCM is proposed. The calculated values of CCM are in satisfactory agreement with experimental data for four classes of investigated detergents.

5. Presence of oxygen, hydroxyl, double bonds, and cyclic groups in the hydrocarbon radical sharply lower the oleophilic properties of detergents.

6. For production of surface-active substances with good oleophilic properties, chain radicals of the optimum length (C_{14}-C_{18}) should be linked with functional hydrophilic groups through primary carbon atoms. Cyclic and mixed hydrocarbon radicals, containing hydrophilic groups and heteroatoms, should be linked with functional groups so as to give molecules of the maximum length and oleophily.

LITERATURE CITED

1. A. V. Dumanskii and P. A. Demchenko, Doklady Akad. Nauk SSSR 78, 277 (1951).
2. P. A. Rebinder, Khim. Nauka i Promylshlennost' 4, 554 (1959).
3. P. A. Demchenko, A. V. Dumanskii, and L. G. Demchenko. Kolloid. Zhur. 14, 164 (1952).*
4. P. A. Demchenko, Masloboino-Zhirovaya Prom. 7, 36 (1959).
5. A. M. Schwartz and J. W. Perry, Surface Active Agents [Russian translation] (IL, Moscow, 1953).
6. Z. N. Markina, K. A. Pospelova, and P. A. Rebinder, Proceedings of the Third All-Union Conference on Colloid Chemistry [in Russian] (Izd. Akad. Nauk SSSR, Moscow, 1956) p. 410.
7. N. P. Apukhtina and A. M. Lyagalova, Kolloid. Zhur. 19, 154 (1957).*
8. M. E. McBain and E. Hutchinson, Solubilization and Related Phenomena (N. Y., 1955).
9. P. A. Demchenko, Masloboino-Zhirovaya Prom. 10, 22 (1959).
10. A. I. Yurzhenko, Zhur. Obshchei Khim. 16, 1171 (1946).
11. A. V. Dumanskii, V. I. Solnyshkin, and P. A. Demchenko. Ukrainskii Khim. Zhur. 22, 635 (1954).
12. A. V. Dumanskii, Ya. F. Mezhennyi, and E. F. Nekryach, Kolloid. Zhur. 9, 335 (1947).
13. P. A. Demchenko, Zavodskaya Lab. 7, 870 (1953).
14. P. A. Demchenko, Doklady Akad. Nauk UkrainSSR 5, 494 (1959).
15. P. A. Demchenko, Ukrainskii Khim. Zhur. 24, 746 (1959).
16. H. B. Klevens, Chem. Revs. 47, 1 (1950).
17. P. Ekwall, Koll.-Z. 136, 37 (1954).
18. A. B. Taubman, Khim. Nauka i Promyshlennost' 4, 554 (1959).
19. H. B. Klevens, Analyt. Chem. 22, 1141 (1950).

* Original Russian pagination. See C. B. translation.

RHEOLOGICAL PROPERTIES OF GLYCEROL SOLUTIONS

I. A. Dumanskii and L. V. Khailenko

Institute of General and Inorganic Chemistry, Academy of Sciences, UkrSSR, Kiev
Translated from Kolloidnyi Zhurnal, Vol. 22, No. 3, pp. 277-281
May-June, 1960
Original article submitted February 25, 1960

The rheological properties of glycerol and its aqueous solutions have been studied in our laboratory for a number of years. The investigations were carried out by the method proposed by Rebinder [1, 2], with studies of deformation kinetics at constant shearing stress and subsequent analytical calculation of the elasticoviscous characteristics from the complete $\xi = \varphi(\tau)_P$ flow curve.

In this investigation the structure formed in the glycerol–water system is characterized by the viscosity of plastic flow of the system, found from the linear region of the flow curve, in the form

$$\eta_1 = \frac{P}{(d\xi / d\tau)}.$$

The $\xi = \varphi(\tau)_P$ flow curves were determined experimentally by means of a highly sensitive Shvedov elastoviscosimeter [3], with some design modifications introduced by us [4].

It is known [5] that the shearing stress (P applied to a system by torsion of a wire through the angle δ is

$$P = \frac{K}{S_{r_0}} \delta \text{ dynes/cm}^2$$

and the relative shearing deformation of the system in the annular gap is $\xi = \frac{2\omega}{r_0^2 (1/r_0^2 - 1/r_1^2)}$.

In these equations $K = M/\delta$, dynes·cm/radian; M is the torque transmitted to the system in the cylindrical gap; $S = 2\pi r_0 h$ is the lateral surface area of the inner cylinder; δ is the torsion angle of the suspension wire, in radians; ω is the angular displacement of the inner cylinder in radians; this determines the relative shearing deformation in the gap between the coaxial cylinders.

Instrument characteristics. Height h of the inner cylinder, less the bottom and top, 23.60 cm; radius of outer cylinder r_1 = 3.65 cm; radius of inner cylinder r_0 = 2.84 cm; distance from the scale center to the suspension wire R = 3.23 cm.

A range of suspension wire with torsional coefficients K_1 = 8.24 dynes/cm; K_2 = 47.35 dynes/cm; K_3 = 306 dynes/cm was used, so that a range of shearing stresses ($P \cdot 10^{-4}$) between 2.1 and 1430 dynes·cm^{-2} was available.

The investigation shows that under isothermal conditions at 20° structure formation in the glycerol–water system is determined by the amount of water in the glycerol and the aging time.

Figure 1, curve 1 shows that the viscosity of 98.8% glycerol is independent of time. However, the viscosity calculated from the experimental data ($\approx$ 40 poises) is 3.5 times the viscosity given in standard tables (11.6 poises). The $\xi = \varphi(\tau)$ P graph for 98.8% glycerol solution was specially investigated in order to explain this excessive discrepancy. As the result of a series of experiments at different shearing stresses it was found that the linear flow graph for this solution has an inflection point, so that there are two viscosity values:

η_1 = 45 poises, calculated as $\eta_1 = \frac{P}{(d\xi/d\tau)}$ before the inflection point, and η = 14 poises, calculated after the inflection point (Fig. 2). Evidently deformation is accompanied by breakdown of the structure formed in the system in presence of 1.2% water in the glycerol. Curves 2, 3, and 4 in Fig. 1 represent viscosity increases in glycerol containing dissolved water in the percentage proportions indicated in Fig. 1.

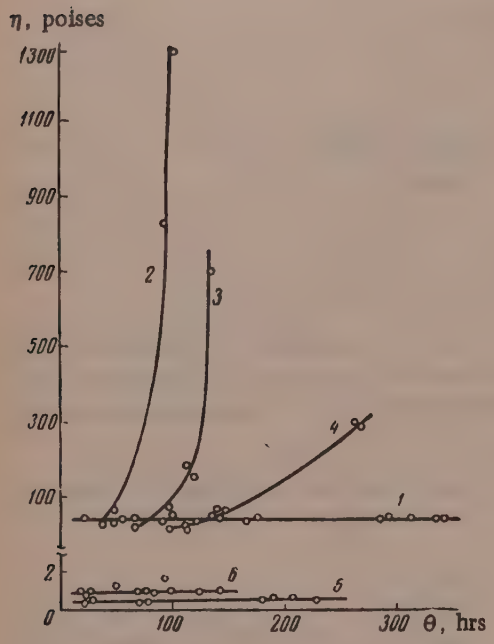


Fig. 1. Variations of viscosity of plastic flow (η_1) with aging time (θ) of glycerol solutions containing: 1) 1.2% water; 2) 5.3% water; 3) 27% water; 4) 50% water; 5) 30% methanol; 6) 30% ethanol.

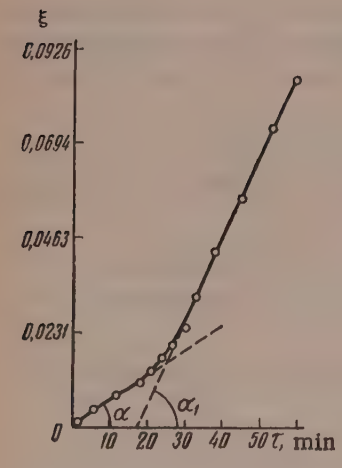


Fig. 2. Dependence of deformation (ξ) on time of deformation (τ) for 98.8% aqueous glycerol solution at $P \cdot 10^{-1}$ = 4.7 dynes/cm^2.

The graphical $\eta_1 = f(\theta)$ relationship shows that structure formation in aqueous glycerol solutions, characterized by the value of η_1, is accelerated to an increasing extent with decrease of the amount of water in the system. For each concentration of the glycerol solution there is a certain initial period θ_0 during which the viscosity of that solution is less than the viscosity of 98.8% glycerol solution. There is a definite value of θ_0 for each concentration, and this value increases with increasing water content in the system. When $\theta > \theta_0$ the solution viscosity η_1 rises rapidly and reaches values above 1000 poises. Further increase of θ may result in total loss of fluidity ($\eta_1 = \infty$), so that the solution acquires an apparent elastic limit P_k and its $\xi = \varphi(\tau)_P$ deformation curve corresponds to the model for a Kelvin body, as was shown earlier [6]. It is possible to find a shearing stress for glycerol–water solutions at which the system exhibits irreversible breakdown deformation.

Figure 3 shows comparative deformation–time curves for 20% solidol (grease) solutions from data in [7] and for 73% glycerol solution after aging time θ = 560 hours.

It is known that glycerol and its aqueous solutions pass into the glassy state when cooled [8]. If the anomalous viscosity is the result of vitrification, then if the liquid is cooled below the crystallization temperature we should expect to have instead of a $\xi = \varphi(\tau)_P$ flow diagram for which the first derivative $d\xi/d\tau$ = const (Newtonian liquid), a diagram for which the first derivative $d\xi/d\tau \neq$ const (elastic liquid). However Fig. 4 shows that this is not the case in practice. It follows from the viscosity values calculated from the graphs in Fig. 4 that decrease of temperature only raises the viscosity of glycerol to η_1 = 196 poises at −9° and to 236-239 poises at −15°.

The thermal breakdown of structure in glycerol–water solution containing 27% water is represented graphically in Fig. 5. The glycerol solution was heated at 90° for 4 hours (point B) and then cooled to 20°; the viscosity determined immediately after the cooling (point A_1) was 33 poises, and rose to 450 poises in 168 hours. The solution was then heated again at 90° for 4 hours (point B_1). Figure 5 shows that the viscosity (η_1) of the glycerol solution corresponding to point A_2 is 5.5 times the viscosity at point A_1. Further structure formation in the solution, represented quantitatively by the value of η_1, is more rapid between point A_2 and B_2 than between A_1 and B_1. The $\xi = \varphi(\tau)_P$ curves for our systems are similar in the form to the flow curves for natural and synthetic rubber solutions studied by Rebinder and Kolbanovskaya [1]. They showed [1] that the elastico-viscous properties of rubber solutions can be correlated with their structural characteristics. The structure of such solutions is taken to consist of individual chain molecules which can undergo deformation in flow by virtue of the flexibility of C–C valence bonds, which gives rise to high-elastic deformation [9].

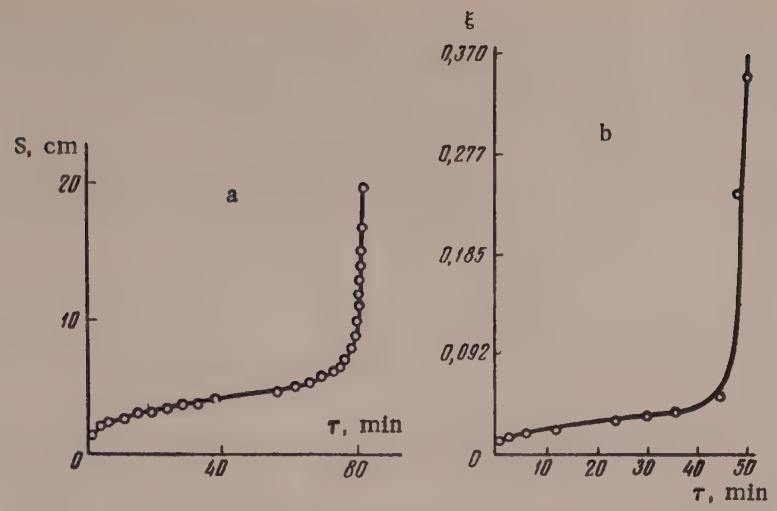


Fig. 3. Comparative deformation–time curves: a) for 20% solidol [7]; b) for 73% aqueous glycerol solution at P = 8.3 dynes/ cm^2.

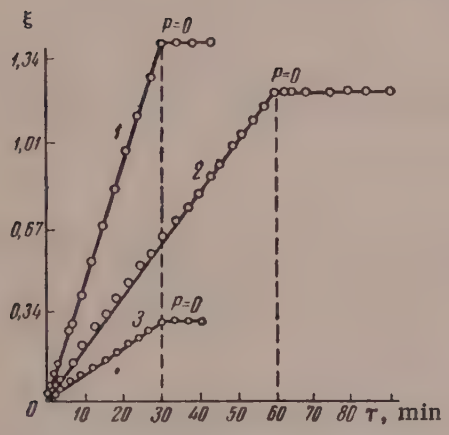


Fig. 4. Deformation–time curves for 98.8% aqueous glycerol solution aged for 122 hours: 1) at −9°, P = 0.143 dyne/cm^2; 2) at −15°, P = 0.0716 dyne/cm^2; 3) at −15°, P = 0.0358 dyne/cm^2.

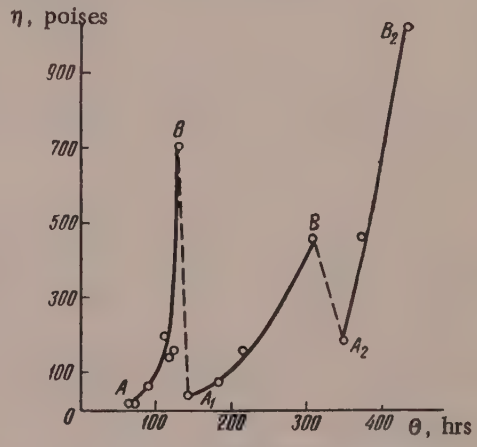
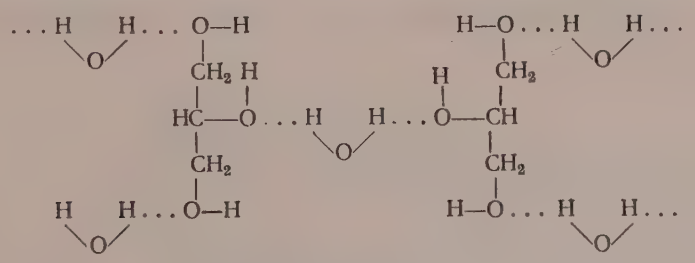


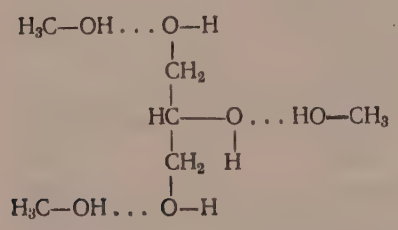
Fig. 5. Viscosity (η_1) as a function of aging time of 73% aqueous glycerol solution subjected to intermittent heating and cooling.

In our systems a chain structure can be produced by hydrogen bonding which results in formation of quasi-polymeric glycerol–water molecules:

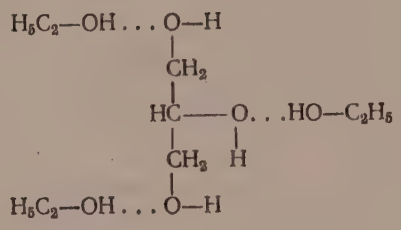


To test our hypothesis that the chain structure and elasticoviscous properties of glycerol–water associated systems are caused by hydrogen bonding, flow diagrams of glycerol–ethanol and glycerol–methanol solutions containing 70% glycerol and 30% alcohol by weight were investigated. The flow diagrams for these solutions are straight lines with constant deformation rates such that $d\xi/d\tau = \text{const}$, while the solutions themselves are ordinary Newtonian liquids. For glycerol–ethanol solutions $\eta_1 \approx 0.7$ poise, and for glycerol–methanol solutions $\eta_1 \approx 0.4$ poise.

The time of structure formation is of no significance for these solutions, as their viscosity remains constant (Fig. 1, lines 5 and 6). It is possible that glycerol interacts with alcohols to form the following compounds:



glycerol + methanol



glycerol + ethanol.

Evidently addition of alcohol by means of hydrogen bonding makes the system incapable of forming further associated groups.

SUMMARY

1. The glycerol–water system is a quasipolymeric structurized liquid in which structure formation is effected by hydrogen bonding; these bonds are assumed to be as mobile as in elastic molecules.

2. When water is replaced by alcohol in glycerol solutions they lose their ability to form structures; this may be attributed to blocking of the hydrogen bonds by CH_3 or C_2H_5 radicals.

3. In glycerol–water solutions the "age" of the system (time θ) is an important factor in structure formation. Evidently θ reflects the kinetics of formation of a quasipolymeric glycerol–water structure by hydrogen bonding. With very large values of θ the solution may completely lose experimentally detectable fluidity.

4. The structure of a glycerol–water solution may undergo breakdown in deformation; this is indicated on the $\xi = \varphi(\tau)_p$ flow curve by an almost instantaneous decrease of the viscosity η_1. It was shown in the case of 98.8% glycerol solution that the viscosity after structural breakdown is approximately equal to the standard tabular value.

5. Transition of the glycerol–water system into the undercooled state does not produce a region of elastic aftereffects on the flow curve; this means that undercooling does not give rise to elastic effects in the liquid but merely raises the total viscosity of the system.

6. The structure of a glycerol–water solution is thermally unstable, but is restored after cooling, and, for equal θ, the preceding value of the viscosity η_1 is exceeded.

7. The structures formed in solutions of the water–glycerol type can be studied by direct mechanical methods used in experimental rheology.

LITERATURE CITED

1. A. S. Kolbanovskaya and P. A. Rebinder, Kolloid. Zhur. 12, 194 (1950).
2. P. A. Rebinder, Tr. In-ta Fiz. Khim. AN SSSR 1, 5 (1950).
3. F. N. Shvedov, J. de Phys. 8, 341 (1889).
4. I. A. Dumanskii and L. V. Khailenko, Kolloid Zhur. 15, 426 (1953).*
5. L. I. Édel'man and P. A. Rebinder, Kolloid. Zhur. 13, 64 (1951).

*Original Russian pagination. See C. B. translation.

6. L. V. Khailenko, Doklady Akad. Nauk SSSR 115, 1135 (1957).*
7. A. A. Trapeznikov and E. M. Shlosberg, Tr. In-ta Fiz. Khim. AN SSSR 1, 49 (1950).
8. Lowry, Glycerols and Glycols [Russian translation] (Goskhimtekhizdat, Leningrad, 1933).
9. V. A. Kargin and G. L. Slonimskii, Zhur. Tekh. Fiz. 11, 341 (1941).

*Original Russian pagination. See C. B. translation.

STUDY OF EQUILIBRIUM IN THE SYSTEM STARCH–AQUEOUS ALCOHOL

O. D. Kurilenko and E. A. Yakovkina

Kiev Technological Institute of the Food Industry
Translated from Kolloidnyi Zhurnal, Vol. 22, No. 3, pp. 282-286
May-June, 1960
Original article submitted February 25, 1960

Among the numerous methods for determination of hydrophily, indicator methods are widely used [1]. The principle of these methods is that the amount of bound water is found from the increase in the concentration of a third component (indicator) in the solution after addition of a weighed quantity of polymer (dry or of known moisture content). It is assumed that the polymer adsorbs water only. This assumption is not always justified, because, on the one hand, in many cases the indicator is adsorbed as well as water, so that errors which are difficult to allow for are introduced into the determination; on the other hand, the indicator is itself hydrophilic (as otherwise it would not dissolve in water). As a rule the indicator alters the activity of water in solution, so that the amount of water taken up by the polymer is also changed. This effect of the indicator is particularly large at high solution concentrations. All this makes studies of equilibria in polymer–aqueous solution systems an urgent problem.

In this paper we present the results of equilibrium studies for the system: starch–aqueous alcohol.

Notation: G = amount of solution in grams; m = weight of dry hydrophilic substance in grams; a = number of grams of water taken up by one gram of the hydrophilic substance (bound water); b = number of grams of the third component taken up by one gram of the hydrophilic substance; P_{os} = the content of the third component in the original solution (%); P_{es} = the content of the third component in solution after addition of the hydrophilic substance (%); W = the moisture content of the hydrophilic substance used.

In (G–ma–mb+mW) grams of solution there is (P_{as} G/ 100-mb) grams of the third component, and 100 g of equilibrium solution contains P_{os} grams of dissolved substance.

From this relationship we have the expression:

$$a - b\frac{P_{ew}}{P_{es}} = W + \frac{G}{m}\frac{P_{es} - P_{os}}{P_{es}}. \qquad (1)$$

All the quantities in the right-hand side of this equation are easy to determine experimentally, but the amounts of water (a) and third component (b) can be only by calculation. If we assume that W = 0, Equation (1) becomes

$$a - b\frac{P_{ew}}{P_{es}} = \frac{G}{m}\frac{P_{es} - P_{os}}{P_{es}}, \qquad (2)$$

which differs only in form from the equations derived by Vilenskii and Pavlova [2] or by Sherer and Crookston [3].

If it is assumed that the third component is not adsorbed by the hydrophilic substance, then Equations (1) and (2) become

$$a = W + \frac{G}{m}\frac{P_{es} - P_{os}}{P_{es}} \qquad (3)$$

or

$$a = \frac{G}{m} \frac{P_{es} - P_{os}}{P_{es}}. \quad (4)$$

Equations (3) and (4) are analogous to the equations given by A. V. Dumanskii for calculation of the amount of bound water by the indicator method. Therefore, the Vilenskii-Pavlova and Dumanskii equations are special cases of our general Equation (1).

Equations (1) and (2) are inconvenient for practical calculations, as they contain two unknowns, a and b. Vilenskii and Pavlova calculated the right-hand side of a somewhat modified form of Equation (2), and thus found the so-called predominant adsorption rather than the amounts of components adsorbed in the solution. Kiselev and co-workers [4] and Ermolenko and co-workers [5] used similar procedures.

Sherer and Crookston [3] have a different approach to the problem. In a study of solvation of cellulose nitrate in acetone–water mixtures they assumed that the Freundlich equation is applicable to adsorption of acetone and can be used as the second equation in a system of two equations with two unknowns. This approach to the problem is correct in principle, but the authors did not justify the applicability of the Freundlich equation either theoretically or experimentally.

It may be assumed that the heat of wetting of a hydrophilic substance by aqueous alcohol is proportional to the amounts of water and alcohol adsorbed

$$q/m = K_1 a + K_2 b, \quad (5)$$

where q is the heat of wetting of the starch sample by the aqueous alcohol mixture, and K_1 and K_2 are constants.

Equation (5) can be used in conjunction with Equation (1). We then have a system of two equations with two unknowns, and can calculate adsorption of both components of the mixture. It is subsequently assumed that the weight m is always 1 g, and W = 0.

Simultaneous solution of Equations (1) and (5) gives

$$a = \frac{qP_{ew} + GK_2(P_{es} - P_{os})}{K_2 P_{es} + K_1 P_{ew}}. \quad (6)$$

All the quantities in the right-hand side of Equation (6) can easily be found by experiment, apart from the constants K_1 and K_2, which must be calculated from experimental data.

The constant K_1 connects the heat of wetting (q) with the amount of bound water (a), and is known from the work of Dumanskii and his associates. We can take $K_1 = 80$ to a sufficient degree of accuracy. The heat of wetting of starch by alcohol is not known to this degree of accuracy. This is because it is difficult to remove traces of water during the experiments, since dry starch and anhydrous alcohol take up water very avidly. According to the results of Dumanskii and Nekryach [6] the heat of wetting of starch by alcohol is 1.7 cal/g of starch. The amount of adsorbed alcohol is known less reliably. Rakovskii and Polyanskii [8] give the value of 1.8 g of alcohol per 100 g of starch. Ulman and Schierbaum [9], who determined adsorption of alcohol from the difference in weight between starch dried after it had been wetted with alcohol and the original weight, found that from 2.4 to 3.3% of alcohol is adsorbed by starch.

If we assume that starch adsorbs 2% of alcohol, then $K_2 \approx 80$. Then, if it is assumed that $K_1 = K_2 = 80$ and $P_{ew} + P_{es} = 100$, Equation (6) becomes

$$a = \frac{qP_{ew} + 80G(P_{es} - P_{os})}{8000}. \quad (7)$$

If a is known, then the amount of adsorbed third component b can be found from the expression

$$b = \frac{q - 80a}{80}. \qquad (8)$$

If a and b are known, the heat of wetting (q) can be calculated from this same Equation (8).

We used the following procedure for studying equilibria in the system: starch–aqueous alcohol. In every case 30 g of solution was added to 10 g of starch. The mixture was shaken at intervals during two days. It was then allowed to settle and the equilibrium compounds of the alcohol–water mixture was determined. The alcohol concentration in the solution was determined with the aid of the IRF-23 refractometer, a sodium lamp being used as the light source.

For convenience, we used standard mixtures to plot a calibration curve showing the refractive index as a function of the percentage alcohol content in solution. It is interesting to note that the refractive index rises to a maximum and then falls with increase of alcohol concentration. The maximum corresponds to ~75% alcohol. In a solution of this composition there is ~1 mole of alcohol per mole of water.

For calculation by Eq. (7) the heat of wetting of 1g of starch by aqueous alcohol must be known. Equilibrium is established between water and alcohol adsorbed by the starch and the solution components as the result of wetting. At constant temperature and with a constant amount of the hydrophilic substance the equilibrium system is invariant. Therefore, a relationship between the heat of wetting and composition must be sought for the equilibrium and not the initial composition of the alcohol–water mixture.

The heat of wetting of starch is plotted against the composition of the aqueous alcohol mixture in Fig. 1 [6, 7]. The scatter of the experimental points is possibly due to the fact that the authors determined the relationship between heat of wetting and the composition of the original rather than the equilibrium solution. In that case the heat of wetting (q) depends on the amounts of starch and solution taken.

We determined the compositions of the original and equilibrium solutions experimentally. The heats of wetting corresponding to our values of the equilibrium solution compositions were found graphically from the curve in Fig. 1. The results are presented in Table 1, which also contains calculated values of the amounts of water and alcohol taken up by 1g of starch from solution. The determinations were performed at 20°±0.1 in an ultrathermostat.

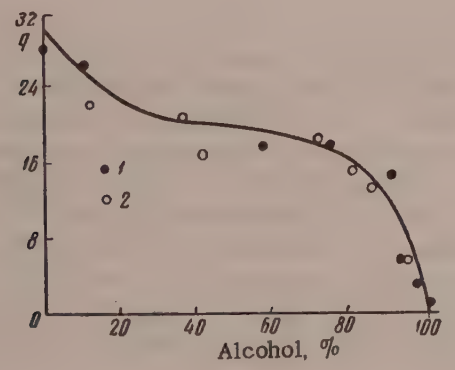


Fig. 1. Heat of wetting of starch (q, cal/g of starch) by aqueous alcohol as a function of alcohol concentration: 1) From data in [6]; 2) from data in [7].

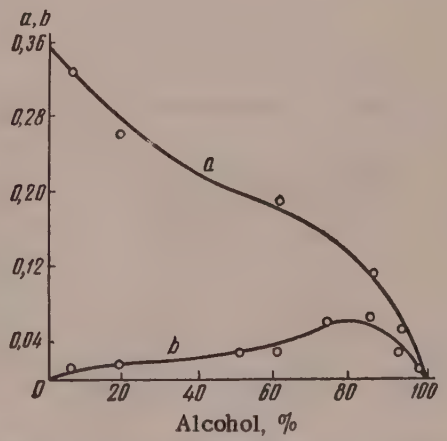


Fig. 2. Amounts of water (a) and alcohol (b) adsorbed by starch, in grams per g of starch, at different concentrations of alcohol in the mixture.

TABLE 1

Compositions of the Original and Equilibrium Alcohol Solutions, Heat of Wetting and Amounts of Water and Alcohol Adsorbed by 1 g of Starch, Calculated by Equations (4), (7), and (8)

Amt of alcohol in soln., %		Heat of wetting found graphically, cal/g	Bound water (a), g		Amt of alcohol (b) by equation (8), g
original, P_{os}	equilibrium, P_{es}		by equation (4)	by equation (7)	
5,5	6,0	27,0	0,25	0,33	0,010
17,8	19,0	22,0	0,20	0,26	0,015
46,2	48,9	18,1	0,16	0,20	0,026
57,2	60,6	18,0	0,17	0,19	0,035
71,0	74,0	17,0	0,11	0,15	0,063
83,2	86,0	14,0	0,10	0,11	0,065
92,4	94,0	6,0	0,050	0,050	0,030
98,6	99,2	2,3	0,018	0,018	0,011

The amounts of bound water calculated by Equation (7), and of adsorbed alcohol calculated by Equation (8), are plotted in Fig. 2.

It is clear from Fig. 2 that the maximum amount of alcohol adsorbed by 1 g of starch corresponds to 75-80% concentration of the equilibrium alcohol–water mixture, which is the concentration corresponding to the maximum refractive index.

Therefore it follows from Fig. 2 that the amount of alcohol adsorbed by 1 g of starch depends not only on the alcohol concentration but also on the water concentration. When the concentration of water in the mixture is below 18%, the amounts of adsorbed water and adsorbed alcohol both decrease.

This leads to the conclusion that either alcohol is adsorbed on starch which is hydrated (even if only partially), or only alcohol hydrates are adsorbed on dry starch. Dry alcohol is not adsorbed by dry starch, or is adsorbed in very slight amounts only.

To verify our calculations, we carried out experiments on wetting of starch containing 0.173 g moisture per g (air-dry) by aqueous alcohol mixtures. The results are given in Table 2. In every case 40 g of solution was added to 20 g of starch.

TABLE 2

Wetting of Starch by Aqueous Alcohol Mixtures

Original concentration, g P_{os}	Equilibrium concentration g P_{es}	Change of conc., g, $P_{es}-P_{os}$
17,3	20,6	3,3
24,6	27,2	2,6
48,0	49,0	1,0
58,0	57,7	—0,3
71,6	70.0	—1,64

It follows from Table 2 that water was predominantly adsorbed at low concentrations of alcohol in water, and alcohol at high. It can be shown graphically that when the alcohol concentration in water is 55% alcohol and water are adsorbed in equal quantities after wetting. Figure 2 shows that at this concentration the amounts of water and alcohol taken up by the starch are 0.2 and 0.026 g respectively. It follows that when starch containing 0.173% moisture is wetted by aqueous alcohol containing 55% alcohol 1 g of starch should adsorb 0.2–0.173 = 0.027 g of water and 0.026 g of alcohol (Fig. 2). The quantity of heat liberated should be q=80(0,026+ +0,027) = 4.2 cal/ g.

This value is in good agreement with the data of A. V. Dumanskii and E. F. Nekryach.

SUMMARY

1. An expression has been derived for calculation of the amounts of water and alcohol adsorbed by starch from aqueous alcohol solutions.

2. The amount of water adsorbed by starch decreases with increase of alcohol concentration.

3. The amount of alcohol adsorbed by starch first increases to a maximum with increase of alcohol concentration in the solution, and then decreases.

4. It is concluded that only hydrated starch can be adsorb alcohol.

LITERATURE CITED

1. A. V. Dumanskii, Hydrophily of Disperse Systems [in Russian] (1940) p. 108.
2. V. A. Vilenskii and V. A. Pavlova, Kolloid. Zhur. 6, 607 (1940).
3. P. C. Sherer and N. J. Crookston, J. Polymer Sci. 14, 129 (1954).
4. A. V. Kiselev, V. V. Khlopina, and Yu. A. El'tekov, Izvest. Akad. Nauk SSSR, Otdel. Khim. Nauk 56, 664 (1958).*
5. N. F. Ermolenko and N. L. Lemets, Uch. Zap. Belorussk. Un-ta, No. 20, 141.
6. A. V. Dumanskii and E. F. Nekryach, Kolloid. Zhur. 10, 103 (1948).
7. M. V. Chapek, A. A. Mozgovoi, and G. I. Tret'yakov, Kolloid. Zhur. 1, 339 (1935).
8. A. V. Rakovskii and G. V. Polyanskii, Zhur. Khim. 2, 151 (1931).
9. M. Ulman and F. Schierbaum, Kolloid. Z. 156, 2, 1956 (1958).

*Original Russian pagination. See C. B. translation.

SORPTION OF WATER VAPOR AND HEAT OF WETTING OF CERTAIN POLYAMIDES

E. F. Nekryach and Z. A. Samchenko

Institute of General and Inorganic Chemistry, Academy of Sciences UkrSSR, Kiev
Translated from Kolloidnyi Zhurnal, Vol. 22, No. 3, pp. 288-292
May-June, 1960
Original article submitted February 25, 1960

Sorption of moisture is one of the most characteristic and technically important properties of fiber-forming polymers, including polyamides. There have been several studies [1-5] concerned with the hygroscopicity of polyamide fibers, but they are not numerous and therefore certain important aspects of polyamide–water interaction have not been adequately studied. The relationship between hydrophily and chemical structure of polyamides is a subject of topical importance. The information available in the literature, which has been published very recently, is scanty and requires verification and confirmation.

The object of the present investigation was a comparative study of the sorptional and hydrophilic properties of polycaprolactam (Capron) and polyhexamethyleneadipamide (Anid); they each have the same number of methylene groups per carbamide group, but their arrangement is different. The repeating unit of Capron has the formula $[OC(CH_2)_5NH]-$, and that of Anid, $-[OC(CH_2)_4CONH(CH_2)_6NH]-$. This problem is of interest because in many instances the properties of polymers of the same chemical composition differ sharply in accordance with the configuration of the monomer unit. For example, starch and cellulose, which differ in the arrangement of the glucose residues in the principal chain, differ in properties. Moreover, study of the hygroscopicity of Capron and Anid is of independent interest from the practical standpoint.

The materials used in the investigation were Capron and Anid polyamide resins in the form of transparent ribbon chips.*

The polyamides were obtained as fine powders by mechanical grinding of the resins or by precipitation from resin solutions. The solvent was 20% solution of calcium chloride in methanol. The resin was dissolved at the boil in a flask under reflux for 6-7 hours. The solution was then cooled and the polyamide precipitated by dilution of the solution with methanol. The liquid was drawn off in a vacuum filter and the precipitate was thoroughly washed, first with methanol and then repeatedly with large amounts of distilled water until no traces of chloride could be detected. The samples were slightly dried in air, ground in a porcelain mortar, passed through a screen with 0.25 mm apertures, and used in that form for determination of water-vapor sorption isotherms and heats of wetting.

The sorption isotherms of Capron and Anid at 20° obtained pycnometrically is described in [6].

The heats of wetting by water were determined at 20° in an adiabatic calorimeter described fully earlier [7-9].

In order to find how the method for making polyamide powders influences their hydrophily and to determine the optimum drying conditions the heats of wetting by water were determined for Capron samples powdered mechanically and powders made by precipitation from solution. The samples were dried at 110° in an automatically regulated drying oven, and at 60 and 100° in vacuum. The results are presented in the table.

The table shows that the heat of wetting of Capron powdered mechanically is considerably less than that of Capron precipitated from solution. The probably explanation is that Capron powder made mechanically is coarser than the precipitated powder. The drying conditions also have a considerable influence on hydrophily of the samples,

* Capron resin was made at the Kiev Synthetic Fiber Factory, and Anid resin at the All-Union Scientific Research Institute of Artificial Fibers.

Effect of Method of Preparation on the Heat of Wetting of Capron Samples

Method of preparation on the Heat of Wetting of Capron Samples	Heat of wetting of dried samples*, cal/g		
	in oven at 110°	in vacuum	
		at 60°	at 100°
Mechanical (grinding)	5.9	7.1	6.2
Precipitation from solution	6.3	7.6	7.7

*Mean of several close values.

The data in the table indicate that vacuum drying at 60° is best. Air drying at 110° is in any case unsuitable, while vacuum drying at higher temperatures is of no advantage because the hydrophily either remains unchanged or decreases. It is interesting to note that the behavior of Capron in this respect is similar to that of cellulose [8].

The Capron and Anid powders used in the subsequent investigations were made by precipitation from solution. The heats of wetting were determined after the samples had been dried in vacuum at 60°. The results plotted in Fig. 1 and 2.

Figure 1 shows that there is hardly any difference between the sorption isotherms of Capron and Anid up to $p/p_s \approx 0.85$. The two isotherms differ considerably in the p/p_s region from 0.85 to 0.98. Up to $p/p_s \approx 0.96$ the sorption isotherm of Capron is above that of Anid, but at $p/p_s = 0.98$ Capron sorbs 30.2% and Anid 41.1% H_2O.

Comparison of our data with sorption values reported in [1] reveals that in the p/p_s region up to 0.80 isotherms for sorption of water vapor by Capron fibers and Capron precipitated from resin solution almost coincide, but above this point, at relative humidities up to $p/p_s \approx 1.00$, the sorptive capacity of precipitated Capron is far greater than that of Capron fibers. At $p/p_s \approx 0.80$ Capron in fiber form takes up 7-8% moisture, which corresponds to approximately one H_2O molecule per two –NHCO– groups. Roughly the same results are obtained for precipitated Anid. The situation changes sharply with increase of relative humidity from 0.80 to 1.00. Whereas at $p/p_s \approx 1.00$ Capron fibers take up 8-13% moisture [3], precipitated Capron takes up over 30% moisture; this is probably because of structural differences between the samples. The fibers have dense structure, low swelling, and bind water by hydration of free carbamide groups. In the p/p_s region up to 0.80 precipitated Capron also binds water only by hydration of free –NHCO– groups. On further increase of relative humidity precipitated Capron swells strongly because of the less dense packing of its macromolecules, and sorption of moisture can occur both by hydration of newly released carbamide groups and by capillary condensation. It follows that sorption of water as the result of capillary condensation exceeds sorption due to hydration of carbamide groups, which theoretically cannot exceed 16% in Capron and Anid if each –NHCO– group can add on one H_2O molecule.

Capron and Anid also differ little in their heats of wetting and variations of heat of wetting with moisture contents of the specimens (x) (Fig. 2).

The $q_{int} = f(x)$ curves in Fig. 2 show that the average decrease of the heat of wetting of Capron over the region of moisture contents up to 4% is ~ 1.3 cal/g; over the 4 to 8% region it is 0.5 cal/g, and over the 8 to 30.2% region it is only 0.05 cal/g; the corresponding values for Anid are 1.3, 0.2, and 0.01 cal/g. It follows that most of the heat is liberated owing to hydration of free carbamide groups in the polyamide macromolecules. This is illustrated very clearly by a graph for variations of the differential heats of wetting with the initial moisture contents of the samples (Fig. 3).

Our values for the heats of heats of wetting of Capron differ from those given in [3], probably because different Capron samples were studied. However, we must draw attention to an error in [3]: extrapolation of $q_{int} = f(x)$ curves to the abscissa axis in order to find the moisture content at which the heat effect is zero is inadmissible.

It follows from our work and from the data in [10] that such extrapolation may lead to serious errors. Mikhailov and Fainberg [3] represented the $q_{int} = f(x)$ curves as consisting of two straight lines and therefore, having found two values for the differential heats of wetting, they concluded that intramolecular and intermolecular hydrogen bonds are formed when water is bound by polycaprolactam. This may be so, but it should have been shown experimentally that at moisture contents of ~6% and higher the heat of interaction of Capron fiber and water is zero.

Our values for bound water (x_b) in Capron and Anid, calculated from the equation $q_{int}/x_b = 80$ [11], are 9.5 and 10.4%, respectively. These values correspond to the amount of water taken up at $p/p_s \sim 0.85$. Calculation of the amount of bound water per polyamid repeat unit shows that there is one water molecule per two carbamide groups.

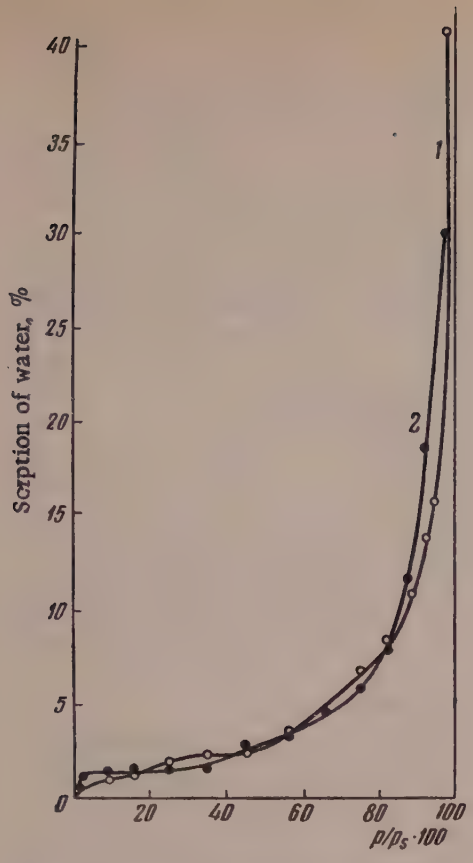


Fig. 1. Isotherms for sorption of water vapor by Anid (1) and Capron (2).

Figure 2 shows that at moisture contents corresponding to the content of bound water heat of wetting is still liberated (q = 1.5 cal/g). This poses the question whether the calculated values of x_b can be regarded as bound water. To settle the point, we determined the integral heats of wetting of Capron and Anid from the $q_{dif} = f(x)$ graph (Fig. 3), i.e., we found the value of $\int_0^{x_b} q_{dif}\,dx$. The values found for q_{int} were close to the experimental results; the doubt was therefore resolved.

An interesting fact is that the values of x_b calculated by means of our equation from the experimental heats of wetting of Capron given in [3] coincide almost exactly with the experimental values for bound water given in that paper. In [3] the value $\int_0^{x_b} q_{dif} = 600$ cal is given. Substitution of this into the equation $x_b = q_{int}/80$ gives $x_b = 7.5\%$, whereas the amount of bound water found experimentally in that study was 7.1%. The probable explanation for the somewhat lower value of bound water is that in this instance extrapolation of the $q_{int} = f(x)$ curve gives somewhat unreliable results, as discussed earlier.

Analysis of the graph in Fig. 3 is of particular interest. It is seen that the $q_{dif} = f(x)$ curve for Capron has two inflection points, at approximately 4 and 8% moisture contents. Over the region of the curve between zero and 4% moisture the differential heat is constant, and considerable (~ 120 cal per g); between 4 and 8% moisture the value falls rapidly to ~ 5 cal/g, and remains unchanged with further increase of moisture content.

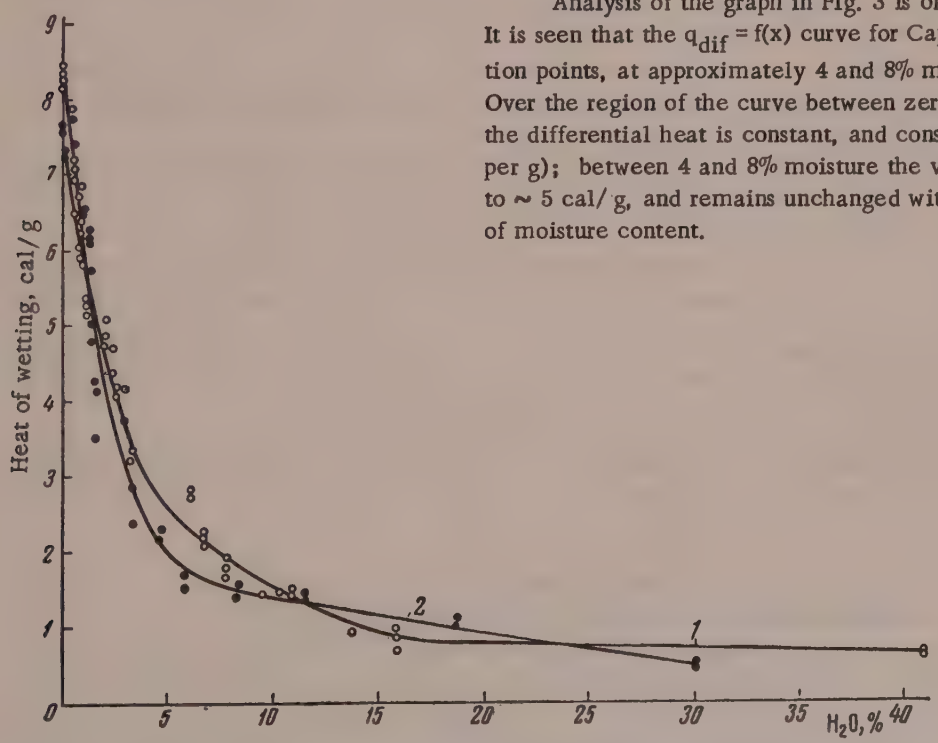


Fig. 2. Heats of wetting of Anid (1) and Capron (2) by water.

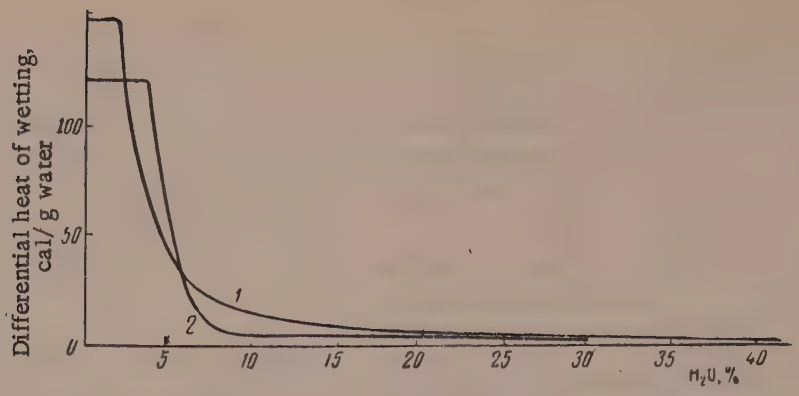


Fig. 3. Differential heats of wetting of Anid (1) and Capron (2).

It is clear from Fig. 3 that most of the heat of wetting (over 90%), probably due to hydration of carbamide groups, is liberated when Capron takes up moisture to 8% content. It is not clear why heat is liberated on further increase of moisture content. It is possible that swelling releases a certain amount of free –NHCO– groups, or that multilayer formation occurs.

Nothing definite can be said about this in absence of additional experimental data.

Analysis of variations of the differential heat of wetting with the initial moisture content leads to the conclusion that hydration of Capron results in one type of hydrogen bonding between free carbamide groups of the polycaprolactam molecule and water molecules.

The $q_{dif} = f(x)$ curve for hydration of Anid takes a similar course.

SUMMARY

1. Isotherms for sorption of water vapor by polycaprolactam (Capron) and polyhexamethyleneadipamide (Anid) at 20° are very similar in the p/p_s range from 0 to 0.85.

2. Curves for the heats of wetting of Capron and Anid with water at 20°, as functions of the moisture contents of the samples, are also very similar in character but differ in magnitude over certain regions.

3. The differential heats of sorption of water by Capron and Anid (q_{dif}) were calculated. It is shown that the $q_{dif} = f(x)$ curve consists of two regions over which these values are constant; these correspond to the heat of hydration of free carbamide groups and to heat liberated as the result of other processes.

4. The amount of bound water per carbamide group is the same for Capron as for Anid. Differences in the structure of the principal macromolecular chains of these polyamides do not affect their hydrophilic properties.

5. The values found for the amount of bound water (x_b) from equation $x_b = q_{int}/80$ are the same whichever value of the integral heat of wetting (q_{int}) is used – either the experimental value, or the value calculated from the graph for the differential heat of wetting as a function of moisture content.

The authors thank Academician of the Academy of Sciences UkrSSR A. V. Dumanskii for his constant interest and valuable advice in discussion of the results.

LITERATURE CITED

1. N. V. Mikhailov, É. Z. Fainberg, and S. M. Skuratov, Kolloid. Zhur. 15, 271 (1953).*
2. S. M. Skuratov, N. V. Mikhailov, and É. Z. Fainberg, Kolloid. Zhur. 16, 58 (1954).*
3. N. V. Mikhailov and É. Z. Fainberg, Kolloid. Zhur. 16, 120 (1954);* 18, 315 (1956).*
4. Z. G. Serebryakova and N. V. Mikhailov, Vysokomolek. Soed. 1, 222 (1959); N. V. Mikhailov and É. Z. Fainberg, Vysokomolek. Soed. 1, 201, 410 (1959); N. V. Mikhailov, Summaries of Papers at the Eighth Mendeleev Congress [in Russian] (Izd. Akad. Nauk SSSR, 1959) No. 6; V. A. Berestnev, T. V. Gatovskaya, V. A. Kargin, and E. Ya. Yaminskaya, Kolloid. Zhur. 20, 694 (1958);* Vysokomolek. Soed. 1, 337 (1959).

5. M. Dole and L. Faller, J. Amer. Chem. Soc. 72, 414 (1950); M. Dole and A. D. McLaren, J. Amer. Chem. Soc. 69, 651 (1947); W. R. Moore, Text. Recorder 1, 66, (1953); S. E. Smith, J. Amer. Chem. Soc. 69, 646, (1947).
6. E. F. Nekryach and A. V. Dumanskii, Ukrain. Khim. Zhur. 26, 3 (1960).
7. A. V. Dumanskii, Ya. F. Mezhennyi, and E. F. Nekryach, Kolloid. Zhur. 9, 355 (1947).
8. A. V. Dumanskii and E. F. Nekryach, Kolloid. Zhur. 15, 91 (1953).*
9. E. F. Nekryach, Zavodskaya Lab. 21, 1248 (1955).
10. R. É. Neiman and O. V. Neiman, Kolloid. Zhur. 4, 3 (1938).
11. A. V. Dumanskii, Ya. F. Mezhennyi, and E. F. Nekryach, Kolloid. Zhur. 10, 103 (1948).

*Original Russian pagination. See C. B. translation.

SORPTION OF WATER VAPOR AND HEAT OF WETTING OF SILICA GELS

E. F. Nekryach and Z. A. Samchenko

Institute of General and Inorganic Chemistry, Academy of Sciences UkrSSR, Kiev
Translated from Kolloidnyi Zhurnal, Vol. 22, No. 3, pp 293-296
May-June, 1960
Original article submitted February 25, 1960

There have been many investigations, both theoretical and practical in character, concerned with the interaction of hydrophilic substances with water. Despite the considerable successes in this field, a number of important questions relating to hydrophily remain unsolved. Further studies are required on the mechanism of water binding, the role of different functional groups in the process, and the influence of structural characteristics of the material and of other factors on it.

The most promising approach to a solution of these problems is provided by the combined use of thermochemical and sorption methods of investigation. Data obtained in this way have already led to a number of important conclusions concerning sorption of water (role of polar groups and degree of crystallinity of hydrophilic polymers in the sorption process, significance of swelling in sorptional hysteresis, etc.). At the same time, some important aspects are either still obscure or have not been studied at all (bonding energy of the first and subsequent layers of bound water, energy of interaction of similar functional groups with water molecules in relation to the chemical composition and structure of hydrophilic substances, nature of bound water close to the saturation pressure, etc.).

The purpose of the present investigation was study of water sorption by silica gels in relation to structure. Silica gels are similar in the nature of their interaction with water to the hydrophilic polymers studied by us earlier—starch and cellulose. All these substances bind water by hydration of free hydroxyl groups by hydrogen bonding. The differences between them lie in their different physical structure—silica gel has a rigid structure, the structure of starch is elastic, while cellulose occupies an intermediate position, having amorphous and highly oriented regions.

Characteristics of the silica gels used are given in the table.

Structural Characteristics of Silica Gels

Characteristics	Silica gels*		
	SI	SII	SIII
apparent density, g/cc	0,73	1,29	1,43
total pore volume, cc/g	0,91	0,32	0,25
maximum sorptional pore volume, cc/g	0,91	0,32	0,25
specific surface, m^2/g	184	493	600

The table shows that all the silica gels have pores accessible to water molecules. Silica gels SII and SIII are similar in porosity and specific surface, but SI differs sharply in both respects from SII and SIII, being coarsely porous and having a much smaller specific surface.

Methods used for preparation of silica gel specimens for sorptional and calorimetric experiments, and the experimental procedures, have been described previously [1].

The sorption isotherms and graphs showing variations of the heat of wetting with the amount of water previously taken up by the silica gels are given in Fig. 1 and 2.

It follows from Fig. 1 and 2 that SI differs sharply in properties from SII and SIII, which are similar to each other.

* The silica gels and their characteristics were kindly supplied by the Laboratory of Sorption Processes of the Institute of Physical Chemistry, Academy of Sciences UkrSSR. The authors thank Prof. I. E. Neimark, the head of the laboratory.

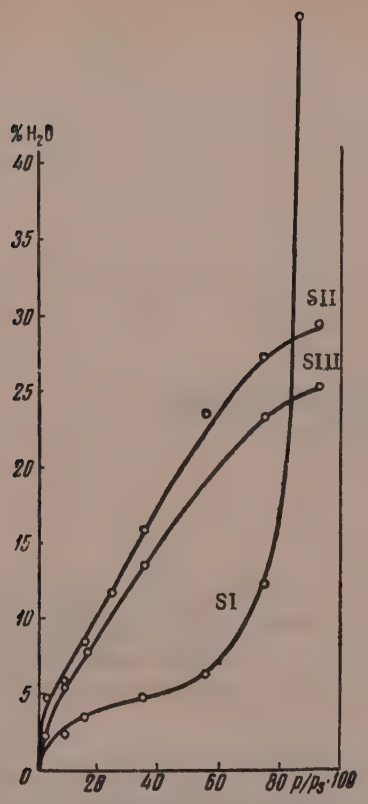


Fig. 1. Isotherms for sorption of water vapor by silica gels SI, SII, and SIII.

At p/p_s from zero to ~0.80 the isotherm for SI lies considerably lower than the isotherms for SII and SIII, and then rises sharply. Whereas at $p/p_s = 0.15$ SII and SIII take up twice as much water as SI, and three times as much at $p/p_s = 0.55$, at $p/p_s = 0.82$ the sorption values are the same, and at $p/p_s = 0.90$ SI takes up three times as much water as SII or SIII. This indicates that these silica gels take up water in different ways. In sorption of water vapor by the finely porous SII and SIII only surface adsorption of water molecules occurs, whereas sorption of water by coarsely porous SI proceeds in two stages—surface adsorption and capillary condensation in the silica gel pores.

When the curves for heat of wetting (q) of silica gels by water as a function of initial moisture content are examined, it is seen that the $q_{int} = f(x)$ curves for SII and SIII, like their isotherms, are similar, whereas the corresponding curve for SI differs sharply from them. The point of inflection on this curve corresponds to the inflection on the SI sorption isotherm—in both cases the amount of bound water x is 12.5-14% per g of silica gel. Beyond this point the heat of wetting decreases very slowly up to high moisture contents (> 80%), but its absolute value at these high moisture contents is very high. Thus, at $x \approx 50\%$ the heat of wetting is ~ 5 cal/g, and at $x \approx 85\%$ it is about 3 cal/g. These high heat effects at moisture contents when the monolayers have been completed are difficult to explain, because formation of further layers of bound water cannot be accompanied by liberation of considerable quantities of heat [2].

A very interesting fact is that the sorption isotherms and $q_{int} = f(x)$ curves for coarsely porous silica gel are very similar to the corresponding curves obtained by us for crystalline polyamides – polycaprolactam and polyhexamethyleneadipamide [3]. This suggests that the structure of precipitated Capron and Anid powders is analogous to that of coarsely porous silica gel, and accordingly sorption of water by these substances proceeds in two stages—the first is adsorption, and the second is capillary condensation.

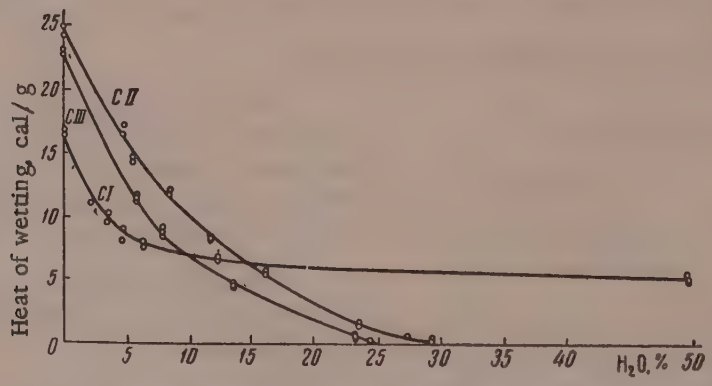


Fig. 2. Heats of wetting of silica gels SI, SII, and SIII by water.

As already stated, the adsorption isotherms and curves for heat of wetting of SII and SIII are similar. However, in both cases the curves for SII lie higher than those for SIII; it follows that SII is more hydrophilic than SIII, which is consistent with the data on their structures in the table. The total pore volume and the maximum sorptional pore volume of SII is greater than that of SIII (0.32 cc/g as against 0.25 cc/g), and therefore, the former can adsorb more water although its specific surface is less. Apparently steric hindrance has an effect here.

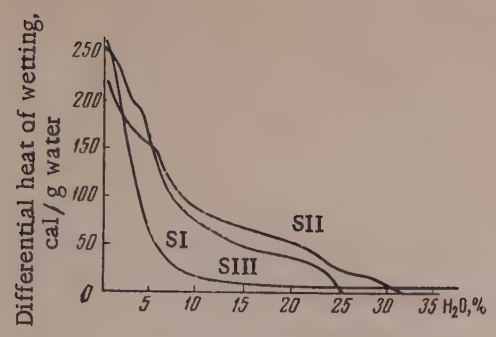


Fig. 3. Differential heats of wetting of silica gels SI, SII, and SIII.

The differential heats of wetting are plotted in Fig. 3 against the initial moisture contents of the silica gels. It is seen that binding of water by these gels is generally of the same character, but differs considerably at different moisture contents. The $q_{dif} = f(x)$ curve for SI has one inflection point at ~12% moisture content, beyond which the differential heat of wetting remains almost unchanged at a low value, little different from the heat of condensation of water vapor. A considerable quantity of heat is liberated in bonding a small proportion of the water; between 260 and 150 cal/g for 2.5%, and between 150 and 50 cal/g for 3%. The corresponding curves for SII and SIII both have two points of inflection, at moisture contents of 5.5 and 21.5% (SII) and 4.5 and 22.5% (SIII). Over these regions the differential heats of wetting fall from 220 to 150 cal/g and from 150 to 50 cal/g, respectively, (SII) and from 225 to 185 cal/g and from 185 to 30 cal/g (SIII). Evidently most of the heat of wetting of SII and SIII is liberated owing to hydration of OH groups, and they differ in their energies of interaction with water molecules. It follows that most of the water taken up is held by hydrogen bond forces. In the case of SI only a small proportion of the water taken up is held by hydration of OH groups, although the heat of wetting, as in the case of SII or SIII, is essentially heat of hydration, as Fig. 3 shows.

As in the interaction of polyamides with water [3], the values of $\int_0^{x_b} q_{dif}\,dx$ calculated from the $q_{dif} = f(x)$ graph were close to the integral heats of wetting found experimentally. The calculated and experimental values of q_{int} were: for SI, 15.7 and 16.5 cal/g; and for SII, 26.7 and 25.0 cal/g; and for SIII, 22.9 and 22.9 cal/g.

SUMMARY

1. Isotherms for sorption of water vapor at 20° by samples of coarsely and finely porous silica gels differ sharply in accordance with their porosities. In the case of finely porous silica gels the predominant role is played by adsorption of water by surface hydroxyl groups, while in coarsely porous silica gels capillary condensation in the pores is predominant.

2. Variations of the heats of wetting of the silica gels by water at 20° as functions of the initial moisture content are also different in character. The $q_{int} = f(x)$ curves for finely porous silica gels fall smoothly and reach the abscissa axis at moisture contents close to the amounts of bound water calculated from the equation $x_b = q_{int}/80$. The heat of wetting of coarsely porous silica gel varies similarly to that of finely porous silica gel at low moisture contents, but with further increase of moisture content it falls very slowly, and is very considerable at very high moisture contents.

3. Investigation of curves for the differential heats of wetting as functions of initial moisture contents showed that finely porous silica gels have two kinds of hydroxyl groups, different in their energy relationships, whereas coarsely porous silica gel contains only one kind.

4. The integral heats of wetting (q_{int}) calculated from the $q_{dif} = f(x)$ graphs are close to the values found experimentally.

The authors are deeply grateful to Academician of the Academy of Sciences Ukrainian SSR A. V. Dumanskii for his constant interest and valuable advice in discussions.

LITERATURE CITED

1. A. V. Dumanskii, Ya. F. Mezhennyi, and E. F. Nekrvach, Kolloid. Zhur. 9, 355 (1947); E. F. Nekryach and A. V. Dumanskii, Ukrain. Khim. Zhur. 26, 3 (1960); E. F. Nekryach, Zavodskaya Lab. 21, 1248 (1955).
2. W. D. Harkins and G. Jura, Coll. Chem. Theor. Appl. 6, 30 (1946).
3. E. F. Nekryach and Z. A. Samchenko, Kolloid. Zhur. 22, 288 (1960).*

*Original Russian pagination. See C. B. translation.

SOLUBILIZATION OF WATER IN HYDROCARBON SOLUTIONS OF LECITHIN

P. A. Demchenko

Institute of General and Inorganic Chemistry, Academy of Sciences UkrSSR, Kiev
Translated from Kolloidnyi Zhurnal, Vol. 22, No. 3, pp. 297-300
May-June, 1960
Original article submitted February 11, 1959

Solubilization of water by soap solutions in organic media was first observed by our compatriot Weichherz [1]. It was subsequently shown that water dissolves in hydrocarbons, immiscible with it under normal conditions, under the influence of various surface-active agents (SA); this is a common effect of interest in various branches of industry. Recent publications [2-5] contain results obtained in studies of individual systems, but there have been no systematic studies of solubilization of water in hydrocarbon solutions by various homologous surface-active agents. In the case of some hydrocarbon solutions of surface-active agents it has been found that solubilization of water increases almost linearly with increase of solubilizer concentration [2, 5, 6].

If SA solutions are used in hydrocarbon mixtures, solubilization of water is governed by more complex relationships [7].

As yet there have not been any comparative studies of the solubilizing effects of different hydrophilic groups in SA molecules, or of the influence of hydrocarbon radicals differing in length and structure on the binding of water.

It is believed that solubilization of hydrocarbons in aqueous soap solutions and of water in hydrocarbon solutions of surface-active agents proceeds by a similar mechanism [8], although the two processes differ greatly from the energy standpoint. Studies of hydrophilic and oleophilic properties of soaps have shown that the energy of bonding between a solubilizing liquid and a soap is the determining factor in solubilization and formation of thermodynamically stable solutions [9, 10].

Phosphatides, including lecithin, are becoming increasingly widely used as surface-active additives in the varnish and paint industry to prevent phase separation in paints [11], in systems of the emulsol type [12], in the food industry for production of high-grade margarine [13], and in other branches of the national economy. Lack of quantitative data on their lyophilic properties hinders studies of the properties of systems containing them, and retards their industrial utilization.

The present investigation is concerned with solubilization of water by lecithin dissolved in aromatic hydrocarbons.

Lecithin is a derivative of choline and the phosphate ester of glycerol in which two hydroxyl groups are esterified by fatty acids [14]. We prepared pure lecithin from crude phosphatides of sunflower oil by repeated treatment with acetone; the product was alternately dissolved in ether and precipitated with acetone 5-6 times until a transparent acetone solution was formed over the precipitate. The precipitated lecithin was separated from the liquid and dried under vacuum on a water bath. The pure lecithin so obtained, in the form of a pale-yellow powder, was used in the investigations.

The experimental procedure was as follows: water (1.5-2 ml) was put into the graduated tube of 1 of the glass apparatus (Fig. 1) through the tube 5 by means of a funnel with a thin drawn-out neck. After this 130-150 ml of lecithin solution of known concentration in an aromatic hydrocarbon was put into the bulb 2; the apparatus was closed by a well-fitting ground-glass stopper 6 and placed in a thermostat (bulb 4 of the apparatus was not immersed in the thermostatic liquid and acted as a pressure buffer). Solubilization of water was studied in benzene

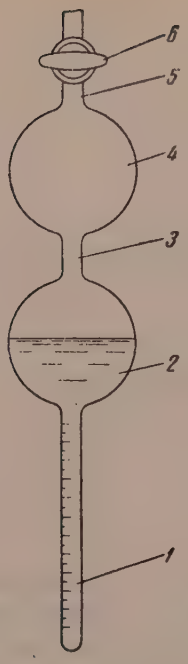


Fig. 1. Apparatus for determination of solubilization of water and of liquids of higher density than the surface-active agent solution. 1) Graduated tube; 2) bulb for solution; 3) connecting tube; 4) air bulb; 5) tube; 6) stopcock.

solutions of lecithin containing 4, 20, and 60 g of lecithin per liter, in toluene solutions containing 10, 20, and 50 g/liter, and in xylene solutions containing 10, 30 and 50 g/liter.

The course of solubilization of water in hydrocarbon solutions of lecithin was studied by observation of changes in the volume of water in the apparatus as indicated in the graduated tube 1. Maximum solubilization is reached more rapidly if water is agitated with the hydrocarbon solution of lecithin. Emulsions are not formed in the process, and excess water rapidly settles at the bottom of the vessel as a separate phase. With the apparatus in a vertical position the water collects in the graduated tube 1 and a clear boundary is formed between the water and the lecithin solution, so that the volume change can be accurately determined. It was assumed that maximum solubilization had been reached when absorption of water by the hydrocarbon solution of lecithin practically ceased and permanent turbidity caused by hydrated lecithin appeared in the solution. The amounts of solubilized water, in grams per gram of lecithin in the hydrocarbon solution, are given in the table.

This apparatus can be used for studying solubilization of various liquids in aqueous and nonaqueous solutions of surface-active agents, when the density of the solubilized liquid is higher than that of the solution.

Solubilization of Water in Hydrocarbon Solutions of Lecithin

Hydrocarbon	Lecithin conc. in solution, g/liter	Solubilization of water by solution, g/liter	Amt. of water solubilized, g/g lecithin	
			from vol. in apparatus	by Fischer titration
benzene	4	1,3	0,32	0,33
	20	6,4	0,32	0,32
	60	19,7	0,33	0,33
toluene	10	3,2	0,32	0,33
	20	6,5	0,33	0,32
	50	16,5	0,33	0,33
xylene	10	3,1	0,31	0,32
	30	9,9	0,33	0,33
	50	16,0	0,32	0,32

In addition to the method described above for determination of the amount of solubilized water the transparent solution of lecithin in the hydrocarbon, containing the maximum amount of solubilized water, was titrated with Fischer reagent [15]. The amounts of solubilized water in hydrocarbon solutions of lecithin as determined volumetrically in the apparatus and as found by means of the Fischer reagent were in close agreement: the value was 0.31-0.33 g of water per g of dissolved lecithin (see table).

Results of studies of the solubilizing action of lecithin solutions in benzene, toluene, and xylene showed that there is a nearly linear relationship between the amount of water solubilized and the concentration of lecithin in solution (Fig. 2). In the concentration range studied the dispersion medium has no effect on the amount of water solubilized by solutions of lecithin in aromatic hydrocarbons.

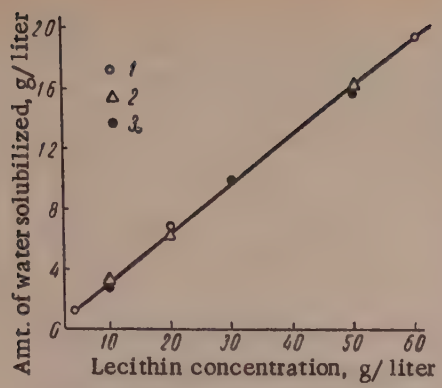


Fig. 2. Effects of lecithin concentration in benzene (1), toluene (2), and xylene (3) solutions on the amount of water solubilized.

To confirm that the nonaqueous lecithin solutions were stable equilibrium solutions, solutions containing 20 to 40 g of lecithin in toluene and xylene were kept in the laboratory for 13 months in contact with water; the amount of water taken was somewhat greater than required for maximum solubilization. Water was then determined in the transparent lecithin solutions by titration with Fischer reagent [15]. It was found that the solubilization of water, calculated on the lecithin present in solution, was 32.5-33.0%; that is, it was almost independent of the time of contact between the hydrocarbon solutions of lecithin and water, and depended only on the content of lecithin in the solutions. Solubilization of water in hydrocarbon solutions of lecithin is caused by interaction of complex polar groups of lecithin with water molecules.

If the molecular weight of lecithin is taken as 778 [16], it can be calculated from the experimental data that one mole of lecithin dissolved in an aromatic hydrocarbon solubilizes about 14 moles of water; $C_{42}H_{84}O_9PN \cdot 14\ H_2O$.

When solubilized water is distilled out of the system xylene–water–lecithin, the liquid remains clear and boils steadily with slight uniform frothing and without splashing. This system may serve as an analog of technically important systems formed in production of greases, margarine, and emulsols. Solubilized water should be regarded as a variety of bound water, as its evaporation requires thermal energy, greater than the heat of evaporation of an equal amount of free water by the amount of energy required for binding the water to the hydrophilic groups of the surface-active solubilizer.

The hydrophilic properties of phosphatides and other surface-active substances can be characterized by determination of solubilization of water by their solutions in hydrocarbons.

SUMMARY

1. Sols of lecithin in aromatic hydrocarbons remain transparent after absorption of water and do not emulsify the water when agitated with it up to the saturation limit. The saturation limit is indicated by the appearance of turbidity due to hydrated lecithin. In presence of water in excess of the solubilization limit large flakes are precipitated and a suspension of lecithin in water is formed.

2. It was shown volumetrically and by titration with Fischer reagent that there is an approximately linear relationship between the amount of water solubilized and the concentration of lecithin in the hydrocarbon solution. The amount of water solubilized by solutions of lecithin in benzene, toluene, and xylene is 0.31-0.33 g per g of lecithin, or about 14 moles of water per mole of lecithin.

3. It is suggested that the hydrophilic properties of surface-active substances differing in nature and structure can be assessed from solubilization of water by their solutions in hydrocarbons.

LITERATURE CITED

1. I. Weichherz, Kolloid-Z. 49, 158 (1929); I. Weichherz and N. Pleteneva, Kolloid. Zhur. 2, 133 (1936).
2. R. C. Pink, J. Chem. Soc., 53, (1939).
3. C. R. Palit and McBain, J. Soc. Chem. Ind., London 66, 3 (1947).
4. G. R. Halpern and I. Biel, J. Biol. Chem. 174, 817 (1948).
5. P. A. Rebinder and K. A. Pospelova, Introductory chapter to W. Clayton's "Emulsions" [Russian translation] (IL, Moscow, 1950) p. 11.
6. A. Kitahara, Bull. Chem. Soc. Japan 29, 15 (1956); 28, 234 (1956).
7. S. R. Palit, J. Colloid Sci. 4, 532 (1949).
8. K. A. Pospelova, Kolloid. Zhur. 11, 187 (1949).
9. A. V. Dumanskii and P. A. Demchenko, Doklady Akad. Nauk SSSR 78, 277 (1951).
10. P. A. Demchenko, A. V. Dumanskii, and L. G. Demchenko, Kolloid. Zhur. 14, 164 (1952).*
11. H. H. Hutt, J. Oil and Colour Chemists, Assoc. 39, 399 (1956).

*Original Russian pagination. See C. B. translation.

12. P. Scherman, J. Colloid. Sci. 10, 63 (1955).
13. G. S. Garmash, Production and Uses of Phosphatides [in Russian] (Izd. N.-T. O-va, Khar'kov, 1958).
14. A. M. Schwartz and J. W. Perry, Surface-Active Agents [Russian translation] (IL, Moscow, 1953).
15. J. Mitchell and D. M. Smith, Aquametry [Russian translation] (IL, Moscow, 1952).
16. Chemist's Handbook [in Russian] (Goskhimizdat, 1951) Vol. II, 622.

• Original Russian pagination. See C. B. translation.

ELECTROKINETIC PROPERTIES OF PEAT

M. P. Volarovich and G. Ya. Voronkov

Department of Physics, the Kalinin Peat Institute
Translated from Kolloidnyi Zhurnal, Vol. 22, No. 3, pp. 301-304
May-June, 1960
Original article submitted February 25, 1960

Electrokinetic effects are of interest in relation to evaluation of the surface properties of solids and various liquids [1-3]. In the case of peat, for example, they determine the course of various physicochemical processes in the deposit and the nature of the principal processes for winning, converting, and drying the peat. The existence of this connection between electrokinetic phenomena and various processes in disperse systems is due to a direct although indefinite relationship [4] between the electrokinetic potential (zeta-potential) and the stability of colloidal systems. There is known to be a connection between the zeta-potential and the hydration properties of peat [5] and clays [6]. Nevertheless, very little is known about the electrokinetic properties of peat.

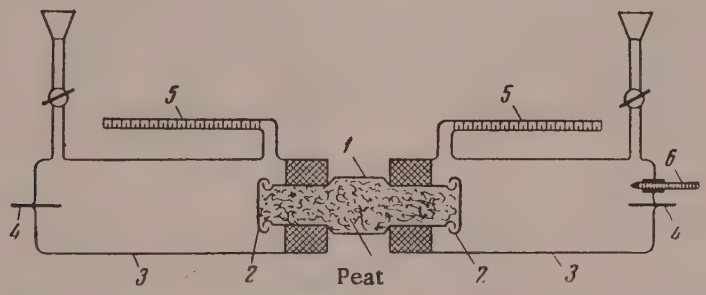


Fig. 1. Apparatus for determination of the zeta-potential of peat by an electroosmotic method: 1) Bulb; 2) Capron gauze caps; 3) chambers; 4) electrodes; 5) capillaries; 6) thermometer.

The electrokinetic potential of peat was determined by an electroosmotic method with an apparatus (Fig. 1) which was a modified form of the Aleshin [7] and Perrin [8] apparatus. A definite weight of processed raw peat was suspended in distilled water to which various reagents could be added. Water was filtered off from the suspension until the peat was at a state of complete saturation. At the end of the filtration the peat was put into the bulb 1 (Fig. 1), covered with Capron gauze caps; the pH of the filtrate was determined and the filtrate was then poured into the chambers 3. The apparatus was then connected to the circuit usual for such determinations, by means of the platinum electrodes 4. Electroosmotic flow of the liquid phase was observed in the capillaries 5.

The zeta-potential was calculated from the Helmholtz–Smoluchowskii equation [1]; viscosities and dielectric constants for free water at the experimental temperatures were taken from tables. It is known that most of the particles in processed peat are in the size range above 2μ [9]. Because of this there is no need to take surface conduction into account [10] in determinations of zeta-potential. Preliminary experiments were carried

out in order to find the length of bulb needed to eliminate any possible errors in determinations of zeta-potential because of the short length of the diaphragm [11]. The limiting current strength below which the electrokinetic potential remains constant [1] was also determined.

The experiments were performed with upper medium peat of degree of decomposition R=10%, and pinewood bottom peat of R=40%. It was shown experimentally that decrease of the peat particle size by mechanical dispersion (according to results obtained with a sedimentimetric balance [9] the specific surface of the material reached 12 m^2/g of dry material) has no effect on the electrokinetic potential.

The influence of pH on the zeta-potential of peat is represented in Fig. 2 (the pH was varied by additions of HCl or NaOH). It follows from Fig. 2 that the zeta-potential of peat increases with increase of pH, whereas the conductivity of the system decreases in every experiment (Fig. 3). The zeta-potential of upper peat is higher than that of bottom peat at the same pH values because of differences in the chemical composition of the peats; in particular, because upper peat has a higher calcium content [12]. Particles of upper peat therefore have thicker diffuse outer layers. This explains why, according to Samarina [13] with the same contents of dry material and at almost the same degree of decomposition upper peat suspensions had higher viscosities than suspensions of bottom peat. In addition, it has been shown [14] that upper peats bind rather more immobilized water.

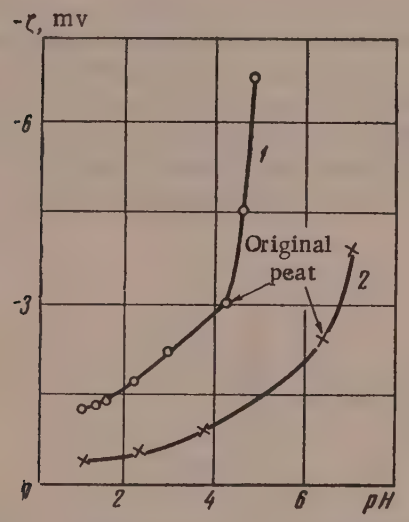


Fig. 2. Influence of pH on the zeta-potential of upper (1) and bottom (2) peat.

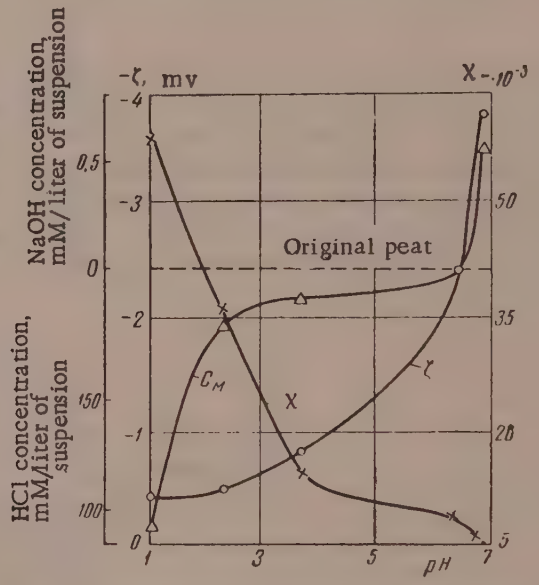


Fig. 3. Influence of pH on the zeta-potential and conductivity (X) of bottom peat with changes in the concentration (C_m) of HCl and NaOH.

To investigate the effects of cations of different valences on the electrokinetic potential of peats, salts (NaCl, $CaCl_2$, and $FeCl_3$) were added to the distilled water used for preparing the suspensions. In agreement with the views of Antipov-Karataev [15] and others [16] we assumed that when these salts are added ion exchange takes place on the particle surfaces. Variations of the zeta-potential of upper and bottom peats as the result of adsorption of uni-, bi-, and trivalent ions are shown graphically in Fig. 4. It is seen that, as in the case of other colloid and capillary systems [1], cations lower the zeta-potential of peat, and the lowering effect increases with increasing valence and concentration of the adsorbed ions. The electrokinetic potential of peat is also lowered by addition of a surface-active agent (NaOl)* (see table).

In addition to changes produced in the electric double layer, characterized by changes of the zeta-potential, the above-named reagents may cause changes in the structure and thickness of the solvation liquid layers. It is known [17] that the disjoining effect of these layers has a strong influence on various properties of disperse systems. Studies of the electrokinetic properties of peat indicate that there are great potentialities for improving the physical and mechanical properties of processed fuel peat by application of the methods of physicochemical mechanics [18].

* Probably refers to sodium oleate.

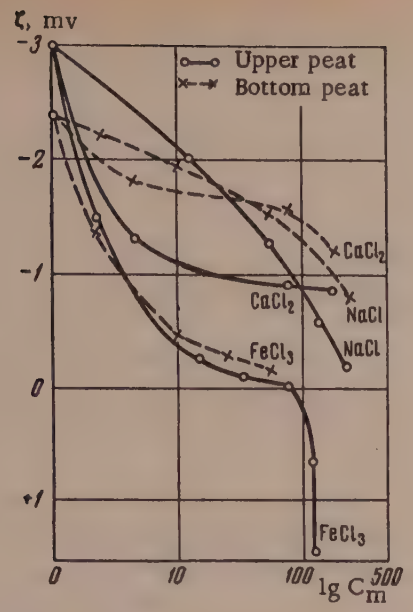


Fig. 4. Effects of cations of different valences on zeta-potential of peats.

Effect of NaOl on the Electrokinetic Properties of Peats

NaOl concentration, g per liter of peat slurry	Zeta-potential, mv	
	upper medium peat, R = 10%	pinewood bottom peat, R = 40%
Original peat	−3.0	−2.45
0.5	−2.8	−2.3
1.0	−2.7	−2.3
5.0	−2.3	−2.05

SUMMARY

1. A technique has been developed for studying the electrokinetic properties of peat by an electroosmotic method, and the zeta-potentials of upper and bottom peats have been determined.

2. Upper peat had a higher zeta-potential than bottom peat because the latter has a higher content of bivalent cations.

3. Increase of pH raises the zeta-potential of peat. Additions of cations of different valences result in corresponding decreases of the zeta-potential of peat in the same way as in other systems.

LITERATURE CITED

1. Electrokinetic Properties of Capillary Systems [in Russian] (Izd. AN SSSR, 1956).
2. A. N. Frumkin, Usp. Khimii 15, 385 (1946).
3. S. Glasstone, Introduction to Electrochemistry [Russian translation] (IL, Moscow, 1951).
4. B. V. Deryagin, Proc. Third All-Union Conference on Colloid Chemistry [in Russian] (Izd. AN SSSR, 1956) p. 225.
5. A. V. Dumanskii and M. V. Chapek, Kolloid. Zhur. 2, 95 (1936); A. V. Dumanskii, Izvest. Akad. Nauk SSSR, Ser. Khim. Nauk 5, 1975 (1937).
6. E. T. Uskova, Kolloid. Zhur. 20, 102 (1958).*
7. S. N. Aleshin, Kolloid. Zhur. 6, 701 (1940).
8. N. P. Peskov, Physicochemical Principles of Colloid Science, 2nd ed. [in Russian] (Khim.-Tekhn. Izd., 1934).
9. M. P. Volarovich and N. V. Churaev, Kolloid. Zhur. 17, 200 (1955);* Proc. 3rd All-Union Conference on Colloid Chemistry [in Russian] (Izd. AN SSSR, 1956) p. 258.
10. L. I. Zhukov and D. A. Fridrikhsberg, Kolloid. Zhur. 11, 163 (1944).
11. O. N. Grigorov and K. P. Tikhomolova, Kolloid. Zhur. 19, 406 (1957).*
12. N. V. Churaev, Trudy Mosk. Torfyanogo In-ta, 5, 113 (1957).
13. N. N. Kulakov, Introduction to the Physics of Peat [in Russian] (GÉI, 1947) p. 153.
14. M. P. Volarovich and N. V. Churaev, Kolloid. Zhur. 21, 157 (1959).*
15. L. N. Antipov-Karataev and G. M. Kader, Kolloid. Zhur. 9, 81 (1947).
16. P. I. Bel'kevich and L. R. Chistova, Trudy In-ta Torfa AN Belorussk. SSR 6, 130 (1957).
17. B. V. Deryagin, Proroda 2, 23 (1943); S. V. Nerpin and B. V. Deryagin, Doklady Akad. Nauk SSSR 100, 17 (1955).
18. P. A. Rebinder, Vestnik Akad. Nauk SSSR 1, 44 (1959); Physicochemical Mechanics, a New Field of Science [in Russian] (Znanie, 1958).

* Original Russian pagination. See C. B. Translation.

EFFECT OF FREEZING ON THE PROPERTIES OF COAGULATED METAL HYDROXIDES

1. INFLUENCE OF FREEZING AND THAWING CONDITIONS ON THE PROPERTIES OF COAGULATED FERRIC HYDROXIDE

V. L. Zolotavin, V. V. Vol'khin and V. V. Rezvushkin

S. M. Kirov Urals Polytechnic Institute, Sverdlovsk
Translated from Kolloidnyi Zhurnal, Vol. 22, No. 3, pp. 305-313
May-June, 1960
Original article submitted June 15, 1959

The coagulating effect of freezing on sols, first discovered by Lyubavin [1], was later studied by a number of investigators [2-3]. The effect of freezing on coagulated metal hydroxides has been studied much less, although it has been reported that such precipitates become granular and shrink considerably after freezing and thawing [4-7]. In view of the favorable effects of freezing on coagulates, further studies of all aspects of this process are of great theoretical and practical interest. Considerable advances have now been made in refrigeration technology, so that even now freezing can be used in improvements to processes of effluent purification, in dehydration and washing of precipitates difficult to filter in chemical technology, and for improving the properties of coagulates in laboratory practice.

The present paper contains data obtained in a study of the effects of various freezing and thawing conditions on the volume, particle size, sedimentation and filtration rates, and moisture content of ferric hydroxide precipitates.

Ferric hydroxide was prepared by the action of 0.2 N NH_4OH on $Fe_2(SO_4)_3$ solution (14-15 g/liter) with continuous stirring in the cold until pH 7.1-7.5 was reached. The precipitate was washed to a negative reaction for SO_4^{2-} ($BaCl_2$ test), and to pH 5.2-5.4. It was then left to settle for 12 hours, the supernatant liquid was decanted off, and iron was determined in the suspension by the Trilon method. The sample volume used in the experiments was 25 ml of hydroxide (about 225 mg Fe_2O_3). The freezing was performed in an air-cooled thermostat based on a Freon refrigeration unit with a BR-RKF-0.9 compressor, at −1, −5, −10, and −15°.

Effect of freezing and thawing conditions on precipitate volume. The effect of the time of exposure at various subzero temperatures on the volume of the precipitate is shown in Fig. 1. The initial value was taken to be the volume of the coagulate occupied in a nonfrozen sample after sedimentation to a constant level. In this experiment all the frozen samples were thawed in air at room temperature.

Figure 1 shows that a sharp decrease of the hydroxide volume corresponds to the instant when the whole sample is completely frozen through. Since the solidification temperature of the electrolyte-free coagulate is almost zero, the times of freezing of equal volumes of coagulate and distilled water are equal.

The effect of further exposure to low temperatures after complete freezing on the precipitate volume was also studied at different temperatures (Fig. 2). The results indicate that the volume of the "zot" * decreases considerably with decrease of the freezing temperature. Exposure in the frozen state has a significant influence only at freezing temperatures close to zero. In the experiments described the samples underwent an average 15-to 25-fold shrinkage.

* Since the properties on the precipitate are altered sharply after freezing and thawing, it has been given the special name of "zot," at S. A. Voznesenskii's suggestion.

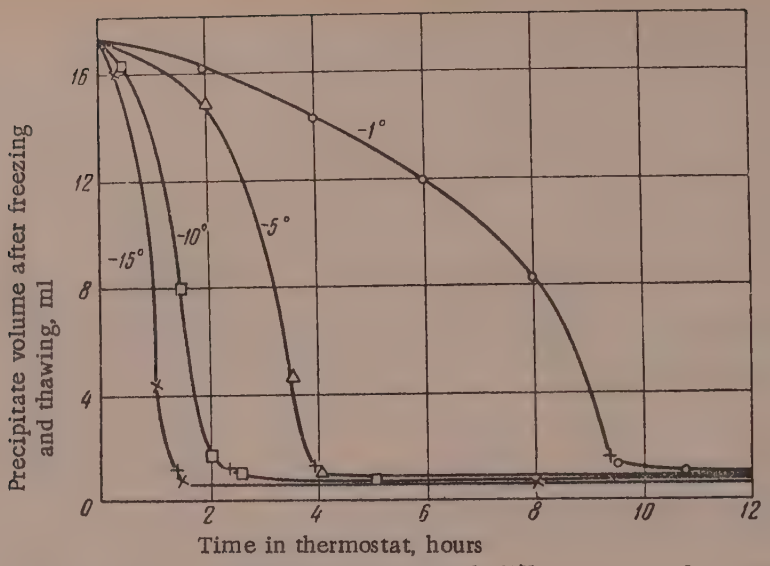


Fig. 1. Changes of coagulate volume with different times of exposure in a thermostatic refrigerator at various temperatures. + indicates the time required for complete freezing of distilled water.

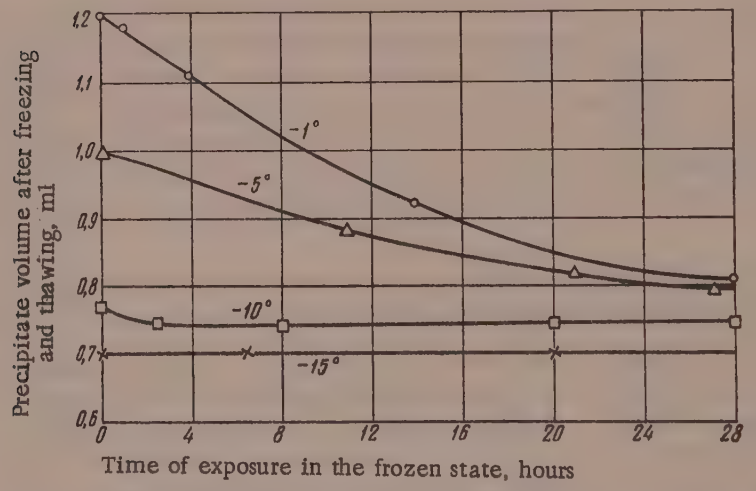


Fig. 2. Changes of zot volume with the time of exposure at different freezing temperatures from the instant of complete freezing.

The effects of various thawing conditions on the zot volume were studied (Table 1), in order to reduce the time of thawing of the frozen precipitate (it must be remembered that thawing may take longer than freezing). In these experiments 570 ml samples of hydroxide were used; this corresponds to 400 ml of precipitate after settling to constant level. The samples were kept in the thermostat for 15 hours.

Table 1 shows that the rate of thawing has no significant influence on the zot volume. Comparison of the results of these and the preceding experiments also shows that the freezing effect is independent of the initial sample volume. The iron content per unit zot volume is roughly the same in both cases, 125-230 mg/ml, in accordance with the temperature of freezing.

Influence of freezing and thawing conditions on precipitate particle size. The size of the ferric hydroxide particles before and after freezing was determined by Figurovskii's method of gravimetric sedimentation analysis [8]. It was found that the particle size of freshly prepared hydroxide is in the 1-10 range. (It must be remembered

that these sizes apply to aggregates of numerous smaller particles). The differential size-distribution curves for the zot particles are given in Fig. 3.

TABLE 1.

Influence of Freezing Conditions on Zot Volume

Freezing temperature deg.	Zot volume after thawing, ml		
	in snow bath, 20 hrs	in air at room temp. 8 hrs	in water at 50°, 15 min
— 1	19,8	20,5	20,1
— 5	18,2	18,6	18,3
—10	17,5	16,9	17,4
—15	15,8	15,4	15,2

It follows from Fig. 3 that the precipitates obtained after thawing become coarser with rise of the freezing temperature; the largest particles are found in the precipitate formed at −1°. Exposure of the precipitate in the frozen state influences the zot particle size appreciably only at temperatures close to zero, when the proportion of coarse particles increases somewhat, (Fig. 4) and has almost no effect at lower freezing temperatures.

At the temperatures investigated, freezing and thawing of ferric hydroxide washed free from electrolytes results in 5- to 15-fold increase of particle size. In these experiments the thawing conditions did not influence the zot particle size.

Influence of freezing and thawing conditions on the sedimentation rate. Sedimentation curves for nonfrozen coagulates and zot prepared at different temperatures are given in Fig. 5. Comparison of these curves show that the sedimentation rate of zot is about 1000 times that of the coagulate. As the size of the zot particles decreases with decrease of freezing temperature, the sedimentation time increases accordingly. As in the previous instance, thawing conditions do not have any appreciable influence on the zot sedimentation rate.

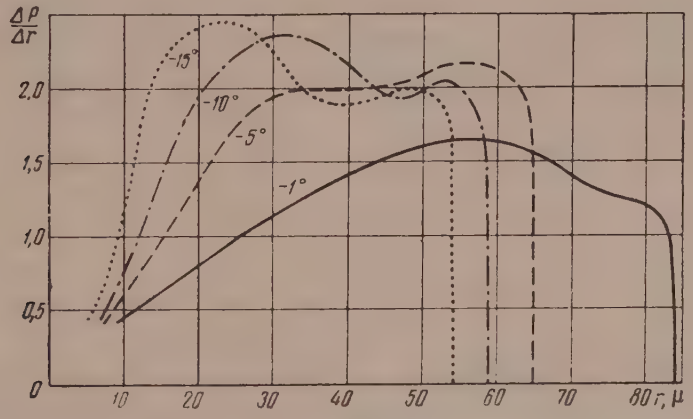


Fig. 3. Particle radii of zot precipitates formed at different freezing temperatures.

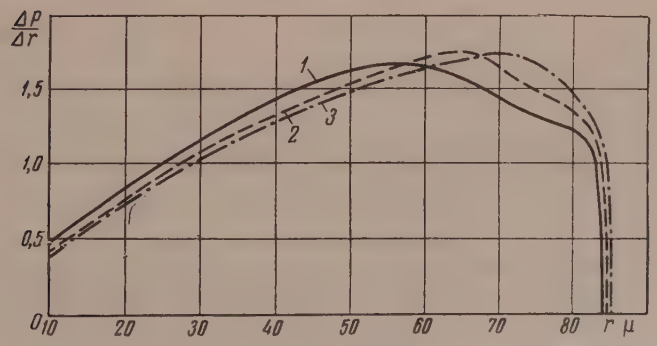


Fig. 4. Particle radii in zot precipitates held for different times in the frozen state at −1°: 1) Immediately after freezing; 2) held in the frozen state for 14 hours; 3) same, 40 hours.

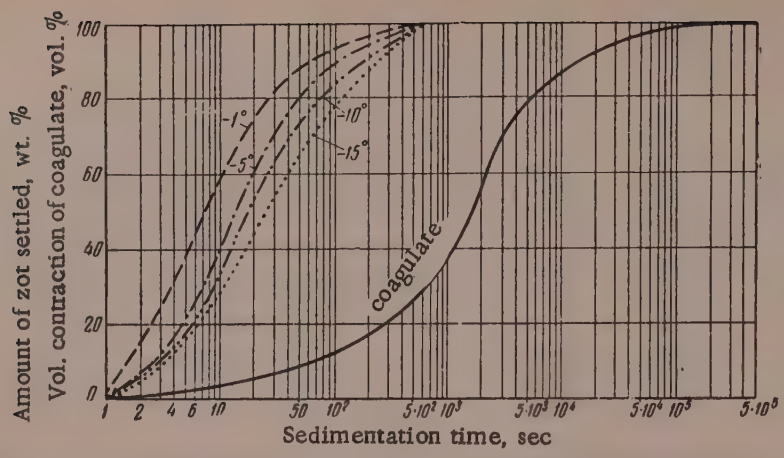


Fig. 5. Sedimentation rates of coagulate and zot precipitates formed at different freezing temperatures.

Influence of freezing and thawing conditions on the filtration rate. As was noted earlier, freezing and thawing of ferric hydroxide coagulates results in formation of granular precipitates with considerably larger particles. The rate of filtration through such precipitates is therefore greatly increased. However, as the liquid passes through the zot layer the filtration channels gradually become plugged, probably because of partial surface disaggregation of the particles, and the filtration rate falls continuously. Since the filtration rate does not remain constant, filtration rate constants cannot be calculated by the usual methods [9]. Therefore, mathematical analysis of the experimental data was performed with the aid of the equation for so-called plugging filtration [10], which takes place when a suspension containing a small number of fine particles is filtered through a cake (or filter layer) of constant thickness. The only difference is that in our case plugging of the filtration channels in the zot precipitates is caused by breakdown products from the precipitate itself and not by particles suspended in the filtered liquid.

Plugging filtration is represented by the equation

$$K\tau = \tau/V - 1/S_0, \tag{1}$$

where V is the volume of filtrate; τ is the time of filtration; S_0 is the filtration rate at the start of the process; K is the filtration constant.

For plugging filtration the (τ/V)–τ relationship is linear, the rate constant is given by the slope factor of this line, and $1/S_0$ is given by the intercept cut off by the straight line along the axis of ordinates in Fig. 6, which shows variation of the rate of filtration through a precipitate frozen at –5° (duration of freezing 48 hours) and held for 45 hours before the start of filtration.

The relationship between the initial filtration rate and the pressure difference is given by the equation

$$S_0 = P/R_0\eta, \tag{2}$$

where P is the pressure difference in filtration, R_0 is the resistance of the precipitate at the start of filtration, and η is the filtrate viscosity.

The filtration constant, which characterizes retardation of the process, depends only on the properties of the precipitate. If the pressure is altered its value should remain unchanged, and the straight line in the graph is merely shifted in a parallel direction.

From the initial rate and the filtration constant we can assess the filtration behavior of the precipitate and calculate the volume of filtrate obtained from 1 m^2 of filter area at a given instant from the start of the process.

$$V = 1/(K + 1/S_0\tau). \tag{3}$$

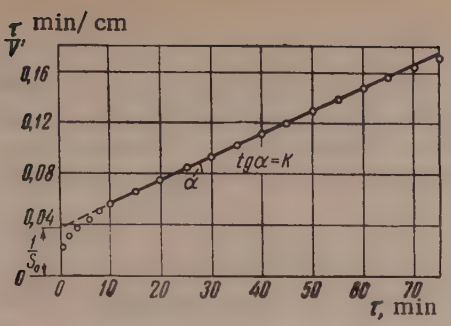


Fig. 6. Rate of filtration through zot precipitate as a function of the time from the start of filtration.

The volume of filtrate at the instant when total plugging occurs is

$$V = 1/K. \qquad (4)$$

In all the cases studied a linear relationship was obtained between τ/V and τ by the method described above. Deviations occur only at the earliest stages of filtration, when the particles are being deposited on the filter, and at the end of the process, because complete plugging is not attained and the filtration rate becomes almost constant, somewhat greater than the rate for nonfrozen coagulate. Table 2 gives the initial filtration rates and constants, determined in glass columns 1 cm^2 in cross sections, with a pressure difference of 550 mm water column. Zot precipitates containing equal weights of hydroxide (corresponding to 225 mg Fe_2O_3) were placed on sand drainage beds, and decanted liquor from frozen and thawed hydroxide (previously passed through a paper filter) was passed through them at 20°.

TABLE 2.

Influence of Freezing Conditions on Rate of Filtration Through Zot Precipitates. The Frozen Precipitates were Thawed in Air At Room Temperature*

Holding time of precipitate after thawing, hrs	S_0, $cm \cdot min^{-1}$	$K \cdot 10^{-5}$, cm^{-1}	S_0, $cm \cdot min^{-1}$	$K \cdot 10^{-5}$, cm^{-1}	S_0, $cm \cdot min^{-1}$	$K \cdot 10^{-5}$, cm^{-1}
	Frozen at —1° during					
	9,5 hr		20 hr		48 hr	
0—4	20,9	630	25,0	550	22,1	400
45—50	21,4	230	27,8	250	25,8	160
165—170	42,4	42	45,4	32	51,0	30
	Frozen at —5° during					
	4 hr		15 hr		24 hr	
0—4	17,2	320	17,3	192	19,9	170
45—50	19,1	157	15,1	118	19,8	90
165—170	18,9	83	23,4	89	22,9	58
	Frozen at —10° during					
	2,5 hr		13 hr		23 hr	
0—4	13,1	192	14,0	176	14,1	134
45—50	13,9	126	14,1	118	14,5	105
165—170	14,3	88	15,1	92	15,1	80
	Frozen at —15° during					
	1,5 hr		12 hr		22 hr	
0—4	11,8	164	12,9	108	13,1	112
45—50	12,2	95	12,8	93	14,1	90
165—170	13,2	91	14,0	83	14,2	84

* The filtration rate through precipitates thawed in a snow bath or in hot water (50°) depends similarly on the freezing conditions, but in some instances it is somewhat higher than the corresponding rate for precipitates thawed in air at room temperature.

Table 2 shows that the filtration rate does not always correspond to the particle size of the zot precipitates, but depends in a complex manner on the freezing and thawing conditions. At the same time, for some time after thawing zot precipitates have increased filterability in proportion to the time of holding before filtration. This increase is especially noticeable in precipitates obtained at freezing temperatures close to zero. For example, the average filtration rate immediately after thawing is greater through a precipitate obtained at −15° than at −1°. The

reverse result is found if the precipitates are held after thawing: in this case the filtration rate is considerably higher with the precipitate frozen at −1°, in accordance with its larger particles.

The explanation of the observed effect is that aging of zot after thawing strengthens its particles [4] it should be remembered that freezing accelerates the aging process) and they break down less during filtration. Since at freezing temperatures close to zero the largest but less strong zot particles are formed, the rate of filtration through freshly prepared precipitates falls rapidly in such cases. This fall is retarded considerably by aging, as the particles become stronger.

Holding of the precipitate in the frozen state and decrease of the freezing temperature both favor compaction of the particles, and the latter become stronger. The precipitates formed under these conditions are more difficult to break down, and the fall of filtration rate is slower.

Since the particles in a precipitate remain longer in the frozen state when the precipitate is thawed in a snow bath, this also results in a certain increase of the filtration rate as compared with precipitates thawed at room temperature. The experiments showed that thawing of frozen hydroxide in hot water also improves its filterability somewhat. This is possibly because increase of temperature favors aging.

In order to compare these results with data on rates of filtration through nonfrozen hydroxide precipitates, analogous experiments were carried out with the latter. The filtration rate for nonfrozen hydroxide is 0.003 m/hr for a precipitate of equal weight to the zot, or 0.0045 m/hr for a precipitate of equal volume to the zot. Comparison of these values with the average values over the whole period for zot shows that freezing and subsequent thawing of ferric hydroxide increases the rate of filtration from 200- to 5000-fold.

It should also be noted that if the zot precipitate is stirred after filtration or frozen again on the filter its filtering power is restored; this is a favorable factor in practical utilization of the freezing method.

Influence of freezing and thawing conditions on moisture content of precipitates. To determine the influence of different freezing conditions on the moisture content of zot precipitates, four sets of moisture determinations were carried out: after settling, after vacuum filtration, after drying in air at room temperature, and after drying at 105°. The moisture contents of nonfrozen coagulates were determined under analogous conditions. The results are presented in Table 3.

TABLE 3

Effects of Freezing Temperature (t_{fr}) and Time on Moisture Content of Precipitates.

Freezing time, hrs	Moisture contents of precipitates after settling to a constant level (A), and after vacuum filtration (B), %							
	$t_{fr} = -1°$		$t_{fr} = -5°$		$t_{fr} = -10°$		$t_{fr} = -15°$	
	A	B	A	B	A	B	A	B
0	98,3	91,5	98,3	91,3	98,3	91,6	98,3	91,3
1	—	—	—	—	95,0	—	95,0	85,4
1,5	—	—	—	—	87,0	—	75,2	66,7
2,5	—	—	—	—	77,7	68,0	—	—
4	98,0	87,6	82,8	69,5	—	—	—	—
6	97,8	87,2	—	—	77,0	67,0	75,2	66,5
9,5	85,5	73,4	82,8	69,3	—	—	—	—
10,5	85,4	72,1	80,4	69,0	—	—	—	—
12	84,5	73,5	—	—	—	—	—	—
22	81,5	71,9	80,1	68,7	77,0	67,0	75,2	66,2
25	—	—	79,0	68,4	77,1	67,5	—	—
48	80,7	70,2	79,1	69,0	—	—	—	—

Note. Below the heavy line the precipitates were completely frozen through.

It follows from Table 3 that the moisture content of freely settled precipitates falls from 99% before freezing to 75-85% after freezing and thawing. The decrease of moisture content is greater at lower freezing temperatures and longer times of holding in the frozen state. The moisture content of zot precipitates filtered under vacuum is 18-25% lower than the moisture content of coagulates.

In the air-dry state and after drying at 105° the moisture contents of coagulates and zots are equal. The moisture content in the air-dry state is 28-29% of the weight of precipitate, which corresponds to the composition $Fe_2O_3 \cdot (3.4\text{-}3.5) \cdot H_2O$. The same value for the moisture content of air-dry ferric hydroxide was obtained by Hepburn [6]. The moisture content of precipitates dried at 105° is 13-12.6%. This agrees with the moisture content at 105° as determined for ferric hydroxide by Rode [11] by thermal analysis.

The moisture content of freely settled and vacuum-filtered zot precipitates therefore decreases with lowering of the freezing temperature and increase of the time of holding at the particular subzero temperature. Analogous effects have been observed in studies of the effects of freezing on bound water in soils and various colloidal systems [12-17], but as yet there is no generally accepted explanation for them. Some authors associate the effect with lowering of the freezing point of water in the precipitate capillaries as their diameter decreases [12], and others correlate it with the degree of undercooling of water in the precipitate pores and hence with the rate of its crystallization [14]. We believe that the more correct explanation in the present instance is that given by Dumanskii [15] and Tsitovich [16, 17] who consider that in immediate contact with the particle surface there is a layer of bound water which is, according to a number of indications, in the solid state and which does not undergo detectable changes at subzero temperatures. Beyond this is a layer of oriented water; the influence of surface forces on these molecules diminishes with increasing distance from the particle surface. The influence of the freezing temperature is considered with respect to this part of the water, because the lower the subzero temperature the deeper is the freezing through of the oriented water. Free water, if it does not contain considerable amounts of dissolved substances, almost always freezes in large volumes at temperatures close to zero.

As yet there are no convincing theories to account for the influence of the time during which the samples are kept in the frozen state, especially as in many instances nonfreezing water has been detected in substances which had been kept for very long periods in the frozen state at fairly low subzero temperatures [13, 14, 17].

In our experiments, carried out at freezing temperatures not below −15° dehydration of ferric hydroxide is due to the loss of the part of the water which is completely removed in air drying, and therefore, the moisture contents of zot and nonfrozen hydroxide are the same.

It should also be noted that the thawing conditions never influence the moisture contents of the hydroxide precipitates.

The results of studies of the effects of freezing on the properties of ferric hydroxide give the following picture of the process. Coagulated ferric hydroxide prepared at room temperature has an extensively developed structure the cells of which contain up to 99% water (on the weight of the precipitate). When the hydroxide is frozen the first stage is crystallization of water, which begins at the walls of the vessel. The hydroxide particles migrate toward the center of the sample and are concentrated in the interlayers between the ice crystals. Growth of the latter breaks down the spatial structure of the coagulate and its particles begin to aggregate. After the thawing process the compact particles settle to the bottom and the water which was previously held in the cells of the precipitate is liberated. The volume of the resultant zot is considerably less than the volume of the coagulate, and the precipitate itself becomes granular in structure.

At lower temperatures solidification extends to layers of water closer to the particle surfaces; accordingly, the particles become more compressed and the resultant zot precipitate undergoes greater dehydration and occupies a smaller volume.

SUMMARY

1. The influence of freezing and thawing conditions on certain properties of coagulated ferric hydroxide was studied; these properties were found to change sharply.

2. When ferric hydroxide is frozen at temperatures from −1 to −15° its volume after thawing is decreased 15- to 25-fold, the moisture content of the filtered precipitate is 15-20% lower, the particle size is increased 5- to 15-fold, the sedimentation rate is increased 1000-fold, and the filtration rate is increased 200- to 5000-fold.

3. There is a complex relationship between the freezing conditions and changes in the properties of ferric hydroxide; the mechanism of the process is discussed.

4. The rate of thawing was not found to have any significant effect on the properties of frozen and thawed ferric hydroxic.

LITERATURE CITED

1. N. N. Lyubavin, Zhur. Russ. Fiz.-Khim. O-va 21, 397 (1889).
2. S. I. Dyachkovskii, Zhur. Russ. Fiz.-Khim. O-va 62, 1285 (1930); Zhur. Obshchei Khim. 1, 964 (1931); A. Lottermoser, Z. Phys. Chem. 60, 462 (1907); V. A. Kargin and M. L. Tolstaya, Zhur. Fiz. Khim. 16, 116 (1942); Shohei Uno, Naoji Ichiji, and Akio Kabayashi, J. Chem. Soc. Japan, Pure Chem. Sect. 72, 877, (1951); Chem. Abstrs. 46, (6465); Tominosuke Katsurai, Bull. Chem. Soc. Japan 24, 142 (1952).
3. A. Buzagh, Koll.-Z. 146, 133 (1956).
4. A. Lottermoser and F. Langenscheidt, Koll.-Z. 58, 336 (1932).
5. E. I. Kvyat, Zhur. Fiz. Khim. 12, 634, 660 (1938).
6. J. R. L. Hepburn, Rec. Trav. Chim. 45, 321 (1926).
7. Shohei Uno, J. Soc. Chem. Ind., Japan 43, 197 (1940).
8. N. A. Figurovskii, Sedimentation Analysis [in Russian] (Moscow–Leningrad, 1948).
9. W. Siegel, Filtration [Russian translation] (GONTI, 1939).
10. T. F. Dmitrieva and A. B. Pakshver, Khim. Prom. 11, 340 (1951).
11. E. Ya. Rode, Izv. Sekt. Fiz.-Khim. Analiza AN SSSR 16, 3 (1948).
12. H. W. Foote and B. Saxton, J. Amer. Chem. Soc. 18, 3, 588 (1916); 6, 1103 (1917).
13. E. A. Fisher, J. Phys. Chem. 28, 4, 360 (1924).
14. S. S. Kistler, J. Amer. Chem. Soc. 58, 901 (1936).
15. A. V. Dumanskii, Izvest. In-ta Kolloidn. Khim. 2, 3 (1934).
16. N. A. Tsitovich, Izvest. Akad. Nauk SSSR, Ser. Geogr. i Geofiz. 9, 5-6, 493 (1945).
17. N. A. Tsitovich, Izvest. Akad. Nauk SSSR, Ser. Geol. 3, 39 (1947).

THEORY OF THE CORPUSCULAR STRUCTURE OF XEROGELS

I. PREPARATION OF SILICA GELS FROM LARGE GLOBULES WITH DIFFERENT NUMBERS OF CONTACTS, AND INVESTIGATION OF THE GELS BY THE ADSORPTION METHOD

A. V. Kiselev and T. A. Pogosyan

Adsorption Laboratory, M. V. Lomonosov Moscow State University
Institute of Physical Chemistry, Academy of Sciences USSR, Moscow
Translated from Kolloidnyi Zhurnal, Vol. 22, No. 3, pp. 314-322
May-June, 1960
Original article submitted March 19, 1959

One of the present authors, in 1936, represented the surface of silica xerogel as the surfaces of the micelles forming its framework [1]. The theory of corpuscular structure of xerogel adsorbents was developed further [2-5] on the basis of comparisons, on the one hand, of absolute isotherms for vapor adsorption on nonporous silica samples and on silica gels, and on the other, of isotherms for vapor adsorption on loose and compressed particles with nonporous spherical particles. The basic idea of this theory is that the framework of a xerogel consists of a collection of contacting primary particles; in the case of silica gels, these are globules. The specific surface of a silica gel is determined mainly by the size of the primary particles. The pores are empty spaces between them. The pore dimensions and shape are determined by the size of the primary particles, their mutual coordination, and packing density. In development of this theory great interest attaches to studies of the formation of xerogel framework structures at different stages, beginning with sols. Electron micrographs indicate that silicic acid sols contain spherical particles [6]. Electron micrographs [7] of dried very-dilute sols made by peptization of a hydrogel revealed the presence of aggregates, but because of their small size the individual particles could not be investigated in detail, although replicas of the aggregates indicated that they consist of spherical particles. Studies of hydrogels by electron microscopy are even more difficult. A hydrogel was studied at an early stage of formation after steam treatment in an autoclave, which led to growth of the primary particles [8]. Electron microscope studies of hydrogels at later stages do not give a fully definite idea of their structure [9]. The diameters of very large particles in stabilized silica sols have been determined [10]. These determinations were performed on the sols themselves, by the light-scattering method, and after they had been dried in film form, by electron microscopy and determinations of specific surface by adsorption of nitrogen vapor by the dry powders obtained from the sols. All three methods gave similar values.

It was of great interest to obtain sols with particles of relatively large diameters, suitable for quantitative electron microscopy, and to study them consecutively at all the three main stages: sol–hydrogel–xerogel. An attempt was therefore made in the present investigation to prepare sols with relatively large primary particles and to study them as far as possible at all these three stages by the adsorption and electron-microscope methods. The present communication deals with the first part of this work–adsorption studies of silica gel specimens formed from stabilized sols with different particle packing densities.

Preparation of sols, hydrogels, and xerogels. Numerous methods for preparation of silicic acid sols are available. The one chosen was replacement of sodium ions in sodium silicate solution by hydrogen ions, by the action of an ion-exchange resin in the H-form. It has been reported [11] that this method gives the purest, most stable sols.

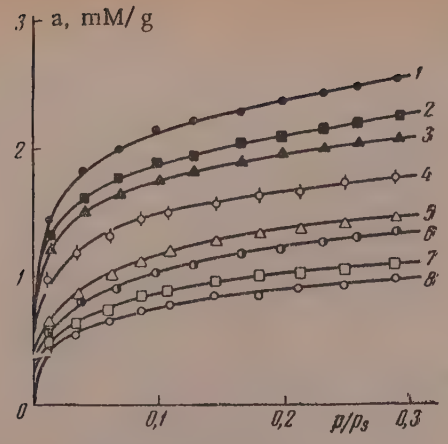


Fig. 1. Isotherms for adsorption of methanol vapor on eight xerogel samples made from sols of different pH: 1) pH 8.1, s = 280; 2) pH 8.4, s = 250; 3) pH 9.3, s = 230; 4) pH 9.5, s = 200; 5) pH 9.6, s = 170; 6) pH 9.8, s = 150; 7) pH 10.2, s = 130; 8) pH 10.7, s = 110 m^2/g.

An aqueous dispersion of KU-1 resin was put in an ion-exchange column. The resin was converted into the H-form by treatment with 7-10% hydrochloric acid solution to a negative reaction for sodium ions, followed by water washing to remove chloride ions. A definite amount of sodium silicate solution containing 2.5% SiO_2 by weight was then passed through. This gave a true solution of silicic acid, which was then stabilized by alkali. The stabilized solution was left to stand for two days at room temperature and then heated almost to boiling. This apparently gave a nucleated solution of silicic acid. To this was added a portion of silicic acid, freshly prepared by the ion-exchange method and of the same pH. The silicic acid condensed on the nuclei and the particles grew, giving rise to a sol. Stable sols were obtained at pH from 9 to 10.7. The sols were then destabilized by addition of small amounts of HCl solution, and passed into hydrogels. To find the optimum pH at which the largest sol particles are formed a series of sols was prepared with pH from 8.3 to 10.7. The solution pH was determined by means of a hydrogen electrode in conjunction with a calomel electrode.

Figure 1 shows isotherms for adsorption of methanol vapor on eight xerogels samples made from these hydrogels by ordinary drying at 110-120°. The xerogel obtained from a sol of pH 10.7 had the least specific surface s = 110 m^2/g, i.e., the largest particles. Therefore, only sols of pH 10.7 were used in the subsequent work. Hydrogels were prepared by decrease of the pH of stabilized sols to ~8.

It was very important to investigate the particles of this hydrogel while avoiding aggregation as far as possible; the method described by Kamakin [12] was used for this purpose.

The hydrogel was put in the pan of a vacuum balance and evacuated. The intermicellar water in the hydrogel solidified and passed into vapor, mainly by sublimation. In this way, it was possible to avoid the formation of liquid meniscuses, which pull the particles of the gel framework together during ordinary drying, in the evaporation of water, so that the particle packing in the dry gel after sublimation of the liquid remained extremely loose. This operation was performed on the hydrogel in the adsorption apparatus with a spring balance, which is described below.

Xerogels were prepared from the same hydrogel by the usual method of drying in a drying oven at 110-120°.

Isotherms for adsorption of methanol and benzene vapors were determined with the aid of the McBain-Baker quartz spring balance apparatus.* A diagram of this apparatus is given in Fig. 2. A similar apparatus was described previously [13], therefore, only certain differences are noted here. The adsorption tubes were placed in a metal thermostat T_1, which was also used as the heater during evacuation of the adsorbents.** The entire unit was enclosed in the thermostat T_2, so that the adsorption could be determined more accurately, especially at high relative vapor pressures in the region of capillary condensation, when fluctuations of the room temperature have a strong influence. The bulb with the adsorbate was also placed in a special thermostat T_3 [14]; the vapor pressure p was regulated in this way.

Four hydrogel samples of pH 10.7 were prepared as described above. The SiO_2 concentration was 10% by weight in samples 1h and 2h, and 5% in samples 3h and 4h. Hydrogel 3h was washed with acetone for seven days after solidification; the acetone was replaced by a fresh portion every 24 hours.

Samples of about 0.5 g of all four hydrogels were placed in the spring balance apparatus and frozen by N. M. Karamakin's method under residual pressure of 10^{-4}–10^{-5} mm Hg; the dispersion medium passed from the solid state into vapor, i.e., sublimed. The weight loss after prolonged evacuation at 20° was ~90% of the initial weight of the hydrogel. The hydrogel volume remained almost unchanged during sublimation of water (as in [12]). In contrast to ordinary aerogels, it had no mechanical strength and crumbled when touched to a fine powder of the "Aerosil" type; this indicates that the cohesion between its particles is very weak.

* The construction of this apparatus was started by the late L. N. Soboleva.

** The design of this thermostat (TSP-4) was developed in our laboratory by G. G. Muttik.

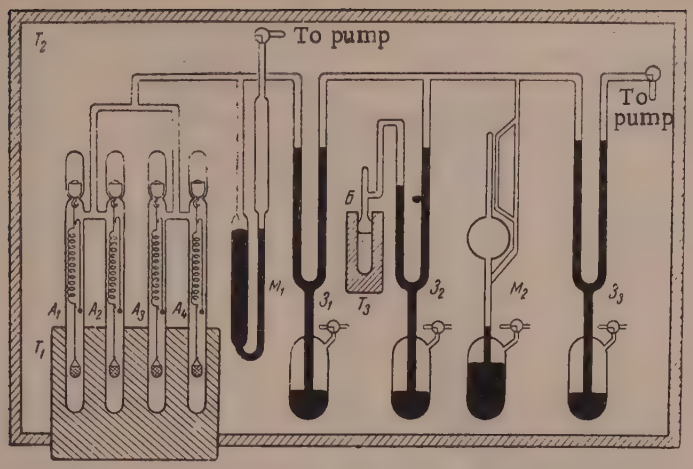


Fig. 2. The McBain-Baker apparatus with a vacuum spring balance.

After these samples (designed as follows: 1h, 20°; 2h, 20°; 3h, 20°; 4h, 20°) had been used for determinations of isotherms of adsorption and desorption of benzene vapor, they were heated to 150° under vacuum (samples: 1h, 150°; 2h, 150°; 3h, 150°; 4h, 150°), and their adsorption isotherms were again determined. Xerogels made from hydrogels by ordinary drying in a thermostat were evacuated in the same apparatus at 150° before determinations of adsorption of benzene vapor (samples: 1x, 150°; 2x, 150°; 3x, 150°; 4x, 150°).

The resultant isotherms for adsorption of benzene vapor are shown in Fig. 3. The specific surface s, the specific surface of the adsorption film at the start of hysteresis, s' [3], the pore volume v_s, the average number of globule contacts n, the most probable pore neck diameter d, and the average globule diameter D are given in the table. The specific surface s of samples 3h, 20° and 3x, 150° was determined in our laboratory by B. G. Aristov* from low-temperature adsorption of nitrogen vapor; the area occupied by a nitrogen molecule in a dense monolayer was $\omega_0 = 16.2$ A^2. The specific surfaces of the other samples were determined from the adsorption isotherms of benzene vapor by the BET method, with $\omega_0 = 49$ A^2 [15]. In the cases of samples 3h and 3x the values were the same as those found from adsorption of nitrogen. The film surfaces s' and pore volumes v were determined from isotherms for adsorption and desorption of benzene. The average number of contacts n was determined from the ratio of the pore volume v_s to the total volume, by extrapolation of the curve for the number of contacts n to percentage voids for ideal packing of similar spheres [16]. The most probable pore neck diameter d [16] was found from the maximum on the curve for pore volume distribution according to neck diameter, with a correction for the thickness of the adsorbed benzene film at the corresponding vapor pressure ratio p/p_s, found from the absolute isotherm for adsorption of benzene vapor in quartz [17]. The average particle diameter was found from the expression $D = 27,300/s$, A [4]. It is clear from Fig. 3 and the table that all these samples have low values of the specific surface s and very large pore volumes v_s. The average numbers of contacts in the investigated samples do not exceed 2.5, i.e., the particles are extremely loosely packed in all of them. All the samples are very uniformly coarse-pored.

The samples prepared in this way largely retained the hydrogel structure, as if frozen in the form in which it existed in the hydrogel. These samples, h, 20°, were then heated under vacuum at 150°, evacuated for a long time (samples h, 150°), and were again used for determination of isotherms for adsorption and desorption of benzene vapor in the initial region (up to $p/p_s = 0.35$). The pore volumes v_s at full saturation were also determined. It was found that the initial region of the isotherms remained unchanged (Fig. 3), while the sorptional pore volume changed by only about 5%. This indicates that when samples evacuated at 20° are heated to 150° no significant changes take place in their structure or pore area.

* The authors offer B. G. Aristov their deep gratitude.

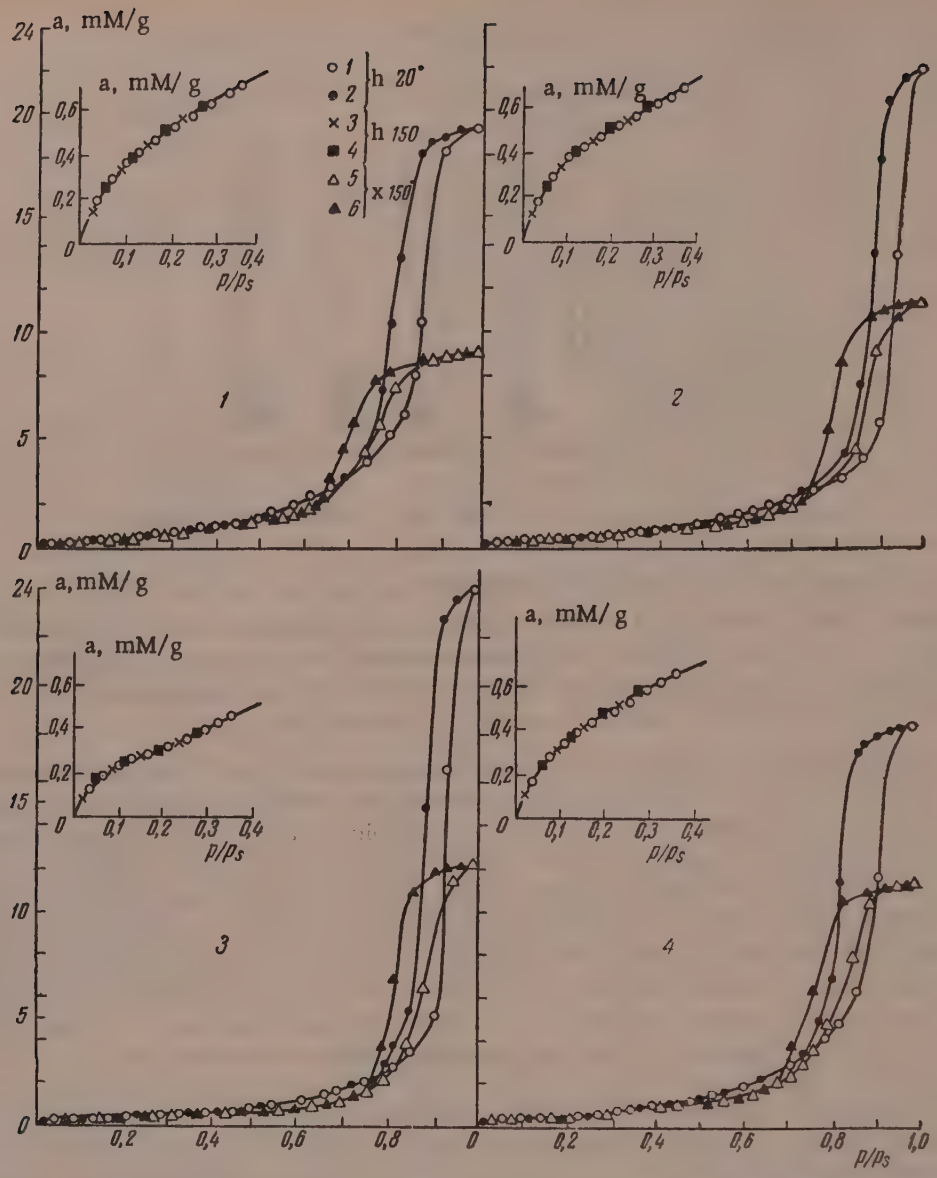


Fig. 3. Isotherms for adsorption of benzene vapor on four gel samples after sublimation, and on four xerogel samples made by ordinary drying. The initial portion of the isotherm for each pair of gel and xerogel samples is given top left. Black points here and subsequently represent desorption.

Isotherms for adsorption of benzene vapor on xerogel samples made from the same hydrogels by normal drying (samples x, 150°) are also given in Fig. 3. This diagram shows that samples obtained from hydrogels frozen and dried by sublimation had the same surface area as xerogels made by normal drying, but the total pore volume of the former was nearly double that of the latter. The constancy of the specific surface is shown particularly clearly in Fig. 4, which gives the initial region of the isotherm for adsorption of benzene vapor on samples of evacuated hydrogel 1h, 20° and 1h, 150°, and of 1x 150° xerogel, made from the same hydrogel [12]; these isotherms coincide.

Samples h, 20° lose a certain amount of water when heated further under vacuum at 150°. However, the constancy of the isotherm for benzene adsorption, which is highly sensitive to the degree of surface hydration [5, 18] shows that samples h, 20° and h, 150° have the same surface properties. This means that the degree of surface hydration of samples h, 20° is approximately the same as that of h, 150° and x, 150°; i.e., during prolonged evacuation the water adsorbed from the liquid dispersion medium is removed from the micelle surfaces

Structural Characteristics of Silica Gel Samples Prepared From Frozen Hydrogels (h) and Samples Made by Ordinary Drying (x)

Samples	Specific surface s, m^2/g	Specific surface of film s', m^2/g	Pore volume v_s, cc/g	Average no. of globule contacts, n	Mean diameter, A	
					pore necks, d	globules D
1h	155	140	1,70	(2,4)	260	180
2h	150	145	1,92	(2,2)	370	180
3h	105	100	2,14	(2)	350	280
4h	133	130	1,6	(2,5)	270	230
1x	150	140	0,8	(4,5)	145	180
2x	150	130	1,00	(3,7)	205	180
3x	100	100	1,06	(3,5)	260	270
4x	130	120	0,97	(3,8)	175	210

of fresh silicic acid gel in the same way as water adsorbed from vapor is removed from xerogel surfaces during evacuation at 20° [3, 5, 19]. A certain amount of structural and possibly also adsorbed water is retained within the micelles of the fresh gel between the intertwined polysilicic acid chains after evacuation at 20°; this water is removed completely when the gel is heated in vacuum at 150-200°; as shown by adsorption [19] and deuterium exchange [20] studies.

In the light of the theory of the corpuscular structure of xerogels this means that the primary silica particles do not lose their individuality but merely become more closely packed in the transition from hydrogel to xerogel. Figure 5 shows curves for pore volume distribution by neck diameters for pairs of specimens of a frozen and sublimation-dried hydrogel (3h) and the corresponding xerogel dried in the usual way (3x). The structural characteristics of all four xerogels are given in the table.

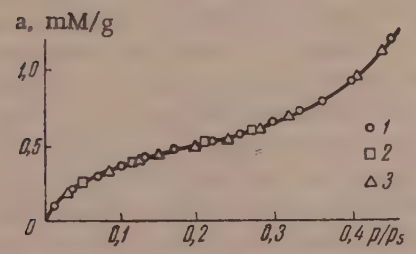


Fig. 4. Initial region of the isotherm for adsorption of benzene vapor on samples: 1) 1h after sublimation (1h, 20°); 2) 1h after evacuation at 150° (1h, 150°); 3) the corresponding xerogel after normal drying (1x, 150°).

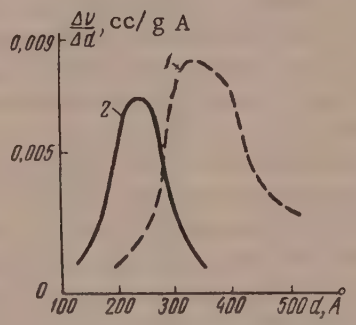


Fig. 5. Curves for pore volume distribution by neck for samples 3h (1) and 3x (2).

Comparison of the tabulated data for frozen sublimation-dried hydrogels and for xerogels made from the same hydrogels by ordinary drying shows that while s, s', and D for corresponding samples were almost unchanged the pore volumes v_s and neck diameters d decreased sharply, and the average coordination numbers n increased considerably in accordance with this. This indicates that the framework of an ordinary xerogel is built of the same primary particles, retaining their individuality, as are present in frozen and sublimation-dried hydrogels; the particles are merely packed more closely.

As stated earlier, acetone was used in washing of sample 3h. Introduction of surface-active substances leads to formation of more coarsely porous samples [22]. In the present instance washing with acetone led to formation of the most coarsely porous xerogel. Use of this method in conjunction with vacuum removal of the intermicellar liquid yielded sample 3h, with the loosest packing of the largest particles.

Thus, the methods used for treatment of hydrogels made from stabilized sols with very large particles (~300 A) yielded silica gel samples built up from the same particles but of different packing densities. In each pair of samples (dried under vacuum after freezing, and dried by the usual method) the silica particles remained the same, and only their packing changed.

Because the primary particles were large and loosely packed (even in the case of xerogels), the samples were virtually free from fine pores; this is shown by the distribution curves and by the closeness of the values of s' and s. It is therefore possible to interpret the vapor adsorption isotherms without the difficulties generally met in the case of fine-pored samples, and to use the samples for electron microscope studies of globules; the results of such studies will be given in the second part of this paper.

In Fig. 6 isotherms for adsorption of benzene vapor on silica gel samples 3h, 20°; 3h, 150°; and 3x, 150° are compared with isotherms for adsorption of benzene on quartz, determined in our laboratory. All these samples had strongly hydrated surfaces. For convenient comparison in the initial adsorption region, we converted relative adsorptions to absolute values calculated per unit area of the adsorbents [3]. The comparison in this region was extended to the uniformly coarse-pored KSK-2 silica gel which had been studied earlier.* Comparison of the isotherms in the initial adsorption region (the portion a of the complete curve is shown at top, left, on a larger scale) shows that the absolute isotherms for adsorption of benzene vapor on all five samples are similar. It follows that the properties of unit surface areas of these samples differ little. This is of special interest, because our sample 3h, 20 was not heated at all above 20° (adsorbed water was removed by prolonged evacuation of a small amount of the substance under high vacuum at 20°). In the region of intermediate relative pressures (Fig. 6b) the adsorption isotherms diverge, not only for the porous samples and nonporous quartz, but also for porous samples with different numbers of contacts between the silica globules: $n \approx 2$ (3h, 20°) and $n \approx 3.5$ (3x, 150°); the isotherm for the sample with $n \approx 3.5$ is first less steep than that for the sample with $n \approx 2$, and then becomes steeper and intersects the latter. The fact that the absolute adsorption isotherms coincide in the initial region of pure adsorption (Fib. 6a) shows that in the case of such coarsely porous samples the geometric factor (presence of pores) does not have any appreciable effect on the shape of the isotherm. However, subsequently two complications develop. First, capillary condensation begins at the points of contact between the globules, so that the isotherms for the two silica gels 3h and 3x move upward away from the isotherm for quartz. Second, decrease of the film area (s') on which multimolecular adsorption occurs begins to have an effect. It has been shown [23] that this reduces adsorption to an extent which increases with the number of contacts between the globules. Accordingly, the isotherms for silica gels 3h and 3x diverge, so that the isotherms for the sample with denser packing of the globules (3x) first lies below the isotherm for silica gel with looser packing of the same globules (3h). On further increase of the relative vapor pressure increased capillary condensation in the denser sample 3x masks the decrease of multimolecular adsorption, and total sorption for this sample becomes greater than for the looser sample 3h. In the region of high relative vapor pressures the isotherms for adsorption of benzene vapor on both coarse-pored silica gels, 3h and 3x, diverge increasingly from the isotherm for quartz, as in this region the main process in silica gel pores is capillary condensation, with a wide hysteresis region, whereas the isotherm for this very coarse quartz sample corresponds to almost pure multimolecular adsorption, and therefore, remains completely reversible [17]. In the case of porous samples the process is completed by filling of the entire pore volume, first in sample x, with the closer packing of the globules, and then in the looser sample 3h. Multimolecular adsorption on quartz continues to increase.

SUMMARY

1. Samples of stabilized sols with large particles were prepared. These were converted into hydrogels and the corresponding silica gels by freezing of the hydrogels and sublimation of the liquid under vacuum, and by ordinary drying in air. The structure of the silica gels was investigated with the aid of isotherms for adsorption and desorption of benzene vapor.

2. Samples dried by sublimation of liquid from frozen hydrogels, and corresponding samples dried by the usual method, are uniformly coarse-pored; they have equal specific surfaces (equal particle sizes) but differ in

* The data for quartz were taken from [17], and were also determined by Yu. A. El'tekov and D. P. Poshkus in our laboratory; date for KSK-2 silica gel at 200° were taken from [15] and [18].

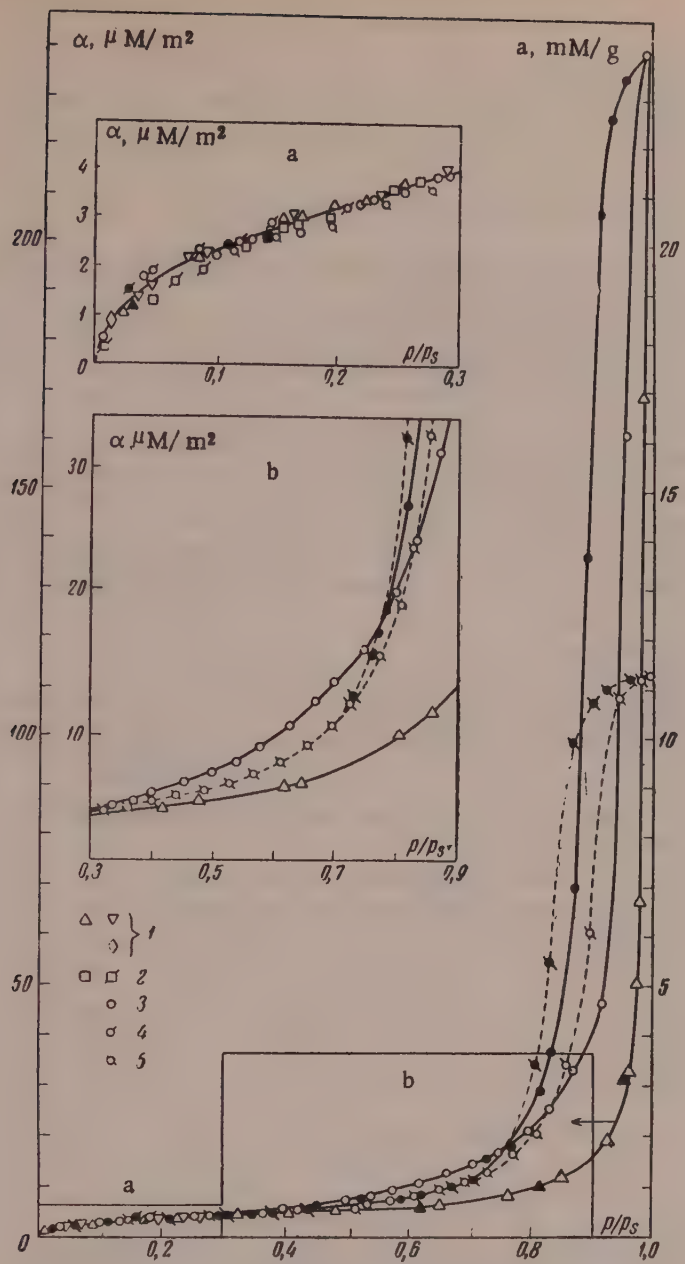


Fig. 6. Comparison of isotherms for adsorption of benzene vapor on quartz (1); silica gel KSK-2, 200° [15, 18] (2); 3h, 20° (3); 3h, 150° (4); and 3x, 150° (5). Ordinates indicate adsorption: relative, a, mM/ g; absolute, α, μM/ m². Parts a and b of the graph are shown separately on a larger scale.

pore volumes and sizes (the particle packing densities are different). The primary particles are packed very loosely in gel samples dried by sublimation; the same particles are packed much more closely in samples made from the same hydrogels by ordinary drying.

3. Before the start of capillary condensation the absolute isotherms for adsorption of benzene vapor on all these silica gels coincide within the limits of experimental accuracy, and are close to the absolute isotherm (determined earlier) for adsorption on quartz and on coarse-pored silica gel with a hydrated surface. Differences of particle packing density in the framework of coarse-pored silica gels become apparent at the stages of multimolecular adsorption and capillary condensation.

LITERATURE CITED

1. A. V. Kiselev, Kolloid. Zhur. 2, 17 (1936).
2. A. V. Kiselev, Doklady Akad. Nauk SSSR 98, 427 (1954); A. V. Kiselev, Collection: Use of Chromatography in Chemical Analysis, Transactions of Commission on Analytical Chemistry [in Russian] (Izd. Akad. Nauk SSSR, 1955) 6 (9), 46.
3. A. V. Kiselev, Collection: Surface Chemical Compounds and Their Role in Adsorption Phenomena [in Russian] (Izd. MGU, 1957) p. 90.
4. A. V. Kiselev, Collection: Methods for Investigation of the Structure of Highly Disperse and Porous Substances [in Russian] (Izd. Akad. Nauk SSSR, 1958) No. 2, p. 47.
5. A. V. Kiselev, in: The Structure and Properties of Porous Materials (London, 1958) p. 195.
6. Z. Ya. Berestneva and V. A. Kargin, Usp. Khimii 24, 249 (1955).
7. A. V. Kiselev, V. I. Lygin, I. E. Neimark, I. B. Slinyakova, and Ch'eng Wen-hang. Kolloid. Zhur. 20, 52 (1958).*
8. H. D. Ashley and W. D. Mc Innes, Ind. Engng. Chem. 44, 2857 (1952).
9. E. A. Hauser and P. D. LeBeau, J. Phys. Chem. 56, 136 (1952).
10. G. B. Alexander and R. K. Iler, J. Phys. Chem. 57, 932 (1953).
11. R. K. Iler, The Colloid Chemistry of Silica and Silicates, (New York, 1955).
12. N. M. Kamakin and Ya. V. Mirskii, Collection: Methods for Investigation of the Structure of Highly Disperse and Porous Substances [in Russian] (Izd. Akad. Nauk SSSR, 1958) No. 2, p. 190.
13. N. N. Avgul', O. M. Dzhigit, A. V. Kiselev, and K. D. Shcherbakova, Zhur. Fiz. Khim. 26, 977 (1952).
14. G. G. Muttik, Zavodskaya Lab. 17, 1403 (1951).
15. A. A. Isirikyan and A. V. Kiselev, Zhur. Fiz. Khim. 32, 679 (1958).
16. A. P. Karnaukhov and A. V. Kiselev, Zhur. Fiz. Khim. 31, 2635 (1957).
17. A. A. Isirikyan and A. V. Kiselev, Doklady Akad. Nauk SSSR 119, 731 (1958).*
18. L. D. Belyakova and A. V. Kiselev, Doklady Akad. Nauk SSSR 119, 298 (1958).*
19. L. D. Belyakova, O. M. Dzhigit, and A. V. Kiselev, Zhur. Fiz. Khim. 31, 1577 (1957); A. V. Kiselev and G. G. Muttik, Kolloid. Zhur. 19, 562 (1957).*
20. R. G. Haldeman and P. A. Emmett, J. Amer. Chem. Soc. 78, 2917 (1956).
21. A. V. Kiselev and V. I. Lygin, Kolloid. Zhur. 21, 581 (1959);* 22 (1960).*
22. I. E. Neimark and F. I. Khatset, Kolloid. Zhur. 9, 289 (1947).
23. A. P. Karnaukhov and A. V. Kiselev, Zhur. Fiz. Khim. 34, No. 9 (1960).

*Original Russian pagination. See C. B. translation.

APPLICATION OF THE SHADOW METHOD OF DETERMINING OPTICAL HETEROGENEITIES TO THE INVESTIGATION OF MASS TRANSFER ACROSS THE SURFACE OF SEPARATION OF DIFFERENT PHASES

Hartmut Linde, Institute of Chemistry of Fats,
German Academy of Sciences, Berlin, German Democratic Republic
Translated from Kolloidnyi Zhurnal, Vol. 22, No. 3, pp. 323-333
May-June, 1960
Original article submitted January 12, 1959

We have been using the shadow method for determining optical heterogeneities extensively for the study and demonstration of mass transfer processes. In the present article, we shall describe an apparatus of simple construction for the investigation of optical heterogeneity of different media and indicate the possibility of applying different modifications of the shadow method.

1. A number of shadow methods can be applied to the investigation of mass transfer processes [1-3]. Our problem was to develop, on the basis of these investigations [1-3], a method which would allow us to follow the creation of heterogeneity of concentration, and occasionally the motion of the liquid, by optical projection of cuvettes or diffusion cells. Aside from obtaining an over-all picture of the optical effects induced by the variation of the concentration and by the motion of the liquid, it was also necessary to ensure the possibility of obtaining quantitative data on the rate of change of the concentration.

The solution of our problem was based on the Töpler method [1]; using the K. Zeiss 80-VEB apparatus for the determination of optical heterogeneity we tried to design a simpler and cheaper apparatus. The apparatus we constructed is based on the design developed for optical detection of flaws in glasses.

The Töpler method, as well as the method in which the projection device is constructed according to diagram A, Fig. 1, makes it possible to determine changes of concentrations within given limits and, according to the conditions, to reveal the presence of currents. However, the Töpler method, as well as the evaluation of the simple projected picture with the apparatus represented in Fig. 1, A (allowing direct appreciation of the deviation angle by measurements of brightness), is too complicated and too inaccurate for quantitative determinations.

For quantitative determination, methods such as the Philpot-Swensen are recommended. We made quantitative determinations by using the Antweiler electrophoresis micromeasuring apparatus (manufactured by Boskamp and Co., Bonn) with an additional shadow attachment. With this apparatus we determined the concentration gradient along an arbitrary straight line crossing the interphase and obtained a photographic record of it. This shadow projection equipment was modified to obtain similar results which allowed quantitative evaluation by simpler means.

We assume that the principle and the operating techniques of the Töpler and the Philpot-Swensen devices are known. Both devices are very sensitive to optical heterogeneities and to small differences in refraction indexes, and therefore, they are very useful for the study of mass transfer.

The Rotsch shadow projection apparatus [4] has the advantage of simple construction. We first assembled our apparatus according to the basic diagram A of Fig. 1. In this apparatus the optical requirements for the condenser and for the illuminating lens are not very high. The quality of the reproduction of the object and of the heterogeneities contained in it depends essentially on the quality of the objective. When using the apparatus

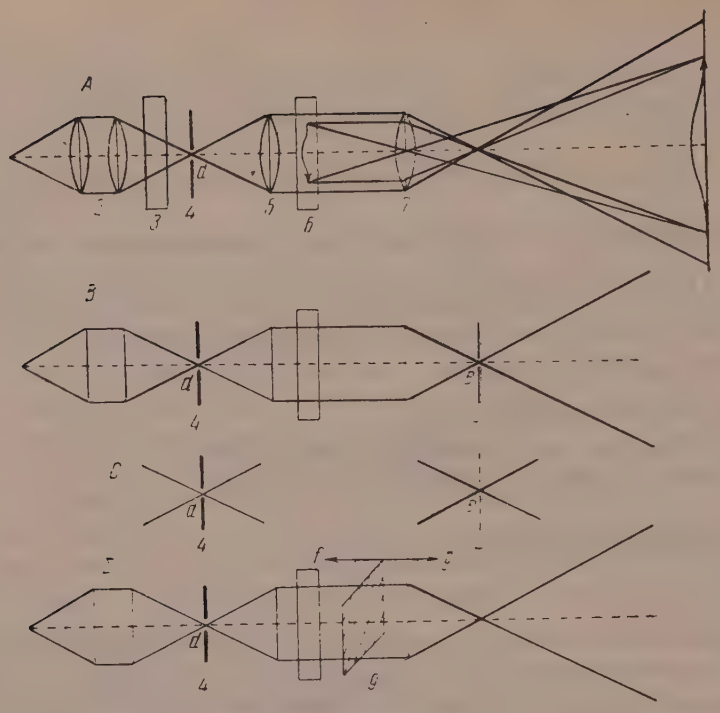


Fig. 1. Shadow apparatus arrangements A, B, C, and D. 1) Point source, 2) Condenser, 3) Heat filter, 4, 4') First and second diaphragms, 4") Grating, 5) Illuminating lamp, 6) Object, 7) Objective, 8) Screen, 9) Inclined raster.

assembled according to diagram A as well as according to later diagrams, special attention must be given to the point source, which must be very bright; this can be achieved with an NVO-107* mercury lamp. If excessive light losses are eliminated one obtains sharp contrasts and high sensitivity to optical heterogeneities of the medium. A sufficient enlargement of the heterogeneities is obtained on the projection by using microscopic objectives of adequate power, or by increasing the sharpness and the contrast of the image (since optical heterogeneities are very sensitive to changes in sharpness and contrast).

When the object to be examined is focused so as to obtain a sharp image in the plane of the screen so that the light (including the deviated light) is combined to form a sharp image of the object, then the image of optical heterogeneities has regions of minimum visibility and contrast. If the image is focused on the plane in front of the screen or behind the screen, then the light refracted by the optical heterogeneity will go from the zone of the heterogeneity to the image of the object. These cases are represented in Fig. 2. If the screen is in position b (beyond the sharp image), the image of the object will still remain sufficiently sharp because the source is a point source and the sharpness of the image is very great. The pencil of light deviated at point W at an angle α will fall on point U of the image instead of point T, and as a result there will be a dark spot at T while the brightness will increase at U. When the screen is positioned at a (in front of the sharp image) the light will be deviated in the opposite direction.

When the screen is placed at b the image of the object corresponds to the image which one obtains by the shadow method when a correspondingly magnified object is placed at c and the light is correspondingly deviated by an angle β in V, the point source being in the focus e of the objective. Only when the screen is placed at a does one obtain an image which cannot be obtained by the simple shadow method. Thus arrangement A of Fig. 1 is a variation of the direct shadow method, a simple and convenient method of obtaining magnified images of small objects. The interpretation of the images is the same as in the shadow method [3].

* The mean brightness of the NVO-107 VEB tube is 10^5 stilb over an illumination field of 0.3 × 0.3 mm; the luminous flux is 10^3 lumens.

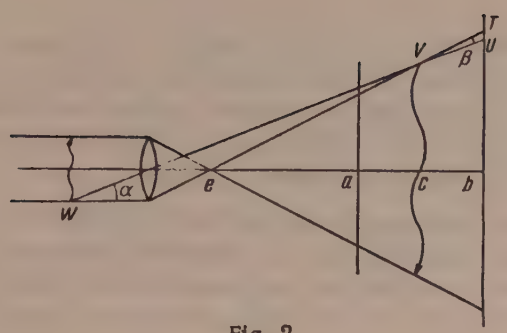


Fig. 2.

Method A of Fig. 1 has the disadvantage that when the apparatus is adjusted to the sensitivity of a given optical heterogeneity the image of the object is not very sharp. Furthermore, even when the image of the object is still sufficiently sharp only very gross gradients are visible, and in places, totally dark areas correspond to optical heterogeneities. When the area of optical heterogeneities is small the light refracted by them often increases the contrasts of the image, but the intensification of contrasts does not occur in the places where the light is deviated and consequently the results, due to the overlapping of light and dark zones, may become erroneous.

This defect is eliminated and the sensitivity is increased (the sharpness of the image of the object remaining constant) in the case of system B (Fig. 1). Also, the beam of light refracted by the optical heterogeneity is limited by the diaphragm 4', placed in the focus of the objective, e. To achieve this as completely as possible, the image of the light source in the focus of the condenser, d, is sharply limited by the diaphragm, which can also be used advantageously in other systems. When the condenser and the illuminating lens are of high optical quality the accuracy of alignment of the diaphragm, 4, increases with the size of the image of the diaphragm at the focus, e.

When the area of the optical heterogeneities is large a considerable part of the image of the object can be darkened (when the B system is used) and this hampers, for example, the observation of the motion of the liquid within the optically heterogeneous space. Also it becomes impossible to measure the change of the index of refraction in the darkened part of the image.

These defects are elminated in system C by replacing the diaphragm, 4', in e, by a grating, 4", (grating method). Since the light source is either a point source or has the shape of a small disk and is limited by the diaphragm, 4, in d, it is preferable to use a grating made of concentric rings. Optical heterogeneities of low intensity occupying a considerable volume are hardly visible with arrangement A, give an extended darkened area with arrangement B, but are resolved into a series of flat isophots allowing measurement of the change of the index of refraction with arrangement C. The absolute value of the deflection angle can be easily derived from the order number N of the isophot. By covering the light fringes given by the grating one obtains the magnitude of deviation N·a for the corresponding isophot and thus one can calculate the tangent of the angle or the corresponding angle in radians; thus $\alpha = Na/f$, where f is the focal length of the objective (Fig. 3).

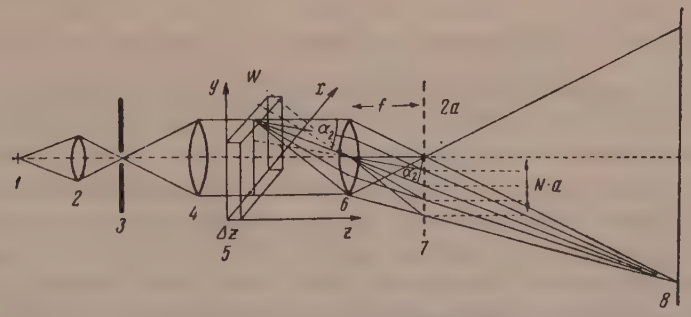


Fig. 3. Path of the light ray diffracted in W, and concentration of light with a grating. 1) Light source, 2) Condenser, 3) Diaphragm, 4) Illuminating lens, 5) Object, 6) Objective, 7) Grating, 8) Screen. α = angle of deviation in radians.

A simple case often occurring in processes of diffusion and mass transfer is characterized by the fact that the state of matter within the optical heterogeneity is constant along the z axis (direction of propagation of light), while the gradients are along x and y axes, perpendicular to z; in this case the gradient of the refraction index is given by the following expression:

$$\frac{\partial n}{\partial (x, y)} = \frac{n_0 Na}{zf},$$

where n_0 is the index of refraction corresponding to the origin of the heterogeneity; z is the thickness of the optically heterogeneous layer (in our case the thickness of the cuvette); Na/f the deviation of the light beam (in radians) determined from the order number, N, the grating spacing, a, and the focal length of the objective. When this method is used to investigate diffusion processes one can replace the concentration, c, by the refraction index, n, (provided n is a linear function of c) in the differential equations describing diffusion.

For simple calculations the curve representing the gradient of the refraction indexes can be identified with the curve representing the concentrations gradient. The temperature distribution is determined by measurements of heat losses from the photographs obtained by the grating method. In this case the temperature gradient can be deduced from the refraction indexes gradient. The relationship between the index of refraction and the density is given by the Lorentz-Lorenz equation:

$$\frac{n^2 - 1}{n^2 + 1} \frac{1}{\rho} = K,$$

which, for gases, takes the following simple form:

$$\frac{n - 1}{\rho} = \frac{3}{2} K.$$

For gases the relationship between the density, the pressure and the temperature is given by the following equation:

$$\frac{p}{\rho} = \frac{R}{M} T.$$

Correspondingly, in the general case one must apply the laws of thermal expansion for real gases and liquids.

A further improvement in the apparatus was arrangement D, Fig. 1; this arrangement allowed us to obtain directly the curves representing the gradient of the refraction indexes in a very simple manner, with the shadow projection equipment used simultaneously with the Philpot-Swensen apparatus. This was achieved by stringing a number of wires on a frame placed as an inclined raster on the path of the light beam at each side of the objective in the space f-g, according to the desired sensitivity. One can also place the raster between the focus of the objective, e, and the screen, but in this case the gradient curves fit less favorably into the rectangular space of the cuvette. The frame can be rotated so that the wire can be inclined at any desirable angle, 45° for example, with respect to the direction of the gradient of refraction indexes to be represented. The image of the wires projected sharply on the screen spreads into the gradient curve in angular coordinates. To avoid deformation of the image of the gradient curve, it is necessary to focus sharply on the object or the middle of the space occupied by the object in the Z direction. One obtains a sufficiently sharp image of the wire by using a point source. By transferring the deviations into a rectangular system of coordinates, according to Fig. 4, one obtains the same normal gradient curve as that provided by the Philpot-Swensen method. Arrangement C has some similarity to the Wiener arrangement [5], although the deviation of the image of the wire is not in the direction of refraction gradient indexes but is perpendicular to it. The photographs obtained by this simple method are easier to compare with the photographs obtained by the Philpot-Swensen method. For small angles between the gradient of refraction indexes and the inclined raster the shape of the curve approaches that obtained by the Philpot-Swensen method although the deviation and, therefore, the sensitivity are decreased.

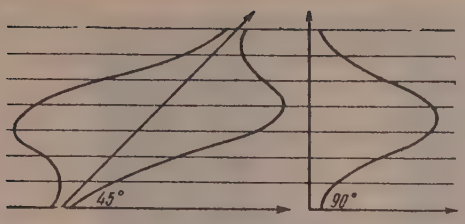


Fig. 4. Gaussian distribution curve as a concentration gradient curve represented in an angular system of coordinates by using an inclined raster.

During the investigation of the process of mass transfer or heat conduction with the shadow projection apparatus one can easily pass from arrangement A to arrangement B by introducing the diaphragm, 4'; then one can pass to the C arrangement by replacing the diaphragm, 4', with the grating 4". Finally, by replacing the grating with the inclined raster, 9, and changing its position and angle of inclination according to the sensitivity desired, one easily passes to arrangement D. In this way one can profit by the advantages of each of these arrangements. The light emitted by the NVO-107 lamp is very intense and allows very short exposure times (for example, 1/25 second when the diaphragm, 4 , is used), and also it becomes possible to photograph the image on the screen directly, so that arrangements A and D are equally well adapted for demonstration and for photographic recording.

2. The simplest investigation of mass transfer processes is that of undisturbed diffusion without passage across an interphase. The sensitive Töpler method can be applied in this case even when the variation of the concentration is very small.

When small differences in the concentration of a diffusing substance are to be studied one cannot use simple cuvettes and create interfaces by introducing a layer of solution under or on top of the original liquid with pipettes. When this method of layer creation is used the difference between the densities of the solutions due to the diffusing substance must be sufficiently large, otherwise, it is impossible to create layers of solutions without disturbing the original conditions of the experiment for a considerable amount of time.

Figure 5 represents the photograph of a cuvette (of a Pulfrich photometer) obtained by the Töpler method, in which a layer of a 4% solution of methyl alcohol in isoamyl alcohol was carefully spread over a layer of pure isoamyl alcohol. The working width of the cuvette was 17 mm and the working height 27 mm. The scale of the photograph obtained by the Philpot-Swensen method was chosen in accordance with the dimensions of the cuvette.

The photographs, especially those obtained by the Töpler method, show that in the case of this primitive means of filling the cuvette, the initial disturbances of homogeneity (as well as later ones created by heat convection), are acting even after 10 minutes. Photographs of the same cuvette obtained by the Philpot-Swensen method for the sake of comparison give a curve of concentration gradients. Layers of solutions can be obtained more precisely by using the special cuvette from the Antweiler microelectrophoresis apparatus, in which case the original disturbance of homogeneity is lessened. As an example one may cite the investigation of the diffusion of methyl alcohol from a 16% aqueous solution of methyl alcohol into water. The sensitivity of the Töpler and the Philpot-Swensen methods can be regulated with a diaphragm, and thus one can easily adapt the methods to the object to be investigated. The Philpot-Swensen method cannot be used in the case of very large differences in concentrations.

The second series of photographs (Fig. 6.1 and 6.2) illustrates the same diffusion process in the case of larger differences in concentrations, the photographs being obtained with the shadow projection apparatus. The photographs were made 6-8 and 25-26 minutes after the creation of layers, by using the different arrangements from A to D consecutively. A 20% solution of methyl alcohol in isoamyl alcohol was spread on a layer of pure isoamyl alcohol. By using arrangement A we obtained photographs in two different positions: a sharp image in front (A_1) and a sharp image behind (A_2) the projection plane; in these photographs the area of the largest drop of concentration is indicated by slight darkening. The deviated light somewhat overlaps the boundary of the darkened area. The image of the less steep gradient is less contrasted. Arrangement B is more sensitive; on photographs obtained by this method zones of complete darkness correspond to the areas deviating light and no details can be distinguished within these zones. With arrangement C the darkened zone is separated into several isophots, which allows quantitative evaluation and further observation of details and of flow processes within the family of isophots. Arrangement D gives the image of the family of concentration gradient curves with clearly observable breaks.

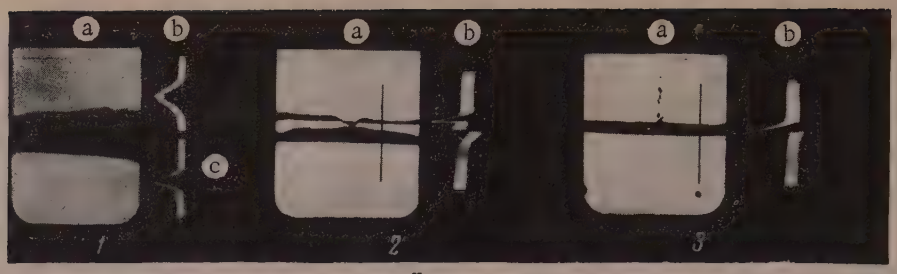


Fig. 5. Photograph according to: a) Töpler method. b, c,) Philpot-Swenson method. 1) Ten minutes after a layer of 4% methyl alcohol solution in isoamyl alcohol was spread over isoamyl alcohol (b) and 2.5 minutes after a layer of 16% methyl alcohol solution in water was spread over water (c): 2) three minutes after a layer of 4% methyl alcohol solution in isoamyl alcohol was spread over water: 3) same as in 2, with addition of 0.1% saponine or $C_{16}H_{33}OSO_3Na$ at phase equilibrium.



Fig. 6. Photograph made with arrangements A, B, C, and D of the shadow projection apparatus. 1) Six to eight minutes after a layer of 20% methyl alcohol solution in isoamyl alcohol was spread over isoamyl alcohol: 2) same, after 25-26 minutes: 3) same, after 60 minutes: 4) three to five minutes after a layer of 4% methyl alcohol solution in isoamyl alcohol was spread over water: 5) same, with addition of saponine at phase equilibrium.

Both series of photographs taken after 6-8 minutes (Fig. 6.1) and after 25-26 minutes (Fig. 6.2) show clearly the widening of the curves representing the concentration gradients. This is indicated by the increase of the darkened area (arrangement B), by the decrease of the number of isophots, and the increase of the distance between them (arrangement C), and is indicated directly by the shape of the curves (arrangement D). By moving the inclined raster from f to g (Fig. 1) one can increase the deflection of the shadow band (arrangement D, Fig. 6.2) and thus the sensitivity of the instrument. This method allows one to see quite clearly the disturbance of normal diffusion due to convection induced by differences in temperature or evaporation. Figure 6.3 represents photographs taken 60 minutes after a layer of methyl alcohol was spread over a layer of isoamyl alcohol. Weak diffusion currents, which after the removal of the cover from the cuvette (photograph C_2) are replaced by violent mixing due to evaporation, occur in methyl alcohol.

3. When matter is transported across the limit of separation of two liquid phases [6, 7] the image becomes distorted due to the deformation of the surface of separation induced by the angle of contact at the wall of the cuvette. The deviation of light in these areas is very large and cannot be controlled, so that the area in direct contact with the phase boundary becomes omitted in shadow photographs. In the cases investigated the conditions of experiment were chosen so that convection currents were eliminated.

The photographs of Fig. 5.2, obtained by the Töpler and Philpot-Swensen method, represent the process of mass transfer from a layer of a 4% methyl alcohol solution in isoamyl alcohol to pure water. The series of photographs of Fig. 6.4, representing the same process, was obtained by the shadow projection method (arrangement A to D). The photographs obtained with the different arrangements supplement each other and show that the transport of mass across the limit of separation of two different phases is not determined by passive diffusion alone. The expected homogeneous darkened zone at the limit of separation of two phases is separated into two zones. The vertical line on the photograph obtained by the Töpler method indicates the position of the plane of the band of light on the photograph obtained by the Philpot-Swensen method. The photographs obtained with the Philpot-Swensen method and with arrangement C of the shadow method show that the most abrupt drop in concentration moves from the separation boundary as a separate dent of concentration gradient; only a relatively small peak of the gradient remains at the surface of separation.

It must be noted that the maximum on the curve representing the concentration gradient must remain at the phase separation boundary, since the diffusion coefficient is independent of the concentration. Only when the diffusion coefficients depend on the concentration may one expect a small displacement of the maximum of the gradient curve. Considerable displacement and splitting of the gradient dent into two parts at the surface of separation would indicate the violation of the simple law of diffusion. This easily reproducible phenomenon is considered to be an acceleration of mass transfer due to convection induced by the unavoidable small difference in concentration of the diffusing substance of low surface activity.

The different processes of mass transfer can be easily distinguished by the method of shadow photographs. Thus, it appeared to be of interest to set up an identical case of mass transfer, but at the same time, depress the possible effects of the surface activity of the diffusing substance at a given phase separation boundary. For this purpose we added saponine, acting as a strong surface-active substance under the conditions of phase equilibrium. A qualitatively analogous effect can be achieved by adding sodium alkylsulfate (cetylsulfate for example— $C_{16}H_{33}OSO_3Na$ under the conditions of phase equilibrium. Then, as can be seen from Fig. 6.5 and 9.1, a homogeneous darkened zone appears at the phase separation boundary. The concentration gradient first is localized, in the shape of steep peaks, at the surface of separation, and then slowly washes out as the result of diffusion. To determine whether in this case we are dealing only with ideal diffusion, (undisturbed by convection) or whether in addition there exists a real retardation of transfer of the diffusing substance at the phase separation boundary it is necessary to make a strict quantitative investigation of the concentration curve (curve representing the concentration gradient [8]). Under favorable conditions this can be done with arrangements C and D (Fig. 1) or by the Philpot-Swensen method. The distribution of concentrations can also be determined very precisely by interferometric methods.

In the examples described the photographs were made at the same time intervals as before so as to make possible a comparison with further very intense processes of mass transfer. Naturally, when the rate of mass transfer is very low it is impossible to follow the changes in concentration at large distances from the phase separation boundary disturbing the optical homogeneity.

The curves of refraction indexes relative to the processes of mass transfer by diffusion in a two-phase system and in a one-phase system can be very different. Thus, when the diffusion coefficients are different the concentration curve shows at the phase boundary a break which appears as a discontinuity on the curve representing the concentration gradient. Figure 7 represents curves of concentration and of concentration gradients as they should look in the case of diffusion when a layer of a solution is spread over a layer of pure solvent, and also in the case of diffusion in a two-phase system in which the diffusion coefficients are different but the initial conditions are comparable.

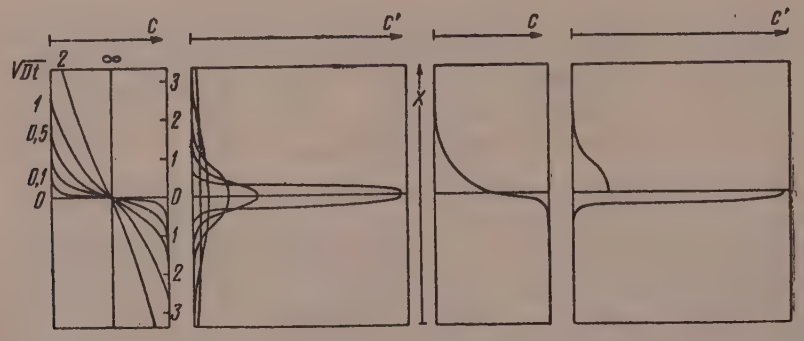


Fig. 7. Shape of concentration curves and of curves representing concentration gradients in the case of diffusion. a) In a monophase system: b) in a two-phase system (when the diffusion coefficients are different; c) concentration: $c' = dc/dx$; x is the distance from the phase separation boundary: $c = c_0/2\ [1 - E_r f\ (x/2\sqrt{Dt'})]$.

Since the distribution coefficient is not equal to unity a discontinuity appears in the concentration curve at the phase boundary. This leads either to an increase or a decrease of the concentration drop in both phases. Usually the fact that the index of refraction varies linearly with the concentration makes it possible to assign to each index of refraction and to the curve of refraction indexes a corresponding value of concentration and a corresponding curve of concentration gradients, or vice versa. Since, in the general case, both phases of a two-phase system have different refraction indexes, a jump in the values of refraction indexes occurs as a rule at the phase boundary, i.e., a discontinuity in the corresponding curve. As a result curves of refraction indexes of different slopes may correspond to a given concentration curve in different phases and the resulting curve of refraction index gradients may show again a discontinuity at the phase boundary (Fig. 8).

The indexes of refraction gradient are different at each side of the phase boundary; they may proportionally increase or decrease or even become negative; when they become negative a "reflection" of the curve representing the gradient of refraction indexes may occur at the phase boundary. These are basically the variations which can be expected, assuming ideal diffusion in a two-phase system with mass transfer across the interphase boundary. Convection processes and specific diffusion anomalies related to mass transfer may very strongly affect the shape of the curves representing the curves of concentration gradients and the curves of indexes of refraction gradients corresponding to them. These circumstances must be taken into account in the interpretation of the photographs.

Our next problem was to investigate the process of transfer of strongly surface-active matter added to a two-phase system in nonequilibrium condition (of one of the members of the sodium alkylsulfate series— $C_n H_{2n+1} OSO_3 Na$, for example.

Figure 9 represents photographs obtained by the Töpler and the Philpot-Swensen methods for the transfer of $C_{16}H_{33}OSO_3Na$ from an initial 2% homogeneous solution in isoamyl alcohol (upper phase) into water. Three minutes after a layer of water is introduced an image of extremely intense mass transfer accompanied by a spontaneous reproducible intense surface convection occurs. The concentration fronts far removed from the separation boundary are observable by the darkening or by the gradient peak.

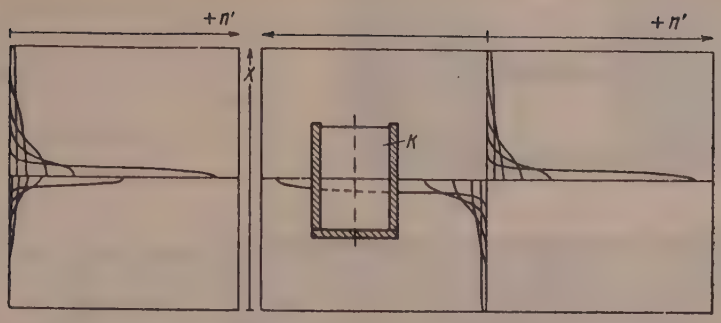


Fig. 8. Discontinuity and "reflection" of curves of indexes of refraction gradients in the upper and lower phase due to the difference in the indexes of refractions: K) Cuvette containing a two-phase system: n) refraction index: n' = dn/ dx, where x is the distance from the phase separation boundary.

Further photographs show how the different arrangements of the shadow projection apparatus supplement each other, giving a clear picture of such a process of mass transfer.

Figure 10 represents photographs made 1-2.5 minutes after layering of the phases. When the processes are very intense each photograph corresponds to a different distribution of concentrations and to a different state of surface convection. Arrangement A, not very effective in the case of normal diffusion with flat concentration fronts, gives very sharply contrasted images in this case. Arrangements B, C, and D give pictures characterizing more precisely the relationship between the concentrations corresponding to those represented in Fig. 9.2.

"Spontaneous surface convection" begins simultaneously at different points immediately after the introduction of layers of solutions; it appears first in the shape of little eddies which under the effect of current further unite into a general eddy motion occupying a large volume. After a period of intensive spontaneous surface convection the current often calms down and steep concentration fronts, up to which spreads the equilibrium state, appear at a large distance from and at both sides of the phase boundary. If the equilibrium distribution is again disrupted as the result of widening of the concentration front due to diffusion, an intense transfer of mass accompanied by spontaneous surface convection starts again.

Figure 10.2 represents a state of relative rest approximately 25 minutes after the layering of phases.

Figure 10.3 represents periods of renewed spontaneous surface convection 15, 25, and 35 minutes after the layering of phases. At the same time a current leaving the localized eddy area and spreading over a large volume is created. This current creates at the phase separation boundary a new nonequilibrium two-phase system either at the right or the left wall or in the middle of the cuvette as the result of separation of the liquid into two zones. As a consequence differences in surface tension [6] are created which basically are responsible for the current near the surface of separation of the phases.

In the next experiment (Fig. 10.4) the distribution of concentrations, with a concentration front at a large distance from the phase separation, stabilized 25 minutes after layering becomes totally homogeneous within each phase on mixing.

The photograph shows how a strong "spontaneous surface convection", which even after 50-51 minutes following the period of temporary rest (Fig. 10.3) still gives a clear picture, already develops anew 30 seconds after the end of mixing.

Since our main purpose was to show the applicability of the shadow method to the investigation of mass transfer, we can only mention these phenomena here. It will suffice to note that these phenomena may also depend to a considerable extent on the structure of the micellae of the diffusing surface-active substance formed at the surface of separation. Thus, all the transported molecules must pass through this micellar surface structure acting as a membrane. We investigated the effect of the length of the chain on the transport process, using compounds of the $C_nH_{2n+1}OSO_3Na$ series as the diffusing substance. We also investigated the transfer of substances from the lower phase (water) into the upper (isoamyl alcohol). We observed analogous phenomena but the effects of chain lengths were different.

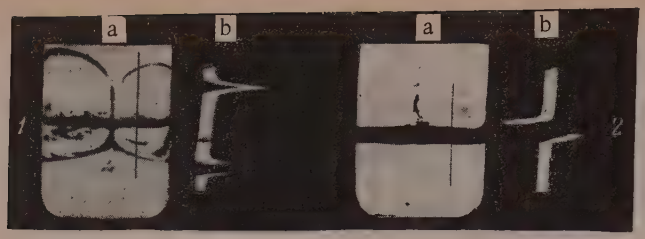


Fig. 9. Photographs made by the Töpler method (a) and the Philpot-Swensen method (b). 1) Three minutes after a layer of 2% solution of $C_{16}H_{33}OSO_3Na$ in isoamyl alcohol was spread over water: 2) three minutes after a layer of isoamyl alcohol was spread over a 2% $C_{16}H_{33}OSO_3Na$ solution in water.

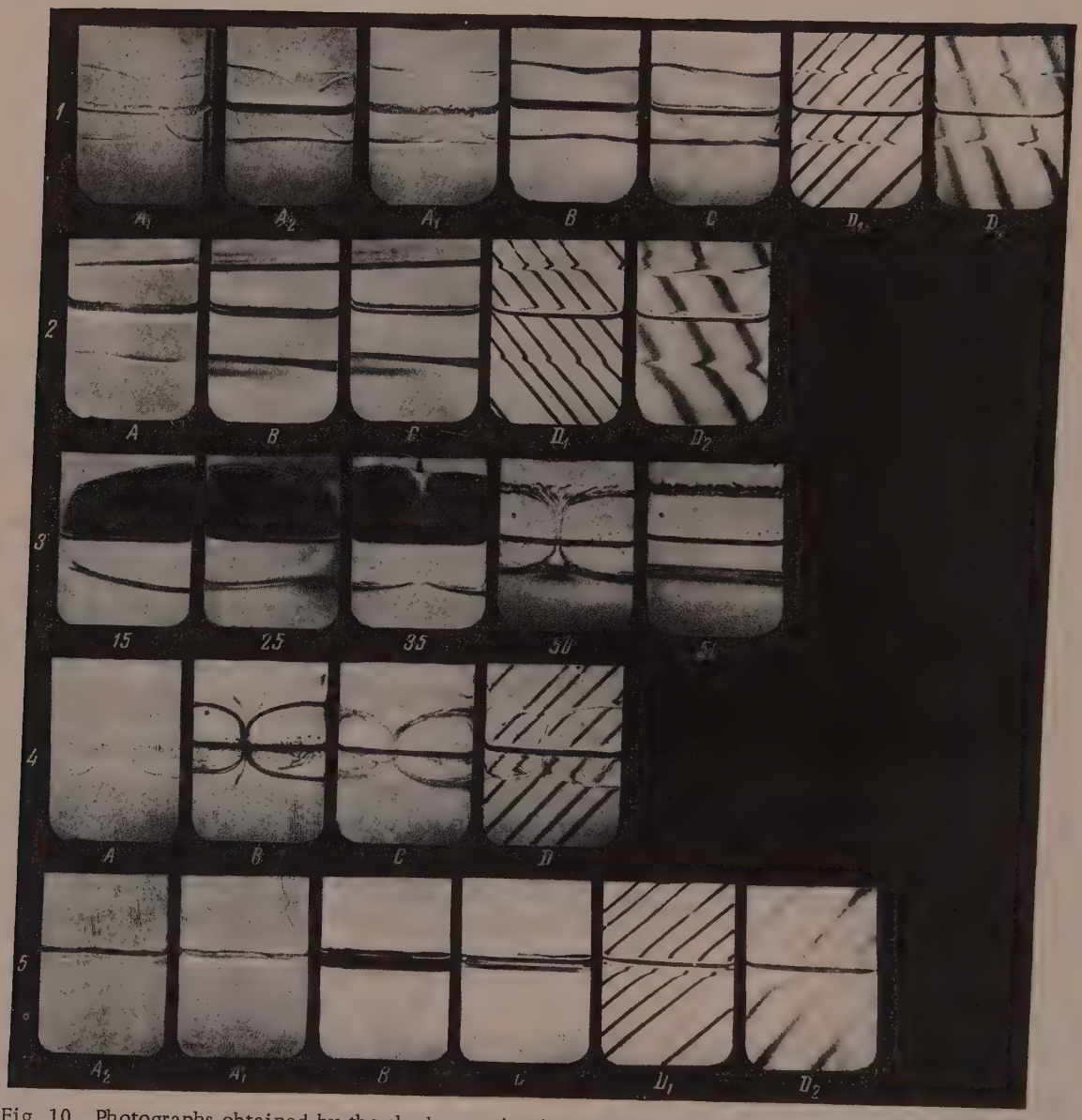


Fig. 10. Photographs obtained by the shadow projection method. 1) With arrangements A, B, C, and D, 1.25 minutes after a layer of 1% $C_{15}H_{31}OSO_3Na$ solution in isoamyl alcohol was spread over water: 2) same, after 25 minutes: 3) arrangement C, 15, 25, and 35 minutes after a layer of 1% $C_{15}H_{31}OSO_3Na$ solution in isoamyl alcohol was spread over water and 50 and 51 minutes after a 2% $C_{15}H_{31}OSO_3Na$ solution in isoamyl alcohol was spread over water: 4) arrangements A, B, C, and D, 3 seconds after the end of mixing carried out to homogenize the different concentrations occurring 25 minutes after a 2% $C_{15}H_{31}OSO_3Na$ solution in isoamyl alcohol was spread over water: 5) three minutes after a layer of isoamyl alcohol was spread over a 4% solution of $C_{15}H_{31}OSONa$ in water.

Figures 9.2 to 10.5 represent photographs relative to the investigation of such reverse transfer in the case of $C_{15}H_{31}OSO_3Na$ and $C_{16}H_{33}OSO_3Na$. It turns out that the phenomena of intense mass transfer described above do not occur in these cases. In the case of $C_{15}H_{31}OSO_3Na$ one observes near the surface of separation a slight disturbance due to convection analogous to the more intense disturbance occurring during the transfer of a less surface-active substance–methyl alcohol.

SUMMARY

1. We have developed a simple shadow projection apparatus allowing a rapid and simple change of parts, which ensures the applicability of different modifications of the shadow method–total darkening method, light deflection method, grating method, and inclined raster method.

2. We have investigated the applicability of the shadow methods to the investigation of the processes of transfer of substances affected to a considerable extent by the addition of surface-active substances.

3. The processes of transfer of atypical surface-active substances (lower homologues) within two-phase systems under the effect of additions of typical surface-active substances are slowed down when these substances are introduced (a) under the conditions of phase equilibrium [6] and are accelerated when they are introduced under the condition of nonequilibrium (b).

4. Typical surface-active substances can be characterized by highly intense mass transfer across a phase interface.

5. In cases when the laws of interaction between forced convection and diffusion hold transport processes under the condition of phase equilibrium [3, a) correspond most closely to an ideal behavior on solid surfaces.

6. The rate of transport processes of substances (as well as of atypical surface-active substances) in pure two-phase systems, particularly in the absence of equilibrium conditions or when the process is very intense, may be determined by spontaneous surface convection and the resulting increased turbulence at the surface of separation of phases.

7. The rate of mass transfer across the surface of separation of two liquid phases may depend on the direction of the transfer.

LITERATURE CITED

1. A. Töpler, Poggendorfs. Ann. 127, 556; 128, 126 (1866); 131, 33 180 (1867); 134, 194 (1868).
2. G. St. L. Philpot, Nature 141, 283 (1938).
3. H. Schardin, Ergebn. exakt. Naturwiss. (Berlin, 1942) p. 20.
4. M. Rötsch, Feingeräte Technik 3, Heft 12, 542 (1954).
5. O. Wiener, Wied. Ann. 49, 105 (1893).
6. V. G. Levich, Disc. Faraday Soc., No. 1, 37 (1947); J. Phys. Chem. 22, 575, 711, 721 (1948); Physical-Chemical Hydrodynamics [in Russian] Second Edition (Moscow, 1959).
7. E. Hutchinson, J. Phys. Chem. 52, 897 (1948); J. T. Davies, J. Phys. Chem. 54, 185 (1950); W. Vielstich, Z. Elektrochem. 57, 646 (1953); J. B. Lewis and H. R. C. Pratt, Nature (London) 171, 1155 (1953); J.B. Lewis, Chem. Engng. Sci. 3, 248 (1954); F. H. Garner and A. H. Skelland, Industr. and Engng. Chem. 46, 1255 (1954); 48, 51 (1956); H. Linde, Dissertation Friedrich-Schiller-Universität, (Jena, May 1954); K. Sigwart and H. Nassenstein, Naturwissenschaften 42, 458 (1955); Z. V. D. I 98, 453 (1956); H. Krŏpelin and H. G. Neumann, Naturwissenschaften, 43, 347 (1956); 44, 304 (1957); 45, 333 (1958); M. Linton and K. L. Sutherland, Proceeding of the Second Intern. Congr. of Surface Activity, (1957) p. 494; P. C. Bloker, Ibid., p. 503; H. Linde, Fette, Seifen, Annstrichmittel 60, 826 (1958).
8. W. Jost, Z. Phys. 127, 163 (1950); P. L. Auer and E. W. Murbach, J. Chem. Phys. 22 1054 (1954).

ADSORPTION PROPERTIES AND INFRARED SPECTRA OF OXIDIZED CARBON BLACKS

V. I. Lygin, N. V. Kovaleva, N. N. Kavtaradze, and A. V. Kiselev.

Institute of Physical Chemistry, Academy of Sciences USSR, Moscow
Translated from Kolloidnyi Zhurnal, Vol. 22, No. 3, pp. 334-339
May-June, 1960
Original article submitted March 9, 1959

The chemical nature of the surface of oxidized carbon blacks is the cause of their reinforcing effect and determinates the physical and mechanical properties of rubbers, plastics, lubricants, and surface coatings in which they are used as fillers. It has been pointed out [1] that it is now necessary to develop fillers with predetermined properties by means of various chemical reactions effected on their surfaces, and to carry out detailed studies of the structure and properties of the surface compounds formed in these processes.

The nature of the chemical compounds on filler surfaces is usually determined by means of chemical reactions characteristic of these compounds. It has been shown with the aid of ion exchange between surface compounds and electrolyte solutions [2], the Grignard reaction [3], and the diazomethane reaction [4, 5], that oxygen may be present in the form of phenolic, quinoid, carboxylic, and lactone surface compounds. The results of polarographic analysis [6] also show that quinoid and phenolic groups are present on carbon-black surfaces. The adsorption properties of carbon blacks also characterize their chemical surface structure [1, 7]. Infrared absorption spectra of carbon blacks can provide direct information on the presence and state of various types of oxygen complexes on their surfaces. However, it is rather difficult to obtain distinct infrared spectra of surface compounds on finely divided materials, including carbon blacks, because of the large losses of infrared radiation due to scattering and continuous absorption background. Therefore, in earlier investigations [2, 6], infrared spectroscopy was used merely as an auxiliary method for investigating surface chemical compounds on only a small number of carbon blacks which are most suitable for spectroscopic studies: oxidized blacks of the Carbolac type [2], and fine channel black with particles 80-100 A [6].

In the present investigation certain adsorption properties and infrared spectra of specially oxidized blacks were studied. This work is a continuation of infrared spectroscopic studies of surface chemical compounds on adsorbents [8, 9].

The materials used were Ukhta channel black, in the original form and after additional oxidation (oxidation with the aid of sodium hypochlorite was carried out in Korolev's laboratory [1]), and carbon black obtained by decomposition of graphitic oxide at 300° [10].

Characteristics of the carbon blacks are given in the table. Chemically combined oxygen was determined by ultimate analysis [1]; acidic groups were estimated by adsorption of caustic soda in an aqueous medium [7].

The table shows that the amount of oxygen in the acidic groups in the original and oxidized blacks, as found from data on adsorption of caustic soda, is considerably less than the total oxygen as given by ultimate analysis. Oxidation of channel black increased the content of total oxygen and of acidic groups capable of reacting with caustic soda. At the same time, in the case of specially oxidized blacks the amount of oxygen present in ion-exchange groups increased somewhat relative to the amount of oxygen present in other functional groups.

Characteristics of Carbon Blacks

Carbon Blacks	Specific surface, m^2/g*	Particle size from electron microscope data, A	Oxygen content meq/g		Adsorption of NaOH, meq/g
Ukhta channel, original	150	250 [11]	4.4	2.7	0.32
Same, oxidized by hypochlorite	80	—	17.3	10.8	1.7
Original, from graphitic oxide	175	100-1000 [4]	25.3	15.8	2.35
Same, treated at 1700° in a stream of hydrogen	130	—	—	—	—

*Specific surface was determined from low-temperature nitrogen adsorption by the BET method by N. N. Avgul', to whom the authors offer their thanks.

To obtain infrared spectra of surface compounds the substances chosen should cause the least loss of infrared radiation due to scattering and continuous absorption background, and give spectra from a large number of surface layers with a high concentration of chemical compounds. Of all the blacks studied by the adsorption method (see table) the one most suitable for spectroscopic investigation was that obtained from graphitic oxide. This had the highest concentration of oxygen compounds and laminar particles, which are the most suitable for repeated penetration of the surface layers by the infrared beam. We were unable to obtain an absorption spectrum for carbon black from graphitic oxide heated at 1700° in a stream of hydrogen, because heating at this temperature results in considerable growth of the microcrystals [12], so that the material becomes complete opaque [2].

Isotherms for adsorption of water vapor on Ukhta channel black were determined by means of the McBain–Baker vacuum spring balance at 30°, and on black from graphitic oxide by means of a vacuum gravimetric apparatus at 20° [13]. The samples were evacuated for a long time at 200° down to 10^{-5} mm Hg before the determinations.

The carbon blacks were mixed in liquid petrolatum for spectral investigation, in order to reduce scattering of infrared radiation. Despite thorough grinding in oil for 4 hours, the original channel black has a strong scattering effect on infrared radiation. In the case of carbon black from graphitic oxide, with particles of laminar structure, prolonged grinding in oil diminishes scattering considerably. In order to diminish scattering by oxidized channel black, fine particles were separated out by dispersion in water [1] and slow evaporation.

The spectra of carbon blacks after adsorption of water show considerable broadening of the absorption bands due to oxygen bonds in the surface compounds. In order to remove adsorbed water, the carbon blacks were evacuated in glass bulbs (10^{-4} mm Hg) at 20° for 4 hours. The bulbs were then sealed off under vacuum and the tips were broken off under oil in order to wet the black with oil. Because of the strong scattering of infrared radiation in the frequency region > 2000 cm^{-1} absorption bands due to valence vibrations of hydroxyl groups could not be observed. The spectra were determined only in the 900-2000 cm^{-1} region, by means of the IKS-12 single beam prism infrared spectrometer. Dried nitrogen vapor was blown through the jacket surrounding the monochromator and light source in order to prevent sorption of atmospheric moisture.

Isotherms for adsorption of water vapor on carbon blacks. Isotherms for adsorption of water vapor on the investigated blacks are given in Fig. 1. The isotherm for the original carbon black from graphitic oxide (Fig. 1, a) is sharply convex in the region of low relative pressures. At $p/p_s = 0.3$ the isotherm passes through an inflection point and rises steeply. The desorption branch is above the adsorption branch throughout. Part of the water is adsorbed irreversibly by the carbon black. The irreversibly adsorbed water is not removed during prolonged evacuation at 25°; it is probably held by activated adsorption and also penetrates into the oxidized regions between the basal planes in this carbon black.

The isotherm for adsorption of water vapor on Ukhta channel black additionally oxidized by hypochlorite (Fig. 1, b), determined earlier [1], is similar in appearance. The isotherm rises steeply even in the region of low relative pressures. The desorption branch lies above the adsorption branch over the entire pressure range, probably for the same reasons as in the case of carbon black from graphitic oxide.

The original Ukhta channel black, with a considerably lower content of chemically combined oxygen (Fig. 1, c), adsorbs water vapor much less – the adsorption isotherm for this black is S-shaped with an initial concave portion [7].

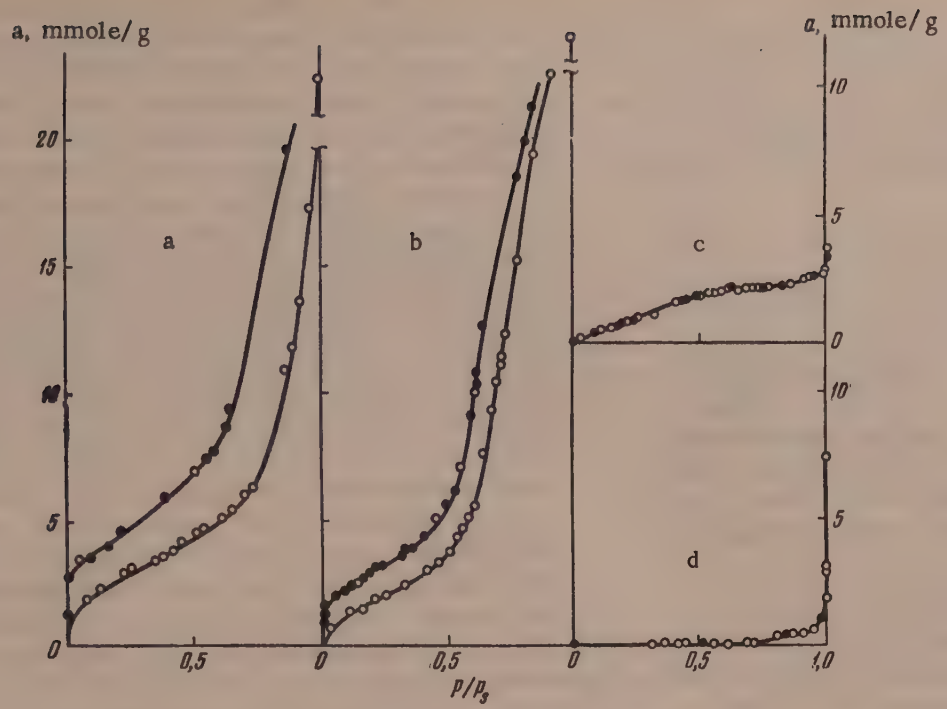


Fig. 1. Isotherms for adsorption of water vapor on carbon blacks: a) from graphitic oxide; b) channel black oxidized by hypochlorite; c) original channel black; d) from graphitic oxide, heated in hydrogen at 1700° (black points represent desorption).

Adsorption of water vapor on carbon black from graphitic oxide, heated in hydrogen at 1700° and free from chemically combined oxygen (Fig. 1, d) as on other types of carbon black subjected to this type of treatment [7], is negligibly small over the entire range of relative pressures. The isotherm for adsorption of water vapor on this black is concave throughout.

Infrared spectra of carbon blacks. The spectra of carbon blacks evacuated (down to 10^{-4} mm Hg) at 20° for 4 hours are given in Fig. 2. The spectra of oxidized black from graphitic oxide (curve 1) and channel black oxidized by hypochlorite (curve 3) contain the following bands: a weak band at 1750 cm^{-1}, bands of moderate intensity at 1585 cm^{-1}, and a strong band at 1070 cm^{-1}. Because of the lower concentration of chemical surface compounds and extensive scattering, it is not possible to obtain an equally clear spectrum for the original channel black (curve 2), but even here weak but quite reproducible absorption bands are found at ~1750, 1585 and 1070 cm^{-1}.

Because of the differences in the scattering power of the carbon blacks and difficulty in reproducing the concentration and thickness of the sample layers it is not possible to draw quantitative conclusions concerning intensity changes of the absorption bands as the result of oxidation, and therefore, concerning the increased contents of surface chemical groups which cause this absorption. However, it is quite possible that the absorption bands in the spectra of carbon black from graphitic oxide and channel black oxidized by hypochlorite (Fig. 2, curves 1 and 3) are more distinct than in the spectrum of the original channel black (curve 2) because of an increase in the number of chemical surface groups as the result of oxidation.

The absorption band at 1750 cm^{-1}, found in the spectra of all the investigated blacks, is due to carbonyl groups, as it lies in the region of absorption of carbonyl groups in various compounds [14]. It is difficult to ascribe this band to any definite type of compound, because it is weak and rather broad, probably owing to interaction with neighboring groups and possibly also because of the presence on the surface of a number of related chemical compounds, such as δ- and γ- saturated or unsaturated lactones, as was suggested earlier [2].

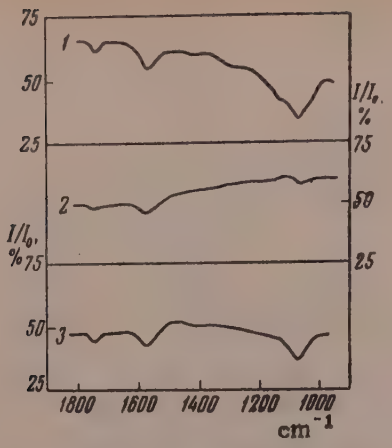


Fig. 2. Infrared spectra of carbon blacks: 1) from graphitic oxide; 2) original channel black; 3) channel black oxidized by hypochlorite.

The band at ~1585 cm^{-1} is stronger than the 1750 cm^{-1} band; it is found in the spectra of all the blacks studied by us, in the spectrum of channel black studied in [6], and in the spectrum of channel black studied in [6], and in the spectrum of Carbolac (~1600 cm^{-1}) [2]. Absorption bands at ~1600 cm^{-1} are also found in the spectra of coals [15]. The interpretation of these absorption bands has been debated [15], since it is known that an absorption band at ~1600 cm^{-1} is found in the spectra of many aromatic compounds containing single or condensed nuclei, and also in the spectra of compounds containing carbonyl groups linked to hydroxyls by hydrogen bonds. It is highly probable that this band in the spectra of carbon blacks is attributable to hydrogen-bonded carbonyl groups in surface compounds, as it has been found that when the carbon blacks are treated with alkali this band broadens and shifts toward lower frequencies [2], in the same way as the absorption band in carboxylic compounds in which hydrogen of the hydroxyl group is replaced by a metal ion [14]. Results of polarographic analysis of the surface compounds on carbon blacks also indicate that bound carbonyl groups are present on their surfaces. Finally, the concept of carbon black structure as a combination of crystallites each of which has a layer lattice analogous to that of graphite [16] is not inconsistent with the possibility of hydrogen bonding between neighboring hydroxyl and carbonyl groups lying in the same plane of the hexagonal carbon rings, since the existence of such bonding has been established experimentally in plane molecules consisting of systems of condensed rings and having such groups [14, 17]. Such bonding is less probably between these groups in neighboring crystallite planes, since the distance between them is usually greater than 3.55 A [16], which is more than the distance within which hydrogen bonding is possible [9].

The spectra of our carbon blacks (Fig. 2) have a strong band with a maximum at 1070 cm^{-1}, which was observed by Hadzi [18] in the spectrum of graphitic oxide and interpreted as due to valence vibrations of C–OH bonds. De Boer and Van Doorn [19] attribute a similar band (1065 cm^{-1}) in the spectrum of graphitic oxide to valence vibrations of the C–OH enol group. Our strong 1070 cm^{-1} band in the spectra of oxidized carbon blacks can also be attributed to valence vibrations of the C–OH bond. It is significant that the 1070 cm^{-1} absorption band in the spectra of strongly oxidized carbon blacks (Fig. 1, curves 1 and 3) is considerably stronger than the absorption band at 1750 cm^{-1} which is due to free carbonyl groups. A similar, although less pronounced, relationship between the intensities of the absorption bands was observed by Hadzi [18] in the spectrum of graphitic oxide; in his opinion, this indicated that in addition to carboxy groups with C–OH bonds hydroxyl groups of another type were present. The considerably higher intensity of the 1070 cm^{-1} band in comparison with the 1750 cm^{-1} band (Fig. 2, curves 1 and 3) found in our spectra may also be attributed to the above-mentioned possibility of hydrogen bonding between surface groups, as a result of which a band due to bound carbonyl groups appears at 1585 cm^{-1} and the band due to free carbonyl groups at 1750 cm^{-1} becomes weaker.

Certain conclusions concerning the structure of surface chemical compounds on oxidized carbon blacks may be drawn from a comparison of the results of adsorption and spectral studies.

The adsorption-desorption hysteresis for water vapor on carbon black from graphitic oxide (Fig. 1, a), channel black oxidized by hypochlorite (Fig. 1, b) and the original channel black (Fig. 1, c) indicates that the action of the oxidizing agent not only resulted in oxidation of hydrocarbon radicals at the corners of the crystallites emerging on the surface, but led to penetration of a part of the oxygen into the spaces between the crystallites and possibly between the planes. Although the adsorption data indicate that the blacks become more acid as the result of oxidation, they do not allow differentiation of the types of surface oxygen compounds. The results of chemical analysis (Table 1) indicate that the proportion of acidic (hydroxyl) groups in specially oxidized blacks increases somewhat.

Infrared spectra of the carbon blacks give a more complete picture of the type of surface compounds. Spectral data indicate that simple functional groups of the hydroxyl, carbonyl, and carboxyl types are present in the structure of surface chemical compounds in carbon blacks. Oxygen combines primarily with carbon atoms in the

prismatic faces and edges of the crystallites and with surface atoms of carbon chains formed in breakdown of carbon rings or by addition of partially undecomposed hydrocarbons. It is therefore reasonable to suppose that these functional groups are components of more complex surface compounds, such as phenol, enol, and lactone compounds, the existence of which is usually postulated from the results of chemical analysis [2]. It is also significant that, as the spectroscopic data indicate, such compounds do not exist in isolation from each other in the surface layers of the carbon-black particles. Phenolic and carbonyl groups in close proximity and favorable orientation form bonds of the intramolecular-hydrogen-bond type between themselves, similarly to the interaction of hydroxyl groups on the surface of porous glass [8] and silica gel [9].

The foregoing spectral data merely characterize the structure of surface compounds on carbon blacks. No less interesting is application of the spectroscopic method to studies of bonding between surface chemical compounds on carbon blacks and the chemical groups of polymers into which the blacks are introduced as fillers. Such investigations involve certain difficulties in view of the above-mentioned strong scattering of infrared radiation by carbon blacks and the consequent low selectivity of their spectra, and also because of possible superposition of filler and polymer absorption bands. It is to be hoped, however, that such an investigation may be carried out on special mixtures of carbon black and polymer in which the polymer serves as a medium which reduces scattering of infrared radiation.

SUMMARY

Chemical analysis and adsorption of water indicate that strongly oxidized carbon blacks contain various oxygen compounds which greatly influence adsorption of water. Infrared spectra give indications of the nature of these compounds and of their mutual interaction.

LITERATURE CITED

1. A. V. Kiselev, N. V. Kovaleva, A. Ya. Korolev, and K. D. Shcherbakova, Doklady Akad. Nauk SSSR, 124, 617 (1959).*
2. V. A. Garten, D. E. Weiss, and J. B. Willis, Austral. J. Chem. 10, 295 (1957).
3. D. I. Villars, J. Amer. Chem. Soc. 70, 3655 (1948).
4. U. Hofman and G. Ohlerich, Angew. Chemie 62, 16 (1950).
5. M. Studebaker, E. W. D. Huffman, A. C. Wolfe, and L. G. Nabors, Ind. and Eng. Chem. 48, 162 (1956).
6. I. V. Hallum and H. V. Druschel, J. Phys. Chem. 62, 110 (1958).
7. A. V. Kiselev and N. V. Kovaleva, Izvest. Akad. Nauk SSSR, Otdel. Khim. Nauk 989 (1959).*
8. A. V. Kiselev and V. I. Lygin, Proceedings of the Second International Congress on Surface Activity (London, 1957) 2, 204; V. I. Lygin, Vestnik Moskovskogo Un-ta 1, 223 (1958).
9. A. V. Kiselev and V. I. Lygin, Kolloid. Zhur. 21, 581 (1959);* A. V. Kiselev, in: The Structure and Properties of Porous Materials (London, 1958) p. 195.
10. V. Kohlschütter and P. Haenni, Z. anorgan.und allgem. Chem. 105, 121 (1919).
11. A. V. Kiselev, V. M. Luk'yanovich, and E. A. Porai-Koshits, Collection: Methods for Investigating the Structure of Highly Disperse and Porous Bodies [in Russian] (1958) part 2, p. 161.
12. W. D. Schaeffer, W. R. Smith, and M. H. Polley, Ind. and Eng. Chem. 45, 1731 (1953); W. D. Schaeffer and W. R. Smith, Ind. and Eng. Chem. 47, 1286 (1955).
13. A. V. Kiselev and N. V. Kovaleva, Zhur. Fiz. Khim. 30, 2775 (1956).
14. L. J. Bellamy, Infrared Spectra of Complex Molecules [Russian translation] (IL, Moscow, 1957).
15. J. K. Brown, J. Chem. Soc. 744 (1955).
16. J. Biscol and B. Warren, Appl. Phys. 13, 3647 (1942).
17. J. M. Hunsberger, R. Ketcham, and H. S. Gutowsky, J. Amer. Chem. Soc. 74, 4839 (1952).
18. D. Hadzi and A. Novak, Trans. Faraday Soc. 51, 1614 (1955).
19. A. VanDoorn, Grafietoxyde, Proefschrift ter verkrijging van de graad van doctor in de technische wetenschap an technische hogeschool (Delft, 1957).

* Original Russian pagination. See C. B. translation.

RELATIONSHIP BETWEEN HEAT OF WETTING, AMOUNT OF BOUND WATER, HYGROSCOPICITY, AND ION EXCHANGE CAPACITY OF CLAYS

I. I. Morachevskii, E. Ya. Shteigel'berg, V. B. Chernogorenko, and M. A. Kirdo

Scientific Research Institute of Constructional Materials and Products, Kiev
Translated from Kolloidnyi Zhurnal, Vol. 22, No. 3, pp. 340-343
May-June, 1960
Original article submitted February 28, 1959

Many physicochemical properties of ceramic pastes, including plasticity and swelling, are determined by hydrophily of the clays. It has been shown [1] that the amount of bound water, which is determined by a variety of methods [2], is a measure of hydrophily. Fairly reproducible data can also be obtained from determinations of heats of wetting. We used the established relationships between the hydrophilic characteristics of clay minerals [1] in a study of the heats of wetting of 14 clays used in ceramic factories in the Ukraine. The results were correlated with the amounts of moisture taken up hygroscopically from the air and with the total cation-exchange capacity.

A calorimeter of the adiabatic type, analogous to that used in Dumanskii's laboratory [3], was used for determination of the integral heats of wetting of clays. The water equivalent of the calorimeter was 186 cal/degree. On the assumption that the heat liberated when clay is wetted by water corresponds to monolayer adsorption, the amount of firmly bound water (A, %) was calculated from the formula [1]

$$A = \frac{Qh\rho}{q} \cdot 100\%,$$

where Q is the heat of wetting (erg/g); h is the thickness of a monomolecular layer of water, equal to $2.76 \cdot 10^{-8}$ cm; q is the surface energy of water, equal to 116 ergs/cm^2; ρ is the density of bound water, taken to be 1 g/cc.

For determination of hygroscopic moisture the clay samples were kept at 20° in a desiccator over saturated calcium nitrate solution (relative humidity 55%) to equilibrium. The total cation-exchange capacity was determined by the method described by Antipov-Karataev [4].

The experimental results are summarized in the table. The results of chemical, mineralogical, and particle-size analyses are given in [5].

The relationship between the heat of wetting by water and the amount of bound water is plotted in Fig. 1. It is seen that there is a linear relationship, represented by the equation Q = 1.15 W, between the heat of wetting (Q) and hygroscopic moisture content (W). According to Andrianov [6] the ratio between the heat of wetting and hygroscopic moisture content for a number of soils varies between 0.78 and 1.25.

Relationships Between the Heats of Wetting of Clays by Water and Benzene, Amounts of Bound Water, and Cation-Exchange Capacities

Clays	Heat of wetting, cal/g		Philicity coeff., $\beta = \frac{Q_{H_2O}}{Q_{C_6H_6}}$	Amt. of bound water, %		T, total exchange capacity, meq/100 g
	Q_{H_2O}	$Q_{C_6H_6}$		from Q_{H_2O}, A	hygroscopic moist., W	
Glukhovo kaolin, beneficiated (Zhitomir prov.)	1,07	0,59	1,8	1,06	0,65	10,1
Belaya Tserkov loess (Kiev Prov.)	2,59	1,61	1,6	2,57	2,18	20,3
Nikiforovo clay (Stalino Prov.)	3,02	1,75	1,7	3,00	2,34	19,2
Pavlograd loam (Dnepropetrovsk Prov.)	3,43	1,65	2,2	3,41	2,53	20,3
Beregov clay (Transcarpathian Prov.)	3,50	2,00	1,7	3,45	2,87	24,7
Chasov Yar clay, G-2 (Stalino Prov.)	3,20	1,21	2,6	3,18	3,00	24,7
Drogobych clay (Drogobych Prov.)	3,66	2,25	1,7	3,64	3,11	26,4
Spondylic clay (Kiev)	4,05	2,43	1,7	4,03	2,79	22,4
Balaklava clay (Crimea)	4,14	2,00	2,0	4,12	3,31	25,3
Vendichany clay (Vinnitsa Prov.)	5,06	2,49	2,0	5,04	3,63	29,5
Krasnogvardeisk clay (Dnepropetrovsk Prov.)	4,63	2,41	1,9	4,61	4,00	32,8
Vasil'kov clay (Kiev Prov.)	6,61	2,83	2,3	6,58	5,12	37,5
Berislav clay (Kherson Prov.)	6,30	3,02	2,1	6,27	5,46	41,0
Gorbsk bentonite (Transcarpathian Prov.)	7,75	3,73	2,1	7,70	7,26	47,6

The relationship between the heat of wetting and the amount of bound water (A, %) calculated from Equation (1) is represented by curve II, the equation for which is $Q = 0.98\,A$.

It is known [1] that heat of wetting is an aggregate effect in the interaction of clay with water: it is made of the heat of wetting of the true clay surface, the heat of reaction with exchange ions, and other factors.

The difference (A–W) between the amount of bound water determined from the heat of wetting and the hygroscopic moisture content increases with increasing exchange capacity. We consider, consistently with the views of Ovcharenko [7] and Rode [8], that this difference is associated with hydration of exchange cations. The difference A–W, calculated from Equation (1), gives the degree of hydration of the cations. For the clays studied the heat of hydration of the cations is ~20% of the integral heat of wetting Q_{H_2O}.

The relationship between the exchange capacity (T) and hygroscopic moisture content (W) is represented by a straight line in Fig. 2. This relationship corresponds to the equation $T = 7.2\,W$. For soils of the chernozem type Aleshin [9] found a value of 7.6 for the coefficient in this equation; this is close to our value (7.2)

As Sergeev [10] points out, the existence of a correlation between the exchange capacity and the amount of firmly bound water involves the existence of a correlation between exchange capacity and heat of wetting. However, the ratio between the exchange capacity and heat of wetting is constant only within each group of clays, as these properties depend on the mineral composition and the composition of the exchange cations [11]. In Fig. 2 the relationship between exchange capacity (T) and the heat of wetting by water Q_{H_2O} is represented by the equation $T \approx 6.5\,Q$*. Jänert [12] found the expression $T = 4.2\,Q$ for a series of clays.

From the curves in Fig. 2 it may be concluded that a relationship exists between the hygroscopic moisture content, heat of wetting by water, and exchange capacity. If the origin of the ordinate representing the hygroscopic moisture in Fig. 2 is lowered, the lines virtually coincide. Figure 2 then becomes a nomogram for calculation in two quantities when the third is given. Ovcharenko [13] showed earlier that hydrophilic properties of

* The heat of wetting is taken in calories per gram of clay, and the cation-exchange capacity is expressed in mg-equivalents per 100 g of clay.

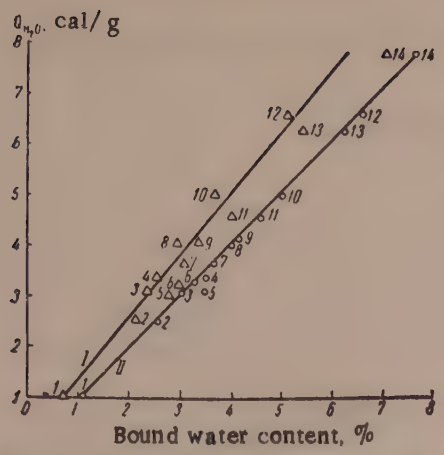


Fig. 1. Relationships between the heats of wetting of clays by water (Q_{H_2O}) and: I) hygroscopic moisture contents, II) amounts of bound water calculated from Equation (1). The numbers at the points correspond to the numbers of the clays in the table.

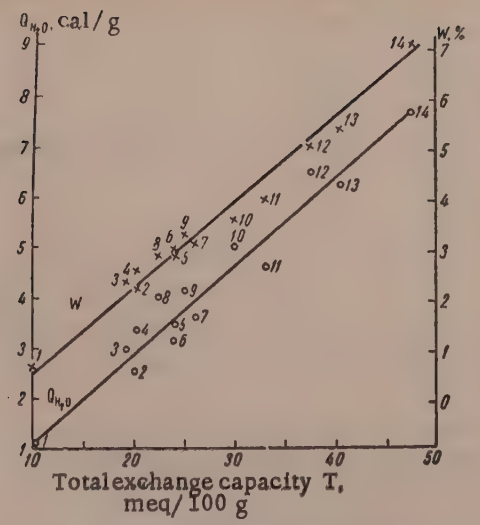


Fig. 2. Relationships between the total exchange capacities, hygroscopic moisture contents (W), and heats of wetting of clays by water (Q_{H_2O}). The numbers at the points correspond to the numbers of the clays in the table.

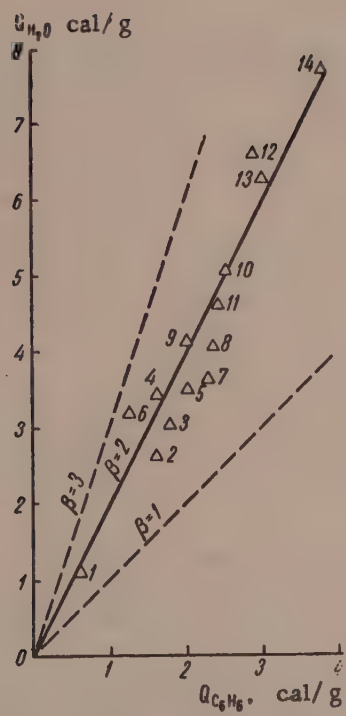


Fig. 3. Relationship between the heats of wetting by water (Q_{H_2O}) and by benzene ($Q_{C_6H_6}$). The numbers at the points correspond to the numbers of the clays in the table.

clays determine the plasticity of clay pastes. This result, with our data taken into account, leads to the conclusion that clay quality may be assessed from one characteristic of the hydrophilic properties. Evidently, this is valid only for clays used in the ceramic industry.

The surface area of a wetted mineral is often estimated from the ratio of the heats of wetting by a polar liquid (water), and a nonpolar medium (benzene). The resultant dimensionless quantity was given the name of philicity coefficient (β) by Rebinder [14]. It is easy to see that a linear relationship exists between the heats of wetting by water and by benzene, and the average value of the philicity coefficient (β) is 2. It is known that the heat of ion solvation in benzene is very small, and therefore, we may assume that benzene wets only the aluminosilicate framework of the clay surface. With increase of surface area, as indicated by the increase of the heat of wetting by benzene $Q_{C_6H_6}$, the heat of wetting by water Q_{H_2O} also increases (Fig. 3). Kelley and Jenny [15] showed in the case of comminuted clay and nonclay minerals that the cation-exchange capacity increases with increasing surface area. Therefore, increase of the heat of wetting cannot be attributed to cation exchange only. The surface area is of decisive significance.

SUMMARY

1. Relationships between the exchange capacity (T), hygroscopic moisture content (W), and the heat of wetting (Q_{H_2O}) were established for 14 clays used in the Ukrainian ceramic industry; these relationships are represented by equations $T = 7.2\ W$ and $T \approx 6.5\ Q_{H_2O}$.

2. The relationship between the heat of wetting by water and the hygroscopic moisture content of clays is represented by the equation $Q_{H_2O} = 1.15\ W$.

3. The heats of wetting of clays by water (Q_{H_2O}) and by benzene ($Q_{C_6H_6}$) are connected by the linear relationship $Q_{H_2O} \approx 2Q\ C_6H_6$.

It is our pleasant duty to thank F. D. Ovcharenko for his interest in the work.

LITERATURE CITED

1. F. D. Ovcharenko, Collection: Physicochemical Principles of Ceramics [in Russian] (Promstroiizdat, Moscow, 1956) p. 31; Reports on the international meeting on clays in Brussels, 1958, (Moscow, 1958) pp. 107, 158.
2. P. I. Andrianov, Tr. In-ta Merzlotovedeniya im. V. A. Obrucheva 3, 27 (1946).
3. A. V. Dumanskii and F. D. Ovcharenko, Kolloid. Zhur. 12, 331 (1950); A. V. Dumanskii, Ya. F. Mezhennyi, and E. F. Nekryach, Kolloid. Zhur. 10, 108 (1948).
4. L. N. Antipov-Karataev, D. I. Kovda, and G. N. Sambur, Instruction on Sulfate Treatment of Solonetz Soils in UkrSSR [in Russian] (Sel'khozgiz, 1939).
5. B. V. Chernogorenko, E. Ya. Shteigel'berg, and L. L. Morachevskii, Tr. NII Stroimaterialov i Izdelii AS i A USSR No. 2, 129 (1960).
6. P. N. Andrianov, Kolloid. Zhur. 6, 695 (1940).
7. F. D. Ovcharenko, Ukrain. Khim. Zhur. 19, 139 (1953).
8. A. A. Rode, Soil Moisture [in Russian] (Izd. Akad. Nauk SSSR, Moscow, 1952) p. 152.
9. S. I. Aleshin, Collection: Soil Physics in the USSR [in Russian] (Sel'khozgiz, Moscow, 1936) 5, p. 540; Khimizatsiya Sotsialist. Zemledeliya 4, 60 (1939).
10. E. M. Sergeev, General Soil Science [in Russian] (Izd. MGU, Moscow, 1952) p. 372
11. E. M. Sergeev, Vestnik MGU 2, 69 (1947).
12. H. Z. Janert, J. Agric. Sci. 24, 136 (1934).
13. F. D. Ovcharenko, Collection: Advances in Building Technology [in Russian] No. 5 (Izd. Akad. Arkhitektury UkrSSR, Kiev, 1954) p. 71.
14. P. A. Rebinder, Collection: Mathematics and Natural Science in the USSR [in Russian] (Izd. Akad. Nauk SSSR, Moscow–Leningrad, 1938) p. 431.
15. W. P. Kelley and H. Jenny, Soil Sci. 41, 367 (1936).

EXTRACTION OF COLLOIDALLY DISSOLVED MIXED FERROCYANIDES OF HEAVY METALS FROM THEIR HYDROSOLS BY MEANS OF GELATIN FOAM

L. D. Skrylev and S. G. Mokrushin

S. M. Kirov Ural Polytechnic Institute, Sverdlovsk
Translated from Kolloidnyi Zhurnal, Vol. 22, No. 3, pp. 344-349
May-June, 1960
Original article submitted March 4, 1959

One of us showed experimentally that it is possible to extract completely colloidal hydroxides, sulfides, and colorants from hydrosols and mixtures of hydrosols with true solutions [1]. Studies of the kinetics of this process showed that the rate of colloid extraction depends on a number of factors, of which the most important are: pH of the medium, concentration of gelatin, temperature of the original solution, and the presence of electrolytes and surface-active substances in the solution [2, 3].

The present paper deals with a kinetic study of extraction of colloidal mixed heavy-metal ferrocyanides by means of gelatin foam.

The materials used in the investigation were hydrosols of mixed ferrocyanides of copper, nickel, cobalt, bivalent manganese, and trivalent iron. The solutions needed for their formation were prepared in distilled water from chemically pure compounds: $K_4[Fe(CN)_6]\cdot 3H_2O$, $CuSO_4\cdot 5H_2O$, $CoSO_4\cdot 7H_2O$, $NiSO_4\cdot 7H_2O$, $MnSO_4\cdot 7H_2O$ and $FeCl_3\cdot 6H_2O$.

Experimental procedure. Solutions of $K_4[Fe(CN)_6]\cdot 3H_2O$ and one of the above-named heavy-metal salts were put into glass beakers 250 ml in capacity, each containing 75 ml of distilled water. The resultant sol was stirred thoroughly, the foaming agent (2 ml of 1% gelatin solution) was added, the volume was made up to 100 ml, and the liquid was poured into a vertical glass tube 1 m long and 40 mm in diameter. The bottom of the tube consisted of a porous plate. Air dispersed by means of this plate was blown through the sol to produce foam. The air rate was measured by means of a flow meter, and was 600 cc/min.

The reagents needed for formation of the ferrocyanides were added in amounts calculated to give 100 mg of solid phase per liter for the compositions: $K_2Cu_3[Fe(CN)_6]_2$, $K_4Co_{10}[Fe(CN)_6]_6$, $K_4Ni_4[Fe(CN)_6]_3$, and 50 mg of solid phase per liter for the compositions $K_2Mn[Fe(CN)_6]$ and $KFe[Fe(CN)_6]$, [4,5]; the potassium ferrocyanate was taken in 50% excess*, to act as the peptizing agent.

* The peptizing action of excess $K_4[Fe(CN)_6]$ is explained as follows. The $Fe(CN)_6^{4-}$ ions introduced into the solution are adsorbed on the precipitate particles, forming an electric double layer; the particles then pass into the sol form but retain their individuality [6]. Beyond a definite excess of $K_4[Fe(CN)_6]$, the sol coagulates. This is probably because the simultaneous tendencies to peptization of the precipitate (influence of $Fe(CN)_6^{4-}$ ions) and to coagulation (influence of K^+ ions), characteristic of the system, vary in accordance with the amount of excess $K_4[Fe(CN)_6]$ present. At high $K_4[Fe(CN)_6]$ concentrations the influence of potassium ions predominates, and the sol therefore coagulates [4].

The degree of extraction of the colloidal substance from the sol was determined colorimetrically by means of a photoelectric colorimeter.

Extraction kinetics. The very first experiments showed that it is possible in principle to apply the foam method to extraction of these colloidal ferrocyanides from aqueous solutions.

Studies of extraction kinetics (Fig. 1) showed that different ferrocyanides are extracted at different rates. An exception is provided by mixed ferrocyanides of copper and cobalt, which are extracted at the same rate. The differences between the extraction rates of ferrocyanides are especially prominent at the start of foam formation. For example, during the first three minutes of air blowing 68.8% of mixed manganese ferrocyanide and only 36.5% of mixed ferric ferrocyanide is extracted. However, the difference between the extraction rates of these ferrocyanides decreases with increase of foaming time. Complete extraction of the mixed ferrocyanides of cobalt, nickel, and manganese is effected after 12 minutes of air blowing through the sols. For complete extraction of mixed ferrocyanides the foaming time should be increased to 18 minutes.

Effect of gelatin concentration. Special experiments on the effect of gelatin concentration in the sol on the kinetics of extraction of colloidal ferrocyanides by the gelatin foam method showed that the gelatin concentration has a considerable influence on the rate of extraction of the disperse phase.

Figure 2 shows that there is an optimum concentration of gelatin in the sol at which the rate of extraction of the colloid is at a maximum. For mixed ferrocyanides of copper and nickel this concentration is 0.02%. At lower gelatin concentrations the amount and strength of the foam formed when air is blown through the sol diminish. As a result some of the bubbles break down, with consequent peptization of the protein–ferrocyanide gel in the structure of the foam films [7], and this in its turn lowers the rate of extraction of the colloid. Excess gelatin in the sol also lowers the rate of extraction of the disperse phase. When air is blown through a sol containing excess gelatin, a large amount of microcellular moist foam is formed, and this does not hold the colloid effectively. A similar effect of gelatin concentration on the degree of extraction of colloidal sulfides of certain metals was reported earlier [3].

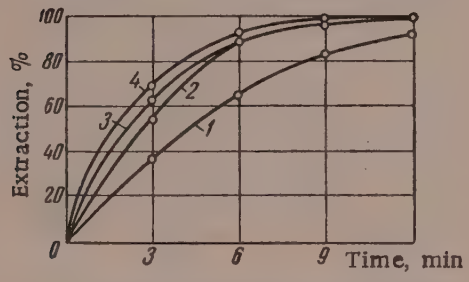


Fig. 1. Extraction kinetics of mixed ferrocyanides of manganese (1), copper and cobalt (2), nickel (3), and iron (4).

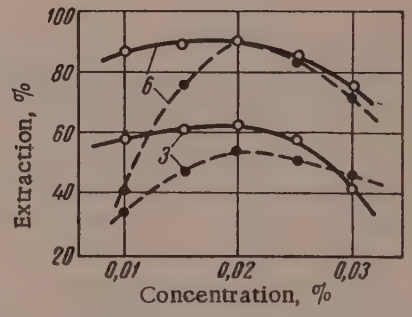


Fig. 2. Effect of gelatin concentration in the sol on the degree of extraction of mixed copper ferrocyanide (continuous curve) and mixed nickel ferrocyanide (dash line). The numbers by the curves represent the time of foam formation in minutes.

Effect of the air blowing rate. The rate of air blowing is one of the principal factors determining the completeness of foam separation of surface-active substances in true solution [8]. The best separation is effected by slow blowing, so that the air bubbles stay in the liquid long enough to allow the surface layers of the bubbles to come into equilibrium with the surrounding liquid and to ensure a high degree of foam draining [9]. Moreover, the stability of the foam increases with decrease of the air blowing rate [10].

Ermolenko and Plenina [1], who studied foam formation in ferric hydroxide sols containing lupine protein as foaming agent, found that the amount of hydroxide entering the foam passes through a maximum with increase of the air blowing rate. The existence of an optimum air rate was also reported by Stark [11], who studied coagulation of ferric hydroxide sols at the sol– gas interface with different gases blown through the sols.

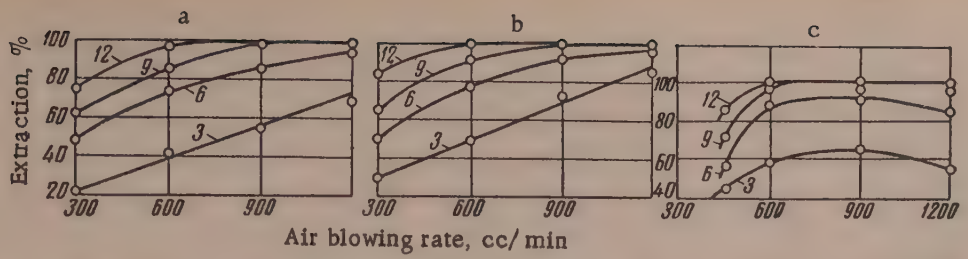


Fig. 3. Effect of the rate of air blowing on the degree of extraction of colloidal mixed ferrocyanides of copper (a) and cobalt (b) from sols containing 0.03% gelatin, and of mixed copper ferrocyanide from a sol containing 0.01% gelatin (c). The numbers by the curves represent the time of foam formation in minutes.

The foregoing facts suggested that the rate of air blowing should have a considerable influence on foam extraction of these ferrocyanides. Experiments carried out with hydrosols of the mixed ferrocyanides of copper and cobalt confirmed this hypothesis. The nature of this influence depends on the concentration of foaming agent (gelatin) in the sol.

When the gelatin concentration is fairly high (0.03%), the amount of foam formed and the amount of colloid taken into the foam increase with increase of the blowing rate. Figure 3, a and 3, b shows the relationship between the air blowing rate and the degree of extraction of the disperse phase in the sols over certain definite time intervals. It is clear from Fig. 4 that when the foaming time is short (3 minutes) the degree of extraction of ferrocyanides is directly proportional to the air blowing rate. However, with increase of the foaming time this direct proportionality breaks down owing to a decrease in the rate of extraction of the colloid from the sol.

The explanation of this effect may be that the concentration of gelatin and of the colloidal ferrocyanide particles sensitized by it decrease continuously during foam formation. After a certain instant the concentration of these particles becomes insufficient for formation of a saturated surface film at the liquid–gas interface, and as a result the amount of colloid taken up by the foam formed by the passage of a given volume of air through the sol decreases. Moreover, a decrease of the concentration of surface-active particles at the liquid–gas interface lowers considerably the strength of the surface film, and therefore, some of the air bubbles break down immediately after emerging to the sol surface. This leads to partial peptization of the gelatin–ferrocyanide gel in the film structure.

The situation is entirely different if foam formation takes place in a sol containing a small amount of foaming agent (Fig. 3, c). Even with a short foaming time there is no direct proportionality between the volume of air passed during a given time and the degree of extraction of the colloid. The curve showing the degree of extraction of the solid phase as a function of the air blowing rate passes through a maximum. Maximum extraction corresponds to an air rate of 900 cc/ min. The existence of a maximum is due to the extreme weakness of the films formed on the surface of bubbles formed when air dispersed by the porous plate is passed through the sol. When the blowing rate is higher than 900 cc/min the surface films undergo mechanical breakdown; this leads to a decrease in the degree of colloid extraction, and fragments of denatured gelatin–ferrocyanide film appear in the sol. These fragments interfere with colorimetric determination of the degree of extraction of the dispersed substance.

Comparison of Fig. 3, a and 3, c shows that at low air rates the degree of extraction of mixed copper ferrocyanide from a sol containing the smallest amount of gelatin (0.01%) is lower than in the case when foaming is carried out in a sol containing a certain excess of gelatin (0.03%).

This is understandable if it is taken into account that the relative concentration (referred to the total number of surface-active particles) of sensitized colloidal particles in the sol and therefore in the surface layer is higher in the first case than in the second.

Influence of surface-active substances. Any foaming process involves transition of surface-active substances from solution to the liquid–gas interface. Studies by numerous workers have established that this transition conforms to a definite sequence, For example, when foam is formed in a dilute solution of gelatin and sodium oleate the upper foam layer contains gelatin only. If the solution contains saponin also, the substances are arranged in the foam column in the following sequence: saponin, gelatin, sodium oleate [12].

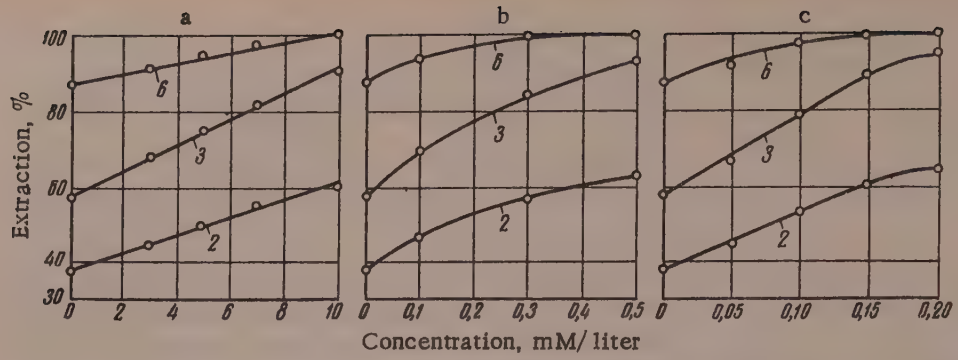


Fig. 4. Effects of the concentrations of ethyl (a), n-butyl (b), and isoamyl alcohols (c) on the degree of extraction of colloidally dissolved mixed copper ferrocyanide from a sol containing 0.01% gelatin. The numbers by the curves represent the time of foam formation in minutes.

When one surface-active substance is added to an aqueous solution of another, foaming may either increase or decrease, because of a change in the solubility of the surface-active substance in water [13]. If the solubility decreases, foaming is intensified; if the solubility rises, foaming is weakened. Additions of small amounts of certain substances such as alcohol or acetone to protein solutions increase foam stability considerably [9]; this was attributed to the strong dehydrating action of alcohol and acetone. Additions of large amounts of these substances, on the other hand, lower foam stability, as an excess of alcohol or acetone molecules in solutions causes them to displace proteins from the foam bubble surfaces. Schutz [9], in a study of foam formation in solutions of various organic substances and mixtures, showed that an aqueous solution of inulin, which gives a highly unstable foam, forms a very stable foam if alcohol or dioxane is added.

Additions of surface-active substances often not only increase the strength of surface films but accelerate their formation. The formation of a surface film on a solution of hydrocinnamic acid was accelerated in presence of propyl alcohol [14]. In presence of ethyl, n-butyl, or isoamyl alcohol the rate of extraction of negatively charged colloidal particles by gelatin foam increases, while the rate of extraction of positively charged colloidal particles decreases. This is because the liquid–gas interface in alcohol solutions is positively charged [15]. The positive interfacial charge favors transition of negatively charged particles into the surface layer, and hinders transition of positive particles.

Experiments to study the effect of surface-active substances on the kinetics of extraction of mixed heavy-metal ferrocyanides by gelatin foam were carried out with a sol of mixed copper ferrocyanide. The surface-active substances used were ethyl, n-butyl, and isoamyl alcohols, and glycerol. The surface-active substances were added to the sol before addition of gelatin. Air was blown through the sol at 600 cc/min.

The results are presented in the table and Fig. 4. The table shows that when the gelatin concentration in the sol is high enough (0.03%) the presence of small amounts of ethyl, n-butyl, or isoamyl alcohol has almost no effect on the extraction kinetics of colloidally dissolved mixed copper ferrocyanide, but increases foaming considerably. When air is blown through sols containing these alcohols a large amount of moist microcellular foam is formed; this entrains a large amount of sol without specific separation of the colloid. The volume and moisture content of the foam increase with the alcohol concentration. Glycerol has no appreciable effect on colloid extraction or foaming even at very high concentrations.

The situation is quite different at low (0.01%) concentrations of gelatin in the sol. In this case addition of a small amount of ethyl, n-butyl, or isoamyl alcohol to the sol sharply increases foam stability and the rate of colloid extraction (Fig. 4). Whereas 12 minutes is needed for complete extraction of mixed copper ferrocyanide from a sol containing gelatin only, only 6 minutes is needed to extract it from a sol containing 0.2 mM/liter of isoamyl alcohol in addition to gelatin. The rate of colloid extraction increases with the alcohol concentration in the sol. The increase of the extraction rate may be explained as follows: when surface-active substances (such as alcohols) are added to an aqueous gelatin solution their polar groups are bonded to the polar groups of the gelatin micelles and thereby exert a dehydrating action; that is, they decrease both surface and volume solvation and make the hydrophilic micelles hydrophobic [16]; this, in its turn, increases the surface activity of the gelatin–ferrocyanide complex. The favorable influence of alcohols on extraction of mixed copper ferrocyanide by gelatin foam increases with increase of their molecular weight.

Effect of the Concentration of Surface-Active Substances (SA) in the Sol on the Degree of Extraction of Mixed Copper Ferrocyanide by Gelatin Foam From 0.03% Gelatin Solution During 3 Minutes of Foaming

Surface-active substance (SA)	SA concentration, mM/liter	Degree of extraction, %	Surface-active substance (SA)	SA concentration, mM/liter	Degree of extraction, %
Ethyl alcohol	0,0	57,2	Isoamyl alcohol	0,1	57,0
	0,5	58,3		0,5	58,4
	1,0	57,6		1,0	58,5
	2,0	56,8			
			Glycerol	1	57,7
n-Butyl alcohol	0,1	57,3		10	57,9
	0,5	58,2		100	56,8
	1,0	57,1			

Additions of glycerol to a sol containing a small amount of gelatin decrease foam stability and the rate of colloid extraction.

SUMMARY

1. It was shown experimentally that colloidal mixed ferrocyanides of copper, nickel, cobalt, bivalent manganese, and trivalent iron can be completely extracted from their hydrosols by means of gelatin foam.

2. There is an optimum concentration of gelatin in the sol at which the rate of colloid extraction is highest.

3. The air blowing rate and additions of surface-active substances have a considerable influence on foam extraction of colloids; the nature of this influence depends on the concentration of gelatin in the sol.

LITERATURE CITED

1. S. G. Mokrushin, Reports on the Scientific Work of Members of the D. I. Mendeleev All-Union Chemical Society [in Russian] (1953) 2, p. 26.
2. R. V. Shveikina and S. G. Mokrushin, Kolloid. Zhur. 20, 233 (1958);* Zhur. Priklad. Khim. 31, 943 (1958);* Izvest. VUZ, Khimiya i Khim. Tekhnologiya 4, 8 (1958).
3. S. G. Mokrushin and K. G. Potaskuev, Kolloid. Zhur. 18, 215 (1956).*
4. I. V. Tananaev and M. I. Levina, Zhur. Anal. Khim. 3, 31 (1948).
5. I. V. Tananaev, Izvest. Akad. Nauk SSSR, Otdel. Khim. Nauk 12, 1421 (1957);* 2, 268 (1957).*
6. D. I. Éristavi and D. N. Barnabishvili, Zhur. Obshch. Khim. 9, 1880 (1939).
7. N. F. Ermolenko and G. N. Plenina, Kolloid. Zhur. 5, 193 (1939).
8. H. G. Cassidy, Fundamentals of Chromatography (Interscience Publishers, N.Y., 1957) p. 341.
9. F. Schütz, Trans. Faraday Soc. 42, 437 (1946).
10. G. O. Erchikovskii, Formation of Flotation Foam [in Russian] (GONTI, 1939).
11. H. M. Stark, J. Amer. Chem. Soc. 52, 2730 (1930).
12. Chromatography [Russian translation edited by M. M. Dubinin] (IL, Moscow, 1949) p. 176.
13. O. Bartsch, Kolloidchem Beihefte 20, 1 (1925).
14. J. Alexander, Trans. Faraday Soc. 37, 1525 (1941).
15. A. N. Frumkin, Trudy In-ta im. L. Ya. Karpova 3, 3 (1924).
16. K. F. Zhigach and P. A. Rebinder, Zhur. Fiz. Khim. 13, 94 (1939).

* Original Russian pagination. See C. B. translation.

STATES OF AGGREGATION OF HIGH POLYMERS

7. INFLUENCE OF TEMPERATURE ON THE STATE OF KERATINS

R. I. Fel'dman

N. K. Krupskaya Moscow Regional Pedagogic Institute
Translated from Kolloidnyi Zhurnal, Vol. 22, No. 3, pp. 351-356
May-June, 1960
Original article submitted June 17, 1959

We showed in the case of collagen, gelatin, and silk fibroin [1] that the behavior of fibrous proteins with variations of temperature can be conveniently studied by means of linear dilatometry [2]. This method was used earlier for studies of other synthetic [2, 3] and natural [4] polymers. We therefore considered that this method should be applicable to keratins. As was noted earlier [4], dilatometric investigations can reveal similarities in the behavior of materials belonging to different classes of polymers and the characteristic features of each.

It is to be expected that keratins, because of their complex morphological structure and variety of forms of water bonding, should, like other protein formations [1], exhibit a complicated behavior pattern under conditions of simultaneously changing temperature and humidity. Changes in the properties of hydrophilic materials such as keratins are directly related to variable amounts of moisture which is taken up by them, which acts as a plasticizing component in the system. The course of variations of the moisture content of a system depends not only on the form of bonding between water and the sorbent, but also on the surface–volume ratio of the specimen. Under the influence of temperature changes the dimensional changes of a hygroscopic specimen in general comprise the aggregate effects of thermal expansion, changes in the degree of orientation, transition of the system into a state with different molecular packing, and moisture content [1, 3].

The purpose of this communication, like that of the earlier papers, is to demonstrate the behavior of materials on heating and cooling under variable conditions which include variations of temperature and moisture content of the surrounding medium.

Keratins, which belong to the keratin–myosin group of fibrous proteins (horn, tendons, muscle myosin, blood fibrinogen and fibroin, silk fibroin, etc.), are regarded as dense spatial networks composed of threadlike molecules. All the above-named substances have a common type of structure and differ from each other in amino acid composition [5]. The interactions between regions of the polypeptide chains is so strong that the system as a whole is regarded as a highly concentrated protein gel in the glassy state [6]. The bonds between protein macromolecules are diverse in character, from covalent disulfide bonds in hair and wool keratin to dispersion bonds between nonpolar regions. Salt-type bonds formed from ionic groups in side branches of the polypeptide chains are also of great significance. The presence of different amino acid regions in keratin molecules prevents close packing of the polypeptide chains and leads to loop formation [7] and packing of the flexural (folded) type [8]. The folded chain molecules straighten out when stretched. Straightening of the microperiodic folds [8] leads to changes in the relative positions of the chains and in distances between them. Therefore x-ray diagrams of stretched and unstretched keratin present different diffraction patterns. A distinction is therefore made [7] between the α-form characteristic of unstretched keratin and with small folds, the β-form of stretched keratin and the supercontracted form with deeper folds than in the α-form. The reversible $\alpha \rightleftharpoons \beta$ transition may occur in accordance with conditions and degree of stretching.

At extensions between 20 and 70%, when residual deformation is possible in the material, changes takes place in it owing to conversion of the α- into the β-form; this is reflected in the x-ray patterns.

In the α-form it is postulated that consecutively alternating amino acid residues along the polypeptide chain are packed relatively closely [9]. There is a disulfide bond at roughly every eighth amino acid residue [6]. Stretching of keratin favors weakening and reduction of the number of existing intermolecular bonds [10 11]. The bonds may be gradually re-formed; this is indirectly confirmed by the existence of a hysteresis loop on the stress—deformation curve. The elongation curve ceases to coincide with the contraction curve beyond the point corresponding to ≈ 25% deformation.

Under the influence of hot water, and especially of steam, keratin passes into an irreversible supercontracted state with even greater breakdown of cross links [5,6]. The polypeptide chains assume a more random configuration—the entropy of the system increases.

Solutions of various substances [5, 6, 12] may influence intermolecular bonds in keratin fibers (human hair and wool). This action alters the physical and mechanical properties of the system [6]. In acetate buffer of pH 4.1 salt bonds are broken down; in aqueous solutions of guanidine nitrate, urethane, Sulfanol, Igepon, and mixtures of urea and Igepon hydrogen bonds break down. Covalent (disulfide) bonds are unaffected by these treatments, so that the elastic properties of keratin fibers are improved but the work of extension becomes less. Rupture of disulfide bonds under the influence of sodium hydrosulfite results in simultaneous lowering of the work of extension and elasticity. As the intermolecular interaction is diminished the entropy factor in the fiber stress at a given extension increases [6]. Heat treatment at 60° does not break down covalent bonds but changes the mechanical properties of hair keratin [11].

The observed lowering of elastic properties and appearance of high elasticity on sorption of molecules of polar substances, leading to breakdown of intermolecular bonds and increased flexibility of the chain segments in the protein macromolecule, may be compared to the plasticization effect of other high polymers [13-16]. In the present instance the plasticizing agents for keratin are the above-named solutions [6] while under ordinary conditions water is the plasticizer. If disulfide bonds are broken and —SH groups are formed in treatment with sodium hydrosulfite, the chains become more flexible and can move more freely relatively to each other. The plastic component of deformation therefore increases.

Two opposing processes take place simultaneously on heating in the investigated protein system as in other polymeric systems containing water as the plasticizing component: one process leads to weakening and the other to strengthening of intermolecular action. When the temperature increases the bonds between water and the sorbent (protein) break down, so that water is removed from the system. The resultant deplasticization of the material leads to increased interaction between the segments of the chain molecules and to changes of the distances between them. Removal of water under isothermal conditions and during heating to a definite temperature increases the rigidity of the material. At the same time, however, all forms of interaction should become gradually weaker with rise of temperature.

If decrease of water content (deplasticization) under isothermal conditions results in increased brittleness of the material then rupture occurs at lower stresses; this appears anomalous at first sight but is really quite natural as the nature of the breakdown changes.

Experimental. Dilatometric determinations were carried out by the method described earlier [2] on keratin in the form of horse hair with average cross-sectional area $S = 3.73 \cdot 10^{-4}$ cm, and goose feather quills of $S = 2.14 \cdot 10^{-2}$ cm^2. The keratin samples were washed several times with benzene, extracted in alcohol and ether, and dried at room temperature to constant weight. The principal determinations of length with changes of temperature were performed at 1° stages at intervals of 3-5 minutes.

Numerous data were obtained on changes in the linear dimensions of the specimens during heating and cooling over various temperature ranges. The experiments were conducted in additionally humidified air (with the relative humidity tending to 100%) and in air without additional humidification. Humidification was effected by the presence of liquid water in the chamber of the measuring apparatus [2]. In addition, the load (P) applied to the specimens to maintain them in the straightened state in the dynamometer used for the dilatometric determinations [2] was varied from 350 to 0.5 g/mm^2. Some specimens were subjected to preliminary 5% stretching. It is not possible to give all the data obtained in this communication.

In view of the fact that the general behavior of keratins has much in common with the behavior of other fibrous proteins and synthetic polyamides, investigations of which were reported earlier [1, 3], we shall describe only the most characteristic effects recorded for two types of keratin formations, and give, in illustration, only one length–temperature curve.

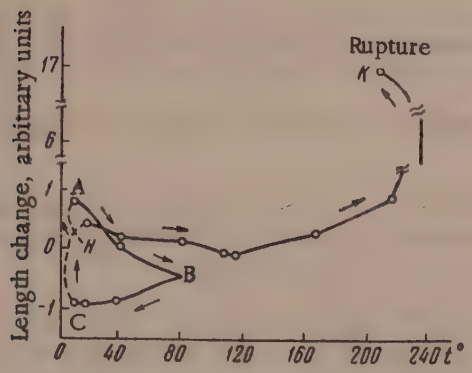


Fig. 1. Length–temperature curve for a specimen of horsehair keratin.

Figure 1 shows one of the dilatometric plots found for horsehair keratin, in the form of two temperature cycles: the first, 20°→7°→80°→7°→14° and the second, 14°→235°→207°. The total duration of the measurements was 7 days. The load P in the tests was 316 g/mm^2. In the first cycle the specimen contracted by 0.79% when heated from 11 (A) to 80° (B), and by 1.12% between 11 (a) and 11° (C). The specimen was kept for 1.5 hours at 80° (B). The length of the specimen under isothermal conditions was almost constant (the maximum change in time was only 0.006%). During the second test cycle, after heat treatment, the contraction was less; it was 0.10% from 20 to 80°, and 0.31% from 20 to 106°. Similar effects were described earler for other polymeric compounds [1-4]. The total elongation of the specimen from the start (H) to the end (K) of the tests was about 29%.

The results of additional determinations performed at intervals at constant temperature or with the temperature changing much more slowly are represented by a dash line in Fig. 1.

The dilatometric curves are complex in character. This follows both from Fig. 1 and from other similar plots determined under experimental conditions ensuring transfer of moisture between the specimens and the surrounding medium.

Over some portions of the dilatometric curves it was possible, in certain limits, to observe a simple linear relationship from which the coefficient of linear thermal expansion α (cm/cm·deg) could be estimated. The most reliable values are found at temperatures above 100°, when the influence of moisture is apparently insignificant. For example, in the case of hair keratin at P = 316 g/mm^2, in the temperature range between ~100 and ~170°, the average value is $\alpha = 0.5 \cdot 10^{-4}$, and for quill keratin $\alpha_{183-38^\circ} = 1.25 \cdot 10^{-4}$ when P = 2.3 g/mm^2 and $\alpha_{210-40} = 0.75 \cdot 10^{-4}$ at P = 0.7 g/mm^2. Between 0 and 100° the variations of linear dimensions with temperature are more complicated, mainly owing to changes of moisture content. Loss of moisture leads to contraction, and sorption of moisture to extension. The higher the moisture content of the surrounding medium the smaller the absolute contraction. However, comparison with the other polymeric materials studied earlier indicates that the degree of orientation may also alter, which also influences the specimen length.

Comparison of the heating and cooling curves shows that in many cases elongation and contraction under the conditions described are subject to pronounced hysteresis effects.

As in the cases described earlier [1-4], the hysteresis loops may be either of the positive type (with the length greater during cooling than during heating) or of the negative type, in accordance with the previous history of the specimens. The latter type is generally attributed to contraction due either to loss of orientation or to loss of moisture. The size and sign of the hysteresis loop also depend on the maximum heating temperature and the load applied during the tests.

All these observations indicate that the linear dimensions of hair keratin and (to a somewhat lesser degree) quill keratin specimens depend not only on the existing conditions but also on the previous history of the specimens, i.e., the preceding states and the kinetics of transition into the new state.

This is one piece of evidence in support of the general principle that polymer systems are capable of prolonged existence in nonequilibrium states of different degrees of stability [2]. Several temperature transition points may be determined by analysis of numerous length–temperature plots found by means of linear dilatometry. Some of these transition points are relatively constant and reproducible despite variations of the experimental conditions, and are characteristic for each of the investigated materials [1-4].

Four transition points are found for keratin: 1) in the ~30-40° region, 2) in the ~100° region, 3) in the ~180-190° region, and 4) in the region between ~210 and 245°.

The transition in the ~30-40° region apparently reflects changes in the form of bonding between the molecules of fibrous protein and water molecules. Considerable increases of length and moisture content during cooling down from ~40° are especially characteristic.

We observed similar effects in studies of other hydrophilic materials [1, 3], and attributed them to hydrogen bonding in the interaction of water with the macromolecules.

The transition point in the region of 100° is probably also associated with a sharp change in the state of water in the material.

The points above 100° are interesting because they characterize the practically dry material and can be used for comparing keratin with such materials as synthetic polyamides, similarities with which may be regarded as being due to the presence of common features in the structures of the respective compounds.

Experiments showed that the positions of the transition points at ~180-190° and ~210-245° depend on the tensile stress applied to the specimen. We therefore compared results obtained under different loads in order to find the true values of the transition points in absence of tensile stresses.

Figure 2 shows the effect of applied load on the transition temperature corresponding to the start of normal elongation after contraction effects. In addition to the points found by analysis of the dilatometric curves, the graph contains points determined by visual observations in a special apparatus. A point for natural silk fiber is given in Fig. 2 for comparison. The transition temperature of 190° for specimens at zero load corresponds, in our opinion, to transition of dry keratin from the glassy into the high-elastic state.

The results of experiments in which the temperature of failure (break) of horsehair specimens under different loads was determined are plotted in Fig. 3. Extrapolation of this curve to zero load gives a temperature of 245°. We regard this point as the flow temperature, i.e., transition from the high-elastic into the viscofluid state. In accordance with the accepted views on keratin structure as outlined above, transition into the viscofluid state is accompanied by rupture of covalent bonds present in the structure, i.e., by irreversible thermal degradation.

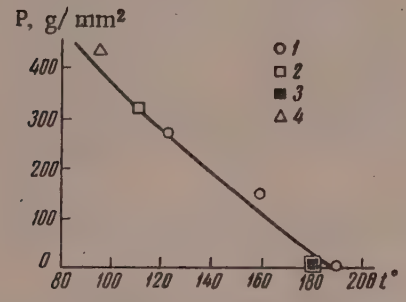


Fig. 2. Effect of load on the transition point of keratins corresponding to the start of elongation after contraction: 1) Horse hair, visual observations; 2) same, dynamometric measurements; 3) feather quill, dynamometric measurements; 4) silk fibroin, dynamometric measurements.

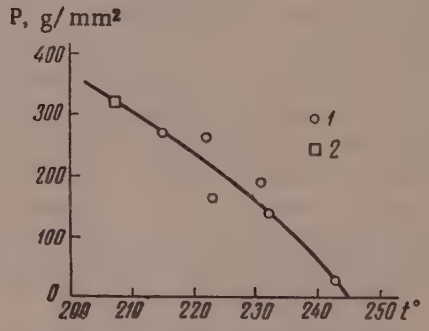


Fig. 3. Effect of load on the failure temperature of horsehair keratin: 1) Visual observations; 2) dynamometric measurements.

The foregoing experimental results show that the conditions of thermal and mechanical treatments to which silk, keratin, and collagen articles are subjected in order to give them the shape and dimensions appropriate for their end uses, may be determined from the results of dilatometric measurements. Problems of this type arise in technological processes in industries where these substances are used as raw materials.

SUMMARY

1. The behavior of keratins with changes of temperature may be investigated by the dilatometric method. This can be used to determine the coefficients of linear expansion, transition temperatures, shrinkage, and hysteresis effects.

2. The states of aggregation of keratins, as of other fibrous proteins and synthetic polyamides, are determined to a considerable extent by the amount of moisture taken up by the material and by its entire previous history, i.e., the preceding states and the kinetics of their changes.

I thank Prof. S. I. Sokolov for his participation in discussion of these results.

LITERATURE CITED

1. R. I. Fel'dman, Kolloid. Zhur. 21, 499 (1959).*
2. R. I. Fel'dman, Kolloid. Zhur. 20, 220 (1958).*
3. R. I. Fel'dman, Kolloid. Zhur. 21, 238 (1959).*
4. R. I. Fel'dman and S. I. Sokolov, Kolloid. Zhur. 20, 388 (1958);* Abstracts of Papers at the 9th Conference on General Questions of Polymer Chemistry and Physics [in Russian] (Izd. Akad. Nauk SSSR, 1952) p. 97; Chemistry and Physical Chemistry of High Polymers [in Russian] (Izd. Akad. Nauk SSSR,1952) p. 159.
5. F. Haurowitz, Chemistry and Biology of Proteins [Russian translation] (IL, Moscow, 1953).
6. A. G. Pasynskii and V. P. Blokhina, Chemistry and Physical Chemistry of High Polymers [in Russian] (Izd. Akad. Nauk 1952) p. 291.
7. W. T. Astbury, Advances in Enzymol. 3, 63, (1943); F. Billmeyer, Introduction to Polymer Chemistry and Technology [Russian translation] (IL, Moscow, 1958) p. 70; S. Mizushima, Structure of Molecules and Internal Rotation [Russian translation] (IL, Moscow, 1957) p. 161; R. D. B. Fraser and T. P. Macrae, Biochem. et biophys. acta 29, 2, 229 (1958).
8. S. I. Sokolov and R. I. Fel'dman, Kolloid. Zhur. 21, 630 (1959).*
9. H. Bull and M. Gutmann, J. Amer. Chem. Soc. 66, 8, 1253 (1944).
10. Corey, Chem. Rev. 26, 227 (1940).
11. H. Bull, J. Amer. Chem. Soc. 67, 533 (1945).
12. A. R. Haly and M. Feughelman, Text. Res. J. 27, 919 (1957); A. R. Haly and J. Griffith, Text. Res. J. 28, 1, 32 (1958); M. Feughelman, A. R. Haly and T. W. Mitchell, Text. Res. J. 28, 8, 655 (1958).
13. R. I. Fel'dman, Doklady Akad. Nauk SSSR 97, 1033 (1954).*
14. S. I. Sokolov, S. A. Reitlinger, and R. I. Fel'dman, Kolloid. Zhur. 19, 624 (1957).*
15. R. I. Fel'dman and A. K. Mironova, Kolloid. Zhur. 17, 465 (1955).*
16. R. I. Fel'dman, S. I. Sokolov, and A. K. Mironova, Kolloid. Zhur. 20, 106 (1958).*

* Original Russian pagination. See C. B. translation.

A STUDY OF THE RELATIONSHIP BETWEEN ELECTRICAL CONDUCTIVITY AND POROSITY OF SOILS

D. A. Fridrikhsberg, Yu. S. Bol'shakova, and T. S. Lipshits

A. A. Zhdanov Leningrad University

Translated from Kolloidnyi Zhurnal, Vol. 22, No. 3, pp. 357-364
May-June, 1960
Original article submitted January 9, 1958

In civil engineering practice, in construction of natural foundations and earthworks, it is important to have reliable data on the density of soils with undisturbed structure. A knowledge of density and its changes during spontaneous or enforced consolidation is necessary for solution of a number of problems of soil mechanics.

For evaluation of soil density a method has been developed based on the linear relationship which has been observed in many instances between the voids ratio ϵ of a soil (ratio of pore volume to volume of the solid phase) and its conductivity κ_d.

If a $\kappa_d = f(\epsilon)$ calibration curve for a given material is available, variations of soil density with time can be evaluated by means of periodic conductivity determinations with the aid of instruments embedded in the soil.

There was found a direct proportionality between κ and ϵ for many soils, but in some instances there were deviations, such that conductivity increased or remained constant with increase of density. Since such observations referred to highly disperse soils of low salt content, it was likely that these anomalies are associated with the "capillary superconduction" effect [1, 2]. Clearly it is necessary to study the causes of these anomalies and the conditions under which they appear for application of the electrometric method.

The purpose of the present investigation was to study the dependence of conductivity on soil porosity for different concentrations of soil solution of definite composition. The experimental curves were also analyzed with the aid of the theory of surface conduction in order to determine whether it is possible to calculate $\kappa_d = f(\epsilon)$ relationships under conditions of different soil salinity.

The conductivity of a capillary system, such as a soil, can be characterized by the quantities κ_v, κ_s, κ_d, K, α and β [2]. The conductivity of solution in the pores (κ) is the sum of the conductivity of the free equilibrium solution (κ_v) and the surface conductivity due to motion of ions in the double layer, $\kappa = \kappa_v + \kappa_s$.

The surface conductivity can be referred to unit interfacial area. The specific surface conductivity (K) is then defined as

$$KS = \varkappa_s W, \tag{1}$$

where S is the total surface area per unit soil volume; W is its total pore volume or volume porosity.

The efficiency ratio α is the ratio of the conductivity of the solution in the pores to the conductivity of the free solution

$$\alpha = \frac{\varkappa_v + \varkappa_s}{\varkappa_v}. \tag{2}$$

The structural resistance coefficient β shows the ratio in which the resistance increases (the "open section" decreases) in the capillary system because of the nonconducting framework

$$\beta = R_d^0/R_v^0, \tag{3}$$

where R_d^0 is the resistance of the capillary system (soil) in the apparatus; R_d^0 is the resistance of free solution in the same apparatus. The sign (0) refers to a solution of high concentration such that $\kappa_V \gg \kappa_S$, so that the surface conductivity may be disregarded ($\alpha \to 1$).

The conductivity of the capillary system as a whole, i.e., of the water-saturated soil, is clearly less by a factor of β than the conductivity of the pore liquid itself, $\kappa_d = \kappa/\beta$, and therefore

$$\varkappa_d/\varkappa_v = \alpha/\beta. \tag{4}$$

When $\alpha > \beta$ the "capillary superconductivity" effect is observed; in this effect the resistance of the diaphragm is less than the resistance of an equal layer of solution in equilibrium with it, since the conductivity which decreases by a factor of β because of the framework, increases by a factor of α because of surface conduction. Therefore, introduction of solid phase into the solution under the condition $\alpha > \beta$ lowers the resistance and may account for the anomalous course of the curves (decreases of κ_d with increasing consolidation) in dilute solutions, since the coefficient α increases on dilution (because of the decrease of κ_V).

Therefore, in order to investigate the relationship between κ_d and consolidation, it is necessary to establish the relationships between α and β and soil porosity. The relationship between α and porosity is easily found from Equations (1) and (3):

$$\alpha = 1 + \varkappa_s/\varkappa_v = 1 + KS/\varkappa_v(1 - p), \tag{5}$$

where p is the volume fraction of the solid phase

$$1 - p = W. \tag{6}$$

Taking the specific surface S_0 (cm^2/g), we can write:

$$S = S_0 dp, \tag{7}$$

where d is the density.

Consequently

$$\alpha = 1 + KS_0 pd/\varkappa_v(1 - p). \tag{8}$$

Since S_0, K, and d do not change in the course of consolidation, it is evident that β should increase with increasing compaction of the soil.

Several equations have been proposed for the relationship between β and porosity; some of these are given in [3-6] and in publications by other authors. The papers [7] give a calculation of the electrical parameters for spherical conducting particles in a dielectric, and the various equations are reviewed and compared in [8, 9]. The Fricke equation [5] is applicable to anisometric particles; this equation assumes the following form for nonconducting solid ellipsoids in a conducting liquid medium in absence of surface conduction ($\kappa = \kappa_V$):

$$\left(\frac{\varkappa_d}{\varkappa_v}\right)_{\varkappa=\varkappa_v} = \frac{1}{\beta} = \frac{1-p}{1+\varphi p}, \tag{9}$$

where φ is the "shape factor," equal to 0.5 for spherical particles and increasing with increasing dissymmetry. It follows from Equation (9) that β also increases with compaction. From ρ we can easily pass to the voids ratio (ϵ)

$$\varepsilon = W/p = (1 - p)/p,$$

and therefore

$$p = \frac{1}{\varepsilon + 1} \tag{10}$$

Substituting into (4) the values of α, β, and $\underline{p}$ from Equations (8), (9), and (10), we have:

$$\varkappa_d = \frac{\varkappa_v \varepsilon + KS_0 d}{\varepsilon + 1 + \varphi} \tag{11}$$

In Equation (11) the slope of the $\kappa = f(\epsilon)$ curves is given by the derivative of κ_d with respect to ϵ. The values of $\kappa_d - \epsilon$ and $\underline{d}$ are independent of ϵ, and therefore

$$\left(\frac{\partial \varkappa_d}{\partial \varepsilon}\right)_c = \frac{\varkappa_v (1 + \varphi) - KS_0 d}{(\varepsilon + 1 + \varphi)^2}. \tag{12}$$

Since the denominator is essentially positive, the sign of the derivative is determined by the difference of the two terms in the numerator. The first of these is proportional to the concentration of the solution, and the second to the specific surface. It follows that the slope of the curve must be increasingly anomalous $\left(\frac{\partial \varkappa_d}{\partial \varepsilon} < 0\right)$, with decrease of salinity and increased dispersity of the soil.

It is interesting to note that the numerator does not contain ϵ, and therefore the slope of the $\kappa_d - \epsilon$ curve does not change sign anywhere. The absolute magnitude of the slope must decrease with increase of ϵ, tending to zero when $\epsilon \to \infty$. In the region studied ($0.3 < \epsilon < 0.6$), which is the one of practical interest, ϵ is condiserably less than $1 + \varphi$, and therefore $\partial \kappa_d / \partial \epsilon = 0$ alters only slightly; the $\kappa_d - \epsilon$ curves should be nearly linear.

The lines become horizontal, i.e., κ_d is independent of ϵ when $\partial \kappa_d / \partial \epsilon = 0$. Putting this values of the derivative into Equation (12), we have

$$\varkappa_v = KS_0 d/(1 + \varphi) \tag{13}$$

To test and apply these expressions it was necessary to carry out an experimental investigation of the $\kappa_d - \epsilon$ relationship and to determine the values of S_0, K, φ and κ_d. This was the purpose of the present investigation.

The apparatus consists of two metal compartments separated by a rigid grid, and a perforated piston lid. The compartments are lined with an insulating layer of vinyl resin, which is also the material used for the grid and lid. The upper and lower compartments and the separating grid are bolted together. Two stainless steel electrodes of 2 × 1 cm in size are mounted in the insulating layer of the upper compartment diametrically opposite each other.

To carry out the experiment, the water-saturated soil in the form of a homogeneous thick fluid mass was put into the upper compartment on the grid which was previously covered with a layer of filter paper. The soil was covered with the piston lid, also fitted with a filter layer, and the resistance of the soil in the initial state was measured. Pressure was applied to the soil by means of a lever press. The soil was consolidated under pressure. The water pressed out collected in the lower compartment and the resultant displacement was recorded by means of a micrometer head to within 5 μ. The pressure on the soil was gradually increased to give a series of displacements and the resistance of the soil corresponding to each compaction stage was measured. The ultimate pressure in the experiments was 10 kg/cm^2.

The voids ratio was calculated from experimental data: the initial and final moisture contents w_0 and w_f (calculated on the absolutely dry soil weight), the final (h_f) and intermediate (h_n) displacements, and the density of the soil (d), by means of the formulas

$$\varepsilon_0 = dw_0;\ \varepsilon_f = dw_f;\ \Delta\varepsilon_f = d(w_0 - w_f);$$

$$\frac{\Delta\varepsilon_n}{\Delta\varepsilon_f} = \frac{h_n}{h_f},\ \varepsilon_n = \varepsilon_0 - \Delta\varepsilon_n.$$

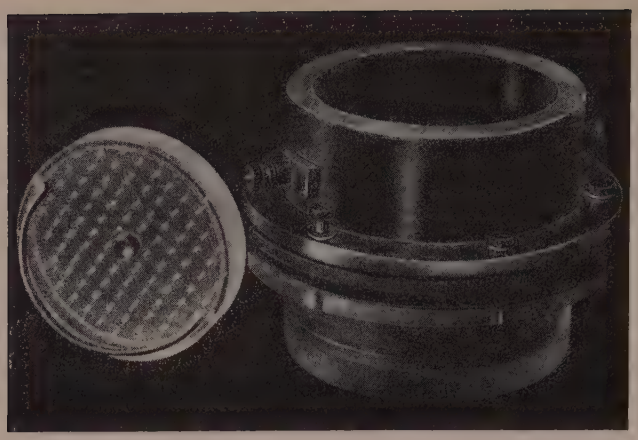


Fig. 1. Apparatus for measurement of conductivity and compaction of soils.

The conductivity of the soil was calculated from the resistance, determined with the aid of a resistance bridge supplied by an alternating-current generator at 800 cps. A low-resistance microphone was used as the null instrument.

The determinations were carried out at 16-19° and reduced to 18° by means of the formula $R_d = R_t [1 + (t - 18)\ 0.02]$.

The resistance constant C_d of the apparatus with the soil was determined in 0.1 N KCl solution. The conductivity of the soil was calculated from the equation $\kappa_d = C_d/R_d$, and the conductivity κ_v of the free solution was determined either in the apparatus without the soil or in an ordinary conductivity cell.

The material used in the investigation, after prelimary experiments, was yellow Ul'ba clay containing an addition of 10% by weight of Oglanly bentonite. The mixture was ground in a mortar and then washed five times with distilled water by decantation (with at least 2-3 days for each settling). The water was then removed by means of a porous cylinder connected to a water-jet pump. The resultant mass was covered with water once more and the water was removed by suction. The material so prepared was free from dissolved salts (this was tested by conductivity determinations on the water). The clay was then saturated with Na^+ by treatment with 0.1 N NaCl for three days, followed by twofold decantation with water and threefold decantation with NaCl solution, with subsequent suction treatment in the cylinder.

Sedimentation analysis of the product by the pipet method gave the following results:

Particle size, μ	<1	1—5	5—10	10—50	>50
Number of particles, %	48,3	14,7	5,5	15	16,5

The density of the clay, determined by the pycnometric method, was 2.79 ±0.01 g/cc. The cell content, determined in standard KCl solution, was 0.54 cm^{-1}. Control experiments showed that displacement of the apparatus lid in compression does not exceed this value. Data on the resistance and porosity in NaCl solutions of different concentrations are given in Table 1.

The dependence of conductivity of clay (κ_d) on the volume fraction of the solid phase (p) for all the investigated concentrations is shown in Figure 2; here, for convenient comparison, the conductivity is expressed as the ratio of κ_d to the conductivity κ_v of the free solution.*

Figure 2 shows the characteristic fan-shaped group of curves with an "anomalous" course at concentrations < 0,01 N NaCl. Vertical sections corresponding to different values of p were taken in order to calculate the main characteristics of surface conductivity. Each such section is essentially analogous to one diaphragm in different

* The slope of $\kappa_d/\kappa_v = f(p)$ curves is opposite to that of the $\kappa_d = f(\epsilon)$ curves, since $p = 1/(\epsilon+1)$, while κ_v is constant for the entire curve.

solutions. By studying the dependence of α and κ_s on concentration at constant p in this way we can compare the results with the predictions of the surface conductivity theory and with the relationships found for rigid diaphragms.

TABLE 1

Conductivity and Porosity of Soil Saturated With Soil Water and With NaCl Solutions

Pressure kg/cm²	Disp., mm	R_d, ohms	$\varkappa_d \cdot 10^3$ ohm⁻¹·cm⁻¹	ε	p	$\varkappa_d/\varkappa_v$
Water: $\varkappa_v = 2{,}4 \cdot 10^{-4}$; $w_0 = 52{,}8\%$; $w_f = 21{,}6\%$						
0	0	610	0,89	1,470	0,404	3,68
1	2,65	570	0,95	1,246	0,445	3,96
3	4,57	485	1,10	1,084	0,481	4,59
7,5	6,24	422	1,28	0,943	0,515	5,33
10	8,11	384	1,40	0,785	0,561	5,84
0,001 *N* NaCl: $\varkappa_v = 3{,}07 \cdot 10^{-4}$; $w_0 = 68{,}2\%$; $w_f = 30{,}8\%$						
0	0	745	0,725	1,902	0,344	2,36
1	5,18	649	0,834	1,447	0,409	2,72
3	8,58	600	0,900	1,134	0,469	2,92
7	10,36	560	0,965	0,974	0,506	3,14
9	11,65	550	0,981	0,859	0,539	3,20
0,003 *N* NaCl: $\varkappa_v = 5{,}6 \cdot 10^{-4}$; $w_0 = 81{,}5\%$; $w_f = 66{,}3\%$						
0	0	755	0,715	2,27	0,306	1,28
1	2,53	718	0,752	2,12	0,320	1,34
3	4,04	710	0,760	2,03	0,330	1,36
7	6,09	677	0,790	1,90	0,345	1,41
9	7,02	675	0,800	1,85	0,350	1,43
0,005 *N* NaCl: $\varkappa_v = 7{,}6 \cdot 10^{-4}$; $w_0 = 55{,}3\%$; $w_f = 33{,}3\%$						
0	0	566	0,950	1,545	0,393	1,26
1	4,00	560	0,964	1,323	0,431	1,27
3	8,04	560	0,964	1,100	0,476	1,27
7	11,19	555	0,975	0,930	0,517	1,28
0,01 *N* NaCl: $\varkappa_v = 1{,}41 \cdot 10^{-3}$; $w_0 = 59{,}7\%$; $w_f = 35{,}2\%$						
0	0	460	1,17	1,665	0,374	0,830
1	0,85	460	1,17	1,541	0,393	0,830
2	1,67	458	1,18	1,421	0,413	0,835
4	2,81	455	1,19	1,254	0,444	0,845
10	4,67	450	1,20	0,981	0,504	0,853
0,05 *N* NaCl: $\varkappa_v = 4{,}43 \cdot 10^{-3}$; $w_0 = 90{,}8\%$; $w_f = 43{,}7\%$						
0	0	195	2,78	2,540	0,280	0,629
1	4,90	213	2,54	2,061	0,327	0,574
3	9,82	236	2,29	1,580	0,388	0,517
7	11,92	238	2,27	1,377	0,421	0,512
10	13,51	242	2,23	1,220	0,450	0,503
1 *N* NaCl: $\varkappa_v = 38 \cdot 10^{-3}$; $w_0 = 67{,}8\%$; $w_f = 42{,}4\%$						
0	0	30,6	17,6	1,890	0,346	0,464
1	3,41	33,0	16,4	1,568	0,389	0,432
4	4,52	40,0	13,5	1,464	0,406	0,355
8,5	7,53	44,0	12,3	1,180	0,460	0,324

The values of α, β, and κ_s calculated from Equations (4) and (2) for three constant values of p (0.3, 0.4, and 0.5) are given in Table 2.

It follows from Table 2 that surface conductance increases with decreasing porosity, and is almost constant for each given pososity, remaining unchanged with variations of solution concentration. These results are in good agreement with data for ceramic and collodion diaphragms. It is evident that the specific surface conductivity K as defined in Equation (1) also remains unchanged with solution concentration.

An expression connecting K and porosity may be derived from Equations (1), (6), and (7):

$$KS_0 = \frac{\varkappa_s (1 - p)}{pd}. \qquad (14)$$

Equation (14) contains the unknown but constant value of the specific surface S_0. Values of KS_0 calculated for different porosities from Equation (14) are given below:

P	0,50	0,45	0,40	0,35	0,30
$\kappa_s \cdot 10^3$ mean	2,8	2,3	1,8	1,4	1,0
$KS_0 \cdot 10^{-3}$	1,0	1,0	1,0	0,9	0,8

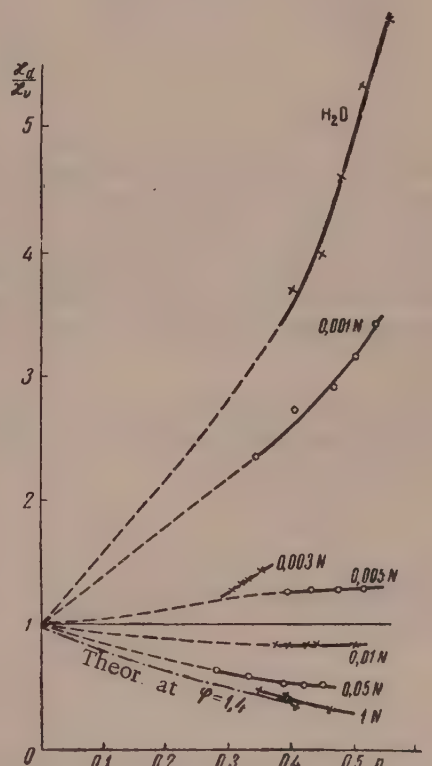


Fig. 2. Relationship between relative conductivity (κ_d/κ_v) and volume fraction of solid phase (p) of soil saturated with water and with NaCl solutions of different concentrations.

These data show that K is in fact independent of porosity, as was to be expected on theoretical grounds; in other words, the variations of κ_s and α with porosity which were found are fully consistent with theory.

The specific surface conductivity K therefore remains constant when the electrolyte concentration and the degree of compaction of the soil are varied.

If we assume tentatively that $K = 1 \cdot 10^{-9}$ ohm^{-1}, we find the order of magnitude to the specific surface $S_0 \approx 1 \cdot 10^6$ cm^2/g, or ≈ 100 m^2/g. This agrees with literature data on the specific surface of plastic clays.

We now consider variations of the structural coefficient β with porosity. The applicability of the theoretical. Equation (9) to polydisperse soils with particles of irregular shape requires experimental verification. Variations of β with p are given by the curve for 1 N NaCl in Fig. 2, where $\alpha \approx 1$ and $\kappa_d/\kappa_v = 1/\beta$. The course of the experimental curve corresponds to Equation (9). Solution of the system of equations by substitution of different pairs of values of β_i and p_i gives the average value $\alpha = 1.4$.* With this value the calculated curve for $\kappa_d/\kappa_v = 1/\beta = (1-p)(+1.4\,p)$ is in good agreement with the experimental data (Fig. 2).

TABLE 2

Values of Conductivity and Coefficients α and β at Constant Volume Fractions of Solid Phase in the Soil

C, equiv/liter	$\varkappa_v \cdot 10^4$	$p = 0{,}5$; $\beta = 3{,}6$			$p = 0{,}4$; $\beta = 2{,}6$			$p = 0{,}3$; $\beta = 2{,}0$		
		$\varkappa_d/\varkappa_v$	α	$\varkappa_s \cdot 10^4$	$\varkappa_d/\varkappa_v$	α	$\varkappa_s \cdot 10^4$	$\varkappa_d/\varkappa_v$	α	$\varkappa_s \cdot 10^4$
1,000	380	0,28	1,0	—	0,38	1,0	—	0,50	1,00	—
0,050	44,3	0,44	1,6	26,6	0,50	1,3	17,3	0,61	1,22	9,8
0,010	14,1	0,86	3,1	29,6	0,84	2,2	17,0	0,83	1,66	9,3
0,005	7,6	1,30	4,7	28,1	1,24	3,2	16,7	1,20	2,40	10,6
0,003	5,6	1,70	6,1	28,6	1,50	3,9	16,2	1,30	2,60	9,0
0,001	3,1	3,0	11,1	31,3	2,66	6,9	18,2	2,24	4,48	10,8
(H_2O)	2,4	(5,00)	(18,0)	(40,8)	3,65	9,5	20,4	—	—	—

To verify the applicability of these results in practice it is necessary to determine how far these concepts can be used in concrete instances for predicting the slope and the entire course of the $\kappa = f(\epsilon)$ curves, both for the given soil solution and for soils with other salt contents. It is clear that if tabulated data on K, α, and S_0 were available for different soils such calculations could be carried out from Equation (11) without the need for experimental determinations. At present it is necessary to carry out at least one determination of the resistance of the soil in its natural state in order to find the constant term KS_0d, which characterizes the solid phase of a given soil.

As an example, we give a specimen calculation for our system in 0.005 N NaCl (close to natural salinity). From the initial data (before compression), namely: $\epsilon = 1.55$; $\kappa_d = 0.954 \cdot 10^{-3}$; $\kappa_v = 0.76 \cdot 10^{-3}$; $d = 2.8$; $\varphi = 1.4$, we find from Equation (12)

$$KS_0d = 2{,}6 \cdot 10^{-3}.$$

Substituting rhis value into Equation (13) we find that the boundary of the "anomalous" (horizontal) course for this soil

$$\varkappa_v = 2{,}6 \cdot 10^{-4} : 2{,}4 = 1{,}1 \cdot 10^{-3} \quad \text{ohm}^{-1} \cdot \text{cm}^{-1}$$

corresponds approximately to 0.01 N NaCl, which is in good agreement with the data in Fig. 2.**

* It follows that for laminar particles of clay minerals the experimental values of $\varphi > 1$.

** Analogous horizontal linear plots were found [10] for petroleum emulsions.

Putting the value found for KS_0d into Equation (13) we have a formula for calculating soil conductivity

$$\varkappa_d = \frac{\varkappa_v \varepsilon + 2{,}6 \cdot 10^{-3}}{\varepsilon + 2{,}4}. \qquad (15)$$

The values of $\varkappa_d$ calculated from Equation (15) for different values of ε and $\varkappa_v$ (Table 2) are compared in Fig. 3 (straight lines) with the experimental points. Comparison shows that calculations by Equation (15) in general give good agreement with experimental data. Therefore, it is possible to calculate, from one determination of the resistance of the original sample, all the compression curves for different salinities over a thousandfold range of NaCl concentration variations (provided that the soil solution is almost free of other salts)

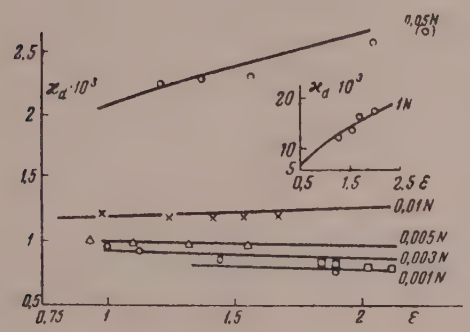


Fig. 3. Comparison of calculated experimental values of soil conductivity in relation to the porosity coefficient at different NaCl concentrations.

SUMMARY

1. When a water-saturated soil with low salinity of the soil solution is subjected to compaction the resistance decreases instead of increasing, as is generally the case. The observed effect is explained in the light of the main principles of the theory of surface conduction.

2. Equations were derived for approximate estimation of the conductivity of a soil in relation to its degree of compaction and concentration of the soil solution, both for normal and for "anomalous" cases.

LITERATURE CITED

1. I. I. Zhukov and D. A. Fridrikhsberg, Kolloid. Zhur. 11, 163 (1949).
2. O. N. Grigorov, Z. P. Koz'mina, A. V. Markovich, and D. A. Fridrikhsberg, Collection: Electrokinetic Properties of Capillary Systems [in Russian] (Izd. Akad. Nauk SSSR, 1956).
3. J. C. Maxwell, A Treatise on Electricity and Magnetism. 1, 440 (1904).
4. J. Runge, Z. techn. Phys. 6, 61 (1925).
5. H. Fricke, Phys. Rev. 24, 575 (1924); J. Appl. Phys. 24, 644 (1953).
6. H. Fricke and H. J. Curtis, J. Phys. Chem. 40, 715 (1936).
7. Ya. I. Frenkel', Kolloid. Zhur. 10, 148 (1948); Ya. I. Frenkel' and B. M. Fradkina, Kolloid. Zhur. 10, 241 (1948).
8. V. P. Mashovets, Zhur. Priklad. Khim. 24, 353 (1951).
9. N. Street, Austral. J. Chem. 9, 3, 373 (1956).
10. V. G. Ben'kovskii, Kolloid. Zhur. 14, 10 (1952).•

• Original Russian pagination. See C. B. translation.

INFLUENCE OF THE MEDIUM OF FINE GRINDING OF SOLIDS

G. S. Khodakov and P. A. Rebinder

Division of Disperse Systems, Institute of Physical Chemistry, Academy of Sciences, USSR;
Institute of New Constructional Materials, Academy of Sciences USSR, Moscow
Translated from Kolloidnyi Zhurnal, Vol. 22, No. 3, pp. 365-375
May-June, 1960
Original article submitted February 26, 1960

It is known as the result of a series of investigations [1, 2] that the degree of adsorption lowering of the strength of solids in surface-active media depends not only on the properties of the solid and the nature of its interaction with the medium, but also on its dispersity and the dispersion conditions. However, in studies of the influence of the external medium on comminution processes [3-6] the dependence of the effectiveness of the medium on the dispersity of the solids or on a number of other factors was not taken into account; this led to sharp discrepancies in estimates of the adsorption effect in facilitation of dispersion. The influence of the medium on fine and ultrafine grinding has been studied very little, largely because of the difficulties involved in these processes and of difficulties in dispersion analysis of the resultant systems. Advances in the technology of vibratory grinding [7, 8] and development of adsorption methods for determination of specific surface* [9] have made it possible to study certain characteristerics of very fine dispersions of such substances as graphite [10] and quartz [11].

In the present investigation we studied dispersion of quartz, corundum, calcite, and talc in a laboratory eccentric vibratory mill [8] operated at 50 cps with vibration amplitudes of 3, 4, or 5 mm. The dispersion was effected in dry air and in various liquids and their vapors; these included polar liquids such as acetone and water, and nonpolar liquids such as benzene and paraffin oil.

The principal material used in the investigations was quartz, primarily because of the ever-increasing use of finely ground quartz sand in a number of industries, and especially in the building materials industry.

Studies of the action of various media on dispersion of quartz—a typical brittle solid—are also of considerable scientific interest. Quartz and a number of silicate glasses have the characteristic ability of forming silicic acid gels of various compositions at interfaces with aqueous media; these gels are decisive in the course of surface dispersion (polishing of glasses) [12].

Investigation of the effect of the medium on dispersion of quartz. When quartz** is ground in water its specific surface becomes many times greater than that of quartz ground in dry air under the same conditions (Table 1). The difference in the fineness of powders obtained by dry and wet grinding increases sharply with increase of the grinding time. Grinding of quartz in acetone, benzene, and alcohol does not produce such a large increase of grinding efficiency.

* The specific surface S_1 is a fairly general characteristic of dispersity; it is connected with the equivalent mean particle size δ by the expression $\delta = 6/\rho S_1$, where ρ is the density.

** Pure quartz sand from the Lyubertsy quarry was used in the experiments. The grain size was between 150 and 300 μ; the specific surface did not exceed 0.02 m^2/g.

These experimental results seemed very strange. The heats of wetting of quartz by the liquids listed in Table 1 differ little from each other [13, 14]. Therefore, in accordance with the theory of adsorptional strength lowering, the dispersibility of quartz should have been increased to approximately the same extent in each case [2, 15, 16]. It was also difficult to explain the results of experiments on prolonged dry grinding of quartz and a number of other solids. The specific surfaces of these powders reached maximum values in the course of grinding, and then decreased appreciably during further grinding in a number of instances.

TABLE 1

Variations of the Specific Surface (m^2/g) of Quartz During Grinding with Various Liquids (80% on the Weight of Quartz)

Grinding time, min	Specific surface of quartz, m^2/g				
	in air	in water	in benzene	in acetone	in alcohol
2	3,8	9,8	—	—	—
4	5,2	17,0	2,8	2,0	4,1
8	4,7	27,0	6,6	6,3	7,1
16	6,5	42,0	8,3	13,2	—
32	5,9	73,0	9,3	13,3	—

It was found that the specific surface was increased severalfold by additional grinding with water of quartz powders obtained by prolonged dry grinding, grinding with acetone, benzene, or alcohol, or with small additions of water or other liquids. The time of additional grinding required was so short that any dispersion effected during the process could be disregarded. In every case the sharp increase of specific surface was completed in less than 40 seconds of additional grinding in water; with further increase of the additional grinding time the specific surface increases in accordance with the kinetics of grinding in water. At the same time, prolonged grinding in the dry state, or with small amounts of water, or in acetone or other liquids, of powders obtained by grinding in water and then dried results in appreciable decreases of the specific surface; this indicates that the observed effect is reversible (Table 2).

TABLE 2

Decrease of the Specific Surface of Fine Quartz During Additional Grinding

Medium	Duration of "grinding", min	Specific surface, m^2/g		Medium	Duration of "grinding", min	Specific surface, m^2/g	
		before "grinding"	after "grinding"			before "grinding"	after "grinding"
air	2	39	30	5,0% water	16	58	35
same	4	39	29	8,0% "	16	60	46
» »	8	39	20	20%	16	60	61
» »	12	39	16	air	10	60	20
» »	16	60	18	40% acetone	10	60	22
» »	16	58	28	air	20	74	22
1,2% water	16	58	32	33% acetone	20	74	40
2,5% water	16	58	34				

In the light of the data in Table 2 and of other experimental results [11, 17], the sharp increase of specific surface as the result of brief additional grinding in water may be attributed to formation and subsequent breakdown of dense but relatively weak aggregates of particles, the pores between which are filled with even finer particles [11, 17]. It seems that aggregates with such dense packing that most of their internal surface becomes inaccessible to adsorption of nitrogen molecules, are formed as the result of high-frequency and rather strong mechanical forces at the points of contact with the grinding balls. In most methods of particle-size analysis, other than such methods as the x-ray method, such particle aggregates are recorded as individual particles of correspondingly larger size. Application of the x-ray method in this case is not successful because the primary particles are too small and amorphous.

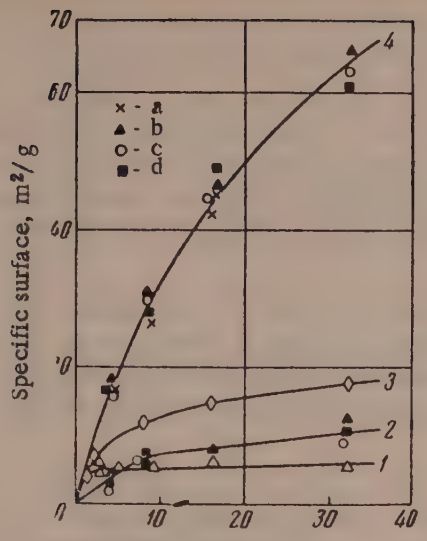


Fig. 1. Grinding of quartz in an eccentric mill at 4 mm vibration amplitude: 1 and 3) Without additions; 2 and 4) with additions of 70-80% of water (a), acetone (b), benzene (c), alcohol (d); 1 and 2) without disaggregation; 3 and 4) with subsequent disaggregation.

The fact that the time of additional grinding in water needed to break down the aggregates is very short indicates that aggregation has no appreciable influence on the dispersion kinetics. As has been pointed out, disaggregation of fine powders is necessary because of the strong distortion of dispersion results so that, in particular, it becomes impossible to assess the influence of different media in grinding. This follows, for example, from a comparison of the data in Table 1 and in Fig. 1 and 2. The kinetic curves for dispersion of quartz in water, acetone, benzene, and alcohol, determined by the usual method, differ very much from each other, but after disaggregation they coincide (Fig. 1), This is fully consistent with the theory of adsorptional strength lowering, according to which the effectiveness of surface-active substances depends only on the decrease of the interfacial tension of solids [2, 15, 16].

Investigations of compact aggregation of solid particles during fine grinding, in conjunction with a simple method for bringing about their disaggregation, made it possible to study fine and ultrafine dispersion of solids and the influence of added liquids in relation to their nature and concentration under different mechanical dispersion conditions. In addition to water, acetone, benzene, and alcohol, the surface-active agents used included triethanolamine, paraffin oil, oleic acid, liquid petrolatum, and others. Since water is one of the most powerful surface-active agents in relation to quartz, as is shown by the heats of wetting of silica and quartz by water [13, 14, 18], the action of added water on the dispersion of quartz was studied most fully.

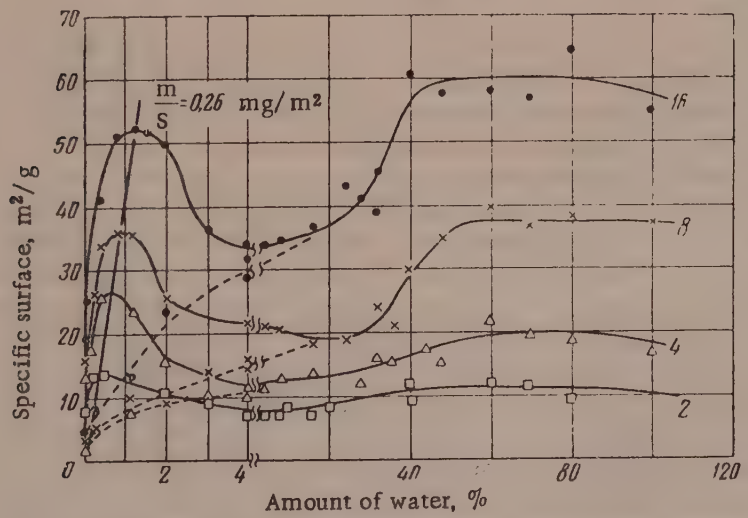


Fig. 2. Effect of added water on the degree of dispersion of quartz. The numbers at the curves represent the duration of grinding in minutes. The dash lines represent grinding without disaggregation.

The data on grinding of quartz sand, presented in Fig. 2, indicate that even very small amounts of water have a very strong influence on the degree of dispersion. For example, with only 0,04% moisture the degree of

dispersion is appreciably greater than in grinding in dry air, and it rises sharply with increase of moisture content to 1%. On further increase of the water content from 2 to 30% the degree of dispersion falls considerably, while with 30-40% it rises sharply again and reaches the optimum level in wet grinding with 50-80% water.

The decrease of the degree of dispersion when the water concentration is increased from 2 to 30% can be explained if we consider the mechanical properties of the moist powder. Observations showed that a finely ground quartz mass containing 2-30% moisture has considerable viscosity and strength, so that some of the powder adheres to the balls and mill walls and the grinding is therefore less effective. It is likely that these mechanical properties of moist powders are due to formation of coagulation structures in a system consisting of quartz particles joined by thin interlayers of water.

The average thickness of the liquid layers between the solid particles, or the surface concentration which can be conveniently expressed in terms of the number of saturated monomolecular layers, can be determined from our experimental values for the specific surface and water contents. The surface concentration of water corresponding to one saturated monomolecular layer is calculated from the area occupied by a water molecule ($11.5 \cdot 10^{-16}$ cm^2) and its weight; the value is 0.26 mg/m^2.

It may be assumed that the lowest grinding efficiency (minima on the curves in Fig. 2) corresponds to the highest strength of the coagulation structure in the moist powder. This minimum efficiency is observed for a medium thickness of the water interlayers between the quartz particles, corresponding to a surface concentration of 5-10 saturated monolayers. Increase of the thickness of water interlayers between the quartz particles weakens the coagulation structure, and this leads to increased grinding efficiency. When the water content corresponds to a surface concentration of 40-100 monolayers (layers ~0.01-0.02 μ thick), the process enters the wet-grinding stage and further increases of moisture content, as the curves in Fig. 2 show, are useless. At the same time these water layers reliably protect the quartz particles against aggregation. These results are in full harmony with the theory of coagulational structure formation, according to which the strength of such structures is determined by van der Waals forces which are effective only over distances corresponding to a few molecular radii.

It follows from the data in Fig. 2 that formation of coagulation structures, breakdown of which consumes a considerable proportion of the mill energy, is a very important factor in studies of the dispersion process with additions of small amounts of surface-active substances to dry powders. Neglect of this factor leads to erroneous conclusions concerning the true magnitude of the adsorption effect in facilitating the grinding of quartz and, as will be shown later, of other solids.

The data in Fig. 2 show that the maximum degree of dispersion in grinding for 2, 4, and 8 minutes is obtained when the average thickness of the water layers is one monolayer. The somewhat lower value of the specific surface at the maximum of the curve for 16 minutes of grinding, as compared with the value with a high moisture content, may be attributed to slowing down of the dispersion during the initial grinding stages, when the surface concentration of water molecules is appreciably in excess of one monolayer and the rate of dispersion diminishes owing to structure formation. Therefore, the most favorable grinding conditions are those in which the amount of liquid corresponds to formation of a monomolecular layer around the solid particles. This is confirmed by the data in Fig. 3, which show variations of the rate of dispersion as a function of the surface concentration expressed in terms of the number of saturated monolayers. The values of the dispersion rate were found by differentiation of curves for dispersion kinetics of powders with specific surfaces of 25 and 35 m^2/g. The left-hand branches of the curves in Fig. 3 apparently represent adsorptional lowering of quartz strength, and the right-hand branches correspond to formation of coagulation structures. The great steepness of the curves in Fig. 3 on each side of the maximum indicates a source of considerable errors in studies of the action of small amounts of water on the degree of dispersion. Slight inaccuracies in the amounts of water added and in dispersity determinations can lead to substantially different results; this must be taken into account in estimations of adsorption effects of fine grinding.

It should be particularly noted that the action of small amounts of surface-active substances becomes quite noticeable even at concentrations considerably less than those corresponding to a single monolayer. An addition of water which corresponds to ~0.1 of a saturated monomolecular layer on a powder with a specific surface of 15 m^2/g increases the rate of subdivision at this degree of dispersion about 2.5-fold in comparison with the rate without additions. Since it is almost impossible to get rid of traces of moisture from solid surfaces, the initial stages of dispersion in practice always take place in presence of adsorbed vapor of water or other active substances. With increase of dispersity the surface concentration of the contaminations diminishes in grinding in airtight cylinders, and the grinding becomes virtually dry.

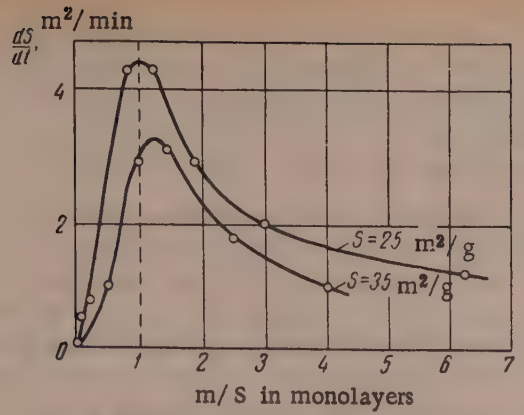


Fig. 3. Effect of the nominal surface concentration of water on the rate of dispersion of quartz.

The effect of small amounts of acetone, ethyl alcohol, and benzene on dispersion of quartz (Table 3) is similar in many respects to the effect of small amounts of water. It also follows from this that the equal effectiveness of dispersion of quartz in acetone, benzene, and alcohol cannot be attributed to contamination of these liquids with water. Otherwise, it should be necessary to assume, for example, the presence of ~30% water in benzene; in reality it was known that the content of impurities in it did not exceed 1%.

The effect of added triethanolamine and aqueous potassium dodecylaminoacetate solution ("amak") on the dispersibility of quartz was almost the same as the effect of small amounts of water, acetone, benzene, or alcohol, additions of oleic acid and paraffin oil (at the optimum concentrations), which have lower heats of wetting of quartz than the above-named liquids, produce an appreciably smaller effect (Fig. 4). Similar results were obtained with additions of petrolatum to the quartz powder. All these experiments confirm the foregoing views concerning the decisive significance of adsorbability of liquids in lowering the strength of solids.

TABLE 3

Effect of Small Amounts of Added Water, Acetone, Ethyl Alcohol, and Benzene on the Dispersibility of Quartz; Grinding Time 16 Minutes, Amplitude 5 mm

Amt. of liquid added, cc	Specific surface of quartz after grinding, m^2/g			
	in water	in acetone	in alcohol	in benzene
dry	19	19	19	19
0,05	25	26	21	29
0,01	41	33	28	29
0,03	52	43	41	41
0,6	—	56	62	59
0,9	—	48	59	41
1,2	35	68	60	49

It follows from the data in Figs 1-5 that the role of added surface-active substances depends very appreciably on the duration of grinding, and becomes more pronounced with increasing dispersity of the quartz. Thus, the rate of dispersion of relatively large particles is little affected by the presence of water if the grinding time is less than 2 minutes. With more prolonged grinding the increase of specific surface almost ceases in dry grinding, whereas in an aqueous medium, the rate of dispersion remains considerable even with powders with specific surfaces of 60-70 m^2/g.

The dependence of increased dispersibility on the dispersity and mechanical parameters of the mill can be conveniently estimated if the effect is measured in terms of $(S_1-S_2)/S_2$, where S_1 is the specific surface in grinding with water and S_2 is the specific surface in dry grinding of the same duration. The data in Fig. 5 show that the influence of added liquids increases approximately linearly with increase of dispersity, and increases with decrease of the mill vibration amplitude from 5 to 3 mm.

At high dispersities, when contamination of the surface by adsorbed moisture in grinding without additions may be disregarded, the effectiveness of dispersion of quartz in certain liquids is 6-8 times as high as in dry grinding with the same expenditure of energy. This great increase in the dispersibility of quartz approaches in magnitude to the effects of strength lowering of single metallic crystals under the influence of liquid metallic coatings [2, 16], and is probably due to analogous causes [19]. The decrease of strength can be estimated [2, 16] from the lowering of specific surface energy, which decreases [18] from 980 erg/cm^2 in vacuum to 416 erg/cm^2 in water in the case of quartz, and from 275 to 130-80 erg/cm^2, respectively, in the case of amorphous silica. This should give an approximately twofold lowering of strength, which may ultimately lead to the observed effects of improved dispersibility.

Fine dispersion of calcite, corundum, talc, and other solids in surface-active media. The decrease in the strength of solids in liquid media is a universal effect which depends on the decrease of their interfacial tension relatively to the value in vacuum. However, it has been shown in the case of graphite [10] and, by ourselves, in the case of quartz that addition of liquids does not always lead to the expected increase of dispersibility. It was noted that this is caused by various effects arising in the course of grinding—formation of coagulation structures,

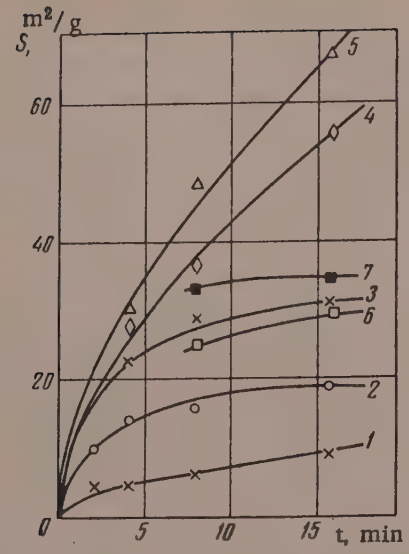


Fig. 4. Dispersion of quartz with various additives: 1) 3% triethanolamine, without disaggregation; 2, 3, 4, 5) respectively, dry, and with 0.2, 0.4, and 1.2% triethanolamine, with subsequent disaggregation; 6 and 7) with oleic acid and paraffin oil (optimum concentrations).

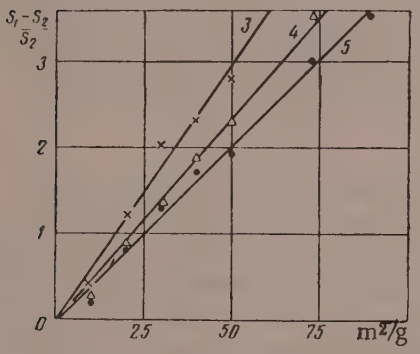


Fig. 5. Effect of degree of dispersion on adsorptional dispersibility increase at different intensities of quartz grinding with vibration amplitudes of 3, 4, and 5 mm.

compact aggregation of particles, and decrease of the coefficient of friction, determined to a considerable extent by the properties of the solids in question. It is of interest in this connection to study the effects of added surface-active substances on the dispersion of solids differing in nature.

It was found in studies of the grinding of calcite ($CaCO_3$), corundum (Al_2O_3), talc ($4MgO \cdot 3SiO_2 \cdot H_2O$) rutile ($TiO_2$), alumina ($AlO_3 \cdot nH_2O$), silicate glass, quartz glass, and cement that many of these substances, like quartz, form compact aggregates during grinding; these are broken down during brief additional grinding with water. If aggregation of fine particles is disregarded, considerable errors are obtained in the results of grinding not only of quartz but also of calcite, corundum, fused quartz, and cement. For example, the specific surface of calcite (the initial specific surface S_0 did not exceed 0.01 m^2 /g) obtained by grinding with additions of oleic acid or triethanolamine but without subsequent disaggregation was considerably less than the specific surface of the same calcite obtained by grinding in water under otherwise the same conditions. Disaggregation produced a sharp increase in the specific surface of calcite ground dry or with additions of triethanolamine or oleic acid. It was found (see Fig. 6) that additions of triethanolamine produce the greatest effect; the effect was less with oleic acid, and less still with water. It is significant that effective grinding and disaggregation of calcite can be performed not only with water, but also with acetone or alcohol. This shows that the aggregates of calcite particles are noticeably weaker than aggregates of quartz particles.

Corundum is one of the hardest and most abrasive materials. It is clear from Fig. 7 that it is impossible in practice to obtain finely divided corundum by grinding in dry air without disaggregation of the powders. For example, in dry grinding of corundum ($S_0 \approx 0.1\ m^2/g$) it is impossible to obtain a powder with a specific surface greater than 6-7 m^2/ g. A specific surface of 50 m^2/ g can be attained by grinding in water. In grinding of corundum as of quartz, the dispersibility greatly depends on the moisture contents of the powders, which is also associated with formation of coagulation structures. Corundum, like quartz, tends to form compact aggregates which are broken down by brief grinding with water.

When fine corundum powder ground in water and then dried are subjected to dry "grinding," the particles become aggregated and the surface accessible to nitrogen adsorption decreases. For example, during 16 minutes of grinding the specific surface of corundum decreased from 33 to 8, from 41 to 13, and from 51 to 19 m^2/g.

Water has considerably less effect on grinding of alumina formed by dehydration of alumina gel. In contrast, to corundum, dry grinding of alumina does not result in an appreciable decrease of specific surface (Fig. 7).

Amorphous solids are also made more easily dispersible by adsorption of surface-active substances. Kinetic curves representing increases of the specific surface during grinding of fused quartz ($S \approx 0.1$-$0.2\ m^2/g$) in the dry state and with water resemble the corresponding curves for crystalline quartz (Fig. 8).

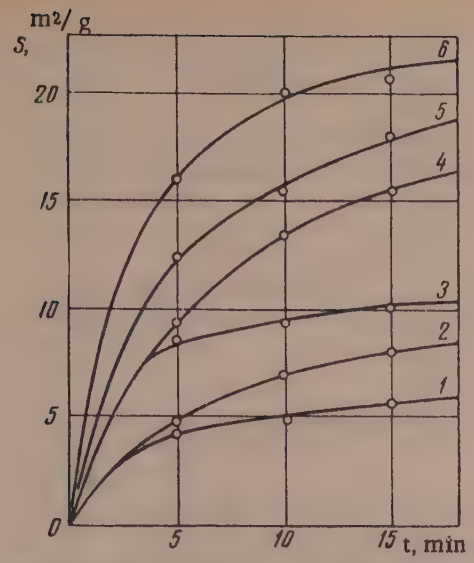


Fig. 6. Effects of additions on the rate of comminution of calcite: 1) Dry, without additions; 2) with 1.2% oleic acid, without disaggregation; 3) dry, with disaggregation; 4) with 80% water; 5 and 6) with 1.2% oleic acid and triethanolamine respectively, with subsequent disaggregation.

In grinding both of fused and of crystalline quartz the rate of dispersion depends on the moisture contents of the powders, and particle aggregation leading to decreased specific surface occurs.

The effects observed when rutile ($S_0 \approx 0.2$ m^2/g) and silicate glass ($S_0 \approx 0.1$ m^2/g) are dispersed in presence of water are relatively small (Fig. 7 and 9); this may be attributed to their chemical activity with respect to water. The aqueous solutions of these substances, formed near the particle surfaces, partially help in closing over surface cracks, similarly to the effect observed in Ioffe's experiments on studies of the strength of rock salt crystals.

The action of the medium has a number of characteristic peculiarities in the dispersion of talc, which has a laminar structure and is lyophobic toward polar liquids. Small additions of water, acetone, and alcohol cause a considerable increase, and somewhat larger additions a decrease in the degree of dispersion of talc (Fig. 9). A similar effect is observed in dispersion of quartz. Calculations show that the maxima of the curves in Fig. 9 correspond to formation of single saturated monomolecular liquid layers, so that the increased dispersion of talc, as of other substances, is associated with formation of the first adsorption layer. However, on further increase of the amount of liquid the dispersion of talc is not increased, in contrast to quartz. This peculiarity in the action of water vapor, acetone, and alcohol on the grinding of talc is probably caused by a decrease of the coefficient of friction in the system composed of the powder and the grinding balls. This, in its turn, is the consequence of mutual slippage of laminar particles separated by fairly thick layers of nonwetting liquid. We did not detect any appreciable decrease of the specific surface of talc powders (aggregation) in either dry or wet grinding.

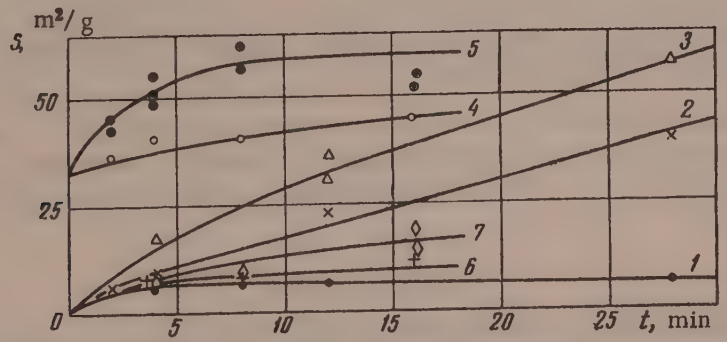


Fig. 7. Grinding of corundum, alumina, and rutile: 1, 2, and 3) Corundum in dry air and with 10-30 and 80% water, respectively; 4 and 5) alumina in dry air with 80% water; 6 and 7) rutile in dry air and with 80% water.

Dry grinding of cement in a vibratory mill causes first an increase and then a considerable decrease of specific surface. Small additions of oleic acid, even without subsequent disaggregation of the cement in water, cause its specific surface to increase throughout the grinding process. Similar results were obtained with additions of naphthenate soap or triethanolamine. Disaggregation of cement particles by additional grinding in water cannot be carried out because of hydration of the clinker minerals.

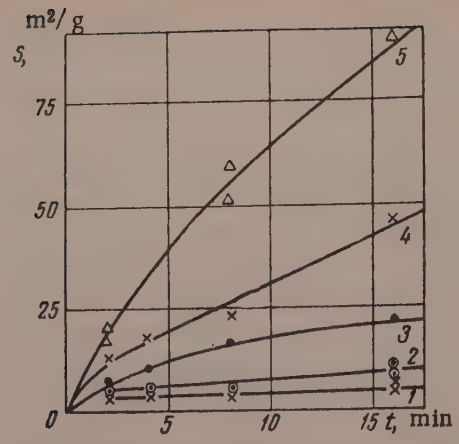


Fig. 8. Grinding of fused quartz and silicate glass: 1 and 2) Silicate glass in dry air and with 80% water; 3, 4, and 5) fused quartz in dry air, and with 20 and 80% water, respectively.

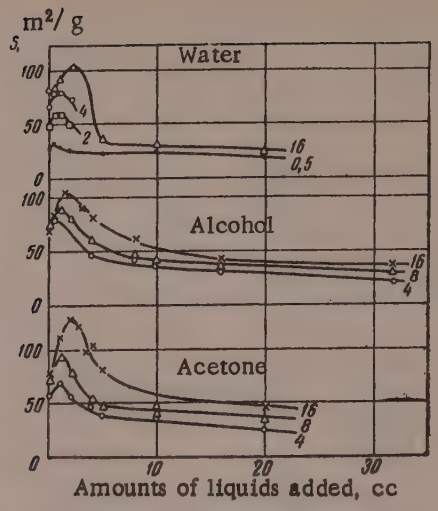


Fig. 9. Effect of concentrations of different liquids on dispersion of talc. The numbers at the curves represent the grinding time in minutes.

Additions of surface-active substances favor increase of the specific surface of cement during grinding; they facilitate dispersion and have a disaggregating and stabilizing effect. This solves the problem, raised in earlier investigations [5, 20], of the role of additives in cement grinding. In each of these investigations only one of these factors was taken into account.

Our experiments show that adsorptional effects of strength lowering of solids do not always come into play during mechanical grinding. In many cases the adsorption effects are masked by aggregation and structure formation effects, which are especially prominent in the case of fine powders. The magnitude of the dispersibility increase in active media depends on the structure and particle size of solids and their interaction with the medium. The results of these investigations account for the discrepancies in estimations of the magnitude of the adsorption effects in facilitating the dispersion of solids, because aggregation of the particles, structure formation during grinding, and the dependence of adsorptional effects on the particle size were not taken into account in any of the investigations, with the exception of [11]. Neither was due attention paid to the role of surface contamination of solids in grinding without additions, although this is especially important for evaluation of the effectiveness of surface-active substances in the coarse particle range.

It is interesting to note that the adsorptional effect in facilitating dispersibility, determined during grinding under comparable conditions, increases with increasing hardness of the solids; for example, in the case of corundum and quartz the effects corresponds to ~600-800%; for fused quartz it is ~500%; for calcite it is ~200% and for talc and alumina, ~150%.

SUMMARY

1. Fine grinding of quartz and certain other solids in vibratory mills is a complex process in which an important part is played by such effects as adsorptional lowering of strength, coagulation structure formation, and peculiar aggregation of the particles which results in a decrease of the surface area accessible to adsorption of nitrogen molecules. Disaggregation of powders after grinding by means of additional brief grinding in water makes it possible to study the influence of the medium on the effectiveness of the dispersion of the primary particles.

2. Dispersion of quartz and other solids is facilitated considerably in presence of vapors of surface-active substances, the effectiveness of which greatly depends on their concentration. The influence of adsorbed vapors becomes quite appreciable when the surface concentration corresponds to about 0.1 of a saturated monolayer and reaches a maximum at concentrations corresponding to one saturated monolayer on the particle surfaces. The decrease of the rate of dispersion of moist powders is due to formation of coagulation structures, the maximum strength of which corresponds to a surface concentration of water equivalent to 5-10 monolayers.

3. In harmony with the theory of adsorptional strength lowering, the adsorption effect in facilitating the dispersion of quartz depends on the degree of lowering of its interfacial tension and is independent of polarity of the liquid.

4. The role of surface-active substances increases considerably with increasing subdivision of solids. The effect of increased dispersibility also depends on the properties of solids; it reaches values of 600-800% for corundum and quartz.

LITERATURE CITED

1. P. A. Rebinder, Paper at the Sixth Congress of Russian Physicists [in Russian] (Moscow, 1928); P. A. Rebinder, L. A. Shreiner, and K. F. Zhigach, Agents of Lowering Hardness in Drilling [in Russian] (Moscow-Leningrad, 1944).
2. E. D. Shchukin and P. A. Rebinder, Kolloid. Zhur. 20, 646(1958).*
3. I. P. Ettinger and I. M. Protod'yakonov, Doklady Akad. Nauk SSSR 84, 1825 (1952); I. Z. Eichborn, Koll.-Z. 149, 128 (1956).
4. A. Götte and E. Ziegler, VDI-Zs 9, 98 (1956).
5. L. I. Édel'man and D. S. Sominskii, Doklady Akad. Nauk SSSR 114, 844 (1957).*
6. G. V. Kukolev and L. G. Mel'nichenko, Ogneupory 13, 447 (1948); V. I. Klassen and É. I. Popova, Doklady Akad. Nauk SSSR 85, 1 (1953); L. I. Chernyi, Trudy Gos. In-ta Gorno-Khim. Syr'ya, 1 (1950); V. I. Byalkovskii and I. A. Kudinov, Keramicheskii Sbornik, 10 (1948); E. B. Matskevich and P. Yu. Butyagin, Kolloid. Zhur. 20, 655 (1958).*
7. M. L. Morgulis, Vibratory Grinding of Materials [in Russian] (Moscow, 1957).
8. M. I. Aronov, Pribory i Tekhn. Éksperimenta 1, 153 (1959).
9. P. H. Emmett, Symposium on New Methods for Particle Size Determination in Subsieve Range (1939); D. S. Sominskii and G. S. Khodakov, Sci. Rep. All-Union Sci. Res. Inst. of Fine Grinding of Structural Materials [in Russian] 29 (1957).
10. L. A. Feigin and V. N. Rozhanskii, Doklady Akad. Nauk SSSR 115, 946 (1957).*
11. G. S. Khodakov and P. A. Rebinder, Doklady Akad. Nauk SSSR 127, 1070 (1959).*
12. I. V. Grebenshchikov, Izvest. Akad. Nauk SSSR, Otdel. Tekhn. Nauk No. 1 (1937).
13. S. Brunauer, Adsorption of Gases and Vapors [Russian translation] (Moscow, Goskhimizdat, 1948) 1.
14. B. S. Shvetsov, Introduction to the Chemistry of Silicon [in Russian] (Moscow–Leningrad, 1953).
15. P. A. Rebinder, V. I. Likhtman, and L. A. Kochanova, Doklady Akad. Nauk SSSR 111, 1278 (1955).
16. E. D. Shchukin and V. I. Likhtman, Doklady Akad. Nauk SSSR 124, 307 (1959).*
17. V. F. Kiselev, K. G. Krasil'nikov, and G. S. Khodakov, Doklady Akad. Nauk SSSR 130, 1233 (1960).*
18. R. K. Iler, Colloid Chemistry of Silica and Silicates [Russian translation] (IL, Moscow, 1959).
19. G. S. Khodakov and P. A. Rebinder, Doklady Akad. Nauk SSSR 131, 1316 (1960).*
20. M. I. Khigerovich, Trudy In-ta Tsementa No. 3 (1950).

* Original Russian pagination. See C. B. translation.

INFLUENCE OF PRIMARY ALIPHATIC ALCOHOLS ON THE SOL–COAGEL TRANSITION TEMPERATURE IN AQUEOUS SODIUM STEARATE SOLUTIONS

A. I. Yurzhenko and G. F. Storozh

Department of Physical and Colloid Chemistry, I. Franko L'vov State University
Translated from Kolloidnyi Zhurnal, Vol. 22, No. 3, pp. 376-381
May-June, 1960
Original article submitted January 27, 1959

Several workers [1, 2] have shown that the sol–coagel phase transition is accompanied by abrupt changes in nearly all the physicochemical parameters of the system, and the properties change at a definite and quite reproducible temperature. The process is accompanied by evolution of a considerable amount of heat and is purely crystallizational in character. Various additives have a significant influence on the transition temperature. Electrolytes raise the temperature of coagel formation [3], whereas surface-active substances [4, 5] lower it.

Coagel formation is regarded [4] as a complex process consisting of formation and spontaneous flocculation of soap microcrystals. Formation of microscopic crystals when an aqueous soap solution is cooled below the Krafft point is probably caused by bonding between the polar groups of the soap molecules. The surface of these crystals is strongly hydrophobic owing to outward orientation of the hydrocarbon molecular chains. When a coagel is formed from solution the surface of the soap microcrystals is partially stabilized by adsorbed molecules and ions of the soap fraction in true solution. Because of their hydrocarbon surface, the primary crystallites have high adsorption power and flocculate extensively in the aqueous phase, and this leads to formation of a coagel with a definite structure.

Evidently, surface-active substances must greatly diminish the flocculation tendency of the microcrystals by replacing the adsorption layer by molecules of the additive, and also by formation of mixed micelles; they should thereby lower the sol–coagel transition temperature. The nature of the additive is significant. Even different members of the same homologous series should have different effects.

The present paper deals with a study of the influence of normal aliphatic alcohols containing from 1 to 18 carbon atoms on the sol–coagel transition temperature of 0.1 M (molal) aqueous sodium stearate solution. The choice of this series of alcohols was suitable for determining the influence of the length of the hydrocarbon chain on the colloidochemical properties of soap and detergent hydrosols.

The materials used were sodium stearate and alcohols* (pure); these were dissolved in redistilled water. In each experiment 50 cc of the sol, previously heated to 80°, was put into a thick-walled test tube with an air jacket; the fall of temperature was recorded at intervals in the stirred liquid. It is known that the duration of cooling of a sol has a significant influence on the transition temperature. Pure soap solutions form coagels at much lower temperatures when cooled rapidly. As has been correctly pointed out [2], this simple distinction between the equilibrium temperature of coagel formation (coinciding with the fusion temperature of the coagel) and the "dynamic" temperature of coagel formation which is usually determined experimentally has been disregarded by most investigators. Therefore, our numerical values for the transition temperatures do not agree with those of

* Undecyl dodecyl, tridecyl, and tetradecyl alcohols were kindly supplied by K. V. Vil'shau to whom the authors are deeply grateful.

Lederer [1], whose experiments were 7-8 minutes in duration at the melting point of ice. All our experiments were carried out at 20°. The average duration of an experiment was 20 minutes. Nevertheless, as will be shown later, our calculated values of the heat effects are in good agreement with the data of other authors.

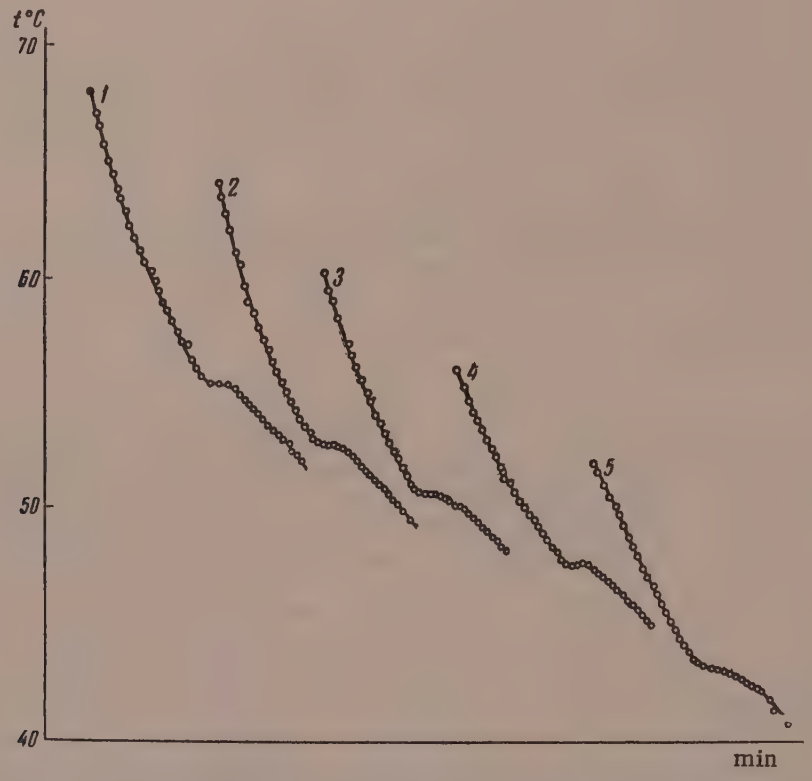


Fig. 1. Cooling curves for 0.1 M aqueous alcohol sols of sodium stearate in presence of various amounts of propyl alcohol: 1) 0; 2) 0.1; 3) 0.2; 4) 0.3; 5) 0.4 moles/liter.

Figure 1 shows some selected cooling curves for 0.1 M solutions of sodium stearate in presence of various amounts of propyl alcohol. The reasons why this particular alcohol was chosen was that in the case of methyl and ethyl alcohols the lowering of the gelatin point is small, whereas with the higher homologs it is very considerable even with relatively small amounts of added alcohols, so that the results are difficult to present visually in the same diagram. We do not describe the nature of the cooling curves, as this has been done in detail earlier [1], but merely note that the sharp breaks seen in the curves in Fig. 1 are found in all cases as a general rule. The discontinuity is somewhat "diffuse" for systems in which the transition temperature is very close to the temperature of the surrounding medium (20°). However, even in these individual cases the break on the curve is easy to determine.

The effect of concentration of the added alcohols on the temperature of the sol–coagel phase transition is shown in Fig. 2. The alcohol concentration is expressed as the ratio of the number of alcohol molecules (n) to the total number of molecules of all the mixture components (Σn). As was to be expected, the data in Fig. 2 show that the transition temperature decreases with increasing concentration of added alcohols. Within the concentration range studied this decrease is linear. The nature of the alcohol is significant. The temperature of coagel formation decreases progressively with the molecular weight of the additive as far as tetradecyl alcohol. Hexadecyl and octadecyl alcohols have less effect on the sol–coagel transition temperature (Fig. 3). Since the temperature of coagel formation is a linear function of the concentration of additive, it is possible to use the ordinary "cryoscopic" equation for calculating the latent heat of sol–coagel phase transition in presence of additives:

$$T - T_0 = \frac{RT_0^2}{\lambda} \frac{n}{\Sigma n}, \quad (1)$$

where T_0 and T are the transition temperatures for aqueous and aqueous–alcoholic solutions respectively; λ is the latent heat of transition calculated per mole of additive; $n/\Sigma n$ is the mole fraction of additive present.

The table contains values of the slope factor K for the relationships between transition temperature and additive concentration (here the alcohol concentrations were expressed in moles per 1000 g of water), and also values of λ for different numbers of carbon atoms in the alcohol molecules, calculated from the data in Figure 2. By analogy with the cryoscopic constant, K evidently represents the lowering of the temperature of coagel formation for solutions containing 1 mole of additive per 1000 g of solvent. Although the values of this constant for the higher alcohols are too high, we believe that it can be used for approximate estimation of the sol–coagel transition temperature for a given concentration of the additive, by means of the equation

$$t_{gel} = -KC + 55{,}4 \quad (2)$$

(55.4 is the gelatin temperature of 0.1 M sodium stearate solution without additives). The concentration range of applicability of this equation becomes narrower with increasing molecular weight of the alcohol, because of the decreasing solubility of the alcohols in this system.

Effect of the Nature of the Alcohol on the Latent Heat of Transition of 0.1 M Sodium Stearate Solution

Number of carbon atoms in alcohol molecule	– K	– λ	Number of carbon atoms in alcohol molecule	– K	– λ
1	2,456	1969,0	9	354,8	10,90
2	7,188	550,7	10	399,2	9,692
3	32,09	114,7	11	447,8	8,646
4	69,05	56,71	12	484,4	7,986
5	111,6	34,98	13	648,9	5,839
6	176,0	21,72	14	907,8	4,268
7	207,9	18,71	16	787,9	4,962
8	260,3	15,09	18	572,0	6,609

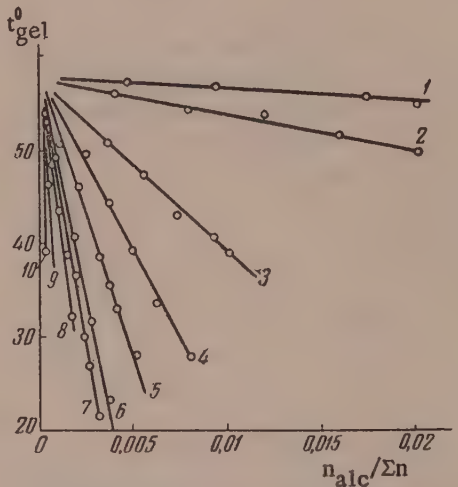


Fig. 2. Variations of the temperature of coagel formation in 0.1 M sodium stearate sol with concentration of alcohols: 1) Methyl; 2) ethyl; 3) propyl; 4) butyl; 5) amyl; 6) hexyl; 7) heptyl; 8) octyl; 9) nonyl; 10) decyl.

The influence of the nature of the alcohol on the latent heat of the sol–coagel transition is represented in Fig. 3 as the reciprocal of the latter plotted against ν, the number of C atoms in the molecule. Similar results were obtained in a study of the biological activity of alcohols in concentrated sodium oleate solution. It is clear from Fig. 3 that the $1/\lambda = f(\nu C)$ relationship is linear over a considerable range, and can be represented by the equation

$$1/\lambda = a + b\nu, \quad (3)$$

where a is the reciprocal of the heat of coagel formation of aqueous stearate solution without additions ($1/\lambda_0$). The numerical value of λ_0, found from Fig. 3, is 28.57 cal/mole. Almost the same value (30.07 cal/mole) was calculated by means of Equation (1) from the data in Fig. 4, which represents the effect of soap concentration on the sol–coagel transition temperature. The values found for the latent heat of transition of 0.1 M sodium stearate solution are very close to the literature data.

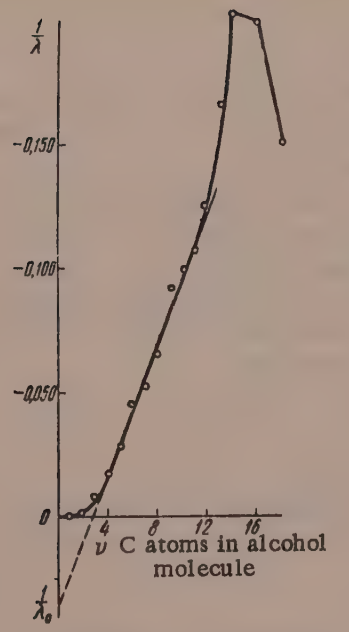


Fig. 3. Effect of the length of the hydrocarbon radical in alcohols on the reciprocal heat of transition of 0.1 M sodium stearate sol.

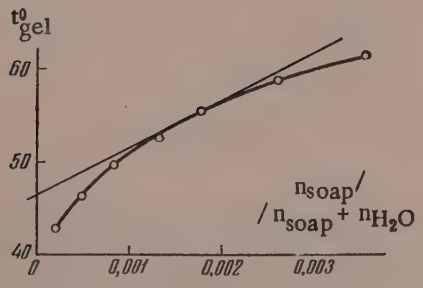


Fig. 4. Variation of the temperature of coagel formation of sodium stearate sols with the concentration of sodium stearate.

For example, Lederer [1] found by analysis of cooling curves that the heats of gelation of 0.25 and 0.125 M solutions of sodium stearate are 47.9 and 34.0 cal/mole, respectively. Although we could not find a numerical value for the heat of transition of 0.1 M sodium stearate hydrosol in the literature, it may be concluded from this comparison that our method for calculating this value from Equation (1) is valid. Moreover, this method of determination is more convenient, as the equation given by Lederer for the heat effect [1] contains a number of values, such as the density and specific heat of the system, which must be determined separately.

The coefficient b in Equation (3) may be interpreted as the degree of influence of the alcohol on the heat of transition of the system, calculated per 1 gram-atom of the additive, and its reciprocal value may be regarded as the change in the heat effect produced by one gram-atom. The numerical value of b is −0.01297 (1/b = λ−77,09). The change of sign of the heat effect in presence of alcohol is quite normal; it follows even from Equation (1). A decrease of the numerical value of the heat of coagel formation in presence of surface-active agents has been reported elsewhere [3]. The value for 0.2 M solution of sodium stearate with 2% cresol added was somewhat over one half of the heat effect for the pure soap solution.

In our opinion our results are consistent with P. A. Rebinder's general theory of coagel formation. When lower aliphatic alcohols are introduced into the soap–water system, anomalously high values for the heat effect of the sol–coagel transition are obtained. Since lower alcohols act as peptizing agents on a system containing colloidal particles, forming solvation layers on the latter, energy must be expended in breakdown of these protective layers for formation of the coagel, which involves consolidation of the primary soap microcrystals. This energy is opposite in sign to the heat effect of the sol–coagel phase transition. The value of −λ decreases with lengthening of the hydrocarbon radical in the alcohol, and although the transition temperature also falls, perhaps owing to formation of mixed micelles, the sol–coagel transition itself requires less energy. The minimum value of −λ is found for the system containing tetradecyl alcohol; beyond this it increases again. Increase of the heat effect (−λ) for systems containing hexa- and octadecyl alcohols, or weakening of the ability of these alcohols to lower the temperature of coagel formation, may be attributed to the fact that, starting with these alcohols, the molecules become comparable in size with the stearate molecules. This evidently leads to formation of mixed micelles the properties of which differ from the properties of micelles formed by molecules of stearate and lower homologs of the series; this leads to a decrease in the magnitude of the heat effect in transition of these systems from the sol to the coagel state.

SUMMARY

1. The temperature of coagel formation in 0.1 M sodium stearate hydrosol falls with increasing concentration of added aliphatic alcohols; the fall is greater for alcohols of higher molecular weight. The lowering of the transition temperature within the alcohol concentration ranges studied is linear.

2. An equation is given for calculating the dynamic temperature of coagel formation in 0.1 M stearate hydrosols in presence of known amounts of additives.

3. The cryoscopic equation was used for calculating the heat effect of the sol–coagel transition of stearate. The relationship between the reciprocal of the heat of transition ($1/\lambda$) and the number of carbon atoms in the alcohol molecule is linear over a considerable region. The fact that the sign of the heat of transition for alcoholic–aqueous solutions of sodium stearate is opposite to the sign of the heat of transition for pure soap hydrosol is attributed to the properties of the mixed soap–alcohol–water micelles formed.

LITERATURE CITED

1. M. Fischer, Koll.-Z. 46, 359 (1923); E. Lederer, Koll.-Z. 57, 16 (1931).
2. V. B. Mokievskii, Usp. Khimii 9, 1025 (1940).
3. Angelescu and Popescu, Koll.-Z. 66, 175 (1934).
4. V. B. Mokievskii and P. A. Rebinder, Doklady, Akad. Nauk SSSR 26, 47 (1940).
5. Angelescu and Popescu, Koll.-Z. 51, 336 (1930).
6. H. L. Booij, Koll.-Z. 125, 21 (1952).

DETERMINATION OF THE SIGN OF THE CHARGE OF COLLOIDAL PARTICLES IN COAGULATED SYSTEMS BY MEANS OF A pH METER

É. A. Levitskii

Institute of Petrochemical Synthesis, Academy of Sciences USSR, Moscow
Translated from Kolloidnyi Zhurnal, Vol. 22, No. 3, pp. 382-383
May-June, 1960
Original article submitted April 24, 1959

The presence of colloidal particles influences the hydrogen ion concentration in solution [1-4]. This phenomenon, known as the Pallmann effect, was discovered by determinations of the pH of the medium with the aid of quinhydrone, hydrogen, and glass electrodes, and is therefore a property of the disperse systems themselves [4].

The cause of the suspension effect is active participation of hydrogen and hydroxyl ions in formation of electric double layers on the colloidal particles [3]. Sedimenting particles in coarsely disperse (coagulated) systems take H and OH ions with them, and make them partially "insoluble" [3].

In a coagulated colloidal system the Pallmann suspension effect is represented by the difference (ΔpH) between the hydrogen ion concentration in the clear solution over the precipitate (solution pH) and the concentration in the zone where the precipitate accumulates (pH of the slurry), such that ΔpH = solution pH-slurry pH. According to Pallmann the difference (ΔpH) may be either positive or negative in sign [2]. Van Laar [1] found that precipitates in the isoelectric state do not exhibit the suspension effect. This effect was used for very accurate determination of the isoelectric pH of silver chloride precipitate [1].

There is a correlation between the sign of the charge on colloidal particles and ΔpH [1, 4]. This made it possible to use the suspension effect in a simple, accurate, and rapid method for determination of the sign of the charge on colloidal particles by means of a pH meter.

This method was used to determine the sign of the charge on colloidal particles in precipitates of nickel and chromium hydroxides, barium sulfate, and silver chloride.

After the precipitate had settled in a beaker and the supernatant liquid became clear, the clear solution was poured off into the pH meter cell and the solution pH was determined. The precipitate was stirred up in the remaining liquid and the pH of the slurry was determined. The difference ΔpH = solution pH–slurry pH was then calculated, and the sign of the charge on the colloidal particles was found from the sign of the pH difference.

The results of the sign determinations from the suspension effect were checked against the results of electrophoretic determinations of sign of the particle charge. Direct current at U = 60 v, I = 150 ma was supplied to the electrodes. The determinations lasted from 5 to 15 minutes.

The results of the charge-sign determinations are given in the table.

For precipitates very close to the isoelectric state determination of sign of particle charge by the suspension effect must be more accurate than the electrophoresis method.

The suspension-effect method is most suitable for determinations of charge sign in coagulated colloidal systems. Poor sedimentation (with turbid solutions) lowers the accuracy of the determination. In systems where the precipitate is in equilibrium with a peptized solution it is sometimes impossible to determine ΔpH at all, as its value is zero in such cases. This was found to occur when precipitates of nickel, aluminum, and chromium

Determinations of the Sign of Particle Charge by the Suspension Effect and by Electrophoresis

Formula of ppt.	Suspension effect method			Sign of particle charge	Sign of particle charge by electrophoresis	Formula of ppt.	Suspension effect method			Sign of particle charge	Sign of particle charge by electrophoresis
	sol. pH	slurry pH	Δ pH				sol. pH	slurry pH	Δ pH		
$Cr(OH)_3$	11,2	11,2	—	—	—	$Ni(OH)_2$	9,70	9,30	+0,40	+	+
	9,60	9,68	—0,08	—	—		8,38	8,43	—0,05	—	0*
	9,00	9,27	—0,27	—	—		8,50	8,80	—0,30	—	—
	8,35	8,95	—0,60	—	—	$BaSO_4$	8,48	8,80	—0,32	—	—
	8,50	9,22	—0,72	—	—		7,60	5,50	+2,10	+	+
$Ni(OH)_2$	7,22	6,85	+0,37	+	+	AgCl	6,3	6,62	—0,32	—	—
	7,50	6,00	+1,50	+	+		5,24	5,14	+0,10	+	+
	7,90	7,80	+0,10	+	+						

* The reason for the discrepancy of sign is that the particle charge was close to zero and could not be determined by electrophoresis.

hydroxides were in equilibrium with solutions containing their cations (Ni^{2+}, Al^{3+}, Cr^{3+}), in incomplete precipitation. However, in general, slight peptization of the precipitate does not interfere with the determination. These results, therefore, showed that the suspension effect can be used for determining the sign of the charge on colloidal particles.

SUMMARY

1. The relationship between the sign of the suspension effect and the sign of the charge on colloidal particles was investigated for a number of systems.

2. In the cases studied the sign of ΔpH = solution pH—slurry pH was the same as the sign of the particle charge.

3. A simple method is proposed for determination of the sign of the charge on colloidal particles by means of a pH meter; the method is not inferior to the electrophoresis method in accuracy.

LITERATURE CITED

1. H. R. Kruyt, Colloid Science [Russian translation] (IL, Moscow, 1955).
2. H. Pallmann, Kolloid. Beihefte 30, 334 (1930).
3. G. Weigner and H. Pallmann, Chem. 24, 5200 (1930).
4. G. Weigner, H. Pallmann, J. Albareda, and A. Musierowicz, Chem. Abs. 28, 1904 (4) (1934).

SIGNIFICANCE OF ABBREVIATIONS MOST FREQUENTLY ENCOUNTERED IN SOVIET PERIODICALS

FIAN	Phys. Inst. Acad. Sci. USSR.
GDI	Water Power Inst.
GITI	State Sci.-Tech. Press
GITTL	State Tech. and Theor. Lit. Press
GONTI	State United Sci.-Tech. Press
Gosenergoizdat	State Power Press
Goskhimizdat	State Chem. Press
GOST	All-Union State Standard
GTTI	State Tech. and Theor. Lit. Press
IL	Foreign Lit. Press
ISN (Izd. Sov. Nauk)	Soviet Science Press
Izd. AN SSSR	Acad. Sci. USSR Press
Izd. MGU	Moscow State Univ. Press
LEIIZhT	Leningrad Power Inst. of Railroad Engineering
LET	Leningrad Elec. Engr. School
LETI	Leningrad Electrotechnical Inst.
LETIIZhT	Leningrad Electrical Engineering Research Inst. of Railroad Engr.
Mashgiz	State Sci.-Tech. Press for Machine Construction Lit.
MEP	Ministry of Electrical Industry
MES	Ministry of Electrical Power Plants
MESEP	Ministry of Electrical Power Plants and the Electrical Industry
MGU	Moscow State Univ.
MKhTI	Moscow Inst. Chem. Tech.
MOPI	Moscow Regional Pedagogical Inst.
MSP	Ministry of Industrial Construction
NII ZVUKSZAPIOI	Scientific Research Inst. of Sound Recording
NIKFI	Sci. Inst. of Modern Motion Picture Photography
ONTI	United Sci.-Tech. Press
OTI	Division of Technical Information
OTN	Div. Tech. Sci.
Stroiizdat	Construction Press
TOE	Association of Power Engineers
TsKTI	Central Research Inst. for Boilers and Turbines
TsNIEL	Central Scientific Research Elec. Engr. Lab.
TsNIEL-MES	Central Scientific Research Elec. Engr. Lab.—Ministry of Electric Power Plants
TsVTI	Central Office of Economic Information
UF	Ural Branch
VIESKh	All-Union Inst. of Rural Elec. Power Stations
VNIIM	All-Union Scientific Research Inst. of Metrology
VNIIZhDT	All-Union Scientific Research Inst. of Railroad Engineering
VTI	All-Union Thermotech. Inst.
VZEI	All-Union Power Correspondence Inst.

Note: Abbreviations not on this list and not explained in the translation have been transliterated, no further information about their significance being available to us. — Publisher.

INVESTIGATION OF CRYSTALLIZATION STRUCTURE FORMATION IN CALCIUM HYDROCHLOROALUMINATE*

E. P. Andreeva and E. E. Segalova

Chemistry Faculty, Moscow University
Translated from Kolloidnyi Zhurnal Vol. 22, No. 4, pp. 385-392,
July-August, 1960
Original article submitted September 10, 1959

Calcium chloride is used very extensively in building [1] because of its ability to accelerate early hardening of Portland cement, even below 0° as well as above. Therefore studies of the mechanism of its action on Portland cement are practical as well as of theoretical interest.

To determine the mechanism of action of calcium chloride on Portland cement at temperatures below 0° it is first necessary to study its influence at the same temperatures on structure formation in suspensions of tricalcium aluminate (C_3A), the individual mineral in cement clinker which determines the nature of structure formation at the first stages of interaction between cement and water.

Several workers showed that calcium chloride reacts chemically with the aluminate component of cement clinker to form complex calcium hydrochloroaluminates of the compositions $3CaO \cdot Al_2O_3 \cdot CaCl_2 \cdot 10H_2O$ [2-6] and $3CaO \cdot Al_2O_3 \cdot 3CaCl_2 \cdot 31H_2O$ [7-9]. It is still not known how formation of these compounds affects the initial stages of structure formation.

It has been suggested [7,10] that their influence is associated with chemical dispersion of the solid phase. However, it is hardly likely that dispersion can be the sole cause of the sharp acceleration of the setting and hardening processes which occurs on addition of fairly large amounts of calcium chloride. Moreover, this hypothesis does not explain why, in presence of small and moderate amounts of calcium chloride, the setting is retarded and not accelerated.

It was of interest to determine whether hydrochloroaluminate can have an effect by being able to form hardening structures. Accordingly a study was made of structure formation at -5 and -10° in suspensions of C_3A (tricalcium aluminate, $3CaO \cdot Al_2O_3$) and its hydrated form $C_3A \cdot aq$ (tricalcium aluminate hydrate, $3CaO\ Al_2O_3 \cdot 6H_2O$) mixed with calcium chloride solutions of various concentrations. Experience has shown that the most suitable mixtures for investigations of this type contain from 2 to 10% of cement and 98-90% of inert filler—ground quartz sand. Concentrated suspensions (pastes) were prepared from such mixtures by addition of calcium chloride solutions. Structure formation was characterized by the kinetics of plastic strength increase [11]. The samples were kept in desiccators over calcium chloride solutions.

The results of studies of structure formation at -5° in C_3A suspensions mixed with calcium chloride solutions of various concentrations (1.5 to 5N) show that calcium hydrochloroaluminate is capable of forming hardening structures (Fig. 1). The hardening structures cannot be formed by some other substance, because our x-ray investigations [12] showed that under these conditions calcium hydrochloroaluminate is the only new substance to arise during the entire period of structure formation. Hydrochloroaluminate hardening structures are formed when it crystallizes out of solution, as the result of formation of stable crystallization contacts between its crystals.

*I. M. Timofeeva, diploma student of the Department of Colloid Chemistry, assisted in the work.

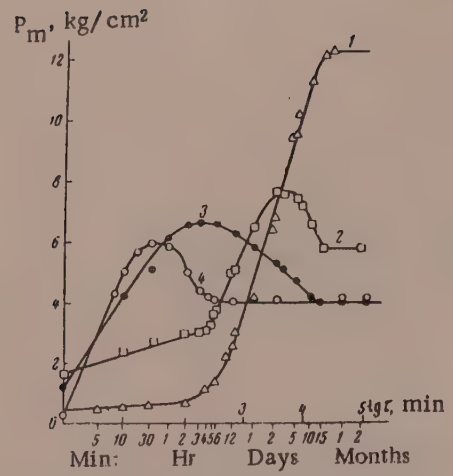


Fig. 1. Kinetics of structure formation at -5° in suspensions of 5% C_3A + 95% Si_2O + 35 ml of calcium chloride solution per 100 g of dry mixture: 1) 1.58 N; 2) 2.5 N; 3) 4 N; 4) 5 N $CaCl_2$.

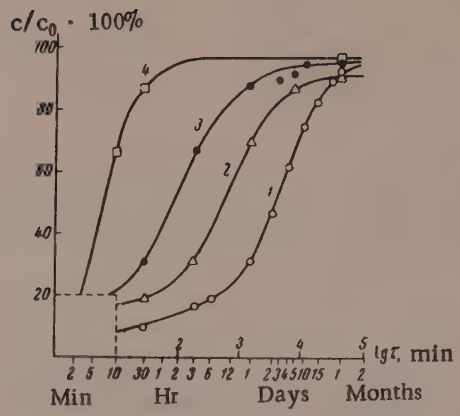


Fig. 2. Kinetics of chemical binding of calcium chloride in suspensions of 5% C_3A + 95% SiO_2 + 35 ml of calcium chloride solution per 100 g of dry mixture: 1) 1.58 N; 2) 3 N; 3) 4 N; 4) 5 N $CaCl_2$; $c/c_0 \cdot 100\%$ is the amount of $CaCl_2$ bound at a given instant, as a percentage of the theoretical amount for the monochloride form of the hydrochloroaluminate.

Fig. 1 shows that the rate of plastic strength increase, its dependence on time, and the maximum and ultimate strengths of hydrochloroaluminate hardening structures greatly depend on the concentrations of the calcium chloride solutions.

Kinetic studies of the chemical reaction between tricalcium aluminate and calcium chloride showed that this dependence is primarily determined by different rates of formation of calcium hydrochloroaluminate. The higher the concentration of calcium chloride solution, the more rapidly is its chemical binding completed (Fig. 2).

The maximum amounts of bound calcium chloride in suspensions of C_3A mixed with solutions of different concentrations are similar in value; the average is 95.2% of the theoretical for the monochloride form of hydrochloroaluminate. Despite the fact that equal amounts of calcium chloride are bound in all the suspensions, in C_3A suspension mixed with 1.58 N $CaCl_2$ solution, where the chemical reaction is relatively slow, a hydrochloroaluminate crystallization structure of high ultimate strength is formed, whereas in suspensions with higher concentrations of calcium chloride, where the reactions are more rapid, weaker structures are produced and these break down spontaneously in time (Fig. 1).

Spontaneous breakdown of the structures begins long before the end of the reaction between tricalcium aluminate and calcium chloride (Fig. 1, 2, and 3) and is accompanied by considerable expansion; it is due to breakdown of the structure at the weakest regions under the influence of stresses arising in the structure during growth of its constituent crystals. Breakdown of the structure during growth of the crystals, however, is not the only process. It is accompanied by reinforcement of the structure because of the increase in the size of its constituent crystals. In consequence the nature of variations of the plastic strength of the suspension during intensive growth of the crystals depends on which of these two processes is predominant at the given instant. This accounts for the second strength maximum on the kinetic curve for structure formation at -10° in tricalcium aluminate suspension mixed with 3 N calcium chloride solution (Fig. 4). In the same suspension, but at -5°, the plastic strength ceases to vary until the end of the reaction, because the spontaneous breakdown and reinforcement processes compensate each other.

It must be pointed out that duration of stirring during the mixing process has a great influence on the kinetics of structure formation and on strength. It was shown in a study of the mechanism of hydration hardening of a number of cements [13] that formation of the hardening structure proceeds in two stages. At the first stage, at high supersaturations, the framework of the crystallization structure is formed as the result of formation of concretion contacts between the newly formed crystals. At the second stage, when a considerable amount of the

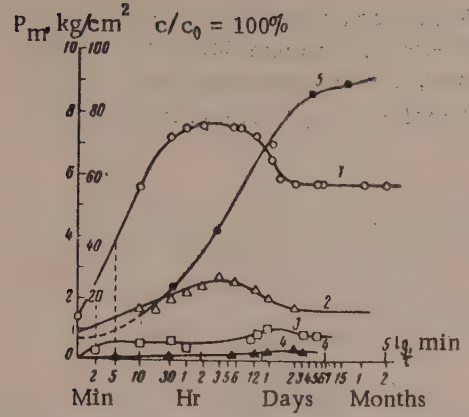


Fig. 3. Kinetics of structure formation at -5° (1-4) and of chemical binding of calcium chloride (5) in suspensions of 5% C_3A + 95% SiO_2 + 35 ml 3 N calcium chloride solution of calcium chloride per 100 g of dry mixture: 1) suspension made by impregnation; 2, 3, 4) suspension stirred again after mixing, after 30 sec, and 2 and 5 min, respectively.

newly formed substances accumulates in the suspension and supersaturation decreases, only the existing framework grows, by growth of its constituent crystals. To account for the influence of stirring on structure formation it was desired to determine the durations of the two stages in formation of hardening structures of calcium hydrochloroaluminate at different solution concentrations. Accordingly, the kinetics of structure formation was studied with repeated breakdown of the structures in the course of formation. Repeated breakdown makes it possible to detect the instant when the suspensions cease to be capable of repeated hardening, and thereby to find the duration of the first stage.

The experiments showed that in tricalcium aluminate suspensions mixed with 3 N calcium chloride solution (Fig. 3, 4) very brief mechanical action leads to considerable lowering of structure strength. Thus, the maximum strength of the structure in a suspension stirred for only 30 seconds during the mixing is already much lower than the strength of a structure made by impregnation.

Two-minute stirring of the suspension is quite enough to prevent structure formation completely, despite the fact that formation of hydrochloroaluminate in it still continues for a very long time (Fig. 3). This shows that the period during which the crystals grow together, with formation of a crystallizational framework, is very short for these suspensions. On the other hand, in a tricalcium aluminate suspension mixed with 1.58 N $CaCl_2$ solution the crystallizational structure of hydrochloroaluminate is formed under conditions in which formation of the crystallizational framework continues for a very long time (Fig. 5). It is only on the fifth day that the crystals cease to grow together and the hydrochloroaluminate loses its power of forming hardening structures.

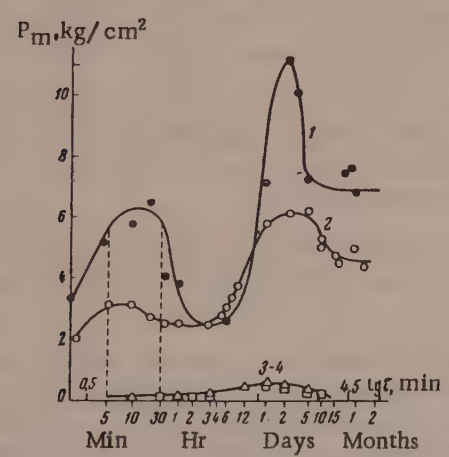


Fig. 4. Kinetics of structure formation at -10° in suspensions of 5% C_3A + 95% SiO_2 + 35 ml of 3 N calcium chloride solution per 100 g of dry mixture: 1) suspension made by impregnation; 2, 3, 4) suspensions stirred again after mixing, after 30 sec, and 5 and 30 min, respectively.

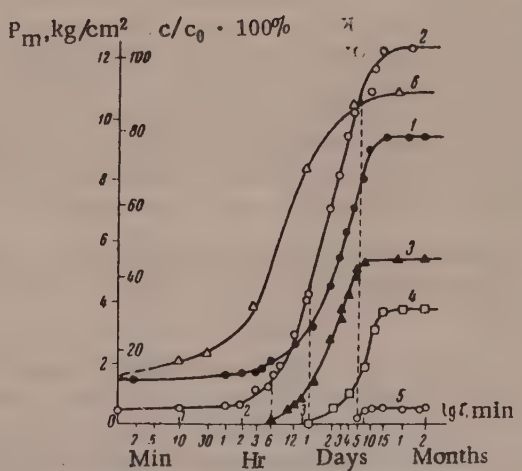


Fig. 5. Kinetics of structure formation (1-5) and chemical binding of calcium chloride (6) in suspensions of 5% C_3A + + 95% SiO_2 + 35 ml of 1.58 N $CaCl_2$ solution per 100 g of dry mixture: 1) suspension made by impregnation; 2, 3, 4, 5) suspensions stirred again after 30 sec, 6 hr, 1 day, and 5 days, respectively.

Kinetics of Chemical Binding of Calcium Chloride at Different Temperatures in Suspensions of Tricalcium Aluminate and Its Hexahydrate, Mixed with 3 N Calcium Chloride Solution (suspension compositions: 5% C_3A + 95% SiO_2 + 35 ml of calcium chloride solution per 100 g of dry mixture; 7% $C_3A \cdot aq$ + 93% SiO_2 + 29 ml of $CaCl_2$ solution per 100 g of dry mixture)

Time	C_3A, at −5°		C_3A, at −10°		$C_3A \cdot aq$, at −5°		$C_3A \cdot aq$, at −10°	
	I	II	I	II	I	II	I	II
5 min	—	—	—	—	0,021	5,3	0,015	3,8
10 »	0,07	17	—	—	—	—	—	—
30 »	0,078	19	0,070	17	0,040	9,73	0,029	7,0
3 hr	0,129	31,5	0,123	29,5	0,237	57,73	0,215	52,5
1 day	0,284	70	—	—	0,328	79,82	—	—
5 »	0,358	87,1	0,349	85	—	—	—	—
7 »	—	—	—	—	—	—	0,274	66,7
10 »	—	—	—	—	0,370	90	0,360	87,6
15 »	—	—	—	—	0,371	90,27	0,360	87,6
1 month	0,373	90,6	0,349	85	0,372	90,4	0,361	87,8

I) in grams per g of C_3A; II) in percent of the theoretical for the monochloride form of hydrochloroaluminate.

Thus, the time during which the crystallizational structure framework is formed differs for suspensions containing different amounts of added calcium chloride; therefore breakdown of their hydrochloroaluminate structures formed at the instant of mixing influences subsequent structure formation in different ways. In suspensions in which the formation of the crystallizational structure framework is a lengthy process and the reaction continues for a long time, breakdown of the structure initially formed does not affect the final strength of the structure. For example, in a suspension mixed with 1.58 N $CaCl_2$ solution, early stirring (after 30 sec) does not lower the final strength of the structure, but even increases it somewhat (Fig. 5). The explanation is that brief stirring produces a more homogeneous suspension than impregnation does. In suspensions in which the first stage is brief and the reaction is rapid, the role of the structure formed at the first instant is very great in creating the final strength. Breakdown of this structure may prevent structure formation altogether, and can give rise to the false impression that no hydrochloroaluminate structure is formed at this solution concentration.

Until now our studies of the mechanism of the influence of calcium chloride on the aluminate component of cement clinker have been carried out with suspensions in which the original cement consisted of anhydrous aluminates. It was of interest to find whether chemical reactions and structure formation in presence of calcium chloride occur in aqueous suspensions of completely hydrated tricalcium aluminate.

Investigations by x-ray [12] and chemical methods (see table) showed that when tricalcium aluminate hexahydrate is mixed with calcium chloride solutions (up to 5 N) the monochloride form of hydrochloroaluminate is produced.

With regard to suspensions of tricalcium aluminate it cannot be assumed with certainty from the results of chemical analyses only that the monochloride form of hydrochloroaluminate is formed, because the reaction may not go to completion because of the presence of films of new compounds on the C_3A grains. In hydroaluminate suspensions formation of hydrochloroaluminate occurs at lower supersaturations with respect to the original cement, as the solubility of hydroaluminate is lower than the metastable solubility of aluminate [14]. Under these conditions protective layers are not formed on the original cement grains and the reaction goes to completion. Because of the absence of these films, most of the hydroaluminate reacts in a shorter time than tricalcium aluminate at a given solution concentration.

Studies of chemical reaction between hydroaluminate and calcium chloride show that when tricalcium aluminate is mixed with calcium chloride solutions (provided that enough calcium chloride is added to bind the C_3A present in the form of a complex salt) hydroaluminate cannot be formed simultaneously with chloroaluminate.

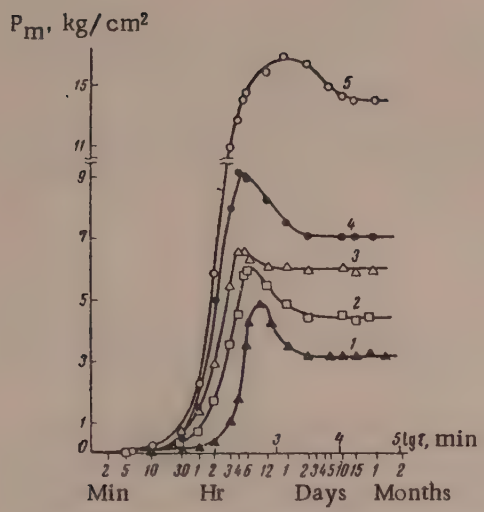


Fig. 6. Kinetics of structure formation at -5° in suspensions containing 7% $C_3A \cdot aq$ + 93% SiO_2 + 29 ml of $CaCl_2$ solution per 100 g of dry mixture; the suspensions were stirred for 30 sec, at mixing. 1) 1.58 N; 2) 2.16 N; 3) 3 N; 4) 4 N; 5) 5 N $CaCl_2$.

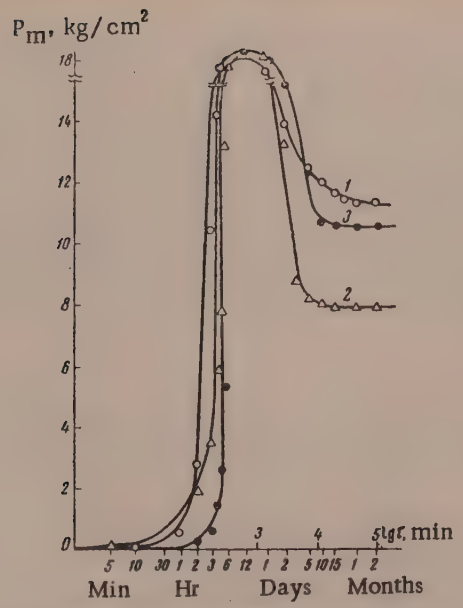


Fig. 7. Kinetics of structure formation at -10° in suspensions containing 7% $C_3A \cdot aq$ + 93% SiO_2 + 29 ml of $CaCl_2$ solution per 100 g of dry mixture. 1) 3 N; 2) 4 N; 3) 5 N $CaCl_2$

It is clear from Fig. 6 that when hydroaluminate is mixed with calcium chloride solutions the plastic strength increases with time; this is due to formation of hydrochloroaluminate structures. In hydroaluminate suspensions, in contrast to C_3A suspensions, structure formation processes have a marked induction period. This is because hydroaluminate dissolves much more slowly than tricalcium aluminate [14], and formation of chloroaluminate during the first 30 min is very slow (see table).

At high concentrations of calcium chloride (3 N and over) the general character of structure formation in hydroaluminate suspensions remains the same as in tricalcium aluminate suspensions. Crystallizational chloroaluminate structures are formed in the suspensions; in the course of time they break down spontaneously under the influence of tensile stresses arising during growth of the crystals. At moderate solution concentrations there is a deviation from the optimum conditions necessary for formation of a strong chloroaluminate structure, such as exist in suspensions of tricalcium aluminate.

In a suspension of hydroaluminate mixed with 1.58 N $CaCl_2$ solution a weak structure which breaks down spontaneously is formed, instead of the very strong and stable structure such as is formed in C_3A suspensions. This once again demonstrates the important role of supersaturations in structure formation.

The kinetics of structure formation depends less on the concentration of calcium chloride solutions in $C_3A \cdot aq$ suspensions than in C_3A suspensions (Fig. 6, 7).

Comparison of the kinetics of structure formation at various temperatures: + 20° [15], -5°, and -10° in suspensions of C_3A and $C_3A \cdot aq$ with added calcium chloride shows that the general character of the processes remains almost unchanged within these temperature ranges. The only difference is that when the temperature is lowered to -10° the processes leading to breakdown of the structures are not so pronounced in C_3A and $C_3A \cdot aq$ suspensions (Fig. 1, 5-7).

In suspensions of C_3A and $C_3A \cdot aq$ mixed with 6.3 N calcium chloride solutions the Debye patterns of the solid phase are identical, but differ from the pattern for calcium hydroaluminate. The chemical composition of the new phase is unknown as yet. Structure-formation processes in the suspensions take the same course as in the mixing of C_3A and $C_3A \cdot aq$ with 5 N $CaCl_2$ solution.

These investigations suggest that calcium hydrochloroaluminate influences structure-formation processes in Portland cement because of its ability to form hardening structures. Retardation of structure formation in Portland cement is due to the fact that at low and moderate concentrations of $CaCl_2$, the period during which the framework of the hydrochloroaluminate crystallizational structure is formed is relatively long. The framework is initially weak and is easily broken down by mechanical action. The acceleration of structure formation is due to the fact that at high solution concentrations chloroaluminate crystallizational structures are rapidly formed, instead of the hydroaluminate structures, which develop more slowly. The influence of breakdown of the chloroaluminate structure itself within the silicate component on the strength is a very important problem which is to be the subject of our future researches.

SUMMARY

1. The kinetics of crystallizational structure formation and chemical reaction has been studied in suspensions of tricalcium aluminate (C_3A) and its hydrate, mixed with calcium chloride solutions (1.5-5N), at -5 and -10°.

2. A hardening structure is formed in the suspension when calcium hydrochloroaluminate crystallizes out of the liquid phase. The strength of this structure and the kinetics of its development depend on the rate of formation of calcium hydrochloroaluminate. Hydrochloroaluminate structures undergo expansion during their growth; this leads to spontaneous breakdown of the structures and a sharp fall in strength.

LITERATURE CITED

1. V. M. Moskvin, Additives for Accelerating Concrete Hardening [in Russian] (Stroiizdat, 1938); S. L. Mironov and V. N. Sizov, Stroit. Prom. 9, 19 (1948); F. M. Ivanov and V. I. Ovcharov, Road Concrete with Additions of Calcium Chloride [in Russian] (Avtotransizdat, Moscow, 1956); A. A. Shishkin, Stroit. Prom. No. 8, 9 (1952); Yu. A. Savvina, V. É. Leirikh, and N. N. Serb-Serbina, Hardening and Properties of Cold Concrete [in Russian] (Orgénergostroi, 1957); V. N. Sizov, Concrete's Hardening in Frost [in Russian] (Orgénergostroi, 1957); E. K. Grabinskii, Experience in the Use of "Salt" Concrete Hardening in Frost [in Russian] (Ugletekhizdat, 1957).
2. J. Egret, Recherches sur les combinaisons entre les sels de calcium et les aluminates de calcium (Paris, 1935).
3. C. R. W. Mylius, Acta Acad. Aboensis Mathematica et Physica 7, 3 (1933).
4. R. Nacken and R. Moseabach, J. anorg. und allgem. Chem. 228 (I), 19, 193 b; Zement, 51ё52 (1942).
5. L. S. Wells and J. Res. Nat. Bur. Standards 1, No. 4, 951 (1928).
6. G. Friedel, Bull. Soc. franc. mineral. 19, 122 (1897).
7. Yu. A. Savvina and N. N. Serb-Serbina, Stroit. Prom. 9, 6 (1954); N. N. Serb-Serbina and Yu. A. Savvina, Tsement 2, 3 (1955); N. N. Serb-Serbina, Yu. A. Savvina, and V. S. Zhurina, Doklady Akad. Nauk SSSR 111, 659 (1956).•
8. E. I. Morozov, Tsement, 3, 24 (1958).
9. P. F. Konovalov and E. I. Morozov, Tsement 2, 25 (1959).
10. V. V. Kind, E. V. Lavrinovich, and R. E. Litvinova, Tsement 3, 7 (1955).
11. E. E. Segalova, P. A. Rebinder, and O. I. Luk'yanova, Vestnik MGU 2 (1954).
12. E. P. Endreeva and E. E. Segalova, Zhur. Priklad. Khim. 33, 1042 (1960).•
13. E. S. Solov'eva and E. E. Segalova, Kolloid. Zhur. 20, 620 (1958).•
14. E. E. Segalova, E. S. Solov'eva, and P. A. Rebinder, Doklady Akad. Nauk SSSR 117, 841 (1957).•
15. E. P. Andreeva, E. E. Segalova, and E. E. Volynets, Doklady Akad. Nauk SSSR 129, 1052 (1958).•

• Original Russian pagination. See C. B. translation.

STREAMING POTENTIAL IN OSCILLATORY FLOW OF A LIQUID IN A POROUS DIAPHRAGM

L. V. Gorelik

B. E. Vedeneev All-Union Scientific Research Institute of Hydraulic Engineering, Leningrad
Translated from Kolloidnyi Zhurnal, Vol. 22, No. 4, pp. 393-397,
July-August, 1960
Original article submitted March 11, 1959

Studies of streaming potential at different streaming oscillation frequencies of the liquid are of considerable interest in relation to investigation and utilization of the seismoelectric effect of the second kind [1], development of various electrokinetic transducers [2], and certain other phenomena.

In the presence investigation a formula was derived for the streaming potential, assuming a pressure gradient varying in accordance with a harmonic law and an oscillating framework of the porous body, and the formula was verified experimentally.

Consider an individual pore, consisting of a cylindrical capillary of circular cross section, vibrating along its axis with acceleration $Ae^{i\omega t}$, where A is the acceleration amplitude and ω is the angular vibration frequency.

The expression for the relative velocity of a liquid in a capillary under a pressure gradient $\partial p/\partial x \cdot e^{i\omega t}$ is of the following form [3]:

$$v = -\frac{\partial p/\partial x + \rho A}{i\omega\rho}\left\{1 - \frac{I_0\left[i\left(\frac{i\omega}{\nu}\right)^{1/2} r\right]}{I_0\left[i\left(\frac{i\omega}{\nu}\right)^{1/2} a\right]}\right\}, \tag{1}$$

where the factor $e^{i\omega t}$ is omitted; ρ is the density of the liquid; a is the capillary radius; ν is the kinematic viscosity of the liquid; r is the distance from the x axis, which coincides with the capillary axis; I_0 is a zero-order Bessel function of the first kind.

When a liquid moves through the capillary the diffuse part of the double layer is displaced, and ions predominantly of one sign are moved out in the direction of the liquid motion. This convective current in a capillary of arbitrary form is represented by

$$i_1 = \int_s v_n \sigma ds, \tag{2}$$

where v_n is the component of the liquid velocity normal to ds; σ is the charge density; s is the capillary cross section.

Owing to charge transfer, a potential difference arises between the capillary ends, leading to a conduction current opposite in direction to the convective current.

The conduction current is:

$$i_2 = -\int_s \varkappa \operatorname{grad}_n U ds, \tag{3}$$

where U is the potential arising as the result of liquid flow; $\varkappa$ is the conductivity of the liquid.

Using Poisson's theorem and assuming that the thickness of the double layer is small in comparison with the radius of curvature of a periphery of cross section s, we may write Equation (2) in the form of [4]:

$$i_1 = -\frac{\varepsilon}{4\pi}\int_l \zeta \frac{dv_n}{dN} dl, \tag{4}$$

where ϵ is the dielectric constant; N is the normal to the capillary wall; dl is an element of the periphery of cross section s.

For a cylindrical capillary of circular section Equation (4) can be rewritten as

$$i_1 = \frac{\varepsilon\zeta}{4\pi}\int_0^{2\pi} \frac{dv}{dr} a\, d\varphi \tag{5}$$

Substitution of v from Equation (1) into (5) and rearrangement gives:

$$i_1 = -\frac{\varepsilon\zeta a^2}{4\mu}(\partial p/\partial x + \rho A)\,\Phi(k), \tag{6}$$

where $\mu = \rho\nu$, the viscosity of the liquid; $k = (\omega/\nu)^{1/2}a$.

$$\Phi(k) = \frac{2J_1(i\sqrt{i}\,k)}{i\sqrt{i}\,kJ_0(i\sqrt{i}\,k)}. \tag{7}$$

It follows from Equation (3) that the conduction current in a cylindrical capillary of circular section is

$$i_2 = -\varkappa\pi a^2 \frac{\partial U}{\partial x}. \tag{8}$$

Assuming that the oscillation period of the liquid in the capillaries is much greater than the time required for establishment of the conduction current, and equating i_1 and $-i_2$ we have

$$\frac{\partial U}{\partial x} = \frac{\varepsilon\zeta}{4\pi\mu\varkappa}(\partial p/\partial x + \rho A)\,\Phi(k). \tag{9}$$

To examine the effect of pore shape on the expression for the streaming potential, we consider a slit capillary formed by plane parallel walls at a distance 2α apart, oscillating in phase in their own planes. Let the x axis lie in the middle between the planes in the direction of the oscillation of the capillary walls, and the y axis perpendicular to the wall planes. If the pressure gradient $\partial p/\partial x \cdot e^{i\omega t}$ exists in the capillary and the walls have acceleration $Ae^{i\omega t}$, then the velocity of the liquid relative to the capillary is [3]

$$v_1 = -\frac{\partial p/\partial x + \rho A}{i\omega\rho}\left\{1 - \frac{ch\left[\left(i\frac{\omega}{\nu}\right)^{1/2} y\right]}{ch\left[\left(i\frac{\omega}{\nu}\right)^{1/2} a\right]}\right\}. \tag{10}$$

We use (10) to find the convection current for a slit capillary of width d from Equation (4):

$$i_1 = -\frac{\varepsilon\zeta d}{2\pi}\cdot\frac{dv_1}{dy} = \frac{\zeta\varepsilon a d}{2\pi\mu}\left(\frac{\partial p}{\partial x} + \rho A\right)F(k), \tag{11}$$

where

$$F(k) = \frac{th(\sqrt{i}\,k)}{\sqrt{i}\,k}. \tag{12}$$

The conduction current for a region of the slit capillary is

$$i_2 = -\varkappa \frac{\partial U}{\partial x} 2ad. \tag{13}$$

Equating i_1 and $-i_2$ we have an expression for the streaming potential gradient in a slit capillary

$$\frac{\partial U}{\partial x} = \frac{\zeta r}{4\pi\mu\varkappa} (\partial p/\partial x + \rho A) F(k). \tag{14}$$

Equations (9) and (14) contain complex frequency functions. The moduli of the frequency functions characterize the decrease of the streaming potential with increasing oscillation frequency. The arguments of the frequency functions give the phase lag of the oscillations of the streaming potential gradient relative to oscillations of the pressure gradient and capillary acceleration. With decrease of the oscillation frequency to zero the amplitudes of the frequency functions tend to unity, and the phase lag tends to zero. The moduli and arguments of the functions Φ (k) and F (k) are shown graphically in Fig. 1. Analysis of these graphs shows that the functions Φ (2k) and F (k) virtually coincide. Therefore it may be approximately assumed that the frequency dependence for a slit pore with 2a distance between the walls is the same as for a cylindrical pore of circular section of radius 2a. Assume that for a pore of any chosen form we can find a radius a_e of an equivalent cylindrical pore of circular section such that the frequency function $\Phi\left(a_e\sqrt{\frac{\omega}{\nu}}\right)$ of the cylindrical pore virtually coincides with the frequency function of the random pore. It is shown below that this assumption is confirmed experimentally for pores in sand. We take the average value of Equation (9) per unit volume of an isotropic solid, and write it in vector form

$$\overline{\operatorname{grad} U} = \frac{\zeta\varepsilon}{4\pi\mu\varkappa} (\overline{\operatorname{grad} p} + \rho\vec{A}) \Phi\left(a_e\sqrt{\frac{\omega}{\nu}}\right). \tag{15}$$

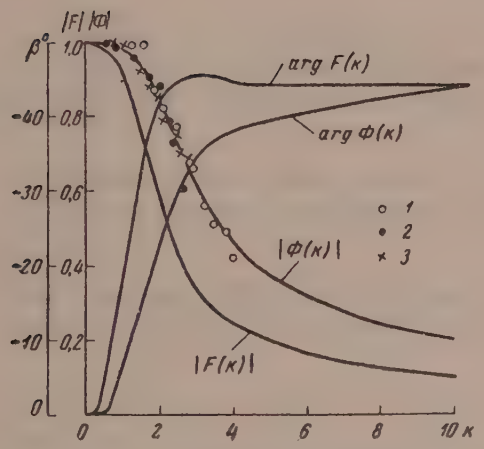


Fig. 1. Moduli and arguments of frequency functions for three sand samples: 1) Medium grain, $a_e = 7.9 \cdot 10^{-3}$ cm; 2 and 3) fine grain $a_e = 4.9 \cdot 10^{-3}$ and $a_e = 5.3 \cdot 10^{-3}$ cm.

If the framework of the porous body is stationary (A = 0) and the vibration frequency is low ($\omega \to 0$), then Equation (15) becomes the usual expression for streaming potential in steady-state filtration.

Streaming potentials at oscillating filtration rates were studied by means of the apparatus shown schematically in Fig. 2.

The design and operating principle of the apparatus are as follows. The rod of a GMK-1 mechanical vibrator carries a cell 1, made of transparent plastic, containing a sample of water-saturated sand. The sand sample is retained by plastic grids 2 and 3 to prevent displacement of the sand framework relative to the cell. Brass grids 4 and 5, which act as electrodes, are placed between the plastic grids and the sand. Polarization of these electrodes may be disregarded as the reactive component of the cell resistance is small relative to the input resistance of the amplifier used in the apparatus.

In order to prevent the formation of a horizontal pressure gradient in the pore water, the cell is provided with cavities 6 and 7, connected to the water in the pores through the grids 2 and 3, and communicating with the atmosphere. The cell is protected from magnetic and electric fields by the screen 8.

When the mechanical vibrator 10 is fed from the audio oscillator 9 (3G -10), the vibrator rod begins to oscillate horizontally. The GMK-1 vibrator contains a velocity converter which gives a voltage proportional to the velocity of the vibrator rod. This voltage, measured by means of the tube voltmeter 11 (MVL-2M), is used to find the amplitude $\underline{w}$ of the vibrator rod velocity. The acceleration amplitude of the cell mounted on the rod is found from the expression $A = \omega w$.

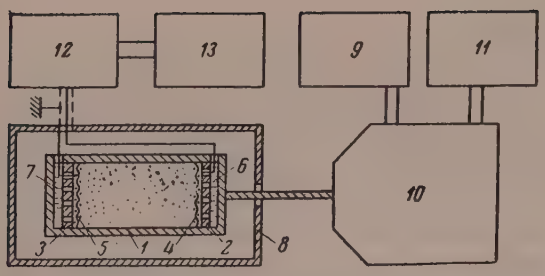


Fig. 2. Block diagram of apparatus for investigating streaming potentials with oscillating velocities of liquid flow.

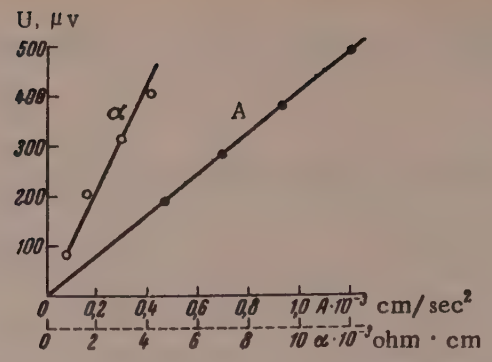


Fig. 3. Variations of streaming potential with acceleration of the sand framework (A) and resistivity of pore water (α).

The potential difference from the electrodes 4 and 5 is fed through a shielded cable to the amplifier 12, and is determined from the deviation of the beam on the screen of a cathode-ray oscillograph (ÉO-7) 13.

Since the sand framework is not displaced relatively to the cell, the acceleration amplitude of the framework is also A, and is constant along the cell. Denoting the distance between electrodes 4 and 5 as L, we use Equation (15) to find for the potential difference between them

$$U = \frac{\zeta\varepsilon}{4\pi\mu\varkappa} L\rho A\Phi\left(a_e\sqrt{\frac{\omega}{\nu}}\right). \qquad (16)$$

The highest value of the streaming potential $U_0 = \zeta\varepsilon L\rho A/4\pi\mu\varkappa$ in relation to the oscillation frequency will be found at $\omega \to 0$.

This apparatus was used for investigations of the dependence of streaming potential on the oscillation frequency of various samples of water-saturated sand. Analysis of the results showed that for each sample of sand a value of a_e can be found such that the experimental points, if plotted in U/U_0 and $a_e\sqrt{\omega/\nu}$ coordinates, fit on the theoretical curve $[\Phi(a_e\sqrt{\omega/\nu})]$ (Fig. 1).

The apparatus was used for investigating the dependence of the streaming potential on acceleration A of the sand framework and on the resistivity $\alpha = 1/\varkappa$ of the pore water at an oscillation frequency of 100 cps in the quartz sand framework.

The results are plotted in Fig. 3. It is seen in Fig. 3 that the streaming potential is proportional to acceleration of the sand framework and resistivity of the solution.* The experiments were performed with KCl solutions of various concentrations.

SUMMARY

1. An equation is derived for the streaming potential through a porous body at pressure and framework-acceleration gradients conforming to a harmonic oscillation law.

2. The streaming potential decreases with increasing oscillation frequency of the liquid velocity. This decrease is determined by the modulus of a complex frequency function. The argument of the frequency function gives the phase lag between oscillations of the streaming potential gradient and oscillations of the pressure gradient and acceleration of the framework of the porous body.

3. An apparatus was designed for measurement of streaming potentials at oscillating filtration velocities; this was used for investigating the dependence of streaming potentials on acceleration and oscillation frequency of the sand framework.

The author thanks B. F. Rel'tov for valuable comments on the work.

* Variations of the zeta-potential may be disregarded for the investigated range of values of α (Fig. 3).

LITERATURE CITED

1. A. G. Ivanov, Izvest. Akad. Nauk SSSR, Ser. Geogr. i Geofiz. 4, 699 (1940); Ya. I. Frenkel', Izvest. Akad. Nauk SSSR, Ser. Geogr. i Geofiz. 5, 133 (1944); M. S. Antsiferov, Doklady Akad. Nauk SSSR 121, 827 (1958).*
2. E. V. Hardway, Instruments, 26, (8), 1186 (1953); N. I. Shapirovskii, Trudy Azerb. N.-I. In-ta po Dobyche Nefti 4, 212 (1956).
3. M. A. Biot, J. Acoustical Soc. Am. 28, No. 2, 179 (1956).
4. H. R. Kruyt, Colloid Science [Russian translation] (IL, 1955), Vol. 1, p. 289.

*Original Russian pagination. See C. B. translation.

STABILITY MECHANISM OF FREE FILMS OF SOLUTIONS OF SURFACE-ACTIVE SUBSTANCES

B. V. Deryagin, A. S. Titievskaya, and V. Kh. Vybornova

Laboratory of Surface Phenomena, Institute of Physical Chemistry,
Academy of Sciences USSR, Moscow
Translated from Kolloidnyi Zhurnal, Vol. 22, No. 4, pp. 398-402,
July-August, 1960
Original article submitted March 11, 1960

The question of the stability mechanism of free films, considered as foam elements, is both complex and highly important for colloid chemistry. Investigations in this field have shown that in a number of cases the stability of free films is due to the action of repulsion forces which arise as the result of approach and overlapping of the ionic atmospheres on the two sides of a free film. An example is provided by our investigations of aqueous sodium oleate solutions [1]. In agreement with theory [2], increase in the concentration of NaCl added to these solutions diminishes the equilibrium thickness of the film.

In many instances decrease of free film thickness under the influence of added electrolytes leads to film rupture. However, this rule is not general, and it does not apply to films of sodium oleate, OT aerosol, OP-10, and other solutions. In these cases the film thickness tends to the limiting value of ~ 120 A with increase of electrolyte concentration; this value is independent of the pressure. To explain this it was postulated that the limiting thickness of a free film is the consequence of hydration of the adsorption monolayers by solvent molecules, leading to formation of multimolecular water layers with special properties.

Our method [3], which involves measurement of the thickness of free films formed between two bubbles pressed against each other in the solution under investigation, also allows observation of the course of film attenuation. Attenuation of free films of some of the substances investigated by us was filmed; individual frames are shown in Fig. 1 and 2. For example, in the case of sodium oleate solution with addition of 0.1 N sodium chloride (Fig. 1, a) a thick nonequilibrium free film is initially formed. When the thickness of this film reaches ~ 400 A as the result of attenuation, dark spots about 135 A thick appear at isolated points. These points gradually grow in size and numbers, and become round islets with thickness of the limiting value; they then coalesce and form a film of the final equilibrium thickness.

Attenuation in 0.1% solution of OP-10 + 0.6% NaCl proceeds analogously (Fig. 1, b). In the case of saponin solutions (Fig. 2) the course of attenuation is somewhat different. At first the film is of very irregular thickness, which is greatest at the center, as is shown by the presence of Newton's rings in the film. Two or three minutes after formation of the film dark spots appear at its extreme edges. These spots then grow and also become rounded islets of the limiting thickness. These islets displace excess liquid in the course of growth; sometimes the excess liquid remains in the center of the film.

For further clarification of the nature of the forces which determine the stability of free films the effect of temperature on film thickness and stability was studied. An apparatus was designed whereby measurements could be made on free films while the temperature of the solution was varied from room temperature (17-18°) to 80°.

The apparatus was made of quartz glass; we found earlier that ordinary and even Jena glass is leached out and contaminates the solution under test. The apparatus is shown schematically in Fig. 3, where A is a vessel

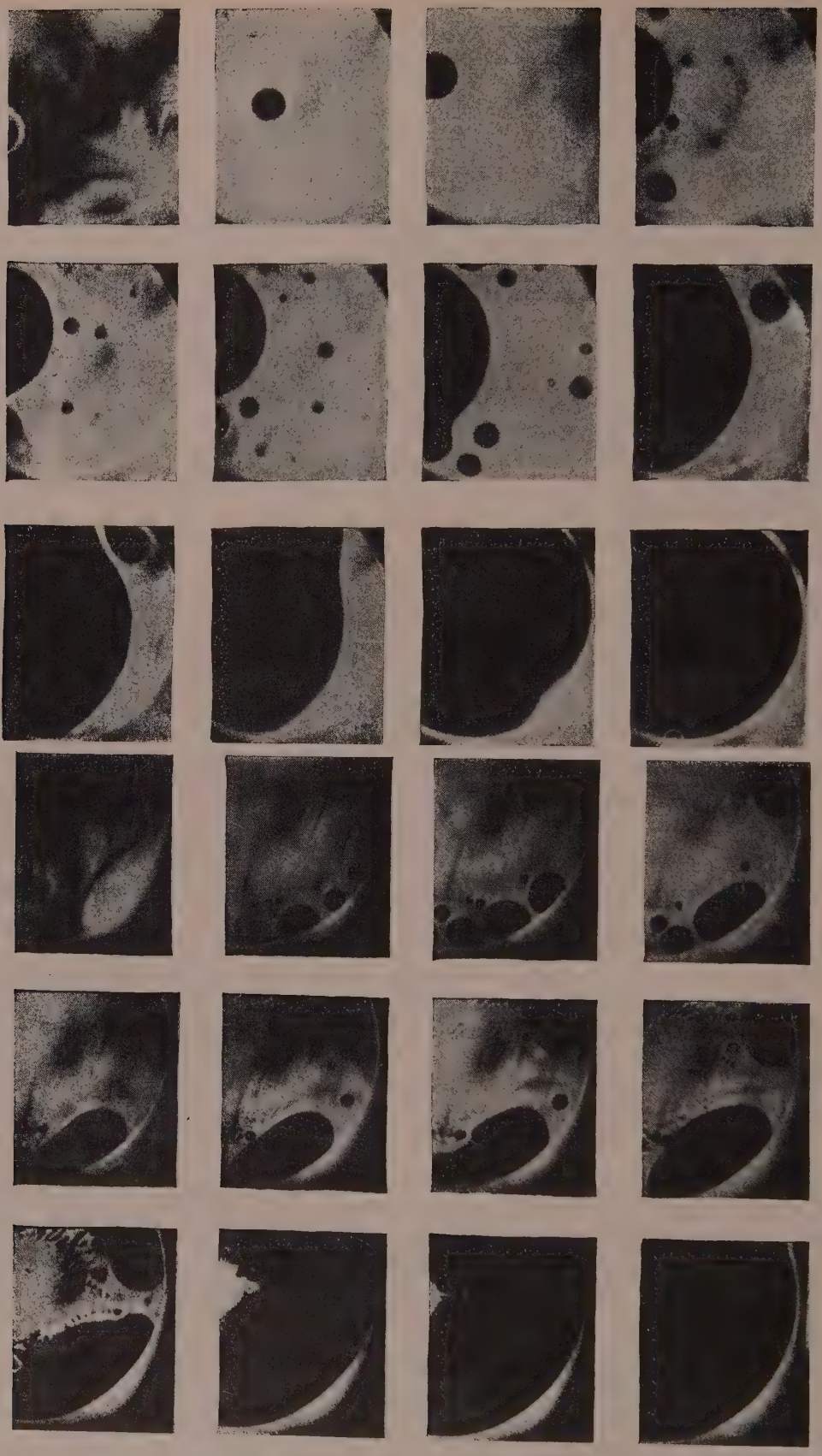


Fig. 1. High-speed photomicrographs of attenuation of free films: a) 0.01 N sodium oleate solution + 0.1 N NaCl; b) 0.1% solution of OP-10 and 0.1 N NaCl.

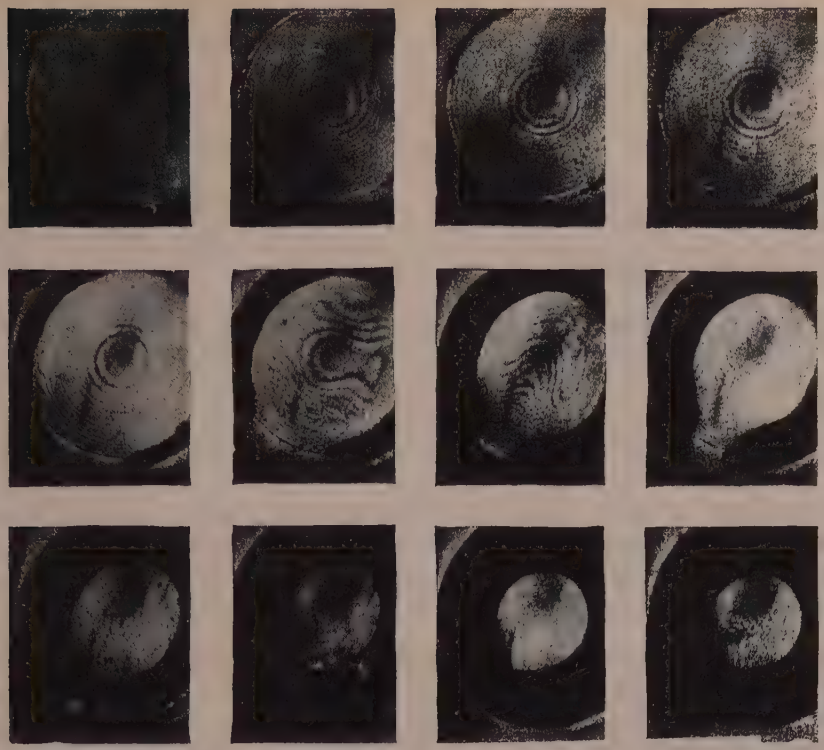


Fig. 2. High-speed photomicrographs of attenuation of a free film from 0.1% solution of saponin + 1 N NaCl.

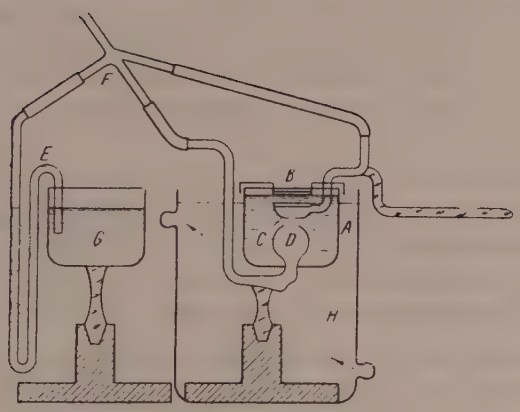


Fig. 3. Diagram of the apparatus.

with the solution. The pressure into the bubbles pressed out of the orifices C and D is applied through the three-way joint F and measured by means of the manometer E as described earlier [3], but with the difference that the manometer tip is immersed in an auxiliary vessel G filled with the same solution. After the apparatus has been filled with the solution it is covered by the lid B with an inspection window, in order to prevent evaporation of the solvent. The behavior of the free film is observed through the window with the aid of a microscope. The apparatus is stood on a metal support in the vessel H; water is circulated in this vessel at the required temperature from a thermostat. A stream of warm air is directed onto the lid of the apparatus in order to prevent cooling of the top layer of solution. The temperature of the air stream is roughly the same as that of the thermostat. The thickness of the free film is measured by means of a microscope with a photometric attachment, from the intensity of the reflected light.

The following solutions were investigated:

1. Sodium oleate, 10^{-3} N, with additions of sodium chloride solutions of various concentrations (from 0.001 to 0.1 N).

2. 0.1% solution of OP-10 (polymeric condensation product of ethylene oxide with alkylated phenol), with addition of 0.01 N sodium chloride.

3. 0.05% solution of the nonionic agent DB (polyoxyethylene ether of di-tert-butylphenol) with addition of 0.01 N sodium chloride.

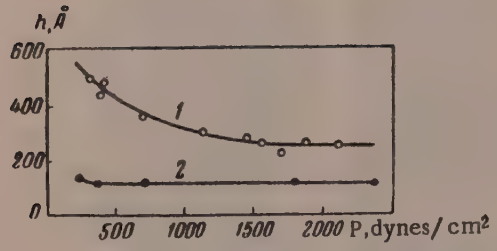


Fig. 4. Isotherm for disjoining pressure of free films of 0.001 N sodium oleate + + 0.001 N NaCl. 1) T = 22.5-23.5°; 2) T = 50°.

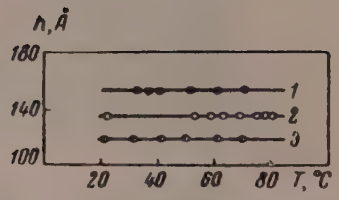


Fig. 5. Effects of temperature on thickness of free films. 1) 0.1% OP-10 with 0.01 N NaCl; 2) 0.1 N sodium oleate with 0.001 N NaCl; 3) 0.05% DB with 0.01 N NaCl.

Repeated measurements of the thickness of free films of 0.001 N sodium oleate with addition of 0.001 N sodium chloride showed that increase of temperature to 45-50° reduces the free film thickness (Fig. 4). However, film stability is not destroyed even at 80°. Curve 2 in Fig. 5 represents the effect of temperature on free film thickness at constant pressure, 284 dynes/cm^2, for 0.1 N sodium oleate solution.

Measurements on 0.05% DB solution with 0.01 N sodium chloride showed that the free film thickness is independent of temperature in the range of 22.2 to 70.1° (Fig. 5, curve 3). The conductivity of 0.05% DB solution was found to be $6.2 \cdot 10^{-6}$ Ω^{-1}; this indicates absence of electrolytes. Earlier we showed that the free film thickness of DB solutions is independent of the added electrolyte concentration; this is evidently associated with the fact that DB is nonionic and cannot charge the film surface, so that the disjoining pressure which arises in its presence is not due to electrostatic repulsion of ionic atmospheres.*

Measurements on free films of 0.1% OP-10 solution with addition of 0.01 N sodium chloride showed that the free film thickness is quite independent of temperature between room temperature and 80°; this is represented by curve 1 in Fig. 5, for a constant pressure of 480 dynes/cm^2. The agent OP-10 is a technical product and contains electrolytes which apparently lead, even in absence of other added electrolytes, to compression of the ionic atmospheres and decrease of free film thickness to the critical value.

Our investigations of the attenuation of free films of sodium oleate and certain other substances indicate that free films in the thickness range between 150 and 400 A are extremely unstable and that stable multimolecular "hydration" layers are separated from the rest of the liquid volume by a sharp boundary. This suggests that these water layers, several tens of molecules thick, differ in structure from the liquid volume—this assumption was put forward earlier to account for multimolecular adsorption of water vapor on smooth hydrophilic surfaces [4].

The fact that, after abrupt attenuation, the remaining limiting film at once acquires a final and completely uniform thickness, which depends little on pressure or temperature, proves quite conclusively that the stability and thickness of the observed films cannot possibly be explained in terms of their mechanical properties, such as the yield value θ due to the structure which arises in the film. Indeed, the speed of the abrupt attenuation indicates that the part of the liquid which is pressed out in the process is devoid of such properties. As regards the surface layers of thickness $h \sim 120$ A/2, which then come in contact, it is easy to calculate what yield value they must have in order to withstand the suction effect of the capillary meniscuses for a long time.

Such a calculation was performed in detail [5] on the basis of capillary rheology equations, which yielded the formula:

$$h = 26{,}0 \ldots R_1^3 \frac{\theta^2}{\sigma^2} = 3{,}25 \ldots R^3 \frac{\theta^2}{\sigma^2},$$

*However, in absence of added electrolyte the equilibrium thickness was reached much more slowly, and therefore the data plotted in curve 3, Fig. 5 were determined in presence of 0.01 N NaCl.

where h is the thickness of the layer not pressed out; R is the bubble radius; * σ is the surface tension; hence we have:

$$\theta = 0{,}56 \ldots \sigma h^{1/2} R^{-3/2} .$$

Multiplying these values of θ by h/2 we find that the two-dimensional shearing stress θ_1 is

$$\theta_1 = 0{,}28 \ldots \sigma (h/R)^{3/2};$$

putting $\sigma \sim 30$ dynes/cm^2; $h \sim 10^{-6}$ cm; $R \sim 10^{-2}$ cm, $R \sim 10^{-2}$ cm, we have $\theta_1 \sim 10^{-5}$. With this value θ_1 should have a noticeable influence in measurements of surface viscosity at solution—air interfaces; this is not found to be the case for DB, OP-10, and sodium oleate.

A mechanical interpretation of the thickness and stability of limiting films must therefore be rejected; they must be attributed to the existence of true (metastable) thermodynamic equilibrium between capillary pressure and repulsion forces (disjoining pressure), which are functions of film thickness.

SUMMARY

1. The thickness of free films of sodium oleate at low electrolyte concentrations decreases with rise of temperature, but the films retain stability.

2. Increases of electrolyte concentration in an aqueous solution of a surface-active substance causes compression of the ionic atmospheres and thereby either destroys the stability of free films or reduces their thickness to about 110-140 A, which is very constant (it depends little on pressure and is independent of further increase of electrolyte concentration or of the temperature).

3. In presence of the nonionic surface-active agent DB the film thickness is $\sim$ 120 A even at very low electrolyte concentrations; this is evidently the consequence of absence of charge on the film surface, and consequent absence of ionic atmospheres. In this case the sole cause of film stability and disjoining pressure, which prevents further attenuation of the film, can be interaction of the adsorbed monolayers with adjacent water layers 10-20 molecules thick by means of forces which are insensitive to temperature.

4. It is reasonable to attribute to such forces also the existence of "limiting" free films (110-140 A thick) observed with ionic surface-active substances in presence of NaCl up to 0.1 N concentrations.

5. The experimental results indicate that boundary water layers $\sim$ 30-40 A thick situated at the surface of the adsorption monolayers differ in structure from the main volume of the liquid, from which they are separated by a sharp boundary. Instability of free films in the intermediate thickness range of 120-300 A can be attributed to incomplete wetting, because of this structural difference, of these boundary layers by thicker layers.

6. Despite the fact that the mechanical properties of adsorbed layers of saponin and other surface-active substances differ very greatly, the course of attenuation of free films and the thicknesses of the limiting (most stable) layers are similar for all the substances studied. This indicates that the mechanical properties of adsorption layers cannot account for the observed results. Calculations also show that the yield values necessary to account for the observed thickness without the participation of repulsion forces (disjoining pressure) are greater by several orders of magnitude than the permissible values.

LITERATURE CITED

1. B. V. Deryagin and A. S. Titievskaya, Discussions of the Faraday Society No. 18, 32 (1954).
2. B. V. Deryagin and M. M. Kusakov, Izvest. Akad. Nauk SSSR, Ser. Khim. 5, 1119 (1937); V. B. Deryagin, M. M. Kusakov, and L. S. Lebedeva, Doklady Akad. Nauk 23, 670 (1939); M. M. Kusakov and A. S. Titievskaya, Doklady Akad. Nauk SSSR 83, 4 (1940); Acta Phys. Chim. URSS 10, 25 (1939); 10, 153 (1939).
3. B. V. Deryagin and A. S. Titievskaya, Kolloid. Zhur. 15, 417 (1953); Doklady Akad. Nauk SSSR 89, 2041 (1952); Discussions of the Faraday Society No. 18, 24 (1954).

*R_1 is the radius of the meridional section of the bubbles near the perimeter of the film separating them. In [5] (III, 58) R is printed in error instead of R_1.

4. B.V. Deryagin and Z. M. Zorin, Doklady Akad. Nauk SSSR 98, 93 (1954); Zhur. Fiz. Khim. 29, 1009, 1755 (1955).
5. B. V. Deryagin and S. M. Levi, Physical Chemistry of the Application of Thin Layers onto Moving Supports [in Russian] (Izd. AN SSSR, 1959) p. 42.

INVESTIGATION OF THE PHYSICAL ADSORPTION OF WATER ON SILICA GEL WITH A HYDRATED SURFACE BY INFRARED SPECTROSCOPY

A. V. Kiselev and V. I. Lygin

Institute of Physical Chemistry, Academy of Sciences, USSR
Chemical Faculty, M. V. Lomonosov Moscow State University
Translated from Kolloidnyi Zhurnal, Vol. 22, No. 4, pp. 403-410,
July-August, 1960
Original article submitted May 21, 1959

In addition to the usual adsorption and calorimetric methods, which give the integral characteristics of the adsorption process, increasing use is being made in adsorption studies of infrared spectroscopy, whereby it is possible to study elementary events in adsorptional interaction between adsorbed molecules and surface chemical groups of adsorbents. Infrared spectroscopy was first applied to adsorption studies by Terenin et al., [1-4], and was subsequently developed by them. In recent years there has been an increasing number of spectroscopic investigations of adsorption abroad [5-17]. Most of the studies were concerned with adsorption of water [1-7, 12, 14-17], usually effected on silicas with partially dehydrated surfaces as the result of vacuum high-temperature treatment [1-4], or as the result of the method used for preparation of the silica itself [12, 16]. It is difficult to interpret the spectral manifestations of the interaction of water with various surface groups of such silicas, because in such cases physical adsorption is accompanied by chemisorption, and this leads to regeneration of the surface hydroxyl layer. Because of this, spectroscopic data have given rise to contradictory conclusions concerning the mechanism of water adsorption [1, 3, 4, 16], and some of these were inconsistent with adsorption data [12, 18, 19].

The present paper is concerned with an infrared spectroscopic study of water adsorption on a fully hydrated silica gel surface, in the regions of both valence and deformational vibrations of hydroxyl groups in water. This work was a continuation of research into the structure of hydroxyl layers on silica surfaces with the aid of infrared absorption spectra [20-22].

The Adsorbent. We used KSK-2 coarse-pored silica gel, the adsorption properties of which were studied earlier [23]. Surface water was removed by evacuation of the silica gel for at least 6 hr at 10^{-4} mm Hg and 200°.

The reversible nature of water adsorption isotherms for silica gel evacuated in this manner [23] indicates that its surface is fully hydrated. The surface hydroxyl groups were then deuterated [3, 6, 16, 22]; for this, D_2O vapor was repeatedly admitted into the cell containing the sample (Fig. 1), and the sample was then evacuated at 200°. The spectra were photographed 1 hr after admission of D_2O vapor.

The spectroscopic method was used to study not only the state of the hydroxyl surface layer on the silica gel, but also the state of the adsorbed molecules of ordinary and heavy water in monolayer coverage (at relative water vapor pressure $p/p_s \approx 0.25$ [23]) and under conditions of capillary condensation ($p/p_s \approx 1$).

The object for the spectroscopic determination was placed in a vacuum cell [24] (Fig. 1) of molybdenum glass. The cell has two openings with NaCl windows 1, attached by BF-2 cement, to transmit infrared radiation. A tube 3 is inserted into the upper part of the cell through the ground-glass joint 2. An aluminum tube 4, with sample holder 5 and a cavity for the windows 6 between which the sample is gripped, is fixed on the tube by

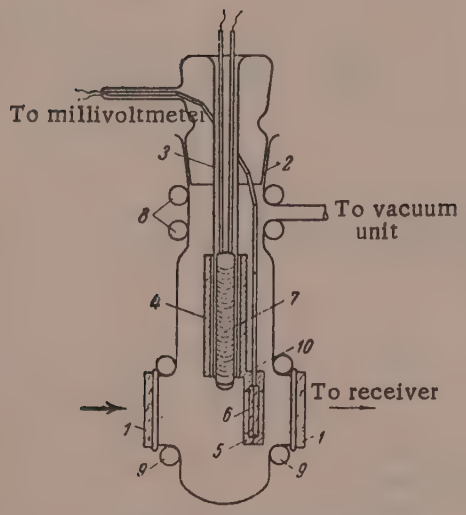


Fig. 1. Cell for spectroscopic study of adsorption.

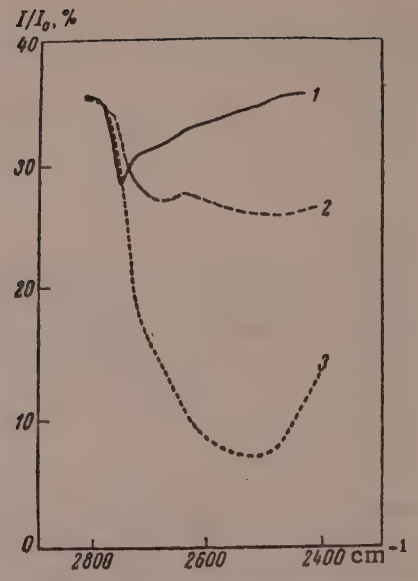


Fig. 2. Infrared spectra of deuterated silica gel after evacuation at 200° (1), after monolayer adsorption of water molecules (2), and after sorption of water under conditions of capillary condensation (3).

means of a groove joint. The holder is displaced sideways to the tube axis; it is thus possible, by a turn of the ground-glass joint, to move the sample away from the radiation beam and to take the spectrum of the radiation or of the gas in the cell. The sample is heated by means of the heater 7 in the tube 3. The temperature is regulated by variation of the heater voltage. For low-temperature determinations the tube of the cell was filled with liquid nitrogen or freezing mixture in order to cool the sample. Corrugated copper tubes 8,9 were fixed to the cell body; water was circulated through these in order to reduce heating of the joint 2 and windows 1 when the sample was heated. If the sample was cooled, warm water was passed through the tube 9 to prevent water condensation on the cell walls. The temperature of the sample was measured by the thermocouple 10, inserted in an opening in the holder in immediate proximity to the sample. The cell is rigidly fixed in front of the spectrometer slit and attached to a vacuum unit.

The spectra were determined, as before [22, 25], with a single-beam infraredspectrometer IKS-12 with a LiF prism in the region of valence vibrations of the hydroxyl groups in H_2O (3800-3000 cm^{-1}) and D_2O (2800-2200 cm^{-1}) and with a NaCl prism in the region of H_2O deformational vibrations (1700-1500 cm^{-1}). The deformational vibrations of D_2O are superposed on a strong absorption band of the silica framework at 1000-1200 cm^{-1} and do not appear in the spectrum [22]. Dry nitrogen was blown through the jacket of the monochromator and light source to eliminate absorption of infrared radiation by atmospheric moisture. A fine silica gel powder fraction (< 0.5 μ), obtained by sedimentation in water, was used in order to reduce scattering. A thin layer of powder was spread between two NaCl plates fixed in the holder 5 (Fig. 1). Nevertheless, scattering of infrared radiation by a sample prepared in this way is considerable, and transmission in the 3700 cm^{-1} region was < 20%. Scattering is considerably less in the long-wave region, and transmission in the region of valence vibrations of OD groups at 2700 cm^{-1} is 35%. The spectral slit width is 8 cm^{-1} in the 3750 cm^{-1} region, and 5 and 10 cm^{-1}, respectively, in the 2600 and 1600 cm^{-1} regions.

In the region of valence vibrations of the hydroxyl groups in deuterated silica gel, owing to absence of strong scattering and absorption of radiation by atmospheric moisture, variations in the nature of the spectrum during adsorption of water are clearly observed. The spectrum of deuterated silica gel evacuated at 200° (Fig. 2, curve 1) contains a sharp band at 2760 cm^{-1} with asymmetrical absorption on the long-wave side. Adsorption of D_2O at $p/p_s \approx 0.25$ (monolayer coverage of the surface [23, 26]) leads to a considerable weakening of the 2760 cm^{-1} band and appearance of new broad bands at 2680 and 2500 cm^{-1} (Fig. 2, curve 2). The spectrum of deuterated silica gel after adsorption of D_2O at $p/p_s \approx 1$ (Fig. 2, curve 3) has one broad band with a maximum at 2500 cm^{-1}. In the region of valence vibrations of OH groups, variations of the silica gel spectrum as the result

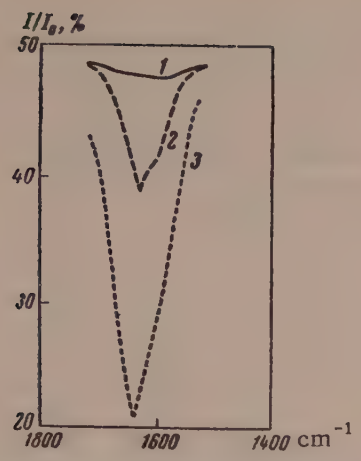


Fig. 3. Infrared spectra of the original silica gel after evacuation at 200° (1), after monolayer adsorption of water molecules (2), and after sorption of water under conditions of capillary condensation (3).

of adsorption of water cannot be observed as distinctly, owing to strong scattering of radiation by the sample and the presence of absorption bands due to atmospheric moisture. However, the general nature of the spectral variations is the same in this case as in adsorption of heavy water on deuterated silica gel (Fig. 2).

There is no appreciable absorption in the region of deformational vibrations of hydroxyl groups in water in the spectrum of the original silica gel evacuated at 200° (Fig. 3, curve 1). The spectrum of silica gel after adsorption of water at $p/p_s \approx 0.25$ (Fig. 3, curve 2) contains a band with a maximum at 1620 cm^{-1}. Water sorbed by silica gel at $p/p_s \approx 1$ gives an absorption band at 1640 cm^{-1} (Fig. 3, curve 3).

Structure of the Hydroxyl Surface Layer on Silica Gel. It has been shown [27] that silica gel dried at 150-200° contains hydroxyl groups linked chemically to the silica framework. In earlier spectroscopic studies of adsorption [1-3] and also in [12] it was concluded that such hydroxyl groups are freely distributed over the silica surface. The observed asymmetry of the absorption bands on the long-wave side, even after evacuation at 500°, was attributed to presence of adsorbed water molecules on the surface [3, 4], or to the Christiansen effect [12]. However, absorption in the long-wave portion of the hydroxyl absorption band in silica gel cannot be attributed to adsorbed water molecules because first, the results of calorimetric, thermal, and adsorption analyses and dehydration experiments [14, 21, 23, 26-29] indicate that adsorbed water is removed completely from silica gel during prolonged evacuation at 200° and second, because the spectrum of the original silica gel evacuated at 200° (Fig. 3, curve 1) does not reveal any appreciable absorption in the region of deformational vibrations of water molecules; this indicates that physically adsorbed water is completely removed by such treatment. Equally, asymmetry of the band cannot be attributed to formation of a Christiansen filter, because hydroxyl group absorption bands of this type are found in spectra of powdered silicas in petrolatum [16, 20], in which the Christiansen scattering effect cannot occur in the same spectral region.

The sharp absorption bands due to valence vibrations of OH and OD groups at 3750 and 2760 cm^{-1} can be attributed to "free" surface hydroxyl groups at considerable distances apart, and absorption in the longer-wave region of the band to surface hydroxyl groups which are in close proximity and favorable orientation, and therefore joined by intramolecular hydrogen bonds [20-22]. Our analysis of the structure of the surface hydroxyl layer on silicas, with data on the average surface concentration of hydroxyl groups taken into account [21, 22], confirms the possibility of intramolecular hydrogen bonding between some of the hydroxyl groups in close proximity to each other. This view of the structure of the surface hydroxyl layer on silicas has now been accepted [4, 13, 16].

The relative proportions of free and bound surface hydroxyl groups differ for silicas prepared by different methods. In crystalline silicas in which the structure of the oxygen–silicon framework is of a high degree of order interaction between surface hydroxyl groups is improbable [16]. In the case of silica gel the random packing of the silicon-oxygen tetrahedrons in the surface layer, and the consequent varying orientation of the surface hydroxyl groups, are more favorable for intramolecular hydrogen bonding between some of the neighboring hydroxyls. The process of silica gel formation by condensation of silicic acid [26, 27] itself favors formation of bound hydroxyl groups on the surfaces of the globules constituting the silica gel skeleton [30].

Mechanism of Water Adsorption on Silica Gel with a Hydrated Surface. The form of interaction of adsorbed water molecules with silica gel surface groups can be deduced, on the one hand, from changes in the absorption spectrum of the surface hydroxyl groups of the silica gel and from the appearance of a new band due to surface hydroxyl groups influenced by adsorbed water molecules. On the other hand, it can be deduced from changes in the spectrum of the adsorbed water molecules themselves, in comparison with their spectrum in the gaseous state. Interpretation of spectra obtained during adsorption of water is rather difficult because of the proximity of the absorption bands due to valence vibrations of hydroxyl groups in silica gel and water, respectively (see table). In all spectroscopic investigations, apart from [15, 17], conclusions are drawn concerning the character

Comparison of Vibration Frequencies (cm^{-1}) of Hydroxyl Groups

Type of vibration	Surface groups in silica gel	Water			
		vapor [32]	adsorbed in monolayer	capillary condensation	liquid [32]
Fundamental frequency of OD valence vibration	2760	2789	2680	2500	2510
Fundamental frequency of H_2O deformational vibration	—	1595	1620 ± 5	1640 ± 5	1640

of water adsorption only from changes in the valence vibrations of the hydroxyl groups, and changes of deformational vibrations in adsorbed water molecules are not considered. As already noted, the observed changes in the spectrum are not correlated with the degree of surface covered by the adsorbed molecules, and the degree of hydration of the silica surface is not taken into account. Conclusions concerning the mechanism of water adsorption on silicas, drawn from spectroscopic studies, must therefore be considered critically, especially as all the conclusions concerning the existence of secondary (nonhydroxyl) active adsorption centers [3, 4, 13] are based on the persistence, after evacuation, of the absorption bands which reappeared after adsorption of water; however, they can be interpreted as absorption bands due to hydroxyl groups regenerated on the surface, since adsorption experiments indicate that water is chemically sorbed on the surface of silica evacuated at high temperatures [23, 26, 29, 31].

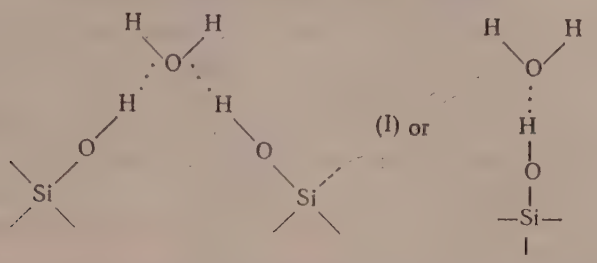
Taking all this into consideration, and wishing to prevent chemisorption of water during determination of the spectra, we investigated the adsorption of water on silica gel which is fully hydrated as far as possible, but freed from adsorbed water.

The spectrograms (Fig. 2, curve 2) show that on monomolecular adsorption of heavy water the intensity of the band due to free hydroxyl groups in deuterated silica gel is greatly diminished, and new bands appear at 2680 and 2500 cm^{-1}. Weakening of the absorption band due to structural hydroxyl groups in silica gel on adsorption of water is the result of their interaction with adsorbed water molecules; this is consistent with the results of spectroscopic studies of water adsorption [12, 16], and with investigations of adsorption [21, 23, 26, 29, 31].

The 2680 cm^{-1} band lies between the absorption bands due to valence vibrations of hydroxyl groups in water molecules in the gaseous and liquid states, respectively (see table), and is therefore attributable to hydroxyl groups more perturbed than the structural hydroxyl groups of the silica surface and of water in the gaseous state, but much less perturbed than water molecules in the liquid state. This fact is generally used as the basis for interpreting these bands as absorption bands due to adsorbed water molecules [3, 4]. The broad band at 2500 cm^{-1}, due to the monomolecular layer of adsorbed water, in the spectrum of deuterated silica gel (Fig. 2, curve 2) lies in the absorption region of liquid water and may be ascribed to hydroxyl groups in silica gel linked by hydrogen bonds to adsorbed water molecules. Absorption in this region cannot be caused by molecules of water in a state of capillary condensation, since the spectra in Fig. 2 (curve 2) refer to cover with only a monolayer of water, and possibly even less than a monolayer, because the sample is heated by infrared radiation. The position of the absorption band due to deformational vibrations of adsorbed water molecules under these conditions (Fig. 3, curve 2) indicates the absence of a liquid phase, since this band differs in position from the absorption band due to liquid water. A difference between the positions of the absorption bands due to deformational vibrations of liquid water molecules and water molecules adsorbed on hydrated silica gel surfaces with less than monolayer cover was also found in [17]. The absorption band due to deformational vibrations of adsorbed water under conditions of capillary condensation is close to the absorption band for liquid water.

It therefore follows from spectroscopic investigations in conjunction with adsorption data that adsorption of water on a fully hydrated silica gel surface occurs at surface hydroxyl groups and that hydrogen of these hydroxyl groups is involved in formation of hydrogen bonds with oxygen of the adsorbed water molecules.

However, it cannot yet be decided from spectroscopic data by which of the possible mechanisms, such as [21],



(II)

water is adsorbed. This would require further investigation, with quantitative determinations of band intensities with known amounts of hydroxyl groups on the silica gel surface and known numbers of adsorbed water molecules per hydroxyl group.

A subject of current interest is calculation of adsorption equilibria based on adsorbate and adsorbent properties only; this reduces to calculations of standard free energies or entropies and heats of adsorption [33]. In investigations of adsorption by the methods of statistical thermodynamics [34] more or less arbitrary assumptions are usually made about the state of the adsorbed substance, and the calculated theroretical values are compared with experimental data in order to assess the validity of the assumptions made concerning the nature of molecular movement in the adsorption layer. However, the same experimental value of entropy may correspond to different arbitrarily chosen states of the adsorbate. It would be better, on the basis of independent methods, to establish a model of the adsorption complex and the possible degrees of freedom of an adsorbed molecule in this complex, and to calculate the thermodynamic characteristics for these. The spectroscopic method offers great potentialities in this respect.

However, spectroscopic investigations in this direction involve considerable experimental difficulties. The published spectroscopic investigations now available give information, far from complete and requiring further verification, on the states of a very limited number of molecules in the adsorption layer. We hope in the future to carry out investigations in order to determine the spectral characteristics necessary for statistical calculations of the thermodynamic functions of adsorbed substances.

SUMMARY

1. The infrared spectra of water adsorbed in a monolayer on silica gel, and under conditions of capillary condensation, were investigated in the valence and deformation vibrations of hydroxyl groups.

2. Weakening of the absorption band due to silica gel hydroxyl groups in monolayer coverage, and the simultaneous appearance of a broad band in the region of absorption of hydroxyl groups perturbed by hydrogen bonds, indicate hydrogen bonding between adsorbed water molecules and hydroxyl groups of silica gel. The hydroxyl groups in silica gel with a fully hydrated surface can therefore be regarded as the main centers for physical adsorption of water. The observed difference between the position of the absorption bands corresponding to deformational vibrations of water molecules in a monolayer and under conditions of capillary condensation, respectively, is consistent with this adsorption mechanism.

3. The possible applications of infrared spectroscopy in studies of thermodynamic properties of adsorption systems are considered.

The authors thank N. N. Kavtaradze for cooperation in this work, and G. V. Kazakova for assistance.

LITERATURE CITED

1. A. N. Terenin, Zhur. Fiz. Khim. 14, 1362 (1940); L. N. Kurbatov and G. G. Neuimin, Doklady Akad. Nauk SSSR 68, 341 (1949); N. G. Yaroslavskii, and A. N. Terenin, Doklady Akad. Nauk SSSR 66, 885 (1949); Zhur. Fiz. Khim. 24, 68 (1950); N. G. Yaroslavskii and A. V. Karyakin, Doklady Akad. Nauk SSSR 85, 1103 (1952); V. N. Filimonov, Optika i Spektroskopiya 1, 490 (1956).

2. A. N. Sidorov, Doklady Akad. Nauk 95, 1235 (1954).
3. V. A. Nikitin, A. N. Sidorov, and A. V. Karyakin, Zhur. Fiz. Khim. 30, 117 (1956).
4. A. N. Sidorov, Zhur. Fiz. Khim. 30, 995 (1956); Opt-Mekh. Prom. 1, 1 (1959).
5. A. Chevet, J. Phys. et. rad. 14, 493 (1953).
6. G. C. Pimentel, C. W. Garland, and G. Jura, J. Amer. Chem. Soc. 75, 803 (1953).
7. J. E. Mapes and R. P. Eischens, J. Phys. Chem. 58, 1059 (1954).
8. R. P. Eichens, W. A. Pliskin, and S. A. Francis, J. Chem. Phys. 22, 1786 (1954); R. O. French, M. E. Wadsworth, M. A. Cook, and B. Cutler, J. Phys. Chem. 58, 805 (1954).
9. T. Yoshino, J. Chem. Phys. 23, 1564 (1955).
10. D. I. C. Yates, N. Sheppard, and C. L. Angel, J. Chem. Phys. 23, 1980 (1955).
11. G. Karagounis and O. Peter, Z. Electrochem. 61, 827, 1094 (1957).
12. R. McDonald, J. Amer. Chem. Soc. 79, 850 (1958).
13. M. Folman and D. I. C. Yates, Proc. Roy. Soc. A 246, 32, (1958); Trans. Faraday Soc. 54, 11 (1958); J. Phys. Chem. 63, 183 (1959).
14. C. I. Young, J. Colloid. Sci. 13, 67 (1958).
15. G. L. Kington, in: The Structure and Properties of Porous Materials (London, 1958) p. 247; G. J. Fronsdorff and G. L. Kington, Proc. Roy. Soc. A 247, 469 (1958).
16. R. Mc Donald, J. Phys. Chem. 62, 1168 (1958).
17. H. A. Benesi and A. C. Jones, J. Phys. Chem. 63, 179 (1959).
18. S. P. Zhdanov, Zhur. Fiz. Khim. 32, 699 (1958).
19. A. N. Sidorov and V. A. Nikitin, Zhur. Fiz. Khim. 32, 1667 (1958).
20. A. V. Kiselev and V. I. Lygin, Proceedings of the Second International Congress on Surface Activity (London, 1957) vol. 2, p. 204; V. I. Lygin, Vestnik Mosk. Un-ta 1, 223 (1958).
21. A. V. Kiselev, in: The Structure and Properties of Porous Materials (London, 1958) p. 195.
22. A. V. Kiselev and V. I. Lygin, Kolloid. Zhur. 21, 581 (1959).*
23. L. D. Belyakova, O. M. Dzhigit, and A. V. Kiselev, Zhur. Fiz. Khim. 31, 1577 (1957); L. D. Belyakova and A. V. Kiselev, Doklady Akad. Nauk SSSR 119, 298 (1958);* Zhur. Fiz. Khim. 33, 2624 (1959).
24. N. N. Kavtaradze and V. I. Lygin, Zhur. Fiz. Khim. 34, 462 (1960).
25. V. I. Lygin, N. V. Kovaleva, N. N. Kavtaradze, and A. V. Kiselev, Kolloid. Zhur. 22, 334 (1960).*
26. A. V. Kiselev, collection: Surface Chemical Compounds and Their Role in Adsorption Phenomena [in Russian] (Izd. MGU, 1957) p. 90.
27. A. V. Kiselev, Kolloid. Zhur. 2, 17 (1936).
28. E. A. Hauser and D. S. Le Beau, J. Phys. Chem. 56, 136 (1952).
29. A. V. Kiselev and G. G. Muttik, Kolloid. Zhur. 19, 562 (1957).*
30. A. V. Kiselev, V. I. Lygin, I. E. Neimark, M. B. Slinyakova, and Chen Wen-hang, Kolloid. Zhur. 20, 52 (1958).*
31. S. P. Zhdanov, Doklady Akad. Nauk SSSR 100, 1115 (1955); 115, 938 (1957);* 120, 103 (1958).*
32. G. Herzberg, Vibrational and Rotational Spectra of Polyatomic Molecules [Russian translation] (Izd. INI, 1949) p. 305.
33. A. A. Isirikyan, A. V. Kiselev, I. A. Lygina, and D. P. Poshkus, Izvest. Akad. Nauk SSSR, Otdel. Khim. Nauk 11, 1312 (1957);* A. V. Kiselev and D. P. Poshkus, Doklady Akad. Nauk SSSR 132, 876 (1960).*
34. C. Kemball, in: Catalysis; Theory and Methods of Investigation [Russian translation] (IL, 1955) p. 256.

*Original Russian pagination. See C. B. translation.

STUDY OF THE NATURE OF FORMS OF MOISTURE BINDING IN GELATIN AND PHOTOGRAPHIC EMULSIONS BY INFRARED SPECTROSCOPY

L. A. Lepilkina

Institute of Physical Chemistry, Academy of Sciences, USSR, Moscow
Moscow Technological Institute of the Meat Industry
Translated from Kolloidnyi Zhurnal, Vol. 22, No. 4, pp. 411-417,
July-August, 1960
Original article submitted May 12, 1959

When photographic gelatin and photographic emulsions containing various amounts of silver are dried, the structures of these materials undergo complex changes which lead to changes in their structural, mechanical, and physicochemical characteristics which are dependent on the type of binding between moisture and the material.

The main distinction between different forms of moisture binding lies in the energy of binding between moisture and the material [1]. If the transition boundaries between these types of water binding during drying are established and the nature of such binding in photographic materials is investigated, it becomes possible to select the drying method and optimum drying conditions. The use of various methods for studying the transition boundaries between different types of water binding in the course of drying showed that the most sensitive method is based on determinations of electrical characteristics.

In the present investigation the electrical characteristics of photographic gelatin and emulsions were studied by means of the KV-1 Q-meter in the frequency range from 50 kc to 25 Mc per second.

1. In Fig. 1 the dielectric loss factor of photographic gelatin during drying is plotted against the moisture content. It is seen that the curve for gelatin has three extremal points, the first of which corresponds to 50-60% moisture content. Analysis of the variants of other physical characteristics (coefficient of temperature gradient, coefficient of moisture conductivity, structural and mechanical properties) indicates that this moisture content corresponds to adsorbed water in the gelatin. The second extremal point is found at 400% moisture. With increase of the moisture content above 400% the strength of the structure falls considerably, especially at 25°, with a sharp rise in the hygrothermal characteristics [2]. With further increase of the moisture content the curve for gelatin exhibits a third extremal point. Data on the effects of moisture content on various physical characteristics show that the position of this point fluctuates in the 600-700% range for a given type of gelatin.

However, determination of the physical characteristics of the material can only give the transition boundaries between different forms of moisture binding, which is not enough for studying the structural changes in the transition of one form of moisture into another.

Studies of photographic materials in relation to the forms of moisture binding during drying are of great practical importance for elucidation of the drying mechanism; regulation of the drying process allows the production of high-quality material with the minimum expenditure of resources and time. In the present investigation an attempt was made to apply infrared spectroscopy to studies of structural changes in photographic materials, caused by transition of one form of moisture binding into another.

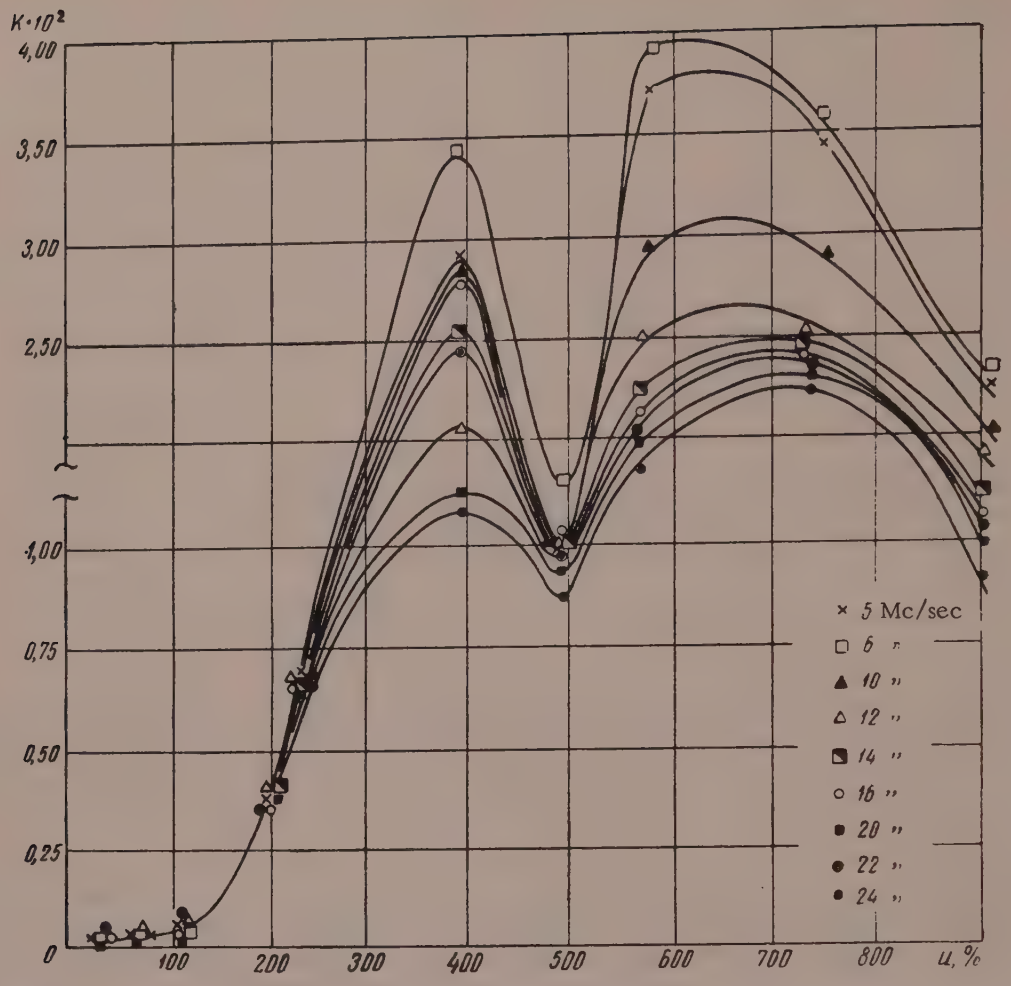
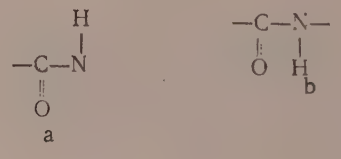


Fig. 1. Variations of the dielectric loss factor of gelatin with moisture content (u) at various frequencies (in Mc/second).

It has been shown [3] that hydrogen bonds play a significant role in the structure of polypeptide chains of substances similar in nature to gelatin. In studies of sorption and desorption of water and other vapors by porous sorbents [4] it was found that hydrogen bonds are the most sensitive to changes of adsorbent structure during sorption and desorption.

For studies of the influence of the form of water binding on gelatin structure the infrared absorption spectra were determined by means of the IKS-12 instrument with a lithium fluoride prism, in the wave length range between 2 and 5 μ.

The transmission curve for dry gelatin (on an arbitrary scale) is given in Fig. 2; it is seen that the spectrum of dry photographic gelatin contains bands at 3100 and 3365 cm^{-1} in the region of valence vibrations of N-H. . . groups. The strongest absorption is found in the region of the 3365 cm^{-1}; this corresponds to vibrations of the hydroxyl groups forming the most stable hydrogen bonds. It was shown by infrared spectroscopy in the studies cited above that there are two possible peptide group configurations corresponding to these valence vibrations of N-H groups, involved in hydrogen bonding in the trans- (a) and cis- (b) positions:



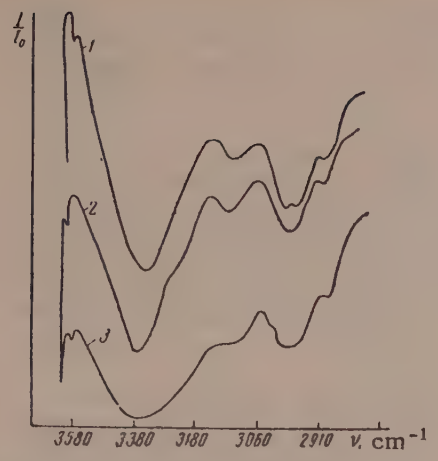


Fig. 2. Spectrograms of various materials: 1) gelatin; 2) type R emulsion; 3) diapositive emulsion.

There is also a narrow band at 3546 cm^{-1}, due to weaker hydrogen bonds. The nature of the spectra changes significantly with increase of the moisture content of gelatin (see table).

The table shows that the frequencies of the groups characterizing changes of hydrogen bonding undergo the most significant changes. With increase of the moisture content above that of adsorbed water, the band due to presence of hydrogen bonds of the trans type between the molecular chains disappears (this band is not found when the moisture content of gelatin is increased up to 1100%), and the band at 3100-3080 cm^{-1} also gradually becomes more and more diffuse. As this band disappears, two new bands appear in the region of lower frequencies, at 3545 and 3585 cm^{-1}. It has been shown by a number of workers [5] that the 3080-3100 cm^{-1} band characterizes weaker intermolecular hydrogen bonds and, like the 3320-3360 cm^{-1} band, it disappears indilute solutions, being replaced by a band at lower frequencies—at 3545 cm^{-1}.

The 3520 cm^{-1} band corresponds to peptides of the glycyl-leucine type, which are present in considerable amounts in gelatin [6]. The existence of a band at this frequency indicates that photographic gelatin contains free groupings in which the end NH_2 groups cannot be involved in hydrogen bonding. This band remains unchanged with increase of the moisture content of photographic gelatin up to 400%.

The band at 3585 cm^{-1} appears when the moisture content of gelatin exceeds the amount of water held by adsorption, persists unchanged up to 400% moisture content, and disappears with further increase of the moisture content. It is likely that this band corresponds to valence vibrations of OH groups forming very weak hydrogen bonds with the soluble gelatin fractions. All the bands described above disappear with increase of the moisture content above 400%.

Dependence of Wave Numbers on Moisture Content of Photographic Gelatin

Water content of gelatin, %	Wave numbers, cm^{-1}								
Air-dry	—	2880	2948	2972	3100	3365	3546	—	—
15	—	2867	2927	2972	3083	3320	3524	—	—
40	—	2871	2928	2956	3091	3322	3527	—	—
80	—	2871	2927	2955	3080	—	3548	—	—
115	—	2868	2917	2964	3086	—	3520	3545	3585
185	2845	2865	—	2958	—	—	3520	3545	3585
233	2845	2872	—	2956	—	—	3520	3545	3585
270	2844	2869	—	2962	—	—	3515	3546	3585
354	2843	—	—	2962	—	—	3520	3545	3585
400	2833	—	—	—	—	—	3522	3545	3585

The above description of changes in the infrared spectrum of gelatin during drying suggests that water at contents between 60 and 400% in gelatin is osmotic in character; 60% represents the limit of water held by adsorption.

The following mechanism of water binding by gelatin can be postulated from these data. As the amount of water in photographic gelatin increases above the adsorption limit, so intermolecular bonds break down. Studies of the structure of gelatin in the 200-300% range of moisture content [2] by electron microscopy suggest that mainly the side-chain intermolecular bonds are broken down, and the structure of gelatin containing osmotic water is of the condensational type. It is also evident from these data that the more soluble gelatin fractions are dissolved, and the main structure holds a considerable amount of water by osmotic forces.

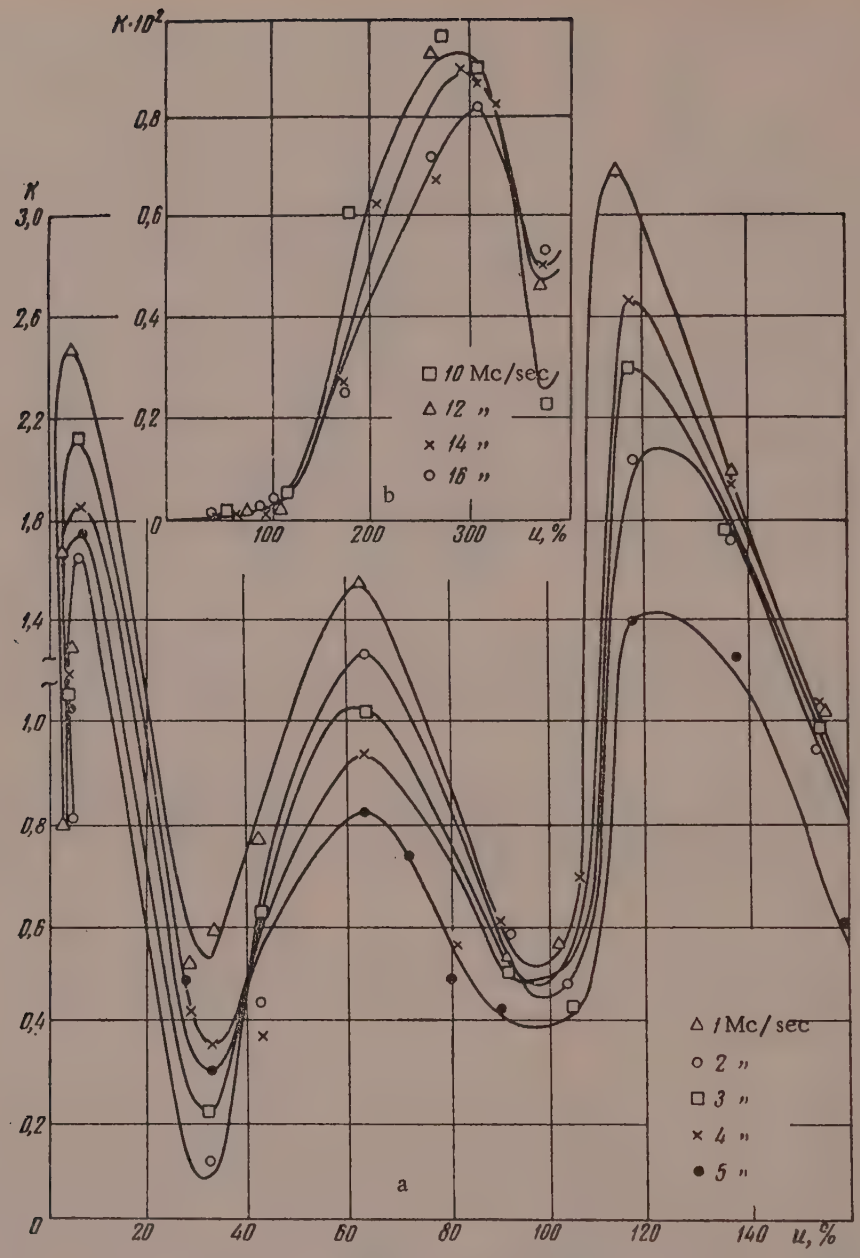


Fig. 3. Variations of the dielectric loss factor with moisture content at various frequencies: a) for diapositive emulsion; b) for type R emulsion.

When the moisture content increases above 400% the structure of gelatin changes qualitatively. It follows from the table that principal bonds are broken at this stage. Evidently the type of structure passes from condensational to coagulational [1]. The appearance of a third extremal point in the 600-700% moisture-content range, as detected in studies of the electrical characteristics of photographic gelatin, is indicative of considerable breakdown of the coagulational structure.

2. Studies of the types of water binding in photographic emulsions containing various amounts of silver are decisive for elucidation of the mechanism of drying of photographic emulsions. The transition boundaries between different forms of water binding during drying of photographic emulsions have not been determined as yet.

Infrared spectroscopy was used for studying the forms of water binding in photographic emulsions. In conjunction with this, the transition boundaries between different forms of water binding were determined from the electrical characteristics. Variations of dielectric loss with moisture content during drying of a diapositive

emulsion are plotted in Fig. 3, a. The first extremal point is in the region of 41% moisture. On further increase of the moisture content a weak extremal point appears; its position fluctuates in the 250-300% range, dependent on frequency. The position of the third extremal point depends considerably on frequency, and lies in the 500-700% range.

Studies of diapositive emulsions by infrared spectroscopy showed that all the bands found for photographic gelatin in the range from 2 to 5 μ are completely reproduced up to 40% moisture content. It therefore follows that 41% moisture content corresponds to the amount of water held by adsorption in diapositive emulsions. It follows from Fig. 2 that, in distinction from photographic gelatin, the spectrum of diapositive emulsion does not contain a band at 3520 cm^{-1}, which characterizes the presence of free amino end groups. On further increase of the moisture content of the emulsion, all the bands observed previously disappear, and do not return at higher moisture contents.

Studies of the structure of moist diapositive emulsion by means of the electron microscope showed that each crystal of silver halide is surrounded with a layer of substance of much lower density than the medium binding the individual silver halide grains. These results suggest that the substance surrounding each silver halide crystal consists of water containing certain soluble gelatin fractions. In order to explain this effect, a study was made of the infrared spectra and changes in them during drying of photographic emulsions with a high silver content. Fig. 2 shows that type-R emulsion gives bands which were also found in the spectra of diapositive emulsion, but in the case of type-R emulsion these bands are shifted somewhat toward higher frequencies and appear only at moisture contents up to 8%. These bands disappear at higher moisture contents.

Investigations of electrical characteristics (Fig. 3) showed that the dielectric-loss curve for type R emulsion has three extremal points. The first is found at 6-8% moisture content, in accordance with frequency.

Investigation of the infrared spectra of photographic emulsions indicate that 40% moisture in diapositive emulsion corresponds to the amount of water held by adsorption. With increase of the amount of silver in the emulsion the region of adsorbed water is displaced toward lower moisture contents, and is 6-8% for type-R emulsion. On further increase of moisture content the extremal point for the diapositive emulsion is found in the 250-300% region. In the case of type-R emulsion this point is the most pronounced, and is found in the region of 60-70% moisture. Studies of the spectra of gelatin and photographic emulsions have shown that certain principal bonds found in the structure of gelatin are fully retained in photographic emulsions, regardless of the silver content. Evidently, in photographic emulsions these bonds belong to the structure of gelatin, which is the carrier of the silver grains.

The spectrograms show that as the moisture contents of photographic emulsions are increased above the level corresponding to adsorbed water the principal bonds are broken down, so that water can penetrate more easily into cells containing silver. Evidently this process can continue up to a certain limit, beyond which the structure of the emulsion begins to break down as the moisture content increases. This breakdown cannot be detected by infrared spectroscopy.

The foregoing results suggest that 250-300% moisture in diapositive emulsion and 60-70% in type-R emulsion corresponds to maximum saturation of the cells with water.

3. The method of drying has a great influence on the structure and physicochemical properties of gelatin. All the results detailed above refer to gelatin dried in slabs which were subsequently ground. The infrared spectra of spray-dried air-dry gelatin contain the same bands as the spectra of slab-dried gelatin. However, the relative absorption intensities in any particular frequency region are much lower for spray-dried than for slab-dried gelatin.

Above 40% moisture bands corresponding to vibrations of the cis and trans configurations of the peptide groups disappear from the infrared spectra of spray-dried gelatin, while above 100% moisture the bands corresponding to vibrations of the other groups and observed for dry gelatin also disappear. Investigations of electrical characteristics showed that spray-dried gelatin contains less adsorbed and bound water than slab-dried gelatin.

It follows that spray drying of gelatin at higher temperatures results in irreversible breakdown of hydrogen bonds. As a result, the structural and mechanical characteristics of gels made from spray-dried gelatin are considerably inferior to those of gels made from slab-dried gelatin. For example, the ultimate breakdown compressive stress for slab-dried gelatin is 20 times that for spray-dried gelatin. From this it follows that photographic emulsions made from spray-dried gelatin would have inferior structural and mechanical properties.

SUMMARY

By determinations of electrical characteristics and infrared absorption spectra of photographic gelatin and emulsions it is possible to find the transition boundaries between different forms of water binding in the course of drying, which is necessary in order to calculate the optimum drying conditions, and also to establish the basic relationships governing the changes in the structure of these materials during drying.

I thank Prof. A. A. Berlin for valuable comments and advice.

LITERATURE CITED

1. P. A. Rebinder, Investigations of the Physical Chemistry of Suspensions [in Russian] (Moscow, 1933); Physicochemical Mechanics [in Russian] (Znanie, Moscow, 1958); Proceedings of the All-Union Scientific and Technical Conference, Plenary Session [in Russian] (1958) p. 20.
2. L. A. Lepilkina, Kolloid. Zhur. 18, 302 (1956)*; 19, 678 (1957)*; L. A. Lepilkina and F. M. Polonskaya, Inzhinerno-Fiz. Zhur. 1, 11, 46 (1958).
3. D. N. Shigorin, N. V. Mikhailov, and O. A. Klyueva, Zhur. Fiz. Khim. 30, 1591 (1956); A. A. Konkin, D. N. Shigorin, and L. M. Novikova, Zhur. Fiz. Khim. 32, 894 (1958); D. N. Shigorin, Problems of Physical Chemistry [in Russian] (1958) No. 1; Zhur. Fiz. Khim. 30, 2753 (1956).
4. S. P. Zhdanov, Doklady Akad. Nauk SSSR 68, 151 (1949); A. N. Sidorov, Physics Collection [in Russian] 1, 8 (1957); L. M. Roev and A. N. Terenin, Doklady Akad. Nauk SSSR 124, 373 (1959).*
5. L. Bellamy, Infrared Spectra of Complex Molecules [Russian translation] (IL, Moscow, 1957) p. 14.
6. G. Steinsby, Recent Advances in Gelatin and Glue Research (London, 1958); I. Beersmans, Industr. Chemiques Belge 20, No. 4, 381, 506 (1955).

*Original Russian pagination. See C. B. translation.

NATURE OF THE INTERACTION FORCES BETWEEN STRUCTURAL PARCELS (LAYERS) IN MICA CRYSTALS

M. S. Metsik

Laboratory of Surface Forces, Institute of Physical Chemistry, Academy of Sciences, USSR
Irkutsk University
Translated from Kolloidnyi Zhurnal, Vol. 22, No. 4, pp. 418-422,
July-August, 1960
Original article submitted November 6, 1958

It is known that a mica crystal can partially regain its strength after it has undergone primary separation into two parts which are subsequently rejoined [1]. This effect is not usually found in other crystals, and is of undoubted scientific interest. Experiments on the cohesion of parts of a crystal after primary cleavage may also shed some light on the nature of the forces acting between the structural elements (parcels) in mica crystals.

We studied the strength of cohesion between parts of a crystal after they had been joined and subsequently separated in moist air, and also after cleavage in water and subsequent drying. The purpose of the latter experiments was to verify the hypothesis concerning the role of water in the bonding of structural parcels in native mica crystals. The experiments were performed with muscovite crystals.

The work of cleavage was measured by means of an adhesion meter; the cleavage was effected slowly, at fractions of a millimeter per second.

In the first experiments the work of consecutive cleavage in moist air was determined, with short intervals during which the parts of the crystal were joined.

The experiments were conducted as follows.

A mica crystal, cut in the form of a long strip, was split to about one half of its length and attached by means of modeling clay to the plate of the adhesion meter [2]. The cleavage region was situated near the instrument axis and a load of a few grams was attached to the end of the part of the crystal which was being split off; the plate of the instrument was then turned through an angle such that cleavage continued for 2-3 mm further. The instrument plate was then turned back so that the parts of the crystal were brought into contact and cohered, and the next cleavage was performed immediately. This procedure was repeated until the parts of the crystal failed to cohere. The air humidity was 30%, and the temperature was 20°. The work of cleavage was usually less at the initial region of the moving front than at the subsequent region, because of the more prolonged contact with air.

Table 1 shows that after the primary cleavage the work of cleavage at once falls from 680 to 290 erg/cm^2; it then rises to 450 erg/cm^2 and subsequently falls gradually, with fluctuations.

A similar experiment was performed with a muscovite plate warmed by an electric lamp (40 w) placed near the crystal. In this case cohesion ceased after 91 cleavages. The work of the last cleavage, after 50 min, was 80 erg/cm^2. It follows that heating of the specimen accelerates the decrease of the work of cleavage. In the second series of experiments the time during which the crystal was in the split state was reduced to a minimum (some tens of seconds), and the specimens were split after various time intervals in the joined state. In this case the work of cleavage passed smoothly through a minimum and then began to increase, approaching the

TABLE 1

Work of Consecutive Cleavages of the Same Crystal, With Short Intervals in the Cohered State (between consecutive cleavages)

Cleavage No.	Time from first cleavage, min	Specific work, erg/cm²	Cleavage No.	Time from first cleavage, min	Specific work, erg/cm²
1	0	680	After specimen had been held in the divided state for 40 min		
2	1,5	290			
5	6	450			
10	25	390	95	155	285
15	33	320	100	160	290
20	44	345	105	164	280
25	49	305	110	168	280
30	52	340	115	172	270
35	56	315	120	178	260
40	62	320	125	182	250
45	67	300			
50	71	305	After specimen had been held in the divided state for 20 hr 35 min		
55	76	300			
60	78	330			
65	84	320	130	1417	225
70	88	305	135	1424	190
75	97	300	140	1427	155
80	101	305	145	1432	130
85	107	295	150	1435	130
90	112	290	151	No Cohesion	

TABLE 2

Changes in the Work of Cleavage of Muscovite Crystals During Repeated Cleavage and Subsequent Joining (with short intervals in the split state)

Cleavage No.	Time after first cleavage	Work of cleavage, erg/cm²		
		crystal No. 1	crystal No. 2	crystal No. 3
1	0	840	755	600
2	5 sec	400	340	—
3	10 "	310	370	—
4	20 "	310	370	—
5	40 "	310	370	—
6	80 "	310	390	—
7	3 min	370	400	—
8	5 min	370	400	—
9	11 "	400	460	—
10	30 "	460	460	—
11	60 "	460	495	—
12	120 "	505	—	—
13	24 hr	550	570	—
14	48 "	665	—	—
15	168 "	840	715	570*

*Data for second cleavage 168 hr from the start of the first.

work of primary splitting (Table 2) under favorable conditions. It follows that the forces of cohesion between the parts of the crystal first diminish and then increase up to the magnitude of the forces acting between the structural parcels in the intact crystal. Table 3 contains data on the work of consecutive cleavages of three mica crystals after primary cleavage in distilled water and subsequent drying in a state such that the parts of the crystal had been placed in contact and the unity of the crystal had been restored.

These results show that the crystal strength is restored in the course of drying and in some particularly favorable instances approximates to the primary value. As a rule, however, the strength is less than this. This is primarily because a certain, sometimes considerable, number of gas bubbles is formed in the cleavage plane; evidently the parts of the crystal do not cohere at the points of their formation.

Similar experiments with once-distilled benzene showed that there was no cohesion of the crystal parts after the interlayer had dried. Benzene leaves some sort of irreversible changes on the crystal surface which prevent multimolecular adsorption of water molecules on the surface. Experiments showed [3] that whereas fresh crystal surfaces split in moist air have high electrical conductivity, if the splitting is effected in presence of benzene, the conductivity remains negligible both immediately after the splitting and after drying of the benzene film.

TABLE 3

Strength of Bonding of Mica by Water Under Different Drying Conditions

Drying time	Work of first cleavage, after preliminary cleavage in distilled water and subsequent drying, erg/cm²		
	A	B	C
0	170	170	170
3 hr	185	250	–
1 day	285	320	500
3 "	350	400	–
7 "	380	–	–
11 "	380	–	–

Drying conditions: A) drying in air at 30% humidity at 20°; B) drying in air air at 20 cm distance from a 0.5 kw reflection heater; C) same, after exposure of wet specimens for 40 min in vacuum at 5 mm Hg.

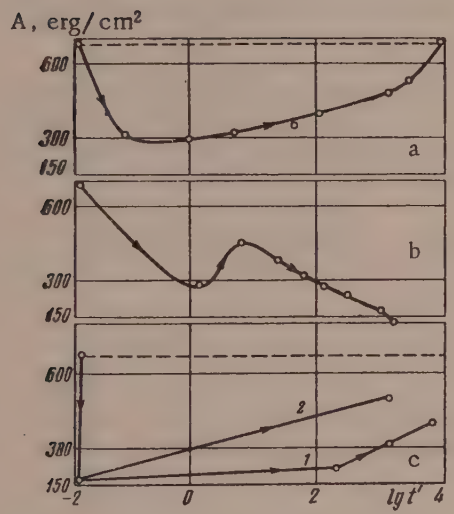


Fig. 1. Dependence of the work of repeated cleavage of a mica crystal (A_0) on time (log t) of contact between its parts (a) and on time of exposure of the parts of the crystal to air (b); restoration of strength of a crystal split in water, during drying (c) in air (1) and vacuum (2). The first point represents the work of primary cleavage in air.

Therefore the cohesion effect is directly connected with the presence of a water film between the crystal parts.

These variations of crystal strength (during repeated cleavages) with time are represented graphically in Fig. 1.

We represent the molecular mechanism of these effects as follows. The aqueous layer between the crystal parts becomes thinner with time, water molecules are pressed out of the layer, and the crystal parts come closer together until the film becomes close to monomolecular. Bonding of two adjacent crystal layers is effected through this water monolayer, and the water dipoles are oriented in the direction of the parcel dipole axes [4]. As a result, an electric double layer is formed between the parcels: the water molecules acquire charges of one sign, and the parcels, of the other. This hypothesis explains why the bonding forces between the crystal parts first diminish and then increase during repeated cleavage in air (Table 2 and Fig. 1). In the first cleavage of the crystal in air, a multimolecular water layer is adsorbed on the fresh cleavage surfaces; the thickness of this layer increases relatively rapidly at first. This is also shown by the higher surface conductivity of fresh cleavage surfaces in mica crystals [4].

Increase of the thickness of the adsorption film is accompanied by a decrease in the bond strength between the crystal parts in contact through this film. Evidently the minimum work of cleavage of a crystal re-formed in this manner must correspond to the maximum film thickness. Subsequently, because of the decreased adsorption capacity of the crystal surfaces, the thickness of the film on them decreases, and the cohesive strength between the crystal parts increases and may reach its initial level in favorable cases (Fig. 1, a and 1 c).

Direct measurements of changes in the thickness of the adsorption film on crystal surfaces, performed in our laboratory by the ellipsometric method, confirm the mechanism outlined above. The results of one such

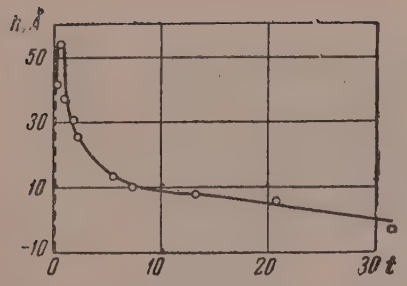


Fig. 2. Changes in the thickness (h) of the adsorbed water film on a mica crystal surface after cleavage (p/p = 20%, T = 20°) with time (t).

preliminary determination, performed under much the same conditions as the experiments with consecutive cleavage, are presented in Fig. 2.

After prolonged exposure to air, fresh surfaces are apparently contaminated by dust from the air, and the cohesive strength gradually decreases (Fig. 1,b).

It follows from these results that water molecules play an important part in the formation of bonding forces between the parcels in mica crystals. The presence of semibound interlayer water in native mica crystals has been reported [5, 6].

The fact that the work of cleavage of a natural crystal is equal to that of a crystal bonded by an adsorbed water film may be regarded as an indication that the bonding forces are the same in both cases.

The experiments described above clarify the physical nature of the effects forming the basis of water bonding of fresh mica crystal surfaces for production of larger mica sheets.

An industrial process has now been developed for production of mica insulating material bonded without the use of adhesives.

SUMMARY

1. When a mica crystal is split in moist air and the parts are then brought into contact the bonding strength reaches the primary value in favorable cases. Crystal strength is partially restored when crystals are split in water and dried in air.

2. It is suggested that changes of secondary bonding strength between the crystal parts with the time can be attributed to changes in the thickness of the film of adsorbed water formed on mica crystal surfaces in cleavage in moist air. The important part played by water molecules in the bonding of structural parcels in mica crystals is noted.

I offer my sincere thanks to Corresponding Member, Acad. Sci. USSR, B. V. Deryagin for certain advice and discussion of the results of this work.

LITERATURE CITED

1. J. W. Obreimoff, Proc. Roy. Soc. A 127, No. A 805, 290, (1930).
2. B. V. Deryagin and N. A. Krotova, Adhesion [in Russian] (Izd. AN SSSR, 1949).
3. M. S. Metsik, Izvest. Vuzov Min. Vysshego Obrazovaniya SSSR, Razd. Fizika, No. 4, 29 (1958).
4. M. S. Metsik, Izvest. Tomskogo Politekhn. In-ta 91, 413 (1956).
5. M. S. Metsik, Trudy Sib. Fiziko-Tekhn. In-ta, No. 35, 60 (1956).
6. M. A. Metsik and R. A. Zhidikhanov, Kristallografiya 3, No. 1, 95 (1958).

*Original Russian pagination. See C. B. translation.

INVESTIGATION OF THE ACTIVITIES OF DIFFERENT TYPES OF CONDENSATION NUCLEI

M. L. Mikhel'son

Mining Scientific Research Institute, Krivoi Rog
Translated from Kolloidnyi Zhurnal, Vol. 22, No. 4, pp. 423-438,
July-August, 1960
Original article submitted June 23, 1959

An important problem in the development of a condensation process for dust removal [1-5] is elucidation of the manner in which volume condensation occurs on nuclei of different types. Because of the different activities* of the nuclei, and of the low degrees of supersaturation attained in high-output condensation filters [4, 5], the possibility is not excluded that condensation would take place on some particles (for example, atmospheric nuclei [6]), but would be inhibited on others (such as the dust particles which are to be removed).

According to the results of a number of authors [7-9] the average radius of atmospheric nuclei lies in the $2.5\text{-}3 \cdot 10^{-6}$ cm range. However, according to others [10, 8] the size distribution curve of atmospheric nuclei reaches values in excess of 10^{-5} cm. In that case atmospheric nuclei, especially if soluble, may be more active than dust particles with radii between 10^{-5} and 10^{-4} cm. It is therefore desirable to investigate the activities of different condensation nuclei. The present communication is concerned with this problem.

We studied the activities of various condensation nuclei: wettable iron-ore dust, coal dust of poor wettability, and smoke particles, by comparison of the course of condensation on each of the components and on atmospheric nuclei.

Volume condensation on the nuclei was effected in a diffusion condensation chamber of the flow type, where air was supersaturated with water vapor by the passage of a turbulent stream between moist surfaces at different temperatures; one was the evaporation surface and the other, the condensation surface. It is known [2] that, in absence of volume condensation, the resultant supersaturation may be represented as follows:

$$S = \rho'/\rho_s(T'), \quad \rho' = \bar{\rho} - (\bar{\rho} - \rho_0)\, e^{-\frac{M_D}{d}x};$$
$$T' = \bar{T} - (\bar{T} - T_0)\, e^{-\frac{M}{d}x}, \qquad (1)$$

where

$$\bar{\rho} = {}^1/_2[\rho_s(T_1) + \rho_s(T_2)]; \quad \bar{T} = {}^1/_2(T_1 + T_2);$$

T_1 is the temperature of the upper surface; T_2 is the temperature of the lower surface ($T_2 > T_1$); T_0 and ρ_0 are

*We define the activity of condensation nuclei as the minimum supersaturation $S_{cr} = \rho/\rho_s$ required for unrestricted growth of droplets by condensation; here ρ is the water vapor density and ρ_s is the density of saturated water vapor at the same temperature.

are the initial temperature and density of the water vapor in the air; M_D and M are the Margulis diffusion and thermal numbers; d is the distance between the moist surfaces; the x axis is in the direction of flow.

With l/d and T_1 fixed (l is the channel length), supersaturation at the end of the chamber, where it is greatest, is easily regulated by the temperature of the lower surface. If the channel is sufficiently long [$Ml/d > 1$], supersaturation at the end of the chamber increases very slowly with increase of x. This creates favorable conditions for loss of supersaturation by condensation on the more active component, so that condensation cannot occur at all on the less active one.

Consider mass and heat transfer in volume condensation on nuclei.

The unknowns ρ, T, and r can be found from the following system of differential equations:

$$\frac{d\rho}{dx} = -\frac{M_D}{d}(\rho - \bar{\rho}) - \frac{4}{3}\pi\gamma n \frac{dr^3}{dx}, \tag{2}$$

$$\frac{dT}{dx} = -\frac{M}{d}(T - \bar{T}) + \frac{4}{3}\pi\gamma \frac{L}{c'\gamma'} \frac{dr^3}{dx}, \tag{3}$$

$$\frac{dr^2}{dx} = \frac{2D[\rho - \rho_s(T)]}{v\gamma(1+b)}, \tag{4}$$

where r is the radius of the condensate droplets; γ is the density of water; n is the concentration of nuclei; c' and γ' are the specific heat and density of the vapor-air mixture; D is the coefficient of diffusion of water vapor in air; v is the average flow velocity; $b = LD\,\rho_s(T)\,\mu/\lambda$; $\mu = mL/RT^2$; m is the molecular weight of water; R is the gas constant; λ is the coefficient of thermal conductivity for air.

Equation (4) gives the rate of condensational growth, account being taken of the increase of drop temperature due to liberation of the latent heat of condensation [5].

We solve the system of Equations (2) and (4) by the method of successive approximations. Suppose that the loss of supersaturation is not great. Then, substituting the expressions for ρ' and T', as zero approximation, from Equation (1) into Equation (4), we have:

$$r^2 = \int_0^x \frac{2D}{v\gamma(1+b)} \left\{\bar{\rho} - (\bar{\rho} - \rho_0)\, e^{-\frac{M_D}{d}x} - \right.$$
$$\left. - \rho_s\left[\bar{T} - (\bar{T} - T_0)\, e^{-\frac{M}{d}x}\right]\right\} dx, \tag{5}$$

where the coordinate origin is taken from the point where condensation starts and not from the point of entry of the air stream into the chamber.

Since condensation in the chamber, when $Mx/d > 1$, begins far from the origin, i.e., at T close to $\bar{T}$, we assume that $b \approx b(\bar{T})$; then, resolving ρ_s into series close to $\bar{T}$ and taking only the first two terms, we have:

$$\rho_s(T) = \rho_s(\bar{T})\left[1 - \mu(\bar{T})(\bar{T} - T_0)\, e^{-\frac{M}{d}x}\right],$$

where $\mu = \partial\rho_s/\rho_s\,\partial T$ from the Clausius-Clapeyron equation.*

Integration of Equation (5) gives

$$r^2 = \frac{2Dd}{v\gamma M}\left[\delta\rho x_1 - (\delta\bar{\rho} - \delta\rho_0)(1 - e^{-x_1})\right], \tag{6}$$

where $\delta\bar{\rho} = \bar{\rho} - \rho_s(\bar{T})$; $\delta\rho_0 = \rho_0 - \rho_s(T_0)$;

$$x_1 = \frac{M}{d}x; \quad M_D \approx M.$$

* We use the approximate expression $\rho_s \approx A - mL/RT$.

Assuming that the start of condensation corresponds to the point where S = 1, we have $\delta\rho_0 = 0$.*

Then we have for the droplet radius, in the first approximation:

$$r^2 = \frac{2Dd\overline{\delta\rho}}{M\upsilon\gamma(1+b)}[x_1 - (1 - e^{-x_1})]. \tag{7}$$

We substitute this expression into Equations (2) and (3); after simple rearrangements we have as the first approximation for ρ and T

$$\rho = \rho' - 2\pi\gamma n\left(\frac{2Dd\overline{\delta\rho}}{\upsilon\gamma(1+b)M}\right)^{3/2} I(x_1)\cdot e^{-x_1}, \tag{8}$$

$$T = T' + 2\pi n\cdot\frac{L}{c'\gamma'}\left(\frac{2Dd\overline{\delta\rho}}{\upsilon\gamma(1+b)M}\right)^{3/2} I(x_1)\, e^{-x_1}, \tag{9}$$

where

$$I(x_1) = \int_0^{x_1}\sqrt{x_1 - (1 - e^{-x_1})}\,(e^{x_1} - 1)\,dx_1 \tag{10}$$

rapidly increases with x_1, while ρ' and T' are zero approximations unaffected by volume condensation.

Data calculated from Equation (10) are plotted in Fig. 1.

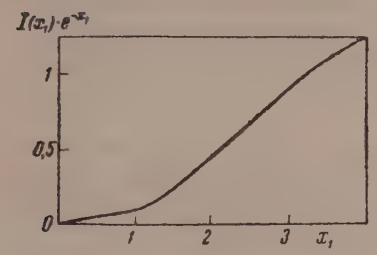


Fig. 1. Plot of the function $I(x_1) \times e^{-x_1} = f(x_1)$.

Thus, with the temperatures T_1 and T_2 fixed, changes of ρ and T, and therefore decrease of supersaturation, depend significantly on two factors only: concentration n of the nuclei and the corrected length $\bar{x}_1$ of the apparatus. If the air stream contains two kinds of nuclei with different S_{cr}, then at sufficiently high concentrations of the more active component supersaturation decreases owing to the more active component, involved considerably earlier in the condensation process (this component corresponds to a higher value of x_1 and therefore of $I(x_1)\, e^{-x_1}$). The greater the difference between the activities of the condensation nuclei, the less is the concentration of the more active component required for decrease of supersaturation, with selective condensation on the more active component.

The experimental unit is shown diagrammatically in Fig. 2. The aerosol was forced into the condensation chamber by means of an air blower attached to a dust chamber 36 m^3 in capacity. The condensation chamber had the following characteristics: 8 zigzag-shaped channels with 180° turns with l = 560 cm, l/d = 158, and rectangular channel section 20 cm; the average flow rate was v = 2.08 m/sec.

The experimental value of the Margulis number was 0.024 $\left(\frac{M}{d}\, l = 3.79\right)$.

The dust chamber was attached to a unit consisting of a fan and a special metering device for introduction of smoke or dust particles into the circulating air stream. If dust particles were used, the coarse fractions were removed from the dusty air in a foam filter [11] so that the radii of the dust particles were in the 0.1-1 μ range.

The numerical particle concentrations at each end of the condensation chamber were determined by means of the flow ultramicroscope designed by Deryagin and Vlasenko [12].

The dispersity of the condensate droplets was determined by means of the photometric wedge of the ultramicroscope.

The technique was initially developed for smoke particles (tobacco smoke); the procedure was as follows. The concentration of the smoke particles before the chamber, and the concentration of the same particles and

* Since $\delta\rho_0 \lesssim 0$ for the condensation nuclei, somewhat high estimates of $\bar{r}$, ρ, and T are given by Equations (7), (8), and (9).

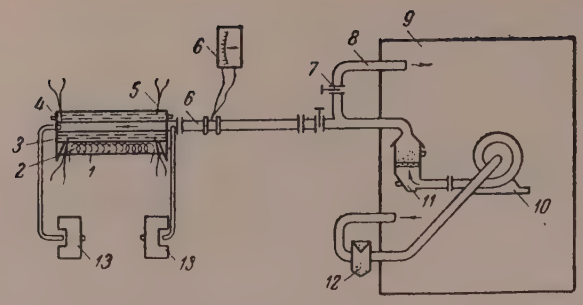


Fig. 2. Diagram of experimental unit: 1) condensation chamber; 2) heater; 3) hot water; 4) cold running water; 5) thermocouples; 6) flow meter; 7) air flow regulators; 8) air ducts; 9) dust chamber; 10) air blower; 11) foam filter; 12) metering device; 13) flow ultramicroscopes.

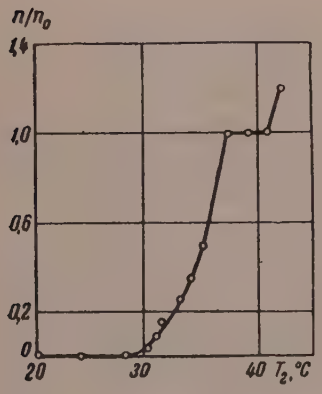


Fig. 3. Selective condensation on smoke particles. $T_1 = 20°$; $n_0 = 7.6 \cdot 10^{-4}$ cm^{-3}.

the droplets formed on them at the end of the condensation chamber were determined. The smoke particles and the droplets formed on them were counted separately by means of the photometric wedge of the ultramicroscope. For this, the concentration of the aerosol particles was found with the wedge fully withdrawn and with the wedge in the position at which all the smoke particles in the ultramicroscope field were darkened, while the droplets were distinctly visible because of their much greater size in comparison with the smoke particles.

With increase of temperature T_2 (at fixed T_1), and therefore with increase of supersaturation, the concentration of the condensate droplets increased, while the total concentration of aerosol particles, determined at the end of the condensation chamber, remained unchanged. This showed that additional nuclei, atmospheric in this case, did not appear. After all the dust particles had become droplets, only the droplet size increased over a small range of T_2 (supersaturations) while the numerical concentration remained unchanged. On further increase of T_2 the numerical droplet concentration $\underline{n}$ began to exceed the concentration n_0 of smoke particles at the entry into the condensation chamber, which indicates that atmospheric nuclei began to appear.

This method was used for comparing the activities of smoke particles and atmospheric nuclei; it was found that the latter are the less active.*

A typical plot of the function $n/n_0 = f(T_2)$ is given in Fig. 3. The course of the curve up to the point $n/n_0 = 1$ is associated with differences in the activities of the smoke particles. The horizontal portion of the graph at $n/n_0 = 1$ indicates that the smoke particles are more active than atmospheric nuclei, condensation on which begins at higher supersaturation.

Since smoke particles proved to be more active than atmospheric nuclei, it was to be expected that when their concentration is high enough there should be a considerable decrease of supersaturation, so that subsequent condensation on atmospheric nuclei would be hindered. A series of experiments was carried out to confirm this, with different concentrations of smoke particles; the results are presented in Fig. 4. It was found that, in general, the higher the activity of a given type of nucleus, the earlier (nearer to the entrance to the channel with different temperatures) does volume condensation begin; the supersaturation diminishes to a greater extent accordingly. Therefore, to ensure condensation on atmospheric nuclei, the more active the other nuclei present simultaneously, the higher the temperatures required. It follows from Fig. 4, c, that atmospheric nuclei begin to grow by condensation at higher temperatures (supersaturation) in presence of mine dust than in presence of coal dust or smoke. This means that the critical supersaturation value diminishes in the aerosol series: tobacco smoke—coal dust—

*By this method it was possible to avoid the very complex problem of highly accurate determination of very small supersaturations for determination of S.

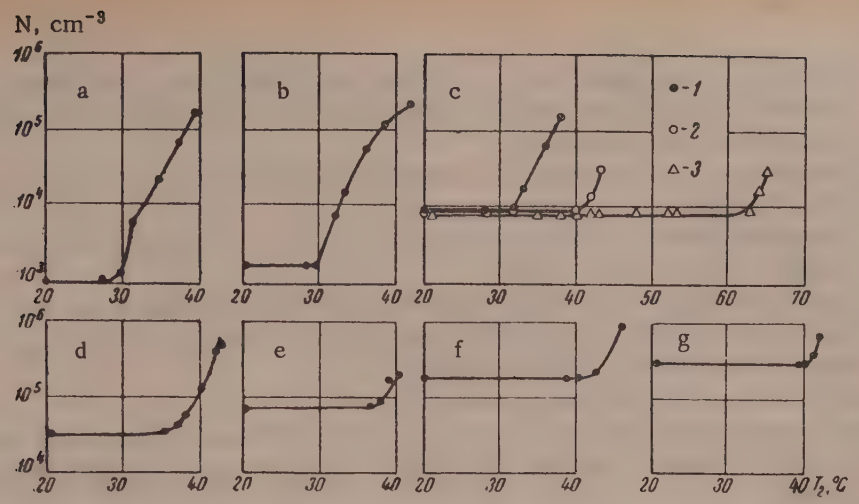


Fig. 4. Effects of concentration and nature of the more active component on the course of condensation on smoke particles, mine dust, and coal dust in presence of atmospheric nuclei: $T_1 = 20°$; 1) smoke particles; 2) coal dust; 3) mine dust. Values of n_0: a) 10^3; b) $1.5 \cdot 10^3$; c) $8.6 \cdot 10^3$; d) $3.3 \cdot 10^4$; e) $7.6 \cdot 10^4$; f) $1.7 \cdot 10^5$; g) $3.2 \cdot 10^5$ cm^{-3}.

mine dust. In these graphs N represents the total particle or droplet concentration at the end of the apparatus, and increase of N means that condensation commences on additional (atmospheric) nuclei.*

In condensation on coal and mine dust (Fig. 4) at concentrations equal to that of smoke particles, atmospheric nuclei begin to appear (especially in condensation on easily wetted mine dust) at considerably higher values of T_2, whereas even at $T_2 = 32°$ all the dust particles are converted into droplets $\sim 2\ \mu$ in radius.

If the value $x_1 = 3.79$ is substituted into Equations (9) and (10), i.e., if it is assumed that condensation begins from the instant the stream enters the chamber (which corresponds to $S_{cr} \approx 1$), it is found that at T_2 of 30-40° and $T_1 = 20°$ supersaturation begins to diminish rapidly even at $n \sim 10^3$ cm^{-3}, which is in agreement with the results of experiments on condensation on wetted dust particles.

SUMMARY

1. By comparison of the course of condensation it was shown that dust particles 0.1-1 μ in size, whether easily wetted or not, are more active than atmospheric nuclei; i.e., lower supersaturations are needed for their unlimited growth by condensation.

2. The investigations showed that the activities of condensation nuclei of different types diminish in the following sequence: mine dust—coal dust—smoke particles—atmospheric nuclei.

3. To prevent condensation on atmospheric nuclei the increase of supersaturation along the stream must be less than the decrease of supersaturation caused by the more active component. Such conditions may be achieved in a long-channel chamber in which a temperature difference is maintained, even at relatively low concentrations ($10^4 \cdot$ cm^{-3}) of dust particles. At even lower concentrations of the dust particles condensation on atmospheric nuclei presents no danger, because relatively little excess moisture is needed for growth of the dust particles, and a deficiency of moisture can arise only at moderate and high concentrations.

In conclusion, I offer my deep gratitude to Corresponding Member, Acad. Sci. USSR, B. V. Deryagin for valuable advice and interest in the work.

LITERATURE CITED

1. B. V. Deryagin, S. S. Dukhin, M. L. Mikhel'son, and V. M. Kaganer, collection: Silicosis Prevention [in Russian] Vol. 2 (Izd. AN SSSR, 1955).

*It follows from Equation (1) that the supersaturations in the condensation chamber (at the values of T_1 and T_2 used in the experiments) are insufficient for spontaneous condensation or condensation on ions.

2. S. S. Dukhin, B. V. Deryagin, and M. L. Mikhel'son, Doklady Akad. Nauk SSSR 105, No. 6 (1955).
3. S. S. Dukhin, V. M. Kaganer, and M. L. Mikhel'son, Byull. Nauchno-Tekhn. Informatsii NIGRI, No. 1 [in Russian] (Metallurgizdat, 1956).
4. M. L. Mikhel'son, B. V. Deryagin, M. S. Binus, and Girik, Bulletin of Nonferrous Metallurgy, No. 2 [in Russian] (1959).
5. B. V. Deryagin and M. L. Mikhel'son, Izvest. Akad. Nauk SSSR, Otdel. Tekhn. Nauk, Problemy Metallurgii i Topliva, No. 2 (1959).
6. R. I. Grabovskii, Atmospheric Condensation Nuclei [in Russian] (Gidrometeoizdat, 1956).
7. I. Nolan, and N. Guerrini, Trans. Faraday Soc. 32, 1175 (1936).
8. M. Kumai, J. Meteorology 8, N 3, 151 (1951).
9. M. L. Mikhel'son, Kolloid. Zhur. 19, 125 (1957).*
10. Dessens, Quart. J. of the Roy. Met. Soc. 75, No. 323 (1949); D. Kuroiwa, J. Meteorology 8, No. 3 (1951).
11. M. E. Pozin, I. P. Mukhenova, and É. Ya. Tarat, Trudy Leningrad. Tekhnol. In-ta im. Lensoveta, No. No. 26 (1953).
12. B. V. Deryagin and G. Ya. Vlasenko, Doklady Akad. Nauk SSSR 63, 155 (1948); Collection: New Ideas in the Study of Aerosols [in Russian] (Moscow, 1949) p. 7; Trudy in-ta Fiz. Khim. Akad. Nauk SSSR 1, 161 (1950); Kolloid Zhur. 13, 249 (1951); Priroda No. 29 (1953).

*Original Russian pagination. See C. B. translation.

INVESTIGATION OF CATION-SUBSTITUTED AGAR SAMPLES

A. A. Morozov and S. N. Stavrov

I. I. Mechnikov Odessa University; Chernovits University
Translated from Kolloidnyi Zhurnal, Vol. 2, No. 4, pp. 429-433,
July-August, 1960
Original article submitted May 24, 1959

Substances extracted from red algae, including agar, agaroid, carrageenin, and iridophycin, are salts of incompletely esterified sulfate esters of polysaccharides. They are all polyelectrolytes containing organic ions which differ in their contents of functional SO_4 groups per unit molecular weight [1, 2]. Agar and carrageenin consist mainly of the calcium salt, and iridophycin of the sodium salt; the agaroid from Iridaea is also a sodium salt, whereas Odessa agaroid from the Black Sea alga Phyllophora contains calcium, magnesium, sodium, and potassium cations [1]. According to some reports, replacement of calcium in agar by univalent cations does not result in any significant changes in gelating power [3, 4], and according to others the gelating power is weakened considerably [1]. All the above-mentioned algal extracts have the properties of natural cation exchangers [3-7].

The object of the present investigation was an experimental study of the properties of solutions and gels of cation-substituted (Li, Na, K, Ca) samples of White Sea agar—dried extract of Ahnfeltia plicata.

For replacement of all the above-mentioned cations by only one, the original agar was subjected to special treatment. In the initial treatment stage agar acid (H-agar) was prepared as described previously [4].

Curves for conductometric titration of 2% suspension (75 ml) of H-agar with Li, Na, and Ca acetates (Fig. 1) indicate that agar acid displaces acetic acid from its salts; the reaction yields cation-substituted products, Li-, Na-, or Ca-agar, respectively.

The agar acid was then treated with 1% solutions of lithium, sodium, potassium, and calcium acetates; it was found (Fig. 1) that the corresponding cation-substituted agar derivatives are formed. Excess acetates and acetic acid were removed from the samples by dialysis through parchment paper (distilled water was used as the external liquid).

The conductivities of the solutions were determined at 65° under thermostatic control in the usual apparatus. The solution concentration and the SO_4 group contents per unit weight of agar dried to constant weight at 110° were taken into account in calculations of equivalent conductivity.

The original agar (not fractionated) contained 6.0% SO_4 groups by weight. During preparation of agar acid, part of the readily soluble agar fractions, richer in sulfur [8], was lost in the course of acid treatment. The agar acid from which the cation-substituted agar samples were prepared, contained only 1.2% SO_4 groups by weight.

The equivalent conductivity of cation-substituted agar solutions (Fig. 2) varies with dilution similarly to that of weak electrolytes [9]. The absolute magnitudes of the conductivity differences between different samples are slight. The positions of the curves correspond to the mobilities of the cations present in the agar samples. Therefore there is reason to believe that under given conditions (concentration, temperature) of conductivity determination, the different agar samples do not differ significantly from each other in degree of electrolytic dissociation.

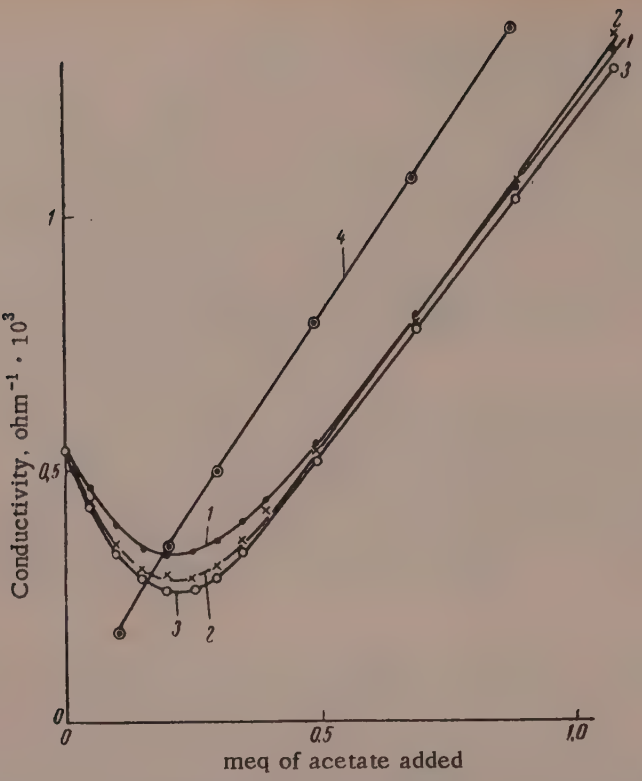


Fig. 1. Conductometric titration of 2% agar acid suspension with acetates: 1) $Ca(CH_3COO)_2$; 2) $NaCH_3COO$; 3) $LiCH_3COO$; 4) conductivity of calcium acetate solutions.

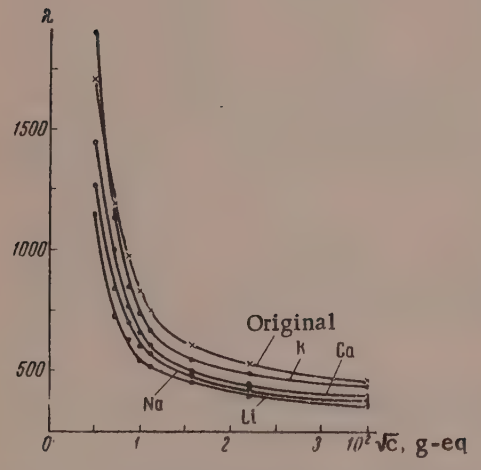


Fig. 2. Variations of equivalent conductivity (λ) of agar solutions with the square root of the concentration (c).

Viscosity was determined by the capillary efflux method at 65°. The observed increase of the reduced viscosity (η_{sp}/c) of agar solutions with dilution (Fig. 3) is the result of straightening of the polymeric anions of the polyelectrolytes. This effect may be caused by repulsion forces between similarly charged centers (SO_4 groups) situated along the entire length of the agar polymeric anion. The repulsion forces and straightening of the anions increase with the degree of electrolytic dissociation of the agar at higher dilutions.

The original agar sample has considerably greater viscosity than the cation-substituted samples, and the viscosities of agar samples containing different cations (Li, Na, K, Ca) differ very little from one another. This is easily explained if viscosity and conductivity data are compared: cation-substituted agar samples differ very slightly in the magnitude of the polymeric anion charges, and hence in the hydrodynamic particle volumes and viscosities of the solutions. The probable reason why the viscosity of the original agar is much greater than the viscosity of cation-substituted samples is that the original material has a much higher content of functional SO_4 groups per unit weight of substance (see above). It follows that under given conditions the charge and hydrodynamic particle volume are greater for the original agar than for the cation-substituted samples.

Variations of η_{sp}/c with concentration of the original agar at various temperatures are plotted in Fig. 4. The dissociation of the polyelectrolyte and the kinetic energy of the agar particles decrease with fall of temperature. The electrostatic repulsion forces between similarly charged particles diminish with decrease of the charge on the agar anions. This results in structure formation in the system, which increases appreciably with fall of temperature and increasing concentration.

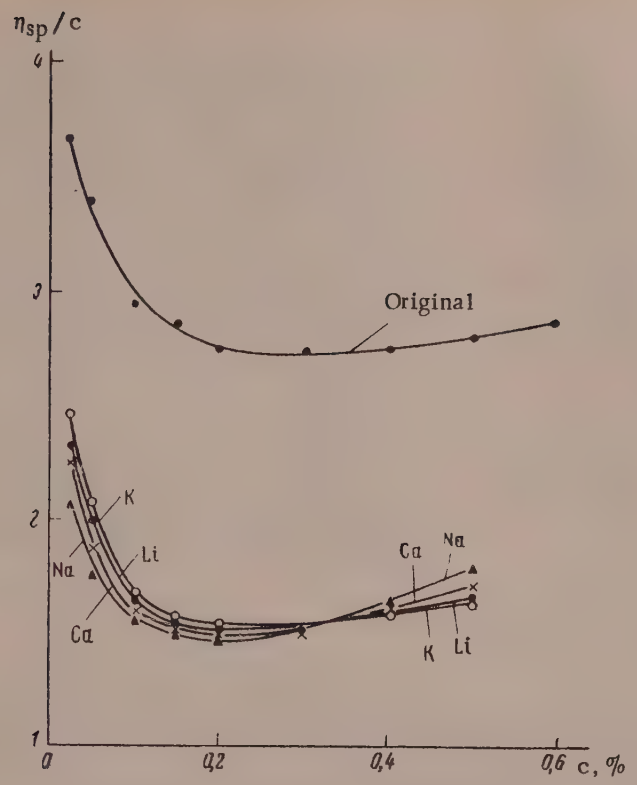


Fig. 3. Variations of reduced viscosity (η_{sp}/c) of agar samples with concentration (c).

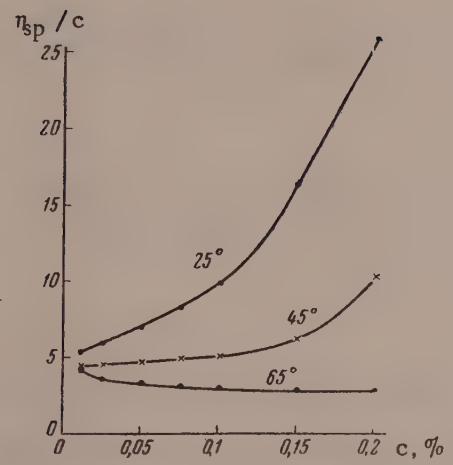


Fig. 4. Variations of reduced viscosity (η_{sp}/c) of agar solutions with concentration (c) at various temperature.

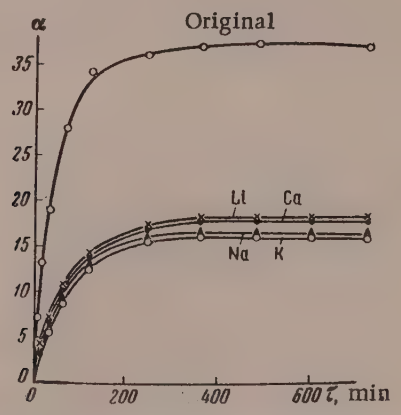


Fig. 5. Kinetic curves for swelling of agar samples in water at 20°.

Swelling of the agar samples in water was determined by the gravimetric method [7]. The resultant kinetic curves (Fig. 5) show that there is a pronounced relationship between the particle charge of the anionic polyelectrolyte and the swelling.

Gel strengths, evaluated from yield-value determinations [7, 10, 11], are represented by a group of curves which differ little for different cation-substituted agars (Fig. 6). Here again the only difference is between the original agar on the one hand, and all the cation-substituted samples on the other. Swelling increases and gel strength decreases with increase of the anion charge.

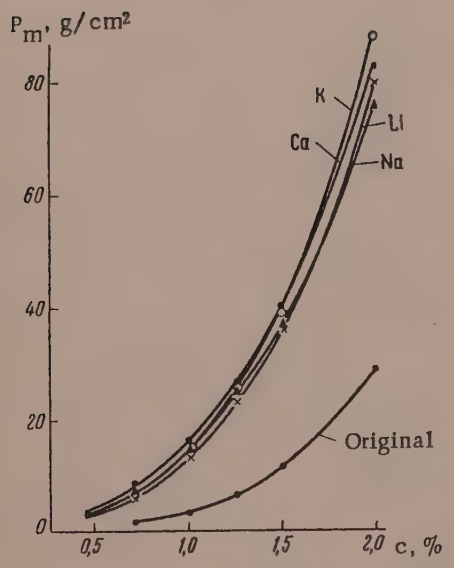


Fig. 6. Variations of yield values of agar gel samples with concentration at 20°.

In conclusion, it is of interest to compare the experimental data found for cation-substituted agar samples with analogous data on cation-substituted agaroids [7]. Data on conductivities, viscosities, swelling, and gel strengths of Black Sea agaroid and White Sea agar reveal a close connection between the magnitude of the charge and the physical and mechanical properties of solutions and gels. The principal difference in properties between agar and agaroid, directly related to their applications in the confectionery industry, lies in their gelating power and gel strengths; in our opinion, this is caused by differences of the sulfur contents of the two materials. Sulfur is present in the functional SO_4 groups both in agar and in agaroid. However, agaroid contains 21.6% sulfur calculated as SO_4 groups, which is nearly four times as much as is present in agar. This explains why agaroid is inferior to agar in technical qualities and gives weaker gels. The properties of agaroid may be modified in a desired direction by substitution of one type of cation by another.

SUMMARY

1. Conductivity studies were carried out with solutions of White Sea agar and cation-substituted samples of Li-, Na-, K-, and Ca-agar prepared from the latter, which behave like weak electrolytes (polyelectrolytes) in aqueous solution.

2. The reduced viscosities of solutions and gel swelling of the cation-substituted samples are less, and gel strengths greater, than those of the original untreated agar. This difference in properties is the consequence of different contents of functional SO_4 groups, i.e., differences in the magnitude of the charge on the polymeric agar anion.

3. Replacement of one type of cation by another in the molecule of cation-substituted agar (containing 1.2% SO_4) cannot result in any significant changes in the physical and mechanical properties of solutions and gels, as is the case with agaroid, which has a considerably higher SO_4 content.

LITERATURE CITED

1. I. V. Kizevetter, Izvest. Tikhookeanskogo N.-I. In-ta Rybnogo Khoz. i Okeanografii 36, 1 (1952).
2. C. K. Tseng. in: Colloid Chemistry, edited by Jerome Alexander (New York, 1946) Vol. 6, p. 629.
3. H. de Waele, Ann. Phys. Physiochim. Biol. 5, 877 (1929).
4. F. Fairbrother and H. Mastin, J. Chem. Soc. 123, 1412 (1923).
5. T. Currie, Chem. Ind. 116, (1955).
6. M. R. Butler, Biochem. J. 28, 759 (1934).
7. S. N. Stavrov and A. A. Morozov, Ukr. Khim. Zhur. 23, 721 (1957); A. A. Morozov and S. N. Stavrov, Kolloid. Zhur. 20, 194 (1958).*
8. S. M. Lipatov and A. A. Morozov, Zhur. Obshchei Khim. 5, 1119, 1359 (1935); A. A. Morozov, Kolloid, Zhur. 1, 37 (1935); S. M. Lipatov, Problems of the Science of Lyophilic Colloids [in Russian] (Izd. AN Beloruss. SSR, 1941) pp. 53 and 84; S. A. Glikman and I. G. Shubtsova, Kolloid. Zhur. 19, 281 (1957).*
9. N. A. Izgaryshev and S. V. Gorbachev, Course of Theoretical Electrochemistry [in Russian] (Goskhimizdat, Moscow-Leningrad, 1951) p. 133.
10. V. P. Rudi and A. A. Morozov, Kolloid. Zhur. 15, 117 (1953).*
11. E. E. Segalova and P. A. Rebinder, Kolloid. Zhur. 10, 223 (1948).

*Original Russian pagination. See C. B. translation.

OPTICAL POLARIZATION STUDY OF PLASTIC DEFORMATION PROCESSES WITH THE AID OF ETHYLCELLULOSE SOLUTIONS AND GELS

D. N. Osokina, M. V. Gzovskii, G. V. Vinogradov

and V. P. Pavlov

O. Yu. Shmidt Institute of Soil Physics, Moscow

Translated from Kolloidnyi Zhurnal, Vol. 22, No. 4, pp. 434-441,
July-August, 1960
Original article submitted April 19, 1959

Optical polarization studies of stresses in models undergoing plastic deformation are very important in the solution of many problems of the mechanics of disperse systems, tectonics, etc. For this it is desirable to have materials consisting of readily available components, the proportion of which can be varied in order to vary the mechanical properties over a wide range while a fairly high optical activity is retained. Among the many systems studied [1-8], special interest attaches to systems containing ethylcellulose, solutions of which were used by Weller [8], and later by Vinogradov and Manin [1], in the photoviscosity method. We have shown that ethylcellulose solutions and gels can be used in preparation of highly effective materials, not only for the photoviscosity but also for the photoplasticity method* [9]. Systems with various physical and mechanical characteristics can be obtained by the use of solvents consisting of mixtures of good and poor solvents in various proportions. Some of the systems described below were used with success for studying the stressed state in models of upheavals of the earth's crust [11, 12]; others may be used for simulation and visualization of flow processes in disperse systems, high polymers, etc. In accordance with the foregoing, this paper contains the results of a study of the optical-polarization and mechanical properties of ethylcellulose solutions in benzyl alcohol (good solvent) and in mixtures of benzyl alcohol with dibutyl phthalate (poor solvent). Benzyl alcohol and dibutyl phthalate are convenient by virtue of their high boiling points and low volatility at room temperature. The ethylcellulose content of the solutions was varied from 10 to 35%, and the experiments were performed at temperatures from 10 to 50°.

In a study of an optically active material it is important to investigate its optical and rheological characteristics simultaneously under identical conditions. This was done with the aid of a rotational apparatus, the photoplastoviscosimeter, which fulfills the functions of a plastoviscosimeter and a dynamooptimeter. Its design was suggested by V. P. Pavlov [13], and the instrument was designed and constructed in the Institute of Soil Physics, Acad. Sci. USSR. The main part of the instrument is a cylindrical body in which a rotor is mounted strictly coaxially with the yy axis (Fig. 1). The rotor consists of a cylinder with radius R_r and length L_r, and two conical surfaces each ΔR high, equal to the gap in the cylindrical part. The shape of the rotor ends is so chosen that the relative deformations and velocity gradients, and therefore the corresponding shearing stresses, are equal, in the first approximation, throughout the deformed material. The stress heterogeneity is $\sim 7\%$ in the annular gap, and not more than 0.1-0.2% at the ends. There are two glass windows at the upper parts of the end surfaces of the cylinder. The entire space between the body and the rotor is filled with the material under test. The

*The photoplasticity method is the term applied to optical polarization studies of the stressed state in plastic deformation, regardless of whether the model material has a yield value, such as polystyrene [7, 10], or is a highly viscous liquid, such as rosin-based materials [3]. The photoviscosity method comprises optical polarization studies of liquid flow, carried out for hydrodynamic purposes.

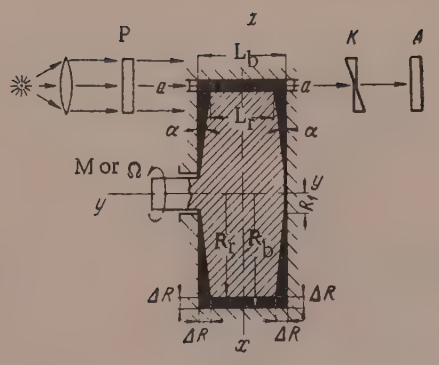


Fig. 1. Diagram of photoplastoviscosimeter.

instrument is placed between the polarizer P and analyzer A of the KSP-5 (coordinated synchronous polarimeter) apparatus so that the optical axis of the latter lies along the window axial line aa. The optical effect is measured by means of the Berek compensator K, and the extinction angles are read off from the rotation angle of the Polaroids.

The moment due to each of the end surfaces of the rotor is

$$M_E = \int_{R_1}^{R_r} \tau 2\pi r^2 dr = \frac{2}{3}\pi (R_r^3 - R_1^3)\tau,$$

where τ is the shearing stress; r is the distance from the instrument axis to a random ring of width dr on the end; R_1 is the radius at which the conical end surface starts. Since $R_1^3 < 2\%$ of R_r^3, we can write

$$M_E = \frac{2}{3}\pi R_r^3 \tau.$$

The moment produced on the cylindrical rotor surface is

$$M_c = 2\pi R_r^2 L_r \tau.$$

Therefore the moment acting on the rotor shaft

$$M = M_c + 2M_E$$

is related as follows to the stress τ:

$$\tau = \frac{M}{2\pi R_r^2 \left(L_r + \frac{2}{3} R_r\right)}.$$

The average deformation rate is

$$D = \frac{v}{\Delta R} = \frac{R_r}{\Delta R} \frac{d\varphi}{dt},$$

where v is the linear velocity of the rotor surface; $d\varphi/dt$ is the angular velocity of the rotor. With the degree of stress uniformity indicated above taken into account, the difference between the true velocity gradient on the rotor surface and the average value does not exceed a few per cent. The present investigations were carried out by the constant shearing-stress method—different constant torques were applied to the instrument rotor. This was done in the usual way by means of weights and pulleys, frictional losses in free running being taken into account. The error in torque measurements did not exceed 5%, and in measurements of the stress τ, 3-4 g/cm^2. The rotor speed was determined visually from its angle of rotation over different time intervals, to an accuracy within 2-3%.

The Pavlov elastoplastoviscosimeter [14] was used for determinations of shearing stress—deformation characteristics and kinetic deformation curves. Soviet ethylcellulose K-290 was used, of molecular weight $7.7 \cdot 10^4$, degree of substitution 46.25%; the viscosity of a 5% solution in alcoholic benzene at 20° was 290 centipoises.

Physical and Mechanical Properties of Ethylcellulose Solutions and Gels

Solutions in Benzyl Alcohol. In the shearing-stress range from 0.5 to 16-18 g/cm^2, at low concentrations and room temperature, ethylcellulose solutions in benzyl alcohol are Newtonian liquids. At concentrations of 15% and over they are non-Newtonian liquids with not very pronounced anomalous viscosity. In such cases small hysteresis effects and thixotropy are observed in consecutive increases and decreases of the deformation rate. The solution viscosities are in the range of 10^2 to 10^6 poises. The viscosities increase exponentially with solution concentration (Fig. 2) and decrease exponentially with rise of temperature.

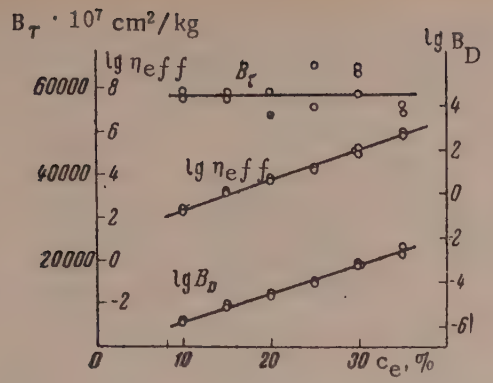


Fig. 2. Effective viscosity η_{eff}, stress-optical coefficient B_τ (determined at τ = 10 g/cm², and strain-rate optical coefficient B_D (mean), as function of ethylcellulose concentration c_e in benzyl alcohol at 20°

Solutions in Mixtures of Benzyl Alcohol and Dibutyl Phthalate. The solutions investigated all contained 30% ethylcellulose, while 1/3, 1/2, and 3/5 of the benzyl alcohol was replaced by dibutyl phthalate. The experiments were performed at τ from 0.5 to 20-23 g/cm². The viscosity increases rapidly and the viscosity anomaly becomes more pronounced with increase of the dibutyl phthalate concentration (c_d) in the solvent. Increase of c_d from 0 to 60% results in a roughly 40-fold increase (from $8 \cdot 10^4$ to $3 \cdot 10^6$ poises) of the effective viscosity η_{eff} at τ = 20 g/cm² (Fig. 3, a). The stress–deformation curves for systems containing considerable amounts of dibutyl phthalate have maxima; this means that the systems now have ultimate shearing strengths. Ultimate shearing strengths are observed at lower deformation rates with increase of ethylcellulose concentration or dibutyl phthalate in the system. Solutions containing considerable amounts of dibutyl phthalate in the solvent exhibit increasing hysteresis. At c_d of 50 and 60% the difference between the values of D at the same values of τ on the ascending and descending branches of the $D = f(\tau)$ curves reaches several hundred per cent.

The viscosity–temperature relationship for solutions with c_d = 33.3% was found to be exponential, as was the case for solutions in benzyl alcohol. With increase of temperature from 11 to 50° at τ = 20 g/cm² η_{eff} decreases from $1.1 \cdot 10^6$ to $1.6 \cdot 10^4$ poises, and log η_{eff} decreases linearly with temperature (Fig. 3, b).

The nominal-instantaneous shear modulus G_1 and high-elastic shear modulus G_2 of these solutions, at ethylcellulose concentrations c_e of about 25-35%, both lie in the 0.01-1 kg/cm² range, and G_1 is considerably larger than G_2.

Thus, ethylcellulose solutions can be used for preparation of a series of materials with mechanical properties varying over a wide range: from Newtonian liquids (10-15% solutions in benzyl alcohol) to plastic and highly structurized systems (30% solutions in a 2 : 3 mixture of benzyl alcohol and dibutyl phthalate).

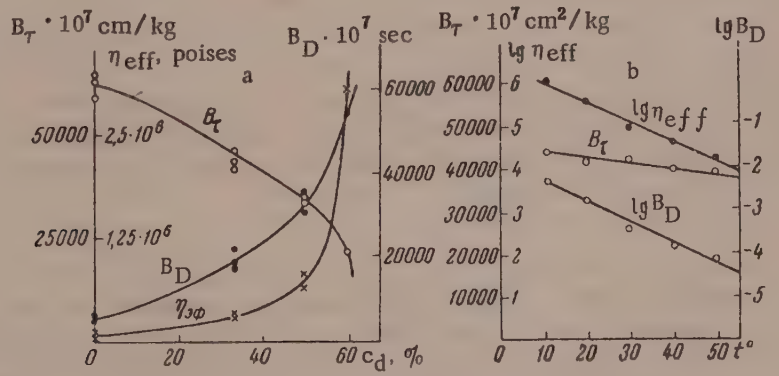


Fig. 3. Variations of η_{eff}, B_τ, determined at τ = 20 g/cm², and B_D, for 30% solutions of ethylcellulose in mixtures of benzyl alcohol and dibutyl phthalate: a) With the dibutyl phthalate content c_d in the solvent at 20°; b) with the temperature, for 33.3% dibutyl phthalate in the solvent; B_D calculated for D = 0.02 sec⁻¹.

Optical Polarization Properties of Ethylcellulose Solutions and Gels

Optical Activity Coefficients of Ethylcellulose Solutions in Benzyl Alcohol. The birefringence Δn of ethylcellulose solutions in benzyl alcohol under constant shearing stress τ is constant in time; this value becomes established in less than 30 sec after application of the stress and disappears just as rapidly when the stress is removed.

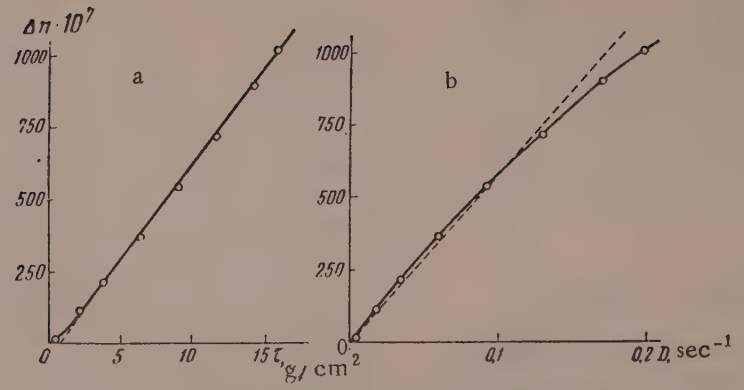


Fig. 4. Optical polarization properties of 30% ethylcellulose solution in benzyl alcohol at 20°: a) variation of the optical effect Δn with the shearing stress τ; b) variation of Δn with the strain rate D.

Plots of the optical effect Δn against stress τ in the range studied, for 10-25% solutions, are straight lines passing through the coordinate origin. For 30 and 35% solutions the function $\Delta n = f(\tau)$ at low values of τ is represented by a curve convex towards the axis of abscissas, while at $\tau > 2$ g/cm^2 it becomes linear (Fig. 4, a). The stress-optical activity coefficient is, as usual, defined as $B_\tau = \Delta n/\tau$. For 10-25% solutions B_τ is independent of τ, while for 30 and 35% solutions it decreases somewhat with increase of τ. Therefore the values of B_τ calculated for equal shearing stresses are compared in the subsequent discussion. The unit of B_τ is taken to be 10^{-7} cm^2/kg, which is equivalent to 0.98 brewster. With increase of solution concentration at 20° from 10 to 35% the value of B_τ (calculated at $\tau = 10$ g/cm^2) remains unchanged (Fig. 2), and is $5.8 \cdot 10^{-3}$ cm^2/kg (with 10% accuracy). The value of B_τ diminishes, but only very slightly, with rise of temperature (at $\tau = 10$ g/cm^2). With rise of temperature from 10 to 50° the value of B_τ for 30 and 35% solutions diminishes by only about one third (whereas the effective viscosities decrease approximately 23-fold and 55-fold with the same change of temperature at $\tau = 10$ g/cm^2). The value of B_τ decreases somewhat during aging of the solutions.

The plots of Δn against D are lines of small curvature, passing through the coordinate origin and convex toward the Δn axis (Fig. 4, b). If these curves are replaced by straight lines through the origin the error does not exceed 20-25%. The coefficient of optical activity based on the strain rate is $B_D = \Delta n/D$. The quantity B_D has the dimensions of time, and is connected with B_τ and η_{eff} by the expression $B_D = B_\tau \eta_{eff}$. Since B_τ changes little with rise of temperature and is almost independent of solution concentration, B_D depends on them in the same way as the viscosity. With increase of ethylcellulose concentration the average value of B_D, calculated from the slope of the above-mentioned straight lines, increases from $1.2 \cdot 10^{-6}$ to $3 \cdot 10^{-3}$ sec (Fig. 2); $B_{D_{av}}$ decreases exponentially with rise of temperature.

The relationship between birefringence Δn and τ, represented by the coefficient B_τ, is less sensitive to temperature than the relationship between Δn and the strain rate, represented by the coefficient B_D. This fact is an advantage in the use of these materials for investigation of stresses, a strict temperature control of the models is not needed. A further advantage of the materials is that the viscosity is greatly influenced by the ethylcellulose concentration, while B_τ is almost independent of the concentration. Solutions of different concentrations can be used for preparation of multilayer models with large variations of mechanical properties but of almost the same stress-optical coefficients.

In the table, values of B_τ for 30% ethylcellulose solution in benzyl alcohol and for certain known elastic and plastic materials are compared. The value of B_τ for ethylcellulose solution in benzyl alcohol is $\sim 6 \cdot 10^4$ brewsters, which is nearly 1000 times the value of B_τ for solid photoelastic materials, hundreds of times the value of B_τ for rosin-based photoplastic materials [3], and about 10 times the value of B_τ for gelatin gels [11]. Ethylcellulose solutions are therefore far superior in optical activity to any other materials known at this time.

Optical Activity Coefficients of Ethylcellulose Solutions in Mixtures of Benzyl Alcohol and Dibutyl Phthalate. If 33.3% of the benzyl alcohol in the 30% ethylcellulose solutions is replaced by dibutyl phthalate, Δn remains constant with time at constant τ, in the same way as for the original solutions in benzyl alcohol. After removal

Optical Activities B_τ, Fringe Values $\tau_0^{(1,0)}$, Elasticity Moduli E, and Viscosities η of Certain Optically Active Materials

Materials	$B_\tau \cdot 10^7$, cm²/kg	$\tau_0^{(1,0)}$, kg/cm²	E, kg/cm²	η, poises
Wischomlit at 20°	91	6,0	$4 \cdot 10^4$	—
Bakelite at 20°	71	7,7	$4 \cdot 10^4$	—
Polystyrene at 20°	83	6,6	$3 \cdot 10^4$	—
Gelatin–glycerol gels at 20°	$4 \cdot 10^3$—$2,4 \cdot 10^4$	0,14—0,023	5—0,2	—
Rosin–rosin oil melt at 21°	248	2,2	—	$2,5 \cdot 10^8$
30% ethylcellulose solution in benzyl alcohol at 20°	$6 \cdot 10^4$	0,009	$\sim 10^{-1}$	10^5

of the stress the optical path difference disappears rapidly, as in the case of solutions in benzyl alcohol. For solutions in which the dibutyl phthalate contents c_d are 50 and 60%, Δn rapidly reaches a certain maximum value after application of the stress, and then decreases with time at constant τ; the decrease is several tens per cent. These solutions still retain a path difference of some tens of millimicrons 1-2 min after removal of the stress; this falls to zero in 20-30 min. It follows from Fig. 5, a, that the optical activity B_τ of the material decreases and B_τ becomes more strongly dependent on τ with increase of c_e. As c_d increases from 0 to 60%, the value of B_τ (at $\tau = 20$ g/cm²) is diminished almost threefold, (Fig. 3, a). The curves in Fig. 5, a, for c_d of 50 and 60% show distinct inflections at τ of about 9 and 18 g/cm², respectively; beyond this the slope relative to the τ axis increases very sharply, sometimes by a factor of two or three. It is interesting to note that the $D = f(\tau)$ curves for the same solutions also have inflections at the same values of τ, beyond which the slope of the curves increases severalfold.

Introduction of dibutyl phthalate into the solvent also changes sharply the nature of the Δn-D relationship. As c_d increases the $\Delta n = f(D)$ curves move further away from the D axis and their curvature increases (Fig. 5, b). With increse of c_d from 0 to 60% the value of B_D at $D = 0.01$ sec^{-1} increases from $6 \cdot 10^{-4}$ to $5.4 \cdot 10^{-3}$ sec (Fig. 3, a). The simple explanation for the increase of B_D is that the decrease of B_τ is slower than the increase of viscosity with increase of c_d.

Structure breakdown of reinforcement effects have a considerable influence on the optical activity B_τ as well as the viscosity characteristics of the material. Thus, if we reach higher values of τ on the $\Delta n = f(\tau)$ curves and then descend to lower values, the new values of Δn are higher than before. The higher the value of c_d, the greater the increase of Δn on the return branch of the curve. When c_d is 0 or 33.3%, the increase of Δn is almost negligible, while at c_d of 50 and 60% it is several tens per cent (Fig. 5, a).

As the age of the material increases, with a corresponding increase of viscosity, the optical activity diminishes.

Extinction Angles. In a photoelastic model the directions of the principal normal stresses σ_1 and σ_3 coincide at every point with the orientation of the principal axes of the refractive-index ellipsoid. Therefore, the isocline parameter uniquely defines the direction of σ_1 and σ_3 at the points in the model through which the isocline passes. The situation is more complex in ethylcellulose solutions. Simple shear is effected in the gap of the photoplastoviscosimeter, where σ_1 and σ_3 are at 45° to the direction of shear (the flow axis). However, the isocline appears in the gap when the direction of one of the principal Polaroid planes forms the angle $\underline{i}$ (extinction angle) less than 45° with the flow axis: $i = 45° - \psi$. This means that the principal axes of the section of the refractive-index ellipsoid which lies in a plane perpendicular to the direction of the incident light deviate by the angle ψ from the directions σ_1 and σ_3. The accuracy with which the extinction angles were determined in this investigation was not high, for a number of reasons (the error was ± 3%), and the values of $\underline{i}$ can be estimated only approximately. Therefore we merely note that for these solutions in benzyl alcohol under constant stress the values of $\underline{i}$ are either constant in time or fall by 2-3° in 40 min. For solutions with added dibutyl phthalate the

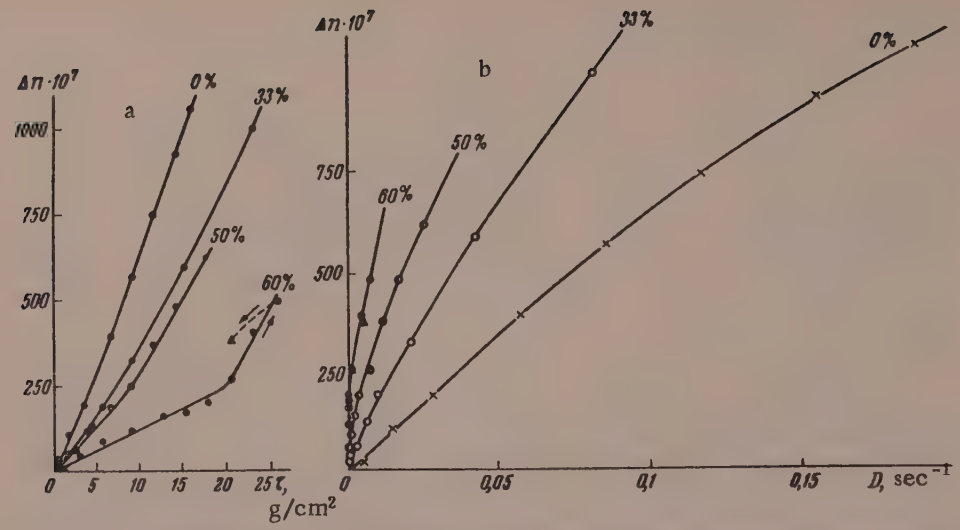


Fig. 5. Optical polarization properties of 30% ethylcellulose solutions in mixtures of benzyl alcohol with dibutyl phthalate: the numbers by the curves represent the dibutyl phthalate contents on the solvent; the dash line indicates transition from higher to lower values of τ, up to the point ▲: a) variation of Δn with τ; b) variation of Δn with D.

decrease of $\bar{i}$ is greater, and may reach 10-12° during the same period. With increase of τ from 0.5 to 3-4 g/cm^2 the values of $\bar{i}$ increase from 15-25° to 33-38°, while at $\tau > 4$ g/cm^2 they remain almost constant at $\sim 35°$, and appear to be independent of solution composition.

The following conclusions concerning the nature of the optical effect in the investigated materials can be drawn from the foregoing data on their optical polarization properties.

1. The optical effect is determined by the magnitude of the shearing stress acting on the system; in other words, by tension of the molecules and their elastic deformation, and not by the deformation rate. This is confirmed by the fact that at constant stress the deformation rate increases very sharply with temperature, whereas B_τ remains constant, in the first approximation (B_D decreases tens of time as rapidly as B_τ with rise of temperature).

2. At constant temperature and concentration, in cases where the structure of the system becomes stronger and less deformable (on addition of a poor solvent to a good one, during aging, etc.), the value of B_τ decreases. The explanation is that B_τ is directly determined by the deformability of the material. Moreover, interaction between the molecules is intensified and their freedom of movement is diminished with strengthening of the structure. Therefore, the number of molecules oriented in the direction of the acting forces and creating the total optical effect decreases at a given τ.

3. The fact that B_τ falls slightly with rise of temperature although deformability of the system increases indicates that B_τ depends on the relaxation time θ of the system. Thermal motion of the molecules increases with rise of temperature, θ decreases, and the number of ordered molecules, which give rise to the optical effect, diminishes. The influence of decreasing θ on B_τ is stronger than the influence of increasing deformability, so that B_τ decreases with rise of temperature.

4. It is possible that B_τ is associated with only a certain part and not all of the elastic deformation (such as the nominal-instantaneous component). This follows from the fact that when a constant stress τ acts on the system a constant value of Δn becomes established almost instantaneously (in 30-60 sec), whereas elastic deformation develops at a very noticeable rate for some 10 or 20 min after application of the stress.

5. The fact that B_τ is independent of concentration in the case of solutions in benzyl alcohol is extremely interesting.

SUMMARY

1. A group of highly active photoplastic materials with shear moduli of the order of 0.01-1 kg/cm^2 and viscosities in the 10^2-10^7 poise range has been prepared from ethylcellulose solutions and gels.

2. The photoplastoviscosimeter was used for simultaneous investigations of the effects of shearing stress τ and strain rate D on the birefringence Δn and viscosity η of these materials.

3. Solutions of K-290 ethylcellulose in benzyl alcohol are close in their mechanical properties to highly viscous Newtonian liquids; their birefringence varies almost linearly with the shearing stress and deformation rate.

4. Solutions of K-290 ethylcellulose in mixtures of benzyl alcohol with dibutyl phthalate tend to become plastic structurized bodies with increase of dibutyl phthalate content; the relationships between the optical effect and the shearing stress and deformation rate accordingly become nonlinear.

5. The stress-optical coefficient B_τ of 10-35% ethylcellulose solutions is almost independent of ethylcellulose concentration, and lies in the range of $5\text{-}7 \cdot 10^4$ brewsters, which is much higher than the activity of any other known optically active materials.

6. The value of B_τ decreases with addition of dibutyl phthalate to benzyl alcohol, and with fall of temperature.

7. These results show that it is possible, in principle, to use the optical polarization method for studying stresses and deformation rates in soft bodies undergoing plastic deformation.

LITERATURE CITED

1. G. V. Vinogradov, Doklady Akad. Nauk SSSR 71, No. 3 (1950); Proceedings of All-Union Conference on Colloid Chemistry [in Russian] (Izd. AN UkrSSR, Kiev, 1952) p. 249.
2. G. V. Vinogradov and V. N. Manin, Zhur. Tekh. Fiz. 28, 279 (1957); N. M. Vyatskikh, Izvest. N.-i. In-ta Gidrotekhniki 20, 257 (1937).
3. S. I. Gubkin, S. I. Dobrovol'skii, and B. B. Boiko, Photoplasticity [in Russian] (Izd. AN Beloruss. SSR, Minsk, 1957).
4. Ya. V. Mamul', Zhur. Tekh. Fiz. 6, No. 11 (1936).
5. A. D. Mikhailov, Zhur. Tekh. Fiz. 8, 885 (1938).
6. A. V. Stepanov, Zhur. Tekh. Fiz. 19, 205 (1949).
7. R. Hiltscher, Z. Vereines dtsch. Ingr. 95, No. 23, 777 (1953).
8. R. Weller, J. Appl. Mech. 14, No. 2, A-103, (1947).
9. D. N. Osokina, V. P. Pavlov, G. V. Vinogradov, and M. V. Gzovskii, Summaries of Papers at the 9th Conference on General Questions of High-Polymer Chemistry and Physics [in Russian] (Izd. AN SSSR, Moscow, 1956) p. 124.
10. R. Hiltscher, Problemy Sovr. Metallurgii No. 1 (25), 120 (1956).
11. M. V. Gzovskii, Coll. Sci. Res. Inst. "Problems of Tectonics" [in Russian] (Gosgeoltekhizdat, 1959).
12. M. V. Gzovskii, Sov. Geologiya No. 4, 53 (1958).
13. V. P. Pavlov and G. V. Vinogradov, "The Photoplastoviscosimeter" Summaries of Papers on Chemistry and Technology of Petroleum and Gas for 1956 [in Russian] (Izd. AN SSSR, In-t Nefti, 1957) p. 71.

INFLUENCE OF CAPILLARY CONTRACTION FORCES ON MECHANICAL PROPERTIES AND STRUCTURE OF DRYING BODIES

M. S. Ostrikov, I. V. Rostovtseva, G. D. Dibrov, and E. P. Danilova

Rostov-on-Don University; Groznyi Petroleum Institute; Rostov-on-Don Institute of Structural Engineering

Translated from Kolloidnyi Zhurnal, Vol. 22, No. 4, pp. 443-450, July-August, 1960
Original article submitted March 27, 1959

We have studied the forces of capillary contraction which develop in the course of physicochemical processes in drying disperse and high-molecular structures. These forces, together with the adsorptional influence of the medium studied by Rebinder and his co-workers [1], constitute an important factor which influences the formation of the outer layers of the disperse body, its shape, internal structure, and mechanical properties.

The experimental results published earlier [2], and the new data presented below were obtained in studies of gelatin, nitrocellulose, wood, hydrated oxides of iron and other metals, highly disperse clays, plates made from cement hardened for different periods, and certain other substances with various additives. The results indicate that the forces in question operate by a common molecular surface mechanism, despite the great differences in chemical composition, structure, and physical properties of the materials studied.

The curves representing the growth of capillary contraction forces (F_σ) during the drying of various systems are always S-shaped. Different portions of these curves (Fig. 1, 2, and 3) reflect three stages in the development of these forces. The lowest, slightly ascending region corresponds to the start of the action of capillary forces, i.e., to the period of initial formation of a surface layer of the system (becoming denser under the action of capillary forces), and the inception of a moisture gradient. The second steep region corresponds to completion of the formation of the upper layer of maximum density [3], its gradual dehydration up to the loss of solvation layers, and spread of the influence of capillary contraction forces into the depth of the body, up to total removal of the liquid phase. The third and top region of the curve, which sometimes passes through a maximum, reflects three effects: 1) balancing of the compressive forces of capillary contraction by opposing forces of elastic resistance of the structure; 2) influence of relaxation processes near the stress maximum; 3) disappearance from the process of the action of capillary forces after evaporation of the remains of the liquid phase, i.e., after disappearance of the meniscuses (thin liquid microbridges) connecting adjacent structural elements.

Influence of the properties of the liquid phase. The data presented graphically in Fig. 1, 2, and 3 indicate that the maximum values of the capillary contraction forces differ greatly in systems of different chemical nature. The latter determines all the qualitative peculiarities and energy relationships in the interaction of the solid phase with the liquid medium in the phenomenon in question.

However, the maximum values of F_σ may vary considerably systems with the same solid disperse phase if the physicochemical properties of the liquid phase are varied by means of additives. For example, an acid medium has a somewhat weakening effect on the capillary contraction forces in silica gel. Additions of naphthenic acids produce a larger decrease of F_σ. Additions of alkali to silica gel increase the capillary contraction forces considerably (Fig. 1).

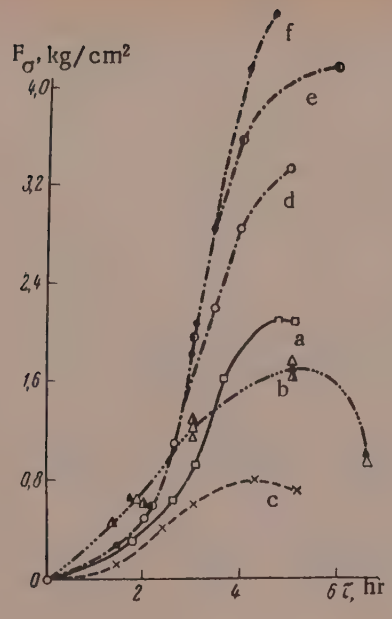


Fig. 1. Development of capillary contraction forces (F_σ) in pure silica gel (a), and in silica gels with additions of hydrochloric acid (b), naphthenic acids (c), and increasing amounts of alkali (d, e, f).

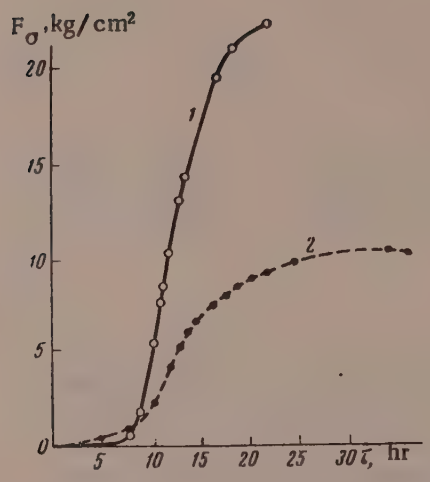


Fig. 2. Effect of polarity of the liquid medium on F_σ in drying wood (aspen): 1) specimen saturated with water; 2) specimen saturated with gasoline by displacement of water by means of progressive treatment with liquids of decreasing polarity.

The effects of hydrochloric acid and caustic soda concentrations in solution on silica gel are shown in Fig. 4. Even at low acid concentrations the hydrogen ions can displace all other cations, forming a saturated and dense double layer and thereby lowering the electrokinetic potential to a minimum. On the basis of the generally accepted electrocapillary concepts it is to be expected that the surface of the silica gel particles should accordingly become less hydrophilic, and the capillary contraction forces, which depend directly on hydrophily, should diminish accordingly . Evidently any further increase of the amount of hydrochloric acid, if it is not too large, should not have any significant effect (Fig. 4).

The action of alkali probably also consists of exchange interaction of sodium cations with the silica gel surface. Sodium ions displace hydrogen ions. This process is fairly rapid and irreversible because the displaced hydrogen ions form undissociated water molecules with hydroxyl ions.

The relationship between capillary contraction forces and the amount of alkali (c) per gram of dry silica gel may be represented by the empirical formula:

$$F_\sigma = a + b \log c,$$

where a and b are empirical constants (Fig. 4, curve b).

At high alkali concentrations there is an abrupt discontinuity in this relationship, when the capillary contraction forces begin to decrease; this indicates a change in the nature of the interaction between the silica gel and the liquid medium, and in particular, a weakening of structure-forming coagulational and crystallizational bonds. These effects of acids and alkalies on F_σ are consistent with adsorption data on the influence of the medium on the structure of silica gel [4].

The influence of polarity of the liquid medium on capillary contraction forces acting in a radial direction was demonstrated in the case of wood. Wood specimens (20 × 4 × 1 cm) were cut from the butt end of the trunk through the middle and at right angles to its length. The wood was first completely saturated with water, and then treated successively with a series of liquids of progressively decreasing polarity (water, ethyl alcohol, butyl alcohol, amyl alcohol, gasoline). Variations of capillary contraction forces in wood during evaporation of gaso-

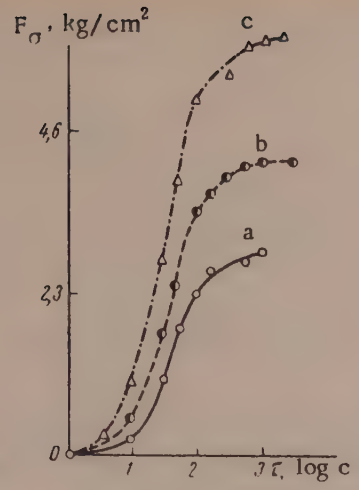


Fig. 3. Development of F_σ in ferric hydroxide (a), and in the same gel with additions of 13% (b) and 3% (c) of asbestos.

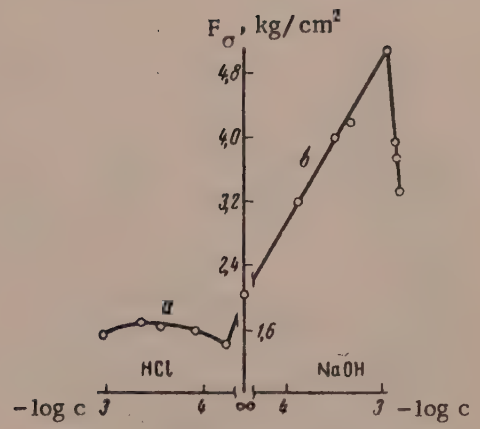


Fig. 4. Dependence of the maximum values of F_σ in silica gel on the amounts (c) of acid (a) and alkali (b) previously added.

line and water are plotted in Fig. 2. When the nonpolar medium is replaced by a polar liquid the capillary contraction forces return to near the original value.

Role of structural and mechanical properties. The role of the mechanical properties of the structure in the effects under consideration, and the interaction between capillary forces and elastic or elasticoplastic resistance forces in the structure, constitute a very important part of the problem in question. If the system is fully wet or is incapable of structure formation, the tension at its surface differs little from the surface tension of the liquid medium. In the course of drying the surface layer of the disperse system becomes more dense, the necks of the micropores become narrower, and capillary forces increase accordingly. The mechanical resistance of the structure increases at the same time. At the start of the process the capillary forces exceed the mechanical resistance of the structure. Subsequently, however, these forces balance each other; this corresponds to the maxima on the curves discussed above. Some decrease of stress in the drying sample is possible during further drying, both as the result of relaxation and owing to disappearance of the micromeniscuses on which the capillary forces act.

Results obtained in measurements of capillary contraction forces in ferric hydroxide films with and without additions of powdered asbestos are given in Fig. 3. These results indicate that small amounts of added asbestos, which acts as a structure-forming and microprotective chemically neutral agent, produce a very considerable increase of the capillary contraction forces; the effect of further increase of the amount of asbestos is to lower these forces rather than to increase them.

The dependence of the maximum capillary contraction forces on the relative proportions of montmorillonite and fine-fiber asbestos in mixtures is shown in Fig. 5, curve a; this is similar to curve b, which represents capillary contraction of gelatin in which the structure has been hardened by treatment with formaldehyde solutions of various concentrations. An interesting fact is that curve b for the same specimen at the initial period of drying follows the opposite course. This means that specimens with a more rigid structure begin to exhibit capillary condensation forces earlier, i.e., at considerable moisture contents. These results provide convincing confirmation of the foregoing general views on the dual role of the mechanical properties of the structure at different stages of drying.

When a gel with an elastic structure is dried, the structure undergoes considerable deformation in directions which correspond to the directions of the capillary contraction forces. The structure of a dry elastic gel in this deformed stressed state is fixed, and can be retained indefinitely by the action of secondary intermolecular and intramacromolecular bonds which arise during contraction of the system in the drying process. The secondary bonds arise and are stable only in absence of the liquid medium. Stresses in the structure can be determined by optical direct or indirect methods [5].

It follows that in a dry elastic gel the work done by capillary forces in deformation of the structural elements and of the structure as a whole is stored as a latent reserve of free energy. This energy is liberated by

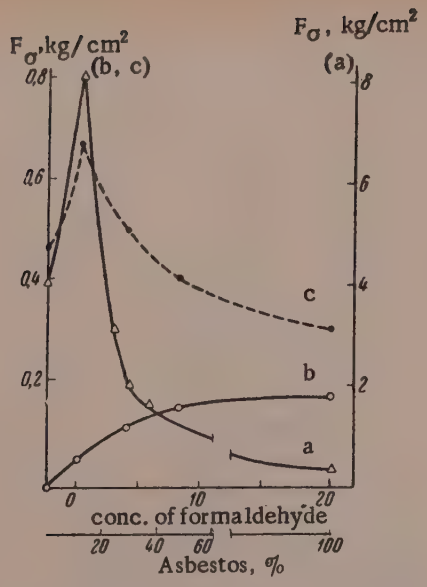


Fig. 5. Effects of structure-forming agents on F_σ of gelatin and montmorillonite: a) montmorillonite with increasing amounts of fine-fiber asbestos; c) gelatin, in relation to the concentration of formaldehyde solution used in its treatment; b) same, at lower moisture content.

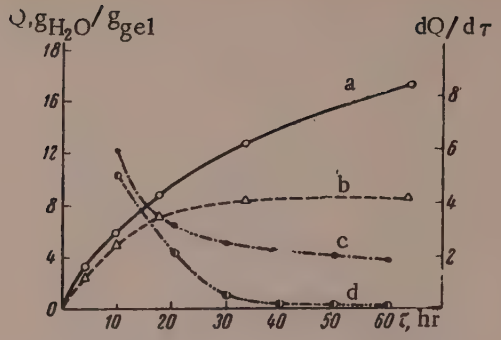


Fig. 6. Decrease of swelling (a, c) and swelling rate (b, d) of gelatin under the influence of moist surface heat treatment: a,c) untreated gelatin; b, d) treated gelatin.

the action of a liquid medium, which breaks down the bonds which are not resistant to it. The elastic forces in the structure, in tending to return the system to its initial shape, then begin to act as forces sucking in the liquid medium. This is the role of elastic forces in the structure as one of the most important factors in swelling.

The significance of this factor is confirmed by the following experiment. If dry gelatin is immersed for one second in boiling water, it has time to swell only slightly. However, its properties are changed very considerably (Fig. 6). The swelling capacity decreases considerably, and the swelling rate diminishes. The decrease of swelling is due to the fact that this treatment causes thermal relaxation and regrouping of the macromolecules [6] in a thin surface layer of the structure, which is under the greatest stress.

A gelatin plate treated in this way has lost a considerable part of the latent reserve of free energy in its structure, which was created by capillary contraction forces when it was dried. The ability of the structure to imbibe water is weakened accordingly. That is why dry gelatin cannot be dissolved in hot water without preliminary swelling at normal temperatures.

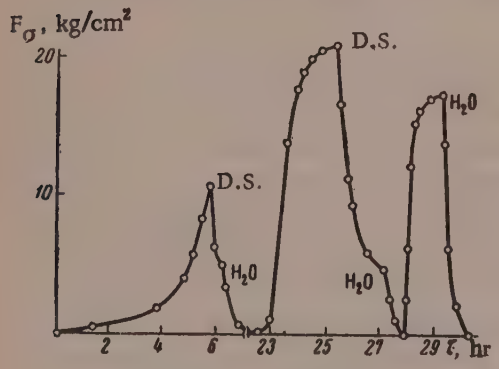


Fig. 7. Reversibility in the drying of montmorillonite: D. S.) Drying stopped; H_2O) humidification by water vapor.

In the transition from drying to humidification of disperse systems the action of molecular surface forces is transferred from the liquid–air interface to the growing solid–liquid interface. The liquid molecules extend their action into the depth of the humidified body and break down the secondary structural bonds formed under the compressive influence of capillary contraction forces during the preceding drying. The intensity of this process depends on the affinity of the liquid for the solid phase and on the stability of the structure to water. Such action can be exerted not only by liquids but also by vapors, which undergo adsorption and capillary condensation in the necks of the micropores and penetrate rapidly into the solid.

Data obtained in experiments with bentonite are plotted in Fig. 7. The curve represents the increase of capillary contraction forces during drying, and their decrease when drying is stopped or under the influence of water vapor. The initial ascending branch represents the first and the start of the second stage in the development of the forces.

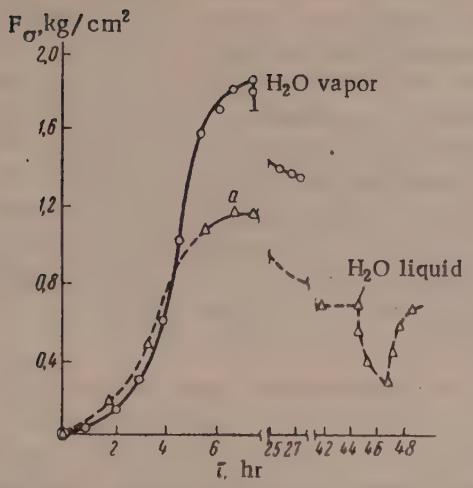


Fig. 8. Irreversible processes in drying of silica gel: a) silica gel with added HCl; b) original silica gel.

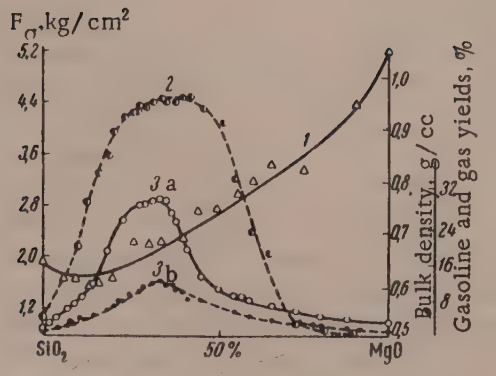


Fig. 9. Effect of composition on properties of magnesia-silica catalysts: 1) F_σ; 2) bulk density; 3a) gasoline yield in gas-oil cracking; 3b) gas yield in the same process.

As soon as drying is stopped F_σ falls rapidly. The fall is caused by the influence of residual liquid water which migrates from the inner layers to the external macrosurface along the internal pore surfaces. In presence of thermal gradients moisture can migrate through the vapor phase, by thermoosmosis, or by the thermal capillarity effect.

The second part of the curve in Fig. 7 indicates the considerable water-holding power of bentonite. After the drying is stopped some water is still retained in the specimen; this water passes into the denser surface layer, humidifies it, and rapidly lowers F_σ. It is evident from this that curves of this type for various disperse materials can be used for assessment of their water-holding power, properties of the structure and of its dense surface layer (which plays an important role in the existence of the body itself), and of the interaction of the layer with the medium. The rate and even the direction of moisture exchange with the medium, and in some instances the principal mechanical properties, depend on the properties and structure of this layer.

The steepest descending (to zero) branches of the curve (Fig. 7), found for the action of water vapor, and all the data discussed above, indicate that the structure of dry bentonite is unstable to the action of water.

Different results are obtained for silica gel, which has a water-resistant and rigid structure in which irreversible crystallizational bonds predominate (Fig. 8). The resistance of the structure to the compressive action of capillary forces during drying is the cause of the very low values of F_σ for silica gels used for preparation of the experimental specimens. It is clear from Fig. 8 that F_σ was decreased only slightly by the action of water vapor on silica gel for 20 hr, whereas in the case of bentonite, with capillary forces ten times that magnitude, less than one hour was needed to remove them completely (Fig. 7).

Silica gels have especially high resistance to water and structural rigidity in an acid medium. The capillary contraction forces do not reach their initial maximum value in alternate moistening and drying; this indicates irreversibility, characteristic for acid silica gel, of the changes which took place under the simultaneous influence of stresses and surface molecular water layers. The irreversibility is intensified by the formation of new crystallizational bonds in the structure.

Action of capillary contraction forces in formation of an active catalyst surface during drying. In view of the action of capillary contraction forces in formation of external and internal microsurfaces in drying disperse systems, it was natural to expect that these forces have a significant influence on structure formation in certain catalysts which are dried in the course of production. Results obtained in a study of magnesia-silica catalysts [7] used in petroleum cracking are of great interest in this respect. Figure 9 shows that the activity of these catalysts is at a maximum with 30-35% MgO in mixtures with SiO_2. This composition also corresponds to the maximum bulk density.

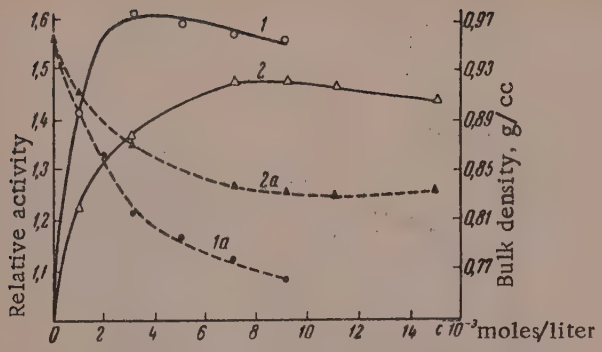


Fig. 10. Activating effect of surface-active substances (c, moles/liter) on magnesia-silica catalyst of the optimum composition (35% MgO): 1 and 2) relative activities of the catalyst as functions of the concentration of added naphthenic acids (1) and butyric acid (2); 1a and 2a) bulk densities of the same catalysts.

A study of the effect of composition of magnesia-silica mixtures on F_σ (curve 1, Fig. 9) revealed a considerable negative deviation from additivity. It appears that the entire surface, where capillary contraction forces develop, is dominated by silicic acid, which acts as a surface-active component. This action of silicic acid is associated with the fact that it can exist in the form of a semicolloid [8]. The increase of bulk density of the mixtures is the consequence of the fact that in the simultaneous presence of the components dispersion proceeds more effectively during preparation of the catalyst.

It was demonstrated experimentally that the activity of the most active magnesia-silica catalyst (35% MgO) can be raised by addition of surface-active substances during preparation. Such substances diminish the capillary contraction forces which compress the formed catalyst grains during drying. Figure 10 gives data on the relative activity increase of magnesia-silica catalysts and decrease of bulk density as functions of naphthenic and butyric acid concentrations. Catalysts activated by surface-active agents exhibited considerably higher sorption of methyl alcohol vapor. The resultant sorption isotherms contained branches representing capillary condensation, with hysteresis loops in desorption.

The specific action of surface-active substances on catalyst pore structure was noted. This is probably associated both with their influence on capillary forces and with the characteristic effects of the additives on structure-forming intermicellar bonds. Further studies of structure formation in catalysts and adsorbents in presence of various surface-active substances should reveal potentialities for production and accurate regulation of predetermined structures.

SUMMARY

1. The development of capillary contraction forces F_σ during the drying of disperse, porous, and high-molecular systems can be divided into three periods: origination and slow growth of F_σ, rapid increase of F_σ, and completion of the drying process. These periods correspond to variations of the relationship between capillary contraction forces and forces of elasticoplastic resistance of the structure.

2. The properties of the liquid medium influence the development of capillary condensation forces. In the case of silica gel an acid medium produces some decrease and an alkaline medium a considerable increase in the capillary contraction forces. An empirical formula for the magnitude of these forces in relation to alkali concentration is given.

3. The relationship between the maximum values of the capillary contraction forces and the growing structural strength is represented by a curve with a sharp maximum; this confirms the concept of the dual role of the structure, which determines the inception of these forces and at the same time gives rise to rigidity in the system, which prevents the appearance of these same forces.

4. The catalytic activity of magnesia-silica cracking catalyst can be raised considerably by introduction of surface-active additives. The concept of a capillary activation mechanism is confirmed by adsorption data which demonstrate the influence of surface-active additives on the catalyst structure.

The authors are deeply grateful to Academician P. A. Rebinder for his interest and very valuable advice.

LITERATURE CITED

1. P. A. Rebinder, Usp. Khimii 26, 1320 (1957); Izvest. Akad. Nauk SSSR, Otdel. Khim. Nauk No. 11, 1284 (1957);* Kolloid. Zhur. 20, 527 (1958);* E. E. Segalova, R. R. Sarkisyan, and P. A. Rebinder, Kolloid.

*Original Russian pagination. See C. B. translation.

Zhur. 20, 610 (1958);* G. M. Bartenev, I. V. Yudina, and P. A. Rebinder, Kolloid. Zhur. 20, 655 (1958);* P. A. Rebinder, Physicochemical Mechanics [in Russian] (Izd. "Znanie," Moscow, 1958) Series 4, No. 39-40.

2. M. S. Ostrikov, S. I. Pakhomov, and N. P. Sinel'nikov, Izvest. Akad. Nauk Beloruss. SSR, Ser. Fiz.-Khim. Nauk No. 4, 119 (1956); M. S. Ostrikov, G. D. Dibrov, and E. P. Danilova, Doklady Akad. Nauk SSSR 118, 751 (1958);* Doklady Akad. Nauk UkrSSR No. 3, 299 (1958).
3. P. V. Kozlov and B. N. Korostylev, Zhur. Fiz. Khim. 31, 653 (1957).
4. I. B. Slinyakova and I. E. Neimark, Kolloid. Zhur. 20, 84 (1958).*
5. S. A. Shreiner and P. I. Zubov, Kolloid. Zhur. 19, 651 (1957).*
6. P. I. Zubov and M. P. Zverev, Kolloid. Zhur. 18, 679 (1956).*
7. I. V. Rostovtseva, Dissertation [in Russian] (Rostov State University, 1954).
8. M. S. Ostrikov and V. T. Gleim, Zhur. Priklad. Khim. 30, 508 (1957).*

*Original Russian pagination. See C. B. translation.

EXCHANGEABLE ACIDITY IN COLLOIDAL SYSTEMS OF NATURAL ALUMINOSILICATES

S. N. Papuashvili, M. E. Shishniashvili, and L. V. Kuridze

Institute of Chemistry, Academy of Sciences USSR; Laboratory of Colloid Chemistry, Tbilisi

Translated from Kolloidnyi Zhurnal, Vol. 22, No. 4, pp. 451-456, July-August, 1960
Original article submitted August 12, 1958

There exist two opposing views on the nature of exchangeable acidity. According to Vernadskii [1] the exchange adsorption properties of aluminosilicates are determined by their strongly acidic properties. Gedroits and his school [2] consider that interaction of neutral salts with acid aluminosilicates consists primarily of direct exchange between hydrogen ions of the acid aluminosilicate and cations of the added electrolyte. Lewis, Squires and Broughton [3] hold the view that electrodialyzed bentonite is "hydrogen bentonite," which is titrated with alkali like an ordinary acid, and even the "equivalent weight" of clay can be calculated. Supporters of the other view [4-7] consider that the exchangeable acidity of acid aluminosilicates is determined by exchangeable aluminum ions.

Some workers [8, 9] report that the exchangeable acidity of aluminosilicates is determined by both hydrogen and aluminum ions, the quantitative proportions of which vary in wide limits in accordance with the nature of the aluminosilicate itself and with the external conditions.

Aleshin and Goletiani [5, 10] showed that the exchangeable acidity of red-soil colloids and electrodialyzed askangel is due to aluminum. They state, however, that the passage of aluminum into solution is the direct result of decomposition of clay minerals by the action of neutral salts. Certain Indian workers [8, 9] found that the quantitative Al^{3+} : H^{+} ratio in salt extracts of electrodialyzed bentonite increased with the concentration of neutral salt. Chernov and his associates [6, 11] state that as the result of a chemical neutralization reaction between the acid sorption complex and free aluminum hydroxide exchangeable hydrogen ions on the particle surfaces are gradually replaced spontaneously by aluminum ions. Mieserov [12] demonstrated that H-aluminosilicates are unstable and gradually pass spontaneously into Al-aluminosilicates.

The object of the present investigation was to study how exchangeable acidity arises, and to investigate the gradual replacement of hydrogen ions by aluminum ions during electrodialysis of askangel bentonite clay.

The materials used were highly disperse askangel isolated from native askangel, and Na-askangel. The Na-askangel was prepared by repeated treatment of highly disperse askangel with NaCl solution to complete saturation with Na ions, with subsequent washing with distilled water until there was no reaction for Cl'. The electrodialysis was performed in the usual three-compartment electrodialyzers [13]. Distilled water was used as the liquid for electrodialysis; the membrane was cellophane. The electrodialysis was effected at a potential gradient of 50-80 v/cm. The amounts of base (exchangeable cations) which passed into the cathodic solutions were determined by titration with acid at each change of the anodic and cathodic solutions.

The following procedure was used for determination of exchangeable aluminum and of hydrogen formed in askangel suspensions during electrodialysis: after desorption (removal) of a certain quantity of the exchangeable cations the electrodialyzed suspension was treated once with 1 N KCl solution. The amounts of aluminum and

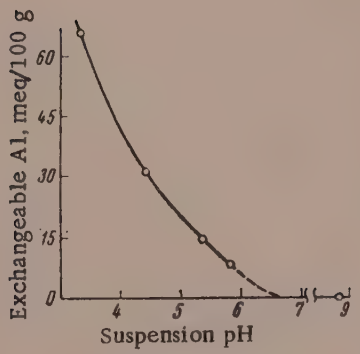


Fig. 1. Variation of the amount of exchangeable aluminum with pH of the askangel suspension during electrodialysis.

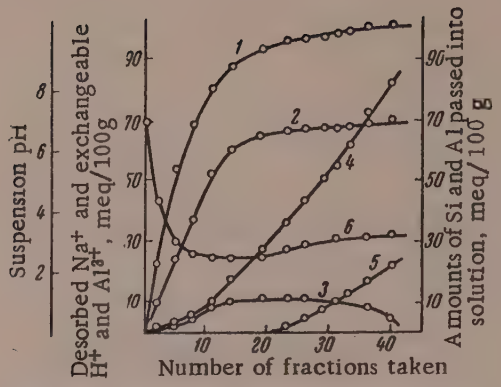


Fig. 2. Kinetics of the occurrence of exchangeable acidity during electrodialysis of Na-askangel: 1) Desorption of Na ions; 2) exchangeable aluminum; 3) exchangeable H ions; 4) SiO_3 ions and 5) Al ions which passed into the cathodic solution; 6) pH of suspension.

hydrogen which passed into the KCl solution were determined from the inflections on the potentiometric titration curves of the KCl extracts. Exchangeable aluminum was also determined in the KCl extracts by the gravimetric method. The kinetics of removal of the main components (silicon, aluminum, and iron) from the askangel suspension into the anodic and cathodic solutions was also investigated.

Preliminary experiments showed that the amount of aluminum contained in the KCl extracts of electrodialyzed askangel varies sharply with the degree of leaching. The greater the desorption of exchangeable cations during electrodialysis, the greater the fall of pH (down to a certain value), and the greater the amount of exchangeable aluminum (Fig. 1). Formation of exchangeable aluminum during electrodialysis begins even when the askangel suspension is very slightly acid.

The data in Fig. 2 show that in electrodialysis of highly disperse Na-askangel exchangeable sodium ions are removed very rapidly at the initial stages of the process. The pH of the suspension falls sharply (to 2.45) at this stage also. Removal of Na ion stops almost entirely during subsequent leaching, and the pH of the suspension begins to rise very slowly (to 3.24).

It is interesting to note that formation of mobile aluminum begins at the earliest leaching stage, and its quantitative course coincides completely with the course of desorption of Na ions (Fig. 2). This fact shows that formation of mobile aluminum proceeds in parallel to removal of exchangeable cations from the askangel. However, the results show that the amount of exchangeable aluminum is always less than the amount of desorbed cations.

The results of our earlier investigations [14, 15] showed that aluminum is removed fairly rapidly, together with the other main components (silicon and iron), during actual leaching of red-soil colloids and askangel. Therefore the direct possibility of conversion of structural aluminum into the exchangeable adsorption state arises in the leaching process itself. Trenel [16] referred to the possible decomposition of the aluminosilicate complex during electrodialysis.

To give a fuller idea of the decomposition of acid aluminosilicates, we present data in Fig. 2 which show that removal of soluble silicic acid from askangel begins at the very start of the leaching process. Transfer of aluminum and iron into the cathodic fractions does not begin at once, but only after the main bulk of the exchangeable cations have been leached out. This lag in the removal of aluminum and iron is partly attributable to the high alkalinity of the cathodic solutions and to partial conversion of aluminum and iron into the exchange adsorption state. The total amounts of SiO_2 and Al_2O_3 which had passed into the anodic and cathodic solutions by the end of electrodialysis were 2.4 and 0.39% of the total amount of Na-askangel dialyzed, while in electrodialysis of highly disperse askangel, the respective amounts were 0.60 and 0.14%.

Amounts of H and Al Ions Passed Into KCl Extracts of Electrodialyzed Suspensions of Na-Askangel as Functions of the Time Between the End of Electrodialysis and the Start of Treatment with KCl Solution. The Original Na-Askangel Contained 101 meq of Exchangeable Na Ions per 100 g; Initial pH of the Suspension was 6.96

Duration of electrodialysis, hr	Amt. of Na^+ desorbed, meq/100 g	Suspension pH	Time,* hr	Amt. of H^+ and Al^{3+} passed into KCl extract, meq/100 g of askangel				$\frac{\Delta Al^{3+}}{\Delta H^+}$
				Al^{3+} by gravimetric method	from potentiometric titration curves		$H^+ + Al^{3+}$	
					Al^{3+}	H^+		
~5	79,4	2,4	1	38,5	34,4	19,4	53,7	—
			240	43,3	38,1	14,7	52,8	0,80
			960	50,6	44,2	9,2	53,4	1,10
6	87,8	2,0	1	40,9	36,0	22,7	58,2	—
			240	45,8	42,2	14,3	56,5	0,74
			960	53,0	44,2	11,9	56,1	0,82
			2064	57,8	48,7	8,6	57,3	1,39
7	99,3	2,61	1	44,1	42,7	15,4	58,1	—
			144	49,1	46,4	13,7	60,0	2,10
			1600	65,5	54,7	10,3	65,0	2,15

*Between the end of electrodialysis and start of treatment with KCl solution.

It is interesting to note that the molar ratio of SiO_2 to aluminum and iron sesquioxides which passed into the dialysis liquid diminished with the duration of electrodialysis. When base removal was largely complete, this ratio approached to the molar ratio ($SiO_2 : Al_2O_3$) in the askangel. This fact also indicates that the clay mineral, montmorillonite, does in fact undergo partial decomposition during leaching.

In the preceding experiments electrodialysis of each askangel specimen was continued for a long time (with fairly long intervals), and moreover the contents of H and Al ions in the electrodialyzed specimens were not determined immediately after electrodialysis had been stopped. However, some workers [11] report that as the result of chemical action, hydrogen ions are gradually replaced by aluminum ions on the surfaces of soil colloid particles which had been treated with acid. Accordingly, Na-askangel suspensions were subjected to intensive, continuous, and brief dialysis, in order to study spontaneous substitution of H ions (formed in the course of leaching) by aluminum ions. Three electrodialyzed suspensions were obtained in this way, with different contents of desorbed sodium cations: 79.4, 87.8, and 99.3 meq/100 g of askangel. In this series of experiments yet another electrodialyzed suspension was taken for comparison; this was prepared by leaching of Na-askangel for 6 months. These suspensions were treated once with 1 N KCl solution immediately after the end of electrodialysis and at various time intervals between the end of electrodialysis and the start of treatment with KCl solutions. The H and Al ion contents and total acidity of the KCl extracts were determined from the inflections on the curves obtained by potentiometric titration with 0.1 N NaOH solution (Fig. 3 and 4).* The Al ion contents were also determined gravimetrically.

The results show (see table and Fig. 3) that for each electrodialyzed suspension the H ion contents of the KCl extracts gradually decrease and the Al ion contents increase with increase of the time between the end of electrodialysis of the askangel and the start of its treatment with KCl solution. Potentiometric titration of a KCl extract of electrodialyzed askangel made by leaching of Na-askangel for 6 months showed total absence of H ions, so that the acidity of the KCl extract was due almost entirely to Al ions (Fig. 4).

It is interesting to note that the ratio between the amount of newly formed Al ions and the amount of sorbed H ions (found from the titration curves) is initially less than unity for the first two suspensions, and later becomes

*Figure 3 shows titration curves for 14 ml lots of KCl extracts, corresponding to 0.244 g of electrodialyzed askangel. Over the region up to the first inflection on each curve the amount of alkali taken approximately corresponds to the H ion content, and between the first and second inflections it corresponds to the Al ion content. For comparison, the titration curve for a mixture of pure $AlCl_3$ and KCl solutions is shown in Fig. 3.

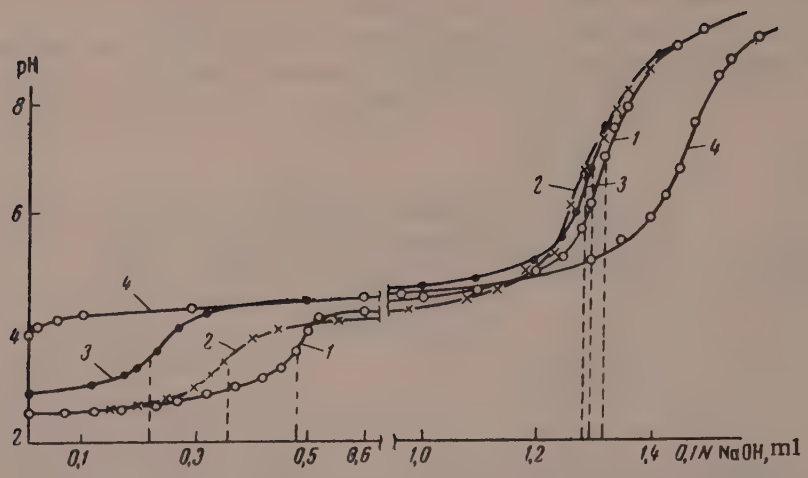


Fig. 3. Potentiometric titration of KCl extracts from electrodialyzed askangel (amount of Na ions desorbed = 79.4 meq) at various time intervals: 1) 1 hr; 2) 10 days; 3) 40 days; 4) mixture of $AlCl_3$ and KCl solutions.

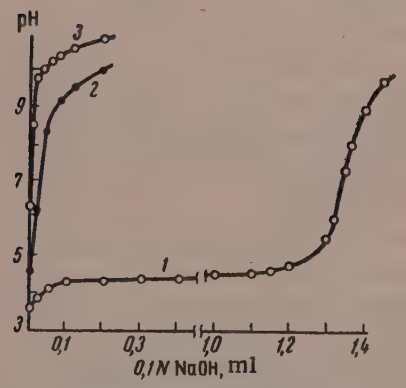


Fig. 4. Potentiometric titration of KCl extract of askangel obtained after 6 months of leaching by electrodialysis: 1) KCl extract of 0.2 g of electrodialyzed askangel; 2) same, with KF; 3) distilled water.

greater than unity. For the third suspension, where removal of exchangeable cations was virtually complete (99.3 meq/100 g) as the result of leaching, this ratio also increases with time, but is always greater than unity (see table). This is probably because incorporation of increasing amounts of H ions (both during the leaching, and after the end of this process) in the crystal lattice of the aluminosilicate minerals gradually raises the degree of conversion of structural aluminum into the mobile state—in the form of basic and trivalent aluminum ions. With incomplete desorption of the exchangeable cations, i.e., with incorporation of an insufficient amount of hydrogen ions, basic forms of mobile aluminum should be predominantly formed; these should mainly be in the structure itself and partially on the particle surfaces in the exchangeable adsorption state. Further sorption of increasing amounts of hydrogen ions by the aluminosilicate minerals converts these basic forms of mobile aluminum into trivalent ions, which are located on the particle surfaces, mainly in the exchangeable adsorption state.

When neutral salts (especially at high concentrations) act on acid natural aluminosilicates, not only the trivalent aluminum ions present in the exchangeable adsorption state on the particle surfaces may pass into the salt solution, but also the basic forms of mobile aluminum, as the result of direct interaction of neutral salts with structural components of the clay minerals which are not resistant to an acid medium. It seems that those side regions of the aluminum-oxygen layers of the crystal lattice which had already been subjected to the action of hydrogen ions are relatively easily susceptible to such action in an acid medium, especially at high salt concentrations. However, after displacement into solution these basic aluminum chlorides apparently react chemically with hydrogen ions and are converted into $AlCl_3$. This perhaps explains why, according to some reports [8, 17] the quantitative ratio of aluminum to hydrogen ions ($Al^{3+} : H^+$) increased in $BaCl_2$ extracts of electrodialyzed bentonite clays with increasing concentration of the salt solutions, while at high concentrations the total acidity became equivalent to the aluminum ion content.

SUMMARY

1. The origin of exchangeable acidity, partial decomposition of the aluminosilicate complex, and gradual replacement of H ions by aluminum ions during electrodialysis of askangel were studied.

2. Hydrogen ions formed during electrodialysis are not only adsorbed in the exchangeable form, but are also incorporated in the crystal lattice and favor partial decomposition of clay minerals which are unstable in an acid medium. As a result, the principal components: SiO_2, Al_2O_3, and Fe_2O_3, are removed fairly rapidly during electrodialysis. Consequently, conditions for direct conversion of structural aluminum into the exchangeable adsorbed state, and into a mobile state in general, are created during the actual electrodialysis process.

3. The amount of mobile aluminum increases sharply at the start of electrodialysis, and after that it varies very slowly. Its quantitative variation corresponds in character to desorption of the exchangeable cations. The amount of H ions formed increases at first to a maximum value, and then diminishes sharply, almost to zero.

4. The ratio of H to Al ions passing into solutions of neutral salts depends both on the nature of the aluminosilicates and on the time of interaction with the H ions formed during leaching. The greater the time after formation of the H ions, the more does this ratio decrease as the result of gradual replacement of H ions by aluminum ions. After very prolonged interaction the salt extracts are almost entirely free of exchangeable H ions, and the total acidity of the extracts is due only to exchangeable aluminum ions.

LITERATURE CITED

1. V. I. Vernadskii, Geochemical Essays [in Russian] (ONTI, 1934); V. I. Vernadskii and S. I. Kurbatov, Soil Aluminosilicates and Their Analogs [in Russian] (ONTI, 1937).
2. K. K. Gedroits, Byull. Pochvoveda 1-4, 3 (1930); D. L. Askinazi, Khimizatsiya Sots. Zemledeliya 2, 45 (1934); A. A. Arbuzov, Pochvovedenie 4, 71 (1940); P. Schachtschabel, Kolloid-Beihefte 5, 199 (1940).
3. W. K. Lewis, L. Squires, and G. Broughton, Industrial Chemistry of Colloidal and Amorphous Materials [Russian translation] (IL, Moscow, 1948).
4. G. Kappen, Soil Acidity [in Russian] (Moscow, 1934).
5. S. N. Aleshin and G. I. Goletiani, Khimizatsiya Sots. Zemledeliya 11, 12 (1935).
6. A. V. Chernov, The Nature of Soil Acidity [in Russian] (Izd. AN SSSR, Moscow-Leningrad, 1947).
7. M. E. Shishniashvili, Izvest. Akad. Nauk SSSR, Otdel. Khim. Nauk 2, 169 (1950); S. N. Papuashvili and I. F. Sarishvili, Trudy Gruz. Sel'-Khoz. in-ta 29, 79 (1948).
8. H. Paver and C. Marshall, J. Soc. Chem. Ind. 53 (1934).
9. I N. Mukherjee and B. Catterjee, Ind. J. Agr. Sci. 12, (1942).
10. S. N. Aleshin, Doklady Akad. Nauk SSSR 61, 693 (1948).
11. A. V. Chernov and L. P. Kislitsyna, Pochvovedenie 3, 7 (1955).
12. K. G. Mieserov, Doklady Akad. Nauk SSSR 84, 1009 (1952); Usp. Khimii 22, 279 (1953); Zhur. Obshchei Khim. 24, 947 (1954).*
13. M. O. Shishniashvili and M. V. Pirtskhalava, Trudy In-ta Khimii Akad. Nauk Gruz. SSR 10B, 21 (1950).
14. S. N. Papuashvili, Trudy In-ta Khimii Akad. Nauk Gruz. SSR 11, 88 (1953).
15. S. N. Papuashvili, M. E. Shishniashvili, and L. D. Agladze, Trudy In-ta Khimii Akad. Nauk Gruz. SSR 12, 23 (1956).
16. M. Trenel, and J. Wunschik, Z. Pflanzenernähr., Düngung, Bodenkunde 17, 257 (1930).
17. S. Mattson, Soil Sci. 25, 345 (1928).

*Original Russian pagination. See C. B. translation.

PHASE TRANSITIONS IN SOAP AND THEIR QUANTITATIVE DETERMINATION

D. A. Rozhdestvenskii, M. N. Zaliopo, and G. A. Borodina

G. V. Plekhanov Institute of National Economy, "Svoboda" Factory, Moscow
Translated from Kolloindyi Zhurnal, Vol. 22, No. 4, pp. 458-463,
July-August, 1960
Original article submitted June 8, 1959

It is known that the properties of soaps of the same composition depend on the mechanical treatment and the temperature conditions during cooling and drying, when the soaps undergo phase transitions in the solid state. It was shown by x-ray studies [1] that soaps may crystallize in different forms under the influence of thermal and other conditions, undergoing first- and second-order phase transitions. In the former case transition of crystals from one modification into another is accompanied by absorption or liberation of heat of transition, and therefore by a change of internal energy. In second-order phase transitions (Thiessen's "genotypes") no changes of crystalline form are observed, but there are far-reaching abrupt changes of dielectric constant, heat capacity, birefringence, viscosity, solubility, micellar state, or other volume properties. The genotype transition points of soaps almost coincide with the melting points of the fatty acids corresponding to the given soaps.

The soap forms which have been studied most fully are the metastable α-form (crystals in the rhombic system) and the stable, final β-form (monoclinic system). The intermediate γ-form has a transition temperature differing only by 1-2° from that of the α-form, and is therefore regarded jointly with the latter, being difficult to distinguish.

In sodium stearate the rhombic form exists only at temperatures up to 52°. Above 52° it passes into the monoclinic β-form. In sodium palmitate the transition of the rhombic into the monoclinic form takes place at 42°, in sodium myristate at 37°, in sodium laurate at 11.5°, and in sodium oleate at -2°. The unit cell parameters for certain soap crystals in the α- and β-forms are given in Table 1.

Table 1 shows that soaps, like their corresponding fatty acids, form double molecules in the crystal lattice. The structure and bonding of these double molecules differ between the α- and β-forms, with consequent differences in the structure and properties of the corresponding crystals.

The structures of the double molecules in the rhombic and monoclinic forms are represented schematically, after Thiessen [1], in Fig. 1. It is clear from Fig. 1 that in α-soaps the double molecules in the crystal lattice are at an angle of 90° to the basal plane, and in β-soaps, at 62.4°. Figure 1 also shows that monoclinic soap should be the more stable form, because of the closer molecular contact and more complete saturation of the bonds between the polar COONa groups in the molecules. This stability is so great that reverse transition of the β-into the α-form by gradual cooling below the transition point is impossible. An irreversible transition of this type is said to be monotropic.

It has also been shown that the two soap forms differ in energy level and in the number of molecules in the unit cell, which contains eight molecules in α-soaps and only four in β-soaps. The molecular packing is less dense in the cell of β- than of α-soap; therefore β-soap is more accessible to the action of water and should accordingly have higher solubility and swelling and should differ from α-soap in a number of other physical properties.

Unit Cell Parameters of Soap Crystals, After Thiessen and Stauff [1]

Soap	Unit cell parameters, A			Angle β	Length of double molecule A, $\frac{c}{\sin \beta}$	Transition temperatures, deg	
	a	b	c			α- and β-forms	genotypes
α-Na palmitate	8,06	9,24	47,7	90	47,7	42	64
β-Na palmitate	7,83	5,40	42,1	62,4	48,0		
α-Na stearate	8,04	9,24	51,77	90	51,77	52	71
β-Na stearate	7,80	5,33	46,1	62,4	52,5		

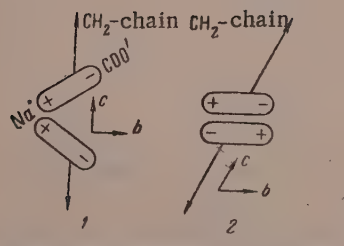


Fig. 1. Molecular arrangement in soap crystals: 1) Rhombic α-form; 2) monoclinic β-form.

In discussions of the monotropic transition of the rhombic form of soap into the monoclinic it must be taken into account that monotropic substances have only one return route to the unstable forms—through supercooled melts, when, in accordance with the Ostwald rule, the most unstable form is initially formed, and this gradually passes into the stable form at the appropriate temperature.

If sodium stearate at 90°, when it should exist in the β-form, is slowly cooled to a temperature below the phase transition point, such as 20°, the β-form is retained. On rapid cooling to 20° at a rate of some 40° per minute the α-form is produced and the phase transition is accompanied by liberation of heat. The unstable forms of monotropic substances may persist indefinitely at temperatures below the phase transition points.

The existence of double soap molecules in the α- and β-forms depends on the nature of the solvent as well as on the crystallization temperature. Crystals of the β-form are always obtained from solvents with nonpolar molecules, such as benzene, as the COONa groups do not become solvated by the hydrophobic solvent and their contact during crystallization is more complete. The α-form crystallizes out of ethyl alcohol at room temperature, because the dipole moment of the alcohol molecule is considerable and the molecules can surround and solvate the COONa groups and thereby prevent complete contact between them, such as is postulated in the formation of the β-form. If the resultant dry α-soap is heated above the phase transition temperature, the α-modification undergoes monotropic transition into the β-form. At temperatures below the transition point soaps also crystallize in the α-form from aqueous dispersions, as water has a greater dipole moment than alcohol.

Electrolytes, by influencing the solubility of soaps, should also influence their crystal structure and therefore phase formation. Usually addition of large amounts of electrolytes causes partial dehydration of the polar groups in soap molecules, which favors formation of the β-phase.

Phase transition characteristics of soaps, determined from studies of individual fatty acids, lead to certain practical conclusions with regard to technical soaps. Soaps in different crystalline modifications, and therefore of different physicochemical properties, can be made if the temperature conditions in cooling, drying, and mechanical treatment are varied. Heat treatment of this kind is now used in production of toilet soaps which, being in the β-form, have high solubility and good lathering characteristics [2].

Differences of crystal structure and the associated physical properties should lead to differences in the technical qualities of soaps. For example, it is known [3, 4] that the detergent action of soaps is determined not only by adsorption processes at interfaces, but also by volume properties of soap solutions which, in their turn, depend on molecular structure.

Double molecules of the α- and β-form are the structural elements in soap micelles, crystallites, and crystals. The structure of soap micelles in aqueous solutions [4] is similar to that of soap crystals, but less ordered. It is also known [1] that in aqueous solutions at concentrations up to 1%, soap is distributed in the form of double molecules, micelles, and crystallites having these double molecules as the structural components. Such solutions contain only very few single molecules and ions. According to Syrkin [5], carboxylic acids exist as double

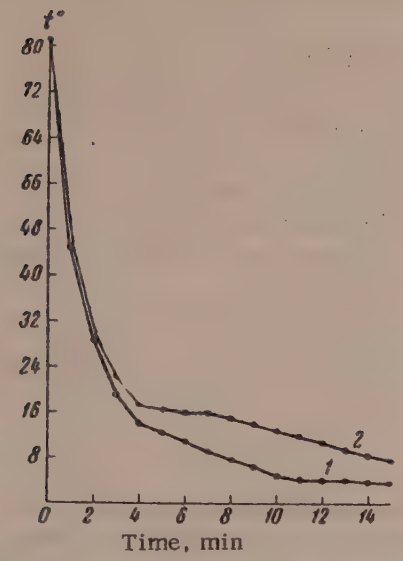


Fig. 2. Cooling curves of 3% solution of strawberry-scented toilet soap from the "Svoboda" factory (2) and of water (1).

molecules in vapors as well as in solutions, and dissociate into single molecules only at relatively high temperatures. Therefore, phase transitions occur in soaps both in the solid state and in the aqueous solutions, and influence their properties. It should be noted that even Fischer [6] found inflections on rapid-cooling curves of 0.5 M solutions of various individual soaps.

A considerable quantity of heat (of the order of 15 cal/mole) was liberated during cooling at the inflection point, similarly to the heat effect in crystallization. This heat effect was formerly known as the heat of gelatinization, but Thiessen [1] showed that this effect is unrelated to the solution concentration and depends only on the cooling procedure. The inflection points on Fischer's cooling curves correspond fairly accurately to the phase transition points determined by Thiessen by means of x-ray structure analysis, and therefore this liberation of heat is a sign of the transition of the β-phase into the α-phase.

McBain [7] also noted the existence of two liquid crystal phases in aqueous solutions. We must also refer to the work of Rebinder and his co-workers [3], who repeatedly drew attention to the influence of heat treatment on the physicochemical properties of aqueous soap solutions. The anomalies of surface tension and foaming of the solutions which were observed by these workers are easily explained by phase transitions in soaps.

To investigate phase transitions of soaps in aqueous solution we compared the temperature changes during cooling of these solutions with the cooling of distilled water. Most of the experiments were performed with 50 ml of soap solution and 50 ml of water in round-bottomed flasks with thermometers. The two flasks were put side by side in a two-liter water bath containing ice. In some experiments the flasks were cooled in air, and other volumes of water and soap solutions were used.

If no phase transitions occur in the soap in the chosen temperature range, the cooling curves for water and the soap solution coincide. If there are phase transitions, which are accompanied by liberation of considerable heat, the coolingcurves diverge sharply beyond a certain temperature.

Figure 2 shows temperature changes during the cooling of 3% solution of strawberry-scented toilet soap from the "Svoboda" factory, down from 78° (the surrounding medium was at 0°). At 30° the soap solution begins to exhibit turbidity, gelation begins at 13°, and is complete at 9°.

Cooling experiments on soap solutions showed that conversion of the monotropic β-phase into the unstable α-phase is possible only by rapid cooling (at a rate of at least 40° per min) of small volumes of solution, when effects associated with supercooling are present. There were no phase transitions when the solutions were cooled less rapidly. These experiments also showed that phase transitions are much slower and take place at lower temperatures in soaps of mixed composition than in individual stearates and palmitates.

Cooling curves can be used for determination of cooling conditions for soap solutions after transition into the β-phase and in production of the α-phase. The presence of the β-phase in soap solutions can be qualitatively detected from cooling curves, and presence of the α-phase from the corresponding heating curves. These curves can also be used for calculation of the heat effect of phase transition; moreover, they provide additional data on phase transitions in soaps in relation to their fat and chemical composition.

The surface and volume properties of α- and β-soap solutions should, in principle, be different. Therefore, the α- and β-phase contents of soap can be determined quantitatively by measurements of such properties.

In preliminary experiments on quantitative determination of α- and β-phases in soap, foaming of their aqueous solutions at concentrations between 0.03 and 0.06% was determined at 20-25°. At this temperature the critical concentration for most soaps is 0.125%, and their foaming power, in this concentration range, is proportional to concentration [3]. Since soap of the same composition was present in these mixtures of the α- and

TABLE 2

Foaming Power and Contents of α- and β -Phases in Investigated Soaps

Soaps	Phases	Foam volume, ml		Nominal phase contents, %	Phase contents of soaps, %	
		instant	after 3-min		α-phase	β -phase
Soap base	α+β	220	130	86	43	57
	β	270	195			
	α	210	120			
Strawberry-scented toilet soap	α+β	280	200	50	25	75
	β	315	240			
	α	260	160			

β -phases, it was assumed that the foaming of such mixtures is an additive function of the foaming powers of the components. Therefore the quantitative proportions of the α- and β -phases, differing in foaminess, in a soap can be calculated on the additivity principle. For determination of foaming power 100 ml of the soap solution was shaken in a graduated separating funnel 250 mm long and 1 liter in capacity for 60 sec at 20°, at the rate of 120 to-and-fro movements per minute. The height of the foam layer was measured after 3 min. Strawberry-scented toilet soap from the "Svoboda" factory, and its soap base, were used for the experiments.

The following characteristics are found for quantitative determination of α- and β -phases in soap: foaming power of the soap, which is usually a mixture of α- and β -phases; foaming power of the soap after complete conversion into the β -phase; and foaming power after partial conversion into the α -phase.

In all cases the soap was dissolved after preliminary swelling; a weighed sample of the soap was kept in water until swelling was complete (3 hr at 20-25°), and then transferred quantitatively into a flask and dissolved with stirring during 15 min.

Swelling under these conditions results in relatively concentrated soap solutions in which hydrolysis and aging are slight. To obtain the soap in the β -form it is convenient to use a gel, rather than an aqueous solution, simultaneously with the swelling procedure, for the heat treatment (i.e., heating to produce the β -phase and subsequent cooling). A soap sample was covered with water in a closed vessel and placed in a thermostat for 3 hr at 70° for swelling and for simultaneous conversion of the existing α-phase into the β -phase. The soap was then gradually cooled for at least an hour, and then transferred quantitatively into a flask for dissolution.

The soap was converted into the α-phase by crystallization from a saturated solution in absolute alcohol, evaporated at 20-25°. The soap sample was dissolved in ethyl alcohol in a flat basin at 20-25°. Alcohol was evaporated from this solution in a vacuum desiccator over calcium chloride at 20-25°. The dry residue was dissolved in the same vessel in water (in portions) after preliminary swelling. A sample for determination of foaming power was taken from the resultant solution.

A simpler but less accurate method for converting soap into the α -phase is by rapid cooling (from 80 to 20-25°) of an aqueous solution. In the case of soaps of new composition the cooling curves are first determined as described above, and the time of exposure in freezing mixture (at 0°) is established accordingly.

The results obtained in determinations of foaming power of toilet soap and its base, in different phase states, are presented in Table 2. The foaminess found for the toilet soap (200 ml) is not the limiting value, as it can be increased by 20% (to 240 ml) by suitable heat treatment.*

The relative proportions of α - and β -phases in the soap at the given temperature can be approximately calculated from these data. In characterization of the phase state of toilet soaps at 20-25° it must be taken into account that laurates, with a transition point of 11.5°, and oleates with a transition point of -2°, are always present

* The soap contained 1% scent, 0.1% sodium silicate, and color, in addition to the soap base.

in the β-form at 20-25°, and only myristates (37°), palmitates (42°), and stearates (52°) may be present in both the α- and the β-form.

In illustration, we give the calculation for the soap base of strawberry-scented soap, with a foaming power of 130 ml. After conversion into the β-phase the foaming power became 195 ml, and after partial conversion into the α-phase, it was 120 ml.

In the case of this soap, at 20°, we shall refer to the sum of the stearates, palmitates, myristates, and other soaps with phase transition points above 20° as "two-phase soaps," and to the sum of the laurates, oleates, and other soaps with transition points below 20° as "one-phase soaps."

The foam volumes in milliliters corresponding to 1% of "two-phase" soaps are denoted by the symbols Tα and Tβ, and the foam volumes of 1% "one-phase" soaps in the β-phase, by Oβ. Further, the required percentages of the β- and α-phases in "two-phase" soaps are denoted by X and 100-X.

From the three values given above for the foaming power of the soap base at different ratios of the α- and β-phases we have the following equations:

$$100\ T\beta + 100\ O\beta = 195, \tag{1}$$

$$100\ T\alpha + 100\ O\beta = 120, \tag{2}$$

$$X T\beta + (100 - X)\ Д\alpha + 100\ O\beta = 130. \tag{3}$$

Subtracting Equations (2) and (3) from (1), we have:

$$100\ (T\beta - T\alpha) = 75, \tag{4}$$

$$(100 - X) \cdot (T\beta - T\alpha) = 65. \tag{5}$$

Replacing (Tβ - Tα) in Equation (5) by 75/100, in accordance with Equation (4), we have (100-X) or content of the α-phase = 65 · 100/75 = 86%. As already stated, the α-phase can be present only in "two-phase" soaps with transition temperatures above 20°. The investigated soap, like most toilet soaps, contains about 50% of such "two-phase" soaps. Therefore, if the nominal value found for the α-phase content (%), which is 86% referred to the "two-phase" soaps, is divided by two, we find the approximate α-phase content of the original soap, 43%. Subtraction of this value from 100, gives 57% for the β-phase content.

For more exact calculations the contents of the principal fatty acids in the soap must be known. In some cases it is necessary to take into account the influence of electrolytes, surface-active impurities, and so-called modifiers (in Rebinder's terminology) on phase transitions; these substances become adsorbed on crystal faces, decrease their rate of growth, and inhibit phase transitions. Such substances include cresol [6] and β-naphthol (our experiments).

SUMMARY

1. The phase state of soaps in aqueous solution may be estimated from the foaming power of the solution in conjunction with cooling curves. A method based on this principle gives results of sufficient accuracy for production purposes when the relative proportions of the phases in soap have to be determined.

2. The suggested method may be useful for establishing the conditions of heat treatment required to ensure the maximum content of a particular phase in the soap.

In conclusion, we thank Academician P. A. Rebinder for his interest and valuable advice.

LITERATURE CITED

1. H. Schönfeld, Seifen und Seifenartige Stoffen, m. 1, Theoretische, (1943).
2. E. T. Webb, "Phase factors affecting soap quality" Soap, Perfumery and Cosmetics 22, 838 (1949).
3. P. A. Rebinder, Physical Chemistry of Detergent Action [in Russian] Pishchepromizdat (1934) p. 108.
4. H. Frotscher, Chemistry of Textile Auxiliaries [Russian translation] (Gizlegprom, 1958) p. 37.
5. Ya. Syrkin and M. Dyatkina, The Chemical Bond and Structure of Molecules [in Russian] (1946).
6. E. Lederer, Colloid Chemistry of Soaps [Russian translation] (Gizlegprom, 1934) Vol. 1, p. 44.
7. E. Valko, Colloidochemical Principles of Textile Technology [Russian translation] (Gizlegprom, 1940) part II, 537.

SUPERSATURATION KINETICS AND TENDENCY TO FORM CONCRETION CONTACTS IN HYDRATION HARDENING OF THE α- AND β-FORMS OF CALCIUM SULFATE HEMIHYDRATE

E. E. Segalova, Ezhi Stoklosa, and Z. N. Markina

Department of Colloid Chemistry, M. V. Lomonosov Moscow State University
Translated from Kolloidnyi Zhurnal, Vol. 22, No. 4, pp. 464-468,
July-August, 1960
Original article submitted January 29, 1959

Crystallization structures are formed during hydration hardening of mineral cements as the result of crystallization of newly formed hydrates from supersaturated solutions formed from the dissolving cement. Previous investigations [1] showed that the hardening structure develops in two stages. During the first stage a crystallization structure framework is formed, with concretion contacts between the newly formed crystals. Partial growth of these crystals is also possible at this stage. During the second stage new crystallization contacts (concretion contacts) are not formed; only the crystals constituting the existing framework grow.

It was natural to assume that the first stage in structure formation is associated with high degrees of supersaturation in the suspension, when new crystallization nuclei and crystallization contacts can arise, whereas the second stage proceeds at lower supersaturations, when growth of the newly formed crystals already existing in the suspension is more probable. To determine the magnitude of the "critical" supersaturation at which formation of crystallization contacts is still possible it was necessary to carry out concurrent determinations of supersaturation kinetics in a hardening calcium sulfate suspension, and of the tendency of this suspension to form crystallization contacts.

No definite conclusions could be drawn from the results of earlier investigations carried out in our laboratory concerning the tendency to structure formation in concentrated suspensions of calcium sulfate hemihydrate as a function of supersaturation, because only dilute suspensions had been used in studies of supersaturation kinetics [2]. It was therefore impossible to make direct comparisons of the kinetic curves representing structure formation with changes of Ca^{2+} and SO_4^{2-} concentration in the liquid phase of the suspension during formation of real hardening structures.

Supersaturation kinetics in hardened plaster was investigated as follows. The liquid phase of the suspension was pressed out at definite time intervals, and the Ca^{2+} concentration was determined by complexometric analysis [3]. The liquid phase was pressed out by means of a stainless steel rod moved by the action of a hydraulic press (150 atm) inside a steel vessel coaxial with the rod, with a filtering bottom.

To test the tendency to formation of crystallization contacts during hardening of a plaster suspension, the suspension was repeatedly stirred at different stages of structure formation and the strength of the crystallization structure which was then formed was determined.

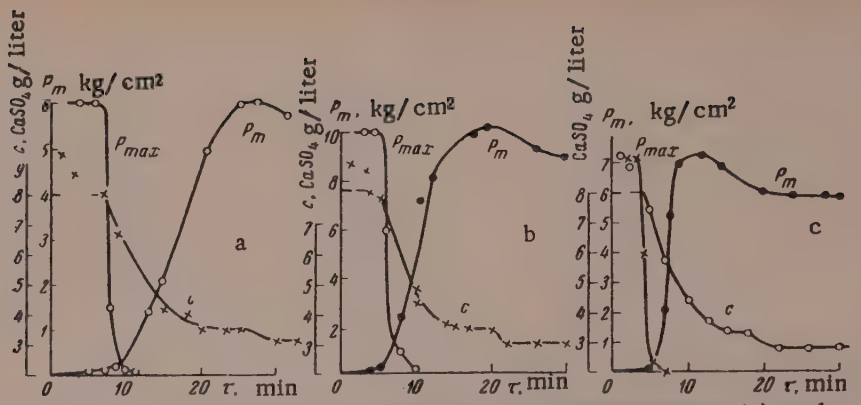


Fig. 1. Kinetics of structure formation (P_m) and of supersaturation (c), and dependence of the strength of the structure on the time of repeated stirring (P_{max}) in a hardening suspension with 30% of β-calcium sulfate hemihydrate and 70% of ground quartz sand, + 83% of water on the dry mixture. Nominal specific surface of the β-calcium sulfate hemihydrate: a) 3.4 m^2/g; b) 10.7 m^2/g; c) 16.5 m^2/g.

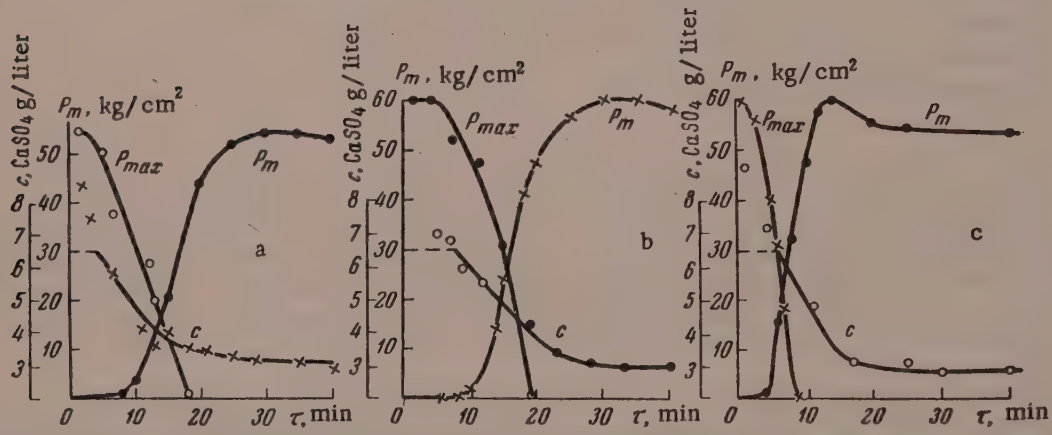


Fig. 2. Kinetics of structure formation (P_m) and of supersaturation (c), and dependence of the strength of the structure on the time of repeated stirring (P_{max}) in a hardening suspension with 30% of α-calcium sulfate hemihydrate and 70% of ground quartz sand, + 50% of water on the dry mixture. Nominal specific surface of the α-calcium sulfate hemihydrate: a) 2.9 m^2/g; b) 3.4 m^2/g; c) 7.7 m^2/g.

Mixtures containing 30% of calcium sulfate hemihydrate and 70% of inert filler (ground quartz sand [1]) were used; the mechanical properties of these suspensions were characterized by their plastic strength.

Figures 1 and 2 show, for the α- and β-forms of calcium sulfate hemihydrate, the kinetics of strength increase (P_m) and of supersaturation (c), and the dependence of the final strength of the crystallization structure (P_{max}) on the time of repeated stirring of the hardening suspension. The portions of the curves corresponding to supersaturation during the induction period are represented by dash lines, as the experimental values in the region are much too high. The explanation is that when the liquid phase of the suspension is pressed out the filter lets through minute crystallization nuclei which have not yet grown into a continuous crystallization framework.

The degree of supersaturation corresponding to metastable solubility of the α- and β-forms of calcium sulfate hemihydrate is taken from literature data [3, 4]. The existence of a constant supersaturation level for α-calcium sulfate hemihydrate, independent of the suspension concentration, was confirmed earlier in our laboratory by conductivity determinations on diluted suspensions [2]. Rozenberg and Ratinov [3] carried out a quantitative study of the solubility of calcium sulfate hemihydrate in various electrolyte solutions.

Conductivity variations in dilute suspensions of the α- and β-forms of calcium sulfate hemihydrate are plotted in Fig. 3. The maximum conductivity in suspensions of the α-form is independent of the concentration

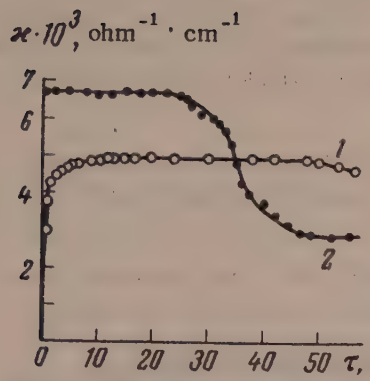


Fig. 3. Variations of conductivity in suspensions of the α - (1) and β - (2) forms of calcium sulfate hemihydrate containing 3 g of hemihydrate per 150 ml of water. The nominal specific surface of the α - and β -forms = = 3.4 m^2/g; t = 20°.

and may therefore characterize the metastable solubility of the compound. It was confirmed by special experiments that the maximum conductivity is independent of the stirring rate and concentration for suspensions of the α-form.

Figure 3 shows that, in agreement with literature data, the solubility of the β -form of calcium sulfate hemihydrate is considerably higher than that of the α -form. Another very important difference between the two compounds is the high rate at which the β -form dissolves. It is seen in Fig. 3 that, at the same suspension concentration and the same nominal specific surface of the original compounds, a constant supersaturation level is reached in 30 sec in suspensions of β -calcium sulfate hemihydrate, and in 10-12 min in suspensions of the α-form; in other words, it takes 20 times as long to saturate the same amount of liquid in the second case.

It is known that the α- and β -modifications of calcium sulfate hemihydrate, while differing in a number of properties (refractive index, specific heat, heat of hydration, solubility, and rate ofdissolution), give quite similar x-ray diffraction patterns.

In [3 and 5] differences between the properties of the α - and β -hemihydrates are attributed to different true specific surfaces of the crystals in these compounds, associated with details of their production. The β -form is made by calcination of ground gypsum in a kettle at 120-170°, when water is removed in the form of steam. The α-form is made by treatment of gypsum under moderate pressure (1.2-1.4 atm), and the hemihydrate crystallizes out of water in regular crystals. The differences between the α- and β -modifications are probably associated not only with differences between the specific surfaces of their crystals, but also with the nonequilibrium character of the crystal lattice in the β -form, which accounts for the fluctuations in the solubility of different samples of the β -hemihydrate [3].

The curves representing the kinetics of supersaturation in the liquid phase of β -hemihydrate suspensions have inflections at ~ 3.5 g/liter; the concentration drops sharply to 2.3-3.2 g/liter and then remains unchanged for a long time. A similar discontinuity in the decrease of supersaturation during hydration of calcium sulfate hemihydrate was observed by Kuznetsov [6]; his explanation was that after the hemihydrate has dissolved completely the liquid phase of the suspension is no longer supplemented with Ca^{2+} and SO_4^{2-} ions, so that the supersaturation drops more rapidly. This discontinuity is imperceptible for suspensions of the α-form, because of the considerably lower rate of dissolution of this form.

It is clear from Fig. 1 that suspensions of β -hemihydrate lose the ability to form crystallization contacts even while fairly high degrees of supersaturation still exist in the liquid phase. The structures formed in such suspensions during the first stage of structure formation are of low strength (this is especially distinct in Fig. 1, a and 1, c); the main strength increase occurs at the second stage, during growth of the framework.

The situation is different in suspensions of the α -hemihydrate (Fig. 2). These suspensions retain for a long time the ability to form crystallization contacts, even at low degrees of supersaturation in the liquid phase. For example, it is seen in Fig. 2, a, that the tendency to form crystallization contacts is lost only when the concentration in the liquid phase of the suspension falls below 3.5 g/liter. This critical concentration increases appreciably with decreasing particle size of the α-hemihydrate, and reaches 5 g/liter at s = 7.7 m^2/g (Fig. 2, c); i.e., it approaches the values found for suspensions of the β -form. In α -hemihydrate suspensions the main strength increase occurs during the first stage of structure formation, and the strength increases only slightly during the second stage.

Comparison of the results obtained for suspensions of the α- and β -hemihydrates shows that the degree of supersaturation reached during hydration of the plaster does not determine uniquely the tendency of the suspension to form concretion contacts between crystals of the newly formed hydrates. The probability of formation of such contacts, as of new crystallization nuclei, is determined not only by the degree of supersaturation, but also by the total surface of the new compounds already formed, on which crystallization may occur. This is confirmed by the fact that in suspensions of β -hemihydrate, where the degree of supersaturation is greater and a more highly

disperse dihydrate is therefore formed, the ability to form crystallization contacts is lost at higher degrees of supersaturation than in α-hemihydrate suspensions. On the other hand, the more disperse the original hemihydrate, the greater must be the dispersity of the dihydrate formed, and the earlier the tendency to form concretion contacts must be lost. This is satisfactorily confirmed with suspensions of α-hemihydrate, for which the determinations are more exact because the process is relatively slow.

It must be pointed out that the concentration of the liquid phase at the end of hydration and hardening of all the investigated suspensions never corresponded to the solubility of calcium sulfate dihydrate (2.8 g/liter), but was always higher, 2.8-3.2 g/liter.

The stable existence of a supersaturated solution in the pores of the hardening structure demonstrates that the latter is thermodynamically unstable, evidently because of the stresses which arise in the structure during growth of crystals of the new compounds already joined into a crystallization framework. Such supersaturation cannot be caused by increased solubility of crystallization contacts not in thermodynamic equilibrium, because this would lead to a very sharp drop of strength, which is not observed under such conditions. Apparently the degree of saturation may act to some extent as a measure of the stress in the formed hardening structure. However, this problem requires further investigation.

SUMMARY

1. The kinetics of structure formation and supersaturation, and the tendency to form crystallization contacts, were studied concurrently in suspensions of the α- and β -modifications of calcium sulfate monohydrate during hydration hardening.

2. The tendency to form crystallization contacts (concretion contacts between crystals of newly formed compounds) is not determined uniquely by the degree of supersaturation attained in the suspension, but also depends on the specific surface of the newly formed compounds present in the suspension at the given instant.

3. When hydration hardening is complete, supersaturations corresponding to $CaSO_4$ concentrations of 2.8-3.2 g/liter are maintained in the pores of the crystallization structure; this is associated with the stresses which develop in the hardening structure during its formation.

LITERATURE CITED

1. V. N. Izmailova, E. E. Segalova, and P. A. Rebinder, Doklady Akad. Nauk SSSR 107, No. 3, 425 (1956).*
2. E. E. Segalova, V. N. Izmailova, and P. A. Rebinder, Doklady Akad. Nauk SSSR, 114, No. 3, 594 (1957).*
3. T. I. Rozenberg and V. B. Ratinov, Coll. Trans. All-Union Ferroconcrete Sci. Res. Inst. [in Russian] (1957) No. 1, p. 36.
4. K. K. Kelley, J. C. Southard, and C. T. Anderson, Thermodynamic Properties of Gypsum [Russian translation by S. S. Pechuro] (BTI MPSM, 1949); W. C. Riddell, Rock Products, 57, 10, 109 (1954).
5. P. P. Budnikov, Investigation and Uses of Gypsum [in Russian] (Stroiizdat, 1943).
6. A. M. Kuznetsov and M. T. Oborina, Izvest. Estestv.-n. in-ta pri Permskom un-te 14, No. 1 (1957).

*Original Russian pagination. See C. B. translation.

COLLOIDAL STABILITY OF LITHIUM SOAP-OIL DISPERSE SYSTEMS*

V. V. Sinitsyn, K. I. Klimov, and E. V. Aleeva

Scientific Research Institute of Fuels and Lubricants, Moscow
Translated from Kolloidnyi Zhurnal, Vol. 22, No. 4, pp. 469-476,
July-August, 1960
Original article submitted March 10, 1959

The colloidal stability of soap-oil dispersions is one of the most interesting problems of physical chemistry in the theoretical sense and one of the most important with regard to practical applications. The stability of such systems is generally taken to mean their ability to retain for a long time the dispersion medium (oil) in the spatial network of disperse phase particles (soap). Oil can separate out spontaneously, in consequence of structural changes in the system, and the process may be accelerated or retarded under the influence of temperature, pressure, and other factors.

The term syneresis is sometimes used with reference to plastic greases [1]. However, soap-oil pseudogels of this type differ significantly from true gels, such as gelatin gels. The syneresis effect, characteristic of gels [2], differs significantly from the segregation of the dispersion medium in soap-oil pseudogels; this is confirmed, in particular, by the data in [1]. We therefore consider that the term "syneresis" is not appropriate for description of the effect considered here.

Early work on stability [3-6] was concerned with methods; the influence of various factors on stability was not considered, or else relegated to a subordinate position. Moreover, these studies have serious defects with regard to the methods used [7, 8]. In later work attention was again devoted mainly to development of methods for estimation of the stability of plastic soap greases [9-13]. In one interesting investigation [14] the vacuum filtration method was used for studying the influence of the nature of the dispersion medium and the disperse phase, temperature, and particle size in the dispersion medium and the disperse phase on stability of oil-soap systems. The effects of viscosity of the dispersion medium, concentration of the disperse phase, structure of the system, pressure, and temperature on separation of oil from plastic greases were studied in [15]. Interesting data on the effects of compression and extension (under gravity) on the rate of oil separation are contained in [6]. Some attention was devoted in [11, 15] to the influence of stability on the properties and behavior of plastic greases in storage and use. The papers [1, 17] are concerned with studies of the mechanism of oil separation from lithium stearate-oil systems. The following facts have been established in our studies, started in 1948 [18]:

1) The poor stability of plastic soap greases is in many cases (low-temperature greases) the cause of their deterioration in storage. Because of this several types of grease cannot be kept for longer than 6-8 months without considerable separation of oil (up to 20%).

2) Different sorts and different batches of one sort of grease differ considerably in stability.

3) The least stable greases are those made from low-viscosity oils thickened with small amounts of soap or solid hydrocarbons. The type of thickener used is of less significance. In the light of modern views on the structure of greases [10, 19], we devised a simple apparatus and method for estimating the tendency of dispersion medium-thickener systems (primarily plastic greases) to lose oil during storage [8, 20]. The method is based on

*Presented at the 4th All-Union Conference on Colloid Chemistry, Tbilisi, May, 1958.

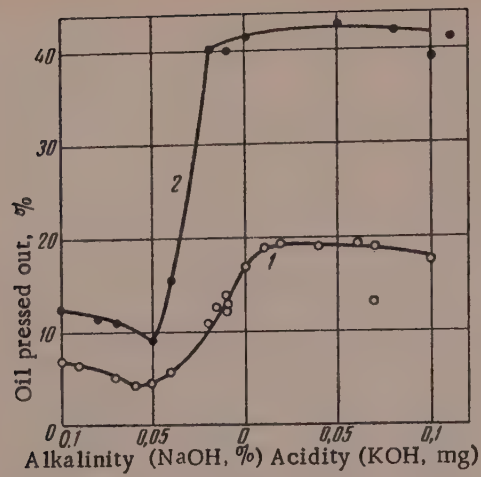


Fig. 1. Variations of stability with acidity in lithium stearate-spindle oil 3 systems made by: 1) rapid cooling; 2) slow cooling. Acid number 0.2 mg KOH.

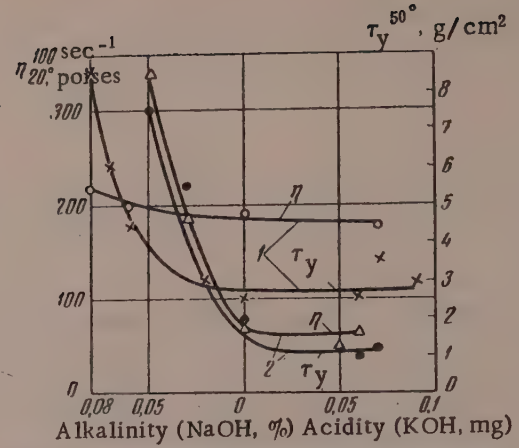


Fig. 2. Variations of yield value and effective viscosity in lithium stearate-spindle oil 3 systems made by: 1) rapid cooling; 2) slow cooling.

mechanical pressing of the dispersion medium from plastic disperse systems in the KSA apparatus. Some results of our later studies [18, 21, 22] may be summarized as follows:

1) Increased concentration of the disperse phase (especially in systems of low concentration) sharply improves stability.

2) Increase of oil viscosity improves stability. However, in sodium soap-oil systems the stability deteriorated somewhat above an optimum viscosity level of the dispersion medium.

3) Increase of the dependence of the viscosity of the dispersion medium on temperature improves stability.

4) The chemical composition of the dispersion medium has only a slight influence on stability.

In continuation of the work published earlier, the present paper deals with the use of lithium stearate-oil model systems for investigating the influence of pH of the disperse phase, cooling rate, properties of the dispersion medium, etc., on stability of soap-oil disperse systems of the pseudogel class.

The following petroleum oils were used for preparation of the samples: spindle oil 3, GOST 1707-51 ($\nu_{20°}$ = 99.8 centistokes; $\nu_{50°}$ = 20.3 centistokes; acid number 0.03 mg KOH) and MK-8, GOST 6457-53 ($\nu_{20°}$ = = 27.5 centistokes; $\nu_{50°}$ = 8.7 centistokes, acid number 0.01 mg KOH). The oils were thickened with prepared air-dry lithium soap with a weak alkaline reaction: the alkalinity of 10% lithium stearate—MK-8 oil systems was roughly 0.02% NaOH (by GOST 6707-57).

The samples were generally prepared as follows. A flask of ~ 500 ml capacity, provided with a stirrer and thermometer, contained 40 g of oil and 10 g of dry soap. Definite amounts of lithium hydroxide or stearic acid were introduced if necessary (in preparation of greases of different degrees of acidity or alkalinity). The flask was stoppered, the contents were mixed thoroughly and warmed for one hour at 220°, and the melt was poured out in a thin layer on a metal tray. Losses due to oil evaporation in this operation did not exceed 1% for spindle oil 3, and 2% for MK-8 oil. To investigate the influence of the cooling rate on stability, the melt in the flask was cooled down from 220° to room temperature during 3-4 hr in a thermostat heated to 150° and then switched off. If additives were used, these were introduced into the flask a short time before the grease was poured onto the tray.

The prepared and cooled soap-oil gel was rubbed through a 200-mesh copper screen. In some instances, to which special reference is made, the greases were broken down in the gap of a rotational viscosimeter at a high deformation rate. The acidity (or alkalinity), pH, stability, viscosity characteristics, and yield value of the greases were determined 24 hr after preparation. Acidity (or alkalinity) was determined in accordance with GOST 6707-57 by titration of an extract in alcohol—water—gasoline mixture in presence of an indicator

(phenolphthalein). Alkalinity was expressed as % NaOH, and acidity (acid number) in mg KOH per gram of grease. The pH and ΔpH of the grease were determined by means of the LP-6 potentiometer with an antimony electrode [23]. Stability was determined in accordance with GOST 7142-54 in the KSA apparatus, from the amount of oil pressed out in 30 min. The viscosity characteristics in yield value, required for additional characterization of certain samples, were determined with the automatic capillary viscosimeter AKV-2 (GOST 7163-54) and the K-2 plastometer (GOST 7143-54). The separation of oil during prolonged storage was observed in some samples. In such cases the sample (50 g) was put in a 100 ml glass beaker. The open beaker was kept in a dark place at 15-22°. The specimens were inspected visually at intervals. If large amounts of oil separated out, it was poured out of the beaker and weighed.

It is important to note that the reproducibility in sample preparation was quite good [22]. Variations in the amount of oil pressed out from duplicate samples did not exceed 2-4%.

Figure 1 shows the influence of acidity (or alkalinity) on stability of lithium stearate-spindle oil systems prepared by rapid cooling (on trays) and by slow cooling (in a thermostat). The samples made by rapid cooling had higher stability. Under otherwise similar conditions the amount of oil pressed out of systems made by slow cooling is about double the amount found for samples made by rapid cooling. Slow cooling also lowers the yield value and effective viscosity of the systems, apart from samples with high contents of free alkali (Fig. 2). Evidently, decrease of the cooling rate results in considerable lowering of the thickening effect of the disperse phase (lithium stearate). Comparison of the electron micrographs in Fig. 3, a and 3, i, and 3, c, and 3, h shows that the lowering of the thickening effect of lithium stearate is associated with a considerable decrease of dispersity and reduction of the length-diameter ratio of the soap fibers as the result of slow cooling. Coarse fibers evidently form a structure of low mechanical strength which does not hold the dispersion medium well.

Data on the effects of acidity (or alkalinity) on stability of soap-oil disperse systems are of great interest. Acidity variations have a very strong influence on stability. For example, not only does the amount of oil pressed out increase from 15 to 40% (Fig. 1, curve 2) on decrease of alkalinity from 0.04 to 0.02% NaOH; the principal influence is seen in the fact that variations of the cooling rate, which have a strong effect on the amount of oil pressed out, have hardly any effect on the stability-acidity relationship (curves 1 and 2 in Fig. 1 are similar in character).

The following main regions may be distinguished on the stability-acidity curves (Fig. 1).

1) Acidity increase has almost no effect on stability of greases which are neutral or acid by GOST 6707-57, or even weakly alkaline (up to 0.02% NaOH), if made by the rapid cooling method. Figure 2 shows that under these conditions the yield value and effective viscosity remain almost unchanged with increased acidity. It is important to note that the size and shape of the lithium stearate fibers which form the structural framework of the system change little (Fig. 3, a, b, c, and d) with increase of acidity (in the range under consideration). It is therefore evident that neutral and acid (acid numbers up to 0.1 mg KOH) lithium stearate-oil systems have almost the same structure and also similar bulk mechanical properties and stability, which are determined by this structure. In comparison with alkaline systems (of the order of 0.02-0.049% NaOH), acid soap-oil disperse systems have lower stability, lower yield values, and lower effective viscosities.

2) Increase of alkalinity above 0-0.02% NaOH (dependent on the cooling rate) improves the stability of the systems considerably. The yield values and viscosities increase also. Comparison of the electron micrographs (Fig. 3, a and 3, d) clearly shows that at moderate alkalinities these systems differ little from neutral or acid soap-oil systems with regard to the size and shape of the soap particles. The soap fibers merely become somewhat less anisodiametric; they are more massive and shorter.

3) Further increase of alkalinity to 0.04-0.06% NaOH and over results in progressive decrease in the amount of dispersion medium pressed out of the system (in stability determinations by GOST 7142-54). The yield value and effective viscosity increase sharply. The minimum amount of oil pressed out corresponds to alkalinity in the range of 0.05 to 0.07% NaOH. Further increase of alkalinity results in a small decrease of stability.

Lithium stearate-spindle oil systems of alkalinity above 0.04% NaOH differ sharply from less alkaline soap-oil systems in their microstructure; this is especially characteristic of systems made by rapid cooling. Greases which are weakly alkaline, neutral, or acid become soft and plastic, with a smooth macrostructure (texture) after being cooled on trays. The disperse-phase particles in such systems are fine long needles (Fig. 3, a-3, d),

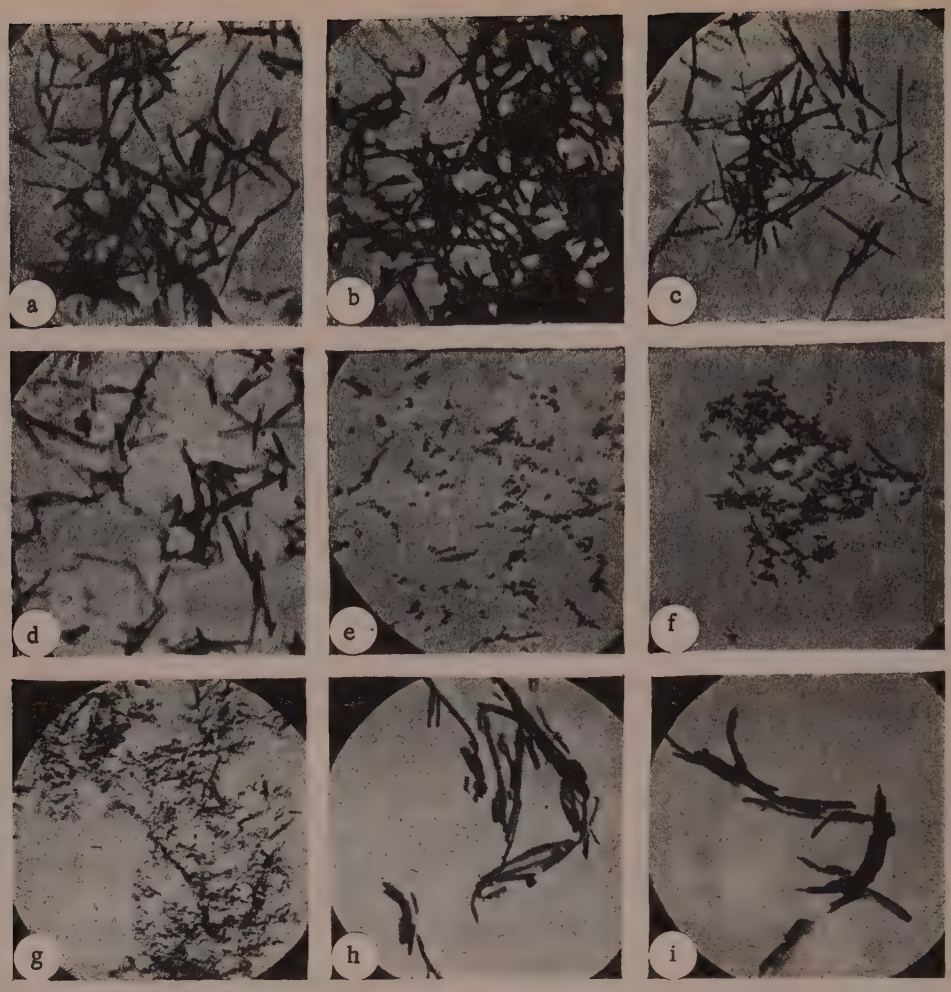


Fig. 3. Electron micrographs of structures in lithium stearate-spindle oil 3 disperse systems: a) acid number (AN) 0.07 mg KOH; b) AN 0.01 mg KOH; c) neutral; d) alkalinity (A) 0.01% NaOH; e) A 0.06% NaOH; f) A 0.08% NaOH; g) A 0.09% NaOH; h) neutral; i) AN 0.1 mg KOH; a-g) rapid cooling; h-i) slow cooling.

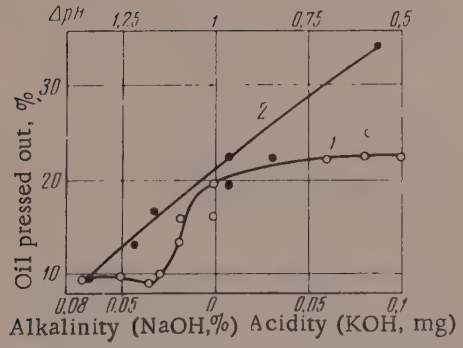


Fig. 4. Variations of stability of lithium stearate–MK-8 oil systems with acidity (1) and pH (2).

characteristic of greases thickened by lithium stearate [10, 22, 24, 25]. When a hot soap-oil melt with alkalinity of 0.04% NaOH or higher is cooled on a tray, up to 3-5% of the oil separates out, and a transparent, hard, brittle gel which readily breaks into irregular pieces remains on the tray.

Electron micrographs of lithium soap-oil systems of alkalinity > 0.04% NaOH present an unusual picture (Fig. 3, e; 3, f; and 3, g). It is seen in Fig. 3, f, and 3, g, that the disperse phase particles are of a shape unusual in soap fibers—very fine rods and fragments of irregular or slightly extended form. This shape and size of the particles constituting the structural framework of the systems partially accounts for the peculiarities of their bulk mechanical properties and stability. The viscosity level and yield value increase somewhat for systems of over 0.04% alkalinity; this is probably due to close packing of the fine soap particles, which form a strong gel-like structure in the grease.

TABLE 1

Effect of Homogenization on Properties of Mineral Oil-LiSt Systems

System	Alkalinity, % NaOH	Acidity, mg KOH	Oil pressed out, %	Yield value at 50°	Viscosity, poises at 20° and 100 sec^{-1}	Viscosity, poises at 50° and 100 sec^{-1}	$\eta_{-50°}/\eta_{50°}$, 10 sec^{-1}
Spindle 3 + 10% LiSt (rapid cooling)							
Original (A)	0,06	—	5,0	4,4	1400	—	—
Homogenized at $2 \cdot 10^4$ sec^{-1} (B)	0,06	—	14,7	2,9	400	—	—
A	0,02	—	10,9	3,0	1500	—	—
B	0,02	—	22,1	2,5	600	—	—
A	—	0,06	19,3	2,6	1500	—	—
B	—	0,06	31,6	0,6	350	—	—
MK-8 + 10% LiSt (rapid cooling)							
A	0,04	—	10,6	12	—	7600	35
B	0,04	—	36,1	0,4	—	4000	50
A	Neutr.	Neutr.	16,4	6,7	—	8900	25
B	Same	Same	44,6	0,3	—	2900	29
A	—	0,09	25,3	9,5	—	8700	23
B	—	0,09	43,6	0,3	—	1900	25

Because of the gel-like granular macrostructure and excessively high yield values, lithium stearate-oil systems of high alkalinity cannot be recommended for use as plastic greases. Moreover, some samples of high alkalinity proved to be unstable on keeping despite the small amounts of oil pressed out in tests. This indicates a peculiar type of binding of the dispersion medium, probably in consequence of the sharp difference between their structure (Fig. 3, e; and 3, g) and the usual structure of lithium soap-oil systems (Fig. 3, d).

In order to investigate the influence of oil properties on stability of soap-oil disperse systems, a series of greases was prepared by thickening of MK-8 oil with 10% lithium stearate. The greases were made by the rapid cooling method.

Data on variations of the amount of oil pressed out with the alkalinity (or acidity) and ΔpH of lithium stearate—MK-8 oil systems are plotted in Fig. 4. It follows from a comparison of Fig. 4 (curve 1) and Fig. 1 that the character of the influence of acidity (or alkalinity) on the stability of soap-oil systems is virtually unchanged when spindle oil 3 is replaced by the less viscous MK-8 oil (the viscosity of the former is 3.5 times that of the latter at 20°). The only effect of the lower viscosity of MK-8 oil is to increase somewhat the amount of oil pressed out from greases made with it. As in the case of spindle oil 3, lithium stearate—MK-8 oil systems with alkalinity of 0.03% NaOH and over have gel-like brittle macrostructure. In addition to the data in Fig. 4, it may be noted that increase of the acid number up to 3.4 mg KOH increases to 30% the amount of oil pressed out of greases made with this oil.

The influence of ΔpH of lithium stearate-oil systems on the amount of oil pressed out is of considerable interest. It is clear from Fig. 4 (curve 2) that the stability increases steadily with increase of ΔpH (i.e., of alkalinity). This confirms earlier results, according to which the amount of oil pressed out of the systems decreases with increase of free alkali content.

In the modern production process soap greases are subjected to mechanical treatment in various homogenizers [10, 24]. In order to study the effect of homogenization on the properties of our systems, the latter were treated in a rotational instrument at 20° for 1 min at a deformation rate of $2 \cdot 10^4$ sec^{-1}.

All the systems of lithium stearate with spindle oil 3 or MK-8 oil, including alkaline systems with a coarse-grained (gel-like) structure, acquired a smooth structure as the result of the treatment. Changes of stability and other properties of these systems are given in Table 1.

Table 1 shows that homogenization increases the amount of oil pressed out and lowers strength and viscosity in all cases. The greatest decreases of stability are found for systems of high alkalinity. Changes of viscosity and

TABLE 2

Effects of Various Additives on Stability of MK-8 oil—LiSt Systems

Additive	Additive concentration, %	Oil pressed out, %	Alkalinity, % NaOH
No additive	—	20.4	0.018
Lithium naphthenate	0.6	22.1	Neutr.
The same	1.0	21.2	The same
" "	2.4	25.2	" "
Calcium sulfonate	1.0	24.1	" "
Lithium naphthenate and acetate	2.0	22.8	" "
Lithium naphthenate and calcium sulfonate (1 : 1)	2.0	39.4	" "
Glycerol	2.0	20.9	0.014
TsIATIM-339	0.6	11.2	0.05
The same	1.0	11.5	0.05
TsIATIM-339 and stearic acid (1 : 1)	1.2	21.1	Neutr.
			The same
Sodium oleate	1.0	14.5	" "
Sodium hydroxide	0.12	15.5	" "
The same	0.20	8.6	0.07

strength characteristics apparently depend to a lesser extent on pH, although increase of acidity tends more to decrease τ_y in systems with spindle oil, and to decrease viscosity in systems with spindle oil, and to decrease viscosity in systems with MK-8 oil.

Various additives have been recommended for improvement of the stability of lithium greases [10, 26, 27].

Data on the effects of various additives on stability of lithium stearate–MK-8 oil systems (made by the rapid cooling method) are given in Table 2.

Table 2 shows that additions of lithium naphthenate, calcium sulfonate, and mixtures of lithium naphthenate and acetate have almost no effect on the stability of lithium stearate–MK-8 oil systems. In one experiment addition of a mixture of lithium naphthenate and calcium sulfonate sharply lowered the stability of the grease (with the reaction unchanged). Glycerol has no effect on stability either. These experimental results contradict literature data [10, 26, 27] according to which the stability of lithium greases is improved by addition of such substances; this may be associated with the composition characteristics of the lithium greases used. It is improbable, however, that additives should have such different effects in greases of much the same type. It is more likely that basic salts of organic acids might have been used as additives; these would raise the alkalinity and thus improve stability. For example, addition of the dispersing agent TsIATIM*-339 results in considerable improvement of stability of lithium stearate–MK-8 oil systems. It might be thought that such additives themselves improve stability of the greases, but in fact the alkalinity is increased, so that the amount of oil pressed out is reduced (Fig. 4). If enough stearic acid is added with the TsIATIM additive to give a grease with a neutral reaction, then, as Table 2 shows, the TsIATIM additive has hardly any effect.

*Central Scientific Research Institute of Aviation Fuels and Oils.

These results show quite convincingly that dispersing agents are unsuitable for improving the stability of lithium greases.

The pronounced effect of added sodium hydroxide on the amount of oil pressed out of lithium stearate–MK-8 oil systems (Table 2) is very interesting. In this case, as with addition of lithium hydroxide, the stability is improved. It is particularly important to note that the amount of oil pressed out at a given degree of alkalinity is approximately the same, whichever alkali (LiOH or NaOH) was used to produce the alkalinity. This can be seen from a comparison of Table 2 and Fig. 4.

SUMMARY

1. Acidity (or alkalinity) has a strong and often decisive effect on the properties of lithium soap-oil systems. The stability is improved on decrease of acidity or increase of alkalinity. However, when the free alkali content is 0.04-0.06% NaOH and over the systems acquire a granular gel-like texture; although the amount of oil pressed out of them is small, their stability in storage deteriorates.

2. The stability of lithium stearate-oil disperse systems is improved if the rate of cooling of soap-oil melts in production is raised. Their bulk mechanical properties are also improved.

3. Intensive breakdown at high deformation rates (up to $2 \cdot 10^4$ cm^{-1}) lowers the yield value and effective viscosity and diminishes the stability of the systems.

4. Additives (lithium or calcium naphthenates, acetates, and sulfonates, and glycerol) which, according to literature data, improve the stability of lithium greases, have almost no effect on the stability of lithium stearate–MK-8 oil systems. Additives with an alkaline reaction and sodium hydroxide improve stability of these systems considerably by increasing the alkalinity of the lithium soap-oil systems.

5. Electron microscope studies of the influence of acidity (or alkalinity) on the structure of lithium stearate–spindle oil 3 systems showed that changes in the pH of the system have a significant effect on the size and shape of the soap crystallites which comprise the disperse phase of such systems. The relationship between structure and stability of lithium soap-oil systems has been established.

LITERATURE CITED

1. V. M. Martynov, Khim. i. Tekhnol. Topliva, 9, 63 (1956).
2. N. P. Peskova and E. M. Aleksandrova-Preis, Course of Colloid Chemistry [in Russian] (Goskhimizdat, 1948).
3. W. H. Herschel, Proc. ASTM 33, 343 (1933).
4. V. P. Varentsov and E. D. Leonova, Neftyanoe Khoz. 1, 50 (1938); E. L. Al'perovich and V. P. Varentsov, Trans. Central Scientific Res. Inst. of Aviation Fuels and Oils, No. 1 [in Russian] (Gostoptekhizdat, 1941).
5. B. B. Farrington and R. L. Humphreys, Ind. Eng. Chem. 31, 230 (1939).
6. D. S. Velikovskii, Neftyanoe Khoz. 5, 35 (1949); Lubricant Greases [in Russian] (Gostoptekhizdat, 1945); D. S. Velikovskii and I. P. Lukashevich, Trudy Moskovskogo Neftyanogo In-ta im. Gubkina 2, 259 (1940).
7. Report CLRC of CRC, NoCLLG 19-43 (August 18, 1947).
8. K. I. Klimov et al., Zavodskaya Lab. 21, 106 (1955).
9. T. G. Roehner and C. R. Robinson, Oil and Gas J 43, No. 29, 76 (1944); T. M. Dosher and R. D. Vold, J. Amer. Oil. Chemists' Soc. 26, 515, (1949); T. D. Smith, Inst. Spokesman 14, No. 4, 10 (1950); S. F. Calhoun, Bull. ASTM, No. 210, 45 (1955); J. L. Dreher and A. L. McClellan, NLGI Spokesman 19, No. 12, 30 (1956).
10. C. J. Boner, Manufacture and Application of Lubricating Greases [Russian translation] (Gostoptekhizdat, 1958).
11. J. S. Aarons, NLGI Spokesman 22, No. 12, 12 (1958).
12. S. G. Ellis, Scient. Lubricat. 10, No. 9, 20 (1958); A. Kinsel and J. Phillips, Petrol. Refiner 27, No. 8, 98 (1948).
13. M. Prasad and V. Sundaram, Proc. Indian Acad. Sci. 33A, 295, 305, 333, 339, 344 (1951).
14. B. W. Hotten and D. H. Birdsall, Industr. and Engng. Chem. 47, 447 (1955).

15. S. F. Calhoun, NLGI Spokesman 22, No. 2, 69 (1958).
16. D. W. Griddles and J. W. Cortes, NLG Spokesman 22, No. 6, 278 (1958).
17. V. M. Martynov, Novosti Neft. Tekhn., Neftepererabotka, 3, 5 (1956); Khim. i Tekhnol. Topliva 6, 61 (1956).
18. V. V. Sinitsyn et al., Novosti Neft. Tekhn. Neftepererabotka, 6, 50 (1955).
19. G. V. Vinogradov, Usp. Khimii, 21, No. 6, 758 (1952).
20. K. I. Klimov et al., Authors' Certificate No. 99049 [in Russian].
21. K. I. Klimov et al., Neftyanoe Khoz. 11, 62 (1954).
22. V. V. Sinitsyn et al., Zhur. Priklad. Khim. 31, 8, 1202 (1958).*
23. V. S. Luneva, Collection: Investigation and Uses of Petroleum Products [in Russian] (1950) part 2, p. p. 126.
24. Motor Fuels and Oils [in Russian] part 2 (Gostoptekhizdat, 1957).
25. G. V. Vinogradov et al., Zhur. Priklad. Khim. 28, 1, 52 (1955).*
26. British Patent 693697 (1953); U. S. Patent 2625510.

*Original Russian pagination. See C. B. translation.

SOLUBILIZATION OF SULFITE CELLULOSE RESIN AND ROSIN

S. L. Talmud, A. N. Turzhetskaya, V. A. Volkov, G. P. Ivashkin, and Yu. M. Fedotov

Department of Physical and Colloid Chemistry, Leningrad Technological Institute
Translated from Kolloidnyi Zhurnal, Vol. 22, No. 4, pp. 477-481, July-August, 1960
Original article submitted December 12, 1958

The systems: resin-water, resin-sulfite liquor-water, and resin-sulfite liquor-fiber-water were studied fully earlier [1]. A method for dealing with the so-called "pitch troubles" was worked out under laboratory conditions, tested, and introduced in paper mills. This method involves coagulation of resin from the sulfite pulp, rosin, and fine cellulose fibers, present in the pulp in the emulsified or suspended state [2]. It was noted that evaporation of the clear filtrate yielded a solid residue resembling resin or rosin in appearance. It is known that transparent emulsions are formed when both liquids have the same refractive index and the same optical dispersion [3]. However, the refractive indices of rosin (1.548) and water (1.333) differ sharply, and therefore formation of transparent emulsions of suspensions in this case could not be attributed to similarity of the optical properties of the two phases.

Formation of various emulsions and colloidal solutions, and the role of surface-active substances, have been studied previously [4-14]. The purpose of the present investigation was to make a thorough check of the above-mentioned individual observations concerning the presence of sulfite pulp resin and rosin in the quite transparent filtrates obtained in coagulation of the substances emulsified and suspended in the pulp; to investigate the phenomenon quantitatively; and to study the possible role of pitch and rosin solubilization in the technological processes of the pulp and paper industry.

Resin–Water Emulsions. Resin (or, more accurately, the resins and fats present in sulfite pulp) was obtained by extraction of fine cellulose fibers from the Solikamsk Pulp and Paper Combine in dichloroethane, with subsequent evaporation of the solvent.

Resin-water emulsions were prepared by the method described earlier [1]. Boiling distilled water was added to the resin in a flask; the contents were shaken ten times during 20 min. The liquid was left to settle for 24 hr, the emulsion was filtered through an ashless filter, and the pitch content was determined.

The amounts of $Al_2(SO_4)_3$ required for complete coagulation of the emulsified resin, i.e., to make the filtrate completely clear, were then determined in separate samples. The emulsified resin in one liter of emulsion was then coagulated.

Evaporation of water from a filtrate sample showed that the filtrate contained a certain amount of resin which could not be determined refractometrically; it was therefore determined gravimetrically. The results are summarized in Table 1.

It follows from Table 1, that with the conditions used in preparation of the resin-water emulsions, after coagulation of the emulsified resin until the filtrate is quite clear, between 1.7 and 3.03% of the added substances remains in the filtration residue. Most of the resin and $Al_2(SO_4)_3$ (96.96-98.3%) remains in the clear filtrate.

It was also impossible, because of the high errors in determination, to estimate the resin and $Al_2(SO_4)_3$ contents separately in the residue and filtrate by combustion of the resin and estimation in the form of Al_2O_3.

Rosin-Water Suspensions. Rosin-water suspensions were prepared from gum rosin* of "Wg-first quality" grade, obtained from the Gor'kii rosin factory. The rosin was passed into the column at 94°, remained there for 25-28 min, and emerged heated to 165°.

*We take this opportunity of thanking S. S. Malevskaya, of the Organic Chemistry Faculty of the Academy of Wood Technology, for the rosin samples.

TABLE 1

Analytical Results for Resin-Water Emulsions Before and After Coagulation

Contents in emulsion		Content of resin + $Al_2(SO_4)_3$			
		in residue		in filtrate	
resin, g/liter	$Al_2(SO_4)_3$, g/liter	g/liter	%	g/liter	%
0,45	0,0704	0,0078	1.5	0,4705	90,4
0,635	0,0919	0,0244	3,3	0,6684	92,0
0,404	0,0919	0,0113	2,28	0,4741	95,7
0,403	0,0913	0,0086	1,7	0,4917	99,3
0,58	0,0919	0,0175	2,6	0,6594	98,4
0,78	0,0919	0,0155	1,78	0,8647	99,0

TABLE 2

Analytical Results for Rosin-Water Suspensions Before and After Coagulation

Contents in suspension		Rosin and $Al_2(SO_4)_3$ contents, g/liter		Rosin content, g/liter		$Al_2(SO_4)_3$ content, g/liter	
rosin	$Al_2(SO_4)_3$	in residue	in filtrate	in residue	in filtrate	in residue	in filtrate
Suspensions prepared by first method							
0,225	0,1378	0,0343	0,2979	0,0309	0,1637	0,0034	0,1342
0,265	0,1838	0,0204	0,4740	0,0147	0,2396	0,0057	0,2244
0,193	0,1838	0,0163	0,3305	0,0136	0,1521	0,0027	0,1784
0,190	0,1838	0,0229	0,3563	0,0022	0,1837	0,0207	0,1726
Suspensions prepared by second method							
0,240	1,8380	0,1838	1,7795	0,1835	0,1070	0,0004	1,6725
0,203	0,7352	0,1178	0,8228	0,1171	0,0845	0,0007	0,7383
0,240	0,9190	0,0670	1,1136	0,0660	0,2048	0,0001	0,9088

The rosin had the following characteristics:

Moisture	0.16%	Softening point	69.7°
Ash	0.045%	Acid number	169.3
Mechanical impurities	0.042%		

Rosin suspensions were prepared: 1) By the same method as resin-water emulsions. 2) By replacement of solvent at room temperature. For this, a solution of 1 g of rosin in 50 ml of ethyl alcohol was made up to 1 liter with distilled water, with shaking. The suspension was left for 24 hr and then filtered. The stable rosin suspensions made by these two methods were turbid. The suspended rosin was coagulated by means of $Al_2(SO_4)_3$, and the resin and $Al_2(SO_4)_3$ contents of the filtrate and residue dried at 105° were determined. In addition, resin and Al_2O_3 were determined separately by calcination of dried residues, the results being calculated as Al_2O_3. The results of the experiments are presented in Table 2, which shows that, with the two methods used for preparation of rosin suspensions, the complete clear filtrate after coagulation contains considerable amounts of suspended rosin.

For suspensions prepared by the first method (by heating at 100°) the amount of suspended rosin and $Al_2(SO_4)_3$ in the dried residues varied between 4.3 and 9.5%, so that 90.5-95.7% of the rosin was present in the clear filtrate. The calcined residues contained from 1.1 to 13.7% rosin, so that the rosin content of the filtrate was 86.3-98.9%.

TABLE 3

Analytical Results for the Liquid Phase from Production Samples from the Solikamsk Pulp and Paper Combine (averages of triplicate determinations)

Sample	Dry substance, g/liter				Appearance		
	sample	sample after addition of $Al_2(SO_4)_3$	residue	filtrate	sample	residue	evaporated filtrate
Pulp from screening section tank	0.0355	0.553	0.1233	0.4338	Turbid	Gray	Brown resin
Return water	0.0252	0.450	0.0950	0.3539	The same	The same	The same
Stock from No. 1 box	0.0620	0.7124	No residue	0.7151	Slight turbidity	"	Light-brown resin
The same	0.0620	0.6200	No residue	0.6207	Clear	"	The same

Different results were obtained with suspensions prepared by the second method. Although the dried residues of rosin and $Al_2(SO_4)_3$ comprised between 5.8 and 12.5% of the amounts taken, their rosin contents were higher (from 27.5 to 76.5%). Therefore the clear filtrate contained from 23.5 to 72.5% of the amount of rosin taken.

Investigation of Production Pulp and Water Samples from the Solikamsk Pulp and Paper Combine. The following samples were taken at the Solikamsk factory: 1) from the pulp mill—pulp from the screening section tank (before bleaching), and return water (from the thickeners); 2) from the paper mill—stock from the box of No. 1 machine for production of photosensitive paper base.

The liquid phase was separated from the pulp samples taken for analysis, and filtered to remove suspended matter. The concentration of dry substance in the samples was determined, $Al_2(SO_4)_3$ being added until the filtrate was quite clear, and the dry substance in the residue and filtrate was then determined (Table 3). Turbidity of the samples indicates that the return water from the thickeners and the liquid phase of the pulp from the screening section both contain emulsified resin. It was found that after addition of $Al_2(SO_4)_3$ there was more emulsified resin in the clear filtrate than in the coagulated residue. The liquid phase from the stock in the box of the machine for production of size paper was clear, or almost clear in the first sample. No precipitate was formed by coagulation of the first sample [$Al(SO_4)_3$ was not added to the second and third samples.] The dry residue after evaporation of the samples was light brown in color and resembled rosin. Therefore the completely clear liquid phase of sized stock contains rosin in colloidal dispersion.

The presence of colloidally dispersed resin and rosin in the transparent liquids obtained after coagulation of resin-water and rosin-water dispersions, demonstrated by us for the first time, may be interpreted as follows.

In the preparation of resin-water emulsions at 100° the system approaches the critical conditions to some extent. As a result of a sharp decrease of the interfacial tension, colloidally dispersed resin particles are formed in the spontaneously forming dilute emulsion, in addition to coarse particles of emulsified resin which are coagulated on addition of $Al_2(SO_4)_3$. The colloidal particles had not been observed previously because the systems are completely transparent. Transparent resin-water emulsions are stable systems of the same character as systems obtained by induced colloidal dissolution or solubilization.

Dispersions of rosin in water obtained at 100° are of the same nature as the resin-water dispersions.

If dispersions of rosin in water are made at room temperature by the solvent replacement method, the weight of coarse rosin particles present increases considerably, while the content of colloidally dispersed particles in the clear filtrate diminishes.

During sulfite cooking of wood chips a considerable proportion of the resins and fats present in the wood passes into the aqueous phase, together with large amounts of various surface-active and protective substances formed during the cook.

In presence of high concentrations of surface-active substances in the liquid phase of the pulp in the digester, at high temperature (145°) and pressure (6-7 atm), almost all the resin is in the solubilized state. This is indicated in particular by the fact that all the liquor samples taken were homogeneous and clear. Obviously, if the liquor is cooled or diluted with cold water its appearance changes because of separation of part of the solubilized resin.

We found that the clear liquid phase in pulp and paper-mill waters, after coagulation of the coarse resin particles, contains solubilized resin which is not all removed with the washing water. Part of it is washed out of the fiber and is present in the liquid phase of the pulp.

Large amounts of resin soaps (resinates) are formed during the cooking of white and high-resin rosin sizes. In the case of high-resin size, sodium caseinate is added during the cooking. Under such conditions there is no doubt that "free resin" (rosin) is intensively solubilized.

In stock-sizing processes, when the rosin dispersion is diluted, the solubilized rosin is distributed throughout the liquid phase of the stock. This is confirmed by the fact that solubilized rosin was found in the clear liquid phase from stock in the machine feed box.

Great interest attaches to studies of factors which influence separation of solubilized resin from the liquid phase of pulp, and also to the question of whether this separation may be one cause of "resin difficulties."

Determinations of the amount of rosin solubilized during production of rosin sizes would help to determine whether solubilization of rosin is an important cause of rosin losses in stock sizing.

To elucidate these problems, it is first necessary to work out a physicochemical technique for determination of solubilized resin and rosin in order to make the investigations more rapid and accurate.

SUMMARY

1. The clear liquors obtained after coagulation of resin-water and rosin-water dispersions contain solubilized resin and rosin.

2. Solubilized resin and rosin were detected in the clear filtrates obtained after coagulation of production samples.

3. During sulfite cooking of wood chips part of the resins and fats passes into the aqueous phase, and is solubilized in it in presence of large amounts of surface-active substances.

4. In the production of rosin sizes, at high concentrations of resinates and sometimes in presence of sodium caseinate, the "free resin" (rosin) is solubilized.

LITERATURE CITED

1. V. P. Derevyagina and S. L. Talmud, Kolloid. Zhur. 15, 20 (1953); * Zhur. Priklad. Khim. 27, 501, 901 (1954);* 29, 133 (1956);*29, 308 (1956).*
2. N. P. Dymarchuk, A.M. Ivanyushkina, L. A. Popova, and S. L. Talmud, Zhur. Priklad. Khim. 29, 610 (1956);* S. L. Talmud, A.M. Ivanyushkina, P. A. Kuznechenko, N. A. Erashova, G. M. Vol'man, and A. N. Turzhetskaya, Trans. Leningrad Technological Inst. [in Russian] (Goslesbumizdat, 1956) No. 4, p. 133.
3. W. Clayton, Emulsions and Their Technical Treatment [Russian translation edited by P. A. Rebinder] (IL, 1950) p. 280; S. S. Voyutskii and M. A. Zaitseva, Usp. Khimii, 16, 68 (1947).
4. J. W. McBain and L. McBain, J. Amer. Chem. Soc. 58, 2610 (1936).
5. P. A. Rebinder, Kolloid. Zhur. 20, 527 (1958).*
6. M. Volmer, Z. Phys. Chem. 125, 151 (1927); 155, 281 (1931).
7. P. A. Rebinder, Izvest. Otdel. Mat. i Estestv. Nauk, Akad. Nauk SSSR, Khim. Ser. 5, 639 (1936).
8. K. A. Pospelova and P. A. Rebinder, Acta Physicochim. URSS 16, 71 (1942).

*Original Russian pagination. See C. B. translation.

9. J. F. Hartley, Aqueous Solutions of Paraffin-Chain Salts (Paris, 1936).
10. Laurence, Trans. Faraday Soc. 33, 815 (1937).
11. J. W. McBain, Nature 145, 702 (1940); Advances in Coll. Sci. 1, 99 (1942).
12. I. Stauff, Koll. Z. 89, 224 (1939).
13. A. I. Yurzhenko, Zhur. Obshchei Khim. 16, 171 (1946).
14. W. D. Harkins, J. Amer. Chem. Soc. 69, 1423 (1947); J. Polymer Sci. 5, 217 (1950).

CHANGES OF THE DAMPING DECREMENT AND OSCILLATION PERIOD OF A TORSION PENDULUM IN TWO-SIDED SOAP FILMS DURING THEIR THINNING TO RUPTURE

A. A. Trapeznikov and K. V. Zotova

Laboratory of Oleocolloids and Monolayers, Institute of Physical Chemistry,
Academy of Sciences USSR, Moscow
Translated from Kolloidnyi Zhurnal, Vol. 22, No. 4, pp. 482-488,
July-August, 1960
Original article submitted October 16, 1959

The thinning of two-sided films formed from solutions of soap-like substances is one of the most interesting and important problems in investigations of foam stability. According to the literature, when a film becomes thinner its surface tension remains unchanged [1] while its thickness diminishes to a certain equilibrium value which depends on the disjoining pressure [2].

As the film becomes thinner, the volume of liquid enclosed in it diminishes; accordingly, the conditions for the action of various effects, such as the Marangoni and Gibbs effects, to which much importance is attached in relation to foam film stabilization, are altered. However, no data are available on these effects, or on methods for investigating them, in films during the thinning process [3]. The film structure can also alter during thinning; for example, Gibbs [4] postulated that "gelatinization" occurs in the transition to the thinnest films ("black" spots).

Our technique for investigation of the mechanical properties of two-sided films [5] yielded certain new data on changes in the properties of films during thinning. Although the results obtained cannot be interpreted quite uniquely at this time, nevertheless they demonstrate a number of important film characteristics and offer certain routes for further investigation of the above-named effects.

The results are also of value for estimation of two-dimensional viscosity effects in two-sided films and of the associated structure.

The method consisted of determination of the logarithmic damping decrement (λ) and torsional oscillation period (T) of a pendulum carrying a platinum ring situated horizontally and concentric with another (outer) ring, fixed rigidly on the walls of the basin in the same plane as the inner ring. The diameter of the ring wires in these experiments was 1.5 mm, the outer radius of the inner (rotating) ring was R_1 = 2.755 cm, and the inner radius of the outer (stationary) ring was R_2 = 3.000 cm; the gap between the rings, carrying the film, was ΔR = = 0.245 cm. The characteristics of the pendulum were: elastic constant of the wire (tungsten, d*= 0.05 mm) of the length used was C_0 = 3.12 dyne·cm/radian, the moment of inertia was 103.958 g.-cm^2, the oscillation period in air T = 36.60 sec, the logarithmic decrement λ_0 = 0.0185. The experiments were conducted with films from 1% solution of an alkylbenzene sulfonate synthesized in A. D. Petrov's laboratory and additionally purified in the F.V. Nevolin (designated as detergent No. 3; for example, see [6] and [7]) laboratory.

Determinations of λ and T were carried out immediately after a film had been formed between the rings, and at different time intervals during its life until it burst spontaneously. The values of λ and T, and also the effective values of film viscosity η_s^{f*} and shear modulus E_s^{f*} calculated from them by means of the formulas used previously [5], are presented in the table and in Fig. 1, for two films.

*This is left a blank in the Russian original, but presumably refers to diameter— Publisher's note.

τ	λ	T, sec	P_s	$\eta_s^{f*} \cdot 10^4$ surf. poises	ΔG	$E_s^{f*} \cdot 10^4$ dynes/cm
Film 1						
10 min	0,0276	37,82	0,045	0,74	—	—
12 hr 20 min	0,0280	37,60	0,049	0,81	—	—
23 hr	0,0298	37,95	0,058	0,96	—	—
32 hr	0,0348	38,14	0,084	1,39	—	—
48 hr 45 min	0,0360	38,00	0,091	1,50	—	—
57 hr	0,0414	38,09	0,119	1,96	—	—
58 hr	0,0460	38,16	0,143	2,36	—	—
59 hr	0,0507	38,12	0,169	2,79	—	—
59 hr 30 min	0,0575	38,09	0,207	3,42	—	—
59 hr 45 min	0,0620	38,08	0,232	3,83	—	—
60 hr 5[illegible] min	0,133	36,30	0,657	10,85	0,0655	0,90
61 hr 07 min	0,149	36,66	0,739	12,20	—	—
61 hr 25 min	0,166	36,69	0,832	13,72	—	—
61 hr 40 min	0,189	36,41	0,954	16,55	0,0409	0,67
62 hr	0,189	36,10	0,972	16,05	0,0901	1,49
62 hr 40 min	0,174	35,38	0,917	15,15	0,250	4,12
63 hr	0,159	34,51	0,849	14,00	0,405	6,68
63 hr 40 min *	0,112	34,40	0,570	9,40	0,414	6,84
Film 2						
7 min	0,0276	37,82	0,045	0,74	—	—
19 hr 45 min	0,0287	38,15	0,051	0,84	—	—
24 hr 50 min	0,0288	38,25	0,051	0,84	—	—
42 hr 40 min	0,0322	38,30	0,069	1,14	—	—
49 hr 10 min	0,036	38,61	0,088	1,45	—	—
50 hr 40 min	0,039	38,50	0,104	1,72	—	—
55 hr 30 min	0,039	38,4	0,108	1,78	—	—
63 hr 45 min	0,0507	38,75	0,172	2,84	—	—
64 hr 30 min	0,103	38,46	0,449	7,41	—	—
64 hr 45 min	0,133	38,09	0,614	10,13	—	—
65 hr	0,162	37,58	0,790	13,05	—	—
65 hr 15 min	0,184	36,21	0,948	15,65	0,0736	1,21
65 hr 30 min	0,11	35,65	0,536	8,85	0,163	2,69
65 hr 45 min	0,099	34,99	0,482	7,94	0,295	4,87
66 hr	0,094	35,08	0,451	7,45	0,278	4,58
66 hr 20 min	0,077	35,07	0,349	5,75	0,278	4,58
66 hr 35 min	0,066	35,34	0,283	4,67	0,232	3,82
66 hr 55 min *	0,056	35,46	0,221	3,64	0,209	3,44

*The film burst before the next determination could be made.

It follows from the curves in Fig. 1 that, in relation to its influence on λ and T, the whole process of film thinning can be divided into three or four stages: I) very slight increase of λ over a long period, and a gradual slight increase of T. II) Rapid increase of λ and rapid decrease of T. III) Decrease of λ after a maximum, and continuing decrease of T. IV) Slight increase of T with continuing decrease of λ (noted only on the curve for film 2, which had the longer life).

The film thickness, observed visually, undergoes parallel changes. Immediately after formation the rapidly thinning film still exhibits interference colors, and its thickness is probably of the order of 3000-4000 A (and possibly more). After only 15 min the color disappears and the film becomes grayish blue, visible only by reflected light; its thickness is probably up to 200-400 A. This appearance persists for a long time, roughly to the end of stage I, and then the film gradually becomes thinner again; it is then hardly visible even by reflected light at small angles, and acquires a darker (pale violet) tint. In stages III and IV the film becomes even less visible. These thinning stages evidently correspond to "black" spots of various thicknesses; at the last stage the thickness is probably close to 100 A.

The curves for λ and T, determined for different films, break off at different stages. The films sometimes burst at the end of stage I, and more often in stages II and III.

It is clear from these results that damping of the pendulum may be higher than λ_0, whereas the oscillation period may be either greater or less than T_0. This is highly important, but difficult to explain.

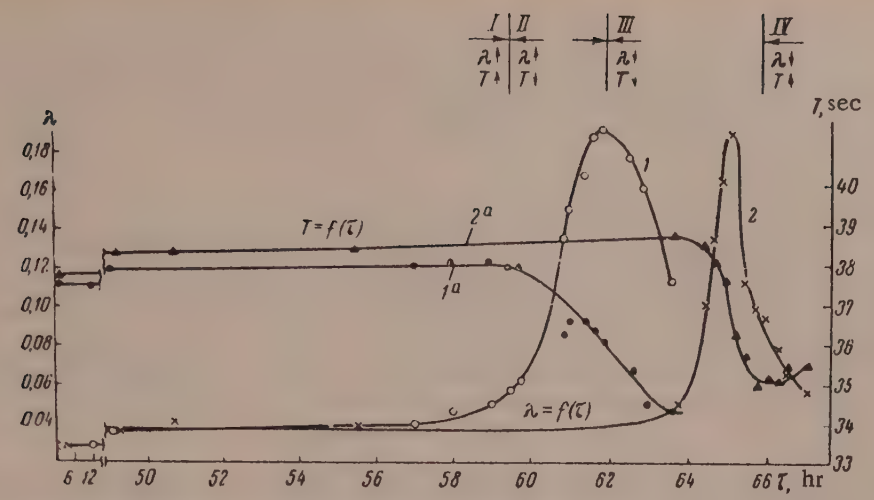


Fig. 1. Variations of λ and T during thinning of films: 1 and 1a) for film 1; 2 and 2a) for film 2.

Naturally, the first attempt at an explanation involved the assumption that a structure is formed which causes increase of λ and, accordingly, of the film viscosity as a whole, i.e., of η_s^f, as in all previous cases [5]. The increase of T could then be attributed to the influence of damping, in conformity to the general equation $T = T_0\sqrt{1 + \lambda^2/4\pi^2}$. However, even the highest observed value λ = 0.19 can increase T to only 36.61 sec. Therefore, the values of T observed in practice must be ascribed to some other mechanism (clearly, in this instance they cannot be attributed to increase of the moment of inertia by entrainment of a fairly thick supporting layer) [8].

The decrease of T in comparison with T_0 indicates the action of an elastic force in addition to the elasticity C_0 of the wire. This elastic force might be the shear elasticity of the wire, and it might formally be possible to calculate the shear modulus E_s^{f*} from T, like the viscosity η_s^{f*} from Δλ or P_s (see table). However, as the elasticity of the structures formed in these cases is far from ideally statistical, but is obviously relaxational, in this case the absolute value of λ would be considerably greater, corresponding to fairly high relaxational viscosity (this follows from the properties of all the monolayers and two-sided films studied earlier). It is therefore more correct to attribute the decrease of T to some other mechanism; the possible influence of true viscosity η_s^{δ} or η_s^f, although of very small magnitude, cannot be completely excluded.

The observed changes of λ and T may be attributed to the influences of surface tension σ and its changes (Δ σ) during deformation of the film and of its surface layers; i.e., to the Gibbs and Marangoni effects. In the Marangoni effect a force Δσ acts in a direction opposite to the motion of any body on the solution surface, caused by compression of the surface layer in front and extension behind the body; this is equivalent to a certain retarding force Δσ, and therefore to a certain apparent surface viscosity. Evidently increase of velocity must increase Δσ at given rates of adsorption and surface migration. Therefore the "frictional force" produced by this effect may be, roughly speaking, proportional to the velocity and may approximately retain the logarithmic damping character of the pendulum. This follows from the observed fact that the decrement is independent of amplitude, for example at stage I and at the end of stage III, when λ is slightly greater than λ_0, and from the slight increase of λ with decrease of amplitude at the highest values of λ in stages II and III (near the maximum).

The Marangoni effect should depend on the concentration and volume of the liquid adjacent to the surface layer; if these are large, the effect is relatively small. As the volume of liquid diminishes and the possibility of adsorption (or desorption) on the "exposed" surface decreases, the effect should become greater. It is therefore to be expected that the role of the Marangoni effect should be intensified as the film becomes thinner. However, when the film thickness is very small, comparable to the thickness of the adsorption layers, "removal" of the adsorption layer and exposure of a "clean" surface becomes almost impossible. In this case the Marangoni effect should become weaker; in the whole thinning process it should pass through a maximum.

The Marangoni effect should appear in translational motion of any body, or in rotation of a noncylindrical body (about its axis). In fact, Plateau [9], the first to investigate surface viscosity, used a magnetic needle and observed that it moved more slowly in the surface layer than in the liquid volume; he attributed this to true surface viscosity. It was this that caused Marangoni to have doubts and to suggest the possibility of the action of "pseudoviscosity" [10].

In our experiments concentric rings were used deliberately; rotating coaxially, they should, in principle, be free of the Marangoni $\Delta\sigma$ effect. Apparently this was mostly the case in all our previous experiments, with monolayers of insoluble substances and also with adsorption layers and two-sided films. In any event, the effect was very small in practice, within the limits of experimental error. However, it cannot be claimed that in experiments with two-sided films the rings are absolutely concentric at every angle of rotation. It must be admitted that, despite tests of the rings by the method of beats on a lathe and the most accurate setting in the apparatus, certain very small radial displacements of the inner ring perimeter may be possible. In such cases the Marangoni effect could be appreciable.

To judge from the magnitude of λ, for a very long time, corresponding to stage I of the film life, damping of the pendulum in the film is indeed very small, and there are virtually no data for taking the Marangoni effect into account. However, changes of T in comparison with T_0 indicate that the Marangoni effect is to some degree superposed on the true viscosity of the film even at stage I. Later it intensifies gradually, and it is only when stage II is reached that it becomes especially prominent, which is reflected in the rapid increase of λ and gradual fall of T. The decrease of λ in stage III may possibly be associated with weakening of this effect. Thus, thinning of the film provides special conditions for manifestation of the Marangoni effect. At the same time it may be assumed that appearance of surface pseudoviscosity is a manifestation of the Marangoni effect.

We now consider pseudoelasticity. According to Gibbs [4], film stabilization is associated with the action of "surface elasticity" which arises during extension of the film. It should be emphasized that what Gibbs considers is the increase of the total film area and the associated increase of surface concentration and of surface tension σ, which is the occurrence of $\Delta\sigma$, leading to contraction of the film. Therefore the Gibbs stabilizing elasticity modulus includes the increase of film area. This effect is taken into account in the stabilization theory [11]. This mechanism differs substantially from the Marangoni mechanism, in which a constant value of the total area is postulated [3].

The elasticity operative under our conditions (decrease of T) may be ascribed to the influence of the surface tension itself. As before, we must assume that rotation of a ring which is not ideally horizontal must inevitably lead to microextension of the film in planes which are not truly horizontal (as distinct from nonideal concentricity of the rings, which merely leads to "removal" of the adsorption layer). This may also be associated with the fact that the film does not adhere absolutely horizontally to the rings.

Extension of the film (and contraction in some regions) increases (or decreases) its area and creates an additional "elastic" surface tension force which acts independently of the magnitude of deformation. This is accompanied by the action of $\Delta\sigma$ which arises, in the Gibbs theory, during extension of the film and the corresponding change of surface concentration. This accelerates the motion of the ring and decreases T. It must be assumed that the film plane is nonuniform right from the start of formation of the film. Therefore T should decrease from the instant the film is formed, and yet under these conditions the decrease begins only at stage III. It follows that something changes in the film by that time, so that its extension exerts an active influence. It was noticed that in the course of time the wetting meniscuses on the film rings gradually disappear; they are either drawn along the wire of the outer ring and pass along the basin walls into the solution, or evaporate. In the latter case the increase of λ in stage II could be attributed simply to increase of the soap concentration in the film. However, this is unlikely, because at stage III λ falls to almost its initial value, which contradicts this explanation. Closer "attachment" of the film to the ring and disappearance of intermediate liquid meniscuses prevents slippage of the film along the ring and the meniscuses, and intensifies its extension. The decrease of the total volume of liquid in the film hinders adsorption on the extended parts of this film, and the consequence is that the film is extended at a higher value of σ, which leads to a greater decrease of T.

The λ (τ) curve (Fig. 1) indicates that the film life, which depends on adequate compensation of its extension and preservation of a low value of σ, is determined by the duration of stage I. Stages II and III are preruptured stages, relatively brief; in other words, the resistance of the film to the possible action of weak

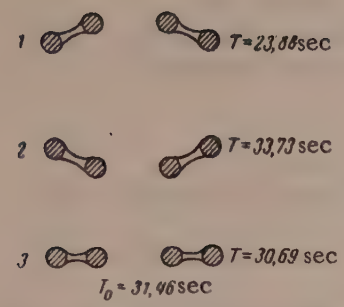


Fig. 2. Influence of the relative positions of the inner and outer rings on the value of T.

deformations is determined principally by the presence of a certain reserve of liquid (the film thickness) and by mobility of the molecules in the layer which aid sealing of ruptures [12] and the action of the Marangoni effect. This situation exists in stages I and II. The Gibbs effect, in its turn, is predominant at stages II and III.

It must be pointed out that T may have different value with a somewhat different relative position of the rings. If the inner ring is placed 1 mm higher than the outer (here the diameter of the ring wires was 1 mm, and the ring diameters and gap width were as indicated above), then T is much lower than T_0 right from the start. At the same time the film drainage is greatly accelerated, together with thinning of its upper part, adjacent to the moving ring. It seems that under such conditions extension of the film has a much stronger influence than it does when the rings are in one plane. Conversely, if the inner ring is placed 1 mm below the outer, then T is appreciably greater than T_0 right from the start.

These experiments show that the Gibbs effect predominates in position 1 (Fig. 2), and the Marangoni effect in position 2; these effects operate mainly near the moving ring. Position 3 represents one instance in which the rings are situated in the same plane.

It follows from the above values of $\Delta\lambda$ and of η_s^f* calculated from them that in presence of the foaming agent used, the film viscosity does not exceed 10^{-4}—10^{-5} surface poise even when the black-spot stage is reached; that is, the films are fluid, and relatively of very low viscosity. Moreover, it may be assumed that if they have a static shearing stress it does not, in any event, exceed $3.4 \cdot 10^{-5}$ dyne/cm, which corresponds to a definite decrease of sensitivity in the instrument equivalent to $^1/_{35}$ of a degree of thread torsion. It is quite legitimate to assume a sensitivity ten times as high, when the upper limit of the static shearing stress becomes $3.4 \cdot 10^{-6}$ dyne/cm.

In foam formation under natural conditions thinning of the meniscuses takes place as described above, with closer joining of the films. Therefore all the effects found in films between rings are reproduced in ordinary foam and are applicable to the latter, certainly, if the specific conditions of film formation are taken into account.

SUMMARY

1. A study was carried out of changes in the logarithmic damping decrement λ and the oscillation period T of a torsion pendulum in a two-sided film containing a foaming agent (Na alkylaryl sulfonate) during prolonged thinning (up to 70 hr).

2. During prolonged thinning of the film changes of λ and T follow a complex course which may, in general, be subdivided into three (or four) stages. The variations of λ and T are considered in the light of possible influence of the Marangoni and Gibbs effects at different stages of film thinning.

It also follows from the results that the film as a whole is fluid and that the static shearing stress cannot exceed $3.4 \cdot 10^{-5}$ or possibly even $3.4 \cdot 10^{-6}$ dyne/cm.

3. The value of T greatly depends on the relative position of the planes of the horizontal rings (mobile and stationary); this is attributed to draining conditions and correlated with changes of T during prolonged thinning of the film.

LITERATURE CITED

1. A. W. Reinold and A. W. Rücker, Phil. Trans. 172, 447 (1881); 174, 645 (1883); E. S. Jochonott, Phil. Mag. 47, 501 (1899); 11, 746 (1906).
2. B. V. Deryagin and A. S. Titievskaya, Kolloid. Zhur. 15, 416 (1953);* 17, 207 (1955);* Second International Congress of Surface Activity 1, 210 (London, 1957).
3. J. A. Kitchener and C. F. Cooper, Quarterly reviews, vol. 13, I (1959).

*Original Russian pagination. See C. B. translation.

4. J. W. Gibbs, Collected Works [Russian translation] (Moscow-Leningrad, 1950) p. 399.
5. A. A. Trapeznikov, Kolloid. Zhur. 19, 252 (1957);* Second International Congress of Surface Activity 1, 242 (London, 1957); K. V. Zotova and A. A. Trapeznikov, Doklady Akad. Nauk SSSR 117, 5, 833 (1957);* 128, 2 (1959).*
6. F. V. Nevolin, Masloboinaya i Zhirovaya Prom. 8 (1958).
7. K. V. Zotova and A. A. Trapeznikov, Zhur. Fiz. Khim. (1959) (in the press).
8. A. A. Trapeznikov, Conference on Viscosity of Liquids and Colloidal Solutions [in Russian] (1947) Vol. 1, p. 67.
9. J. Plateau, Ann. Physik 141, 44 (1870).
10. C. Marangoni, Nuovo Cimento 2, 5-6, 239 (1872).
11. J. K. Ewers and K. L. Sutherland, Austral. J. Sci. Res. 5, 697 (1952).
12. A. A. Trapeznikov, Zhur. Fiz. Khim. 14, 821 (1940).

*Original Russian pagination. See C. B. translation.

INVESTIGATION OF SURFACE CONDUCTIVITY IN THE ISOELECTRIC REGION

D. A. Fridrikhsberg, N. G. Gerasimova, and L. P. Popkova

Department of Colloid Chemistry, A. A. Zhdanov Leningrad University
Translated from Kolloidnyi Zhurnal, Vol. 22, No. 4, pp. 489-496,
July-August, 1960
Original article submitted February 13, 1959

The literature contains hardly any reports of studies of surface conductivity at interfaces between nonconductors and solutions in the region close to the isoelectric point. The only reference found was by Briggs [1] who, in a study of the surface conductivity of cellulose in various electrolyte solutions, did not find any changes in the case of $ThCl_4$ in the region of charge reversal. It is difficult to judge the value of the results of these early experiments, because the method of measurement is not described. Nevertheless, this unsolved problem is of great importance, not only in relation to real systems capable of undergoing surface charge reversal (proteins, hydroxides, etc.), but also for deeper insight into the properties of the electric double layer. Indeed, if at the isoelectric point (IEP) the outer layer is dense and the neighboring regions include both a dense and a diffuse layer, then it follows that studies of surface conductivity changes close to IEP would permit resolution of the conductivity into two components, which would give an idea of ion mobilities in both the dense and the diffuse layer.

It is known [2, 3] that the conductivity (κ) of a solution in the pores of a diaphragm exceeds the conductivity in the free solution (κ_v) by the value of the surface conductivity (κ_s) which is due to mobility of the ions in the double layer

$$\varkappa = \varkappa_v + \varkappa_s. \tag{1}$$

The conductivity increase is represented by the effectiveness factor

$$\alpha = \frac{\varkappa_v + \varkappa_s}{\varkappa_v}. \tag{2}$$

Determinations of surface conductivity are not only necessary for calculations of zeta-potential, but are of independent significance, as for estimating mobilities of ions in the double layer, in conjunction with adsorption determinations, since in the first approximation [2]

$$\varkappa_s \approx Fua,$$

where a is the concentration of adsorbed ions (eq/cc of pore solution); u is the mobility; F is the Faraday number.

However, this gives only the average mobility u for all the ions of the double layer. The true mobilities of the ions in the diffuse and dense layers are as yet unknown. Mobility of ions in the diffuse layer apparently differs from the mobility in free solution. The question of ion mobility in the dense layer has not been solved even qualitatively. The absence of electrokinetic effects at high ionic concentrations indicates that the dense layers are not involved in electroosmotic transfer. On the other hand, there are a number of arguments in favor of the mobility of ions in the dense layer, namely:

1) existence of two-dimensional diffusion [4] and surface pressure, caused by molecules adsorbed on the solid interface;

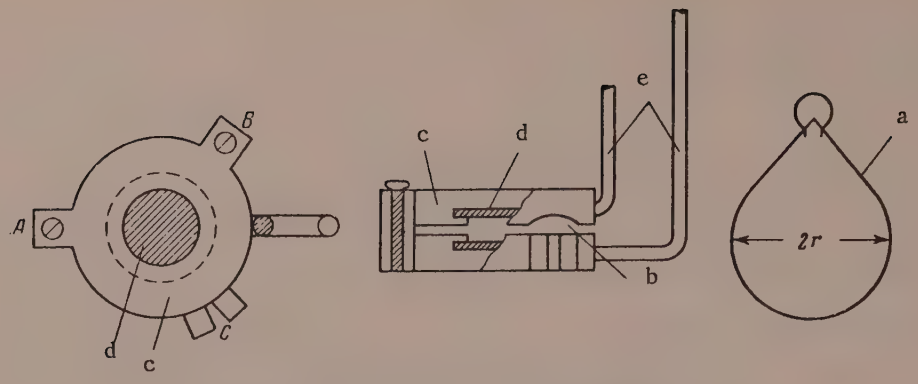


Fig. 1. Slit cell for resistance measurement.

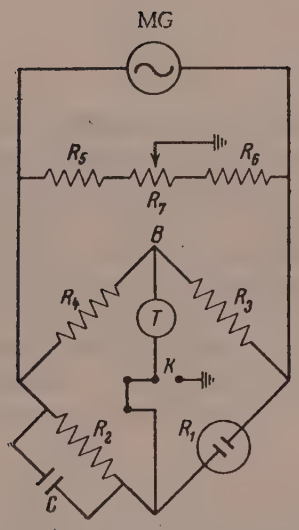


Fig. 2. Diagram of the resistance measurement circuit.

TABLE 1

Resistance Determinations (in ohms) for Two Duplicate Specimens

Specimen	R	R_v	ΔR
1	1257	1220	37
	1259	1218	41
	1256	1218	38
	1257	1218	41
2	1267	1217	50
	1266	1216	50
	1267	1216	51
	1267	1217	50
Mean	1262	1217	45

Note: r = 7 mμ; d = 0.03 cm; methylene blue (MCl) 5 M + KCl $5 \cdot 10^{-4}$ N; t = 20°.

2) absence of any appreciable change of surface conductivity with increase of solution concentration; i.e., with the passage of counter ions from the diffuse into the dense layer which has been reported [3, 5];

3) the fact that the measured surface conductivity does not coincide with the value calculated from the Gouy theory [6] (the calculated value is only 5-10% of the experimental) [8, 9].

The lack of information on the mobility of the dense layer determined the purpose of the present investigation, which was to investigate surface conductivity at the IEP in presence of an outer layer, as in the case of adsorption of counter ions causing charge reversal. Under such conditions there can be no doubt about the existence of a dense layer even at the IEP, whereas there is no diffuse layer.

The materials used for investigation were collodion membranes of different dispersities [2] in equilibrium with aqueous solutions of methylene blue and quinine hydrochloride. Cations of these salts cause charge reversal.

In order to equalize the conductivity, KCl was added to a concentration of $5 \cdot 10^{-4}$ N to all the solutions studied. One series of specimens cut from the membrane was put into 1 N KCl solution, and another in a solution of the adsorbate of high concentration; the specimens were then kept for a long time in the solutions, which were changed daily, until the determined values became equal (within the limits of experimental error) in both series. The surface conductivity in the preliminary experiments was measured by the method described in [2, 3]. Since the calculation error was ~ 10%, the main experiments were conducted by a somewhat modified method [7]. The apparatus is depicted schematically in Fig. 1 and 2. The cut membrane specimen with a silver wire loop a was introduced by means of a glass hook into a narrow slit b 0.5 mm wide between two Plexiglas disks c with

TABLE 2

Mean Values of Surface Conductivity and Zeta-Potential for a Collodion Membrane (r = 7 mμ) in Solutions of Methylene Blue + KCl $5 \cdot 10^{-4}$ N

MCl concentration, M	R_1, ohms	R_V, ohms	$C_V^0 \cdot 100$, cm^{-1}	d/l	$C_d^0 \cdot 100$, cm^{-1}	ΔR	R_h	R_d	$\kappa\ 10^5$ ohm^{-1} cm^{-1}	$\kappa_V\ 10^5$ ohm^{-1} cm^{-1}	$\kappa_S\ 10^5$, ohm^{-1} cm^{-1}	α	ζ, mv	g, $\mu M/cm^2$
0	1133	1230	9,10	0,186	2,98	—97	229	132	22,57	7,40	15,17	3,05	—4,0	—
0,5	1482	1318	9,95	0,165	2,88	+164	217	381	7,56	7,55	0,01	1,00	—0,14	0,32
1	1524	1351	9,95	0,165	2,88	173	223	396	7,27	7,36	—0,09	0,99	0	0,27
2	1479	1347	9,95	0,165	2,88	132	222	354	8,14	7,39	0,75	1,10	+0,49	0,31
3	1330	1236	9,10	0,186	2,98	94	230	324	9,20	7,36	1,84	1,25	0,42	0,33
4	1303	1231	9,10	0,186	2,98	72	229	301	9,90	7,39	2,51	1,34	0,96	0,37
5	1262	1217	9,10	0,186	2,98	45	226	271	11,00	7,48	3,52	1,47	1,14	0,40
6	1237	1218	9,10	0,186	2,98	19	226	245	12,16	7,47	4,69	1,63	1,51	0,43
10	1209	1222	9,10	0,186	2,98	—13	227	214	13,92	7,45	6,47	1,87	2,16	0,47
14	1161	1195	9,10	0,186	2,98	—34	222	188	15,85	7,62	8,23	2,08	2,94	0,51
18	1149	1198	9,10	0,186	2,98	—49	223	174	17,12	7,60	9,52	2,25	3,70	—
25	1130	1195	9,10	0,186	2,98	—65	222	157	18,98	7,62	11,36	2,49	3,93	—
100	1122	1264	9,00	0,188	2,98	—142	238	96	31,04	7,12	23,92	4,35	—	—
500	773	861	9,00	0,188	2,98	—88	162	74	40,27	10,50	29,77	3,84	10,6	—
KCl 0,05*N*	18,7	16,6	9,95	0,165	2,88	1,9	2,7	4,8	(599)	599	—	(1,00)	—	—

Note: There are certain variations in the values of C_d^0 and C_V^0 owing to slight changes in the thickness of the membrane specimens (± 0.01 mm) and interelectrode distance.

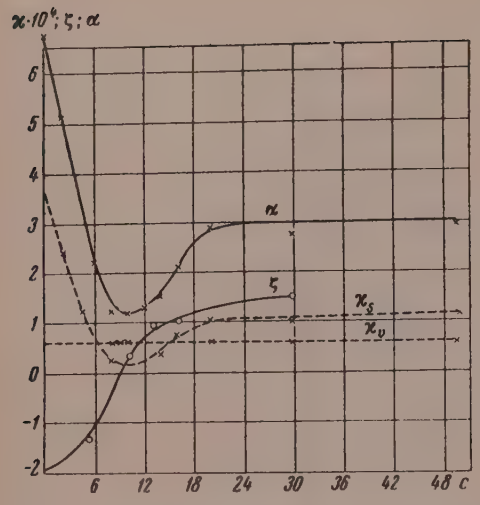


Fig. 3. Variations of surface conductivity (κ_s and α) and zeta-potential of a collodion membrane with concentration of methylene blue (c).

attached platinized platinum electrodes d. The insulated leads e were connected to contact rings fixed on a shaft; further contact was effected through mercury filling circular grooves cut in the rings. The cell was rotated uniformly in a beaker containing the solution, placed in a thermostat, to ensure that solution flowed over the diaphragm during the determination and thus to eliminate indeterminate errors associated with the passage of current (heat liberation, gas formation, changes of concentration). The measurement circuit [8], based on the Wheatstone bridge principle, consisted of an audio-frequency oscillator ZG 10, the cell R_1, plug resistance boxes R_3 and R_4, a knob resistance box R_2 (0.1-10^5 ohms), an R-523 capacitor box (0.001-1 μf), and a supplementary Wagner bridge [9] consisting of two resistances R_5 and R_6 and a grounded 50 ohm potentiometer R_7.

A sharp sound minimum recorded by the microphone T was obtained owing to the presence of a capacitor in parallel with the cell and the supplementary branch; the determination error did not exceed 0.2%.

The resistance determinations with the membrane (R) and without (R_v) were performed consecutively, 3-4 times for each specimen. In illustration, the results for two specimens are given in Table 1 (the scatter was slight in all cases).

The difference of the measured resistances $R-R_v = \Delta R$ is equal to the membrane resistance R_d less the resistance of the solution layer replacing it (R_h), and hence

$$R_d = \Delta R + R_h. \tag{3}$$

R_h was found from measurements of the solution resistance R_v in the cell without the membrane, the interelectrode distance l, and membrane thickness d

$$R_h = R_v \frac{d}{l}. \tag{4}$$

The membrane thickness (d) was measured with a micrometer, and the distance l was found from the cell constant $C_v^0 = l / F_e$; $l = C_v F_e$, where F_e is the area of the electrodes.

From (3) and (4), the membrane resistance is

$$R_d = R_v \frac{d}{l} + \Delta R.$$

To find κ, the membrane resistance constant C_d^0 was measured in 0.1 N KCl solution, in which $\kappa \approx \kappa_v$ $\alpha \approx 1$

$$C_d^0 = \varkappa_v^0 R_d^0,$$

where the sign (^{0}) refers to 0.05 N solution

$$\varkappa = C_d^0 / R_d \text{ and } \varkappa_v = C_v^0 / R_v.$$

These results and Equations (1) and (2) were used to find κ_s and α, and also the structure factor $\beta = R_d^0 / R_h^0$.

The values of the zeta-potential required for determinating the IEP were found by the streaming potential method with the apparatus described earlier [10], and calculated from the equation

$$\zeta = 6{,}75 \cdot 10^7 \cdot \frac{4\pi\eta E(\varkappa_v + \varkappa_s)}{Dp},$$

where p is the pressure (mm Hg); η is the solution viscosity; D is the dielectric constant; E is the streaming potential. The values of ζ and E are expressed in the same units. The pore membrane radius (r) was found by the usual method [3]; $r = \sqrt{8\eta\Phi d\beta}$, where Φ is the filtration coefficient.

Dye adsorption was determined by direct photometry of the membranes with the MF-2 microphotometer. Absorption was measured at 10-12 points in the membrane. The adsorption by the membrane g, in μmole/cm^2, was calculated for mean values (root mean square error $\approx$ 5%) with the aid of a calibration curve plotted from the results of measurements on standards made from specimens of the same membrane.

Solutions of Methylene Blue. The preliminary experiments were performed in a dismountable apparatus with two collodion membranes (r = 7 and 15 mμ) in solutions of methylene blue (MCl). Variations of $\varkappa_s$, α and ζ with the dye concentration are plotted in Fig. 3. In the region of the isoelectric point ($\zeta = 0$) there is a distinct minimum of surface conductivity, but as the error was up to 10% it was not possible to solve the main problem: whether a certain surface conductivity of the ions in the dense layer (up to 10% of the total conductivity) is retained, or whether these ions are devoid of directed motion in the electric field, i.e., do not take part in transfer of electricity.

The results of the main experiments, carried out by the more exact method, are summarized in Table 2. These data confirm the general effects of concentration shown graphically in Fig. 3.

It is interesting to note that the difference $R-R_V = \Delta R$, which is the value found by direct experiment, is negative in pure KCl; with increase of dye concentration the resistance of the membrane near the IEP becomes higher than that of an equivalent layer of solution ($\Delta R > 0$), and with further increase of concentration and surface conductivity R again becomes less than R_V. The region of negative values corresponds to the condition $\alpha > \beta$, i.e., to the "capillary superconductivity" effect [3].

The data in Table 2 show that the surface conductivity values ($\varkappa_s$ and α) fall sharply with increase of concentration, with a deep minimum at the IEP ($\zeta = 0$).

The minimum values of α are almost exactly unity (0.99-1.02), and the values of $\varkappa_s$ are zero. We consider that a definite conclusion may be drawn from this: the dye cations in the dense layer do not move along the interface under the influence of the electric field. The surface conductivity reappears with further increase of dye concentration and increases throughout the range studied, up to 500 M. Thus very asymmetric curves with minima are obtained; in the left-hand branch of the curve, at low dye concentrations, the composition of the double layer varies more sharply than in the right.

The adsorption isotherm $g = f(c)$, on the other hand, increases steadily. At the IEP the adsorption is $\sim$ 45% of the limiting value found by extrapolation. Approximate calculations* show that the dye covers only $\sim$ 1.5% of the total internal surface at the IEP, and $\sim$ 3% at maximum adsorption. Further increase of the charge density is apparently confined to mutual repulsion of similarly charged dye ions.

Causes of Surface Conductivity Changes in the Isoelectric Region. At low concentrations the dye ions are held firmly by their positive charges on the ionic groups of the wall and are immobile. Shielding of the surface charge is completed at the IEP, when the dye ions are stationary ($\varkappa_s = 0$). With increasing concentration additional dye cations are adsorbed; their positive charges are apparently directed toward the solution and are balanced by the chloride ions. This new layer causes increase of the surface conductivity, represented by the ascending branch of the curve.

* The specific surface of the membrane is $s/Q \approx 2/r$ (where s is the internal surface; Q is the pore volume per cm^2 area). For r = 7 mμ we have: $s/Q = 280$ m^2/cc. The adsorption per cc of solution is $a = g/dW$, where d is the membrane thickness and W is the porosity. When $g = 0.27\mu$mole/cm^2 at the IEP d = 0.029 and W = 0.76; $a = 0.27/0.022 = 12.3$ μmole/cc. From the value for the closest packing of the dye, 0.33 m^2 per μmole [4] (p. 295) we have that at the IEP the dye covers $s/Q = 0.33 \cdot 12.3 = 4.1$ m^2, or $4.1 \cdot 100/280 = 1.5\%$ of the total internal surface.

The mobility of these adsorbed chloride ions can be estimated from the equation

$$\varkappa_s = c_s U = \frac{g - g_0}{Q} U, \text{ where } U = Fu$$

TABLE 3

Comparison of Surface Conductivity and Dye Adsorption on a Collodion Membrane

MCl concentration, M	$\kappa_s \cdot 10^5$ ohm^{-1} · cm^{-1}	$(g-g_0)\cdot 10^6$, mole/cm^2	$\frac{\kappa_s}{g-g_0} \cdot 10^3$
3	1,84	0,06	0,31
4	2,51	0,10	0,25
5	3,52	0,13	0,27
6	4,69	0,16	0,36
10	6,47	0,20	0,32
14	8,23	0,24	0,32

and hence

$$U = \frac{\varkappa_s Q}{g - g_0},$$

where g and g_0 are the adsorption at the given concentration and at the IEP, respectively, (per cm^2 membrane area); Q is the volume of liquid in the pores, 0.022 cc per cm^2 membrane area. The values of κ_s and $g-g_0$ (Table 2) are given in Table 3.

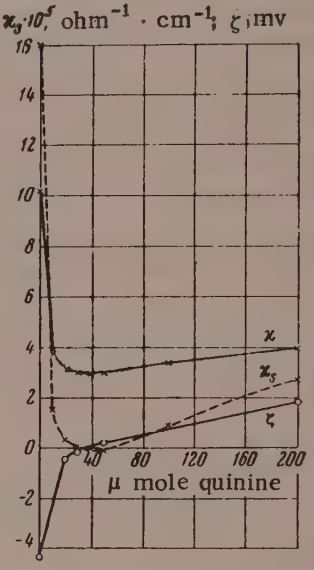


Fig. 4. Variations of surface conductivity (κ_s and α) and zeta-potential of a collodion membrane with concentration of quinine hydrochloride (c).

The data in Table 3 show that surface conductivity increases in proportion to the amount of dye adsorbed, and therefore the mobility is constant, within the limits of experimental error

$$U = 0{,}31 \cdot 10^{-3} \cdot 2{,}2 \cdot 10^{-2} = 6{,}8 \text{ cm}^2/\text{eq} \cdot \text{ohm}$$

which is ~ 10% of the mobility of Cl^- in free solution.

Quinine Hydrochloride Solutions. Membranes prepared: I) from 4% collodion without addition of water; II and III) with additions of 1 and 3% water, respectively, were studied in quinine hydrochloride solutions. The slit apparatus (Fig. 2) was used for the determinations. Equilibrium was reached in 6-10 days. The reproducibility of the measurements was the same as in the dye solutions (error of $R \leq 0.5\%$). The mean experimental values of β, κ_s, α and ζ are given in Table 4.

TABLE 4

Mean Values of Surface Conductivity and Zeta-Potential of Collodion Membranes in Solutions of Quinine + $5 \cdot 10^{-4}$ KCl

Quinine concentration, μM	Membrane I: r=9,2; β=1,62			Membrane II: r=12,2; β=1,5			Membrane III: r=36,3; β=1,3		
	$\varkappa_s \cdot 10^5$	α	ζ	$\varkappa_s \cdot 10^5$	α	ζ	$\varkappa_s \cdot 10^5$	α	ζ
0	15,9	3,4	—4,3	11,7	2,7	—4,25	4,52	1,68	—10,0
10	1,52	1,23	—	1,20	1,19	—	0,25	1,04	—
20	0,33	1,05	—0,49	0,17	1,02	—0,76	—0,15	0,98	—2,04
30	0,08	1,01	—0,12	0,16	1,02	+0,29	0,06	1,01	+0,15
40	0	1,00	—	0,0	1,0	—	0,09	1,02	—
50	—0,08	0,99	+0,27	0,16	1,02	—	0,27	1,04	+0,45
100	0,90	1,12	—	1,10	1,15	—	0,64	1,08	—
200	2,55	1,30	1,77	2,51	1,30	2,14	1,22	1,14	+5,0

The results obtained with adsorption of quinine conform to the same basic relationship as in the case of methylene blue, namely: the values of α and κ_s pass through a minimum at the IEP, corresponding to absence of surface conductivity. It must be pointed out that here the IEP corresponds to a concentration 30 times that of the dye, and the region of low values of α (0.98-1.05) is accordingly spread over some tens of micromoles per liter; this indicates that the values for adsorption of quinine and the dye differ (by a factor of about 30).

However, if the abscissa scale is reduced in the same proportion we again have typical curves with a sharp fall and slow rise (Fig. 4).

Comparison of the results found for membranes of different structures shows that the IEP is shifted somewhat toward higher equilibrium concentrations with decrease of pore radius; it seems that adsorption of quinine is hindered in narrow pores by the influence of the opposite wall, bearing the same charge. On either side of the IEP the surface conductivity increases, as usual, with decreasing pore radius.

It must be pointed out that the data in this paper on the absence of surface conductivity at the IEP do not refute the concept of ion mobility in the dense layer, as the results found for large organic cations evidently cannot be extended to all ions.

SUMMARY

1. The electrokinetic potentials, surface conductivity, and adsorption on collodion membranes in solutions of methylene blue and quinine hydrochloride have been determined. The surface conductivity—concentration curve passes through a minimum at the isoelectric point, where the surface conductivity is zero. The results show that adsorbed organic cations in the dense layer are devoid of mobility.

2. Adsorption at the isoelectric point is $\sim$ 45% of the limiting value, with $\sim$ 1.5% of the internal surface covered.

3. The isoelectric point is shifted somewhat toward higher concentrations with decrease of the membrane pore radius.

LITERATURE CITED

1. D. Briggs, Colloid Symposium Monograph 6, 41 (1928).
2. O. N. Grigorov, Z. P. Koz'mina, A. V. Markovich, and D. A. Fridrikhsberg, in: Electrokinetic Properties of Capillary Systems [in Russian] (Izd. AN SSSR, 1956).
3. I. I. Zhukov and D. A. Fridrikhsberg, Kolloid. Zhur. 11, 3, 163 (1949).
4. S. Brunauer, Adsorption of Gases and Vapors [Russian translation] (1949) Vol. 1.
5. I. W. McBain and C. R. Peaker, Proc. Roy. Soc. (Lond) A125, 394 (1929); H. White, B. L. Monaghan, and F. Urban, J. Phys. Chem. 45, 500, (1941); A. J. Rutgers and M. de Smet , Trans. Faraday Soc. 36, 69 (1940).
6. K. S. Cole, Physics 3, 114 (1932); A. J. Rutgers, Trans. Faraday Soc. 36, 69 (1940).
7. G. Schmid and H. Schwartz, Z. Elektrochem. 55, No. 4, 295 (1951).
8. J. Jones and H. Josephs, J. Amer. Chem. Soc. 50, 1049 (1928).
9. W. Grallert, Z. Elektrochem. 42, No. 6, 330 (1936).
10. I. I. Zhukov and D. A. Fridrikhsberg, Kolloid. Zhur. 12, 1, 26 (1950).

INFLUENCE OF INTERNAL STRESSES ON THE ADHESION PROPERTIES OF GELATIN FILMS*

S. A. Shreiner and P. I. Zubov

Polymer Section, Institute of Physical Chemistry, Academy of Sciences USSR
Leningrad Technological Institute of the Food Industry
Translated from Kolloidnyi Zhurnal, Vol. 22, No. 4, pp. 497-502,
July-August, 1960
Original article submitted March 30, 1959

The formation of adhesive films proceeds by the same mechanism as the formation of concentrated gels [1, 2]. The strength characteristics of adhesive layers are determined not only by the nature of the local bonds between the macromolecules but also by the conditions in which these layers are formed: concentration of the original solution, thickness of the layer, structure and chemical composition of low-molecular impurities, drying conditions, etc.

From data on the mechanical properties of gels [2] and the concepts developed by Kargin and his co-workers [3], we concluded that the formation conditions primarily influence the character of the relaxation processes and the magnitude of the internal (shrinkage) stresses which arise in adhesive layers and which, by weakening the forces acting between the chains, tend to reduce bonding strength. The magnitude of these stresses can be determined from the value of the birefringence which arises in the thickness of an elastic isotropic glass support when a film is formed on its surface [4]. This method can be used for observing changes of internal stresses in relation to the formation time and thickness of the film.

The experimental section of this paper contains experimental data on the influence of low-molecular impurities on the magnitude and distribution of internal stresses which arise both in adhesion and in formation of a film on a rigid support.

Data on increase of internal stresses in adhesive films and visual observations of the state of contact with the support were used to establish the existence of a limiting (critical) value for the internal stresses; this value is proposed as a criterion for estimating adhesion and surface strength of rigid supports.

The adhesive films were formed from gelatin solutions. The method used for preparation of the solutions, the conditions of film formation, and measurements of bonding strength were the same as before [1].

The rigid supports and plates for lapped joints were optically polished four-sided rectangular prisms 10 × 20 × 20 mm in size, made from TF-1 glass. The length of the overlap was the same in each case (6 mm). Birefringence was measured in a layer of the support at a distance of 0.2 mm from the surface of contact between the support and the film, by means of a polarization microscope fitted with a KPK rotating calcite compensator.

Figure 1 shows that the stress distribution in the adhesive layers is not uniform. The stresses are greatest at the ends of the overlap, and least in the middle. The shape of the curves (Fig. 1) indicates that relaxation processes develop irregularly throughout the volume of the adhesive layer; this is associated with the conditions of layer formation and, in particular, with the rate of evaporation of the solvent. As was to be expected, low-molecular impurities do not influence the internal stress distribution. However, the magnitude of the internal

*Communication 20 in the series: Structure of Gels.

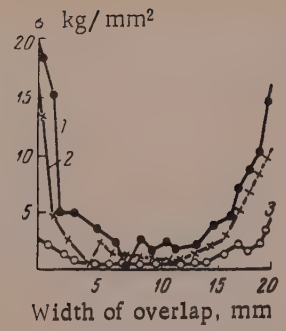


Fig. 1. Distribution of internal stresses (σ) across the overlap in specimens bonded by 20% gelatin solution prepared with: 1) 0.45 M sodium sulfate solution; 2) water; 3) 2M urea solution. Thickness of adhesive layers 0.1 mm.

stress distribution. However, the magnitude of the internal stresses depends on the nature of the additive; sodium sulfate decreases and urea increases the stresses in the layer.

Visual observations of the adhesive layers, especially under the microscope, indicate that additives also influence the character of the defects (cracks) which form in the adhesive layer.

In presence of sodium sulfate, which tends to increase internal stresses, the layers are more defective than those containing urea (Fig. 2). The layers also become more defective with increasing thickness (Fig. 3).

The bonding strength decreases in presence of sodium sulfate and with increasing thickness of the layer (table and Fig. 2 and 3).

The nonuniform distribution of internal stresses becomes apparent to some extent if the layers are formed on rigid supports, especially in the case of thick adhesive films, the surfaces of which are marked by peculiar alternating depressions and projections.

We studied the kinetics of internal stress increase in an adhesive gelatin film in relation to concentration and the rate of evaporation of the solvent (water). The stress increase is closely correlated with decrease of water concentration in the films (Fig. 4). As was to be expected, very sharp stress increases are observed only in the region of high gelatin concentrations in the films (~ 70-75%), i.e., in

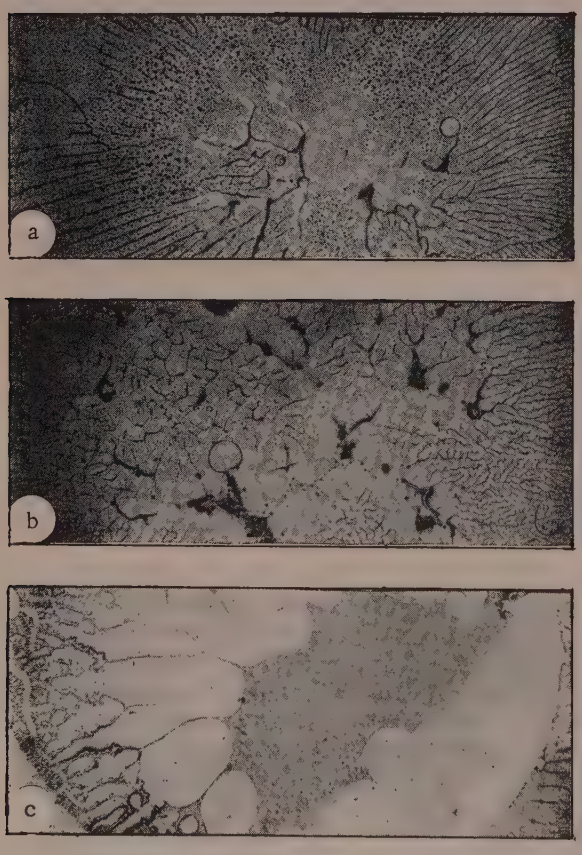


Fig. 2. Photographs of adhesive layers 0.1 mm thick in specimens bonded by 20% gelatin solutions prepared with: a) 2M urea solution; b) 2M acetamide solution; c) 0.45 M sodium sulfate solution. Magnification 12.

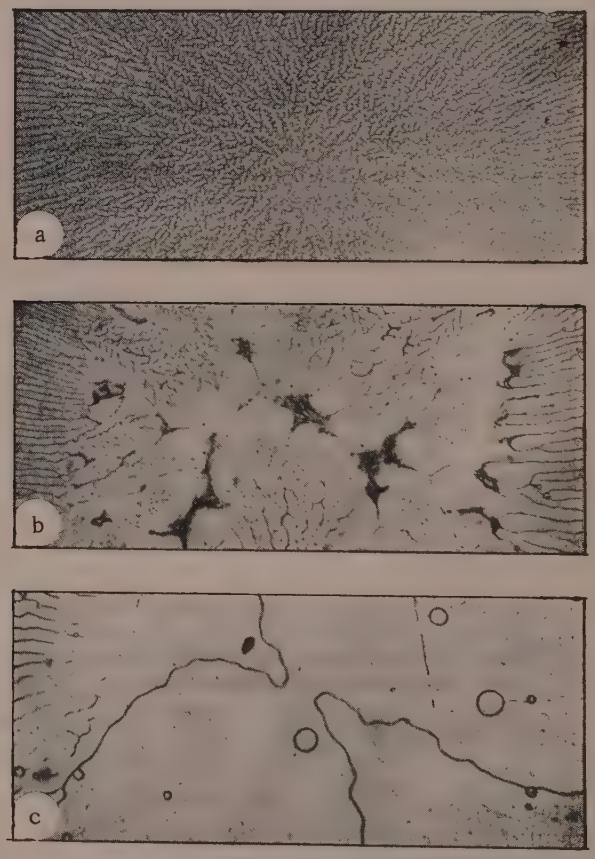


Fig. 3. Photographs of adhesive layers in specimens bonded by 20% gelatin solution with different layer thicknesses: a) 0.02 mm; b) 0.1 mm; c) 0.2 mm.

Dependence of Bonding Strength on the Conditions of Formation of Adhesive Layers from 20% Gelatin Solutions With and Without Additives

Solvent	Layer thickness, mm	Bonding strength, kg/cm²	Solvent	Layer thickness, mm	Bonding strength kg/cm²
2 M urea	0.1	103	Water	0.02	105
2 M acetamide	0.1	94	"	0.1	58
0.45 M sodium sulfate	0.1	26	"	0.2	46

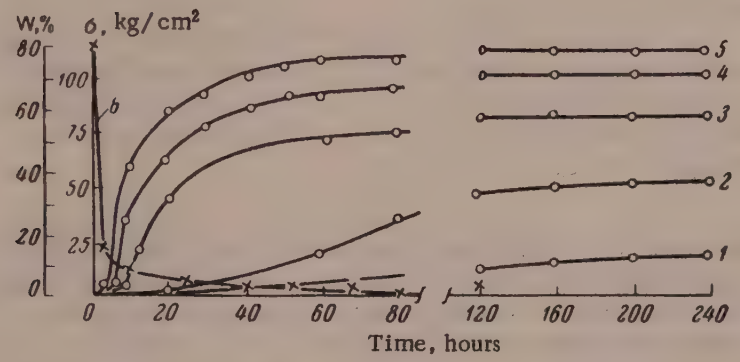


Fig. 4. Effects of low-molecular additives on the development of internal stresses (σ) at the interphase boundary in formation of films from 20% gelatin solutions prepared with: 1, 2, 3) 2 M, 1 M, and 0.5 M urea solution; 4) water; 5) 0.45 M sodium sulfate solution; 6) decrease of water content (W, %).

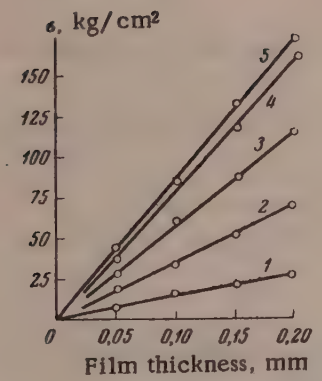


Fig. 5. Variations of internal stresses (σ) in relation to thickness of gelatin films made from 20% solutions: 1, 2, 3) 2 M, 1 M, and 0.5 M urea solutions; 4) water; 5) 0.5 M sodium sulfate solution.

the region of retarded relaxation processes. Addition of sodium sulfate increases stress (curve 5) while urea, as was to be expected, decreases stress, the decreases being greater at higher urea concentrations (Curves 1-3).

The stresses in all the experiments increase linearly with the film thickness [4]. However, Fig. 5 shows that the linear relationship holds only up to a definite film thickness (in the case of gelatin films, up to 200 μ). In thicker films the stress begins to diminish sharply beyond a certain maximum value, and in some cases falls to zero. A special study was made of this peculiar effect. It was found that the decrease of stress in the thickness of the support, observed beyond a certain limiting value, is associated with breaks in the contact between the film and support, and the total disappearance of the stress is determined by breakdown of contact between the gelatin and support over the entire film—support interface.

The experimental data can be plotted in a system of rectangular coordinates in the form of a triangle (Fig. 6). The vertex A of this triangle corresponds to the limiting (critical) value of internal stress, which we regard as equivalent to the adhesive strength. This value naturally depends on the conditions in which the adhesive film was formed, in addition to its composition; the reproducibility of this value is directly related to the film formation conditions, which cannot always be fulfilled exactly. Therefore deviations are inevitable in duplicate experiments.

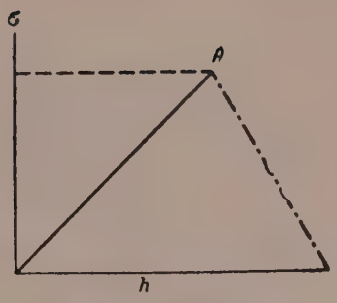


Fig. 6. Effect of adhesive film thickness (h) on the internal stresses (σ) which arise in formation of films on glass surfaces.

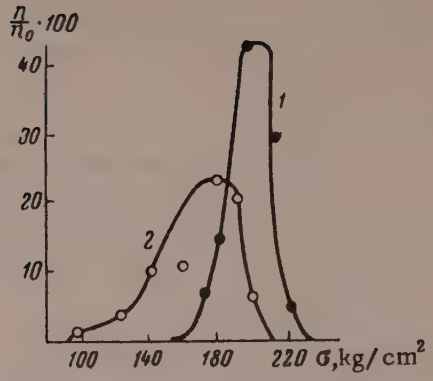


Fig. 7. Distribution of the force of separation of a forming film from glass-film (1) and glass-glass (2) interfaces under the influence of internal stresses: n) number of specimens in which separation took place at the given σ; n_0) number of specimens tested.

The results of statistical analysis of 50 cases of spontaneous separation of gelatin films from glass surfaces (Fig. 7, curve 1) show that the most probable value for the adhesion strength is in the range of 180-200 kg/cm².

In these experiments, together with spontaneous separation of the gelatin film from the glass surface, detachment of the film together with the glass (cohesive rupture) was sometimes observed. This effect, which we attribute to defects in the glass surface, was very common. Out of our 80 experiments, 50 resulted in adhesional separation, and 30 in cohesive rupture (Fig. 7, curve 2).

These results show that birefringence variations within glass on the surface of which an adhesive film is formed can give an indication of the glass surface quality as well as of the degree of adhesion.

SUMMARY

1. The internal stress distribution between the surfaces of adhesive layers has been shown to be nonuniform by an optical method.

2. The course of development of internal stresses in film formation on glass surfaces was investigated; the stress was found to be a linear function of film thickness.

3. In thick films formed on glass supports stresses arise which lead to separation of the film from the film-glass interface or to cohesive rupture of the support.

4. The limiting (critical) value of the internal stresses arising in the formation of adhesive films can serve as a criterion for evaluation of the adhesion properties of films and the surface strength of rigid supports.

LITERATURE CITED

1. S. A. Shreiner and P. I. Zubov, Kolloid. Zhur. 19, 651 (1957);* Summaries of Papers at the 4th All-Union Conference on Colloid Chemistry [in Russian] (Izd. AN SSSR, 1958).
2. P. I. Zubov, Z. N. Zhurkina, and V. A. Kargin, Kolloid. Zhur. 9, 109 (1947).
3. V. A. Kargin and M. N. Shteding, Zhur. Fiz. Khim. 20, 727 (1946).
4. S. A. Shreiner and P. I. Zubov, Doklady Akad. Nauk SSSR, 124, 1102 (1959).*

*Original Russian pagination. See C. B. translation.

LETTER TO THE EDITOR

KINETICS OF STRUCTURE FORMATION IN SUSPENSIONS OF TRICALCIUM AND β-DICALCIUM SILICATES IN PRESENCE OF CALCIUM CHLORIDE*

E. P. Andreeva and E. E. Segalova

Department of Colloid Chemistry, M. V. Lomonosov Moscow University
Translated from Kolloidnyi Zhurnal, Vol. 22, No. 4, pp. 503-505,
July-August, 1960
Original article submitted April 1, 1960

For investigation of the mechanism of action of calcium chloride on silicate minerals in cement clinker during hydration, we studied the kinetics of structure formation in calcium trisilicate (C_3S) and β-dicalcium silicate (β-C_2S) when mixed with solutions of calcium chloride of various concentrations.

Processes of structure formation were characterized by the kinetics of plastic strength increase, measured by means of a cone plastometer. The specimens were kept in desiccators over water or appropriate solutions of calcium chloride.

Before the chemically combined $CaCl_2$ and H_2O were determined, the pastes containing silicates mixed with finely ground quartz sand were washed with ethyl alcohol to a negative reaction for Cl^-. Chemically bound water was determined as described in [1]. For determination of bound $CaCl_2$ the paste was treated with 5% HNO_3 solution, the filler was filtered off, and the Cl^- content in the neutralized filtrate was determined by Mohr's method.

Table 1 shows that calcium chloride lengthens sharply the induction period of structure formation; this was reported earlier [2]. Despite the retardation of the initial stage of structure formation, subsequently the strength of suspensions containing $CaCl_2$ increases rapidly; at concentrations of $CaCl_2 \leq 3.2$ N this leads to formation of hardening structures of considerably higher strength than in suspensions made with water. When the concentration of $CaCl_2 > 3.2$ N the strength of the forming hardening structures diminishes.

To elucidate the nature of the interaction in C_3S and β-C_2S suspensions, combined Cl^- in the solid phases of the suspensions was determined by chemical analysis 5 min, 1, 3, and 10 days, and 1 and 1.5 months after the silicates had been mixed with 0.6, 1.6, and 3.2 N $CaCl_2$ solutions (these are the concentrations most widely used in practice for acceleration of hardening processes) (Table 1). The analytical results showed that when C_3S and β-C_2S are mixed with solutions of $CaCl_2 < 3.2$ N the calcium chloride is not combined chemically at all. In suspensions in which 3.2 N solution was used, a small amount of $CaCl_2$ is combined.

It is clear from Table 2 that the amount of combined calcium chloride corresponds to 0.08 mole per mole of silicate in the case of C_3S, and 0.01 mole per mole in the case of β-C_2S; in all probability, the hydroxychloride $3Ca(OH)_2 \cdot CaCl_2 \cdot 12H_2O$ [4] is formed by the action of calcium chloride on calcium hydroxide formed by hydrolysis. Accordingly, the amount of combined $CaCl_2$ is considerably less in β-C_2S suspensions.

The results of chemical analysis thus show that no direct chemical action takes place between calcium silicates and calcium chloride. Calcium chloride accelerates hydration (Table 2) and structure formation (Table 1) in calcium silicates; it acts through the solution, by changing the solubility for the original silicates and the crystallization conditions for their hydrates.

*Student E. I. Brodova took part in the experimental work.

TABLE 1

Kinetics of Structure Formation in C_3S and β-C_2S Suspensions. Duration of Stirring in Mixing, 25 min

Time after end of mixing	Calcium chloride concentration in water, N					
	H_2O	0,6	1,6	3,2	6,3	8,0
	Plastic strength P_m, kg/cm²					
10% C_3S + 90% sand + 34 ml water or $CaCl_2$ solution per 100 g of dry mixture						
1 min	0,120	0,100	0,080	0,050	0,040	0,030
1 hr	0,26	0,72	0,38	0,31	0,130	0,070
3 »	0,77	1,14	1,20	2,52	0,61	0,42
5 »	1,67	1,86	7,00	11,00	1,70	0,48
1day	7,0	12,00	25,0	36,0	5,00	2,00
5 »	28,0	40,0	60,0	76,0	20,0	11,0
15 »	65,0	82,0	105	127	57,0	25,0
30 »	80,0	96,0	118	146	71,0	36,0
60 »	82,0	97,0	120	150	72,0	38,0
25% β-C_2S + 90% sand + 33 ml water or $CaCl_2$ solution per 100 g of dry mixture						
1 min	0,10	—	0,080	0,060	0,050	0,010
30 »	0,40	—	0,33	0,080	0,060	0,30
6 hr	1,72	—	1,50	0,80	0,30	0,20
1 day	8,00	—	12,0	27,5	4,00	2,00
5 »	35,0	—	53,2	85,0	22,5	14,0
15 »	76,5	—	116	154	51,0	36,0
20 »	84,0	—	122	160	55,0	41,0
30 »	84,0	—	122	160	55,0	41,0

TABLE 2

Amounts of Chemically Combined Water * and $CaCl_2$ ** (grams per gram of silicate taken) in Suspensions of C_3S and β-C_2S. Composition of Suspensions 10% C_3S + 90% SiO_2 + 34 ml H_2O or 3.2 N $CaCl_2$ per 100 g Dry Mixture; 25% β-C_2S + 75% SiO_2 + 34 ml 3.2 N $CaCl_2$ per 100 g of Dry Mixture; 1 and 2) Amounts of Combined H_2O in Mixing with Water and 3 N $CaCl_2$; 3 and 4) Amounts of Combined $CaCl_2$ in Mixing with 3 N $CaCl_2$

Time after mixing	C_3S			β-C_2S
	1	2	3	4
5 min	—	—	0	0
1 day	0,055	0,115	0,020	0,003
3 »	0,106	0,162	0,034	0,005
7 »	0,121	—	—	—
10 »	—	—	0,035	0,008
20 »	—	0,246	—	—
30 »	0,137	0,248	0,038	—
45 »	—	—	0,040	—

*Complete conversion of C_3S into $C_2S \cdot 4H_2O$ and $Ca(OH)_2$ corresponds to 323 g of water per gram of the original silicate.

**Formation of hydroxychloride does not influence the analytical results, as it decomposes at 50° into $CaCl_2$, $Ca(OH)_2$ and H_2O [3].

SUMMARY

Structure formation in concentrated suspensions of tricalcium and β-dicalcium silicates is much more rapid if calcium chloride solutions ($c \leq 3.2$ N) are used for mixing than in water. This acceleration is not connected with chemical reactions of calcium chloride with the silicate minerals; it is caused by accelerated hydration of anhydrous calcium silicates in presence of the added electrolyte.

LITERATURE CITED

1. Yu. M. Butt, Manual of Cement Technology [in Russian] (Moscow, 1953) p. 320.
2. Yu. M. Butt, Trans. Sci. Res. Cement Institute [in Russian] (1949), No. 2, p. 29.
3. I. I. Vol'nov, Izvest. Sekt. Fiz.-Khim. Analiza Akad. Nauk SSSR, 27, 251 (1956).
4. S. Z. Makarov and I. I. Vol'nov, Izvest. Sekt. Fiz.-Khim. Analiza Akad. Nauk SSSR 25, 320 (1954).

CURRENT EVENTS

THE 25TH ANNIVERSARY OF THE LABORATORY OF SURFACE PHENOMENA OF THE INSTITUTE OF PHYSICAL CHEMISTRY, ACADEMY OF SCIENCES, USSR

N. N. Zakhavaeva

Translated from Kolloidnyi Zhurnal, Vol. 22, No. 4, pp. 506-511, July-August, 1960

March 1960 was the twenty-fifth anniversary of the founding of the Laboratory of Surface Phenomena of the Institute of Physical Chemistry, Academy of Sciences USSR. The founder and permanent head of the laboratory is Corresponding Member, Acad. Sci. USSR, B. V. Deryagin. At first this was a small laboratory with only four scientists on the staff. The present staff of the laboratory numbers over forty.

The initial scope of the laboratory (1935-1941) included problems concerned with the studies of special properties of multimolecular liquid layers and with the influence of these layers on interaction between solid surfaces. The disjoining action and other thermodynamic properties of thin liquid layers were discovered and studied experimentally (M. M. Kusakov, L. S. Lebedeva, and A. S. Titievskaya). Special mechanical properties of thin liquid layers were also studied; in particular, variations of viscosity with distance from the solid wall. Important work was done on the mechanism of friction and its relationship to adhesion forces in relation to the theory of friction developed by B. V. Deryagin in 1934; the mechanism of oiliness of lubricant layers of limiting thickness during friction was studied (V. P. Lazarev M. M. Kusakov, and N.N. Zakhavaeva). At the same time B. V. Deryagin was conducting a number of theoretical investigations; a theory of particle interaction in presence of electric double layers and of the stability of lyophobic colloids was worked out (this has been widely accepted and applied), and also a theory of capillary condensation and other capillary effects, with the disjoining action of multimolecular liquid films taken into account.

During the Second World War the scope of the laboratory was widened in accordance with wartime requirements; lubricants, aerosols, etc., were investigated.

After the war special attention was devoted to surface phenomena and forces, and their role in the kinetics of heterogeneous systems, the adhesion problem, and aerosols. The problem of direct measurement of molecular attraction as a function of distance between surfaces was brilliantly solved by the use of a reverse-linkage balance. (I. I. Abrikosova and B. V. Deryagin). The Lomonosov Prize of the Academy of Sciences, USSR, was awarded for this work in 1958.

To provide a new approach to problems of colloid stability and coagulation, a technique was developed for observing the adhesion of crossed filaments (A. D. Malkina and M. F. Futran), in the clean state and coated with polymer films. Investigations were started on the activation force barrier in adhesion of metal surfaces with different degrees of polarization, by means of the crossed-filament method (T. N. Voropaeva and B. N. Kabanov). Colloidal processes could be modeled by this method. The thermodynamic theory of interaction between convex particles with smooth surfaces at close distances in any medium, developed by B. V. Deryagin in 1934, provided the necessary basis for such modeling.

Work on adsorption was also carried on in the laboratory; the influence of adsorption layers on external friction was investigated. Multimolecular adsorption and condensation of vapors on glass was investigated by an optical method (G. I. Izmailova and V. V. Karasev).

Methods for investigating viscosity by the blow-off method were developed further. The concept of boundary liquid phases as a special state of aggregation was advanced and substantiated; the lubricating action of films was studied from this standpoint (V. V. Karasev and N. N. Zakhavaeva).

In 1946 a series of researches was started on the physics of porous and disperse materials; filtration and diffusion of liquids and gases in such materials were investigated, and practical applications of these processes (determination of specific surfaces of powders and porous materials, determinations of filtration coefficients of liquids) were studied. Instruments were designed (N. N. Zakhavaeva and M. V. Talaev) which have been widely adopted in industry. The prize of the Presidium of the Academy of Sciences USSR was awarded for this work in 1953. The theory of pseudomolecular gas flow in porous materials was developed and confirmed experimentally (B. V. Deryagin, S. P. Bakanov, and M. V. Talaev).

B. V. Deryagin advanced and verified experimentally the electrical theory of adhesion, and discovered and investigated the emission of electrons when high-polymer films are detached from glass, metal, and other surfaces in high vacua, and when crystalline materials are split (N. A. Krotova and V. V. Karasev). A method was developed for determining the velocities of emitted electrons from their penetration through obstacles of different thicknesses and from their deflection in a magnetic field. The influence of the external medium on adhesion was studied; it was found that adhesion phenomena conform to the laws of gaseous discharge (N. A. Krotova and I. N. Aleinikova). It was shown that the adhesion of certain polymers diminishes to zero in the region of charge reversal when contact between the joined surfaces is disturbed (L. P. Morozova and N. A. Krotova). The prize of the Presidium of the Academy of Sciences USSR was awarded for the work on adhesion in 1957.

The aerosols group of the laboratory studied elementary effects in clouds and mists; the work of this group included elucidation of the causes of noncoalescence of liquid drops on contact (P. S. Prokhorov and L. F. Leonov), the influence of moisture deficiency on the effectiveness of collision between water droplets, and on the coagulation rate in an aqueous mist in an ascending current of air in a pipe (for simulation of natural processes).

I. S. Artemov studied the influence of aerosol coagulation rate in presence of extraneous vapors, and of an electric field, on coagulation. The flow ultramicroscope for counting particles of aerosols and other disperse bodies was developed and widely adopted (G. Ya. Vlasenko).

Development work was carried out on new methods of acting on warm clouds by adsorptive modification of atmospheric condensation nuclei or by introduction of new and more active nuclei (B. V. Deryagin, P. S. Prokhorov, G. I. Izmailova, and L. F. Leonov).

Theoretical researches in the aerosol field are being developed on the basis of analysis of acting surface forces (the theory of diffusiophoresis and thermophoresis) (S. S. Dukhin and S. P. Bakanov).

Members of the laboratory have taken part in numerous conferences and discussions and have published more than 600 papers; many candidates' and doctors' dissertations have emanated from the laboratory.

Thus, in a period of 25 years the small laboratory concerned with studies of the properties of thin multimolecular liquid layers has grown into a research section where the various investigations cover a wide range of surface phenomena.

On the occasion of the laboratory jubilee a series of measures were taken in order to summarize the activities of the laboratory during the last 25 years. A jubilee exhibition was organized, where instruments, demonstrations, books, reprints of papers, etc., were shown. A scientific conference was held; members of the laboratory took active part in this and presented 17 papers. In addition, 11 papers were given by members of other institutions (from Moscow, Leningrad, Kiev, Tula, Irkutsk, etc.), either associated with the work of the laboratory or interested in its subject field. The conference program included papers from various branches of the science of surface phenomena.

The following subjects were considered at the conference meetings: 1) general aspects of surface forces; 2) polymer adhesion; 3) surface forces in thin liquid layers; 4) surface phenomena in disperse systems; 5) surface forces in aerosols.

The conference was opened by V. I. Spitsyn, Director of the Institute of Physical Chemistry, Academy of Sciences USSR; in his opening address he summarized the activity of the laboratory of surface phenomena during the 25 years of its existence.

In his introductory paper, the head of the Laboratory of Surface Phenomena, B. V. Deryagin, described the development of researches in the field of molecular and electrical surface forces and their influence on the properties of heterogeneous (including colloidal and aerodisperse) systems. Researches on the theory of disjoining pressure and its applications to studies of colloid stability and heterocoagulation and flotation effects were summarized.

Nonequilibrium surface forces, in particular those of diffusional origin, in electrolyte solutions and in gases were also discussed. The role of surface forces in the kinetics of important physicochemical heterogeneous processes was stressed.

M. M. Kusakov and L. I. Mekenitskaya reported on an experimental study of the state of bound water in the form of thin wetting layers in petroleum and gas collectors. It was found that, when thin layers of aqueous electrolyte solutions or oil-field waters are formed at air interfaces in glass or quartz capillaries, equilibrium thin wetting layers may exist; the thickness of such a layer depends on temperature, valence and concentration of the salts in solution, and the capillary radius.

The thin water layers formed between the solid phase and oil may be either equilibrium or nonequilibrium in character. The nature of the solid phase, interfacial tension between water and oil, and surface-active substances all exert an influence. Investigations showed that if the oil-filled waters are highly mineralized and the oils are of low activity then the continuous film in the gas-bearing and oil-bearing strata is held by a capillary mechanism. If the water is weakly mineralized and the tension at its interface with oil is very low, then bound water in the porous medium is present both in film form and in the capillary-held state.

L. M. Shcherbakov discussed the general theory of capillary effects of the second kind, which arise when one, two, or three dimensions of the phase are small. In the first case interpretation of capillary effects of the second kind must be based on considerations of disjoining pressure and other thermodynamic functions of thin layers.

In the third case, capillary effects of the second kind must form the basis of an exact theory of the origin of new phases; the speaker presented certain new results based on this theory.

S. S. Dukhin described investigations of surface forces arising in deformation of electrolyte solution—gas or solution—liquid interfaces as the result of diffusion streams which restore adsorption equilibrium. The influence of these forces on adherence of mineral particles to bubbles in flotation was demonstrated.

Six papers were presented in the section on polymer adhesion. N. A. Krotova and L. P. Morozova reported on a study of the nature of adhesive bonding of polymers with the aid of the luminescence method. Different systems were found to differ sharply in accordance with the chemical structure of their components. Systems formed from nonpolar polymers of similar structure form very diffuse interfaces as the result of diffusion of polymer chain segments from one volume into the other. Systems with components differing sharply in chemical structure (polar and nonpolar), one of which contains characteristic polar groups, form sharp interfaces, and electrical effects are observed when they are separated.

The same authors presented a paper on the application of infrared spectroscopy in studies of the nature of the adhesion bond between polymers and glass. When a monomer is adsorbed from the gas phase on dry glass and subsequently polymerized, the resultant spectra indicate that hydrogen bonds are formed between the hydroxyl groups of the glass and carboxyl groups of methacrylic acid. If the monomer in the liquid phase remains in prolonged contact with glass, deeper chemical changes take place which lead to disappearance of the hydroxyl groups in the glass.

V. P. Smilga presented the theory of formation of an electric double layer as the result of donor-acceptor bonding when two polymers (or two dielectrics) come into contact. The effect of temperature on this reaction was studied. The conditions for formation of double layers of maximum thickness at the interface were investigated. It was shown that in some instances the double layer formed can give rise to adhesion forces of the order of tens of kilograms per square centimeter.

I. N. Aleinikova reported on measurements of the true density of the electric double layer at the metal-polymer interface. The relationship between the apparent surface charge density and the polymer film thickness was determined. The experiments were conducted at small thicknesses; losses of charge due to neutralization

by gaseous discharge were very small, and the measured value of the charge was at the maximum and close to the true value.

V. L. Vakula, V. E. Gul', Hei Yung-tsui, and S. S. Voyutskii investigated the influence of molecular weights of butadiene–acrylonitrile polymers differing in polarity on their adhesion to polar (polyamide) and nonpolar (polyisobutylene) substrates. It was shown that the adhesion of each of the copolymers studied decreases with increase of the molecular weight of the fraction, up to a certain limit (300,000-350,000), beyond which it remains almost constant. It was shown that adhesion of butadiene–acrylonitrile copolymer fractions to a nonpolar substrate is independent of the polarity and molecular weight of the fractions and of the contact temperature. The results were discussed inthe light of the diffusional theory of adhesion.

M. S. Metsik reported on the results of investigations on the role of surface forces in the mechanical and electrical properties of mica crystals.

Six papers are given in the section on surface forces in thin liquid layers.

D. M. Tolstoi, R. L. Kaplan, and Lin Fu-shen presented some new experimental data on external friction. To investigate the influence of static and kinetic frictional characteristics on frictional autovibrations, they used the apparatus devised by D. M. Tolstoi, whereby oscillograms of the frictional autovibrations could be obtained or the autovibrations eliminated, and the force of kinetic friction measured as a function of uniform sliding velocity, or the force of static friction as a function of duration of static contact. Several relationships were discovered; for example, at low sliding velocities the force of kinetic friction depends not only on velocity but on the entire kinetic history of the frictional system. The radius of microcurvature of the bearing surface of a slide bar has a strong influence on steel-lead friction but does not affect steel–steel friction.

D. M. Tolstoi also put forward some ideas concerning the laws of external friction. It was concluded from the experimental data of a number of authors that the velocity characteristic of friction of the first and second kind always commences with a rising region and has a maximum in the region of very low velocities; this represents the "boundary force of static friction." An analogy between the form of the rheological curve at low velocity gradients and the form of the velocity–friction curves at low sliding velocities was postulated and substantiated. This analogy is incomplete, because of the existence of a descending region in the velocity–friction curve; an explanation of this was put forward. A quantity which was hitherto disregarded in expressions of frictional force as a function of normal forces was taken into account; molecular adhesion on regions of the surfaces which are not in direct contact,but lie within the fields of mutual attraction. Introduction of this quantity makes it possible to explain the influence of microcurvature of slide bar bearings on the coefficient of friction.

In a paper entitled: "Properties of solutions of organic acids in liquid hydrocarbons on solid surfaces," G. I. Fuks showed that such solutions exert disjoining pressure, the magnitude of which depends on the nature and concentration of the acid and the properties of the solid. At the same time, the boundary layers were found to offer nonequilibrium resistance to thinning, manifested in their elasticity (under relatively rapid loading) and increased viscosity. In the case of benzoic acid and dicarboxylic acids these effects are small. They increase in the fatty acid series with the length of the hydrocarbon radical. The nature of the solvent hydrocarbons has an influence; this indicates that the solvent molecules are involved in the formation of boundary solution layers, with differing orientation with respect to the acid molecules.

It was shown that the resistance to shear in boundary lubrication by solutions of fatty acids decreases in proportion to the length of the hydrocarbon radical. If the gap between the solid surfaces in these solutions is constant, their resistance to relative shearing is independent of the molecular weight of the fatty acid. Therefore, the observed effect of the length of the hydrocarbon radical is associated with its influence on the thickness of the solution which remains.

B. V. Deryagin, N. N. Zakhavaeva, and S. V. Andreev gave an account of a method for measuring the viscosity of thin boundary liquid layers applied to solid surfaces; the method is suitable for polymeric liquids and polymer solutions. The liquid was blown off the surface by a stream of air, and the residual wedge-shaped film exhibited interference bands in reflected monochromatic light. The slope of the wedge, which is proportional to the viscosity, can be estimated from the distance between the bands. The interference pattern was photographed. The method of motion photography was also used; this has a number of advantages over still

photography of the pattern. By this method it was possible to follow the course of flow processes in the wedge-shaped film and to establish many interesting characteristics of the flow of thin polymer and monomer layers. These methods were used for studying variations of viscosity with distance from a solid surface, and showed the existence of a sharp transition from boundary to volume viscosity.

The paper by A. S. Akhmatov and Liu Chau-tsen dealt with the physical interpretation of the binomial friction law. The results of determinations of friction and adhesion of specular steel surfaces (of finite length) in presence of various lubricants showed that the results obtained by extrapolation of $s = \mu(sp_0 + N)$ curves agree, within the limits of experimental error, with the results of direct measurement of adhesion.

These authors also found the absolute values of molecular adhesion and true frictional coefficient for lubricants of various types. It was found that at relatively high pressures the boundary layer structure is changed, with an abrupt change in the value of μ.

The paper by T. N. Voropaeva, B. V. Deryagin, and B. N. Kabanov contained an account of the effect of electrolyte concentration on the magnitude of the force barrier in cohesion of platinum filaments. Relationships were found for the magnitude of the force barrier as a function of the electrolyte concentration and filament potentials in solutions of KCl, $ZnCl_2$, $MgSO_4$, H_2SO_4. In dilute electrolyte solutions the magnitude of the force barrier diminishes with increasing concentration, and it is at a minimum at the electrocapillary maximum for platinum (0.2 v). The results are fully consistent with the theory of interaction of hydrophobic convex surfaces, worked out by B. V. Deryagin for dilute electrolyte solutions. This theory was used to calculate the van der Waals constant for platinum from experimental data; the reasonable magnitude of the result once again confirmed the applicability of the theory to dilute electrolyte solutions.

In concentrated electrolyte solutions (from 0.1 N upward for univalent electrolytes, and from 0.01 N upward for bivalent electrolytes) the magnitude of the force barrier is independent of the filament potential but varies with the electrolyte concentration.

The paper by V. N. Yashin, A. V. Gorodetskaya, A. S. Titievskaya, and B. V. Deryagin contained the results of a study of the disjoining pressure of aqueous films between polarized mercury and glass.

Six papers were presented in the section on surface phenomena in disperse systems.

M. P. Volarovich and M. P. Churaev reported the results of a radioactive tracer study of moisture migration in peat. S. V. Nerpin discussed (on a quantitative basis) applications of the concepts of surface forces and disjoining pressure to mechanical and hydrological properties of soils, and demonstrated the great engineering importance of the theory and of the results obtained by the author and his associates.

Yu. M. Glazman's paper contained an account of the application of the modern physical theory of lyophobic colloid stability to the coagulant action of binary electrolyte mixtures. It was shown that the theory fully explains all the effects observed experimentally: antagonism, synergism, and superadditivity; the mechanism of these effects was discussed in relation to both strongly and weakly charged soils.

The paper by B. V. Deryagin, N. N. Zakhavaeva, and A. M. Lopatina described an investigation of the percolation of electrolyte solutions through fine powders. The filtration coefficient of the liquid was determined at the initial stages of impregnation, before the filtration rate was slowed down by the resistance of the impregnated layer. Air in advance of the impregnation front was pumped out to prevent possible capture of air bubbles between the powder particles, which could retard impregnation and give erroneous results. The results obtained experimentally with this new technique were compared with theoretical values calculated from the Carman equation. The experimental data show that: 1) increase of electrolyte concentration gradually lowers effective viscosity in filtration to its normal (volume) value; 2) the mechanical properties and filtration characteristics of soils are determined not only by the particle size but also by the composition and concentration of the substance dissolved in the water.

The paper by N. M. Kudryavtseva contained the results of a study of slow coagulation of gold hydrosols on addition of the electrolytes KCl and $BaCl_2$ in various concentrations. A variant of the flow ultramicroscope designed by B. V. Deryagin and G. Ya. Vlasenko was used for measurement of slow coagulation. The flow method of particle counting is free from the defects of Zsigmondy's classic ultramicroscopic method. A laboratory unit was constructed whereby concentrations of hydrosol particles up to about 10^{10} particles per cc could be

determined; this is sufficient for studies of sol coagulation. Curves showing variations of particle (numerical) concentration with time at various concentrations of added electrolyte were plotted; these showed sharp differences from the hyperbolic relationship which follows from the Smoluchowski coagulation theory. The role of surface forces in these differences was discussed.

Six papers were given in the section on surface forces in aerosols. The paper by B. V. Deryagin, S. P. Bakanov, S. S. Dukhin, and G. A. Batova, entitled: "Diffusiophoresis of aerosol particles" dealt with the behavior of aerosol particles in a diffusion field. A strict theory, based on the methods of the kinetic theory of gases, was worked out for aerosol particles small relatively to the mean free path of gas molecules. For larger particles the theory is based on the methods of diffusion hydrodynamics. In either case movement of the particles relatively to the Stefan flow was demonstrated. The results predicted by the theory were confirmed by experiments on capillary osmosis and also by P. S. Prokhorov and L. F. Leonov's model experiments on direct measurement of forces acting on solid spheres in a diffusion stream.

In his paper: "Influence of thermal diffusion on the behavior of aerosol particles in a heterogeneous gaseous medium" S. P. Bakanov examined theoretically the problem of the motion of a small particle in an unequally heated mixture of gases. As an example, the motion of an aerosol particle near a drop of CCl_4 in helium was considered. It was found that the particle velocity undergoes inversion; in a definite temperature range a heated drop can attract aerosol particles, while a cold drop can repel them. This effect does not occur in a one-component gas.

The paper by S. P. Bakanov and G. A. Martynov: "Gravitational coagulation of cloud droplets" contained a theoretical examination of the coagulation kinetics at the initial stage of the process. The kinetic equation for coagulation was solved by resolution into a power series of the relative change of the number of particles. It was found that the n-th term of the series represents the change of the total number of particles by coalescence of n initial particles.

A. I. Storozhilova's paper: "Differential counter of condensation nuclei" described a method, developed by the author, for producing supersaturations so that nuclei can be grown in a stream in a zone of predetermined constant supersaturation. The "developed" nuclei were counted with the aid of a flow ultramicroscope. The method can be used for determining the activity spectrum of the condensation nuclei from counts of nuclei which "develop" at various supersaturations.

The paper by L. F. Leonov, M. V. Velichko, B. V. Deryagin, and P. S. Prokhorov: "Diffusion chamber with constant volume supersaturation" contained a description of a diffusion chamber with wetted walls subjected to periodic thermal conditions. The average vapor pressure in the main volume of this chamber is higher than the saturation value at the mean temperature established in this volume; i.e., there is a constant supersaturation in the chamber volume. The chamber is designed for laboratory studies of condensational mist formation at low supersaturations. At high supersaturations it is suitable for studies of high-energy particles; it differs advantageously from the usual diffusion chambers by having uniform supersaturation in most of the chamber volume.

The main conclusion of the conference, emphasized by the participants, was that the science of surface forces is an original and a highly important branch of the science of surface phenomena considered in three dimensions.

This approach proved necessary for explanation and interpretation of the kinetics of most important heterogeneous systems, and has been widely accepted and applied both here and abroad. This field is at the stage of rapid growth and expansion.

The addresses by the conference participants lead to the conclusion that the Laboratory of Surface Phenomena has a considerable scientific influence.

The theoretical principles elaborated in the laboratory are widely applied by workers in various organizations. The techniques and original instruments developed in the laboratory are used in many scientific research institutes and other organizations. Thus, during the twenty-five years of its existence the Laboratory of Surface Phenomena has greatly assisted the development of Soviet science and helped to establish its priority in various aspects of surface phenomena.

SIGNIFICANCE OF ABBREVIATIONS MOST FREQUENTLY ENCOUNTERED IN SOVIET PERIODICALS

FIAN	Phys. Inst. Acad. Sci. USSR.
GDI	Water Power Inst.
GITI	State Sci.-Tech. Press
GITTL	State Tech. and Theor. Lit. Press
GONTI	State United Sci.-Tech. Press
Gosenergoizdat	State Power Press
Goskhimizdat	State Chem. Press
GOST	All-Union State Standard
GTTI	State Tech. and Theor. Lit. Press
IL	Foreign Lit. Press
ISN (Izd. Sov. Nauk)	Soviet Science Press
Izd. AN SSSR	Acad. Sci. USSR Press
Izd. MGU	Moscow State Univ. Press
LEIIZhT	Leningrad Power Inst. of Railroad Engineering
LET	Leningrad Elec. Engr. School
LETI	Leningrad Electrotechnical Inst.
LETIIZhT	Leningrad Electrical Engineering Research Inst. of Railroad Engr.
Mashgiz	State Sci.-Tech. Press for Machine Construction Lit.
MEP	Ministry of Electrical Industry
MES	Ministry of Electrical Power Plants
MESEP	Ministry of Electrical Power Plants and the Electrical Industry
MGU	Moscow State Univ.
MKhTI	Moscow Inst. Chem. Tech.
MOPI	Moscow Regional Pedagogical Inst.
MSP	Ministry of Industrial Construction
NII ZVUKSZAPIOI	Scientific Research Inst. of Sound Recording
NIKFI	Sci. Inst. of Modern Motion Picture Photography
ONTI	United Sci.-Tech. Press
OTI	Division of Technical Information
OTN	Div. Tech. Sci.
Stroiizdat	Construction Press
TOE	Association of Power Engineers
TsKTI	Central Research Inst. for Boilers and Turbines
TsNIEL	Central Scientific Research Elec. Engr. Lab.
TsNIEL-MES	Central Scientific Research Elec. Engr. Lab.–Ministry of Electric Power Plants
TsVTI	Central Office of Economic Information
UF	Ural Branch
VIESKh	All-Union Inst. of Rural Elec. Power Stations
VNIIM	All-Union Scientific Research Inst. of Metrology
VNIIZhDT	All-Union Scientific Research Inst. of Railroad Engineering
VTI	All-Union Thermotech. Inst.
VZEI	All-Union Power Correspondence Inst.

Note: Abbreviations not on this list and not explained in the translation have been transliterated, no further information about their significance being available to us. – Publisher.

THE SCIENTIFIC WORK OF PROFESSOR MIKHAIL PAVLOVICH VOLAROVICH (ON THE OCCASION OF HIS SIXTIETH BIRTHDAY)

The Editorial Board

Translated from Kolloidnyi Zhurnal, Vol. 22, No. 5, pp. 513-519, September-October, 1960

M. P. Volarovich graduated as a physicist in the Physicomathematical Faculty of Moscow University in 1926, and while still a student began to do scientific work in the Institute of Physics and Biophysics of the People's Commissariat of Public Health under the guidance of Academician P. P. Lazarev. His first research was concerned with sensitization of photographic plates for infrared photography by means of dye solutions. He then worked under the guidance of Corresponding Member of the Academy of Sciences USSR N. K. Shchodro in the Magnetism Laboratory of the Commission for Investigation of the Kursk Magnetic Anomaly, and studied the magnetic properties of pure magnetite in powder form by the magnetometer method with a Helmholtz double tangent compass. This work showed that iron-ore quartzites with high magnetite contents have high residual magnetism and considerable coercive force; this provided the basis for P. P. Lazarev's explanation of the large anomalies of the elements of the earth's magnetic field in the region of the Kursk magnetic anomaly.

Volarovich then started independent work on viscosity and plasticity of silicate melts and dispersions, and concentrated his attention on studies of the physicochemical properties of highly viscous liquids and disperse systems. He has been now developing this line of research for 34 years, first in the Institute of Physics and Biophysics, from 1933 in the Moscow (now the Kalinin) Peat Institute, and from 1941 to 1950 in the Institute of Machine Technology of the Academy of Sciences USSR. In his work in the Institute of Mineral Raw Materials from 1932, and subsequently in the Petrographic Institute of the Academy of Sciences USSR (1935) on the physicochemical and colloidal properties of rock melts, Volarovich became interested in geological and geophysical problems; he is now working in this field in the Institute of Geophysics of the Academy of Sciences USSR.

The work of M. P. Volarovich and his associates has been especially prolific in the following directions: 1) Investigations of the viscosity and other properties of glassy systems at high temperatures; 2) investigations of the rheological properties of disperse systems, especially with high disperse-phase concentrations; 3) research into the physical chemistry of peat; 4) studies of lubricant oils at low temperatures; 5) experimental studies in the field of high-temperature mineralogy and petrography – the molecular physical properties of fused rocks; 6) investigation of the influence of high pressure on the physical properties of rocks in relation to geophysical problems.

Between 1926 and 1935 M. P. Volarovich carried out and published a series of researches on the viscosity of glasses and binary glassy systems in the fused state at temperatures up to 1400°; he developed a special technique for this purpose and built a rotational viscosimeter with platinum cylinders and a thermostat in the form of a high-temperature furnace. The results, and in particular the simultaneous determinations of viscosities and conductivities of fused silicates, are of great interest in relation to the theory of the amorphous state of matter. Jointly with D. M. Tolstoi, he discovered maxima on the viscosity–composition isotherms of a number of glassy systems, corresponding to definite chemical compounds, in agreement with Academician N. S. Kurnakov's theory of physicochemical analysis. Volarovich showed that the sharp increase in the viscosity of silicate melts (slags, rocks, etc.) observed in a number of instances is associated with deposition of a primary



Mikhail Pavlovich Volarovich

crystalline phase, i.e., high-temperature formation of a peculiar disperse system – a suspension with anomalous viscosity and plasticity. He then used his own method for measuring the density of silicate melts at 1400°, and determined in what cases silicate systems conform to Bachinskii's viscosity law and in what cases deviations occur.

Apart from its significance for the physical chemistry of the glassy state, this work is of special practical importance in metallurgy (work carried out jointly with L. V. Zverev on the viscosity of slags) and in the glass industry. His methods for determination of viscosities at high-temperatures is widely used in the Institute of Glass and other institutes, and in a number of factory laboratories. The results of these investigations are fully described in numerous monographs and text books on the physics and physical chemistry of silicates (O. K. Botvinkin and others), on glass technology (I. I. Kitaigorodskii, etc.), including foreign publications (the monographs by Morey, Eitel, and others). Some of the data determined by M. P. Volarovich are included in the Landolt–Börnstein tables. It should be emphasized that Volarovich was the first scientist in the USSR to measure the viscosity of fused glasses and slags. He was the first to determine the viscosity of quartz glass, a number of simple glasses, rocks, and meteorites.

Since 1937 M. V. Volarovich and his co-workers (A. A. Leont'eva, L. I. Korchemkin, R. S. Fridman, and others) in the Geological Institute of the Academy of Sciences USSR have conducted extensive studies of viscosity and other properties (density, elasticity, electrical conductivity, surface tension, crystallizability, flow structures, etc.) of fused rocks, and, in particular, under high pressures. Apart from their importance in geology and petrography, these researches are of interest in geophysics. The results are included in the well-known Handbook of Physical Constants, published in 1942 by Birch, Schairer, and Spicer in the USA.

Concurrently with this work, since 1928 Volarovich undertook for the first time in the USSR systematic investigations of the rheological properties of various disperse systems – clays, peats, lubricants, printing and other inks, glues, graphite masses, food products, etc. Apart from a number of interesting and original results, the special significance of these researches lies in the fact that Volarovich stated and solved the problem of the scientific basis of the rheological characteristics of disperse systems (plasticity and viscosity), which were formerly regarded purely from an empirical standpoint and without correlation with modern experimental physics and physical and colloid chemistry. The values found by M. P. Volarovich and his associates for the rheological parameters of disperse systems form the basis of design calculations relating to processing and conveying equipment in various branches of industry. In the course of these investigations, which played an important role in the development of viscosimetry in the USSR, M. P. Volarovich developed a number of new instrument designs, theoretically substantiated and of a high degree of accuracy. Among the instruments built by Volarovich, which total more than twenty, mention must be made of several original variants of rotating-cylinder viscosimeters for disperse systems which are now being made in large numbers and are used in numerous institutes and industrial laboratories. Volarovich's rotational viscosimeters are used in many universities in practical courses on physics and on physical and colloid chemistry.

In a discussion of the results of these investigations it should be mentioned that M. P. Volarovich, jointly with his associates D. M. Tolstoi, G. B. Ravich, N. N. Kulakov, N. V. Lazovskaya, A. A. Bagrov, L. Ya. Ginsburg, V. V. Vasil'eva, M. F. Nikishina, V. P. Lobanov, and others, showed that the parameters of the Shvedov–Bingham equation of viscoplastic flow – the yield value and plastic viscosity – are applicable to many quasisolid disperse systems over considerable ranges of velocity gradients and shearing stresses. The effects of various factors on these parameters were studied: concentration of the disperse phase, degree of dispersion, temperature, added electrolytes and surface-active agents, etc. In addition to studying flow in disperse systems under steady conditions, since 1939 Volarovich and his pupils (R. A. Branopol'skaya, T. Ya. Gorazdovskii, and N. I. Malinin) have studied kinetic elastic effects (stress, relaxation, creep, etc.) in bread dough, clays, peats, and other systems with high disperse-phase concentrations. Complete rheological diagrams, or series of deformation–time curves at constant shearing stresses from the lowest values, causing only elastic deformation, to stresses corresponding to the yield value and breakdown in the continuity of the system, were plotted for substances such as peat.

Apart from his experimental investigations, since 1932 M. P. Volarovich with his associates (D. M. Tolstoi, A. M. Gutkin, P. K. Shchipanov, and A. Kh. Kim) has been systematically developing the theory of viscoplastic flow of disperse systems. It was shown that the Hencky – Il'yushin system of differential equations is a generalization, for the three-dimensional case, of the Shvedov – Bingham equation of viscoplastic flow. These equations were integrated for a number of cases of practical importance: relative rotation of coaxial cylinders, flow-

through slit and annular capillaries, axial displacement of a cylinder, plane flow of two contacting viscoplastic masses, flow along an inclined plane, relative rotation of cones with common vertex, rotation of a shaft in a bearing with a viscoplastic grease, motion between two planes forming an acute angle, compression of a bar of rectangular section for the case of two simple shears, screw motion of a cylinder, flow of a system on a rotating disk, etc. It was shown that in solution of problems of this type it must always be remembered that a viscoplastic substance under stress in flow may contain regions of both plastic and elastic deformations. In regions where only elastic irreversible deformations occur the stress does not reach the yield value. Conversely, in regions of plastic deformation the stresses exceed the yield value, and irreversible flow occurs in these regions. The elastic and plastic regions in the flow of disperse systems (greases, printing inks, peat, etc.) can be distinguished very conveniently by the x-ray transmission method which was suggested and worked out by M. P. Volarovich. Together with his pupils (N. V. Lazovskaya, S. N. Markov, and N. P. Perov), M. P. Volarovich obtained valuable results with this method, whereby it is possible to determine the deformation fields and deformation rates over the entire volume of a flowing plastic disperse mass.

The numerous researches carried out by Volarovich in rheology and microrheology are very important for colloid science. The work on microrheology is also of great interest in molecular physics. Such studies include determinations of activation energies and effective molecular weights of silica and boric anhydride in the fused state from viscosity data, determinations of the thickness of layers of the dispersion medium (liquid petrolatum) in suspensions of colloidal mica with a yield value, determinations of (true) dipole moments of fatty acids in dioxane solutions (with N. N. Stepanenko), studies of the thixotropy of lubricating oils in relation to their structure and chemical composition, x-ray studies of peats in relation to their hydration properties, x-ray investigations of rubbers milled to different extents in relation to the viscoplastic and adhesive properties of their solutions, etc.

At the start of the Second World War M. P. Volarovich began to study the low-temperature properties of lubricating oils, which are of great importance in the use of motors and other machinery in winter. At the end of 1941 he moved to Kazan' to work in the Institute of Machine Technology of the Academy of Sciences USSR, and in a short time completed extensive studies of the viscosity and plasticity of lubricants. Being a highly skilled specialist in the rheological field, in conformity with wartime requirements he quickly developed a number of methods and instruments for low-temperature investigations of oils, and carried out a large number of viscosity determinations on various lubricating oils, including oils containing high-polymer additives. The results of these investigations were published in articles by Volarovich and his pupils (V. L. Val'dman, K. I. Samarina, N. N. Agranat, T. M. Kuz'minskaya, O. V. Lazovskaya, and D. V. Zelikovich); these articles contained a variety of practical information on cold starting of engines, liquefaction of oils with gasoline and kerosene, temperature – viscosity curves of oils with various additives, thixotropy of lubricating oils, etc. He designed and built special apparatus for low-temperature studies of the motion of a piston in a cylinder and of a shaft in a bearing. The applicability of the hydrodynamic theory of lubrication to a sliding bearing at low temperatures was demonstrated for the first time. At Volarovich's suggestion the All-Union Standards Committee ratified several new standards, based on his work, on methods for testing lubricating oils: GOST 2878-45, GOST 33-46, GOST 2878-48, and GOST 1939-51.

For 27 years M. P. Volarovich has been head of the Department of Physics of the Moscow (since 1958 the Kalinin) Peat Institute; during this time he undertook and completed extensive studies of the physics and colloid chemistry of peat. It may be claimed that this field of peat science was created by the work of M. P. Volarovich and his pupils. Since 1948 the curriculum of this institute has included a special course of peat physics, given by Volarovich during the entire period. The collection entitled: New Physical Methods for Investigation of Peat (1960) summarizes the experimental work in this field. The research on peat – a natural polydisperse system of a special kind, where the particles of the disperse phase vary in size from several millimeters to fractions of a micron – has been carried out in the following four principal directions.

Particle-size distribution curves for numerous samples of peat (and also certain sapropels) were determined by means of sedimentometric methods specially developed for peat (N. V. Churaev, V. P. Tropin) and by electron microscopy. These curves are now the principal characteristics used in the technology of peat winning, processing, and drying. The work on peat rheology, noted earlier, was extensively developed in relation to peat conveying, processing, molding, drying, etc. By means of x-ray structure studies of peats, Volarovich and K. F. Gusev were able to establish a continuous series of x-ray patterns, from peat-forming plants to brown coals;

this is of great interest in relation to the genesis of solid mineral fuels. In particular, it was shown that the so-called peat bitumens and waxes are paraffins, isostructural with normal paraffinic hydrocarbons in petroleum.

In the field of peat physics the greatest interest attaches to the work of Volarovich and his co-workers (N. V. Churaev, N. I. Malinin, B. Ya. Minkov, G. I. Kuzhman, N. I. Gamayunov, F. D. Sysoeva, V. V. Chernyavskaya, Z. A. Starikova, and others) on a number of processes in peat studied by means of radioactive tracers. This work was done in the special laboratory of radioactive isotopes organized by M. P. Volarovich in the Peat Institute. The use of the sulfur-35 isotope in the form of sodium sulfate, which is not adsorbed by the solid phase of peat, made it possible to elucidate the nature of water percolation through peat, to determine the dimensions of water-conducting pores, to establish the amounts of different forms of bound water, etc. On the other hand, problems of peat mixing in machines could be solved successfully by the use of the phosphorus-32 isotope in the form of a sodium compound, which is completely adsorbed by the solid phase in peat. Equipment was also designed for determinations of density and moisture variations in peat under field conditions, both with the aid of cobalt-60 gamma radiation by scattering ("radio drill") and absorption ("radio fork") of gamma quanta, and by neutron scattering. Work carried out under field conditions directly in peat deposits is also very important. A solution of sodium sulfate with labeled sulfur was poured into specially drilled wells; it was thus possible to study the movement of soil water in the peat deposit, to determine the direction of flow, to calculate the filtration coefficient, to establish the nature of the motion of water in sediments, etc. These investigations were carried out extensively at a number of peat deposits and under various drying conditions, and led to important conclusions of great practical significance. Several aspects of the use of radioactive isotopes for the above-named purposes were studied for the first time. It should be pointed out that the results of these investigations go far beyond the scope of the peat industry; they are of great interest to agriculture (soil amelioration, etc.), pedology, hydraulic engineering, etc.

Since 1950 M. P. Volarovich has been working in the O. Yu. Shmidt Institute of Geophysics of the Academy of Sciences USSR (formerly the Geophysical Institute); together with his co-workers Z. I. Stakhovskaya, D. B. Balashov, E. I. Bayuk, I. S. Tomashevskaya, V. A. Pavlogradskii, A. T. Bondarenko, and A. I. Levykin he has carried out a series of investigations of the physical, mechanical, and electrical properties of rocks under high all-round pressures in the laboratory of high pressures which he organized. The problems studied included the effect of pressure on the velocity of elastic waves in rock specimens, determined by an ultrasonic pulse method; effect of pressure on Young's modulus, investigated by the bending method; and compressibilities of rocks at pressures up to 5000 kg/cm^2. Suitable equipment and techniques were developed for these experiments; numerous very serious difficulties had to be surmounted. The investigations showed that the elastic characteristics of rocks — which are peculiar multiphase disperse systems — vary most sharply when the pressure is raised to 1000-1500 kg/cm^2; this is due to closing of the pores and compaction of the rocks in this pressure range. The elastic characteristics alter less rapidly at higher pressures owing to the absence of the gas phase. The effect of pressure on rock strength was also studied. The results are of great interest for the physics of earthquakes, since pressures of 5000 kg/cm^2 correspond to depths of 20 km in the earth, and the sites of destructive earthquakes are at these depths. In addition, M. P. Volarovich and D. B. Balashov measured the velocity of ultrasonics in nitrogen at pressures up to 5000 kg/cm^2; this enabled them to carry out a number of calculations related to verification of the equation of state for gases at high pressures.

Volarovich has carried out a series of investigations on sudden ejection of coal and gas in mines, when many tons of coals are ejected unexpectedly in the form of fine dust. The effect of high pressure on the velocity of elastic waves in coal specimens was studied. In experiments performed jointly with É. I. Parkhomenko sudden ejection of coal was reproduced under laboratory conditions by two methods: compression of the specimens in cylinders with lateral orifices, and torsion of thin plates under unilateral pressure (Bridgman's method). It was found that coal from seams liable to sudden ejection in mines exhibits "laboratory" ejection at lower pressures. Volarovich is the compiler and editor of the Collected Papers of the Geophysical Institute of the Academy of Sciences USSR (1956) on control of sudden ejections of coal and gas. In addition, M. P. Volarovich, jointly with É. I. Parkhomenko discovered for the first time (in 1953) the existence of the piezoelectric effect in rocks containing quartz grains. This effect has now been studied both theoretically (on the basis of Academician A. V. Shubnikov's work on piezoelectric structures) and experimentally. The piezo moduli of numerous rock specimens — granites, gneisses, quartzites, etc., with structures containing quartz microcrystals — were determined under laboratory conditions by both static and dynamic methods. In 1957-1959 special expeditions organized by Volarovich established the existence of the piezoelectric effect in quartz-containing rocks under

field conditions. The results of these experiments, while of interest in the physics of earthquakes, may serve as the basis for a new method of electrical prospecting.

Volarovich has made a thorough study of the history of Russian science, and in his papers and addresses he demonstrated the role played by Russian scientists (in particular F. N. Shvedov) in the foundation of various branches of rheology. He has written an interesting biography of the founder of the hydrodynamic theory of lubrication N. P. Petrov, and at the All-Union Colloid Conference in Kiev in 1951 he read a paper entitled: "History of the development of rheological work in Russia up to 1917." In 1939, jointly with R. A. Branopol'skaya, he built for the first time in the USSR the classic instrument designed by Shvedov, the founder of the rheology of disperse systems, and investigated kinetic elastic effects in a number of colloids. Works on the history of science include biographies of scientists (Academician P. P. Lazarev, Corresponding Member of the Academy of Sciences USSR N. K. Shchodro, F. N. Shvedov, and A. I. Bachinskii) written by Volarovich, and also a collection of P. P. Lazarev's "Essays on the History of Russian Science"(1950), prepared for publication by Volarovich jointly with Academician S. I. Vavilov.

For a number of years M. P. Volarovich has been successfully coordinating the work of Soviet rheologists. At his suggestion a conference on the viscosity of liquids and colloidal solutions was held at the beginning of 1941; he took a very active part in its organization and activities. This conference was concerned with the theory of viscosity, viscosity of lubricants, colloids, and melts at high temperatures. He was the Editor-in-Chief, with the assistance of E. A. Chudakov, of three volumes of Proceedings of the Conference on Viscosity, published by the Academy of Sciences USSR. He was one of the organizers of the Conference on Low-Temperature Properties of Petroleum Products (1947) and edited the proceedings of this conference jointly with G. V. Vinogradov and A. S. Irisov. He was a member of the Organizing Committee of the Second All-Union Conference on Friction and Wear in Machines, and leader of the lubricants section; he took an active part in the organization of this conference and the publication of the four volumes of its proceedings (1947-1951). He was the chairman of a discussion conference on the structural and mechanical properties of colloidal and polymeric systems, held in the Institute of Physical Chemistry of the Academy of Sciences USSR in 1952-1953. In August,1953,he was sent by the Academy of Sciences USSR to Poland to attend a conference on the theory of elasticity, plasticity, and rheology, where he presented a paper entitled "Rheological investigations of disperse systems" (a review of USSR work), and in September,1958,he went to the Third International Congress of Rheology held in Federal Germany, when he also gave a paper on his rheological work. He was the organizer and chairman of the rheology section at the conference on the theories of elasticity and plasticity and theoretical aspects of construction mechanics, held by the Institute of Mechanics of the Academy of Sciences USSR and the Mechanics and Mathematics Faculty of the Moscow State University in December 1954, and of the rheology subsection of the All-Union Conference on Theoretical and Applied Mechanics. He has been a constant and active member of All-Union conferences on colloid chemistry and has served on the Editorial Board of Kolloidnyi Zhurnal for a number of years. He played a prominent part in compilation of the section on molecular physics in the "Physics Dictionary" (1935-1938), and wrote a number of articles for the 2nd edition of the Great Soviet Encyclopedia (1950-1956). The total number of his publications is over 200.

Volarovich is prominent in the training of highly qualified research workers and university teachers. Many of his pupils have presented doctorate and candidates' dissertations. The fruitful scientific and teaching activity of M. P. Volarovich has been rewarded by high Government awards — the Order of Lenin and the Red Star.

THE MOST IMPORTANT SCIENTIFIC PUBLICATIONS OF M. P. VOLAROVICH

Translated from Kolloidnyi Zhurnal, Vol. 22, No. 5, pp. 520-523, September-October, 1960

1. "Investigation of the viscosity of molten glass," Zhur. Priklad. Fiz. 5, 185 (1928); 6, 1 (1929).

2. "Investigation of the viscosity of the binary system $Na_2B_4O_7$–NaH_2PO_3," Zhur. Priklad. Fiz. 6, 131 (1929); J. Soc. Glass Technol. 18, 201 (1934).

3. "Investigation of the plastic properties of clay by the rotating cylinder method," Zhur. Priklad. Fiz. 9, 5 (1930).

4. "Investigation of the viscosity of the binary system $Na_2B_4O_7 - B_2O_3$ in the molten state," (with D. M. Tolstoi) Izvest. Akad. Nauk SSSR 9, 897 (1930); J. Soc. Glass Technol. 18, 209 (1934).

5. "Investigation of the thermal expansion of the binary system $Na_2B_4O_7 - B_2O_3$ at high temperatures," Izvest. Akad. Nauk SSSR 5, 663 (1933); Acta Physicochim. URSS 2, 695 (1935).

6. "Determination of the plastic-flow constants of mineral suspensions," (with D. M. Tolstoi) Zhur. Fiz. Khim. 4, 6, 815 (1933).

7. "Investigation of the viscosity of fused slags and rocks," Zhur. Fiz. Khim. 4, 6, 807 (1933); C. R. Acad. Sci. Paris 202, 78 (1936).

8. "Measurement of the viscosity of molten glass and verification of the formula of H. Le Chatelier," (with B. V. Deryagin) J. Chim. Phys. 31, 471 (1934); 32, 143 (1935) [in French].

9. "Investigation of the viscosity of molten rocks," Doklady Akad. Nauk SSSR 9, 561 (1934).

10. "Effect of electrolytes on the plasticity of kaolin," (with D. M. Tolstoi) Doklady Akad. Nauk SSSR, 9, 557 (1934).

11. "Investigations of the viscosity of titanium-containing slags," (with L. V. Zverev) Dommenoe Pr-vo., 5, 22 (1934).

12. "Applications of viscometry and plastometry to problems of applied mineralogy," Trans. Inst. Appl. Mineral. [in Russian] No. 66, 1934.

13. "Investigation of the specific volume of fused diabase at high temperatures" (with A. A. Leont'eva) Doklady Akad. Nauk SSSR 2, 533 (1935).

14. "Investigation of the plasticoviscous properties of peat" (with N. N. Kulakov and A. N. Romanskii) Izvest. Akad. Nauk SSSR, 10, 1371 (1935); Kolloid. Zhur. 3, 163 (1937).

15. "Viscosity of fused salts, glasses and slags at high temperatures," supplement to E. Hatschek's book: The Viscosity of Liquids [Russian translation] 2nd Ed., 1935.

16. "Plasticity of disperse masses," Kolloid Zhur. 2, 557 (1936); The Rheology Leaflet (Soc. of Rheol., USA) No. 5, 12, 1937.

17. "Viscosity as a method of high-temperature physicochemical analysis," Izvest. Sektora Fiz.-Khim. Analiza Akad. Nauk SSSR, 8, 1935 (1936).

18. "Effect of surface-active substances on the plastic properties of kaolin" (with D. M. Tolstoi), Kolloid. Zhur. 2, 621 (1936).

19. "Simultaneous measurement of viscosity and electrical conductivity of silicate melts at high temperatures" Zhur. Fiz. Khim. 7, 496 (1936).

20. "Investigation of the elasticity of amorphous bodies in the softening range" (with B. V. Deryagin and A. A. Leont'eva), Zhur. Fiz. Khim. 8, 479 (1936); Acta Physicochim. URSS 5, 617 (1936).

21. "Investigation of the elasticity of molten rocks" (with A. A. Leont'eva), Doklady Akad. Nauk SSSR 3, 225 (1936).

22. "Investigation of the densities of fused salts" (with A. A. Leont'eva), Doklady Akad. Nauk SSSR 2, 535 (1935); Zeits. anorg., allg. Chem. B225, 327 (1936).

23. Sur la densité des roches fondues, Compt. rend. Acad. Sci., Paris, 202, 143 (1936).

24. "Investigation of the viscosity of quartz glass in the softening range" (with A. A. Leont'eva), Zhur. Fiz. Khim. 8, 335 (1931); Journ. Soc. Glass, Techn. 20, 139 (1936).

25. "Viscosimetric and x-ray investigations of hydrogenated fats (with G. V. Ravich and K. F. Gusev), Kolloid. Zhur. 2, 787 (1931).

26. "Physicochemical investigations of silicate melts," Proc. 2nd Conf. on Exptl. Mineralogy and Petrography [in Russian] (1937) p. 109.

27. "Investigation of the viscosity of the binary system $K_2B_4O_7 - B_2O_3$ in the fused state" (with R. S. Fridman), Zhur. Fiz. Khim. 9, 177 (1937); Acta Physicochim. URSS 6, 393 (1937).

28. "The viscoplastic properties of printing inks," Trudy In-ta Poligraf. Prom. OGIZ, 5, 261 (1937).

29. "Determination of the effective molecular weights of B_2O_3 and SiO_2 in melts" (with A. A. Leont'eva), Zhur. Fiz. Khim. 10, 439 (1937); Acta Physicochim. URSS, No. 3, 357 (1937).

30. "Relation between the viscosity of fused rocks and the acidity coefficient of F. J. Levinson-Lessing" (with L. I. Korchemkin), Doklady Akad. Nauk SSSR 17, 413 (1937).

31. "Viscosity of obsidians in relation to the genesis problems" (with A. A. Leont'eva), Doklady Akad. Nauk SSSR 17, 419 (1937).

32. "External friction and adhesion of fats" (with A. E. Pukhlyanko), Kolloid. Zhur. 3, 621 (1937); 5, 89 (1939).

33. "Thickness of the layers of dispersion medium in a plastic mica suspension" (with I. S. Erokhin), Zhur. Fiz. Khim. 12, 277 (1938); Acta Physicochim. URSS 9, 89 (1938).

34. "Experimental study of flow structure in melts," Izvest. Akad. Nauk SSSR, Ser. Geol. 4, 599 (1938).

35. "Falling velocity of liquid drops in melts" (with A. A. Leont'eva) Zhur. Fiz. Khim. 13, 846 (1939); Acta Physicochim. 11, 251 (1939).

36. "Investigation of the viscosity of meterorites" (with A. A. Leont'eva), Doklady Akad. Nauk SSSR, 22, 594 (1939); Collection: Meteorites [in Russian] No. 1, 33 (1941).

37. "Calculation of activation energy and latent heat of fusion of feldspars from viscosity measurements;" Doklady Akad. Nauk SSSR 24, 393 (1939).

38. "Calculation of activation energies of fatty acids from viscosity measurements" (with G. B. Ravich), Doklady Akad. Nauk SSSR 23, 251 (1939).

39. "Experiments for investigating flow structures and filtration of rock melts," Proc. 3rd Conf. on Exptl. Mineralogy and Petrography [in Russian] (1940) p. 69.

40. "Experiments on heating rocks under pressure up to 1000 kg/cm^2," Proc. 3rd Conf. on Exptl. Mineralogy and Petrography [in Russian] (1940) p. 46.

41. "Use of high pressures in experiments in geological sciences and geophysics," Izvest. Akad. Nauk SSSR, Otdel. Khim. Nauk 6, 935 (1940).

42. "Viscosity of lubricating oils at high pressures," Izvest. Akad. Nauk SSSR,Otdel. Tekh. Nauk 3, 49 (1940); Proc. 1st Conf. on Friction and Wear [in Russian] 2, 281 (1940).

43. "Investigation of the viscosity of fused rocks," Zap. Miner. Obshch-va, 69, 310 (1940).

44. "Determination of the dipole moments of fatty acids in solutions" (with N. N. Stepanenko), Zhur. Éksp. Teoret. Fiz. 10, 317 (1940); 14, 313 (1944); Kolloid Zhur. 7, 232 (1941).

45. Investigation of the Physicomechanical Properties of Dough (with R. A. Branopol'skaya) [in Russian] (Pishchepromizdat, 1940), 6.5 pages.

46. "Investigation of melt viscosities at high temperatures," Conference on Viscosity of Liquids and Colloids [in Russian] (1941) Vol. 1, p. 249.

47. "Viscosity and crystallization of blast-furnace slags," Collected Papers on the Uses of Blast-Furnace Slags in Building [in Russian] (Stroiizdat, 1941) p. 82.

48. "Effect of pressures up to 500 kg/cm^2 on the relation between viscosity and linear crystallization rate" (with A. A. Leont'eva), Zhur. Fiz. Khim. 17, 45 (1943); Zap. Miner. Obshch. 3-4, 177 (1943).

49. Viscosity of Mineral Oils at Low Temperatures [in Russian] (Izd. AN SSSR, 1944), 10 pages.

50. "The present state of the theory of viscosity of liquids and its practical applications," Conference on Viscosity of Liquids and Colloids [in Russian] (1944) Vol. 2, p. 18.

51. "New viscosimeters for petroleum products," Conference on Viscosity of Liquids and Colloids [in Russian] (1944) p. 132; Zavodskaya Lab. 1, 49 (1945).

52. "Investigation of the velocity profile and dependence of pressure drop; flow rate of peat slurry through pipes 440, 570, and 750 mm in diameter" (with N. N. Kulakov, E. P. Semenskii, N. D. Bezzubov, and K. I. Samarina), Zhur. Tekh. Fiz. 14, 448 (1944); Kolloid. Zhur. 8, 9 (1946).

53. "Heating of obsidian under pressure in relation to the genesis of pumice," Zap. Mineral. Obshch-va 73, 50 (1944).

54. "New model of the rotational viscosimeter (RV-7)," Zavodskaya Lab. 9, 832 (1945).

55. "Low-temperature properties of lubricating oils in relation to cold starting of engines," Vestnik Akad. Nauk SSSR 10-11, 90 (1945).

56. "Method for determination of the kinematic viscosity of petroleum products," Friction and Wear in Machines [in Russian] 2, 72 (1946).

57. "Viscosity of lubricating oils at low temperatures" (with V. L. Val'dman), Friction and Wear in Machines [in Russian] 2, 80 (1946).

58. "Rheological properties of greases" (with E. P. Loshakova), Kolloid. Zhur. 8, 127 (1946).

59. "Calculation of the motion of a viscoplastic mass between two plane parallel walls and in the annular space between two coaxial tubes" (with A. M. Gutkin), Zhur. Tekh. Fiz. 16, 321 (1946).

60. "Experimental investigations in the field of rheological kinematics of disperse systems," Kolloid Zhur. 9, 325 (1947).

61. "Study of the displacement of a piston in a cylinder in relation to cold starting of an engine," Friction and Wear in Machines [in Russian] 3, 100 (1948); Proc. 2nd Conference on Friction and Wear [in Russian] (1948) Vol. 2, p. 463; Wear, 2, 203 (1959).

62. "Flatness of lubricating-oil temperature curves," Proc. 2nd Conference on Friction and Wear [in Russian] (1948) Vol. 2, p. 538.

63. "Conditions of flow of two contacting disperse masses with the properties of viscoplastic bodies" (with A. M. Gutkin), Kolloid Zhur. 10, 329 (1948).

64. "Relaxation effects in disperse systems" (with R. A. Branopol'skaya), Kolloid. Zhur. 10, 406 (1948).

65. "Application of the hydrodynamic theory of friction to sliding bearings in the low-temperature region" (with O. V. Lazovskaya) Izvest. Akad. Nauk SSSR, Otdel. Tekh. Nauk 10, 1607 (1948); Friction and Wear in Machines [in Russian] 4, 142 (1949).

66. "Low-temperature properties of lubricating oils," Collection: Low-Temperature Properties of Petroleum Products [in Russian] (Gostoptekhizdat, 1949) p. 3.

67. "Investigation of viscosities of liquids for hydraulic systems at low temperatures" (with T. N. Tikholaz and D. V. Zelikovich). Collection: Low-Temperature Properties of Petroleum Products [in Russian] (Gostoptekhizdat, 1949) p. 172.

68. "Low-temperature properties of Nigrol transmission oil with various additions," Proc. 2nd Conference on Friction and Wear [in Russian] (1949) Vol. 3, p. 266.

69. "Use of rheological methods in the food industry," Collection: Colloids in the Food Industry [in Russian] No. 2, 40 (1949).

70. "Calculation of the motion of peat with variable viscosity and yield value" (with P. K. Shchipanov), Kolloid. Zhur. 11, 384 (1949).

71. Description and Instructions for the PV-3 Ball-Fall Viscosimeter for Field Use [in Russian] (Izd. AN SSSR, 1950); 2nd Edn. 1951; Automobil, 2, 29 (1952).

72. "Viscosity of road bitumen" (with M. F. Nikishina), Kolloid. Zhur. 12, 169 (1950).

73. "Problem of the quality of lubricating oils in relation to the development of lubrication technology," Proc. 2nd Conference on Friction and Wear [in Russian] (1951) Vol. 4, p. 323.

74. "Investigation of the flow of peat in conical ducts" (with N. V. Lazovskaya), Doklady Akad. Nauk SSSR 76, 211 (1951).

75. Determination of the yield value of peat by Rebinder's cone plastometer method" (with S. N. Markov), Zavodskaya Lab. 12, 1461 (1951); Torf. Prom. 10, 23 (1951); Collection: New Physical Methods for Investigation of Peat [in Russian] (Gosénergoizdat, 1960) p. 95.

76. "Study of deformation in peat under various conditions by the x-ray transmission method," Trudy Mosk. Torf. In-ta, 2, 112 (1953).

77. "X-ray investigations of peats" (with K. F. Gusev), Trudy Mosk. Torf. In-ta, 2, 97 (1953); 5, 3 (1957); Collection: New Physical Methods for Investigation of Peat [in Russian] (Gosénergoizdat, 1960) p. 155.

78. "Investigation of the rheological properties of disperse systems," Kolloid. Zhur. 16, 227 (1954);* Archiwum Mechaniki Stosowanej (Warsaw) No. 2, 171 (1954).

79. "Investigation of the dispersity of peat suspensions by means of the sedimentometer and electron microscope" (with N. V. Churaev), Kolloid. Zhur. 16, 241 (1954);* 17, 200 (1955);* Trudy Mosk. Torf. In-ta, 3, 33 (1955); Proc. 3rd All-Union Colloid Conference [in Russian] (1956) p. 258.

80. "The piezoelectric effect in rocks" (with É. I. Parkhomenko), Doklady Akad. Nauk SSSR 119, 239 (1954); Izvest. Akad. Nauk SSSR Ser. Geofiz. 3, 215 (1955); Assoc. Seismol. et phys. de la terre (Toulouse) (1959) p. 289.

81. "Some problems in the theory of flow of a viscoplastic medium" (with A. M. Gutkin), Izvest. Akad. Nauk SSSR, Otdel. Tekh. Nauk 9, 37 (1955).

82. "Effect of high pressures on the molecular structure of coals" (with V. I. Kasatochkin and L. L. Razumova), Doklady Akad. Nauk SSSR 103, 1033 (1955).

83. "Investigation of the effects of high pressures up to 1000 kg/cm^2 on the velocity of elastic waves in coal specimens" (with D. B. Balashov), Trudy Geofiz. In-ta Akad. Nauk SSSR, 34, 164 (1956).

*Original Russian pagination. See C. B. translation.

84. "Investigation of sudden ejection of coal by compression of cylindrical specimens in steel cylinders with lateral orifices" (with É. I. Parkhomenko), Trudy Geofiz. In-ta Akad. Nauk SSSR 34, 179 (1956).

85. "Simulation of sudden ejection of coal by unilateral compression of thin disks with simultaneous torsion" (with É. I. Parkhomenko), Trudy Geofiz. In-ta Akad. Nauk SSSR 34, 193 (1956).

86. "Viscosity structure and adhesive properties of glue solutions" (with L. Ya. Ginzburg and K. F. Gusev), Proc. 3rd All-Union Colloid Conference [in Russian] (1956) p. 155.

87. "Plastic deformations and failure under shear in torsion of thin rock specimens under unilateral pressures up to 40000 kg/cm^2 (with É. I. Parkhomenko), Izvest. Akad. Nauk SSSR Ser. Geofiz. 2, 85 (1957).

88. "Calculation of yield values of disperse systems in measurements with the cone plastometer" (with N. N. Agranat), Kolloid. Zhur. 19, 3 (1957).*

89. "Propagation velocities of elastic waves in rock specimens under all-round pressures up to 5000 kg/cm^2" (with D. B. Balashov), Izvest. Akad. Nauk SSSR Ser. Geofiz. 3 (1957).

90. "Viscosity of liquids," International Conference on the Thermodynamic Properties of Fluids (London] [Russian translation] (Gosénergizdat, Moscow, 1957).

91. "Effect of temperature on the dynamic elasticity modules of rocks" (with A. S. Gurvich), Izvest. Akad. Nauk SSSR, Ser. Geofiz. 4, 417 (1957).

92. "Physicomechanical properties of rocks under various pressures," Summaries of Papers at the Tectophysics Conference of the Geophysics Institute of the Academy of Sciences USSR, 1957 [in Russian] (Gosgeolizdat, 1960) p. 5; Freiberger Forschungshefte, Geophysik, C 81, 231 (1960).

93. "Investigation of the dispersity of sapropels by means of the sedimentometer and electron microscope" (with V. P. Tropin), Kolloid. Zhur. 20, 1 (1958).

94. "Determination of Young's modulus of rock specimens under all-round pressures up to 5000 kg/cm^2 by the bending method" (with Z. I. Stakhovskaya), Izvest. Akad. Nauk SSSR Ser. Geofiz. 5 (1958).

95. "Investigation of the elastic properties of rocks at high pressures up to 5000 kg/cm^2" (with D. B. Balashov and Z. I. Stakhovskaya), Proc. 5th Conference on Experimental Mineralogy and Petrography [in Russian] (1958) p. 203; Assoc. Seismol et phys. de la terre (Toulouse) (1959) p. 277.

96. "Research Work of the Physics Department of the Moscow Peat Institute on the physics of peat," Trudy Mosk. Torf. In-ta, Jubilee Issue on the 40th Anniversary of the Great October Socialist Revolution [in Russian] 8, 115 (1958).

97. "Rheological properties of peats of low moisture contents" (with N. I. Malinin), Kolloid. Zhur. 20, 3 (1958).*

98. "Investigation under field conditions of the piezoelectric effect in rocks in a massif" (with É. I. Parkhomenko and G. N. Sobolev), Doklady Akad. Nauk SSSR 128, 3 (1959).*

99. "X-ray structural analysis of the interaction between paper and binders in printing inks" (with V. T. Ivanova, E. M. Afanas'eva, and K. F. Gusev), Kolloid. Zhur. 21, 544 (1959).*

100. "Velocity of ultrasonic waves in nitrogen at pressures up to 1050 kg/cm^2" (with D. B. Balashov), Applications of Ultrasonics to Investigations of Matter [in Russian] No. 8, 83 (1959).

101. "Compressibility of volcanic rocks at pressures up to 5000 kg/cm^2" (with D. B. Balashov and V. A. Pavlogradskii), Izvest. Akad. Nauk SSSR, Ser. Geofiz. 5, 693 (1959).

102. "Plane problem of the motion of a viscoplastic disperse system between two planes forming an acute angle" (with A. Kh. Kim), Kolloid. Zhur. 22, 2 (1960).*

103. "Electrokinetic properties of peat" (with G. Ya. Voronkov), Kolloid. Zhur. 22, 301 (1960).*

104. "Extinction of elastic waves in rock specimens" (with A. I. Levykin and V. P. Sizov), Izvest. Akad. Nauk SSSR, Ser. Geofiz. 5 (1960).

* Original Russian pagination. See C. B. translation.

105. "Electrical resistance of rock specimens at pressures up to 1000 kg/cm^2" (with A. T. Bondarenko), Izvest. Akad. Nauk SSSR, Ser. Geofiz. 6 (1960).

106. Investigation of the Properties of Peat and of Processes in it by Means of Radioactive Isotopes (with N. V. Churaev) [in Russian] (Izd. AN SSSR, 1960).*

* Other publications by M. P. Volarovich and his co-workers, concerned with radioactive tracer studies of peat, are cited in the next article by M. P. Volarovich in this issue.

RADIOISOTOPE STUDIES OF PROCESSES IN AND PROPERTIES OF PEAT

M. P. Volarovich

Kalinin Peat Institute
Translated from Kolloidnyi Zhurnal, Vol. 22, No. 5, pp. 524-534,
September-October, 1960
Original article submitted July 19, 1960

Research on peat was begun in the early years of soviet power in connection with plans for developing the peat industry. Lenin [1, 2] directed that intensive work should be devoted to mechanization. Much detailed information was required in order to develop new mechanized processes of preparing peat for fuel, chemical, and agricultural purposes, in order to design new machines, in order to modernize old processes, and so on. There has been an intensive study of the colloidal behavior of peat during the last four decades [3-5] in which many institutes have participated. Peat research has been a subject largely neglected abroad; there are very few foreign papers on the properties of peat.

Peat forms a typical polydisperse system containing humus and plant remains; the particles vary greatly in size (from millimeters to microns), and the spread in size is increased by cutting, drying,etc.; the humidity, structure, and related properties are also affected by those processes. Naturally enough, classical methods of examining polydisperse systems were the first to be used [3, 6], namely sedimentometry, rheological methods, measurements of free and bound water, x-ray analysis, and (more recently) electron microscopy.

Peat resembles other polydisperse systems in that the processes in it are very complicated; the above methods were not able to provide the required information in some cases. Radioisotopes have been used on this account to investigate processes and properties not susceptible of analysis by means of the older methods [7, 8]. This work was begun in the physics department of the Moscow (now Kalinin) Peat Institute in 1956; a special laboratory was set up [3, 9, 10].

The main lines of work [11] in this laboratory have been laboratory studies of the structure and hydration of peat, and of the transport of heat and water in peat, and also field studies of the movements of water in peat bogs drained in various ways; further, a study has been made of the detailed movements of the peat in peat-working machines, and nuclear radiations have been used to measure the density and water content. Some special methods have been developed in order to deal with the great variety of problems encountered.

A special filtration plant [12-14] has been made for use in hydration and filtration studies, the isotope used as tracer for the water being S-35 (a soft-β-emitter) in the form of sodium sulfate. This compound is adsorbed to a negligible extent (2-3%) by the solid. Diffusion also was unimportant at the flow rates used in the experiments. The natural radioactivity of peat is slight [15], so suitable corrections can be made. A sample of peat having the native structure was cut and was inserted in a Plexiglas tube; it was then soaked with distilled water. The radioactive water (0.005 to 0.01 μc/ml) was run in up to a fixed mark above the peat; the level was kept constant. The filtrate was collected and was run into tubes at known times. The tubes were held in a rotating holder. Samples of the filtrate were evaporated to dryness on metal holders, which were tested for activity with a T-25-BFL end-window counter coupled to an ordinary B-2 radiometer. The activity curve was found to rise to a limiting value (the activity of the original water); curves of this kind were analyzed to derive the quantity of water as a function of rate of motion and as a function of pore size. The rate of

displacement of the original free water by the tracer water gave an indication of the amount of fixed water, i.e., of the amount of water not participating in exchange with slow flows.

Secondly, the amount of bound water was measured by means of negative adsorption or in terms of the volume unavailable for solution [16-19]. The weakest forms of binding are detected when the concentration of tracer is very small. Here again it was found convenient to use S-35 sodium sulfate. Concentrations as low as 10^{-10}% were used in order to avoid the errors that occur when comparatively large amounts of sucrose or electrolytes are used for the same purpose. The degree of hydration has been measured as a function of the dispersion (degree of decomposition) for various fractions of peat; these parameters have been found to vary during dispersion and compression processes [20-25]. Other methods that have been used to measure the bound water have been Dumanskii's (negative adsorption of sugar), Pokrovskii's (freezing), and Kurnakov's (vapor pressure) [26]. These experiments gave estimates of the various classes of bound water as classified in Dumanskii and Rebinder's scheme for the bound forms of water in disperse systems.

The results were that the total water capacity of a peat from the upper layers (i.e., Fuscum or 20% decomposed weathered top peat) is 1600-1700%, of which 400-600% is fixed water. The difference, 1100-1200%, represents the capillary water. The 400-600% consists of bound water (here 300-400%) and of structural water in the micropores (100-200%). The bound water itself consists mainly of intracellular (immobilized) water (250-350%), the physically and chemically bound water being only about 50%. There is little chemically bound water, most of the last quantity being physically bound. The layers of such water are about 30 molecules thick. The intracellular water is prominent, especially in undecomposed peat; it is trapped within the undecomposed cells of the plant remains. Dispersion (processing) and compression eliminate much of this water, because the cells are ruptured, but part of it is transformed to physically bound water on account of the increase in the specific surface.

We used only a crude model having straight circular capillaries in our early [12-14] calculations of size distributions for water-bearing pores. More recent results [18-22] have been used in conjunction with Deryagin's theories to derive more interesting structural parameters. We can calculate the specific kinetic surface, for example, from the Karman formula in terms of the active porosity. These two parameters together give the hydraulic radius of the capillaries. The active porosity varied only from 0.3 to 0.7 in the peats used, whereas the kinetic specific surface varied from 3 to 30 m^2/g; the hydraulic radius varied from 1.25 to 0.15 μ. The kinetic specific surface is much larger than the specific surface found from dispersion analysis (0.3-3 cm^2/g), because no allowance is made in the latter case for internal porosity and for the irregular and reentrant shapes of the particles. Radioautography has proved of value in this connection.

We need to know the laws governing heat and water transport in order to perform certain technical calculations on peat. These transport effects are very complex and little is known about them. We need methods of measuring the transport parameters, especially as functions of water content, particle size, etc. Radioisotope methods have enabled us to solve some of these transport problems and have added much to our knowledge of the processes [4, 11, 27-35].*

Several distinct methods have been devised. In one of them, peat is mixed with a solution of S-35 sodium sulphate and then placed in a demountable insulating cylinder 3-5 cm long and 5 cm in diameter. One end is closed by a brass plate, which is heated by an infrared lamp. The other end is closed by paraffin wax, which represents a semiinfinite medium. The heat supplied by the lamp causes the water to take up a new distribution within the cylinder. After a measured time the specimen is removed and is cut up into slices 0.5 cm thick, each of which is assayed for water content and activity.

The water is found to be distributed in the same way as the activity when the heating time is short (40-50 min). The water is transferred as a liquid in this case. The water tends to migrate to the hot end, where it begins to evaporate. The effects of this process become apparent when the heating lasts a day or so; much of the activity is found at the hot end (on account of evaporation), whereas much of the water is at the other end. The two distributions can be used to calculate the amounts of water evaporated and condensed at any point. Other radioisotope methods may be used to follow the flow of liquid directly; that flow may be towards the hot end (thermoosmosis, capillary motion) or towards the cold end (thermocapillary motion), according to Deryagin. These types of motion can be detected by using thin (3-5 mm) layers of peat containing the tracer (sodium sulfate); alternatively, plastic grids wetted with the solution can be used. Probe methods [34] have been used in conjunction with this technique to show that the water flows mainly in liquid form when the heat flux is small.

*See the paper by Volarovich, Churaev, and Gamayunov in this issue.

Larger fluxes caused the transfer to occur as steam, at least near the hot areas; the subsequent motion follows the direction of flow of the heat. The water flows in liquid form to the heated area in the latter case.

A thermostatic drying oven has been used in studies of isothermal drying, in which air of a fixed humidity was passed through the oven [33]. A sphere of peat 1-1.5 cm in diameter and treated with S-35 sodium sulfate solution is suspended from a hook at the top of the oven. Shadowgraphs are used to measure the changes in volume during drying; an end-window counter records the specific activity of the surface. The soft β-rays from S-35 are absorbed within a short distance in the peat, so only a layer about 0.1 mm thick can affect the counter. The dissolved salt is left behind as the free water evaporates from the surface, but the activity does not change as the water within the pores evaporates. The method thus enables us to distinguish between evaporation of free (tagged) water and of bound (inactive) water. In particular, the arrival of a concentrated solution of the tracer at the surface towards the end of the drying is (Deryagin and Nerpin) to be explained in terms of initial evaporation within the specimen followed by film transport down the humidity gradient. It appears from these experiments that it is possible to determine the bound water, since the results agree well with those obtained from other methods. These studies are closely related to other studies of the hydration and structure of peat. The use of a tracer for the free water makes it possible to study capillary rise in unbroken peat, flow paths during drying in stacks, redistribution effects in trimmings, etc.

These laboratory results have been utilized in field studies of the movements of ground water in turbaries [3, 7, 12, 14, 20, 18, 36-44]. There is currently a great deal of interest in means of draining peat bogs and marshy soils; the best solution can be chosen in any particular case only on the basis of results from studies of the flow patterns produced by natural and artificial means. The problems are extremely complicated. Radioisotopes have enabled us to elucidate the movements of ground water, to measure flow rates and filtration coefficients, and to solve many important problems.

We have experimented on peat beds drained by pipe drains or by open ditches; a hole 10-15 cm in diameter is bored in the middle of such a bed, with five or six similar holes in a ring around it. The S-35 sulfate was placed in the central hole, and the water in each hole was sampled at intervals throughout the day. The samples were assayed in the field laboratory. The results were worked up in three ways which gave concordant results. The first method was based on the fall in the activity remaining in the central hole; the logarithm of the relative activity is a linear function of time. The slope of the line gives the flow at the hole and the mean filtration factor for the ground in its natural state. Calculations and tests showed that diffusion is important only when the filtration rate is less than 0.001 m/day; the actual rate usually lies between 0.05 and 1 m/day. The second method was based on the activity appearing in the other holes; these results give the direction and the maximum and minimum rates of the flow.

The third method was based on samples of peat taken from various depths at a variety of distances from the central hole at certain times (5-20 days) after the start. Measurements on these samples (e.g., by means of a portable meter) gave a complete picture of the movements of the water from the hole. Other isotopes that can be used in this case are I-131 and Br-82 as compounds with sodium [41, 44]. The observations become much simpler in this case, because the peat need not be sampled; the penetrating gamma rays emitted by these isotopes can be detected directly from the surface. For this purpose we used a probe consisting of a duralumin tube containing an STS γ-ray counter. The probe is pushed into the peat and is coupled to a field ratemeter. The flow patterns are extremely variable, since they depend on the structure of the deposit and on the method of drainage. Very often the water moves in a thin saturated layer located above the water table in the peat, which is very finely divided at that level. In some cases we have detected two such layers. Rainwater usually moves vertically. Finally, flow rates in drains and the effective areas of channels may be measured by means of radioisotopes [45]. All of these methods gave similar values for the flow rates, filtration factors, etc.

Very little is known about the mixing processes in machines for processing, pressing, and chopping peat. We have used radioisotopes to study these processes [46, 47]. We have shown above that S-35 sodium sulfate is not adsorbed by peat, and we have used it repeatedly in studies of hydration and so on. The movements of peat itself are best studied by means of P-32 used as compounds that are adsorbed almost completely. For this purpose we have used peat balls weighing 10-30 g suitably treated with the isotope. These balls are introduced into the machine. The degree of mixing is established by recording the distribution of activity in the processed peat emerging from the machine; for this purpose we have used ordinary counting methods and radioautography. The two methods gave consistent results. A measure of the effectiveness of mixing is the length corresponding to half the area under the curve (the total length of the pattern is difficult to measure). That length, divided by the radius of the ball, minus unity, may be taken as an index to the process; but this index alone is insufficient,

for we may need to know the evenness of the mixing. For the latter purpose we may use the ratio of the length containing 90% of the activity to twice the length containing 45%; the ratio is one if the mixing is ideal, but is larger than one if it is not. Some machines were found to give good mixing and to distribute the activity over a large volume of peat, but with the activity unevenly distributed in length and width. The converse situation also occurred. The best machines are those that perform well in both tests, of course.

It is necessary to be able to measure the density and humidity of peat simply and quickly. We have produced methods and apparatus [12, 48-55] for the purpose, in which we used the γ -rays from cobalt-60 (and other isotopes) as well as neutrons. The best method of measuring the density is by means of γ -ray scattering. The energy and paths of the γ -rays are altered by collisions with electrons, whose number is proportional to the density of the material, so the scattering γ -ray intensity is proportional to the density. The instrument we designed has been called a radioprobe. It consists of a duralumin tube containing a source (1.5 μc of cobalt-60) at one end; at the other end, behind a lead screen that cuts out the direct radiation, there is an STS γ -ray counter coupled to a portable radiometer. The counting rate increases rapidly with the density of the peat, but only for densities not exceeding 1 g/cm^2. Again, we have found that the count rate as a function of density has a maximum at a certain density (the same is true for materials other than peat) on account of multiple scattering. The falling branch of the curve slopes gently, whereas the rising branch is steep between 0 and 1. The density of peat varies from 0.3 to 1, so we use the rising branch, which gives the most accurate readings. Trials under actual working conditions have shown that the readings are made rapidly and reliably. Several of these instruments are now in use at peat works.

The humidity may be measured in terms of γ -ray absorption. An instrument we have designed for the purpose has come to be called a radiofork; it consists of two duralumin tubes 4-5 m long placed 20-80 cm apart. The lower end of one tube contains a source (10-15 μc of cobalt-60) enclosed in a lead shield having a small hole. The other tube contains an STS counter coupled to a portable radiometer. The two prongs are inserted together into the peat to a suitable depth. The γ -ray intensity is recorded; the fork may be left in position throughout the season to record the variations in water content if a sample is taken at the start to establish the variation of water content with depth. Another instrument for the same purpose uses a γ -ray flux directed at an angle to the horizontal. This instrument is used to assess the total water content of the upper layers of the peat, and to follow any changes associated with evaporation, precipitation, etc.

It is more difficult to measure the humidity directly and in absolute terms, although changes may be followed easily by the above means. Neutron moderation can be used [49, 52, 54] and has been applied to soils. The moderation is most rapid in a medium containing much hydrogen, e.g., water. The slow neutron flux produced by peat exposed to a fast neutron flux may be used as a measure of the hydrogen (i.e., water) content of the peat. The hydrogen content of the solid part varies little, and appropriate corrections can be applied. We have made a neutron radioprobe for this purpose. A duralumin tube contains a polonium-beryllium source producing about 10^6 neutrons per sec; the tube also contains an STS-1 (or STS-6) counter behind a lead shield; the counter is surrounded by 1 mm of cadmium foil. Thermal neutrons are captured by the cadmium (foil enriched in cadmium-113 is best), which emits γ -rays; the STS counter records these. The probe is calibrated by reference to samples of peat having known water contents; then it may be inserted into a peat bed to measure the humidity. Tests have shown that the instrument is satisfactory. The density and humidity can be measured simultaneously by placing the neutron and γ -ray sources in one probe, together with STS counters with and without cadmium foil.

The list of references shows that the results from this work have been discussed repeatedly at conferences and meetings. Several of the methods developed in the radioisotopes laboratory of the Peat Institute, and some of the results from our researches, have already been put to use in the peat industry and in other laboratories and institutes [56-58]. Some of the results were presented at the second Geneva Conference on the Peaceful Uses of Atomic Energy [59]. It is likely that some of the radioisotope methods developed for use with peat will be found of value in studies of other such systems.

LITERATURE CITED

[1] Government Decrees and Regulations, Lenin's Letters and Statements on the Peat Industry; 40 Years of the Peat Industry of the USSR, edited by A. F. Bausin [in Russian] (Gosénergoizdat, Moscow-Leningrad, 1957) p. 10.

[2] S. G. Solopov, "Lenin on peat and its uses," Trudy Kalinin. Torf. Inst. No. 9, 3 (1958).

[3] M. P. Volarovich, "Research in the physics department of the Moscow Peat Institute on the physics of peat:" Paper Read at a Conference in Honor of the 40th Anniversary of the October Revolution on October 24, 1957 in Moscow, Trudy Kalinin. Torf. Inst. No. 8, 115 (1958).

[4] M. P. Volarovich, "Recent research on the physics of peat:" Paper Read at a Conference in Kalinin Peat Institute on March 31, 1960 in Kalinin; Summaries of Papers [in Russian] (Izd. Kalinin. Torf. Inst., Moscow, 1960) p. 8.

[5] M. P. Volarovich, "History of the physics of peat:" Summaries of Papers at a Conference of Higher Educational Institutions on the History of the Physicomathematical Sciences [in Russian] (Izd. Mosk. Gos. Univ., Moscow, 1960) p. 74.

[6] N. N. Kulakov, Introduction to the Physics of Peat (edited by M. P. Volarovich) [in Russian] (Gosénergoizdat, 1947).

[7] M. P. Volarovich, "Use of radioisotopes in studies of some drying processes in peat bogs:" Paper Read at a Conference in Moscow Peat Institute on February 2, 1956 in Moscow; Summaries of Papers [in Russian] (Izd. Mosk. Torf. Inst., Moscow, 1956) p. 20.

[8] M. P. Volarovich, "Use of radioisotopes in studies of peat:" Paper Read at a Conference in Moscow Peat Institute on March 11, 1957 in Moscow [in Russian]: (Conference program, Moscow, 1957) p. 2.

[9] S. G. Solopov, "Training of engineers and technicians for the peat industry of the USSR:" 40 Years of the Peat Industry of the USSR, edited by A. F. Bausin [in Russian] (Gosénergoizdat, Moscow-Leningrad, 1957) p. 265.

[10] Moscow Peat Institute, MVO SSSR (Izd. Pavil'ona "Torf," Vses. Prom. Vystavka, Moscow, 1958).

[11] M. P. Volarovich, "The main results from the use of radioisotopes in studies of peat and the prospects for further research:" Paper at a Conference of Higher Educational Institutions on the Use of Peat in the National Economy held in Moscow on March 31, 1959; Summaries of Papers [in Russian] (Izd. Kalinin. Torf. Inst., Moscow, 1959) p. 5.

[12] M. P. Volarovich, N. V. Churaev, and B. Ya. Minkov, "Radioisotope studies of some technical parameters of peat bogs," Report of Moscow Peat Institute [in Russian] (1956).

[13] M. P. Volarovich, N. V. Churaev, and B. Ya. Minkov, "Radioisotope studies of the behavior of water in peat," Dokl. Akad. Nauk SSSR 114, No. 5, 964 (1957); Koll. Zh. 19, No. 2, 159 (1957).*

[14] M. P. Volarovich, N. V. Churaev, and B. Ya. Minkov, "Radioisotope studies of the movements of water in peat in the laboratory and in the field," Paper at the All-Union Conference on the Uses of Radioisotopes in the National Economy and in Science held on April 10, 1957 in Moscow, Transactions of the Conference [in Russian] (Gosénergoizdat, Moscow-Leningrad, 1958) vol. 4, p. 72.

[15] M. P. Volarovich, N. N. Stepanenko, and N. A. Sokolov, "Determination of the natural radioactivity of peat and lignite," Trudy Mosk. Torf. Inst. No. 5, 57 (1957).

[16] M. P. Volarovich, N. V. Churaev, and B. Ya. Minkov, "Radioisotope studies of the behavior of water in peat in the laboratory," Report of Moscow Peat Institute [in Russian] No. 11 (1957); Paper at the Conference on Methods of Work in the Physics of Soils held on April 12, 1958 in Leningrad: Conference Program [in Russian] (Izd. VASKhNIL, Leningrad, 1958) p. 3.

[17] M. P. Volarovich, F. D. Sysoeva, V. V. Chernyavskaya, and N. V. Churaev, "Negative adsorption of a radioactive tracer as means of measuring the bound-water content of peat," Koll. Zh. 20, No. 1, 122 (1958).*

[18] M. P. Volarovich, N. I. Gamayunov, N. I. Malinin, Z. A. Starikova, and N. V. Churaev, "Radioisotope studies of the structure and hydration of peat:" Paper at the Fourth All-Union Conference on Colloid Chemistry held on May 23, 1958 in Tbilisi; Summaries of Papers (Izd. Akad. Nauk SSSR, Moscow, 1958) p. 19.

*Original Russian pagination. See C. B. translation.

[19] M. P. Volarovich, N. V. Churaev, N. I. Gamayunov, Z. A. Starikova, and V. V. Chernyavskaya, "Use of trace atoms in physicochemical studies of peat:" Paper at the Conference on the Use of Isotopes in Agriculture held on April 23, 1958 in Moscow; Summaries of Papers [in Russian] (Izd. VASKhNIL, Moscow, 1958) p. 67.

[20] M. P. Volarovich, N. V. Churaev, N. I. Malinin, and A. N. Fedorov, "Radioisotope studies of the behavior of water in peat;" Report of Kalinin Peat Institute, Topic No. 11, 1958 [in Russian].

[21] M. P. Volarovich and N. V. Churaev, "Hydration and structure of peat," Koll. Zh. 21, No. 2, 159 (1959).*

[22] M. P. Volarovich, N. I. Gamayunov, Z. A. Starikova, and N. V. Churaev, "Changes in the hydration and structure of peat resulting from compression," Koll. Zh. 21, No. 3, 258 (1959).*

[23] M. P. Volarovich and N. V. Churaev, "Radioisotope studies of the hydration and structure of peat " Paper at the Section on Colloid Chemistry of the Eighth Mendeleev Meeting held on March 19, 1959 in Moscow: Program of the Meeting [in Russian] (Izd. Akad. Nauk SSSR, Moscow, 1959) p. 67.

[24] N. V. Churaev, "Radioisotope studies of the behavior of water in peat under laboratory conditions:" Paper at a Conference held at Moscow Peat Institute on February 20, 1958; Program of Conference [in Russian] (Izd. Mosk. Torf. Inst., Moscow, 1958) p. 2.

[25] N. V. Churaev, "Radioisotope methods in studies of the hydration and structure of peat:" Coll.: New Physical Methods of Studying Peat (edited by M. P. Volarovich and N. V. Churaev) [in Russian] (Gosénergoizdat, Moscow-Leningrad, 1960) p. 125.

[26] F. D. Zhitetskaya (Sysoeva), "Methods of determining bound water in peat," [in Russian] (Gosénergoizdat, Moscow-Leningrad, 1960) p. 238.

[27] M. P. Volarovich, N. V. Churaev, N. I. Gamayunov, Z. A. Starikova, and V. V. Chernyavskaya, "Radioisotope studies of the colloidal and physicochemical parameters of peat:" Report of Kalinin Peat Institute, Topic No. 11b, 1958 [in Russian].

[28] M. P. Volarovich, N. V. Churaev, N. I. Il'in, and N. I. Gamayunov, "Radioisotope studies of the colloidal and physicochemical parameters of peat and of the movements of water in peat bogs:" Report of Kalinin Peat Institute, Topic No. 11, 1959 [in Russian].

[29] N. V. Churaev, "Radioisotope studies of the hydration and structure of peat and of the movements of water in peat bogs:" Paper at the Tashkent Conference on the Peaceful Uses of Atomic Energy held on October 2, 1959; Summaries of Papers [in Russian] (Izd. Akad. Nauk Uzbek. SSR, Tashkent, 1959) p. 59.

[30] N. I. Gamayunov, "A new method of measuring heat- and mass-transfer factors," Inzh.-Fiz. Zh. 2, No. 11, 35 (1959).

[31] M. P. Volarovich and N. V. Churaev, "Radioisotope studies of the movement of water in peat:" Paper at the Conference on Surface Forces held at IMKh** AN SSSR, on April 13, 1960; Conference Program [in Russian] (Moscow, 1960) p. 3.

[32] N. V. Churaev, "Studies of the movement of eater in peat:" Paper at the Conference of Kalinin Peat Institute held on March 31, 1960 in Kalinin; Summaries of Papers [in Russian] (Izd. Kalinin. Torf. Inst., Moscow, 1960) p. 9.

[33] N. V. Churaev, "Radioisotope studies of the movement of water in peat:" Coll.: New Physical Methods of Studying Peat (edited by M. P. Volarovich and N. V. Churaev) [in Russian] (Gosénergoizdat, Moscow-Leningrad, 1960) p. 180.

[34] N. I. Gamayunov, "Probe methods of measuring heat- and mass-transfer factors": Coll.: New Physical Methods of Studying Peat (edited by M. P. Volarovich and N. V. Churaev) [in Russian] (Gosénergoizdat, Moscow-Leningrad, 1960) p. 168.

*Original Russian pagination. See C. B. translation.

**Institute of World Economics and Politics.

[35] N. I. Gamayunov, "Transfer of heat and water in a finite rod," Inzh.-Fiz. Zh. 3, No. 4, 11 (1960).

[36] M. P. Volarovich, N. V. Churaev, and N. I. Malinin, "Radioisotope studies of the movements of water in peat in the laboratory and in the field:" Report of Moscow Peat Institute, Topic No. 6b, 1957 [in Russian].

[37] M. P. Volarovich, N. V. Churaev, and B. Ya. Minkov, "Experience in radioisotope studies of the behavior of water in peat," Torf. Prom. No. 7, 26 (1957).

[38] M. P. Volarovich, "Use of radioisotopes in studying the movements of water in a peat bog:" Paper read at a conference in Moscow Peat Institute on February 20, 1958 in Moscow; Conference Program (Izd. Mosk. Torf. Inst., Moscow, 1958).

[39] M. P. Volarovich, N. V. Churaev, and N. I. Malinin, "Radioisotope studies of the movements of water in peat deposits:" Paper at the Conference on the Use of Isotopes in Agriculture held on April 23, 1958 in Moscow; Summaries of Papers [in Russian] (Izd. VASKhNIL, Moscow, 1958) p. 66.

[40] M. P. Volarovich, "Use of radioisotopes in studying the movements of water in peat workings:" Paper at a Joint Meeting on the Exploitation of Marsh and Bog Soils held on August 9, 1958 in Minsk at VASKhNIL and the Academy of Agricultural Sciences of the Beloruss.SSR; Program of Meeting [in Russian] (Izd. Akad. Sel'koz. Nauk Beloruss.SSR, Minsk, 1958) p. 10.

[41] M. P. Volarovich and N. V. Churaev, "Use of radioisotopes in studies of some drying processes in peat bogs:" Paper at a Conference of Higher Educational Institutions on the Use of Peat in the National Economy held in Moscow on March 31, 1959; Summaries of Papers [in Russian] (Izd. Kalinin. Torf. Inst., Moscow, 1959) p. 26.

[42] M. P. Volarovich, N. I. Malinin, and N. V. Churaev, "Use of radioisotopes in studying the movements of water in a peat bog:" Paper at the Hydrogeology Section, Moscow Society of Field Naturalists, in Moscow on January 22, 1959: Program of the Meetings of the Society for January 1959 [in Russian] (Izd. Mosk. Obshch. Ispyt. Prirod.); Conference on Sediments (Moscow Society of Naturalists, Moscow, January, 1959).

[43] M. P. Volarovich and N. V. Churaev, "Use of radioisotopes in studies of some drying processes in peat bogs:" Paper at the Tashkent Conference on the Peaceful Uses of Atomic Energy held on October 2, 1959; Summaries of Papers [in Russian] (Izd. Akad. Nauk Uzbek.SSR, Tashkent, 1959) p. 59.

[44] M. P. Volarovich and N. V. Churaev, "Use of radioisotopes in studying the movements of water in a peat bog:" Coll.: New Physical Methods of Studying Peat (edited by M. P. Volarovich and N. V. Churaev) [in Russian] (Gosénergoizdat, Moscow-Leningrad, 1960) p. 192.

[45] N. V. Churaev, "Use of radioisotopes in studying the working of a drainage system," Nauch. Dokl. Vyssh. Shkoly, ser. Gorn. Delo No. 1, 21 (1959).

[46] M. P. Volarovich, G. I. Kuzhman, I. F. Makov, and N. V. Churaev, "Use of radioisotopes in studying the working of peat-handling machines" Izv. Akad. Nauk SSSR, Otdel. Tekh. Nauk No. 12, 87 (1957).

[47] M. P. Volarovich, G. I. Kuzhman, N. V. Churaev, and I. F. Makov, "Use of radioisotopes in studying the working of peat in peat-processing plants," Nauch. Dokl. Vyssh. Shkoly, ser. Gorn. Delo No. 1, 275 (1958).

[48] M. P. Volarovich, N. V. Churaev, and B. Ya. Minkov, "Use of radioisotopes to measure the humidity and density of cut peat," Report of Moscow Peat Institute, Topic No. 11a, 1957 [in Russian].

[49] M. P. Volarovich, N. V. Churaev, B. Ya. Minkov, and A. A. Sysoev, "Use of radioactive materials for monitoring and automatic-control purposes in peat cutting and processing," Report of Kalinin Peat Institute, Topic No. 11a, 1958 [in Russian].

[50] M. P. Volarovich, N. V. Churaev, and B. Ya. Minkov, "Use of radioisotopes to measure the humidity and density of cut peat:" Paper at the Conference on the Use of Isotopes in Agriculture held on April 23, 1958 in Moscow; Summaries of Papers [in Russian] (Izd. VASKhNIL, Moscow, 1958) p. 73.

[51] B. Ya. Minkov, "Development of a method of using γ-rays to measure the humidity and density of cut peat:" Paper at a Conference held at Moscow Peat Institute on February 20, 1958; Program of Conference [in Russian] Izd. Mosk. Torf. Inst., Moscow, 1958) p. 3.

[52] M. P. Volarovich, N. V. Churaev, B. Ya. Minkov, A. A. Sysoev, L. G. Rode, and S. F. Shebalin, "Use of radioactive materials for monitoring and automatic-control purposes in peat cutting and processing," Report of Kalinin Peat Institute, Topic No. 11a, 1959 [in Russian].

[53] M. P. Volarovich, B. Ya. Minkov, and N. V. Churaev, "A study of the working of instruments that measure the humidity and density of cut peat," Nauch. Dokl. Vyssh. Shkoly, ser. Gorn. Delo No. 1, 75 (1959).

[54] B. Ya. Minkov, "Results from full-scale tests of radiometric instruments for weighing cut peat and development of new instruments for measuring the humidity and density of peat simultaneously:" Paper at a Conference held at Kalinin Peat Institute on March 31, 1960; Summaries of Papers [in Russian] (Izd. Kalinin. Torf. Inst., Moscow, 1960) p. 9.

[55] B. Ya. Minkov and N. V. Churaev, "Methods and instruments for measuring the humidity and density of peat simultaneously by means of γ-rays:" Coll.: New Physical Methods of Studying Peat (edited by M. P. Volarovich and N. V. Churaev) [in Russian] (Gosénergoizdat, Moscow-Leningrad, 1960) p. 203.

[56] M. P. Volarovich, B. Ya. Minkov, and N. V. Churaev, "Experience with the use of radioisotopes and nuclear radiations in the peat industry:" Paper at a Conference on the Use of Radioisotopes and Nuclear Radiations in the National Economy held on April 13, 1960 at Riga; Conference Program [in Russian] (Izd. SM Latv.SSR, Riga, 1960) p. 48.

[57] N. V. Churaev, "Use of radioisotopes in studies on peat," Information Letter No. 102 of the Technical Section of the Ministry of the Fuel Industry of the Russian Federation [in Russian] (Izd. Giprotopprom, 1957).

[58] Use of Radioisotopes in Determining the Physical Properties of Peat; Information Letter No. 446 of the Ministry of Power Stations of the USSR [in Russian] (Izd. NII Torf. Prom., Leningrad, 1958).

[59] A. V. Topchiev, I. T. Alad'ev, and P. S. Savitskii, "Use of radioisotopes in the USSR," Nauka i Zhizn' No. 12, 17 (1958).

INVESTIGATION OF HEAT AND MOISTURE CONDUCTION IN PEAT

M. P. Volarovich, N. I. Gamayunov, and N. V. Churaev

Kalinin Peat Institute

Translated from Kolloidnyi Zhurnal, Vol. 32, No. 5, pp. 535-542,
September-October, 1960
Original article submitted April 5, 1960

Processes of heat and moisture transfer constitute the physical basis of peat drying and processing technology. Calculation and control of these processes require determination of the transfer coefficients and elucidation of the mechanism of moisture transfer [1-5] in peats of different degrees of dispersion, moisture content, and structure.

The coefficients of heat and moisture transfer of different peat specimens were determined by means of constant-power probes, whereby all the transfer coefficients and the criterion of phase transition may be found from the results of a single experiment [6, 7]. At the same time, methods developed earlier [8] were used for studying the hydration properties and structural characteristics of the peat specimens. The mechanism of moisture transfer was analyzed by methods based on the use of radioactive tracers [9]. The experiments were carried out with bottom sedge peat (35% decomposition) in its original state and dispersed by repeated mechanical treatment in a meat chopper.

Table 1 contains the results of all the experiments carried out by the probe method in which all the transfer coefficients were determined, including the thermal-gradient coefficient δ and the phase-transition criteria ϵ.

The values of the transfer coefficients (Table 1) determine the processes of internal heat and mass transfer in peat, and can be used in the relevant calculations.

In Fig. 1 and 2 the principal transfer coefficients: thermal conductivity λ* (Fig. 1a), temperature conductivity a (Fig. 1b), and potential conductivity a' (Fig. 2) are plotted against the moisture content for samples of different degrees of dispersion. Results of separate experiments on the same peat, by the heat-probe method, which are not included in Table 1, were also used in the plotting of these curves. The moisture contents are given in grams per gram of solid peat phase in all cases. Points corresponding to equal experimental temperatures were chosen for the plots. The moisture-transfer potentials were determined by the methods and with the apparatus devised by Korchunov [10].

Figure 1a shows that the values of λ (curves 1-4) increase with water content at low moisture contents, reach a maximum, and then decrease. This form of relationship is associated with the thermal-moisture conductivity effect. Curve 5 (Fig. 1a) shows variations of the coefficient of thermal conductivity λ_0 calculated from the contents of water, solid phase, and air in the samples, on the assumption that heat is transferred independently in each of these phases.** It should be noted that the values of λ_0 calculated by this method were

* The coefficients of thermal conductivity determined by the probe method are equivalent [1].

** This case corresponds to a model consisting of three parallel layers, thermally insulated from each other, each of a thickness corresponding to its volume in the sample.

TABLE 1

Coefficients of Heat and Moisture Transfer for Sedge Peat of 35% Decomposition

u, g/g	γ, g/cc	Mean values during expt.		q · 10², cal/cm² · sec	Transfer coefficients						δ · 10², degree⁻¹	ε, %
					heat			moisture				
		Φ · 10⁻⁵, erg/g	t, °C		a · 10³ cm²/sec	λ · 10³, cal/cm · sec · deg	C, cal/g · deg	a' · 10³ cm²/sec	λ' · 10⁹ g · sec/cc	C' · 10⁵ g/erg		
Original peat												
4,50	0,780	0,765	40,9	15,5	3,62	2,64	5,10	3,17	6,61	1,46	0,75	4,4
3,10	0,670	4,00	29,0	6,95	4,99	2,88	3,54	3,85	1,78	0,28	2,44	26,5
2,75	0,640	6,75	18,0	2,36	3,59	2,04	3,28	2,49	0,91	0,21	1,00	0,6
Peat passed once through chopper												
4,05	0,680	0,560	44,1	11,95	5,31	3,31	4,62	4,22	6,71	1,18	1,24	46,1
3,60	0,620	1,25	29,0	8,35	3,50	1,97	4,18	5,50	2,97	0,40	0,53	4,2
3,40	0,875	1,06	43,3	17,80	3,93	2,96	3,86	8,75	7,21	0,42	0,55	69,5
2,65	0,862	4,06	29,0	2,95	2,00	1,50	3,20	4,95	15,6	1,34	3,87	6,9
2,65	0,862	3,31	36,0	6,84	2,36	1,77	3,20	5,00	2,12	0,18	0,93	39,6
2,65	0,862	2,94	44,1	11,48	2,57	1,93	3,20	5,34	1,37	0,11	0,80	46,0
2,65	0,862	3,74	45,0	27,42	3,44	2,60	3,20	4,88	1,08	0,09	0,24	100,0
Peat passed three times through chopper												
4,50	0,780	0,367	34,2	24,0	4,06	3,02	5,19	8,75	13,9	1,12	0,56	50,0
2,50	0,600	3,97	37,7	8,66	2,82	1,47	3,03	1,46	0,36	0,14	1,97	11,0
Peat passed five times through chopper												
3,50	0,700	0,054	29,7	6,11	4,45	2,65	3,83	3,67	68,5	12,1	8,64	2,8
3,30	0,665	1,22	34,2	13,1	3,80	2,24	3,80	8,15	21,1	1,67	1,19	26,2
3,10	0,655	0,382	29,6	4,75	5,45	3,00	3,44	6,70	30,7	2,87	3,24	5,6
2,55	0,848	1,41	36,6	13,9	3,82	2,72	3,01	3,86	2,62	0,29	1,43	11,8

Symbols: u, moisture content; γ, density; Φ, heat transfer per unit probe area; a and a', coefficients of temperature and potential conductivity; λ and λ', coefficients of thermal and moisture conductivity; C and C', coefficients of specific heat capacity and specific mass capacity; δ, temperature-gradient coefficient; ε, criterion of phase transition.

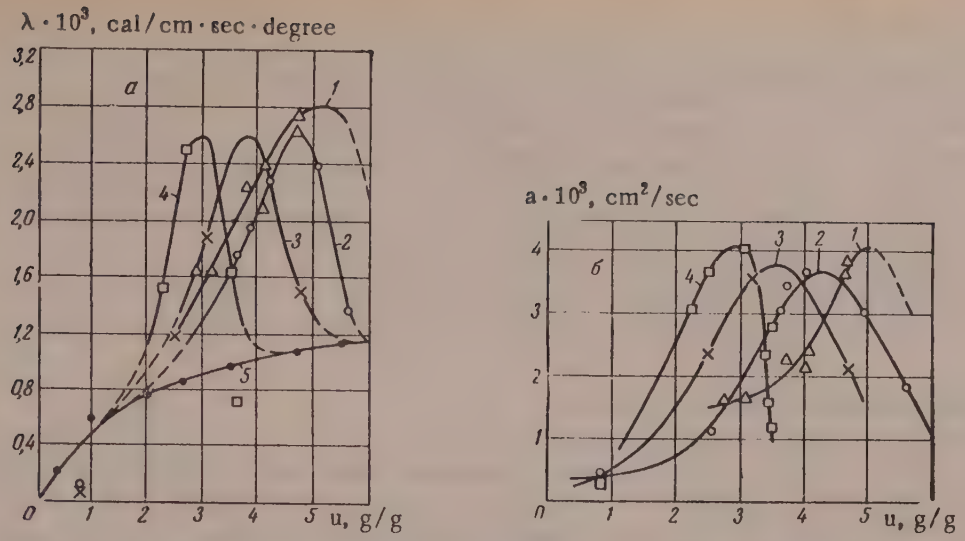


Fig. 1. Effects of moisture content and dispersity of peat on the coefficients of thermal conductivity (a) and temperature conductivity (b) (t = 20°): 1) Original peat; 2,3, and 4) peat chopped once, three times, and five times, respectively; 5) calculated values of λ_0.

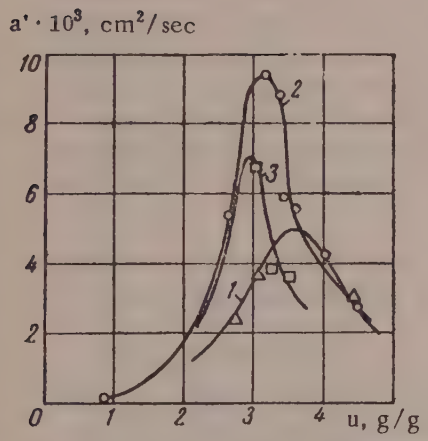


Fig. 2. Variation of the coefficient of potential conductivity (a') with the moisture content and dispersity of peat (at 35-40°): 1) Original peat; 2 and 3) peat chopped one and five times, respectively.

close to the coefficients of thermal conductivity actually found for peat under conditions such that the influence of moisture transfer was slight [11].

Deviations of the experimental values of λ (Fig. 1, curves 1-4) from λ_0 should indicate the existence of convective heat transfer by the migrating moisture. It is seen in Fig. 1 that λ begins to deviate from the calculated values at a moisture content which approximately corresponds to the content of immobile water. The amount of immobile water, determined by filtration of a radioactive tracer [8], was 3 g/g for the original peat and 2.0-2.5 g/g for dispersed peat. However, it must be borne in mind that the amount of residual immobile water (or water of low mobility) depends on the mechanism of moisture transfer in the peat, and may not coincide for pressure filtration and thermal-moisture conductivity. Therefore the above numerical data should be regarded as approximate.

The increase in the coefficient of thermal conductivity at higher moisture contents is due to additional transfer of heat by the migrating moisture. As the system approaches the two-phase state the possibility of moisture redistribution in it diminishes, and λ therefore decreases. The maximum of the coefficient of thermal conductivity in all probability corresponds to the greatest mobility of moisture in the sample. This hypothesis is confirmed by the fact that the moisture contents corresponding to the intersections of curves 1-4 with curve 5 in Fig. 1a, coincide with the moisture contents of the samples in the two-phase state. The latter values were determined by extrapolation of the moisture potential – moisture content plots to zero.

The positions of maximum λ are shifted as the result of dispersion of peat toward lower moisture contents, because of transition of part of the immobilized moisture into the capillary form as the result of dispersion [12], and decrease in the moisture capacity of the peat. The coefficients of thermal conductivity increase with rise of temperature because of intensification of the transfer processes. Maxima on the curves showing variations of the equivalent coefficients of thermal conductivity with moisture contents have been observed for certain other disperse materials [1, 2, 13].

TABLE 2

Structural Characteristics of Peat Samples Passed Once through the Chopper

Moisture content u, g/g	γ_0, g/cc	Active porosity, m	Pore sizes D, μ			Kinetic specific surface s, m^2/g
			D_{min}	D_{max}	D_{av}	
7,3*	0,10	0,46	1,3	9,8	2,6	6,0
0,40	0,44	0,46	0,08	0,55	0,26	12,2
2,80	0,316	0,43	0,02	0,16	0,06	53,1
4,0—6,0	0,20	0,48	0,05	0,30	0,10	55,0

* Original peat.

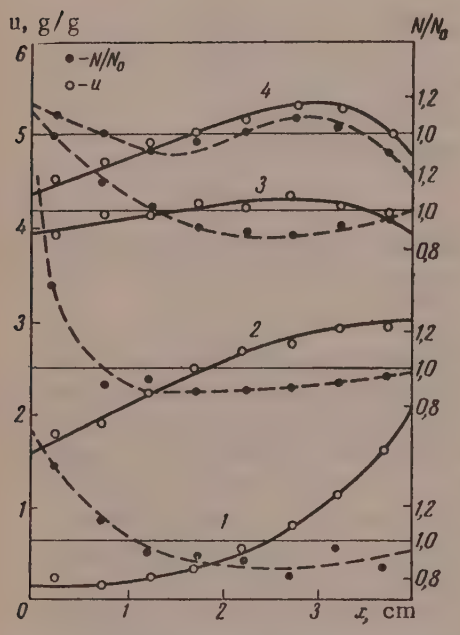


Fig. 3. Distribution of specific activity N/N_0 and moisture content u along the length x of peat samples of different moisture contents (at 50-60°), from the results of four experiments: 1) u_0 = 0.62 g/g, Δt = 5.8 degrees/cm; 2) u_0 = 2.50 g/g, Δt = 4.5 degrees/cm; 3) u_0 = 4.20 g/g, Δt = 3.3 degrees/cm; 4) u_0 = 5.00 g/g, Δt = 2.3 degrees/cm.

Moisture content has a similar influence on the coefficients of temperature conductivity (Fig. 1b), which are connected with λ by the simple relationship $a = \lambda/C\gamma_0$, where γ_0 is the mass of the solid phase per unit volume. The values of the specific heat capacity C of peat, found in probe experiments, as was to be expected, vary linearly with the moisture content, and are in good agreement with Bespalov's results [14].

Analysis of the values found for the coefficients of heat transfer show that they depend to a considerable extent on the moisture content, dispersity, and mechanism of heat and moisture transfer in peat. The connection between the coefficients of heat transfer and the hydration properties of peat is more complex than for other disperse materials, where the inflection points on the λ(u) and a(u) graphs correspond to definite types of bound water [15-19].

One of the moisture-transfer coefficients, the coefficient of potential conductivity a', is plotted against the moisture content and dispersity in Fig. 2. It is known that the variation of a' is determined by the forms of moisture binding in the material and by the mechanism of moisture transfer. The fact that the a'(u) function for colloidal substances passes through a maximum is attributable to transition from transfer of moisture in vapor form to a liquid mechanism, predominantly diffusional [1, 2, 20].

Figure 3 represents the results of four experiments with radioactive tracers, carried out in order to clarify the mechanism of moisture transfer in peats of different moisture contents. The graphs show the distribution of moisture u (continuous lines) and specific activity N/N_0 (dash lines) along the specimens in a state close to equilibrium. The horizontal lines represent the initial values ($u = u_0$ and $N/N_0 = 1$). The abscissas represent the distance along a cylindrical specimen from the heated end. The tracer was Na_2SO_4 containing the radioactive S^{35} isotope which, as was shown earlier [21], is not taken up by peat to any appreciable extent. The experiments were carried out with once-chopped peat at an average temperature of 50° in the peat specimen, and with temperature gradients of 3-5 degrees/cm.

The structure of the specimens studied is characterized by the data in Table 2, determined by filtration of a radioactive tracer [8]. The pore sizes given in Table 2 determine the equivalent diameters of the moisture-conducting pore channels.

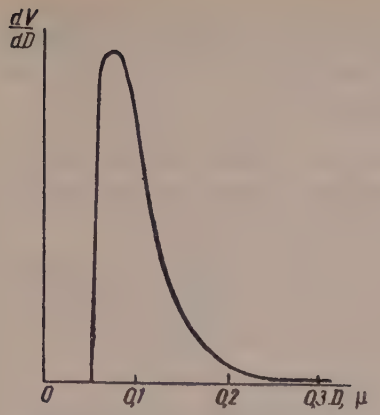


Fig. 4. Pore-size distribution in once-chopped peat (u = 4 g/g).

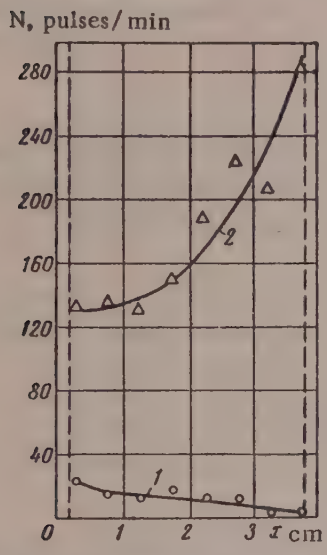


Fig. 5. Results of observations of liquid flow in two samples of dispersed peat (u = 4 g/g, t = 45°) by the tracer-atom method.

Table 2 shows that dispersion of the peat results in a sharp decrease of pore size. The size of the pore channels in dispersed peat decreases owing to swelling of the disperse phase. The active porosity m remains roughly the same for dispersed peat with various moisture contents as for the original peat, because of different concentrations of the dry substance per unit volume, γ_0, in the samples. The kinetic specific surface is considerably greater in dispersed peat than in the original material. In processed peat of low moisture content the specific surface decreases owing to aggregation of the peat particles, which leads to a corresponding increase in the size of the pore channels.

The results of structure investigations show that whereas in natural unprocessed peat the pore channels are macrocapillaries, in dispersed peat (apart from specimens of low moisture contents) most of the pores are microcapillaries. A typical curve showing the size distribution of equivalent pores in moist dispersed peat is given in Fig. 4.

We now use Fig. 3 to examine the mechanism of thermal moisture conduction in dispersed peats of various moisture contents. Comparison of the curves for distribution of specific activity and moisture content along the specimens shows that at a low moisture content (experiment 1) moisture is predominantly transferred in vapor form in the cold direction, and this is accompanied by a return flow of liquid caused by the moisture gradient which arises in the material. In this case the pores in the sample are of considerable size, so that vapor can pass without hindrance along the entire specimen.

With increase of moisture content the air-conducting channels decrease in size, but at moisture content u = 2-3 g/g (experiment 2) the effect of moisture transfer in vapor form is still large.

The character of moisture transfer changes at moisture contents above 3 g/g. The regions where condensation of moisture occurs, indicated by maximum u and minimum N/N_0, approach the heated end. This leads to partial blockage of the water-conducting pores by moisture, including the condensed water. Local overhumidification of the specimen leads to a transition from moisture transfer in vapor form to transfer in liquid form. Thus, at moisture contents above 3 g/g the role of moisture transfer in vapor form diminishes, while the role of the liquid mechanism increases. Thus, at u = 5 g/g (experiment 4) the curves for u and N/N_0 are similar in character over most of the specimen length, with the exception of layers immediately adjacent to the heated end.

At high moisture contents moisture transfer in the cold direction is effected by a thermocapillary mechanism [3], and by the pressure of air expanding in closed pores [22]. Thermoosmotic transfer of moisture in the hot direction [3], the role of which may be significant in view of the considerable interfacial area in dispersed peat, may be superposed on this motion.

The moisture content u = 3 g/g, which marks the boundary between transfer predominantly in the form of vapor and a liquid transfer mechanism, corresponds to the maximum value of a' (Fig. 2), which confirms Lykov's views [1, 2, 20]. Therefore the maximum point of the coefficient of potential conductivity corresponds to the moisture content at which the air-conducting pores become sealed by water, with a sharp decrease in gas permeability of the material. Naturally, the decrease in the size of the pore channels which occurs when the peat is subdivided leads to a decrease in the moisture content corresponding to the maximum value of a'; this is confirmed by data (Fig. 2) for specimens of different degrees of dispersion.

It should be noted that the transfer mechanism considered in relation to changes of a' applies when the peat is at fairly high temperatures, above 35-40°. Table 1 shows that at lower temperatures the phase-transition criterion ϵ is not large. At a given temperature ϵ increases with decrease of moisture content. Therefore moisture transfer in vapor form may be significant in dry peat even at lower temperatures.

To determine the dependence of the other moisture-transfer coefficients on the moisture content and dispersity of peat more experimental points must be determined for equal temperatures. The order of magnitude of the moisture-transfer coefficients for the peat samples studied is clear from the data in Table 1.

It should also be pointed out here that the values found for the coefficients of heat and moisture transfer in peat are approximate, as they depend to a considerable extent on structural homogeneity of the samples. Undetected structural defects lead to scattering of the transfer coefficients, which must be investigated in detail by statistical methods.

In experiments with moisture-insulated peat specimens (Fig. 3) when 20-30 hours had elapsed from the start of heating the so-called quasisteady state became established, accompanied by circulation of moisture within the specimen without any significant changes in moisture distribution along its length. In this case transfer of moisture in the cold direction under the influence of the temperature gradient is compensated by a return flow of moisture in the hot direction under the influence of the moisture gradient. The existence of circulating flows in the specimens is confirmed by the results of experiments which pieces of netting previously impregnated with a solution of radioactive tracer [9] were placed in the specimens.

The results of one experiment carried out by this method are plotted in Fig. 5. Capron nets impregnated with Na_2SO_4 solution containing S^{35} were put in cylindrical specimens of dispersed peat at 0.3 cm from the ends: at the hot end in the first specimen, and at the cold end in the second. At the end of the experiments, which were conducted under strictly similar conditions, the distribution of specific activity along the first (curve 1) and second (curve 2) specimen was determined.

Since the tracer could migrate in the specimens mainly in liquid streams which washed it from the netting (the effect of diffusion was negligible), the results of the experiments indicate the existence of intensive flow of water in the hot direction, and a much weaker flow in the opposite direction. Since the quasisteady state was reached in the experiments, moisture was also transferred in the cold direction in vapor form; this was not detected in the experiments with nets, but was clearly demonstrated in experiments where the whole peat was labeled (curves 3, Fig. 3). Figure 5 shows that at $u = 4$ g/g migration of water in the cold direction is effected not only by transfer in vapor form but also in liquid streams which begin to develop.

These experiments show that heat and moisture transfer in peat is a highly complex process which depends to a significant extent on the structure, hydration properties, and dispersity of the specimens and on the external experimental conditions. Thermal-moisture conduction in peat can be studied with a multiple approach by means of the methods for determination of heat and moisture transfer coefficients and for investigation of structure and transfer mechanisms.

SUMMARY

1. Coefficients of heat and moisture transfer in bottom-peat specimens differing in moisture contents and degree of dispersion were determined by probe methods.

2. The structure of the specimens and mechanism of moisture transfer in peat were investigated by means of methods based on the use of radioactive tracers.

3. The results of these investigations account for the experimental relationships between moisture content and dispersity on the one hand, and the coefficients of heat, temperature, and potential conductivity on the other.

LITERATURE CITED

[1] A. V. Lykov, Transfer in Capillary Porous Bodies [in Russian] (GITTL, 1954).

[2] A. V. Lykov, Heat and Mass Transfer in Drying Processes [in Russian] (GÉI, 1956).

[3] B. V. Deryagin, M. K. Mel'nikova, and S. V. Nerpin, Paper at the 6th International Congress of Soil Science, Physics of Soils [in Russian] (Izd. AN SSSR, 1956) p. 101.

[4] B. V. Deryagin and M. K. Mel'nikov, Collection: Problems of Agricultural Physics, edited by A. F. Ioffe and N. N. Samoilova [in Russian] (VASKhNIL, 1957) p. 30.

[5] S. V. Nerpin and B. V. Deryagin, Doklady Akad. Nauk SSSR 100, 1 (1955).

[6] N. I. Gamayunov, Inzhenerno-Fiz. Zhur. 2, 11, 35 (1959).

[7] N. I. Gamayunov, Collection: New Physical Methods for Investigation of Peat, edited by M. P. Volarovich and N. V. Churaev [in Russian] (GÉI, 1960) p. 170.

[8] M. P. Volarovich and N. V. Churaev, Kolloid. Zhur. 21, 157 (1959).*

[9] N. V. Churaev, Kolloid. Zhur. 22, 5, 631 (1960).*

[10] S. S. Korchunov, Summary of Work on the Cutting Method for Peat Winning [in Russian] (GÉI, 1959) p. 87.

[11] S. S. Korchunov, Torfyanaya Prom. 2, 23 (1948).

[12] M. P. Volarovich, N. I. Gamayunov, Z. A. Starikova, and N. V. Churaev, Kolloid. Zhur. 21, 257 (1959).*

[13] M. I. Makovozov, Inzhenerno-Fiz. Zhur. 2, 6, 96 (1959).

[14] S. G. Bespalov, Dissertation: Determination of the Specific Heat of Peat [in Russian] (Moscow Peat Institute, 1954).

[15] L. A. Lepilkina and F. M. Polonskaya, Inzhenerno-Fiz. Zhur. 1, 10, 55 (1958); 11, 46 (1958).

[16] M. F. Kazanskii and A. N. Kulandina, Inzhenerno-Fiz. Zhur. 2, 5, 88 (1959).

[17] M. F. Kazanskii, Zhur. Tekh. Fiz. 29, 2, 247 (1959).

[18] M. F. Kazanskii, A. N. Kulandina, and P. P. Lutsik, Inzhenerno-Fiz. Zhur. 3, 2, 67 (1960).

[19] A. F. Myaglichenko, Inzhenerno-Fiz. Zhur. 3, 2, 25 (1960).

[20] A. V. Lykov and F. M. Polonskaya, Trudy N.-i. Kino-Foto In-ta, 2 (25) 170 (1958).

[21] M. P. Volarovich, N. V. Churaev, and B. Ya. Minkov, Kolloid. Zhur. 19, 159 (1957).*

[22] N. A. Nasedkin and G. I. Pokrovskii, Zhur. Tekh. Fiz. 9, 16 (1939).

* Original Russian pagination. See C. B. Translation.

COMPRESSION OF A VISCOPLASTIC DISPERSE SYSTEM IN THE FORM OF A BAR OF RECTANGULAR SECTION

M. P. Volarovich and A. M. Gutkin

Kalinin Peat Institute

Translated from Kolloidnyi Zhumal, Vol. 22, No. 5, pp. 543-545,
September-October, 1960
Original article submitted April 5, 1960

The Shvedov–Bingham differential equation, which represents fairly accurately the viscoplastic properties of many disperse systems [1], has been solved for a number of special cases [1-4]. However, the compression of a viscoplastic medium in the form of a rectangular bar has not yet been considered. Nevertheless, the force required in the pressing of a viscoplastic disperse system of a particular shape is a problem of great practical importance.

Consider a viscoplastic body in the form of a rectangular bar, unlimited in the z direction. Let the height 2a of the bar be much less than its width 2b (see Figure). The rigid plates A and B compressing the medium under the force F approach each other, each with velocity U. It is assumed that the medium does not slip at the boundary with the plates. Since the width of the bar is much greater than its height, some simplifying assumptions may be introduced. The velocity v_y is considerably less than the velocity v_x everywhere apart from a small region. The velocity derivatives along the y coordinate are much greater than the velocity derivatives along the x coordinate. Therefore in this approximation the deformation rate h is $|dv_x/dy|$. The only tangential stress which is not equal to zero is τ_{xy}.

The equilibrium equation representing variations of τ_{xy} with the coordinate y is of the form

$$-\frac{\partial p}{\partial x}+\frac{\partial \tau_{xy}}{\partial y}=0. \tag{1}$$

Suppose further that $\partial p/\partial x$ varies little with the coordinate y. This follows from a consideration of the second equilibrium equation

$$-\frac{\partial p}{\partial y}+\frac{\partial \tau_{xy}}{\partial x}=0. \tag{2}$$

The second term in Eq. (2) is known to be small, because the width of the bar is much greater than its height, and hence

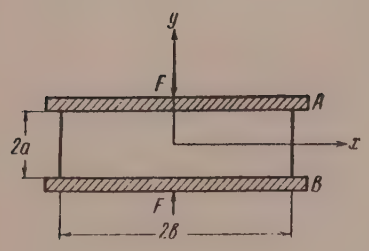
$$\frac{\partial \tau_{xy}}{\partial x} \ll \frac{\partial \tau_{xy}}{\partial y}.$$

It therefore follows that

$$\frac{\partial p}{\partial x} \gg \frac{\partial p}{\partial y} \approx 0. \tag{3}$$

Integration of Eq. (1) with respect to y gives

$$-\frac{\partial p}{\partial x} y + \tau_{xy} = C. \tag{4}$$



The integration constant C must be zero, because otherwise the absolute values of the tangential stresses corresponding to values of y equal in absolute magnitude but opposite in sign cannot be equal. If τ_{xy} is known, $\partial v_x/\partial y$ can be found. We have

$$\tau_{xy} = \frac{\partial p}{\partial x} y = \eta \frac{\partial v_x}{\partial y} + \tau_0 \frac{\partial v_x/\partial y}{\left|\partial v_x/\partial y\right|}, \tag{5}$$

where τ_0 and η represent the yield value and plastic viscosity of the disperse system. From Eq. (5) it follows that $\partial v_x/\partial y = 0$ if

$$|y| < y_0 = \frac{\tau_0}{|\partial p/\partial x|}. \tag{6}$$

Integrating the equations for the remaining range of values of y, under the condition that the velocity v_x at the boundaries of the medium becomes zero, we have

$$v_x = \frac{(y^2 - a^2)}{2\eta} \frac{\partial p}{\partial x} + \frac{\tau_0}{\eta}(y - a) \tag{7}$$

when $|y| \geq y_0$, and

$$v_x = v_0 = \frac{y_0^2 - a^2}{2\eta} \frac{dp}{dx} + \frac{\tau_0}{\eta}(y_0 - a) \tag{8}$$

when $|y| \leq y_0$, where y_0 is found by means of expression (6).

The flow rate Q of the viscoplastic medium is

$$Q = 2v_0 y_0 + 2\int_{y_0}^{a} v_x\, dy = \frac{2}{3}\frac{dp}{dx}(a^3 - y_0^3) - \frac{\tau_0}{\eta}(a^2 - y_0^2). \tag{9}$$

The very simple consideration that a definite relationship must exist between the amount of medium flowing across the section x and the velocity of the rigid plates shows that

$$Q = 2Ux. \tag{10}$$

Equating (9) and (10) and using expression (6) to find y_0, we have

$$-\frac{a^3}{3\eta} - \frac{\partial p}{x\partial}\frac{\tau_0}{2\eta}a^2 + \frac{\tau_0^3}{6\eta\left(\frac{\partial p}{\partial x}\right)^2} = Ux. \tag{11}$$

Equation (11) is a cubic equation in the unknown quantity $\partial p/\partial x$. We solve it first for the case when it is simplest, namely, when the third term in the left-hand side may be disregarded. This simplification does not invalidate the equation if

$$\tau_0 \ll \sqrt{3}a\frac{\partial p}{\partial x}. \tag{12}$$

It then follows from Eq. (11) that

$$\frac{\partial p}{\partial x} = -\frac{3\eta U x}{a^3} - \frac{3}{2}\frac{\tau_0}{a}. \tag{13}$$

We then have from Eq. (13):

$$p = C - \frac{3\eta U x^2}{2a^3} - \frac{3}{2}\frac{\tau_0 x}{a}. \tag{14}$$

The value of C can be found if the pressure in any cross section of the specimen is known. Suppose that in the section x = b the pressure is zero; then

$$p = \frac{3U\eta}{2a^3}(b^2 - x^2) + \frac{3}{2}\frac{\tau_0}{a}(b - x). \tag{15}$$

We now calculate the magnitude of the force F required to compress the bar with velocity U:

$$F = \int_{-b}^{+b} p\,dx = 2U\eta\frac{b^3}{a^3} + \frac{3}{2}\tau_0\frac{b^2}{a}. \tag{16}$$

Formula (16) cannot be used for calculating the minimum force necessary to produce flow in the viscoplastic disperse system. The whole derivation of Formula (14) is invalidated when U $\rightarrow$ 0. Formula (16) can be used only if the first term in the right-hand side is greater than the second.

SUMMARY

1. Velocity and pressure distribution has been calculated for a specimen of a viscoplastic disperse system in the form of a rectangular bar compressed between two rigid plates, in absence of slip.

2. The force with which the rigid plates must be compressed in order that they should approach each other at a given velocity has been calculated for cases when this velocity is not too low.

LITERATURE CITED

[1] M. P. Volarovich, Kolloid. Zhur. 16, 3, 227 (1954).*

[2] M. P. Volarovich and A. M. Gutkin, Zhur. Tekh. Fiz. 16, 3, 321 (1946).

[3] A. M. Gutkin, Proceedings of 2nd All-Union Conference on Friction and Wear [in Russian] (1947), vol. 1, p. 31; Kolloid. Zhur. 17, 6, 421 (1955);* 19, 1, 31 (1957).*

[4] A. Kh. Mirkhadzhanzade, Hydrodynamics of Viscoplastic and Viscous Liquids in Relation to Oil Production [in Russian] (Baku, 1959).

* Original Russian pagination. See C. B. Translation.

STUDIES OF PEAT HUMIN SOLS

1. STRUCTURAL AND MECHANICAL PROPERTIES AND THE INFLUENCE OF ADDITIVES ON THEM

M. P. Volarovich, I. I. Lishtvan, and N. V. Churaev

Kalinin Peat Institute
Translated from Kolloidnyi Zhumal, Vol. 22, No. 5, pp. 546-552,
September-October, 1960
Original article submitted June 9, 1960

Utilization of peat as fuel and a chemical source and improvements in peat technology require detailed studies of structure formation processes, which determine the properties of the product to a considerable extent. Up to the present the structural and mechanical properties of peat have been regulated mainly by dispersion of the peat with the aid of various mechanisms. This results in breakdown of the coarse particles, consisting of plant residues, increase of the content of particles of colloidal dimensions, and equalization of the structural properties in the peat volume as the result of mixing. However, mechanical dispersion does not produce any significant changes in the colloidochemical properties of peat, which depend on its natural characteristics.

Rebinder and his co-workers [1, 2] have shown that processes of structure formation can be regulated; in particular, for production of building materials of predetermined properties. These problems have also been studied in relation to other disperse systems and polymer solutions [3]. The use of colloidochemical methods for changing the properties of peat as required for practical purposes is a matter of interest. Since the main constituents of peat which determine the properties of the colloidal fraction are humin substances (humic acids and their salts [4-7]), it was first necessary to study their structural and mechanical properties, and the influence of various additives on these properties.

Humin substances were isolated from raw peat (medium peat of degree of decomposition R = 25%) by treatment with 0.1 N NaOH [7], followed by precipitation with HCl and washing with water until the start of peptization. When the humin paste was diluted with water a humin sol was obtained; this was used for the investigation. The concentration of the original sol was varied from 2.52 to 0.252% (in terms of the dry substance) by dilution with distilled water. The structural and mechanical properties were varied by addition of aqueous 0.1-5 N solutions of $CaCl_2$, HCl, or NaOH in the proportion of 1ml of solution to 10 ml of sol; to each sample of sol without additives 1 ml of water was added. The rheological characteristics were studied in capillary viscosimeters with manostats under isothermal conditions.

The rheological $1/t = f(P)$ curves plotted for sols of various concentrations with additions of $CaCl_2$ and NaOH (Fig. 1) are S-shaped, which is characteristic of quasiliquid hydrophilic systems [1, 2]. This justifies characterization of the rheological properties of humin sols in terms of the viscosity of the virtually intact structure η_0, the viscosity of the structure at maximum breakdown η_m, the nominal limit of the virtually intact structure P'_r, the nominal limit of the structure at maximum breakdown P'_m, the dynamic yield value Θ, and the minimum plastic (Bingham) viscosity η_{pl} [8]. Values of these characteristics for humin sols of various concentrations, both original and modified by additives, are given in the table.

The table shows that increase of the disperse-phase concentration increases all the rheological parameters associated with development of coagulation structures. The presence of structural bonds even at low concentrations of the disperse phase (0.2-0.3%) indicates that the particles are anisometric and elongated.

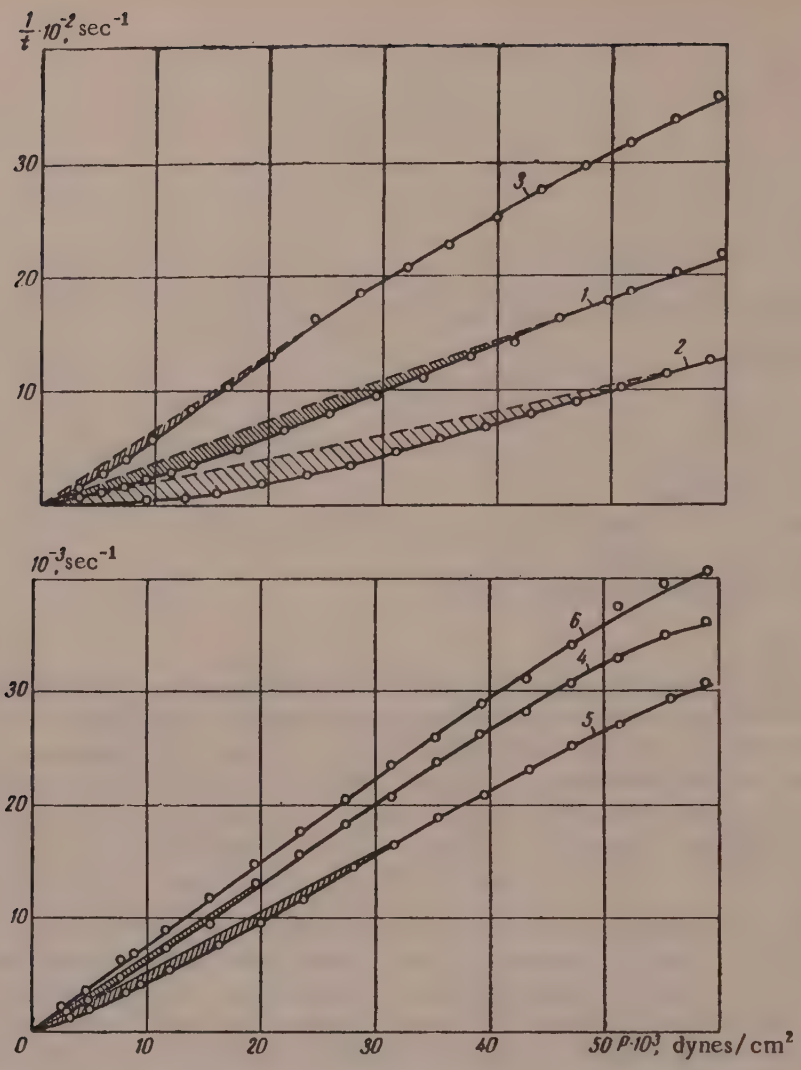


Fig. 1. Rheological $1/t = f(P)$ curves for humin sols. 1) Original humin sol, c = 2.29%; 2) same, with addition of 0.25 N $CaCl_2$; 3) same, with addition of 0.25 N NaOH; 4) original humin sol, c = = 0.57%; 5) same, with addition of 5 N $CaCl_2$; 6) same, with addition of 5 N NaOH.

Calculation of the ratio f = b/a (ratio of the largest to the smallest dimension of the particle) from the Einstein equation and the Simha formula [9] shows that f = 20 for the diluted sol with added NaOH, and somewhat greater for the original sol. The results are close to the values given by Dragunov [6], who considered that the molecule of humic acid (sodium humate) is about 35 × 2 A in size, which corresponds to f = 17.5.

From the point of view of colloid chemistry humins can be classified with the hydrophilic semicolloidal systems [1, 7, 10]. Variations of the disperse-phase concentration shift the gel ⇌sol ⇌true solution equilibrium in one direction or the other; this accounts for changes in the rheological properties of these systems. However, because of the considerable size of the macromolecules and the disperse-phase particles, equilibrium is not established immediately after introduction of additives or change of concentration. Because of this, the viscosimetric determinations were performed immediately after preparation of the suspensions so as to make the results comparable.

Interaction between the hydrophilic disperse-phase particles leads to formation of typical coagulational thixotropic structures. The greater the dispersity of the system, i.e., the greater the shift of the dynamic

Variations of Rheological Characteristics with Concentration of the Humin Sol and Concentrations of the Added Electrolyte Solutions

Concentration of added electrolyte	Contents of disperse phase in solution, %					
	Θ, dynes/cm^2	$P'_r \cdot 10^3$, dynes/cm^2	$P'_m \cdot 10^3$, dynes/cm^2	η_{pl}, poises	η_0, poises	η_m, poises
			2,29			
No addition	13,65	6,3	46	0,0355	0,0764	0,040
$CaCl_2$ 0,1 *N*	29,3	6,88	50,1	0,0375	0,1005	0,0437
0,25 *N*	42,7	7,36	53,7	0,054	0,2625	0,0727
0,5 *N*	37,5	7,82	57	0,040	0,2940	0,053
1 *N*	38,3	8,0	58,5	0,0346	0,332	0,051
5 *N*	41,2	8,35	61	0,0385	0,408	0,0505
NaOH 0,1 *N*	9,87	4,65	34	0,0334	0,0605	0,036
0,25 *N*	4,6	3,27	23,8	0,0205	0,0318	0,0229
0,5 *N*	4,92	3,27	23,8	0,0198	0,0314	0,0211
1 *N*	3,04	2,41	17,6	0,0184	0,0297	0,0194
5 *N*	1,59	2,18	15,9	0,0182	0,0248	0,0192
HCl 0,25 *N*	26,9	6,56	48,2	0,0375	0,0995	0,045
5 *N*	37,2	8,24	59,9	0,0435	0,346	0,054
			1,72			
No addition	6,03	4,42	32,4	0,0276	0,0501	0,03
$CaCl_2$ 0,1 *N*	14,3	5,11	37,2	0,0295	0,0825	0,0334
0,25 *N*	18,65	5,74	41,3	0,0313	0,1048	0,0375
0,5 *N*	22,0	5,90	43,3	0,0321	0,123	0,0388
1 *N*	17,9	5,40	39,3	0,0278	0,0986	0,0328
5 *N*	24,8	6,47	47,2	0,038	0,1570	0,0458
NaOH 0,1 *N*	4,92	3,57	26,2	0,0232	0,0372	0,0257
0,25 *N*	2,52	2,79	20,4	0,0173	0,0237	0,018
0,5 *N*	1,59	1,71	12,5	0,0173	0,0232	0,0178
1 *N*	1,74	2,02	14,75	0,0177	0,0248	0,0188
5 *N*	1,46	2,02	14,75	0,0168	0,0220	0,0174
HCl 0,25 *N*	17,7	6,05	44,2	0,0302	0,1000	0,0345
5 *N*	22,6	5,30	46,1	0,0312	0,1305	0,0377
			0,57			
No addition	2,33	1,47	10,7	0,0133	0,0182	0,0141
$CaCl_2$ 0,1 *N*	2,79	1,53	11,1	0,0135	0,0195	0,0148
0,25 *N*	3,14	1,59	11,6	0,0142	0,0210	0,0156
0,5 *N*	3,49	1,64	12,0	0,0145	0,0232	0,0161
1 *N*	3,72	1,7	12,4	0,0147	0,0242	0,0169
5 *N*	4,07	1,76	12,85	0,0158	0,0260	0,0177
NaOH 0,1 *N*	1,47	1,14	8,3	0,0122	0,0149	0,0126
0,25 *N*	1,11	1,01	7,3	0,0120	0,0145	0,0125
0,5 *N*	0,83	0,87	6,3	0,0119	0,0135	0,0122
1 *N*	0,621	0,67	4,9	0,0118	0,0129	0,0120
5 *N*	0,276	0,54	3,92	0,0118	0,0125	0,0120
HCl 0,25 *N*	3,02	1,7	12,45	0,0158	0,0245	0,0178
5 *N*	4,42	2,0	14,9	0,0168	0,0284	0,0190
			0,23			
No addition	1,04	0,736	5,47	0,0118	0,0142	0,0119
$CaCl_2$ 0,1 *N*	1,16	0,793	5,78	0,0119	0,016	0,0121
0,25 *N*	1,28	0,853	6,23	0,0121	0,0172	0,0125
0,5 *N*	1,405	0,91	6,64	0,0122	0,0185	0,0126
1 *N*	1,51	0,962	7,05	0,0123	0,0195	0,0127
5 *N*	1,62	1,02	7,43	0,0123	0,0205	0,0129
NaOH 0,1 *N*	0,41	0,47	3,42	0,0117	0,0128	0,0117
0,25 *N*	0	0	0	—	—	0,0117
0,5 *N*	0	0	0	—	—	0,0117
1 *N*	0	0	0	—	—	0,0117
5 *N*	0	0	0	—	—	0,0117
HCl 0,25 *N*	1,275	0,853	6,23	0,0121	0,0172	0,0125
5 *N*	1,39	0,9	6,65	0,0122	0,0183	0,0126

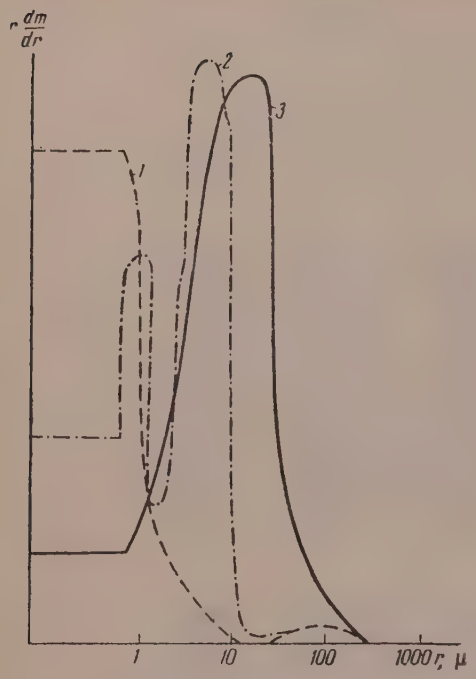


Fig. 2. Particle-size distribution curves for the original humin sol (1) and for the same sol with additions of 0.1 N (2) and 0.25 N (3) $CaCl_2$ (calculated for 1.89% sol concentration). Suspension concentration in sedimentometer 0.025%.

equilibrium to the right, the more rapid the restoration of the rheological parameters. Whereas in sols with added peptizing agent the rheological properties are fully restored within 20-25 days after stirring, in the case of suspensions with added $CaCl_2$ the time is 100 days or more.

The decrease in the dispersity of the system in the latter case is confirmed by the results of sedimentometric analysis plotted in Fig. 2, and by electron-microscope studies [11, 12]. Figure 2 shows that the maximum on the particle-size distribution curve is shifted toward larger sizes. The existence of a characteristic network coagulational (gel) structure in electron micrographs of dried humin sols has been demonstrated [11].

The effects of additives on the structural and mechanical properties of humin sols are illustrated in Fig. 3.

Figure 3 shows that small amounts of additives are the most effective in altering the rheological properties. Graphs showing variations of Θ and η_m^* with concentration of the added solutions pass through maxima, which are displaced toward the coordinate origin with increase of the humin sol concentration.

This effect of added $CaCl_2$ is attributable to the fact that the sol particle surfaces become increasingly hydrophobic with increase of the Ca^{2+} content in the exchange complex of the humic acids; this leads to particle aggregation and loss of solubility. At low Ca^{2+} contents cohesion at hydrophobic regions leads to formation of stable coagulational structures which on further increase of the Ca^{2+} content pass into hydrophobic compactly coagulated aggregates of low strength [10]. The same effect is produced by added HCl, which leads to loss of solubility in the humins. The progressive decrease in the hydrophily of humin pastes in substitution of cations in the exchange complex in the sequence: Na > Ca > Fe > Al is confirmed by Volkov's investigations [13]. The conditions for formation of stable coagulational structures are naturally more favorable with increasing concentration of the disperse phase. For the same reason, at low concentrations of the disperse phase the effect of additives is slight.

Addition of NaOH leads to formation of soluble humates and a shift of the sol $\rightleftharpoons$ solution dynamic dispersional equilibrium to the right. Increase of NaOH concentration gradually lowers the structural and mechanical characteristics and even leads to total loss of structure at low concentrations of the disperse phase. The stabilization of Θ and η_m on further increase of the amount of NaOH added may be attributed to limited exchange capacity, increase of the number of particles per unit volume, and possibly to increased forces of interaction between the humate macromolecules owing to increase of the dipole moment [13]. The existence of rigid dipole moments in disperse-phase particles of native humin sols was demonstrated by G. I. Kuzhman, N. V. Churaev, and G. Ya. Voronkov by the electrooptical method with the Tolstoi apparatus [14]. However, variations of the dipole moment under the influence of additives have not been studied as yet.

These experimental results show that the greatest relative changes in the structural and mechanical properties are obtained at high concentrations of the disperse phase by the action of small amounts of electrolytes. The table shows that the rheological characteristics of humin sols may be varied within fairly wide limits by the action of additives. For example, the yield value can be varied by a factor of 25, the viscosity of the undestroyed structure by a factor of 15, and η_m and η_{pl} by a factor of 3 or 4. This provides possibilities for regulating the structure of peat and creation of conditions for production of a material of improved quality. Possibilities include partial replacement of energy-consuming mechanical dispersion by spontaneous chemical

* Of all the rheological characteristics, Θ and η_m could be determined the most accurately in these experiments.

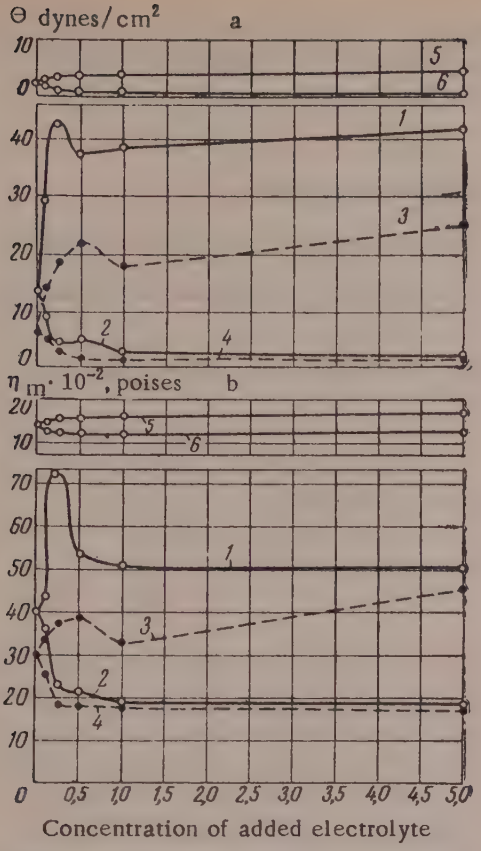


Fig. 3. Effect of concentration of added electrolyte on the yield value Θ (a) and viscosity of the structure broken down to the limit η_m (b): 1, 3, and 5) $CaCl_2$; 2, 4, and 6) NaOH; concentration of humin sol: 1 and 2) 2.29%; 3 and 4) 1.72%; 5 and 6) 0.57%.

dispersions, increase of strength, decreased crumbling, and lowered water sorption of fuel peat.

The results of our early experiments in this direction indicate that additions of sodium salts to peat increase the strength of the lump peat produced from it, while calcium salts reduce its water sorption. Kurdyumov [15] reported that the dispersity of peat was increased and its crumbling reduced by addition of Na salts.

The results therefore show that it is possible in principle to control the structural, mechanical, and colloidal properties of peat; this provides extensive possibilities for improving peat technology.

SUMMARY

1. The rheological properties of humin sols isolated from medium peat, with various concentrations of the disperse phase, were investigated by means of capillary viscosimeters.

2. The influence of added electrolytes on the structural and mechanical properties of humin sols was studied. Changes of these properties are explained in the light of the colloidochemical structure of the sols, which are semicolloidal hydrophilic systems.

3. The greatest changes in the rheological parameters are produced by the action of small amounts of electrolytes at higher concentrations of the disperse phase. Additions of $CaCl_2$ and HCl increase the rheological parameters, and NaOH reduces them. The use of small amounts of electrolytes for directed variation of the properties of peat in technological processes is recommended.

LITERATURE CITED

[1] P. A. Rebinder, Proceedings of the Third All-Union Conference on Colloid Chemistry [in Russian] (Izd. AN SSSR, Moscow, 1956); Kolloid. Zhur. 20, 527 (1958).

[2] N. N. Serb-Serbina, Proceedings of Conference on the Viscosity of Liquids and Colloidal Solutions [in Russian] (Izd. AN SSSR, Moscow-Leningrad, 1941): Kolloid. Zhur. 20, 563 (1958);* L. A. Abduragimova, P. A. Rebinder, and N. N. Serb-Serbina, Kolloid. Zhur. 17, 184 (1955);* E. E. Segalova, S. I. Kontorovich, and P. A. Rebinder, Kolloid. Zhur. 22, 74 (1960);* L. A. Abduragimova and N. G. Alekperova, Kolloid. Zhur. 20, 681 (1958).*

[3] M. P. Volarovich and D. M. Tolstoi, Doklady Akad. Nauk SSSR 1, 1 (1934); B. V. Deryagin, S. M. Levi, and V. S. Kol'tsov, Doklady Akad. Nauk SSSR 79, 2 (1951); S. S. Voyutskii, High-Polymer Solutions [in Russian] (Leningrad, 1958); S. A. Glikman, Introduction to the Physical Chemistry of High Polymers [in Russian] (Izd. Saratovskogo Un-ta, 1959).

[4] V. E. Rakovskii, General Chemical Technology of Peat [in Russian] (Gosénergoizdat, 1948).

[5] M. M. Zhuravleva and V. E. Rakovskii, Trudy In-ta Torfa Akad. Nauk Beloruss.SSR 2 (1952).

[6] S. S. Dragunov, Trudy Moskovskogo Torfyanogo In-ta, 8 (1958).

[7] A. A. Berezin and I. D. Belovilov, Trudy Moskovskogo Torfyanogo In-ta, 8 (1958).

*Original Russian pagination. See C. B. translation.

[8] N. V. Mikhailov, Kolloid. Zhur. 17, 242 (1955)*; N. V. Mikhailov and A. M. Likhtgeim, Kolloid. Zhur. 17, 364 (1955)*; A. I. Ivanov and N. V. Mikhailov, Kolloid. Zhur. 22, 176 (1960);* N. V. Mikhailov and P. A. Rebinder, Kolloid. Zhur. 17, 107 (1955).*

[9] R. Simha, J. Phys. Chem. A 44, 25 (1940).

[10] Chiang Lung, Dissertation [in Russian] (Inst. Fiz. Khim. Akad. Nauk SSSR, 1960).

[11] M. P. Volarovich, T. S. Mukhina, V. P. Tropin, and N. V. Churaev, Kolloid. Zhur. 22, 553 (1960).*

[12] N. V. Churaev, Kolloid. Zhur. 16, 220 (1954);* M. P. Volarovich and N. V. Churaev, Kolloid. Zhur. 16, 4 (1954);* 17, 3 (1955).*

[13] G. M. Volkov, Dissertation [in Russian] (IGI Akad. Nauk SSSR, 1960); Doklady Akad. Nauk Beloruss.SSR 4, 3 (1960).

[14] N. A. Tolstoi, Doklady Akad. Nauk SSSR 10, 5 (1955).

[15] S. S. Kurdyumov, Introduction to the Physics of Peat [in Russian] (Kiev, 1957).

* Original Russian pagination. See C. B. Translation.

ELECTRON MICROSCOPY OF PEAT AND ITS CONSTITUENTS

M. P. Volarovich, T. S. Mukhina, V. P. Tropin, and

N. V. Churaev

Kalinin Peat Institute

Translated from Kolloidnyi Zhurnal, Vol. 22, No. 5, pp. 553-556,
September-October, 1960
Original article submitted June 9, 1960

Because of the polydispersity of peat, three methods of dispersion analysis have to be used with this material: sieve analysis for particles larger than 250 μ, sedimentometric analysis for fractions between 250 and 1 μ, and electron microscopy for particles smaller than 1 μ [1]. The combined results of such multiple analyses can be used for plotting of complete curves for the particle-size distribution of peat [2, 4], which is the main characteristic of its physical properties. It is known that the physical, mechanical, and technological properties of peat are determined to a considerable extent by its contents of fine fractions [5, 6]. Detailed studies of the particle structure and particle-size composition are therefore necessary. The methods of electron microscopy can be used for this purpose.

The methods used for preparation of the peat specimens and analysis of the electron micrographs, and the first results obtained in investigations of peat, were published earlier [3, 7]. In this paper we present the results of statistical analysis of more than 300 electron micrographs obtained in a series of experiments with 12 peat samples, representing the main types. The size of the particles in the fine fraction was measured on a screen (at constant magnification of 50,000) with the aid of a transparent celluloid gauge marked with concentric rings corresponding to particle sizes from 3 to 0.1 μ. The shapes of the particles were noted, together with the densities of the images on the micrographs; it is known that the density is proportional to the particle thickness multiplied by the specific gravity of its constituent material. An average of 1500-2000 particles was measured for each sample.

The results of analysis of the electron micrographs of the fine peat fractions used in this series of experiments are presented in the table. The weighted mean diameter D and the specific surface $\underline{s}$ of the fine fraction (< 1 μ) were calculated for each sample; the percentage contents (K) of this fraction, determined by sedimentometric analysis [1, 2] are given. In addition, the table shows the number (N) of particles counted for each sample, and the percentage distribution of particles by shape is given.

It is clear from the table that differences in the botanical composition and degree of decomposition of peat have little effect on the dispersion characteristics of its fine fraction. This is because this fraction consists mainly of humin substances, the disperse state of which bears little relation to the botanical composition of the peat. It is determined to a much greater degree by the chemical structure of the decomposition products and by the composition of the dispersion medium. This, in particular, accounts for difference in the densities of the particle images in the micrographs. The specific surface of the fine fraction lies in the range of 5-10 m^2/g. The weighted mean particle size varies accordingly; its value lies in the 0.5-0.8 μ range. These characteristics have somewhat greater variations for upper peats. Increase of the degree of decomposition of the latter diminishes $\underline{s}$ and increases D.

Round particles are the commonest in peat (up to 75-80% of the total); of the other types of particles, elliptical particles are commonest in bottom peats, and irregular in upper peats. Intermediate peat is closer

Results of Statistical Treatment of Electron Micrographs of Peat

Peat type	Deg. of decomp. R, %	K, %	D, μ	s, m^2/g	N	Contents of particles, %			
						rounded	elliptical	elongated	irregl. shape
Upper peats									
Spruce-cotton grass	75	50,0	0,74	5,75	2270	75,2	14,0	1,6	9,2
Cotton grass-sphagnum	30	4,3	0,81	5,14	1290	83,0	8,0	0,3	8,7
Scheuchzeria-sphagnum	30	10,5	0,73	6,18	630	71,8	11,3	2,8	14,1
Sphagnum moss	20	6,9	0,78	5,75	1590	77,1	1,7	0	21,2
Fuscum	15	6,7	0,54	8,91	1200	74,1	5,1	1,6	19,2
Complex	10	2,6	0,47	9,95	900	77,3	2,1	2,5	18,1
Mean	—	—	0,68	6,95	—	76,5	7,0	1,5	15,0
Intermediate sedge-sphagnum	45	11,3	0,74	5,90	1780	77,9	5,7	0,2	16,2
Bottom peats									
Wood-reed	50	15,1	0,64	7,10	1670	75,5	6,1	1,5	16,9
Birch	40	13,3	0,74	6,36	5230	61,7	32,8	0,4	5,1
Reed	35	5,4	0,75	5,81	1910	85,9	10,7	0,1	3,3
Scheuchzeria	25	12,4	0,78	5,77	1010	68,2	28,3	0	3,5
Sedge-hypnum	15	8,0	0,78	5,57	3580	80,1	17,2	0,7	2,0
Mean	—	—	0,74	6,12	—	74,4	19,0	0,5	6,1

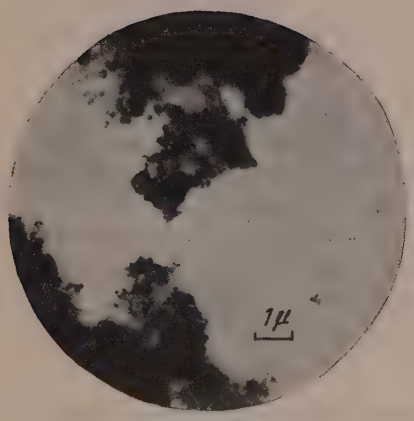


Fig. 1. Electron micrograph of peat humic acid isolated by the Institute of Peat's method.

to upper peat in its particle-size and structural characteristics. Elongated particles, generally 6-8 μ long and ~ 0.1-0.3 μ in diameter, are the least common in peat; they may differ in nature; some of them are different types of bacteria. The fact that most of the peat particles are spherical is confirmed by the results obtained with the oblique shadowing method [2]; their surface can therefore be determined with the aid of formulas for spheres. However, the value of s so found does not take into account either the internal porosity or the roughness of the particles.

The diversity of size, shape, and image density on the micrographs indicates that the particles vary in chemical nature. Investigations of individual components of the colloidal fraction of peat by electron microscopy are therefore of interest. It is known [8, 9] that a considerable proportion of this fraction consists of humic acids, which can be isolated from peat by a number of methods. In analysis of the properties of fine peat fractions mild methods of isolation, which do not cause serious structural changes in the colloidal particles, are to be preferred; these methods include the direct peptization of crude peat by NaOH [10], which is also used for purely practical purposes [11].

The electron micrographs of humic acids are shown in Figs. 1 and 2. These micrographs show that the method used for isolation of the humic acid largely determines its colloidal structure. Humic acid isolated by a less mild method* [12] is lumpy and flocculent in structure (Fig. 1). The disperse phase of humic acids isolated by mild methods (Fig. 2a,b, and c) has a characteristic network structure, the same for different peat samples. Similar network and chain formations are found fairly often in micrographs of colloidal peat fractions.

* The samples were provided by B. F. Sergeev [13].

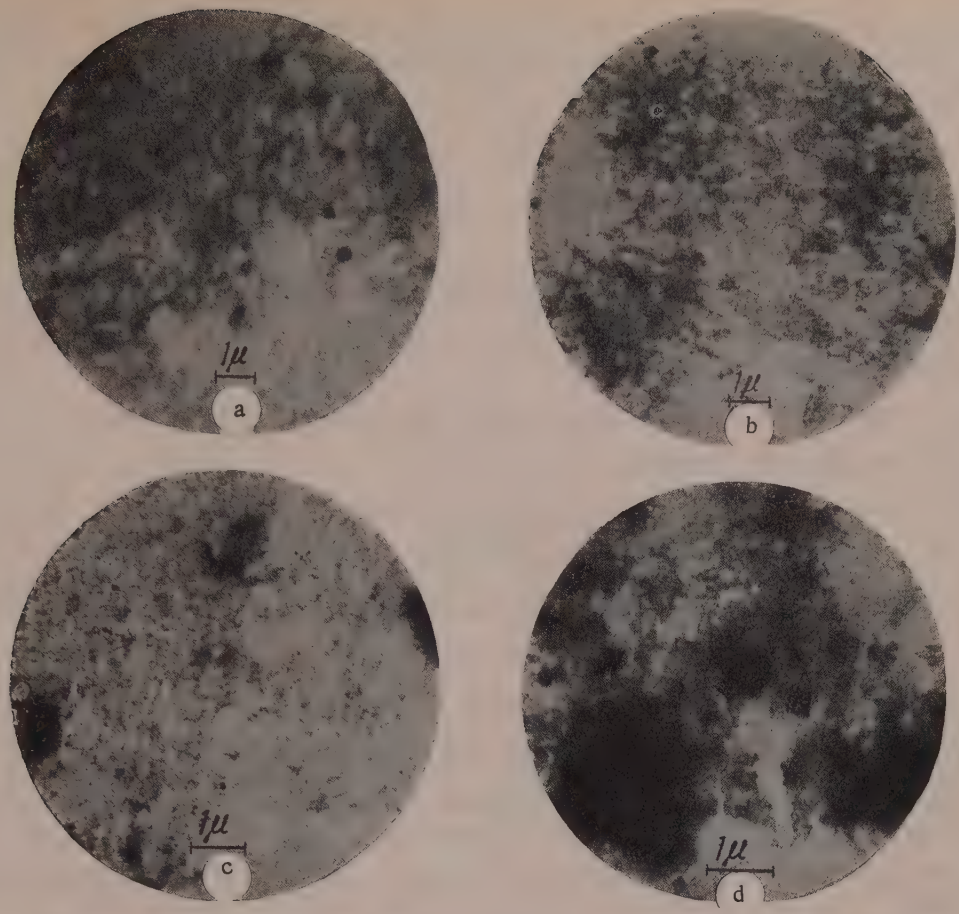


Fig. 2. Electrom micrographs of humic acids isolated from peat by the mild method: a) wood bottom peat, R = 40-45%; b) sedge bottom peat, R = 20%; c) medium upper peat, R = 25%; d) same, with added $CaCl_2$.

It should be noted that a similar type of structure was found by electron microscopy in humic acids isolated from coals [14, 15] and soils [16, 17]. At maximum peptization the humic acid particles are spherical, and their size approaches 60-100 A [16].

Addition of salts of bivalent metals causes particle aggregation (Fig. 2d). Aggregates of considerable size (5-10 μ) are formed. With small amounts of added salts the aggregates are apparently not compact but have considerable internal porosity. The gradual blackening of the image from the edges to the center indicates that the aggregates are three-dimensional and approximate to the spherical form.

The electron micrographs of humic acids (Fig. 2) can be used as reference standards for identification of particles originating from humus in micrographs of fine peat fractions. Identification of particles of other types requires further electron-microscope investigations of the other peat components – bitumens, lignin, etc. Since chemical isolation of these components from peat may involve fairly extensive breakdown of the colloidal structure, individual narrow fractions isolated by mechanical methods such as decantation and sedimentation, which may differ considerably in chemical composition [18, 19], should be investigated in the electron microscope. Studies of peat by these methods would give a deeper insight into the nature and properties of its colloidal fraction, which plays the most important part in the physical, mechanical, and technological properties of peat.

SUMMARY

1. The fine fractions of 12 different types of upper and bottom peat were investigated by electron microscopy. The weighted mean particle sizes and specific surfaces were determined by statistical analysis of over 300 micrographs. The shapes of the particles in fine peat fractions were studied.

2. Electron micrographs of one component of peat, humic acids, isolated by different methods, were obtained. Humic acid aggregates have a characteristic network or chain structure; accordingly, particles originating from humus can be identified in micrographs of peat.

LITERATURE CITED

[1] M. P. Volarovich and N. V. Churaev (editors), New Physical Investigations of Peat [Russian] (Gosénergoizdat, 1960).

[2] M. P. Volarovich and N. V. Churaev, Kolloid. Zhur. 17, 200 (1955).*

[3] M. P. Volarovich and N. V. Churaev, Proceedings of 3rd Conference on Colloid Chemistry [in Russian] (Izd. AN SSSR, 1956) p. 258.

[4] V. P. Tropin, College Scientific Reports, Mining Series [in Russian] 2, 91 (1958).

[5] E. P. Semenskii, Torfyanaya Prom. No. 7 (1953).

[6] S. G. Solopov, Trudy Mosk. Torfyan. In-ta, 8, 140 (1958).

[7] M. P. Volarovich and N. V. Churaev, Kolloid. Zhur. 16, 241 (1954).*

[8] V. E. Rakovskii, General Chemical Technology of Peat [in Russian] (Gosénergoizdat, 1949).

[9] M. M. Zhuravlev, Torfyanaya Prom. 5, 22 (1954).

[10] A. A. Berezin and I. D. Belovidov, Trudy Mosk. Torfyan. In-ta, 8, 167 (1958).

[11] Prevention of Water Percolation in Loess Soils [in Russian] (Izd. AN UkrSSR, Kiev, 1954).

[12] V. E. Rakovskii and M. M. Zhuravleva, Proceedings of the First All-Union Conference on the Chemistry and Origin of Solid Mineral Fuels [in Russian] (Izd. AN SSSR, 1953).

[13] B. F. Sergeev and T. P. Soldatkina, Trans. All-Union Sci. Res. Inst. of the Peat Industry [in Russian] No. 13, 64 (1956).

[14] T. A. Kukharenko, Trudy In-ta Torfa Akad. Nauk Beloruss. SSR 3, 120 (1954).

[15] T. A. Kukharenko, Origin of Solid Mineral Fuels [in Russian] (Izd. AN SSSR, 1959) p. 319.

[16] W. Flaig and H. Beutelspacher, Optik 7, N. 4-6 (1950).

[17] E. Kuster, Z. Pflanz. Dung. and Bodenkunde 57, No. 1, 51 (1952).

[18] V. E. Rakovskii and M. A. Rakovskaya, Collection of Scientific Transactions of the Institute of Peat, Acad. Sci. Belorussian SSR [in Russian] 1, 112 (1951).

[19] Zhitkute and Vidmantas, Tr. Kaunas Politekh. In-ta 7, 263 (1957).

CRYSTALLIZATION MECHANISM OF COLLOIDAL TITANIUM DIOXIDE

Z. Ya. Berestneva, M. B. Konstantinopol'skaya, and V. A. Kargin

L. Ya. Karpov Physicochemical Scientific Research Institute
Translated from Kolloidnyi Zhurnal, Vol. 22, No. 5, pp. 557-559, September-October, 1960
Original article submitted February 25, 1960

It was shown in the preceding investigation [1] that in the formation of colloidal titanium dioxide spherical colloidal particles of amorphous structure are formed first. Crystallization then begins within these particles and they disintegrate into numerous fine but now crystalline particles. It was desired to determine the influence of interfacial tension at the colloidal particle–intermicellar liquid interface on the crystallization of titanium dioxide. Unfortunately, there are no direct methods for studying interfacial tension in such systems. However, the interfacial tension at the colloidal particle–intermicellar liquid boundary can be varied by variation of the composition of the liquid. In such cases the course of crystallization in these systems can be followed by means of electron microscopy in conjunction with electron diffraction.

To study the crystallization mechanism of colloidal titanium dioxide the colloidal solutions were prepared by addition of titanium tetrachloride to redistilled water at temperatures between − 2 and +1°. The freshly prepared sol was concentrated by ultrafiltration, diluted with previously cooled redistilled water, and again concentrated by the same method. This operation was repeated from five to ten times at temperatures between −2 and +21° in order that the intermicellar liquid should be practically free from electrolytes. In some of the experiments the concentrated colloidal solution, after three or four cold washings, was washed several times with hot water. The resultant titanium dioxide sol was investigated in the electron microscope and by electron diffraction.

Regardless of the washing method used, all the sols presented the usual picture of spherical particles of colloidal titanium dioxide in the electron microscope (Fig. 1). Electron-diffraction data indicate that these particles are amorphous in structure. If these systems are kept at room temperature, crystallization begins 24 hours after preparation, whereas in titanium dioxide sols not washed free from electrolyte [1] crystallization begins 1-2 hours after preparation. It follows that removal of electrolytes from the intermicellar liquid changed the crystallization rate of colloidal titanium dioxide.

Addition of protective substances such as gelatin or polyvinyl alcohol in amounts of 0.001 to 0.005% did not have any significant influence on the crystallization rate of colloidal titanium dioxide. With these additions the titanium dioxide sols again started to crystallize 24 hours after preparation. Addition of such surface-active agents as sodium oleate and caproic acid to colloidal titanium dioxide solutions gave the same results: crystallization of titanium dioxide began 24 hours after preparation.

It follows that additives have no significant influence on the crystallization process; they lower the rate of crystallization somewhat. This effect of additives shows that either interfacial tension between the colloidal particles and the intermicellar liquid changes little with change in the composition of the liquid in these systems, or this tension has no significant influence on crystallization.

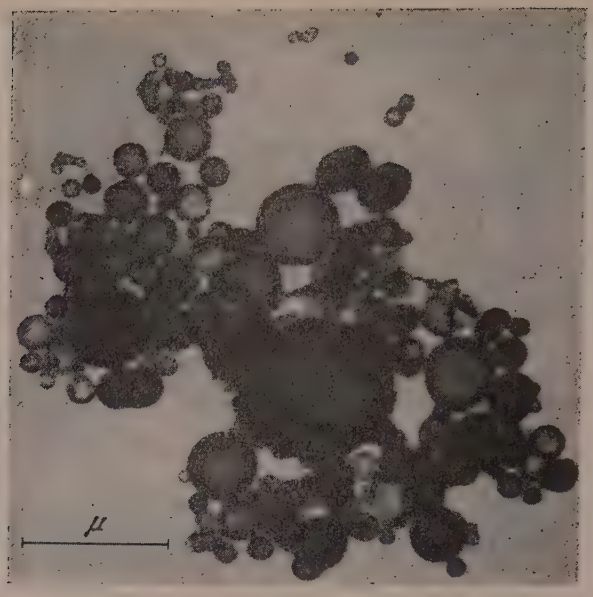


Fig. 1.

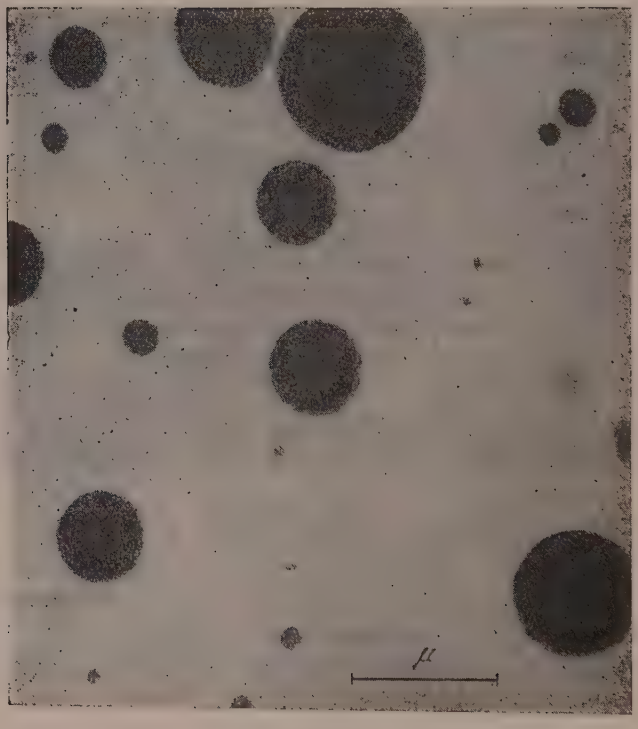


Fig. 2.

Electron micrographs of colloidal titanium dioxide prepared in: 1) Water; 2) organic solvents (benzene, toluene, or heptane).

Organic solvents, such as benzene, toluene, and heptane, were used as the intermicellar liquids in order to change substantially the interfacial tension between the colloidal particles and the liquid. Colloidal titanium dioxide solutions were prepared by addition of titanium tetrachloride to benzene, toluene, or heptane. These freshly prepared titanium dioxide sols were also found under the electron microscope to consist of spherical

particles (Fig. 2). However, in this case the spherical particles do not join in chains or aggregates as they do in water, but are separate from each other. Therefore these particles differ in surface character from particles in an aqueous medium. Colloidal particles of freshly prepared titanium dioxide solutions in organic solvents are amorphous, but crystallization begins in them also after 24 hours. Hence it may be concluded that interfacial tension at the colloidal particle–intermicellar liquid interface does not have any significant effect on crystallization of colloidal titanium dioxide.

It seemed possible that the presence of water in the system should influence the crystallization rate of titanium dioxide. In fact, the crystallization rate of colloidal titanium dioxide in organic solvents varied with the amount of water added to the organic solvent. For example, the particles in a colloidal solution of titanium dioxide prepared by the action of titanium tetrachloride on freshly distilled toluene began to crystallize 24 days after preparation when kept in a desiccator at room temperature. If water equivalent to 25% of the titanium tetrachloride is added to this solution, crystallization begins 10 days after preparation. Addition of 75% of water (calculated on the same basis) results in crystallization within 24 hours. Similar results are obtained with other organic solvents. If follows that the presence of water in the system has a very important influence on crystallization of colloidal titanium dioxide.

SUMMARY

1. Interfacial tension at the boundary between the colloidal particles and the intermicellar liquid does not have any significant effect on the crystallization of colloidal titanium dioxide.

2. Presence of water in the system has a considerable effect on the crystallization of colloidal titanium dioxide.

LITERATURE CITED

[1] Z. Ya. Berestneva, T. A. Koretskaya, and V. A. Kargin, Kolloid. Zhur. 12, 338 (1950).

MODEL STUDIES OF RHEOLOGICAL PROCESSES IN SOLID-STRESS INVESTIGATION BY OPTICAL POLARIZATION METHODS*

M. V. Gzovskii and D. N. Osokina

O. Yu. Shmidt Institute of Geophysics, Academy of Sciences of the USSR
Translated from Kolloidnyi Zhurnal, Vol. 22, No. 5, pp. 560-568,
September-October, 1960
Original article submitted May 13, 1960

Evaluation of stress and strain distributions inside large solids over very long periods is extremely important in construction of buildings intended to last several centuries, in the building of large machines, and in relation to prospecting for useful minerals which do not appear on the earth's surface. Direct tests of such bodies and locations (dams, mineral deposits, etc.) over hundreds of years are impossible in practice. Therefore, in addition to theoretical calculations (which often involve various assumptions and simplifications), a very promising method is the testing of models on greatly reduced geometrical and time scales. Tests of models on greatly increased geometrical and time scales may also be needed in development work on small complex instruments and studies of processes developing during very short time intervals.

Principles of Simultation of Elastic and Plastic Deformation Processes, the Stressed State, and Breakdown of Solids with Large Variations in Geometrical Dimensions and Time

Newton's laws, represented by equations for equilibrium and motion, are valid for any element of a stressed body undergoing deformation. Deformations of two types, reversible and irreversible, develop to some extent in each element; in the simplest case they are represented [1, 2] by the well-known equation for deformation kinetics of the type

$$\gamma_i = \frac{\tau_i}{2G_1} + \frac{\tau_i}{2G_2}(1 - e^{-t/\theta_2}) + \frac{\tau_i}{2\eta_3}t, \tag{1}$$

where γ_i is the shear deformation rate; τ_i is the rate of tangential stress. This equation includes the characteristics of mechanical properties G_1 and G_2, the elasticity moduli; θ_2, the relaxation time of the elastic aftereffect; η_3, the coefficient of effective viscosity; these are functions of the stressed state and of the thermodynamic conditions of deformation. These factors have the greatest influence on viscosity as represented, for example, by the Frenkel equation:

$$\eta_3 = \eta_0 e^{\frac{u - a\sigma_m}{kT}}, \tag{2}$$

which gives the increase of viscosity η_3 with increase of total pressure σ_m, or by the equation

$$\lg \eta_3 = (\eta_3)_0 - N\tau_i, \tag{3}$$

* Paper presented at the Rheology Subsection of the First All-Union Conference on Mechanics, January-February, 1960.

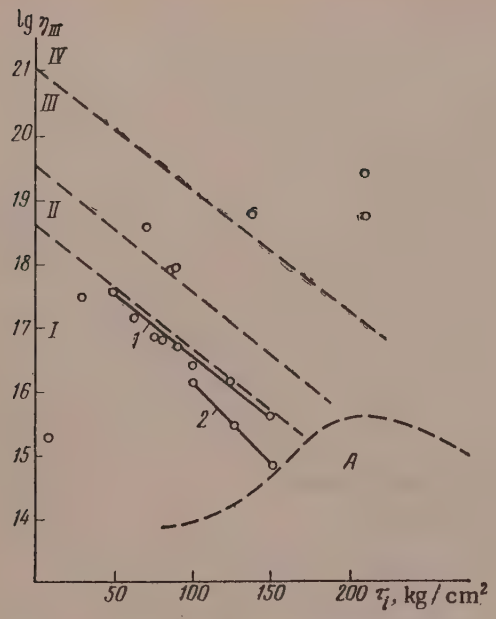


Fig. 1. Variations of the effective viscosity η_3 of rocks with the tangential stresses τ_i at atmospheric pressure and 20°. The dash lines divide rocks into the following four groups according to viscosity: I) clay, salt, and gypsum strata; thin-layered aleuritic–clay strata; II) thin-layered limestone–marl, sand–clay, and flysch strata; III) weakly layered sandstone, conglomerated, carbonate, volcanic, and previously strongly dissociated and weakly metamorphosed sand–clay strata; IV) granites and other intrusive rocks (apart from ultrabasic), gneisses, crystalline shales; A) Region of quasiinstantaneous breakdown; 1 and 2) Variations of η_3 with τ_i for gypsum, at total pressures of 1 and 1000 kg/cm² [3].

showing the dependence of η_3 on τ_i, which has proved useful for approximate characterization of the viscosity of solid rocks, which has been studied very little. Here η_0, u, a, and N are constants for the material.

We used experimental results [3-5] and a number of geological data to plot (for the first time) a graph representing the viscosities of large masses of various rocks under natural conditions (Fig. 1).

Stresses of certain magnitudes and durations of action produce macroscopic breakdown in addition to deformation, no matter whether the bodies in question are regarded as solid or liquid under everyday conditions. For solids the breakdown conditions in relation to time [6] and total pressure (Mohr's theory) can be unified in the following form:

$$p_d = p_{1(0)} - q\sigma_m - \zeta \ln d, \qquad (4)$$

where p_d is long-term shear (or tensile) strength; $p_{1(0)}$ is the quasiinstantaneous strength at total compression $\sigma_m = 0$; ζ, q are coefficients representing the properties of the material; d is the duration of the stress action. Of course, the strength of materials also depends on the temperature. There is a definite relationship between the elasticity moduli, viscosity, and strength of any material under given thermodynamic conditions. For this reason the relative elastic deformation in metals and rocks cannot exceed 0.01.

These characteristics of the macroscopic properties are common to a great variety of materials. If model tests are confined to macroscopic studies of deformations and failure, then the equations of equilibrium and motion and equations of types (1)-(4) are sufficient for determination of the similarity conditions by theoretical analysis by the method of dimensionless equations [7]. If the factor of geometrical similarity (ratio of the dimensions of the object) is C_l, the time ratio C_t, the acceleration ratio C_g, the density ratio C_ρ, the viscosity ratio C_η, the relaxation-time ratio C_θ, the elasticity-modulus ratio C_G, the strength ratio C_p, and the stress ratio C_τ, then we have the following relationships between the similarity ratios, which must hold for similarity to exist:

$$C_G = C_\rho C_g C_l, \quad C_\eta = C_G C_t, \quad C_\theta = C_t, \quad C_p = C_G = C_\tau. \qquad (5,6,7,8)$$

Variations of G, θ_2, η_3 and p in model must be such that the similarity ratios for G, θ_2, η_3 and p remain constant over the entire range of thermodynamic conditions in the model and the object. For example, it is required that, in Eq. (3)

$$C_N = C_\tau^{-1}, \qquad (9)$$

and, for Eq. (4)

$$C_\zeta = C_p. \qquad (10)$$

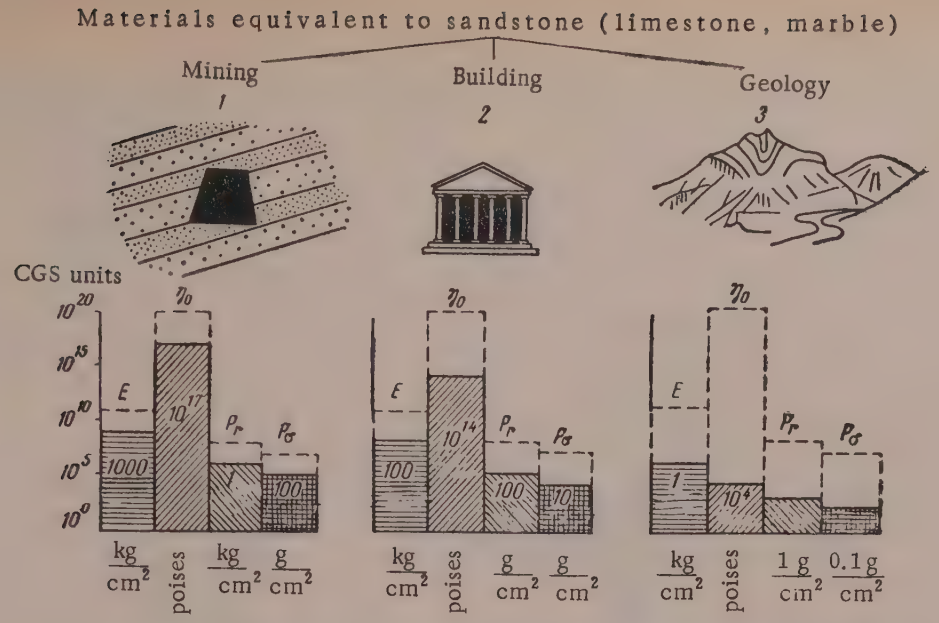


Fig. 2. Mechanical properties of materials equivalent to sedimentary rocks (sandstones, limestone, marble) with greatly differing geometrical and time scales: E) Elasticity modulus; η_0) viscosity; p_r) shearing strength; p_σ) tensile strength. The mechanical properties of the rocks are indicated by dash lines. One cm corresponds to: 1) 1 m; 2) 10 m; 3) 1000 m; 1 day corresponds to: 1) 10 days; 2) 1 year; 3) 10^8 years.

	C_l	C_t	C_E	C_η	C_p
1	10^{-2}	10^{-1}	10^{-2}	10^{-2}	10^{-2}
2	10^{-3}	10^{-3}	10^{-3}	10^{-6}	10^{-3}
3	10^{-5}	10^{-11}	10^{-5}	10^{-16}	10^{-5}

The similarity ratios for dimensionless quantities, such as the Poisson ratio and $\underline{q}$ in Eq. (4), must be unity for all relative deformations. It is obvious that the similarity ratios of quantities with interrelated dimensions are themselves interrelated [7].

For modeling of a definite group of objects with different boundary and initial conditions but with a common given variation of geometrical dimensions C and time C_t Eqs. (5)-(10) can be used to calculate all the characteristics of the mechanical properties of the model materials.

It is possible to determine theoretically, in accordance with the specific nature of the group of effects in question, reflected by the equations representing them, which similarity conditions are obligatory in the given case and which may be disregarded [7]. The more the dimensions and times of the models differ from those of the objects, the more should all the mechanical properties of the models differ from those of the objects [8, 9]. For example, in simulating the behavior of roofings the models must be made from materials with elasticity moduli of the order of 10^3 kg/cm^2, viscosity of 10^{14} poises, and strengths of 10^{-1} kg/cm^2. In models of slowly rising mountains, scaled down by a factor of 10^5 in dimensions and 10^{12} in time, the same sandstones and limestones must be represented by materials with elasticity moduli of the order of 10^0 kg/cm^2, viscosity of 10^4 poises, and strengths of 10^{-3} kg/cm^2. In model experiments it is often necessary to make large changes in the relationships between the elasticity moduli, relaxation times of elastic after-effects, and viscosity coefficients, measured in CGS units (Fig. 2). This can be done in principle, but it is first necessary to develop considerably the theory of possible independent variations of all these values in materials. The greatest difficulties arise in regulation of macroscopic tensile and shearing strengths of materials.

Stresses in models can be studied most effectively and strictly by the optical polarization method; this method is applicable if the model materials are transparent and optically active, in addition to having the required mechanical properties. To reveal regions of different stresses in a model the stress-optical coefficient must be connected with the strength similarity factor C_p [9] and the strength of the material in the object p_{ob} as follows:

$$B_\tau > 550/p_{ob} C_p. \qquad (11)$$

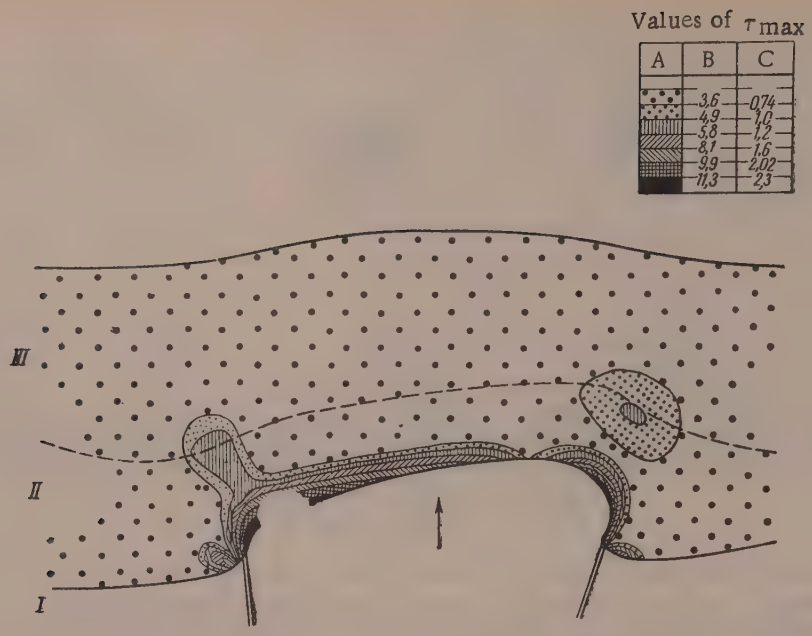


Fig. 3. Stress distribution in a model of a transverse anticline formed in a two-layer sedimentary stratum in ascent of granite bedrock (I); model under plastic deformation. Materials of layers II and III = 30 and 35% solutions of ethylcellulose in benzyl alcohol, with viscosities of the order of $1.7 \cdot 10^5$ and $9 \cdot 10^5$ poises, respectively, at $\tau = 2$ g/cm^2. For both layers $B_\tau = 61500 \cdot 10^{-7}$ cm^2/kg. Similarity factors: $C_l = 5 \cdot 10^{-4}$; $C_t = 4 \cdot 10^{-11}$, $C_\eta = 10^{-14}$. A) Layers; B) absolute values, g/cm^2; C) relative values.

Gels of gelatin [10] and acetylcellulose* are elastic materials with mechanical and optical properties close to those required, for large dimensional variations. If not only the dimensions but also time is greatly varied, plastic materials are required; the best of these are concentrated ethylcellulose solutions** [11, 12] and modified glyptal and epoxy resins*** [13]. Examples of models made from these materials are described in earlier papers [8, 9].

The results of tests on the new models are given in Fig. 3; this reproduces a section of the earth's crust in a foothill region or lowland between mountains; regions of this type often contain large accumulations of coal, oil, gas, or salts. The width of the model represents 4 km. The upper (sedimentary) stratum of the earth's crust, consisting of two layers, is deformed in such regions under the influence of vertical displacements, limited by faults in the underlying granite bedrock. The rate of rise of the blocks in the model is such that 1 minute corresponds to 50,000 years of the natural process. Since the viscosity of the lower layer of the sedimentary stratum is less than that of the upper, the models exhibited stress concentrations within the sedimentary stratum at some distance from the corners of the underlying rigid blocks pressing on it. This form of stress distribution is unusual. The knowledge of its existence makes it possible to predict, under natural conditions, regions in the depths of which there should be sites of increased fissuring, favorable for accumulation of oil and gas.

Relationships between Artificial Birefringence, Deformations, and Stresses in Certain Optically Active Materials

Optically active materials exhibit a great variety of relationships between the birefringence Δn on the one hand, and shearing deformation γ and shearing stress τ on the other. In many elastic and plastic materials, usually of the polymer type, Δn appears simultaneously with elastic deformation and disappears with it when the stress is removed. In transparent soaps a considerable proportion of the birefringence is determined by elastic

* Developed by the authors jointly with L. S. Gembitskii and S. A. Glikman.
** Developed by the authors jointly with G. V. Vinogradov and V. P. Pavlov.
*** Developed by authors jointly with S. I. Sokolov and N. A. Shchegolevskaya.

Effects of Temperature on the Shearing Modulus G and the Optical Activity Coefficients B_γ and B_τ of Various Materials

Material	Temp., deg.	G, kg/cm^2	$B_\tau \cdot 10^7$, cm^2/kg, from stress	$B_\gamma \cdot 10^7$, from elastic shearing deformation
Wischomlite (M-44)	20	(1,46—1,53)·10^4	0,91·10^2	(1,33—1,39)·10^6
	110	0,704·10^2	6,07·10^2	4,27·10^4
Bakelite VT 61-893	21	1,58·10^4	0,709·10^2	1,11·10^6
	110	0,287·10^2	1,91·10^3	5,47·10^4
ÉD6-M	Room	(1,2—1,27)·10^4	(1,09—0,99)·10^2	(1,3—1,26)·10^6
	Freezing	(0,867—1,0)·10^2	(3,64—3,21)·10^3	(3,16—3,21)·10^5
Epoxyphthamal	20	(1,28—1,46)·10^4	0,993·10^2	1,27·10^6
	120	0,5·10^2	5,46·10^3	2,73·10^5
30% gelatin-glycerol gel 1 min after loading	18	0,687	7,6·10^3	5,22·10^3
	22	0,32	1,29·10^4	4,13·10^3

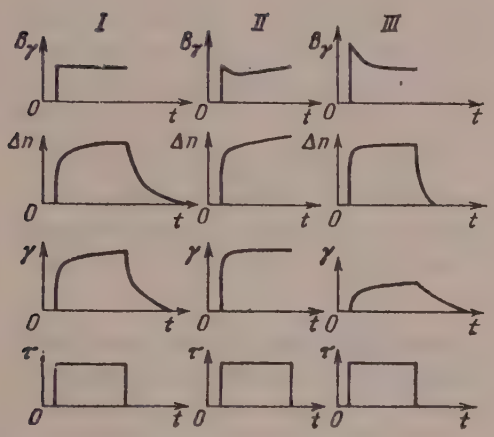


Fig. 4. Different types of relationships between the birefringence Δn and elastic deformation γ, leading to different variations in time of the deformation-optical coefficient B_γ at constant stress τ.

deformation, but most of it is associated with irreversible deformation.* Finally, it is known that in solid greases [14, 15] and bentonite clay pastes virtually all the birefringence is associated with irreversible deformation.

Optical investigation of stresses is possible only with materials in which Δn can be correlated with the magnitude of the stress; this can be done only if the birefringence disappears after removal of the load. It is found that in such materials, used in optical studies, the birefringence Δn is determined primarily by the magnitude of the elastic deformation. This is confirmed by the fact that the stress-optical coefficient B_τ in most cases varies qualitatively in the same way as the deformability of the material, i.e., the reciprocal of the elasticity modulus. For example, in the aging of gelatin gels and ethylcellulose solutions, increase of the elasticity moduli is accompanied by decrease of B_τ. The same is found if in these materials part of a good solvent is replaced by a poor one (water by glycerol in gelatin gels, and benzyl alcohol by dibutyl phthalate in ethylcellulose solutions [10, 12]). Increase of temperature results in decrease of the elastic modulus G with a simultaneous increase of B_τ in many materials, such as Bakelite, Wischomlite, and Fosterite [16], epoxyphthamal [17], ÉD6-M, gelatin and acetylcellulose gels, etc (table).

The quantitative relationship between the birefringence Δn and elastic deformation γ is represented by the strain-optical coefficient $B_\gamma = \Delta n/\gamma$, which must be regarded as an important physical characteristic of the optical activity of the material.** Optical activities of different materials should be compared by their values of B_γ, but only provided that the materials have the same values of G. An important fact is that B can vary

* Birefringence in transparent soap was observed by us jointly with G. V. Vinogradov. The soap consisted of 11% beef fat, 10.5% coconut oil, 3% castor oil, and 6.1% glycerol; to this mixture at 70-75° there was added a mixture of 3.9% NaCl, 9.8% ethyl alcohol, and 13.7% distilled water, followed by 13.2% sugar solution in distilled water (28.9%). [As in the original Russian].

** The coefficient B_γ, to the accuracy of the constant factor, is equal to the quality factor $Q[Q = E/2\tau_0^{(1,0)}]$ where E is the elasticity modulus and $\tau_0^{(1,0)}$ is the fringe value. The higher the quality factor, the better a given optically active material is considered to be [16].

in different ways with time at constant stress. This is because various molecular processes associated with the development of reversible deformation are accompanied by birefringence effects which differ in magnitude and even in sign. The following examples may be noted: a) B_γ remains virtually constant in time, as Δn and γ vary to the same extent with time (gelatin gels, Fig. 4, group I) [10]; b) after a constant equilibrium elastic deformation has become established Δn continues to increase, i.e., B_γ increases with time (gelatin gels with additions of HCl, Na_2SO_4 and $CO(NH_2)_2$, Fig. 4, group II*); c) after Δn has reached a constant value high-elastic deformation continues to develop at an appreciable rate, and B_γ decreases in time (solution of ethyl-cellulose in benzyl alcohol, Fig. 4, group III) [12]. An attempt can be made to explain these relationships between birefringence and elastic deformation on the assumption that in the above-mentioned cases: a) elastic macroscopic deformation and birefringence are determined by the same molecular process; b) increase of birefringence after equilibrium elastic deformation has been attained is caused by gradual orientation of optically anisotropic groups of rigidly bonded atoms forming branches in the principal chains; rotation of such groups is not accompanied by macroscopic deformation; c) birefringence is caused only by the processes which determine only the quasiinstantaneous component of the macroscopic elastic deformation.

The values of B_γ and B_τ depend on a number of factors, foremost among which are composition of the material and temperature. As already stated, B_τ of many materials increases with rise of temperature and increase of the deformability $1/G$. However, its increase is slower than the decrease of G, and therefore B_τ, $B = B_\gamma$ decrease with rise of temperature (see table). One possible cause of the retarded increase of B_τ is the disorientating effect of thermal motion, which diminishes the number of similarly orientated optically anisotropic particles involved in the total optical effect [12]. If the temperature change is so great that the material passes from the solid into the high-elastic state, then another cause of the retarded increase of B_τ may lie in the difference in magnitude of the birefringence effects accompanying instantaneous (Hooke-type) elastic and high-elastic deformations.

It would be of interest to examine the actual mechanism which gives rise to birefringence in elastic and viscoplastic materials used for stress investigations by the optical polarization method. This problem must be solved with the aid of data on the physicochemical molecular characteristics and structure of each material in conjunction with the principles of molecular optics which correlate the birefringence of high polymers with the nature and structure of their molecules.

Whereas the main cause of birefringence in solid compounds of low molecular weight is probably variation of interatomic distances in different directions, in the case of high polymers, their solutions and gels, and disperse systems, in addition to this mechanism we must postulate the existence of definite particles, molecules or molecular segments, which are carriers of optical activity because of their form or optical anisotropy (constant, or arising as the result of elastic deformation). With this approach we may assume that the birefringence of a given material may be correlated with elastic or residual deformation, depending on whether the orientation of these elements is destroyed or not as the result of thermal motion after removal of the load. For example, in the case of solid greases, soaps, and bentonite clay pastes the considerable proportion of birefringence corresponding to residual deformation shows that very large particles are the carriers of optical activity in this group of materials. In the case of greases and soaps these particles are probably anisotropic soap crystallites, and in the case of bentonite clay pastes, crystalline mineral scales. Because of the large size of the dispersed particles and the high viscosity of the dispersion medium the crystallites or microcrystals cannot lose their acquired orientation under the influence of thermal motion. It would be very useful to determine for every highly active material whether it has such definite structural elements which are responsible for birefringence, and to establish their nature. It might then be possible to say, for example, that in cellulose ethers or esters the high optical activity is determined by the presence of rigid glucose residues, in polystyrene and epoxy resins by the presence of benzene rings, in gelatin gels by rigid side chains of imino acids, etc. A solution of this problem would be of great value, as the optical method of stress study, which is being applied to an ever-increasing number of problems, requires the development of new materials of high optical activity and various predetermined mechanical properties. A deliberate approach to the production of such requires a knowledge of the compounds and their constituent elements which have the requisite optical properties.

* This type of variation of B_γ was discovered by Fang Wei-ch'ing of the Institute of Geophysics, Academy of Sciences USSR.

Further development of the modeling technique and the value of the results obtained with it depend on the success obtained in investigations in a number of directions. To find equivalent materials with the required optical polarization properties it is necessary to extend physicochemical studies of processes which cause birefringence in the deformation of elastic, viscous, and plastic bodies.

To obtain the required rheological properties in equivalent materials it is necessary to extend our knowledge of the general laws governing deformation and breakdown of various real bodies; in particular, to define more precisely the fundamental rheological equations on which the similarity conditions are based.

In addition, deeper studies into the rheological properties of various solids are needed. Much credit in this field is due to M. P. Volarovich, who is developing rheological studies of rocks.

SUMMARY

1. Equations representing deformation and breakdown processes in solids and relationships between the mechanical properties of materials and the thermodynamic conditions of deformation were used to derive similarity conditions, i.e., relations between scales of physical quantities which ensure similarity between the rheological processes in a model and the modeled object. It is shown that the mechanical properties of equivalent materials must vary in accordance with variations of the geometrical and time scales.

2. The condition which the stress-optical coefficient B_τ of an equivalent material must satisfy in order that the stressed state of the model can be studied by the optical polarization method has been derived.

3. The optical method can be used for studying stresses in models of solids, with geometrical scales from 10^0 to 10^{-5} and time scales from 10^0 to 10^{-13}, with the aid of previously known and newly developed optically active materials: of the elastic type with elasticity moduli between 10^{-1} and 10^4 kg/cm^2, and of the plastic type with viscosities from 10^2 to 10^8 poises.

4. There is a close connection between B_τ and the deformability of a material; i.e., the reciprocal of its elasticity modulus. In most optically active materials, B_τ increases while the elasticity modulus E decreases with rise of temperature.

5. Three types of relationship between the birefringence Δn and the elastic component γ of the total deformation have been demonstrated experimentally. The proportionality factor $B_\gamma = \Delta n/\gamma$ was considered; the variations of B_γ in time show that there are several different molecular causes of the macroscopic elastic deformation and birefringence.

6. Attention is drawn to the need for studying the chemical components and molecular structure elements in each material which cause optical activity.

LITERATURE CITED

[1] P. A. Rebinder and E. E. Segalova, Doklady Akad. Nauk SSSR, 71, 1, 85 (1956).*

[2] M. P. Volarovich, Kolloid. Zhur. 16, 3, 227 (1954).*

[3] D. T. Griggs, J. Geol. 47, No. 3 (1939).

[4] G. N. Kuznetsov, Mechanical Properties of Rocks [in Russian] (Ugletekhizdat, 1947).

[5] C. Lomnitz, J. Geol. 64, No. 5, 473 (1956).

[6] S. N. Zhurkov and B. N. Narzullaev, Zhur. Tekh. Fiz. 23, 10 (1953).

[7] L. S. Éigenson, Modeling [in Russian] (Gosizdat Sovetskaya Nauka, Moscow, 1952).

[8] M. V. Gzovskii, Izvest. Akad. Nauk SSSR, Ser. Geofiz. 6, 527 (1954).

[9] M. V. Gzovskii, Sov. Geol. 4, 53 (1958).

[10] D. N. Osokina, Kolloid. Zhur. 19, 6, 713 (1957).*

[11] M. V. Gzovskii, D. N. Osokina, and I. M. Kuznetsova, Proceedings of the Conference on the Optical Polarization Method of Stress Study [in Russian] (Izd. Leningrad. Univ., 1960) p. 290.

* Original Russian pagination. See C. B. Translation.

[12] D. N. Osokina, M. V. Gzovskii, G. V. Vinogradov, and V. P. Pavlov, Kolloid. Zhur. 22, 434 (1960).*

[13] N. A. Shchegolevskaya, D. N. Osokina, M. V. Gzovskii, and S. I. Sokolov, Izvest.vyssh. ucheb. zaved. Khim. i Khim. Tekhnol. 3, 1, 172 (1960).

[14] G. V. Vinogradov, Doklady Akad. Nauk SSSR 71, 3 (1950).

[15] G. V. Vinogradov, Proc. All-Union Conference on Colloid Chemistry [in Russian] (Kiev, 1952) p. 249.

[16] M. M. Frocht, Photoelasticity [Russian translation] (Gostekhizdat, Moscow-Leningrad, 1950).

[17] N. A. Shchegolevskaya and S. I. Sokolov, Zavodskaya Lab. 4, 511 (1958).

[18] N. I. Prigorovskii, A. K. Preis, M. F. Bokshtein, and N. A. Kupryakova, Models from the New Optically Active Material ÉD6-M for Stress Studies by Optical Polarization [in Russian].

* Original Russian pagination. See C. B. Translation.

SCREW MOTION OF A CYLINDER IN A VISCOPLASTIC SYSTEM

A. M. Gutkin

Moscow Power Institute
Translated from Kolloidnyi Zhurnal, Vol. 22, No. 5, pp. 569-572,
September-October, 1960
Original article submitted February 25, 1960

One important case in the rheology of viscoplastic disperse systems is screw flow, which belongs to the class of flows with double shear [1].* Suppose that this type of flow of the medium is produced by the screw motion of a long circular cylinder of radius a. The viscoplastic medium is considered to be infinite. We denote the forward velocity of the cylinder by u, and its angular velocity by ω_0. It is assumed that there is no slippage between the surface of the cylinder and the viscoplastic medium in which it is immersed. The problem is solved in the cylindrical coordinate system r, z, θ.

The boundary conditions for the viscoplastic medium when r = a are of the form $v_\theta = \omega_0 a$, $v_z = u$ and $v_r = 0$. It is reasonable to assume that in this case the velocity component v_r is everywhere zero, and v_θ and v_z depend on r only. We consider the case when flow of the medium is caused by the motion of the cylinder and there is no pressure gradient along the z axis, which coincides with the cylinder axis. In this case the equilibrium equations are:

$$\frac{d\tau_{r\theta}}{dr} + \frac{2\tau_{r\theta}}{r} = 0, \tag{1}$$

$$\frac{d\tau_{zr}}{dr} + \frac{\tau_{zr}}{r} = 0, \tag{2}$$

where τ represents tangential stresses.

The stress tensor components $\tau_{z\theta}$ and τ_{rz} depend as follows on the flow velocity, in accordance with the Hencky-Il'yushin equation [2]:

$$\tau_{r\theta} = \left(\mu + \frac{\tau_0}{h}\right)\left(\frac{dv_\theta}{dr} - \frac{v_\theta}{r}\right), \tag{3}$$

$$\tau_{rz} = \left(\mu + \frac{\tau_0}{h}\right)\frac{dv_z}{dr}, \tag{4}$$

where

$$h = \sqrt{\left(\frac{dv_\theta}{dr} - \frac{v_\theta}{r}\right)^2 + \left(\frac{dv_z}{dr}\right)^2}, \tag{5}$$

where τ_0 and μ are, respectively, the yield stress and the plastic viscosity of the disperse system.

* The theory of this effect was studied by the author; the results were presented at the 1st All-Union Congress on Mechanics in 1960.

Integration of Eqs. (1) and (2) gives

$$\tau_{r\theta} = A/r^2, \tag{6}$$

$$\tau_{rz} = B/r, \tag{7}$$

where A and B are the integration constants.

The velocities of peripheral and axial motion of the medium can be interconnected by means of Eqs. (6) and (7).

Division of one of these equations by the other and the substitution $v_\theta = r\omega$ gives

$$\frac{dv_z}{dr} = \alpha r^2 \frac{d\omega}{dr}, \tag{8}$$

where $\alpha = B/A$.

With the aid of Eq. (8), Eq. (5) is transformed into

$$h = r\left|\frac{d\omega}{dr}\right|\sqrt{1+\alpha^2 r^2}. \tag{9}$$

From Eqs. (3), (6), and (9) we have

$$\frac{d\omega}{dr} = \frac{A}{\mu r^3} - \frac{\tau_0 \frac{d\omega}{dr}}{\mu r\left|\frac{d\omega}{dr}\right|\sqrt{1+\alpha^2 r^2}}. \tag{10}$$

Since $d\omega/dr < 0$, Eq. (10) may be written in the form

$$\frac{d\omega}{dr} = \frac{A}{\mu r^3} + \frac{\tau_0}{\mu r\sqrt{1+\alpha^2 r^2}}. \tag{11}$$

This last expression can be used to find the dependence of dv_z/dr on r. With the aid of Eq. (8) we have:

$$\frac{dv_z}{dr} = \frac{\alpha A}{\mu r} + \frac{\alpha\tau_0 r}{\mu\sqrt{1+\alpha^2 r^2}} = \frac{B}{\mu r} + \frac{\alpha\tau_0 r}{\mu\sqrt{1+\alpha^2 r^2}}. \tag{12}$$

Integrating Eqs. (11) and (12), we have

$$\omega = -\frac{A}{2\mu r^2} - \frac{\tau_0}{\mu}\ln\frac{1+\sqrt{1+\alpha^2 r^2}}{r} + C_1, \tag{13}$$

$$v_z = \frac{B}{\mu}\ln r + \frac{\tau_0}{\mu}\sqrt{1+\alpha^2 r^2} + C_2. \tag{14}$$

The constants C_1 and C_2 are found from the condition that the angular velocity ω and the velocity v_z at the boundary of the flow zone are zero, i.e., when $r = R$.

We then have

$$\omega = \frac{A}{2\mu}\left(\frac{1}{R^2} - \frac{1}{r^2}\right) + \frac{\tau_0}{\mu}\ln\frac{r(1+\sqrt{1+\alpha^2 R^2})}{R(1+\sqrt{1+\alpha^2 r^2})}, \tag{15}$$

$$v_z = \frac{B}{\mu}\ln\frac{r}{R} + \frac{\tau_0}{\mu}\left(\sqrt{1+\alpha^2 r^2} - \sqrt{1+\alpha^2 R^2}\right). \tag{16}$$

The constants A and B are determined if we know the axial force F and the torque M acting on each unit of the cylinder length. For example, to find F we must divide the external force acting on the cylinder by the length of the cylinder surface in contact with the viscoplastic medium.

When r = a the following equations must be satisfied:

$$-2\pi\tau_{r\theta}a^2 = M \text{ and } -2\pi\tau_{rz}a = F,$$

and therefore

$$A = -\frac{M}{2\pi}, \tag{17}$$

$$B = -\frac{F}{2\pi}, \tag{18}$$

$$\alpha = \frac{F}{M}. \tag{19}$$

The value of R is found from the condition that when r = R the tangential stresses are represented by

$$\sqrt{\tau_{r\theta}^2 + \tau_{rz}^2} = \tau_0 \text{ when } r = R. \tag{20}$$

With the aid of Eqs. (6), (7), (17), and (18), Eq. (20) can be written in the form

$$\frac{M^2}{R^4} + \frac{F^2}{R^2} = 4\pi^2\tau_0^2. \tag{21}$$

From Eq. (21) we find R:

$$R^2 = \frac{F^2}{8\pi^2\tau_0^2} + \sqrt{\frac{F^4}{64\pi^4\tau_0^4} + \frac{M^2}{4\pi^2\tau_0^2}}. \tag{22}$$

The negative root of the quadratic equation (21) in R^2 is rejected, as it has no physical meaning.

We now consider some special cases.

1. The viscoplastic disperse system fills the gap between two coaxial cylinders of radii R_1 and R_2. The inner cylinder rotates and moves along the common axis of the two cylinders. The velocities of both motions can be measured. The torque and axial force are given. Then, if the tangential stresses are such that the shear spreads to the end, the plastic viscosity μ and the yield stress τ_0 can be calculated from the results of a single experiment by means of the equations

$$\omega = \frac{M}{4\pi\mu}\left(\frac{1}{R_1^2} - \frac{1}{R_2^2}\right) + \frac{\tau_0}{\mu}\ln\frac{R_1\left(M + \sqrt{M^2 + R_2^2F^2}\right)}{R_2\left(M + \sqrt{M^2 + R_1^2F^2}\right)}, \tag{23}$$

$$v_z = \frac{F}{2\pi\mu}\ln\frac{R_2}{R_1} - \frac{\tau_0}{\mu}\left(\sqrt{M^2 + R_2^2F^2} - \sqrt{M^2 + R_1^2F^2}\right) \tag{24}$$

After τ_0 has been found from Eqs. (23) and (24) it is necessary to verify whether the shear had, in fact, spread to R_2, i.e., whether the inequality

$$R > R_2,$$

where R is found from Eq. (22) and the value of τ_0 already found, is satisfied.

2. The observations and measurements refer to a cylinder in screw motion when the flow has spread over a very small region, so that $R - a = \Delta$ is small in comparison with a. Here a represents the radius of the inner cylinder; it is assumed that the outer cylinder is absent, although this is of no significance. In this case, since

$$\frac{\Delta}{a} \ll 1,$$

Equations (15) and (16) become the following approximate equations:

$$\omega = \frac{M\Delta}{2\pi\mu a^3} - \frac{\tau_0}{\mu}\frac{\Delta}{a} + \frac{\tau_0 F^2 a\Delta}{\mu\left[(\mu^2 + F^2a^2) + M\sqrt{M^2 + F^2a^2}\right]}; \tag{25}$$

$$v_z = \frac{F\Delta}{2\pi\mu a} - \frac{\tau_0 F^2 a\Delta}{\mu M\sqrt{M^2 + a^2F^2}}. \tag{26}$$

If v_z, ω, F, and M are known, the formula obtained by division of Eq. (25) by (26) gives the value of τ_0.

Equation (22) is used to find Δ from the known τ_0. If Δ and τ_0 are known, μ can be found from Eqs. (25) or (26).

The main advantage of using screw motion in plastometric determinations is that both characteristics of the viscoplastic medium in a given state can be found from a single experiment.

SUMMARY

1. The velocity distribution caused by the screw motion of a cylinder in a viscoplastic medium has been determined.

2. The relation has been found between the torque and axial force acting on the cylinder and the velocity components of the screw motion of the cylinder.

3. A method is proposed for experimental determination of the yield stress and plastic viscosity from the screw motion of a cylinder in a viscoplastic disperse system.

LITERATURE CITED

[1] G. V. Vinogradov, A. A. Mamakov, and V. P. Pavlov, Doklady Akad. Nauk SSSR 27, 2, 362 (1959).*

[2] M. P. Volarovich and A. M. Gutkin, Zhur. Tekh. Fiz. 16, 3, 321 (1946).

* Original Russian pagination. See C. B. Translation.

FLOW OF A VISCOPLASTIC DISPERSE SYSTEM ON A ROTATING DISK

A. M. Gutkin

Moscow Power Institute
Translated from Kolloidnyi Zhurnal, Vol. 22, No. 5, pp. 573-575,
September-October, 1960
Original article submitted February 25, 1960

To investigate the behavior of viscoplastic solid greases in rotating regions of friction we must consider the simplest case – the flow of a viscoplastic medium on a rotating disk. This problem was solved previously [1], but a wrong result was obtained because the solution was based on incorrect initial theoretical assumptions.

Consider the case when a grease layer of small thickness h is initially applied to a disk of radius a. The disk is brought into rotation so rapidly that the grease layer does not change anywhere in thickness during the time required for the disk to reach angular velocity ω.

The equilibrium equations for the grease on a rotating disk, in the cylindrical coordinates r, z, and θ, are of the form

$$\frac{\partial \sigma_r}{\partial r} + \frac{\partial \tau_{rz}}{\partial z} + \frac{\sigma_r - \sigma_\theta}{r} = -\rho\omega^2 r, \tag{1}$$

$$\frac{\partial \tau_{rz}}{\partial r} + \frac{\partial \sigma_z}{\partial z} + \frac{\tau_{rz}}{r} = 0. \tag{2}$$

Here, as usual, σ and τ represent the normal and tangential stresses; ρ is the density of the grease.

It was shown previously that if the radius of the layer of plastic grease is less than a certain value r_0, such that $r_0 = \tau_0/\rho\omega^2 h$, then the grease does not spread over the disk (τ_0 is the yield value of the grease).

Suppose that the radius of the elastic layer is much greater than its thickness, i.e., that the following inequality holds:

$$\rho\omega^2 h^2/\tau_0 \ll 1. \tag{3}$$

For grease of $\tau_0 = 10$ g/cm^2 and layers of thickness h = 1 mm, inequality (3) holds up to rotation speeds $n = 3 \cdot 10^4$ rpm. Then the velocity v_z in the region $r > r_0$ is much less than v_r.

Moreover, the derivatives of the velocity v_r with respect to r are much smaller than the derivatives with respect to z. In that case Eq. (2) contains only quantities of the second order of smallness, and should be disregarded in the first approximation of the solution.

Accordingly, Eq. (1) becomes

$$\partial \tau_{rz}/\partial r = -\rho\omega^2 r. \tag{4}$$

Integration of Eq. (4) gives

$$\tau_{rz} = -\rho\omega^2 rz + C. \tag{5}$$

Since $\tau_{rz} = 0$ when $z = l$, Eq. (5) becomes

$$\tau_{rz} = \rho\omega^2 r(l - z). \tag{6}$$

Here l is the new thickness of the grease layer at the given point on the disk at the given time instant.

In the first approximation the tangential stress intensity is represented by $|\tau_{rz}|$, since τ_{rz} is the greatest of the stress tensor components. Therefore flow does not begin in the grease so long as $\tau_{rz} < \tau_0$.

The derivative of v_r with respect to z differs from zero only in the region $z < z_0$, where z_0 is determined from the equation

$$\tau_0 = \rho\omega^2 r(l - z_0). \tag{7}$$

To find the radial velocity component we must integrate the equation derived from the Shvedov-Bingham equation

$$\mu\frac{\partial v_r}{\partial z} + \tau_0 = \rho\omega^2 r(l - z), \tag{8}$$

where μ is the plastic viscosity of the grease.

If the value of τ_0 from Eq. (7) is substituted into Eq. (8), we have:

$$\frac{\partial v_r}{\partial z} = \rho\frac{\omega^2 r}{\mu}(z_0 - z). \tag{9}$$

Since $v_r = 0$ when $z = 0$, Eq. (9) gives

$$v_r = \frac{\rho\omega^2 r}{\mu}\left(z_0 z - \frac{z^2}{2}\right). \tag{10}$$

The velocity of the upper layer of grease, where $\tau_{rz} < \tau_0$, is

$$v_{or} = \frac{\rho\omega^2 r z_0^2}{2\mu}. \tag{11}$$

The flow rate Q of the grease through the cylindrical surface of radius r is

$$Q = 2\pi r(l - z_0)v_{or} + 2\pi r\int_0^{z_0} v_r dz = \frac{2\pi\rho\omega^2 r^2 z_0^3}{\mu}\left(l - \frac{z_0}{6}\right). \tag{12}$$

If z_0 in Eq. (12) is replaced by its form as given by Eq. (7), we have

$$Q = \frac{\pi\rho\omega^2 r^2}{3\mu}\left(l - \frac{\tau_0}{\rho\omega^2 r}\right)^3\left(5l - \frac{\tau_0}{\rho\omega^2 r}\right). \tag{13}$$

Equation (13) makes it possible to calculate the rate of flow through a cylindrical surface of any radius $r > r_0$ if l is known. However, l is everywhere constant and is equal to h only at the instant $t = 0$, when the disk starts to rotate at angular velocity ω.

At every point on the disk where $r > r_0$ the value of l will change with time, and as t increases it will tend to the value given by Eq. (7) with $z_0 = 0$

$$l_{t\to\infty} = \tau_0/\rho\omega^2 r.$$

The flow rate Q can be connected with the rate of change of l by simple reasoning.

The value of $Q(r + dr)\,dt$ is equal to the volume of the viscoplastic medium flowing in time dt through a cylinder of radius$(r + dr)$.

The value of $Q(r)\,dt$ is equal to the volume of the viscoplastic medium flowing in time dt through a cylinder of radius r. The difference $[Q(r) - Q(r + dr)]\,dt$ is equal to the increase of the volume of the medium between cylinders of radii r and $r + dr$. This leads to the obvious equation

$$[Q(r) - Q(r + dr)]\,dt = 2\pi r\,dr\,dl. \tag{14}$$

From Eq. (14) we have the differential equation

$$\frac{\partial l}{\partial t} = -\frac{1}{2\pi r}\frac{\partial Q}{\partial r}. \tag{15}$$

Substituting Q by its equivalent from Eq. (13), we have the differential equation for l

$$\frac{\partial l}{\partial t} = -\frac{\rho\omega^2}{6\mu}\left(l - \frac{\tau_0}{\rho\omega^2 r}\right)\left[\left(10l^2 - \frac{\tau_0 l}{\rho\omega^2 r} - \frac{\tau_0^2}{\rho^2\omega^4 r^2}\right) - \left(15l - \frac{7\tau_0}{\rho\omega^2 r}\right) r\frac{\partial l}{\partial r}\right]. \tag{16}$$

Equation (16) can be integrated by the method of successive approximations.

In the first approximation we put in the right-hand side of Eq. (16) the values of l and $\partial l/\partial r$ at the initial instant. The expression for l and $\partial l/\partial r$ so found, when substituted into the right-hand side of Eq. (16), makes it possible to calculate in the next approximation.

In the second approximation for the region of values when $h \gg \tau_0/\rho\omega^2 r$, i.e., the region where the initial height is much greater than the thickness of the layer of elastic deformations, we have after simple calculations (the second approximation)

$$l = h - \frac{h^2}{3\mu}\left(5\rho\omega^2 h - \frac{11}{2}\frac{\tau_0}{r}\right)t + \frac{25\rho^2\omega^4 h^5}{6\mu^2}t^2. \tag{17}$$

Replacing l in Eq. (13) by its value from Eq. (17), we find the flow rate of the grease as a function of time. However, the resultant formula is valid only for not very large t, so long as the thickness l of the grease at the edge of the disk is much greater than its limiting value of $\tau_0/\rho\omega^2 a$.

SUMMARY

1. The velocity distribution in a viscoplastic disperse system on a rotating disk has been determined.

2. The relationship between the flow rate, rotation velocity, and the viscoplastic characteristics of the medium has been established.

LITERATURE CITED

[1] N. V. Tyabin, A. A. Shklyar, E. P. Mosikhin, and G. V. Vinogradov, Trans. S. M. Kirov Kazan Inst. of Chemical Technology [in Russian] (1953) No. 18, p. 123.

[2] A. M. Gutkin, Kolloid. Zhur. 19, 1, 31 (1957).*

* Original Russian pagination. See C. B. Translation.

POSSIBILITY OF STUDYING THE STRUCTURE OF VULCANIZATES WITH CARBON BLACK FILLERS BY MEASUREMENTS OF THEIR DIELECTRIC PROPERTIES

A. I. Lukomskaya and B. A. Dogadkin

Scientific Research Institute of the Tire Industry
Translated from Kolloidnyi Zhurnal, Vol. 22, No. 5, pp. 576-586,
September-October, 1960
Original article submitted March 17, 1960

Studies of the dielectric properties of rubber mixtures containing carbon black present a fairly complicated problem both with regard to the apparatus (selection of the method for measurement and calculation of the dielectric constant ϵ' and the dielectric loss coefficient ϵ'', or the tangent of the dielectric loss angle $\tan\delta = \epsilon''/\epsilon'$) and because of the lack of the relevant theory for direct interpretation of the results. Therefore, while there are numerous publications on measurements of ϵ' and $\tan\delta$ for raw rubbers and unfilled vulcanizates, which are summarized in review articles [1-5], there are relatively few scattered reports on the dielectric properties of loaded vulcanizates (including those containing carbon black) [6-18]. Some of these [10-18] may be regarded as more or less systematic.

Measurements of ϵ' and ϵ'' for vulcanizates without fillers [1-5] demonstrated the existence of dipole polarization and of associated temperature and frequency regions of dispersion of ϵ' and maximum $\tan\delta$ or ϵ'' (dipole losses). The theory of polar dielectrics was developed by Debye [19] and subsequently perfected in relation to polar polymers [20]. It was found for vulcanizates of natural [2] and synthetic [3] rubbers that raw stocks do not exhibit maximum $\tan\delta$, which is associated with rotation of "sulfur dipoles," formed during vulcanization, in an electric field. The frequency at which the maximum occurs at room temperature is 10^6-10^7 cps; this frequency increases with temperature and depends on the degree of vulcanization, type of rubber, and other factors which influence the number and mobility of "sulfur dipoles."

When carbon black is introduced into a rubber mixture the dielectric properties are partially lost. Electron-microscope investigations of rubber mixtures with small amounts of carbon black [21] showed that the carbon black is distributed in them somewhat irregularly in the form of individual particles and aggregates of various sizes. When the carbon black content is increased, chain and network structures are formed while the distribution remains irregular. The carbon chains act as conductors of electricity in the mixture. A sharp increase in the direct-current conductivity occurs at the point when a continuous structure of carbon black is formed.

From these data on the structure of rubbers containing carbon black one should expect the existence of dielectric losses, characteristic of a heterogeneous dielectric (a suspension of conducting carbon particles in the dielectric medium of the rubber phase) at low rubber contents, and conductivity losses which increase sharply with increased loading.

The formal Maxwell-Wagner theory can account for the variations of ϵ' and ϵ'' (ϵ'_h and ϵ''_h for a heterogeneous dielectric) with temperature and frequency. Jager [23] described a practical method for calculation of ϵ'_h and ϵ''_h for various temperatures and frequencies from Wagner's formulas.

Variations of ϵ' and ϵ'' with frequency $f = \omega/2\pi$, or temperature T,* for a heterogeneous dielectric are represented by the equations

$$\epsilon'_h = \epsilon_{\infty h}\left[1 + \frac{kb}{\sqrt{\pi}} \cdot e^{-b^2u^2} \frac{\mathrm{ch}\,[(2b^2z_0 - 1)\,u]}{\mathrm{ch}\,(u)}\,du\right], \tag{1}$$

$$\epsilon''_h = \frac{\epsilon_{\infty h}}{\sqrt{\pi}}\, kb \cdot e^{-b^2u^2} \frac{\mathrm{ch}\,(2b^2z_0u)}{\mathrm{ch}\,(u)}\,du, \tag{2}$$

where $u = \ln \omega\tau$; $z = \ln \tau/\tau_0$; τ is the relaxation time, and $u = z + z_0$.

The parameters of these equations are found with the aid of tables [23] of calculated integrals of $\epsilon''_h/k\epsilon_{\infty h}$ and $(\epsilon'_h - \epsilon_{\infty h})/k\epsilon_{\infty h}$, corresponding to the parameter of the relaxation-time distribution $\underline{b}$ between 0.08 and ∞ in the frequency range where $z_0 = \ln \omega\tau_0$ has values from -6 to $+6$. These tables in practice cover the entire range of ϵ' and ϵ'' variations for the most usual relaxation-time distributions.

To determine f_M and $\underline{b}$ we introduce the variable $\theta = \epsilon''_a/\epsilon'_x$, the ratio of the loss factor ϵ''_a at a randomly chosen frequency f_a to ϵ''_x at frequency f_x, which is one order of magnitude lower than f_a when $f_x > f_M$ (descending branch of the ϵ'' curve), and one order of magnitude higher than f_a when $f_x < f_M$ (ascending branch of the ϵ'' curve). The values of ϵ''_a and ϵ''_x are taken from the experimental relationship. Under the specified conditions θ is never greater than unity, and has the same value for $-z_x$ and $+z_x$, where $z_x = -\ln(f_M/f_x)$. Variations of θ with z_x at different values of $\underline{b}$ have also been tabulated [23].

By choosing θ_1 and θ_2 at f_{x_1} and f_{x_2}, respectively, and using the table for θ as a function of z_x we can plot the curve for θ_1 = constant in $b - z_{x_1}$ coordinates. Since $z_{x_1} = z_{x_2} + \ln(f_{x_1}/f_{x_2})$, it follows that if we calculate the values of z_{x_2} corresponding to z_{x_1} from this and then plot the curve for θ_2 = constant in the same $b - z_{x_1}$ coordinates, the intersection of the θ_1 = constant and θ_2 = constant curves gives a point which determines $\underline{b}$ and $\underline{z}$ simultaneously. From the expression $z_{x_1} = \ln(f_{x_1}/f_M)$ we find f_M.

If the experimental data give a satisfactory fit with Eqs. (1) and (2), then the relationship between the experimental value of ϵ''_h and $\epsilon''_h/k\epsilon_{\infty h}$, found theoretically at the corresponding frequencies is represented by a straight line the slope of which is $k\epsilon_{\infty h}$. Moreover, $\epsilon'_M = \epsilon_{\infty h}(1 + 0.5k)$, where ϵ'_M is the experimental value of the dielectric constant at frequency f_M. Hence $\epsilon_{\infty h}$ and $\underline{k}$ can be found.

The variations of ϵ'_h and ϵ''_h with frequency are determined at a given temperature, and all the corresponding parameters of Eqs. (1) and (2), namely $f_M(\tau_0)$, $\underline{b}$, $\epsilon_{\infty h}$ and $\underline{k}$, refer to that temperature. At a given frequency the dependence of ϵ' and ϵ'' on temperature is determined by the variations of $f_M(\tau_0)$, $\underline{b}$, $\epsilon_{\infty h}$ and $\underline{k}$ with temperature.

The effect of frequency on the dielectric loss factor due to conductance current ϵ'' is determined by the expression

$$\epsilon''_{con} = \frac{9 \cdot 10^{11} \cdot 4 \cdot \pi\Delta}{\omega}, \tag{3}$$

where Δ is the direct-current conductance at the given temperature and ω is the angular frequency of the alternating current. The value of ϵ''_{con} falls sharply with increasing frequency.

The first attempt at a theoretical analysis of the experimental relationships between ϵ' and ϵ'' and frequency for tread vulcanizates from different rubbers was made by Schneider et al., [11, 12]. In the case of neoprene rubbers two very indistinct maxima were found, at frequencies of $7 \cdot 10^3$ and $5 \cdot 10^6$ cps, which were attributed to losses in a heterogeneous dielectric (Maxwell–Wagner) and dipole losses (Debye). Analogous maxima were found for other mixtures containing carbon blacks. The ϵ'' curves were broken up into three components, conforming to: 1) the relationship established earlier for polar polymers [20]; 2) the simplified Maxwell– Wagner theory, and 3) Eq. (3) for conductance losses. However, such separation of the curves with

* The temperature determines the frequency f_M corresponding to maximum ϵ'' (since $f_M = 1/2\pi\tau_0$, where τ_0, the most probable relaxation time, is a function of temperature).

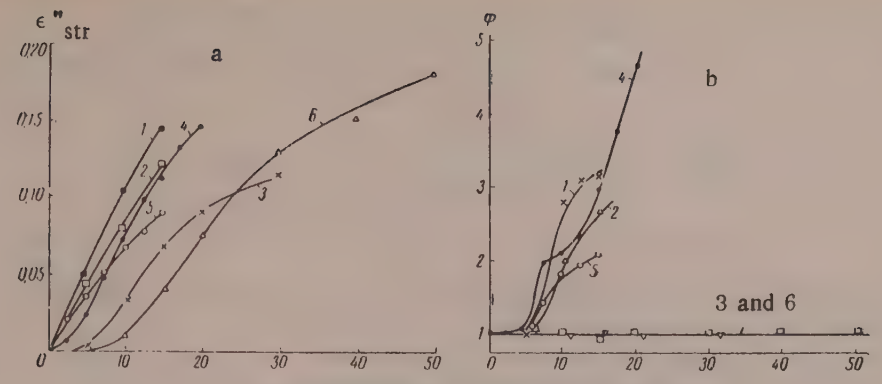


Fig. 1. Variations of the structural loss factor ϵ''_{str} (a) and shape factor (b) with the carbon-black contents of two-component mixtures: 1) Natural rubber (NR) + channel-gas black; 2) NR + extracted channel-gas black; 3) NR + thermal black; 4) sodium butadiene rubber (SKB) + channel-gas black; 5) SKB + extracted channel black; 6) SKB + thermal black.

almost imperceptible maxima could not be convincing, since the authors did not have the data on the corresponding effects of temperature and, without a progressive study of the effects of added carbon black in the range from unfilled vulcanizates to filled, used a very approximate calculation method.

A more detailed investigation and careful analysis of the effects of temperature and frequency on ϵ' and ϵ'' revealed the following characteristics [13-16]:

1. The dielectric properties of a pure nonpolar rubber are determined by its electronic polarization and are independent of frequency and temperature.

2. In two-component nonpolar rubber–carbon black mixtures there are losses characteristic of a heterogeneous dielectric ϵ''_h, conductance current losses ϵ''_{con}, and a change of the dielectric constant ϵ' (dispersion) corresponding to the loss maximum in a heterogeneous dielectric.

3. It is possible to segregate quantitatively ϵ''_h and ϵ''_{con} from the total losses (the experimental values of the dielectric loss factor ϵ''_e) in accordance with Eqs. (1)-(3)* if the presence of another constant term is postulated; this does not depend on frequency or temperature, but is determined by the type and amount of carbon black and the type of rubber (Fig. 1a). These losses were termed structural, since they vary in accordance with the structure formed by the carbon black in the mixture. The structure was assessed, on the one hand, from the direct current conductivity [21], and on the other from the dielectric constant ϵ'_∞ at high frequencies, when it is virtually constant.

If we know ϵ'_∞ as a function of the content p of carbon black in the mixture, we can calculate the "shape factor" Φ of the carbon black particles:

$$\varepsilon'_\infty = \varepsilon'_1(1 + 3\Phi p), \tag{4}$$

where ϵ'_1 is the dielectric constant of the rubber phase.

If Φ is independent of the carbon black content, then it represents the ratio of the dimensions (longitudinal to transverse) of individual particles, and characterizes their shape: when $\Phi = 1$ the particles are spherical, and when $\Phi > 1$ they are elongated. If Φ increases with the carbon black content this can only mean that the particles join together to form "structures" (chains or a network).

Variations of Φ with the contents and type of carbon black in two-component mixtures are represented in Fig. 1b.

* The direct-current conductivity of the mixtures was determined in the same capacitor and at the same temperatures as ϵ' and ϵ''.

At high frequencies, when the losses due to conductance and to heterogeneity of the dielectric are very small, structural losses determine the experimental value of the dielectric loss factor.

4. Variations of ϵ' and ϵ'' of unfilled vulcanizates with frequency f and temperature T satisfy the expressions [20]

$$\varepsilon'_{dip} = \varepsilon_\infty + \frac{1}{2}(\varepsilon_0 - \varepsilon_\infty)\left[1 - \frac{\operatorname{sech}(\alpha x)}{\operatorname{ch}(\alpha x) + \operatorname{ch}\frac{1}{2}(1-\alpha)\pi}\right], \tag{5a}$$

where ϵ_0 and ϵ_∞ are the "static" and "infinite" dielectric constants, corresponding to frequencies $f = 0$ and $f = \infty$, and

$$\varepsilon''_{dip} = \varepsilon''_M \cdot \operatorname{sech}(\alpha x), \tag{5b}$$

where ϵ''_M is the value of ϵ''_{dip} at the maximum (at $f_{M\cdot dip}$), $x = \ln[f_{M\cdot dip}/f]$; α is the parameter of the dipole relaxation time distribution.

Determination of α is performed graphically, from experimental data on the effects of frequency on ϵ'_{dip} and ϵ''_{dip} at the given temperature. The parameter α is equal to the tangent of the angle of inclination of the linear plot of the relationship between

$$ch^{-1}\left\{\frac{\varepsilon''_M[2 + (1/\varepsilon'_M)^2]}{\varepsilon''[2 + 1/\varepsilon')^2]}\right\} \text{and } \ln f,$$

where ϵ''_M and ϵ'_M are the values of ϵ_{dip} at $f_{M\cdot dip}$ (at the maximum).

If the values of ϵ''_M and ϵ'_M at the given temperature are unknown, they are also found from the linear relationship between

$$ch^{-1}\left\{\frac{\varepsilon''_M[2 + (1/\varepsilon'_M)^2]}{\varepsilon''[2 + (1/\varepsilon')^2]}\right\} \text{and } \ln f,$$

with several known experimental values of ϵ' and ϵ''.

It has been shown [13, 16] that in the first approximation the dependence of $f_{M\cdot dip}$ on $1/T$ is linear (the temperature coefficient of the function is found experimentally from the change of the temperature of the dipole maximum with frequency). From this relationship it is always possible to determine x for a given frequency and temperature. From $\epsilon' - \epsilon''$ vector diagrams [25] for a given temperature it is possible to find the "static" (ϵ_0) and "infinite" (ϵ_∞) dielectric constants.

5. All four types of dielectric loss can be distinguished in vulcanizates with carbon black: dipole, structural, conduction, and loss due to the heterogeneous dielectric.

Figures 2 and 3 illustrate the separation of the variations of the experimental loss factor with frequency and temperature into their individual components.*

* The experimental values of the dielectric constant ϵ'_e can also be divided into their components:

$$\varepsilon'_e = \Delta\varepsilon'_{dip} + \Delta\varepsilon'_h + \Delta\varepsilon'_{str} + \varepsilon_{\infty h},$$

where $\Delta\epsilon'_{dip} = (\epsilon'_e - \epsilon_\infty)$ in accordance with Eq. (5a)

$$\Delta\varepsilon'_h = (\varepsilon'_h - \varepsilon_{\infty h}),$$

in accordance with Eq. (1),

$$\Delta\varepsilon'_{str} = (\varepsilon_\infty - \varepsilon_{\infty h}),$$

where $\Delta\epsilon'_{str}$ is a constant quantity, independent of frequency and temperature.

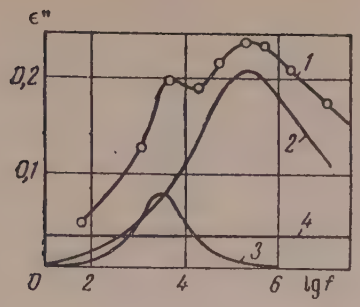


Fig. 2. Variations of the experimental dielectric loss factor ϵ''_e with log f at 20° for a natural rubber vulcanizate containing 30 parts by volume of thermal black. Here ϵ''_e (1) is separated into ϵ''_{dip} (2), ϵ''_h (3), and ϵ''_{str} (4).

The height of the dipole maximum $\epsilon''_{M\cdot dip}$ is almost unchanged in presence of carbon black; this indicates that the dipole moment of the vulcanizate remains constant or that there is no interaction between the carbon black and rubber at the locations of the "sulfur dipoles." As in the case of two-component rubber–carbon black mixtures, in filled vulcanizates the structural losses have the following distinguishing characteristics:

1) they are independent of frequency and temperature;

2) they are determined by the type of rubber and carbon black and by the content of the latter; they vary symbatically with the shape factor Φ found from the component of the dielectric constant which is due to polarization in a heterogeneous dielectric, as is seen in Fig. 4. Thus, structural losses are determined by the structure of the mixture containing carbon black.

At high frequencies, when ϵ''_{con} and ϵ''_h are negligibly small, ϵ''_{str} forms a "background" of constant height under the dipole loss maximum ϵ''_{dip}.

The experimental data presented by Chasset and Thirion [10, 17, 18], which were not always interpreted correctly by the authors owing to lack of appropriate analysis, should also be examined in the light of the foregoing relationships. One of these investigations [10] was concerned with dielectric losses in filled vulcanizates at high frequencies and low temperatures; in view of the fact that, as was already noted earlier, conduction losses due to heterogeneity of the dielectric occur both at low and at high temperatures in rubber stocks and vulcanizates containing carbon blacks, these losses naturally escaped detection. At the same time dipole maxima were observed; their height and position in relation to frequency and temperature remained almost unchanged with the degree of loading, but they appeared above a constant "background" which was a definite function of the carbon black type and content. As is clear from Fig. 5 [10], this background is not present in the case of rubber without carbon black; it follows from [13-16] that it is due to structural losses. Thirion and Chasset describe these losses as "supplementary." They also note that the magnitude of these losses appears to be associated with the structure formed by the carbon black in the mixture. It is known [26, 17] that carbon black structures are broken down when the rubber is stretched. Thirion and Chasset measured tan δ for both stretched and swollen rubbers and found that the magnitude of the supplementary loss is considerably less in such cases; in the case of vulcanizates containing 10 parts by volume of MPC channel black the loss vanishes almost entirely on swelling in 80% n-heptane solution. The explanation offered [10] for the supplementary losses is that the carbon black particles in the structure formed by them constitute a succession of microcapacitors in series, with a dielectric medium of unloaded rubber. The particles move further apart during extension or swelling, and the capacity of the microcapacitors becomes negligible.

At first sight this explanation seems plausible, but it contradicts a number of experimental facts. First, if the explanation is valid, the supplementary losses should depend on frequency and temperature, which is not the case. Further, measurements of the direct-current conductivity Δ of a rubber mixture containing channel-gas black, in the form of chains or networks at sufficiently high loadings, show [21] that Δ is a linear function of the voltage. This indicates the existence of direct contacts between the channel black particles. Under such conditions the carbon black particles cannot form microcapacitors which could play any significant role.

Thus, although the supplementary losses are undoubtedly associated with the carbon black and depend on the structure formed by the latter in the rubber stock or vulcanizate, their nature was not actually established.

Subsequently Chasset and Thirion [17, 18] measured conductivity at low frequencies and high temperatures. As was to be expected, they obtained the following results, analogous to those found earlier [13-16].

1. Dielectric losses varied in the course of vulcanization symbatically with direct-current conductivity (Fig. 6 from [17]). Such losses should be described simply as conduction losses. The authors attribute them to "absorption" currents which are known to flow in dielectrics consisting of regions differing sharply in conductivity and dielectric constant, i.e., in heterogeneous dielectrics.

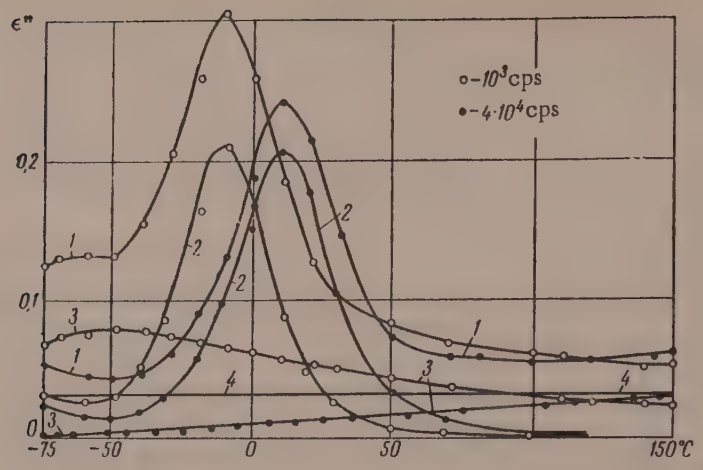


Fig. 3. Variations of the experimental dielectric loss factor ϵ''_e with temperature for a natural rubber vulcanizate containing 30 parts by volume of thermal black. Here ϵ''_e (1) is separated into ϵ''_{dip} (2), ϵ''_h (3), and ϵ''_{str} (4).

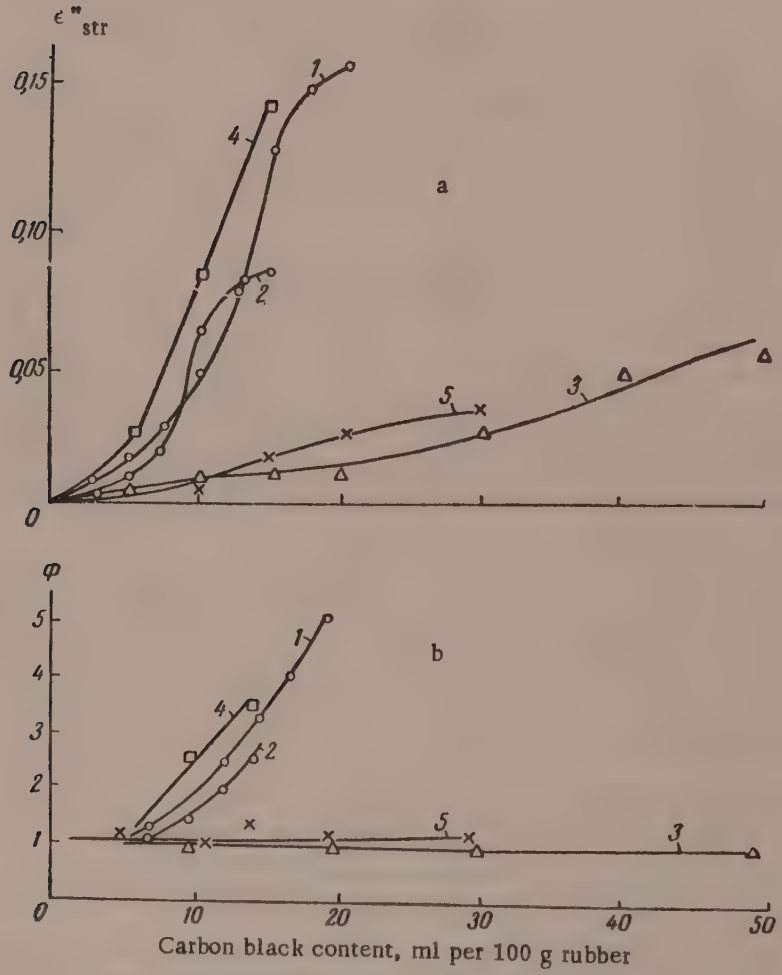


Fig. 4. Effects of carbon black content on the structural loss factor ϵ''_{str} (a) and shape factor (b) for vulcanizates of: 1) SKB with channel gas black; 2) SKB with extracted channel-gas black; 3) SKB with thermal black; 4) NR with channel-gas black; 5) NR with thermal black.

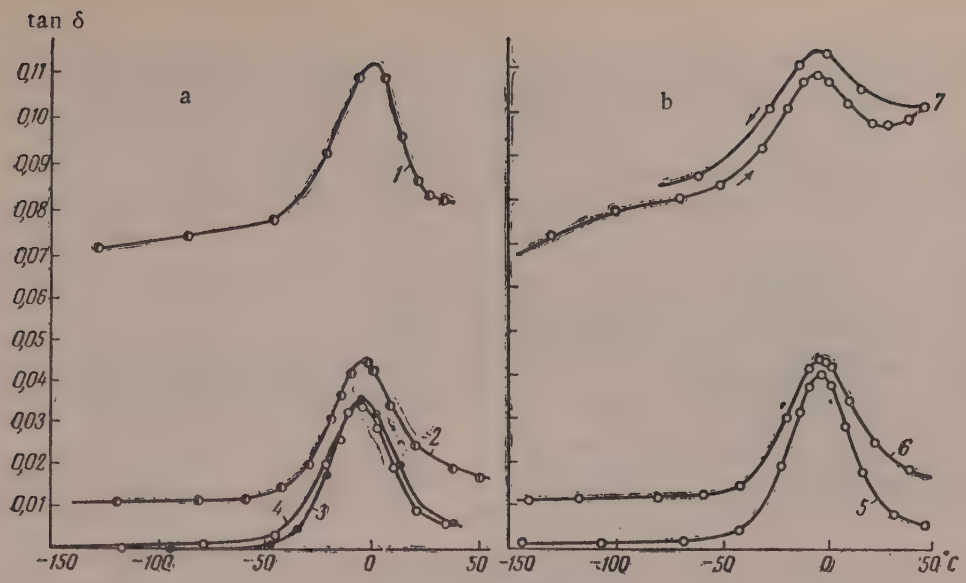


Fig. 5. Effects of temperature on the tangent of the dielectric loss angle tan δ at $120 \cdot 10^3$ cps for vulcanizates containing: a) 10 parts by volume of acetylene black (1), MPC channel black (2), fine furnace black (3), or colloidal chalk (4); b) without carbon black (5), and with 10 (6) and 20 (7) volume parts of MPC channel black.

2. Natural rubber vulcanizates with MPC carbon black exhibited a maximum of ϵ''_h (Maxwell–Wagner), which depended on the carbon black content with respect to height but not to frequency [18]. This maximum should be displaced with fall of temperature toward lower frequencies of the order of $10^3 - 10^4$ cps, where it was found earlier [13-16]; Chasset and Thirion found it at the frequency of $4 \cdot 10^5$ cps at 135°[18].

It should be noted that losses in heterogeneous dielectrics occur apart from conduction losses, but Thirion and others could not establish this fact since they did not perform a quantitative analysis.

3. Thirion et al., [17,18] observed increases of ϵ' and ϵ'' with increasing contents of carbon black and another filler (mixtures of natural rubber with Hi-Sil silica were investigated). It was found that ϵ' and ϵ'' varied linearly with the silica content, whereas they rise sharply with increase of MPC channel black content.

We consider that these data on the variations of dielectric constant ϵ' with the filler content p should be used to calculate the shape factor Φ [24].

4. Vulcanization of an unloaded stock containing sulfur and accelerators, and of the same stock with MPC carbon black or Hi-Sil silica [17, 18] is accompanied by changes of ϵ' and ϵ''. However, in pure rubber or natural rubber–filler binary mixtures ϵ' and ϵ'' do not change. The variations of ϵ' and ϵ'' are attributed to the structure of the mixture. This seems to be correct: changes in the structure of a loaded mixture during vulcanization were observed directly by means of the electron microscope, and also from changes in electrical conductivity as the result of vulcanization (the conductivity increases by several orders of magnitude as the result of vulcanization) [21]. Vulcanization causes growth of the carbon aggregates, joined in rough chains, and makes them join in a network structure.

5. With more than 20 parts of MPC carbon black by volume it becomes practically impossible to measure ϵ'' at low frequencies (120-1000 cps), and high temperatures (125-150°). Here, as already stated, considerable conductance losses should occur, owing to formation of a continuous conducting carbon phase in the mixture [21]. In comparison with these, all other types of loss are negligibly small. This gives rise to an abrupt increase of direct-current conductivity. As is to be expected from Eq. (3), ϵ'' decreases sharply with increase of frequency ($3 \cdot 10^4$ cps).

6. As vulcanization proceeds all the values of the dielectric constant ϵ' tend to a certain limit which depends little on the vulcanization temperature. This shows that the structure of the vulcanizate becomes stabilized during vulcanization, and in this case depends little on the temperature (the 125-150° range was investigated).

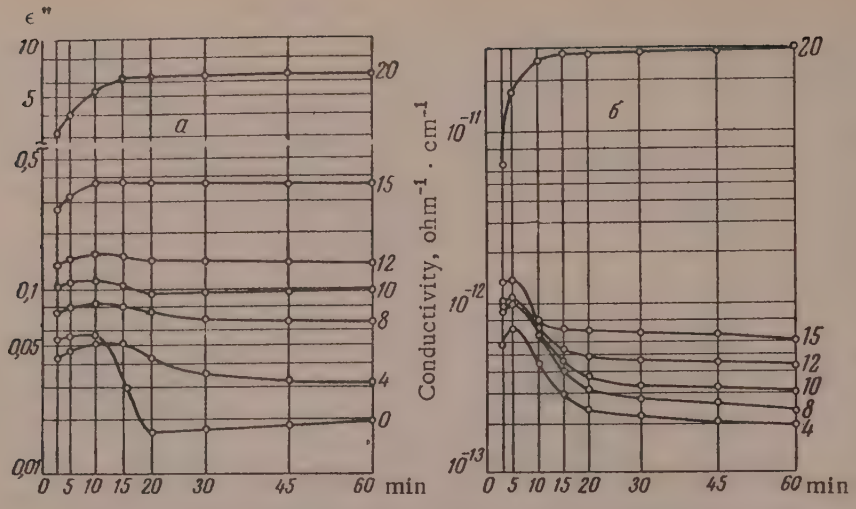


Fig. 6. Effect of the content of MPC channel black in a natural rubber stock on its dielectric loss factor ϵ'' during vulcanization at 135° (a) (measurements at 10^3 cps) and on direct-current conductivity (b). The numbers on the curves correspond to the volume contents of carbon black.

The method developed by Thirion and Chasset for measuring ϵ' and ϵ'' in the course of vulcanization is one possible route for investigating the structure of rubber mixtures.

To summarize the work discussed above, we may indicate the following ways of studying the structure of vulcanizates with carbon black by means of measurement of their dielectric constants and dielectric loss factors:

1. Investigations of the height and position of the dipole maximum on the dielectric loss factor curve and of the height of constant "background" (structural losses) at high frequencies and low temperatures [10] in relation to the type of rubber; contents and nature of the vulcanizing agent, fillers, and other ingredients; degree of extension and swelling, and other factors which influence the structure of the material.

2. Investigations of the effects of frequency and temperature on the dielectric constant ϵ' and the dielectric loss factor ϵ'' over wide ranges in relation to the above-named factors, with separation of the following components of the dielectric loss factor: a) conductance loss ϵ''_{con}; b) loss in a heterogeneous dielectric ϵ''_{h}; c) dipole loss ϵ''_{dip}; d) "structural" loss ϵ''_{str}, and the following components of the experimental dielectric loss factor:

$$\varepsilon'_e = \varepsilon'_\infty + \Delta\varepsilon'_{dip} + \Delta\varepsilon'_{str} + \Delta\varepsilon'_h,$$

where $\epsilon'_\infty = n^2$, the dielectric constant at a high frequency $f \to \infty$, due to electronic polarization (here $\underline{n}$ is the index of optical refraction); $\Delta\epsilon'_{dip}$, $\Delta\epsilon'_{str}$, and $\Delta\epsilon'_h$ are the components of the dielectric constants associated respectively with dipole polarization, structural polarization, and polarization in a heterogeneous dielectric [13-16].

This method, which is the most detailed, gives an indication of the structure of the vulcanizate formed by the reaction between the rubber and the vulcanizing agent, characterized by the dipole components $\Delta\epsilon'_{dip}$ and ϵ''_{dip}, and of the structure of the carbon black phase, characterized by the shape factor Φ and the values of ϵ''_{con} and ϵ''_{str}.

3. Studies of variations of ϵ' and ϵ'' in the course of vulcanization at given frequencies and temperatures. This is a useful supplementary method when the principal laws governing variations of ϵ' and ϵ'' with temperature and frequency are known. Otherwise its results are difficult to interpret; it indicates whether the structure of the rubber mixture changes in the course of vulcanization, and to what extent, with variations in the formulation of the mixture [17, 18].

SUMMARY

1. Analysis of the temperature and frequency relations of the dielectric properties of vulcanizates with carbon blacks shows that they lend themselves to quantitative treatment. The resultant characteristics give an indication of the structure of filled vulcanizates.

2. The tendency of a carbon black to form chain and network structures and the degree of their development are evaluated in terms of the "shape factor," calculated by separation of the experimental dielectric constant into its components.

3. Since the "shape factor" alters symbatically with the "structural" dielectric loss ϵ''_{str}, the development of carbon black structures can be assessed from this component of the experimental loss factor ϵ''.

4. At high frequencies and low temperatures ϵ''_{str} coincides with ϵ''. At low frequencies and high temperatures (as in direct current) the conductance losses are a measure of the development of carbon black structures.

5. Direct measurements of ϵ' and ϵ'' in the course of vulcanization provide additional information on structural changes in filled vulcanizates.

LITERATURE CITED

[1] C. C. Davis and J. T. Blake, Chemistry and Technology of Rubber (N. Y., 1937) p. 557; Chemistry of Large Molecules [Russian translation] (IL, 1948), Vol. 2, p. 265; H. Schurer, J. Rubber Res. 17, 3, 35 (1948); Raw and Cured Rubber [Russian translation] (IL, 1949) Vol. 3.

[2] A. Scot, A. McPherson, and H. Curtis, J. Res. Bureau Stand. 11, 713; Res. Paper 585 (1933); Rubber. Chem. Techn. 7, 341 (1934); Scient. Paper Bur. Stand. 22 (S 560) 398 (1927).

[3] A. M. Zolotareva, Dissertation [in Russian] (Leningrad Pedagogic Inst., 1941); Zhur. Tekh. Fiz. 16, 8, 937 (1946).

[4] L. T. Ponomarev, Zhur. Tekhn. Fiz. 10, 7, 588 (1940).

[5] A. Schallamach and P. Thirion, Trans. Faraday Soc. 42, 495 (1946); 45, No. 319, 7,605 (1949); J. R. S. Waring, Trans. Inst. Rubber Ind. 27, No. 1, 16 (1951); A. Schallamach, Trans. Inst. Rubber Ind. 27, 1, 40 (1951).

[6] H. Curtis and A. McPherson, Bur. Stand. Techn. Paper 19, 669 (1925); Industr. and Engng. Chem. 11, 1258 (1930).

[7] A. R. Kemp and D. B. Hermann, Proc. 1st Rubber Tech. Conf. (London, 1938) p. 893; Rubber Chem. Technol. 12, 2, 317 (1939); Dunsheath, Trans. Inst. Rubber Ind. 2, 460 (1936); W. B. Wiegand and C. R. Boggs, Ind. Eng. Chem. 22, 822 (1930); R. W. Williams and A. R. Kemp, J. Franklin Inst. 203, 1, 35 (1927); A. J. Wildschut, India-Rubber J. 92, 18a, 19 (1936); C. Zwikker, Proc. Rubber Tech. Conf. (London, 1938) p. 912.

[8] E. Guth, J. Appl. Phys. 16, 20 (1946).

[9] A. Scott and A. McPherson, J. Res. Nat. Bur. Standards 28, 279, (1942); Rub. Chem. Technol. 15, No. 4, 879 (1942); A. Scott, J. Res. Nat. Bur. Standards 43, 355 (1949).

[10] P. Thirion and R. Chasset, Trans. Inst. Rubber Ind. 27, No. 6, 364 (1951).

[11] W. G. Schneider, W. C. Carter, M. Magat, and C. P. Smyth, J. Amer. Chem. Soc. 67, No. 6, 959 (1945).

[12] W. C. Carter, M. Magat, W. G. Schneider, and C. P. Smyth, Trans. Faraday Soc. 42A, 213 (1946).

[13] A. I. Lukomskaya, Dissertation [in Russian] (Institute of Fine Chemical Technology, Moscow, 1951).

[14] B. A. Dogadkin and A. I. Lukomskaya, Doklady Akad. Nauk SSSR 88, 6, 1015 (1953); Proc. 3rd All-Union Conference on Colloid Chemistry [in Russian] (1956) p. 363.

[15] B. A. Dogadkin and A. I. Lukomskaya, Kolloid. Zhur. 15, 3, 183 (1953).*

* Original Russian pagination. See C. B. Translation.

[16] A. I. Lukomskaya and B. A. Dogadkin, Kolloid. Zhur. 15, 4, 259 (1953);* 16, 1, 36 (1954).*

[17] H. Desanges, R. Chasset, and P. Thirion, Rev. gén. caoutchouc 34, 893 (1957); Rubber Chem. Technol. 31, 631 (1958).

[18] R. Chasset, P. Thirion, and Vinh-Binh Ngyuen, P. Rev. gén. caoutchouc 36, 857 (1959).

[19] P. Debye, Phys. Z. 36, 100, 193 (1935); Chem. Rev. 19, 171 (1936); Polar Molecules [Russian translation] (GTTI, 1931); Physics of Dielectrics, edited by A. F. Val'ter [in Russian] (GTTI, 1932); G. I. Skanavi, Physics of Dielectrics, Region of Weak Fields [in Russian] (GTTI, 1949).

[20] R. M. Fuoss, J. Amer. Chem. Soc. 63, No. 2, 369, 378 (1941); R. M. Fuoss and J. G. Kirkwood, J. Amer. Chem. Soc. 63, No. 2, 385 (1941); J. Chem. Phys. 9, No. 4, 329 (1941); K. S. Cole and R. H. Cole, J. Chem. Phys. 9, No. 341 (1941).

[21] B. A. Dogadkin, K. A. Pechkovskaya, and I. I. Dashevskii, Kolloid. Zhur. 10, 5, 357 (1948); Trans. Sci. Res. Inst. of the Tire Ind. [in Russian] (Goskhimizdat, 1950) pp. 103, 120, 134.

[22] K. W. Wagner, Arch. Electrotechnik 2, 371 (1914); Ann. d. Physik. 40, 817 (1913); E. T. Z., 1279 (1913).

[23] A. Jager, Phys. 7, 434 (1936).

[24] A. Voet, J. Phys. Coll. Chem. 51, 1037 (1937); R. W. Sillars, J. Inst. Electr. Engrs. 80, No. 481, 378 (1937).

[25] A. P. Aleksandrov and Yu. S. Lazurkin, Kauchuk i Rezina, 10, 34 (1939).

[26] L. Mullins, J. Rubber. Res. 16, 277 (1947).

[27] B. A. Dogadkin and K. A. Pechkovskaya, Proc. 3rd Conference on Colloid Chemistry [in Russian] (1956) p. 371.

* Original Russian pagination. See C. B. Translation.

THE ELECTRICAL FIELD OF A MOVING UNCHARGED DROP*

2. THEORY OF THE ELECTRICAL FIELD OF A DROP CONTAINING A NONIONIC SURFACE-ACTIVE SUBSTANCE

S. S. Dukhin and B. V. Deryagin

Institute of Physical Chemistry, Academy of Sciences of the USSR, Moscow
Translated from Kolloidnyi Zhurnal, Vol. 22, No. 5, pp. 588-592,
September-October, 1960
Original article submitted December 2, 1959

The preceding paper [1] was concerned with the electrical field of a moving drop, which originates if the drop surface is mobile owing to circulatory motion of liquid within the drop, with adsorption of ions on the drop surface.

In the present paper it is shown that motion of the drop surface generates an electrical field even in absence of ions if the drop contains a nonionic surface-active substance. The mechanism of this effect is very simple. In a resting drop the electrical double layer formed by the adsorbed molecular dipoles has a spherically symmetrical structure, so that it has no external electrical field. Motion of the drop surface disturbs the spherical symmetry of the double layer and this leads, in accordance with laws of the electrostatics, to formation of an electrical field. It should be noted, of course, that an electrostatic field arises in steady motion of the drop. An alternating field arises in nonsteady motion of the drop, which we do not consider here.

The theory of this effect can be presented in general form covering both the case of a drop falling in another nonconducting liquid and the case of a drop falling in a gaseous medium, which is assumed to be free from ions.

Let us consider the electrical field of a fairly small drop, the motion of which is characterized by a Reynolds number $\mathrm{Re} \ll 1$.

The distribution of adsorption of a surface-active substance along the surface of a liquid drop falling in another liquid at $\mathrm{Re} \ll 1$ was found [2] on the assumption that the deviation of the number of molecules adsorbed from the equilibrium value is small, so that we may write

$$\Gamma(\theta) = \Gamma_0 + \Gamma'(\theta), \tag{1}$$

$$\Gamma'(\theta) \ll \Gamma_0, \tag{2}$$

where Γ_0 is the equilibrium surface concentration; $\Gamma' = \Gamma - \Gamma_0$ is the deviation of the surface concentration from the equilibrium value.

When $\mathrm{Re} \ll 1$ this assumption does not limit the general nature of the discussion, because it has been shown [3] that Eq. (2) is valid under the condition that

$$a < a_c = \left[\frac{3(\sigma_0 - \sigma)}{|\rho' - \rho| g}\right]^{1/2}, \tag{3}$$

* Paper presented at the IVth All-Union Conference on Colloid Chemistry in Tbilisi, 1958.

where a is the drop radius; σ_0 is the surface tension in absence of adsorption; σ is the surface tension at equilibrium surface concentration of the adsorbed substance; ρ is the density of the medium; ρ' is the density of the drop substance. Even if we assume the small value of $\sigma_0 - \sigma = 1$ dyne/cm² and $a_c \approx 0.06$ cm, at Re < 1, a < 0.02 cm, so that condition (3) and therefore condition (2) are satisfied automatically, but to a low degree of accuracy.

It is known [4] that the orientation of the dipole moment of an adsorbed molecule depends on the molecular surface concentration. Since, in accordance with condition (2), the latter varies negligibly along the surface in this instance, we may assume that the average value of the normal component of the dipole moment $\bar{\mu}_n$ is the same for all regions of the drop surface.

Then the potential difference between the two sides of the drop surface may be expressed as follows:

$$\Delta U(\theta) = \frac{4\pi\bar{\mu}_n \Gamma(\theta)}{\bar{\varepsilon}} = \frac{4\pi\bar{\mu}_n \Gamma_0}{\bar{\varepsilon}}\left(1 + \frac{\Gamma'(\theta)}{\Gamma_0}\right) = \Delta U_0\left(1 + \frac{\Gamma'(\theta)}{\Gamma_0}\right), \tag{4}$$

where $\Delta U_0 = 4\pi\bar{\mu}_n\Gamma_0/\bar{\epsilon}$ is the experimentally determined [4] potential difference between the two sides of a stationary plane interface which has adsorbed the equilibrium amount of surface-active substance; $\bar{\epsilon}$ is the average dielectric constant in the electrical double layer. We adopt a spherical system of coordinates with the origin in the center of the drop and the $\theta = 0$ axis directed vertically upward, and we represent the potential distribution by the sumbols $\varphi'(r, \theta)$, within the drop and $\varphi(r, \theta)$ outside the drop. Equation (4) can now be written as follows:

$$\varphi'(a, \theta) - \varphi(a, \theta) = \Delta U_0\left(1 + \frac{\Gamma(\theta)}{\Gamma_0}\right). \tag{4a}$$

Since the total density of free charges at the interface is zero, the normal components of the electrical field must satisfy the following condition at the interface:

$$\varepsilon' \frac{\partial\varphi'}{\partial r}(a, \theta) - \varepsilon\frac{\partial\varphi}{\partial r}(a, \theta) = 0, \tag{5}$$

where ϵ' and ϵ are the dielectric constants of the drop substance and medium, respectively; $\varphi'(r, \theta)$ and $\varphi(r, \theta)$ must conform to the Laplace equation; there are no free charges either in the drop or in the medium:

$$\Delta\varphi'(r, \theta) = 0, \quad \Delta\varphi(r, \theta) = 0. \tag{6}$$

With Eq. (6), the axial symmetry of the problem, and the obvious condition $\varphi(\infty, \theta) = 0$ taken into account, the required functions are $\Gamma'(\theta)$ should be expressed in the form of series of spherical functions

$$\varphi(r, \theta) = \sum_{n=0}^{\infty} A_n\left(\frac{a}{r}\right)^{n+1} P_n(\cos\theta), \tag{7}$$

$$\varphi'(r, \theta) = \sum_{n=0}^{\infty} B_n\left(\frac{r}{a}\right)^{n} P_n(\cos\theta), \tag{8}$$

$$\Gamma'(\theta) = \sum_{n=0}^{\infty} C_n P_n(\cos\theta). \tag{9}$$

Substituting Eqs. (7), (8), and (9) into (5) and (4), we obtain algebraic equations for determination of A_n and B_nC_n:

$$A_0 = 0, \quad B_0 = \Delta U_0, \tag{10}$$

$$-\varepsilon(n+1)A_n = \varepsilon' n B_n, \tag{11}$$

$$A_n - B_n = \frac{\Delta U_0}{\Gamma_0} C_n. \tag{12}$$

Values of $\Gamma'(\theta)$ have been determined [2] for two limiting sets of conditions for processes determining the supply of surface-active molecules from the solution volume.

1. In the first limiting case the supply rate of the molecules to the drop surface is determined by the low rate of the adsorption–desorption process

$$\Gamma'(\theta) = \frac{2\Gamma_0 v_0}{\alpha a}\cos\theta, \tag{13}$$

where α is a constant characterizing the adsorption–desorption process; $v_0\sin\theta$ is the velocity distribution along the drop surface. Substituting into Eq. (13) the value found for v_0 [2]

$$v_0 = \frac{8}{2}\, u\, \frac{\eta+\eta'}{2\eta+3\eta'+3\gamma_1}, \tag{14}$$

(where $u = 2(\rho'-\rho)ga^2/9\eta$ is the falling velocity under the same conditions, determined by means of the Stokes formula) and the retardation coefficient $\gamma_1 = (2\Gamma_0/3\alpha a)(\partial\sigma/\partial\Gamma)$, we have

$$\Gamma'(\theta) = \Delta\Gamma\cos\theta = \frac{3\Gamma_0 u}{\alpha a}\,\frac{\eta+\eta'}{2\eta+3\eta'+3\gamma_1}\cos\theta. \tag{15}$$

2. In the second limiting case, when the resultant rate of transfer of the surface-active substance is determined by the low rate of transfer from the volume to the surface, i.e., by the slowness of convective diffusion, the angular relationship $\Gamma'(\theta)$ and velocity distribution may be represented in terms of $\cos\theta$ as a rough approximation only

$$\Gamma'(\theta) = \Delta\Gamma\cos\theta = -\frac{\delta}{D}\,\frac{2v_0\Gamma_\infty}{a\dfrac{\partial c}{\partial\Gamma}}\cos\theta, \tag{16}$$

$$v_0 = \frac{3}{2}\, u\, \frac{\eta+\eta'}{2\eta+3\eta'+3\gamma_2}, \tag{17}$$

where c_0 is the volume concentration of the surface-active substance; δ is the average thickness of the diffusional boundary layer at the drop surface, where the retardation coefficient $\gamma_2 = 2/3\,(RT\Gamma_0^2\delta/Dac_0)$; D is the molecular diffusivity of the surface-active substance. Substitution of Eq. (17) into (16) gives

$$\Gamma'(\theta) = \frac{3}{2}\,\frac{\delta}{D}\,\frac{2u\Gamma_\infty}{a\dfrac{\partial c}{\partial\Gamma}}\,\frac{\eta+\eta'}{2\eta+3\eta'+3\gamma_2}\cos\theta. \tag{18}$$

The quantities α, $\partial\sigma/\partial\Gamma$ and $\partial c/\partial\Gamma$ which appear in Eqs. (15) and (18) may be expressed directly in terms of volume concentrations with the aid of the Gibbs equation and Langmuir's adsorption isotherm [2].

Assuming, for calculation of the electrical field, that

$$\Gamma'(\theta) = \Delta\Gamma\cos\theta, \tag{19}$$

we obtain a formula which, with $\Delta\Gamma$ determined from Eqs. (15), gives the distribution of electrical potential for the first limiting case; with $\Delta\Gamma$ determined from Eq. (18) we have the distribution of potential in the second limiting case. From a comparison of Eqs. (9) and (19) it follows that

$$C_1 = \Delta\Gamma,\ C_n = 0\ (n \neq 1). \tag{20}$$

Substituting these values into Eqs. (11) and (12), we have, after simple transformations

$$A_1 = -\frac{\varepsilon'}{2\varepsilon' + \varepsilon}\frac{\Delta\Gamma}{\Gamma_0}, \quad B_1 = \frac{2\varepsilon}{2\varepsilon' + \varepsilon}\frac{\Delta\Gamma}{\Gamma_0}\Delta U_0, \tag{21}$$

$$A_n = B_n = 0 \quad (n \neq 1),$$

and hence, from Eqs. (7) and (8), it follows that

$$\varphi(r, \theta) = -\frac{\varepsilon'}{2\varepsilon' + \varepsilon}\frac{\Delta\Gamma}{\Gamma_0}\Delta U_0 \frac{a^2}{r^2}\cos\theta, \tag{22}$$

$$\varphi'(r, \theta) = \frac{2\varepsilon}{2\varepsilon' + \varepsilon}\frac{\Delta\Gamma}{\Gamma_0}\Delta U_0 \frac{r}{a}\cos\theta. \tag{23}$$

When Eq. (22) is used to calculate the external electrical field of the drop

$$E(a, \theta) = \frac{2\varepsilon'}{2\varepsilon' + \varepsilon}\frac{\Delta\Gamma}{\Gamma_0}\frac{\Delta U_0}{a}\cos\theta. \tag{24}$$

it should be remembered that ΔU_0 depends on Γ_0 $\Delta U_0 = (4\pi\bar{\mu}_n/\bar{\epsilon})\Gamma_0$.

The maximum potential difference ΔU_0 is attained at fairly high concentrations, when the adsorption tends to a maximum value Γ_∞ corresponding to saturation of the adsorption layer, and is equivalent to several tenths of a volt. However, with increased adsorption the movement of the surface is increasingly retarded by the surface-active substance and therefore $\Delta\Gamma/\Gamma_0$, as is clear from Eqs. (15) and (18), decreases. It is therefore easy to see that the maximum possible field strength $E(a,\theta)$ is obtained when the adsorption layer is close to saturation and the retardation coefficient is small.

If the retardation coefficient is disregarded in comparison with the largest of the viscosity coefficients in substitution of the expressions (13) or (16) into Eq. (22), the resultant estimate shows that the maximum possible values of $E(a,\theta)$ may be as much as several thousand volts per centimeter.

However, with a single-phase adsorption film such considerable electrical fields do not arise, because in such cases the ratio $\Delta\Gamma/\Gamma_0$ is less than unity by several orders of magnitude. This is because it is impossible to have a low retardation coefficient and a sufficiently high value of adsorption simultaneously.

At high concentrations of the reagent large potential differences are obtained, but the surface retardation is then very large and the relative variation of the potential difference along the surface is correspondingly small; at low reagent concentration the retardation is small, and the relative variation of the potential difference is correspondingly large, but because of the low value of adsorption the absolute potential difference is also small.

Large relative variations of the potential difference while its absolute value is high are possible with two-phase adsorption films, the compressibility of which is known to be considerable, so that in this case retardation of the surface is negligible. If the volume concentration of the reagent in the drop is high enough, the adsorption layer is in the liquid or crystalline state over its entire surface, and at low enough concentrations it is in the gaseous state. There is also a region of intermediate concentrations, where part of the adsorption layer is in the gaseous state and part in a condensed state. In the latter case it is possible to define a boundary line $\theta = \theta_0$ on the drop surface, on one side of which the adsorption layer is gaseous and on the other it is in a condensed state.

We assume that the adsorptions Γ_1 and Γ_2 are constant within the gaseous and condensed regions, respectively, as variations of adsorption within each of these regions are much smaller than the difference $\Gamma_1 - \Gamma_2$.

Accordingly, the angular variation of the potential difference, which we transform by resolution into series by Legendre polynomials, becomes

$$\varphi'(a, \theta) - \varphi(a, \theta) = \sum_n \delta_n P_n(\cos\theta) = \begin{cases} \Delta U_1 & \theta > \theta_0 \\ \Delta U_2 & \theta < \theta_0 \end{cases},$$

where ΔU_1 and ΔU_2 are the potential differences between the two sides of a stationary plane interface the adsorption on which is Γ_1 and Γ_2, respectively. Without writing explicit expressions for the coefficient δ_n, we derive the equation for the field strength in general form:

$$E(a, \theta) = \sum_n \frac{\varepsilon' n (n+1)}{\varepsilon' n + \varepsilon (n+1)} \frac{\delta_n}{a} P_n (\cos \theta). \qquad (25)$$

It may be noted that at small values of n the coefficients δ_n will be of the same order of magnitude as ΔU_0. It follows that with drops 1-10 μ in size two-phase adsorption films can give rise to field strengths of the order of some thousands or hundreds of volts per centimeter, whereas with a one-phase adsorption layer the electrical fields of this type have much lower strengths owing to considerable capillary retardation.

SUMMARY

1. A theoretically new effect is defined and considered: an electrical field arises during the motion of an uncharged drop with an adsorbed layer of a nonionic surface-active agent.

2. If the adsorption film is of the two-phase type the electrical field strength may be thousands of volts per centimeter; with one-phase films it is less by several orders of magnitude.

LITERATURE CITED

[1] S. S. Dukhin and B. V. Deryagin, Kolloid. Zhur. 21, 37 (1959).*

[2] V. G. Levich, Physicochemical Hydrodynamics [in Russian] (Izd. AN SSSR, 1955) p. 59-63.

[3] V. G. Levich, Physicochemical Hydrodynamics [in Russian] (Izd. AN SSSR, 1955) p. 64.

[4] N. K. Adam, Physics and Chemistry of Surfaces [Russian translation] (Gostekhizdat, Moscow, 1947).

* Original Russian pagination. See C. B. Translation.

STUDIES OF ELECTROKINETIC PROCESSES AND SEDIMENTATION IN DISPERSE SYSTEMS BY THE RADIOACTIVE TRACER METHOD

Yu. S. Zaslavskii, G. I. Shor, and I. A. Morozova

Scientific Research Institute of Petroleum and Gas Conversion and Production of Synthetic Liquid Fuel, Moscow

Translated from Kolloidnyi Zhurnal, Vol. 22, No. 5, pp. 593-598, September-October, 1960
Original article submitted August 11, 1959

The mechanism of action of detergent additives to oils for modern high-performance internal combustion engines has not been studied sufficiently. In particular, little is known about the action mechanism of the so-called "dispersing" additives, which raise the ability of oils to retain in colloidal form the insoluble oil oxidation products and fuel combustion products [1].

The existing laboratory methods for estimation of the detergent properties of oils with such additives cannot be used for establishing the mechanism of their action in sufficient detail; engine methods are even less suitable. Recent investigations [2], in which attempts were made to study the connection between the dispersing (or, more correctly, the deflocculating) action of additives and electrokinetic processes, have yielded some new and interesting data on the action of such additives.

We have developed a radioactive tracer method for studying the electrokinetic processes associated with the action mechanism of many "dispersing" additives to engine oils. A distinguishing feature of this method is that radiation counters are used simultaneously as electrodes for creation of an electric field and for recording the migration of the labeled disperse phase.

Carbon black was used as the model substance to represent the disperse phase — products of oil oxidation and fuel combustion — and was labeled with the thallium-204 radioactive isotope. This isotope has a fairly long half life (3.5 years) and emits only β-radiation at the relatively low energy of 0.76 Mev. It is therefore possible to detect very efficiently the appearance of labeled particles in a given narrow zone.

For activation with thallium-204 a sample of the carbon black was wetted in thallium chloride solution (activity 1-2 mC), washed with distilled water, and dried. The dried radioactive carbon black was added to 50 g of the oil under investigation in order to form the labeled disperse system.

In each experiment 1 cc of the labeled disperse system was added to the oil sample containing the additive. The experimental unit shown schematically in Fig. 1 was used for the experiments.

The glass cylinder 1 (38 mm in diameter and 120 mm high) had a bottom made of brass foil 0.05 mm thick, attached to the end of the cylinder by means of BF-2 adhesive. An end-window β-counter (T25 BFL) 2 was pressed against it from below. The second counter 2, with a similar piece of brass foil glued to its end, was immersed from above into the cylinder, which was filled with 100 g of the oil under investigation. The counters were connected to radiometric units ("Bambu" type) the readings of which were recorded continuously by the electronic potentiometers 4 (ÉPP-09 and PS-1).

The high-voltage rectifier 5 (VSM type), carefully insulated from the radiometric equipment, was used for applying potentials to the bottom of the cylinder and to the foil on the upper counter. The current in the circuit between the counters was measured by the microammeter 6.

The upper β-counter recorded the settling rate of the labeled carbon black onto the foil of the counter under the electric field's influence, i.e., the electrophoresis rate in oils with the investigated additives.

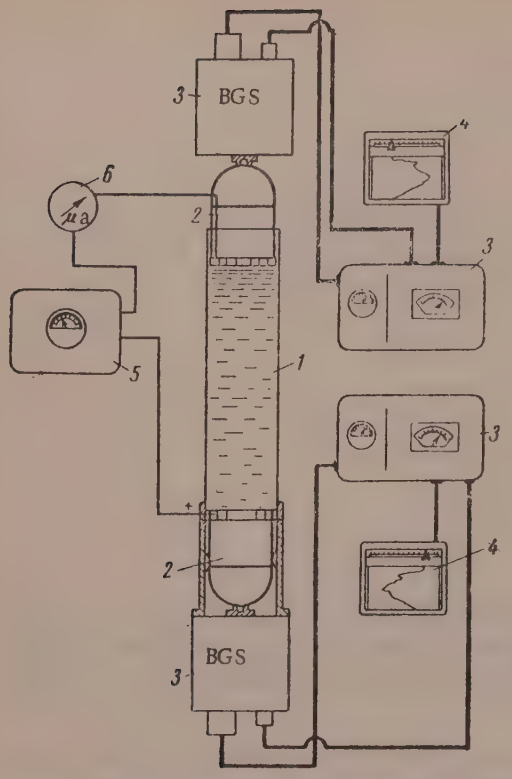


Fig. 1. Apparatus for radioactive tracer studies of electrokinetic processes and sedimentation in disperse systems.

The lower β-counter recorded the settling of labeled carbon black from the oil both in presence and in absence of the electric field. In the latter case the variation of the average concentration of labeled carbon black in the oil was recorded as a check with the aid of the upper counter.

The curves for electrophoresis and sedimentation of the carbon black were recorded automatically with this apparatus.

Figure 2 is an electrophoresis diagram of labeled carbon black in AS-5 engine oil made from sulfur-containing petroleum, with addition of VNII NP-354 additive. The diagram was recorded by means of the ÉPP-09 potentiometer from the readings of the upper β-counter with a potential of +1000 v applied to its foil. The diagram can be used to find tan α, which is a measure of the electrophoresis rate, and also indicates repulsion of the labeled carbon black from the electrode on reversal of the charge sign.

It is clear from Fig. 3 that the diagram recorded by means of the ÉPP-09 electronic potentiometer from the readings of the lower T-25 BFL counter has fairly distinct regions I and II, corresponding to rapid and slow settling of the labeled carbon black; i.e., the sedimentation curve is similar to the usual curves obtained by numerous workers [3]. The sedimentation rate was determined from the slope of the curve as described above.

In the electrokinetic investigations, in which sedimentation of the labeled black was not studied, the cylindrical vessel was replaced by a U-shaped tube containing oil, with β-counters either of the T-25 BFL type with attached brass foil or of AS-1 or AS-2 type at its ends. The disperse tracer system was introduced through a third branch of the tube.

These radioactive tracer methods were used to obtain data on the mechanism of detergent action of high-ash calcium sulfonate PMS-19,* an effective additive for engine oils.

The electrode–counter apparatus (Fig. 1) was used for studying the electrophoresis rate in engine oils made from sulfur-containing petroleum in presence of additives: mixtures containing various proportions of high-ash PMS-19 calcium sulfonate and barium alkylphenolate.** It was found that the electrophoresis rate increases linearly with the calcium sulfonate content in the mixture. Electrophoresis did not occur in experiments with oil containing barium alkylphenolate only.

Our earlier radioactive tracer studies [4] showed that the effectiveness of this binary mixture in prevention of corrosive wear increased linearly with the barium alkylphenolate content. It was then noted that this result was due to the high degree of dissociation of barium alkylphenolate in the oil.

Therefore in the selection of the optimum proportions of the components in this mixture, used in oils for modern high-efficiency engines [5], it is necessary to take into account changes in the oil performance resulting from variations in the composition of the mixture.

* PMS-19 sulfonate of 17.0% ash content, prepared by V. N. Monastyrskii, T. K. Aval'yani, and their co-workers, was used.

** Mixtures of high-ash PMS-19 calcium sulfonate and barium alkylphenolate were prepared to give a total metal content equivalent to 2% barium or 0.6% calcium on the oil.

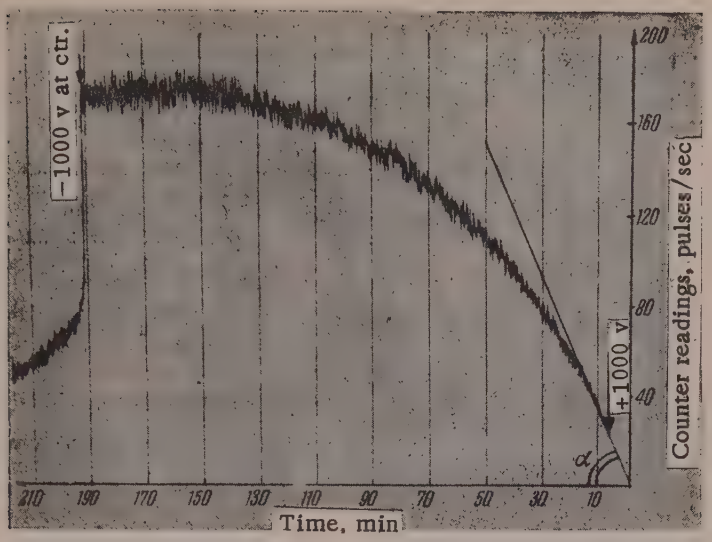


Fig. 2. Electrophoresis diagram of labeled carbon black in AS-5 engine oil with VNII NP-354 additive.

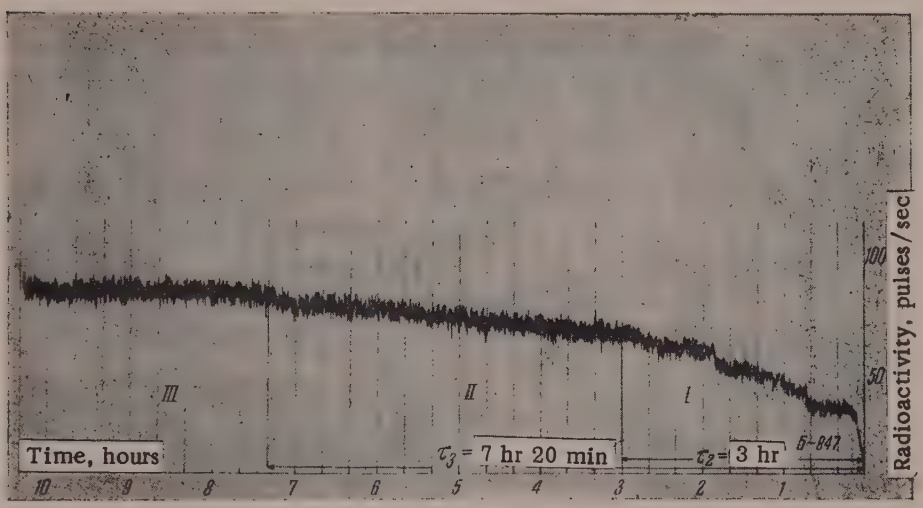


Fig. 3. Automatic trace of the sedimentation of labeled carbon black in AS-5 engine oil containing PMS-19 detergent additive.

Study of the electrophoresis in oil containing calcium sulfonate only showed that the carbon particles with adsorbed surface-active sulfonate additives PMS-19 are positively charged, as they are deposited on the electrode if the latter is negatively charged and repelled when the charge is reversed.

Carbon black particles can acquire positive charges both in cationic and in molecular adsorption; in the latter case the additive molecules are located with their positive charges in the oil direction. The greater the dissociation of the additive in the oil, the greater should cationic adsorption be. However, as already stated, barium alkylphenolate, which is strongly dissociated in oil, did not induce electrophoresis of the carbon black.

Accordingly, it seems likely that the deflocculating mechanism of high-ash PMS-19 calcium sulfonate is based on molecular adsorption, in which the additive molecules are orientated with their negative charges toward the colloidal particles and their positive charges toward the oil.

At the same time, investigations of numerous detergent additives introduced in various concentrations into engine oils showed that the mechanism of detergent action can be considered more fully on the basis of the micellar theory of surface-active solutions.

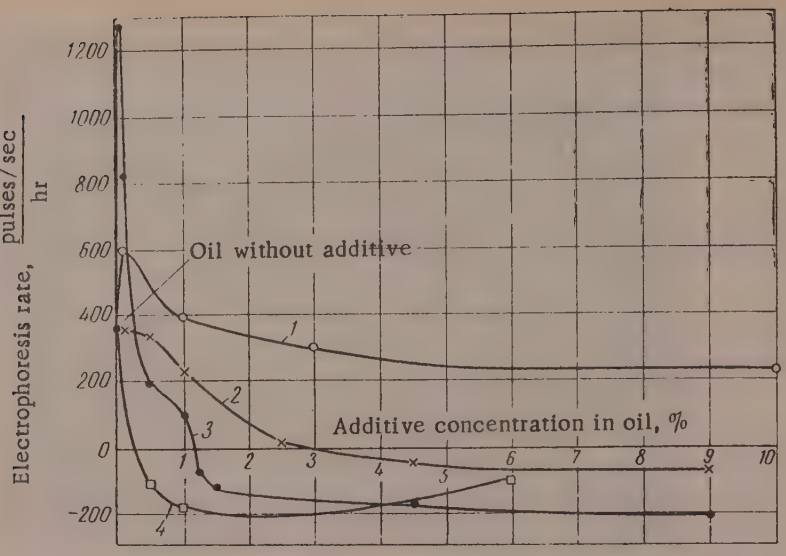


Fig. 4. Effects of the concentrations of various additives on the electrophoresis rate of labeled carbon black in AS-5 engine oil from sulfur-containing petroleum: 1) TsIATIM-339; 2) VNII NP-354; 3) VNII NP-353; 4) PMS-19.

As an example, Fig. 4 shows variations of the rate of electrophoresis with concentrations of various additives in AS-5 oil from sulfur-containing petroleum. It is seen in Fig. 4 that in presence of PMS-19 additive at any concentration the labeled carbon black migrated to the cathode only, TsIATIM-339 additive (barium alkylphenolate and disulfide) caused migration of the carbon black toward the anode only.

The dialkyldithiophosphate additives VNII NP-353 and 354 caused migration of carbon black to the anode up to certain concentrations, and at high concentrations the carbon black migrated to the cathode.

The form of the curves in Fig. 4 can be explained by means of McBain's theory, according to which solutions of surface-active substances contain micelles differing in type and size in accordance with concentration, and in the light of the analogy found between the volume properties of aqueous and hydrocarbon solutions of surface-active substances [6].

Thus, when VNII NP-353 and 354 additives are present in oil in low concentrations, small and strongly charged ionic micelles are evidently formed, solubilize the carbon black, and ensure a high rate of electrophoresis of the latter. With increasing concentration of these additives large and weakly charged micelles begin to predominate, and the electrophoresis rate of the carbon black decreases accordingly. When a certain concentration of the additive in the oil has been reached, counter ions begin to associate with the micelles and change the direction of electrophoresis.

SUMMARY

1. A radioactive tracer method has been developed for studying electrokinetic processes in disperse systems. In this method radiation counters are used simultaneously as electrodes to provide an electric field and for recording migration of the labeled disperse phase.

2. A radioactive tracer method for studying sedimentation of a disperse phase labeled with a radioactive isotope has been developed.

3. High-ash calcium sulfonate PMS-19 is adsorbed on the carbon black particles and confers positive charges on them. The mechanism of the deflocculating action of PMS-19 calcium sulfonate is probably based on molecular adsorption in which the additive molecules are orientated with their negative charges toward the colloidal particles and their positive charges toward the oil.

4. The effect of concentration of certain additives in engine oil on the electrophoresis rate of labeled carbon black has been demonstrated.

*Central Scientific Research Institute of Aviation Fuels and Lubricants

LITERATURE CITED

[1] G. I. Fuks and E. V. Tsyganov, Collection: Investigation and Use of Petroleum Products [in Russian] (Gostoptekhizdat, 1948) Vol. 1, p. 266; N. I. Chernozhukov, S. É. Krein, and B. V. Losikov, Chemistry of Mineral Oils [in Russian] (Gostoptekhizdat, 1959); W. D. Bascom, S. Kaufman, and C. R. Singleterry, Paper No. 18 at the 5th International Petroleum Congress, June 1959.

[2] F. H. Garner, C. W. Nutt, and M. F. Mohtadi, J. Inst. Petrol. 38, No. 348, 986 (1952); J. L. Van der Minne, Rec. Trav. Chim. Pays-Bas. 65, No. 9, 549 (1946); P. Y. Agius and D. Mulvey, J. Inst. Petrol. 44, No. 416, 229 (1958); B. Bernelin, Rev. l'Inst. Francais du Pétrole 14, No. 10, 1295 (1959); J. Briant and B. Bernelin, Rev. l'Inst. Francais du Pétrole 14, 1767 (1959).

[3] N. A. Figurovskii, Sedimentometric Analysis [in Russian] (Izd. AN SSSR, 1948).

[4] Yu. S. Zaslavskii, G. I. Shor, and V. N. Monastyrskii, Khim. i Tekhnol. Topliv i Masel, 2,51 (1959).

[5] G. H. Denison and F. W. Kavanagh, Proceedings of the 4th International Petroleum Congress [Russian translation] (Gostoptekhizdat, 1957) Vol. 7, p. 326.

[6] R. Courtel and I. Larbre, Rev. l'Inst. Francais du Pétrole 14, No. 12, 1763 (1959).

INVESTIGATION OF THE STRUCTURAL AND MECHANICAL PROPERTIES OF GELATIN*

S. M. Levi

Motion Picture and Photography Scientific Research Institute, Moscow
Translated from Kolloidnyi Zhurnal, Vol. 22, No. 5, pp. 599-604,
September-October, 1960
Original article submitted March 16, 1960

A number of investigations [1, 2], starting with the classic work of Shvedov [1], have been concerned with the structural properties of gelatin solutions and gels [3]. However, despite the great practical importance of the problem of structure formation of gelatin solutions, very little information is available on the subject in the literature.

The physical and mechanical properties of gelatin solutions are determined by the configuration of the gelatin molecules and depend on the temperature and gelatin concentration in solution. At temperatures above 38-45° the viscosity of gelatin solutions conforms satisfactorily to Frenkel's [4] equation

$$\eta = Ae^{u/RT}, \tag{1}$$

where T is the absolute temperature; A is a constant; R is the gas constant; u is a certain energy value characteristic of the given liquid.

In Fig. 1 the viscosity of gelatin solutions is represented as a function of the reciprocal of the absolute temperature T for three gelatins differing in molecular weight. The molecular weight is expressed in terms of the intrinsic viscosity $[\eta]$, which was 0.65 for gelatin 1, 0.32 for gelatin 2, and 0.27 for gelatin 3.

In the coordinates chosen, the experimental data for temperatures above 38-45° are represented by a linear relationship between T^{-1} and $\log \eta$

$$\lg \eta = K\left(\frac{1}{T}\right) + \lg \eta_0, \tag{2}$$

where η is the viscosity of the gelatin solution at T° K; $\lg \eta_0$ is the intercept cut off along the axis of ordinates by the continuation of the straight line; K is the slope of the line, known as the temperature coefficient of viscosity (K = 0.4).

These results show that the temperature coefficient of viscosity is constant for all the gelatins tested, regardless of their molecular weight. In the region of constant temperature coefficient of viscosity, gelatin solutions behave as Newtonian liquids with yield value of zero. Beyond this temperature limit gelatin solutions acquire the properties of an elasticoviscous liquid. Experimental data on variations of the yield value with temperature are plotted in Fig. 2; it is seen that structure formation in gelatin solutions occurs at a temperature below the temperature limit (38-45°) above which the coefficient K remains constant. Similar temperature limits have been reported by others [5, 6].

* Paper at the Rheology Subsection of the All-Union Congress on Theoretical and Applied Mechanics, February 2, 1960.

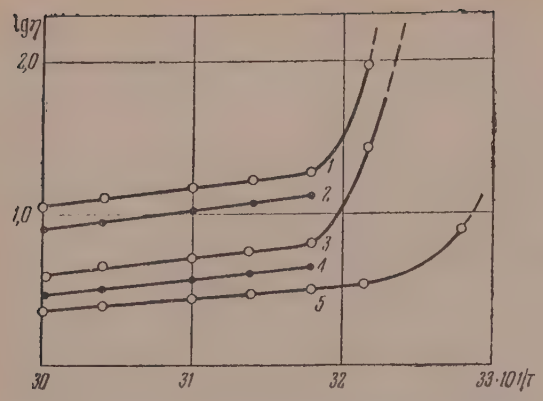


Fig. 1. Viscosity–temperature graphs for 10% (1, 3, 5) and 6% (2, 4) gelatin solutions, plotted in $1/T - \lg \eta$ coordinates: 1 and 2) $[\eta] = 0.65$; 3 and 4) $[\eta] = 0.32$; 5) $[\eta] = 0.24$.

It has been shown [6, 7] that in the 28-40° temperature range, in which gelatin solutions behave as elasticoviscous bodies, the viscosity–temperature behavior of the solutions can be represented by the following equation, or one of similar form:

$$\eta = \eta_0 e^{K_1/\sqrt{T-T_0}}, \qquad (3)$$

where η is the solution viscosity at T° K; T_0 is a constant close in value to the gelatin temperature; $K_1 = 0.44$ for all the gelatins tested. Comparison of the values of the coefficients K and K_1 in Eqs. (1) and (3), with constant values of gelatins differing in structure, indicates that they can be regarded as identical with the coefficient u/R in the Frenkel' Eq. (1). For gelatin solutions at temperatures below 38-45°, 1/T in the exponent is replaced by the more complicated temperature coefficient $1/(T - T_0)^{1/2}$.

The values of the exponent in Eqs. (2) and (3) are different because in the first case the gelatin solution behaves like a true Newtonian liquid and is devoid of structure, i.e., its yield value is zero; in the second case the gelatin solution behaves like a quasidisperse system which forms a structure with a yield value.

Structure formation in gelatin solutions is closely associated with thermal motion of the molecules: when this motion is sufficiently intense, stable bonds are not formed between the molecules and therefore the solutions have neither yield value nor elasticity. As the temperature falls the velocity of thermal motion of the molecules diminishes sharply and the gelatin solution is transformed from a true Newtonian liquid into a quasidisperse system with the properties of a Shvedov liquid. Variations of viscosity and yield value in very rapid changes of the solution temperature were studied in order to investigate structure formation as the result of changes of the solution temperature.

The experiments were performed with the dual-temperature viscosimeter (Fig. 3) [8], consisting of two vertical capillaries 1 and 2 of different diameters, fixed vertically along a common axis. Both capillaries were sealed into a spherical reservoir 3 communicating with the atmosphere through the tube 4. The upper capillary 1 (with the greater internal diameter) was connected to the tube 5 supplying the liquid. This tube was connected to a source of excess pressure. The lower capillary 2 (with the smaller internal diameter) passed into the U-tube 6 joined to a vacuum pump. The tube 5 was contained in a thermostat 7 maintained at temperature t_2. The capillaries 1 and 2 together with the bulb were in a second thermostat 8 maintained at temperature t_1 ($t_1 < t_2$). The liquid at temperature t_2, under a pressure of P_1 mm, flowed at a definite rate through the capillary 1; during this time its temperature fell from t_2 to t_1. By the action of the vacuum the cooled liquid flowed through the measuring capillary 2; the time required for a definite volume (A – B) of liquid passing through this capillary was noted, and from the result its viscosity and yield value could be calculated. The size of the capillary 1 was so designed that the temperature of the liquid flowing through it fell from t_2 to t_1.

Viscosity variations of gelatin solution after rapid cooling are plotted in Fig. 4. Gelatin solution of viscosity $[\eta] = 0.32$ was cooled from 40 to 35, 32, 30, and 29°. It follows from Fig. 4 that a certain time interval is needed before the solution reaches a constant viscosity corresponding to the solution viscosity at the given temperature. This time is much longer than the time required to cool the solution. The solution viscosity remains constant for some time, and then increases thixotropically; this characterizes structure formation. Data obtained in these experiments are compared with some values obtained in prolonged cooling of the solutions to the lower temperature limit.

The data in Table 1 show that when the solution has reached the final cooling temperature it acquires a viscosity value corresponding to that temperature. Formation of a gelatin structure in the solution takes a definite period of time; the greater the temperature drop in cooling and the lower the cooling temperature, the shorter this time is. After the time necessary for formation of the gelatin structure there is a continuous

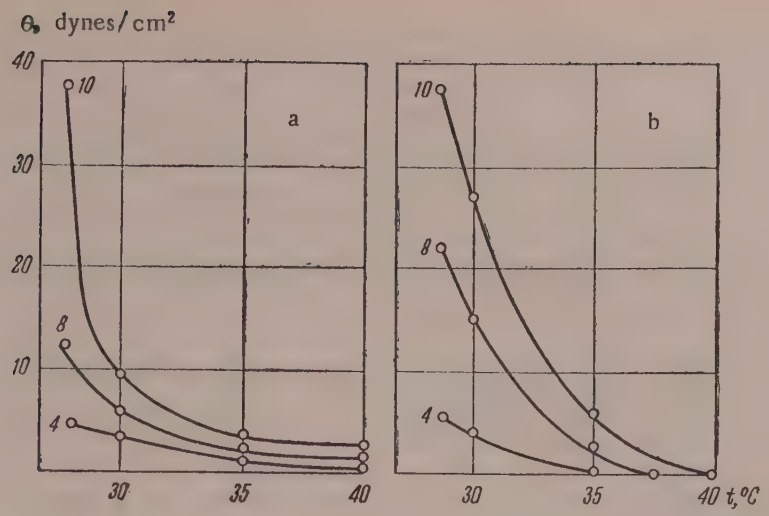


Fig. 2. Variations of yield value with temperature for 10, 8, and 4% gelatin solutions: a) $[\eta] = 0.32$; b) $[\eta] = 0.65$.

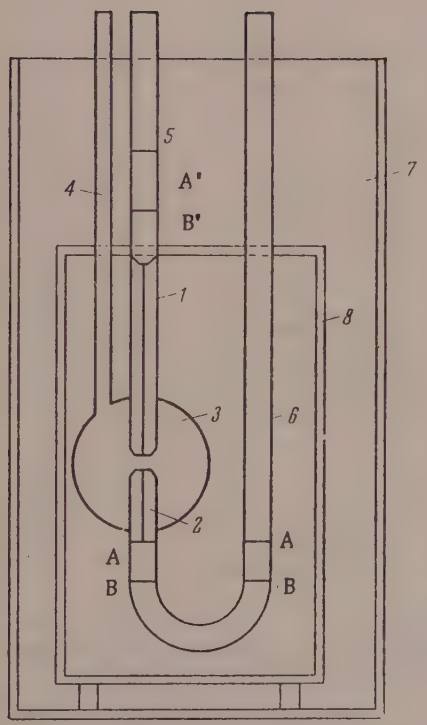


Fig. 3. The Deryagin–Levi dual-temperature viscosimeter.

thixotropic increase of viscosity and yield value. Data on the thixotropic increase of yield value and viscosity in relation to the degree of structural buildup are plotted in Fig. 5. Longer observations of structure development may give rise to errors because of thermal hydrolysis of gelatin solutions on standing, and therefore such experiments would not be of value.

The gelatin solution loses mobility and forms a gel after a decrease of temperature which is specific for each type of gelatin. This process is usually accompanied by a sharp increase of the yield value, due to rapid development of intermolecular bonds, as the result of the loss of mobility by the gelatin molecules. The gelatin then passes from an elastico-viscous liquid into an elastic body. This process is accompanied by rapid increase of the yield value (Table 2).

Data on the increase of the elasticity modulus of gelatin in solution as the result of prolonged standing are contained in an interesting paper by Roloff and Schinie [9].

Further mutual approach of the gelatin molecules, which occurs when the gelatin passes into the xerogel form, i.e., during drying, results in formation of very considerable intermolecular forces and also, apparently, in deformation of the molecules. This structural change is accompanied by further increase of elasticity in gelatin films. In Fig. 6 the tensile curve for a film of gelatin xerogel is plotted in deformation (ϵ), stress (τ) coordinates. It follows from Fig. 6 that gelatins are elastic bodies with a very small region of plastic deformation, and break down like brittle solids. It is interesting to note that in the Hookeian region a gelatin film exhibits, within the limits of experimental error, completely reversible deformation (without elastic hysteresis loops) when loaded during times up to 150 hours. In Fig. 6 (curve 1) the points corresponding to extension and contraction of the gelatin film fit almost exactly on the same straight line. Figure 6 also shows the effect of molecular weight on the behavior of gelatin films in deformation under identical conditions. It is clear from Fig. 6 that the range of plastic deformation of gelatin films increases in proportion to the molecular weight.

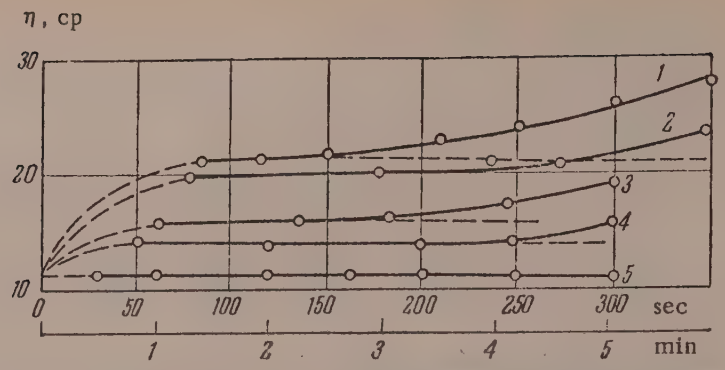


Fig. 4. Changes of viscosity with time after rapid cooling of gelatin solutions: 1) from 40 to 29°; 2) from 40 to 30°; 3) from 40 to 32°; 4) from 40 to 35°; 5) 40°.

TABLE 1

Variations of the Physical and Mechanical Properties of Gelatin on Cooling

Cooling temperature, °C	35	32	30	29
Temperature drop, °C	5	8	10	11
Time to reach constant η, sec	50	60	100	100
Duration of constant η, sec	150	80	80	15
Viscosity increase after 300 sec	0.8	1.6	0.8	4.5
Yield value after 300 sec, dynes/cm^2	2.8	–	8.2	28.5
Plastic viscosity	13.6	16.0	20.9	27.6

TABLE 2

Variations of the Yield Values of Gelatin Solutions (at 35°) and Gels with Concentration and Viscosity of the Original Solutions

Viscosity [η]	0.32	0.32	0.65	0.65
Concentration of original solution, %	5	10	5	10
Yield value of solution, dynes/cm^2	0	3.0	0.63	3.4
Same, of gel	600	1500	950	1850

It seems that the elasticity of gelatin stems from a molecular configuration at which the molecules lose mobility both as the result of their own rigidity and owing to formation of intermolecular bonds. Therefore gelatin films could be plasticized by altering the configuration of the gelatin molecules, which causes hardness, or by weakening of the intermolecular bonds. This can be effected either by addition of surface-active substances or by introduction of filler inert toward gelatin. Changes in the configuration of gelatin molecules can be characterized by the molecular asymmetry factor [3]. It has been shown [10] that a number of surface-active substances, such as succinic acid sulfonic esters, increase the asymmetry factor from 18 to 38. This increase is accompanied by increase of solution viscosity and plasticization of gelatin xerogels. The plasticizing action of sodium di-2-ethylhexylsulfosuccinate is illustrated in Fig. 7 (curve 2).

In experiments performed jointly with O. K. Smirnov the inactive fillers used were methyl- and ethylsiloxanes in the form of emulsions containing particles comparable in size to microcrystals of silver halides in photographic emulsions; their plasticizing effects are shown in Fig. 7 (curve 3). It follows that structural properties arise in gelatin in consequence of its specific molecular configuration and formation of intermolecular bonds.

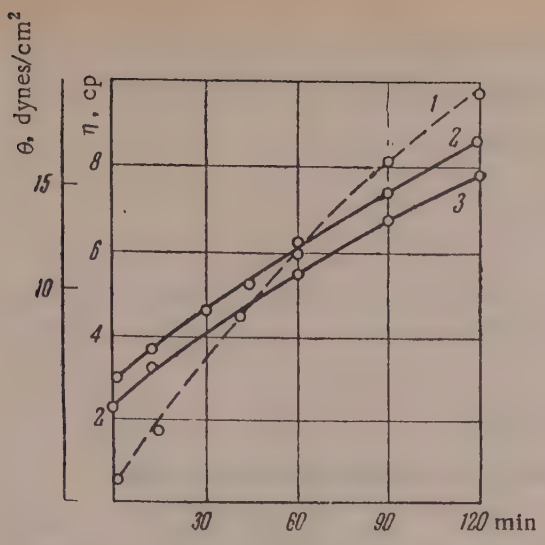


Fig. 5. Variations of yield value (1) and viscosity at maximum water-gauge pressures of 40 cm (2) and 10 cm (3) with time.

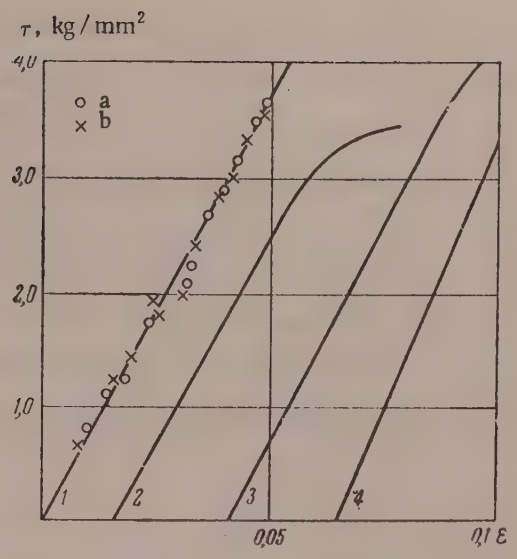


Fig. 6. Extension curves for gelatin xerogels: 1) Extension (a) and contraction (b) of gelatin films; 2) gelatin of $[\eta] = 0.65$; 3) gelatin of $[\eta] = 0.32$; 4) gelatin of $[\eta] = 0.12$.

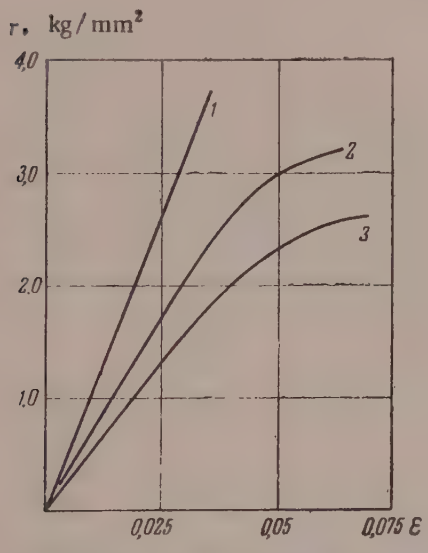


Fig. 7. Extension curves for gelatin films: 1) Not plasticized; 2) plasticized with sodium diethylhexylsulfosuccinate; 3) plasticized with inactive filler.

SUMMARY

1. Gelatin solutions are either Newtonian liquids or elasticoviscous bodies, dependent on temperature and concentration. At temperatures above 38-40° and < 15% concentration gelatin solutions have the properties of Newtonian liquids; below 40° they have the properties of elasticoviscous bodies.

2. Structure formation during the cooling of gelatin solutions requires a definite time, during which the solutions exhibit viscosity only; the duration of the structure formation period depends on the temperature drop.

3. As soon as a structure has been formed in a gelatin solution the solution exhibits continuous thixotropic increase of viscosity and of yield value, in proportion to the molecular weight of the gelatin. As the result of this process the gelation solution loses fluidity and becomes a gel.

4. When the gelatin passes into the gel form the solution structure undergoes a significant change which leads to an abrupt increase of yield value and elasticity modulus.

5. The rheological properties of gelatin gels and xerogels are determined by molecular configuration and intermolecular bonding. If the configuration of gelatin molecules is altered, by uncoiling by the action of surface-active substances or by breakdown of intermolecular bonds by inert fillers, gelatin gels and xerogels are plasticized.

LITERATURE CITED

[1] F. N. Shvedov, J. de Phys. 8, (2) 341 (1889); 9 (2) 34 (1890).

[2] M. P. Volarovich and S. M. Levi, Kolloid. Zhur. 18, 2, 129 (1956).*

[3] S. M. Levi, Collection: Advances in Scientific Photography [in Russian] (Izd. AN SSSR, 1960) No. 7.

[4] Ya. I. Frenkel', Kinetic Theory of Liquids [in Russian] (Izd. AN SSSR, 1945).

[5] R. N. Boque, J. Amer. Chem. Soc. 43, 1767 (1921).

[6] E. E. Schepperd, J. Phys. Chem. 29, 1224 (1925).

[7] M. I. Shor, Zhur. Priklad. Khim. 24, 748 (1951).

[8] B. V. Deryagin and S. M. Levi, Kolloid. Zhur. 15, 29 (1953).*

[9] Roloff and Schinie, Phys. Z. No. 64 (1906).

[10] B. V. Deryagin and S. M. Levi, Author's Certif. No. 114314.

[11] B. V. Deryagin and S. M. Levi, Izvest. Akad. Nauk SSSR, Otdel. Tekhn. Nauk 9, 43 (1950).

* Original Russian pagination. See C. B. Translation.

STRUCTURE FORMATION IN SUSPENSIONS OF ASKANGEL AND ITS DERIVATIVES

O. M. Mdivnishvili, G. V. Vinogradov, and S. A. Gol'din

Caucasian Institute of Mineral Raw Materials, Tbilisi
Translated from Kolloidyni Zhurnal, Vol. 22, No. 5, pp. 606-610,
September-October, 1960
Original article submitted July 21, 1960

There have been relatively few studies of structure formation in clay suspensions by optical and electron microscopy, although correlation of rheological studies of various structures with direct observations is of great theoretical and practical interest.

The results of ultramicroscope observations of the gelation of bentonite suspensions are given in the first reported studies of structure formation in bentonite [1] and in somewhat later publications [2]. Unfortunately, the disadvantage of ultramicroscope observations is that the observer sees only the light reflected and scattered by the particles but does not see the configuration of the particles themselves. Therefore much more interest attaches to the work of Hauser [3-5], who prepared films from bentonite suspensions and gels on smooth, hard surfaces of film materials. Hauser observed film formation under the microscope in a dark field and found that the individual colloidal clay particles join into chains when dried. These aggregates intersect and interweave, forming a coherent fabric-like microstructure. X-ray studies of these films showed that the particles which are of plate shape are all orientated with their flat surfaces parallel to the support, with their crystallographic c-axis perpendicular to it. However, Hauser does not state anywhere that similar chains can exist in undried suspensions, and does not associate the formation of a fibrous microstructure in bentonite films with characteristics of structure formation in bentonite suspensions. Moreover, Hauser used gels of fine fractions of native bentonite, and did not refer to the influence of the nature of exchange cations on the structure of the films formed by drying of the suspensions on solid smooth surfaces.

The first attempt to study under the microscope the nature of structure formation in clays saturated with various cations [6] was made with previously coagulated systems (coagels) which were subsequently dried; this restricts the scope of the investigation considerably and limits the validity of the author's conclusions.

In recent years the structures of various disperse systems have been extensively studied by electron microscopy; this is a method of great potentialities, in particular for the characterization of such finely divided materials as clay minerals in askangel suspensions, and sodium and calcium derivatives of askangel [7]. A network structure was discovered in suspensions of native askangel [7].

We used microscopy and electron microscopy for studying structure formation in suspensions of bentonite saturated with various cations. A Zeiss biological microscope with a photographic attachment was used for microscope studies of the nature of structure formation in bentonite suspensions. By means of photographic enlargement an ultimate magnification of 1300 was obtained. The advantage of the optical over the electron microscope is that much more concentrated suspensions can be used. This is a factor of considerable importance in studies of structure formation.

The monosubstituted askangel derivatives were prepared by the method described previously [8]. The concentration of the original bentonite suspension was 5-6%. The suspension was spread in a very thin layer on a microscope slide and dried at room temperature. In some instances wet specimens were also examined,

but the structure in the latter is visible only at low moisture contents. The specimens were examined by transmitted ordinary and polarized light; a phase-contrast device was also used. The results obtained in all three cases were similar, and therefore only the micrographs obtained by ordinary transmitted light are given here (Fig. 1).

It is evident from these photographs that the type of structure formed by the particles of Na-bentonite (Fig. 1a) differs considerably from that formed by particles of native askangel (Fig. 1b), Ca-bentonite (Fig. 1c), and Al-bentonite (Fig. 1d). The main structural difference of the latter lies in the degree of structural homogeneity, which diminishes in the series from askangel to Ca- and Al-bentonite; this is due to differences in the packing density of primary particles in secondary aggregates, which increases in the series from askangel to Ca- and Al-bentonite.

Specimens of askangel, Ca-bentonite, and Al-bentonite exhibit a granular structure (by grains we mean aggregates of irregular shape, formed by coagulative cohesion of the primary platelets). The grains are of a low degree of asymmetry.

In contrast to this, Na-bentonite specimens show the formation of a fibrous structure, consisting of sharply anisodiametric fibers of few microns across. Experiments with the fine askangel fraction, isolated by prolonged sedimentation from a native askangel suspension, give results qualitatively similar to those with Na-bentonite. In this case aggregates in the form of fine fibers (Fig. 1e), are seen in addition to the granular aggregates. These fibers do not form the continuous spatial network seen in Fig. 1a. The structure formed in such systems is of a mixed character, i.e., it contains both granular and fibrous particles. The present investigation therefore shows that the fibrous structure found by Hauser in dried films of Wyoming bentonite is typical for Na-bentonite.

In suspensions of Na-bentonite, the exchange complex of which is almost completely saturated with sodium ions, the predominant and perhaps the principal structural type is the fibrous type, formed from aggregates of sharply anisodiametric form (Fig. 1a). Such fibers can be formed only if the clay is peptized to the limit and the system contains sufficient primary particles of plate shape. This is the case to the greatest extent in Na-bentonite suspensions. Interaction of the primary particles may occur either by cohesion of the plates by their corners and edges through thin water interlayers, or by decrease of the charge at these regions of the plate surfaces (owing to suppressed dissociation of the compound $Na^+AlO_2^-$ in a neutral medium) [9], or perhaps in consequence of the large dipole moments of colloidal clay particles [10], so that the particles are attracted to each other and are orientated in a definite direction to form fibers.

It has been suggested [11] that a fibrous structure exists in Na-bentonites before the systems are dried. To confirm this hypothesis, the structure was subjected to orientation in flow or in an electric field, and then dried. An orientated fibrous structure is clearly seen in the dried specimens (Fig. 1f and 1g).

Specimen 1f was obtained as follows. A drop of Na-bentonite suspension was placed on a slide. On it was placed a cover glass which was moved in the direction indicated by the arrow in Fig. 1f, past the specimen, and the specimen was then dried in air. Figure 1g represents the structure of a Na-bentonite film dried on glass after the suspension had been subjected to a direct electrical field (gradient of ~10 v/cm). The field was applied to two copper wires immersed in the drop of Na-bentonite suspension. Figure 1g shows orientation of the particles at the anode. The situation at some distance from the electrode is typical for nonorientated specimens of Na-bentonite. Longer action of the electrical field results in orientation of all the particles in the space between the electrodes.

The following experiment was also of certain interest. A drop of bentonite suspension was placed on a slide and frozen. The ice was sublimed under vacuum. This gave a specimen of air-dry bentonite (aerogel) which was examined under the microscope. It was found that crystallization of water produces a threadlike structure (Fig. 1h), where the direction of the threads is determined by the direction of growth of the ice crystals.

These results of microscopic examination of dry Na-bentonite films lead to the important conclusion that the structures formed by bentonite are highly labile (mobile). This characteristic of Na-bentonite is closely associated with the rheological and, in particular, with the thixotropic properties of its suspensions [8]. Suspensions and gels of Na-bentonite are characterized by a high rate of thixotropic buildup with a sharp transition between the states in which the systems behave as Newtonian liquids at moderate and at high rates of deformation in steady flow; i.e., the transition from one state to the other occurs in a narrow range of deformation rates.

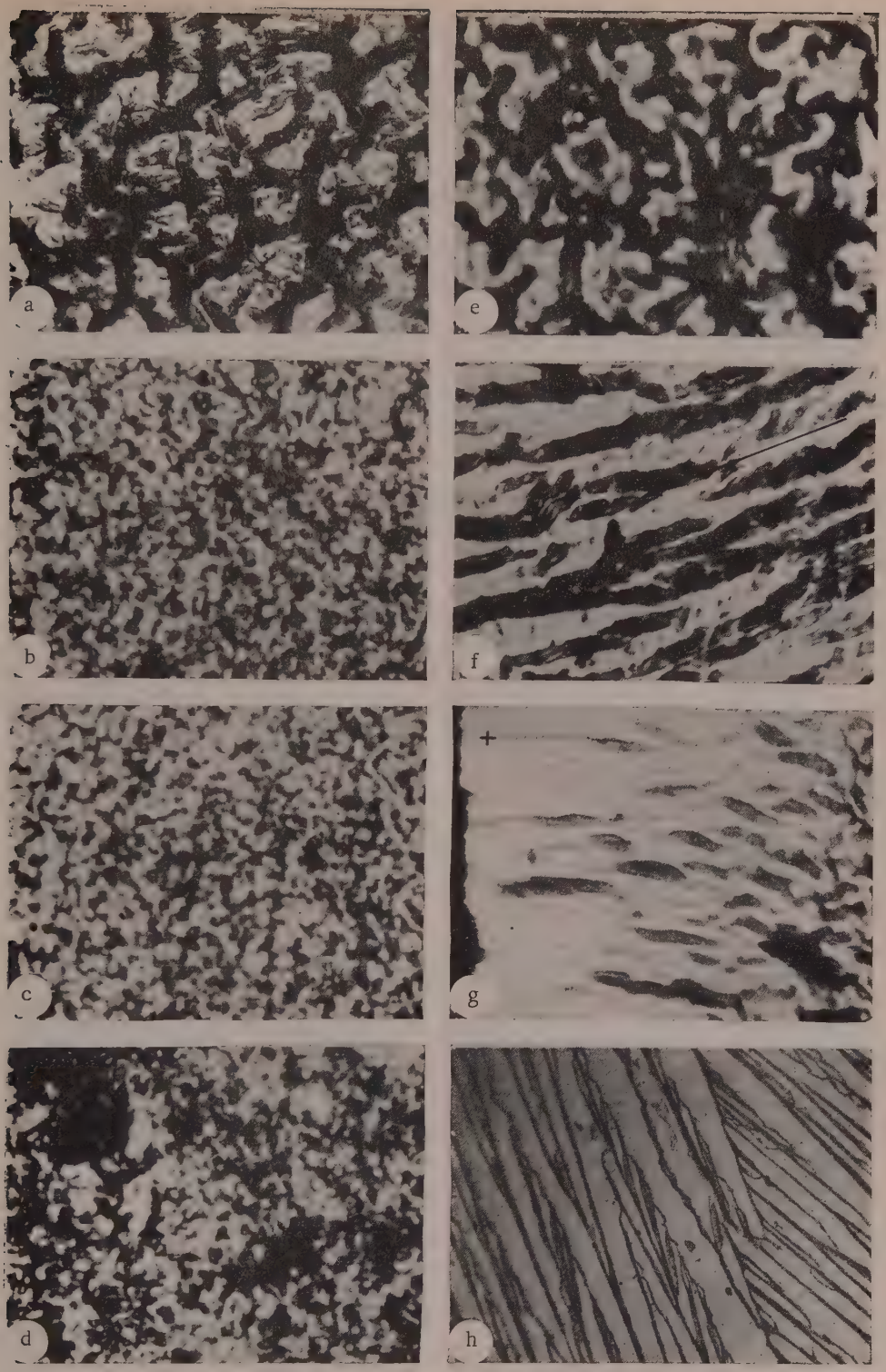


Fig. 1. Microphotographs of dry films: a) Na-bentonite (× 900); b) native askangel (× 900); c) Ca-bentonite (× 900); d) Al-bentonite (× 900); e) fine fraction of native askangel; f, g, and h) Na-bentonite orientated in flow, an electrical field (× 900), and by crystallization of water (× 60).

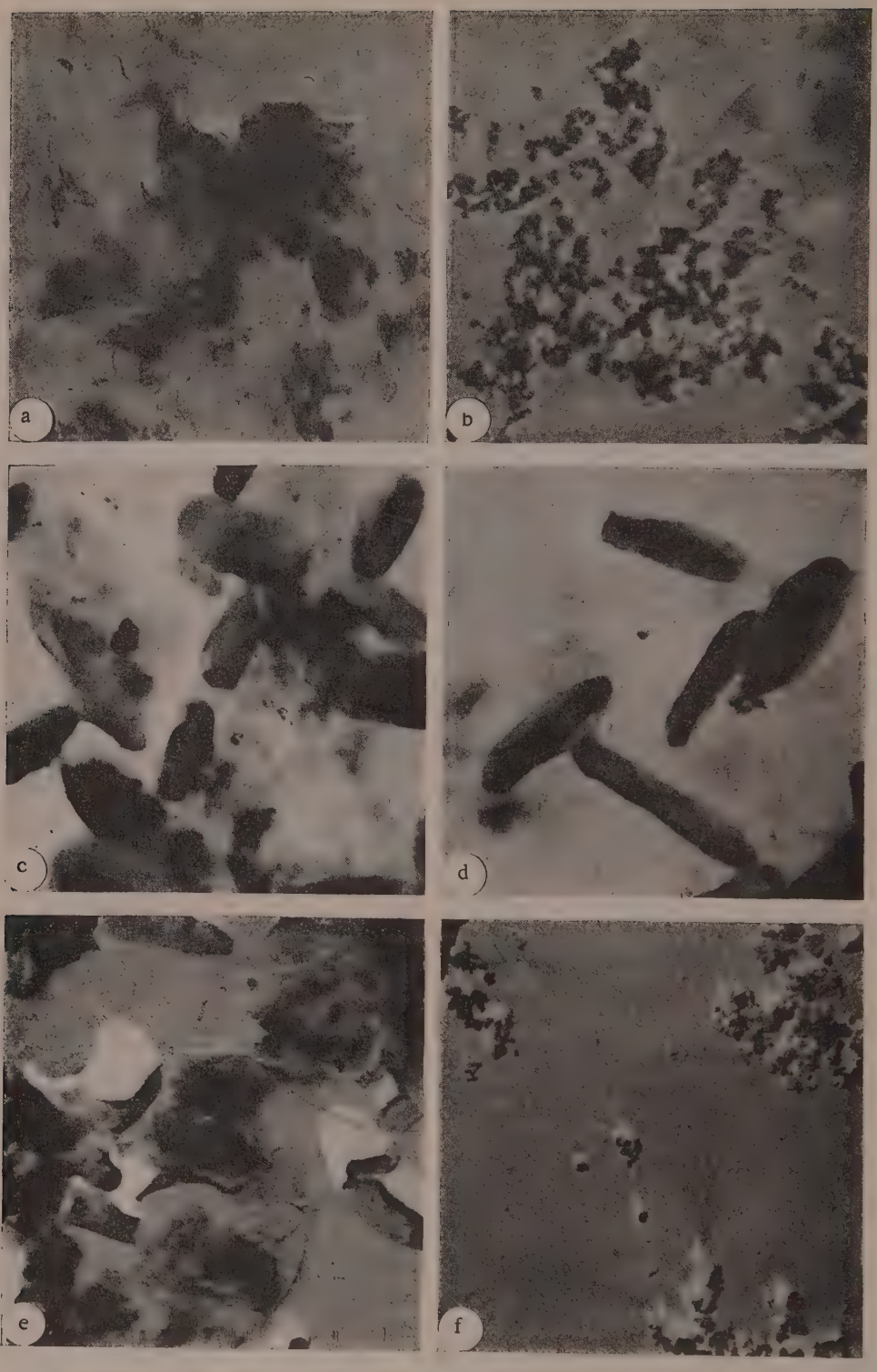


Fig. 2. Electron micrographs of films (× 20,000): a) Native askangel; e) Al-bentonite; b and f) silica particles; c and d) Ca-bentonite.

The micrographs in Fig. 1f and 1g, although not a direct proof, are in our opinion convincing indirect evidence for the possible existence of a fibrous structure in undried Na-bentonite suspensions and gels.

In addition to the structure studies by means of the optical microscope, we investigated the same materials by means of the ÉM-3 electron microscope. Very dilute clay suspensions, in which structure formation is weak,

were used. The bonds between the individual fine particles, which arise when such systems are dried, may be the result of accidental cohesion and need not always correspond to the type of structure found at high concentrations of the disperse phase in the system. This applies especially to easily peptized systems such as Na-bentonite suspensions. Coagulated suspensions of Na- and Al-bentonites are not peptized even at very high dilutions and retain fragments of coagulative structure. In view of all this, specimens of native askangel and of Ca- and Al-bentonites were prepared in the usual way by application of a drop of the suspension on a support, with subsequent drying. The concentration of the original suspension did not exceed 0.1%. A different technique was used with Na-bentonite. A suspension of Na-bentonite containing 4-5% of the disperse phase was applied onto glass in a thin layer and dried. The dried film was then covered with a solution of nitrocellulose in amyl acetate and dried again. The resultant film was trimmed at the edges and removed from the glass. The clay layer previously applied onto the glass came off with the film. The film with its thin clay layer was immersed in distilled water, which was changed several times. This caused gradual peptization of the clay in water and removal of clay from the film. The washing was terminated when the clay layer on the film became so thin that it was visible only under the microscope. The film with its very thin clay layer was then dried and immersed in amyl acetate. Nitrocellulose dissolved in the amyl acetate and the thin clay film remained in the solution; it was then taken out onto a support, dried, and examined in the electron microscope.

Examination of such films in the electron microscope (Fig. 2) showed that the particles of native askangel consist of very thin semitransparent platelets of irregular form (Fig. 2a). The width and length of these plates vary in fairly wide limits, from 0.05 to 1.5 μ; the thickness varies from 0.05 to 0.1 μ. Examination of native askangel specimens in the electron microscope reveals network and cluster formations consisting of chains and aggregates of spherical particles (Fig. 2b). Similar clusters of spherical particles are seen in Al-bentonite specimens (Fig. 2f). The size (average diameter) of these particles is in the 0.05-0.2 μ range. The picture presented by Fig. 2d and 2e corresponds to what is known for silica and aluminum hydroxide gels [12]. We therefore consider that the network structure shown in Fig. 2b and 2d, and described earlier [6, 7] is to be attributed to the silica present in native askangel.

As already noted, Na-askangel in an aqueous medium is a well-peptized system; the clay particles are therefore so small that they are difficult to distinguish even under the electron microscope, especially if the specimens are prepared in the usual way from very dilute suspensions. When the specimens were prepared by the technique described above from much more concentrated suspensions, they were too thick for individual particles to be seen; only large aggregates were visible, and these can be approximately regarded as elements of the fibrous structure. To determine the structure of cellular – fibrous Na-bentonite films it is necessary to work out a special replica technique, as attempts to prepare replicas by the usual methods proved unsuccessful.

Interesting micrographs were obtained in studies of Ca-bentonite specimens (Fig. 2e and 2f). Individual particles forming the structure are seen distinctly here, as they are fairly large and very markedly anisodiametric. In this case the crystallites are 1.0-3.0 μ long, 0.5-1.0 μ wide, and up to 0.1 μ thick. These crystallites are joined by the edges, mainly at their ends. Similar particles are observed in Al-bentonite specimens (Fig. 2c), but larger aggregates formed from laminar particles are seen here; there are also clusters of particles close to spherical in form (Fig. 2d).

SUMMARY

1. The structure of dried gel specimens of native askangel and its Na-, Ca-, and Al-derivatives has been studied by optical and electron microscopy.

It is shown that the cellular–fibrous structure in dry films of Wyoming bentonite, described by Hauser, is typical of Na-bentonite only.

2. The structure of the film varies in accordance with the treatment of the suspension (action of an electrical field, shear, freezing) before it is dried. This confirms the hypothesis that a cellular–fibrous structure, which is highly labile, also exists in Na-bentonite suspensions. The high lability and the character of the cellular–fibrous structure in Na-bentonite accounts for the rheological characteristics of Na-bentonite suspensions.

3. Native askangel contains three types of structure: 1) cellular–fibrous structure of Na-bentonite; 2) a granular mass consisting of aggregates of laminar particles of mixed Na, Ca-bentonite; 3) a granular mass consisting of chain formations and clusters of spherical particles; it is suggested that these are silica particles.

4. Primary individual particles could not be revealed in Na-bentonite under the electron microscope. A specialized replica technique must be evolved for interpretation of the structure in cellular–fibrous Na-bentonite films.

The particles of Ca- and Al-bentonite are anisodiametric platelets easily distinguishable in the electron microscope.

LITERATURE CITED

[1] A. Szegvari and H. Schalek, Koll. Z. 33, 326 (1923).

[2] B. S. Kandelaki, Kolloid. Zhur. 3, 395 (1937).

[3] E. A. Hauser and D. S. LeBeau, J. Phys. Chem. 42, 961 (1938).

[4] E. A. Hauser and D. S. LeBeau, in the Collection: Physical Chemistry of Clay Suspensions [Russian translation] (Gostoptekhizdat, 1947) p. 60.

[5] E. A. Hauser, Silicic Science (Van Nostrand, 1955).

[6] I. V. Popov, Collection: Problems of Soviet Soil Science [in Russian] (1949) No. 15, p. 174.

[7] E. I. Kobakhidze and M. E. Shishniashvili, Kolloid. Zhur. 19, 59 (1957);* É. D. Uznadze and M. E. Shishniashvili, Kolloid. Zhur. 19, 368 (1957).*

[8] O. M. Mdivnishvili and G. V. Vinogradov, Kolloid. Zhur. 20, 569 (1958).*

[9] I. A. Uskov and E. T. Uskova, Kolloid. Zhur. 19, 361 (1957).*

[10] N. A. Tolstoi, Doklady Akad. Nauk SSSR 100, 893 (1955).

[11] O. M. Mdivnishvili, Dissertation [in Russian] (Georgian Polytechnic Institute, Tbilisi, 1959).

[12] Z. Ya. Berestneva and V. A. Kargin, Kolloid. Zhur. 17, 196 (1955).*

* Original Russian pagination. See C. B. Translation.

DEPENDENCE OF THE SEDIMENTATION RATE OF A SUSPENSION ON THE SOLUTION VELOCITY

G. A. Ostroumov

Perm' University

Translated from Kolloidnyi Zhurnal, Vol. 22, No. 5, pp. 611-614,
September-October, 1960
Original article submitted November 15, 1959

Decantation of suspensions is commonly used in various industries. Sedimentation and sedimentometric analysis are the laboratory and metrological analogs of this process [1]. It is known that even slow motion of the solution slows down sedimentation substantially, while rapid motion (in stirring or shaking) leads to resuspension of the sediment. However, no calculations relating to this process could be found in the available literature. It is not clear what solution velocities are permissible for sedimentation to proceed without serious hindrance, at what velocities it ceases, and at what velocities sedimentation is replaced by resuspension of the sediment formed.

Some simple considerations leading to an approximate theory of the problem are put forward below; for the sake of definiteness the range of ideas utilized is defined by enumeration of the known formulas.

Let us assume that the suspension or emulsion obeys the laws of ideal gases up to the high concentration which the precipitate possesses. The upper limit to the concentration of the uncoagulated particles will be $C_0 = 1/8\ a^3$, ml, where a is the radius of the suspended particles which we will assume to be spherical and have granulometric homogeneity.

On the assumption that Stokes' law is valid, the sedimentation rate (v) in an absolutely still solution is

$$v = \frac{2}{9}\left(\frac{\rho}{\rho_0} - 1\right)\frac{a^2 g}{\nu}, \tag{1}$$

where g = 981 cm/sec^2, the acceleration due to gravity; ρ/ρ_0 is the ratio of the densities of the particle material and the solvent; ν is the coefficient of kinematic viscosity of the solvent.

The number of particles q_m deposited per unit area per second is

$$q_m = vc_0 = (\rho/\rho_0 - 1)\, g/36\, \nu a. \tag{2}$$

To find the mass of the deposited particles, the above expression is multiplied by the mass of a single particle and the area of the floor of the vessel.

The distribution of particle concentration over the completely settled sediment is given by the barometric formula

$$c(h) = c_0 e^{-h/H};\ H = D/v;\ D = kT/6\pi a\rho_0\nu, \tag{3}$$

where h is the height of a layer of concentration c above the sediment surface; D is the diffusivity of the particles in this layer; k is the Boltzmann constant; T is the absolute temperature; H is the characteristic height over which the concentration decreases by a factor e.

The average concentration in a vessel at a height of B cm over the sediment is

$$c_1 = c_0 H(1 - e^{-B/H})/B = H(1 - e^{-B/H})/8a^3 B. \tag{4}$$

If the average concentration is less than c_1 a sediment is not formed at all. The greater the value of B, the lower the average concentrations which give sediments.

The barometric equilibrium concentration distribution may be represented as the superposition of two countercurrent particle streams. A stream vc of settling particles moves downward, and an equal diffusional stream moves upward:

$$q_d = D \cdot dc/dh. \tag{5}$$

When these two flows are equal, the barometric distribution is in dynamic equilibrium. In particular, on the bottom of the vessel

$$q_{d_0} = Dc_0/H. \tag{6}$$

If the liquid now flows parallel to the horizontal bottom of a vertical cylindrical vessel of diameter Φ at an average velocity U, then a hydrodynamic boundary layer [2, p. 16] is formed at the bottom; its thickness is

$$\delta_1 = \sqrt{\Phi\nu/U};\ U = \Phi\nu/\delta_1^2. \tag{7}$$

The following velocity gradient is established in it:

$$\frac{du}{dh} = U/\delta_1 = \Phi\nu/\delta_1^3;\ \delta_1 = \left(\frac{\Phi\nu}{du/dh}\right)^{1/3}. \tag{8}$$

The presence of the hydrodynamic boundary layer leads to the formation of diffusional boundary layer [2, p. 46] the thickness of which is of the following order of magnitude:

$$\delta_2 = \delta_1 (D/\nu)^{1/3} = \left(\frac{\Phi D}{du/dh}\right)^{1/3} \tag{9}$$

Over this layer the particle concentration varies from c_0 at the sediment surface to c_2 in the solution, and the second concentration is virtually constant throughout the vessel (because of agitation of the liquid by the stream). The diffusional flow of particles upward within the boundary layer is now not q_0 but

$$q_d = D(c_0 - c_2)/\delta_2 = (c_0 - c_2) \cdot \left(\frac{D^2 du/dh}{\Phi}\right)^{1/3}. \tag{10}$$

This may be less than, equal to, or greater than the flow of settling particles v_0. In the first case the role of such weak flow would have little effect on the process and the sedimentation rate, and in the last case sedimentation is replaced by resuspension of the sediment. The boundary case is represented by the equation

$$(c_0 - c_2) \cdot \left(\frac{D^2}{\Phi} \cdot \frac{du}{dh}\right)^{1/3} = Dc_0/H. \tag{11}$$

Hence the critical velocity gradient for sedimentation is:

$$\frac{du}{dh} = \frac{\Phi D}{H^3(1 - c_2/c_0)^3} = \frac{32\pi^2 g^3}{81} \cdot \frac{\rho_0^2(\rho/\rho_0 - 1)^3 a^8}{\nu} \cdot \cdot \frac{\Phi}{(kT)^2} \cdot \left[1 + 3\frac{c_2}{c_0} + 6\left(\frac{c_2}{c_0}\right)^2 + 10\left(\frac{c_2}{c_0}\right)^3 + 15\left(\frac{c_2}{c_0}\right)^4 + \ldots\right]. \tag{12}$$

The great significance of the density ratio ρ/ρ_0 is very striking here: the critical velocity gradient decreases in proportion to the cube of the difference between this ratio and unity. The particle size is even more significant: if the diameter is halved, the critical velocity gradient is diminished 256-fold.

The solvation layers on the particles play a peculiar role. Suppose that a particle of true radius a and density ρ is surrounded by a solvation layer a_1 thick, with the density of the solvent ρ_0. The effective mass of the particle, multiplied by $^3/_4 \pi$, then becomes

$$(a + a_1)^3 \rho_1 = (a + a_1)^3 \rho_0 - a^3\rho_0 + a^3\rho. \quad (13)$$

Hence its effective relative density is

$$\rho_1/\rho_0 = 1 + (\rho/\rho_0 - 1)\, a^3/(a + a_1)^3 = 1 + (\rho/\rho_0 - 1)/(1 + a_1/a)^3. \quad (14)$$

The critical velocity gradient is altered in such a manner that $(\rho/\rho_0 - 1)^3 a^8$ is divided by $1 + a_1/a$, i.e., the critical flow velocity is reduced in that proportion. This may partially account for the fact that solvated particles settle with more difficulty than nonsolvated.

Thermal convection currents are said to be one of the causes of flow in sedimenting suspensions [1]. The nature of these currents in unilateral heating may be represented by reversal of Fig. 3 in [3], and also from [4].

SUMMARY

1. With certain simplifying assumptions (that the suspension conforms to the ideal gas laws and that the particles are spherical and of uniform size) it is possible to derive theoretically the basic laws of sedimentation in a liquid completely at rest.

2. These basic laws may be extended to the case of a flowing liquid by means of the known concepts of hydrodynamic and diffusional boundary layers.

3. A mathematical expression for the critical flow velocity gradient has been derived: at lower velocities the sediment grows, while at higher velocities it is resuspended.

4. The critical velocity gradient depends greatly on the relative density and relative concentration of the particles, and very greatly on the particle size: if the size is halved, the critical flow velocity is diminished 256-fold.

5. Particle solvation decreases the critical liquid velocity in a ratio equal to the ratio of the diameter of the solvation layer to the diameter of the particle proper.

LITERATURE CITED

[1] N. A. Figurovskii, Sedimentometric Analysis [in Russian] (Moscow-Leningrad, 1948).

[2] V. G. Levich, Physicochemical Hydrodynamics [in Russian] (Izd. AN SSSR, 1952).

[3] G. A. Ostroumov, Free Convection in the Conditions of an Internal Problem [in Russian] (GTTI, Moscow-Leningrad, 1952).

[4] A. A. Boyarshinova, Uch. Zap. Molotovskogo Gos. Univ. 9, 4, 61 (1955).

THEORY OF COLLOID HETEROCOAGULATION IN COMPLEX SOLUTIONS OF ELECTROLYTES

V. P. Smilga

Institute of Physical Chemistry, Academy of Sciences of the USSR, Moscow
Translated from Kolloidnyi Zhurnal, Vol. 22, No. 5, pp. 615-624,
September-October, 1960
Original article submitted June 18, 1959

The theory of interaction of particles of unlike charge in solutions of binary electrolytes was developed in earlier publications [1, 2].

In the present paper we consider interaction in an electrolyte consisting of a mixture of different ions of any desired complexity.

We first solve the problem of the interaction of two plane-parallel plates with potentials ψ_1 and ψ_2 and separated by a layer of solution of thickness H.

The potential φ in solution can be found from the equation:

$$\frac{d^2\varphi}{dx^2} = -\frac{4\pi e}{\varepsilon}\left(\sum_c z_c n_{c0} e^{-\frac{z_c e\varphi}{kT}} - \sum_a z_a n_{a0} e^{\frac{z_a e\varphi}{kT}}\right). \quad (1)$$

Here e is the electronic charge; ϵ is the dielectric constant; n_{c0} and n_{a0} are the numbers of cations and anions, respectively, per unit volume of solution; x is the distance of the given point from the surface of the plate of potential ψ_1; $z_c e$ and $-z_a e$ are the charges of cations and anions of definite types.

In absence of a field the electrolyte is, naturally, electrically neutral, i.e.,

$$\sum_c z_c n_{c0} - \sum_a z_a n_{a0} = 0. \quad (2)$$

It follows from Eq. (1) that the charge density depends only on φ. Therefore, representing the right side of Eq. (1) by $\rho(\varphi)$ and integrating, we easily find the first integral

$$\frac{\varphi'(x)^2}{2} = \int_{\varphi(0)}^{\varphi(x)} \rho(\varphi)\, d\varphi + \frac{\varphi'(0)^2}{2}. \quad (3)$$

The boundary conditions for solution of Eq. (1) are of the form $\varphi(0) = \psi_1$ and $\varphi(H) = \psi_2$.

It should be pointed out that repeated integration of Eq. (1) is necessary only insofar as it is otherwise impossible to find $\varphi'(0)$ and $\varphi'(H)$; in general, the force between the plates is determined by the first integral of Eq. (1).*

* It is interesting to note in this connection that for determination of the interaction force it is, in general, sufficient, without solving Eq. (1), to formulate the Neumann boundary problem for it, equivalent to the Dirichlet problem under consideration.

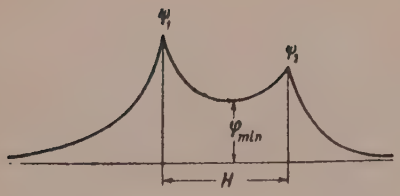


Fig. 1. Integral curve of Eq. (3) for the variant ($H_m < H < \infty$). Here φ_{min} is the minimum value of the potential in the space between the plates.

In fact, it is known [3] that the force on interaction per unit area (F) is:

$$F = \frac{\varepsilon}{8\pi}[E_1^2(0) - E_2^2(0)] = \frac{\varepsilon}{8\pi}[E_1^2(H) - E_2^2(H)]. \quad (4)$$

Here $E_1(0)$, $E_1(H)$, and $E_2(0)$, $E_2(H)$ are the forces acting on the outer and inner sides of the first and second plates. To determine $E_1(0)$ and $E_1(H)$ we use Eq. (3), remembering that $d\varphi/dx = 0$ when $\varphi = 0$. We then have

$$E_1^2(0) = 2\int_0^{\psi_1} \rho(\varphi)\, d\varphi \quad (5)$$

$$E_1^2(H) = 2\int_0^{\psi_2} \rho(\varphi)\, d\varphi. \quad (5a)$$

It follows from Eq. (4) that when the interaction forces are positive the plates repel each other. We now integrate Eq. (1) for the case when the plate potentials ψ_1 and ψ_2 are of the same sign. For example, suppose that $\psi_1 > \psi_2 > 0$. If the potentials of the plates are of different signs, analysis of the problem is trivial, and will be presented at the end of this article.

Three variants are possible in the present case, such that the integral curve of Eq. (1) has a minimum in the range of values from 0 to H^*; 2) has no minimum, but

$$\varphi'(0)^2 \leqslant 2\int_0^{\psi_1} \rho(\varphi)\, d\varphi;$$

3) has no minimum, but

$$\varphi'(0)^2 > 2\int_0^{\psi_1} \rho(\varphi)\, d\varphi.$$

Any of these variants may occur, in accordance with the distance between the plates, with given ψ_1 and ψ_2.

We now consider each of these three variants in turn.

Variant 1. $H_m \leq H \leq \infty$ (Fig. 1), where H_m is the least distance between the plates at which the integral curve of Eq. (3) still has a minimum in the middle region.

Integrating Eq. (3) with the second boundary condition taken into account, we have:

$$\sqrt{2}\,H \equiv D_1(\psi_1;\ \psi_2;\ \varphi_{min}) = \int_{\varphi_{min}}^{\psi_1} \frac{du}{\sqrt{\int_{\varphi_{min}}^{u} \rho(t)\, dt}} + \int_{\varphi_{min}}^{\psi_2} \frac{du}{\sqrt{\int_{\varphi_{min}}^{u} \rho(t)\, dt}}. \quad (6)$$

When H is known from Eq. (6), φ_{min} can be uniquely determined.

It can be shown that when H is varied from ∞ to a certain value H_m, φ_{min} changes correspondingly from 0 to ψ_2.

When the distance between the plates is less than

$$H_m \equiv \frac{1}{\sqrt{2}} D_1(\psi_1;\ \psi_2;\ \psi_2) = \frac{1}{\sqrt{2}} \int_{\psi_2}^{\psi_1} \frac{du}{\sqrt{\int_{\psi_2}^{u} \rho(t)\, dt}} \tag{6a}$$

the minimum disappears from the integral curve. It is easily seen that the repulsion force between the plates is greatest at $H = H_m$.

In fact, F is determined by the difference between the forces acting on the outer and inner sides of the plate. The force acting on the outer side of either plate is completely determined by the plate potential and is independent of the distance between the plates. Naturally, the interaction force may be determined in relation to either plate [in accordance with Newton's third law, the validity of which for the given system is confirmed most simply by establishment of the relation between $\varphi'(0)$ and $\varphi'(H)$ from Eq. (3)]. Therefore the repulsion force between the plates is greatest at $\varphi'(H) = 0$, when no force acts on the inner side of the plate charged to the lower potential. Indeed, if there should be such a force, it must always act in the direction of the other plate.

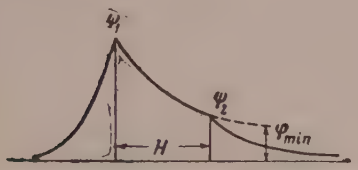


Fig. 2. Integral curve of Eq. (3) for variant 2.

It follows from (5a) that the maximum force of interaction is

$$F(H_m) = \frac{\varepsilon}{4\pi} \int_0^{\psi_2} \rho(\varphi)\, d\varphi. \tag{7}$$

Thus, the height of the force barrier created by the electrical forces is determined only by the potential of the plate of lower charge. The integral in the right-hand side of Eq. (7) is calculated very simply for any electrolyte.

The general expression for the interaction force in this instance is of the form [see Eqs. (4), (5), (5a)]

$$F = \frac{\varepsilon}{4\pi} \int_0^{\varphi_{min}} \rho(\varphi)\, d\varphi. \tag{8}$$

As stated earlier, φ_{min} can be found from Eq. (6); in the general case, the integrals in Eq. (6) are not reduced to elementary functions, and therefore φ_{min} is found by numerical calculation. However, this analysis shows that a qualitative examination is somewhat trivial.

Variant 2. $H_0 \leq H \leq H_m$, such that $\varphi'(0^2) \leq 2 \int_0^{\psi_1} \rho(\varphi)\, d\varphi$ (Fig. 2).

It will be shown that in this case $\varphi'(0)$ increases steadily with decrease of H. The value H_0 represents the distance between the plates such that $\varphi'(0)^2 = 2 \int_0^{\psi_1} \rho(\varphi)\, d\varphi$. In this case we can find a value $\varphi_{min} > 0$ when

$$\varphi'(0)^2 = 2 \int_{\varphi_{min}}^{\psi_1} \rho(\varphi)\, d\varphi. \tag{9}$$

Then we again have

$$F(H) = \frac{\varepsilon}{4\pi} \int_0^{\varphi_{min}} \rho(\varphi)\, d\varphi. \tag{10}$$

Now φ_{min} no longer corresponds to a real point on the integral curve at which $\varphi'(x) = 0$. We may say, however, that φ_{min} is the potential at which $\varphi'(x)$ would be zero if the solution were continued analytically into the region $x > H$. The plates are mutually repelled as before, and the force falls from the maximum value to zero as H varies from H_m to H_0.

The nature of F(H) is easily found by analysis of the equation for φ_{min} which is obtained by integration of Eq. (3)

$$\sqrt{2}H \equiv D_2(\psi_1, \psi_2, \varphi_{min}) = \int_{\psi_2}^{\psi_1} \frac{du}{\sqrt{\int_{\varphi_{min}}^{u} \rho(t)\,dt}}. \tag{11}$$

Indeed, it is clear from Eq. (11) that $D_2(\psi_1, \psi_2, \varphi_{min})$ is a steadily increasing function of φ_{min}. Therefore smaller values of φ_{min} and correspondingly smaller interaction forces correspond to smaller values of H.

The distance H_0 at which φ_{min}, and therefore F, is zero is found from the expression:

$$\sqrt{2}H_0 = \int_{\psi_2}^{\psi_1} \frac{du}{\sqrt{\int_{0}^{u} \rho(t)\,dt}}. \tag{12}$$

Variant 3. When $H < H_0$ we have $\varphi'(0)^2 > 2\int_0^{\psi_1} \rho(t)\,dt$ (Fig. 3). In this case, as Eq. (4) shows, the plates attract each other. If we introduce a certain potential $\varphi_0 > \psi_1$, such that

$$\varphi'(0)^2 = 2\int_0^{\varphi_0} \rho(t)\,dt, \tag{13}$$

then the force may be represented as follows:

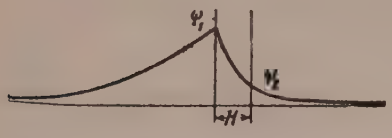


Fig. 3. Integral curve of Eq. (3) for variant 3.

$$F(H) = -\frac{\varepsilon}{4\pi}\int_{\psi_1}^{\varphi_0} \rho(t)\,dt. \tag{14}$$

Integration of Eq. (3) gives

$$\sqrt{2}H \equiv D_3(\psi_1, \psi_2, \varphi_0) = \int_{\psi_2}^{\psi_1} \frac{du}{\sqrt{\int_{0}^{u} \rho(t)\,dt + \int_{\psi_1}^{\varphi_0} \rho(t)\,dt}} \tag{15}$$

Equations (15) and (11) are easily reduced to the same form; this gives the explicit relation between F and H.

In fact, for the region $0 < H < H_m$ we can write

$$\sqrt{2}H = \int_{\psi_2}^{\psi_1} \frac{du}{\sqrt{\int_{0}^{u} \rho(t)\,dt - \frac{4\pi}{\varepsilon}F}}, \tag{15a}$$

and $F \gtrless 0$ when $H \gtrless H_0$.

Analogous modification of Eq. (6) is inappropriate, since φ_{min} is within the integration limits and the relation between F and H is no longer expressed in explicit form.

When H approaches zero, φ_0 tends to infinity and

$$F \sim H^{-2} \tag{16*}$$

This asymptotic law has a quite obvious interpretation: at small distances between the plates the electrolyte is incapable of shielding the field between them, and the field may be regarded simply as a field in a vacuum between two capacitor plates. From Eq. (15) we find that the asymptotic law for F holds under the condition

$$\int_0^{\psi_1} \rho(t)\,dt \ll \int_{\psi_1}^{\varphi_0} \rho(t)\,dt, \tag{17}$$

which may also be written in the form

$$F \gg F(0) \tag{17a}$$

where F(0) is the force acting on the outer side of the plate with the higher potential. Taking into account Eq. (17) and retaining terms of the first order, we can write Eq. (15) as

$$\sqrt{\frac{2\pi}{\varepsilon}}\, HF(H)^{1/2} = \int_{\psi_2}^{\psi_1} \left(1 - \frac{\varepsilon}{8\pi F(H)} \int_0^u \rho(t)\,dt\right) du \tag{18}$$

or

$$\sqrt{\frac{2\pi}{\varepsilon}}\, HF(H)^{1/2} = (\psi_1 - \psi_2) - \frac{\varepsilon}{8\pi F(H)} \int_{\psi_2}^{\psi_1} \int_0^u \rho(t)\,dt\,du. \tag{18a}$$

The integral in (18a) is calculated very easily for any electrolyte, and F(H) is found for the given H as the root of a cubic equation. If we discard first-order terms, in the zero approximation we have the above-mentioned asymptotic expression: $F \sim H^{-2}$.

It is interesting to note that the general character of interaction is quite the same in a complex electrolyte solution as in a solution of a binary electrolyte.

Variations of F with H are plotted in Fig. 4. Positive values of F correspond to repulsion and negative, to attraction.

For analysis of the case in which the plates are charged by potentials opposite in sign we can use Eq. (15), bearing in mind that $\psi_2 < 0$. Under all conditions a force of attraction acts between the plates, decreasing steadily with increase of H. Since $\rho(\varphi) \gtrless 0$ at $\varphi \gtrless 0$, $\int_0^{\varphi} \rho(t)\,dt > 0$ regardless of the sign of the potential φ. Therefore the expression under the root sign in (15) is always positive, F decreases steadily with increase of H, and when $H \to \infty$, $F \to 0$. Under the condition $\varphi_0 = \psi_1$ (or F = 0) the function $D_3(\psi_1 - |\psi_2|, \psi_1)$ becomes infinite. This can be seen if it is remembered that the integration limits with respect to u include the point u = 0, and when $t \to 0$, $\rho(t) \to 0$, near the point u = 0 the integrand diverges, like 1/u, which leads to logarithmic divergence of the whole integral.

* To avoid misunderstandings it should be remembered that at distances of the order of several interatomic distances the influence of the Stern double layer must be taken into account, and the theory developed here is not applicable to such small distances.

We now again consider the interaction of plates charged by potentials of the same sign ψ_1 and $\psi_2 < \psi_1$. Integrating Eq. (7), we find for the maximum repulsion force

$$F(H_m) = kT\left[\sum_a n_{a0}\left(e^{\frac{z_a e\psi_2}{kT}} - 1\right) + \sum_c n_{c0}\left(e^{-\frac{z_a e\psi_2}{kT}} - 1\right)\right]. \tag{19}$$

At sufficiently high potentials ψ_2, when

$$\frac{z_a e\psi_2}{kT} \gg 1, \quad F(H_m) \approx kT \sum_a n_{a0} e^{\frac{z_a e\psi_2}{kT}}. \tag{19a}$$

In the opposite case, when the potential ψ_2 is so small that $e^{\frac{z_a e\psi_2}{kT}} \approx 1$, we have from (19)

$$F(H_m) \approx \frac{e^2\psi_2^2}{2kT}\left\{\sum_a n_{a0} z_a^2 + \sum_a n_{c0} z_c^2\right\}. \tag{19b}$$

(Terms of the first order in $e\psi/kT$ become zero owing to the condition of electrical neutrality).

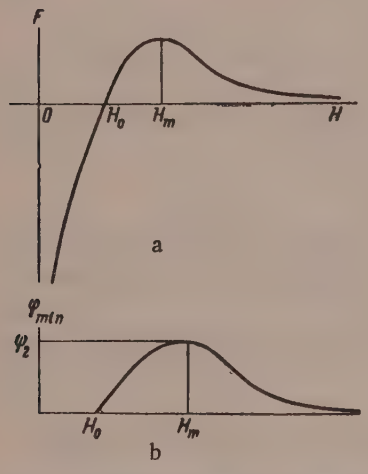


Fig. 4. General scheme of electrostatic interaction of charged plates (a). Dependent on the distance between the plates, F is given by the expressions:

$$F = \begin{cases} = -\frac{\varepsilon}{4\pi}\int_{\psi_1}^{\varphi_0} \rho(t)\,dt & 0 < H < H_0 \\ = \frac{\varepsilon}{4\pi}\int_0^{\varphi_{min}} \rho(t)\,dt & H_0 < H < \infty \\ = \frac{\varepsilon}{4\pi}\int_0^{\psi_2} \rho(t)\,dt & H = H_m \end{cases}$$

Variations of φ_{min} with the distance between the plates (b).

In general, the laws of heterocoagulation cannot be assessed from the height of the force barrier for electrostatic interaction alone, because van der Waals forces, in addition to electrical forces, act between the particles. However, some qualitative conclusions may be drawn even without derivation of an expression for the force of interaction between the plates with van der Waals forces taken into account.

For example, in considering two electrolytes in which the force barriers for the electrostatic forces are

$$F^{(1)}(H_m^{(1)}) = F^{(2)}(H_m^{(2)}), \tag{20}$$

but $H_m^{(2)} > H_m^{(1)}$ (the symbols (1) and (2) refer to the two electrolytes), we can claim that the total force barrier with van der Waals forces taken into account must be higher in the first case than in the second. Therefore, under otherwise equal conditions heterocoagulation must be more difficult in the first electrolyte. It follows from Eqs. (7) and (6a) that if we increase the electrolyte concentration and consequently $\rho(\varphi)$, we increase $F(H_m)$ on the one hand, and decrease H_m on the other. Therefore, beyond a certain concentration, the resultant force barrier may diminish owing to the influence of van der Waals forces. Naturally the maximum resultant force of repulsion (with van der Waals forces taken into account) is now found not at H_m, but at a certain value of $H > H_m$.

It will be shown later that if we consider heterocoagulation of convex particles there is another characteristic distance H_0 (see Eq. 12). Therefore we must take into account variations of H_0 in order to extend the foregoing concepts concerning the influence of composition of the mixture on heterocoagulation involving convex particles.

Equality of the force barriers means that

$$\int_0^{\psi_2} \rho^{(1)}(t)\,dt = \int_0^{\psi_2} \rho^{(2)}(t)\,dt \tag{20}$$

or, in expanded form:

$$\left\{\sum_a n_{ao}^{(1)}\left(e^{\frac{z_a^{(1)} e\psi_2}{kT}} - 1\right) + \sum_c n_{co}^{(1)}\left(e^{-\frac{z_c^{(1)} e\psi_2}{kT}} - 1\right)\right\} =$$
$$= \left\{\sum_a n_{ao}^{(2)}\left(e^{\frac{z_a^{(2)} e\psi_2}{kT}} - 1\right) + \sum_c n_{co}^{(2)}\left(e^{-\frac{z_c^{(2)} e\psi_2}{kT}} - 1\right)\right\}, \tag{20a}$$

when $e\psi_2/kT \approx 1$ Eq. (20)becomes

$$\sum_a n_{ao}^{(1)} e^{\frac{z_a^{(1)} e\psi_2}{kT}} = \sum_a n_{ao}^{(2)} e^{\frac{z_a^{(2)} e\psi_2}{kT}}. \tag{20b}$$

For the inequality $H_m^{(1)} > H_m^{(2)}$ to be satisfied the following expression must hold for any value of u satisfying the condition $\psi_2 < u < \psi_1$:

$$\int_{\psi_2}^{u} \rho^{(1)}(t)\,dt < \int_{\psi_2}^{u} \rho^{(2)}(t)\,dt. \tag{21}$$

With Eq. (20) taken into account, Eq. (21) is written in the form

$$\int_0^{u} \rho^{(1)}(t)\,dt < \int_0^{u} \rho^{(2)}(t)\,dt. \tag{21a}$$

From Eq. (12) it follows, incidentally, that if condition (21a) is satisfied not only is $H_m^{(1)} > H_m^{(2)}$, but $H_0^{(1)} > H_0^{(2)}$. As will be clear later, the latter is important for analysis of the interaction of convex particles. Conditions (20) and (21a) are quite compatible and very simply interpreted. In order that they should be satisfied it is sufficient, for example, that with increase of φ the value of $\rho^{(2)}(\varphi)$ should rise more sharply than $\rho^{(1)}(\varphi)$, while $\rho^{(1)}(\varphi)$ should be greater than $\rho^{(2)}(\varphi)$ in the region of low potentials. The growth of $\rho^{(2)}(\varphi)$ may be more rapid if the anions of electrolyte (2) have larger charges than the anions of electrolyte (1).

In this case, although the concentration of electrolyte (1) is higher than that of electrolyte (2) [since $\rho^{(1)}(\varphi) > \rho^{(2)}(\varphi($ at low $\varphi)]$ while the force barriers of electrostatic repulsion are equal in height, heterocoagulation in electrolyte (1) is much more difficult than in electrolyte (2). Of course, a more detailed analysis is needed for each specific instance. Nevertheless, ways of regulating heterocoagulation by variation of the electrolyte composition may be found from the considerations presented here.

In view of the fact that in the example under consideration H_0 varied symbatically with H_m, our reasoning is valid for convex particles to the same extent as for plane particles [see below, formula (22)].

Interaction of particles with convex surfaces. The electrostatic force between particles with convex surfaces can be determined from the following approximate formula, which is general in character [1-3]:

$$N = G\int_y^{\infty} F(H)\,dH. \tag{22}$$

where $\underline{y}$ is the width of the gap in the narrowest place; G is the shape factor, determined by the radii of curvature of the two surfaces near the proximity region and by mutual orientation of their principal normal sections. In the case of two equal spheres $G = \pi r$.

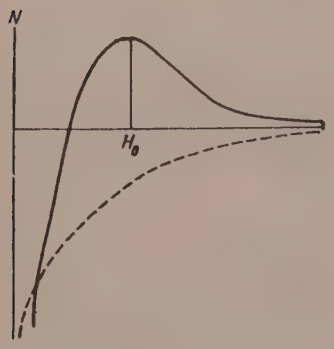


Fig. 5.

Formula (22) is valid so long as the radii of curvature are considerably greater than the radius of action of the forces between the surfaces. Naturally, we are interested in the case of like charges (ψ_1 and ψ_2 of the same sign).

Since van der Waals forces decrease steadily with the distance, for investigation of the force barrier we can restrict ourselves to the region where $y > H_0$ (H_0 is the distance at which the electrostatic force between plane plates is zero).

It is clear from expression (22) that the force barrier caused by electrostatic forces is at a maximum when the least distance $\underline{y}$ between these particles is H_0. It is easy to show that as $\underline{y}$ increases the force barrier tends to zero, remaining positive all the time (repulsion), and as $\underline{y}$ diminishes it decreases to zero, after which the sign of the force changes. Thus, the variation of N with $\underline{y}$ is of the form shown in Fig. 5.

If van der Waals forces are taken into account, the steadily decreasing attraction force (dash line in Fig. 5) should be added to the electrostatic forces. In this case the value of y_{max} at which the repulsion force is at a maximum changes, and, as Fig. 5 shows, $y_{max} > H_0$. Of course, this last result can be derived more rigorously, but this is hardly necessary.

With expressions (8) and (10) taken into account, we write Eq. (22) in the form

$$N = \frac{\varepsilon}{4\pi} G \int_{H}^{\infty} \int_{0}^{\varphi_{\min}(H)} \rho(\varphi)\, d\varphi\, dH. \tag{23}$$

In accordance with Eq. (23)

$$N_{max} = \frac{\varepsilon}{4\pi} G \int_{H0}^{\infty} \int_{0}^{\varphi_{\min}(H)} \rho(\varphi)\, d\varphi\, dH. \tag{24}$$

Changing the order of integration in expression (24), we have (see Fig. 4a)

$$N_{max} = \frac{\varepsilon}{4\pi} G \int_{0}^{\psi_2} \rho(\varphi)\, d\varphi \int_{H_2(\varphi)}^{H_1(\varphi)} dH. \tag{24a}$$

Here $H_2 < H_m < H_1$, and $H_2(\varphi)$ and $H_1(\varphi)$ are determined by formulas (11) and (6). Integrating expression (24a), we have

$$N_{max} = \frac{\varepsilon G}{4\pi\sqrt{2}} \int_{0}^{\psi_2} \rho(\varphi)\, d\varphi \left[\int_{\varphi}^{\psi_2} \frac{du}{\sqrt{\int_{\varphi}^{u} \rho(t)\, dt}} + \int_{\varphi}^{\psi_2} \frac{du}{\sqrt{\int_{\varphi}^{u} \rho(t)\, dt}} - \int_{\psi_2}^{\psi_1} \frac{du}{\sqrt{\int_{\varphi}^{u} \rho(t)\, dt}} \right] =$$

$$= \frac{G}{\sqrt{2}} \frac{\varepsilon}{4\pi} \int_{0}^{\psi_2} \rho(\varphi)\, d\varphi \int_{\varphi}^{\psi_2} \frac{du}{\sqrt{\int_{\varphi}^{u} \rho(t)\, dt}}. \tag{25}$$

In other words, the force barrier N_m depends only on the potential of the more weakly charged particle. Therefore this result, established previously for binary electrolytes [1], is quite general in character.

By changing the order of integration in expression (25) we can express N_{max} in a more convenient form. We first introduce the auxiliary function

$$F(\varphi, u) = \int_{\varphi}^{u} \rho(t)\, dt. \tag{26}$$

Then

$$\partial F(\varphi, u)/\partial\varphi = -\rho(\varphi).$$

Changing the order of integration in expression (25) we have

$$N_{max} = \frac{\varepsilon}{4\pi}\frac{G}{\sqrt{2}}\int_0^{\psi_2} du \int_0^{u} \frac{\rho(\varphi)\, d\varphi}{\sqrt{F(\varphi, u)}} = \frac{G}{\sqrt{2}}\frac{\varepsilon}{4\pi}\int_0^{\psi_2} du \int_0^{u} \frac{-dF(\varphi, u)}{\sqrt{F(\varphi, u)}} =$$

$$= \frac{\varepsilon}{4\pi}\sqrt{2G}\int_0^{\psi_2} du\,[\sqrt{(F0, u)} - \sqrt{F(u, u)}] = \frac{\varepsilon}{4\pi}\sqrt{2G}\int_0^{\psi_2}\sqrt{\int_0^{u}\rho(t)\,dt}\cdot du. \tag{27}$$

Integration under the root sign finally gives:

$$N_{max} = \sqrt{\frac{\varepsilon kT}{2\pi}}\, G\int_0^{\psi_2}\sqrt{\sum_a n_{ao}\left(e^{-\frac{z_a e\psi}{kT}} - 1\right) + \sum_c n_{co}\left(e^{-\frac{z_c e\varphi}{kT}} - 1\right)}\, du. \tag{28}$$

We thus derive a simple expression for the maximum value of the force barrier in the interaction of convex particles.

SUMMARY

1. Electrostatic interaction of charged particles in complex electrolyte solutions has been investigated.

2. The maximum value of the electrostatic repulsion force is determined only by the potential of the particle with the weaker charge, both in interaction between plane surfaces and with convex particles. Therefore the results of [1] and [2] can be extended to the case of any complex electrolyte solution.

3. The character of particle interaction in complex systems is, in general, analogous to that in binary electrolyte solutions.

4. Expressions have been derived for calculation of the maximum electrostatic repulsion force between two plane plates and two convex particles.

5. It can be shown that by means of an analysis similar to that presented in the paper it is possible to determine the general principles for variation of interaction forces between particles and changes of concentration during coagulation in relation to the composition of a complex electrolyte system.

I am deeply grateful to B. V. Deryagin for his constant interest and valuable comments.

LITERATURE CITED

[1] B. V. Deryagin, Kolloid. Zhur. 16, 6, 425 (1954);* Discussion Faraday Soc. No. 18 (1954).

[2] B. V. Deryagin and V. G. Levich, Doklady Akad. Nauk SSSR 98, 6 (1954).*

[3] B. V. Deryagin, Izvest. Akad. Nauk SSSR, Otdel Matem. Estestv. Nauk, Ser. Khim. 5, 1153 (1937); Kolloid. Zhur. 7, 285 (1941).

* Original Russian pagination. See C. B. Translation.

APPLICATION OF THE SIMILARITY PRINCIPLE TO DETERMINATION OF INLET EFFECTS IN FLOW OF RUBBER STOCKS ALONG DUCTS OF CIRCULAR SECTION*

R. V. Torner

Scientific Research Institute of the Rubber Industry
Translated from Kolloidnyi Zhurnal, Vol. 22, No. 5, pp. 625-630,
September-October, 1960
Original article submitted March 7, 1960

It is known that the flow of viscoplastic liquids through ducts of circular section is accompanied by inlet effects which are considerably greater than the inlet effects observed in the flow of Newtonian liquids [1, 2]. A similar effect is found in the flow of rubber stocks through such ducts [3, 4]. The pressure field established along the axis of the duct carrying a rubber stock was investigated experimentally [5] in order to determine the magnitude of the inlet effect and its connection with the kinematic flow characteristics and the rheological properties of the material. It was found that two essentially distinct flow zones exist in the duct: a region of steady flow in which the pressure gradient is constant, and an inlet region where the pressure gradient diminishes from the maximum value at the entry into the duct to the constant value corresponding to the region of steady flow.

Typical diagrams of the pressure fields which become established along a duct are shown in Fig. 1. Each such pressure-field curve can be used to calculate the pressure gradient for the region of steady flow, and to determine the inlet losses. If the average flow velocity and the pressure gradient over the region of steady flow are known, the flow curve of the material under investigation can be plotted. The flow of two rubber stocks T_1 and T_2, of the composition given below (in parts by weight) was investigated:

T-1		T-2	
SKN-26	100.0	SKB 30-35	100.0
Channel black	30.0	Lamp black	72.0
Lamp black	70.0	Aktinap	5.0
Aldol	1.0	Pine resin	4.0
Zinc oxide	6.5	Petrolatum	12.0
Technical stearin	1.0		
Rosin	3.0		
Total	211.5	Total	193.0
Defoe plasticity	5000-5300		1500-1600
Density, g/cc	1.3		1.2

These experimental data show that in the range of velocity gradients (from 10^{-1} to 10^{2} sec^{-1}) and temperatures (from 60 to 140°) investigated the rheological characteristics of both stocks are represented with satisfactory

* Paper at the Rheology Subsection of the All-Union Congress on Theoretical and Applied Mechanics, February 2, 1960.

TABLE

	Stock T-1 **					Stock T-2			
Temperature, °C	60	85	95	122	140	60	80	95	122
n	3,64	3,71	3,71	3,71	3,71	5,13	5,13	5,13	5,13
c, kg/cm²	3,4	2,7	2,2	1,53	1,29	1,36	1,13	0,99	0,77

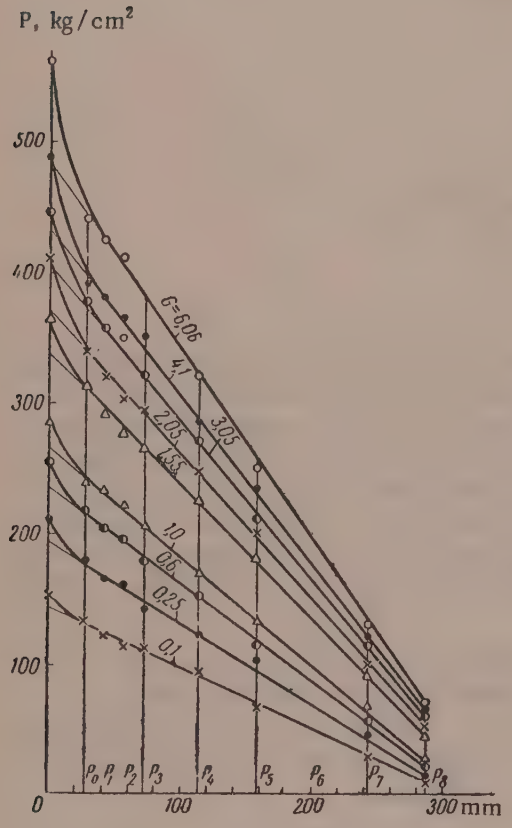


Fig. 1. Typical graphs for the pressure field established along the axis of a duct carrying a rubber stock (T-1), t = 85°.

approximation by the power equation

$$\dot{\gamma} = (\tau/c)^n, \qquad (1)$$

where γ is the velocity gradient; τ is the shearing stress; n and c are empirical constants.

Values of the constants n and c for T-1 and T-2 stocks, found from the linear sections of the pressure plots, are given in the table above.

The absolute magnitude of the inlet loss can be found from the same pressure-field graph. It follows from the results that the relation between the inlet loss ΔP_i and the average flow velocity $\bar{v}$ can be represented by an equation of the form

$$\Delta P_i = B\bar{v}^{\alpha}, \qquad (2)$$

where B and α are empirical constants which depend both on the composition and on the temperature of the stock.

For correlation of the results Eq. (2) was put into a dimensionless form, the terms in the first part being grouped in such a way that one of the criteria was the effective Reynolds number. The following expression was obtained:

$$Eu_i = \frac{\Delta P_i}{\rho \bar{v}^2} = W^{\frac{\alpha}{2n-1}} Re_r^{\frac{\alpha n}{2n-1}} \qquad (3)$$

where ρ is the density of the rubber stock; r is the duct radius; Re_r is the effective Reynolds number:

$$W = B^{\frac{2n-1}{\alpha}} \frac{c^n (n+3)^{1-n}}{\rho^{\frac{n(2+\alpha)-1}{\alpha}} \bar{v}^{\frac{4n-2}{\alpha}} r}; \quad Re_r = \frac{\rho v^{2-1/n} r^{1/n}}{c (n+3)^{1/n+1}}.$$

Equation (3) can be used to find the dimensionless pressure drop at the inlet, which we term the Euler inlet number (Eu_i), as a function of two dimensionless parameters Re_r and W. Each of these parameters, in its turn, depends on the kinematic and dynamic flow characteristics, and on the rheological properties of the material. However, it was found that the effects of the two criteria are not equal, and that the effective Reynolds number is predominant.

The experimental results for all nine series of experiments, plotted in $\lg Eu_i - \lg Re_r$ coordinates, fit satisfactorily on one straight line (Fig. 2). The equation corresponding to the straight line in Fig. 2 is of the form:

$$Eu_i = 224\, Re_r^{-0.935}. \qquad (4)$$

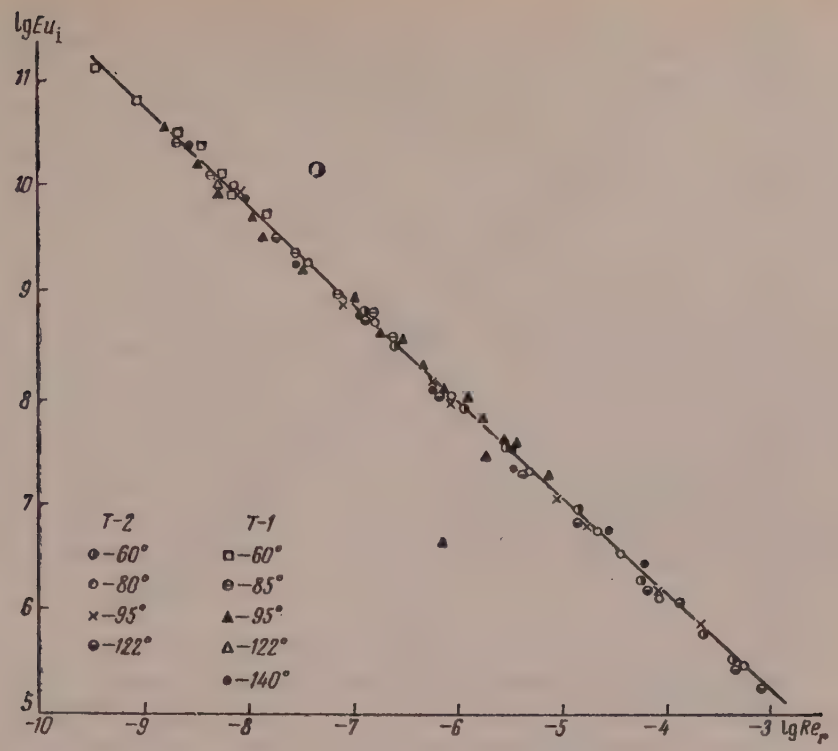


Fig. 2. The $\lg Eu_i - \lg Re_r$ correlation.

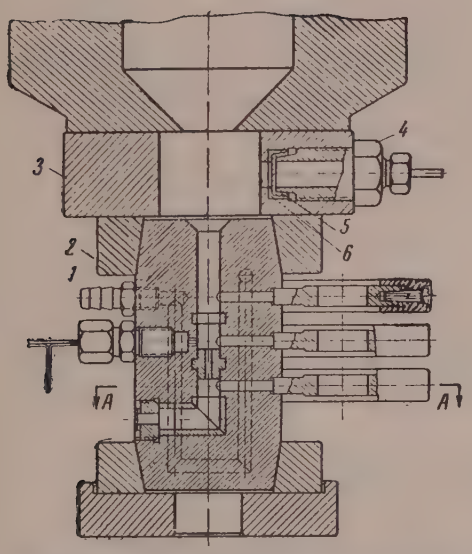


Fig. 3. Diagram of mold used for determination of pressure losses in flow of a rubber stock through inserts of internal diameters: 4.0, 3.18, and 2.34 mm.

The resultant expression can be used for calculating inlet losses in a circular duct for rubber stocks of any rheological characteristics, as the effective Reynolds number* is the determining criterion.

Since all the experiments described above on determination of inlet losses were performed with a duct 10 mm in diameter, it was required to verify the validity of Eq. (4) for the flow of the same stocks through ducts of other sizes. Three inserts were made for this purpose, with central orifices 4.0, 3.18, and 2.34 mm in diameter. Each insert could be placed between two pressure gauges in the duct of an experimental mold, as shown in Fig. 3. It was therefore possible to determine the pressure drop between the ends of the insert at any given flow rate. The experiments were performed with T-1 stock at 85°.

The pressure loss in these experiments was the sum of the inlet effect and loss of steady flow. The pressure loss ΔP_L corresponding to the region of steady flow can be determined from the equation:

$$\Delta P_L = \frac{2Lc}{R^{\frac{n+1}{n}}} \bar{v}^{1/n} (n+3)^{1/n}, \qquad (5)$$

* The effective Reynolds number is the ratio of the forces of viscous friction at the duct walls to the inertia forces in the cross section.

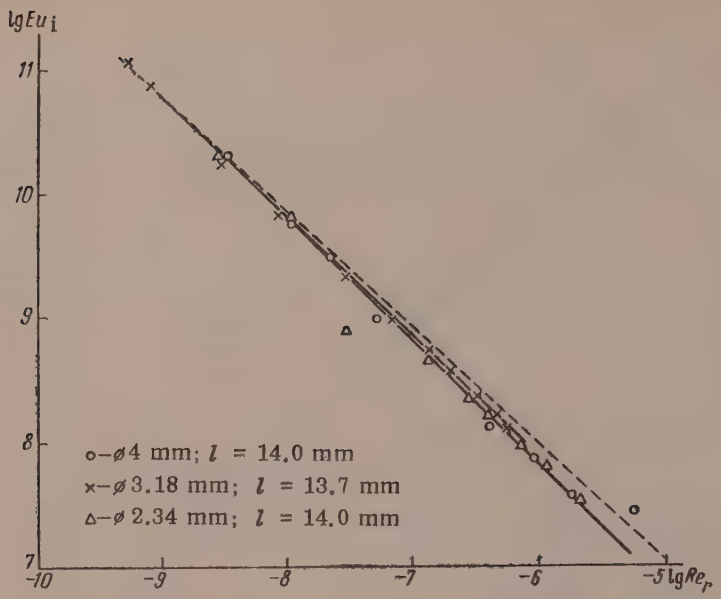


Fig. 4. The $\lg Eu_i' - \lg Re_r$ correlation calculated from results of experiments with inserts 4.0, 3.18, and 2.34 mm in internal diameter. Stock T-1, t = 85°.

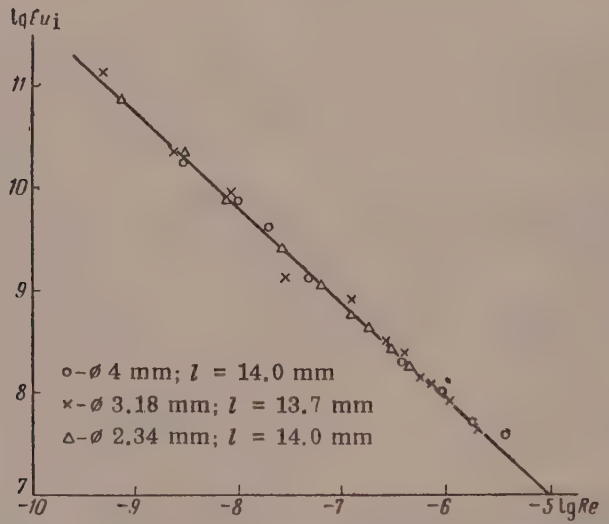


Fig. 5. Comparison of values of $\lg Eu_i$ for a stepped duct, calculated from Eq. (6), with Eq. (4).

where L is the length of the insert and R is its internal radius. By subtraction of ΔP_L from the total pressure drop we can find the inlet loss as the difference between the total pressure drop and the pressure drop calculated from Eq. (5).

Values of $\lg Eu_i'$ and the corresponding values of $\lg Re_r$, calculated from the experimental results, are plotted in Fig. 4. It is seen that the values found for $\lg Eu_i'$ deviate systematically from the straight line corresponding to Eq. (4), and the deviation increases with the effective Reynolds number. We consider that this deviation can be explained as follows: the energy expended to break down the structure and in high-elastic deformation is proportional, in the first approximation, to the specific work of the inlet effect per unit volume of the flowing stock. It follows that the inlet effect is approximately equal to the specific power of structural breakdown and high-elastic deformation of the material at entry. Therefore in a stepped duct the work of structural breakdown

and high-elastic deformation at the entry to the second step should be less than in a straight uniform duct of the same diameter of the step; the difference should be equal to the inlet loss at the entry into the duct. In other words, the pressure losses in the second and all subsequent sections of a stepped duct must be determined with the preliminary structural breakdown taken into account.

In a two-step duct the inlet loss at the region of the smaller diameter can be found from the formula:

$$Eu'_{id} = Eu_{id} - Eu_{iD}\frac{d^4}{D^4}, \tag{6}$$

where Eu_{iD} is the dimensionless loss at the inlet to the duct of larger diameter; Eu'_{id} is the dimensionless loss at the inlet to the duct of smaller diameter; Eu_{id} is the dimensionless inlet loss in a stepped duct over the region of smaller diameter. If we use the values of Eu'_i found from experimental data and calculate Eu_i from them for ducts 2.34, 3.18, and 4.0 mm in diameter, we can compare the experimental data with the graphical plot of Eq. (4). It is seen in Fig. 5 that the values of $\lg Eu_i$ calculated in this way fit satisfactorily near the plot of $\lg Eu_i = 224\ Re_r^{-0.935}$, and therefore the experimental Eq. (4) is also valid for duct diameters of 2.34, 3.18 and 4.0 mm. The pressure drop for the region of steady flow can also be reduced to a dimensionless form [6-9]. The dimensionless pressure loss Eu_L for the region of steady flow can be calculated from the formula

$$Eu_L = \frac{2L(n+3)}{r} Re_r. \tag{7}$$

The total dimensionless pressure loss is equal to the sum of Eu_i and Eu_L. Therefore calculation of flow in a duct of circular section can be reduced to calculation of the dimensionless criteria Eu_i and Eu_L.

SUMMARY

1. A general expression is derived for the relation between the dimensionless flow parameters and dimensionless inlet losses in flow of rubber stocks through circular ducts.

2. The determining criterion for dimensionless inlet losses Eu_i is the effective Reynolds number, which is the ratio of the inertia forces in flow to the forces of viscous friction at the duct walls.

3. The relation between Eu and the effective Reynolds number is represented by the equation:

$$Eu_i = 224\ Re_r^{-0,935}.$$

4. In two consecutive ducts of a larger and smaller diameter the inlet loss in the duct of smaller diameter decreases in proportion to the work of structural breakdown at the entry into the duct of larger section. In this case Eu_i is found from the formula:

$$Eu'_{id} = Eu_{id} - Eu_{iD}\frac{d^4}{D^4}.$$

5. A method has been devised for calculating the flow behavior of rubber and raw stocks through circular ducts; it consists of consecutive determination and subsequent addition of the criteria Eu_i and Eu_L.

LITERATURE CITED

[1] E. V. Kuvshinskii, Dissertation: Studies of the efflux of high-polymer solutions [in Russian] (1950).

[2] A. H. Nissan and F. H. Garner, J. Inst. Petrol. 33, 71 (1947).

[3] M. Mooney and S. A. Black, Rubber Chem. Techn. 26, 311 (1953).

[4] S. Eccher, Ind. Eng. Chem. 43, 479 (1951).

[5] R. V. Torner and M. M. Maizel', Trudy MTILP, 811 (1958).

[6] N. V. Tyabin, Kolloid. Zhur. 14, 270 (1952).*

[7] B. R. Bird, A. I. Ch. E. Journal 2, 428 (1956).

[8] A. B. Metzner, Advances Chem. Eng. 6, No. 4 (1956).

[9] R. N. Weltman, Ind. and Eng. Chem. 48, 386 (1956).

* Original Russian pagination. See C. B. Translation.

USE OF RADIOACTIVE ISOTOPES FOR STUDYING MOISTURE TRANSPORT IN PEAT

N. V. Churaev

Kalinin Peat Institute
Translated from Kolloidnyi Zhurnal, Vol. 22, No. 5, pp. 631-637,
September-October, 1960
Original article submitted July 21, 1959

Problems of water migration in peat are highly complex and have not been studied sufficiently. Nevertheless, investigation of these processes and elucidation of the mechanism of moisture transport is an urgent task in peat technology, and especially in the technology of peat drying and dewatering [1].

The complexity of moisture transfer processes in peat is due to its high hydrophily and dispersity, the presence of diffuse layers of adsorbed ions, the presence of several phases, and the diversity of the forms of bonding between the water and the material. Because of all this, water in peat moves under the influence of various forces (gradients of pressure, concentration, moisture, temperature, capillary and electrical potentials, etc.) which are difficult to estimate quantitatively. Whereas many of these may be disregarded in the case of coarsely dispersed capillary-porous bodies, in the case of peat disregard of secondary factors may lead to serious errors. In such systems the rates of moisture migration under the influence of osmotic forces and temperature gradients may in some cases greatly exceed the rate of percolation by gravity [2, 3]. The action of electroosmotic forces may be equally important [4-6].

An important role in moisture transport is played by the effect of thermal moisture conduction [7], which essentially determines the course of drying of peat during processing and the moisture conditions in the upper layers of peat deposits.

Modern methods for calculation of heat and moisture transfer are based on the potential theory and thermodynamics of irreversible processes [1,7-9]. In these cases the transfer processes are characterized by the heat and moisture transfer coefficients, which can be determined by a number of methods [7, 8, 10]. However, it is not always possible to obtain satisfactory solutions, especially if the properties of the material change substantially during the process, or the process conditions are not steady.

For proper evaluation of the acting factors the thermodynamic methods should be supplemented by a consideration of transfer processes in the light of the molecular kinetic theory. The results of such investigations help to reveal the physical bases and mechanisms of many processes in disperse systems [2, 3, 11, 12].

A very promising method for studying moisture transport in disperse material is with the use of water labeled with a radioactive tracer; the migration of such water can be systematically observed. For example, the radioactive tracer Na_2SO_4 labeled with the S^{35} isotope [13] can be used with peat.

In assessment of the results obtained by these methods it must be remembered that the radioactive tracer does not dissolve in the bound water and is therefore a "label" for free water on peat only. Likewise the radioactive tracer does not evaporate from the water and therefore cannot be transported with water vapor.

In studies of thermal moisture conduction the dispersed peat was mixed with a solution of radioactive $Na_2S^*O_4$ tracer and left for 1-2 days to ensure uniform distribution. The amount of added tracer was ~ 1 microcurie per g of the moist peat. To test the uniformity of the mixing a series of samples was taken and their specific activities and moisture contents were determined.

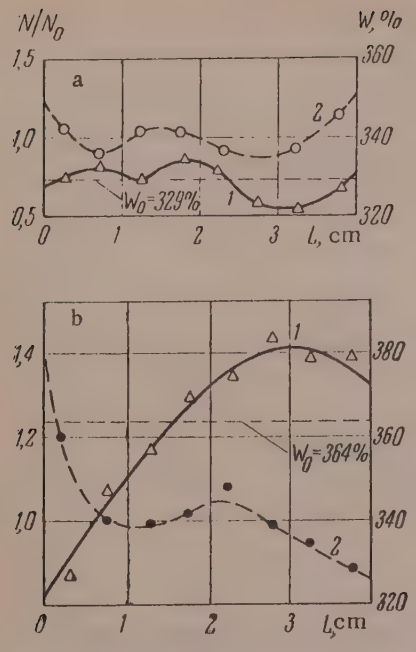


Fig. 1. Distribution of moisture content (1) and specific activity (2) along a heated peat specimen: a) heating time 53 min, average temperature 31.5°; b) heating time 30 hours, average temperature 55°.

The peat containing the tracer was put in a separable cylinder 5 cm in diameter, made from a heat-insulating material. The specimen length was from 3 to 5 cm. The peat, packed compactly in the cylinder, was in contact with a brass foil screen on the left, and with paraffin (to simulate a semiinfinite medium) on the right. As the peat was well insulated from the surroundings, the moisture in it could move only along the specimen under the influence of thermal flow. The specimen was heated by means of a lamp with a reflector which directed heat onto the brass screen.

After a definite heating time the specimen was taken out of the apparatus and cut into pieces 0.5 cm long. Each piece was put in a weighing bottle, weighed, and dried at 105° to determine the moisture content. The dry residue was then ground in a mortar and analyzed for determination of the radioactive tracer content. The peat powder samples were put by the standard method into foil cups; these were placed in a fixed position under a T-25 BFL counter connected to a B-2 radiometer for the activity determinations. Since "thick" layers [14] were used for the activity determinations, it was not essential to weigh the samples. Three replicate samples for determination of specific activity were taken from each portion of the specimen.

The results of two experiments are shown in Fig. 1, where the ratios of the average specific activity N of different parts of the specimen to the initial activity N_0 of the peat are plotted against the distance L from the heated end of the specimen. The length of the specimen was 4 cm; moisture and specific activity were determined in eight regions. The peat used for the experiments was sedge peat of degree of decomposition R = 35%, passed once through a meat chopper.

Analysis of the results gives an indication of the mechanism of moisture transport in peat. If the moisture moves in the specimen during the experiment in liquid form only, then the curves for variations of moisture content and specific activity along the specimen should be similar in character. Deviations from this may be due to evaporation or condensation of moisture. Evaporation of moisture increases the tracer concentration in the peat, because the radioactive tracer remains at the evaporation region and is not carried with the vapor. Condensation results in dilution of the tracer, which leads to a decrease in the specific activity of the peat. With a short time of heating (Fig. 1, a) the moisture and activity curves are similar in shape, which indicates that moisture is transported in liquid form. At this stage of the experiment migration of moisture in the hot direction occurs, and evaporation begins at the "hot" end of the specimen (the activity curve rises at the heated end).

If the heating time is considerable and the average temperature higher, the activity and moisture distributions differ in character. The specific activity at the "hot" end of the specimen increases considerably, indicating that moisture is evaporated in this region. Moisture condenses at the "cold" end, so that the region becomes moister and its specific activity falls below the initial value, taken as unity. In this case moisture is transported mainly in vapor form, toward the cold end of the specimen. Since a steady state was reached in the experiment (confirmed by the gravimetric method [15, 16]), transport of vapor to the cold end was balanced by the flow to the hot end due to the resultant moisture gradient.

Because dynamic equilibrium has been established, the distribution of moisture and temperature along the specimen remain almost unchanged. However, such is not the case with the radioactive tracer. The activity distribution curve alters continuously during the process because of the continuing internal mass transfer: transport of moisture in vapor form in the cold direction, and return transfer of condensing moisture in the hot direction. As a result of this process the radioactive tracer is completely transferred to the surface of the hot specimen end if the process continues long enough.

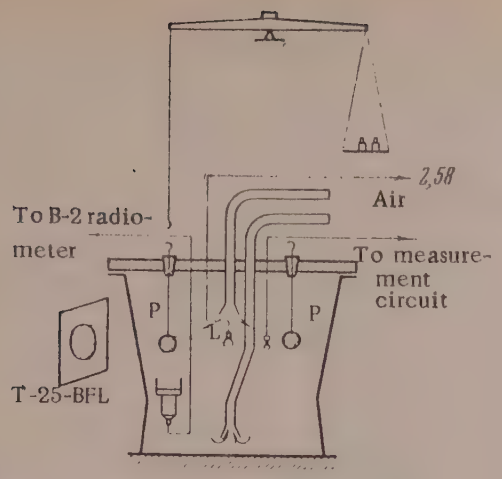


Fig. 2. Diagram of drying unit for work with radioactive tracers.

The results of radioactive tracer experiments reveal the transport mechanism and the zones of moisture evaporation and condensation in peat specimens differing in moisture content, dispersity, and composition. Generally such experiments are accompanied by determinations of the transfer coefficients by the weighing or probe methods [16], so that a more complete idea of the nature of the processes is obtained.

The method described above makes it possible to distinguish between moisture transport in liquid and in vapor form. However, in many cases it is desired to study liquid flows in a specimen, directed both toward the hot end (thermoosmosis, capillary suction) and the cold end (thermocapillary migration). Labeling of individual regions of a specimen can be used for this purpose. A layer of labeled peat of the same moisture content and 3-5 mm thick, or a capron net previously soaked in a solution of the radioactive tracer and dried, is placed in the middle portion of a clean specimen. At the end of the experiment samples are taken and their moisture contents and activities determined; the direction of liquid streams causing transport of the tracer can be determined from the spread of the tracer on either side of the net or labeled layer.

A special drying chamber (Fig. 2) was devised for studying isothermal drying processes with the aid of the radioactive tracer method.

The chamber is a desiccator with a textolite lid, contained in a thermostat. Air is pumped through the desiccator; the air is conditioned to a definite moisture content by being bubbled through sulfuric acid solutions of various concentrations. The relative humidity of the air passed into the desiccator is recorded on the band of a recording hygrometer installed in an intermediate chamber. The air flow rate is recorded by means of a rheometer.

The radioactive tracer was first added to the moist peat and mixed thoroughly with it. The peat was then molded into several pellets 1-1.5 cm in diameter; these were suspended on threads from corks inserted in the desiccator lid. The peat was dried isothermally under constant conditions. The changes in the weight of the pellets were determined by means of an analytical balance. Contraction was determined from measurements of the area of a shadow of the pellet on a screen. The point source of light was a small lamp placed in the center of the desiccator and switched on only when the measurements were being made. The shadow was outlined on tracing paper and its area was measured by means of a planimeter. An end-window counter of the T-25-BFL type, connected to a B-2 radiometer, was placed under one pellet for measurement of the specific activity of its surface. The counter was screened from radiation from neighboring pellets by a foil cylinder which was opaque to radiation from S^{35}. Because of self-absorption of soft β-radiation from S^{35} in peat, the measurement data referred only to the surface layer of the pellet, less than 0.1 mm thick. A semiconductor thermoresistor connected to a measurement bridge was suspended in the desiccator to measure the air temperature.

Changes of the weight P, surface area $\underline{s}$, and volume V of the pellet, amount of tracer carried out onto the surface, and moisture content and bulk density of the peat were recorded in the course of drying.

The rate of evaporation of water from the pellet surface was calculated from the formula:

$$i = \frac{\Delta P}{s\Delta\tau}, \qquad (1)$$

where ΔP is the weight loss of the specimen in time $\Delta\tau$; $\underline{s}$ is the surface area of the pellet.

The specific activity of the surface was determined from counts of the pulse rate (N) in the B-2 unit. Since the geometrical conditions for activity measurement alter as the pellet shrinks, a correction for the change

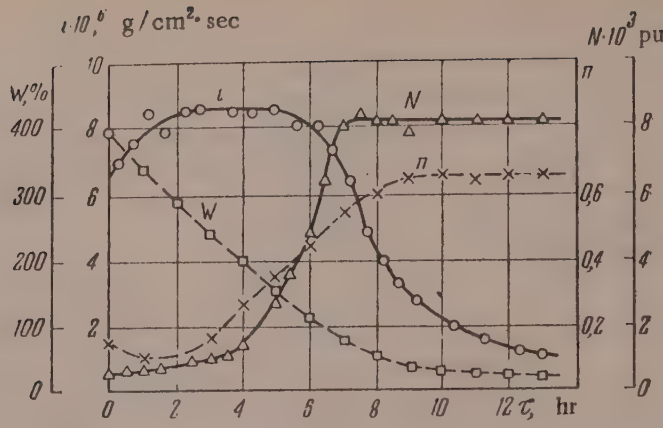


Fig. 3. Results of observations of the drying of labeled peat.

of pellet volume during the experiment was applied to the values obtained for N. The magnitude of this correction was determined previously from a series of measurements on pellets of different diameters made from the same labeled peat.

For studies of the mechanism of moisture transport it is also of interest to determine, in addition to the quantities named above, the ratio of the air-filled pore volume V_a to the total pore volume V_p in the peat; this can be calculated as follows:

$$n = \frac{P - P_d}{(V - P_d/\rho_d)\,\rho_w}, \tag{2}$$

where P_d is the mass of the dry peat material in the pellet; ρ_d is the density of the dry substance, assumed to be 1.5 g/cc; ρ_w is the density of water.

The results of one experiment with sedge peat of R = 35%, passed once through the meat chopper, are given in Fig. 3. The graph shows variations of the absolute moisture content W of the pellet, water evaporation rate i, specific activity N, and the ratio $n = V_a/V_p$, in the course of the experiment.

When free water containing the tracer evaporates, the radioactive tracer remains at the point of evaporation. Therefore the specific activity N is a measure of the amount of water evaporated from the pellet surface. However, the specific activity of the surface does not change as the result of evaporation of moisture in the pores within the pellet. Therefore the radioactive tracer makes it possible to distinguish between: 1) evaporation of free water from the pellet surface and within the pores, and 2) evaporation of free (labeled) and bound (nonlabeled) water.

It is seen in Fig. 3 that the ratio n begins to increase soon after the start of the experiment; this shows that the evaporation front recedes into the pellet. For this reason the specific activity of the pellet surface alters little at the start of the experiment. The tracer is carried out onto the surface with some delay. This may be attributed to increase of the tracer concentration during evaporation within the specimen, with subsequent transport of the concentrated solution to the surface by a film mechanism in consequence of the resultant moisture gradient, in agreement with the concepts put forward by Deryagin and Nerpin [17, 18].

When the moisture content of the specimen W reaches 70%, transport of the tracer to the surface ceases. This moisture content corresponds to the amount of bound water remaining in the specimen; it is in good agreement with the results of determinations of bound water by other methods [19]. After removal of free water the mechanism of water transport changes, and the evaporation rate drops sharply.

A somewhat different technique was used for studies of capillary rise of water in monolithic peat blocks. The specimens, cut from the deposit and placed in separable tubes (from 10 to 80 cm long), were stood vertically with the lower ends immersed to a depth of 1-2 cm in water containing the radioactive tracer in solution. The top ends of the blocks were open and could lose moisture by evaporation. The amount of water evaporated was found by weighing of the specimens.

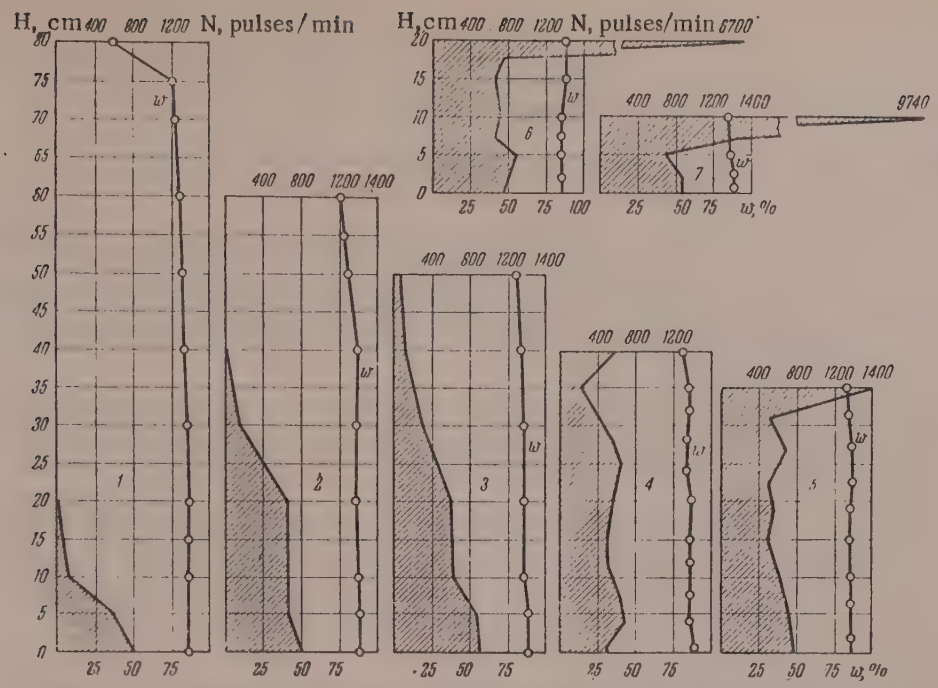


Fig. 4. Distribution of moisture content w and specific activity N at different heights of peat blocks. Specimen heights: 1) 80; 2) 60; 3) 50; 4) 40; 5) 35; 6) 20; 7) 10 cm.

Migration of water in the peat was indicated by the spread of the radioactive tracer along the specimens. After 10-20 days the blocks were removed from the apparatus and cut into 2-5 cm pieces along the specimen height. The pieces were tested for moisture content and then for content of radioactive tracer. The dry powdered samples were prepared and their activity measured by the same methods as before.

Figure 4 shows the distribution of relative moisture content w and specific activity N (hatched regions) of samples at different heights of the blocks at the end of the experiments. The conditions for evaporation from the block surfaces were kept constant by means of an electric annular heater. Evaporation was observed by the method described by Panferov [20].

The distribution of labeled water in blocks of different heights is associated with the mechanism of water transport in peat. In specimens of small height (up to 35 cm) capillary rise of water to the evaporation surface predominates. In this case the evaporation rate remained constant. The tracer brought out onto the evaporation surface accumulates on it in considerable amounts. Labeled water filling the water-conducting pores is distributed uniformly along the specimen height.

If the specimen height exceeds 35 cm, which is the height of capillary rise in this type of peat [20], the rate of transport of labeled water falls, which is also indicated by a decrease in the evaporation rate. The rate of moisture access to the evaporation surface is determined in this case by the conditions of its hydraulic connection with the bottom water level. The film transport of moisture, which takes place in the upper layers of tall specimens and which replaces the capillary mechanism, lowers the rate of water migration to the peat surface. In each case a quite definite evaporation rate becomes established, corresponding to the conditions of film transport of water in the upper layers of the specimen. The distribution of the radioactive tracer in the specimens (Fig. 4) shows that the rate of water transport in peat dimishes with increasing height of the block.

The use of radioactive tracers for studying percolation of water through peat under pressure has been described earlier [13, 19, 21].

SUMMARY

1. Methods have been worked out for studying the transport of moisture in peat by means of labeled water containing a radioactive tracer in solution.

2. These methods were used for studying thermal moisture conduction, isothermal drying, capillary imbibition, and filtration of water in peat.

3. These methods can be used for investigating the mechanism of moisture transport in peat and other disperse materials in the course of various technological processes.

In conclusion, I thank Prof. M. P. Volarovich for valuable comments in discussion of the work, and N. I. Gamayunov for help in the experiments.

LITERATURE CITED

[1] Proceedings of the Scientific and Technical Conference on Acceleration of Processes and Improvement of Product Quality in Drying in the Main Branches of Industry and Agriculture, Plenary Sessions [in Russian] (Izd. VTsSPS, Profizdat, 1958).

[2] B. V. Deryagin and M. K. Mel'nikova, Proceedings of the 6th International Congress of Soil Science, Soil Physics [in Russian] (Izd. AN SSSR, 1956) p. 119; Problems of Agricultural Physics [in Russian] (Izd. VASKhNIL, Leningrad, 1957) p. 30.

[3] B. V. Deryagin, M. K. Mel'nikova, and S. V. Nerpin, Proceedings of the 6th International Congress of Soil Science, Soil Physics [in Russian] (Izd. AN SSSR, 1956) p. 101.

[4] Electrokinetic Properties of Capillary Systems [in Russian] (Izd. AN SSSR, 1956).

[5] M. N. Gol'dshtein, Kolloid. Zhur. 21, 30 (1959).*

[6] G. M. Lomidze and A. V. Netushil, Gidrotekhnich. Str-vo, 3, 26 (1956).

[7] A. V. Lykov, Transfer in Capillary Porous Bodies [in Russian] (Gostekhizdat, 1954).

[8] A. V. Lykov, Heat and Mass Transfer in Drying Processes [in Russian] (Gosénergoizdat, 1956).

[9] K. Denbigh, Thermodynamics of the Steady State [Russian translation] (IL, Moscow, 1954).

[10] S. S. Korchunov, Trudy Vses. N.-I. In-ta Torfyanoi Prom. 13, 74 (Gosénergoizdat, 1956).

[11] W. A. Hadley and R. Eisenstadt, Piping and Air Cond. No. 6, 111 (1953).

[12] J. M. Kuzmak and P. J. Sereda, Soil Sci. 84, 291, 419 (1957).

[13] M. P. Volarovich, N. V. Churaev, and B. Ya. Minkov, Kolloid. Zhur. 19, 159 (1957);* Doklady Akad. Nauk SSSR 114, 964 (1957).*

[14] S. M. Raiskii and V. F. Smirnov, Physical Principles of the Radioactive Tracer Method [in Russian] (GITTL, 1956).

[15] N. A. Nasedkin and G. I. Pokrovskii, Zhur. Tekh. Fiz. 9 (1939); N. N. Bab'ev, Trudy MTIPP, 6 (1956).

[16] N. I. Gamayunov, Inzh-Fiz. Zhur. 2, 35 (1959).

[17] S. V. Nerpin, Trudy Leningrad. In-ta Vodnogo Transporta, 21, 126 (Gosizdat. Vodn. Transporta, 1954).

[18] S. V. Nerpin and B. V. Deryagin, Doklady Akad. Nauk SSSR 100, 17 (1955).*

[19] M. P. Volarovich and N. V. Churaev, Kolloid. Zhur. 21, 157 (1959).*

[20] P. V. Panferov, Trudy Kalininskogo Torf. In-ta, 10, 90 (Gosénergoizdat, 1959).

[21] M. P. Volarovich, N. V. Churaev, and B. Ya. Minkov, Torfyanaya Prom. 7, 26 (1957).

* Original Russian pagination. See C. B. Translation.

LETTER TO THE EDITOR

PHASE SEPARATION IN THE SYSTEM: POLYMER–POLYMER–SOLVENT VOLUMES OF THE LAYERS AND MOLECULAR WEIGHTS OF THE POLYMERS

S. M. Lipatov

Institute of Physical Organic Chemistry, Academy of Sciences Belorussian SSSR, Minsk

Translated from Kolloidnyi Zhurnal, Vol. 22, No. 5, pp. 639-640, September-October, 1960
Original article submitted July 10, 1960

If equal weights of two polymers are placed in the same vessel containing saturated vapor of a liquid which is a solvent for each polymer, each polymer takes up the vapor independently of the other. Equilibrium sorption of each of the polymers is the same as in separate sorption of the same vapor by the polymers. Polystyrene has a higher sorptive capacity than acetylcellulose, and after three days is converted from a powder to a concentrated solution.

If solutions of these polymers are prepared separately in dioxane, and equal volumes of the two solutions are mixed, phase separation takes place and the solvent becomes redistributed in accordance with the sorption capacity of each polymer. As the result of such separation the upper layer contains pure polystyrene and the lower pure acetylcellulose. Mixing of two polymer solutions should not be confused with polymer–polymer mixing. If two polymers differing in polarity are fairly well soluble in a liquid and do not form distinct structures in it, their solutions are miscible although the macromolecules of the two polymers need not necessarily interact.

Consider a system consisting of two layers, one of which contains m_1 grams of polymer p_1 in volume V_1, and the other contains m_2 grams of polymer p_2 in volume V_2

$$\begin{array}{c|c} m_1 p_1 & m_2 p_2 \\ V_1 & V_2 \end{array}$$

Since the solvent is common to both layers and the phase separation is in equilibrium, the vapor pressures of the two layers must be equal. In fact, the free energy of dilution of the first layer is

$$\Delta F_1 = RT \ln p_1/p_0,$$
$$\Delta F_2 = RT \ln p_2/p_0.$$

Since $\Delta F_1 = \Delta F_2$, it follows that $p_1 = p_2$. But it follows from the above scheme that V_1 is not equal to V_2 and m_1 is not equal to m_2, whereas the ratios

$$\frac{m_1}{V_1}\frac{1}{M_1} = \frac{m_2}{V_2}\frac{1}{M_2},$$

where M_1 and M_2 are the molecular weights of the two polymers, are equal. If the molecular weight of one of the polymers is known, the molecular weight of the other can be calculated from these expressions. The volumes and osmotic pressures of the layers formed when solutions of polystyrene and polyvinyl acetate in benzene, dioxane, and toluene are mixed were investigated. The volumes and compositions of the layers were determined after 24 hours. When a polystyrene solution was mixed with 4% polyvinyl acetate solution two layers were formed; the upper contained polystyrene and had a volume of 38.2 ml, and the lower contained polyvinyl acetate and had a volume of 19.8 ml. It follows from these results that benzene is a good solvent for polystyrene and is the worst solvent for polyvinyl acetate.

If 20% of acetone (which is a poor solvent for polystyrene and a good one for polyvinyl acetate) is introduced into this system, the layers disappear. It follows that formation of two layers is associated with aggregation (structure formation) in the solutions or with changes in the shape of the macromolecules. When the relative proportions of the polymers are varied, the proportions of the layers also vary or the layers disappear. It should be remembered in this connection that the flexibility of the macromolecules of one polymer may change considerably in presence of another, and this would influence the equilibrium vapor pressure of the two layers. In this case the apparent molecular weight may be determined from the above relation. Investigation of the osmotic properties of polystyrene and acetylcellulose layers in dioxane showed that the osmotic pressures of the two layers were equal: the values were 0.0126 atm for polystyrene and 0.0130 atm for acetylcellulose.

SUMMARY

1. Phase separation of mixtures of two polymers in a common solvent was studied. It is shown that miscibility of polymer solutions does not denote miscibility of the polymers themselves. Phase separation is caused by differences in the molecular structure (shape of the macromolecules and tendency to structure formation) of the polymers. Phase separation does not occur in liquids in which both polymers saturate their fields of force; niether does it occur when two polymers are mixed in a binary solvent mixture one of the components of which is a good solvent for one polymer and the other is a good solvent for the other.

2. Equilibrium polymer layers have equal osmotic pressures. It is therefore possible to determine the molecular weights of the polymers from the layer volumes and concentrations by weight.

BOOK REVIEW

NEW PHYSICAL METHODS FOR INVESTIGATION OF PEAT

COLLECTED PAPERS OF THE KALININ PEAT INSTITUTE, EDITED BY M. P. VOLAROVICH AND N. V. CHURAEV, GOSENERGOIZDAT, 1960, 228 pp. price 8 r. 75 k.

P. A. Rebinder

Translated from Kolloidnyi Zhurnal, Vol. 22, No. 5, pp. 641-642, September-October, 1960

The physics of peat, a new branch of applied molecular physics and physical chemistry, has been developed extensively in recent years, mainly by the work of Professor M. P. Volarovich and his school in the Physics Department of the Kalinin (formerly Moscow) Peat Institute. Even before the Second World War fundamental investigations of the viscoplastic properties of aqueous peat slurries had been carried out in relation to problems of hydraulic conveying of peat, in addition to studies of external friction and adhesion of peat; subsequently, at the initiative and under the direct guidance of M. P. Volarovich, several other aspects of peat physics were studied: rheological properties of peat over a wide range of moisture contents; characteristics of peat dispersity and its variations in technological processes of peat winning and conversion; the macro- and microstructure of peat; the hydration properties of peat in relation to studies of the forms of moisture binding in peat and moisture transport under the influence of various gradients. A considerable number of experimental and theoretical papers on various aspects of peat physics has been published by Volarovich and his co-workers in various periodicals: Kolloidnyi Zhurnal, Doklady Akademii Nauk SSSR, the journal "Torfyanaya Promyshlennost'," Trudy Torfyanogo Instituta, and in reports of conferences at which these papers were presented. The book under review contains a number of articles, describing mainly the new methods for investigation of the physical properties of peat which have been developed by Volarovich and his pupils (A. A. Bagrov, G. Ya. Voronkov, N. I. Gamayunov, K. F. Gusev, F. D. Zhitetskaya, N. V. Lazovskaya, N. I. Malinin, S. N. Markov, B. Ya. Minkov, V. V. Prokimnov, V. P. Tropin, and N. V. Churaev) and by members of other departments of the Institute (I. D. Belovidov and L. M. Zaitseva). Some of the methods described had been proposed earlier for use with other disperse systems, but they were applied to peat for the first time in the Physics Department of the Kalinin Peat Institute.

The section entitled "Dispersity of Peat" contains methods of dispersion analysis of peat, which is a polydisperse system of complex composition. It includes a description of the design of a weight sedimentometer with a counterpoised cup (a special variant of N. A. Figurovskii's apparatus) which can be used for exact measurements with deposits of small weight, and gives an account of a new and convenient method for mathematical analysis of sedimentometric data. The results of dispersion analysis of peat are presented in the form of distribution curves based on data obtained by three methods: sieve analysis, sedimentometric analysis, and electron microscopy. In analysis by electron microscopy the photographs are projected onto a screen and the particle sizes are then determined by means of transparent circular gauges.

The peculiar character of the size-distribution curves for peat, which is a mixture of coarse vegetable fragments and highly disperse humus, made it necessary to introduce a series of statistical parameters characterizing its dispersity. Comparative evaluation of the dispersion of peat is effected by an interesting technique which involves the plotting of a "differential" distribution curve and introduction of the concept "dispersibility range," which characterizes the dispersing power of various mechanisms.

The same section includes a number of methods for investigating the dispersity of dry peat. The method of filtration of rarefied air (as devised by B. V. Deryagin) was used for determination of the specific surface of peat briquets and developed for determination of the dispersity of peat dust fractions.

The section "Rheology of Peat" first contains a description of the successful use of D. M. Tolstoi's well-known apparatus for studying kinetic elastic effects in peat in the range of small shearing stresses. This is followed by an account of an original technique for studying the deformation of peat by means of x-ray transmission, whereby the motion of peat during complex flow processes can be studied. Our conical plastometer was used successfully with peat. The appended graph shows that this plastometer can be used for determining the yield value of peat over a very wide range of moisture contents: between 15 and 55% of the dry substance in peat. A variant of the method based on uniaxial compression of a cylinder was also developed for determination of the yield value of peat. The well-known RV-4 rotational viscosimeter is recommended for determination of both parameters of viscoplastic flow in the Shvedov–Bingham equation for peat with 90-75% moisture. For peat of lower moisture contents a new rotational instrument has been devised, in which the peat under test is placed between two concentric spherical surfaces. It must be noted that all these rheological methods and instruments are provided with a theoretical basis.

The section "Aqueous Properties and Structure of Peat" contains descriptions of a number of known methods (A. V. Dumanskii's method of the negative adsorption of sugar, N. S. Kurnakov's tensimetric method, and G. I. Pokrovskii's freezing method) which have been improved by the authors, and some new methods of investigation. An instrument of considerable interest is a special x-ray camera of high resolving power which can be used for studying the structure of peats of different moisture contents, and of peat components such as cellulose, paraffins, etc. In particular, methods based on the use of radioactive tracers proved especially fruitful. Such methods are used very widely in investigations of peat properties. The methods which have been developed can be used for studying different types of bound and immobilized water in peat on the basis of the classification of the forms of water binding in disperse systems; they can also be used for determining a number of new parameters characterizing the structure of peat – pore size, active porosity, and kinetic specific surface (after B. V. Deryagin).

The tracer-atom method is also used for studying moisture transport in peat. The authors have succeeded in developing a range of methods for investigating the physical aspects of various processes – thermal moisture conduction, drying, capillary rise, etc. The radioactive-tracer method and nuclear radiations are used for studying the transport of water in a peat deposit being dried, i.e., under field conditions. The successful development of a method for determining the bulk density of peat with the use of γ-radiation from the cobalt isotope should also be mentioned here.

Theoretically and experimentally new probe methods (thermal and moisture variants) have been devised for determination of heat and moisture transfer coefficients in peat; the quantitative aspects of the transfer processes can thereby be evaluated. This section also contains a description of an instrument for electroosmotic determination of the electrokinetic potential of peat.

The methods devised by M. P. Volarovich and his co-workers for investigation of peat are also of more general significance, since they can be used with equal success with a number of other disperse materials. It should be pointed out that this is the first time that the tracer-atom method has been used for solving such a wide range of problems in the physics of disperse materials. Accordingly, this book may be a valuable manual for investigation of other disperse systems in addition to peat.

CHRONICLE

WORK OF THE SUBSECTION ON RHEOLOGY OF THE ALL-UNION CONGRESS ON MECHANICS

N. V. Lazovskaya

Translated from Kolloidnyi Zhurnal, Vol. 22, No. 5, pp. 643-647, September-October, 1960

The first All-Union Congress on theoretical and applied mechanics, which was convened by the National Committee on theoretical and applied mechanics of the USSR, jointly with the Division of Technical Sciences of the Academy of Sciences of the USSR and the Moscow State University, took place in Moscow from January 27 through February 3, 1960. The papers were divided into three sections: a section on general applied mechanics, a section on the mechanics of fluids and gases, and a section on solids. The subsection on rheology fell in the last section.

Forty papers were presented in seven sessions of the rheology subsection (presided over by M. P. Volarovich). These papers elucidated theoretical work in the field of rheology, as well as experimental investigations of the rheological nature of various easily deformed materials—dispersed systems and macromolecular compounds. The papers which were read, and the debates which grew out of their discussion, show that research in the field of rheology in our country has continued to develop, and significant successes have been achieved in the various areas of rheology in the past few years. The theory of Shvedov—Bingham on the flow of a viscoplastic substance has been developed further. The general equations of Hencky—Il'yushin, corresponding to a rheological model of such a substance, have been solved for a number of new special cases having great practical significance. At the same time, much experimental work has been carried out in order to study the various types of rheological bodies, and several new methods of investigating the rheological nature of materials have been worked out. In this short review it is not possible to explain fully the contents of the papers. Therefore, the questions which were considered in the various reports will only be mentioned.

In the introductory paper, M. P. Volarovich, speaking of the general problems of rheology, recalled, in particular, the problems which were posed in the area of rheology at the 1954 conference on the theory of elasticity, plasticity and structural mechanics. He indicated that at the present time several of these problems are already solved (see the article by N. I. Malinin, Kolloidnyi Zhurnal 17, 4, 332, 1955).* Then M. P. Volarovich gave a report on the third International Congress on Rheology, which took place under the chairmanship of Professor Müller (Marburg) in 1958 in the Federal Republic of Germany, in the operation of which he participated on the staff of a delegation of Soviet scientists (N. V. Mikhailov, G. V. Vinogradov, A. A. Trapeznikov, and Yu. A. Dainega). The Soviet scientists participated in the meeting of the International Committee on Rheology, at which Professor Saal of Holland presided. Having described the instruments for rheological investigations, which were shown at the exhibits devoted to the congress (principally rotational viscosimeters), M. P. Volarovich noted that these instruments did not exceed domestic viscosimeters of the rotational type in quality. He recalled, in particular, that F. N. Shvedov, born 120 years ago, constructed the first viscosimeter for rheological investigations. Having indicated the wide publication of papers in various fields of rheology in the USSR, M. P. Volarovich noted that in the Soviet Union, however, there have been few monographs published on rheology.

P. A. Rebinder in his paper, "Types of high molecular and dispersed structures and their characteristic mechanical properties," elucidated the basic concept of the new branch of science being developed by him—

* Original Russian pagination. See C. B. translation.

physicochemical mechanics. Having indicated the connection of problems of rheology and physicochemical mechanics, P. A. Rebinder reported his new work and that of his collaborators, pointing out the way in which rheological methods of investigation permit one to ascertain the type of structure of macromolecular compounds and dispersed systems, and also obtain new materials having preassigned properties.

G. V. Vinogradov and V. P. Pavlov came out with a paper on the theme, "Fundamental characteristics of the mechanical properties of consistent (plastic) lubricants as solids," in which they gave the results of the investigation of consistent greases while changing the deformation rate by eight to ten orders of magnitude. The change of the maximum shear stress with a sharp increase and with a decrease of the deformation rate was examined. It was established that a significant change in the degree of homogeneity of the state of stress strongly affects the sharpness of the maximum of the curves expressing the dependence of the shear stress on the deformation, whereas the value of the maximum shear stress changes insignificantly. In the paper of G. V. Vinogradov, A. A. Mamakov, and V. P. Pavlov, "Investigation of soft plastic substances under conditions of complicated states of stress," the flow of highly viscous liquids and nonlinear plastic substances was examined in the presence of two simultaneously occurring simple shears. The circulation and the axial motion in the narrow space between two coaxial cylinders was investigated. These observations also cover a wide range of deformation rates (several decimal orders).

N. V. Mikhailov in his paper dwelt on the investigation of the rheological properties of elastoplastic materials during their deformation. Cases of deformation both under constant shear stress and constant velocity gradient were examined, and an evaluation of the rheological behavior of the indicated materials under these conditions was given. For bitumens, structural solutions, and other dispersed systems, Mikhailov cited considerable experimental data confirming these concepts. The paper of G. M. Bartenev was devoted to investigations of the rheological properties of rubber-like polymers both at small and at large shear stresses. A different character of the development of the deformation in these cases was established. In the first case, the deformation rate curve has a minimum, after which a steady state begins – the deformation rate becomes constant. In the second case, the deformation rate first gradually increases, and then, having attained a certain value, becomes constant.

A. A. Trapeznikov and T. G. Shalopalkina came out with a report giving the results of experimental investigations of the dependence of the maximum elastic and rupture deformation of aluminum naphthenate gel on the deformation rate. They used a complex elastoviscosimeter and an elastorelaxometer in the work. The data cover different stages of deformation and different deformation rates. In the report of T. V. Assonova, T. I. Zatsepin, and A. A. Trapeznikov, "Shear strength and limiting reversible deformation of solutions and the gels of certain rubbers," they reported work on the investigation of the strength and high elastic properties of structuralized solutions of rubber gels, on the basis of which they observed an analogy of the curves expressing the dependence of the deformation on the stress for solutions and rubber gels with curves for rubber in the solid state. The investigations were carried out for large deformation rates, measured by means of an elastorelaxometer.

The papers of S. S. Vyalov were devoted to an investigation of the processes of the deformation of ice and the laws of motion of glacial deposits in conformity with the theories of the flow of viscoplastic bodies, based on investigations carried out in Antarctica. He cited data on the mechanical investigations of ice in the village of Mirny, which permitted him to establish the dependence of the deformation and deformation rate on the stress. In the theoretical solution of the corresponding problem, a power law dependence of the shear stress on the rate of flow was assumed. According to the data it was found possible to determine the change of the rate of flow in different directions (along the height and length) of the glacial deposit and to establish the profile of the glacier deposit of eastern Antarctica (regular semiellipse).

S. E. Frainfel'd discussed the possibility of a certain simplification of the rheological equation in conformity with experimental data. Experiments showed the absence of a well-defined relation between the "instanteous" stress increment and the corresponding deformation. An effect of the initial deformation was also established. However, applications of "hereditary theories" and "aging theories" are very limited. The advantage of the new rheological equation obtained is its simplicity; however it does not permit the possibility of the use of the principle of superposition, even for small deformations. In the report of N. I. Malinin, creep deformation associated with the rupture of molecular chains of high polymers was examined. During investigation of the mechanism of the process of rupture of polymer chains, Eyring's theory of absolute reaction rates was used. T. D. Shermergor reported investigations of the mechanical deformation of an elastoviscous body at

constant rate. The dependence of the elastic modulus on the deformation rate was studied for the simplest distributions of relaxation time, namely, S-shaped, truncated power law, and Gaussian.

A. A. Abbasov, A. F. Kasimov, and Ya. A. Shvarts presented a solution of the problem of the gradual motion of immiscible viscoplastic liquids in the structural regime for several cases of motion in a vertical cylindrical tube and between two coaxial cylinders. The results obtained found practical application in calculations of processes associated with the cementation of oil wells. In the paper by A. A. Abbasov, V. M. Mekhtiev, and A. A. Mirzoyan, the problem of the motion of viscous and viscoplastic liquids in plane and circular ducts considering heat transfer, which has great practical significance for spiral oil pipes and oil wells was examined. The solution of the problem was carried out by applying the method of G. L. Grinberg* and the approximation method of Ritz. As a result, formulas are quoted which permit one to calculate, in particular, the Nusselt number. A. I. Leonov presented solutions of a number of problems in the nonstationary flow of an incompressible viscoelastic Maxwellian fluid, among which were examined: 1) rectilinear motion in the gap between two parallel planes; 2) axially symmetric flow in a cylinder with constant pressure gradient along the tube; 3) motion in a cylinder which rotates with constant angular velocity about its axis. It was shown that from these solutions, one can obtain solutions of corresponding problems of the motion of a Newtonian fluid as the elastic modulus tends to infinity. The paper of A. I. Leonov and M. D. Nusinov was devoted to solutions of certain problems of the quasistationary flow of a Maxwellian fluid. They studied: 1) axially symmetric flow in the gap between two coaxial infinite cylinders; 2) rotation in the gap between two coaxial cylinders; 3) rectilinear motion in the gap between two infinite parallel planes. The solutions under assumptions of incompressibility of the medium and the absence of body forces were carried out on the basis of the general equations of the mechanics of continuous media and the three-dimensional equations of the Maxwellian rheological state. G. T. Gasanov and S. G. Gurbanov examined nonstationary problems of the hydrodynamics of viscous and viscoplastic liquids. It was established that for problems of circular motion with fixed boundaries, the method of Schwartz gives better results than the method of averaging. An exact solution of the approximate equations of the nonstationary motion was carried out by the operational method for viscous and viscoplastic liquids. I. M. Astrakhan came out with a report in which the equations of motion of a viscoplastic liquid in a boundary layer on an arbitrary surface were examined. Such a boundary layer is formed in viscoplastic liquids during motion at high Reynolds numbers. Various cases of flow, depending on the ratio between the dimensionless parameters determining the motion, were investigated. With the help of the boundary layer equations, problems of stationary and nonstationary rotation of a cylinder and of a viscoplastic liquid and other problems were solved.

The paper by G. I. Fuks was devoted to investigations of the viscoplastic flow of structuralized systems (grease, clays, etc.), carried out by differential methods. In the observation of the flow process, the velocity and stress in separate small portions of the moving medium were simultaneously measured in weak suspensions of paraffin in oil, suspensions of clay, and pigments. At small velocities, zones with a different flow character (Newtonian and Binghamian) are observed in the direction perpendicular to the velocity. However, these zones become unstable upon increasing the velocity. V. P. Pavlov reported fundamental results of the investigations of creep, elasto-strength properties, and anisotropy in the deformation of plastic greases under conditions of a homogeneous shear stress field. At stresses whose magnitude is about 3% of the strength limit, creep deformation appears, and a strengthening of the sample with the passage of time is observed. A connection of the strength limit with the rate and direction of deformation was established, and a dependence of the shear modulus on the magnitude of the deformation was also found. V. V. Vainshtok reported investigations of the thixotropic properties of greases as bases for their rheological characteristics. The speaker indicated the absence of a correspondence between the values of rheological parameters and the behavior of consistent greases, which is associated with the peculiarities of their structure, in particular with the presence in them of both a solid skeleton and a liquid medium, whose deformations have a different character. Yu. M. Ivanov reported on the evaluation of the strengths of polymer materials as a function of time and temperature. V. V. Andreev, A. M. Kosevich, and L. V. Tanatarov devoted their paper to investigations of nonelastic and residual deformations of a plane solid lamina during an allotropic transformation. Deformations associated with the displacement of the interface separating two solid phases having different specific volumes were examined, in the case in which the deformations corresponding to the elastic limits of the two phases are less than the change of volume during the phase transformation. Residual deformations occurring as a result of the complete transition of the specimen from one phase to another were found, for the case in which the stress relaxation time is large. The case of fast relaxation was examined subject to a number of simplifying assumptions.

* Translator's note; Possibly H. Greenberg.

A. M. Gutkin examined the problem of the limit equilibrium of an elastoplastic medium during its compression between two solid surfaces in the absence of slip. In this case a dependence of the static coefficient of lateral pressure on the limiting shear stress and the dimensions of the specimen under investigation was also found. A second paper by A. M. Gutkin was devoted to the problem of the flow of a viscoplastic medium under double shear. A plane problem of the motion of a viscoplastic medium between two planes forming an acute angle was presented in the paper of M. P. Volarovich and A. Kh. Kim. For the solution of this problem, a stream function was introduced which satisfies the conditions of continuity, and the velocity components were expressed in terms of this function. As a result of the elimination of the pressure from the equations which were found, they obtained an equation for the velocity components which is nonlinear relative to the stream function Ψ. The solution was carried out under the assumption that the medium sticks to the wall and the shear extends throughout the entire volume of the medium. As a consequence of this, the result obtained is correct for a sufficiently large pressure and a comparatively small value of the limiting shear stress, when the angle between the planes is not very small. A. Kh. Kim, in his paper, reported a solution of a problem of the motion of a viscoplastic dispersion medium in a cone. A solution was found for the case in which the shear extends throughout the entire region, and the system completely sticks to the wall. The solution of a problem in the flow of an elastoviscoplastic medium in a boundary layer was examined by N. V. Tyabin. It was shown that the general equations of motion of an elastoviscoplastic medium occupying the entire region relative to a solid body can be significantly simplified by evaluating the order of magnitude of the individual terms, and as a result, equations for the flow of an elastoviscoplastic medium in a boundary layer are obtained. Several special cases of motion in a boundary layer were presented.

F. S. Fadeeva reported results of the investigation of compression and shear deformation processes in plastic clayey substances, which occur during the molding of ceramic parts; she noted that during the deformation in the pug mill, there is observed a densification of the clayey substance and the formation of a front of motion, which has the form of a paraboloid of revolution. The absence of "dead" zones and the presence of plastic deformations throughout the entire region were established on the basis of experimental investigations. V. V. Vedeneev devoted his paper to investigations of the flow of bitumens, and bitumens with fillers, in tubes; it was pointed out that in solving the flow problem for bitumens, it is necessary to consider mechanical characteristics which are consistent with the complete rheological curves of the bitumens under investigation. It was established that the calculation of the flow of bitumens can be carried out with relations which are well known from hydraulics for purely viscous and structuralized liquids. However, a determination of the coefficient of hydraulic resistance of structuralized bitumens cannot be carried out with the formulas which are correct for purely viscous bitumens. R. V. Torner presented results of the application of the method of the theory of similarity to the calculation of the process of isothermal flow of rubber mixtures in a channel of circular cross-section. It was shown that the value of the dimensionless pressure loss both at the inlet and in the portion where the flow becomes established depends on the value of the effective Reynolds number. In the paper of M. V. Gzovskii, I. Ya. Kuznetsova, and D. I. Osokina, results were presented of the experimental investigation of stress, carried out by application of an optical polarization method. These investigations were for the purpose of modelling the deformation and rupture processes in solids (for large time intervals). The observations were carried out on special materials, which had mechanical properties such as to provide similarity of the processes in the model to the processes taking place under essentially natural conditions. N. V. Lazovskaya reported on x-ray investigations of the deformation of drains on a loaded model for draining peat bogs. Yu. I. Kosterin and I. V. Kragel'skii came out with a report in which rheological processes observed during dry friction were considered. S. V. Levi reported results of the investigation of the rheological properties of a solution of gelatins, which, depending on the concentration and temperature, in some cases exhibited the properties of Newtonian liquids, and in others behaved similarly to elastoviscous bodies. The mechanism of the process of transformation of a solution of gelatin into a gel as the temperature is lowered was examined, and it was established that this process is accompanied by a change in the value of the limiting shear stress, and also of the elastic modulus. The paper of A. E. Desov was devoted to experimental investigations of the process of the propagation of oscillations of different frequencies in concrete mixtures. Observations were carried out at frequencies from 25 to 250 cps; the damping coefficient of the oscillations was determined as a function of the viscosity of the concrete mixture and the duration of the vibration. Thixotropic changes were investigated, and the corresponding limiting vibration amplitudes were established. It was explained that at oscillation frequencies of from 25-50 cps, propagating from the lower base of a concrete prism, the exponential law of damping of the vibrations along the height of the prism is altered. For frequencies of from 100 to 200 cps, the oscillations are damped by a law which is nearly exponential. S. K. Noskov reported investigations of the viscous properties of elastoplastic

materials during their vibration. In a report by M. P. Volarovich, G. Ya. Voronkov, E. P. Kovalevskii, and G. I. Kuzhman, the propagation velocity of longitudinal waves in a sample of peat, the pores of which were filled with air or water, was investigated. The observations were carried out by a pulse method at a frequency of the order of 1000 kc. It was established that the propagation velocity of elastic waves depends on the porosity of the peat sample. A decrease of the wave propagation velocity with an increase of porosity was observed. This change is larger upon filling the pores with air and smaller upon filling them with water. An increase in the absorption coefficient for elastic waves with an increase in porosity is associated with an accompanying change in the viscous properties of the medium.

B. A. Dogadkin came out with a report which was devoted to chemical stress relaxation and the flow of three-dimensional polymers. The kinetic laws of stress relaxation as they depend on the energy of the bonds which are subject to decay under thermomechanical action, were established. The role of the substances which affect the character of the secondary processes of recombination of radicals formed during the decay of the three-dimensional structure of the polymers was clarified. The technical aspects of chemical relaxation and flow for a wide class of substances and phenomena were examined.

In conclusion it should be stated that all of the papers were heard with great interest, which indicates that they elucidated new and essential problems in the realm of theoretical and experimental rheology. Solutions of the general system of the Hencky–Il'yushin equations for certain special cases were of the greatest interest. In addition to the solutions of these equations for new cases of flow in circular and annular tubes (flow considering heat transfer, unsteady flow, sequential flow of two media, flow with two simultaneously acting shears), the problem of the limit equilibrium of a disc under compression between two solid surfaces in the absence of slipping was solved, which thereby clarified the role of the "lateral pressure," and motion in plane* and circular cones was also studied. Cases of the flow of an elastoviscoplastic medium in a boundary layer were examined. Certain new problems of elastokinetic phenomena were developed further: quasistationary and nonstationary flow of a Maxwellian fluid, elastic aftereffect deformations, creep (as applied to high polymers).

Along with these theoretical papers, the experimental investigations of rheological processes and the properties of various materials are very important, in particular those, which find wide practical applications. New methods were used in a number of experimental investigations, and what is particularly essential, in certain papers, structural peculiarities of the system being investigated were considered. In addition, investigations covering a very wide range of shear stresses and velocity gradients (10 orders) are of great interest, and also investigations lasting for very long times (more than 1000 hours). Dynamic methods of investigation, in particular, the use of ultrasonic setups, etc., are also currently applied for dispersed systems. The results obtained enable the classification of rheological bodies to be made more precise. Thus, the significant role of the limiting shear stress (limiting strength of the structures) for solid-like systems and of the effective viscosity for liquid-like materials was confirmed. There has been an expansion of work devoted to problems of complex states of stress. The investigation of certain rheological processes has been carried out by modelling methods with the application of the theory of similarity. The experimental data obtained for a number of materials (ice, high molecular compounds and their solutions, plastic greases, bitumens, peat, clays, etc.) find application in practice for the interpretation of the processes of deformation and flow of materials, for the design of machines, and for the regulation of technological processes.

However, it is nevertheless necessary to note that certain important rheological problems have not yet been sufficiently developed, and they should receive particular attention in future work. Some of these most essential rheological questions which should be investigated follow: 1) by means of a generalization of the experimental investigations, the establishment of the fundamental rheological equations which govern the processes of deformation and flow of real nonlinear materials – dispersed systems and high polymers, and also ice in connection with geophysical investigations in the Arctic and Antarctica, with the application of the methods of mechanics and thermodynamics; 2) further theoretical investigation of various cases of high elastic deformations, and also the flow of relaxing and viscoplastic media; 3) development of the theory of similarity and modelling of rheological processes; 4) further work to relate phenomenological investigations with the molecular mechanism in the nonlinear flow of a material, 5) additional thorough experimental investigation of the rheological characteristics of materials,considering their structural peculiarities; 6) perfection and standarization of methods and apparatus used for rheological investigations; 7) working out of standard methods of investigation of full rheological characteristics; 8) necessity for the output of a series of apparatus with wide ranges of shear stress, velocity

* Translator's note: the translator presumes (but has not been able to verify) that a "plane cone" is a two-dimensional converging or diverging channel.

gradients, temperature, and pressure for use in scientific investigations and for the automation of production; 9) the clearing up of the molecular mechanism of rheological phenomena in structuralized dispersed systems on the basis of wide applications of up-to-date methods of investigating the structure of materials – the electron microscope, ultrasonic and vibrational methods, radioactive isotopes and infrared spectrometers, etc.; 10) the working out of unified definitions of rheological quantities, and the standardization of rheological definitions, terms, and designations.

INFLUENCE OF THE STRUCTURAL AND MECHANICAL PROPERTIES OF PRINTING INKS ON THEIR BEHAVIOR IN THE PRINTING PROCESS*

T. I. Gudkova, L. A. Kozarovitskii, and N. V. Mikhailov

The All-Union Scientific Research Institute of the Printing Industry, Moscow
Translated from Kolloidnyi Zhurnal, Vol. 22, No. 6, pp. 649-657, November–December, 1960
Original article submitted September 21, 1959

Printing inks undergo considerable periodic stress changes, due to sharp differences in rates of deformation, at various stages of the printing process and during interaction with paper. Abrupt stress differences arise when the ink enters the inking system, as it enters and leaves the narrow gap between the rollers, when the ink is applied to the printing form, and during distribution of the layer between the form and the impression. Our calculations show that the maximum velocity gradients may be $1 \cdot 10^4$ sec $^{-1}$ or even greater. The initially structurized ink undergoes complete structural breakdown and its behavior at these stages of the process can be reliably and uniquely characterized, in the main, by the minimum viscosity of the structure broken down to the limit [1,2].

After the impression has been formed, the pressure reduced, and a thin layer of ink on the impression has started to separate from the form, there is a rapid decrease of stress and deformation rate in the ink. The destroyed structure of the ink is restored. Increase of the pigment concentration at the surface of the impression as part of the binder is absorbed also leads to a rapid increase of effective viscosity, up to complete restoration of the destroyed structure and transition of the ink from a sol to a gel and then to a xerogel when the thin layer of ink is completely fixed on the paper. At this stage the most important characteristics of the ink are the kinetics of viscosity increase and structure strengthening, and the ultimate gel strength [1].

For an understanding of the effects taking place when the ink is fed into the inking system, during the feeding process, in separation of the ink layers on the ink rollers, in transfer of the ink from the form to the paper, and during fixation of the ink on the paper, it is also very important to know the character of the structures formed and the nature of the elements of the destroyed structure.

All these characteristics of the ink can be determined from the complete rheological curve; relative shear rate $\dot{\epsilon} = d\epsilon/d\tau$ (velocity gradient) against the shear stress P [2-5]. Hitherto it has not been possible to obtain complete rheological curves for printing inks because velocity gradients of the order of $1.5\text{-}2.5 \cdot 10^3$ sec^{-1} were required in most cases for ultimate structural breakdown, whereas in investigations of printing inks the gradients used generally did not exceed 450 sec^{-1} [6,7].

We were able to obtain, for the first time, complete rheological curves for a series of printing inks by viscosity measurements in two instruments: an instrument of the Veiler-Rebinder type with a vertically moving plate in a plane gap [8], and the NII-200 selsyn rotational elastoviscosimeter [9]. The first instrument was used for investigating regions of the $\dot{\epsilon}$ (P) curves corresponding to constant viscosity η_0 of the undestroyed structure at constant P. The selsyn elastoviscosimeter was used for determining the regions of the curves corresponding to the complete range of effective viscosities and the minimum viscosity of the structure broken down to the limit (η_m) at constant $\dot{\epsilon}$ [2,5].

*Presented at the Fourth All-Union Conference on Colloid Chemistry, May 1958.

Two groups of inks differing sharply in the degree and character of structure formation and in the kinetics of structural strength increase were used for determinations of the complete rheological curves and for correlation of their rheological properties with their behavior in the printing process. Group I contained model inks containing 30% of printing gas black by volume in linseed drying oils of different degrees of polymerization (ink 1, in boiled linseed oil of 0.7 poise viscosity; ink 2, -in polymerized oil of 20.2 poise viscosity; in ink 3 in 200 poise polymerized oil). Group II included industrial samples of black inks 53 and 54 * and a blue ink **, which differ in their printing behavior.

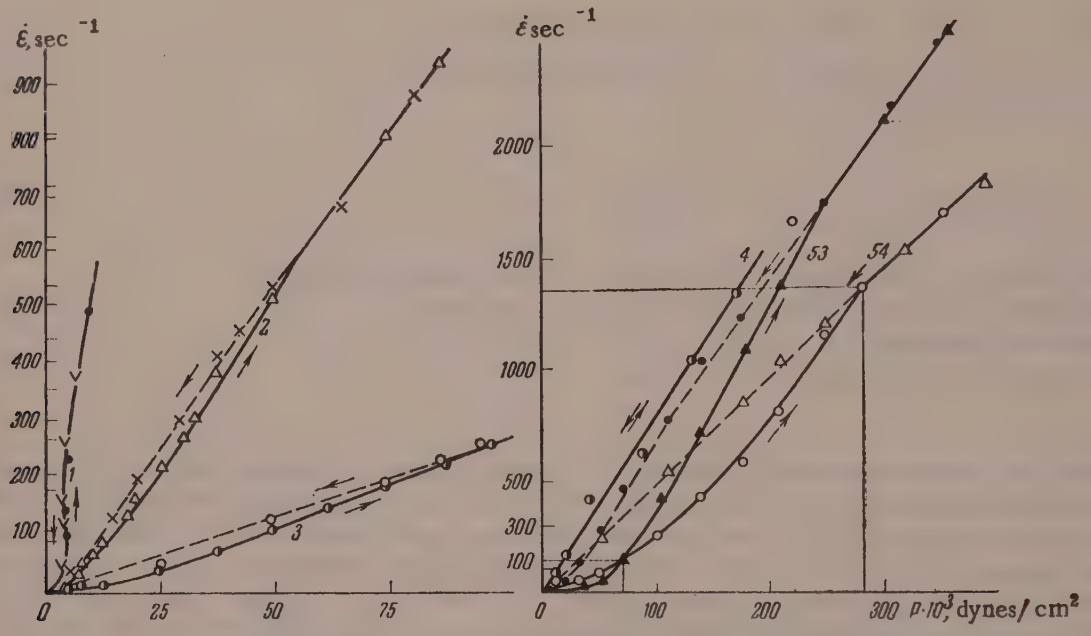


Fig. 1. Complete rheological curves for inks No. 1, 2, 3, 4, 53, and 54. Arrows indicate the directions of the ascending and descending curves.

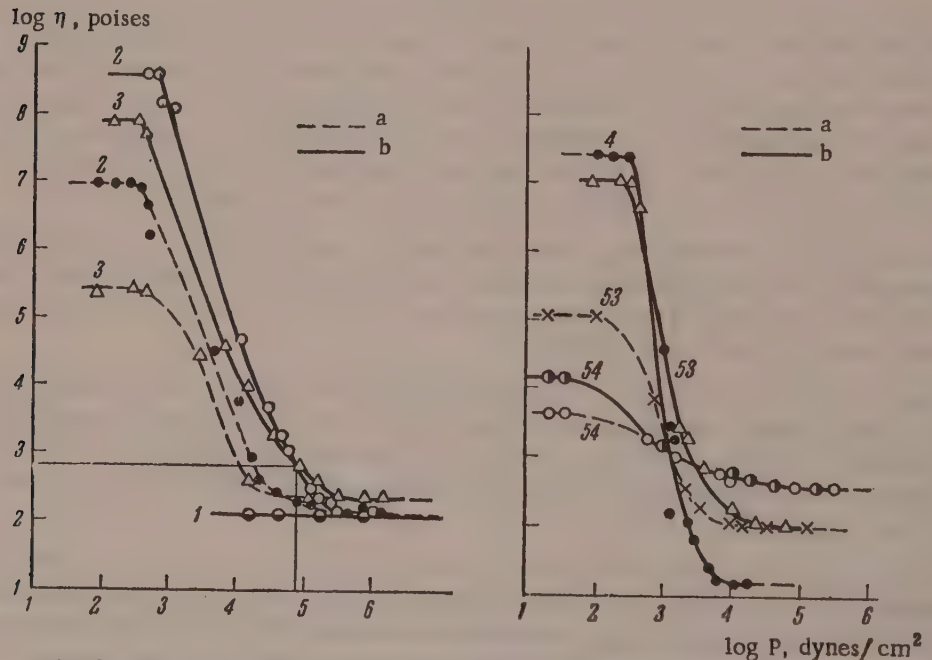


Fig. 2. Variations of the viscosities of inks No. 1, 2, 3, 4, 53, and 54 with shear stress with destroyed (a) and restored (b) structure.

*Ink 53 consists of carbon black and Milori pigments in a mixture of polymerized oils; ink 54 contains carbon black and alkyd resin.

**Consists of Milori pigment and weak-weak drying oil in 1:1 ratio by volume.

TABLE 1

Structural and Mechanical Characteristics * of Printing Inks

inks	η_m, poises	η_0, poises	η_0/η_m	P_m^1, dynes/cm^2	P_m^1, dynes/cm^2	$\dot{\epsilon}_m$, sec^{-1}	$\dot{\epsilon}_r^1$, sec^{-1}	$E \cdot 10^{-5}$	$E_1 \cdot 10^{-4}$	$\theta = \frac{\eta_0}{E_1}$, sec	$\lambda = \frac{E_1}{E_1+E_2}$
1	20,2	$3,0 \cdot 10^7$	$1,5 \cdot 10^6$	$6,0 \cdot 10^3$	317	293	$1 \cdot 10^{-5}$	1,8	8,0	150	0,68
2	93,0	$8,3 \cdot 10^6$	$9,0 \cdot 10^4$	$6,0 \cdot 10^4$	251	645	$3 \cdot 10^{-5}$	0,57	2,0	91,0	0,77
3	370	$2,5 \cdot 10^4$	$6,7 \cdot 10$	$9,0 \cdot 10^4$	50,2	243	$2 \cdot 10^{-3}$	0,08	0,1	3,6	0,90
4	133	$1,3 \cdot 10^2$	1,0	—	—	—	—	—	—	—	—
53	144	$3,1 \cdot 10^8$	$2,1 \cdot 10^6$	$2,4 \cdot 10^5$	1000	1700	$0,3 \cdot 10^{-5}$	13,0	75,0	230	0,65
54	212	$3,6 \cdot 10^7$	$1,7 \cdot 10^5$	$2,9 \cdot 10^5$	501	1300	$1,4 \cdot 10^{-5}$	2,8	9,0	128	0,75

* η_m and η_0 = minimum and maximum viscosities; P_m^1 and P_r^1 = nominal stress limits for the ultimately destroyed and undestroyed structure; $\dot{\epsilon}_m$ and $\dot{\epsilon}_r$ = nominal limits of the velocity gradients for the ultimately destroyed and undestroyed structure; E_1 and E_2 = moduli of quasi-instantaneous deformation and elasticity; θ = true relaxation time; λ = elasticity.

The complete flow curves for these inks and graphs showing variations of their effective viscosity with shear stress are presented in the form of $\dot{\epsilon}$ (P) and log η (log P) graphs in Fig. 1 and 2. The principal rheological characteristics calculated from these graphs are given in Table 1.

Analysis of these graphs leads to the following conclusions: inks 1 and 53 have the highest values of maximum creep viscosity, with relatively low values of the constant viscosity of the destroyed structure. The ratios of their constant viscosities η_0/η_m are $1.5 \cdot 10^6$ and $2.1 \cdot 10^6$ respectively.

Ink 3 has a considerably lower creep viscosity than inks 1 and 53, and the highest constant viscosity of the destroyed structure ($\eta_m = 3.7 \cdot 10^2$). The remaining inks occupy intermediate positions, being systems structurized to different extents. The Milori ink is virtually unstructurized; its viscosity is independent of the velocity gradient over the whole range.

Analysis of Fig. 2 shows that for ink 1 the transition from η_0 to η_m occurs over a relatively narrow stress range, from $3.2 \cdot 10^2$ to $6.0 \cdot 10^3$. The branches of the $\dot{\epsilon}$ (P) curves (Fig. 2) representing decreases of stress and velocity gradient after ultimate structural breakdown show that inks 1 and 53 become structurized even during the experiment; in the case of ink 1 the ascending and descending curves do not form hysteresis loops and almost coincide, while in the case of ink 53 the descending curve ceases to be linear when P has fallen to 10^5 dynes/cm^2 and $\dot{\epsilon}$ to 800 sec^{-1}.

Measurements of the kinetics of thixotropic increase of structural strength, performed in the cone plastometer, showed that the structural strength of ink 1 increases 2.5-fold during the first 3 minutes and fivefold during 60 minutes after breakdown of the structure; in the case of ink 53 the structure is appreciably strengthened after 20 minutes. Inks 3 and 54 do not show any noticeable increase of structural strength during one hour.

This difference between the rheological curves, due to differences in the character of the ink structures, is clearly reflected in the behavior of these inks as they pass from the reservoir into the ink system.

The reservoir for feeding ink into the system of ink rollers in the printing machine consists of a metal cylinder (ductor) with a flexible steel blade adjacent to it at a certain angle. The amount of ink fed onto the rotating ductor is regulated by the size of the gap between it and the blade. The ink should be fed onto the ductor uniformly for normal feeding of the inking system. In very mobile inks, as in truly viscous liquids in general, any stress (no matter how small) arising owing to rotation of the ductor cylinder causes the whole ink mass to flow. The flow rate falls steadily and continuously from the maximum value, equal to the rotation velocity of the cylinder at its surface, to a velocity close to zero at the back wall of the reservoir. In highly structurized

inks like No. 1 or 53 the viscosity drops sharply in the narrow gap and the thin boundary layer on the cylinder, owing to ultimate breakdown of the structure. In layers further from the ductor the viscosity remains fairly high and increases with time after initial mixing of the ink in the reservoir. The liquid boundary layer serves as a lubricant between the ductor and the rest of the ink. Therefore the stresses arising during rotation of the ductor are relaxed in the boundary layer and lead to only very low flow rates and even to small elastic deformations in the ink layers away from the ductor [10]. In such cases flow of ink to the ductor gradually diminishes or stops completely, and the impression becomes gray. The ink has to be agitated in the reservoir at intervals to restore normal flow.

A clear picture of the deformation field and ink flow near the ductor cylinder may be obtained by transmission of x rays through the ink in a model ink reservoir during rotation of the ductor cylinder [11]. The complete rheological curve can be used for predicting the behavior of an ink in the reservoir and the uniformity of its supply to the ductor cylinder. Our investigations show that quasisolid elasticobrittle systems with a sharp drop of constant viscosities in a narrow stress range, provided that the structure is rapidly restored or a certain critical value of the effective viscosity is reached in less than 1 hour, will undoubtedly cause considerable difficulties in feeding of the ink system. Normal feeding would be obtained with unstructurized inks or inks with a quasifluid mobile thixotropic structure which is restored very rapidly after breakdown. The rate of structural buildup, a characteristic of great importance for assessment of normal feeding of the ink system, can be estimated from the descending branch of the complete rheological curve for the ink with different experimental times.

When rolled in the inking system the ink becomes heated; for example, in high-speed printing machines its temperature rises by 20-30° above the temperature of the surrounding air. As a result, the true viscosity of the ultimately destroyed ink structure in the printing machine is lower than that found by viscosimetric measurements. We studied the effect of temperature on the viscosity of a sample of an experimental ink for high-speed machines.

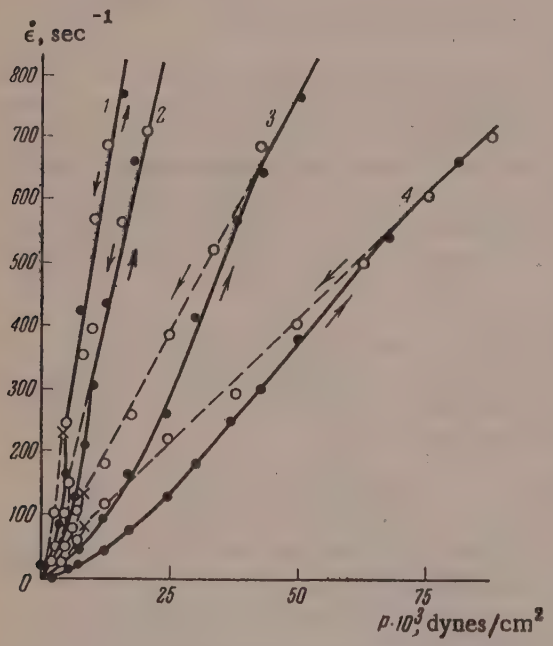


Fig. 3. Complete rheological curves of an experimental ink for a high-speed printing machine: 1) t = 80°; η_m - 20; 2) t = 50°, η_m = 27; 3) t = = 30°, η_m = 67; 4) t = 20°, η_m = 125.

The complete rheological curves for this ink in the 20-80° range are given in Fig. 3, the log η_m - t relationship is shown in Fig. 4, and the quantitative characteristics calculated from these curves are given in Table 2.

It follows from Fig. 3 and 4 and Table 2 that the sharpest drop of the minimum viscosity η_m occurs with a temperature change from 20 to 50°. An initial temperature increase of 30° produces an almost fivefold decrease of η_m. A further temperature increase from 50 to 80° causes only a relatively small viscosity decrease. The nature of the rheological curves also alters with rise of temperature. The stress at which ultimate structural breakdown occurs (minimum constant viscosity) decreases sharply(more than 11-fold with increase of t from 20 to 80°). Structure formation in the inks begins at higher velocity gradients with increase of temperature.

The plot of log η against t is a straight line with a break at about 50° (Fig. 4). The temperature coefficient of thermal sensitivity is $18.6 \cdot 10^{-3}$ and $4.3 \cdot 10^{-3}$.

It is interesting to note that similar results were obtained by Shakhkel'dyan [12] for a large series of polymerized drying oils; he showed that at 50-60° the linear log η (1/T) plots intersect.

The fact that printing inks in the working temperature range and drying oils exhibit the same relationship between viscosity of the ultimately destroyed structure and temperature suggests that in the region of ultimate structural breakdown in the printing machine the nature of the viscosity-temperature relationships for printing inks should be determined primarily by the corresponding variations in the viscosity of the binder.

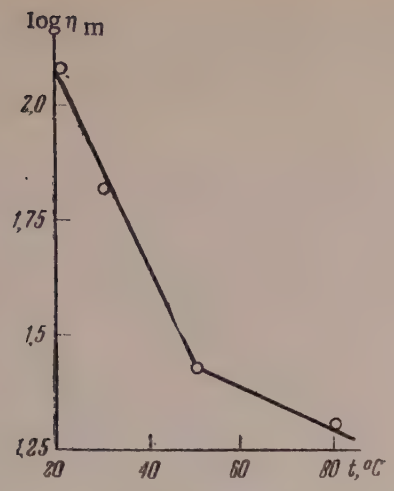


Fig. 4. Effect of temperature on the viscosity of ultimately destroyed structure of printing ink.

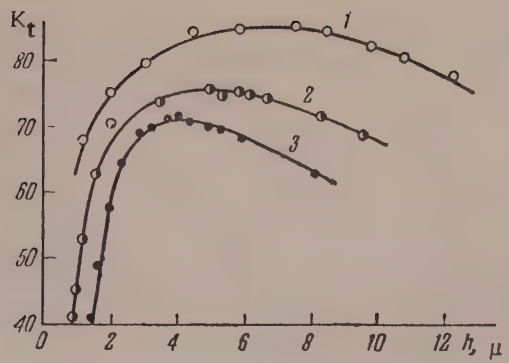


Fig. 5. Variations of transfer coefficient with the thickness of the ink layer on the form (h_f) for inks of different viscosities (η_m): 1) 31.0 poises; 2) 93.0 poises; 3) 370.0 poises.

In the decisive stage of the printing process when the ink is transferred from the form to the paper, i.e., at the instant when the impression is made, the rheological properties of the ink are highly important.

The transfer coefficient (K_t) is usually represented as the ratio of the amount of ink G_o transferred to the paper during printing to the amount initially present on the form (G_f); $K_t = G_o/G_f \cdot 100\%$.

TABLE 2

Effect of Temperature on Rheological Properties of an Ink Sample.

t, °C	η_m, poises	d log η_m/dt	p_m^1, dynes/cm²	$\dot{\epsilon}_m^{-1}$, sec	$\dot{\epsilon}^{-1}$, sec *
20	125	$18{,}6 \cdot 10^{-3}$	$70 \cdot 10^3$	560	70
30	66		$37{,}5 \cdot 10^3$	560	120
50	27	$4{,}3 \cdot 10^{-3}$	$12{,}0 \cdot 10^3$	350	160
80	20		$6{,}0 \cdot 10^3$	300	250

* $\dot{\epsilon}_x$ = the velocity gradient at which structure restoration in flow begins.

$$K_t = \frac{G_o}{G_f} \cdot 100\%$$

The plot of $K_t - G_f$ is a curve with a maximum. The position and value of the maximum depends on the ink capacity of the paper, which is determined by the minimum amount of ink required to cover all the surface irregularities of the paper (the free spaces between them).

Under static, equilibrium conditions the amount of ink required to fill the irregularities (including the ink absorbed by the paper) must evidently be independent of its rheological properties. On the other hand, under dynamic conditions, if the time of contact and layer separation does not exceed 0.1-0.01 sec, the proportion of ink transferred from the form to the paper must evidently depend not only on the nature of the paper surface but also, and to a considerable degree, on the viscosity of the ink. However, data on the influence of ink viscosity on the transference, reported by some workers [13-15], are somewhat indefinite. This is evidently because the viscosities of structurized inks were measured at low and arbitrarily chosen velocity gradients, i.e., at different degrees of structural breakdown for each of the inks. And yet, as was pointed out earlier, the viscosity of any ink at the instant of transfer corresponds to the ultimately destroyed structure.

Our investigations of the $K_t(G_f)$ and $K_s^*(G_f)$ relationships for inks of different viscosities, and of the direct $K_t(\eta_m)$ and $K_s(\eta_m)$ relationships (Figs. 5, 6, and 7) show that with increase of the ink viscosity the

* K_s is the coefficient of saturation of the paint with ink.

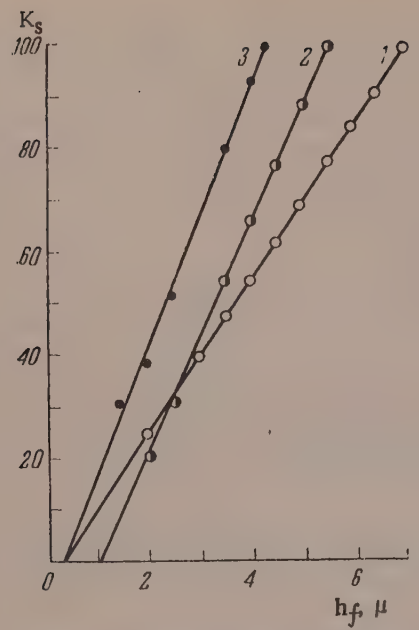


Fig. 6. Variations of saturation coefficient with the thickness of the ink layer on the form (hf) for inks of different viscosities (η_m): 1) 31.0 poises; 2) 93.0 poises; 3) 370.0 poises.

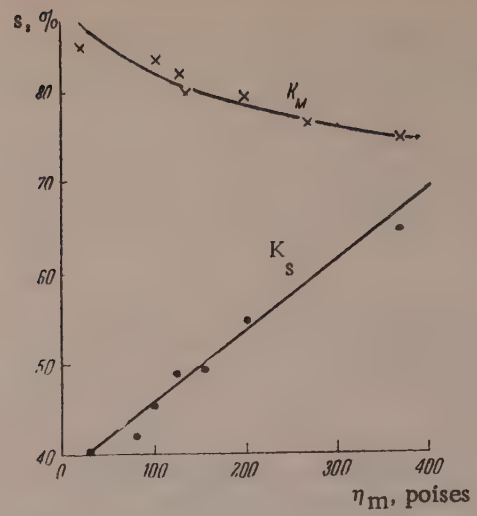


Fig. 7. Variations of the transfer coefficient at the maximum point (K_M) and the saturation coefficient (K_s) with the viscosity η_m corresponding to ultimate structural breakdown.

transfer coefficient in the region of the maximum (K_M) decreases; this means that the relative proportion of ink remaining on the form increases with increasing η_m. The ink acceptance of the paper in the range of working thickness of the ink layer, or the degree of saturation of the paper with ink $K_з = G_o/G_{Mo}$, increases with increasing viscosity for a given layer thickness; i.e., the lower the viscosity, the more ink is required at a given layer thickness on the form for saturation of the paper. This applies to ordinary printing papers with relatively high ink acceptance. For papers with mineral coatings (chalk), of high smoothness and low ink acceptance, the reverse is true, and K_M is higher for inks of lower viscosity. However, the general differences between the values of K_M for inks of different viscosities diminish; for example, K_s decreases appreciably with increase of η_m from 20 to 100 poises. On further increase of η_m up to 270 poises, K_s changes very little. The small variations of K_M with changes of ink viscosity can probably be attributed to the fact that if the paper is very smooth and the ink has high adsorptional activity with respect to the mineral coating on the paper even a short contact time is enough for even a viscous ink to fill almost all the surface irregularities.

SUMMARY

1. The usual characterization of structurized printing inks in terms of effective or plastic viscosity, determined at arbitrarily chosen velocity gradients (i.e., at different degrees of structural breakdown), does not give a correct indication of their behavior in the printing process. Such characteristics are devoid of absolute meaning and cannot be compared for different inks. Our calculated values of the velocity gradients to which the ink is subjected in the inking system reach 10^4 sec^{-1}. Under such conditions the ink structure is broken down to the limit.

2. Complete rheological curves, including the constant viscosity values for the ultimately destroyed structure, have been determined for printing inks for the first time. The principal rheological characteristics of printing inks at entry into the inking system are: ratio of the constant viscosities η_0/η_m; the stress region in which the viscosity drop occurs; and the kinetics of thixotropic structural buildup. In the rolling stage and in the printing process proper the main rheological constant is the constant minimum viscosity of the ultimately destroyed structure.

3. Increase of temperature in the 20-50° range diminishes the minimum constant viscosity almost 5-fold. The viscosity decrease on further rise of temperature is small. The form of the log η_m–t curve in the region of the ultimately destroyed structure is analogous to that of the curve for the ink binder at the same temperatures.

4. The influence of η_m on transfer of ink from the printing form to the paper has been investigated. The proportion of ink transferred from the form to the paper depends primarily on the viscosity of the ink structure after ultimate breakdown. This proportion increases with decrease of η_m for the ink.

LITERATURE CITED

1. L. A. Kozarovitskii and P. A. Rebinder, Zhur. Pologràf. Pr-vo, No. 6 (1951).
2. N. V. Mikhailov and P. A. Rebinder, Kolloid. Zhur. 17, 107 (1955).*
3. W. Philippof, Koll.-Z. 4, 71 (1935); Viskositat des Kolloide (1942).
4. E. E. Kalmykova and N. V. Mikhailov, Kolloid. Zhur. 16, 350 (1954);* N. V. Mikhailov and E. E. Kalmykova, Doklady Akad. Nauk SSSR 99, No. 4, (1954); S. Ya. Shalyt and N. V. Mikhailov, Kolloid. Zhur. 18, 609 (1956).*
5. L. A. Abduragimova, P. A. Rebinder, and N. N. Serb-Serbina, Kolloid. Zhur. 17, 184 (1955)*; N. N. Serb-Serbina, Kolloid. Zhur. 20, 563 (1958)*; L. A. Abduragimova and N. G. Alekperova, Kolloid. Zhur. 20, 681 (1958).*
6. B. N. Shakhkel'dyan, Kolloid. Zhur. 18, 111 (1956).*
7. A. A. Trapeznikov and T. G. Shalopalkina, Kolloid. Zhur. 19, 282 (1957).*
8. S. Ya. Veiler and P. A. Rebinder, Doklady Akad. Nauk SSSR 49, 354 (1945); S. Ya. Veiler, Zavodskaya Lab. 14, 432 (1948).
9. N. V. Mikhailov, Doctorate Dissertation: New Building Characteristics of Bitumens and Cements Based on their Structural and Mechanical Properties [in Russian] (Moscow, 1955).
10. L. A. Kozarovitskii, Poligraf. Pr-vo, No. 1 (1953).
11. L. A. Kozarovitskii and S. Ya. Shalyt, Proc. Third All-Union Conference on Colloid Chemistry [in Russian] (Izd. AN SSSR, Moscow, 1956); Kolloid. Zhur. 15, 437 (1953).*
12. B. N. Shakhkel'dyan, Masloboino-Zhirovaya Prom., No. 3 (1959).
13. J. Olsson and L. Phile, Svensk Papperstidning 12 (1952).
14. J. Fetsko and W. Walker, Am. Ink. Maker 33, 12 (1955).
15. A. Zettlemoyer, R. F. Scarr, and W. D. Schaeffer, Abstracts of Papers Given at the Fourth International Conference of the Scientific Research Institute of Printing in Munich (1957).

*Original Russian pagination. See C. B. translation.

COLLOIDOCHEMICAL PRINCIPLES OF THE VARIATIONS OF OPTICAL PROPERTIES AND WEATHERING RESISTANCE OF LACQUERS PIGMENTED WITH CARBON BLACK

Ya. M. Gurevich and R. F. Minaeva

Scientific Research Institute of the Lacquer and Paint Industry, Moscow
Translated from Kolloidnyi Zhurnal, Vol. 22, No. 6, pp. 658-662,
November-December, 1960
Original article submitted September 18, 1959

This paper deals with a study of the relationship between the optical properties of lacquer films pigmented with carbon black and the colloidochemical processes which occur in them during drying and under the influence of atmospheric factors: light, water, and heat.

We investigated enamel films made from six samples of carbon black (see table) and two binders: alkyd and nitrocellulose resins. The carbon-black concentration in the nonvolatile part of the enamel (in the dry film) was 17% for alkyd enamels and 6% for nitrocellulose enamels.

TABLE 1

Physicochemical Characteristics of Carbon Blacks

Sample No.	Carbon black	Particle diameter,* mμ	Specific surface**, m^2/g	Volatile content**, %	Roughness coefficient *
1	Thermal	250-300	10-15	1.5	1
2	Lamp	150	16-20	3	1
3	Furnace	60-80	30-35	1.5	1
4	Channel, regular	25-30	100	5.5	1.5
5	Channel, special	—	200	7.5	—
6	American channel for paints	10	300	11.5	4.5

*From literature data [1].

**For Samples No. 1-4, from data of the Scientific Research Institute of the Tire Industry; for Samples No. 5 and 6, from data of the Carbon Black Laboratory of VNIIGAZ.

Films of two types, of the same composition but differing in the methods of lacquer preparation, were made from the nitrocellulose lacquers. The nitrocellulose lacquers were made by two methods:

1. All the components were mixed simultaneously and ground in a ball mill (films of the first type).

2. The pigment was ground with semidissolved nitrocellulose (films of the second type).

The principle of the second method is that the pigment is ground with a mixture of the lacquer components which contains nitrocellulose but has a lowered solvent power for it. This is achieved in practice by addition of small portions of active solvent mixed with a diluent to the usual mixture of the nonvolatile nitrocellulose lacquer components (nitrocellulose, alkyd resin, and plasticizer) and treatment in a paint grinder. The paste so obtained is diluted with the usual mixture of solvents and diluents.

TABLE 2

Gloss and Brilliance of Alkyd Films and Nitrocellulose Films of the First and Second Types

Carbon black	Gloss			Brilliance		
	original	polished	polished, after irradiation	original	polished	polished, after irradiation
Alkyd films						
Thermal	57	64	28	1.3	1.5	5.3
Lamp	50	62	48	1.8	1.2	3.4
Furnace	56	70	30	1.1	1.3	3.4
Channel, regular	40	66	50	0.7	1.0	1.3
Channel, special	8	72	70	4	0.8	1.5
Channel, American for paints	1	68	56	4.3	0.7	1.1
Nitrocellulose films of the first type						
Thermal	11	70	20	3	1.9	6.8
Lamp	12	68	15	3.1	1.8	5.7
Furnace	13	65	–	2.7	1.5	5.5
Channel, regular	7	68	17	3.3	1.2	5.2
Channel, special	2.5	67	6	4.1	1.1	5.3
Channel, American for paints	2.5	68	34	4.1	1.0	3.2
Nitrocellulose films of the second type						
Thermal	57	68	40	1.7	1.6	5.2
Lamp	45	68	44	1.1	1.4	3.7
Furnace	60	73	37	1.2	1.2	4
Channel, regular	68	71	*	1.1	1.1	3.2
Channel, special	60	70	77	0.5	0.4	1.1
Channel, American for paints	70	69	66	0.2	0.3	0.95

The enamels were applied in thin layers onto steel plates and allowed to dry; the films were then polished and irradiated by means of a quartz lamp for 3 hours in a bath containing heated water. The following characteristics were determined at each of the three treatment stages:

1) gloss, characterizing the ability of the film to reflect light specularly; 2) brilliance (coefficient of diffuse reflection) or its reciprocal, blackness, representing the absorption of light by the film; 3) stability of these characteristics under the influence of atmospheric factors which stimulate oxidation reactions in the films.

Data on the gloss and brilliance of the films, expressed as percentages of the gloss and brilliance of the plates which were taken as the reference standards, are summarized in Table 2.

The following conclusions may be drawn from Table 2:

1. The blackness of high-gloss films increases with the degree of subdivision of the carbon black, i.e., is determined by the blackness of the carbon black (the finer the carbon black, the blacker the film).

2. In films differing in gloss the depth of the black color depends on the gloss: the weaker the gloss, the less the blackness (the greater the brilliance).

3. The films can be arranged as follows in order of gloss and depth of blackness: nitrocellulose films of the first type < alkyd films < nitrocellulose films of the second type.

4. With increase of the degree of subdivision of the carbon black the gloss and depth of blackdiminish in alkyd films and in nitrocellulose films of the first type, while in nitrocellulose films of the second type the depth of blackness increases while the gloss remains almost unchanged.

5. Irradiation of the films in heated water diminishes their gloss and depth of blackness.

* Number is obscured in the Russian original.

6. Films pigmented with coarse blacks all have weak resistance to irradiation. Nitrocellulose films of the first type, pigmented with fine blacks, also have weak resistance to irradiation, whereas alkyd films and nitrocellulose films of the second type pigmented with fine blacks have high resistance to irradiation.

These results can be satisfactorily explained as follows. The power of films pigmented with carbon black to absorb or reflect light is determined by the degree of aggregation of the carbon black particles in them; the effect of aggregation is equivalent to that of increased particle size, i.e., their power of absorbing light is reduced and the films acquire greater microroughness so that specular reflection of light is reduced.

This interpretation explains the relationship between gloss and depth of blackness. In high-gloss films, i.e., in films in which the carbon black particles are not aggregated, the depth of color is determined by the depth of color of the carbon black: the finer and hence blacker the carbon black, the blacker the film.

In films of lower gloss, where the carbon-black particles are aggregated, the depth of color loses its significance; the predominant factor determining the depth of color of the film becomes the degree of aggregation of the carbon-black particles in it; the greater the aggregation of the carbon black, the weaker the gloss and the less deep the black color of the film.

We had shown [2] that when molecules containing considerable numbers of polar groups are adsorbed on pigment surfaces part of these groups interact with polar active centers of the solid surface, with mutual saturation of the subsidiary valences of both; the rest of the polar groups remain in the free state with unsaturated subsidiary valences, and interaction of these leads to cohesion of the pigment particles if they are near enough to each other.

This accounts for the dependence of the optical properties of the films on the type of film former, particle size of the carbon black, and method of preparation.

Nitrocellulose films prepared by the first and second methods respectively differ sharply in their properties. It is reasonable to suppose that in preparation of nitrocellulose films by the first method (films of the first type) the pigment particles adsorb individual molecules of the dissolved nitrocellulose, and the adsorption layers contain numerous polar groups with unsaturated subsidiary valences. In preparation of nitrocellulose films by the second method (films of the second type) the pigment particles adsorb groups of associated molecules, in which the subsidiary valences of the polar groups are mutually saturated, as the nitrocellulose is in a state of incomplete solution in the binder. This difference in the structure of the adsorption layers determines the difference in the degree of aggregation of the pigment particles. In films of the first type, as the pigment particles approach each other they become easily joined through their adsorption layers in regions with unsaturated subsidiary valences, whereas in films of the second type such cohesion may not occur at the same distances between the particles, because the adsorption layers contain few if any polar groups with unsaturated subsidiary valences.

The difference in the degree of aggregation of the pigment particles determines the differences between the optical properties of the two types of nitrocellulose films. Films of the first type have lower gloss and lower depth of blackness than films of the second type. With increasing subdivision of the carbon black, i.e., with decreasing distance between the particles, aggregation is intensified in films of the first type, so that the gloss and depth of blackness diminish. Under the same conditions aggregation does not occur in films of the second type, the gloss remains unchanged, while the depth of blackness increases with decreasing particle size of the carbon black.

The molecules of alkyd resin are small in comparison with nitrocellulose molecules, and contain few polar groups. Accordingly the degree of aggregation of pigment particles is considerably lower in alkyd films than in nitrocellulose films of the first type. With 17% carbon black (as against 6% in nitrocellulose films) alkyd films have higher gloss and greater depth of blackness than nitrocellulose films of the first type. As the particle size of the carbon black decreases and the distances between the particles diminish aggregation is intensified and the gloss and depth of blackness are reduced.

When molecules of a film former are adsorbed on a pigment surface, regions of higher activity and therefore of greater chemical reactivity are formed in them. This follows from the considerations presented earlier in [2]. The activity of the polar groups which remain free becomes higher because of weaker influence of the neighboring groups which have interacted with the active centers of the pigment surface.

Thus, the pigment has a dual role in the film: on the one hand, by absorbing or reflecting light rays it protects the film against oxidation reactions; on the other, the adsorption layers on the pigment particles in the

surface layers of the film are themselves regions in which oxidation reactions originate and develop rapidly. A similar conclusion was reached in [3].

Addition of oxygen to film-former molecules adsorbed on the pigment particles in the surface layer of the film leads to formation of new polar regions with unsaturated subsidiary valences in them, and to intensified aggregation, as a result of which absorption and specular reflection of light by the film are diminished. This is the mechanism of the effects which, in irradiation, lead to rapid decrease of gloss and blackness of nitrocellulose films of the first type and of alkyd films and nitrocellulose films of the second type pigmented with coarse carbon blacks.

Alkyd films and nitrocellulose films of the second type, pigmented with finely divided channel blacks, are highly resistant to irradiation. The special feature of these films is that they combine two factors: few polar groups with unsaturated subsidiary valences in the adsorbed film-former molecules, and a very extensive pigment surface, rich in active polar centers which are formed as the result of activated adsorption of oxygen by the carbon black surface during the channel process for production of carbon black [1].

Under such conditions all the polar groups with unsaturated subsidiary valences in the adsorbed film-former molecules interact with the polar active centers on the carbon black pigment surface, and no regions of higher activity arise in the adsorption layers. Therefore in these systems the adsorption layers on the pigment particles in the surface layer of the film are not sites of rapid development of oxidation reactions, such as occurs in similar films pigmented with coarse blacks and in all nitrocellulose films of the first type, including those pigmented with finely divided carbon blacks.

SUMMARY

1. Variations of the gloss and brilliance of lacquer films pigmented with carbon black depend on the degree of aggregation of the pigment particles in them.

2. Variations of the gloss and brilliance of films during irradiation in heated water are caused by the presence of regions of higher activity in the adsorbed layers on the pigment particles; oxidation reactions originate and develop in these regions.

3. Films have been prepared in which the adsorption layers on the pigment particles are free from regions of higher activity; accordingly, development of oxidation reactions in them is retarded.

We thank Academician P. A. Rebinder for his interest and valuable advice in discussion of the work.

LITERATURE CITED

1. V. V. Kol'tsev and P. A. Tesner, Carbon Black [in Russian] (1952).
2. Ya. M. Gurevich, Kolloid. Zhur. 18, 158 (1956). *
3. A. V. Pamfilov and A. D. Bochkov, Zhur. Priklad. Khim. 26, 227 (1953). *

*Original Russian pagination. See C. B. translation.

INFLUENCE OF THE CHEMICAL NATURE OF CARBON BLACK SURFACE ON ITS INTERACTION WITH RUBBER AND SULFUR AND ON THE VULCANIZATION KINETICS

B. A. Dogadkin, Z. V. Skorodumova, and M. S. Fel'dshtein

Scientific Research Institute of the Tire Industry, Moscow
Translated from Kolloidnyi Zhurnal, Vol. 22, No. 6, pp. 663-670,
November-December, 1960
Original article submitted June 6, 1960

It is known that introduction of active fillers into rubber stocks has a significant influence on the vulcanization kinetics and the properties of the vulcanizates formed. A series of facts demonstrating the sharp variations in the activity of the vulcanizing group with the nature of the filler has been established [1]. For elucidation of this relationship it was decided, as a first step, to investigate the nature of the interaction between active fillers and the principal components of vulcanization mixtures in very simple systems. Earlier [2,3] we investigated the carbon black-sulfur system and showed that when carbon black is heated with a solution of sulfur in toluene the sulfur reacts chemically with the carbon black surface. It was found that the sulfur reacts with active regions, not occupied by oxygen-containing groups, of the carbon black surface.

It was required to obtain data on carbon black-rubber interaction and to determine which regions of the carbon black surface interact with rubber in rubber-carbon black and rubber-carbon black-sulfur systems.

Interaction of Carbon Black with Rubber

Adsorption of Rubber from n-Heptane Solution by Carbon Blacks. A considerable number of investigations have been concerned with adsorption of rubber on carbon blacks [4]. The adsorption method was used in the present work in order to determine which types of carbon black are the most active with respect to rubber.

The experiments on adsorption of rubber on carbon blacks were conducted in sealed tubes at 25°. A weighed sample of the black (1 g of channel black; 2 g of thermal, lamp, or furnace blacks; 0-1.5 g of Philblack) was put in the tube, followed by a 0.11% solution of butadiene-styrene rubber (SKS-30 A), reprecipitated four times, in n-heptane; 10 ml of the solution was taken for the channel, gas furnace, thermal, and Philblack 0 blacks, and 15 ml for lamp black. The tubes were sealed and shaken in a water thermostat at 25°. After the shaking the carbon black was separated from the solution by centrifugation. The solution concentration before and after the adsorption was determined from a calibration curve, which was plotted from data obtained in measurements of the refractive index difference between a standard liquid (solvent) and solutions of known concentration, based on displacement of the interference spectrum in the ITR-2 interferometer.

With the proportions of black to rubber in the solutions as indicated above, the final rubber concentration after the adsorption was almost the same in all cases, in the range of 0.037 to 0.04%. We are therefore inclined to believe that although these adsorption data do not represent the limiting equilibrium saturation, nevertheless they can be used for comparative characterization of the adsorption activity of the carbon blacks.

Figure 1 shows that the carbon blacks form the following series in order of the amount of rubber adsorbed per unit surface area of carbon black: lamp > thermal > furnace > channel = Philblack 0. The composition of the carbon blacks is given in Table 1.

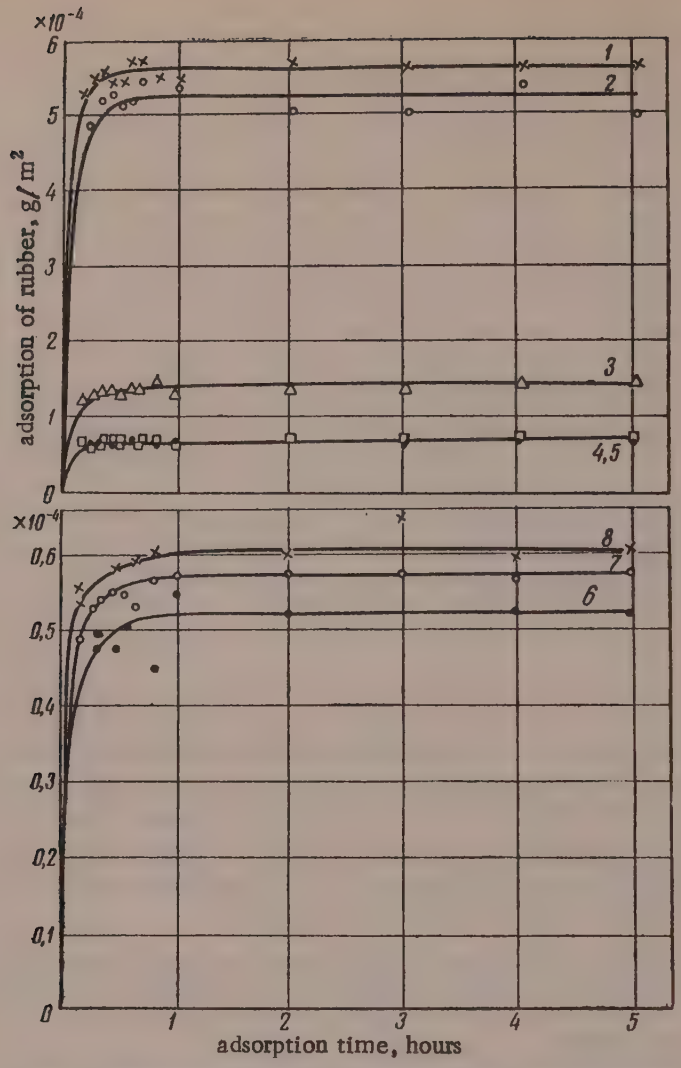


Fig. 1. Adsorption of SKS-30A rubber from n-heptane solutions on carbon blacks: 1) Lamp; 2) thermal; 3) furnace; 4) Philblack 0;5,6) channel; 7) channel heated in hydrogen at 300° under 300 atm pressure; 8) channel, calcined at 3200°.

Experiments were carried out on adsorption of rubber on samples of channel black after heat treatment: in one case the channel black was heated in hydrogen at 300° under 300 atm pressure*, and in the other the channel black was calcined in absence of air** at 3200°.

The composition of the carbon blacks after these treatments is given in Table 2.

The adsorption data in Fig. 1 show that here again the amount of rubber adsorbed per unit surface area increases with decrease of the number of oxygen-containing groups on the carbon black surface.

Rubber-carbon black interaction at the vulcanization temperature. Rubber-carbon black interaction during milling was studied in investigations [5] which dealt in detail with formation of rubber-carbon black gels in relation to the type of rubber and carbon black, filler content, and the nature of the milling treatment.

*Carbon black kindly provided by B. V. Lukin.

** Carbon black kindly provided by K. A. Pechkovskaya.

TABLE 1

Elementary Composition of Carbon Blacks (%)

Blacks	C	H	O by difference
Channel	93.04	1.25	5.71
Philblack 0	96.23	1.13	1.99
Thermal	99.26	0.65	0.09
Lamp	99.54	0.39	0.07
Furnace	97.45	0.68	1.87

TABLE 2

Elementary Composition of Carbon Blacks (%)

Blacks	C	H	O by difference
Channel black	92.75	1.08	6.22
Channel, heated at 300° under 300 atm in hydrogen	96.45	1.2	2.35
Channel, heated at 3200° in absence of air	99. 43	0.46	0.11

We were interested in rubber-carbon black interaction in mixtures made on rolls and heated at the vulcanization temperature, in relation to the chemical nature of the filler surface.

It was important to establish whether the interaction observed by us in studies of rubber-carbon black interaction in n-heptane solution would be of the same character in this case.

TABLE 3

Amount and Composition of Rubber-Carbon Black Gels

Composition, wt. parts		Rubber-carbon gel content, %	Contents in rubber-carbon black gel of				
			carbon black,%	rubber, %	carbon black, g/g rubber	rubber, g/g carbon black	rubber g/m^2 carbon black $\cdot 10^{-3}$
Channel	30	45.0	57.92	42.8	1.38	0.726	6.6
	40	53.0	58.8	41.2	1.43	0.700	6.36
	50	64.3	59.42	40.58	1.46	0.696	6.35
	60	78.5	61.64	38.36	1.60	0.623	5.66
Philblack 0	30	39.9	61.3	38.7	1.58	0.632	8.44
	40	46.3	62.2	37.8	1.64	0.609	8.12
	50	60.0	62.8	37.2	1.69	0.593	7.9
	60	67.0	63.2	36.8	1.71	0.583	7.78
Furnace	30	Dissolves completely	—	—	—	—	—
	40	Very loose gel	—	—	—	—	—
	50	Same	—	—	—	—	—
	60	48.1	73.19	26.81	2.73	0.367	15.1
Lamp	30	Dissolves completely	—	—	—	—	—
	40		—	—	—	—	—
	50		—	—	—	—	—
	60	37.6	84.31	15.69	5.77	0.186	18.2

Accordingly, mixtures of SKS-30A butadiene-styrene rubber were made on cold rolls in air with the following carbon blacks: channel, Philblack 0, furnace, and lamp, in the proportions of 30, 40, 50, and 60 parts by weight to 1000 parts of rubber. The mixtures were heated in the press at 143° for 2 hours and then extracted with benzene in conical flasks; the benzene was changed every two days until all soluble rubber had been completely removed. The amounts of rubber-carbon black gel were determined, and the contents of rubber and carbon black in the gel were found by decomposition of the rubber with nitric acid (Table 3).

It is seen in Table 3 that the amount of bound rubber per unit surface area of the carbon black increases (as in the case of adsorption of rubber from solution) with decrease of the amount of oxygen-containing groups in the carbon black surface.

Interaction of Rubber with Sulfur Bound Chemically on the Carbon Black Surface

It has been shown [2, 3] that when carbon black is heated with toluene dissolved in sulfur the latter is chemically combined with the carbon black surface. It was desired to determine whether this sulfur (present on the carbon black surface) reacts with rubber. Two mixtures were prepared for this purpose on laboratory rolls, each containing 100 parts of rubber and 60 parts of carbon black by weight: 1) SKS-30A rubber with sulfurized black. For the sulfurization the carbon black was heated with crystalline sulfur in 1 : 1 ratio at 145° for 6 hours. The carbon black was extracted with acetone for 30 hours until free sulfur had been completely removed. The content of chemically bound sulfur was 0.7%. The carbon black used in the first mixture was also heated and extracted to ensure the same degree of dispersion of the black in the rubber in both cases. The mixtures were heated in the press at 143°. The maximum swelling was determined, and Shvarts' nomograms [6] were used to calculate the number of cross links in the vulcanizates.

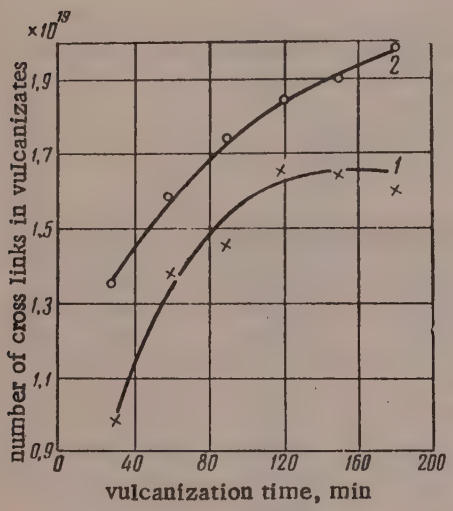


Fig. 2. Kinetics of cross-link formation during heating of systems: 1) SKS-30A + + channel black; 2) SKS-30A + sulfurized channel black.

It follows from Fig. 2 that the mixture containing sulfurized carbon black has a higher content of cross links than the mixture with the original carbon black. This indicates that the sulfur on the carbon black surface forms additional active centers and takes part in cross linking of the vulcanization structure.

However, these data are contrary to the data of an earlier investigation [7], which indicate that the dipole moment of vulcanized rubber is almost unchanged as the result of filling. It follows that filling does not lead to appreciable chemical interaction between the rubber and the filler, and that this rubber-filler interaction does not occur at the "sulfur dipoles." The data in the review article [8] lead to the same conclusion. It follows that the problem of the nature of rubber-carbon black interaction has not found an agreed solution, but requires further investigation and discussion.

Effect of Oxidation of Philblack 0 on Vulcanization Kinetics

Variations of the chemical nature of carbon black surfaces have a strong influence on vulcanization kinetics. We showed earlier [2] that if channel black is heated in hydrogen at 300° under 250 atm pressure (which removes oxygen-containing groups from the carbon black surface) the modulus of the mixtures, the vulcanization rate, and the amount of bound sulfur are all increased.

In the present work we studied the effect of oxidation of the carbon black (increase of the number of oxygen-containing functional groups on its surface) on vulcanization kinetics. The carbon black Philblack 0 which is now widely used in the tire industry, was investigated. It was oxidized in air at 400° for 1.5 hours. The oxygen content of the carbon black increased as a result. The decrease of the pH of the carbon black indicates an increased content of carboxyl and phenolic groups. The results of elementary analysis of these carbon blacks are given in Table 4.

TABLE 4

Elementary Composition of Carbon Blacks (%)

Carbon black	C	H	O	pH
Philblack 0	96.23	1.13	1.99	8.4
Philblack 0 oxidized at 400° for 1.5 hours	96.01	0.46	2.93	4.2

The mixtures were made with SKS-30AM rubber and vulcanized in the press at 143°. It follows from Fig. 3-5 that increase of the amount of oxygen-containing groups on the carbon black surface reduces the vulcanization rate, decreases the strength and modulus, lowers the content of bound sulfur, and increases maximum swelling.

This action of functional oxygen-containing groups is also confirmed by data on bound sulfur determined during heating of rubber-carbon black-sulfur systems containing commercial carbon blacks: lamp, channel, Philblack 0, and furnace. In this series of experiments the mixtures contained 100 weight parts of SKS-30AM rubber, 60 weight parts of carbon black, and 7 weight parts of recrystallized sulfur.

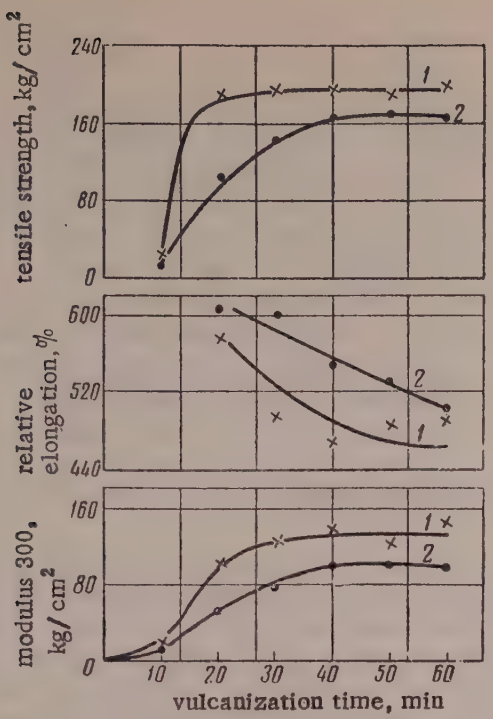


Fig. 3. Variations of the physical and mechanical properties of vulcanizates of SKS-30AM with Philblack 0 (1) and with Philblack 0 oxidized at 400° (2).

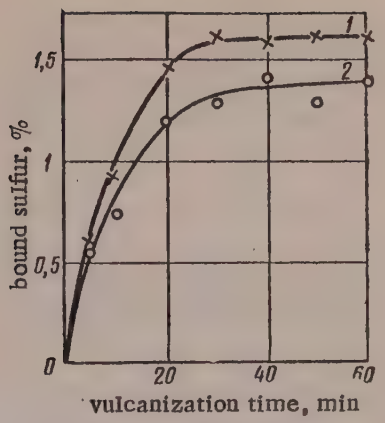


Fig. 4. Kinetics of sulfur addition in vulcanization of SKS-30AM rubber with Philblack 0 (1) and Philblack 0 oxidized at 400° (2).

It follows from Fig. 6 that the amount of bound sulfur is least in the case of channel black and greatest in the case of Philblack 0. Lamp black does not conform to our qualitative relationship between oxygen content and the activity toward sulfur. This type of carbon black is almost free from oxygen, but its activity in the kinetics of addition of sulfur to rubber is lower than the activity of Philblack 0. It follows that, as was to be expected, not only the oxygen content of the carbon black but also the properties of the regions of the carbon black surface which are not occupied by functional oxygen-containing groups play an important part in this property of carbon blacks.

The data presented in this paper on adsorption of rubber and on the interaction of rubber with carbon black on heating, and earlier data [2, 3] on activated adsorption of sulfur, lead to the conclusion that the most active regions on the surface of carbon black with respect to activated adsorption of sulfur and interaction with rubber are regions which do not contain functional oxygen-containing (including carboxyl) groups. The active centers here may be trivalent carbon atoms or olefinic double bonds of the surface hexacarbon groups [9].

Garten and Weiss [10] showed that furnace blacks have high concentrations of benzopyran groups in comparison with channel black, and since the benzopyran group contains an α-methylene group (adjacent to the double bond) it follows that sulfur can interact with carbon black by reactions analogous to the reactions between sulfur and rubber.

We showed [3] that sulfur is bound on the carbon black surface in the form of mono- or disulfides which are incapable of isotope exchange with elemental sulfur. It was shown [2] that the interaction of sulfur with carbon black in toluene solution results in an approximately twofold increase in the size of the carbon black aggregates.

In the course of milling and subsequent vulcanization the aggregates of carbon black particles, bonded by sulfur, may break up at the S bonds, and the sulfur can then react with the rubber, forming additional cross links.

It is likely that the higher vulcanization rates and the larger total amounts of bound sulfur in mixtures with alkaline blacks as compared with channel black are due to the activity of the carbon black surface, which contains large numbers of benzopyran and other active groups capable of taking part in vulcanization reactions, and also to differences in the catalytic effects of the carbon black surface on rubber-sulfur reactions.

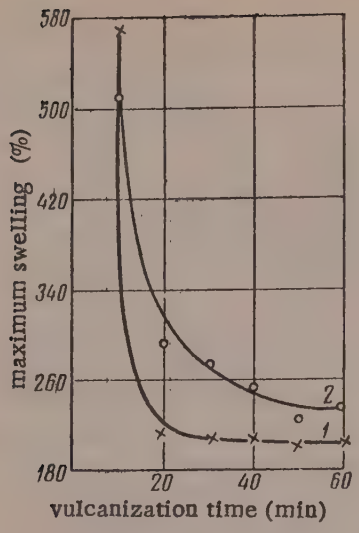


Fig. 5. Variations of the maximum swelling of SKS-30AM vulcanizates with Philblack 0 (1) and Philblack 0 oxidized at 400° (2).

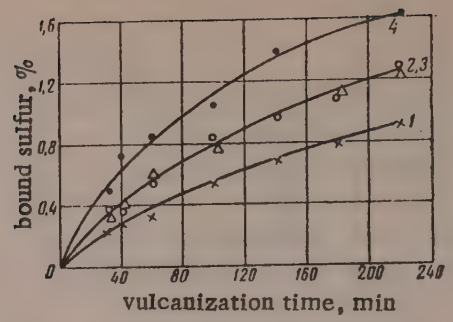


Fig. 6. Kinetics of sulfur addition in vulcanization of the system SKS-30 AM+ carbon black + sulfur: 1) Channel black; 2) lamp black; 3) furnace black; 4) Philblack 0.

It is known [8] that carbon blacks with high oxygen contents and pH values in the acid range are less effective catalysts for decomposition of hydrogen peroxide than carbon blacks with pH in the alkaline range; this is associated with their electron-donor characteristics. Amberg and Willis [11] showed that vulcanization with cumene hydroperoxide in a neutral or alkaline medium proceeds by a radical mechanism. In presence of channel black the peroxide undergoes a certain amount of ionic decomposition. This leads to a higher vulcanization rate in presence of alkaline blacks, and retarded vulcanization in presence of acid blacks.

Thus, there is every reason to assume that alkaline -blacks catalyze such reactions taking place during vulcanization as decomposition of accelerators and polysulfides [12], which lead to formation of free radicals which activate the vulcanization process.

In the case of Philblack 0 the higher vulcanization rate and the greater total amount of bound sulfur are possibly also determined by the sulfur content on its surface.

Oxidation of carbon blacks leads to formation of surface oxygen-containing functional groups; this leads to a decrease of the retardation rate, modulus, and the amount of bound sulfur.

SUMMARY

1 1. The amount of rubber adsorbed from n-heptane solution by carbon black, calculated per unit surface area, increases with decrease of the number of oxygen-containing functional groups on the carbon black surface. Commercial carbon blacks form the following series in order of the amount of rubber adsorbed: lamp > thermal > > furnace > channel. Philblack 0 is equivalent to channel black in adsorption capacity for rubber.

2. The amount of rubber combined with carbon black in mixtures made on rolls and heated at the vulcanization temperature, calculated per unit surface area, increases with decrease of the number of oxygen-containing functional groups on the carbon black surface.

3. Sulfur which is chemically adsorbed on the carbon black surface is involved in formation of additional cross links in the rubber-carbon gel.

4. Oxidation of carbon blacks leads to formation of additional surface oxygen-containing functional groups which increase the acidity of the carbon black; this retards vulcanization, lowers the maximum amount of chemically combined sulfur, and decreases the modulus.

LITERATURE CITED

1. M. S. Fel'dshtein, P. N. Orlovskii, and B. A. Dogadkin, Kauchuk i Rezina, No. 1 (1957).
2. B. A. Dogadkin, et al., Kolloid. Zhur. 18, 413 (1956).*

*Original Russian pagination. See C. B. translation.

3. B. A. Dogadkin, Z. V. Skorodumova, and N. V. Kovaleva, Kolloid. Zhur. 20, 272 (1958).*
4. I. M. Kolthoff and R. G. Gutmacher, Rub. Chem. Techn. 26, 102 (1953); G. Kraus and J. Dugone, Ind. Eng. Chem. 47, 1809 (1955); A. Yurzhenko and I. Maleev, Trudy L'vovskogo Univ., 7, part 3 (1957).
5. Z. V. Chernykh and V. G. Epshtein, Kolloid. Zhur. 19, 644 (1957)*; D. S. Villars, J. Polymer. Sci. 21, 257, (1956); C. W. Sweitzer and T. Lyon, Rub. Chem. Techn. 25, 557 (1952).
6. A. G. Shvarts, Kauchuk i Rezina, No. 7 (1957).
7. A. I. Lukomskaya and B. A. Dogadkin, Kolloid. Zhur. 15, 259 (1953).*
8. M. L. Studebaker, Rub. Chem. Techn. 30, 1401 (1957).
9. V. A. Garten and G. K. Sutherland, Proc. Third Rub. Techn. Conf. (London, 1954) p. 536; V. A. Garten and D. E. Weiss, Austral. J. Chem. 8, 68 (1955); P. S. Stearns, and B. L. Johnson, Ind. Eng. Chem. 43, 146 (1951).
10. V. A. Garten, and D. E. Weiss, Austral. J. Chem. 10, 309 (1957).
11. L. O. Amberg and W. D. Willis, Proc. International Rubb. Conference (Washington, November, 1959), p. 565.
12. B. A. Dogadkin and I. A. Tutorskii, Kolloid. Zhur. 20, 279 (1958).*

*Original Russian pagination. See C. B. translation.

EFFECT OF THE DEGREE OF CHEMICAL MODIFICATION OF SILICA SURFACE BY TETRAMETHYLCHLOROSILANE ON ADSORPTION OF NITROGEN AND KRYPTON VAPORS

A. V. Kiselev, A. Ya. Korolev, R. S. Petrova,

and K. D. Shcherbakova

Adsorption Laboratory, Chemical Faculty, M. V. Lomonosov Moscow State University

Translated from Kolloidnyi Zhurnal, Vol. 22, No. 6, pp. 671-678, November-December, 1960
Original article submitted September 24, 1959

The nature and chemical modification of solid surfaces not only have a significant influence on the behavior of adsorbents and catalysts, but also determine the technical properties of heterogeneous polymeric materials containing fillers. Adsorption is the primary physicochemical stage in the formation of such systems. Great interest therefore attaches to studies of the influence of the chemical composition and structure of surfaces on the adsorption properties of various highly disperse and other solid materials.

Research work on chemical modification of silica surfaces by dehydration, alkoxylation, and halogenation reactions, and on the influence of such modification on adsorption properties, has been reviewed [1,2]. Modification of the surfaces of porous crystals by reactions with amines is considered in [3], oxidation of carbons in [4], and the influence of chemical and crystallochemical modification of carbon blacks, as the result of heat treatment on adsorption of various vapors is discussed in [5].

In studies of the effects of chemical modification of the surface on the adsorption properties of Aerosil and carbon black [6-11] it was shown that replacement of a part of the hydrogen atoms in the surface hydroxyl groups by trimethylsilyl $Si(CH_3)_3$ groups reduces the adsorption of various substances to an extent which increases with the degree of replacement. Adsorption is decreased not only in the case of substances which are adsorbed mainly by electrostatic interaction with hydroxyl dipoles, but also in the case of such a typically nonpolar hydrocarbon as hexane, which is adsorbed essentially by the action of dispersion forces. Calculations of the energy of adsorption showed that the decrease of adsorption in this case is due to removal of adsorbate molecules, reaching the surface of the film of $Si(CH_3)_3$ groups, from the silicon-oxygen framework of the adsorbent [12]. No such weakening of the dispersion force potential is observed in simple surface modification by dehydration, i.e., by simple removal of hydroxyls [2, 13] or in replacement of OH groups by Cl atoms, which are of similar dimensions [14].

It was desired to determine how modification of a silica surface affects adsorption of nitrogen and krypton, the "standard" gases widely used for determinations of adsorbent areas by the BET method. In such determinations the nature of the surface is generally disregarded, and the area occupied by these molecules in a dense monolayer (ω_m) is assumed to be constant and the same for the most diverse adsorbents. It had even been stated in [15] that "changes in the nature of the adsorbent surface, even in the transition from hydrophilic to hydrophobic adsorbents, have no significant influence on the adsorption and energy of adsorption of nitrogen."

However, it is known that the energy of adsorption and the state of adsorbed molecules in an adsorption layer are determined both by the nature of these molecules and the nature of the adsorbent [16]; in particular,

the energy of adsorption of nitrogen, which has a quadrupole moment, is sensitive to the electrostatic field of the surface [17], and the energy of dispersional interaction of both nitrogen and krypton is determined by the structure of the adsorbent and by its electrical and magnetic properties [18]. It has been shown experimentally that the heat and degree of adsorption of nitrogen and argon vapors on carbon black alter if the carbon black is graphitized [19, 20]; adsorption of nitrogen on a silica surface alters if the surface is dehydrated [21]. It is also known that ω_m for nitrogen depends on the distribution of force centers on the surface [22], while in the case of krypton comparison with the surface areas determined by the BET method with nitrogen, with $\omega_{mN_2} = 16.2A^2$, gives different values of ω_{mKr} for different adsorbents (between 15 and 22 A^2); the more uniform the surface, the lower are these values [23-27].

Theoretical investigation of vapor adsorption isotherms [28] shows that, even for adsorption on homogeneous surfaces, the Langmuir and BET equations are merely limiting cases of more general equations which take adsorbate-adsorbate interaction into account. This limiting case corresponds only to relatively very strong adsorbate-adsorbent interactions. Even in low-temperature adsorption of nitrogen vapor on graphitized carbon black with a homogeneous surface the adsorption isotherm is concave at first and only becomes convex at a surface coverage $\theta > 0.3$; it is therefore described by the Langmuir and BET equations only in a narrow range of θ. Over a much wider range, including the concave region, this isotherm is represented by an equation derived by one of us [28], which approximately takes into account adsorbate-adsorbate interaction [29]. All this suggests a certain degree of caution in interpreting the constants a_m in the Langmuir and BET equations as the capacities of the dense monolayer in determination of these constants by a formal description of a certain part of the adsorption isotherm by these equations. Theoretical analysis [28] suggests that low-temperature adsorption of nitrogen and inert gases, generally used for determination of the capacity a_m of the dense monolayer and of the specific surface $s = a_m \omega_m$, should be so greatly changed by a sharp decrease of adsorbate-adsorbent interaction, as the result of chemical surface modification, that it can no longer be used in such cases for determination of these values.

In the present investigation a sharp decrease in the energy of adsorbate-adsorbent interaction was effected by replacement of hydrogen in the hydroxyl groups of the silica surface by trimethylsilyl groups, which greatly increase the distance between the adsorbate molecules and the layer of oxygen atoms which are the main force centers in silica [12]. Adsorption of nitrogen and krypton vapors was studied with five samples of Aerosil, a nonporous highly disperse silica, treated with trimethylchlorosilane in vapor form or in petroleum benzine solution. As the result of this treatment the Aerosil surface is covered with chemically bound groups as the result of the reaction [6, 7, 9-12, 30]:

$$\equiv Si{-}OH + ClSi(CH_3)_3 \rightarrow \equiv Si{-}O{-}Si(CH_3)_3 + HCl. \quad (1)$$

It is evident that under otherwise constant conditions the number of trimethylsilyl groups bound by the surface increases with the number of hydroxyl groups on it [10]. Therefore, in order to prepare the most highly modified sample the original Aerosil was hydrated by the action of water in an autoclave for 19.5 hours at 350 and 169 atm, and then treated with $ClSi(CH_3)_3$.

The content of chemically adsorbed groups on the surface was determined by microanalysis for carbon*. The degree of surface coverage by trimethylsilyl groups was found as the ratio of the number of $Si(CH_3)_3$ groups per 100 A^2 of surface area to the maximum possible number, ~2.4 $Si(CH_3)_3$ groups per 100 A^2. The latter value was calculated from the van der Waals area of $Si(CH_3)_3$ groups, $\omega_m = 42$ A^2, assuming that its configuration is regular [12]. The analytical results and the specific surfaces of the original samples, determined by the BET method from isotherms of strong adsorption of nitrogen vapor on the original Al sample and the hydrated AlH sample at $\omega_{mN_2} = 16.2$ A^2, are given in Table 1.

Formal application of the BET method to the regions of the adsorption isotherms, described by that equation, for nitrogen and krypton vapors on modified samples with the same values of ω_m gives lower values for the specific surface (see below). This is due to the inapplicability of the BET method to weak adsorption and possibly also to the looser packing of nitrogen molecules on the weakly adsorbing surface. Since the reaction

*This value was close to that found from the weight increase of the sample after modification by means of reaction (1).

TABLE 1

Characteristics of the Original and Modified Aerosil Samples

Aerosil samples		Number of groups per 100 A^2 of surface	Degree of surface coverage by $Si(CH_3)_3$ groups, %
designation	treatment of sample	$\alpha_{Si(CH_3)_3}$	$\theta_{Si(CH_3)_3} = \frac{\alpha_{Si(CH_3)_3}}{2.4}$
Series I; specific surface by nitrogen adsorption $s_{N_2} = 170\ m^2/g$			
A1	Original	0	0
$A1M_V$	With $ClSi(CH_3)_3$ vapor	1.4	~60
$A1M_S$	With $ClSi(CH_3)_3$ sol.	2.0	~80
Series II; specific surface by nitrogen adsorption $s_{N_2} = 50\ m^2/g$			
A1H	Hydrated in autoclave	0	0
$A1HM_V$	Same, then treated with $ClSi(CH_3)_3$ vapor	2.2	~90

of surface modification was conducted under conditions which excluded losses of Aerosil, the modified portions differed from the corresponding original samples only by the surface layer of $Si(CH_3)_3$ groups. Therefore in calculations of the analytical results we regarded it as more correct to assume that the modified samples retained the same specific surface as the corresponding samples before modification.

The isotherms of nitrogen and krypton vapor adsorption were determined at the temperature of liquid nitrogen. Adsorption of nitrogen was measured by means of a volumetric apparatus [20]*, and adsorption of krypton, by means of a simplified volumetric apparatus, by a method similar to that used by Wooten and Brown [31]**; the saturated vapor pressure p_s of krypton at the temperature of liquid nitrogen is only ~2 mm for solid krypton and ~3 mm for the supercooled liquid [23], so that a U-tube manometer is not necessary; the initial and equilibrium gas pressures were determined at room temperature by means of a McLeod gauge with a constant of $6.2 \cdot 10^{-5}$. In the pressure region of p 0.25 mm a correction was applied for the thermomolecular effect [20]. The value taken for p_s of krypton was obtained by extrapolation of the saturation pressure of the supercooled liquid [32], calculated from the Meihuizen and Crommelin empirical equiation [33]. Before the experiments all the samples were evacuated at 150°.

The absolute isotherms for adsorption of nitrogen and krypton vapors are given in Fig. 1. The specific surface of A1, $A1M_V$, and $A1M_S$ samples was taken to be 170 m^2/g, and of A1H and $A1HM_V$ as 50 m^2/g, in accordance with the above assumption that in the conditions of our experiments the specific surface of Aerosil is unchanged after trimethylchlorosilane treatment***.

The adsorption both of nitrogen and of krypton decreases rapidly with increased degree of modification. The shape of the isotherms also changes; they become much less convex. The decrease of adsorption is especially pronounced with the most highly modified sample, $A1HM_V$.

The adsorption isotherms in coordinates of the BET equation are shown in Fig. 2. The isotherms for the original and hydrated samples, and for samples of 60 and 80% modification, are satisfactorily linear in these coordinates over a fairly wide p/p_s range. In the case of sample $A1HM_V$, with the highest degree of surface modification (90%), the p/p_s range in which the isotherm is linear is appreciably shortened for nitrogen, and even more so for krypton. Comparison of Fig. 2 with Fig. 1, b shows that as the absolute adsorption decreases the BET equation becomes less satisfactory, because as adsorbate-adsorbent interaction becomes weaker adsorbate-adsorbate interaction can no longer be disregarded [28].

* The authors thank V. P. Dreving for developing the design of this apparatus.

** The isotherm for nitrogen adsorption on sample AlH was determined by B. G. Aristov, to whom the authors offer their thanks.

***It must be pointed out that different portions of the original Al Aerosil had somewhat different specific surfaces, from 170 to 200 m^2/g (see also [34]).

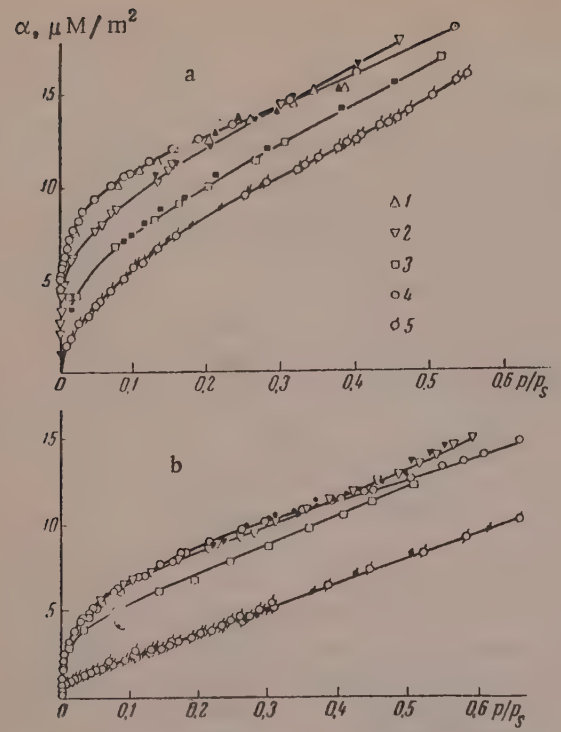


Fig. 1. Absolute isotherms for adsorption of nitrogen vapor (a) and krypton vapor (b) at −195° on Aerosil samples A1(1), $A1M_V$(2), $A1M_S$ (3), A1H (4), and $A1HM_V$(5). The black points represent desorption. (The absolute isotherms for adsorption of krypton vapor, like those of nitrogen vapor, on samples A1 and A1H almost coincide).

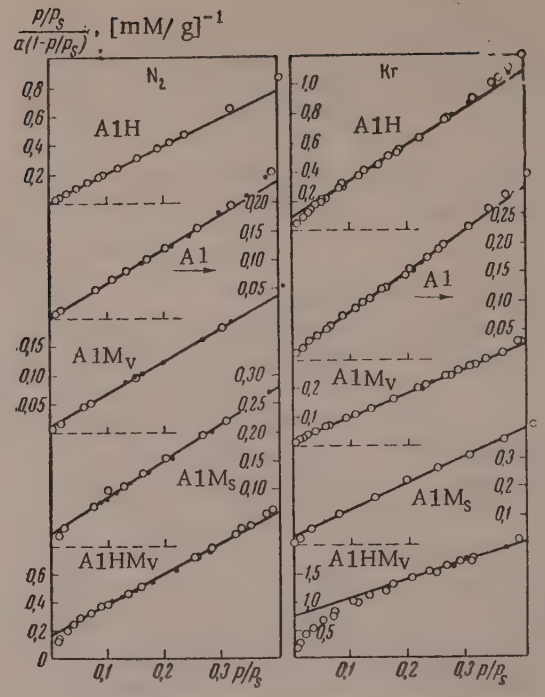


Fig. 2. Isotherms for adsorption of nitrogen and krypton vapors at −195° on Aerosils, in coordinates of the BET equation.

In the case of silica samples not modified by the reaction with trimethylchlorosilane the BET method can be used for determining the specific surface; for example, from adsorption of nitrogen through the constant a_{mN_2}, assuming the constant value $\omega_{mN_2} = 16.2\ A^2$, for nitrogen; then, conversely, ω_{mKr} can be found from a_{mKr}. The corresponding values are given in Table 2.

In the case of samples modified by trimethylchlorosilane it is, of course, formally possible to represent at least a small portion of the nitrogen and krypton adsorption isotherms by the BET equation and to find the corresponding values of the constant a_m. If these values are given the meaning, as in the BET theory, of the "capacity of the dense monolayer," and if it is assumed, as for the nonmodified samples, that $\omega_{mN_2} = 16.2A^2$, and $\omega_{mKr} = 21.5A^2$ (Table 2), then the values given in Table 3 are obtained for the specific surfaces of the Aerosils.

It follows from Table 3 that the values for the specific surfaces of both modified samples, formally determined by the BET method, decrease appreciably with increased modification $\theta_{Si(CH_3)_3}$; the decreases for nitrogen and krypton are different (approximately 15 and 45%, respectively, for the sample with the highest $\theta_{Si(CH_3)_3} = 90\%$). We believe that such a large decrease cannot be attributed either to differences of molecular packing in the dense monolayer, or to changes of specific surface by application of the modifying layer under the conditions of our experiments. It follows that adsorption of nitrogen and krypton vapors is so strongly influenced by the degree of modification of the silica surface by $Si(CH_3)_3$ groups that it cannot be used for determining the specific surfaces of highly modified samples by the BET method.

It should be noted that surface heterogeneities, for example those associated with a certain degree of mosaic structure in the modifying layer [10], are more pronounced against the background of general weakening of the dispersion potential of the surface; as a result, the initial region of the krypton adsorption isotherm remains steep. It is highly probable that the isotherms for adsorption of nitrogen and krypton vapors on a completely homogeneous nonmosaic surface film of $Si(CH_3)_3$ groups would be initially concave. It is therefore most important to prepare the geometrical and chemical structure of the original silica surface and to perform the modi-

TABLE 2

Areas Occupied by a Krypton Molecule in a Dense Monolayer on Surfaces of Different Silicas, Determined by the BET Equation; Silica Surfaces Determined from Adsorption of Nitrogen Vapor with $\omega_{mN_2} = 16.2\,A^2$.

Sample	Specific surface, m^2/g	ω_{mKr}, A^2	Sources
Porous glass	121	21.5	[23]
Glass balls, 200 mesh	5.51	22.0	[26]
Glass balls, 7 μ	0.434	20.4	[26]
Glass balls	4.17	21.6	[27]
Linde Aerosil	321	22.0	[25]
KSK-2 silica gel [35]	330	22.5	Our data
A1H Aerosil	50	22.0	" "

fication reaction in such a manner as to give as dense and homogeneous a layer of modifying groups as possible on the external surface. In such a case the isotherms for adsorption of gases and vapors would have initial regions very close to linear at very low values of the Henry constant. Modified adsorbents of this type could be used in an adsorption variant of gas chromatography, which is thus made closer to the gas-liquid distribution variant while the advantages of chemical and thermal stability and a large surface area are retained. It is highly probable that sufficiently complete modification by means of long chains with appropriate functional groups on the outside of the modifying layer would confer the advantages of the gas-liquid chromatographic method (symmetrical character of the peaks) on the adsorption variant.

Let us now compare the isotherms for adsorption of nitrogen and krypton vapors with the isotherms, obtained earlier, for adsorption of n-hexane, benzene, methanol, and water vapors [6, 7, 10]. The adsorption of these vapors was determined with four Aerosil samples, A1, $A1M_V$, $A1H_S$, $A1HM_V$ of these two series. Figure 3 shows the initial regions of the isotherms of all six adsorbates for the two extreme cases - the Aerosil with the most highly hydrated surface (A1H) and the Aerosil with the most highly modified surface (90%, sample $A1HM_V$). Modification results in a sharp decrease of adsorption with all the adsorbates.

TABLE 3

Values of Monolayer Capacity a_m and Specific Surface $\underline{s}$ Determined Formally by the BET Method from the Graphs in Fig. 3 and the Values ω_{mN_2} 16.2 A^2 and ω_{mKr} = 21.5 A^2

Samples	Degree of modification, %	Monolayer capacity a_m, μM/g		Specific surface			
				nitrogen		krypton	
		nitrogen	krypton	m^2/g	relative	m^2/g	relative
Series I							
A1	0	1.72	1.44	168*	1.00	185*	1.00
$A1M_V$	~60	1.70	1.18	165	0.99	153	0.83
$A1M_S$	~80	1.49	1.04	145	0.87	135	0.73
Series II							
A1H	0	0.52	0.38	50	1.00	50	1.00
$A1HM_V$	~90	0.44	0.21	43	0.86	28	0.56

*Different portions of Aerosil.

Figure 4 represents the approximate course of decreasing adsorption at $p/p_s = 0.1$ with increasing surface coverage by $Si(CH_3)_3$ groups. Water, methanol, and benzene, which form hydrogen bonds with hydroxyls [2], lower adsorption sharply even at $\theta_{Si(CH_3)_3} = 60\%$ [10]. The decrease of adsorption becomes more pronounced as the role of interaction of the adsorbate molecule with the hydroxyl dipole increases, and becomes greater in the sequence: benzene, methanol, water. Adsorption of methanol and water decreases fairly steadily with increasing degree of surface coverage by $Si(CH_3)_3$. Water is an exception; adsorption of water by the most highly

modified sample is perhaps even greater than by the sample of 60% modification. In the case of the small polar molecules of water the contribution of dispersion forces in adsorption is small, and water is adsorbed on silica mainly by formation of hydrogen bonds with surface hydroxyls. The original A1 Aerosil is not completely hydrated, and therefore the surface regions unaffected by modification on the surface of modified sample $A1M_V$ are almost entirely devoid of hydroxyl groups; this is the cause of the sharp decrease in the adsorption of water. The hydrated sample, even after modification, still retains in the remaining gaps of the film of $Si(CH_3)_3$ groups enough hydroxyl groups for appreciable adsorption of the small water molecules, which are capable of penetrating into these gaps [10].

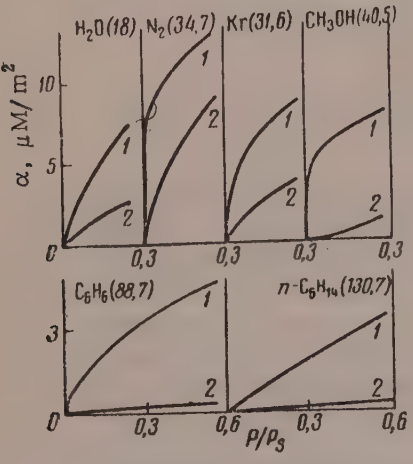


Fig. 3. Initial regions of the absolute isotherms for adsorption of water, nitrogen, krypton, methanol, benzene, and n-heptane on Aerosil samples A1H (1) and $A1HM_V$ (2). The numbers in parentheses are the molar volumes of the adsorbates.

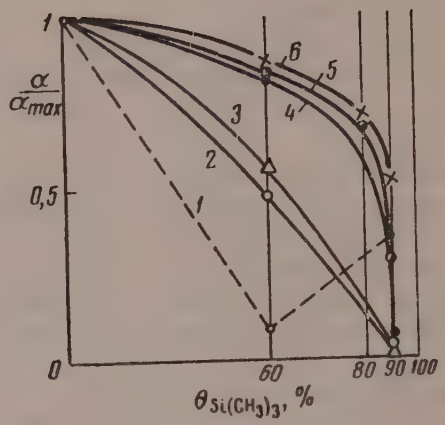


Fig. 4. Variations of the relative adsorption on Aerosil, at $p/p_s = 0.1$, of water (1), methanol (2), benzene (3), n-hexane (4), krypton (5), and nitrogen (6) vapors with the degree of surface coverage of Aerosil by $Si(CH_3)_3$ groups.

The adsorption of three nonpolar adsorbates — hexane, krypton, and nitrogen — caused mainly by dispersional interaction, decreases only slightly with the sample of 60% modification. The adsorption of hexane and krypton then drops sharply with increase of the degree of modification to 90%, when the almost continuous layer of $Si(CH_3)_3$ groups shields the silica surface and makes it almost inaccessible to these large molecules. The decrease of adsorption is relatively somewhat less for nitrogen, because the nitrogen molecules are small and are strongly adsorbed on the accessible hydrated regions in the surface of $A1HM_V$ sample.

SUMMARY

1. The isotherms for adsorption of nitrogen and krypton vapors at the temperature of liquid nitrogen have been determined for two series of finely divided silica (Aerosil), with the surface modified chemically to different extents (up to 90%) by trimethylsilyl groups.

2. Modification of the silica surface by trimethylsilyl groups lowers the adsorption of both nitrogen and krypton vapor; at high degrees of modification the decrease of krypton adsorption is especially pronounced. The form of the adsorption isotherms changes sharply, particularly in the case of krypton.

3. Since fairly complete modification of silica surfaces by trimethylsilyl groups results in a sharp decrease of adsorbate-adsorbent interaction, determination of the specific surface by the BET method gives erroneous (low) results in such cases.

LITERATURE CITED

1. Collection: Surface Chemical Compounds and Their Role in Adsorption Phenomena, edited by A.V. Kiselev [in Russian] (MGU, 1957).
2. A. V. Kiselev, in collection: The Structure and Properties of Porous Materials, Ed. D. H. Everett and F. Stone, (London, 1958) p. 195.
3. R. M. Barrer, British Chemical Engineering (May, 1,1959).
4. M. M. Dubinin, Uspekhi Khim. 24, 513 (1955); R. N. Smith, J. Swinehart, and D. Lesnini, J. Phys. Chem. 63, 544, (1959).
5. A. V. Kiselev and N. V. Kovaleva, Izvest. Akad. Nauk SSSR, Otdel. Khim. Nauk, 989 (1959). *
6. A. V. Kiselev, et al., Doklady Akad. Nauk SSSR 124, 617 (1959).*
7. A. V. Kiselev, A. Ya. Korolev, and K. D. Shcherbakova, Summaries of Papers at the 8th Mendeleev Congress [in Russian] (Izd. AN SSSR, 1959) p. 129.
8. V. I. Lygin, et al., Kolloid. Zhur. 22, 334 (1960).*
9. A. V. Kiselev, Proceedings of Conference on Gas Chromatography [in Russian] (Izd. AN SSSR, 1960).
10. I. Yu. Babkin, et al., Doklady Akad. Nauk SSSR 129, 131 (1959).*
11. A. V. Kiselev, Adsorption, Brief Description of Exhibits on the Stand at Soviet Science, Technology and Culture Exhibition in New York, [in Russian] (Izd. AN SSSR, 1959); A. V. Kiselev and K. D. Shcherbakova, in collection: Gas Chromatographie 1959, Material zum 2 Symposium uber Gas Chromatographie in Bohlen Akademie - Verlag (Berlin, 1959). p. 198.
12. I. Yu. Babkin and A. V. Kiselev, Doklady Akad. Nauk SSSR 129, 357 (1959).*
13. A. A. Isirikyan and A. V. Kiselev, Doklady Akad. Nauk SSSR 115, 343 (1957);* L. D. Belyakov and A. V. Kiselev, Doklady Akad. Nauk SSSR 119, 298 (1958);* in collection: Production, Structure, and Properties of Adsorbents [in Russian] (Goskhimizdat, Leningrad, 1959) p. 180.
14. K. D. Shcherbakova and K. I. Slovetskaya, Doklady Akad. Nauk SSSR, 111, 855 (1956);* R. S. Petrova, Diploma Thesis [in Russian] (MGU, 1957).
15. G. I. Aleksandrova, et al., Doklady Akad. Nauk SSSR 108, 283 (1956);* K. G. Krasil'nikov, et al., Zhur. Fiz. Khim. 31, 1448 (1957).
16. A. V. Kiselev, Vestnik Akad. Nauk SSSR, 10, 43 (1957).
17. G. L. Kington, in collection: The Structure and Properties of Porous Materials, Ed. D. H. Everett, and F. Stone (London, 1958) p. 59.
18. N. N. Avgul', Izvest. Akad. Nauk SSSR, Otdel, Khim. Nauk, 1314 (1957);*N. N. Avgul', et al., Izvest, Akad. Nauk SSSR, 1196 (1959);* B. B. Fisher and W. G. McMillan, J. Chem. Phys. 28, 562 (1958).
19. R. A. Beebe et. al., J. Am. Chem. Soc. 69, 95 (1947); R. A. Beebe, B. Mellard, and Synarski, J. Am. Chem. Soc. 75, 839 (1953); R. A. Beebe and D. M. Young, J. Phys. Chem. 58, 95 (1954).
20. A. V. Kiselev and E. V. Khrapova, Izvest. Akad. Nauk SSSR, Otdel. Khim. Nauk, 389 (1958).*
21. A. V. Kiselev and E. V. Khrapova, Kolloid. Zhur. 19, 572 (1957).*
22. W. C. Walker, and A. C. Zettlemoyer, J. Phys. Chem. 57, 182 (1953); A. V. Kiselev and D. P. Poshkus, Kolloid . Zhur. 21, 590 (1959);* A. A. Isirikyan and A. V. Kiselev, Zhur. Fiz. Khim. 34, 12 (1960).
23. R. A. Beebe, J. B. Beckwith, and J. M. Honig, J. Am. Chem. Soc. 67, 1554 (1945).
24. A. J. Rosenberg, J. Am. Chem. Soc. 78, 2929 (1956).
25. R. A. W. Haul, Angew. Chemie 68, 238 (1956).
26. R. T. Davis, J. W. De Witt, and P. H. Emmett, J. Phys. Coll. Chem. 51, 1246 (1947).
27. J. Wolock and B. L. Harris, Ind. and Eng. Chem. 42, 1347 (1950).
28. A. V. Kiselev, Doklady Akad. Nauk SSSR 117, 1023 (1957);* A. V. Kiselev and D. P. Poshkus, Izvest. Akad. Nauk SSSR, Otdel. Khim. Nauk, 520 (1858);* A. V. Kiselev, Kolloid. Zhur. 20, 338 (1958).*
29. A. V. Kiselev, et al., Kolloid. Zhur. 20, 444 (1958).*
30. H. W. Kohlschütter, P. Best, and G. Wirzing, Z. anorg. und allgem. Chem. 285, 236 (1956).
31. L. A. Wooten and C. Brown, J. Am. Chem. Soc. 65, 113 (1943).
32. A. V. Kiselev and V. V. Kulichenko, Zhur. Fiz. Khim. 29, 663 (1955).
33. J. J. Meihuizen and C. A. Crommelin, Physica 4 1, (1937).
34. G. Bauer and W. Stöber, Koll. Z. 160, 142 (1958).
35. L. D. Belyakova, O. M. Dzhigit, and A. V. Kiselev, Zhur. Fiz. Khim. 31, 1577 (1957).

* Original Russian pagination. See C. B. translation.

INVESTIGATION OF THE SALT STABILITY OF PALYGORSKITE

E. G. Kister

All-Union Scientific Research Institute of Drilling Technology, Moscow
Translated from Kolloidnyi Zhurnal, Vol. 22, No. 6, pp. 680-688,
November-December, 1960
Original article submitted June 23, 1960

It is widely known that clays and clay suspensions of various types – kaolinite, montmorillonite, hydromica, monothermite, allophanoid, and others - are highly sensitive to salt additions and are coagulated even at low salt contents. This effect is of great importance in geology, pedology, and various branches of technology; like other coagulation processes, it is based on an adsorption mechanism which makes the clay particles hydrophobic and causes them to form more or less compact aggregates. Either syneretic phase separation with partial liberation of immobilized water or formation of a continuous gel-like coagulum takes place, in accordance with the concentration of the disperse phase. If clay strata, lumps, or powders are subjected to the action of salts, coagulation processes again make the systems less hydrophilic and sharply reduce swelling and water sorption. Various factors, such as the composition of the exchange complex, nature of the clays and the active ions and the concentration of the latter, may influence and even distort these processes, but in every case the system undergoes significant changes in filtration and rheological characteristics, stability, etc.

Minerals of the palygorskite group are an exception; they differ markedly in their stability to coagulation by salts. Palygorskites are used in the United States of America for production of salt-resistant drilling muds, but their anomalous behavior has not been investigated or explained. Moreover, the numerous mineralogical and physicochemical investigations of palygorskites do not refer to their salt stability at all, although the question is one of considerable theoretical and practical interest.

Palygorskite, also known as attapulgite, is an aluminum magnesium silicate; it has been named "mountain leather," "mountain cork," "mountain wood," etc., and its outer appearance justifies these names. According to Fersman [1], palygorskites are of variable composition, being transitional between the magnesium silicate sepiolite and the magnesium silicate paramontmorillonite. These limits contain a wide range of minerals (those richer in aluminum are α- and β-palygorskites, and those richer in magnesium are α- and β-pilolites). The peculiarities of these minerals are satisfactorily explained by the hypothesis that they have a ribbon structure (of the amphibole type), in contrast to the ordinary clay minerals which have a layer structure (of the mica type). On this basis Bradley [2] put forward a model of the structure of palygorskite (attapulgite), which is consistent with its principal properties and x-ray data (Fig. 1).

From the side perpendicular to the fiber axis, palygorskite bands are continuous twinned chains of SiO_4 silicon-oxygen tetrahedrons which extend along the C axis and are linked through oxygen atoms at their longitudinal edges. The vertices of alternate tetrahedrons are situated in opposite directions, so that a peculiar ribbed double layer is formed in which pairs of rows of tetrahedron vertices are situated at alternating intervals in the base and overlapping of the layers; they are linked with magnesium (or aluminum) octahedrons, of the same kind as in layer silicates, but extended in one direction only. The layers of octahedrons also contain OH groups at the centers and at the free edges. Good cleavage along the fiber axis is ensured by weak bonding of the silicon-oxygen chains through oxygen atoms in the ribbed layer. It is clear from Fig. 1 that the spaces between

the amphibole chains along the C axis form channels which can contain up to four water molecules. These channels are 3.7-6.0 A across, which is even greater than in zeolites [3]. The lattice parameters, according to Bradley, are : $a_0 \sin \alpha = 12.9$ A; $b_0 = 18$ A; $c_0 = 5.2$ A. The distance between the oxygen layers is 6.45 A. The unit cell includes two molecules. The structure is balanced and is represented by the formula: $(OH_2)_4(OH)_2Mg_5Si_8O_{20} \cdot 4H_2O$, where some of the Mg and Si atoms are replaced by Al. These substitutions weaken the structure, and therefore the existence of the end members of the series is doubtful.

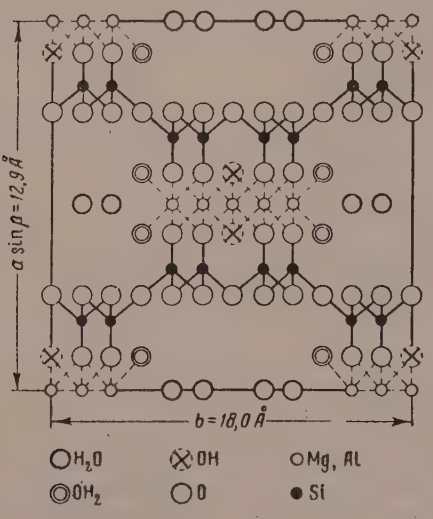


Fig. 1. Structure of palygorskite. Projection onto the plane perpendicular to the C axis [2].

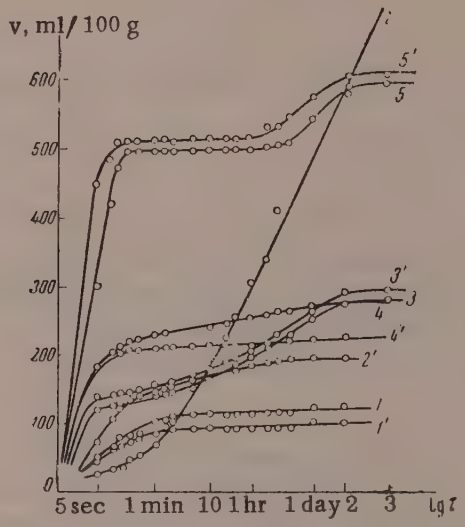


Fig. 2. Kinetics of absorption and swelling in distilled water and 10% NaCl: 1 and 1') Isotherms for Kudinovo clay in distilled and salt water; 2 and 2') askangel; 3 and 3') samples Z; 4 and 4') GK; 5 and 5') GD.

Samples of the following materials were used for the investigation: Kurtsov palygorskite (Crimean region of the Ukrainian SSR), samples A, Aob, B, C, and M; Gor'kii palygorskite from the regions of Velikii Vrag and Ketovo, samples G. and GD; sample GK from the Zeravshan range; and attapulgite sample Z (an American salt-resistant clay, "Zeogel.").

The samples of Kurtsov palygorskite (density from 2.07 to 2.41 g/cc, moisture content 4-10%, refractive index 1.537) contained from 35 to 77% of carbonates. Microscopic examination in immersion liquids showed the minerals to be anisotropic, with interference colors of not higher than the first order (yellow), with positive elongation.

The salt stability of the samples was determined from the following characteristics: kinetics of absorption and swelling in distilled and salt water, determined by a modification of the Freundlich method [4]; the sedimentation volumes of suspensions of various concentrations in saturated salt solution; rheological characteristics of destructurized salt clay suspensions after additions of palygorskite*.

Figure 2 shows that palygorskite swells equally well in salt and fresh water. In contrast to certain clays of low activity (such as Kudinovo monothermite clay), the maximum water sorption of palygorskite is 5-6 times as high, 600 and 590% for the pure sample (GD). The isotherms of water absorption by palygorskite are stepwise, probably because of the alternation of two effects: 1) binding of hygroscopic water, and 2) filling of the intracrystalline channels. The logarithmic abscissas (Fig. 2) show that the second effect is hindered and occurs only after it has been prepared by the first stage, when all the material is impregnated with water in excess, the whole system is in a unified water balance, and the intercrystalline bonds are weakened. The GK sample does not exhibit such swelling kinetics. The isotherm for askangel in distilled water differs sharply from the others. This is because water-impermeable layers which retard further absorption are formed at the initial stages as the result of swelling of the surface regions. As the moisture distribution in the system becomes equalized by the action of diffusion forces, the system becomes more colloidal but binding of water is slowed down further, because penetration of water into the spaces between the sheets rather than into the intercrystalline spaces

*T. I. Kolesnikova performed these determinations and calculated the palygorskite formulas.



Fig. 4. Electron micrographs of various palygorskite samples: a) GK, carbon replica, × 10,000; b) GD, pseudoreplica, × 10,000; c and d) B, two-stage cellulose-carbon replica, × 12,000 and 64,000; d and e) Z and Aob from suspensions after ultrasonic dispersion, × 16,000.

becomes more important. In the case of askangel the discrepancy between the maximum swelling values in distilled and salt water (1770 and 178%) is significant. This may serve as a measure of the sensitivity of clay to the action of salts.

In saturated salt solutions the stability even of dilute suspensions of palygorskite is very high (Table 1). Whereas after half an hour 53% of a 6% askangel suspension settles out, palygorskite forms no sediment. Only low-grade varieties containing up to 50% gangue give a sediment, which amounts to 10% after 24 hours. More highly concentrated suspensions give no sediment even after 24 hours.

The rheological behavior of destructurized salt clay suspensions treated with carboxymethylcellulose and thickened with palygorskite was assessed from their nominal viscosity and static yield value after 1 and 10 minutes of rest (Table 2). Whereas suspensions thickened with even 8% askangel or Kudinovo clay remain liquid after heating and stirring, have virtually zero yield values, and form sediments, even a small addition of palygorskite (samples GD and Aob) thickens the suspension so much that these characteristics cannot be measured. Here again sample GK (a typical mountain leather in appearance, and a typical palygorskite) proved unexpectedly to be an exception.

For a more detailed study, the palygorskite samples were analyzed by the spectroscopic and chemical methods, and investigated by the thermographic, x-ray, and electron microscope methods.

Some of the differential heating and dehydration curves determined in A. I. Tsvetkov's laboratory are given in Fig. 3. The curve for sample Aob shows a deep endothermic minimum, commencing at ~870°, which corresponds to dissociation of the carbonates present in this sample as impurities. The other samples do not give this minimum, and they may be considered without any reservations over the entire range; their thermographic curves are similar in character and are free from any pronounced effects. The curve for the standard attapulgite Z differs somewhat from the typical curve for a sample from Georgia [5], but is similar to the curve for North African palygorskite [6]. All the samples give minima between 125 and 175°; these approximately correspond to the inflections on the dehydration curves which mainly represent loss of hygroscopic water, and also of zeolite water from the structural channels, which is calculated to be up to 10% of the mineral weight. We did not observe the intensive dehydration up to 100° which has been reported by others [7]. The slight minimum at about 250-350° represents, according to Bradley, dehydration of Mg ions in the octahedron layers. A further minimum at ~500°, and at 600° in the case of GK, corresponds to loss of water from the silicate layers and changes in the lattice, indicated in the x-ray pattern by replacement of the very strong line at 10.5 kX by a diffuse ring. The intrastructural channels disappear as the result of displacements in the octahedron layers, the fibers contract in the longitudinal direction, and the capacity for rehydration is irreversibly lost. According to Longchambon et al. [8], these changes represent transition into another mineral form, palygorskite II. The remaining hydroxylic water is lost at ~900°. The changes in the 900-1100° range are apparently associated with recrystallization and formation of enstatite, and subsequently of sillimanite and cristobalite.

A sharper differentiation of the samples is given by x-ray Debye diagrams taken with the RKG camera of d = 86 mm with copper radiation and a nickel filter *. Here again the presence of carbonate impurities in samples A, Aob, and B had a very adverse effect on the x-ray patterns. The interplanar spacings and intensities for all the samples, with the exception of GK, are close to the values calculated for the structure shown in Fig. 1 and to the values found for the typical mineral from Attapulgus (USA). The data in Table 3, calculated from some of the x-ray patterns, show that the most characteristic are the intense reflections at 10.48-10.50 kX and at 2.15 kX. There are also characteristic lines at 6.45 and 3.23 kX

The x-ray pattern of sample GK did not correspond to palygorskite; the most characteristic lines were absent, but it contained lines by which montmorillonite is usually identified; for example, at 4.49 kX and also at 2.58 and 1.515 kX. This is consistent with the view [9] that palygorskites are close to fibrous montmorillonites.

The x-ray data are supplemented by electron micrographs obtained by the replica technique, and also from suspensions which were dispersed by means of ultrasonic vibrations in order to avoid mechanical damage to the fibers. Micrographs b and c in Fig. 4 clearly show the tangled fibrous character of the minerals, with fiber bundles and individual fibers; at high magnification (micrograph d) fragments up to 4-5 μ long and 50-100 A thick may be seen. In contrast to halloysite, in this case there are no signs of a tubular particle structure and there is a tendency to orientation parallel to the fiber axis, with formation of intertwined bundles. The structure of sample GK (micrograph a) is very different from that described above; the continuous leathery surface indicates that the main mineral has a layer rather than a ribbon structure, although morphologically it is a typical palygorskite.

* The micrographs and x-ray patterns were obtained in the Institute of Geology and Mineralogy of the Academy of Sciences USSR under the guidance of S. I. Berkhin and G. S. Gritsaenko.

TABLE 1

Sedimentation Kinetics in Salt-Saturated Clay Suspensions

Sedimentation time, hrs	Sediment, %				
	askangel	Kudinovo clay	kaolin	Aob	G
		6% clay			
0.5	53	72	58	0	0
1.0	71	80	68	2	0
1.5	75	82	70	3	0
2.0	78	85	73	5	0
24.0	80	83	70	10	2
		10% clay			
0.5	40	58	2	0	0
1.0	60	65	8	0	0
1.5	62	68	13	0	0
2.0	68	70	16	0	0
24.0	74	76	58	0	0
		14% clay			
0.5	27	38	6	0	0
1.0	48	47	12	0	0
1.5	51	50	15	0	0
2.0	54	53	18	0	0
24.0	65	60	48	0	0

For a more precise determination of the structural formulas of the various samples the appropriate calculations were performed from the results of chemical analyses [10]. In calculations of the water contents it was assumed that the calcination losses correspond to 20 OH^-, $4H_2O^+$ and H_2O^-, which is represented by the structural formula of ideal palygorskite. The total cation valence is then 42. In the case of sample GK an additional calculation was made, as for montmorillonite with the $[(OH)_2O_{10}]^{22-}$ "anionic framework."

TABLE 2

Viscosities and Yield Values of Destructurized Suspensions with Additions of Various Clays (Composition of the Original Suspension: 25% Kudinovo Clay, 25% NaCl, 2% CMC; Characteristics: T_{100} = 6; θ_1/θ_{10}= o/o *)

Characteristic	Kudinovo clay	Askangel	GK	Aob	GD
		5% added			
T_{100}	9	8	12	20	10
θ_1/θ_{10}	0/18	0/3	0/3	3/27	8/96
		After 24 hours			
T_{100}	8	8	11	36	57
θ_1/θ_{10}	0/9	0/6	0/9	42/60	63/108
		3% more added			
T_{100}	19	15	17		
θ_1/θ_{10}	12/30	6/15	3/42	159/210	400/400
		After 2 hours of heating and stirring			
T_{100}	11	12	15	63	
θ_1/θ_{10}	0/9	0/6	0/6	39/72	400/400

* T_{100} is the nominal viscosity (sec), the efflux time of 100 cc of suspension from a funnel with 5 mm tube (SPV-5), filled with 150 cc of suspension; θ_1 and θ_{10} are the static yield values after 1 and 10 minutes of rest (mg/cm^2).

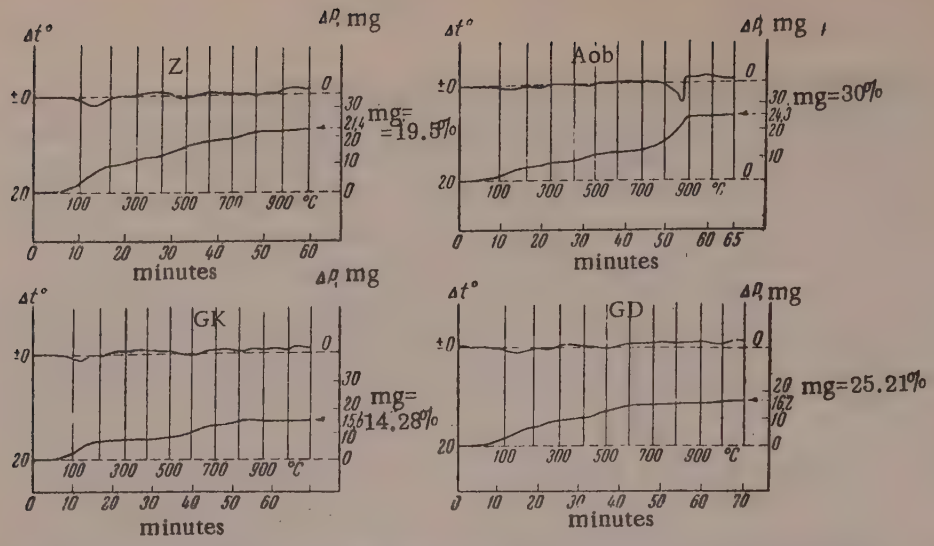


Fig. 3. Differential heating and dehydration thermograms for the following samples: Z (108.9 mg); GK (109.2 mg); Aob (81 mg); and GD (64.5 mg).

TABLE 3

Interplanar Spacings of Different Palygorskite Samples, in kX

GK		Aob		GD		Z		Attapulgite (standard) [2]	
d	*I*	*d*	*I*	*d*	*I*	*d*	*I*	*d*	*I*
12,3	10	—	—	—	—	—	—	—	—
—	—	—	—	—	—	~11	8	—	—
—	—	10,49	10	10,49	9	—	—	10,50	10
—	—	6,49	3	6,45	3	—	—	6,44	6
5,32	2	5,48	3	5,44	3	—	—	5,42	5
—	—	—	—	—	—	—	—	—	—
4,99	2 db	—	—	—	—	—	—	—	—
4,49	10	4,56	4	4,50	5	4,47	3	4,49	2db
—	—	4,34	3	4,18	3 d	4,27	6	4,18	3
—	—	3,89	6	—	—	—	—	—	—
3,76	2	—	—	—	—	3,73	4	—	—
—	—	3,69	2	3,69	3	—	—	3,69	5
3,37	10 з	3,36	3	3,49	3 з	3,36	10	—	—
—	—	3,20	3	3,23	5 d	3,24	2	3,23	10
3,05	3 p	3,03	10	3,04	4 з	—	—	3,03	1
2,97	4	—	—	—	—	2,97	5	—	—
—	—	2,61	3	2,62	4	2,60	4	2,61	8
2,58	10	2,51	8 b	2,56	4	—	—	2,55	3
2,45	3 b	—	—	—	—	2,46	4	—	—
—	—	—	—	—	—	—	—	2,38	3
2,31	3	—	—	—	—	2,28	4	—	—
2,20	3	2,23	30	2,15	3 d	2,19	2	2,15	5
2,14	—	—	—	—	—	2,12	4	—	—
2,00	—	2,10	8	2,10	6	2,02	1	—	—
—	—	1,91	8	—	—	1,98	2	—	—
—	—	1,87	8	—	—	—	—	—	—
1,82	4 з*	—	—	1,815	2	1,83	8	1,82	1
1,70	3	—	—	—	—	—	—	—	—
1,66	3	—	—	1,68	2	1,67	3	1,66	3
—	—	1,60	4	1,61	1 d	—	—	1,62	1
—	—	—	—	1,57	1 d	1,57	7	—	—
1,546	5	—,	—	1,55	1 d	—	—	1,56	3
1,515	8 b	1,519	3 d	1,50	5 d	—	—	1,50	5

* Meaning of symbol not determined.

The composition of the calcined mineral residue was also calculated by the usual stoichiometric method. In view of possible isomorphic substitutions, Al and Fe^{3+} were calculated as Mg, and Mg and Fe^{3+}, in their turn, were calculated as Al. Since Si atoms in the tetrahedron layers may be replaced by Al and Ti atoms, and some-

times by Fe^{3+}, the deficient numbers of Si atoms were supplemented by Al. Similar substitutions are also possible in the octahedron layers with Al, Mg, Fe^{3+}, Ca. The number of oxygen atoms was calculated from their content in the ideal palygorskite structure. Components present in small amounts (P, Mn, etc.) were not taken into account.

TABLE 4

Calculated Formulas of the Various Samples

Sample	Formula
	Complete formula of mineral
theoretical palygorskite [2]	$Mg_5 [Si_8O_{20}] (OH)_2 (H_2)_4 \cdot 4H_2O$
Z	$K_{0,12}Ca_{0,54} (Mg_{1,85}Fe^{2+}_{0,034}Fe^{3+}_{0,4}Al_{1,3}) [Al_{0,3}Si_{7,7}O_{20}] (OH)_2 (H_2)_4 \cdot 4,8H_2O$
same, Al and Fe^{3+} calculated as Mg	$K_{0,12}Ca_{0,54}Mg_{4,45} [Al_{0,3}Si_{7,7}O_{20}] (OH)_2 (H_2)_4 \cdot 4,8H_2O$
GD	$Ca_{0,54}(Mg_{2,14}Fe^{2+}_{0,076}Fe^{+3}_{0,137}Al_{1,52}) [Al_{0,47}Si_{7,53}O_{20}] (OH)_2 (H_2)_4 \cdot 7,3H_2O$
same, Al and Fe^{3+} calculated as Mg	$Ca_{0,54}Mg_{4,7} [Al_{0,47}Si_{7,53}O_{20}] (OH)_2 (H_2)_4 \cdot 7,3H_2O$
GK	$R_{0,65}Ca_{0,62} (Mg_{0,46}Fe^{2+}_{0,011}Fe^{3+}_{0,185}Al_{2,6}) [Al_{1,28}Si_{6,72}O_{20}] (OH)_2 (H_2)_4 \cdot 2,05H_2O$
same, Al and Fe^{3+} calculated as Mg	$R_{0,65}Ca_{0,62}Mg_{4,61} [Al_{1,28}Si_{6,72}O_{20}] (OH)_2 (H_2)_4 \cdot 2,05H_2O$
same, for a total cation valence of 22 (as montmorillonite)	$R_{0,34}Ca_{0,32} (Mg_{0,24}Fe^{2+}_{0,006}Fe^{3+}_{0,09}Al_{1,46}) [Al_{0,58}Si_{3,42}O_{10}] (OH)_2 \cdot 2,68H_2O$
same, Al and Fe^{3+} calculated as Mg	$R_{0,34}Ca_{0,32}Al_{1,71} [Al_{0,58}Si_{3,42}O_{10}] (OH)_2 \cdot 2,68H_2O$
theoretical montmorillonite	$\{Al_2 [Si_4O_{10}] (OH)_2 \cdot nH_2O\}_2$
	Formula for calcined substance
theoretical palygorskite with Al calculated as Mg	$Mg_5 [Si_8O_{20}]$ — —
Aob	$Ca_{0,2}Mg_{1,8}Fe^{3+}_{0,6}Al_{1,5} [Si_8O_{20}]$ 3 1,17
same, Al and Fe^{3+} calculated as Mg	$Ca_{0,2}Mg_{4,8} [Si_8O_{20}]$ — —
GD	$Ca_{0,6}Mg_{2,4}Fe^{3+}_{0,24}Al_{2,0} [Si_{8,0}O_{20}]$ 2 1,0
same, Al and Fe^{3+} calculated as Mg	$Ca_{0,6}Mg_{5,7} [Si_{8,0}O_{20}]$ — —
Z	$Ca_{0,6}Mg_{2,0}Fe^{3+}_{0,68}Al_{1,8} [Si_{8,4}O_{20}]$ 2 1,24
same, Al and Fe^{3+} calculated as Mg	$Ca_{0,6}Mg_{5,6} [Si_{8,4}O_{20}]$ — —
GK	$Ca_{0,68}Mg_{0,5}Fe^{3+}_{0,32}Al_{4,4} [Si_{8,2}O_{20}]$ 2 9,44
same, Al and Fe^{3+} calculated as Mg	$Ca_{0,68}Mg_{7,5} [Si_{8,2}O_{20}]$ — —

Table 4 shows that samples GD, Z, A, and Aob are close to ideal palygorskite. This is also shown clearly by the $(Al + Fe^{3+})$: Mg ratio, which is unity in the theoretical case, while a value of 0.5 indicates, according to Fersman [1], that the mineral belongs to the pilolites. This ratio is about 9 for GK, while for the other samples it is in the range of 1.3-0.8; this shows that GK is close to paramontmorillonite and is consistent with the sharp deviations of its behavior from the typical behavior of palygorskite.

Therefore the $(Al + Fe^{3+})$: Mg ratio can be regarded as an important and sensitive criterion for evaluation of salt-resistant materials.

The available experimental data give only a tentative explanation for the anomalous behavior of palygorskite, in particular, in salt water.

The characteristics of the fibrous structure of this material are the most significant. Even ordinary dispersion in water gives rise to a random feltlike structure, distinctly seen in the electron microscope. This structure is so extensively developed and has such a high thickening effect on palygorskite suspensions that this material is used successfully in drilling practice as a plugging agent [12]. Other fibrous materials, such as chrysotiles, amphiboles, etc., cannot produce this effect because they are not hydrophilic enough to ensure stability of the system. The cause of the higher hydrophily and of the salt stability lies in the peculiarities of the adsorption processes in palygorskite.

The main causes of adsorptional activity in clays are: 1) the presence of uncompensated charges due to breakdown of bonds around the edges of the aluminosilicate monomers; 2) replacement of high-valence ions by ions of lower valence in the tetrahedron and octahedron layers; 3) presence of exchangeable hydrogen in the external hydroxyls.

All these factors generally operate simultaneously, but their significance differs with different minerals. The first factor is most important with kaolinite and halloysite. Its significance increases with the degree of dispersion, and the adsorption capacity increases accordingly. The relative significance of this factor is small in the case of palygorskite. In contrast to the other minerals, in the case of palygorskite bond breakdown occurs not at the cleavage planes but in planes perpendicular to the C axis (Fig. 1), i.e., in the fiber cross section. The total area of the regions which become accessible to coagulating ions is then very small, and the stability to coagulation rises sharply. The same microfibrous structure as is present in absence of salts is essentially retained.

This mechanism applies to systems of low adsorptional activity; mainly systems of low colloidal and hydrophilic characteristics. However, palygorskite does not belong to such systems; although its adsorption capacity is inferior to that of montmorillonite, it is considerably higher than that of kaolinite or halloysite, and is at a level characteristic of the hydromicas, which nevertheless lack stability to coagulation. This apparent contradiction is eliminated if the adsorptional activity of palygorskite is attributed to the presence of free charges in the octahedron and tetrahedron layers, arising as the result of partial replacement of Al^{3+} by Mg^{2+} in the former, and of Si^{4+} by Al^{3+} in the latter.

These charges are neutralized by adsorption of ions at the inner surfaces, within the channels of the crystal structure. Here the exchange sites are much more numerous than on the fiber surface. It was found with the aid of radioactive isotopes [13] that the sorption capacity of a typical palygorskite (attapulgite) is 34 meq/100 g, and the sorption is effected primarily by adsorption within the inner voids, where Al and Mg in octahedral configuration are often exchangeable.

It follows that in palygorskite, as in montmorillonite, the main adsorption processes take place within the crystal structure. However, there is a significant difference. In the case of montmorillonite adsorption takes place on the interlayer planes, which are extremely mobile, and at the external surfaces of the layers; this readily accounts for its high hydrophily and sensitivity to coagulation. In palygorskite the adsorbed ions, including those causing coagulation, are localized within rigid channels. Because of the isolated location of the hydrophobic surfaces within the crystal structure, the particles do not coagulate when they come into contact by their external surfaces, which are inert with respect to adsorption.

A peculiar geometrical factor in stabilization of colloidal systems is significant in the case of palygorskite. Intrastructural adsorption of coagulant ions has virtually no effect on the total hydrophily of the system, so that the system has kinetic and aggregative stability. It is likely that this effect is general for all cases where the structure of the solid phase contains internal channels and voids which act as regions of localized coagulation.

SUMMARY

1. Suspensions of palygorskite, in contrast to suspensions of other clay minerals, are very resistant to the coagulating action of salt. This is characterized by high viscosities and yield values in salt solutions, absence of syneresis even saturated with salt, high and similar maxima of absorption and swelling in fresh and salt water, and stepwise isotherms for this process. This last effect must be attributed to alternation of two effects: binding of water between the particles and on the particle surfaces, and filling of intracrystalline voids.

2. The salt stability of palygorskite is correlated with characteristics of the crystal structure of the mineral, its feltlike structure which is easily seen in the electron microscope, high hydrophily, and the location of most of the sites of exchange adsorption in the intracrystalline channels. Therefore the coagulant ions are localized at the inner surfaces and have virtually no influence on the total hydrophily of the system and on its aggregative and kinetic stability.

3. Palygorskite can be distinguished fairly precisely among other morphologically similar materials by x-ray diffraction, electron microscopy, chemical analysis from the $(Al + Fe^{+3})/Mg \approx 1$ ratio (calculated for the calcined substance), and direct determinations of salt stability.

LITERATURE CITED

1. A. E. Fersman, Investigations of Magnesium Silicates [in Russian] (Izd. An SSSR, St. Petersburg, 1913).
2. W. E. Bradley, Am. Mineralogist 25, 405 (1940).
3. C. E. Marshall and O. G. Caldwell, J. Phys. Coll. Chem. 51, 1,311, (1947).
4. E. G. Kister, Neft. Khozyaistvo, 12, 23 (1947).
5. R. E. Grim, Clay Mineralogy [Russian translation] (IL, 1956).
6. S. Caillère and S. Henin, in collection: X-Ray Identification and Crystal Structures of Clay Minerals [Russian translation] (IL, Moscow, 1955) p. 251.
7. G. Migeon, Bull. Soc. France. Min. 59, No. 6 (1936).
8. H. Lonchambon, Compt. rend Ac. Sci. 203, 672 (1936); 204, 55 (1937).
9. D. P. Serdyuchenko, Mineralogical Collection of the L'vov Geological Society [in Russian] (1955) Vol. 9, p. 156.
10. B. B. Zvyagin, Collection of the All-Union Geological Institute: Manual of Petrographic and Mineralogical Investigation of Clays [in Russian] (Gosgeoltekhizdat, 1957) p. 298.
11. D. M. C. MacEwan, in collection: X-Ray Identification and Crystal Structures of Clay Minerals [Russian translation] (IL, Moscow, 1955) p. 103.
12. D. R. Ruffin, Oil and Gas J. 55, 43, 96 (1957).
13. C. Neale Merriam Jr., and H. C. Thomas, J. Phys. Chem. 5, 993 (1956).

KINETICS OF HYDRATION AND GROWTH OF CRYSTALLIZATIONAL CONCRETION STRUCTURES IN MONOMINERAL CEMENTS OF THE PLASTER OF PARIS TYPE

A. F. Polak

Bashkir Scientific Research Institute of Building, Ufa
Translated from Kolloidnyi Zhurnal, Vol. 22, No. 6, pp. 689-701,
November-December, 1960
Original article submitted November 2, 1959

New concepts of the hardening processes in hydrated cementing materials have been developed by the investigations of Rebinder and his school [1-8]. The experimental data accumulated over many years are in need of correlation. Such a correlation may be performed, somewhat schematically, in the light not only of the laws of hydration kinetics, i.e., the course of formation of the stable crystalline hydrates [9], but also of the laws of contact formation or concretion of crystals, which account for the conversion of a suspension (paste) into a crystallizational structure or monolithic stone.

This article represents a first attempt in this field; the equations which have been derived represent not only the qualitative but also some quantitative aspects of the hardening process. First, the dependence of hydration kinetics during hardening $y(\tau)$, and the ultimate duration of the processes which jointly constitute the hydration process: hydration τ_1 and contact formation τ_k on a number of factors was determined. These factors were: the amount Γ of cementing material per unit volume of suspension, its specific surface s_0, the nominal (metastable) solubility c_m of the original substance, the solubility c_n of the newly formed hydrate, the coefficient of diffusion D, and the thickness of the diffusion layers δ_x and δ_y on the surfaces of the dissolving particles and growing hydrate crystals, respectively.

It is assumed that the particles of all the solid phases in the suspension are not polyhedral but spherical and that at any instant of the hydration process a large number of particles of different diameters may be replaced by the same number of equivalent particles all of the same average diameter. The presence in the suspension of a small fraction of very fine particles, differing considerably in size from the average diameter, cannot have a prolonged effect on the hydration kinetics because these particles dissolve at the initial stages of the process owing to their higher solubility.

Since the solid particles are assumed to be spherical, it is evidently necessary to regard the specific free surface energy σ as the average of the values σ_i for different faces i (of area s_i) of the crystals:

$$\sigma = \sum \sigma_i s_i \Big/ \sum^{i} s_i.$$

For the original cement the particle radius r_x and the total area s_x of all the particles per unit volume of suspension are found from the formulas

$$r_x = \frac{3}{\gamma_x s_0}\left(\frac{x}{\Gamma}\right)^{1/3}, \qquad (1)$$

$$s_x = \Gamma s_0 \left(\frac{x}{\Gamma}\right)^{2/3}. \quad (2)$$

Similarly, for the new substance

$$r_y = r_0 \left(\frac{y}{y_0}\right)^{1/3}; \quad (3)$$

$$s_y = \frac{3y_0}{\gamma_y r_0} \left(\frac{y}{y_0}\right)^{2/3}, \quad (4)$$

where γ_x, γ_y are the densities of the original and new substance; $\underline{x}$ and $\underline{y}$ are the total masses of the respective nuclei at the instant of formation per unit volume of suspension.

The calculations are based on the following physicochemical concepts.

1. Crystal hydrate nuclei are formed on solid surfaces from solution at maximum supersaturation with respect to the new substance. Since the probability of nucleation from supersaturated solution falls very sharply (by an exponential law) with decreasing supersaturation, it is assumed that the time of formation of crystallization centers τ_0 is very small in comparison with the hydration time $\tau_1 (\tau_1 \gg \tau_0 \approx 0)$.

2. The subsequent hydration kinetics is determined by the simple laws for dissolution and crystallization of solid phases from solution. The duration of this process is determined by the condition of complete dissolution of the original substance.

3. At a definite stage of the hydration process conditions again arise for formation of nuclei; it will be shown in this paper that these nuclei cause contact formation, i.e., concretion of the microcrystals and gradual conversion of the suspension (paste) into a crystallizational (stonelike) structure.

The calculations were based on the Nernst diffusion theory of solution [10]. The solubility of the solid phases was determined in relation to their particle size in accordance with the Kelvin law. The kinetics of nucleation was determined as described by Volmer [11]. The α- and β-modifications of calcium sulfate hemihydrate were used as the experimental material.

Hydration kinetics. The rate of weight decrease of the original solid phase (calcium sulfate hemihydrate) as it dissolves $(-dx/dt)$, and the rate of weight increase of the growing crystals of the new substance (calcium sulfate dihydrate $(dy/d\tau)$, are determined in accordance with the Nernst diffusion theory [10] from Formulas (5) and (6)

$$-\frac{dx}{d\tau} = k_x s_x (c_x - c), \quad (5)$$

$$\frac{dy}{d\tau} = k_y s_y (c - c_y), \quad (6)$$

where $\underline{c}$ is the concentration in the volume of the solution; c_x and c_y are the concentrations and s_x and s_y the absolute surface areas of the dissolving and growing particles respectively; $k_{x(y)} = D/\delta_{x(y)}$. The concentrations c_x and c_y are found from the Kelvin equation and, being functions of the radii r_x and r_y, can be presented, with Equations (1) and (3) taken into account, as functions of $\underline{x}$ and $\underline{y}$:

$$\ln \frac{c_y}{c_n} = \frac{2M_y\sigma_y}{RT\gamma_y} \frac{1}{r_y} = \frac{2M_y\sigma_y}{RT\gamma\, r_0} \left(\frac{y_0}{y}\right)^{1/3}, \quad (7)$$

$$\ln \frac{c_x}{c_m} = \frac{2M_x\sigma_x}{RT\gamma_x} \frac{1}{r_x} = \frac{2}{3} \frac{M_x\sigma_x}{RT} s_0 \left(\frac{\Gamma}{x}\right)^{1/3}, \quad (8)$$

where M_x and M_y are the molecular weights of the original and newly formed substance respectively; σ_x, σ_y are the specific free surface energies of these phases; R is the universal gas constant; T is the absolute temperature.

Let us consider the limiting values of the concentrations c_x and c_y. For $\tau = 0$ we have

$$\ln \frac{c_{y_0}}{c_n} = \frac{2M_y\sigma_y}{RT\gamma_y}\frac{1}{r_0},$$

but r_0, which is the radius of a particle formed at solution concentration c_m, must be equal to or somewhat greater than the equilibrium radius determined from the Kelvin equation:

$$r_0 = \beta r_m = \rho \frac{2M_y\sigma_y}{RT\gamma_y}\frac{1}{\ln \frac{c_m}{c_n}}, \tag{9}$$

where $\beta \geqslant$ is a dimensionless coefficient. Substituting Equation (9) into the equation for c_{y_0}, we have

$$\frac{c_{y_0}}{c_m} = \left(\frac{c_n}{c_m}\right)^{1-\frac{1}{\beta}}. \tag{10}$$

When $r_0 = r_m$, $\beta = 1$ and therefore $c_{y_0} = c_m$; if $r_0 > r_m$ then $\beta > 1$ and in that case $c_{y_0} < c_m$.

At the end of the hydration process ($\tau = \tau_1$) $y = y_1$, and therefore

$$\ln \frac{c_{y_1}}{c_n} = \frac{2M_y\sigma_y}{RT\gamma_y}\frac{1}{r_0}\left(\frac{y_0}{y_1}\right)^{1/3},$$

or, with Equation (9) taken into account,

$$\frac{c_{y_1}}{c_n} = \left(\frac{c_m}{c_n}\right)^{1/\beta}\left(\frac{y_0}{y_1}\right)^{1/3} \tag{11}$$

It follows from Equation (6) that crystal growth is proportional to the concentration gradient $(c - c_y)/\delta_y$. At the start of the process the supersaturation in the volume of the solution is c_m. Equation (10) shows that the concentration c_{y_0} at the surface of the growing particles is only slightly less than c_m. Therefore at the start of hydration the rate of this process is very low, $(dy/d\tau)_{\tau=0} \approx 0$. Numerous observations of changes in supersaturation have shown that at the end of hydration the value of the supersaturation tends to c_n (the solubility of calcium sulfate dihydrate), remaining somewhat higher than the latter, and $\underline{c}$ becomes equal to c_n only several hours after completion of the hydration process. It follows that here again $(c_1 - c_{y_1})/\delta_y$ is close to zero, and therefore $(dy/d\tau)_{\tau_1} \approx 0$; accordingly, the hydration process dies down.

If the degree of supersaturation of the solution at the end of hydration is known, then Equation [11] can be used for determining the dimensionless coefficient β from the formula

$$\beta = (y_0/y_1)^{1/3}\frac{\ln (c_m/c_n)}{\ln (c_{y_1}/c_n)}. \tag{12}$$

Experimental work showed that $1.5 < \beta < 2.2$.

We now determine the order of magnitude of the concentration at the surface of the dissolving particles. Substituting into Equation (6) the values: $x = \Gamma$; $M_x = 145$; $\sigma_x \approx 400$ ergs/cm^2; $R = 8.31 \cdot 10^7$ ergs/degree · mole; and $T = 290°$, we have $c_{x_0} = c_m e^{1.6 \cdot 10^{-6} S_0}$.

This equation shows that in the case of calcium sulfate with a large specific surface ($s_0 \approx 10^4$ cm^{2}g^{-1}) the initial solubility is again practically equal to c_m. Therefore at the instant the concentration c_m is reached in the volume of the solution the gradient $(c_{x_0} - c_m)/\delta_x \approx 0$; this means that the dissolution is halted and subsequently recommences only with decrease of the concentration $\underline{c}$.

Toward the end of the dissolution process the calcium sulfate hemihydrate becomes used up and, in accordance with Equation (8), the concentration c_x should increase; at the limit, when $x = 0$ ($\tau = \tau_1$), it should

have the value $c_x = \infty$. In practice, however, this does not happen, because at that instant the dissolving substance is no longer present; in fact even when $x/\Gamma = 0.01$ the value of c_x differs little from c_m.

From the condition that the number of moles of $CaSO_4$ involved in the hydration is constant we have a further equation:

$$x/M_x + y/M_y + c/M = \Gamma/M_x. \tag{13}$$

For suspensions (pastes) in which the calcium sulfate content $\Gamma \geqslant 200$ g/liter the maximum solution concentration is always considerably lower than Γ ($c_m = 8.6$ g/liter $\leqslant 0.043 \cdot \Gamma \ll \Gamma$). Therefore for such suspensions it may be assumed that

$$x/M_x + y/M_y = \Gamma/M_x. \tag{13a}$$

We thus have eight unknown functions: x, y, c, c_x, c_y, s_x, s_y, τ and seven equations: (2), (4), (5), (6), (7), (8), and (13a); seven required values can therefore be represented as a function of the eighth as an independent variable. The most convenient procedure is to take the weight of dihydrate (y) formed in unit volume of the suspension (paste) as this variable and then, $\tau = \tau(y)$ having been found, to represent all the other required variables in terms of time τ.

From these equations we have the differential equation for hydration

$$d\tau = \frac{1}{k_x \Delta c s_0} \frac{d(y/y_1)}{(1 - y/y_1)^{2/3}} + \frac{r_0 \gamma_y}{3 k_y \Delta c} \frac{d(y/y_0)}{(y/y_0)^{2/3}}, \tag{14}$$

where $\Delta c = c_x - c_y$.

Substitution of the numerical values into Equations (7) and (8) shows that $1/\Delta c$ varies over a relatively narrow range with variation of y/y_1 between 0.10 and 0.99. For the α-semihydrate we have $0.33 > 1/\Delta c > 0.22$, and for the β-semihydrate, $0.20 > 1/\Delta c > 0.16$. Accordingly, we make the approximation

$$1/\Delta c = 1/\Delta c_{av} = \text{const}. \tag{15}$$

Integration of Equation (14) with Equation (15) taken into account gives the required function for the hydration kinetics in the form

$$\tau = K_x \xi + K_y \eta, \tag{16}$$

where

$$\left.\begin{gathered} K_x = \frac{1}{k_x \Delta c s_0}, \quad K_y = \frac{1}{k_y \Delta c} \frac{r_0 \gamma_y}{3}, \\ \xi = 3[(1 - y_0/y_1)^{1/3} - (1 - y/y_1)^{1/3}] \approx 3[1 - (1 - y/y_1)^{1/3}], \\ \eta = 3[(y/y_0)^{1/3} - 1]. \end{gathered}\right\} \tag{17}$$

From Equation (16), when $y = y_1$, we find the duration of the hydration process τ_1

$$\tau_1 = \frac{(1 - y_0/y_1)^{1/3}}{k_x \Delta c} \frac{3}{s_0} + \frac{(y_1/y_0)^{1/3} - 1}{k_y \Delta c} r_0 \gamma_y, \tag{18}$$

and from Equations (5), (6), (7), and (8), with Equation (17) taken into account, we find the expression for concentration variations in the bulk of the solution (with the assumption that $c_x = c_m$)

$$\frac{c}{c_m} \approx \frac{K_y/K_x (y_1/y_0)^{1/3} (y_1/y_0 - 1)^{2/3} + c_y/c_m}{K_y/K_x (y_1/y_0)^{1/3} (y_1/y - 1)^{2/3} + 1}. \tag{19}$$

and

$$c_y/c_n = (c_m/c_n)^{\frac{1}{\beta}} \left(\frac{y_0}{y}\right)^{1/3} \tag{20}$$

To assess the accuracy of Equations (16) and (17) we use the results obtained in experimental studies in the Department of Colloid Chemistry of the Moscow State University, where the kinetics of hydrate formation was studied (by calculations based on heat liberation data) in relation to the particle size of α- and β-calcium sulfate hemihydrate at constant W/S ratio of 0.40 (Fig. 1). Figure 1 shows that at $s_0 = 9700$ cm^2/g, the hydration time τ_1 is approximately 27 minutes, and at $s_0 = 3900$ cm^2/g, $\tau_1 \approx 45$ minutes. Substituting these values into Equation (16), and taking $y_0/y_1 = 0.02$ from the diagram, we have $K_x = 3.95 \cdot 10^4/s_0$ and $K = 1.84$. Therefore the kinetics of hydrate formation is represented by the equation

$$\tau = (3{,}95 \cdot 10^4/s_0)\,\xi + 1{,}84\eta, \tag{a}$$

where

$$\xi = 3[0{,}995 - (1 - y/y_1)^{1/3}], \tag{b}$$

$$\eta = 3[(y/y_0)^{1/3} - 1]. \tag{c}$$

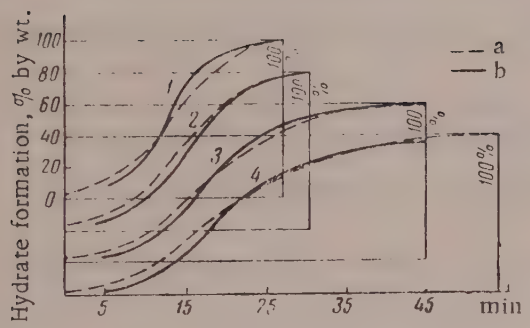


Fig. 1. Kinetics of the formation of hydrate from α-calcium sulfate hemihydrate at W/S = 0.40 from experimental (a) and calculated (b) values: 1) $s_0 = 9700$ cm^2/g, $\tau_1 = 27$ min; 2) $s_0 = 8000$ cm^2/g, $\tau_1 = 30$ min; 3) $s_0 = 3900$ cm^2/g, $\tau_1 = 45$ min; 4) $s_0 = 3000$ cm^2/g, $\tau_1 = 54$ min.

The dash lines in Fig. 1 represent values calculated from Equations (a), (b), and (c) for different degrees of fineness s_0. It follows from Fig. 1 that the kinetics of hydrate formation can be represented with adequate accuracy by means of the proposed equations.

It follows from Equation (15) that the hydration time decreases with increased specific surface, solubility difference between the starting material and the new substance, and increase of y_0/y_1, which represents the rate of nucleus formation.

Table 1 gives the results obtained in determinations of the time of hydration of α- and β-calcium sulfate hemihydrates of different specific surfaces and with different amounts Γ of calcium sulfate.

In the first and third group of experiments the hydration times of α- and β-calcium sulfate hemihydrates were determined with constant amounts of hemihydrate and different specific surfaces. The calculated values of τ_1 found from Equations (d) and (e)* are found to be in good agreement with the actual values:

$$\tau_{1\alpha} = 15 + 11{,}8 \cdot 10^4/s_0, \tag{d}$$

$$\tau_{1\beta} = 7{,}5 + 15{,}5 \cdot 10^4/s_0. \tag{e}$$

It follows from the second and fourth groups of experiments that the duration of the process, both for α- and for β-calcium sulfate hemihydrate, is independent of the water-solid ratio (at constant specific surface); this is fully consistent with the theoretical Equation (16).

*Equation (d) is obtained by the substitution $\tau = \tau_1$ into Equation (a), while Equation (e) was derived from Equation (16) in the same way as Equation (1) with the data in Table 1.

TABLE 1

Duration of the Hydration Process

	α-Calcium sulfate hemihydrate				β-Calcium sulfate hemihydrate			
	Expt. 1, W/S = 40				Expt. 3, W/S = 40			
s_0, cm²/g	3000	3900	8000	9700	5000	8000	11700	13700
$10^4/s_0$	3,33	2,56	1,25	1,03	2,00	1,25	0,855	0,730
τ_1, calc.	54	45	30	27	38	28	22	19
τ_1, exptl.	52—55	53—47	28—31	25—27	36—40	24—26	20—23	18—20
	Expt. 2, s_0 = 3900 cm²/g				Expt. 4, s_0 = 8000 cm²/g			
W/S	0,3	0,4	0,5	0,6	0,3	0,4	0,5	0,6
τ_1	42—45	42—45	40—43	38—42	28—30	25—27	24—27	25—2

It is of interest to verify the coefficients in Equations (d) and (e). Equation (17) cannot be used for calculation of K_x and K_y (since $\underline{k}$ and k_y are not known); we therefore consider the ratio $K_{y\alpha}/K_{y\beta}$. Since

$$\frac{\Delta c_{0\beta}}{\Delta c_{0\alpha}} = 0{,}27/0{,}18\ ^*, \text{ and } \frac{r_{0\alpha}}{r_{0\beta}} = \frac{\ln (c_{m\beta}/c_n)}{\ln (c_{m\alpha}/c_n)} = \frac{0{,}624}{0{,}512},$$

assuming that $y_{0\alpha} \approx y_{0\beta}$ and remembering that k_y is independent of the properties of the starting material, we have from Equation (17)

$$K_{y\alpha}/K_{y\beta} = (\Delta c_{0\beta}/\Delta c_{0\alpha})(r_{0\alpha}/r_{0\beta}) = 1{,}83.$$

In fact, Equations (d) and (e), i.e., substitution of the experimental data into Equation (16) gave $K_{y\alpha}/K_{y\beta}$ = = 15 / 7.5 = 2 (fairly good agreement).

Further, we have from Equations (d) and (e) that $K_{x\alpha}/K_{x\beta}$ = 11.8 / 15.7. This result cannot be verified directly, because from Equation (17) it follows that

$$K_{x\alpha}/K_{x\beta} = (\Delta c_{0\beta}/\Delta c_{0\alpha})(k_{x\beta}/k_{x\alpha}) = (0{,}27/0{,}18)(k_{x\beta}/k_{x\alpha}),$$

$k_{x\alpha} \neq k_{x\beta}$. Comparison of these expressions shows that $K_{x\beta}/k_{x\beta}$ = 0.50. This indicates that the diffusion layer is twice as thick at the surface of the β-hemihydrate as at the surface of the α-hemihydrate, which is in good agreement with the general views on this problem if it is taken into account that the dissolution rate of the β-hemihydrate, with a higher energy capacity, is higher than that of the α-hemihydrate.

Kinetics of contact formation. According to Volmer [11], the probability of formation of crystallization centers is given by the equation

$$W = Ce^{-\frac{A}{kT}}, \tag{21}$$

where A is the energy of nucleus formation according to Gibbs [12], $\underline{k}$ is the Boltzmann constant, T is the absolute temperature, and C is a dimensionless constant. It is known that

$$A = \frac{4\pi}{3} r^2 \sigma. \tag{22}$$

It follows from Equation (21) that the less the energy of formation A, the greater the probability W of nucleation. The most probable nucleus diameter in a solution of concentration c_k should correspond to the minimum radius of stable particles at that concentration. According to Kelvin

$$r_k = \frac{2M\sigma}{RT\gamma} \frac{1}{\ln (c_k/c_n)}. \tag{23}$$

There is no doubt about the formation of nuclei at maximum supersaturation (corresponding to the solubility of calcium sulfate hemihydrate), and therefore the highest probability of nucleus formation (W) would occur at $c_k = c_m$, $A = A_m$ and $r = r_m$, where

$$A_m = \frac{4\pi}{3} r_m^2 \sigma, \tag{22}$$

$$r_m = \frac{2M\sigma}{RT\gamma} \frac{1}{\ln (c_m/c_n)}. \tag{23a}$$

M. Volmer also gave a proof for the predominant formation of nuclei from supersaturated solution on solid surfaces. This suggests that the hardening of a suspension consisting of dihydrate and water, i.e., concretion of individual dihydrate particles and formation of a monolithic stone (crystallizational structure) may be attributed to predominant formation of nuclei between the dihydrate crystals if these are close enough to each other. It follows from the theory that such concretion is possible if the energy of contact formation A_k is less than or equal to the energy of nucleus formation. Therefore the condition for such contact formation is

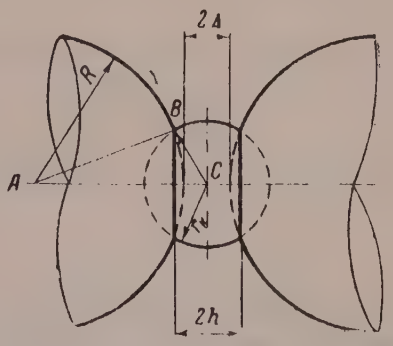


Fig. 2. Model of spherical contacts.

$$A_k \leq A_m. \tag{24}$$

For determination of the energy of contact formation we use a sphere model, on the assumption that a spherical contact of radius r_k is formed between spherical particles of radius r_i (Fig. 2).

It follows from Fig. 2 that

$$2h = \frac{r_k^2 + 2r_i\Delta + \Delta^2}{r_i + \Delta}. \tag{25}$$

Hence

$$A_k = \frac{2\pi}{3} \sigma \frac{\Delta^2 (r_i + r_k) + 2\Delta r_i r_k + r_k^2 (r_k - r_i)}{r_i + \Delta}, \tag{26}$$

where 2Δ is the distance between the particles. From Equations (26), (22a), and (24) we have the thermodynamic conditions for contact formation

$$\left(\frac{\Delta}{r_m}\right)^2 \left(\frac{r_i}{r_m} + \frac{r_k}{r_m}\right) + 2\frac{\Delta}{r_m}\left(\frac{r_i}{r_m}\frac{r_k}{r_m} - 1\right) + \left(\frac{r_k}{r_m}\right)^2 \left(\frac{r_k}{r_m} - \frac{r_i}{r_m}\right) - 2\frac{r_i}{r_m} \leq 0. \tag{27}$$

From Equations (3) and (9) we have

$$\frac{r_i}{r_m} = \beta \left(\frac{y}{y_0}\right)^{1/3}, \tag{28}$$

and from Equations (23) and (23a)

$$\frac{r_k}{r_m} = \ln \frac{c_m}{c_n} \frac{1}{\ln (c_k/c_n)}, \tag{29}$$

therefore it follows from Equation (27) that contact formation is possible if, at a given particle size of the hydrates (r_i) and a given concentration (c_k), the distance between the particles is less than a certain critical value ($2\Delta_k$), given by Equation (27). The variables $r_i(\tau)$, $c_k(\tau)$ as functions of time were determined in the

preceding section of this paper. Therefore determination of $\Delta_k(\tau)$ presents no difficulties. However, Equation (27) is unsuitable for elucidation of the kinetic relationships.

We first determine the order of magnitude of $\Delta(\tau)$ with the approximation

$$c = c_m - (c_m - c_n)(\tau/\tau_1). \tag{a}$$

We have c_m = 8.6 g/liter; c = 2.04 g/liter; therefore, taking $\beta = 2$ and $y_0/y_1 = 0.05$, we have

$$r_i/r_m = 2\left[1 + 1{,}72\frac{\tau}{\tau_1}\left(2 - \frac{\tau}{\tau_1}\right)\right]; \tag{b}$$

$$\frac{r_k}{r_m} = \frac{0{,}626}{\ln (c/2)}. \tag{c}$$

We now take individual values of τ/τ_1 in the range $0 < \tau/\tau_1 < 1$, and calculate c from Equation (a), and r_i/r_m and r_k/r_m from Equations (b) and (c). The results of these calculations are given in Table 2 and Fig. 3

TABLE 2

Determination of Δ/r_m

τ/τ_1	0,00	0,10	0,30	0,50	0,70	0,90	1,00
c_k	8,60	7,94	6,62	5,30	3,98	2,66	2,04
r_k/r_m	1,00	1,05	1,20	1,48	2,10	5,04	—
r_i/r_m	2,00	2,65	3,75	4,58	5,12	5,40	5,44
Δ/r_m by (27)	1,00	1,00	0,90	0,88	0,67	0,34	—
Δ/r_m by (32)	1,00	0,97	0,92	0,87	0,81	—	—

It follows from Table 2 that the function $\Delta(\tau)/r_m$ depends on τ in a very complex manner but, as will be shown, it can with a certain degree of approximation be replaced by a linear function, the tangent to the $\Delta(\tau)/r_m$ curve at the point $\tau = 0$ (Fig. 3). Evidently, the mathematical expression of this approximation is

$$\frac{\Delta}{r_m} = \left(\frac{\Delta}{r_m}\right)_{\tau=0} + \left[\frac{d}{d\tau}\left(\frac{\Delta}{r_m}\right)\right]_{\tau=0}\frac{\tau}{\tau_1}. \tag{30}$$

Substituting values of $(\Delta/r_m)_{\tau=0}$ and $[(d/d\tau)(\Delta/r_m)]_{\tau=0}$, calculated from Equations (27) and (28) into Equation (30), we have

$$\left(\frac{\Delta}{r_m}\right)_k \leqslant 1 - \frac{1}{\beta}\frac{1 - c_n/c_m}{\ln c_m/c_n}\frac{\tau}{\tau_1}. \tag{31}$$

Hence, for c_m = 8.6 g/liter, c_n = 2.04 g/liter, and $\beta = 2$, we have

$$(\Delta/r_m)_k \leqslant 1 - 0{,}263\,\tau/\tau_1. \tag{32}$$

It follows from Table 2 and Fig. 3 that in the range of interest, $0 < \tau/\tau_1 < 0.6$, Equation (32) gives a satisfactory approximation.

We use the following model for calculation of $(\Delta/r_m)_f$: it is assumed that spherical particles of calcium sulfate dihydrate are arranged in space along the edges of a cube; in addition to the spheres at the corners there are n further spheres along each edge. The radius of these spheres is r_i, and the distance between them $2\Delta f$. The volume of the cube is

$$O_1 = (n+1)^3(\Delta f + r_i)^3 \cdot 8, \tag{a}$$

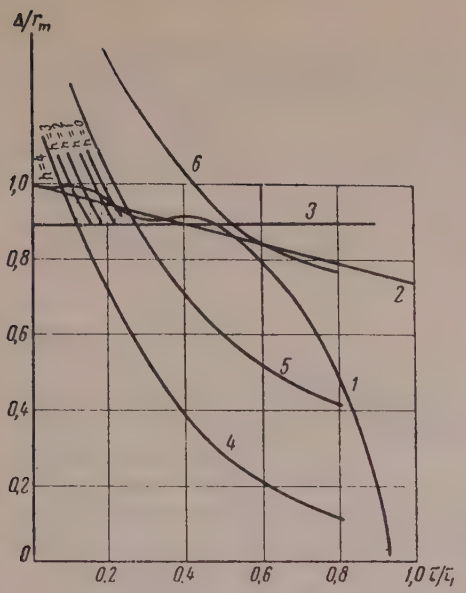


Fig. 3. Kinetics of contact formation: 1 and 2) Δ / r_m from Equations (27) and (31); 3) $(\Delta / r_m)_{min}$; 4,5, and 6) $\Delta\varphi / r_m$ for plaster contents Γ_1, Γ_2 and Γ_3 respectively ($\Gamma_1 > \Gamma_2 > \Gamma_3$) from Equation (33).

and the volume of the spheres within the cube is

$$O_2 = \left(\frac{4\pi}{3} + 4n\pi\right) r_i^3. \qquad (b)$$

Equations (a) and (b) give the following expression for the density y/γ_y:

$$\frac{y}{\gamma_y} = \frac{\pi}{6} \frac{(1+3n)}{(1+n)^3} \frac{r_i^3}{(\Delta f + r_i)^3}. \qquad (c)$$

Since $r_1^3 y_0 = r_0^3 y$, and also $y_1 = \Gamma (M_y / M_x)$ we have from Equation (c)

$$\frac{\Delta f}{r_m} = \beta \left[\frac{\pi}{6} \frac{1+3n}{(1+n)^3} \left(\frac{y_1}{y_0}\right) \frac{M_x}{M_y} \frac{\gamma}{\Gamma} \right]^{1/3} - \frac{r_i}{r_m}. \qquad (33)$$

Figure 3 gives $(\Delta f / r_m)i$ curves for different amounts of sulfate Γ_i, where $\Gamma_1 > \Gamma_2 > \Gamma_3$. These data show that with a small amount of calcium sulfate (high water-solid ratio) the $(\Delta f / r_m)\Gamma_3$ curve does not cut the Δ_k / r_m curve at any point. Therefore $(\Delta_k / r_m) < (\Delta f / r_m)\Gamma_3$ throughout the whole hydration process and contacts cannot be formed; i.e., the suspension does not harden. This is satisfactorily confirmed both by laboratory experiments and by production experience, since it is known that building plasters with low plaster contents gradually thicken but never harden.

Figure 3 also shows that the greater the amount of sulfate Γ_i, the earlier do the $\Delta f / r_m$ curves cut the Δ_k / r_m curve; i.e., the earlier is the instant reached when $\Delta f = \Delta_k$. This means, in full agreement with practice, that the greater the amount of sulfate Γ_i the earlier does contact formation or hardening begin.

Let us now consider how contact formation depends on the number n. The greater the value of n, the greater is the distance between the individual crystal points, i.e., the looser is the structure of the crystalline framework formed. Curve 4 in Fig. 3 was calculated for different values of n; it may be seen that the greater the value of n the earlier is the point reached when $\Delta f / r_m = \Delta_k / r_m$. This means that at first a very loose crystalline hydrate chain is formed at first, and as n diminishes and the radius r_i increases this gradually becomes more dense. This fact is also in good agreement with general ideas on the hardening process.

Finally, Equation (33) indicates that $\Delta f / r_m$ depends on y_0 / y_1, i.e., on the proportion of calcium sulfate dihydrate deposited from solution in the form of crystallization centers. The greater the value of y_0 / y_1 the greater the number of nuclei and the less (under the same conditions) is the distance $\Delta f / r_{m_0}$ (a fact which may be of great technological significance).

We now consider the process in which the hydrate particles approach each other. First, it must be pointed out that all the newly formed crystals are in Brownian movement. Therefore the distance Δf must be regarded only as an average, the most probable distance. Further, it must be taken into account that these particles have certain kinetic energy, sufficient to overcome the stabilizing effects of the solvate and adsorption layers. It is known that Brownian motion of the individual crystals and the action of convection currents lead to coagulational structure formation. If groups of several particles form first loose and then more compact aggregates, the individual elements of which are separated by thin water layers of approximate thickness $h = 10^{-7}$ cm, then compaction of the particles in the aggregates must inevitably lead to the distance between the aggregates being greater than the value found from Equation (33).

Formation of coagulational contacts also leads to other consequences. First, since $h \ll \Delta_k$, it is evident that sites of coagulational contacts become sites of crystalline contacts. Moreover, the velocity of Brownian motion of such aggregates, like the velocity of the larger crystals, is considerably less than the velocity of indi-

dividual nuclei of fine crystals. Therefore, as hydration proceeds, i.e., as the crystals grow and crystalline aggregates are formed, the stabilizing effects of the diffuse double layers of ions separating the aggregates [13, 14] become significant and these layers constitute an insuperable obstacle to the mutual approach of aggregates and crystals above a certain size. It follows that there is a definite limit to the approach of particles of a given size

Let us denote the minimum distance between the particles (aggregates) by $2\Delta_{min}$. If this distance is greater than the distance $2\Delta_k$ required for contact formation

$$\Delta_{min} > \Delta_k, \tag{34}$$

then the formation of new contacts is no longer possible. The instant when this occurs can be found from Equations (33) and (31), so that the duration of contact formation τ_k can be found:

$$\frac{\tau_k}{\tau_1} \leqslant \left[1 - \left(\frac{\Delta}{r_m}\right)_{min}\right]_\beta \frac{\ln (c_m/c_n)}{1 - c_m/c_n}. \tag{35}$$

Comparison of this formula with the experimental data obtained by E. E. Segalova under the guidance of P. A. Rebinder is of considerable interest.

A hardening suspension was ground and the subsequent strength increase was observed; in this way the point was determined at which the strong crystallizational structure is not restored after previous breakdown.

The fact that crystallizational structure formation does not occur in such cases indicates that contact formation has ceased. The time τ_k was determined for the α- and β-forms of calcium sulfate hemihydrate of various specific surfaces at W/S = 0.4.

TABLE 3

Duration of Contact Formation in α- and β-Calcium Sulfate Hemihydrates

	α-Hemihydrate				β-Hemihydrate			
s_0, cm²/g	3000	3900	8000	9700	5000	8000	11700	13700
τ_1, min	54	45	30	27	38	28	22	19
τ_k, min	22	20	14	12	11	8	8	6
τ_k/τ_1	0,41	0,44	0,42	0,44	0,29	0,29	0,36	0,32

The experimental data are summarized in Table 3. The table also contains values of τ_k/τ_1 (for the α-hemihydrate $\tau_k/\tau_1 \approx 0.43$, and for the β-hemihydrate $\tau_k/\tau_1 \approx 0.32$); these are fairly constant, which is consistent with Equation (35). In this case $c_{m\alpha} = 6.5$ g/liter; $c_{m\beta} = 8.6$ g/liter; $c_n = 2.04$g/liter; $\ln(c_{m\alpha}/c_n) = 1.18$; $\ln (c_{m\beta}/c_n) = 1.44$; therefore from Equation (35) we have

$$\left(\frac{\Delta}{r_m}\right)_{min,\,\alpha,\,\beta} = 1 - \left(\frac{\tau_k}{\tau_\alpha}\right)_{\alpha,\,\beta} \frac{1 - c_n/c_m}{\ln (c_{m,\,\alpha,\,\beta}/c_n)} \frac{1}{\beta} \tag{36}$$

and

$$\left(\frac{\Delta}{r_m}\right)_{min,\,\alpha} = 0{,}833; \quad \left(\frac{\Delta}{r_m}\right)_{min,\,\beta} = 0{,}887. \tag{36a}$$

Therefore it follows from the experimental data that $(\Delta/r_m)_{min} = 0.86 \pm 0.03$.

If Equation (35) is used for an approximate estimate of the influence of the solubility of the starting material on the duration of contact formation, the following expression is obtained:

$$\frac{\tau_{h\alpha}}{\tau_{h\beta}} = \frac{\tau_{1\alpha}}{\tau_{1\beta}} \frac{\ln (c_{m\alpha}/c_{m\beta})}{\ln (c_{m\beta}/c_n)} \frac{1 - c_n/c_{m\beta}}{1 - c_n/c_{m,\alpha}} \approx \frac{\Delta c_{0\beta}}{\Delta c_{0\alpha}} \frac{\ln (c_{m\alpha}/c_n)}{\ln (c_{m\beta}/c_n)} \frac{1 - c_n/c_{m\beta}}{1 - c_n/c_{m\alpha}} \tag{37}$$

or, with the corresponding numerical values

$$\frac{\tau_{h\alpha}}{\tau_{h\beta}} = \frac{0,27}{0,18} \cdot \frac{1,18}{1,44} \cdot \frac{0,763}{0,683} = 1,37.$$

We now compare this theoretical result with the actual data for $s_0 = 8000$ cm^2/g. The value found for α- and β-hemihydrate (Table 3) is $(\tau_{k\alpha}/\tau_{k\beta})_f = (0.43 \cdot 30)/(0.32 \cdot 28) = 1.44$, which is in very good agreement with the calculated values.

It is interesting to determine the approximate thickness of the minimum hydration films $2\Delta_{min}$ separating the individual crystals (or aggregates) at the end of contact formation. Since

$$r_{m,\alpha} = \frac{2M_y\sigma_y}{RT\gamma_y} \frac{1}{\ln (c_{m\alpha}/c_n)} \approx \frac{2,172 \cdot 300}{8,31 \cdot 10^7 \cdot 290 \cdot 2,3} \cdot \frac{0,434}{0,52} = 1,55 \cdot 10^{-6} \text{ cm},$$

$$r_{m,\beta} = \frac{2M_y\sigma_y}{RT\gamma_y} \frac{1}{\ln c_{m,\beta}/c_n} \approx \frac{2,172 \cdot 300}{8,31 \cdot 10^7 \cdot 290 \cdot 2,3} \cdot \frac{0,434}{0,624} = 1,29 \cdot 10^{-6} \text{ cm},$$

therefore

$$2\Delta_{min,\alpha} = 0,833 \cdot 1,55 \cdot 10^{-6} \cdot 2 = 2,58 \cdot 10^{-6} \text{ cm},$$

$$2\Delta_{min,\beta} = 0,887 \cdot 1,29 \cdot 10^{-6} \cdot 2 = 2,29 \cdot 10^{-6} \text{ cm},$$

or $2\Delta_{min,av} \approx 240$ A. This value is in good agreement with the general idea of the thickness of such diffuse double ionic layers.

In view of what was said earlier about the influence of the minimum thickness (Δ_{min}) of the hydration layers between microcrystal aggregates, it is appropriate to discuss briefly certain technological aspects.

Intense vibration of concretes not only results in denser packing of the microparticles present in the concretes. High-frequency vibration confers an additional external impulse to all the particles and this, of course, aids them in overcoming the disjoining pressure of the diffuse double layers. It must also be noted that in hard concrete mixes, where capillary forces begin to operate as soon as the concrete has been mixed, the individual aggregates are also brought closer together. In this case the approach is effected through the capillary forces, which counteract the disjoining pressure to a considerable extent. This suggests that intensive vibration, especially of hard concretes, leads to intensification and prolongation of contact formation; this is manifested by the high strength of such concretes.

We now consider Equation (33) again, in the light of what has been said about the minimum distance $2\Delta_{min}$ between the particles, and find from it the "looseness number" (n) with the condition that the distance $\Delta f/r_m = \Delta_{min}/r_m \approx 1$, we then have

$$\frac{1 + 3n}{(1 + n)^3} = \frac{6}{\pi} \left(\frac{y_0}{y_1}\right) \frac{M_y}{M_x} \frac{\Gamma}{\gamma_y} \left(\frac{1 + \frac{r_i}{r_m}}{\beta}\right)^3. \tag{38}$$

Substituting into Equation (38) the following values: $M_y = 172$; $M_x = 145$; $\gamma_y = 2.3$ g/cc, $\beta \approx 2$; $y_0/y_1 \approx 0.05$, and taking into account (Table 3) that when $\tau/\tau_1 \approx 0.35$, $r_i/r_m \approx 4.0$, we obtain

$$(1 + 3n)/(1 + n)^3 \approx 0,78\ \Gamma. \tag{38a}$$

It follows from Equation (38a) that, even when the amount of plaster $\Gamma = 1.30$ g/cc, at the end of the process of contact formation the packing density reaches its maximum, i.e., $n = 0$. With increase of Γ the looseness value $n = 0$ is reached before the end of contact formation. This indicates that if the proportion of plaster is high enough the process of contact formation and subsequent growth of the calcium sulfate dihydrate crystals is inevitably associated with expansion of the hardening plaster and development of tensile stresses in the crystalline framework. These stresses, the existence of which was first demonstrated in [2], account for the considerable strength loss of hardening plaster of Paris. It is also noted in the same publication that increase of the number of crystallization centers increases the absolute values of the tensile stresses in the crystalline hydrate framework. This is fully confirmed by Equation (38), as increase of y_0 / y_1 (weight fraction of the crystallization centers) leads to a decrease of the looseness number (n) at an earlier stage of hardening and thus increases tensile stresses in the framework.

SUMMARY

P. A. Rebinder's theory of cement hardening was used for derivation of equations which represent both qualitative and quantitative aspects of the kinetics of hydration and contact formation in monomineral cements of the calcium sulfate hemihydrate type. These include equations for the duration of hydration and contact formation (concretion). The theoretical relationships derived are in good agreement with experimental data.

The author takes this opportunity to express his deep gratitude to Academician P. A. Rebinder for several joint discussions of this work.

LITERATURE CITED

1. P. A. Rebinder and E. E. Segalova, Priroda, 12, 45 (1952).
2. P. A. Rebinder and E. E. Segalova, Proceedings of Conference on Cement Chemistry [in Russian] (Promstroiizdat, 1956) p. 125.
3. E. S. Solov'eva and E. E. Segalova, Proceedings of Conference on Cement Chemistry [in Russian] (Promstroiizdat, 1956).
4. Ezhi Stoklosa and Z. N. Markina, Kolloid. Zhur. 21, 708 (1959).*
5. E. E. Segalova, V. N. Izmailova, and P. A. Rebinder, Doklady Akad. Nauk SSSR 110,875 (1956).*
6. E. E. Segalova, V. N. Izmailova, and P. A. Rebinder, Doklady Akad. Nauk SSSR 114, 594 (1957).*
7. P. A. Rebinder, Syllabus of a General Course of Colloid Chemistry [in Russian] (Izd. MGU, 1949).
8. P. A. Rebinder, Izvest. Akad. Nauk SSSR, Otdel. Khim. Nauk 11 (1957).*
9. V. B. Ratinov, in collection: Hardening Mechanism of Cement and Plaster Materials [in Russian] (Gosizdat Lit-ry po Stroitel'nym Materialam, 1957).
10. W. Nernst, Z. Phys. Chem. 47, 52 (1904).
11. M. Volmer, Kinetik der Phasenbildung (Dresden und Leipzig, 1939).
12. J. W. Gibbs, The Equilibrium of Heterogeneous Substances, Scientific Papers, No. 1 (1905).
13. B. V. Deryagin, Zhur. Fiz. Khim. 5, Nos. 2-3 (1934).
14. B. V. Deryagin and M. Musakov, Izvest. Akad. Nauk SSSR, Otdel. Khim. Nauk (1936).

*Original Russian pagination. See C.B. translation.

FILTRATION OF RAREFIED AIR THROUGH POROUS BODIES IN THE TRANSITIONAL PRESSURE REGION

M. V. Talaev

Institute of Physical Chemistry, Academy of Sciences of the USSR, Moscow
Translated from Kolloidnyi Zhurnal, Vol. 22, No. 6, pp. 702-704,
November-December 1960
Original article submitted October 24, 1959

Deryagin's theory [1,2] of molecular flow of a rarefied gas through a porous body made it possible to establish the relationship between the resistance to flow and the specific surface of the porous body. This theory provided the basis of the method and apparatus which have been developed for estimation of specific surfaces.

Deryagin's method gives results for nonporous powders in good agreement with the results obtained by other modern methods for determination of the specific surfaces of porous bodies.

It is found in practice that experimental data are in good agreement with Deryagin's formula even under pressures such that the gas flow is known not to be of the molecular or Knudsen type. Therefore much scientific interest attaches to studies of the effect of pressure on the resistance to gas flow beyond the limits of the Knudsen flow regime. It is usually considered that molecular flow of a gas in a porous body gradually passes into viscous flow with increase of pressure, and accordingly the gas flow rate (in moles/$cm^2 \cdot$ sec) becomes a steady and, in the first approximation linear, increasing function of the pressure. The experiments of Knudsen [3], Gaede [4], and other workers have shown, for capillaries of various cross sections, that the gas flow rate as a function of pressure passes through a minimum corresponding to a transitional region where the mean free path of the molecules is of the same order of magnitude as the capillary size. However, no explanation has been given hitherto for the existence of this minimum on the gas flow rate curve. Deryagin and Bakanov [5] performed a theoretical investigation of the flow of gases through highly porous bodies in the transitional pressure range, where the theoretical treatment is simplified; they considered the diffusion of a gas through a model of a porous body, consisting of spheres at considerable distances apart and rigidly joined (for example, by means of thin and ideally elastic rods).

Deryagin and Bakanov [5] showed that in the flow of a rarefied gas through a highly porous body in the low-pressure range in addition to molecular (Knudsen) flow and laminar-viscous flow there is a third, pseudomolecular type of flow between the other two.

In view of the fact that in this type of flow there is as yet no velocity profile, mutual collisions of the gas molecules, although numerous, have only an indirect effect on the resistance to flow; they give rise to the convection component of gas motion by equalizing the impulses of the molecules during their collisions. This is the cause of the difference between resistance in pseudomolecular flow and in molecular flow. However, this difference does not influence the form of the equation representing the gas flow rate as a function of the pressure gradient, but merely has a slight effect on the value of the numerical coefficient, which is somewhat lower than in Knudsen flow. Therefore the rate of flow of a gas through a partition in the low-pressure region should decrease with increase of pressure. At high pressures the flow per unit cross section should be directly proportional to the pressure (viscous flow). It follows that the curve for the gas flow rate against concentration or gas pressure should pass through a minimum.

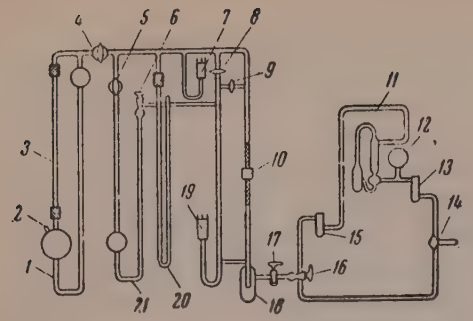


Fig. 1. Diagram of apparatus for studying the flow of gases through highly porous bodies. 1) Rheometer; 2) air inlet tube in rheometer; 3) capillary; 4 and 7) micrococks; 5,8,9) two-way cocks 6) rubber connection; 7 and 19) LT-2 tubes for manometers; 10) cell for specimens; 11) diffusion pump; 12) preliminary vacuum bulb; 13, 15, 18) traps; 14, 16) angle cocks; 20) vacuum meter; 21) differential manometer.

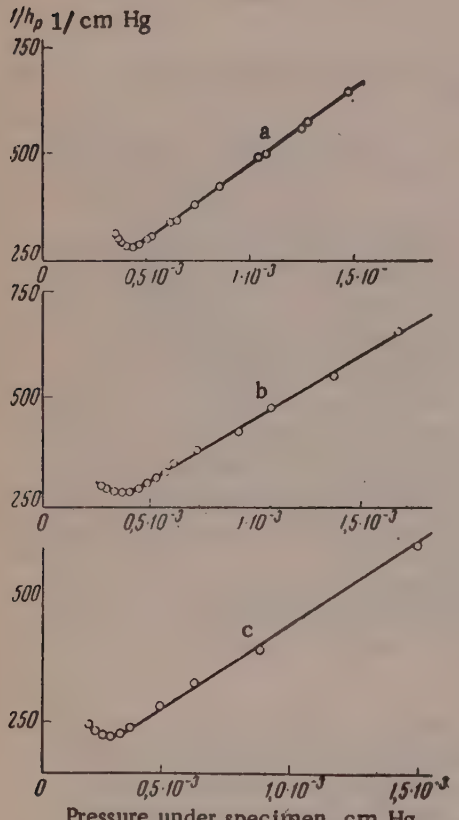


Fig. 2. Flow rate of air as a function of pressure in the pseudo-Knudsen region, in flow through cardboard, $\delta = 0.85$ (a) a glass filter (b), and cotton wool, $\delta = 0.8$ (c).

Although pure pseudomolecular flow cannot occur in cylindrical capillaries, there is no doubt that this theory indicates the physical nature of the minimum observed by Knudsen. For final confirmation of the theory it is necessary to show that this minimum exists in flow of gases through porous bodies with high porosity coefficients, i.e., in cases when the theory is applicable without any reservations.

The apparatus shown in Fig. 1 was designed for investigations of gas flow in highly porous bodies.

The porous body, previously dried, was placed in the cylindrical cell 10. The apparatus was then evacuated down to 10^{-2} mm Hg. The microcock 4 was opened and, with continuing evacuation, steady flow of air through the specimen was established. When the pressure in the system reached 10^{-2}mm the diffusion pump was switched on and the system was evacuated down to 10^{-4}mm with continuous steady flow of air. The air entered through the rheometer tube 2, passed through the capillary 3 and the microcock 4, and filtered through the specimen 10. The pressure difference between the two sides of the specimen was measured by means of two thermocouple manometers.

By variations of the pressure above and below the specimen it is possible to investigate the flow of air through porous bodies at various degrees of evacuation and to plot the corresponding air flow rate against the average pressure.

This method was used for studying the filtration of gases through such materials as pressed cotton wool, glass filters, cardboard, etc., with porosities of 0.8-0.9; it was found that the flow rate-pressure curves have minima at low pressures (10^{-3}–10^{-4} mm). The results are plotted in Fig. 2.

SUMMARY

1. An apparatus was designed for studying the flow of gases through highly porous bodies in the pseudomolecular region.

2. The experimental data on filtration of air through porous bodies show that the curve for the rate of flow of air through a porous partition as a function of the average pressure passes through a minimum, as in the flow of gases through capillaries. The minimum is more pronounced for bodies of higher porosity coefficients and disappears with decrease of the latter, in agreement with the Deryagin-Bakanov theory.

LITERATURE CITED

1. B. V. Deryagin, Doklady Akad.Nauk SSSR 53, 627 (1946).
2. B. V. Deryagin, et al., Determination of the Specific Surfaces of Powdered Substances by the Resistance to Flow of Rarefied Air [in Russian] (Izd. AN SSSR, 1957).
3. M. Knudsen, Ann. d. Physik 28, 75 (1909).
4. N. Gaede, Ann. d. Physik 41, 289 (1913).
5. B. V. Deryagin and S. P. Bakanov, Zhur. Tekh. Fiz. 27, 2056 (1957); Doklady Akad. Nauk SSSR 115, 267 (1957).*
6. S. P. Bakanov, Dissertation [in Russian] (Institute of Physical Chemistry, Izd. AN SSSR, 1957).

* Original Russian pagination. See C. B. translation.

ELECTROOPTICAL PROPERTIES OF LYOPHOBIC COLLOIDS

1. STATEMENT OF THE PROBLEM, BASIC METHODS, AND RESULTS *

N. A. Tolstoi, A. A. Spartakov, and G. I. Khil'ko

Department of Physics, Lensovet Leningrad Technological Institute
Translated from Kolloidnyi Zhurnal Vol. 22, No. 6, pp. 705-716,
November-December, 1960
Original article submitted December 14, 1959

Macroscopically all liquids are isotropic substances**. It is only when we turn to the problem of the molecular structure of liquids that we are convinced of the anisotropic character of the particles of which they are formed: In the great majority of cases the molecules do not possess spherical symmetry in their physical and chemical properties (geometrical, electrical, optical, structural, etc.). The macroscopic isotropy of liquids is a result of the disordered orientation of its anisotropic elements, i.e., the statistical averaging brought about by thermal motion which "smears" all the elementary anisotropic properties.

Since the microscopic molecular characteristics of matter are of primary interest, several methods of investigation have been developed, based on the following idea: the liquid is subjected to an external action which to some extent orders the orientation of the particles, as a result of which the liquid as a whole acquires an anisotropy. For example, if the external action is the application of an electric field and the anisotropy is in the index of refraction of the liquid, we have the electrooptical Kerr effect. If a magnetic field is applied, we have the magnetooptical Cotton-Mouton effect. If a laminar current is created in the liquid, we have the dynamooptical Maxwell effect.

The theories of these phenomena have been more or less worked out suitably for molecular ("pure") liquids. The chief problem of such theories is to associate an observed macroscopic quantity (the amount of birefringence) with the molecular constants of the substance. If from a quantitative point of view better agreement between theory and experiment is not desired, then the basic mechanism of the phenomena of orientation in external fields can be considered as completely explained. Quantitative discrepancy between theory and experiment is caused mainly by the difficulty in evaluating the molecular interactions. In those cases in which it was possible to carry out experiments in the gaseous phase (the work of Stewart and his school on the Kerr effect in gases) the agreement of theory and experiment seemed to be excellent.

For heterogeneous liquids - lyophobic colloids, which are the subject of this article - analogous theories have been proposed (e.g., [1]) which associate the properties of induced anisotropy of the colloidal solution as a whole with the physical and chemical properties of the individual colloidal particles and with the macroscopic properties (viscosity, dielectric strength, etc.) of the dispersion medium. Being based essentially on the same ideas as the theories of induced anisotropy in molecular liquids, the "colloid" theories have certain features which make them in some respects simpler and in others more complex than the "molecular" theories. We shall indicate a series of circumstances on which these features depend, wherein we shall keep in mind only

---

*Presented at the Fourth All-Union Conference on Colloid Chemistry in Tbilisi in 1958.

**With regard to volumetric properties. The role of the liquid surface is not considered here.

theories which refer to electrooptical phenomena or, in other words, to the phenomena of optical anisotropy caused by the application of an electric field to the liquid.

The Role of Brownian Motion. The appearance of optical anisotropy in the case of a colloidal solution in a field is determined by the orientation of the particles. Thermal motion (rotational Brownian motion) tends to destroy this orientation. In contrast with the case of molecular liquids, for which the energy of thermal motion is much larger than the energy acquired by the molecule in the electric field, in the case of colloidal liquids these energies can be comparable. Moreover, for sufficiently strong (but completely reasonable) fields and for not-too-small particles the energy of a particle in the field can considerably exceed its kT. This leads to two results: 1) the orientation of the particles can approach the state of saturation, i.e., can be "almost total" (we note that for molecular liquids, for example, for nitrobenzene, the limiting degree of orientation which can be obtained in electric fields at the limit of breakdown of the liquid amounts to about 1%); 2) in investigating the kinetics of orientation (i.e., studying the process of establishing the orientation in an alternating electric field) we are correct in considering the motion of a colloidal particle to a considerable degree to be mechanical, i.e., in using the equations of motion of a macroscopic body in a viscous medium. On the contrary, the motion of a molecule caused by an electric field in a molecular liquid is not described by such equations; this motion can be described as purely statistical. Below we shall indicate a convenient macroscopic criterion which makes it possible to relate the motion to mechanical, statistical, or intermediate types. We note in passing that for particles of colloidal dimensions we can at the same time neglect the effect of mechanical inertia because of the small moment of inertia of the particles: Physically this means that the motion will always take on a relaxational rather than an oscillational character; mathematically this means that the motion will be described by first-order differential equations.

The Role of Interactions. Considering a colloidal particle as a small, but macroscopic, body to which the properties of a continuum are attributed, we can treat the behavior of colloidal particles in a field as the behavior of independent bodies.* Here the effect of the medium is taken into consideration through macroscopic parameters (viscosity, dielectric strength, index of refraction, etc.). Thus, from this point of view "colloidal theories" have a "quasi-gaseous" character.

Quantitative Factors. No less an important feature of the phenomena of induced anisotropy in colloidal systems in comparison with molecular ones is the very magnitude of the anisotropic effect and also the length of the relaxation time. The fact that the magnitude of the anisotropy in a colloidal solution can, for a given field strength, be many orders of magnitude greater than the anisotropy of a molecular liquid explains the decrease in the disorienting role of Brownian motion in going over to large particles. From a practical standpoint this indicates the possibility of studying electrooptical phenomena in colloids in comparatively weak fields (10^1–10^3 v/cm). The sharp increase in the magnitude of the relaxation time of induced anisotropy is more important: In the case of the molecular Kerr effect reliable determinations of the relaxation time are at present lacking (it is clear only that these times are shorter than 10^{-9} sec), but in the case of colloids they fall in a region completely accessible to radio techniques (in the interval 1-10^{-5} sec).

We have indicated several facts known to be favorable to the "colloidal theories" in comparison to the "molecular" ones. We now turn to certain complicating factors.

Secondary Electrical Phenomena. Anisotropy of a molecular liquid is caused directly by orientation of the molecules by the field (deformation of the molecules almost always can be completely neglected), and the electric field, moreover, does not in principle cause any physical or chemical changes in the liquid.** In the case of a colloidal solution, generally speaking, there can arise various complications. Thus, for example, electrophoretic and electroosmotic motion can be additional factors in orientation which are found to be either in cooperation or in competition with the direct orientating action of the field [2]. The polarization of the electrodes which create the field in the liquid can introduce quantitative and temporary (for alternating fields) alterations of the field. Finally, the coagulating action of the current passing through the colloidal solution can cause irreversible changes in the system.

*For sufficient dilution of the colloidal solution. The problem of where the limit of this dilution is located has not yet been solved.

**Complications caused by the presence of a noticeable ionic conductivity of the liquid (which leads to disturbance of the homogeneity of the field of a plane condensor) can be removed by the use of a sufficiently high-frequency field. In any case, these complications are not significant in the case of a molecular liquid.

Optical Phenomena. The optical heterogeneity of a colloidal solution creates specific and occasionally very great difficulties for the interpretation of electrooptical phenomena. Actually, a molecular liquid is optically homogeneous because the average period of its structure is much less than the wavelength of light λ. Optical methods for homogeneous media are comparatively well-developed.

The other extreme, macroscopic (smooth) bodies with reference to which it is possible to speak of light of a "homogeneous" structure (λ is much less than the dimensions of the body), is encompassed by methods of light optics. The particles of sols and suspensions lie right around a limited region - their dimensions are comparable with λ. To this it should be added that electrooptical anisotropy can be observed in principle only for nonspherical ("anisodimensional") particles. In spite of a series of achievements in the optics of "small bodies" (the works of Rayleigh, Mie, Debye, Gans, Shuleikin, and Shifrin), we were unable to find definite data on the optical and, in particular, the polarization properties of nonspherical particles with dimensions of the order of λ.* From this it follows that we have not previously been able to answer the question of just what is the nature of an anisotropy induced in a colloidal solution by a field. The answer can only be given by experiment.

Polydispersion and Polymorphism. In the overwhelming majority of cases colloidal particles of a given solution have various dimensions (polydispersion). For nonspherical particles there are in addition variations of form (polymorphism).** It is possible in principle to obtain monodispersive spherical particles by means of repeated fractional centrifuging, but the separation of monomorphic particles is as yet an unsolved problem. Polydispersion and polymorphism should make quantitative comparison between theory and experiment extremely difficult. The difficulties arise from two directions: 1) Geometrical variations of the particles imply variations in the torques acting on them because of the field. The complication comes because these forces can be due to both volume and surface properties of the particle; for a variation in dimensions of a particle, even though the form is preserved, the relative role of volume and surface forces changes. 2) From facts known about the optical properties of spherical particles with diameters comparable with λ (theory of Mie and experiments with monodispersive sols) it follows that even the most insignificant variations (of the order of a percent) in the dimensions of particles often strongly affects the optical properties of these systems.

Thus, even if we were to lay out a complete theory of electrooptical anisotropy on one side and the necessary experimental data on the other, in order to compare theory and experiment we would have to carry out the extensive and detailed work of evaluating which conclusions of the theory are retained after the unavoidable averaging and "cleaning out" and which must be thrown out. Such evaluations must be made also with regard to experiment in order to understand which part of the experiment is associated with specific effects of polydispersion and polymorphism (we have in mind, for example, the possibility of creating in an actual colloidal solution certain preferential groups of dimensions and forms; this case introduces certain specific points which, it is understood, must be considered in the comparison of theory and experiment).

Now, we are convinced that the problem of electrooptical anisotropy in colloids is associated with a series of features which both favor investigation and complicate it. The "specific weight" of these features has not yet been evaluated. Only experiment is able to show which of the above circumstances (and under what conditions) can be thrown out in practice and which, on the other hand, must be included in the first plan. We hope that the experimental material which we expect to report in subsequent publications will permit these evaluations to be carried out.

---

*The theory of Rayleigh [3] refers to spherical particles with dimensions much less than λ. The theories of Love [4] and Mie [5] refer to spherical particles of arbitrary diameter (for large particles the calculations are very complex). Several authors have given approximate theories for large spherical particles (Stratton and Houghton [6], Blumer [7], Jobst [8], Shuleikin [9], and Shifrin [10]). For ellipsoids of arbitrary dimensions there are the formulas of Mäglich [11], which are so complex that for 28 years after their appearance there were no attempts to use them for calculations. The theory of Gans [12] refers to birefringence of ellipsoids which are very small in comparison with λ. The theory of Shifrin [10] refers to the scattering of light by similarly small ellipsoids.

**The methods described in the literature for directly obtaining strictly monodispersive sols are concerned only with isodimensional sols.

NEW METHODS OF INVESTIGATION

Let us ask two questions: 1. What sort of electric fields can be created with expedience in colloidal solutions? 2. What kind of optical anisotropy can be studied with expedience as a basic electrooptical phenomenon?

The answers to these two questions to a considerable degree predetermine the choice of the method of investigation as well as the apparatus required for its accomplishment.

The Electric Fields. In the investigation of very many physical phenomena it is customary to study first the simpler laws of stationary phenomena caused by the constant action of a disturbing force and then the more complex laws of relaxation phenomena caused by varying disturbances. In our case one troublesome circumstance obstructs this natural course: colloids possess an ample electrical conductivity, and with the application of a constant electric field the constant current which arises disrupts the colloidal system. Thus only alternating fields remain at our disposal, and therefore, it would seem, we are forced to begin with the study of nonstationary, very complex phenomena. This difficulty, however, is at a maximum only if, following the example of previous investigators, we produce the alternating field using a sinusoidal voltage, which is the most convenient from the standpoint of its practical production but very complex with regard to the mechanism of its effect on the colloidal system. If we give up sinusoidal voltages and manage to overcome certain technical difficulties, creating electric fields of a special form, then it is possible to economize substantially in the simplicity of the physical conditions of the experiment. We shall indicate three forms of electric fields which are favorable for the study of colloids.

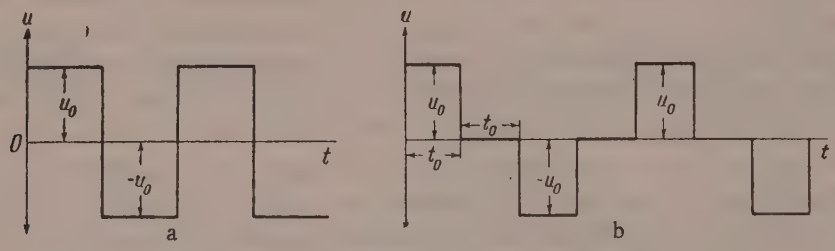


Fig. 1. Rectangular impulses of the first (a) and second (b) types.

1. Rectangular impulses of the first type (F_1) are depicted in Fig. 1a. The field of these impulses is constant in magnitude but changes sign. The transition time from voltage u_0 to voltage $-u_0$ can be practically instantaneous ($< 10^{-6}$ sec). It is obvious that for electrooptical phenomena which depend only on the magnitude and not on the direction of the field (we shall call these phenomena nonpolar) the field F_1 does not differ from a constant one. Moreover, the static component of this field is equal to zero.

2. Rectangular impulses of the second type (F_2) are depicted in Fig. 1b. The field of these impulses has a constant magnitude u_0 for a time t_0, then it is equal to zero for the same time interval, whereupon it has a constant magnitude but the opposite sign ($-u_0$) for a time t_0, etc. The field F_2 appears to be the most favorable for the investigation of relaxation phenomena. Actually, the establishment of an electrooptical phenomenon is accomplished under the influence of a constant factor, and the relaxation of the electrooptical phenomenon proceeds with the sudden disappearance of this influence. The field F_2 also has no static component.

3. A rotating field (R) is an electric field of constant magnitude whose direction continuously changes (remaining in one plane) with a constant angular velocity ω. The field R also has no static component; it can, as we shall see later, create a constant rotating disturbance in the colloid and lead to a uniform rotational motion of the colloidal particles, the character of which depends both on the electrical force (associated with the electrooptical properties of the particle) and on a frictional force connected with the geometrical properties of the particles and with the viscosity of the solution. Rotating fields (electric and magnetic) have been used previously in the study of liquid crystals [13] and colloids [14].

A detailed description of the methods involved with the fields F_1, F_2, and R will be given in subsequent publications.

Basic Electrooptical Experiment

In 1948 a new method was developed for the investigation of physical relaxation processes (the "taumeter" method [15]). This was used by the authors and then by other investigators for the study of luminescence, photoconductivity, gaseous discharge, and several other phenomena. It seemed that it would be of interest to utilize certain procedures from this method in order to shed some light on the nature of electrooptical phenomena in colloids. To this end we carried out some experiments [16] which led to rather unexpected results.

The basic setup of the experiment is shown in Fig. 2. A beam of light from the source S is polarized by the polarizer P and proceeds through a cell with parallel plates K which is filled with the colloidal solution. Next the light passes through the analyzer A and falls on a photoelement, the signal from which is displayed on the screen of a cathode-ray oscilloscope KO.* The recording part of the apparatus makes note only of changes in the amount of light passing through the solution.

If the polaroids P and A are crossed and their optic axes O_P and O_A (Fig. 2) make 45° angles with the direction of the electric field in K, then the setup is designed to record birefringence, which is observed experimentally in that light passes through the crossed polaroids. This form of optical anisotropy, as is well-known, means that the light vibrations polarized along the field are propagated with a different velocity from vibrations transverse to the field. In the overwhelming majority of experiments described in the literature concerning electrooptical phenomena in colloids it is just birefringence that has been measured, i.e., two polaroids P and A have been used. If, besides birefringence, the colloidal solution in a field also exhibits dichroism (i.e., vibrations polarized along the field are absorbed or attenuated differently from vibrations polarized perpendicular to the field), the direct measurement of birefringence may be strongly altered because dichroism also is characterized experimentally by the fact that light will pass through the crossed polaroids P and A even in the absence of any birefringence. This circumstance has unfortunately not been considered in many works, and the experimental results presented in them are, therefore, devoid of significance (e.g., [2]).

The experiments that we have carried out lead to a directly contradictory conclusion: the basic, most strongly expressed form of electrooptical anisotropy in all colloidal solutions we investigated is dichroism.

This is shown by the fact that changes in the luminous flux incident on the photoelement are most effectively recorded with the second polaroid removed. It is obvious that in this case any birefringence cannot effect a change in luminous flux. Therefore, an observable change in flux caused by a change in the electric field in an experiment with one polaroid is associated exclusively with dichroism.

Since from general considerations of symmetry the principle axis of electrooptical anisotropy must be parallel to the field, the recording of dichroism should be most effective when the axis of the polarizer P is oriented parallel or perpendicular to the field (and not at an angle of 45° to the field). Experiment accurately confirms this.

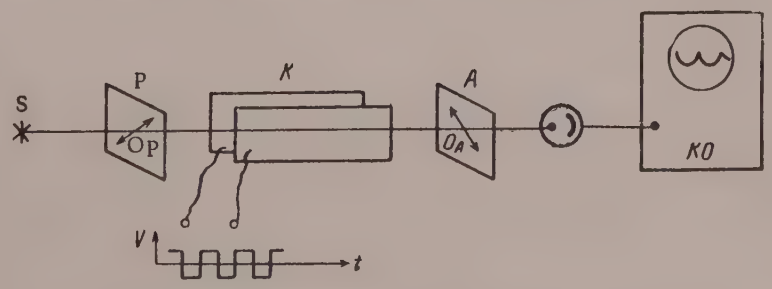


Fig. 2. Diagram of apparatus for the investigation of electrooptical properties of colloids in rectangular pulsed electric fields.

Thus, we now can answer the question asked at the beginning of the second section of this article: As a basic electrooptical phenomenon in colloids it is most expedient to study the anisotropic absorption of light, i.e., dichroism.

* The details of the method developed below will be reported in subsequent publications.

Birefringence, which has been studied by a majority of investigators, is, in general, a weak secondary effect.* That this essentially deciding circumstance escaped the attention of previous investigators is connected, apparently, with the fact that the majority of the early work in electrooptics was done visually. The setup with one polaroid in this case is not used since changes of luminous flux proceed "on a background" of strong unchanging light which blinds the eyes. In the case using the objective method (photoelement) the signal is easily separated from the "background" light by simple procedures.

Let us turn to a description of further results of the basic experiment. When the field F_1 is applied to the condensor K (Fig. 1a) the average value of the luminous flux changes, i.e., the solution becomes less transparent or more transparent, and a modulation of the light with a period equal to half the period of the field F_1 is observed. Both these effects, stationary and modulated, almost always depend essentially on the orientation of the polaroid P, i.e., on whether the light is polarized along or across the field.

The light modulation curves for comparatively high (a) and comparatively low (b) field frequencies are given in Fig. 3.

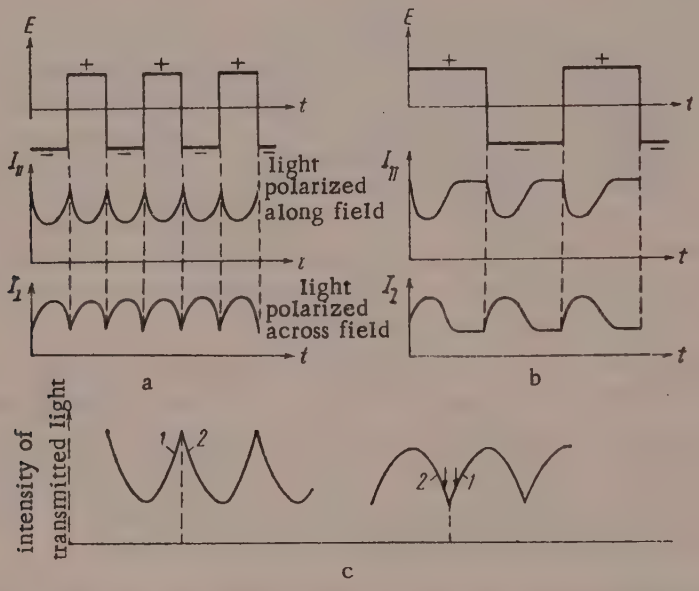


Fig. 3. Light modulation curves in an impulse field F_1. a) Field of comparatively high frequency; b) field of comparatively low frequency; c) time plot of increase (1) and decrease (2) of transparency of a colloidal solution at the instant the field changes sign (3).

As is seen from Fig. 3, at the moment at which the field changes sign the light modulation curve not only undergoes a sharp break but the very process of increasing transparency (or opacity) of the solution is quickly replaced by a process of decreasing transparency (or opacity) (Fig. 3c). If the modulation curve in any way reflects the change in orientation of colloidal particles, then we must conclude that after each change in sign of the field the orientation changes its direction (Fig. 3a). In other words, if a given colloidal particle is rotated under the action of the field in some direction, then after an instantaneous change in sign of the field it reverses the direction of its rotation. The most important conclusion [16, 17] about the electrical structure of colloidal particles follows directly from this: Colloidal particles in water possess a rigid (permanent) dipole moment of

* The statement in any case is correct for lyophobic colloids with not-too-small particles, e.g., for such as colloidal graphite, benzopurpurin, bentonite, and many others. The external feature of colloids of this class is visibility of the Tyndall cone. It may be more proper to consider them as suspensions and not as sols. The question of the relationship of dichroism and birefringence for "amicron" we still leave open.

considerable magnitude. Actually, let us take a nonspherical colloidal particle (in the case of spherical isotropic particles we would not in principle be able to observe any induced anisotropy):

1. The torque experienced by a nonspherical particle in an electric field depends on its form and dimensions and on the difference in the dielectric constants of the particle (ϵ_p) and the medium (ϵ_m).

A particle will always * tend to place its longest axis along the line of the field. The torque is proportional to the square of the field intensity E^2, and consequently the direction of the torque will not change when the field changes sign.

2. The torque may be dependent on the anisotropy of the electric polarizability of the colloidal particle (e.g., if it is an electrically anisotropic crystalline particle). In this case the torque is also $\sim E^2$ and does not change sign when the field changes sign. The particle tends to place its axis of greatest polarizability parallel to the field.

3. The torque may also be caused by an anisotropic polarizability of an electric double layer surrounding the particle. All the above statements refer also to this case.

In all three cases the particle assumes an induced dipole moment in the electric field. When the field changes sign this induced ("soft") dipole also changes sign (practically without inertia), and therefore the direction of the mechanical torque remains unchanged. **

Thus in the electric field F_1 all factors of nonpolar orientation can cause only stationary orientation and cannot be responsible for the modulation of light, which is associated with a change of orientation. Consequently, the only factor that brings about a reorientation of a particle when the field changes sign can be the rigid dipole moment of a colloidal particle. In this case the sign of the torque changes together with the sign of the field. The orientation caused by a rigid dipole we shall designate as polar.

Now, we see that the very fact of light modulation by a colloidal solution in a field F_1 serves as a well-defined, direct indication that the particles have a rigid dipole. From this the great advantage of using fields of special form instead of the usual sinusoidal fields is understandable. Light modulation by a sinusoidal field would show nothing since it could be ascribed to thermal disorientation of particles during periods of weak field.

Let us turn to a qualitative explanation of the form of the modulation curves in the field F_1 starting with the existence of a rigid dipole which we have proved.

Let the colloidal particle be an isotropic, elongated body of revolution. We shall assume for definiteness that the long axis of the particle coincides with the axis of greatest light absorption. In other words, light polarized parallel to the long axis is absorbed (or scattered to the side) the most, that polarized parallel to the short axis, the least, and that polarized at any angle to the long axis, to an intermediate degree. Let us consider two cases:

1. Rigid Dipole Moment Perpendicular to the Long Axis of the Particle. Under the action of the field the particle tends, because of nonpolar orientation, to set its long axis parallel to the field and, because of polar orientation, to turn such that the rigid dipole (as a vector) would be parallel to the field, i.e., such that its long axis would be perpendicular to the field. As a result of a compromise between polar and nonpolar orientations the equilibrium position of the particle will be one in which the direction of the long axis of the particle makes some angle α_0 with the direction of the field. When the field changes sign the torque associated with the rigid dipole changes sign, and the particle begins to assume a new position of equilibrium corresponding to an angle α_0 between the long axis of the particle and the field (Fig. 4).

This rotation of a particle can be performed in any plane parallel to the field. Thus, considering simultaneously the whole collection of particles in a given solution, we see that in positions of equilibrium their axes form a cone with apex angle $2\alpha_0$ and with axis parallel to the field (Fig. 5a). When the field changes sign

---

*Except for a dependence on the sign of the difference $\epsilon_p - \epsilon_m$.

**The considerations presented above preserve their strength under the joint existence of all considered causes of nonpolar orientation.

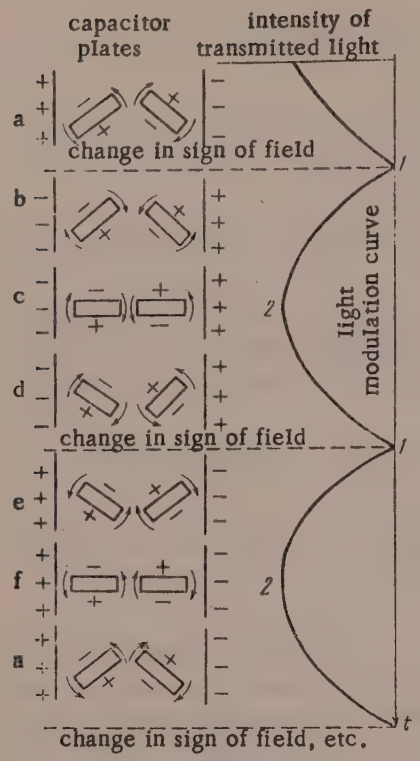


Fig. 4. Diagram of the rotational motion of a colloidal particle with a transverse rigid dipole in a field F_1. a-f) Consecutive instants of time. 1) Change of torque, break in modulation curve; 2) best orientation, maximum or minimum of modulation curve.

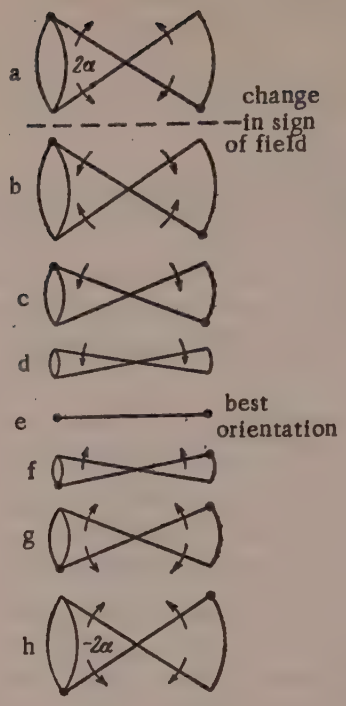


Fig. 5. Schematic representation of the spatial distribution of particle axes at different instants of time. a-h) Successive instants of time.

(Fig. 5b) the apex angle of the cone begins to decrease (Fig. 5c, d), reaches zero (Fig. 5e) (at this instant the axes of all particles are parallel to one another and to the electric field), and then increases again to the value $-2\alpha_0$ (Fig. 5f, g, h). During the time of this process the axis of each particle goes over from some genatrix of the original cone to a diametrically opposite genatrix of the final cone (heavy dots in Fig. 5a-h). If the period of the field F_1 is sufficiently long, then during the time of action of a field with a single sign an equilibrium orientation will be achieved which corresponds to a cone with maximum apex angle $2\alpha_0$ or $-2\alpha_0$. If the period of the field is sufficiently short, the equilibrium orientation will not be achieved, and the cone will not open out completely; its maximum angle will be $2\alpha < 2\alpha_0$.

The explanation presented above clears up the seemingly paradoxical fact that the maximum and minimum transparency of the colloidal solution is attained at some intermediate instant during the application of a field of a given sign (for a field of sufficiently high frequency this instant occurs at the middle of this interval). Actually, the maximum and minimum transparency ought to correspond to the most complete orientation of the particles. According to our explanation, the most complete orientation can be achieved not in equilibrium but in the momentary, transitional condition corresponding to the passage of the cone angle 2α through zero.

2. Rigid Dipole Moment Parallel to the Long Axis of the Particle. Under the action of the field the particle tends, because of nonpolar orientation, to set its long axis parallel to the field. From the two possible positions "along the field" the particle chooses that which corresponds to an energetically favorable orientation of the rigid dipole. Let us consider the motion of particles in the special case in which the period of the field F_1 is rather large. Then toward the end of each half-period of the field the particles will arrive in an equilibrium state (Fig. 6a). After the field changes sign they find themselves in a state of unstable equilibrium * (Fig. 6b)

* The initial impulse knocking particles out of unstable equilibrium is associated with rotational Brownian motion of the particles.

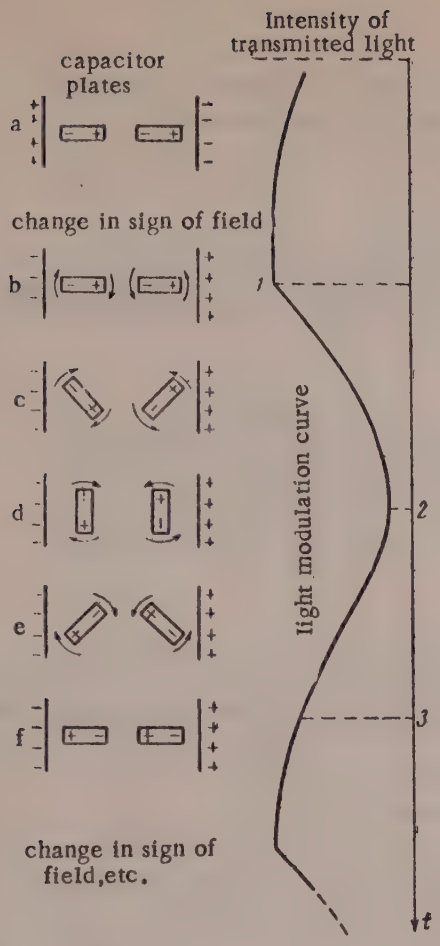


Fig. 6. Diagram of rotational motion of colloidal particles with longitudinal rigid dipoles in a field F_1 of rather low frequency. a-f) Successive instants of time. 1) Start of rotation, break in modulation curve; 2) maximum or minimum of modulation curve, corresponding to relatively best orientation; all particles lie in a plane perpendicular to the field.

and will proceed to a new equilibrium state (Fig. 6c, d, e, f). At some intermediate instant (Fig. 6d) the orientation of the particles will be relatively the best; they will all lie in a plane perpendicular to the field. Thus, the motion of these particles with a "longitudinal" rigid dipole will lead to a phenomenon of light modulation more or less analogous to that which took place with the motion picked above for particles with a "transverse" rigid dipole.

The picture of the motion of particles with a "longitudinal" rigid dipole in the case of a field F_1 with a short period (where equilibrium is not attained toward the end of a half-period) is somewhat more complex.

A more complete discussion of the problem of particle motion in F_1-fields will be given in subsequent publications. Here we have limited ourselves to qualitative illustrations.

Fundamental Problems of the Electrooptics of Colloids

In connection with the above results of the basic electrooptical experiment and their projected interpretation, certain fundamental problems in the further development of the electrooptics of colloids may be pointed out.

1. The Mechanics of Particle Motion in Fields F_1, F_2, and R. Here we refer to the questions of stable forms of motion of the particles, of the role of Brownian motion, and of the connection, between the geometrical and electrical properties of particles and the forms of their motion.

2. The Optics of Colloidal Particles. Here we refer to the questions of scattering and absorption of polarized light by nonspherical particles with dimensions small compared to λ, and, in particular, to the question of the dependence of scattering on particle orientation.

3. The Physical Chemistry of Colloidal Particles. Here we refer to the questions of the role of the medium in the formation of a particle's rigid dipole, of the connection between the rigid dipole and an electric double layer, of the effect of chemical affinity of the particle in the general electrooptical picture, and of the interaction between particles.

As is evident from the above, many aspects of these problems are directly connected, if not simply coincident, with the general interests of colloidal chemistry or physics. Therefore, progress toward the solution of these problems promises to shed light on several questions which arise in colloidal science and in someof its subdivisions. In particular, it seems to us that electrooptics can give important hints about the nature and scale of interactions between colloidal particles in dilute solutions. It is not difficult to see that the field created by the rigid dipoles of colloidal particles can play an important role in the general picture of equilibrium in a colloidal solution as a heterogeneous system.

This article is in certain measure introductory to a series of prospective publications concerned with electrooptical phenomena in colloids. The general direction of our work consists of an attempt to develop the electrooptics of colloids as a branch of colloid physics.

SUMMARY

1. The problem of electrooptical anisotropy in hydrophobic suspensions (in comparison with molecular liquids) is associated with a series of features which favor investigation as well as complicate it.

2. The investigation of electrooptical effects is expediently carried out in rectangular pulsed electric fields or in rotating electric fields.

3. The basic electrooptical effect in hydrophobic suspensions is dichroism, and not birefringence.

4. Modulation of light by rectangular electrical impulses of the first type gives direct proof that colloidal particles in water possessa rigid dipole moment.

LITERATURE CITED

1. Peterlin and Stuart, Z. Phys. 112, 129 (1939); Hand-und Jahrbuch der chem. Physik 8, Abschn. 1 B (1943).
2. W. Heller, Rev. Mod. Phys. 14, 390 (1942).
3. Lord Rayleigh, Phil. Mag. 41, 107, 274, 447 (1871); 44, 28 (1897); 47, 375 (1899).
4. A. E. H. Love, Proc. Lond. Math. Soc. 30, 308, (1899).
5. G. Mie, Ann. Phys. 25, 377 (1908).
6. J. Stratton and H. G. Houghton, Phys. Rev. 38, 159 (1931).
7. H. Blumer, Z. Phys. 32, 115 (1925), 38, 304, 920, (1926).
8. G. Jobst, Ann. der Phys. 76, 863 (1925), 78, 157 (1925).
9. V. V. Shuleikin, Physics of the Sea [in Russian] (Izd. An SSSR, 1953).
10. K. S. Shifrin, Scattering of Light in a Turbid Medium [in Russian] (Gostoptekhizdat, Moscow-Leningrad, 1951).
11. F. Măglich, Ann. der Phys. 83, 609 (1927).
12. R. Gans, Ann. der Phys. 37, 881 (1912), 47, 270 (1915); 62, 331 (1920).
13. V. I. Tsvetkov, Acta Phys. Chim. USSR 10, 555 (1939), 11, 537 (1939).
14. V. I. Tsvetkov and M. Sosinskii, Kolloid. Zhur. 11, 197 (1949).
15. N. A. Tolstoi and P. P. Feofilov, Uspekhi Fiz. Nauk 41, 44 (1950).
16. N. A. Tolstoi and P. P. Feofilov, Doklady Akad. Nauk SSSR 66, 617 (1949).
17. N. A. Tolstoi, Doklady Akad. Nauk SSSR 110, 893 (1955).

THE RESIDUAL BOTTOM LAYER IN MOTION OF A VISCOPLASTIC MEDIUM

S. M. Fleishman

All-Union Scientific Research Institute of Transport Construction, Moscow
Translated from Kolloidnyi Zhurnal, Vol. 22, No. 6, pp. 717-719,
November-December, 1960
Original article submitted November 21, 1958

The laws of flow of multiphase coagulative viscoplastic systems with liquid dispersion media differ from the laws of liquid flow. In particular, the former are characterized by an initial resistance to shear, not exhibited by ordinary liquids. The rheological and physicochemical properties of such systems have been studied in detail by Volarovich, Rebinder, and others [1]. One characteristic of the flow of a viscoplastic medium, the consequence of the initial resistance to shear, is the layer which remains in the bed after the flow has ceased.

We consider the question of this layer for the case of the motion of flood streams [2] which arise in mountain basins as the result of saturation with rain (or thaw) waters and carry down with them into the beds soil masses containing numerous colloidal clay particles. In flowing down from the slopes into the beds and moving further down in definite bedded streams, such flows move to their full depth only in the transit zones, where the bed slopes are fairly steep. When they emerge onto the plain zones, with low gradients and with a considerable decrease of the flow rate, the lower layers cease to move and are deposited, covering roads, inhabited places, and cultivated land.

By the Bernoulli energy equation, the specific energy of flow is greater in the upper than in the lower cross section ($e_1 > e_2$), as a part of the energy is expended to overcome resistance along the length L of the stream.

Denoting the resistance of structural bonds in the flood stream by C_s, we can write

$$e_1 = e_2 + C_s. \tag{1}$$

For viscoplastic flow, as for any fluid flow, the basic equation is the continuity equation, which is represented as follows for steady motion:

$$Q = FV = \text{const}.$$

If the resistance to flow C_s for a certain minimum mass m_0 exceeds the shear stress due to the level difference between z_1 and z_2 (i.e., the value of τ), then a layer of depth h_0 in the stream, corresponding to m_0, remains in the bed and is not carried along with the layers above it. It is evident that

$$m_0 h_0 = f[C_s(z_1 - z_2)].$$

Since $(z_1 - z_2)/L = i$, and C_s is determined by the viscosity of the stream and the roughness of the bed, it follows that

$$C_s = f(\eta, n, \gamma);\ \tau = f(i, H);\ h_0 = f(\eta, n, i),$$

where η is the viscosity of the stream; H is the full depth of the stream (or R, the hydraulic radius for a plane stream); n is the roughness of the bed, and i is the slope of the bed floor.

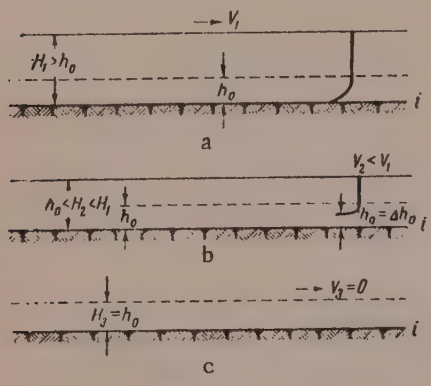


Fig. 1.

It is clear from the diagram that in the motion of a stream of depth $H_1 > h_0$ the layer h_0 is involved in the motion by transfer of motion from the higher layers (a). As the stream depth is decreased from H_1 to H_2 (and therefore, when $V_2 < V_1$) the quantity of motion is no longer sufficient to impart motion to the whole layer h_0, and its lower portion Δh_0 is not involved in the motion (b); finally, when the depth is decreased to $H_{cr} = h_0$ the motion stops (c) because a state is reached when the resistance C is greater than the shear stress τ.

To ensure the motion of the layer h_0 in the continuous stream as a whole the following condition must be satisfied:

$$(z_1 - z_2)/L > i_0 \quad \text{or} \quad i > i_0, \tag{2}$$

where i_0 is the slope corresponding to $C_s = \tau_0$, or the slope of the static shear stress τ.

Variations of h_0 with η and i for a Laboratory Specimen of Soil Mass of the Flood Water Type

Slope of bed, i	Effective flow viscosity, poises			
	3	7	12	20
	Depth of layer h_0, cm			
0.01	18	30	50	90
0.02	10	20	30	60
0.03	8	15	20	35
0.04	7	12	16	25
0.05	6	10	13	20
0.08	3	6	7	14
0.10	1	4	5	10

Roughness of the bed can be disregarded in practice in this instance, because the viscoplastic stream forms a lubricating layer which covers the projections (in relatively smooth bed surfaces). Evidently $i_0 = f(\eta)$, i.e., for a stream of a given structure i_0 and h_0 are constant. Therefore, if a bed carries a stream of depth H, the stream will move if $H > h_0$.

Experiments for verification of the above consideration, performed in a special pan of variable slope, showed that the depth h_0 of the residual layer is a direct function of the effective viscosity η and varies inversely with the slope of the bed floor (Table 1). These experiments also confirmed that h_0 depends on i and η only, and is independent of the flow velocity V, the density γ of the stream, and the total depth H of the stream.

SUMMARY

1. When a viscoplastic medium moves, without application of external pressure, along a bed (pan, tube) of slope $i < i_0$ a residual layer h_0 is deposited on the floor of the bed; the depth of this layer depends on the slope i of the bed and on the effective viscosity η of the moving medium.

2. Quantitative values of the function $h_0 = f(i, \eta)$ were determined.

3. The physical principle of the effect and the experimental relationships which were obtained are applicable to any hydrophilic viscoplastic system: clay suspensions, cement paste, liquid concrete, etc.

LITERATURE CITED

1. M. P. Volarovich, Kolloid. Zhur. 16, 2, 27 (1954);* M. P. Volarovich and A. M. Gutkin, Kolloid. Zhur. 15, 155 (1953);* N. V. Mikhailov and P. A. Rebinder, Kolloid. Zhur. 17, 107 (1955);* N. N. Kulakov and and K. I. Samarina, Kolloid. Zhur. 6, 497 (1940).
2. S. M. Fleishman, Doklady Akad. Nauk, 114, 281 (1957).*

*Original Russian pagination. See C. B. translation.

INVESTIGATION OF BOUNDARY FRICTION AND ADHESION IN RELATION TO STUDIES OF THE INTERACTION OF FINELY DISPERSED PARTICLES

COMMUNICATION 3. INFLUENCE OF NEUTRAL ELECTROLYTES ON THE FRICTION OF QUARTZ, RUBY, AND AGATE AT HIGH CONTACT PRESSURES

G. I. Fuks and A. S. Mikhailyuk

Scientific Research Institute of the Watch Industry
Translated from Kolloidnyi Zhurnal, Vol. 22, No. 6, pp. 720-729,
November - December, 1960
Original article submitted November 4, 1959

In the previous investigation [1] a scale-model method [2,3] was used to show that at contact pressures less than 8-10 kg/cm^2 electrolytes prevent cohesion of solid particles in water owing to electrostatic repulsion of the diffuse layers of hydrated ions. The force of repulsion and certain laws determining it are functions of the distance between the particle surfaces or, accordingly, of their contact pressure. Below 1-2 kg/cm^2 remote hydration of the ions and therefore the ionic radius is of predominant importance; at contact pressures above ~2 kg/cm^2 electrostatic pressure of the diffuse layers is almost the only factor and the effect is determined mainly by the valence and concentration of the ions.

In many cases the contact pressures between particles in real disperse systems do not exceed 10 kg/cm^2, but in highly disperse systems higher contact pressures may develop because of the low radii of curvature of the particles. Calculations, based on the assumption that the ordinary methods for solving contact problems in the theory of elasticity are applicable to microscopic particles, show that the axial gravitational pressure of a spherical quartz particle 10 μ in diameter on a similar particle lying on the bottom of a vessel containing water is 93 kg/cm^2. The gravitational pressure calculated in this way decreases with decreasing particle size (it is ~20 kg/cm^2 for quartz particles 0.1 μ in diameter). When the particle becomes small enough, this pressure is eliminated completely or partially by the energy of Brownian movement. However, the specific contact pressures of particles, including those of small size, can be greatly increased by crystallization pressure, the addition and concentration of the gravitational forces due to many particles, forces of mutual attraction, and their pronounced anisotropy of shape.

This raised the question of the effects of electrolytes on coagulative interaction of particles under high contact pressures. In the present investigation this question was solved by means of model experiments in which particle bonding was simulated by friction of macroscopic solid bodies of simple shape and, as far as possible, of definite chemical composition (for the general principle of the method, see [2,3]).

The experiments were performed with mineral specimens in the shape of small cylinders terminating, at the working ends, in hemispheres with radii of curvature of 1.5 and 2.5 mm. The spherical surfaces were polished to class 13-14 finish (GOST 2789-51). Before the experiments the specimens were washed with redistilled solvents, repeatedly rubbed over with activated charcoal, and then washed with the solution used for the experiments.

The crystalline quartz used contained >99.8% SiO_2; the synthetic ruby consisted of Al_2O_3 colored by 1.5% Cr_2O_3 and 0.004% TiO_2; the agate was an amorphous variety of quartz with an admixture of the oxides of iron and certain other metals.

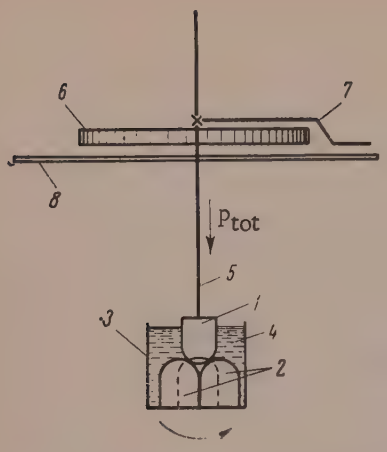


Fig. 1. Diagram of four-ball tribometer.

Static and kinetic friction was measured by means of the four-ball tribometer [4], modified by one of us; a line diagram of the instrument is given in Fig. 1. The upper specimen 1 rests on the three lower specimens 2 under variable pressure P_{tot}. When the vessel 3 with solution 4 is rotated, the frictional forces exert a drag on the specimen 1. The elastic suspension 5 and the calibrated spring 6 exert a reaction to the frictional force, and the latter is indicated by the pointer 7 on the circular scale 8 or by means of an optical lever. Kinetic friction was measured with the lower vessel rotated at 60 rpm (which corresponds to a linear velocity of 0.54 cm/sec); static friction was measured at 0.25 rpm. Displacement of specimen 1 in relation to specimens 2 in measurements of static friction is found from the difference between the angles of rotation of the vessel 3 and the suspension 5. In determinations of kinetic friction round imprints remained on the contact surfaces of the specimens 2; the diameters of these imprints were taken as the measure of wear.

The measurement errors did not exceed ± 0.002 for the coefficient of friction, and 1 μ for the diameter of the imprint (wear trace).

The contact area, needed for determination of the specific pressure, was claculated on the basis of the original Hertz equation [5] from the formula

$$z_s = 0{,}88\sqrt[3]{PR/E},$$

where z_s is the radius of the contact area; P is the pressure applied to the area of contact between two specimens; R is the radius of curvature of the specimens; E is the elasticity modulus of the mineral used. The data presented below refer to the pressure range between 50 and 550 kg/mm^2.

The microhardness of the specimens was determined by the method of Khrushchov and Berkovich [6] with the aid of their PMT-3 instrument; microbrittleness was estimated by Ikornikov's method [7], based on the use of the same instrument.

TABLE 1

Coefficients of Static Friction of Minerals in the Dry State, in Water, and in Electrolyte Solutions (1 meq/liter) under Contact Pressures between 100 and 400 kg/mm^2. Up to 10 Minutes of Contact with Water and Solutions.

Minerals		Dry							
name	microhardness, kg/mm^2	friction	H_2O*	LiCl	NaCl	KBr	$SrCl_2$	$AlCl_3$	$Th(NO_3)_4$
Ruby	2070	0,20	0,19	0,11	0,11	0,09	0,11	0,16	0,14
Quartz	1160	0,62	0,61	0,44	0,48	0,54	0,53	0,50	0,46
Agate	1030	0,64	0,61	0,52	0,60	—	—	0,49	0,42

* Here and subsequently, water redistilled in platinum vessels.

Static Friction.* Under high contact pressures the coefficients of static friction of the minerals in water and in aqueous electrolyte solutions, and therefore the bonding forces between the surfaces of these minerals, depend on their microhardness and are correlated with their coefficients of dry friction** (Table 1); in other words, the bonding force is primarily determined by the properties of the contacting solids. This is the essential

*E. I. Piskunova and L. S. Lupina took part in the experimental work.

** The connection between the coefficients of dry friction and microhardness of minerals is discussed in another paper [8].

difference between particle interaction in the range of contact pressures under consideration and the analogous effect at low and moderate pressures, when properties of the boundary layers at the solid-liquid interface have the predominant influence [1,2].

Nevertheless neutral electrolytes influence the static friction of minerals even at pressures of hundreds of kilograms per square millimeter (Table 1), which are only a little less than the microhardness values of these minerals as determined by the indentation method. The coefficient of friction may vary, in accordance with the solution composition, between 60 and 20% of its value in water; this is a considerable variation for this property.

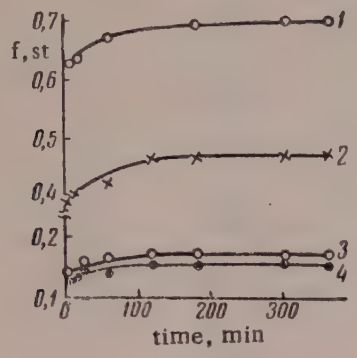


Fig. 2. Effect of the interaction time of liquids and minerals on static friction: 1) Quartz in water (P_{tot} = 700 g); 2) quartz in 0.005 N $Th(NO_3)_4$ (P_{tot} = = 700 g); 3) ruby in 0.005 N $K_4Fe(CN)_6$ (P_{tot}=2100g); 4) ruby in water (P_{tot}= 2100 g).

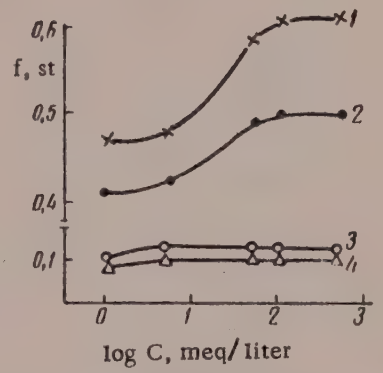


Fig. 3. Effect of solution concentration on the coefficients of static friction of minerals: 1) Quartz in KCl; 2) quartz in LiCl; 3) ruby in KCl; 4) ruby in LiCl.

The action of water and aqueous salt solutions depends on the time of exposure of the minerals in them, but after 1-2 hours the magnitude of the effect becomes stabilized (Fig. 2). The coefficients of friction (static and kinetic) given subsequently in this paper are the constant or nearly constant values obtained after exposure of the minerals to the solutions for an hour or more. Very dilute solutions reduce the static friction of minerals below the values for dry friction or friction in water. As the solution concentration is increased the coefficient of friction rises to a value equal to or higher than that in water (Fig. 3). Quartz, which is more brittle than ruby [8], is also more sensitive to the solution concentration and, as will be shown below, to the nature of the ions.

The relationship between the coefficient of static friction and the ionic charges of solutions of equal concentrations proved to be specific for the region of high contact pressures. If the laws of surface interaction at moderate contact pressures [1] were applicable, it would be expected that increase of the anion valence would lead to a decrease in the protective action of the boundary layer (because the diffuse layer is compressed) at the surface of positively charged aluminum oxide (before charge reversal) and the friction of ruby should increase accordingly; on the same grounds it is to be expected that increase of the cationic charge in solution should increase the friction of negatively charged silica. In reality (Table 2) as the cationic charge increases the friction of ruby increases slightly and the friction of quartz diminishes appreciably, while as the anionic charge increases the friction of ruby remains unchanged (within the precision limits of the method) while that of quartz increases.

The static friction of the minerals in solutions of neutral salts depends not only on the ionic charge but also on the cation radii and in some instances on the specific action of the ions. For example, in the series of 0.001 N solutions of LiCl, NaCl, KCl, and RbCl the coefficient of friction increases from 0.32 to 0.49 for quartz and from 0.11 to 0.12 for ruby. The size of the univalent anions investigated has little effect on the coefficient of friction. The coefficient of friction of quartz only decreased slightly with increase of the halide ion radius.

Kinetic friction and wear.* Kinetic friction is not a direct model of an elementary event of interaction between two fine particles, but investigations of kinetic friction together with wear are of interest for elucidation of the mechanism of mutual displacement of combinations of particles (for example, in the flow of structurized

*L. S. Lupina took part in the experimental work.

TABLE 2

Coefficients of Static Friction of Ruby and Quartz in Electrolyte Solutions. Contact Pressures: Ruby 530 kg/mm^2, Quartz 145 kg/mm^2.

Electrolyte	Electrolyte concentration, meq/liter	Coefficients of static friction	
		ruby	quartz
KCl	1	0.093	0.47
	50	0.113	0.59
$CaCl_2$	1	0.100	0.44
	50	0.114	0.55
$AlCl_3$	1	0.112	0.42
	50	0.116	0.52
$Th(NO_3)_4$	1	0.114	0.34
	50	0.117	0.47
KI	1	0.114	0.45
	50	0.116	0.54
K_2SO_4	1	0.114	0.49
	50	0.116	0.56
$K_3Fe(CN)_6$	1	0.114	0.55
	50	0.116	0.59
$K_4Fe(CN)_6$	1	0.112	0.60
	50	0.117	0.67

disperse systems) and of the nature of the action of electrolytes on the static friction, described above. Studies of the kinetic friction and wear of solids in electrolyte solutions are of independent significance for solid-state physics and certain branches of technology.

As was to be expected, at high contact pressures the coefficients of kinetic friction of the minerals studied are higher than their coefficients of static friction, and the former are higher in dry friction than in friction in water (Table 3).

In all cases the kinetic friction of minerals is greater in electrolyte solutions than in water.

TABLE 3

Coefficients of Kinetic Friction and Wear of Minerals in 10 Minutes in Dry Friction, in Water, and in Different Electrolyte Solutions

Minerals	Contact pressure kg/mm^2	Dry friction		H_2O		0.001 N KCl solution		0.05 N $Th(NO_3)_4$ solution	
		A	B	A	B	A	B	A	B
Ruby	530	0.27	68	0.15	71	0.25	89	0.23	120
Quartz	108	0.58	270	0.27	290	0.28	295	0.31	350
Agate	108	0.62	235	0.29	310	0.30	310	0.33	370

* A = coefficient of friction; B = diameter of wear area in microns.

Kinetic friction decreases with increasing solution concentration (Fig. 4), but does not reach the value for water even in the most concentrated solutions (1.0 N). An interesting fact is that wear increases with decrease of kinetic friction (Fig. 5).

Decrease of the cation or anion charges in solutions of neutral electrolytes of the same concentration increases the coefficient of kinetic friction (Table 4) and wear (Table 5) both of positively charged ruby and of negatively charged quartz. In agreement with the data on static friction, this also shows that the action of electrolytes on mineral interaction in solutions at high contact pressures is determined by a different mechanism from that operating at low contact pressures.

TABLE 4

Coefficients of Kinetic Friction of Ruby and Quartz in Electrolyte Solutions. Contact Pressures: Ruby 530 kg/mm^2, Quartz 108 kg/mm^2.

Electrolytes	Electrolyte concentration, meq/liter	Coefficients of kinetic friction	
		ruby	quartz
NaCl	1	0.160	0.280
	50	0.170	0.290
$CaCl_2$	1	0.180	0.290
	50	0.195	0.300
$AlCl_3$	1	0.220	0.300
	50	—	—
$Th(NO_3)_4$	1	0.220	0.350
	50	0.235	0.315
KCl	1	0.160	0.330
	50	0.160	0.345
K_2SO_4	1	0.170	0.370
	50	0.185	0.350
$K_3Fe(CN)_6$	1	0.200	0.375
	50	0.220	0.400
$K_4Fe(CN)_6$	1	0.210	0.390
	50	0.225	0.420

The experimental results, especially those related to the influence of the ionic charge on friction of minerals, and the different directions of the changes in their static and kinetic friction respectively with increase of solution concentration, show conclusively that at high contact pressures the influence of neutral electrolytes on surface interaction between macroscopic solid bodies and small particles in solutions cannot be attributed to variations in the electrostatic repulsion forces of the diffuse layers of adsorbed ions or to differences in their hydration. This raises the question of the mechanism whereby the ions act under these conditions.

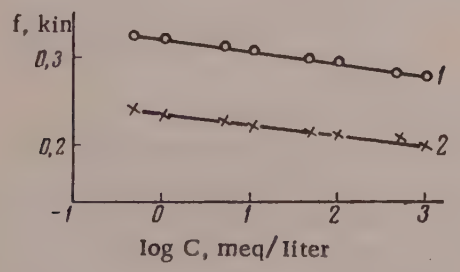


Fig. 4. Effects of concentration of NaCl solution on the coefficients of kinetic friction of minerals: 1) Quartz; 2) ruby.

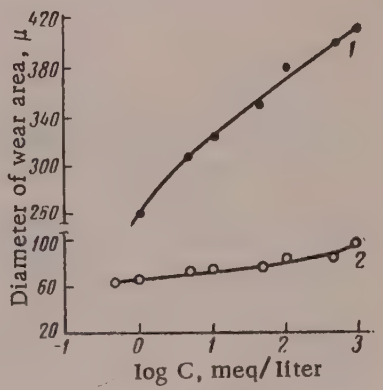


Fig. 5. Effect of concentration of KCl solution on the diameter of the wear area in friction of minerals: 1) Quartz, friction for 2 min; 2) ruby, friction for 10 min.

Since the absolute magnitude of the frictional force for minerals in salt solutions depends primarily on the coefficients of dry friction of these materials (and these coefficients, in their turn, depend on their hardness and brittleness [8-10]), and only secondarily on the solution composition, it is natural to look for an explanation of the influence of the ions in changes in the properties of the solids rather than in the properties of the boundary layer of solution. The literature contains data [11-13] which indicate that the surfaces of high-silica glasses and even of quartz in contact with water and salt solutions undergo physicochemical changes, which in-

TABLE 5

Diameter of the Wear Areas of Ruby and Quartz in Friction in Water and 0.05 N Electrolyte Solutions Contact Pressures: Ruby 530 kg/mm², Quartz 108 kg/mm²

Medium	Duration of friction, min			
	10	20	2	10
	Diameter of wear area, μ			
	Ruby		Quartz	
H_2O	66	71	180	290
NaCl	79	93	200	305
$CaCl_2$	80	94	220	330
$AlCl_3$	89	94	225	335
$Th(NO_3)_4$	90	120	240	350
KCl	80	94	190	310
K_2SO_4	87	109	210	315
$K_3Fe(CN)_6$	91	118	230	330
$K_4Fe(CN)_6$	93	118	240	345

clude hydration and swelling. We showed [14] that after ruby and quartz have been in contact with water or with aqueous electrolyte solutions the hardness and wear resistance of these minerals diminish. This is a manifestation of adsorptional decrease of strength, an effect which was discovered by Rebinder [15] and was studied in detail by him [16] and his associates for metals [17], glasses [18], and certain other materials [16]. Occurrence of the Rebinder effect in homogeneous crystalline minerals, including such a hard one as ruby, in solutions of electrolytes rather than of surface-active agents, is in our opinion of some general interest, but it does not differ in principle from the "classic" cases and essentially fits into the general theory. Electrolytes, like other substances with adsorption activity, bring into operation two main factors which cause the effect in question [19]; they decrease the surface free energy and they increase the two-dimensional pressure of the adsorbed layer at the vertices of microcracks or other structural defects and thereby assist in their development. The criterion of spontaneous dispersion of stressed solids in active media, put forward by Rebinder, Likhtman, and Kochnova [20], is of the following form:

$$W \approx \exp\left[(\delta b^3\sigma - b^2/\lambda)RT\right],$$

where W is the probability of the process; σ is the stress; δ is a dimensionless factor; α is the surface tension; b is the average linear size of the particles formed by dispersion of the body. For the process to take place, the surface tension must not be greater than

$$\alpha \approx RT/b^2 + \delta b\sigma.$$

Electrolyte solutions cannot lower α to the limit at which quartz and ruby undergo spontaneous dispersion, but they diminish microbrittleness (Table 6); in other words, they plasticize the surface. According to Shchukin and Rebinder [21] to effect such plasticization it is sufficient to reduce the surface tension by some tens of ergs per cm². An interesting fact is that the plasticizing effect increases with increase of ionic charge and solution concentration.

TABLE 6

Microhardness and Microbrittleness (Number of Imprints with Cracks) of Ruby and Quartz in Electrolyte Solutions (After Exposure of 1 Hour to the Solutions)

Medium	Microhardness kg mm²	Microbrittleness, % (load 60 g)	Microhardness kg/mm²	Microbrittleness, % (load 60 g)
	Ruby		Quartz	
Air	2270	64	1170	56
Water	2110	50	1130	38
0,05 *N* NaCl	2010	32	1000	34
0,005 *N* KCl	2090	—	1010	—
0,05 *N* KCl	2010	20	980	28
0,05 *N* KCl	1960	16	930	—
0,05 *N* $CaCl_2$	1950	16	910	24
0,05 *N* $AlCl_3$	1850	0	910	22
0,05 *N* $Th(NO_3)_4$	1540	0	900	20
0,05 *N* K_2SO_4	1940	20	910	26
0,05 *N* $K_3Fe(CN)_6$	1740	8	910	18
0,05 *N* $K_4Fe(CN)_6$	1660	0	900	0

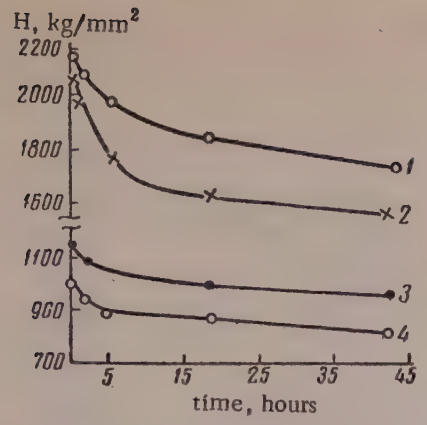


Fig. 6. Effects of the time of action of water and KCl solutions on microhardness of minerals; 1) Ruby in water; 2) ruby in 0.5 N KCl; 3) quartz in water; 4) quartz in 0.5 N KCl.

The adsorbability of ions increases with the solution concentration and, in the absence of interfering effects, with increase of the ion valence [22, 30]. The microhardness of ruby or quartz * decreases in the same manner (Table 6). Adsorptional strength decrease develops in the course of time (Fig. 6); this is the direct consequence of the influence of time on the adsorption process, including the time required for migration of the ions into microcracks in the minerals.

The influence of hardness on friction has been the subject of many theoretical and experimental studies [9, 10, 23-25], but the quantitative expressions which have been derived for this function are not universal in character and sometimes even in direction, as variations of hardness are accompanied by variations of other frictional parameters. In our case it was to be expected that the coefficient of friction would decrease with decrease of the mineral strength, because of lowering of the work of surface dispersion, which constitutes a considerable proportion of the work of friction. This applies primarily to kinetic friction, which is accompanied by continuous destruction of the material, but is also significant in static friction**.

In fact, it is clear from Fig. 7, which contains data on the friction and wear of ruby and quartz in salt solutions, that the kinetic friction of these minerals always increases, irrespectively of the composition and concentration of the solution, with decreasing microhardness which results from interaction with the solutions. The static friction of ruby varies similarly, but its coefficient of static friction varies within a narrow range (curve 1, Fig. 7,a). The corresponding relationship for the static friction of quartz is, in general, indefinite (curve 1, Fig. 7, b); in some groups the coefficient of static friction increases and in others it diminishes with decreasing microhardness. The scatter of the points on the curves in Fig. 7, which are in general definite in direction, indicates that although the influence of ions on hardness of minerals is the main cause of their effect on friction, the influence of the solution composition is superposed on this effect as a secondary factor.

An explanation of these results follows from the molecular theory of friction put forward by Deryagin [26] and from Kragel'skii's molecular-mechanical theory of friction [27, 28]. According to [28], the frictional force T is given by the expression

$$T = (A_1 + B_1 q) S_a' + (A_2 + B_2 q) S_a'',$$

where q is the actual specific pressure; A_1 is the stress of normal molecular interaction; B_1 is a coefficient characterizing molecular "roughness" (one of the forms of expressing molecular interaction in Deryagin's theory); A_2 is the resistance to shear in absence of normal load; B_2 is a coefficient representing the strength increase of the material under compressive load; S_a' and S_a'' are the actual molecular and mechanical contact areas. Decrease of the strength of mineral surfaces by electrolytes makes deformation easier and leads to destruction of the microrelief projections; friction may increase by increase of S_a' and S_a'', or decrease owing to decrease of q and A_2. The resultant change in the friction depends on the numerical values of the terms in the equation and their variations, the properties of the materials, and the type of friction.

Our results show that electrolytes should increase the actual contact area between the minerals studied when they are pressed against each other by high loads. This is a consequence of the adsorptional strength decrease and the associated plasticization of the surface, and it is confirmed by the increase of kinetic friction and diameter of the wear area with decreasing microhardness, regardless of the solution composition. As it is improbable that

* It follows from this that the sorption capacity of adsorbents in the stressed state may increase with increased adsorbability of ions.

** Elin [29] showed that even very small relative displacements (0.5 mm) of metals in contact under high loads result in surface destruction. Similar observations have been described by Bowden and Tabor [31].

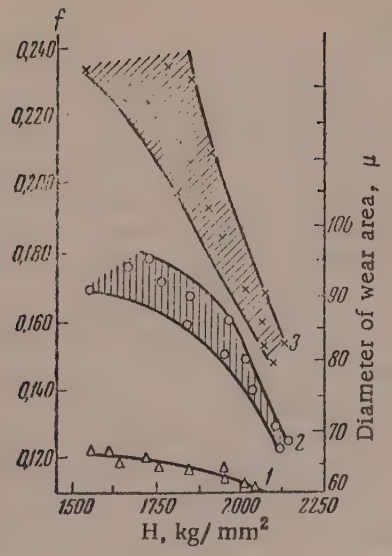


Fig. 7a

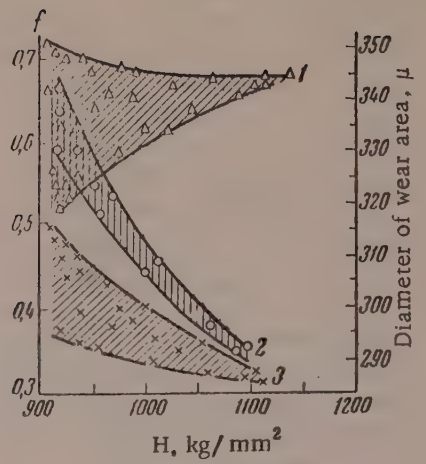


Fig. 7b

Fig. 7. Variations of the friction and wear of minerals in various electrolyte solutions with the microhardness (H) of ruby (a, friction for 10 minutes) and quartz (b, friction for 2 minutes) in these solutions: 1) Coefficient of static friction; 2) wear; 3) coefficient of kinetic friction.

electrolytes decrease the specific force of intermolecular interaction*, we conclude that they must increase the total interaction energy. This effect is associated with the action of the ions on the solid surfaces and not on the boundary liquid layer.

Evidently this third mechanism (supplementing the electrostatic and hydration mechanisms) of the action of electrolytes on coagulative interaction is specific for high contact pressures, when the two surfaces are in direct contact and undergo mutual deformation; apparently it does not operate in coagulation of dilute sols and suspensions by electrolytes, but it may appear in coagulation structure formation and may facilitate conversion of coagulation structures into the crystallization type.

SUMMARY

1. Water and aqueous solutions of neutral electrolytes cause adsorptional decreases of strength in ruby, quartz, and agate, and also the associated surface plasticization of these minerals. The effect appears after the minerals have been exposed to the solutions for some time, and increases with increases of the anionic and cationic charges and with solution concentration.

2. At high contact pressures the coefficients of friction and degree of wear of these minerals are of the same order of magnitude in electrolyte solutions as in dry friction, but the influence of the solution composition can also be considerable; this influence generally increases with increase of the adsorptional strength lowering effect (quartz in solutions of salts with univalent ions is an exception).

3. Coagulative interaction in neutral electrolyte solutions depends on the solution composition, not only when the surfaces are separated by a liquid boundary layer but also when the surfaces are in direct contact and undergo mutual deformation. In the latter case the action of the ions depends on the adsorptional lowering of the strength of solids which they cause; this effect leads to an increase of the actual contact area and thereby increases the total interaction energy.

*In particular, the disjoining pressure cannot increase, because it is an inverse exponential function of the charge of the ions in the diffuse layer and of the square root of the solution concentration [1].

LITERATURE CITED

1. G. I. Fuks and N. I. Kaverina, Kolloid. Zhur. 21, 6, 718 (1959);* Doklady Akad. Nauk SSSR 121, 322 (1958).*
2. G. I. Fuks, Proceedings of the 3rd All-Union Conference on Colloid Chemistry [in Russian] (Izd. AN SSSR, (1956) p. 301.
3. G. I. Fuks, Kolloid. Zhur. 20, 748 (1958)*; Doklady Akad. Nauk SSSR 113, 635 (1957).*
4. G. I. Fuks, Zavodskaya Lab., 5, 594 (1956).
5. A. E. H. Love, Mathematical Theory of Elasticity [Russian translation] (IL, 1935); L. Orton, Applying theory of elasticity in practical design (N.Y., 1941).
6. M. M. Khrushchov and E. S. Berkovich, The PMT-2 and PMT-3 Instruments for Microhardness Testing [in Russian] (Izd. AN SSSR, 1950).
7. N. Yu. Ikornikova, Proceedings of Conference on Microhardness [in Russian] (Izd. AN SSSR, 1951) p. 211.
8. A. S. Mikhailyuk and G. I. Fuks, Priborostroenie, 9, 18 (1957).
9. M. M. Khrushchov and M. A. Babichev, Doklady Akad. Nauk SSSR 107, 75 (1956).*
10. F. Bowden, J. Inst. Petroleum 40, 364 (1954).
11. A. A. Grebenshchikov, Izvest. Akad. Nauk SSSR, Otdel Tekhn. Nauk, 1, 3 (1937).
12. N. Kachalov, Principles of Glass Grinding and Polishing Processes [in Russian] (Izd. AN SSSR, 1946).
13. H. E. Simpson, J. Am. Ceram. Soc. 41, 43 (1958).
14. G. I. Fuks, Kolloid. Zhur. 22, 256 (1960).*
15. P. A. Rebinder, Z. Phys. 72, 191 (1931); Zhur. Tekh. Fiz. 2, 726 (1932); Collection: The 30th Anniversary of the October Socialist Revolution [in Russian] (Izd. AN SSSR, 1947), Part 1, p. 535.
16. P. A. Rebinder, Physicochemical Mechanics [in Russian] (Znanie, Moscow, 1958).
17. V. I. Likhtman, P. A. Rebinder, and G. V. Karpenko, Influence of Surface-Active Media on Metal Deformation [in Russian] (Izd. AN SSSR, 1954).
18. M. S. Aslanova, Doklady Akad. Nauk SSSR 95, 1215 (1954); M. S. Aslanova and P. A. Rebinder, Doklady Akad. Nauk SSSR 96, 299 (1954).
19. G. M. Bartenev, I. V. Yudina, and P. A. Rebinder, Kolloid. Zhur. 20, 655 (1958).*
20. P. A. Rebinder, V. I. Likhtman, and L. A. Kochnova, Doklady Akad. Nauk SSSR 111, 1278 (1956).*
21. E. D. Shchukin and P. A. Rebinder, Kolloid. Zhur. 20, 645 (1958).*
22. K. K. Gedroits, The Sorption Capacity of Soils [in Russian] (Sel'khozgiz, 1933).
23. P. A. Rebinder, Izvest. Akad. Nauk, SSR, Ser. Khim. 5, 639 (1936).
24. F. Bowden, "The physics of rubbing surfaces," J. and Proc. Roy. Soc. N. S. Wales 78, (1944), F. Bowden and L. Leben, Proc. Roy. Soc. A169, 371 (1939).
25. A. Ernst and M. Merchant, Surface Treatment of Metals (Soc. of Metals, New York, 1941). p. 299; M. Merchant, J. Appl. Phys. 11, 230 (1940).
26. B. V. Deryagin, Zhur. Fiz. Khim. 5, 1165 (1934); What is Friction: Essays on the Nature of Friction [in Russian] (Izd. AN SSSR, 1952).
27. I. V. Kragel'skii, Proceedings of the 2nd All-Union Conference on Friction and Wear in Machines [in Russian] (Izd. AN SSSR, 1949) Vol. 3, p. 178.
28. I. V. Kragel'skii and V. S. Shchedrov, The Theory of Friction; Dry Friction [in Russian] (Izd. AN SSSR, 1956).
29. L. V. Elin and M. D. Krylov, Vestnik Metalloprom., 12, 33 (1939); Proceedings of the 1st All-Union Conference on Friction and Wear in Machines [in Russian] (Izd. AN SSSR, 1939) p. 277.
30. A. I. Rabinerson, Problems of Colloid Chemistry [in Russian] (Khimteoretizdat, 1937) Chap. 1.
31. F. Bowden and J. Tabor, Friction and Lubrication of Solids (Oxford, 1950).

*Original Russian pagination. See C.B. translation.

INVESTIGATION OF THE SYSTEM CHASOV YAR CLAY–WATER BY THE ELECTRICAL CONDUCTIVITY METHOD

V. B. Chernogorenko*

Scientific Research Institute of Constructional Materials, Kiev

Translated from Kolloidnyi Zhurnal, Vol. 22, No. 6, pp. 730-734,
November-December, 1960
Original article submitted August 7, 1959

One method for investigating disperse systems and processes taking place in them is based on conductivity measurements [1]. Conductivity measurements are often used for determinations of the moisture contents of various disperse systems, including the clay-water system. It is therefore important to establish how the conductivity of the system varies with the concentration of the disperse phase and the temperature. The surface conductivity, and the influence of surface conductivity on the total conductivity of the system, are important for correct interpretation of the conductivity of such disperse systems as the clay-water system.

We investigated the system Chasov Yar clay-water. The chemical composition of the clay (in %) was: SiO_2-54.86; Al_2O_3-32.18; Fe_2O_3-0.72; TiO_2-0.97; CaO-0.70; MgO-0.70; SO_3-0.34; calcination loss 8.12; total, 98.59. The total ion-exchange capacity of the clay was 24.7 meq/100 g; the content of soluble salts was 5 meq/100 g.

The conductivity measurements were performed by means of a Wheatstone bridge, with an electronic oscillograph as the null instrument. The capacitive reactance in the cell circuit was balanced by a variable capacitance in parallel to the resistance box [2]. Resistance-frequency curves for clay suspensions and the standard solution used for determination of the cell constant showed that a frequency of 2 kc/sec is suitable. Two electrode types were used: needle-shaped platinum electrodes for suspensions, and rigid nickel plates for stonelike masses. Concentrated stonelike masses were prepared by drying of moister pastes. Because of their rigidity, thenickel electrodes immersed in the paste were not deformed during drying. The cell constant was checked at intervals; it remained virtually unchanged between 20 and 80°. The glass vessel containing the electrodes immersed in the suspension or paste was inserted in a metallic vessel, which was placed in an ultrathermostat. Samples were taken for moisture determination after each experiment.

Figure 1 shows that the conductivity polytherms for suspensions with different concentrations of the disperse phase, up to 20%, are linear. The increase of conductivity with temperature slows down as the concentration of the disperse phase is increased. In the case of a 20% suspension the retardation of the conductivity increase begins at 70° (Fig. 1), and in the case of a 72% suspension, at 55°. For pastes of higher concentrations the conductivity-temperature relationship is linear again.

In view of the large specific surface of clay, it is necessary to estimate the proportion of its conductivity which is due to surface conduction. The surface conductivity κ_s is the difference between the conductivity κ_a ** of the solution within the spaces in the framework of a structurized system and the conductivity κ_v of the filtrate from the same system [3].

*In the article by V. B. Chernogorenko, Kolloid. Zhur. 22, 1, 101 (1960) the ordinates in Fig. 1-3 should be designated as sec^{-1} [See C. B. translation].

** The conductivity of the solution within the spaces of the framework was calculated from the formula $\kappa_a = \kappa V/(V-V_1)$ where κ is the conductivity of the suspension ($ohm^{-1} \cdot cm^{-1}$); V is the volume of the suspension (cc); V_1 is the volume occupied by the disperse phase in a suspension of volume V (cc).

Conductivity of Suspensions, Solutions from the Interstitial Spaces of the Structurized System, and the Filtrate, and Surface Conductivity of Chasov Yar Clay at 20°

Concentration of disperse phase, % by wt.	Conductivity, 10^5 ohm^{-1} · cm^{-1}			Surface conductivity		$\frac{\kappa_s}{\kappa} \cdot 100\%$
	of suspension, κ	of solution, κ_a	of filtrate, κ_v	κ_s, 10^5 ohm^{-1} · cm^{-1}	Specific $K \cdot 10^9$, ohm^{-1}	
1	10.0	10.4	7.9	2.5	2.20	25
5	41.0	41.9	37.2	4.7	0.82	12
20	82.0	89.7	77.1	12.6	0.49	15
30	103.0	119.6	97.0	22.6	0.51	22

The results of determinations of the conductivities of certain suspensions and filtrates at 20° are given in the table.

In an earlier investigation [4] the effective specific surface of Chasov Yar clay, s = 1.14 · 10^6 cm^2/g, was determined from heats of wetting. From the known amount (A) of clay in 1 cc of suspension we calculated the surface conductance per cm^2 of the clay surface; this is known as the specific surface conductivity (K, ohm^{-1}). The following formula was used for the calculation:

$$K = \kappa_s / sA,$$

where κ_s is the surface conductance (ohm^{-1} · cm^{-1}); s is the specific surface of the clay (cm^2/g); A is the concentration of clay per cc of suspension (g/cc).

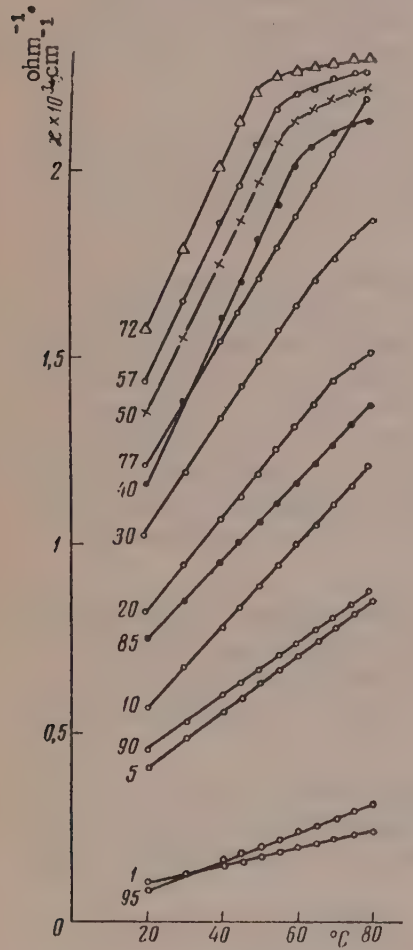


Fig. 1. Conductivity polytherms for Chasov Yar clay suspensions and pastes with different concentrations of the disperse phase (% by weight).

Our values for the specific surface conductivity (see table) are close to the results obtained by other workers for quartz (glass)-water (solution) systems [3]. A knowledge of the specific surface conductivity of clays is important for correct calculations of the electrokinetic potentials of clays [3, 5].

It is seen in the table that the proportion of the conductivity due to surface conductivity [$(\kappa_s/\kappa) \cdot 100$] is, on the average, 18% of the total conductivity in suspensions containing up to 30% of the disperse phase.

The numerical data were used for plotting conductivity isotherms for the system Chasov Yar clay-water (Fig. 2). Despite the fact that the components of the system are nonconducting or of low conductivity, a system with ionic conductance is formed as the result of clay-water interaction*.

Each isotherm (Fig. 2) has a maximum, which becomes flatter in the direction of higher water contents with increase of temperature. The maximum of the 20° isotherm corresponds to 72% concentration of the disperse phase, which coincides with the concentration of the disperse phase in Chasov Yar clay pastes of the normal moisture content for molding. It follows that the normal molding moisture content, i.e., the moisture content corresponding to maximum plasticity, has a definite physical meaning. At this moisture content the diffuse layers of hydration ions on the surfaces of clay materials overlap. The diffuse ionic layers coalesce into one, common for the whole mass [6].

With increase of the amount of water in the paste the ionic double layers become separated by interlayers of the volume solution. Decrease of the clay concentration leads to a decrease in the concentration of dissolved salts in the dispersion medium. The conductivity decreases accordingly. As the amount of free water in the paste decreases,

* The conductivity of distilled water is 1.5 · 10^{-6} ohm^{-1} · cm^{-1}, and of solid dried clay, < 10^{-11} ohm^{-1} · cm^{-1}.

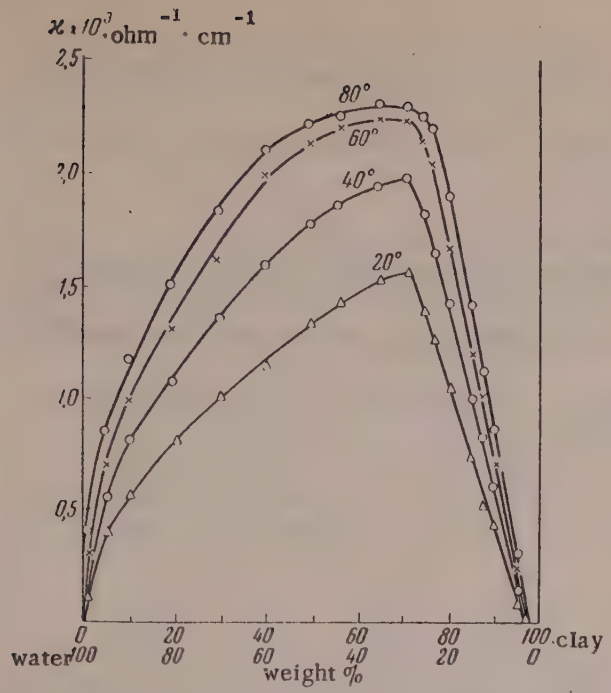


Fig. 2. Conductivity isotherms for the disperse system Chasov Yar clay-water, for temperatures from 20 to 80°.

the content of nonconducting clay particles per unit volume and the air content of the pores increase. The two-phase system passes into a three-phase system: clay-water-air. Therefore the conductivity of pastes with moisture contents below the normal amount for molding must decrease with decrease of moisture content.

It follows from Fig. 2 that each conductivity isotherm has two large branches, and one small branch (not shown in Fig. 2) from the point corresponding to 97%* concentration to the point corresponding to absolutely dry clay. This small portion of low conductivity is the region for the conductivity of the gradually forming monolayer of adsorbed water. The conductivity increases sharply with further increase of water content; this shows that bound water can be determined by the conductivity method.

The lower part of the left-hand branch of the isotherm represents conductivity of the suspension, and the lower part of the right-hand branch corresponds to the conductivity of an elasticobrittle body. The plastic state of the clay-water system corresponds to the transition from a system with coagulational structure formation to a system with condensational structure formation [6, 7]. The highest conductivities on the conductivity isotherms (Fig. 2) correspond to pastes of the maximum plasticity.

The right-hand branch of the isotherm is almost linear from the normal molding moisture content (72% concentration of the disperse phase) to the point corresponding to 97% concentration. It is thus possible to determine the moisture contents of clays and soils over this concentration range; this confirms Dolgov's investigations [8]. In moisture determinations by the conductivity method it is necessary to bear in mind a number of complications which may be caused by compression in processing, the time of aging, etc.

SUMMARY

1. The system Chasov Yar clay-water has been studied by the conductivity method over the entire concentration range at temperatures from 20 to 80°.

2. The maxima on the conductivity isotherms correspond to the normal moisture content for molding, i.e., the maximum plasticity of the pastes.

3. The conductivity isotherm is linear from the point corresponding to the normal molding moisture content to the point corresponding to the hygroscopic moisture content in air. Accordingly it is possible to determine the amount of the dispersion medium in the system from the conductivity.

It is my pleasant duty to thank Academician P. A. Rebinder and N. N. Serb-Serbina for valuable comments in discussion of the experimental data.

LITERATURE CITED

1. B. Dogadkin, K. Pechkovskaya, and M. Dashevskii, Kolloid. Zhur. 10, 358 (1948); S. S. Voyutskii, et al., Kolloid. Zhur. 13, 333 (1951); B. A. Yampol'skii, Kolloid. Zhur. 18, 621 (1956)**; B. Ya. Yampol'skii and E. S. Solov'eva, Proc. 3rd All-Union Conference on Colloid Chemistry [in Russian] (Izd. AN SSSR, Moscow, 1956) p. 42; E. E. Segalova, V. N. Izmailova, and P. A. Rebinder, Doklady Akad. Nauk SSSR 114, 594 (1957).**

*This represents clay of hygroscopic moisture content [4].

**Original Russian pagination. See C. B. translation.

2. G. A. Abramov, et al., Theoretical Principles of the Electrometallurgy of Aluminum [in Russian] (Metallurgizdat, Moscow, 1953) p. 145.
3. O. N. Grigorov, et al., in Collection: Electrokinetic Properties of Capillary Systems [in Russian] (Izd. AN SSSR, Moscow-Leningrad, 1956).
4. I. I. Morachevskii, et al., Kolloid. Zhur. 22, 340 (1960).*
5. I. A. Geller, Kolloid. Zhur. 4, 739 (1938); V. B. Chernogorenko, Kolloid. Zhur. 22, 101 (1960).*
6. I. M. Gor'kova, Proceedings of the F. P. Savarenskii Laboratory of Hydrogeological Problems [in Russian] (Izd. AN SSSR, Moscow, 1957) Vol. 15, p. 26.
7. P. A. Rebinder, Collection in Memory of Academician P. P. Lazarev [in Russian] (Izd. AN SSSR, Moscow, 1956) p. 113.
8. S. I. Dolgov, Investigation of the Mobility of Soil Moisture and its Availability to Plants [in Russian] (Izd. AN SSSR, Moscow-Leningrad, 1948).

*Original Russian pagination. See C. B. translation.

EFFECT OF THE DEFORMATION RATE ON THE ULTIMATE HIGH-ELASTIC AND RUPTURE DEFORMATION OF A GEL SOLUTION OF ALUMINUM NAPHTHENATE*

T. G. Shalopalkina and A. A. Trapeznikov

Institute of Physical Chemistry, Academy of Sciences USSR, Moscow
Translated from Kolloidnyi Zhurnal, Vol. 22, No. 6, pp. 735-742,
November-December, 1960
Original article submitted March 11, 1960

The high-elastic deformational properties of colloidal systems and of polymers in block form are closely interrelated, and therefore considerable interest attaches to comparisons of these properties and investigations by similar methods. Solutions and gels of polymers and many high-elastic colloidal systems differ from polymers in block form by having much higher relaxation rates. High rates of deformation are therefore needed for detection and estimation of large reversible deformations in such systems.

Many workers have used the sinusoidal vibration method [1] for investigations at high deformation rates, but the deformations so obtained were relatively very small. Large deformations can be measured at high rates by the method of deformation at constant rate, for example under shearing conditions. It was shown in earlier investigations that the characteristic parameters of the $P(\epsilon)$ stress-deformation curve determined at constant deformation rates $\dot{\epsilon}$ is the ultimate shearing strength P_r of the structure and the corresponding rupture deformation $\epsilon = \epsilon_r$ [2]. Parallel determinations, by a direct method, of the magnitude of high-elastic deformation in relation to a given ϵ_e (ϵ) showed that in this case the characteristic parameters are the maximum high-elastic deformation $\epsilon_e = \epsilon_{e\,max}$ and the corresponding deformation $\epsilon = \epsilon_m$ [3]. It was found that ϵ_r and ϵ_m need not coincide [4].

Variations of the ultimate high-elastic and rupture deformations with the deformation rate are of special interest with respect to the determinations of general rheological laws. The purpose of the present work was to investigate the $\epsilon_e(\epsilon)$ and $P(\epsilon)$ relationships, in conjunction with $\epsilon_{e\,max}$ and $\epsilon_r(\dot{\epsilon})$, over the widest possible range of $\dot{\epsilon}$, for fluid aluminum naphthenate gel, which is a typical high-elastic colloidal system with not too short relaxation times.

Method. A 2% gel solution of aluminum naphthenate (batch No. 24) in nonpolar medical liquid petrolatum was used. This solution was prepared through the concentrate at 130° and aged for 20 months. An elastorelaxometer (model 2) [5] was used in the range of high $\dot{\epsilon}$ (from 35 to 1100 sec^{-1}), and an elastoviscosimeter (model 3), the recording system of which was described previously [6], was used in the range of lower $\dot{\epsilon}$ (from 0.46 to 46 sec^{-1}). For determination of $\epsilon_e(\epsilon)$ curves a special automatic attachment for the elastoviscosimeter was devised (Fig. 1); it resembles the device in the elastorelaxometer, but its design is adapted to the components already present in the elastoviscosimeter.

The inner hollow ($M \approx 10$ g · cm^2) cylinder 1, made of Dural (R_1 = 1.4 cm, L = 8.0 cm), has upper and lower axes terminating in conical tips. The cylinder is mounted coaxially with the outer cylinder 2 (R_2 = 1.5 cm). The upper bearing for the inner cylinder is the intermediate part 3 gripped in the jaws of the stop device 4. The stop device slides along the instrument support and can be used to regulate the pressure in the upper bearing. A socket

*Presented at the Rheology Subsection of the All-Union Conference on Mechanics, 1960.

with cotter pins 5 is fitted onto the upper portion of the intermediate part 3. The lower end of the measuring wire 6 is gripped in this socket from above, while the upper end is fixed in the lid of the magnetic clutch 7. The latter is inserted in a hole in the moving arm 8 of the elastoviscosimeter (generally used for attachment of the upper end of the rigid measuring wire). A crosspiece 9 is placed on the rod of the inner cylinder so that the pins of the socket are below it. The outer cylinder is turned by hand to bring the crosspiece in contact with the pins which transmit the torque to the wire.

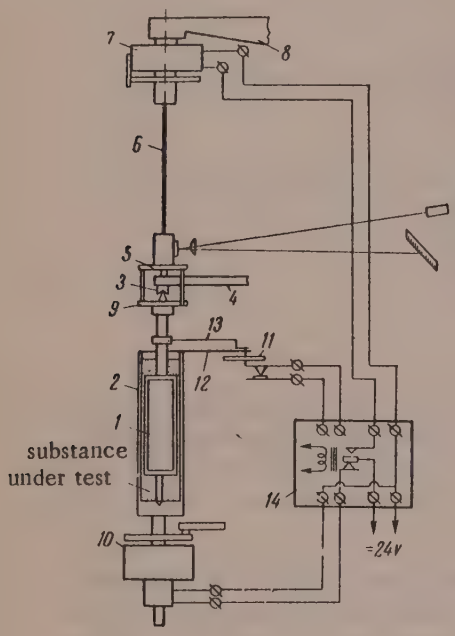


Fig. 1. Diagram of elastoviscosimeter attachment.

For deformation of the system, the outer cylinder is turned through a predetermined angle through the electromagnetic clutch 10, with the motor rotating at constant speed. The angle is restricted by a special moving contact which travels along an annular groove containing electrolyte. The angle is read off on the scale 11. The outer cylinder has a pointer 12 which swings the moving contact over into the electrolyte when the predetermined deformation has been exceeded. The circuit of the lower magnetic clutch 10 is then broken through a relay. Simultaneously the upper magnetic clutch 7 is engaged through the relay, detaching the pins from the crosspiece and breaking the connection between the wire and the inner cylinder. Under the influence of the elastic forces in the gel the inner cylinder begins to move in the direction of rotation of the outer cylinder and passes through an angle, indicated by the pointer 13, corresponding to the elastic deformation (recoil). This device extends the range of the elastoviscosimeter by making possible the measurement of large elastic deformations. The upper rate limit to the applicability of this method is the time for demagnetization of the lower magnetic clutch. This is avoided in the elastorelaxometer by the use of a mechanical brake.

Figure 2 shows $\epsilon_e(\epsilon)$ curves for $\dot{\epsilon}$ between 9.46 and 1112 sec^{-1}. It follows from Fig.2,a,that in the range from 0.46 to 45.8 sec^{-1} the $\epsilon_e(\epsilon)$ curves lie progressively higher, i.e., the elastic deformation increases with the rate at any predetermined deformation. Here ϵ_m, the deformation corresponding to $\epsilon_{e\ max}$, increases with $\epsilon_{e\ max}$. If the system is regarded as containing a range of structural elements characterized by different critical deformations and relaxation times, this means that relaxation of the longer and more mobile structural elements becomes more difficult as $\dot{\epsilon}$ increases [4].

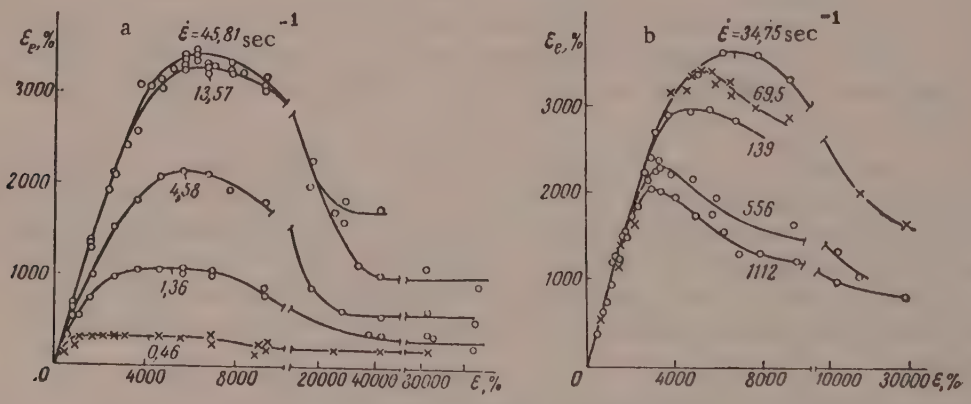


Fig. 2. Curves for the elastic deformation ϵ_e as a function of the predetermined information ϵ at various deformation rates $\dot{\epsilon}$.

The reverse situation is found with increase of $\dot{\epsilon}$ from 34.75 to 1112 sec^{-1} (Fig. 2, b). The higher the value of $\dot{\epsilon}$, the lower the position of the entire $\epsilon_e(\epsilon)$ curve; this means that as the deformation rate increases the maximum elastic deformation which may appear at the given rate diminishes. The decrease of $\epsilon_{e\ max}$ is

accompanied by decrease of ϵ_m. The explanation of this type of variation of ϵ_e and ϵ_m is that as $\dot{\epsilon}$ increases the long intertangled chains of the structural network begin to break without uncoiling completely, i.e., without reaching their maximum elastic (and rupture) deformation. In other words, elastic deformation does not have time to develop fully on considerable increase of $\dot{\epsilon}$; the high-elastic colloidal system becomes more "brittle," just as rubber undergoes brittle failure at high deformation rates. It is likely that with further increase of $\dot{\epsilon}$ it is possible to lower $\epsilon_{e\ max}$ to values characteristic of solids.

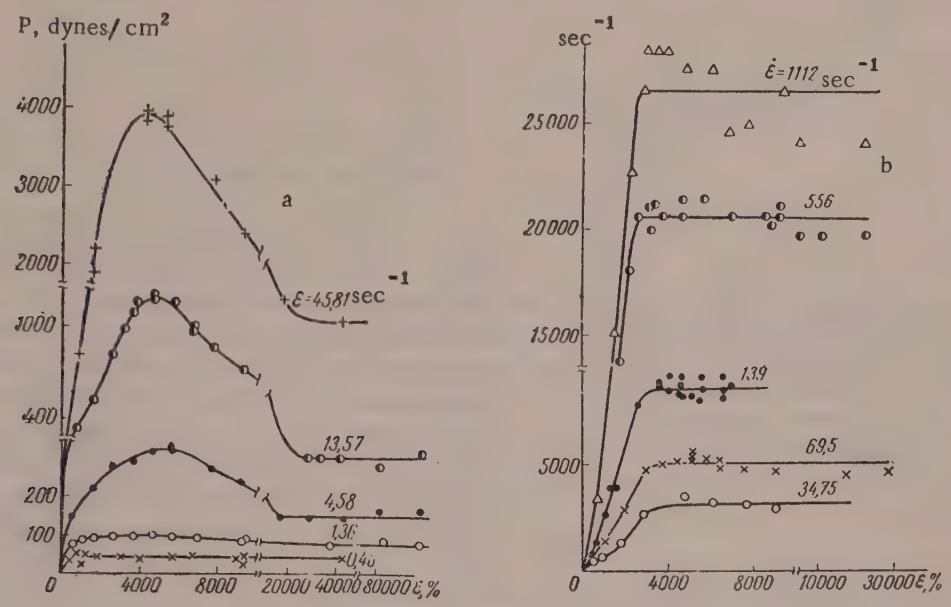


Fig. 3. Curves for the shear stress P as a function of the predetermined deformation ϵ at various deformation rates $\dot{\epsilon}$.

The $P(\epsilon)$ curves (Fig. 3) determined simultaneously with the $\epsilon_e(\epsilon)$ curves (Fig. 2) are noteworthy. The stress maximum is found at $\epsilon = \epsilon_r$ (Fig. 3, a). In the case of the curves in Fig. 3, b this deformation ϵ_r, because of the specific characteristics of elastorelaxometer operation with visual observation of the maximum deviation of the light spot, corresponds to the start of the horizontal region of the $P(\epsilon)$ curve *

It follows from Fig. 3, a and Fig. 3, b that as $\dot{\epsilon}$ increases the values of P_r rise rapidly whereas ϵ_r steadily decreases. This corresponds to our earlier results [6].

Comparison of Fig. 2 and 3 shows that $\epsilon_{e\ max}$, ϵ_m and ϵ_r vary in different ways with increase of $\dot{\epsilon}$, and therefore the maxima on the $P(\epsilon)$ and $\epsilon_e(\epsilon)$ curves represent different stages of structural breakdown during deformation of the system at constant $\dot{\epsilon}$. In Fig. 4 variations of $\epsilon_{e\ max}$, ϵ_m and ϵ_r with $\dot{\epsilon}$ are plotted in semilogarithmic coordinates. The meaning and the symbatic nature of the values of $\epsilon_{e\ max}$ and ϵ_m indicate that they are interrelated and represent, respectively, the maximum elasticity of the system and the deformation at which this is reached at each given $\dot{\epsilon}$. The fact that the values of $\dot{\epsilon}_{e\ max}$ are much less than ϵ_m at low $\dot{\epsilon}$ can be attributed to relaxation of the rapidly relaxing long structural elements; this process has time to occur during deformation of the system (rotation of the outer cylinder) and during contraction of the elastic deformation (movement of the inner cylinder after it has been released). Moreover, relaxation during deformation of the system is probably accompanied by rupture of short bonds. Therefore ϵ_m (and also ϵ_r) includes a considerable proportion of the irreversible plastic deformation. For example, when $\dot{\epsilon} = 0.46\ sec^{-1}$, $\epsilon_{e\ max}$ is only 320%, whereas ϵ_m may be 4000% or even more. Since the role of relaxation and the relative influence of breakdown of the short structural elements diminish with increase of $\dot{\epsilon}$, the value of $\epsilon_{e\ max}$ rapidly approaches ϵ_m but does not reach it (for this system).

When the deformations $\epsilon > \epsilon_r$, at high $\dot{\epsilon}$, the eye registers only the extreme maximum deviation, corresponding to $P = P_r$ at the instant when $\epsilon = \epsilon_r$, despite the fact that P is actually lower at $\epsilon > \epsilon_r$. This was subsequently confirmed by an oscillographic method.

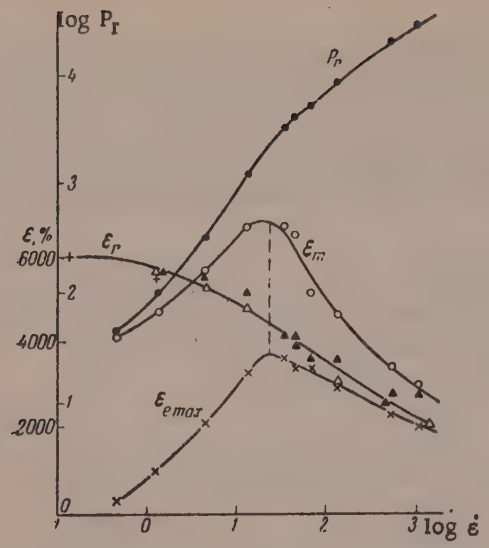


Fig. 4. Variations of the maximum elastic deformation ϵ_e, the deformation ϵ_m at which $\epsilon_{e\,max}$ is reached, rupture deformation ϵ_r, and structural strength P_r with the deformation rate $\dot{\epsilon}$.

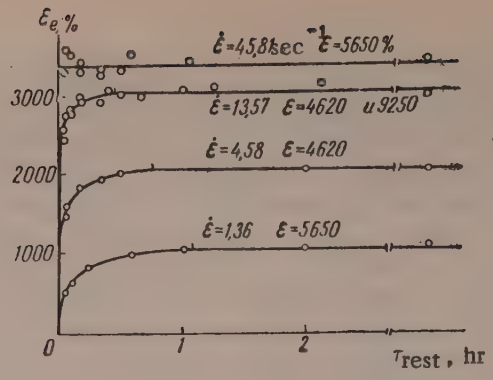


Fig. 5. Curves for thixotropic restoration of the elastic deformation ϵ_e.

As has already been stated, the value of ϵ_r decreases with increase of $\dot{\epsilon}$ in the range of $\dot{\epsilon}$ used in this case. It follows from a comparison of the curves in Fig. 4 that for this system $\epsilon_r = \epsilon_m$ only at one point of intersection of the $\epsilon_r(\dot{\epsilon})$ and $\epsilon_m(\dot{\epsilon})$ curves. This means that the maxima on the $P(\epsilon)$ and $\epsilon_e(\epsilon)$ curves coincide with respect to deformation at only one value of $\dot{\epsilon}$. The fact that ϵ_r and ϵ_m do not coincide [4] is of great interest for an understanding of the structural breakdown process. It shows that not $P(\epsilon)_e$ curves but $\epsilon_{\dot{e}}(\epsilon)_{\dot{\epsilon}}$ curves should be used for evaluation of the high-elastic properties of colloidal systems.

Figure 4 shows that ϵ_r can be either greater or less than ϵ_m for the same system. The relationship $\epsilon_r > \epsilon_m$ is found in the region of low $\dot{\epsilon}$. This means that, in the course of deformation, elastic deformation mainly develops first, and this is followed by an increase of plastic deformation owing to gradual breakdown of the short structural elements. The stress is then redistributed to the longer structural elements, the breakdown of which determines the appearance of P_r. The maximum elastic deformation is found at $\epsilon_m < \epsilon_r$, evidently because the unrelaxed elastically deformed long structural elements are not numerous enough to ensure rotation of the inner cylinder in the highly viscous medium formed by the destroyed structural elements. With increase of $\dot{\epsilon}$ the number of unrelaxed long structural elements increases, and therefore ϵ_m and $\epsilon_{e\,max}$ increase also. However, ϵ_r decreases. This is because the greatest stress corresponds not to the longest structural elements but to those of intermediate length, which are fairly numerous in the system; high stresses are required for their deformation and breakdown, especially at higher $\dot{\epsilon}$, when the viscosity term in the development of high-elastic deformation begins to be significant. With an even greater increase of $\dot{\epsilon}$, when the $\epsilon_m(\dot{\epsilon})$ and $\epsilon_{e\,max}(\dot{\epsilon})$ curves pass through maxima, the longest elements no longer have time to uncoil and elastic deformation begins to diminish. However, ϵ_m decreases much more rapidly than $\epsilon_{e\,max}$ and approaches the latter. This shows that nearly all the deformation ϵ_m is elastic. All three values, ϵ_m, $\epsilon_{e\,max}$ and ϵ_r, become similar and the system becomes almost elasticobrittle in its behavior. Nevertheless, ϵ_m still remains the greatest; this shows that after a part of the bonds causing the structural strength has been destroyed at ϵ_r, a certain proportion of longer structural elements, giving rise to ϵ_m, still remains intact.

The rapid increase of P_r in the $\dot{\epsilon}$ range corresponding to the descending branches of the $\epsilon_m(\dot{\epsilon})$ or $\epsilon_{e\,max}(\dot{\epsilon})$ (Fig. 4) is due to an increase in the number of branch points and entanglements in the network, which is a consequence of hindered uncoiling of the chainlike particles and their rupture in a more entangled state. The decrease of rupture deformation is equivalent to formation of a more compact structure.

Thixotropic changes of ϵ_e. It was shown earlier [3] that the decrease of ϵ_e as $\epsilon_{e\,max}$ is passed in the $\epsilon_e(\epsilon)$ curve is due to breakdown of the structural network. On repeated deformation to $\epsilon = \epsilon_m$ the value of ϵ_e is found to be lower, and it increases and reaches the initial value only after the system has been allowed to rest and the structure has been gradually restored; P_r varies correspondingly. Further it was shown [4] that the nature of the breakdown and restoration of the structural elements in the network may greatly depend on the gel con-

centration and the magnitude of the predetermined deformation; this is associated with the range of the structural elements. It was found that the longer structural elements are the more mobile and the structure which they form is restored more rapidly.

TABLE 1

$\dot{\epsilon}$, sec^{-1}	69,5				139			556			
ϵ, %	5160–5080				4070–4600			3260–3210			
τ_{rest}, min	5	15	50	100	10	35	150	5	18	150	1000
ϵ_e, %	3450	3400	3410	3460	3020	3040	3030	2310	2260	2370	2220

In this investigation the influence of deformation rate on the character of the thixotropic restoration of elastic deformation was demonstrated.

The curves in Fig. 5 show increases of ϵ_e with the time of rest, for different deformation rates at predetermined deformations (ϵ) of 4620 and 5650%, which are close to the maxima of the $\epsilon_e(\epsilon)$ curves in Fig. 2, a. It is easy to see that the time for total thixotropic restoration of the structure, estimated from ϵ_e, decreases with increase of $\dot{\epsilon}$. The values of ϵ_e at even greater $\dot{\epsilon}$ are given in Table 1.

It follows from Table 1 that the limiting value of ϵ_e is reached in a rest time as short as 5 minutes, as at $\dot{\epsilon}$ = 45.8 sec^{-1} (Fig. 5), whereas at lower $\dot{\epsilon}$ restoration of the structure (less by the absolute values of ϵ_e) takes considerably longer; for example, 30 minutes at $\dot{\epsilon}$ = 13.57 sec^{-1}, 40 minutes at $\dot{\epsilon}$ = 4.58 sec^{-1}, and 65 minutes at $\dot{\epsilon}$ = 1.36 sec^{-1} (indicated by short strokes on the curves in Fig. 5).

The explanation of the more rapid restoration of the structure at high $\dot{\epsilon}$ is that the structural elements are more mobile after deformation at high $\dot{\epsilon}$. Apparently this is largely because at higher $\dot{\epsilon}$ the network undergoes greater structural breakdown during deformation up to the predetermined value, and this is equivalent to a viscosity decrease.

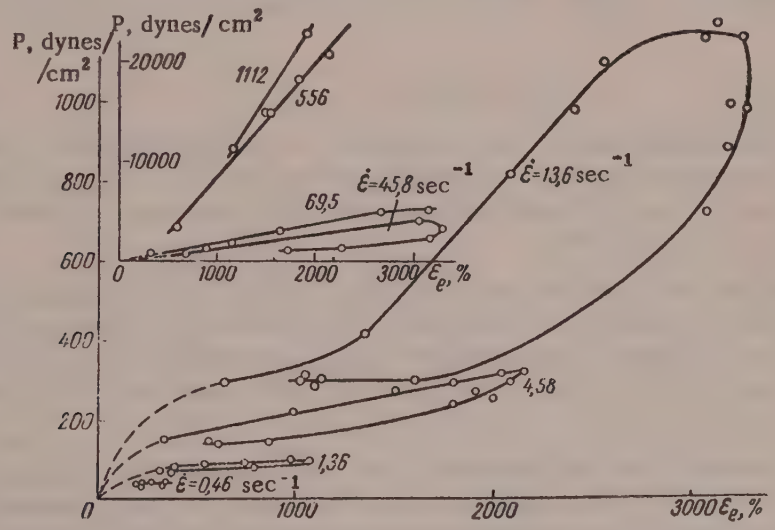


Fig. 6. Curves for variations of the stress P with the elastic deformation ϵ_e.

Stress-elastic deformation curves. The values of P which develop by the instant the inner cylinder is released and the corresponding values of ϵ_e can be used for plotting $P(\epsilon_e)$ curves at different $\dot{\epsilon}$ (Fig. 6). The character of the curves changes as $\dot{\epsilon}$ increases. The curves corresponding to not very high $\dot{\epsilon}$ have forward and return branches, forming loops, which is due to transition through P_r and $\epsilon_{e\,max}$ and structural breakdown. The loop becomes wider at higher $\dot{\epsilon}$.

TABLE 2

$\dot{\epsilon}$, sec^{-1}	Range of ϵ_e, %	$E = \frac{dP}{d\epsilon_e}$, dynes/cm^2
1,36	400	$\gg 2$
	400—1050	2
4,58	400	$\gg 9,5$
	400—2100	9,5
13,6	600	$\gg 15,4$
	600—1350	15,4
	1350—2600	54,7
45,8	0—3000	133
69,5	0—3000	192
556	~600—2100	1180

The curves at the lowest values of $\dot{\epsilon}$ (both branches of the loop) are almost flat in the experimental range studied. Therefore, the initial (hypothetical) regions of these curves, indicated by dash lines, show that at the very lowest values of ϵ_e the stress increases rather steeply.

With increase of $\dot{\epsilon}$ the slope of the flat portions of the curves increases, and at moderate $\dot{\epsilon}$ the flat region is followed by a steeper "strengthening" region of the curve. At even higher $\dot{\epsilon}$ the $P(\epsilon_e)$ curves become very steep and approximately linear throughout. It follows that several types of deformation may be distinguished. Evidently, the horizontal portion of the $P(\epsilon_e)$ curve, which corresponds to a very low (differential) shear modulus $E_{el} = dP/d\epsilon_e$ (Table 2), may be regarded as reflecting typical high elasticity of the system, i.e., very high reversible deformability with very small changes of stress; it is most pronounced at the lowest $\dot{\epsilon}$. With increase of $\dot{\epsilon}$ the value of E_{el} becomes greater, and the range of this elasticity becomes narrower. A strengthening region appears; this is evidently associated with cessation of relaxation of the longest and most mobile structural elements.

The fact that the curves are linear throughout at $\dot{\epsilon} > 46$ sec^{-1} shows that the whole structure of the system begins to act as a single entity, as an elastic system of relatively high E. This is evidently caused by incomplete uncoiling of the long structural elements and an increase in the number of elements being deformed simultaneously. Moreover, increase of $\dot{\epsilon}$ results in a rapid increase of the proportion of the stress corresponding to the viscosity term in the Kelvin deformation contour equation $P = \eta_T \dot{\epsilon} + E\epsilon_e$. It should be noted that in general, as was pointed out earlier [7], $\eta_T = f(\dot{\epsilon}, \epsilon)$.

The dash lines in the region of small ϵ and low $\dot{\epsilon}$ show that at the initial deformation stage ($\epsilon_e \approx 200 - 500\%$) the shearing modulus has a higher value and corresponds to "elastic" deformation of the original structure.

The decrease of E at higher ϵ_e suggests that here the original part of the structure is broken down and the long structural elements begin to uncoil; this corresponds to the earlier conclusions drawn from the general $P(\epsilon)$ curve [8].

SUMMARY

1. Variations of the elastic deformation ϵ_e and shear stress P with the predetermined deformation ϵ have been studied for a 2% gel of aluminum naphthenate in liquid petrolatum over a wide range of deformation rates $\dot{\epsilon}$, from 0.46 to 1112 sec^{-1}. The $\epsilon_e(\epsilon)$ and $P(\epsilon)$ curves pass through maxima at all values of $\dot{\epsilon}$ and tend to constant values corresponding to steady flow.

2. The values of the maximum elastic deformation $\epsilon_{e\,max}$ and the corresponding predetermined deformation ϵ_m pass through maxima with increase of $\dot{\epsilon}$. The value of ϵ_r corresponding to maximum $P = P_r$ decreases continuously in this range of $\dot{\epsilon}$. This fact, and the decrease of $\epsilon_{e\,max}$ in the range of high values of $\dot{\epsilon}$, is attributed to difficulties in uncoiling of the chain particles of aluminum naphthenate in the gel and to their premature rupture.

3. The relationship between ϵ_e and the time of rest of the system at each value of $\dot{\epsilon}$ studied shows that the time of thixotropic restoration of the structure decreases with increase of $\dot{\epsilon}$. The explanation is that when $\dot{\epsilon}$ is increased only the most mobile and rapidly relaxing structural elements are retained and form a structure.

4. The results were used for plotting $P(\epsilon_e)$ curves for various values of $\dot{\epsilon}$; these curves demonstrate the existence of:

a) an initial deformation region with a high shear modulus, which corresponds to "elastic" deformation;

b) an intermediate deformation region with a relatively very low shear modulus, corresponding to high-elastic deformation;

c) a final deformation region with a higher modulus, which corresponds to high-elastic deformation of the strengthened structure. Different types of deformation may predominate at different values of $\dot{\epsilon}$.

LITERATURE CITED

1. A. Aleksandrov and Yu. Lazurkin, Zhur. Tekh. Fiz. 9, 1249 (1939); P. I. Zubov, Z. I. Zhurkina, and V. A. Kargin, Kolloid. Zhur. 9, 109, 367 (1947); E. R. Fitzgerald, L. D. Grandine, Jr., and J. D. Ferry, J. Appl. Phys. 24, 650 (1953); W. Philippoff, Phys. Z. 35, 383 (1933); 35, 900 (1934); A. A. Trapeznikov and E. M. Shlosberg, Doklady Akad. Nauk SSSR 62, 791 (1948); J. G. Oldroyd, D. J. Strawbridge, and B. A. Toms, Proc. Phys. Soc. 64, 44 (1951).
2. A. A. Trapeznikov and V. A. Fedotova, Doklady Akad. Nauk SSSR 81, 1101 (1951); 82, 97 (1952).
3. A. A. Trapeznikov and T. G. Shalopalkina, Doklady Akad. Nauk SSSR 111, 2, 380 (1956).*
4. A. A. Trapeznikov, Kolloid. Zhur. 20, 4, 476 (1958).*
5. A. A. Trapeznikov, Pribor. i Tekh. Eksp. 3, 93 (1958); Kolloid. Zhur. 21, 108 (1959).*
6. T. G. Shalopalkina and A. A. Trapeznikov, Doklady Akad. Nauk SSSR 118, 994 (1958).*
7. A. A. Trapeznikov, Doctorate Dissertation [in Russian] (Moscow, 1955).
8. A. A. Trapeznikov and T. G. Shalopalkina, Kolloid. Zhur. 17, 471 (1955).*

*Original Russian pagination. See C. B. translation.

STUDY OF THE NATURE OF BONDING IN THE RUBBER-FILLER SYSTEM

V. A. Shvetsov, A. P. Pisarenko, and A. S. Novikov

Scientific Research Institute of the Rubber Industry, Moscow
Translated from Kolloidnyi Zhurnal, Vol. 2, No. 6, pp. 743-747,
November-December, 1960
Original article submitted August 27, 1959

Dogadkin and his co-workers [1] have shown that active fillers in rubber mixes, at definite concentrations, form thixotropic chain structures the extent of which influence the physical and mechanical properties of the rubber. Later these workers passed to studies of the distribution of colloidal silica in rubber mixes [2], taking advantage of the solubility of colloidal silica in dilute caustic soda solutions, in which rubber is not soluble.

We used this technique for studying the distribution of calcium silicate and aluminum hydroxide in rubber mixes and vulcanizates based on nitrile rubber, both with formation of the fillers during coagulation of the latex and with the fillers made separately and introduced into the rubber during milling.

Removal of filler from rubber mixes by dissolution in alkali is a more suitable method for aluminum hydroxide than for calcium silicate or silicic acid, because aluminum hydroxide is completely soluble in alkali whereas calcium silicate and silicic acid dissolve only partially (the solubility of calcium silicate in 1% NaOH solution is 36%). Data for aluminum hydroxide only are presented in this paper.

For removal of the filler the samples of rubber, rubber mixes, or vulcanizates in the form of $2 \times 2 \times 0.05$ cm plates were extracted in boiling 1% caustic soda solution for different times, from 30 minutes to 24 hours. The residual filler contents of the samples were determined from their ash contents. The upper extraction limit (24 hours) does not correspond to equilibrium, but it is quite sufficient for determination of the types of structure in reinforced rubbers.

It is clear from Fig. 1 that for unmilled rubbers leaching is complete in 2 hours with 60 weight parts of filler, and in 3 hours with 40 weight parts, while with 20 weight parts 85% of the filler is extracted in 24 hours. The shortest leaching time corresponds to the optimum loading, 60 parts by weight; i.e., to the maximum development of the structure, when the presence of a continuous filler phase which facilitates penetration of the solvent through the rubber is clearly revealed. The chain structure of the filler is less pronounced at lower loadings, and the leaching time is longer. With 20 parts of aluminum hydroxide by weight the filler forms a discontinuous structure; its particles are separated by a film of rubber which hinders diffusion of the solvent.

This leaching behavior is also found in milled rubbers (two-component rubber-filler systems), but leaching is somewhat slower in this case than with unmilled rubbers. For example, with 60 weight parts of filler complete leaching is effected after 6 hours and not 2.

Retardation of filler leaching after milling of the rubber may appear contradictory at first sight, because milling favors better distribution of the filler, making diffusion of the solvent easier. However, unmilled rubber has a looser structure than milled rubber. Moreover, when rubber is milled its globular structure is broken down, protective substances are removed from the surfaces of the rubber particles, and therefore the active surface of the rubber which can be adsorbed by the filler particles is increased. Increase of the structural density and of the number of rubber-filler bonds leads to retardation of the leaching process. Milling of latex mixes is of great importance in increasing the number of rubber-filler bonds.

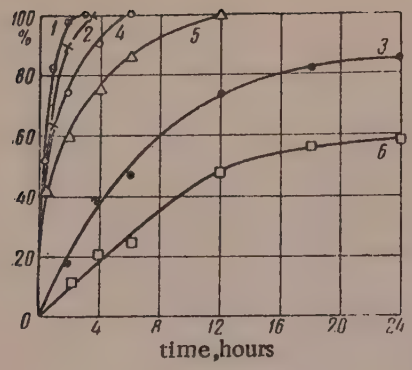


Fig. 1. Kinetics of leaching of aluminum hydroxide, prepared in the latex, from rubber, not milled (1, 2, 3) and milled for 10 minutes (4, 5, 6). Loading: 60 weight parts (1, 4); 40 weight parts (2, 5); 20 weight parts (3, 6).

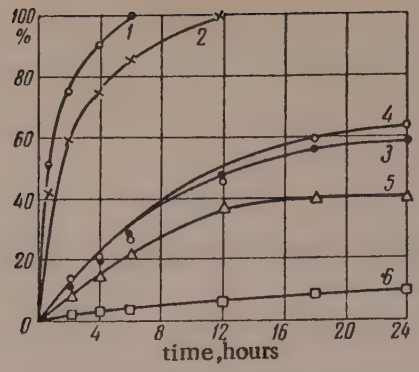


Fig. 2. Kinetics of leaching of aluminum hydroxide, prepared in the latex (1, 2, 3; rubber milled for 10 minutes) and introduced into the rubber during milling (4, 5, 6). Loading: 60 weight parts (1, 4); 40 weight parts (2, 5); 20 weight parts (3, 6).

The influence of milling on the mechanical strength of vulcanizates based on SKN-26 rubber, filled with aluminum hydroxide during coagulation of the latex, is illustrated by the following data:

	Not milled	Milled for 5 minutes
Tensile strength, kg/cm^2	41	192
Elasticity modulus (300%)	35	28
Relative elongation, %	457	820
Residual elongation, %	20	29

Figure 2 shows that with 60 parts of aluminum hydroxide by weight, formed in the latex, the filler is extracted completely with alkali from the rubber within 6 hours, whereas if the same amount of filler is introduced during milling only 63% is extracted in 24 hours. A similar effect is observed at lower loadings.

The data in Fig. 2 indicate that filler introduced during milling does not form chain structures; this is confirmed by mechanical tests. When aluminum hydroxide is introduced during milling the rubbers formed are of lower strength than those containing the filler which was formed in the latex. Finally, the results of electron microscope studies [3] show that aluminum hydroxide introduced at the milling stage does not form chain structures whereas the filler formed in the latex is distributed better in the rubber and forms chain structures; this is confirmed in [4].

For a more complete investigation of the reinforcing effects of aluminum hydroxide on nitrile rubber the influence of stearin as a dispersing agent on the properties of the rubbers was studied. Stearin was added in the proportion of 1.5 parts by weight to 100 parts by weight of rubber.

It is seen in Fig. 3 and 4 that stearin increases the rate of leaching of aluminum hydroxide, both formed in the latex and introduced during milling. When aluminum hydroxide is introduced into rubber during milling the dispersing effect of stearin is more pronounced than in the case of aluminum hydroxide formed in the latex; the probable explanation is that when the rubber and filler are precipitated simultaneously the particles are effectively distributed even without addition of a dispersing agent, as the filler particles become hydrophobic by adsorption of the surface-active substances which are always present in considerable amounts in latexes.

Leaching of fillers from vulcanizates was also of interest for elucidation of the interaction between aluminum hydroxide and nitrile rubber. Figure 5 shows that leaching of aluminum hydroxide from vulcanizates is quantitatively similar to leaching from nonvulcanized systems. The time needed for extraction of the filler is longer because the system is more compact owing to the use of high pressures and to the formation of a spatial network during vulcanization.

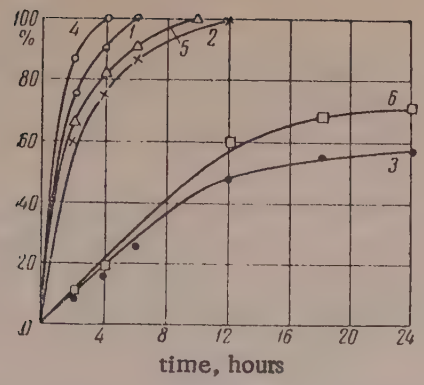


Fig. 3. Kinetics of leaching of aluminum hydroxide from two-component (1, 2, 3) and three-component (4, 5, 6) systems at various loadings. Filler formed in the latex. Loading: 60 weight parts (1, 4); 40 weight parts (2, 5); 20 weight parts (3, 6).

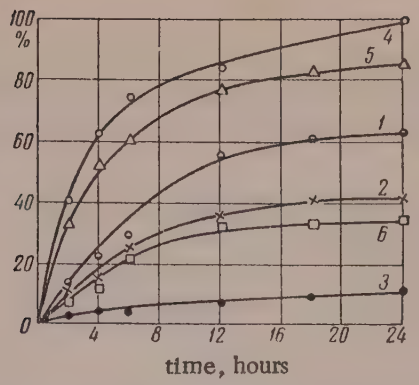


Fig. 4. Kinetics of leaching of aluminum hydroxide from two-component (1, 2, 3) and three-component (4, 5, 6) systems. Filler introduced during milling. Loading: 60 weight parts (1, 4); 40 weight parts (2, 5); 20 weight parts (3, 6).

The fact that aluminum hydroxide can be extracted relatively easily from rubber mixes and vulcanizates indicates that mainly physical bonds, probably of the adsorption type, are formed between this filler and nitrile rubber. Stable bonds of the chemical type are either not formed at all, or formed in only small amounts.

Rubber-filler interaction by formation mainly of secondary bonds of the adsorption type leads to the formation of a rubber-filler network in the system; this, in addition to primary bonds, is the cause of formation of an insoluble gel. Some authors [5] consider that formation of an insoluble rubber-filler gel is due to chemical valence bonding between the rubber and the filler. The data in [2, 6, 7] do not support this one-sided view on the structure of rubber-filler gels. It was shown in [2] that after removal of silica the residual rubber was insoluble in the usual solvents for rubber. This indicates that bonds may be formed directly between individual molecules by means of active substances (oxygen, peroxides) adsorbed on the filler particles, causing structure formation in the rubber.

Our studies of the properties of SKN-26 rubber reinforced with aluminum hydroxide showed that introduction of this filler at the latex stage with subsequent complete extraction from the rubber with alkali solution does not give a rubber with the same properties as before. In this case the rubber was not milled. Neozone D was not removed from the rubber in the extraction.

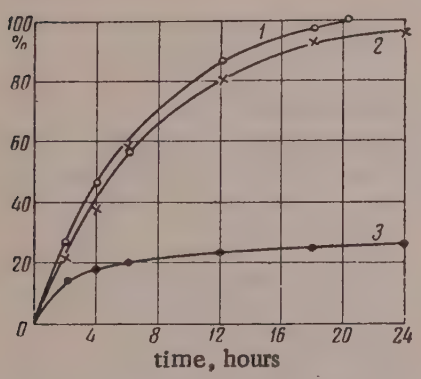


Fig. 5. Kinetics of leaching of aluminum hydroxide from vulcanizates. Filler formed in the latex. Loading: 60 weight parts (1); 40 weight parts (2); 20 weight parts (3).

Studies of rubber solubility showed that SKN-26 rubber deposited from latex without filler is 45.3% soluble in chlorobenzene. The same rubber, deposited from latex together with aluminum hydroxide (60 weight parts per 100 weight parts of rubber), is only 21.2% soluble in chlorobenzene. This solubility decrease indicates that the rubber has undergone structural changes. Evidently a certain number of bonds is formed between the polymer molecules by the action of heat during drying. It is interesting to note that the solubility of SKN-26 rubber in chlorobenzene after extraction of the filler diminishes with increase of the temperature at which the rubber-filler system is dried:

Drying temperature of the system SKN-26 rubber + 60 wt. parts of aluminum hydroxide	100°	120°	150°
Solubility of rubber in chlorobenzene after extraction of filler, %.	23.7	21.2	16.2

Consequently, increase of the drying temperature favors structure formation in SKN-26 rubber.

According to the data in [8], heat treatment of rubber-filler systems tends to increase the number of bonds between the filler and the rubber. Our results and the data in [9] indicate that increase of the drying temperature of rubber-filler systems from 100 to 150° gives vulcanizates of higher strength but with lower relative elongation.

Mixes based on SKN-26 rubber obtained after complete extraction of aluminum hydroxide from it (60 weight parts of filler) give vulcanizates of higher strength than unfilled vulcanizates based on ordinary SKN-26 rubber deposited from latex. The tensile strength of the vulcanizates was 45 kg/cm^2 (relative elongation 480%) in the former case, and 31 kg/cm^2 (relative elongation 510%) in the latter. The rubbers were dried at 120°.

The higher strength of vulcanizates based on rubber after extraction of the filler also indicates that rubber may be structurized by the action of aluminum hydroxide, with formation of bonds directly between the polymer molecules during heat treatment of the rubber-filler system. This is consistent with the data presented above on the solubilities of rubbers.

SUMMARY

1. Aluminum hydroxide may be removed partially or completely from rubber mixes and vulcanizates based on SKN-26 rubber by the action of boiling dilute NaOH solutions.

2. The degree and rate of extraction of the filler depend on its concentration and on the manner in which it is introduced into the rubber.

3. The nature of the bonding and structure in rubber mixes containing aluminum hydroxide is discussed.

LITERATURE CITED

1. B. Dogadkin, K. Pechkovskaya, and L. Chernikina, Kolloid. Zhur. 8, 31, (1946); B. Dogadkin, K. Pechkovskaya, and M. Dashevskii, Kolloid. Zhur. 10, 357 (1948); K. Pechkovskaya, P. Mil'man, and B. Dogadkin, Kolloid. Zhur. 14, 250 (1952);* B. Dogadkin, K. Pechkovskaya, and Ts. Mil'man, Kolloid. Zhur. 14, 346 (1952);* B. Dogadkin, and A. Lukomskaya, Proceedings of the 3rd All-Union Conference on Colloid Chemistry [in Russian] (Izd. AN SSSR, 1956) p. 363.
2. B. Dogadkin, K. Pechkovskaya, and E. Gol'dman, Kauchuk i Rezina, No. 8 (1957).
3. V. A. Shvetsov, et al., Kolloid. Zhur. 22, 233 (1960).*
4. V. A. Shvetsov, A. P. Pisarenko, and A. S. Novikov, Kauchuk i Rezina, 12, 4 (1959); V. A. Shvetsov, A. S. Novikov, and A. P. Pisarenko, Kauchuk i Rezina, 4, 12 (1960).
5. Braber, Kautschuk and Gummi No. 7 (1951); Garten, Nature 173, 997 (1954).
6. F. Menadue, India Rubber J. 109, 711 (1945).
7. F. Endter, Kautschuk und Gummi 5, 17 (1952).
8. A. F. Blanchard and D. Parkinson, Ind. and Eng. Chem., 4, 799 (1952).
9. A. P. Emel'yanov, Candidate's Dissertation [in Russian] (Mosk. Tekh. Inst. Legkoi Prom.).

* Original Russian pagination. See C. B. translation.

PARTICLE-SIZE DISTRIBUTION OF THE DISPERSE PHASE IN A POLYDISPERSE AEROSOL SYSTEM

M. M. Yakubovich

Translated from Kolloidnyi Zhurnal, Vol. 22, No. 6, pp. 748-751,
November-December, 1960
Original article submitted December 18, 1958

Regardless of the method whereby a mist (aerosol) is formed, a polydisperse system is always obtained, and therefore dispersion is characterized by the particle-size distribution of the liquid. However, determination of such distribution presents considerable difficulties because of the low stability of aerosol systems, especially at high weight and particle concentrations. Artificial stabilization of the system by means of dilution inevitably disturbs the initial distribution and complicates the problem.

The following symbols are used in our theoretical analysis of the problem: R, droplet radius; H, height of the aerosol layer; c, concentration by weight; N, particle concentration; Q, the volume of dispersed liquid; δ, the density of the aerosol; γ_l, the density of the disperse phase; γ_a, the density of the dispersion medium; t, the time; η, the coefficient of viscosity; V, droplet volume; n, particle concentration determined experimentally. It is also assumed that there are no convection current, evaporation, or isothermal distillation in the aerosol. This condition is satisfied if a liquid of low volatility is used for the experiments.

The weight and particle concentrations as functions of time, c(t) and n(t), were determined by direct experiment. Samples were taken at a certain constant distance H from the upper boundary of the space occupied by the mist. It was assumed that spherical particles of all sizes were initially distributed uniformly in the aerosol volume.

In absence of coagulation, the particle-size distribution function

$$F(R) = dQ/QdR \tag{1}$$

can be determined by Figurovskii's sedimentometric method [1], according to which the relationship between the density of the aerosol and the time and sampling level is given by the equation

$$\delta = \gamma_a + c_0 \frac{\gamma_e - \gamma_a}{\gamma_e} \int_0^R F(R)\, dR. \tag{2}$$

Evidently, at the initial instant $\int_0^\infty F(R)\, dR = 1$. The value of R in Equation (2) is found from the Stokes equation

$$R = 3\sqrt{\frac{H\eta}{2g(\gamma_e - \gamma_a)}}\, t^{-1/2}. \tag{3}$$

At constant height H differentiation of Equation (2) with respect to time, with Equation (3) taken into account, gives

$$\frac{d\delta}{dt} = -\frac{3}{2} c_0 \sqrt{\frac{H\eta}{2g(\gamma_e - \gamma_a)}} \left(\frac{\gamma_e - \gamma_a}{\gamma_e}\right) F(R)\, t^{-3/2}, \tag{4}$$

and hence

$$F(R) = -\frac{2\gamma_e}{\gamma_e - \gamma_a} \frac{1}{c_0} \frac{t}{R} \frac{d\delta}{dt}. \tag{5}$$

Since at the initial instant

$$\delta = \delta_0 = \gamma_a + c_0 \frac{\gamma_e - \gamma_a}{\gamma_e} \tag{6}$$

and, moreover, $c = \delta - \gamma_a$, we finally have for the distribution function

$$F(R) = -\frac{2t}{R} \frac{d}{dt}\left(\frac{c}{c_0}\right). \tag{7}$$

Of no less interest than the particle-size distribution function is the function for numerical distribution of the particles by volume:

$$\Psi(V) = \frac{dN}{NdV}. \tag{8}$$

The volume of liquid dc corresponding to droplets in the radius range between R and R + dR is distributed between dN droplets, such that

$$dN = \frac{dc}{V}, \tag{9}$$

where $V = 4/3\ \pi\ R^3$. From Equation (1), $dc = cF(R)\,dR$ and then

$$dN = cF(R)\,dR/V. \tag{10}$$

Using Equation (7), we have

$$dN = -\frac{2ct}{RV} \frac{d}{dt}\left(\frac{c}{c_0}\right) dR \tag{11}$$

and, substituting V for the variable R,

$$dN = -\frac{c_0 t}{3} \frac{dV}{V^2} \frac{d}{dt}\left(\frac{c}{c_0}\right)^2. \tag{12}$$

Then the function for the numerical distribution of particles by volume is

$$\Psi(V) = -\frac{c_0 t}{3NV^2} \frac{d}{dt}\left(\frac{c}{c_0}\right)^2. \tag{13}$$

Equations (7) and (13) would be valid for an aerosol system in which the weight (and particle) concentration alters only as the result of sedimentation; there would then be a definite functional relationship between variations of the weight and particle concentrations.

In fact, after time t all particles of volume greater than V will have passed through a certain control plane at a distance H from the upper boundary of the aerosol volume; the number of this particle is

$$N_V = N \int_0^V \Psi(V)\, dV, \tag{14}$$

and for the subsequent differential time interval dt

$$dN = N\Psi(V)\, dV. \tag{15}$$

Using Equations (3) and (13), we obtain

$$dN = -\frac{c_0 t^{3/2}}{72\pi}\left[\frac{2g(\gamma_e - \gamma_a)}{\eta H}\right]^{3/2} d\left(\frac{c}{c_0}\right)^2. \tag{16}$$

Then the loss of particles owing to sedimentation is

$$\Delta N = \int_0^t dN = -\frac{c_0}{72\pi}\left[\frac{2g(\gamma_e - \gamma_a)}{\eta H}\right]^{3/2} \int_0^t t^{3/2} d\left(\frac{c}{c_0}\right)^2. \tag{17}$$

A relationship is thus established between the particle and weight concentrations

$$N(t) = N_0 + \frac{c_0}{72\pi}\left[\frac{2g(\gamma_e - \gamma_a)}{\eta H}\right]^{3/2} \int_0^t t^{3/2} d\left(\frac{c}{c_0}\right)^2, \tag{18}$$

where N_0 is the particle concentration at the initial time instant.

Discrepancies are always found if the results of calculations from Equation (18), easily performed by numerical integration, are compared with the results of experimental determinations of the particle concentration n(t). The difference $N(t) - n(t) = \nu(t)$ remains positive and increases continuously with time.

This discrepancy between the calculated and numerical values of particle concentration shows that the loss of aerosol particles is caused not only by sedimentation but also by coalescence or coagulation.

A very approximate qualitative estimate of the coagulation factor may be made by formal application of the Smoluchowski equation [2] for coagulation kinetics:

$$-\frac{dn}{dt} = -kn^2, \tag{19}$$

which gives the coagulation rate constant for our problem:

$$k = \frac{1}{n^2}\frac{d}{dt}[\nu(t)]. \tag{20}$$

This solution is approximate and therefore tentative, because it does not take into account the opposite effect of coagulation on the sedimentation rate of the mist.

A complete solution of the problem of the influence of coagulation on the particle-size distribution of a dispersed liquid must be based on a particle and mass balance for a fixed control plane through which sedimenting particles of different sizes pass and undergo coagulation.

SUMMARY

The discrepancy between the particle concentration calculated by the Figurovskii method and the particle concentration of an aerosol found by direct measurement indicates that coagulation occurs in the system. The extent of this coagulation can be qualitatively assessed from the discrepancy.

LITERATURE CITED

1. N. A. Figurovskii, Sedimentometric Analysis [in Russian] (Izd. AN SSSR, Moscow-Leningrad, 1948).
2. M. Smoluchowski, Collection: Coagulation of Colloids [Russian translation] (ONTI, Moscow, 1936).

PRODUCTION OF PERIODIC (BANDED) PRECIPITATES ON FILTER PAPER BY MEANS OF IONOPHORESIS

Stoico Jancov

Institute of National Economy, Varna, Bulgaria
Translated from Kolloidnyi Zhurnal, Vol. 22, No. 6, pp. 752-755,
November-December, 1960
Original article submitted June 5, 1959

Banded precipitates have been the subject of numerous investigations; their formation has been studied not only on glass plates but also on paper [1-4]. In this paper we describe a new method for production of banded precipitates on filter paper; here natural diffusion of ions on the paper surface is replaced by ionophoresis induced by a direct current of low strength.

Paper filters of moderate density and 9 cm in diameter were used. The surface of the filter paper was covered uniformly with 1 ml of 4% gelatin or agar solution containing a known amount of internal electrolyte. After 15 minutes of drying and film formation the filter paper was placed on a copper ring 8.5 cm in external and 7 cm in internal diameter. The copper ring was connected to one pole of a direct-current source (for example, a storage battery). One drop (0.02 ml) of a solution of the external electrolyte was placed in the exact center of the filter paper by means of a micropipet. The tip of a platinum wire electrode was immersed in the spherical drop. A milliammeter and a rheostat were connected in series in the circuit. The best results were obtained at 5-10 ma.

Formation of banded precipitates started immediately when the current was switched on. Usually two or three bands could be distinguished on the filter paper within 5 minutes. The high rate of precipitation made it possible to observe the course of formation of banded precipitates in a short time.

The experiments were carried out with the following systems: $AgNO_3$-$K_2Cr_2O_7$; $CuSO_4$-NaOH; $AsCl_3$-Na_2S; $SbCl_3$-Na_2S; $SnCl_2$-Na_2S; $Hg_2(NO_3)_2$-$K_2Cr_2O_4$.

A gelatin solution was used to form the film on the paper in every case, with the exception of the $CuSO_4$-NaOH system, when an agar solution was used.

More detailed experiments were carried out with the systems: $AgNO_3$-$K_2Cr_2O_7$ and $CuSO_4$-NaOH. In the experiments with $AgNO_3$-$K_2Cr_2O_7$ the best results were obtained with 4% gelatin solution, with 0.1 N $AgNO_3$ solution as the external electrolyte, and 0.1-0.5% $K_2Cr_2O_7$ solution as the internal electrolyte. The weighed potassium dichromate was first dissolved in water and gelatin was then added. Experiments with solutions of lower and higher dilutions than those indicated above were carried out with the $AgNO_3$-$K_2Cr_2O_7$ system. The band formation was relatively less distinct and uniform when $K_2Cr_2O_7$ solution was used as the external and $AgNO_3$ solution as the internal electrolyte. In this case the gelatin film soon became dark owing to reduction of $AgNO_3$ by the action of light. Similar broad dark bands at the film edge and between the precipitate bands were also formed when more highly concentrated $AgNO_3$ solutions (1 and 2 N) were used as the external electrolyte.

Banded precipitation in the $AgNO_3$-$K_2Cr_2O_7$ system was most effective if the filter paper was first impregnated with 0.1 N NaOH solution, and the gel film containing the internal electrolyte was applied after that. In experiments without impregnation with NaOH the bands broke rapidly and most of the precipitate dissolved.

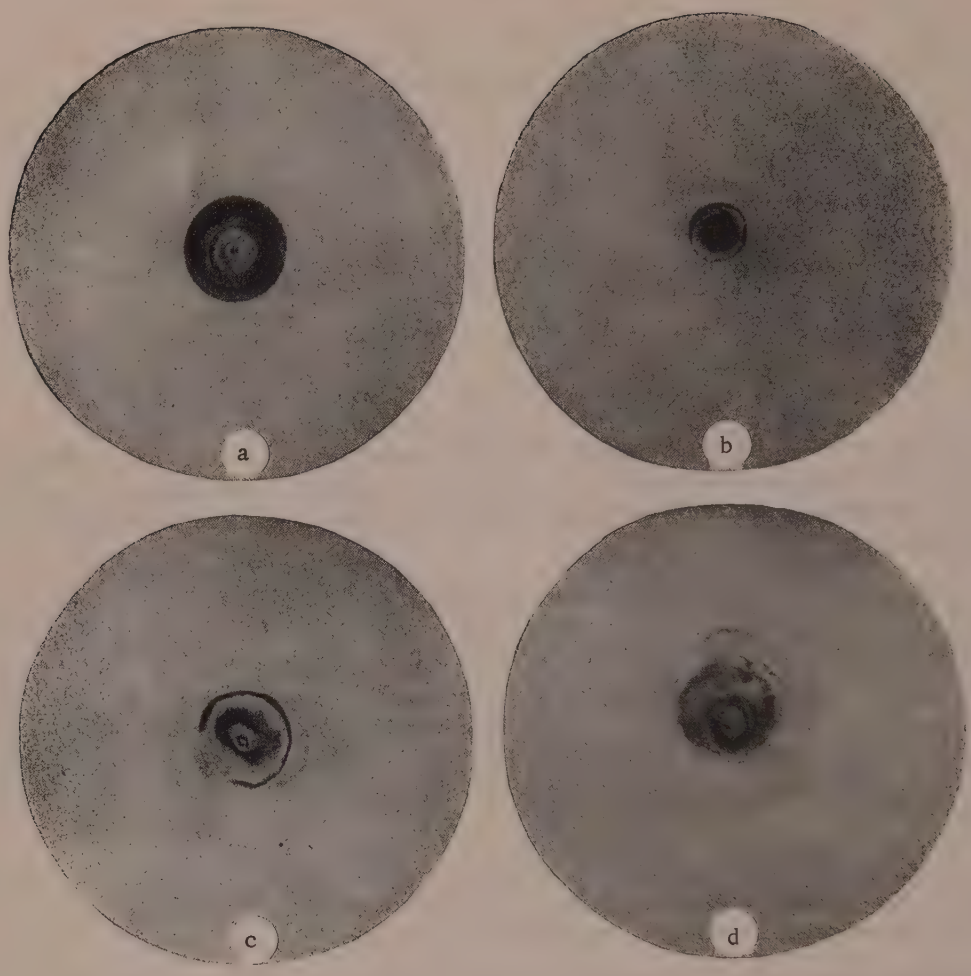


Fig. 1. Banded precipitates from $AgNO_3$ and $K_2Cr_2O_7$ solutions: a) 2 N $AgNO_3$ and 0.1% $K_2Cr_2O_7$, current on for 5 minutes; b) 0.1 N $AgNO_3$ and 0.1% $K_2Cr_2O_7$, current on for 5 minutes; c and d) same, current on for 1 hour.

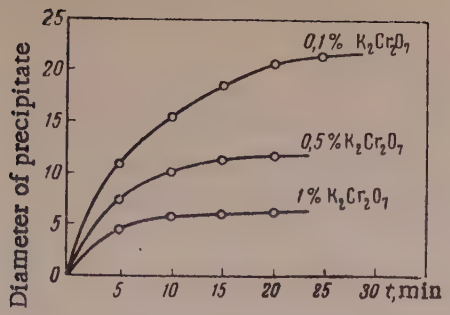


Fig. 2. Variation of the diameters of banded precipitates (in arbitrary units) with the time of passage of the current, at various concentrations of the internal electrolyte.

Figure 1, a shows precipitates formed from 2 N $AgNO_3$ solution, 0.1% $K_2Cr_2O_7$ solution, and 4% gelatin solution with the current on for 5 minutes. Figure 1, b shows the results of an experiment with 0.1 N $AgNO_3$ solution, 0.1% $K_2Cr_2O_7$ solution, and 4% gelatin solution with the current on for 5 minutes; Fig. 1, c and d shows results with the same solutions but after the current had been on for one hour. The colors of the banded precipitates in these experiments depended on the silver nitrate concentration. Bands of different colors were obtained with $AgNO_3$ solutions. For example, the bands shown in Fig. 1, a had the following colors (from the center): orange, red, orange, and red-brown; with 0.1 N $AgNO_3$ solution the precipitates were brick red.

In control experiments with 4% gelatin, 0.1 N $AgNO_3$ (external electrolyte), and 0.1-0.5% solutions of $K_2Cr_2O_7$ (internal electrolyte) without application of direct current (in absence of ionophoresis) dark brown spots roughly circular in shape, without distinct banding, were formed on the paper.

In experiments with $CuSO_4$-NaOH the filter paper was impregnated with 1 ml of 1 N $CuSO_4$ solution and then coated with a uniform layer of 0.7% agar solution. After 15-20 minutes the filter was fixed on the copper ring and 0.02 ml of NaOH solution was placed in the center from a micropipet. The experiments were performed with both 1 N and 2 N NaOH solutions. In the experiments with $CuSO_4$-NaOH the copper ring was connected to the positive pole and the platinum electrode to the negative pole. The experiments were performed at 5.5 v and 5-10 ma. With a current of 50 ma frothing occurred near the platinum electrode and the bands became broken. With the electric current passed for 5 minutes the banded precipitates consisted of three or four bands, usually of different colors. For example, the band nearest the cathode was pale blue, the next was a faded blue, and the third and fourth were pale blue with a greenish tinge.

Similar banded precipitates were obtained with the other systems named above. The most distinct bands were obtained in the experiment with $Hg_2(NO_3)_2$-$K_2Cr_2O_7$, in which the internal electrolyte was 0.1 N $Hg_2(NO_3)_2$ and the external electrolyte was 0.1% $K_2Cr_2O_7$. Three bands were formed: the first black (owing to liberation of metallic mercury) and the others red.

Rate of formation of banded precipitates. Variations of the formation rate of banded precipitates with current strength, time, gelatin concentration, and properties of the external and internal electrolytes were studied. Variations of precipitate diameter with time are shown in Fig. 2, and with concentrations of gelatin and internal electrolyte, in Fig. 3. The diameter of the precipitates increases rapidly at the start of the experiments (usually during the first 5 minutes), after which their growth slows down. As the gelatin concentration is increased the colors of the rings become much less intense and the distances between the rings diminish. For example, the distance between the rings was 3-4 mm in experiments with 4% gelatin, and not more than 2 mm with 8% gelatin. Similar weak stratification is observed if the external electrolyte is used at higher concentrations; for example, with 2 N $AgNO_3$ in the system $AgNO_3$-$K_2Cr_2O_7$ (Fig. 1, a).

In some experiments the ring diameters increased at higher concentrations of the external electrolyte. With the system $CuSO_4$ + NaOH, with 1 N NaOH solution (current strength 10 ma, duration 10 min), the diameter of the outer ring was 15 mm, whereas in the same system under the same conditions but with 2 N NaOH solution the diameter of the outer ring was 18 mm. The rate of diametric growth of banded precipitates decreases with increasing concentration of the internal electrolyte, and the stratification itself is weak and irregular.

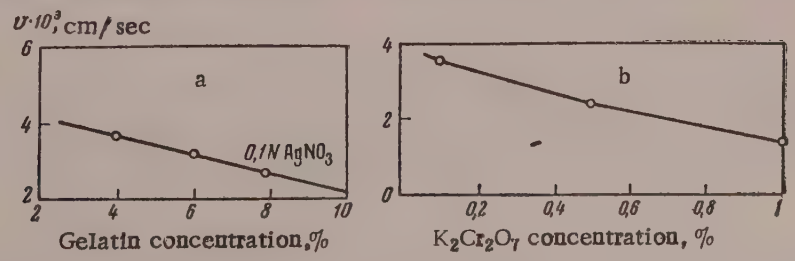


Fig. 3. Rate of diametric growth (v, cm/sec) of banded precipitates: a) At different gelatin concentrations; b) at different concentration of the internal electrolyte.

The current strength has a strong influence on the rate of growth of the bands. If the current strength is increased from 10 to 20 ma the growth rate in the system $AgNO_3$-$K_2Cr_2O_7$ is increased nearly 5-fold during the first minute. However, this increase is accompanied by disintegration of the rings with formation of irregular shapes.

SUMMARY

1. Well-defined banded precipitates can be obtained within a few minutes on paper impregnated with gelatin or agar solutions by application of direct current of low strength.

2. The banded precipitates grow rapidly in diameter during the first few minutes after the current has been switched on, and the growth then gradually slows down.

3. Increase of current strength increases the diametric rate of growth of the precipitates, but it also makes them discontinuous and disperses them.

4. Increases in the concentrations of gelatin and the internal electrolyte reduce the growth rate of the precipitates.

5. It was found in experiments with $CuSO_4$-NaOH that the rate of growth of the precipitates increases with increasing concentration of the internal electrolyte.

LITERATURE CITED

1. DeLoach, School Sci. and Math, No. 8, 56, 1956.
2. A. C. Chatterji, Hary Bhahwan, J. Coll. Sci 13, 232, 1958.
3. G. Cetini, F. Ricca, J. chim. phys. et phys. chim. biol. 55, No. 4, 323, 1958.
4. M. Milone, G. Cetini, F. Kicci, J. chim. phys. et phys. chim. biol. 55, No. 4, 320, 1958.

LETTERS TO THE EDITOR

PLASTICIZER–FILLER INTERACTION

M. P. Zverev and P. I. Zubov

Institute of Physical Chemistry, Academy of Sciences of the USSR
M. V. Lomonosov Institute of Fine Chemical Technology, Moscow
Translated from Kollodinyi Zhurnal, Vol. 22, No. 6, pp. 756-757,
November-December 1960
Original article submitted May 17, 1960

It was shown earlier [1] that filled vulcanizates of butadiene-styrene rubber have higher mechanical strength in presence of polar plasticizers than in presence of nonpolar plasticizers. Data on the sorption of rubber macromolecules in various plasticizers on the surface of gas channel black indicated that the cause of this effect lies in the shielding of active groups, present on the surfaces of the filler particles, by polar groups of the plasticizer. To verify this hypothesis we measured the heats of interaction (wetting) of carbon blacks with plasticizers of various polarities.

The fillers used were a gas channel black with specific surface 110 m^2/g, containing 4.8% oxygen, and a gas channel black with specific surface 100 m^2/g, heated at 900° in a current of hydrogen and free from oxygen-containing groups.

The specific surfaces of the carbon blacks were determined from the amounts of phenol adsorbed. The polarities of the plasticizers were estimated from their dipole moments, determined in benzene solutions at 25° by the method of beats. The dielectric polarizations were extrapolated to infinite dilution by the Hedestrand method. The heats of plasticizer-filler interaction were measured in an adiabatic calorimeter [2]*.

The table gives the heats of wetting of the fillers by plasticizers differing in their dipole moments.

Plasticizer	Dipole moment of plasticizer, debyes	Heats of wetting of blacks, cal/m^2	
		channel	channel, heated in H_2 at 900°
Ditolylmethane	1,33	0,036	—
Dicumylmethane	1,45	0,035	0,036
Dibutyl sebacate	2,48	0,050	0,034
Dibutyl phthalate	2,88	0,055	0,034

The table shows that the heat of wetting of gas channel black by polar plasticizers (dibutyl sebacate, dibutyl phthalate) is approximately double the heat of wetting by nonpolar plasticizers. Therefore introduction of polar plasticizers makes the surface of gas channel black hydrophobic; as was shown earlier [1], this increases the adsorption of butadiene-styrene macromolecules on the filler surface.

*We take this opportunity to thank N. V. Mikhailov and E. Z. Fainberg for their kind help in the thermochemical experiments.

It also follows from the table that the heats of wetting of fillers without functional groups are almost independent of the dipole moment of the plasticizer. These results lead to the conclusion that the better mechanical properties of filled butadiene-styrene rubbers in presence of polar plasticizers are due to shielding of the functional groups of the carbon black by the polar molecules of the plasticizers. We believe that this fact is of interest in relation to the problem of production of oil-filled butadiene-styrene rubbers.

LITERATURE CITED

1. M. P. Zverev, E. A. Eroshkina, and P. I. Zubov, Kolloid. Zhur. 20, 329 (1958).*
2. S. M. Skuratov, Kolloid. Zhur. 9, 133 (1947).

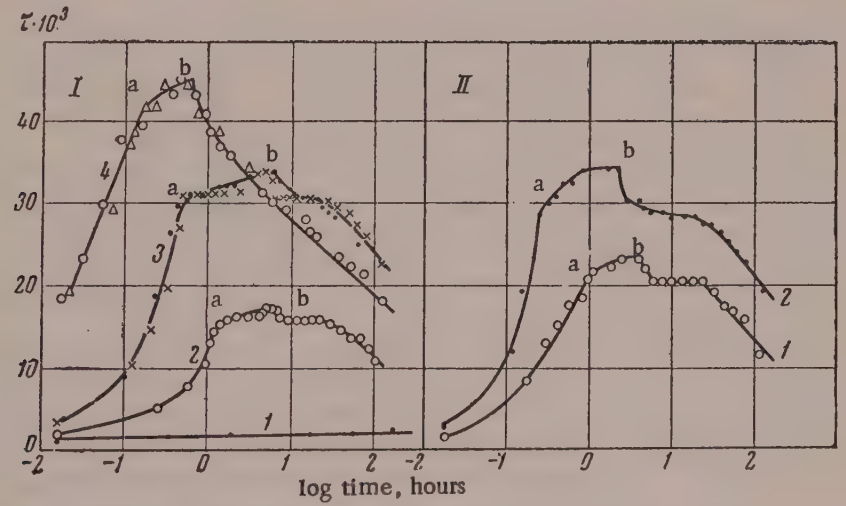
*Original Russian pagination. See C. B. translation.

KINETICS OF TURBIDITY VARIATIONS IN DILUTE SYNTHETIC LATEXES DURING COAGULATION BY ELECTROLYTES

R. É. Neiman and O. A. Lyashenko
Chemistry Faculty, Voronezh University
Translated from Kolloidnyi Zhurnal, Vol. 22, No. 6, pp. 757-759,
November-December, 1960
Original article submitted July 8, 1960

We used the light-scattering method for investigating globule agglomeration and slow coagulation of dilute synthetic latexes on addition of electrolyte.

Different electrolytes ($CaCl_2$ or NaCl) were added to nondialyzed SKS-30-AR butadiene-styrene latex (with Nekal as emulsifier) after 10^4-fold dilution, and the variations of turbidity with time were observed up to complete coagulation of the latex. The turbidity was measured by use of the NFM nephelometer. The concentration gradient of the refractive index was determined with the IRF-23 refractometer. Kinetic curves for the turbidity variations of one latex sample* are given in the diagram. Duplicate experiments gave good reproducibility.



Kinetics of turbidity variations in dilute latex: I) Additions of $CaCl_2$ (mM/liter): 1) Without electrolyte (not coagulated); 2-0.5; 3-2.3; 4-9.0. II) Additions of NaCl (mM/liter; 1) 8.5; 2) 17.5.

Addition of electrolyte causes agglomeration of the globules. However, after some time the increase of turbidity, indicative of this agglomeration, slows down sharply (points a in figures). This retardation evidently occurs because the primary contacts between the globules are effected at regions of the surface which are not

*Properties of the sample: dry residue 14%; pH 10; surface tension 43 dynes/cm; 70% saturation of the globule surfaces with emulsifier; mean globule radius (from turbidity data) r = 19 mμ.

protected by the emulsifier. The consequent increase of surface saturation with the emulsifier during aggregation of the globules leads to formation of a saturated adsorption-solvation layer, and this determines the end of the first stage of the process. The subsequent coagulation is slower (regions a-b on the curves) because the potential barrier associated with the protective action of this layer must be overcome. This may be a general characteristic of latex coagulation, and the coagulation stage the course of which depends on the structural and mechanical properties of the adsorption-solvation layer formed by the emulsifier is inevitable even with latexes in which the initial saturation of the globule surfaces with emulsifier is relatively low.

	$CaCl_2$				NaCl	
Electrolyte concentration, mM/liter	0,5	1,6	2,3	9,0	8,5	17,5
Duration of primary agglomeration, min	100	60	33	9	72	31
Radius of primary agglomerates (from points a), mμ	44	52	52	58	45	52
Duration of second coagulation stage, min	340	—	300	15	180	120

The table shows that primary agglomeration is accelerated with increasing concentration of the added electrolyte, and the primary aggregates formed are larger. The explanation is that the degree to which the electrolyte influences the state of the adsorption-solvation layer depends on the electrolyte concentration; increase of the latter evidently tends to lower the potential barrier of the solvation layer. The observed decrease of turbidity (beyond the points b on the curves) occurs because the coagulated dispersion floats up onto the surface.

Similar results were obtained with several other samples of this latex.

CAUSES OF GELATION IN RUBBER LATEXES

D. M. Sandomirskii and I. D. Pil'menshtein

M. V. Lomomosov Moscow Institue of Fine Chemical Technology
Translated from Kolloidnyi Zhurnal, Vol. 22, No. 6, pp. 759-761,
November-December, 1960
Original article submitted May 30, 1960

Interaction of rubber latexes with electrolytes leads either to coagulation or to gelation, depending on the conditions. The cause of gelation is usually held to be slow and incomplete destabilization of the rubber globules, occurring over only a part of the globule surfaces, which leads to formation of network structures consisting of chains of adhering globules, with serum in the interstices [1,2]. Such destabilization may occur in slow formation of destabilizing ions in the latex [1], or in diffusion of such ions from the form surface [2,3]. In contrast to this, when coagulation occurs (for example, when a suitable electrolyte solution is added to the latex) the globules are destabilized over their entire surfaces and cohere to form a dense coagulum.

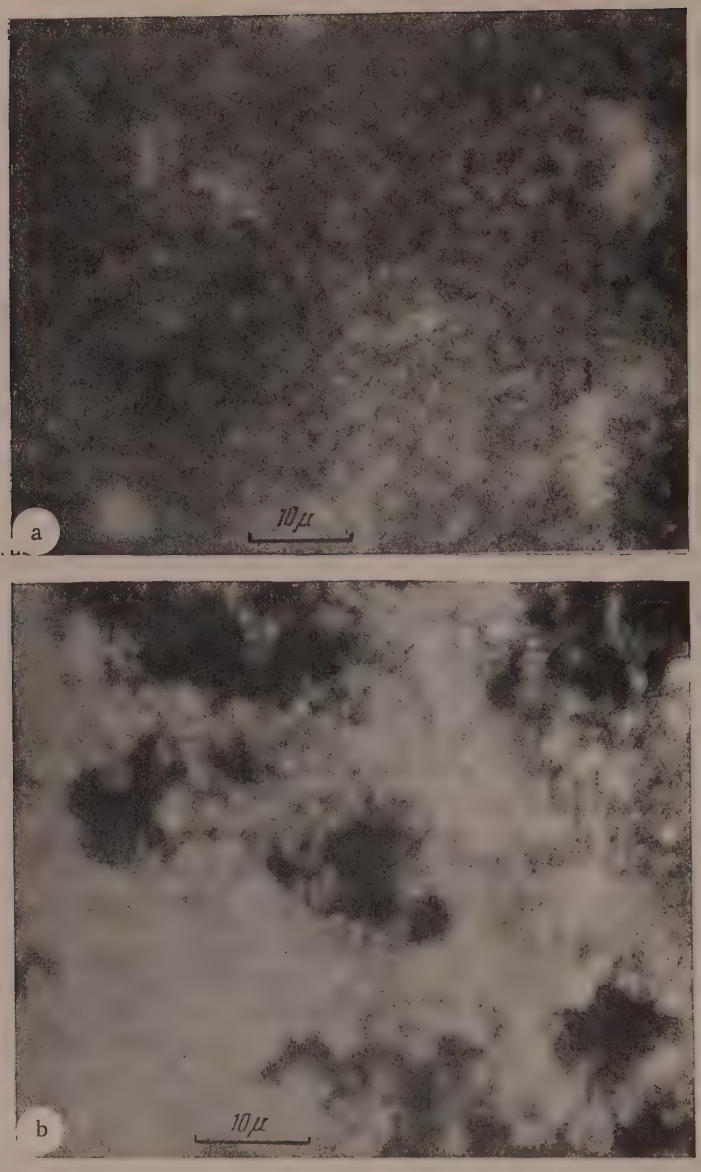
This explanation of gel formation is evidently based on the assumption that the degree of destabilization of the globules, and accordingly the proportion of the surface by which they can cohere, is proportional to the amount of electrolyte introduced into the latex by one method or another. However, this assumption is inconsistent with existing experimental data. For example, a well-known method for estimating the stability of a latex is determination of its coagulation threshold, which is the minimum amount of electrolyte required to cause coagulation [4]. If less electrolyte is added, neither coagulation nor gelation occurs.

We have made an attempt to carry out visual observations of the processes taking place in the course of gelation in natural latex on addition of zinc oxide paste in presence of ammonia. In distinction from other workers [1,5], we used high magnifications (950 and 1340) and the method used (observation in reflected light) made it possible to distinguish clearly both the latex globules and the zinc oxide particles. The MKU-1 apparatus for micromotion photography at 950 magnification was used to obtain a motion film in which individual stages of latex gelation could be observed.

Two frames from this film show that a coagulum grows around each zinc oxide particle as the result of surface formation of zinc-ammonium ions and diffusion of these ions into the latex. After some time (which depends on the number of coagulation centers, temperature, latex concentration, etc.) this growth leads to a formation of a spatial network throughout the whole volume of the latex; this network consists primarily of ordinary coagulum and not of chains of globules joined at individual points.

Therefore in our view the distinction between a gel and a coagulum in a rubber latex lies in the structure of the system formed and not in the nature and degree of globule destabilization. In ordinary coagulation, when an electrolyte solution is added to the latex, the coagulation centers are molecularly dispersed throughout the latex and a continuous coagulum is formed. In gelation, which is always effected by substances of low water solubility which are added to the latex or are formed in it, and which serve as the source of destabilizing ions, the coagulation centers are relatively far apart, so that a network and not a continuous coagulum is formed.

In ionic deposition the latex first comes into contact with the layer of electrolyte solution on the form, and a layer of coagulum is produced around the latter [6]. The electrolyte then diffuses through this layer, apparently at different rates in different points; as a result the coagulation centers are distributed irregularly and



Micrograph frames showing natural latex in the course of gelation (light spots are zinc oxide particles). a) Initial stage; b) final stage.

at some distances apart, and a coagulum network is formed. In systems used in practice this irregularity is increased still further by the use of electrolyte solutions containing various powders such as kaolin, silica, etc.

The fact that a coagulum of the network type (gel) has a looser structure than an ordinary coagulum explains why much more of the protective substance in the latex is bound in the course of gelation than in coagulation [7]. The gel formed is not an obstacle to ion migration [8], and the zinc-ammonium ions can diffuse to any point on the globule surface and interact with all the protective substance. Ordinary rapid coagulation gives rise to a very dense coagulum which is a substantial obstacle to diffusion of the electrolyte ions.

LITERATURE CITED

1. S. S. Voyutskii and B. V. Shtarkh, Physical Chemistry of Film Formation from Polymer Dispersions [in Russian] (Gizlegprom, Moscow, 1954) p. 132.
2. D. M. Sandomirskii and V. V. Chernaya, Trudy Nauch-Issl. Inst. Rezinovoi Prom. 1, 20 (1954).
3. D. M. Sandomirskii and M. K. Vdovchenkova, Kolloid. Zhur. 21, 132 (1959).*
4. B. A. Dogadkin and B. M. Kovarskaya, Kauchuk i Rezina, 1, 33 (1938); V. N. Reikh and B. A. Fainberg, Methods of Technical Quality Control of Synthetic Rubbers and Latexes [in Russian] (Goskhimizdat, Moscow-Leningrad, 1951) p. 201.
5. G. Van Nederveen, and K. Houwink, Chem. Weekblad. 37, No. 1902, 122, 1940.
6. D. M. Sandomirskii and B. Korsunskii, Kauchuk i Rezina (in press).
7. D. M. Sandomirskii and M. Vdovchenkova, Kolloid. Zhur. 22, 69 (1960).*
8. D. M. Sandomirskii, V. Fogel', L. Khazen, and Hu Yu-mu, Kauchuk i Rezina (in press).

*Original Russian pagination. See C. B. translation.

NORMAL STRESSES IN COLLOIDAL STRUCTURIZED SYSTEMS AND THE EFFECT OF THIXOTROPIC STRUCTURE RESTORATION ON THEM

A. A. Trapeznikov, A. S. Morozov, and G. G. Petrzhik

Laboratory of Oleocolloids and Monolayers, Institute of Physical Chemistry, Academy of Sciences of the USSR, Moscow

Translated from Kolloidnyi Zhurnal, Vol. 22, No. 6, pp. 761-762, November-December, 1960
Original article submitted September 27, 1960

Weissenberg [1] was the first to draw attention to the special role of the normal stresses which arise in shear in liquid colloidal systems [1]. They were subsequently studied by numerous workers, who used the method of shear in cone-disk, disk-disk gaps, etc. [2,3]. The stage of steady fluid flow was studied.

In conjunction with a special study of the initial deformation stage in colloidal systems and of the consequent elastic deformation and strength characteristics [4], we developed a technique for investigating normal and shearing stresses in the intial and transitional deformation stages of the system from the state of rest to steady flow [5]. A cone-disk system was used, with measurements of the vertical displacement and rotation of the disk with the aid of capacity transducers, the curves being recorded by means of an electronic potentiometer or oscillography. The forces in the dynamometers were calculated from these displacements.

Aluminum naphthenate gel and natural-rubber solutions were investigated. It was found that when the velocitygradients are not too low stress maxima are found on both the tangential and the normal stress curves; in every case the normal-stress maximum corresponds to deformations which are approximately double the deformations corresponding to the tangential stress maximum (structural strength P_r). In addition, in the case of aluminum maphthenate second maxima of the normal and tangential stresses were found at similar values of ϵ. There is reason to believe that second maxima may also be found for certain rubber solutions.

Relative shearing deformation ϵ	Normal stress P_n, dynes/cm², after different periods of thixotropic structure restoration						Relative shearing deformation ϵ	Normal stress P_n, dynes/cm², after different periods of thixotropic structure restoration					
	2 min	10 min	30 min	1 hr	3 hr	18 hr		2 min	10 min	30 min	1 hr	3 hr	18 hr
20	1020*	—	—	—	—	—	1400	660	850	1200	1550	2300	—
40	970	1610*	—	—	—	—	2000	640	830	1060	1500	2560	2600
80	820	1400	2700*	3980*	—	—	2800	600	780	1040	1260	2500	—
100	765	1300	2500	3800	5970*	5800*	3500	600	740	950	1100	2050	2000
200	700	1100	2000	2500	4500	—	5000	600	710	810	880	1380	1440
400	700	980	1370	1630	2520	2500	8000	600	700	720	800	1000	1000
800	700	870	1250	1600	2100	2030							

*Points on the first ascending branch of the P_n (ϵ) curve are not given, as a three-point automatic potentiometer was used for the recording; with this instrument the time required for traverse of the slider is comparable with the time needed to reach the first maximum.

The fact that the first and second normal-stress maximum for the naphthenate gel are both directly associated with breakdown of the gel structure is confirmed by the values of the $P_n(\epsilon)$ stresses determined for different periods of rest of the system after it has been deformed to the stage of steady flow.

The table gives values of the average normal stresses P_n (dynes/cm^2) for a 2% aluminum naphthenate gel in petrolatum, determined for different rest times τ_{rest} at a velocity gradient $\dot{\epsilon} = 8.75$ sec^{-1}.

The shearing stresses which were recorded simultaneously also reveal the corresponding thixotropic changes, in agreement with earlier results [4].

LITERATURE CITED

1. K. Weissenberg, Proc. I-st Intern. Congr. Rheology, Amsterdam, 1, 29, (1948).
2. N. Pilpel, Trans. Faraday Soc. 50, 1369 (1954).
3. A. Jobling, I. E. Roberts, Rheology, Theory and Applications, Ed. F. R. Eirich, II, N. Y., (1958) p. 503, v. 2.
4. A. A. Trapeznikov, Vestnik Akad. Nauk SSSR, 6, 70 (1960).
5. A. A. Trapeznikov, A. S. Morozov, and G. G. Petrzhik, Doklady Akad. Nauk SSSR 138, 637 (1960).*

*Original Russian pagination. See C. B. translation.

–INDEX–

COLLOID JOURNAL

VOLUME 22, NUMBERS 1-6

1960

AUTHOR INDEX — COLLOID JOURNAL

Volume 22, Numbers 1-6, 1960

Andreeva, E. P. - 395
Andreeva, E. P. - 503
Andres, U. Ts. - 145
Angert, L. G. - 1
Aleeva, E. V. - 471
Alekseeva, V. A. - 259
Arkhangel'skaya, M. I. - 267

Barkan, A. S. - 273
Bartenev, G. M. - 177
Berestneva, Z. Ya. - 557
Bol'shakova, Yu. S. - 367
Borodina, G. A. - 461

Chekunov, A. A. - 95
Chernogorenko, V. B. - 107
Chernogorenko, V. B. - 351
Chernogorenko, V. B. - 725
Churaev, N. V. - 535
Churaev, N. V. - 547
Churaev, N. V. - 553
Churaev, N. V. - 631

Danilova, E. P. - 447
Deinega, Yu. F. - 17
Demchenko, P. A. - 283
Demchenko, P. A. - 309
Deryagin, B. V. - 155
Deryagin, B. V. - 227
Deryagin, B. V. - 407
Deryagin, B. V. - 587
Dibrov, G. D. - 447
Dmitrenko, O. I. - 161
Dobychin, D. P. - 255
Dogadkin, B. A. - 267
Dogadkin, B. A. - 577
Dogadkin, B. A. - 661
Dukhin, S. S. - 133
Dukhin, S. S. - 587
Dumanskii, A. V. - 17
Dumanskii, A. V. - 137
Dumanskii, A. V. - 283
Dumanskii, I. A. - 287
Dunskii, V. F. - 167

Éskin, V. E. - 121
Everett, D. H. - 139

Fedortsev, V. F. - 95
Fedotov, Yu. M. - 479
Fel'dman, R. I. - 103
Fel'dman, R. I. - 361
Fel'dshtein, M. S. - 661
Fialkov, A. S. - 239
Fleishman, S. M. - 711
Fodiman, N. M. - 151
Fridrikhsberg, D. A. - 367
Fridrikhsberg, D. A. - 491
Fuks, G. I. - 271
Fuks, G. I. - 715

Gamayunov, N. I. - 535
Gerasimova, N. G. - 491
Gol'berg, I. I. - 261
Gol'din, S. A. - 605
Gorelik, L. V. - 401
Gudkova, T. I. - 649
Gurevich, Ya. M. - 657
Gutkin, A. M. - 543
Gutkin, A. M. - 569
Gutkin, A. M. - 573
Gutman, A. M. - 9
Gzovskii, M. V. - 439
Gzovskii, M. V. - 561

Ivanchov, S. S. - 125
Ivanov, A. I. - 185
Ivanova, N. Ya. - 39
Ivashkin, G. P. - 479

Jancov, Stoico - 745

Karasik, E. É. - 259
Kargin, V. A. - 557
Kavtardze, N. N. - 345
Kazakov, E. M. - 23
Khailenko, L. V. - 287
Khil'ko, G. I. - 701
Khodakov, G. S. - 375
Kim, A. Kh. - 195
Kirdo, M. A. - 351
Kiselev, A. V. - 27
Kiselev, A. V. - 325
Kiselev, A. V. - 345
Kiselev, A. V. - 413
Kiselev, A. V. - 669
Kister, É. G. - 677
Kitaev, G. A. - 23
Kitaev, A. V. - 167
Klimov, K. I. - 471
Konstantinopol'skaya, M. B. - 557
Kontorovich, S. I. - 79
Kontorovich, S. I. - 205
Korchagin, L. V. - 259
Korolev, A. Ya. - 669
Korvaleva, N. V. - 345
Kozarovitskii, L. A. - 649
Krotova, N. A. - 87
Kuridze, L. V. - 455
Kurilenko, O. D. - 293
Kuz'minskii, A. S. - 1

Lepilkina, L. A. - 419
Levi, S. M. - 599
Levitskii, É. A. - 391
Lipatov, S. M. - 637
Lipshits, T. S. - 367
Lishtvan, I. I. - 547
Lukash, A. E. - 265
Lukomskaya, A. I. - 577
Lyashenko, O. A. - 751
Lygin, V. I. - 345
Lygin, V. I. - 413

Maiboroda, V. I. - 233
Malinin, N. I. - 211
Markina, Z. N. - 221
Markina, Z. N. - 467
Medvedeva, A. M. - 227
Metsik, M. S. - 425
Mdivnishvili, O. M. - 605
Minaeva, R. F. - 657
Mikhailov, N. V. - 185
Mikhailov, N. V. - 233
Mikhailov, N. V. - 649
Mikhailyuk, A. S. - 715
Mikhel'son, M. L. - 429
Mokrushin, S. G. - 23
Mokrushin, S. G. - 355
Morachevskii, I. I. - 351
Morozov, A. A. - 435
Morozov, A. S. - 757
Morozova, I. A. - 593
Mukhina, T. S. - 553

Neiman, R. E. - 751
Neimark, I. E. - 265
Nekryach, E. F. - 299
Nekryach, E. F. - 305
Nikolaeva, S. S. - 233
Novikov, A. S. - 45
Novikov, A. S. - 243
Novikov, A. S. - 737

Osokina, D. N. - 439
Osokina, D. N. - 561
Ostrikov, M. S. - 447
Ostroumov, G. A. - 611

Panich, R. M. - 151
Papuashvili, S. N. - 53
Papuashvili, S. N. - 455
Parfenova, E. I. - 249
Pavlov, V. P. - 17
Pavlov, V. P. - 439
Pavlova, G. A. - 161
Pchelin, V. A. - 67
Petrova, S. B. - 267
Petrova, R. S. - 669
Petrzhik, G. G. - 757
Pil'menshtein, I. D. - 753
Piontkovskaya, M. A. - 265
Pisarenko, A. P. - 61
Pisarenko, A. P. - 243
Pisarenko, A. P. - 737
Pogodaev, A. K. - 255
Pogosyan, T. A. - 325
Polak, A. F. - 687
Popkova, L. P. - 491
Poshkus, D. P. - 27

Rebinder, P. A. - 79
Rebinder, P. A. - 205
Rebinder, P. A. - 375
Rebinder, P. A. - 641
Rezvushkin, V. V. - 317
Rostovtseva, I. V. - 447
Rotleider, V. M. - 9
Rozhdestvenskii, D. A. - 461

Samchenko, Z. A. - 299
Samchenko, Z. A. - 305
Sandomirskii, D. M. - 73
Sandomirskii, D. M. - 151
Sandomirskii, D. M. - 753
Segalova, E. E. - 79
Segalova, E. E. - 205
Segalova, E. E. - 221
Segalova, E. E. - 395
Segalova, E. E. - 467
Segalova, E. E. - 503
Serebrenaya, M. F. - 87
Shakhkel'dyan, B. N. - 111
Shalopalkina, T. G. - 729
Shapovalova, A. I. - 61
Shcherbakov, L. M. - 115
Shcherbakova, K. D. - 669
Shishniashvili, M. E. - 53
Shishniashvili, M. E. - 455
Shor, G. I. - 593
Shreiner, S. A. - 491
Shtarkh, B. V. - 243
Shteigel'berg, E. Ya. - 351
Shvetsov, V. A. - 737
Shvetsov, V. A. - 243
Sinitsyn, V. V. - 471
Skrylev, L. D. - 355
Skorodumova, Z. V. - 661
Smilga, V. P. - 615
Sokolov, S. I. - 103
Solomchenko, N. Ya. - 67
Spartakov, A. A. - 701
Starobinets, G. L. - 273
Stavrov, S. N. - 435
Stoklosa, Ezhi - 221
Stoklosa, Ezhi - 467
Stone, F. S. - 139
Storozh, G. F. - 385

Talaev, M. V. - 699
Talmud, S. L. - 479
Tarasova, Z. N. - 267
Temkin, I. V. - 239
Titievskaya, A. S. - 407
Todes, O. M. - 95
Tolstoi, N. A. - 701
Tolstukhina, F. S. - 45
Tolstukhina, F. S. - 177
Toporova, V. P. - 239
Torner, R. V. - 625
Trapeznikov, A. A. - 485
Trapeznikov, A. A. - 729
Trapeznikov, A. A. - 757
Tropin, V. P. - 553
Turzhetskaya, A. N. - 479
Tyutyunnik, R. S. - 265
Ustinova, Z. M. - 151

Vanina, V. I. - 9

Vashchenko, Z. M. - 137
Vdovchenkova, M. K. - 73
Vinogradov, G. V. - 17
Vinogradov, G. V. - 439
Vinogradov, G. V. - 605
Volarovich, M. P. - 195
Volarovich, M. P. - 313
Volarovich, M. P. - 527
Volarovich, M. P. - 535
Volarovich, M. P. - 543
Volarovich, M. P. - 547
Volarovich, M. P. - 553
Volkov, V. A. - 479
Vol'khin, V. V. - 317
Voronkov, G. Ya. - 313
Voyutskii, S. S. - 61
Voyutskii, S. S. - 138
Voyutskii, S. S. - 151
Vybornova, V. Kh. - 407

Yakovkina, E. A. - 293
Yakubovich, M. M. - 741
Yarilova, E. A. - 249
Yastrebova, L. S. - 255
Yurzhenko, A. I. - 39
Yurzhenko, A. I. - 125
Yurzhenko, A. I. - 385

Zakharenko, N. V. - 177
Zakhavaeva, N. N. - 507
Zakoshchikov, A. P. - 9
Zakoshchikov, S. A. - 9
Zaliopo, M. N. - 461
Zaslavskii, Yu. S. - 593
Zenchenko, A. I. - 1
Zherebkov, S. K. - 227
Zhinkin, G. N. - 33
Zolotavin, Z. I. - 317
Zotova, K. V. - 485
Zubov, P. I. - 499
Zubov, P. I. - 749
Zverev, M. P. - 749

COLLOID JOURNAL

Vol. 22, No. 1 January-February, 1960

CONTENTS

	PAGE	RUSS. PAGE
Volatilization of Ingredients from Polymers. L. G. Angert, A. I. Zenchenko and A. S. Kuz'minskii	1	2
A Study of the Adsorption Properties of Hydrolytic Lignin. V. I. Vanina, A. M. Gutman, A. P. Zakoshchikov, S. A. Zakoshchikov and V. M. Rotleider	9	9
Investigation of the Dielectric and Rheological Properties of Plastic Disperse Systems. Yu. F. Deinega, A. V. Dumanskii, G. V. Vinogradov and V. P. Pavlov	17	16
Experimental Investigations of Laminar Systems. 25. Electron-Microscopic Investigation of the Structure and Formation Mechanism of Ultrathin Films of Copper Hydroxide Forming on a Solid Surface. E. M. Kazakov, G. A. Kitaev and S. G. Mokrushin	23	23
Heat and Entropy of Adsorption of Benzene and n-Hexane Vapors on Magnesium Hydroxide A. V. Kiselev and D. P. Poshkus	27	25
Strengthening of Structural Bonds in Clay Soils as the Result of Electrochemical Stabilization. G. N. Zhinkin	33	31
Emulsion Polymerization of Styrene in Presence of Emulsifiers of Different Molecular Weights. N. Ya. Ivanova and A. I. Yurzhenko	39	37
Influence of Fillers on the Properties of Polydimethylsiloxane. A. S. Novikov and F. S. Tolstukhina	45	42
Surface-Chemical Effects and Structure Formation in Askangel Suspensions*. S. N. Papuashvili and M. E. Shishniashvili	53	49
Adhesion of High Polymers. 4. Influence of Mechanical Factors on Adhesion of High Polymers. A. P. Pisarenko, A. I. Shapovalova and S. S. Voyutskii	61	57
Structural and Mechanical Properties of Solutions, Gels, and Coagulates (Coacervates) of Gelatin. V. A. Pchelin and N. Ya. Solomchenko	67	63
Radioactive Tracer Studies of the Gelation of Rubber Latexes. D. M. Sandomirskii and M. K. Vdovchenkova	73	69
Structure Formation During Hydration Hardening of Calcium Oxides of Different Degrees of Dispersion. E. E. Segalova, S. I. Kontorovich and P. A. Rebinder	79	74
Effects of Deformation and Dispersion of Colloidal Systems in the Vicinity of Electrified Surfaces. M. F. Serebrenaya and N. A. Krotova	87	82
Experimental Investigations of the Scattering of Light by a Coagulating Aerosol. O. M. Todes, V. F. Fedortsev and A. A. Chekunov	95	90
States of Aggregation of Compounds of High Molecular Weight. 6. Tensile Characteristics of an Anisotropic Polycaprolactam Film. R. I. Fel'dman and S. I. Sokolov	103	97

CONTENTS (continued)

	PAGE	RUSS. PAGE
Effect of Temperature on Certain Structural and Mechanical Characteristics of Clay Pastes*. V. B. Chernogorenko.	107	101
Influence of Drying Oil on Stabilization of Carbon-Black Suspensions. B. N. Shakhkel'dyan	111	106
Thermodynamics of Thin Liquid Layers. L. M. Shcherbakov	115	111
Effect of the Angle of Scattering on the Second Virial Coefficient of Polymer Solutions, Determined by the Light-Scattering Method. V. E. Éskin	121	117
Influence of Salts of Fatty Acids on Polymerization of Styrene in Emulsion. A. I. Yurzhenko and S. S. Ivanchov.	125	120
Letter to the Editor		
Theory of Drift of an Aerosol Particle in a Standing Acoustic Wave. S. S. Dukhin	133	128
Book Reviews		
Bibliographical Survey of Colloid Chemistry in the USSR [in Russian]. A. V. Dumanskii and Z. M. Vashchenko	137	131
Solutions of High Polymers [in Russian]. S. S. Voyutskii	138	131
The Structure and Properties of Porous Materials. D. H. Everett and F. S. Stone.	139	133

COLLOID JOURNAL

Volume 22, Number 2 March-April, 1960

CONTENTS

	PAGE	RUSS. PAGE
Experimental Study of the Rheological Properties of Highly Disperse Mineral Suspensions. U. Ts. Andres	145	137
Investigation of the Mechanism of Formation of Films From Vulcanized Latex. 2. Formation of Films From SKS-30 ShKhP Butadiene-Styrene Latex. S. S. Voyutskii, D. M. Sandomirskii, N. M. Fodiman, R. M. Panich, and Z. M. Ustinova	151	143
Effect of Diffusion on the Streaming Potential. B. V. Deryagin	155	148
Binding of Water by Finely Divided Sediments. 3. Influence of Adsorbent Structure, Degree of Hydration, and Charges on the Cations Accompanying the Indicator Ion. O. I. Dmitrenko and G. A. Pavlova	161	154
Precipitation of a Unipolarly-Charged Aerosol in an Enclosed Space. V. F. Dunskii and A. V. Kitaev	167	159
Flow of Rubberlike Polymers and Their Mixtures with Carbon Black. N. V. Zakharenko, F. S. Tolstukhina, and G. M. Bartenev	177	168
Structural and Mechanical Properties of Bitumens Oxidized by Different Methods. A. I. Ivanov and N. V. Mikhailov	185	176
Two-Dimensional Problem of the Motion of a Viscoplastic Disperse System Between Two Planes Forming an Acute Angle. A. Kh. Kim and M. P. Volarovich	195	186
Influence of Added Surface-Active Substances on Development of a Crystallization Hardening Structure in Calcium Oxides of Different Degrees of Dispersion. S. I. Kontorovich, E. E. Segalova, and P. A. Rebinder	205	195
The Weissenberg Effect. N. I. Malinin	211	201
Effect of the Dispersity of the Original Plaster on Structure Formation in Hardening of Calcium Sulfate Hemihydrate. Z. N. Markina, E. E. Segalova, and Ezhi Stoklosa	221	211
Investigation of Adhesion Effects in Bonding of Rubber to Metal by "Leukonat" Adhesive. 3. Reaction of Sodium Butadiene Rubber with Triphenylmethane Triisocyanate. A. M. Medvedeva, B. V. Deryagin, and S. K. Zherebkov	227	217
Preparation and Some Properties of Lyophobic Colloidal Forms of Fiber-Forming Polymers. N. V. Mikhailov, V. I. Maiboroda, and S. S. Nikolaeva	233	223

CONTENTS (continued)

	PAGE	RUSS. PAGE
Influence of Vibratory Milling on the Reinforcing Properties of Carbon Black. A. S. Fialkov, I. V. Temkin, and V. P. Toporova	239	229
An Electron Microscope Study of Reinforced-Rubber Structures. V. A. Shvetsov, A. P. Pisarenko, B. V. Shtarkh, and A. S. Novikov	243	233
Investigation of Clay Minerals in Soil Colloids. E. A. Yarilova and E. I. Parfenova	249	237
Influence of the Surface State of Glass on the Pore Structure of Films Produced by Acid Etching on Unstable Glasses. L. S. Yastrebova, A. K. Pogodaev, and D. P. Dobychin	255	243
Letters to the Editor		
Effect of the Thickness of the Support on the Force of Detachment V. A. Alekseeva, E. É. Karasik, and L. V. Korchagin	259	247
Maximum Stress in Deformation at a Constant Rate. I. I. Gol'berg	261	249
Preparation and Adsorption Properties of a Synthetic Zeolite. I. E. Neimark, M. A. Piontkovskaya, A. E. Lukash, and R. S. Tyutyunnik	265	251
Structure and Properties of Vulcanizates from Carboxyl-Containing Polymers Made by the Simultaneous Action of Metal Oxides and Ionizing Radiations. Z. N. Tarasova, B. A. Dogadkin, M. I. Arkhangel'skaya, and S. B. Petrova	267	253
Adsorptional Lowering of the Strength of Quartz and Ruby in Solutions of Neutral Electrolytes. G. I. Fuks	271	256
Nikolai Fedorovich Ermolenko (On his 60th Birthday and Completion of 36 Years of Scientific, Teaching, and Social Activity). G. L. Starobinets and A. S. Barkan	273	259

COLLOID JOURNAL OF THE USSR

Volume 22, Number 3 May-June, 1960

CONTENTS

	PAGE	RUSS. PAGE
A. V. Dumanskii. (On His 80th Birthday).	277	265
Influence of the Structure and Length of Hydrocarbon Radicals in Detergents on their Oleophilic Properties. P. A. Demchenko and A. V. Dumanskii	283	272
Rheological Properties of Glycerol Solutions. I. A. Dumanskii and L. V. Khailenko.	287	277
Study of Equilibrium in the System Starch–Aqueous Alcohols. O. D. Kurilenko and E. A. Yakovkina.	293	282
Sorption of Water Vapor and Heat of Wetting of Certain Polyamides. E. F. Nekryach and Z. A. Samchenko.	299	288
Sorption of Water Vapor and Heat of Wetting of Silica Gels. E. F. Nekryach and Z. A. Samchenko.	305	293
Solubilization of Water in Hydrocarbon Solutions of Lecithin. P. A. Demchenko.	309	297
Electrokinetic Properties of Peat. M. P. Volarovich and G. Ya. Voronkov.	313	301
Effect of Freezing on the Properties of Coagulated Metal Hydroxides. 1. Influence of Freezing and Thawing Conditions on the Properties of Coagulated Ferric Hydroxide. Z. L. Zolotavin, V. V. Vol'khin, and V. V. Rezvushkin.	317	305
Theory of the Corpuscular Structure of Xerogels. I. Preparation of Silica Gels from Large Globules with Different Numbers of Contacts, and Investigation of the Gels by the Adsorption Method. A. V. Kiselev and T. A. Pogosyan.	325	314
Application of the Shadow Method of Determining Optical Heterogeneities to the Investigation of Mass Transfer Across the Surface of Separation of Different Phases.	333	323
Adsorption Properties and Infrared Spectra of Oxidized Carbon Blacks. V. I. Lygin, N. V. Kovaleva, N. N. Kavtaradze, and A. V. Kiselev.	345	334
Relationship between Heat of Wetting, Amount of Bound Water, Hygroscopicity, and Ion Exchange Capacity of Clays. I. I. Morachevskii, E. Ya. Shteigel'berg, V. B. Chernogorenko, and M. A. Kirdo.	351	340
Extraction of Colloidally Dissolved Mixed Ferrocyanides of Heavy Metals from their Hydrosols by Means of Gelatin Foam. L. D. Skrylev and S. G. Mokrushin.	355	344
States of Aggregation of High Polymers. 7. Influence of Temperature on the State of Keratins. R. I. Fel'dman.	361	351
A Study of the Relationship between Electrical Conductivity and Porosity of Soils. D. A. Fridrikhsberg, Yu. S. Bol'shakova, and T. S. Lipshits.	367	357
Influence of the Medium on Fine Grinding of Solids. G. S. Khodakov and P. A. Rebinder.	375	365
Influence of Primary Aliphatic Alcohols on the Sol–Coagel Transition Temperature in Aqueous Sodium Stearate Solutions. A. I. Yurzhenko and G. F. Storozh.	385	376
Determination of the Sign of the Charge of Colloidal Particles in Coagulated Systems by Means of a pH Meter. É. A. Levitskii.	391	382

Volume 22, Number 4 July-August, 1960

CONTENTS

	PAGE	RUSS. PAGE
Investigation of Crystallization Structure Formation in Calcium Hydrochloroaluminate. . . E. P. Andreeva and E. E. Segalova.	395	385
Streaming Potential in Oscillatory Flow of a Liquid in a Porous Diaphragm. L. V. Gorelik.	401	393
Stability Mechanism of Free Films of Solutions of Surface-Active Substances. B. V. Deryagin, A. S. Titievskaya, and V. Kh. Vybornova.	407	398
Investigation of the Physical Adsorption of Water on Silica Gel with a Hydrated Surface by Infrared Spectroscopy. A. V. Kiselev and V. I. Lygin.	413	403
Study of the Nature of Forms of Moisture Binding in Gelatin and Photographic Emulsions by Infrared Spectroscopy. L. A. Lepilkina.	419	411
Nature of the Interaction Forces Between Structural Parcels (layers) in Mica Crystals. M. S. Metsik.	425	418
Investigation of the Activities of Different Types of Condensation Nuclei. M. L. Mikhel'son.	429	423
Investigation of Cation-Substituted Agar Samples. A. A. Morozov and S. N. Stavrov. . .	435	429
Optical Polarization Study of Plastic Deformation Processes with the Aid of Ethylcellulose Solutions and Gels. D. N. Osokina, M. V. Gzovskii, G. V. Vinogradov, and V. P. Pavlov.	439	434
Influence of Capillary Contraction Forces on Mechanical Properties and Structure of Drying Bodies. M. S. Ostrikov, I. V. Rostoytseva, G. D. Dibrov, and E. P. Danilova. . . .	447	443
Exchangeable Acidity in Colloidal Systems of Natural Aluminosilicates. S. N. Papuashvili, M. E. Shishniashvili, and L. V. Kuridze.	455	451
Phase Transitions in Soap and Their Quantitative Determination. D. A. Rozhdestvenskii, M. N. Zaliopo, and G. A. Borodina.	461	458
Supersaturation Kinetics and Tendency to Form Concretion Contacts in Hydration Hardening of the α- and β-Forms of Calcium Sulfate Hemihydrate. E. E. Segalova, Ezhi Stoklosa, and Z. N. Markina.	467	464
Colloidal Stability of Lithium Soap—Oil Disperse Systems. V. V. Sinitsyn, K. I. Klimov, and E. V. Aleeva.	471	469
Solubilization of Sulfite Cellulose Resin and Rosin. S. L. Talmud, A. N. Turzhetskaya, V. A. Volkov, G. P. Ivashkin, and Yu. M. Fedotov.	479	477
Changes of the Damping Decrement and Oscillation Period of a Torsion Pendulum in Two-Sided Soap Films During Their Thinning to Rupture. A. A. Trapeznikov and K. V. Zotova.	485	482
Investigation of Surface Conductivity in the Isoelectric Region. D. A. Fridrikhsberg, N. G. Gerasimova, and L. P. Popkova.	491	489
Influence of Internal Stresses on the Adhesion Properties of Gelatin Films. S. A. Shreiner and P. I. Zubov.	499	497
LETTER TO THE EDITOR		
Kinetics of Structure Formation in Suspensions of Tricalcium and β-Dicalcium Silicates in Presence of Calcium Chloride. E. P. Andreeva and E. E. Segalova	503	503
CURRENT EVENTS		
The 25th Anniversary of the Laboratory of Surface Phenomena of the Institute of Physical Chemistry, Academy of Sciences, USSR. N. N. Zakhavaeva.	507	506

COLLOID JOURNAL

Volume 22, Number 5 September-October, 1960

CONTENTS

	PAGE	RUSS. PAGE
The Scientific Work of Professor Mikhail Pavlovich Volarovich (On the Occasion of His Sixtieth Birthday). The Editorial Board	515	513
The Most Important Scientific Publications of M. P. Volarovich	521	520
Radioisotope Studies of Processes in and Properties of Peat. M. P. Volarovich	527	524
Investigation of Heat and Moisture Conduction in Peat. M. P. Volarovich, N. I. Gamayunov, and N. V. Churaev	535	535
Compression of a Viscoplastic Disperse System in the Form of a Bar of Rectangular Section. M. P. Volarovich and A. M. Gutkin	543	543
Studies of Peat Humin Sols. 1. Structural and Mechanical Properties and the Influence of Additives on Them. M. P. Volarovich, I. I. Lishtvan, and N. V. Churaev	547	546
Electron Microscopy of Peat and its Constituents. M. P. Volarovich, T. S. Mukhina, V. P. Tropin, and N. V. Churaev	553	553
Crystallization Mechanism of Colloidal Titanium Dioxide. Z. Ya. Berestneva, M. B. Konstantinopol'skaya, and V. A. Kargin	557	557
Model Studies of Rheological Processes in Solids Stress Investigation by Optical Polarization Methods. M. V. Gzovskii and D. N. Osokina	561	560
Screw Motion of a Cylinder in a Viscoplastic System. A. M. Gutkin	569	569
Flow of a Viscoplastic Disperse System on a Rotating Disk. A. M. Gutkin	573	573
Possibility of Studying the Structure of Vulcanizates with Carbon Black Fillers by Measurements of Their Dielectric Properties. A. I. Lukomskaya and B. A. Dogadkin	577	576
The Electrical Field of a Moving Uncharged Drop. 2. Theory of the Electrical Field of a Drop Containing a Nonionic Surface-Active Substance. S. S. Dukhin and B. V. Deryagin	587	587
Studies of Electrokinetic Processes and Sedimentation in Disperse Systems by the Radioactive Tracer Method. Yu. S. Zaslavskii, G. I. Shor, and I. A. Morozova	593	593
Investigation of the Structural and Mechanical Properties of Gelatin. S. M. Levi	599	599
Structure Formation in Suspensions of Askangel and its Derivatives. O. M. Mdivnishvili, G. V. Vinogradov, and S. A. Gol'din	605	606
Dependence of the Sedimentation Rate of a Suspension on the Solution Velocity. G. A. Ostroumov	611	611
Theory of Colloid Heterocoagulation in Complex Solutions of Electrolytes. V. P. Smilga	615	615
Application of the Similarity Principle to Determination of Inlet Effects in Flow of Rubber Stocks Along Ducts of Circular Section. R. V. Torner	625	625
Use of Radioactive Isotopes for Studying Moisture Transport in Peat. N. V. Churaev	631	631
LETTER TO THE EDITOR		
Phase Separation in the System: Polymer–Polymer–Solvent Volumes of the Layers and Molecular Weights of the Polymers. S. M. Lipatov	637	639

CONTENTS (continued)

	PAGE	RUSS. PAGE
BOOK REVIEW		
"New Physical Methods for Investigation of Peat." Collected Papers of the Kalinin Peat Institute, edited by M. P. Volarovich and N. V. Churaev. Reviewed by P. A. Rebinder	639	641
CHRONICLE		
Work of the Subsection on Rheology of the All-Union Congress on Mechanics. N. V. Lazovskaya	641	643

COLLOID JOURNAL

Volume 22, Number 6 November-December, 1960

CONTENTS

	PAGE	RUSS. PAGE
Influence of the Structural and Mechanical Properties of Printing Inks on Their Behavior in the Printing Process. T. I. Gudkova, L. A. Kozarovitskii, and N. V. Mikhailov	649	649
Colloidochemical Principles of the Variations of Optical Properties and Weathering Resistance of Lacquers Pigmented with Carbon Black. Ya. M. Gurevich and R. F. Minaeva	657	658
Influence of the Chemical Nature of Carbon Black Surface on Its Interaction with Rubber and Sulfur and on the Vulcanization Kinetics. B. A. Dogadkin, Z. V. Skorodumova, and M. S. Fel'dshtein	661	663
Effect of the Degree of Chemical Modification of Silica Surface by Tetramethylchlorosilane on Adsorption of Nitrogen and Krypton Vapors. A. V. Kiselev, A. Ya. Korolev, R. S. Petrova, and K. D. Shcherbakova	669	671
Investigation of the Salt Stability of Palygorskite. E. G. Kister	677	680
Kinetics of Hydration and Growth of Crystallization Concretion Structures in Monomineral Cements of the Plaster of Paris Type. A. F. Polak	687	689
Filtration of Rarefied Air through Porous Bodies in the Transitional Pressure Region. M. V. Talaev	699	702
Electrooptical Properties of Lyophobic Colloids. 1. Statement of the Problem, Basic Methods, and Results. N. A. Tolstoi, A. A. Spartakov, and G. I. Khil'ko	701	705
The Residual Bottom Layer in Motion of a Viscoplastic Medium. S. M. Fleishman	711	717
Investigation of Boundary Friction and Adhesion in Relation to Studies of the Interaction of Finely Dispersed Particles. 3. Influence of Neutral Electrolytes on the Friction of Quartz, Ruby, and Agate at High Contact Pressures. G. I. Fuks and A. S. Mikhailyuk	715	720
Investigation of the System Chasov Yar Clay–Water by the Electrical Conductivity Method. V. B. Chernogorenko	725	730
Effect of the Deformation Rate on the Ultimate High-Elastic and Rupture Deformation of a Gel Solution of Aluminum Naphthenate. T. G. Shalopalkina and A. A. Trapeznikov	729	735
Study of the Nature of Bonding in the Rubber–Filler System. V. A. Shvetsov, A. P. Pisarenko, and A. S. Novikov	737	743
Particle-Size Distribution of the Disperse Phase in a Polydisperse Aerosol System. M. M. Yakubovich	741	748
Production of Periodic (Banded) Precipitates on Filter Paper by Means of Ionophoresis. Stoico Jancov	745	752
LETTERS TO THE EDITOR		
Plasticizer–Filler Interaction. M. P. Zverev and P. I. Zubov	749	756

CONTENTS (continued)

	PAGE	RUSS. PAGE
Kinetics of Turbidity Variations in Dilute Synthetic Latexes During Coagulation by Electrolytes. R. E. Neiman and O. A. Lyashenko	751	757
Causes of Gelation in Rubber Latexes. D. M. Sandomirskii and I. D. Pil'menshtein	753	759
Normal Stresses in Colloidal Structurized Systems and the Effect of Thixotropic Structure Restoration on Them. A. A. Trapeznikov, A. S. Morozov, and G. G. Petrzhik	757	761
AUTHOR INDEX, VOLUME 22, 1960	759	
TABLES OF CONTENTS, VOLUME 22, 1960	763	